



Abstract Volume 9th Swiss Geoscience Meeting

Zurich, 11th – 13th November 2011

sc | nat 

Geosciences
Platform of the Swiss Academy of Sciences

ETH

Eidgenössische Technische Hochschule Zürich
Swiss Federal Institute of Technology Zurich

Edited by the Swiss Academy of Sciences

Cover page images (author: Pierre Dèzes, SCNAT):

Large picture: Mammoth Hot Springs, Yellowstone National Park, Park County, Wyoming, USA

Small picture: Alpine ibex, (*Capra ibex*). Brienzer Rothorn, Berner Oberland, Switzerland.

9th Swiss Geoscience Meeting, Zurich 2011

Table of contents

Organisation	2
Abstracts	
0. Plenary Session	4
1. Structural Geology, Tectonics and Geodynamics	10
2. Mineralogy – Petrology – Geochemistry	82
3. Low-Temperature Isotope Geochemistry	138
4. Perspectives on batholith formation and evolution in 4D	156
5. Geomorphology	184
6. Quaternary Research	200
8. Hydrology and Sustainable Water Resources Management in View of Global Changes	230
9. Open Cryosphere Session	254
10. Meteorology and Climatology	286
11. Greenhouse Gases: Linkages between Biosphere and Climate	286
12. Natural or man-made mineral dust and its influence on humans, environment and climate	294
14. Traces of life on planet Earth: A tribute to the late Professor Lukas Hottinger	306
15. Geoscience and Geoinformation - From data acquisition to modelling and visualisation	332
16. Earth System Science related Earth Observation	350
17. Synergies between Advancements in Geodesy and other Geosciences	364
18. Advances in GIScience and Remote Sensing	378
20. Deep Geothermal Energy	394
21. Geophysics and Rockphysics	410
22. Special symposium in honor of Daniel Bernoulli & Albert Matter	434

Organisation

Host Institution

Departement of Earth Sciences of the ETH Zurich

Patronnage

Platform Geosciences, Swiss Academy of Sciences

Program Committee

Daniel Ariztegui	Karl Föllmi	Franziska Nyffenegger
Stefano Bernasconi	Markus Furger	Nils Oesterling
Rizlan Bernier-Latmani	Isabelle Gärtner-Roer	Adrian Pfiffner
Gilles Borel	Alain Geiger	Rolf Philipona
Hugo Bucher	Bernard Grobéty	Eric Reusser
Beat Bürki	Irka Hajdas	Bruno Schädler
Lionel Cavin	Kurt Hanselmann	Michael Schaepman
Nathalie Chèvre	Elena Havlicek	Jürg Schweizer
Reynald Delaloye	Christoph Heinrich	Manfred Thüring
Pierre Dèzes	Adrian Jakob	Peter Ulmer
Hans-Rudolf Egli	Christophe Joerin	Dea Voegelin
Markus Egli	Edi Kissling	Helmut Weissert
Werner Eugster	Florian Kober	Adrian Wiget
Charles Fierz	Rainer Kündig	
David Floess	Neil Mancktelow	

Local Organizing Committee

Helmut Weissert	Peter Bayer	Peter Brack
Neil Mancktelow	Stefano Bernasconi	Paul Tackley
Peter Ulmer	Alain Geiger	Hugo Bucher
Eric Reusser	Florian Kober	Christophe Schneble

Participating Societies and Organisations

Federal Office of Meteorology and Climatology (MeteoSwiss)
Federal Office of Topography (swisstopo)
Forum for Climate and Global Change (ProClim-)
International Geosphere-Biosphere Programme, Swiss Committee (IGBP)
International Union of Geodesy and Geophysics, Swiss Committee (IUGG)
International Union of Geological Sciences, Swiss Committee (IUGS)
Kommission der Schweizerischen Paläontologischen Abhandlungen (KSPA)
Steering Committee NRP 61 (SNSF)
Swiss Association of Geologists (CHGEOL)
Swiss Commission for Oceanography and Limnology (COL)
Swiss Commission for Phenology and Seasonality (CPS)
Swiss Commission for Remote Sensing (SCRS)
Swiss Commission on Atmospheric Chemistry and Physics (ACP)
Swiss Geodetic Commission (SGC)
Swiss Geological Society (SGG/SGS)
Swiss Geological Survey (swisstopo)
Swiss Geomorphological Society (SGGm/SSGm)
Swiss Geophysical Commission (SGPK)
Swiss Geotechnical Commission (SGTK)
Swiss Group for Engineering Geology (SFIG)
Swiss Hydrogeological Society (SGH)
Swiss Hydrological Commission (CHy)
Swiss Meteorological Society (SGM)
Swiss National Science Foundation (SNSF)
Swiss Paleontological Society (SPG/SPS)
Swiss Snow, Ice and Permafrost Society (SIP)
Swiss Society for Hydrology and Limnology (SGHL / SSSL)
Swiss Society for Microbiology (SSM)
Swiss Society for Quaternary Research (CH-QUAT)
Swiss Society of Mineralogy Petrography (SMPG / SSMP)
Swiss Soil Science Society (SSSS)
Swiss Tectonics Studies Group (Swiss Geolocial Society)

0. Plenary Session

- 1 Halliday, Alex N.: The origin of the Earth and its volatiles
- 2 Kump, Lee R.: Emergence of an Aerobic Biosphere during the Archean-Proterozoic Transition
- 3 MacLeod, Norman: 'Mass Extinctions' in the Geological Record: Causes and Consequences
- 4 Boetius, Antje: Geosphere-Biosphere Interactions: Methane-based life at the ocean floor
- 5 Imboden, Dieter: Will research save planet Earth?

1

The origin of the Earth and its volatiles

Alex N Halliday

Oxford University

The origin of Earth is well explained by oligarchic accretion of planetesimals and planetary embryos over tens of millions of years. The last major event is thought to have been the Moon forming Giant Impact which added about 10% of the planet's mass. Tungsten isotopic evidence demonstrates that the Earth's core grew during accretion. Comparisons with meteorite data for other bodies suggest that it may also have grown in relative proportion over time. The depletion of slightly siderophile elements such as vanadium is consistent with a primitive mantle that was more reduced during the earlier stages of accretion. This is confirmed by isotopic evidence that the core had sequestered a significant amount of silicon before the Giant Impact. Despite these advances in our understanding of the past 20 years there are significant issues that have not been resolved. The timing of the Giant Impact is still argued about with recently proposed ages ranging from 30 to 200 million years after the start of the solar system, extending to the ages of the oldest detrital zircon grains yet discovered on Earth. Similarly there still is no consensus about how water and other highly volatile elements were added to Earth. The final (<1%) stage of accretion is often thought to be the addition of a late veneer that provided the mantle and crust inventory of highly siderophile elements (gold, platinum etc) and volatiles such as water, carbon and nitrogen. The fact that this veneer is a far smaller proportion of the Moon's budget is hard to explain unless it was added to Earth by just a few very large bolides. It is generally modelled as relating to the last stages of accretion of all terrestrial planets. The isotopic and relative elemental abundances of highly volatile elements (noble gases, H, C, N) provide evidence of accretion from chondrite-like, as opposed to solar reservoirs. On this basis carbon and nitrogen are the most depleted elements in the silicate Earth. Some process, possibly core formation, removed them prior to partial reinstatement via the late veneer. However, it can be shown that a major fraction (>70%) of the hydrogen (water) budget is earlier, which is hard to reconcile with the hot dry early Earth models advocated by some.

2

Emergence of an Aerobic Biosphere during the Archean-Proterozoic Transition

Lee R. Kump

Department of Geosciences, Pennsylvania State University, University Park, Pennsylvania 16802, USA. (lkump@psu.edu)

The Archean-Proterozoic transition witnessed a revolution in the biosphere attendant upon the establishment of an oxygen-rich atmosphere. Perhaps for the first time, and apparently for the rest of Earth history, oxygen, the most potent of electron acceptors, became widely available to fuel aerobic metabolism and oxidative weathering of reduced materials on land. The timing for the passage of the rise of oxygen through the threshold for the cessation of mass-independent fractionation of sulfur isotopes ($\sim 10^{-5}$ of the present atmospheric level) is fairly well established (ca. 2.4 Ga). However, the reason that the atmosphere was anoxic in the Archean and oxygenated thereafter is not conclusively known. We have hypothesized that the transition to an aerobic biosphere was effected by a reduction in the volcanic sink for oxygen driven by a shift from a predominance of submarine volcanism to a more equal expression of both subaerial and submarine volcanism, itself a result of the stabilization of continents at the end of the Archean. In addition, we have discovered what may be the largest negative carbon isotope excursion of Earth history, occurring at the end of a ~ 400 m.y. interval of atmospheric oxygen rise (at ~ 2.0 Ga), and possibly reflecting the initial deep oxidative weathering of Archean and Paleoproterozoic organic-rich sedimentary rocks exposed on land. This oxidative weathering event may also be linked to the generation of the Oklo natural fission reactors and the widespread supergene enrichment of iron ores at this time.

3

'Mass Extinctions' in the Geological Record: Causes and Consequences

MacLeod Norman*

*Palaeontology Department, The Natural History Museum, Cromwell Road, London, UK SW7 5BD, (N.MacLeod@nhm.ac.uk)

With its decidedly biblical overtones, the phenomenon of 'mass extinction' has intrigued and puzzled scientists in many different disciplines ever since the first summaries of (palaeo)biodiversity data began to appear in the middle 1800s. Over the intervening 150 years an impressive number of hypotheses and mechanisms have been suggested to account for these global biotic turnover events (e.g., Benton 1990). Unfortunately, few of these hypotheses have been tested via reference to empirical observations.

This situation changed in 1980 with the proposal of the bolide extinction hypothesis for the Cretaceous-Tertiary extinction event (Alvarez et al. 1980) which predicted the existence of a globally distributed layer of sediments enriched in rare earth elements (e.g., Ir) coincident with the extinction. When an enriched zone of the predicted magnitude was recovered from many K-T boundary localities worldwide in sediments that appeared to be biostratigraphically coincident with a mass faunal and floral turnover the *prima facie* case for an extraterrestrial cause of this mass extinction appeared to have been made; especially in the light of subsequent discoveries of additional physical impact markers (e.g., shocked quartz) and the likely impact crater. However, most palaeontologists remained skeptical of the bolide impact hypothesis as a sufficient explanation for the K-T (or now, K-P) extinction event (Archibald et al. 2010). Moreover, despite initial claims for a 26 million year periodicity in extinction intensity peaks (Raup & Sepkoski 1984, 1986), little credible evidence has been produced to support the idea of bolide impact as a general cause for 'mass extinctions'.

For most palaeontologists very notion of 'mass extinction' is problematic insofar as there is no generally accepted technical definition of the term. Raup & Sepkoski (1984) identified five stage-level extinction-intensity peaks that 'stood apart' in terms of magnitude from the remaining data. These became the 'big five mass extinctions'. However, the distinctiveness of these intensity peaks was always the result of *a priori* filtering of these data (e.g., elimination of Cambrian stage data). More importantly, when new stage-level palaeobiodiversity data are plotted in rank order the resulting extinction-intensity distribution is continuous. This suggests there is no objectively definable 'mass extinction' class and implies that the mechanisms responsible for smaller extinction events are also responsible for the larger events. The 'big five' peaks stand out not because they are intrinsically large, but because the stage level intensities surrounding them are small. In other words the explanatory signal is not in the magnitude of the larger events, but in their temporal placement.

Results of statistical simulation studies localized extinction-intensity peaks and the temporal distribution of causal mechanism activity are instructive in terms of identifying the causes of these larger events. Evaluations of stage-level coincidences between the distributions of extinction intensity peaks and causal mechanisms against a randomized null model shows that LIP volcanism exhibits the only mechanism-based time series that exhibits a statistically significant association ($p=0.05$) with the 'mass extinction' record. Additionally, if a multiple-cause model involving LIP volcanism, large bolide impact, and sea-level regression is also evaluated against the extinction peak record, this association is also found to be significant. The multiple cause model is favoured by most palaeontologists because it provides a better fit with the complex taxonomic and ecological responses exhibited by different groups to environmental changes across the K-P boundary.

The quality of data collected from the stratigraphic literature of mass extinction intervals also remains suspect. For example, initial reports of the planktonic foraminiferal extinction event listed all but 1-3 members of the diverse Maastrichtian fauna as becoming extinct coincident with the K-P boundary and the Ir anomaly. It is now known that at least 30% of Maastrichtian fauna survived the K-P event (whatever its cause) and numerically dominated the lowermost Palaeocene oceans for up to 500,000 years before giving way to indigenous Danian forms. Until and unless similar investigations can be carried out in other groups the true character of these turnover episodes will remain uncertain. Regardless, it's not just the fine-scale patterns that are influenced by this source of error. Stage level summaries of planktonic foraminiferal biodiversity at the genus and family levels are also erroneous.

Although controversy continues to dog the issue of 'mass extinction' causality, there is much less disagreement over the significance of extinction to the process of evolution. Whether the extinction of the non-avian dinosaurs happened in less than a year as a result of a bolide impact or progressively over tens of thousands of years as a result of a chance coincidence of major extinction mechanisms, it happened and the result was that ecological space was opened up for colonization by new groups. But in addition to the traditional stories told about evolutionary contingency and the rise of the mammals, a key but under-appreciated macroevolutionary trend that appears to be driven by extinction is the accumulation of extinction resistance in the survivors of previous extinction events. Evidence for this can be seen in the character of the smaller stage-level extinction events, whose magnitude undergoes a substantial and highly structured decrease over time.

REFERENCES

- Alvarez, L. W., F. Alvarez, F. Asaro, and H. V. Michel. 1980: Extraterrestrial cause for the Cretaceous-Tertiary extinction, *Science*, 208,1095-1108.
- Archibald, J. D., 28 others. 2010: Cretaceous Extinctions: Multiple Causes, *Science*, 238, 973.
- Benton, M. J. 1990: Scientific methodologies in collision: The history of the study of the extinction of dinosaurs, *Evolutionary Biology*, 24, 371-400.
- Raup, D. M., and J. J. Sepkoski, Jr. 1984: Periodicity of extinctions in the geologic past. *Proceedings of the Natural Academy of Sciences*, 81, 801-805.
- Raup, D. M., and J. J. Sepkoski, Jr. 1986: Periodic extinction of families and genera, *Science*, 231, 833-836.

4

Geosphere-Biosphere Interactions: Methane-based life at the ocean floor

Antje Boetius

HGF MPG research group on Deep Sea Ecology and Technology, Alfred Wegener Institute for Polar and Marine Research, and Max Planck Institute for Marine Microbiology

Natural gas and oil are currently the most important sources of energy to mankind. The ocean floor contains large quantities of these hydrocarbons. But although they are constantly escaping from natural seeps, neither oil nor gas accumulate in the sea. This can be attributed to the activity of hydrocarbon-degrading microorganisms, comprising specialists for consuming the simplest hydrocarbon – methane – as well as those oxidizing complex substrates contained in petroleum and tar. The ability of marine hydrocarbon degraders to clean the ocean from oil and gas spills has been recently stressed in the aftermath of the catastrophic explosion of the Deep Horizon drilling platform in the Gulf of Mexico. But still surprisingly little is known on the development and activity of environmental microorganisms responsible for oil and gas degradation. This presentation makes a journey from some of the hot spots of microbial methanotrophy in the deep sea such as methane hydrate deposits and erupting mud volcanoes, to natural asphalt seeps and its fascinating tar-degrading microbial consortia, which form the basis of a chemosynthetic food web. All of these extreme environments host the anaerobic methanotrophic archaea (ANME), which may be the most relevant group in controlling methane fluxes from the seafloor to the hydro- and atmosphere. The ANME represent special lines of descent within the Euryarchaeota and appear to gain energy exclusively from the anaerobic oxidation of methane (AOM), with sulfate as the final electron acceptor. They are widely distributed in the marine seafloor, and can form the densest biomasses of microorganisms known on Earth if both methane and sulfate are available as energy sources. The presentation will summarize the current knowledge on AOM habitats and its challenges.

5

Will research save planet Earth?

Dieter Imboden*,**

** President of the Swiss National Science Foundation Research Council*

*** Institute of Biogeochemistry and Pollutant Dynamics, ETH Zurich, Universitätstrasse 16, 8092 Zurich (dieter.imboden@env.ethz.ch)*

Politics and scientific research have well defined goals and tasks - so the general wisdom. The latter produces knowledge (some would say 'true facts', what ever true means), the former normative boundary conditions for society which, in an ideal world, would be based on scientific facts and not contradict them. – Yet, this idealistic picture of the partition of responsibilities between science and politics has never hold. Science has never been just a fact finding enterprise, not now and not in the past. It has always (consciously or inadvertently) included a normative component, and thus scientists have always played politics, as well. This holds true not only for the 'softer social sciences and humanities', but also for the 'hard' sciences like physics and chemistry. In turn, politics has always been selective regarding the incorporation of scientific knowledge into its action. While there is hardly any government which would ignore the basic laws of statics in its regulations for the construction of buildings and bridges, things are more complex when it comes to issues like sustainability, a term once invented by science but meanwhile taken over (conquered?) by politics. Conflicts of interest exist on both sides, in politics because of some 'inconvenient truth', in science because of the enormous financial means invested in research. In order to avoid a disturbance of the research system similar to the collapse of the financial bubble it is of vital importance to critically analyze the role of science in society with respect to its real potential as well as to its inherent limits.

1. Structural Geology, Tectonics and Geodynamics

Neil Mancktelow, Guido Schreurs, Paul Tackley

Swiss Tectonics Studies Group of the Swiss Geological Society

TALKS

- 1.1 *Antić M., Kounov A., Trivić B., Peytcheva I., von Quadt A., Gerdjikov I., Serafimovski T., Tasev G.:* Unravelling of continued magmatic activity along the Serbo-Macedonian massif since the Precambrian (south Serbia, southwest Bulgaria and Macedonia)
- 1.2 *Baillieux P., Schill E., Moresi L.:* Development of permeable structures in Graben systems – geothermal reservoirs in the Upper Rhine valley
- 1.3 *Bauville A., Epard J.-L., Schmalholz S.:* A simple thermo-mechanical shear model for the Morcles fold nappe
- 1.4 *Buchs D., Bagheri S., Martin L., Hermann J., Arculus R.:* The role of seamount subduction in the evolution of convergent margins: constraints from the Paleo-Tethys suture zone in Iran
- 1.5 *Cochrane R., Spikings R., Wotzlaw J.:* Apatite ID-TIMS U-Pb Thermochronology: An example from southern Ecuador.
- 1.6 *Crameri F., Tackley P., Meilick I., Gerya T., Kaus B.:* Causes of single-sided subduction on Earth
- 1.7 *Frehner M.:* The neutral lines in buckle folds
- 1.8 *Gerya, T.:* 3-D numerical modelling of oceanic spreading initiation
- 1.9 *Härtel M., Herwegh M.:* Linking titanium-in-quartz thermometry and quartz microstructures: strong evidence of continued vein formation during strain localization
- 1.10 *Lechmann S. M., May D. A., Kaus B. J. P., Schmalholz S. M., Hetényi G.:* Comparing thin-sheet to fully 3D models with application to the India-Asia collision
- 1.11 *Pec M., Stünitz H., Heilbronner R.:* Slow pseudotachylites
- 1.12 *Peters M., Herwegh M., Wehrens P.:* Spatial distribution of quartz recrystallization microstructures across the Aar massif
- 1.13 *Pfiffner O. Adrian:* Structure of the Helvetic nappe system of the Swiss Alps and adjoining France and Austria.
- 1.14 *Pirouz M., Simpson G., Bahroudi A., Azhdari A.:* Neogene sediments and modern depositional environments of the Zagros foreland basin system
- 1.15 *Reitsma M., Spikings R., Schaltegger U., Ulianov, A.:* A late Paleozoic back-arc basin on the western Gondwana margin: age and geodynamic setting of Permo-Carboniferous sedimentary rocks of South-East Peru.
- 1.16 *Rolf, T., Coltice, N., Tackley, P.:* Thermal evolution in a spherical convection model with plate generation and mobile continents
- 1.17 *Ruh J., Kaus B.J.P., Burg J.-P.:* Effect of single and multiple décollement layers on thrusting dynamics in fold-and-thrust belts
- 1.18 *Ruiz, G.M.H., Negro, F., Babault, J., Frizon de Lamotte, D., Stuart, F., Stockli, D., Foeken, J., Thomsen, T.:* Tectono-thermal evolution of the Atlas system (SW Morocco), insights from low-temperature thermochronology and Raman spectroscopy on carbonaceous material
- 1.19 *Van der Lelij R., Spikings R., Ulianov A., Chiaradia M.:* Did Laurentia and Gondwana play terrane tennis in the Palaeozoic? The implications of a Iapetus convergent margin in the Merida Terrane, Venezuela

POSTERS**«Global & Planetary»**

- 1.A.1 Leone G., Gerya T., Tackley P.J., Moore W.B.: Evidence of transition tectonic regime as seen at Hi'iaka and Zal regions on Io.
- 1.A.2 Li Y., Deschamps F., Tackley P.J.: Thermo-chemical convection in spherical geometry: influence of core's size
- 1.A.3 Tackley P., Ammann M., Brodholt J., Dobson D., Valencia D.: Effect of rheology on mantle dynamics and plate tectonics in super-Earths
- 1.A.4 Yao C., Deschamps F., Tackley P., Sanchez-Valle C.: Thermal convection in the outer layer of icy satellites

«Subduction, Lithosphere-scale»

- 1.B.1 Baitsch Ghirardello B., Nikolaeva K., Stracke A., Gerya T.V.: Pb, Sr and Nd in intra-ocean subduction zone: 2D geochemical-thermo-mechanical modeling
- 1.B.2 Duretz T., Gerya T.V., Spakman W.: Long term evolution of subduction-collision systems: numerical modelling
- 1.B.3 Liao J., Gerya T.: Extension of chemically stratified mantle lithosphere: numerical modeling
- 1.B.4 May D. A.: Decoupled and coupled multilevel preconditioners for problems in elasticity and variable viscosity Stokes flow
- 1.B.5 Zhu G., Gerya T., Tackley P., Kissling E.: Crustal Growth at Active Continental Margins : Numerical studies

«Shear zones etc.»

- 1.C.1 Kilian R., Heilbronner R., Stünitz H.: Quartz microstructures and crystallographic preferred orientation: which shear sense do they indicate?
- 1.C.2 Maeder X., Ghisleni R., Michler J.: Plastic deformation of quartz micropillars under uniaxial compression at room temperature
- 1.C.3 Maeder X., Schmalholz S., Bauville A.: Control of temperature, pressure gradient and flow law on the formation of crustal-scale shear zones: results from 1D thermo-mechanical modeling
- 1.C.4 Maeder X., Trullenque G., Drury M., De Bresser H.: Texture development and hybrid deformation mechanisms in fine grained calcite aggregates deformed in direct shear: constraints from electron backscatter diffraction analysis
- 1.C.5 Misra S., Burg J.-P.: Mechanics of kink-bands during torsion deformation of muscovite aggregate
- 1.C.6 Pleuger J., Zwingmann H., Manser M. & Mancktelow N.: K-Ar dating of some synkinematic clay fault gouges from Neoalpine faults
- 1.C.7 Précigout J., Hirth G.: The Origin of Olivine B-type Fabric in naturally deformed Peridotite: insight from the Ronda large-scale Mantle Shear Zone (Spain)
- 1.C.8 Thielmann M., Rozel A., Kaus B., Ricard Y.: Grain size evolution in 2D numerical simulations: Implications for lithospheric localization

«Alpine Studies»

- 1.D.1 *Abednego M., Vouillamoz N., Wust-Bloch H.G., Mosar J.*: Nano-seismology on the Fribourg Lineament - Switzerland
- 1.D.2 *Beltrán-Triviño A., Winkler W., von Quadt A.*: Triassic magmatism recorded by detrital zircons in pre-alpine sedimentary units
- 1.D.3 *Campani M., Mulch A., Kempf O., Schlunegger F. & Mancktelow N.*: Paleotopography of the Miocene European Central Alps
- 1.D.4 *Cardello G.L., Mancktelow N.*: Fault architecture at the brittle-ductile transition in sedimentary rocks – examples from the SW Helvetic (Swiss Alps)
- 1.D.5 *Egli D., Mancktelow N.*: Dextral movements between the Pennine Front and Mont Blanc massif in the Courmayeur area
- 1.D.6 *Mauri G., Negro F., Abdelfettah Y., Vuataz F-D., Schill E.*: Multi-disciplinary study for the exploration of deep low enthalpy geothermal reservoirs, Neuchâtel, Switzerland
- 1.D.7 *Psimoulis P., Feng L., Newman A., Stiros, S., Moschas F., Lycourghiotis S., Farmer G.*: Strong rupture and postseismic response of the 8 June 2008 Achaia-Elia earthquake in Western Peloponnese, Greece
- 1.D.8 *Ragusa, J., Ospina-Ostios, L.M., & Kindler, P.*: Fault-controlled formation of a primary turbiditic channel within the Gurnigel Flysch at the Voirons Massif (Haute-Savoie, France) during the Late Eocene.
- 1.D.9 *Scheiber T., Pfiffner O.A., Schreurs G.*: Large-scale geometry and structural evolution of the Bernhard nappe complex, Valais, Switzerland
- 1.D.10 *von Tschanner M., Schmalholz S.*: 3D FEM modeling of fold nappe formation in the Western Swiss Alps

«Extra-Alpine Studies»

- 1.E.1 *Bagheri S., Madhani-Fard R., Zahabi F., Javadi-Zadeh L.*: Kinematics of Doruneh Fault in central Iran: two different behaviors since Eocene time
- 1.E.2 *Bejaoui J., Samaali M., Baccouche S., Reguigui N., Ben Hamouda M. F., Azzouz Z., Trabelsi A., Bouhleb S. & Salim B.*: New information on radionuclides concentration in phosphorites originating from Tunisia and Algeria
- 1.E.3 *Bouilhol P., Jagoutz O., Hanchar J.M., Dudas F.O.*: Constraining collision events through arc magmatic record: The India / Arc / Asia collision
- 1.E.4 *Buchs D., Baumgartner P., Pilet S., Cosca M., Flores K., Bandini A.*: Petit-spot-like volcano exposed in Costa Rica
- 1.E.5 *Eugster P., Nagel S., Castellort S., Kaus B. J. P.*: Basin Dynamics in Taiwan
- 1.E.6 *Haghipour N., Burg J-P., Kober F., Zeilinger G., Ivy-Ochs S., Kubik P., Faridi M.*: Active crustal shortening in the Makran Accretionary Wedge (SE, Iran) revealed by deformed fluvial terraces
- 1.E.7 *Kais Aridhi, Sabri Aridhi, Mohamed Abdoullah Ould Bagga, Saâdi Abdeljaouad, Fouad Zargouni & Eric Mercier*: Paleogeographical restoration and ramp tectonic evidence in Tunisian Tellian domain: Ain El Bey-Bou Awen area (northwestern Tunisia).
- 1.E.8 *Mandal S K., Burg Jean-Pierre., Haghipour, N.*: Link between topography and large-scale tectonics of Southern India: A preliminary study based on river profile analysis
- 1.E.9 *Ruiz, G.M.H.*: Direct versus indirect thermochronology: What do we truly trace? An example from SE Peru and its implication for the geodynamic development of the Andes
- 1.E.10 *Tin Tin N., Winkler W., Mario N., Albrecht von Q.*: Provenance studies in sands and sandstones from the Bay of Bengal, Myanmar

1.1

Unravelling of continued magmatic activity along the Serbo-Macedonian massif since the Precambrian (south Serbia, southwest Bulgaria and Macedonia)

Antić Milorad¹, Kounov Alexandre¹, Trivić Branislav², Peytcheva Irena³, von Quadt Albrecht⁴, Gerdjikov Ianko⁵, Serafimovski Todor⁶ and Tasev Goran⁶

¹ Geologisch-Paläontologisches Institut, Universität Basel, 4056 Basel, Switzerland. (m.antic@unibas.ch)

² Faculty of Mining and Geology, University of Belgrade, 11000 Belgrade, Serbia

³ Geological Institute, Bulgarian Academy of Sciences, 1113 Sofia, Bulgaria

⁴ Institute of Geochemistry and Petrology, ETH-Zürich, 8092 Zürich, Switzerland

⁵ Faculty of Geology and Geography, St. Kl. Ohridski University of Sofia, 1504 Sofia, Bulgaria

⁶ Faculty of Natural and Technical Sciences, University "Goce Delčev" - Štip, 2000 Štip, Republic of Macedonia

Serbo-Macedonian massif (SMM) is a crystalline terrane, situated between the northeast-vergent Carpatho-Balkan and southwest-vergent Dinaride chains of the Eastern Mediterranean Alpine orogenic system. It is outcropping in southeastern Serbia, southwestern Bulgaria, eastern Macedonia and southern Greece. Its affiliation to European or African plate basement is still questionable due to the lack of reliable geochronological dating and detailed structural investigation along its boundaries. The massif is also a key area to understand the bipolarity of the Alpine orogenic system, as well as the interaction of the Pannonian and Aegean back-arc extension during the Cenozoic time.

SMM is generally considered as comprising an Upper (low-grade) and a Lower (medium to high-grade) unit (Dimitrijević, 1959). The protoliths of the both units are reported as volcano-sedimentary successions, which have later been intruded by magmatic rocks during several consecutive pulses. On our mission to discern the main magmatic episodes and understand the evolution of the SMM, we have dated metamorphic rocks from both units, as well as undeformed igneous rocks from the area. Conventional U-Pb zircon datings were carried out on multiple grains from the total of nineteen samples. For the first time the presence of Permo-Triassic (253 ± 13 Ma), as well as late Variscan magmatism (315 ± 9 Ma), is recognised in the Serbian part of the SMM together with Ordovician (483-442 Ma) and Cadomian (562-525 Ma) ones.

These datings, together with a careful examination of the field relationships, allowed us to conclude that the Lower SMM is consisting of pre-Ordovician volcano-sedimentary sequences and magmatics, intruded by Ordovician magmatic rocks. The Upper SMM (Vlasina and Morava units) contains gneissic basement, intruded by Ediacaran (Cadomian) magmatic rocks, all together covered by Silurian-Devonian volcano-sedimentary sequence. The youngest magmatic episode in the SMM occurred in the late Eocene and was related to the intrusion of Surdulica granodiorite and subsequent latitic volcanism lasting until the early Oligocene.

REFERENCES

Dimitrijević, M. D. 1959. Osnovne karakteristike stuba Srpsko-makedonske mase. (Basic characteristics of the column of the Serbo-Macedonian Mass). First symposium of the SGD, Abstracts.

1.2

Development of permeable structures in Graben systems – geothermal reservoirs in the Upper Rhine valley

Baillieux Paul¹, Schill Eva¹, Moresi Louis²

¹Centre d'Hydrogéologie et de Géothermie, Université de Neuchâtel, Rue Emile-Argand 11, CH-2000 Neuchâtel (paul.baillieux@unine.ch)

²School of Mathematical Sciences, Monash University, Wellington Rd Clayton 3800 VIC, Australia

Many geothermal anomalies occurring in non-volcanic graben systems (France, Germany, Turkey) are found to be linked to special tectonic structures of naturally enhanced hydraulic conductivity allowing heat transport by fluid circulation. In the Upper Rhine Graben, it has been observed that the localization of the thermal anomaly of the European EGS site Soultz corresponds to an area in the horst structure where seismic sections reveal high fault density (Baillieux et al., 2011). Similar interpretation has been deduced for magnetotelluric studies (Geiermann & Schill, 2010). This thermal anomaly has been explained by fluid convection through the two major reservoir faults (Soultz and Kutzenhausen faults) with permeability between 10^{-14} and 10^{-16} m² in the reservoir area (Kohl et al., 2000). For the example of Landau fluid convection cells have been simulated parallel to the two main faults (Bächler et al., 2003). This shows that fault zones are of particular interest for EGS.

In this study, we aim at simulating the development of an asymmetric graben with its internal fault distribution using key geodynamic information of the Upper Rhine Graben. The results are interpreted in terms of distribution of deformation pointing to geothermal favorable zones of naturally enhanced hydraulic conductivity.

The geometry of rifting and its type of extension is linked to the amount of strain softening (the relation which describes the decrease of strength of a rock when subject to faulting) in the brittle upper crust, the thickness of the upper crust, the viscosity and strength of the lower crust, the extension rate and other processes such as gravitationally driven deformation, isostasy, magmatism and necking (Buiter et al., 2008).

The recent thermo-tectono-stratigraphic forward modeling of the Upper Rhine Graben (Hinsken et al., 2010) suggest plane strain deformation and rifting at very low strain rate of about 1.7×10^{-16} s⁻¹ involving brittle-elastic deformation of the crust and ductile deformation of the highly viscous, high strength upper mantle.

We have simulated the development of deformation of the Upper Rhine Graben using “Underworld”, a geodynamic platform using a Lagrangian particle-in-cell finite element scheme (Moresi et al., 2007).

The results are benchmarked using the 3D geological model and deep seismic information from the Soultz site and the graben structure, respectively (Brun et al., 1992; Baillieux et al., 2011). For lower crust viscosity values of 5×10^{21} to 10^{22} Pa.s we approach the patterns of deformation observed in the Upper Rhine Graben.

For an intermediately strong to a strong lower crust, we find that after development of symmetrically conjugated faults, a preferential orientation develops into one main fault crossing the entire upper crust, which accommodates the deformation in this phase of graben formation. The presence of such a fault is suggested in the crustal-scale seismic exploration of the Rhine Graben (Brun et al., 1992). In the following phase a second boundary fault appears and the minor fault density is increasing in the area next to that boundary fault. This is also observed in the seismic results and provides indication for an asymmetric distribution of fault zones within a larger tectonic unit. This may explain also the fault density and temperature distribution in the horst structure of Soultz.

REFERENCES

- Bächler, D., Kohl T., et al. (2003). ‘Impact of graben-parallel faults on hydrothermal convection - Rhine Graben case study’. *Physics and Chemistry of the Earth* 28(9-11): 431-441.
- Baillieux, P., Schill E., et al. (2011). ‘3D structural regional model of the EGS Soultz site (northern Upper Rhine Graben, France): insights and perspectives’. *Proceedings, Thirty-Sixth Workshop on Geothermal Reservoir Engineering, Stanford University, Stanford, California, SGP-TR-191.*
- Brun, J. P., Gutscher M. A., et al. (1992). ‘Deep crustal structure of the Rhine Graben from seismic reflection data: A summary’. *Tectonophysics* 208(1-3): 139-147.
- Buiter, S. J. H., Huismans R. S., et al. (2008). ‘Dissipation analysis as a guide to mode selection during crustal extension and implications for the styles of sedimentary basins’. *Journal of Geophysical Research-Solid Earth* 113(B6): -.
- Geiermann, J. & Schill E. (2010). ‘2-D Magnetotellurics at the geothermal site at Soultz-sous-Forets: Resistivity distribution to about 3000 m depth’. *Comptes Rendus Geoscience* 342(7-8): 587-599.
- Hinsken, S., Schmalholz S. M., et al. (2010). ‘Thermo-Tectono-Stratigraphic Forward Modeling of the Upper Rhine Graben in reference to geometric balancing: Brittle crustal extension on a highly viscous mantle’. *Tectonophysics* In Press, Accepted Manuscript.
- Kohl, T., Bächler D., et al. (2000). ‘Steps towards a comprehensive thermo-hydraulic analysis of the HDR test site Soultz-sous-Forêts’. *Proc. World Geothermal Congress 2000, Kyushu-Tohoku, Japan, May-June 2000*, pp. 2671-2676.
- Moresi, L., Quenette S., et al. (2007). ‘Computational approaches to studying non-linear dynamics of the crust and mantle’. *Physics of The Earth and Planetary Interiors* 163(1-4): 69-82.

1.3

A simple thermo-mechanical shear model for the Morcles fold nappe

Bauville Arthur, Epard Jean-Luc & Schmalholz Stefan Markus

Institut de Géologie et Paléontologie, Anthropole, Université de Lausanne, CH-1015 Lausanne (arthur.bauville@unil.ch)

The Morcles nappe in the western Swiss Alps is a kilometer scale recumbent fold. It exhibits a uniform top-to-the-north shear sense and a shear strain that increases from the top (in the normal limb) to the bottom (in the overturned limb). We present a simple one-dimensional (1D) mathematical shear zone model to explain the first order geometry and strain pattern of the Morcles fold nappe. The applied simple shear model set-up is motivated by previous kinematic models for the formation of the Morcles nappe (Dietrich & Casey 1989, Epard & Escher 1996).

Our model is based on fluid dynamics and also considers a temperature dependent viscosity. In our model strain localization at the base of the nappe is controlled by a decrease in the temperature dependent viscosity. We derive an analytical solution for the horizontal (i.e. parallel to the shear zone) velocity which varies vertically across the shear zone. The velocity variation is controlled only by a single dimensionless parameter β . β depends on the activation energy of the applied flow law and the temperature profile across the shear zone which both are relatively well constrained by rock deformation experiments of calcite (e.g. Schmid et al., 1979 and Schmid et al., 1980) and thermometry (e.g. Kirschner et al. 1995). We use the calculated velocity to deform an initially straight line that makes an initial angle α with the shear direction. The final shape of the deformed line, including shapes of recumbent folds, depends on three parameters: β , α , and the finite shear strain, γ (i.e. total horizontal displacement across the shear zone divided by shear zone thickness, Figure 1).

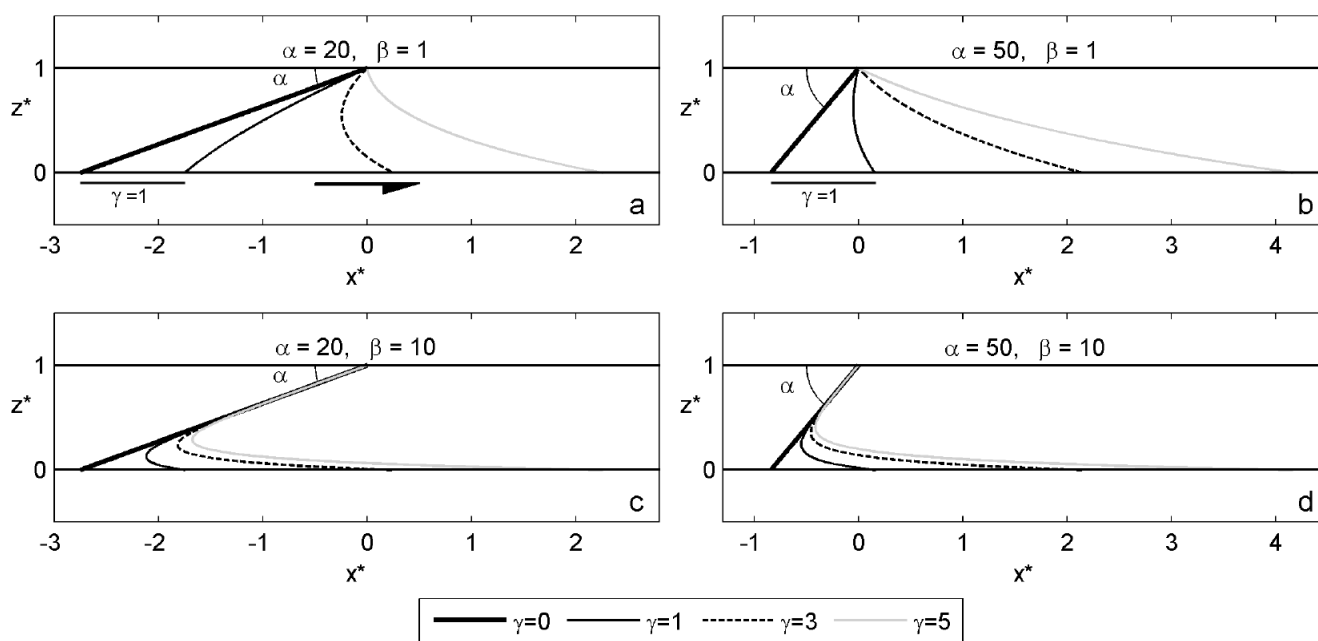


Figure 1. Results of numerical simulations showing the deformation of an initially straight and oblique line for various sets of parameters $\alpha - \beta - \gamma$. The upper boundary is fixed while the bottom boundary moves to the right with a constant velocity. The horizontal axis x^* and vertical axis z^* are normalized by the shear zone thickness. The strain localization, controlled by β , needs to be high enough to create an overturned limb that develops for high enough values of γ .

We apply our model to simulate the formation of the first order features of the Morcles fold nappe. We use the Schrattekalk (Urgonian) unit in the Morcles nappe to define a curved reference line which represents the first order geometry of the frontal part of Morcles fold nappe, i.e. the north dipping normal limb and the overturned limb. We perform a large number of shear zone simulations to determine the set of values for β , α and γ which fit the reference line best. The obtained range of best fit values for β is in agreement with field-based temperature estimates and flow laws of calcite.

Our 1D fluid dynamic shear zone model can explain several first order features of the Morcles fold nappe, such as (1) the recumbent fold geometry, (2) the uniform top-to-north shear sense and (3) the increase of shear strain towards the base of the nappe in the overturned limb.

Our first order model results are, therefore, in agreement with (1) geometrical constrains for the shape of the Morcles nappe, (2) kinematic constrains for the finite shear strain distribution within the nappe and (3) physical constrains for rheology (flow law) and temperature.

We use the best fit parameters to retro-deform the reference line which provides estimates for the horizontal movement of the Morcles nappe between 10 and 15 km. We further apply an elaborated 1D shear zone model in which the deformation is driven by a horizontal pressure gradient. The results indicate that for standard calcite flow laws and temperature profiles constrained from field data the shear zone thickness is of the order of a few kilometers in agreement with the size of the Morcles fold nappe. Horizontal pressure gradients in the order of 1 to 10 MPa/km are necessary to yield horizontal velocities in the order of centimeters per year.

Our simple thermo-mechanical model provides important results for a better understanding of the dynamics of fold nappe formation and yields the basis for further, more elaborated, 2D models for the formation of the Morcles nappe.

REFERENCES

- Schmid, S., Boland, J. & Paterson, M. 1977: Superplastic flow in fine-grained limestone. *Tectonophysics* 43(3–4), 257–291.
- Schmid, S., Paterson, M. & Boland, J. 1980: High temperature flow and dynamic recrystallization in Carrara marble. *Tectonophysics* 65, 245–280.
- Dietrich, D. & Casey, M. 1989. A new tectonic model for the Helvetic nappes. In: *Alpine Tectonics* (edited by Coward, M. P., Dietrich, D. & Park, R. G.). Geological Society special publication, 47-63.
- Epard, J. L. & Escher, A. 1996. Transition from basement to cover: A geometric model. *Journal of Structural Geology*, 18(5), 533-548.
- Kirschner, D. L., Sharp, Z. D. & Masson, H. 1995. Oxygen-isotope thermometry of quartz-calcite veins - unraveling the thermal-tectonic history of the subgreenschist facies Morcles nappe (Swiss-Alps). *Geological Society of America Bulletin*, 107(10), 1145-1156.

1.4

The role of seamount subduction in the evolution of convergent margins: constraints from the Paleo-Tethys suture zone in Iran

Buchs David¹, Bagheri Sasan², Martin Laure³, Hermann Joerg³ & Arculus Richard³

¹IFM-GEOMAR, Kiel, Germany (dbuchs@ifm-geomar.de)

²University of Sistan and Baluchestan, Iran

³Research School of Earth Sciences, Australian National University

Seamounts of volcanic origins are very abundant in modern oceans and may play a significant role in the evolution of convergent margins. Integrated satellite and ship-track bathymetry data show that >200'000 seamounts occur today in the world, covering >12% of the ocean floor (Hillier & Watts, 2007). Seamounts are morphologically and compositionally distinct from the “normal” ocean floor, and geophysical and geochemical observations along modern convergent margins show that seamount subduction is an important process, which can notably trigger: (1) mass-wasting of the forearc wedge and subduction erosion by abrasion of the upper plate (e.g. Ranero & von Huene, 2000); and (2) compositional changes of the arc magmatism (e.g. Hoernle et al., 2008). In addition, field observations indicate that accreted seamount material is abundant along some margins (e.g. Buchs et al., 2011), indicating that seamounts can contribute to the construction of convergent margins at shallow depth. However, processes of seamount subduction or accretion are still poorly constrained in space and time, and poorly documented in deeper levels of the subduction zone. We have investigated a Variscan accretionary complex exposed along the Paleo-Tethys suture zone in Iran, which provides new constraints on the role of seamount subduction in the long-term evolution of convergent margins.

The studied accretionary complex belongs to the Anarak-Jandaq composite terrane, which formed along the northern Paleo-Tethyan margin between the Devonian and Triassic and was exhumed during the closure of the Paleo-Tethys in Triassic times (Bagheri & Stampfli, 2008). Combined field observations, satellite multispectral data and geochemical analyses allow recognition of four types of lithologic assemblage in the complex: (1) meta-igneous rocks and marble that represent accreted fragments of seamounts; (2) arc-derived meta-igneous rocks; (3) meta-greywacke considered to represent accreted forearc or trench-fill sediment; and (4) serpentinitized peridotite bodies of undefined origin, which locally contain altered volcanic intrusives and pillow lavas in blueschist facies conditions. These lithologies occur as kilometer-sized slices preserved in low, greenschist and blueschist facies conditions. Most of the fragments of seamounts and arc-derived meta-igneous rocks are embedded within a matrix of accreted meta-greywacke. This suggests that subducting seamounts were

disembled and partly underplated during their transit to deeper levels of the subduction zone. Similarly, the occurrence of arc-derived meta-igneous rocks in the accretionary complex is interpreted to record underplating of mass wasting products.

Our results show that subducting seamounts that have the potential to trigger mass wasting and subduction erosion in the shallowest parts of the subduction zone may contribute to the construction of the margin at greater depth. This is an important result, because the accretionary or erosive nature of modern convergent margins is commonly inferred based on the nature and evolution of the outermost, shallower part of the margins, and subducting seamounts are generally thought to cause net subduction erosion (e.g. Ranero & von Huene, 2000).

In addition, the geochemistry of the accreted seamounts in Iran is similar to that of typical ocean island basalts, with only minor differences in fluid-mobile element contents. We calculated that seamount subduction occurs today at a rate of ~ 0.34 seamount $\text{km}^{-1} \text{Ma}^{-1}$ along the Pacific margins. High rate of seamount subduction at a global scale, distinct composition of seamounts relative to that of the “normal” ocean floor, and preservation of the seamount composition to deep levels of subduction zones indicate that seamounts are likely to play a major role in the chemical cycle of the silicate Earth; an estimation of the chemical flux related to seamount subduction is in progress.

REFERENCES

- Bagheri, S. & Stampfli, G., 2008: The Anarak, Jandaq and Posht-e-Badam metamorphic complexes in central Iran: New geological data, relationships and tectonic implications. *Tectonophysics* 451, 123-155.
- Buchs, D.M., Arculus, R.J., Baumgartner, P.O. & Ulianov, A., 2011: Oceanic intraplate volcanoes exposed: Example from seamounts accreted in Panama. *Geology* 39, 335-338.
- Hillier, J.K. & Watts, A.B., 2007: Global distribution of seamounts from ship-track bathymetry data. *Geophysical Research Letters* 34, L13304.
- Hoernle, K., Abt, D.L., Fischer, K.M., Nichols, H., Hauff, F., Abers, G.A., van den Bogaard, P., Heydolph, K., Alvarado, G., Protti, M. & Strauch, W., 2008: Arc-parallel flow in the mantle wedge beneath Costa Rica and Nicaragua. *Nature* doi:10.1038/nature06550.
- Ranero, C.R. & von Huene, R., 2000. Subduction erosion along the Middle America convergent margin. *Nature* 404, 748-755.

1.5

Apatite ID-TIMS U-Pb Thermochronology: An example from southern Ecuador.

Ryan Cochrane¹, Richard Spikings¹, Jörn Wotzlaw¹

¹ Department of Mineralogy, University of Geneva, Switzerland (ryan.cochrane@unige.ch)

Thermochronological methods assume that daughter isotopes are lost by a temperature-dependant mechanism, e.g. fission track diffusion and that isotope loss by fluid assisted mechanisms is negligible. If these assumptions are true, a combination of age and a second variable, which provides information about daughter isotope loss can provide thermal history information over a given temperature range. The $^{40}\text{Ar}/^{39}\text{Ar}$ (biotite and alkali feldspar), fission track (zircon and apatite) and (U-Th)/He (zircon and apatite) methods have been extensively applied to the Andean cordilleras of Ecuador (e.g. Spikings et al., 2001, 2010), and reveal thermal history information during the previous ~ 75 Ma, since the time of collision of the Caribbean Large Igneous Province (CLIP) with the north-western Andean margin. Partial daughter isotope loss occurs at temperatures between $\sim 350 - 400^\circ\text{C}$ with these methods. The thermally activated diffusion of Pb in titanite and apatite occurs at temperatures of $\sim 650-550^\circ\text{C}$ and $\sim 550-450^\circ\text{C}$ (e.g. Schoene and Bowring, 2007) and hence may be suitable to constrain the cooling and exhumation histories of the northern Andean margin prior to the collision of the CLIP.

This study aims to investigate the pre-CLIP tectonic history of Ecuador by combining titanite and apatite U-Pb data with hornblende and white mica $^{40}\text{Ar}/^{39}\text{Ar}$ data to quantify the post-anatectic thermal and burial/exhumation histories of Triassic migmatites and granites.

We present preliminary apatite U-Pb ID-TIMS dates obtained from a Triassic (247.2 ± 4.3 Ma, zircon U-Pb LA-ICP-MS) S-Type granite collected from southern Ecuador, which formed during early rifting of western Pangaea. U-Pb ages have been acquired from seven grain size aliquots in which the grain size diameters vary from 90 ± 10 μm to 350 ± 10 μm (all euhedral grains), spanning a closure temperature range of $450 - 510^\circ\text{C}$ for cooling rates of $10^\circ\text{C}/\text{my}$ (assuming that Pb is lost

by thermally activated diffusion). The grain size aliquots yield very precise concordant $^{238}\text{U}/^{206}\text{Pb}$ ages that range between 137.87 ± 0.34 and 94.53 ± 0.47 Ma. Furthermore, a positive age-to-grain size correlation implies that volume diffusion is the dominant process controlling Pb loss. We have obtained a set of time (t)-temperature (T) solutions (Figure 1) for the preliminary data using a controlled random search procedure provided by the HeFTy software (version 1.6.7; Ketcham 2009), using the diffusion parameters of Cherniak et al. (1991; Activation Energy of 54.6 Kcal/mol; Absolute Diffusivity of $1.27 \times 10^{-4} \text{cm}^2 \text{s}^{-1}$). Geological constraints for the t-T solutions provided considerable freedom, and are i) zircon crystallization at ~247 Ma during a thermal spike that caused widespread anatexis (Figure 1, A), and ii) cooling during 75-65 Ma as a consequence of the collision of the CLIP. The thermal history solutions satisfy the U-Pb ages obtained from four size aliquots. The best fit t-T solutions (Kolmogorov-Smirnoff goodness of fit > 0.4) reveal a period of Early Cretaceous heating from ~200°C to ~510°C during 140-100 Ma (Figure 1, B), at rates of ~10°C/my, followed by a period of rapid cooling from ~510°C to ~300°C that started at 100-95 Ma (Figure 1, C).

We propose that the Jurassic trench migrated westward, accompanied by slab rollback that forced the arc axis to migrate oceanwards, and drove rapid extension in the upper plate forming the Alao/Salado Basin. We attribute heating of the Triassic basement rocks to i) asthenospheric upwelling that accompanied extension and the formation of transitional crust, and ii) basin sedimentation burial. Rapid cooling at ~100Ma is attributed to exhumation that accompanied rock uplift, which was driven by closure of the marginal Alao Basin during the rapid westward migration of the South American Plate during the Early Cretaceous.

The thermal history solutions obtained from apatite U-Pb data acquired from a single rock corroborate independent geological observations. Additional U-Pb thermochronology is scheduled to further assist in constraining the tectonic evolution of the Ecuadorian and Colombian margin prior to 75 Ma.

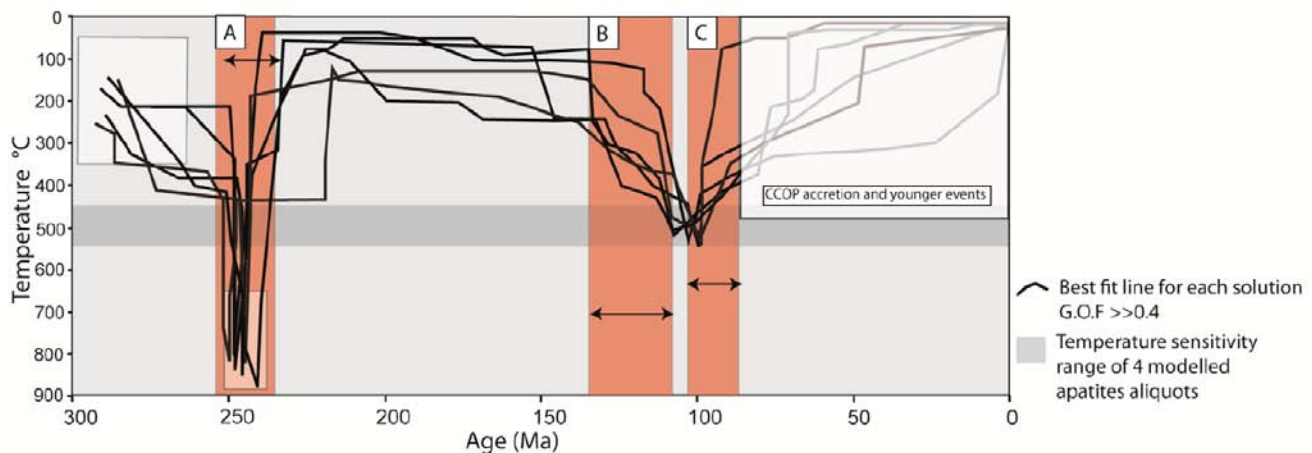


Figure 1: Time-temperature (t-T) history produced for 4 apatite $^{238}\text{U}/^{206}\text{Pb}$ ages.

REFERENCES:

- Cherniak, D.J., Lanford, W.A., Ryerson, F.J. (1991). Lead diffusion in apatite and zircon using ion implantation and Rutherford Backscattering techniques. *Geochim. Cosmochim. Acta* 55, 1663–1673.
- Schoene, B., & Bowring, S.A. (2007). Determining accurate temperature-time paths from U-Pb thermochronology: an example from the SE Kaapvaal Craton, Southern Africa. *Geochim. Cosmochim. Acta* 71, 165-185.
- Spikings, R.A., Seward, D., Winkler, W., Ruiz, G.M. (2001). Low-temperature thermochronology of the northern Cordillera Real, Ecuador: Tectonic insights from zircon and apatite fission track analysis. *Tectonics* 19, 649–668.
- Spikings, R.A., Crowhurst, P.V., Winkler, W., Villagomez, D. (2010). Syn- and post-accretionary cooling history of the Ecuadorian Andes constrained by their in-situ and detrital thermochronometric record. *Journal of South American Earth Sciences* 30 (2010) 121e133

1.6

Causes of single-sided subduction on Earth

Fabio Cramer, Paul Tackley, Irena Meilick, Taras Gerya, Boris Kaus

¹Departement Erdwissenschaften, ETH Zürich, Sonneggstrasse 5, CH-8092 Zürich (fabio.cramer@erdw.ethz.ch)

Subduction zones on present-day Earth are strongly asymmetric features (Zhao 2004) composed of an overriding plate above a subducting plate that sinks into the mantle. While global self-consistent numerical models of mantle convection have reproduced some aspects of plate tectonics (Moresi & Solomatov 1998, Tackley 2000, van Heck & Tackley 2008), the assumptions behind these models do not allow for realistic single-sided subduction. Here we demonstrate that the asymmetry of subduction results from two major features of terrestrial plates: (1) the presence of a free deformable upper surface and (2) the presence of weak hydrated crust atop subducting slabs. We show that by implementing a free surface on the upper boundary of a global numerical model instead of the conventional free-slip condition, the dynamical behaviour at convergent plate boundaries changes from double-sided to single-sided. Including a weak crustal layer further improves the behaviour towards steady single-sided subduction by acting as lubricating layer between the sinking plate and overriding plate.

For this study we perform experiments in 2-D and 3-D global, fully dynamic mantle convection models with self-consistent plate tectonics. These are calculated using the finite volume multigrid code StagYY (Tackley 2008) with strongly temperature and pressure-dependent viscosity, ductile and/or brittle plastic yielding, and non-diffusive tracers tracking compositional variations (the 'air' and the weak crustal layer in this case).

In conclusion, a free surface is the key ingredient to obtain thermally single-sided subduction, while additionally including a weak crust is essential to obtain subduction that is both mechanically and thermally single-sided.

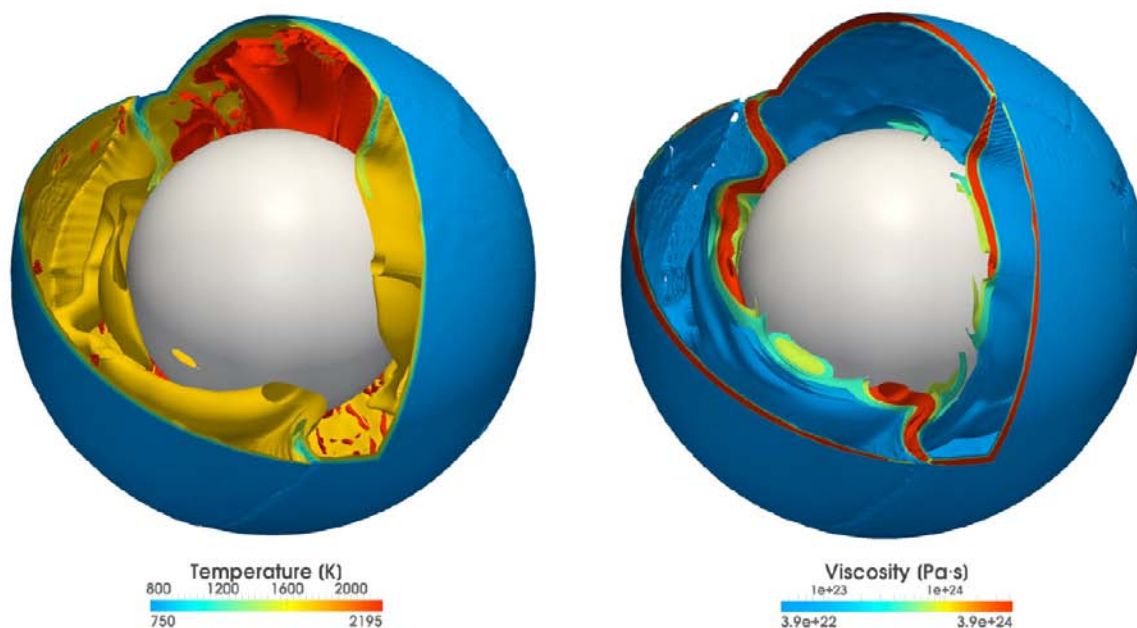


Figure 1. 3-D spherical single-sided subduction shown for temperature (left) and viscosity isosurfaces (right).

REFERENCES

- Zhao, D. P. (2004). Global tomographic images of mantle plumes and subducting slabs: insight into deep Earth dynamics. *Phys. Earth Planet. Inter. (Netherlands)* 146, 3-34, doi:Doi 10.1016/J.Pepi.2003.07.032.
- Moresi, L. & Solomatov, V. (1998). Mantle convection with a brittle lithosphere - Thoughts on the global tectonic styles of the Earth and Venus. *Geophys. J. Int.* 133, 669-682.
- Tackley, P. J. (2000). Self-consistent generation of tectonic plates in time-dependent, three-dimensional mantle convection simulations Part 1: Pseudo-plastic yielding. *Geochem., Geophys., Geosys.* Volume 1.
- van Heck, H. & Tackley, P. J. (2008). Planforms of self-consistently generated plate tectonics in 3-D spherical geometry. *Geophys. Res. Lett.* 35, doi:10.1029/2008GL035190, doi:doi:10.1029/2008GL035190.
- Tackley, P. J. (2008). Modelling compressible mantle convection with large viscosity contrasts in a three-dimensional spherical shell using the yin-yang grid. *Phys. Earth Planet. Int.*, doi:10.1016/j.pepi.2008.1008.1005, doi:doi:10.1016/j.pepi.2008.08.005.

1.7

The neutral lines in buckle folds

Marcel Frehner¹

¹Geological Institute, ETH Zurich, Sonneggstrasse 5, CH-8092 Zurich (marcel.frehner@erdw.ethz.ch)

The neutral line in a buckle fold is a fundamental concept in structural geology. It divides areas of outer-arc extension from areas of inner-arc shortening. Indeed, in natural folds so-called outer-arc-extension structures (Figure 1) or inner-arc-shortening structures (Figure 2) can occur.



Figure 1: Folded Carboniferous quartzwacke-layer near Almogrove, Portugal. Extension in the outer arc of the fold is evident from outer-arc-extension structures, i.e., quartz-filled extensional fractures perpendicular to the folded layer.



Figure 2: Folded Triassic limestone-marl multilayer sequence near Bad Eisenkappel, Austria. Shortening in the inner arc of the multilayer fold is evident from an inner-arc-shortening structure, i.e., a brittle thrust of approximately 20 cm offset.

In the past, folds have been constructed kinematically from a given neutral line geometry using the tangential longitudinal strain (TLS) pattern. In this study, a mechanical finite element (FE) model is used to numerically buckle single-layer folds with Newtonian and power-law viscous rheology. Two neutral lines can be distinguished:

The incremental neutral line (INL) (zero layer-parallel strain rate)

The finite neutral line (FNL) (zero finite layer-parallel strain)

The former develops first and migrates through the layer from the outer towards the inner arc ahead of the latter (Figure 3). Both neutral lines are discontinuous along the fold and terminate either at the bottom or top interface of the layer. For decreasing viscosity ratio between layer and matrix and for decreasing initial amplitude, the neutral lines develop later during folding and, for some cases, no neutral line develops (Figure 4). The dynamical behaviour of the neutral lines is similar for Newtonian and power-law viscous rheology if the viscosity ratio is large, but substantially different for small viscosity ratios (Figure 5).

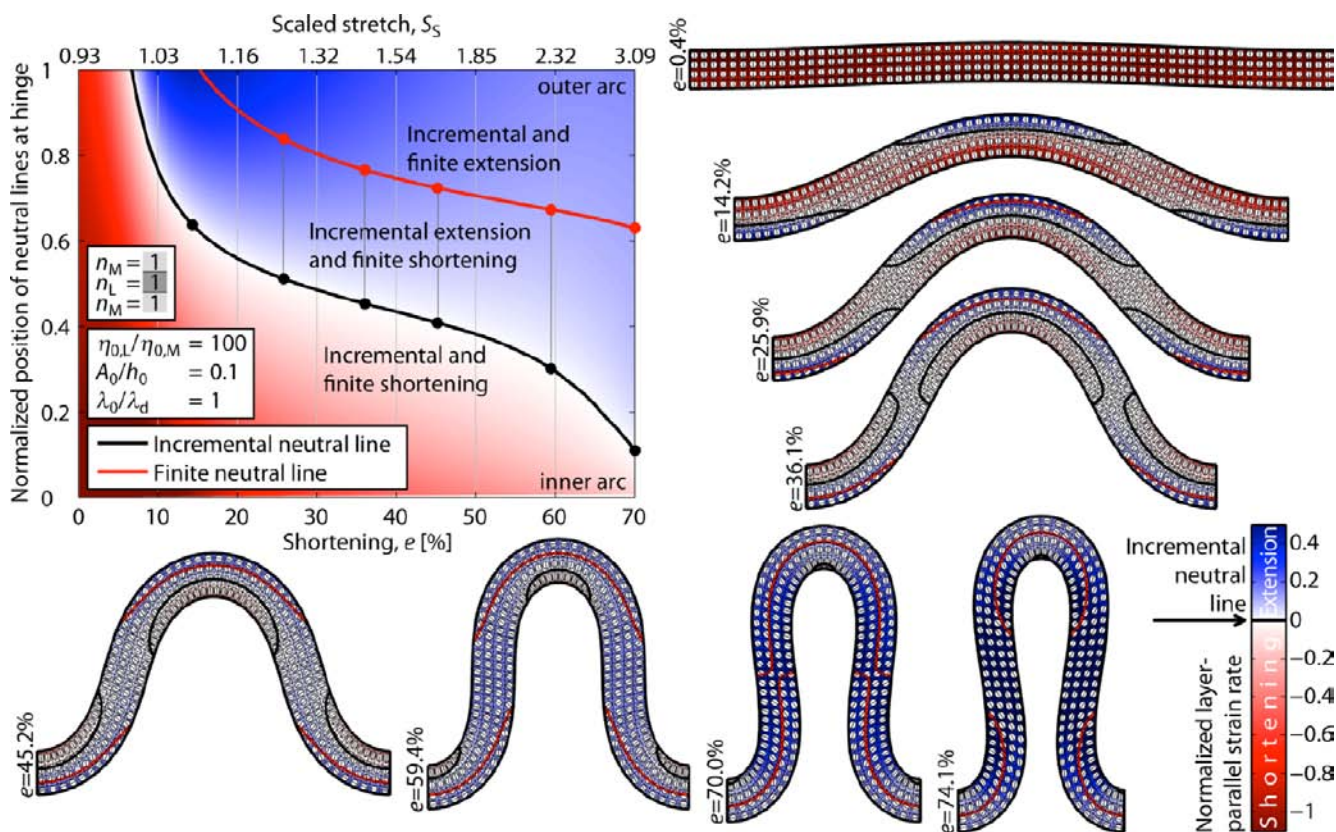


Figure 3. Simulation snapshots of a progressively shortened Newtonian single-layer fold with the indicated modelling parameters. Colours represent the layer-parallel strain rate normalized by the absolute value of the externally applied strain rate. The INL is drawn as a thick black line. The FNL is drawn as a thick red line. Finite strain ellipses with their major axis and a passive, initially orthogonal marker-grid are plotted. The upper-left diagram shows the layer parallel strain rate and the positions of the two neutral lines on the axial plane trace, normalized by the current thickness of the layer at the hinge, with increasing shortening (and scaled stretch). The dots indicate the shortening for which the different simulation snapshots are plotted.

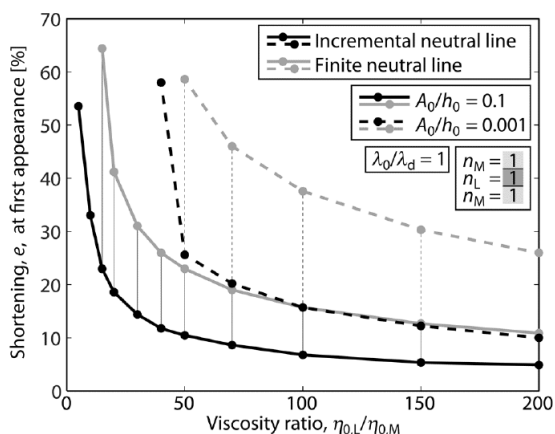


Figure 4. Shortening value at the first appearance of the neutral lines in the single-layer fold for all simulations using a Newtonian rheology.

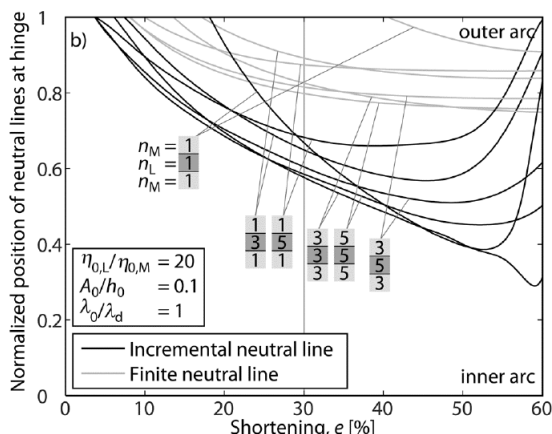


Figure 5. Positions of the two neutral lines on the axial plane trace of different power-law single layer folding simulations, normalized by the current thickness of the layer at the hinge.

REFERENCE

Frehner, M. 2011: The neutral lines in buckle folds, Journal of Structural Geology, doi:10.1016/j.jsg.2011.07.005.

1.8

3-D numerical modelling of oceanic spreading initiation

Gerya Taras¹

¹ *Institut of Geophysics, ETH-Zurich, Sonneggstrasse 5, CH-8057 Zurich (taras.gerya@erdw.ethz.ch)*

Mid-ocean ridges sectioned by transform faults represent prominent surface expressions of plate tectonics. A fundamental problem of plate tectonics is how this orthogonal pattern has formed and why it is maintained. Gross-scale geometry of mid-ocean ridges are often inherited from respective rifted margins. Indeed, transform faults seem to nucleate after the beginning of the oceanic spreading and can spontaneously form at a single straight ridge.

Due to the limited availability of data, detailed interpretations of nucleation and evolution of the orthogonal spreading pattern are difficult and controversial. Analogue and numerical modeling have to be additionally employed. Two main groups of analogue models were implemented (Gerya, 2011 and references therein): (i) thermomechanical freezing wax models with accreting and cooling plates and (ii) mechanical models with viscous mantle and brittle lithosphere. The freezing wax models reproduced characteristic orthogonal ridge - transform fault patterns but often produced open spreading centers with exposed liquid wax, which is dissimilar to nature. On the other hand, in the mechanical models, new lithosphere is not accreted in spreading centers, which is conflicting with oceanic spreading. Numerical models of transform fault nucleation (Gerya, 2011 and references therein) mostly focused on short-term plate fragmentation patterns and strain reached in these numerical experiments was too small to test the long-term evolution of transform faults. Recent large-strain numerical experiments (Gerya, 2010) studied spontaneous nucleation of transform faults at a pre-existing single straight ridge but the initiation and maturation of the orthogonal pattern after continental plate breakup remained unaddressed.

I present new 3-D numerical thermomechanical model of oceanic spreading initiation suggesting that orientation and geometry of transform faults and spreading centers changes with time as the result of accommodation of new oceanic crust growth. The resulting orthogonal ridge-transform system is established on a timescale of millions of years from an arbitrary plate breakup pattern. By its fundamental physical origin, this system is a crustal growth pattern and not a plate fragmentation pattern. In particular, the characteristic extension-parallel orientation of oceanic transform faults is a steady state orientation of a weak strike-slip fault embedded in between simultaneously growing offset crustal segments.

REFERENCES

- Gerya, T., 2010. Dynamical instability produces transform faults at mid-ocean ridges. *Science*, 329, 1047-1050.
 Gerya, T. (2011) Origin and models of oceanic transform faults. *Tectonophysics*, doi: 10.1016/j.tecto.2011.07.006

1.9

Linking titanium-in-quartz thermometry and quartz microstructures: strong evidence of continued vein formation during strain localization

Härtel Mike¹, Herwegh Marco¹

¹*Institute of Geological Sciences, University of Bern, Baltzerstrasse 1+3, 3012 Bern*

Detailed microstructural examinations on mylonites from the Simplon Fault Zone (SFZ) in southern Switzerland revealed the transition of different recrystallization processes in quartz veins of the footwall, ranging from Grain Boundary Migration Recrystallization (GBM) over Subgrain Rotation Recrystallization (SGR) to Bulging Nucleation (BLG), from the rim towards the centre of the shear zone. GBM-microstructures can be recognized at distances of more than 4400 m from the centre and at around 1200 m distance they start to be progressively overprinted by SGR (in the northern part), producing a kilometer-wide mylonite zone comprising ribbon textures in the quartz veins. Near the centre of the SFZ, core-mantle-structures develop and bands of bulging grains transect older quartz ribbons. This microstructural sequence displays the cooling-related localization of strain from initial temperatures over 600 °C down to temperatures lower than 350 °C with respect to their dynamically recrystallized grain sizes. However, the age relations between all the quartz veins remained unknown and some microstructures do not fit into this pattern. The application of Ti-in-quartz geothermometry revealed highest temperatures of 535 ± 17 °C as formation temperatures of GBM-samples, which is lower than the ex-

pected formation temperature. The reason for this discrepancy is the continuous adjustment of Ti-concentrations in quartz, during dynamic recrystallization in the GBM-regime. Within the zone of SGR-affected mylonites a very wide spread of temperatures occurs, ranging from 376 ± 6 °C up to 509 ± 4 °C. Taking into account that SGR overprints former microstructures, but inhibits the readjustment of Ti-concentration in quartz, these temperatures are considered to display the formation temperatures of the subsequently precipitating quartz veins, following the localization of strain. These data allow us to differentiate between veins by their relative age relations and to follow the path of the inhomogeneous overprint of the old microstructures with ongoing strain localization during exhumation and cooling.

1.10

Comparing thin-sheet to fully 3D models with application to the India-Asia collision

Sarah M. Lechmann¹, David A. May², Boris J. P. Kaus³, Stefan M. Schmalholz⁴ & György Hetényi⁵

¹ Geological Institute, ETH Zurich, CH-8092 Zurich (sarah.lechmann@erdw.ethz.ch)

² Institute of Geophysics, ETH Zurich, CH-8092 Zurich

³ Institute of Geosciences, Johannes Gutenberg-University Mainz, D-55128 Mainz

⁴ Inst. of Geology and Palaeontology, University of Lausanne, CH-1015 Lausanne

⁵ Swiss Seismological Service, ETH Zurich, CH-8092 Zurich

Various models have been proposed to explain tectonic deformation during continent collision. A frequently applied model is the thin viscous sheet model which is however not fully three-dimensional (3D) and assumes a priori diffuse thickening as the dominant deformation style.

We compare a fully 3D multilayer numerical model with a corresponding thin viscous sheet numerical model for the scenario of continent indentation. In our comparison we focus on the three basic viscous deformation styles thickening, buckling (folding) and lateral crustal flow. Both numerical models are based on the finite element method (FEM) and employ either a linear or power-law viscous rheology. The 3D model consists of four layers representing a simplified continental lithosphere: strong upper crust, weak lower crust, strong lithospheric mantle and weak asthenospheric mantle. The effective viscosity depth-profile in the 3D model is used to calculate the depth-averaged effective viscosity applied in the thin-sheet model allowing a direct comparison of the models.

We quantify the differences in the strain rate and velocity fields, and investigate the evolution of crustal thickening, buckling and crustal flow resulting from the two models for two different phases of deformation: (1) indentation with a constant velocity and (2) gravitational collapse after a decrease of the indenting velocity by a factor 5. The results indicate that thin-sheet models approximate well the overall large-scale lithospheric deformation, especially during indentation and for a linear viscous rheology. However, in the 3D model, additional processes such as multilayer buckling and lower crustal flow emerge. These are ignored in the thin-sheet model but dominate the deformation style in the 3D model within a range of a few hundred kilometers around the collision zone and indenter corner. Differences between the 3D and thin-sheet model are considerably larger for a power-law viscous than for a linear viscous rheology and especially buckling and lower crustal flow are significant in the 3D model.

3D multilayer models provide a more complete picture of continental collision than thin-sheet models as they enable studying the timing, location and relative importance of different processes simultaneously which is especially important for the 100 km scale around the collision zone and indenter corners.

In a second study we apply the 3D model to the India-Asia collision, where we distinguish between the Indian and the Asian domain, i.e. material parameters are varying both in the vertical and horizontal directions. The model geometry is set up using available geophysical data. From the CRUST2.0 dataset topography and depths of the lithospheric layers are used to set up the vertical layering, and measured Bouguer anomalies are applied to constrain the density structure. The viscosity distribution is controlled by comparing viscous and gravitational stresses. Viscosities must be large enough to counteract or equilibrate gravitationally induced stresses, so that the model does not flow under its own weight (i.e. collapse). We then perform instantaneous indentation of India into Asia to represent the present day state of the continent-continent collision. The impact of various rheological profiles on the velocity, stress and strain rate fields is studied and compared to geophysical observations, such as GPS velocities and anisotropy directions.

1.11

Slow Pseudotachylites

Matej Pec¹, Holger Stünitz² and Renée Heilbronner¹

¹Geological Institute, Basel University, Basel, Switzerland (matej.pec@unibas.ch)

²Department of Geology, Tromsø University, Tromsø, Norway

Tectonic pseudotachylites as solidified, friction induced melts are believed to be the only unequivocal evidence for paleo-earthquakes. Earthquakes occur when fast slip ($1 - 3 \text{ ms}^{-1}$) propagates on a localized failure plane and are always related with stress drops. The mechanical work expended, together with the rock composition and the efficiency of thermal dissipation, controls whether the temperature increase on a localized slip plane will be sufficient to induce fusion.

We report the formation of pseudotachylites during steady-state plastic flow at slow bulk shear strain rates ($\sim 10^{-3} \text{ s}^{-1}$ to $\sim 10^{-5} \text{ s}^{-1}$ corresponding to slip rates of $\sim 10^{-6} \text{ ms}^{-1}$ to $\sim 10^{-8} \text{ ms}^{-1}$) in experiments performed at high confining pressures (500 MPa) and temperatures (300°C) corresponding to a depth of $\sim 15 \text{ km}$.

Crushed granitoid rock (Verzasca gneiss), grain size $\leq 200 \mu\text{m}$, with 0.2 wt% water added was placed between alumina forcing blocks pre-cut at 45° , weld-sealed in platinum jackets and deformed with a constant displacement rate in a solid medium deformation apparatus (modified Griggs rig).

Microstructural observations show the development of an S-C-C' fabric with C' slip zones being the dominant feature. Strain hardening in the beginning of the experiment is accompanied with compaction which is achieved by closely spaced R1 shears pervasively cutting the whole gouge zone and containing fine-grained material ($d < 100 \text{ nm}$). The peak strength is achieved at $\gamma \sim 2$ at shear stress levels of 1350-1450 MPa when compaction ceases.

During further deformation, large local displacements ($\gamma > 10$) are localized in less densely spaced, $\sim 10 \mu\text{m}$ thick C'-C slip zones which develop predominantly in feldspars. In TEM, they appear to have no porosity consisting of partly amorphous material and small crystalline fragments with the average grain size of 20 nm. After the peak strength, the samples weaken by $\sim 20 \text{ MPa}$ and continue deforming up to $\gamma \sim 4$ without any stress drops. Strain localization progresses in the C'-C slip zones and leads to the formation of pseudotachylites. Rough estimates of slip rates in the deforming slip zones are 2 to 4 orders of magnitude higher ($\sim 10^{-2} \text{ ms}^{-1}$ to $\sim 10^{-6} \text{ ms}^{-1}$) than the bulk induced slip rate but clearly slower than seismic.

The composition of the pseudotachylites is usually more ferro-magnesian and less silicic than that of the bulk rock. Microstructural observations show the presence of corroded clasts of especially quartz, injection veins and bubbles with a strong shape preferred orientation within the molten material following the local flow pattern. The pseudotachylites are locally folded; their thickness varies between $< 1 \mu\text{m}$ to $10 \mu\text{m}$. Pseudotachylites have a distinct CL signal compared to any other material present in the less deformed experiments.

Our results indicate that pseudotachylite formation at the bottom of the seismogenic layer may not necessarily be connected with stress drops and thus with earthquakes.

1.12

Spatial distribution of quartz recrystallization microstructures across the Aar massif

Peters Max¹, Herwegh Marco¹, Wehrens Philip¹

¹Institut für Geologie Balzerstraße 1+3, CH-3012 Bern (max.peters@students.unibe.ch)

In the Aar massif, main foliation and major deformation structures were developed during NW-SE compression associated with the Alpine orogeny (Steck 1966). To be precise, shearing at the brittle to ductile transition may have initiated at different stages between 22-20 myr and 14-12 myr, followed by purely brittle deformation at around 10 myr (Rolland et al. 2009). In light of the onset of dynamic recrystallization in quartz, Bambauer et al. (2009) defined a quartz recrystallization isograd in the northern part of the Aar massif. To the south, the grain size of recrystallized grains increases due to an increase of metamorphic temperatures from N to S.

The aim of the current project is to carry out quantitative analysis on changes of the dynamic and static recrystallization behavior of quartz. A series of thin sections, covering an entire N-S transect from Guttannen to Gletsch, gives insights into the long lasting deformation and exhumation history of the crystalline rocks of the Aar massif. In addition, Titanium-in-quartz geothermometry (Kohn and Northrup 2009) was performed to learn more about the deformation temperatures and associated microstructural changes on the retrograde path.

In this N-S section, two general types of microstructures have to be discriminated: (i) weakly to moderately deformed host rocks and (ii) intensely deformed mylonites to ultramylonites out of high strain shear zones. (i) Volume fraction and size of recrystallized quartz grains increases towards the south showing grain size changes from around 5 μm up to ca. 250 μm . Southern microstructures are characterized by complete recrystallization.

In terms of recrystallization processes, a transition from bulging recrystallization in the N to subgrain rotation recrystallization in the S occurs. Such a change in recrystallization processes combined with grain size increase points towards a reduced differential stresses with increasing temperature (Bambauer et al. 2009). (ii) In contrast to the granitic host rocks the mylonites and ultramylonites show smaller recrystallized grain sizes. compared to their host rocks, but they They also reveal a general grain size increase from N to S. Here, enhanced strain rates compared to the host rocks result in overall smaller quartz grains.

In the S, microstructures from (i) and (ii) show equidimensional grains with 120° triple junctions and straight grain boundaries. Such microstructures are typical for static annealing. For that reason, we suggest a post-deformational temperature pulse mainly affecting the southern part of the Aar massif. This annealing stage might correlate with the fluid pulse between 12-10 myr suggested by Challandes et al. (2008).

REFERENCES

- Bambauer, H.U., Herwegh, M., Kroll, H. 2009: Quartz as indicator mineral in the Central Swiss Alps: the quartz recrystallization isograd in the rock series of the northern Aar massif. *Swiss Journal of Geosciences*, 102, 345-351.
- Kohn, M.J., Northrup, C.J. 2009: Taking mylonites' temperatures. *Geology*, 37, 47-50.
- Rolland, Y., Cox, S.F., Corsini, M. 2009: Constraining deformation stages in brittle–ductile shear zones from combined field mapping and ⁴⁰Ar/ ³⁹Ar dating: The structural evolution of the Grimsel Pass area (Aar Massif, Swiss Alps). *J. Struct. Geol.*, 31, 1377-1394.
- Stipp, M., Stünitz, H., Heilbronner, R. and Schmid, S.M. 2002: The eastern Tonale fault zone: a 'natural laboratory' for crystal plastic deformation of quartz over a temperature range from 250 to 700°C. *J. Struct. Geol.*, 24, 1861-1884.
- Stipp, M. & Tullis, J. 2003: The recrystallized grain size piezometer for quartz. *Geophysical Research Letters*, 30 (21).

1.13

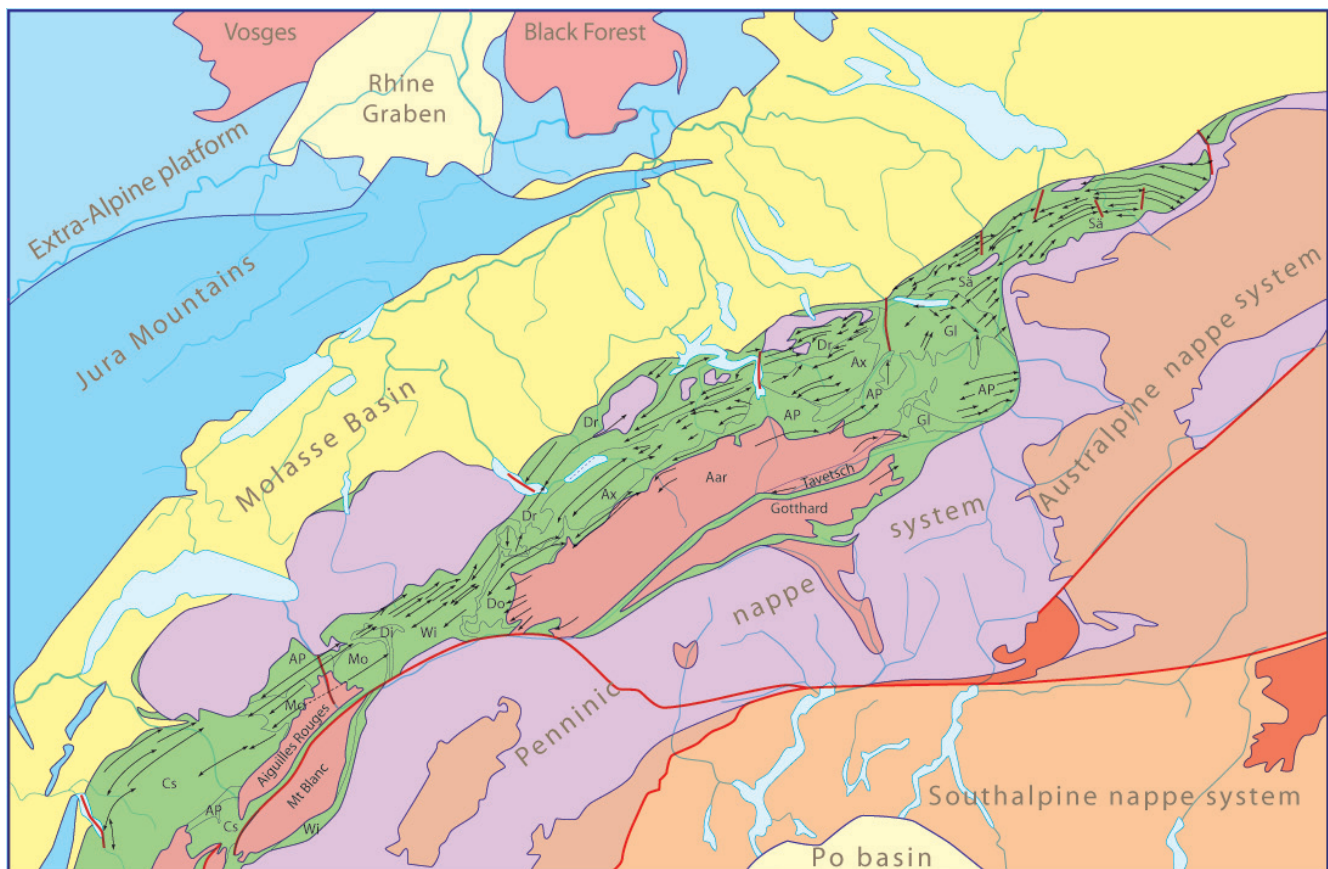
Structure of the Helvetic nappe system of the Swiss Alps and adjoining France and Austria.

Pfiffner O. Adrian

Institut für Geologie, Universität Bern, Baltzerstr. 1+3, Bern (adrian.pfiffner@geo.unibe.ch)

A new structural map of the Helvetic nappe system at the scale 1:100'000 has been prepared in the course of the past years based on a project initiated by John Ramsay in 1978. After revisions and expansion of the map area a digital version is now available (Pfiffner et al. 2009). The map consists of 7 individual sheets, each with a cross section and its own legend and . Considerable overlay between the map sheets help to facilitate lateral correlations. The map contains the traces of faults as well as the axial surfaces of large-scale folds. Lithologic units have been kept simple and adapted to the scale of the map.

The aim of the structural map series of the Helvetic zone is to show the lateral continuity of folds and thrusts, their spatial orientations and mutual interference as well as to highlight the characteristics of the fold-and-thrust structures in individual regions and units. The Helvetic zone, or nappe system, is subdivided into two zones with rather different structural style, the Helvetic nappes proper and the underlying Infrahelvetice complex. The Helvetic nappes comprise allochthonous sediments that were dislocated along a basal thrust fault over distances of several tens of kilometers. The Infrahelvetice complex encompasses all units beneath the basal thrust of the Helvetic nappes. It consists of pre-Triassic crystalline basement rocks and their autochthonous Mesozoic and Cenozoic sedimentary cover. The simplified map in Fig. 1 gives an overview of the nappe systems and foreland basins of the Central Alps. The major basal thrusts of the Helvetic nappes as well as the major transverse faults are also included along with the orientations of the fold axes of large-scale folds. As example a cross section of the Helvetic nappe system in central Switzerland ranging from the Molasse Basin to the rear of the Gotthard massif is shown in Fig. 2.



Cs = Châbles subalpines
Mo = Morcles nappe
AP = Autochthonous-Parautochthonous cover

Wi = Wildhorn nappe
Di = Diablerets nappe
Do = Doldenhorn nappe

Dr = Drusberg nappe
Ax = Axen nappe
AP = Autochthonous-Parautochthonous cover

Sä = Säntis nappe
Gl = Glarus-Mürtschen nappe
AP = Autochthonous-Parautochthonous cover

Fig. 1

The lateral continuity of the Helvetic nappes must be considered separately for the basal thrusts and the nappes as a whole, and the internal fold-and-thrust structures of the nappes. From west to east, the following units constitute the major nappes: Chaînes subalpines in Haute Savoie (France), Diablerets and Wildhorn nappe in western Switzerland, Axen and Drusberg nappe in central Switzerland, Glarus nappe complex and Säntis nappe in eastern Switzerland, with the Säntis nappe extending into Vorarlberg (Austria). The lateral change from the Diablerets-Wildhorn pair to the Axen-Drusberg pair occurs across the Kandertal, and the change to the Glarus-Säntis pair across the Lintlthal. In both instances the change is associated with a subvertical N-S striking fault with transform character. The change from the Chaînes subalpines to the Diablerets-Wildhorn pair must be sought across the Rhone valley. But erosion removed a substantial part of the originally neighboring nappes prohibiting a more thorough interpretation. The displacement along the basal thrust of the nappes is on the order of 10 to 50 km.

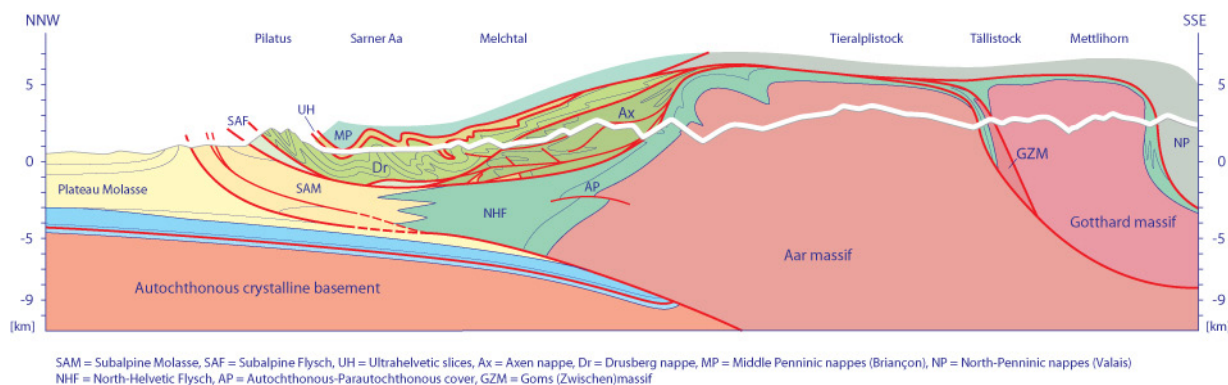


Fig. 2

At several locations relatively small imbricates occur in the footwall of the basal thrusts. They include the Gellihorn nappe and the Plammis and Jägerchrüz slices in the Kandertal-Leukerbad area, the Wissberg slice near Engelberg and the Griesstock and Clariden slices south of Klausenpass. In all of these cases the units can be interpreted as pieces detached either from the footwall dragged along the base of the nappes or as pieces detached from the hanging wall and overridden by the nappes.

The nappe-internal deformation includes large-scale folds and thrust faults with displacements typically being between 1 and 5 km. Very often folds and thrust faults are kinematically linked (fault-propagation and fault-bend folds). Detachment folds are observed where mechanically weak sediments are originally had a significant thickness. Examples include the Early and Middle Jurassic sequences in the Axen nappe in the areas around Interlaken and Engelberg and the Palfris Shale at the base of the Drusberg and Säntis nappes. In map view the fold axes trend parallel to the general strike at first sight. At some localities, however, the fold axes are arcuate in shape. Examples are found in the Chaînes subalpines, in the Axen and Drusberg nappes east of Kandertal and the Glarus nappe south of Walensee. The fold arcs are caused basin inversion and owe their shape to the original basin geometry.

A number of subvertical faults with transform character are responsible for major changes in the internal structure of the nappes. The faults are oriented at high angle to the fold axes of the nappes and have a strike-slip component. The most prominent ones are located in the valley of Lac d'Annecy, east of Samoëns, between Wildhorn and Wildstrubel, along Thunersee, NE of Pilatus, at Engelberg, along Urnersee, west of the Rhine Valley (Sax-Schwende), east of Au and from Sonthofen to the south.

In the Infrahelvetetic complex imbricate thrusting is more pervasive and folds display a more ductile behavior of the strata. Two large-scale recumbent folds that developed a thrust fault on the inverted limb after extensive shearing. The western example, the Morcles nappe, has its fold axes forming a culmination above the Aiguilles Rouges and Mont Blanc massifs that is due to the late updoming of the two basement units. In the eastern example, the Doldenhorn nappe, the fold axes define a fold arc. Their SW plunge in the west prohibit a direct connection with the fold axes of the Morcles nappe, which plunge to the NE where the folds disappear into the subsurface. In both nappes, the core of the recumbent anticline is made of thick Early and Middle Jurassic strata and can be interpreted as an inverted basin.

From the Jungfrau area to Urnersee, the autochthonous cover sediments of the Aar massif are intricately folded and faulted. Most of the axial surfaces and thrust faults dip to the NNW owing to rotation in conjunction with the late, Miocene uplift of the massif. Farther east a major recumbent fold, the Windgällen fold, has a core of Permian volcanics and involves the crystalline basement, too. From here to the east thrust faults and axial surfaces in the Infrahelvetetic complex dip generally speaking to the SSE.

Several deformation phases can be recognized in the Helvetic zone. A first event (Plaine Morte and Pizol phase, resp.) implies the emplacement of allochthonous strip sheets of Penninic, Ultra- and South-Helvetic origin along thrust faults that were parallel to bedding in the footwall (footwall flats) towards the close of the Eocene. The thrust faults were subsequently passively folded. The next event encompasses thrusting and internal deformation of the Helvetic nappes (Prabé and Calanda phases, resp.) in Oligocene times. It was followed by thrusting and internal deformation of the autochthonous cover of the pre-Triassic basement rocks that resulted in the formation of the Aiguilles Rouges – Mont Blanc and Aar – Gotthard massifs (Kiental phase in the west, Calanda phase in the east) in Late Oligocene – Early Miocene times. Continued uplift of the western Aar massif (Grindelwald phase) and the Aiguilles Rouges – Mont Blanc massifs took place in Mid to Late Miocene times, coeval with folding and faulting in the Jura Mountains.

REFERENCE

- Pfiffner, O.A., Burkhard, M., Hänni, R., Kammer, A., Kligfield, R., Mancktelow, N.S., Menkveld, J.W., Ramsay, J.G., Schmid, S.M. & Zurbriggen, R., 2009, Structural Map of the Helvetic Zone of the Swiss Alps, including Vorarlberg (Austria) and Haute Savoie (France), 1:100'000. Geological Special Map 128.
- 7 Map Sheets (1: Haute-Savoie, 2: Col du Pillon, 3: Oberwallis, 4: Brünigpass, 5: Panixerpass, 6: Toggenburg, 7: Vorarlberg)
 - 10 Plates (maps and cross-sections)
 - Explanatory notes (128 pp.)

1.14

Neogene Sediments and modern depositional environments of the Zagros foreland basin system

Pirouz Mortaza¹, Simpson Guy¹, Bahroudi Abbas², Azhdari Ali³

¹ Université de Genève, Département de Géologie et Paléontologie, Rue des Maraîchers 13, CH-1205 Geneva, Switzerland (Mortaza. pirouz@unige.ch)

² Exploration Department, Mining Engineering Faculty, University College of Engineering, University of Tehran, North Kargar St, P.O. Box 1439, 957131, Tehran, Iran

³ Geological Survey of Iran, Ahwaz Branch, Ahwaz, Kiyān Abad, Shahid Vahabi St, No. 130, P.O. Box 6155656371, Iran

A sedimentological investigation of the Neogene deposits of the Zagros foreland basin in SW Iran reveals a continuous and largely gradational passage from supratidal and sabkha sediments at the base (represented by the Gachsaran Formation) to carbonates and marine marls (Mishan Formation with basal Guri carbonate member) followed by coastal plain and meandering river deposits (Agha Jari Formation) and finally to braided river gravel sheets (Bakhtyari Formation). This vertical succession is interpreted to represent the southward migration of foreland basin depozones (from distal foredeep and foredeep to distal wedge-top and proximal wedge-top, respectively) as the Zagros fold-thrust belt migrated progressively southward towards the Arabian foreland. This vertical succession bears a striking similarity to modern depositional environments and sedimentary deposits observed in the Zagros region today, where one passes from mainly braided rivers in the Zagros Mountains to meandering rivers close to the coast, to shallow marine clastic sediments along the northern part of the Persian Gulf and finally to carbonate ramp and sabkha deposits along the southeastern coast of the Persian Gulf. This link between the Neogene succession and the modern-day depositional environments strongly suggests that the major Neogene formations of the Zagros foreland basin are strongly diachronous (as shown recently by others) and have active modern-day equivalents.

Today the Zagros foreland exhibits a variety of different active depositional environments. From the Arabian craton towards the Zagros Mountains in the north, one typically observes a transition from sabkha and supratidal environments to carbonate ramp (distal foredeep), marine basin and coastal plain (foredeep) and finally to meandering and braided river systems (wedge-top). This horizontal transition in depozones also approximately matches the vertical passage in interpreted palaeoenvironments for sedimentary deposits of the foreland basin during the Neogene. These deposits include the mainly evaporitic Gachsaran Formation (dominantly supratidal and sabkha), the Mishan (mainly shallow to open marine marls), Agha Jari (mainly meandering river and flood plain deposits), and the Bakhtyari Formation (dominated by braided river deposits). We interpret this vertical succession to reflect the progressive evolution of the basin from distal to proximal as the mountain front and foredeep migrate southwards with time. Moreover, we suggest that the link between modern and Neogene deposits implies that the various formations are strongly diachronous. Thus, rather than being regarded as time surfaces, the Neogene formations in the Zagros are probably best thought of as diachronous depozone markers.

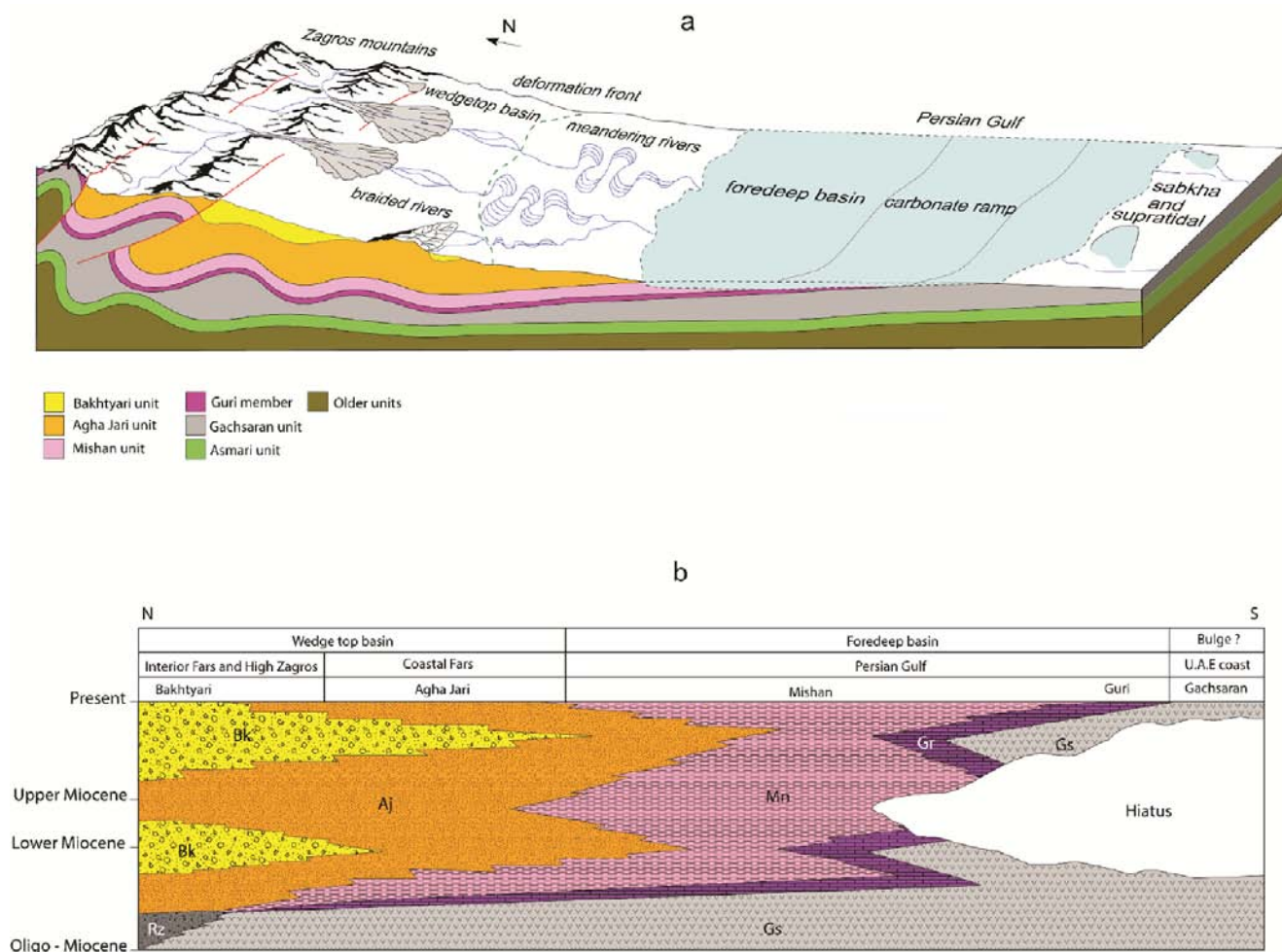


Figure 1. Schematic block diagram (a) and chronostratigraphic diagram (b) of the Zagros foreland basin showing the proposed link between Neogene units and the modern-day environments.

REFERENCES

- Fakhari, M.D., Axen, G.J., Horton, B.K., Hassanzade, J. & Amini, A. 2008. Revised age of proximal deposits in the Zagros foreland basin and implications for Cenozoic evolution of the High Zagros. *Tectonophysics* 451, 170–85.
- Homke, S., Verges, J., Garces, M., Emami, H. & Karpuz, R. 2004. Magnetostratigraphy of Miocene-Pliocene Zagros foreland deposits in the front of the Push-e Kush arc (Lurestan Province, Iran). *Earth and Planetary Science Letters* 225, 397–410.
- Khadivi, S., Mouthereau, F., Larrasoana, J.C., Verges, J., Lacombe, O., Khademi, E., Beamud, E., Melintedobrinescu, M. & Suc, J.-P. 2010. Magnetostratigraphy of synorogenic Miocene foreland sediments in the Fars arc of the Zagros Folded Belt (SW Iran). *Basin Research* 22, 918–32.

1.15

A late Paleozoic back-arc basin on the western Gondwana margin: age and geodynamic setting of Permo-Carboniferous sedimentary rocks of South-East Peru.

Mariël Reitsma¹, Richard Spikings¹, Urs Schaltegger¹ & Alexey Ulianov²

¹ University of Geneva, Earth and Environmental Sciences, Rue des Maraîchers 13, Genève (martje.reitsma@unige.ch)

² University of Lausanne, Department of Mineralogy and Geochemistry, Lausanne

After a long period of igneous quiescence during the Siluro-Devonian, magmatic arc activity recommenced along the western Gondwana margin in the early Carboniferous (~345 Ma; Bahlburg et al., 2009). During the same period sediments of the Ambo Group accumulated in the dominantly continental basins of Peru. At many locations plant remains are preserved indicating a late Viséan – earliest Serpukhovian age and a warm-temperate, humid climate (Azcuy and di Pasquo, 2005). In the Pennsylvanian a marine transgression covered a significant part of Peru and largely overflowed the limits of the Mississippian Ambo basins. Transgression continued and reached its maximum extent in the lower Permian. The platform carbonates deposited in this epeiric sea are referred to as the (Tarma)-Copacabana Group. The upper levels of the Copacabana Group are assigned to the Artinskian (lower Permian) based on palynology and foraminifera (Doubinger and Marocco, 1981).

In this study we present Laser Ablation ICP-MS U-Pb age determinations on detrital and volcanic zircons, and whole rock geochemical compositions on lavas from 5 stratigraphic sections and several key samples from central and south-east Peru. For the first time isotopic age constraints for the Ambo and Copacabana groups are available. Maximum detrital ages for the Ambo sandstones fit well with ages assigned to the plant fossils in the literature. Subsequent flooding of the Ambo basins at the Mississippian-Pennsylvanian boundary coincides with global sea level rise (Haq and Schutter, 2008). However, our study shows that the basin did not remain exclusively marine till the Artinskian but rather experienced important sea level fluctuations tentatively coupled to Permo-Carboniferous glaciation cycles. Most significantly we discovered that the Copacabana Group ends with a continental interval of red bed and volcanic deposits that was previously attributed to the Triassic Mitu Group. Emersion of the Copacabana basin continued until sediments were exposed above base level creating the erosional hiatus with the overlying Mitu Group, this disruption coincides with the eustatic low across the Permo-Triassic boundary (Haq and Schutter, 2008).

U-Pb ages for the Ambo and Copacabana groups overlap with those for the peraluminous granitoids of the Cusco-Vilcabamba area obtained in this study. The Permo-Carboniferous plutons of north and central Peru have been interpreted as a continental arc based solely on their whole rock geochemistry (Nb, Ta, Pb anomalies; Miskovic et al., 2009). However, we argue that the same geochemical signature can be explained by recycling of continental crust in the melt. We therefore reinterpret the late Paleozoic granitoids and sediments from the Eastern Cordillera as remnants of a back-arc system. The research area is too far inboard from the present day trench (~400 km) to be simply related to a subduction zone, neither is there evidence for Phanerozoic terrane accretation to the Peruvian margin. It seems more likely that the coexisting Permo-Carboniferous continental arc was removed at the time of extensive subduction erosion associated with the break-up of Pangea.

REFERENCES

- Azcuy, C.L., Di Pasquo, M. & Valdivia Ampuero, H. 2002: Late Carboniferous miospores from the Tarma Formation, Pongo de Mainique, Peru: review of palaeobotany and palynology, 118, 1-28.
- Bahlburg, H., Vervoort, J.D., Du Frane, S.A., Bock, B., Augustsson, C. & Reimann, C.R. 2009: Timing of crust formation and recycling in accretionary orogens: Insights learned from the western margin of South America: *Earth-Science Reviews*, 97, 215-241.
- Doubinger, J. & Marocco, R. 1981: Contenu Palynologique du Groupe Copacabana (Permien Inférieur et Moyen) sur la bordure Sud de la Cordillère de Vilcabamba, région de Cuzco (Pérou): *International Journal of Earth Sciences*, 70, 1086-1099.
- Haq, B.U. & Schutter, S.R. 2008: A chronology of Paleozoic sea-level changes: *Science*, 322, 64-68.
- Miskovic, A., Spikings, R., Chew, D.M., Kosler, J., Ulianov, A. & Schaltegger, U. 2009: Tectonomagmatic evolution of Western Amazonia: Geochemical characterization and zircon U-Pb geochronologic constraints from the Peruvian Eastern Cordilleran granitoids: *Geological Society of America Bulletin*, 121, 1298-1324.

1.16

Thermal evolution in a spherical convection model with plate generation and mobile continents

Rolf Tobias¹, Coltice Nicolas², Tackley Paul¹

¹ETH Zurich, Institute of Geophysics, Sonneggstrasse 5, CH-8092 Zürich, Corresponding author: (Tobias.Rolf@erdw.ethz.ch)

²Universite Claude Bernard Lyon 1, 43 Boulevard du 11 Novembre 1918, F-69622 Villeurbanne cedex

The thermal budget of a planet is balanced by the generation of heat, e.g. by the decay of radioactive elements, and the heat loss at the surface. On Earth, plate tectonics has been proved to be an efficient mechanism of mantle cooling: it transports hot material to the surface, which then cools, and recycles cold slabs back into the mantle by subduction. On Earth, however, plate tectonics is limited to the oceanic part of the surface, while continents does not actively take part in it and are thought to thermally insulate the mantle. It has formerly been shown, that thermal insulation does not necessarily decrease the total heat flow, but can even enhance it leading to a more efficient cooling of the mantle. Although being counter-intuitive at a first glance, this idea is reasonable as thermal insulation increases the average mantle temperature, which can lead to a more rapid mantle overturn and increased oceanic heat flow as it reduces the viscosity [1].

Here we use 3D spherical numerical simulations with self-consistently evolving oceanic plates and continents floating on top of the mantle. In these models we investigate the evolution of temperature and heat flow below continents and oceans, using different initial configurations of continents.

In the simplest case with only one continent we find a generally high, strongly time-dependent oceanic heat flow. Its time-dependence is driven by the generation of new plate boundaries: the formation of a new boundary leads to smaller oceanic plates, i.e. shorter wavelength, accompanied with peaks in heat flow and a decrease in suboceanic temperature. On the other hand very large oceanic plates correlate with periods of hot oceans. In the case of large plates, their boundaries might be far away from the continental margin, which implies less insulation of the continental convective cell and a relatively low subcontinental temperature. The temperature below continents is highest when plate boundaries are close to the margin as this corresponds to the maximum possible insulation. Consequently, a notable anti-correlation between suboceanic and subcontinental temperatures can be observed.

In cases with multiple continents the anti-correlation is less pronounced as the assembly and dispersal of continents additionally influence subcontinental temperature. In these cases fluctuations of temperatures below individual continents can be much larger and during selected periods the temperature can be lower than below the oceans. If several continents are assembled in a chain-like structure, these cool continents are located at the edges of the chain.

REFERENCE

- [1] Lenardic, Moresi, Jellinek & Manga (2005), Continental insulation, mantle cooling, and the surface area of oceans and continents, *Earth Planetary Science Letters*, 234, 317-333

1.17

Effect of single and multiple décollement layers on thrusting dynamics in fold-and-thrust belts

Jonas B. Ruh¹, Boris J.P. Kaus², Jean-Pierre Burg¹

¹Department of Earth Sciences, Geological Institute, Zurich, Switzerland (jonas.ruh@erdw.ethz.ch)

²Department of Earth Sciences, Institute of Geophysics, Zurich, Switzerland

Thin-skinned fold-and-thrust belts related to convergence tectonics develop by scraping off a rock sequence along a weaker basal décollement. Such décollements are often formed by water-saturated shale layers or low-viscosity salt horizons. A two-dimensional finite element model with a visco-elasto-plastic rheology is used to investigate the structural evolution of fold-and-thrust belts overlying different décollement horizons. In addition, the influence of several weak layers in the stratigraphic column is studied. The characteristics of the layered rock sequence are identical, applying an internal friction angle of 30° and a viscosity of 10²⁵ Pa·s for all simulations. Model shale décollements are purely frictional, with friction angles ranging from 5° - 25° and the same viscosity as the layered overburden. Model salt layers have viscosities ranging from 10¹⁷ - 10²⁰ Pa·s and same friction angle and cohesion as the layered sequence.

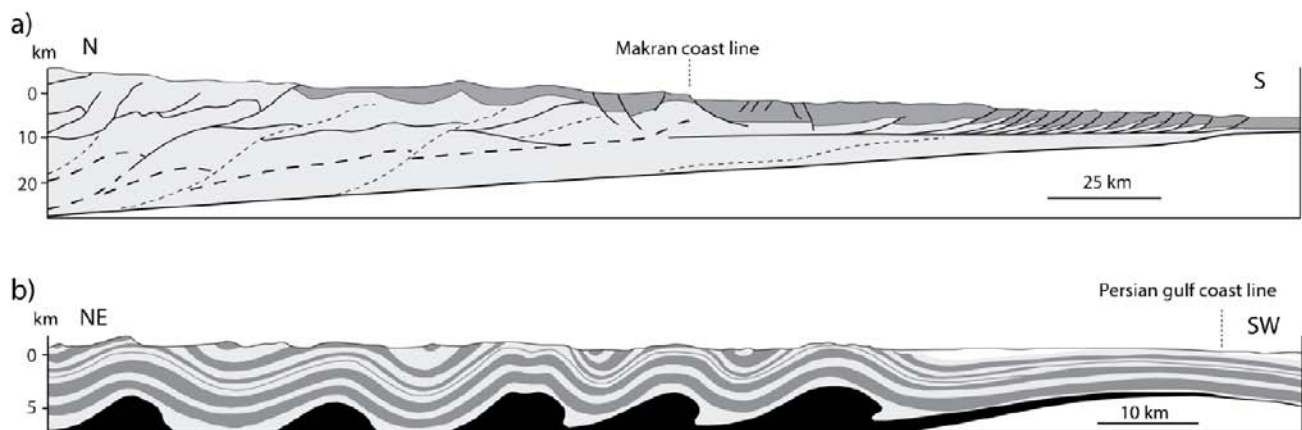


Figure 1: Profiles of selected fold-and-thrust belts comprising different detachment types. a) Cross-section through the Makran accretionary wedge, SE Iran (adapted from [1]). Detachments are frictional and consist of over-pressured shale. Additional detachments exist within the deformed sedimentary pile. b) Profile through the South-western part of the Simply Folded Zone in Zagros, SW Iran (adapted from [2]). The Zagros is an example of a fold belt related to thick salt layers acting as detachment. Several weak salt layers within the sedimentary pile were detected [3].

Results show that fold-and-thrust belts with a single frictional basal décollement generate thrust-systems ramping from the décollement to the surface. Spacing between thrust ramps depends on the thickness of the overlying sequence. If the “salt” décollement has low viscosity (10¹⁸ Pa·s), isolated box-folds (detachment-folds) occur. Multiple viscous salt layers with the same viscosity (10¹⁸ Pa·s) lead to long-wavelength folding. The structural evolution of simulations with an additional low-frictional layer strongly depends on the strength relationship between the basal and the additional, within-sequence décollement. If the within-sequence décollement is weaker, underplating occurs and leads to antiformal stacking at the rear of the fold-and-thrust belt. In the distal part, where deformation is restricted to the upper part of the rock pile, imbrication occurs with a wavelength depending on the depth of the intermediate weak layer.

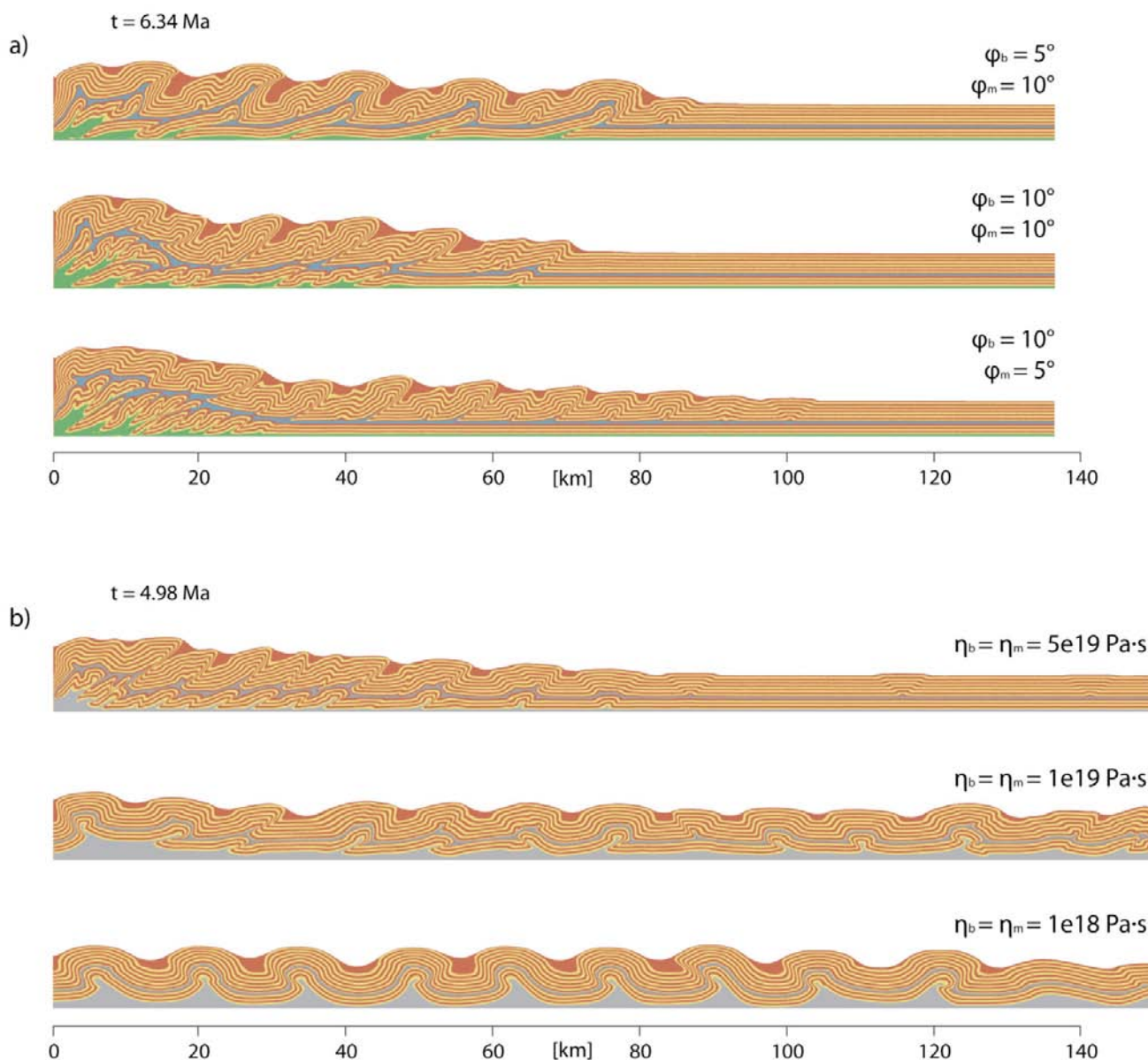


Figure 2: Simulations with multiple décollements. a) Base and intermediate décollement consist of shale (green and blue). All shale related simulations are compressed for 6.34 Ma. Upper subfigure: Intermediate décollement stronger than basal décollement. Total wedge taper is dependent on strength of base décollement. Middle subfigure: Intermediate and base décollement have same strength. Lower subfigure: Basal décollement stronger than intermediate one. Underplating leads to antiformal stacking at the rear of the wedge. Imbrication at the toe of the rock pile with wavelength depending on depth of décollement. b) Simulations with two salt layers (grey scale) compressed during 4.98 Ma. Upper subfigure: High salt viscosity produces drag towards the backstop. Middle subfigure: Fault-propagation folds with no preferred vergence. Very low surface taper Lower subfigure: Low salt viscosity and increased salt thickness form open folds with long wavelengths .

REFERENCES

- [1] Burg, J.-P., Dolati, A., Bernoulli, D., and Smit J., in press, Structural style of the Makran Tertiary accretionary complex in SE-Iran: *GeoArabia*
- [2] Hessami, K., Koyi, H.A., Talbot, C.J., Tabasi, H., and Shabanian, E., 2001, Progressive unconformities within an evolving foreland fold-thrust belt, Zagros Mountains: *Journal of the Geological Society*, v. 158, p. 969-981.
- [3] Motiei, H., 1993, *Geology of Iran: Stratigraphy of Zagros*, Geological Survey of Iran, 536 p.

1.18

Tectono-thermal evolution of the Atlas system (SW Morocco), insights from low-temperature thermochronology and Raman spectroscopy on carbonaceous material

Ruiz Geoffrey¹, Negro Francois², Babault Julien³, Frizon de Lamotte Dominique⁴, Stuart Fin⁵, Stockli Dani⁶, Foeken Jurgen⁷, Sebti Samira⁸, Saddiqi Omar⁸, Di Nicola L.⁵ & Thomsen Tonny⁹

¹IMG, Uni. Lausanne, CH-1015 (geoffrey.ruiz@unil.ch)

²CHYN, CH-2009 Neuchâtel

³UAB, Spain

⁴Uni. Cergy-Pontoise, France

⁵SUERC-Glasgow, UK

⁶Uni. Kansas, USA

⁷VU Amsterdam, NL

⁸Uni. Casablanca, Morocco

⁹Uni. Stockholm, Sweden

In Morocco, the High and Middle Atlas of Morocco are intra-continental fold-thrust belts situated in the southern foreland of the Rif orogen (Fig. 1). It is a key natural laboratory because it 1) is the southern and westernmost expression of Alpine-Himalayan orogeny, and 2) possibly encompasses Pre-Cambrian to recent evolution of the region. Phases of shortening and exhumation of this orogen remain however ill constrained and the few available quantitative data do not allow the present-day high topography (over 4000m) to be explained.

In order to put constraints on the recent orogenic growth of the Atlas system, we investigated the temperature-time history of rocks combining extensive low-temperature thermochronological analysis (Fission tracks and (U-Th)/He on zircon and apatite) and peak temperature estimation by Raman spectroscopy of carbonaceous material (RSCM) and U-Pb ages.

The target area is a NE-SW oriented transect crossing the different structural segments of the western Atlas away from present-day fault systems (Fig. 1). Results are much contrasted from one domain to the other. Pre-Cambrian bedrocks from the Anti-Atlas domain yield old Fission-Track ages on zircon (340-300 Ma), apatite (180-120 Ma) but also U-Th/He (150-50 Ma) still on apatite.

These datasets are interpreted, with the help of thermal modelling, to record passive margin up and down movements during the break-up of the Pangea. U-Th/He pair dating on both apatite (80-55°C) and zircons (200-160°C) minerals are much younger in the High-Atlas once the Tizi N'Test Fault System (TNT), or SAF (Fig. 1) passed to the north, ranging between ~35-5 Ma and 85-30 Ma respectively. Similarly, maximum peak temperatures vary across the TNT, with maximum temperatures of 500-450°C in the axial zone and less than 250-200°C in the Souss plain to the south. Once all datasets combined, they indicate that uplift occurred in the Axial Zone in the Oligocene due to tectonic inversion and crustal shortening and remain constant since allowing a 6-7 km thick pile to be eroded.

Low-thermochronological analyses have also been performed on Cretaceous deposits in the region. Results indicate that these deposits have been reset to temperatures greater than 80°C. This suggests that a post Cretaceous sedimentary pile of at least 3 km in thickness is missing, and as a result that a 3-4 km thick pile of substratum have been eroded in the Axial Zone. Our extensive thermochronological dataset provide for the first time constraints that evidence heterogeneous exhumation history across and along the chain.

All these constraints are put together with structural, geochemical and geophysical informations to discuss the recent tectono-thermal evolution of the Atlas system in the frame of the Africa-Europe convergence and thinning of the lithosphere.

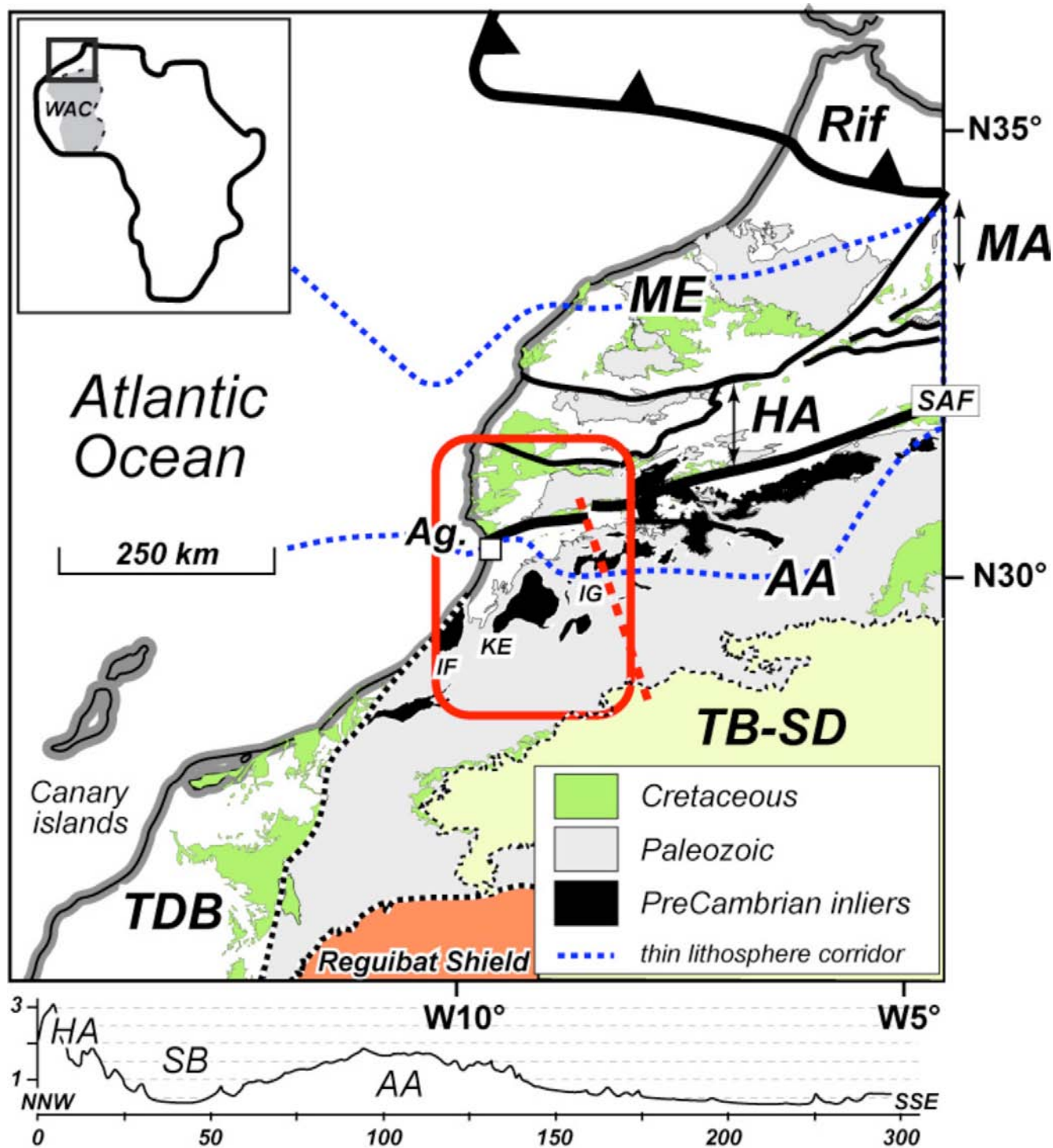


Figure 1. Top: Schematic map of northern Africa showing the main domains in Morocco, i.e. from north to south Rif-Tell, Meseta (ME), Middle-Atlas (MA), High-Atlas (HA), Anti-Atlas (AA), Tindouf Basin (TB) -Saharan Domain (SH) and Reguibat Shield towards the West Africa Craton (WAC) and finally the Tarfaya-Dakhla Basin (TDB) to the SW along the Atlantic Ocean. The studied area (red rectangular) south of Agadir corresponds to the western segment of the Atlas system than encompasses Precambrian inliers, i.e. the Ifni (IF), Kerdous (KE) and Igherm (IG) within the Paleozoic Anti-Atlas domain. SB: Souss Basin. Ag.: Agadir. Thin dashed blue line: corridor for <110 km thick lithosphere (Fullea et al., in press). Bottom: Topographic profile across the region against the strike of the orogen (x10 vertical exaggeration) - see thick dashed red line for location, horizontal and vertical axis in kilometres.

1.19

Did Laurentia and Gondwana play terrane tennis in the Palaeozoic? The implications of a Iapetus convergent margin in the Merida Terrane, Venezuela

Van der Lelij Roelant¹, Spikings Richard¹, Ulianov Alexey², & Chiaradia Massimo¹

¹Département de Minéralogie, Section des Sciences de la Terre et de l'Environnement, Université de Genève, Rue des Maraîchers 13, CH-1205 Genève, roelant.vanderlelij@unige.ch

²Institute of Mineralogy and Geochemistry, University of Lausanne, Switzerland

The tectonic, metamorphic and palaeogeographic origin of the basement terranes of the circum-Maracaibo region, Venezuela and Colombia, are poorly understood. A majority of the reconstructions of western Pangaea place the Merida Terrane of western Venezuela between the Guyana Shield, Mexican and Central American terranes, and hence unravelling its tectonic history is a key step to reconstructing western Pangaea. We aim to develop a robust framework for the age and tectonic origin of the Merida Terrane by using new, in-situ LA-ICP-MS zircon U-Pb geochronology on isotopically and geochemically characterised igneous and metamorphic rocks of the basement complexes.

Widespread I- and S-type arc magmatism and amphibolite facies metamorphism of sedimentary rocks of the Iglesias Complex occurred between the late Cambrian and early Devonian (500-415 Ma), corresponding to a north facing Iapetus continental arc. Detrital zircons from these metasedimentary rocks are early Cambrian and older, which provide a maximum age for deposition. A magmatic hiatus in the Merida Terrane spans the Devonian to Permian, from ~415- 75 Ma.

A compilation of previous work suggests that faunal assemblages from several locations in the Merida Terrane reveal significant assemblage transitions. Faunal affinities change from Gondwanan in the Cambrian, to Acado-Baltic in the Ordovician, to Appalachian in the Silurian. This shift is also characteristic of the Avalonia microcontinent, which rifted off Gondwana in the Cambrian and accreted to Baltica and finally Laurentia in the Silurian.

To the south of the Merida Andes, the Apure Fault separates the Early Palaeozoic igneous and metamorphic belt from the Guyana Shield. The latter exhibits extensive Cambrian rifts which were reactivated in the Jurassic, and K/Ar dates obtained from biotite and feldspar from the basement rocks of the Guyana Shield suggest that the Palaeoproterozoic crust has not experienced a significant thermal event since ~1Ga. Therefore, we propose that the Apure Fault is the south-eastern boundary of the Merida Terrane.

We propose two contrasting scenarios for the evolution of NW Gondwana and the Iapetus and Rheic oceans:

- A) The Merida Terrane may be autochthonous or para-autochthonous to Gondwana, which would imply that the NW corner of Gondwana was a Cambrian to Silurian active margin. This implicitly means that the rift to drift transition which led to the opening of the Rheic Ocean in the Cambrian-Ordovician did not occur this far west, precluding the Rheic Ocean separating NW Gondwana from Laurentia, which in turn suggests that these two supercontinents were close or perhaps connected by the Silurian. A simultaneous back-arc to rift-to drift transition, as required for the opening of the Rheic Ocean in the Cambrian-Ordovician, would lead to scenario B:
- B) The Merida Terrane may be an allochthonous, Avalonia type terrane which separated from Gondwana in the Cambrian-Ordovician due to back-arc basin becoming an oceanic spreading centre (Figure 1). In this scenario, NW Gondwana would become the southern passive margin of the Rheic Ocean; the Merida Terrane would at the same time be the southern Iapetus active margin and the Rheic Ocean northern passive margin (Figure 1). In the Silurian, the Merida Terrane would, like Avalonia, collide with Laurentia during as the Iapetus closed, resulting in the Acadian orogeny in the Appalachians. Following the Amalgamation of Pangaea it would have been re-accreted to Gondwana.

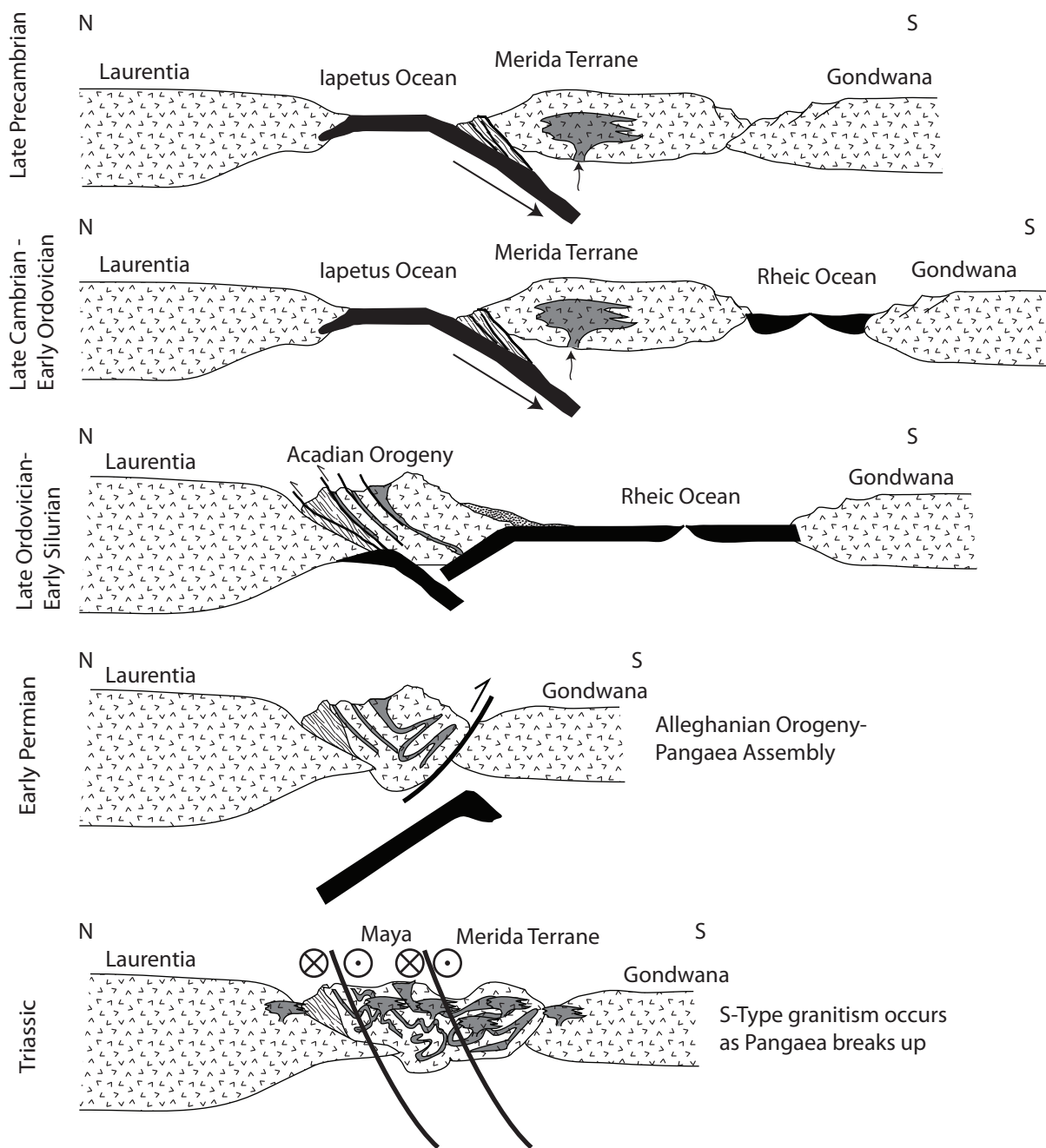


Figure 1. Tectonic sketch for an allochthonous Merida Terrane as described in Scenario B (see text). Drawing is not to scale.

1.A.1

Evidence of transition tectonic regime as seen at Hi'iaka and Zal regions on Io.

Leone Giovanni¹, Gerya Taras¹, Tackley Paul, J.¹, & Moore William, B.²

¹Institute of Geophysics, ETH Zürich, Sonneggstrasse 5, CH-8092 Zürich (giovanni.leone@erdw.ethz.ch)

²Department of Atmospheric and Planetary Sciences, Hampton University, 21 Tyler Street, VA 23668 Hampton

Io is the most volcanically active body of our Solar System, its average global thermal output of 2.4 W/m^2 is higher than that of the Earth. It has been suggested that its mantle may be vigorously convecting (Tackley et al., 2001), but no signs of plate tectonics have been seen so far on its surface. In some cases, mountains appear to be cut and laterally displaced along a transform fault that seems to be a rifting margin (Figure 1 taken from Bunte et al., 2008) and occur as isolated massifs also characterized by lineaments typical of tectonic activity (Figure 2a). A similar morphological pattern that occurs in parts of the Earth oceanic crust (Figure 2b-c), although the timescale and the process differ according to the different tectonic regimes and resurfacing rates.

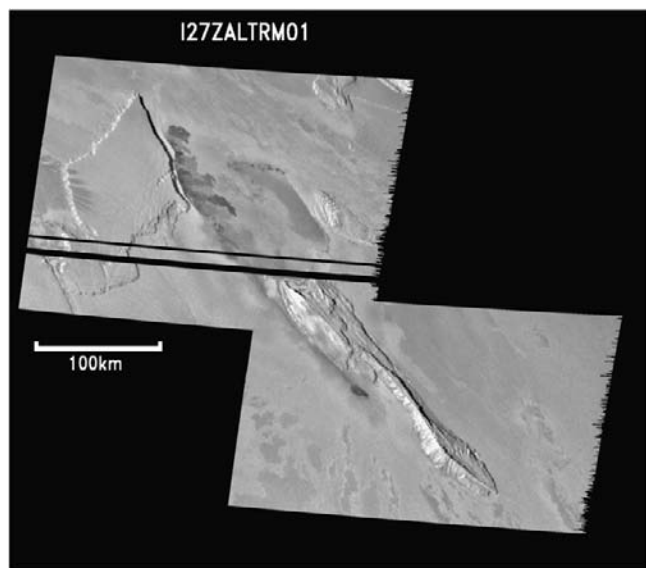


Figure 1. “Galileo SSI mosaic obtained during orbit I27 flyby in February 2000 from image I27ZALTRM01. Resolution is 335 m/pixel. North is up. Illumination is from the left.” (from Bunte et al., 2008). Zal mountains along with associated Zal Patera are displaced along a transform fault from which lava flows erupted on the surface.

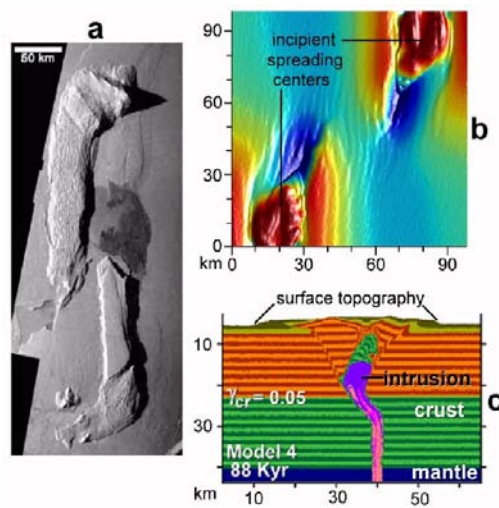


Figure 2. Comparison of Io surface structures (a) with numerical models of magma-assisted spreading under terrestrial conditions (b-c). (a) Galileo image PIA02540 showing Hi'iaka Mons along with the associated Hi'iaka Patera (the darker semi-circular feature in the middle of the image). (b) topographic pattern for oceanic spreading associated with shallow elongated magma chambers (Gerya, submitted). (c) topography rise associated with an emplacement of large dike-like intrusion into the crust (Gerya and Burg, 2007)

O'Neill et al. (2007) identified conditions in which mantle convection may lead (or not) to lithospheric failure and include Io (as well as Venus and Europa) in a transition regime between stagnant and active (mobile) lid, being the latter on Earth regarded as the unique case seen in the Solar System.

However, although failure of the lithosphere does occur (Figs. 1 and 2a), we think that a good coupling between the mantle and the asthenosphere is not achieved on Io due to the low viscosity of the partially-molten asthenosphere and thus the induced lithospheric stresses would be too small to form the observed mountains, which may instead be caused by ‘heat pipe’ resurfacing being more rapid in some areas (above regions with high tidal dissipation) than others, causing lateral differences in lithosphere-crust thickness and, hence, in stress. We plan to perform new simulations including the effect of volatiles on partial melting, heat-pipe resurfacing, mantle-asthenosphere coupling, and laterally variable lithosphere-asthenosphere thicknesses, in order to understand lithospheric stresses and hence the formation of mountains, which should allow us to better match the new models to the available spacecraft and groundbased data.

REFERENCES

- Bunte, M.K., Williams, D.A., & Greeley, R. 2008: Geologic mapping of the Zal region of Io. *Icarus*, 197, 354-367.
- Gerya, T., & Burg, J-P., 2007: Intrusion of ultramafic magmatic bodies into the continental crust: Numerical simulation. *Physics of the Earth and Planetary Interiors*, 160, 124–142.
- Gerya, T. 2011: Initiation and origin of orthogonal oceanic spreading patterns. (submitted)
- O'Neill, C., Jellinek, A.M., & Lenardic, A. 2007: Conditions for the onset of plate tectonics on terrestrial planets and moons. *Earth and Planetary Science Letters*, 261, 20-32.
- Tackley, P.J., Schubert, G., Glatzmaier, G.A., Schenk, P., Ratzcliff, J.T., & Matas, J-P. 2001: Three-Dimensional simulations of mantle convection in Io. *Icarus*, 149, 79-93.

1.A.2

Thermo-chemical convection in spherical geometry: influence of core's size

Yang Li, Frédéric Deschamps & Paul. J. Tackley

Institute of Geophysics, ETH Zürich, CH-8092 Zürich (yang.li@erdw.ethz.ch)

Seismological observations indicate that strong lateral compositional anomalies are present in the deep mantle (Trampert et al., 2004). Meanwhile, numerical models of thermo-chemical convection have shown that reservoirs of primitive dense material can be maintained at the bottom of the system. In particular, Studies in 3D-Cartesian geometry pointed out the parameters that control the stability of dense reservoirs include the chemical density contrast between the dense and regular material, and the thermal viscosity contrast (Deschamps & Tackley, 2008,2009). In addition, the Clapeyron slope of the 660-km phase transition may act as a filter for the dense material.

We continue this work in 3D-spherical geometry, which is the geometry of planetary mantle, using the code STAGYY (Tackley, 2008). We study the influence of several parameters on the stability of primitive dense reservoirs, including the ratio of the radius of the core to the whole shell (f), the buoyancy ratio (B), which is the chemical density contrast between dense material and regular material, and the volume fraction of dense material (X).

Preliminary results suggest that 1) the ratio f doesn't have much influence on the stability of the dense reservoirs, but it has an influence on the detailed structure (shape) of these reservoirs (Fig.1). 2) The buoyancy ratio is the most sensitive parameter (Fig.2). For small (<0.18) buoyancy ratio, the initial layer of dense material is swept out. On the contrary, for buoyancy ratio larger than 0.3, we observe stable layering. For intermediate buoyancy ratio, pools of dense material are forming and remain stable in the bottom of the spherical shell. Future work will explore the influence of the volume fraction of the dense reservoirs.

REFERENCES

- Trampert, J. et al. 2004: Probabilistic tomography maps significant chemical heterogeneities in the lower mantle, *Science*, 306, 853-856.
- Tackley, P.J. 2008: Modelling compressible mantle with large viscosity contrasts in a three-dimensional spherical shell using the yin-yang grid, *Phys. Earth Planet. Inter.*, 171, 7-18.
- Deschamps, F., & Tackley, P.J., 2008: Searching for models of thermo-chemical convection that explain probabilistic tomography I – Principles and influence of the rheological parameters. *Phys. Earth Planet. Inter.*, 171, 357-373.
- Deschamps, F., & Tackley, P.J., 2009: Searching for models of thermo-chemical convection that explain probabilistic tomography II – Influence of physical and compositional parameter. *Phys. Earth Planet. Inter.*, 176, 1-18.

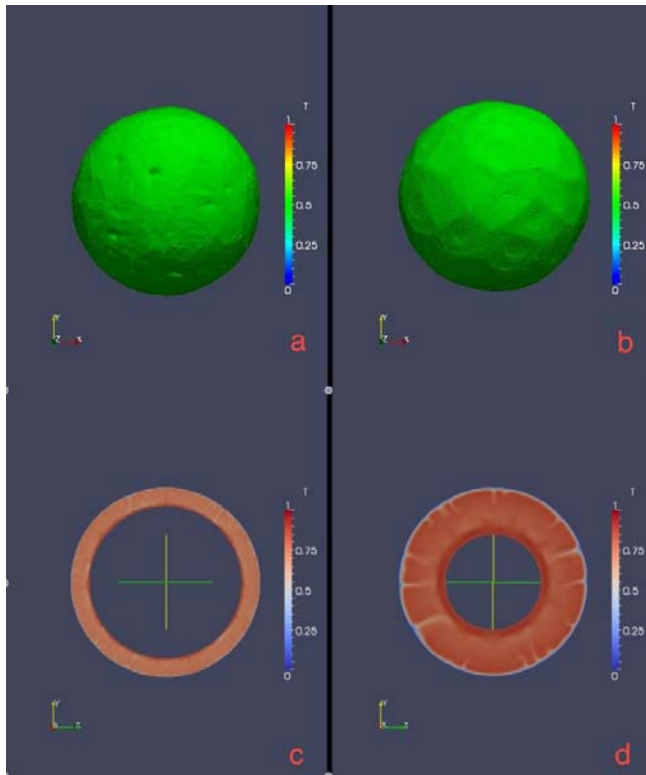


Figure 1. (a-b) isosurfaces of composition $c=0.5$ ($f=0.8$ for a, $f=0.5$ for b), (c-d) snapshots of temperature field ($f=0.8$ for c, $f=0.5$ for d) at $t=0.0106(4.5 \text{ Gyr})$.

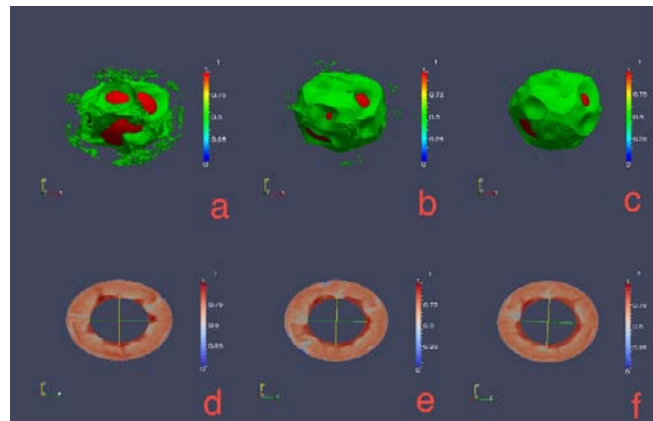


Figure 2. (a-c) isosurfaces of composition $c=0.5$ for $B=0.18$ (a), 0.22 (b), 0.25 (c) and (d-f) snapshots of temperature field for $B=0.18$ (d), 0.22 (e), 0.25 (f) at time $t=0.0170(7.2 \text{ Gyr})$.

1.A.3

Effect of rheology on mantle dynamics and plate tectonics in super-Earths

Tackley Paul¹, Ammann, Michael², Brodholt John¹, Dobson David¹ & Valencia Diana^{3,1}

¹Department of Earth Sciences, ETH Zürich, Switzerland (ptackley@ethz.ch)

²Department of Earth Sciences, University College London, UK

³Department of Earth Atmospheric and Planetary Sciences, MIT, USA

The discovery of extra-solar “super-Earth” planets with sizes up to twice that of Earth has prompted interest in their possible lithosphere and mantle dynamics and evolution. Simple scalings (Valencia et al., 2007; van Heck and Tackley, 2011) suggest that super-Earths are more likely than an equivalent Earth-sized planet to be undergoing plate tectonics. Generally, viscosity and thermal conductivity increase with pressure while thermal expansivity decreases, resulting in lower convective vigor in the deep mantle, which, if extrapolated to the largest super-Earths might, according to conventional thinking, result a very low effective Rayleigh number in their deep mantles and possibly no convection there. Here we evaluate this. (i) As the mantle of a super-Earth is made mostly of post-perovskite we here extend the density functional theory (DFT) calculations of post-perovskite activation enthalpy of Ammann et al. (2010) to a pressure of 1 TPa. The activation volume for diffusion creep becomes very low at very high pressure, but nevertheless for the largest super-Earths the viscosity along an adiabat may approach 10^{30} Pa s in the deep mantle, which would be too high for convection. (ii) We use these DFT-calculated values in numerical simulations of mantle convection and lithosphere dynamics of planets with up to ten Earth masses. The models assume a compressible mantle including depth-dependence of material properties and plastic yielding induced plate-like lithospheric behavior, solved using StagYY (Tackley, 2008). Results confirm the likelihood of plate tectonics and show a novel self-regulation of deep mantle temperature. The deep mantle is not adiabatic; instead internal heating raises the temperature until the viscosity is low enough to facilitate convective loss of the radiogenic heat, which results in a super-adiabatic temperature profile and a viscosity increase with depth of no more than ~ 3 orders of magnitude, regardless of what is calculated for an adiabat. It has recently been argued (Karato, 2011) that at very high

pressures, deformation by interstitial diffusion may become more effective than by vacancy diffusion, possibly causing in a decrease of viscosity with pressure along an adiabat. This would allow \sim adiabatic temperatures in the deepest mantle. (iii) In the context of planetary evolution: If, as is likely, a super-Earth was extremely hot/molten after its formation, it is thus likely that even after billions of years its deep interior is still extremely hot and possibly substantially molten with a “super basal magma ocean” – a larger version of the proposal of Labrosse et al. (2007) although this depends on presently unknown melt-solid density contrast and solidus.

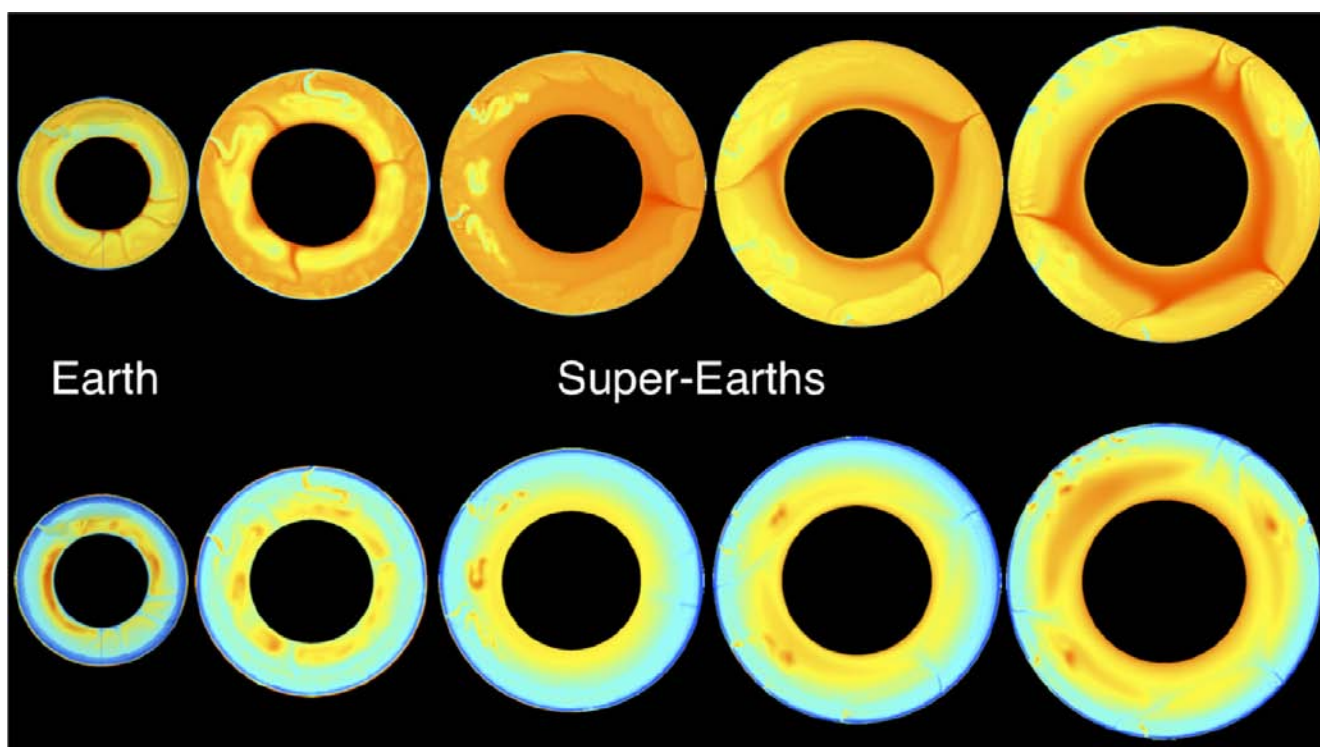


Figure 1. Convection and plate tectonics in planets with 1, 3, 5, 7 and 10 Earth masses (from left to right). Plotted are temperature (top) and viscosity (bottom).

REFERENCES

- Valencia, D., O’Connell R. J. & Sasselov D. D. 2007: *Astro. J.* 670, L45-L48.
 van Heck, H. & Tackley P. J. 2011: *Earth Planet. Sci. Lett.*, in press.
 Ammann, M.W., Brodholt, J.P., Wookey, J., Dobson, D.P. 2010: *Nature* 465, 462-465.
 Tackley P. J. 2008: *Phys. Earth Planet. Inter.* 171, 7-18.
 Karato, S. 2011: *Icarus*, 212, 14-23.
 Labrosse, S., Hernlund, J.W., Coltice, N. 2007: *Nature* 450, 866-869.

1.A.4

Thermal convection in the outer layer of icy satellites

Yao Chloé¹, Deschamps Frédéric¹, Tackley Paul¹ & Sanchez-Valle Carmen²

¹ETH Zurich, Institute of Geophysics, Sonneggstrasse 5, CH-8092 Zurich (chloe.yao@erdw.ethz.ch)

²ETH Zurich, Institute of Geochemistry and Petrology, Clausiusstrasse 25, CH-8092 Zurich

Recent spacecraft missions exploring the outer planets of the Solar System provided new data that increased our knowledge about the internal structure of icy satellites. The existence of a global sub-surface ocean located between an outer layer of ice I and a basal layer of high pressure ices have been proposed forty years ago (Lewis, 1971). As the primordial ocean cools down, ice crystallizes both at its top and its bottom, and if the heat transfer in the outer ice I layer is not efficient enough, a liquid ocean can be maintained in between the two layers of ice. The presence of an ocean is thus controlled by the heat transfer in the outer ice layer. Convection is likely the most efficient way to transfer heat through this ice layer (McKinnon, 2006; Deschamps & Sotin, 2001), but the regime of convection (and therefore the heat transfer) depends on the rheology of the fluid. In the case of ice, viscosity is strongly temperature dependent and thermal convection in the outer ice shell follows a stagnant lid regime. A rigid stagnant lid forms at the top of the system, and convection is confined in a sublayer (Davaille & Jaupart, 1993).

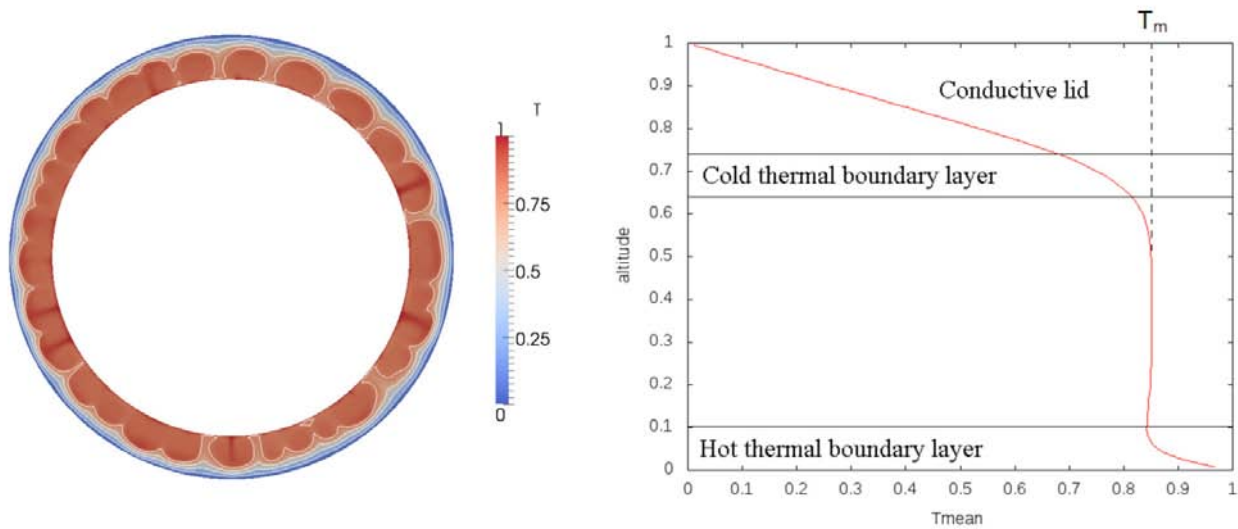


Figure 1. Thermal structure of the convective layer for $Ra=5.7.10^5$ and $\Delta\mu=105$

Many numerical studies including strongly temperature-dependent viscosities have been performed in 2D Cartesian geometry allowing the determination of scaling laws between the temperature of the well-mixed interior and the ratio of the top viscosity to the bottom viscosity.

In this work, we present new models of thermal convection in spherical geometry, which we use to model the heat transfer through the outer layer of icy moons. We use STAGYY (Tackley, 2008) to run simulations in 3D spherical geometry (fig. 1) with a ratio of the core radius to the total radius of 0.80 (meaning that the ice shell represents 20% of the satellite's radius). We consider the only source of heat to be from the bottom of the ice layer (internal heating is neglected). Under these conditions, we study the dependence of the temperature of the well-mixed interior (T_m) on the effective Rayleigh number (Ra) (describing the vigor of convection) and the ratio of viscosity ($\Delta\mu$) (fig. 2). For a range of Ra between 105 and 107 and a range of $\Delta\mu$ between 104 and 106, we obtained the scaling law:

$$(1 - T_m) = 2,287 \frac{1}{\gamma} - 0,056$$

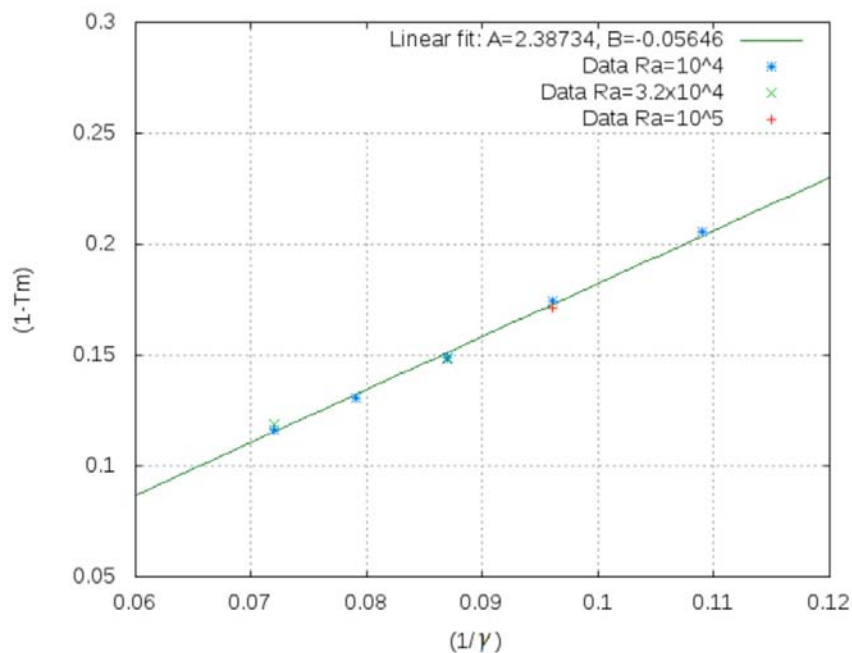


Figure 2. Determination of the temperature of the well-mixed interior T_m as a function of the parameter $\gamma = \ln(\Delta\mu)$.

Compared to Cartesian geometry, the average temperature in the convective layer (T_m) is lower which means that the conductive lid is less developed.

REFERENCES

- Davaille, A., & Jaupart, C., 1993: Transient high-Rayleigh-number thermal convection with large viscosity variations, *J. Fluid. Mech.*, 253, 141-166.
- Deschamps, F. & Sotin, C., 2001: Thermal convection in the outer shell of large icy satellites, *J. Geophys. Res.*, 106, 5107-5121.
- Lewis, J.S., 1971: Satellites of the outer planets: Their physical and chemical nature, *Icarus*, 15, 175-185.
- McKinnon, W.B., 2006: On convection in ice I shells of outer solar system bodies, with detailed application to Callisto, *Icarus*, 183, 435-450.
- Tackley, P., 2008: Modelling compressible mantle convection with large viscosity contrast in three-dimensional spherical shell using the ying-yang grid, *Phys. Earth Planet. Inter.*, 171, 7-18.

1.B.1

Pb, Sr and Nd in intra-ocean subduction zone: 2D geochemical-thermo-mechanical modeling

Baitsch Ghirardello, B.¹, Nikolaeva, K.², Stracke, A.³, Gerya, T.V.¹

¹*Geophysical Institute, ETHZ, Switzerland, baitsch@erdw.ethz.ch*

²*Faculty of Earth and Life Sciences, VU Amsterdam*

³*Institut für Mineralogie, Westfälische Wilhelms-Universität Münster, Germany*

Isotopes behave differently in different processes involved in a subduction zone such as slab dehydration, mantle wedge hydration and partial melting. Therefore, they are indicative of when and where different processes are active. The aim of this study is to extend the 2D coupled petrological-thermo-mechanical numerical model (I2ELVIS) of intra-oceanic subduction processes to include a treatment of isotopic signatures. With this extension we hope to gain more insights into the recycling system within the mantle wedge and are able to visualize the interaction between slab components and the depleted mantle. This will allow us to draw conclusions from isotopic signatures in arc lavas about the involved chemical processes.

The hydration and dehydration processes in subduction zones release chemical components from the subducting slab into the overlying wedge, where arc magma sources are established. These sources can geochemically be considered as a three-fold mixture of wedge peridotite, basaltic ocean crust and sediment (Klimm et al., 2008). A chemical contamination of slab components with wedge peridotite leads to specified signatures in arc magmas. It is widely accepted that two slab components play a key role in this contamination: first, the altered oceanic basalt crust, and second its thin layer of sediment (e.g. Poli & Schmidt, 2002). The chemical contribution of the oceanic crust is restricted to a few trace elements, most notably Pb and the large alkalis (e.g. Rb) and alkaline earths (e.g. Sr) (Klimm et al., 2008). For these reasons, there is a general consensus that the sediment contributes its isotopes to the wedge via a silicate melt, whereas the basalt makes its contribution via an aqueous fluid (Elliott et al., 1997). Based on these results and the well known enrichment of LILE and Pb, U, Th, and B in island arcs in respect to the N-MORB as well as the decrease of HFSE, and Nd, Ta, Zr, and Hf (McCulloch et al. 1991, Tatsumi et al. 1995, 2003, Elliott 2003, Stern 2002), we focus on a limited number of elements (Pb, Hf, Sr and Nd) for our numerical model.

Our first results show a significant increase of Strontium and Lead and a slight increase of Hafnium and Neodymium in the newly formed crust relative to the depleted mantle (DMM), comparable with data from the literature. In addition, the evidence for slab derived fluid /melt (basalt and sediments) in the new crust is obvious.

1.B.2

Long term evolution of subduction-collision systems: numerical modelling

Duretz Thibault¹, Gerya Taras V.¹, Spakman Wim²

¹*Institute of Geophysics, ETH Zürich, Sonneggstrasse 5, CH-8092 Zürich (thibault.duretz@erdw.ethz.ch)*

²*Institute of Earth Sciences, Utrecht University, Budapestlaan 4, 3584 CD Utrecht, the Netherlands*

Subduction-collision zones are natural systems that are controlled by both deep lithospheric and surface processes. In order to model the dynamics of such regions, we have conducted two dimensional and three dimensional numerical simulations of long lasting subduction-collision systems. The study takes into account complex rheological behaviour (plasticity, viscous creep and Peierls creep) as well as a quasi free surface.

We show that continental collision is likely to lead to slab detachment and/or slab rollback. Slab detachment can occur over a large range of depths (40 to 400 km) and is mainly controlled by the thermal age of the subducting oceanic slab. Each of those breakoff types displays a complex rheological behaviour during the plate necking stage. For initially old slabs (50-80 My), olivine's Peierls creep in olivine is a key mechanism for slab detachment that can effectively weaken the slabs, causing them to break at shallower depths.

Models involving different depths of breakoff are subject to different topographic evolution, but always display a sharp breakoff signal. Each slab breakoff end-member is characterised by a subsequent surface uplift in both foreland and hinterland basins. Time averaged (over 5 My) uplift rates range between 0.1 km/My for deep detachment and 0.8 km/My for shallow detachment. In contrast, instantaneous surface uplift rates may reach larger values and vary drastically through time. Our study indicates an quasi linear relationship between the depth of detachment and the rate of time averaged surface uplift.

Continental crust subduction was observed in the experiments involving oceanic lithosphere initially older than 30 My. Different extensive (late-collisional) processes such as slab rollback and slab eduction were modelled and are responsible for the exhumation of buried rocks. The exhumation rates of HP material are generally found than larger than surface uplift rates. These models are likely to undergo large rebound following breakoff and plate delamination if the subducted oceanic slab is old enough.

1.B.3

Extension of chemically stratified mantle lithosphere: numerical modeling

Jie Liao, Taras Gerya

Department of Earth Sciences, Swiss Federal Institute of Technology, Sonneggstrasse 5, CH-8092 Zurich (jie.liao@erdw.ethz.ch)

Using a 2D coupled thermo-mechanical numerical mode, we investigate the extension and breakup of the continental lithosphere. Different from the 'standard' lithospheric model setup where the mantle lithosphere is a homogeneous layer, we introduce a hydrated mantle layer in the mantle lithosphere in our model.

By changing the depth and thickness of the hydrated layer, we find out, the extension and breakup of the compositional layered mantle lithosphere significantly differ from the 'standard' case, and the deformation is mainly affected by the depth rather than the thickness of this hydrated layer (Figure. 1). In a low depth, the hydrated layer is only a low viscosity layer emplacing into the overlying mantle and crust. In a deep depth, due to the water, partial melting occurs in the hydrated layer. The partial melting upwells and thins the overlying mantle, and this may apply to North China Craton where the old, depleted continental lithospheric mantle has been replaced by young, fertile 'oceanic' mantle (Menzies et al., 2007).

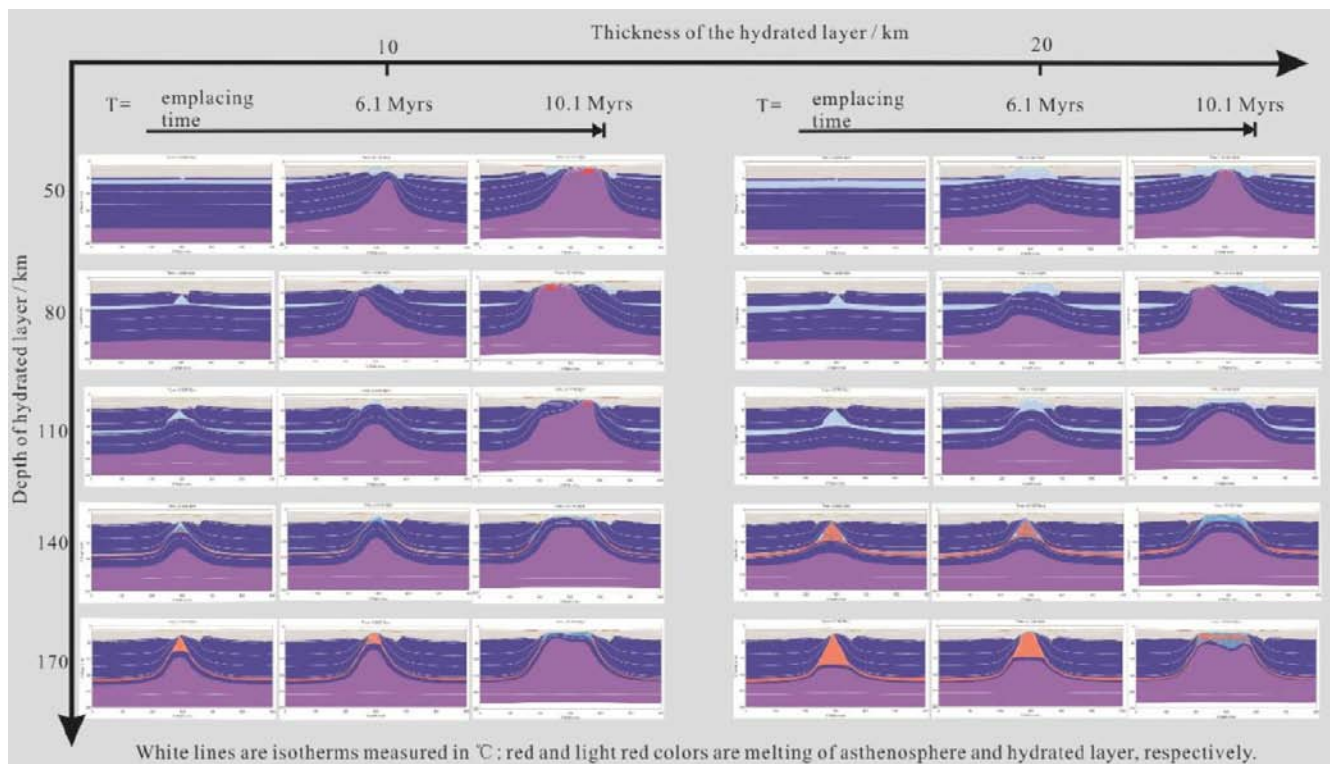


Figure 1. Modeling results with the hydrated layer at different depth and thickness.

REFERENCES

Menzies M, Xu Y G, Zhang H F, et al. 2007: Integration of geology, geophysics and geochemistry: A key to understanding the North China Craton, *Lithos*, 96, 1-21

1.B.4

Decoupled and coupled multilevel preconditioners for problems in elasticity and variable viscosity Stokes flow

Dave A. May¹

¹ *Institute of Geophysics, Department of Earth Sciences, ETH Zurich, Sonneggstrasse 5, CH-8092 Zurich, Switzerland (dave.mayhem23@gmail.com)*

In this work, we focus on the development and comparison of several multilevel preconditioners for solving problems in elasticity and Stokes flow applied to geodynamic applications. The main stumbling block to developing robust, scalable multilevel preconditioners for these applications is that the coefficients in the differential operator (e.g Youngs modulus, viscosity) typically exhibit large variations in space. We consider that our methods should be able to solve problems which exhibit coefficient variations which are either continuous or discontinuous.

When considering coupled partial differential equations, we have several options in how to construct the multilevel preconditioner. For example we can (i) choose to split the PDE into individual scalar components and apply a multilevel preconditioner to each scalar sub-problem and couple the entire system with a stationary block iterative method like Jacobi, or SOR(SSOR), (ii) generate the multilevel hierarchy of the coupled problem and on each level, define the smoother using a node based decoupling of the individual fields or (iii) consider some hybrid method where we generate the multilevel hierarchy of the coupled problem and define the smoother by splitting the discrete coarse grid PDE into individual scalar components (as in (i)).

The performance of the three styles of multilevel preconditioners are compared for a range of different coefficient structures associated with elasticity and Stokes flow for prototypical geodynamic problems. The problems consist of setups with rigid inclusions employing a range of different geometries (dimensionality) and length scales. We also examine some cases in the Stokes regime involving a von-Mises yield surface. The trade-offs between the different strategies are compared and discussed.

1.B.5

Crustal Growth at Active Continental Margins : Numerical studies

Guizhi Zhu*, Taras Gerya*, Paul Tackley*, Eduard Kissling *

¹ Department of Earth Sciences, ETH Zurich, Sonneggstrasse 5, CH-8092 Zurich (guizhi.zhu@erdw.ethz.ch)

Active margins are important sites of new continental crust formation by magmatic processes related to the subduction of oceanic plates. We investigate these phenomena using a three-dimensional coupled petrological-geochemical-thermo-mechanical numerical model, which combines a finite-difference flow solver with a non-diffusive marker-in-cell technique for advection (I3ELVIS code, Gerya and Yuen, PEPI,2007). The model includes mantle flow associated with the subducting plate, water release from the slab, fluid propagation that triggers partial melting at the slab surface, melt extraction and the resulting volcanic crustal growth at the surface. The model also accounts for variations in physical properties (mainly density and viscosity) of both fluids and rocks as a function of local conditions in temperature, pressure, deformation, nature of the rocks, and chemical exchanges.

Our results show different patterns of crustal growth and surface topography, which are comparable to nature, during subduction at active continental margins. Often, two trench-parallel lines of magmatic activity, which reflect two maxima of melt production atop the slab, are formed on the surface, see Figure 1. The melt extraction rate controls the patterns of new crust at different ages (Zhu et al., Journal of Earth Science,2011). Moving free water reflects the path of fluids, and the velocity of free water shows the trend of two parallel lines of magmatic activity. The formation of new crust in particular time intervals is distributed in finger-like shapes, corresponding to finger-like and ridge-like cold plumes developed atop the subducting slabs (Zhu et al., G-cubed,2009; PEPI,2011). Most of the new crust is basaltic, formed from peridotitic mantle. Granitic crust extracted from melted sediment and upper crust forms in a line closer to the trench, and its distribution reflects the finger-like cold plumes. Dacitic crust extracted from the melted lower crust forms in a line farther away from the trench, and its distribution is anticorrelated with the finger-like plumes.

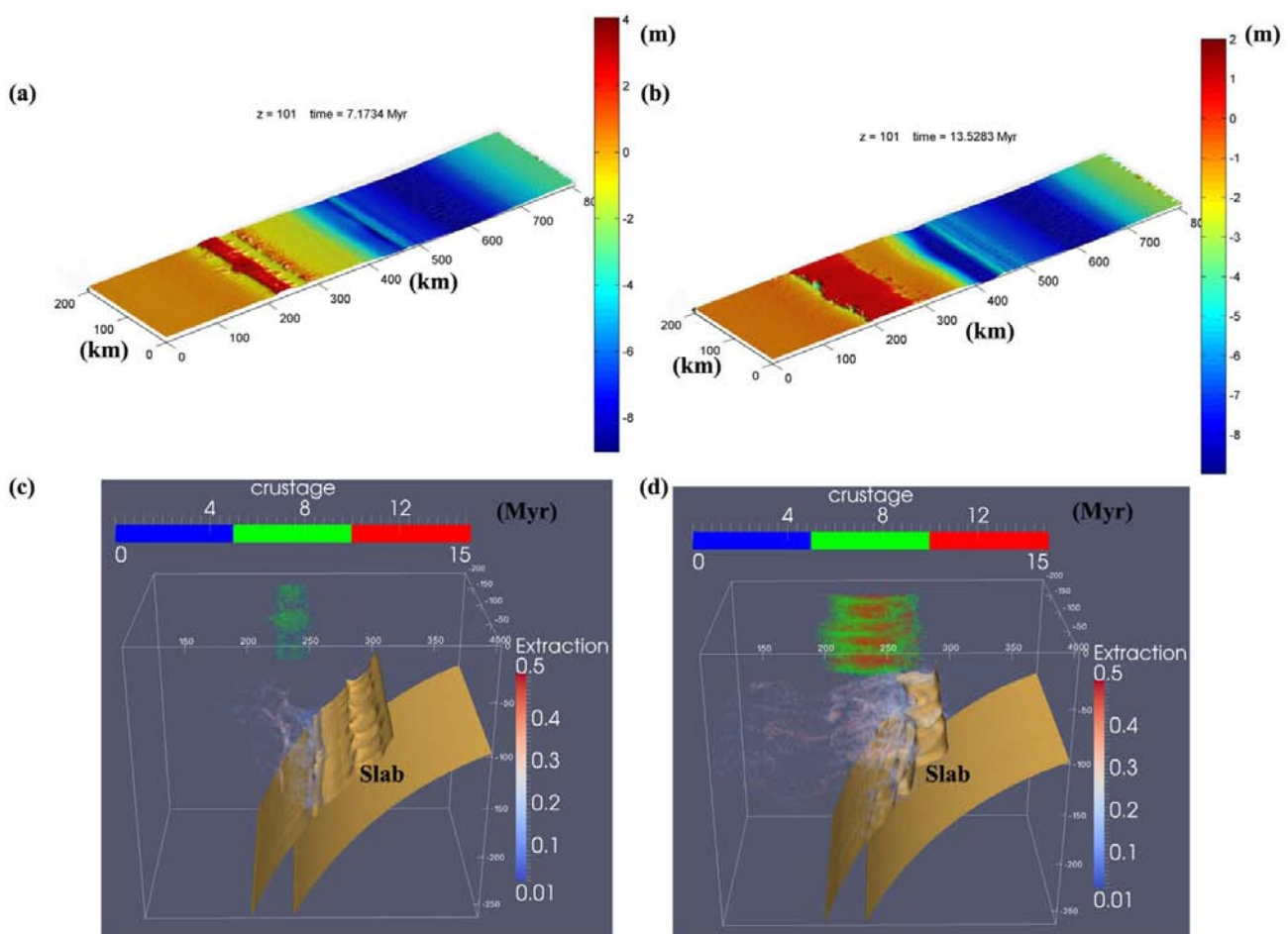


Figure 1. Topography evolution at (a) 7.2 Myr and (b) 13.5 Myr since the beginning of the model calculation and new crust development

with time (c) 7.2 Myr and (d) 13.5 Myr, which corresponds to melt extraction fraction atop the subduction slab, shown as the temperature isosurface of 1200K in gold yellow.

We demonstrate the potential applicability of our model to clustering of arc magmatism in several subduction zones, such as Baja California (Ramos-Velázquez et al., *Revista Mexicana de Ciencias Geológicas*, 2008), North Island of New Zealand (Booden et al., *J. Volcanol. Geotherm. Res.*, 2010), Northeast Japan (Kimura and Yoshida, *Journal of Petrology*, 2006); Ecuador (Schütte et al., *Tectonophysics*, 2010) and Lesser Antilles (Labanieh et al., *EPSL*, 2010).

REFERENCES

- Booden, A.A., et al., 2010. Geochemistry of the Early Miocene volcanic succession of Northland, New Zealand, and implications for the evolution of subduction in the Southwest Pacific. *Journal of Volcanology and Geothermal Research* 199 (2011) 25–37
- Gerya, T. V., Yuen, D. A., 2007. Robust characteristics method for modelling multiphase visco-elasto-plastic thermo-mechanical problems. *Phys. Earth Planet. Inter.*, 163, 83-105.
- Kimura, J., and T. Yoshida (2006), Contributions of slab fluid, mantle wedge and crust to the origin of quaternary lavas in the NE Japan arc, *J. Petrol.*, 47, 2185–2232.
- Labanieh, S., Chauvel, C., Germa, A. et al. 2010. Isotopic hyperbolas constrain sources and processes under the Lesser Antilles arc, *Earth and Planetary Science Letters*. 298(1-2), 35-46
- RAMOS-VELAZQUEZ, Ernesto et al. 2008. U-Pb and ⁴⁰Ar/³⁹Ar geochronology of the coastal Sonora batholith: New insights on Laramide continental arc magmatism. 2008, 25(2), 314-333.
- Schütte, P. et al., 2010. Geodynamic controls on Tertiary arc magmatism in Ecuador: Constraints from U–Pb zircon geochronology of Oligocene–Miocene intrusions and regional age distribution trends. *Tectonophysics*, 489:159-176.
- Zhu, G., Gerya, T.V., Yuen, D., Honda, S., Yoshida, T., Connolly, J.A.D., 2009. Three-dimensional dynamics of hydrous thermal-chemical plumes in oceanic subduction zones. *Geochem. Geophys. Geosyst.*, 10, Q11006, doi:10.1029/2009GC002625.
- Zhu, G., Gerya, T.V., Honda, S., Tackley, P. and Yuen, D., 2011. Influence of the buoyancy of Partially molten rock on 3-D plume patterns and melt productivity above retreating slabs. *Phys. Earth Planet. Inter.*, Doi: Doi:10.1016/j.pepi.2011.02.005.
- Zhu, G., Gerya, T.V., Yuen, D., 2011. Melt evolution above a spontaneously retreating subducting slab in a three-dimensional model. *Journal of Earth Science*, 22(2).137-142. DOI:10.1007/s12583-011-0165-x.

1.C.1

Quartz microstructures and crystallographic preferred orientation: which shear sense do they indicate?

Rüdiger Kilian¹, Renée Heilbronner¹, Holger Stünitz²

¹Geological Institute, Department of Environmental Sciences, Basel University, Bernoullistrasse 32, CH-4056 Basel, Switzerland. (ruediger.kilian@unibas.ch)

²Department of Geology, University of Tromsø, Dramsveien 201, 9037 Tromsø, Norway

Crystallographic preferred orientation (CPO) and shape fabrics of dynamically recrystallized quartz are currently used as shear sense indicators. We show that the CPO and shape fabric in a polyphase rock do not necessarily indicate the shear sense at the global scale of the shear zone but rather at the local scale of the deforming and recrystallizing quartz aggregates.

In lower amphibolite facies shear zones in the Gran Paradiso metagranodiorite, magmatic quartz grains have recrystallized dynamically by subgrain rotation and grain boundary migration to a constant grain size and deform inside a very fine grained feldspar-mica matrix. The polycrystalline quartz aggregates behave as objects with a higher viscosity embedded in a lower viscosity matrix.

A global and a local reference frame are distinguished, the former with respect to the entire shear zone width (~centimeter to decimeter scale), the latter with respect to each deforming quartz aggregate (~micrometer to millimeter scale). Quartz develops a strong CPO with the [c]-axes forming a peripheral maximum inclined synthetically with the inferred local shear sense. At low strain the local shear sense of porphyroclasts is systematically opposite to the global shear sense. The original crystallographic orientation of the magmatic quartz grains has a minor influence on the developing CPO.

The orientation of the surface fabric is related to the orientation of the [c]-axis maximum and the microscopic shear sense in the quartz aggregate. The geometry of the surface fabric ranges from monoclinic to symmetric depending on the relative contribution of grain boundary migration.

It is inferred that flow partitioning between the quartz aggregates and the matrix controls the local kinematics. CPOs are only reliable shear sense indicators in polyphase rocks if the most highly strained parts are analyzed where spin of the aggregates with respect to the shear zone boundary has ceased.

1.C.2

Plastic deformation of quartz micropillars under uniaxial compression at room temperature

Maeder Xavier^{1,2}, Rudy Ghisleni¹ & Michler Johann¹

² *Mechanics of Materials and Nanostructures - Empa, Swiss Federal Laboratories for Materials Science and Technology, Feuerwerkstrasse 39, 3602 Thun, Switzerland (Rudy.Ghisleni@empa.ch, Johann.Michler@empa.ch)*

¹ *Faculté des géosciences et de l'environnement, institut de géologie et paléontologie, UNIL, CH - 1015 Lausanne (xavier.maeder@unil.ch)*

Quantification of the mechanical properties of crystalline materials at micro and nano length-scales is as important as it is challenging. It has been recently discovered that the mechanical behaviour of a crystalline material can change as the size of the system in question approaches any characteristic length scale associated with the dislocation processes of the material (Michler et al. 2007). Several properties are affected by a material's internal and in some cases external length scales, such as the yield stress, the brittle-to-ductile transition temperature and the fracture toughness. Such length-scale dependent values of the mechanical properties of rocks materials and minerals may constrain the deformation behaviour of mylonite or ultramylonite where the grain size reaches micro- to nano-meter scale. In order to address this issue, SEM insitu micropillar compression of natural quartz has been performed. Two sets of samples have been tested with compression axis perpendicular to respectively the c- and the z-planes. The result show that ductile deformation occurs at room temperature with pillar of 1 micron diameter for both orientations, with yield stress between 3 to 4 GPa. Pillar oriented parallel to the c-axis show rhombohedra slip planes and the ones parallel to the z-axis show basal slips. SEM insitu micropillar compression is a very promising method to study plastic deformation behaviour at small scale of rock minerals.

REFERENCES

Michler, J., Wasmer K., Meier S., Ostlund F. & Leifer K. 2007: Plastic deformation of gallium arsenide micropillars under uniaxial compression at room temperature. *Applied Physics Letters* 90, 043123.

1.C.3

Control of temperature, pressure gradient and flow law on the formation of crustal-scale shear zones: results from 1D thermo-mechanical modeling

Maeder Xavier¹, Schmalholz Stefan¹ & Bauville Arthur¹

¹ *Faculté des géosciences et de l'environnement, institut de géologie et paléontologie, Quartier UNIL-Dorigny, CH - 1015 Lausanne (xavier.maeder@unil.ch, Stefan.Schmalholz@unil.ch, Arthur.Bauville@unil.ch)*

Localization of deformation plays a major role during tectonic processes. It is at the origin of many geological structures at all scale from the formation of deformation bands within single grains up to crustal and lithospheric scale shear zones. Deformation in continental collision belts is typically driven by such localizations, which especially result in the formation of fold nappes and thrust sheets. There is considerable speculation as to which process dominates the localization behavior. We present a dynamically self-consistent pressure-driven thermo-mechanical 1D numerical model to study the formation of shear zones in the upper crust. The numerical model is based on the finite element method. Our model consists of a sediment layer and its underlying basement. For the sediment layer we consider several calcite flow laws for diffusion creep and dislocation creep (both power-law and Peierls law). For the basement we apply several flow laws for quartz and granite. We study under what thermal and pressure conditions the shear zones form either at the base of the basement unit or at the base of the sediment layer, or at both locations simultaneously. We also investigate the impact of thermal coupling through shear heating on shear zone formation. We further apply our model to the Morcles fold nappe in the western Swiss Alps by considering previously published estimates for strain rates, stresses, flow laws and temperatures. We identify the thermal and pressure conditions for which the model results fit best the field observation and estimates for stress and strain rate. The advantage of the applied 1D dynamic shear zone model is that neither the strain rate nor the stress is prescribed at any point in depth but is controlled by the applied overall pressure gradient, the temperature profile and the fluid dynamic force balance within the shear zone. The results of our simplified 1D model will be used to set up a more elaborated 2D model for the formation of crustal scale shear zones and nappes.

1.C.4

Texture development and hybrid deformation mechanisms in fine grained calcite aggregates deformed in direct shear: constraints from electron backscatter diffraction analysis

Maeder Xavier^{1,2}, Ghislain Trullenque³, Marty Drury¹ & Hans De Bresser¹

¹ *Departement of Earth Sciences, P.O. box 80021, 3508 TA Utrecht, The Netherlands. (martynd@geo.uu.nl, j.h.p.debresser@geo.uu.nl)*

² *Faculté des géosciences et de l'environnement, institut de géologie et paléontologie, Quartier UNIL-Dorigny, CH - 1015 Lausanne (xavier.maeder@unil.ch)*

³ *Institute for Geosciences-Geology, University of Freiburg, Albertstr. 23-B, D-79104 Freiburg i. Br. (ghislain.trullenque@geologie.uni-freiburg.de)*

Studies on naturally and experimentally deformed calcite and olivine aggregates have demonstrated that even fine grained materials that are expected to exclusively deform by grain size sensitive (GSS) mechanisms, develop a weak but distinct LPO (texture) at high strain. This raises the question to what extent the evolution of the microstructure results in a change from simple GSS or grain size insensitive (GSI) creep to complex composite flow, with related change in the rheology of the material.

To investigate this behaviour, we conducted new deformation experiments on fine grain calcite aggregates (Solnhofen limestone). In one type of experiments, square samples of 8x8x0.5 mm have been deformed in a direct shear piston configuration mounted in an axial loading set-up in a constant volume, internally heated argon gas medium deformation apparatus. Samples have been deformed to a shear strain of $\gamma = 6$, at temperatures of 600, 700, 800 and 900 °C, 300 MPa confining pressure and a shear strain rate of $1.7 \times 10^{-4} \text{ s}^{-1}$.

Conditions have been chosen such after Schmid et al., 1977, that the experiments represent deformation in the GSI (lower temperature) and GSS (higher temperature) creep fields. We used Electron Backscatter Diffraction (EBSD) to determine the texture strength of the samples, the distribution of misorientation axes and the grain size distributions.

The results show an oblique shape preferred orientation at 35° to 40° to the shear plane and a moderate LPO in all samples. The c-axis preferred orientation shows a girdle with one main maximum at a variable angle to the shear plane. The c-axis maxima girdle becomes slightly stronger, more steeply oriented and oblique to the shear plane with increasing temperature. All samples show a similar misorientation distribution with a main peak at low angle. Subgrain formation and rotation with misorientations up to 10° occurred in the coarser grains even in the experiments at high temperatures. This shows the formation of new high angle boundaries. Starting grain size of the experimentally treated Solnhofen limestone was 3.4 micrometer. While no change in grain size occurred during shearing at 600°C, we observed an increase with temperature at higher temperature, to 8.4 micrometer at the end of the experiment at 800°C.

The formation of subgrains and subgrain rotation, along with the fact that the misorientation rotation axes plot preferentially in the center of the figures for the low angle boundaries (5-15°), subparallel to the rotation axes of the imposed simple shear, suggest a component of dislocation creep to the overall deformation in all the samples.

We used the same gas medium apparatus for a second type of experiments on samples of Solnhofen limestone, namely axi-symmetric compression tests in strain rate stepping mode. The results of these tests show an increase of the power law stress exponent with increasing strain at high temperature (1100-1200 K), suggesting grain growth influencing the creep behaviour. Low stress exponents ($n \sim 2$) were found at lower temperature, remaining constant with strain except at high stress.

All these observations suggest that the GSS regime inferred for fine grained calcite aggregates at relatively low strain may be a transient stage evolving into hybrid deformation and GSI regime at high strain, mainly due to grain growth during the deformation. Thus natural superplastic behaviour, in impure calcite rocks like Solnhofen limestone, would be limited to low temperatures, where grain growth is slow, or limited to low strains at high temperatures.

REFERENCES

Schmid, S.M., Boland, J.N. & Paterson, M.S., 1977: Superplastic flow in finegrained limestone. *Tectonophysics*, 43, 257-291.

1.C.5

Mechanics of kink-bands during torsion deformation of muscovite aggregate

Misra Santanu and Burg Jean-Pierre

¹*Structural Geology and Tectonics Research Group, Geological Institute, ETH Zurich, CH-8092, Switzerland
(santanu.misra@erdw.ethz.ch)*

The growth, geometry and mechanical behaviour of grain-scale kink-bands were investigated during layer parallel non-coaxial deformation (torsion) of synthetic polycrystalline aggregates of muscovite at constant displacement rate ($\dot{\gamma} = 3 \cdot 10^{-4} \text{ s}^{-1}$) and various confining pressures (CP = 50 - 300 MPa), temperatures (T = 300 - 800 °C) and finite shear strains ($\gamma = 0.2 - 5.0$). The kink-instabilities developed during elastic to plastic transition (yield) at finite shear strain of ca. 0.2. The shear stress required to form the instabilities is a function of pressure and temperature and range from ca. 20 to 90 MPa within the experimental conditions. The kink bands formed in non-coaxial torsion tests are asymmetric, involve strain partitioning, show complex microstructures with incremental deformation and have a life time as the structure destroys at ca. $\gamma = 5$. These results suggest a domain of pressure and temperature conditions where kink-band structures should be common. Results obtained from torsion experiments are compared to those of layer parallel axial compression conducted with the same displacement rate at 600 °C and 300 MPa for 5, 10 and 17% bulk shortening. Combining microstructures viewed on surfaces parallel and perpendicular to the torsion plane, a schematic 3D geometrical model is constructed to discuss the kink mechanism, the microstructural evolution and the mechanical behaviour.

1.C.6

K-Ar dating of some synkinematic clay fault gouges from Neoalpine faults

Pleuger Jan¹, Zwingmann Horst², Manser Monika¹ & Mancktelow Neil¹

¹*Geologisches Institut, ETH Zürich, Sonneggstrasse 5, CH-8092 Zürich (jan.pleuger@erdw.ethz.ch)*

²*CSIRO Division of Petroleum Resources, School of Applied Geology, Curtin University, Bentley WA 6102, Australia*

In the Central Alps, several large-scale, localised faults were active during the same, though not always the entire, Oligocene to Miocene time span (Neoalpine fault array, including the Insubric Fault). These faults are generally interpreted as to result from the partitioning of strain induced by the crustal convergence between the European and Adriatic plates.

The progressive uplift of the Penninic nappe stack with respect to the Southern Alps is reflected by increasingly brittle style of deformation. Due to the absence of syntectonic sedimentary basins west of the Giudicarie Fault, the timing of faults has to rely on isotopic mineral dating and low-temperature geochronological data, e.g. fission track dating. We provide K-Ar ages of clay fault gouges collected from some prominent faults of the Neoalpine fault array, namely the Canavese Fault, the Giudicarie Fault, and faults along the southern border of the Aar Massif.

The Giudicarie Fault separates two segments of the Periadriatic Fault with an apparent offset of c. 80 km. The Passeier segment of the Giudicarie Fault was active at c. 17 Ma which is the age of a pseudotachylite from that fault (Müller et al. 2001, *Int. J. Earth Sci.* 90, 623-653). A 16.84 ± 0.38 Ma K-Ar age of a fault gouge from the North Giudicarie Fault confirms the c. 17 Ma age of fault activity.

The Canavese Fault accounts for vertical relative displacement between the Penninic Alps and the Southern Alps and a poorly constrained amount of dextral displacement between the two blocks. Two clay-rich fault gouges from the pass between Valle Loana and Val Grande (20.18 ± 0.54 Ma) and Valle Sessera (20.92 ± 0.63 Ma) represent late stages of dextral faulting along the Canavese Fault. A 33.05 ± 0.69 Ma age from south of Val Sessera is either inherited from adjacent Early Oligocene andesites or represents thrusting of the Ivrea Zone over the andesites.

Between the Aar and Gotthard external “massifs”, the trend of the Rhone, Urseren, and Vorderrhein valleys follows the ENE-WSW strike of the Urseren-Garvera Zone and several low-grade ductile shear zones and brittle faults. There is no continuous fault along the southern boundary of the Aar Massif but brittle displacements were dispersed over numerous parallel smaller faults which overlap along strike. Fault gouges collected from these faults yielded ages of c. 13.5 to 11.7 Ma. The displacement sense could only locally be determined. The average fault orientation is 161/79 and the average displacement direction 245/31 implying a north-side-up component in addition to the dextral sense of displacement. Our data thus constrain the onset of uplift of the Aar Massif with respect to the Gotthard “Massif” and confirm the change from ductile to brittle tectonics in Serravallian times. They demonstrate that dextral displacement took place along large segments of the southern boundary of the Aar Massif and suggest a kinematic link to coeval dextral shearing along the Rhone Fault and orogen-parallel extension along the Simplon Fault.

1.C.7

The Origin of Olivine B-type Fabric in naturally deformed Peridotite: insight from the Ronda large-scale Mantle Shear Zone (Spain)

Précigout Jacques¹ and Hirth Greg²

¹Department of Structural Geology and Tectonics, ETH-Zürich, Zürich, Switzerland (jacques.precigout@erdw.ethz.ch)

²Department of Earth Sciences, Brown University, Providence R.I., USA

Strain-induced olivine Lattice Preferred Orientation (LPO) mostly controls the propagation of seismic waves in the mantle. Hence, it strongly affects the imaging of mantle structures through analyzing of elastic waves coming from deep earthquakes (Ismail and Mainprice, 1998). Understanding the relationships between mantle deformation and olivine LPO is thus crucial to objectively interpret the deep mantle structures. Here, based on detailed documentation of olivine LPOs in the Ronda peridotite (southern Spain), we provide evidences of flow-normal a-axis LPO, i.e., B-type fabric, within a kilometer-scale ductile shear zone. This fabric occurs upon entering the shear zone and describes a progressive transition from A-type fabric (parallel-flow a-axis LPO) to B-type fabric. While B-type fabrics have been described from several localities, to our knowledge this is the first olivine fabric transition ever observed in naturally deformed peridotites. Furthermore, while the olivine fabric strength (Jindex) increases in the A-type fabric domain towards the center of the shear zone, the Jindex progressively decreases in the B-type fabric domain.

Based on deformation experiments, A-type fabric occurs during high-temperature/low-stress deformation of anhydrous olivine aggregates (Zhang and Karato, 1995; Jung and Karato, 2001). In contrast, the B-type fabrics have been observed under a wide range of conditions: 1) at high-temperature/low stress conditions in the presence of melt (Kohlstedt and Holtzman, 2009); 2) at high-stress in the presence of water (Jung and Karato, 2001); 3) under dry conditions at very high pressure (> 3 GPa; Jung et al., 2009); and 4) during diffusion-creep in the presence of orthopyroxene (Sundberg and Cooper, 2008). In our natural example, we conclude that the B-type fabric arises from enhancing diffusion creep at the expense of dislocation creep, because: 1) the B-type fabric is observed to overprint the typical fabric of anhydrous peridotite (A-type), 2) the Ronda peridotites were deformed at pressures lower than 2 GPa at sub-solidus conditions (Garrido et al., 2011), and 3) the A-type/B-type transition correlates with a decrease of temperature, grain size and fabric strength (Jindex) towards the inner shear zone. Our results moreover indicate that B-type fabric is somehow related to large-scale mantle shear zones, and hence it could characterize a signature of lithosphere-scale mantle strain localization.

REFERENCES

- Garrido, C.J., Gueydan, F., Booth-Rea, G., Précigout, J., Karoly, H., Padrón-Navarta, J.A. & Marchesi, C. Garnet Lherzolites and Garnet-spinel mylonites in the Ronda Peridotite: Vestiges of Oligocene Back-arc mantle lithospheric extension in the Western Mediterranean. *Geology*, in press.
- Ismail, W.B. & Mainprice, D. An olivine fabric database: an overview of upper mantle fabrics and seismic anisotropy. *Tectonophysics* 196, 145-157, 1998.
- Jung, H. & Karato, S.-I. Water-induced Fabric Transitions in Olivine. *Science* 293, 1460-1463, 2001.
- Jung, H., Mo, W. & Green, H.W. Upper mantle seismic anisotropy resulting from pressure-induced slip transition in olivine. *Nature geoscience* 2, 73-77, 2009.
- Kohlstedt, D.L. & Holtzman, B.K. Shearing Melt Out of the Earth: An Experimentalist's Perspective on the Influence of Deformation on Melt Extraction. *Annu. Rev. Earth Planet. Sci.* 37, 561-593, 2009.
- Sundberg, M. & Cooper, R.F. Crystallographic preferred orientation produced by diffusional creep of harzburgite: Effects of chemical interactions among phases during plastic flow. *JGR* 113, B12208, 2008.
- Zhang, S. & Karato, S.-I. Lattice preferred orientation of olivine aggregates deformed in simple shear. *Nature* 375, 774-777, 1995.

1.C.8

Grain size evolution in 2D numerical simulations: Implications for lithospheric localization

Marcel Thielmann¹, Antoine Rozel², Boris Kaus³ & Yanick Ricard²

¹*Institute of Geophysics, ETH Zürich, Sonneggstrasse 5, CH - 8092 Zürich*

²*Laboratoire des Sciences de la Terre, CNRS, Université de Lyon 1, ENSL, F-69364 Lyon, Cedex 07*

³*Institute of Earth Sciences, Johannes Gutenberg University Mainz, J.-J.-Becher-Weg 21, D-55128 Mainz*

Grain size reduction along with a switch in deformation mechanism (dislocation creep to diffusion creep) has been proposed to result in lithospheric-scale localization, thus being a mechanism to promote subduction initiation (e.g. Braun et al. (1999), Montési and Hirth (2003)). Recently, Rozel et al. (2011) proposed a grain size evolution law for olivine derived from first principles. This law differs from most previously published laws as it relates grain size reduction to deformational work (the tensor product of stress and strainrate).

We implemented this evolution law in the 2D finite element code MILAMIN_VEP and investigate the effect of grain size reduction on deformation style.

First results indicate that grain size reduction does promote localization for a range of parameters. However, due to the rapid grain growth, the memory effect of grain size reduction is rapidly lost once deformation stops.

REFERENCES

- Rozel, A., Ricard, Y. & Bercovici, D. 2011: A thermodynamically self-consistent damage equation for grain size evolution during dynamic recrystallization, *Geophysical Journal International*, 184, 719-728.
- Montési, L. & Hirth, G. 2003: Grain size evolution and the rheology of ductile shear zones: From laboratory experiments to postseismic creep, *Earth and Planetary Science Letters*, 211, 97-110.
- Braun, J., Chéry, J. & Poliakov A. 1999: A simple parameterization of strain localization in the ductile regime due to grain size reduction: A case study for olivine. *Journal of Geophysical Research*, 104, 25167-25181

1.D.1

Nano-seismology on the Fribourg Lineament - Switzerland

Abednego Martinus¹, Vouillamoz Naomi¹, Wust-Bloch Hillel Gilles², Mosar Jon¹

¹University of Fribourg, Departement of Geosciences, Earth Sciences, Chemin du Musée 6, CH-1700 Fribourg, Switzerland
(martinus.abednego@unifr.ch, naomi.vouillamoz@unifr.ch, jon.mosar@unifr.ch.)

²Tel Aviv University, Department of Geophysics and Planetary Sciences, P.O.B. 39040, Tel Aviv, 69978, Israel

As part of two joint PhDs, we study the very small seismicity along the Fribourg Lineament and in the larger Fribourg area. The Fribourg Lineament or Fribourg Zone is represented by an alignment of weak seismic events that seems to show recent signs of increased activity (Kastrup 2007). The lineament runs in a South-North direction west of the city of Fribourg – Switzerland, and is parallel to the Fribourg structure (Figure 1). The orientation of these two features differs strongly from the structures in the surrounding areas that show a general SW-NE trend.

To date, the Fribourg Zone is monitored by two seismic mini-arrays (SNS- Seismic Navigating System) located around the lineament (Figure 1). Each array consists of one 3D central sensor and three 1D sensors with an aperture of about 100 m (Joswig 2008). Such a configuration permits localization of events using recorded data from one station only. However, to complete the monitoring, data from the Swiss Permanent Network are downloaded via the Swiss Seismological Service. Detection of seismic events is enhanced by a pattern recognition method applied on spectrograms of recorded data. Spectrograms show amplitude or energy content for the frequency range of the data. This permits to extract and recognize earthquake signals from noise and therefore allows detection to near zero local magnitude. Localization of detected events is then done interactively through HypoLine, a software especially suited for SNS records. In addition, signals from all kind of networks can be processed too. HypoLine is very different from other well established programs for hypocenter location (Hypo71, HypoLayer, etc) because it doesn't work like a black box. In HypoLine, every onset change induces immediate simulation update in affected parameter space. This means that it is possible to see direct effects of phase picking change on location solution or vice versa to see simulated phase picks while choosing one probable location. This trial- and -error process is very powerfull since it makes it possible to take into account the geological sense in the manifold of possible choices.

In order to obtain a better understanding of the observed seismicity and its links to the tectonics of the Fribourg Structure, a 3D faults plane model was built in ArcGIS (ArcScene). The model was elaborated using data from InterOil (for Resun AG) based on oil company seismic surveys of the Western Molasse Basin (Mosar 2011). Interpretation of lines yielded five interpolated stratigraphic surfaces (base Tertiary, base Malm, top Lias, top Muschelkalk and base Mesozoic) and fault cut lines on respective levels.

First results show that all the seismicity is confined in the sedimentary cover, most of it in the Tertiary cover. A cluster of recent aftershocks SW of lake Murten shows no correlation with known faults. This shows that despite the most precise 3D model available to date, reinterpretation of seismic lines in some areas, may lead to new structural models (Figure 1). It also documents the importance of combining studies on week seismicity and tectonics.

REFERENCES

- Joswig, M., 2008. Nanoseismic monitoring fills the gap between microseismic networks and passive seismic, *First Break*, 26, 2008.
- Kastrup, U., Deichmann, N., Fröhlich, A., Giardini, D., 2007. Evidence for an active fault below the northwestern Alpine foreland of Switzerland, *Geophys. J. Int.* (2007) 169, 1273-1288.
- Mosar, J. et al., 2011. Du Jura central aux Préalpes romandes – Une tectonique active dans l'avant-pays des Alpes, *Géochroniques* n°117, Mars 2011, p.52-55.

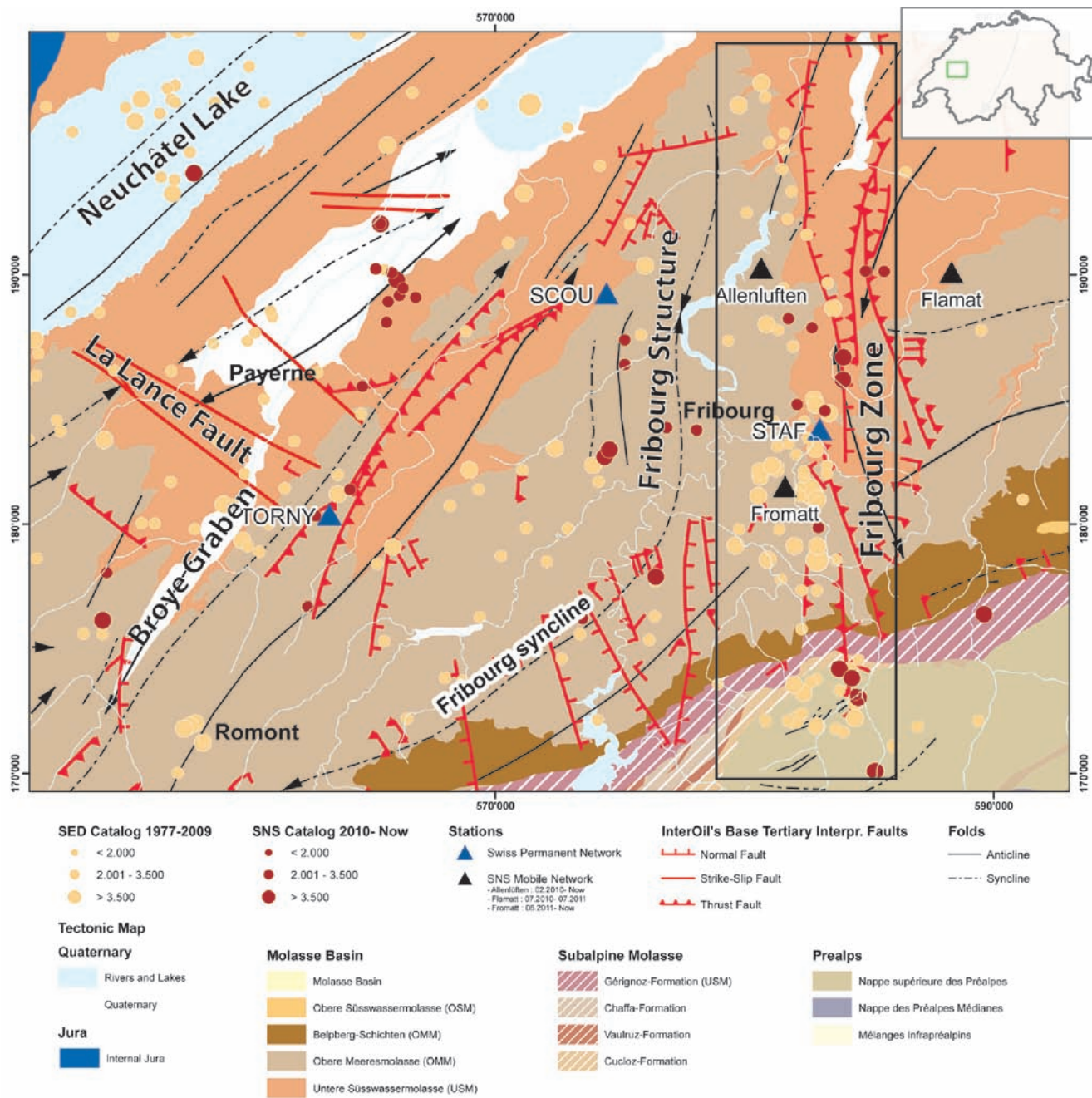


Figure 1: Tectonic Map of the Fribourg Zone showing location of detected earthquakes

1.D.2

Triassic magmatism recorded by detrital zircons in South Alpine sedimentary units.

Beltrán-Triviño Alejandro¹, Winkler Wilfried¹ & von Quadt Albrecht²

¹Geologisches Institut, ETH Zürich, Sonneggstrasse 5, CH-8092 Zürich, Switzerland (alejandro.beltran@erdw.ethz.ch)

²Institut für Geochemie und Petrologie, ETH Zürich, Clausiusstrasse 25, CH-8092 Zürich, Switzerland

Since decades, Triassic magmatism in the Alpine Tethys zone has been matter of controversial discussions. According to Crisci et al. (1984), Triassic magmatic products in Lombardy (Southern Alps) are interbedded with Anisian - Ladinian (245-228 Ma) carbonatic sequences and Ladinian - Carnian (237-216 Ma) continental terrigenous or transitional deposits. K/Ar and Rb/Sr ages on biotites dated the beginning of the volcanism at 225 Ma (Crisci et al. 1984). Petrographic and geochemical data of those volcanics reveal a calc-alkaline affinity, suggesting a continental convergent margin environment. However, according to these authors, geological evidence indicates dominating extensional movements during the Middle Triassic in the Southern Alps.

Garzanti (1985, 1986) suggested that the erosion of a southern volcanic belt provided the bulk of fine-grained and moderately sorted siliciclastic detritus in the deltaic to lagoonal Carnian (228-216 Ma) sequence of the Bergamasco Alps. The volcanic input should have started in the Early Carnian (Calcare Metallifero Bergamasco Fm) and became prominent in Early - Middle (Val Sabbia Fm) and Late Carnian (S. Giovanni Bianco Fm), and a final diminished supply in the topping Gorno Fm. According to mineralogical and chemical data, the sandstones would be comparable with such as derived from modern Pacific-type magmatic arcs, depicting an evolution of the source rocks from andesites and dacites during the deposition of the Val Sabbia sandstones towards rhyodacitic ignimbrites present in the S Giovanni Bianco Fm.

Castellarin et al. (1988) focused on compressional structures in the Central Dolomites. Those structures would be incompatible with an extensional geodynamic setting (crustal rifting) as assumed by other authors. The calc-alkaline character of the Triassic magmatic series is considered to be more in agreement with a compressional geodynamic setting rather than with an extensional one. Furthermore, the time-space distribution of the Middle Triassic magmatic rocks in the Southern Alps coupled with their petrochemical affinity, would closer fit with modern volcanic arcs. Nevertheless, Castellarin et al. (1988) also conclude that the general geodynamic context of the Southern Alps due to their ensialic character, does not fit their oceanic model.

With regard to the controversial interpretation of the origin of Triassic magmatism, we present in this work first geochemical data (laser ablation U-Pb ages, Hf isotopes and trace elements concentrations) on detrital zircons extracted from the Carnian Val Sabbia Formation (Fig. 1a) and other Triassic Alpine sandstones. These results are complemented with petrographical and standard modal grain analysis of the sandstones.

The Val Sabbia Fm sandstone reveals a prominent age population ranging between \approx 256 - 220 Ma, with a peak at 240 Ma (Fig. 1a, b). The ratio of Hf isotopes ($\epsilon_{\text{Hf}}(t)$) shows a constant and narrow range between - 4 and - 6. Such values would indicate a young crustal component dominating the magma formation. A driving continental rifting environment can be suggested. These result will be compared with other Triassic sandstones from the southern Alpine Tethys margin.

REFERENCES:

- Castellarin, A., Lucchini, F., Rossi, P. L. & Simboli, G. 1988: The Middle Triassic magmatic-tectonic arc development in the Southern Alps. *Tectonophysics*, 146, 79-89.
- Crisci, C. M., Ferrara, G., Mazzuoli, R. & Rossi, P. M. 1984: Geochemical and geochronological data on Triassic volcanism of the Southern Alps of Lombardy (Italy): Genetic implications. *Geologische Rundschau*, 73, 279-292.
- Garzanti, E. 1985: The sandstone memory of the evolution of a Triassic volcanic arc in the Southern Alps, Italy. *Sedimentology* 32, 423-433.
- Garzanti, E. 1986: Source rock versus sedimentary control on the mineralogy of deltaic volcanic arenites (Upper Triassic, northern Italy). *Journal of Sedimentary Petrology*, 56, 267-275.

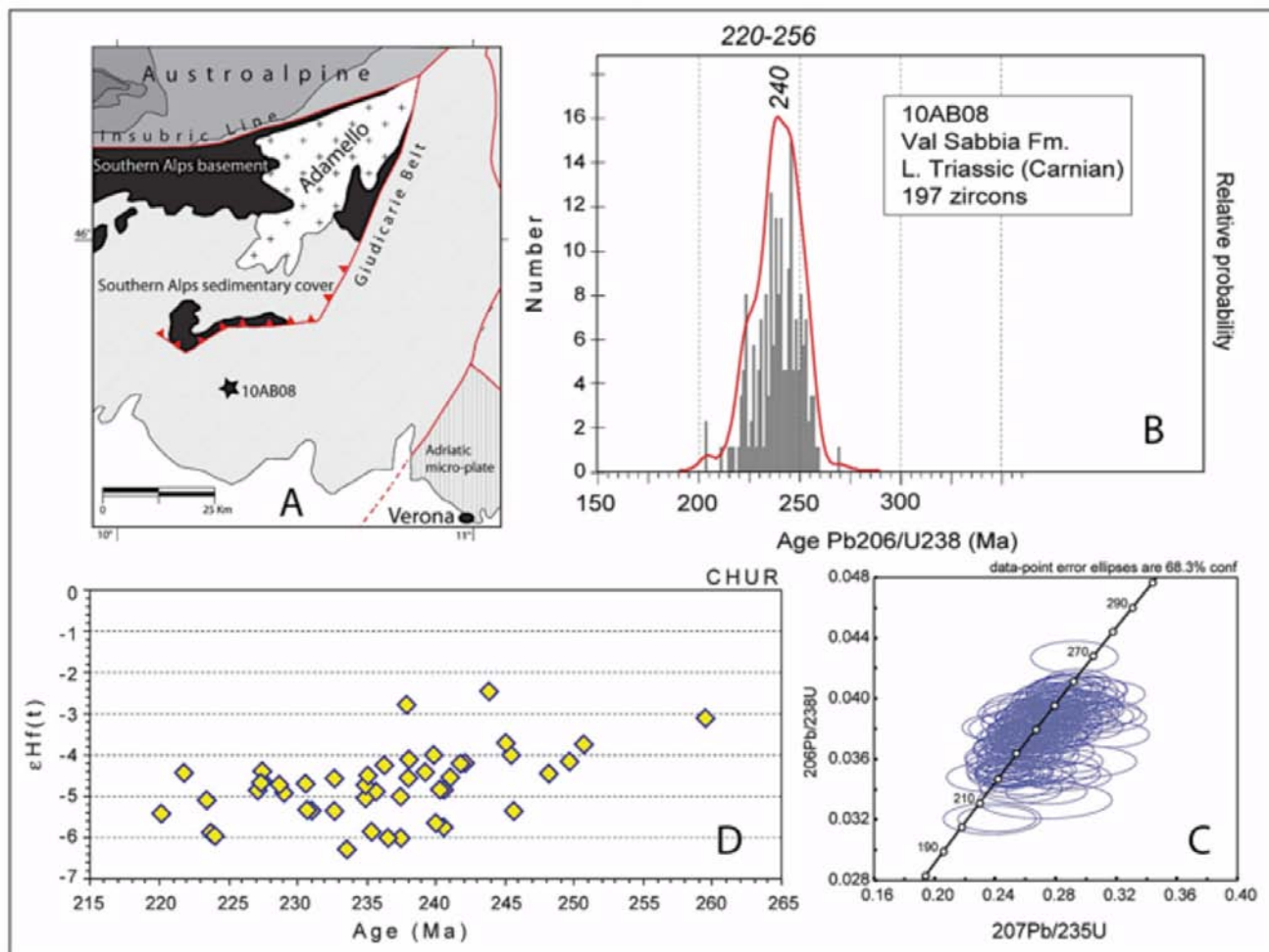


Figure 1: Geographical location (N 45° 41' 57.8" / E 10° 20' 43.1") of the investigated Val Sabbia Fm outcrop (a), histogram of measured detrital zircon U/Pb ages with probability curve (red) (b), concordia diagram (c), and the Hf isotope ratios plotted against age (d).

1.D.3

Paleotopography of the Miocene European Central Alps

Campani Marion¹, Mulch Andreas¹, Kempf Oliver², Schlunegger Fritz³ & Mancktelow Neil⁴

¹ Biodiversity and Climate Research Centre (BiK-F), Senckenberganlage 25, D-60325 Frankfurt, (marion.campani@senckenberg.de/ +496975421883)

² Bundesamt für Landestopografie swisstopo, Geologische Landesaufnahme, Seftigenstr. 264, CH-3084 Wabern

³ Institute of Geological Sciences, University of Bern, Baltzerstrasse 1+3, CH-3012 Bern

⁴ Geologisches Institut, ETH Zürich, CH-8092 Zürich

Recent geologic and geodynamic models for the Central European Alps propose that the bulk of topography was built through the Pliocene, mainly based on the observation of a strong increase in sedimentation and erosion rates during the last 5-6 Ma, suggesting that the Alps never attained elevations as high as today. Here, we aim to quantify the Miocene (20-14 Ma) paleoelevation of the Central Alps through stable isotope paleoaltimetry. The novelty of the approach presented here, which renders it rather insensitive to past climate change, is to analyze stable isotope proxies of identical age, both from high internal parts of the Alpine orogen and from the adjacent foreland basin that was at or near sea level. We compare hydrogen isotopic ratios (δD) in mica and chlorite that interacted with meteoric water along the Simplon detachment, a major normal fault that developed at high elevations, with meteoric water compositions deduced from carbonate-bearing paleosols of the North-Alpine foreland basin.

In the North-Alpine foreland basin, we present oxygen and carbon isotopic compositions of pedogenic mudstones and carbonate concretions. These terrestrial paleosols, dated with ca. 100 ka precision, serve as our point of reference for stable isotope paleoaltimetry, since they formed at or near sea level. Here, $\delta^{18}\text{O}$ and $\delta^{13}\text{C}$ values vary between +19 to +25‰ (SMOW) and -7 to +1‰ respectively and show close correspondence to global climate change during the mid-Miocene climatic optimum. In the Simplon fault zone, detachment-related muscovite (-126‰) and chlorite (-135‰) δD values from the brittle hanging wall provide unequivocal evidence for syntectonic meteoric water interaction. This result is supported by a strongly localized pattern of meteoric water interaction in the footwall mylonites where recrystallized muscovite and biotite have δD values of -108‰ and -140‰, respectively. Detailed $^{40}\text{Ar}/^{39}\text{Ar}$ and fission track geochronology constrains the timing of isotopic exchange during the ductile to brittle transition of the detachment to ca. 14-15 Ma.

Using the relative differences between meteoric water composition in the foreland and internal regions of the orogen, our isotope data are consistent with an average altitude difference of 2300 m \pm 500 m during the mid-Miocene. Our results do not necessarily agree with the proposition that the main formation of topography started only 5-6 Ma ago, since the Alpine elevations were similar or even higher than those of today already in the mid-Miocene. This implies that the bulk of Alpine topography was built during the construction stage of the Alpine orogenic wedge when accretion rates outpaced erosion and sediment evacuation rates.

1.D.4

Fault architecture at the brittle-ductile transition in sedimentary rocks – examples from the SW Helvetics (Swiss Alps)

Cardello Giovanni Luca¹ & Mancktelow Neil S.¹

¹Geological Institute, Sonneggstrasse 5, CH-8092 Zurich. (luca.cardello@ethz.ch)

Most crustal earthquakes are triggered on faults at the brittle-ductile transition, which in the continental crust commonly occurs in sedimentary rocks buried to depths of 8 to 13 km, depending mainly on the geothermal gradient and the tectonic regime (in particular, whether faults are dominantly normal, thrust or strike-slip). In the SW Helvetics, oblique normal faults that cross-cut the Alpine nappe-stack and developed during Neogene time under very low metamorphic grade are currently exposed at the surface. Some of these faults are quite long (5-12 km) and show significant accumulated displacement (> 1 km), which makes them good candidates for past seismogenic structures with earthquakes of similar or even higher magnitude ($M_w \geq 6.0$) compared to those presently recorded in this highly active seismic area (Rhône Valley). The current study investigates the fault architecture as preserved in the field with the aim of establishing the processes involved in fault slip accumulation. Locally, it is possible to establish a transition from mylonitic to cataclastic fabrics (e.g. on the Rezli fault), with a complex interplay of processes including pressure solution, veining, mineralization on fault planes and repeated brecciation. Generally, the fault architecture, as well as the vein distribution and composition, changes with the lithology, and therefore varies both along and across major faults. Where fault displacement is large and different formations are juxtaposed across a fault, the fault core and damage zones develop a complex architecture involving more important fluid circulation, veining and fluid-rock interaction, whereas faults with minor displacement (a few metres) are generally simpler and narrower, with veining concentrated close to the fault. This implies that the damage zone tends to broaden with increased displacement, rather than the fault increasingly localizing on a narrower zone. Despite that, there are also many examples of fault broadening. Nevertheless, veining and pressure solution are apparently always related with the initial stages of faulting. Mode-1 veins, commonly developed in an en-echelon pattern, are locally dissolved by stylolites, which are themselves later crosscut by veins and, finally, also by discrete fault planes. This implies multiple and interrelated processes of dissolution, crack opening, and mineralization and therefore faulting. Such a succession of events is better developed and more broadly distributed in basinal limestones (e.g., Early Lias, Quinten and Seewenkalk Fm.) and in boudinaged limy horizons (e.g. Nummulitenkalk), rather than in shales (e.g. Oxfordian, Zementstein), slates (e.g. Late Lias), limey-sandstones (Wildstrubel Fm.) and platform grainstones (Schrattenkalk), where such processes tend to localize close or inside the damaged zone. Shale-rich formations tend to develop S/C structures in the fault core whereas the more calcareous or sandy units show more discrete faulting. Despite the similar kinematics of the fault planes mapped in the field to the focal mechanisms calculated for recent earthquakes (Maurer et al. 1997), there is no hard evidence of faulting in Quaternary deposits. The fossil fault structures described represent exhumed faults developed at the brittle-ductile transition, which experienced little significant late brittle faulting during exhumation.

REFERENCES

Maurer H.R., Burkhard M, Deichmann N. & Green A.G. 1997: *Active tectonism in the central Alps: contrasting stress regimes north and south of the Rhone Valley*. Terra Nova. 9. Issue 2. Pp 91-94

1.D.5

Dextral movements between the Pennine Front and Mont Blanc massif in the Courmayeur area

Egli Daniel¹ & Mancktelow Neil¹

¹Geologisches Institut, ETH-Zürich, Sonneggstrasse 5, CH-8092 Zürich. (daniel.egli@erdw.ethz.ch)

The area of Courmayeur, located in the uppermost Aosta Valley (I), is geologically very interesting, as several major tectonic units occur in close proximity and the relative relationship between these units is not unequivocally established. The Helvetic and Ultrahelvetic meta-sediments (HU) form a narrow band ca. 4 kilometres wide between the Pennine Front and the Mont Blanc backthrust. They include a small basement sliver, the Mont Chétif slice (MC), forming a 7 kilometre long and few hundred metres wide outcrop that is lithologically comparable to the Mont Blanc external crystalline massif (MB).

Due to its footwall position in the immediate vicinity of the Pennine Front (PF), the observed deformation structures are considered to reflect movements on the PF itself. The PF, separating the internal (Penninic and Briançonnais) and the external (Helvetic and Ultrahelvetic) part of the Alps, is a major fault zone that can be followed around the bend of the western central Alps (e.g. Ceriani et al., 2001). The MC itself is heterogeneously deformed, ranging from mylonites, through weakly foliated granites, to effectively undeformed granite. It is made up of many shear zones, as well as brittle structures. The main mylonitic foliation dips steeply toward SE, with a stretching lineation plunging shallowly toward ENE. Shear sense criteria consistently show that the PF had an oblique dextral-reverse sense of movement in this area.

To the NW, the HU are bound by the Mont Blanc backthrust (MBbt), a steeply NW-ward dipping reverse fault zone that locally places the MB over its sedimentary cover. It has, similar to the PF, an oblique dextral thrust geometry, but with the opposite thrust sense and moderately steep SW-ward plunging lineations. The HU are wedged between these two shear zones and show a multi-stage folding history, with the main foliation being a spaced crenulation cleavage (regional S2), which mainly records NW-directed thrusting. Transcurrent movements in the cover units are restricted to abundant calcite slickenfibres and striae, mainly dextral but with infrequent sinistral faults forming conjugate sets.

These different tectonic structures indicate a long history of dextral transpressive movement, since these structures are supposed to be active at markedly different times. The main activity along the PF is generally considered to be Oligocene (Ceriani et al., 2001), whereas the shear zones related to the MBbt are dated to be active around 16 Ma (Rolland et al., 2007). It is planned to date the shear zones in the MC that overprint the main mylonitic fabric as part of the current study. These shear zones are themselves later overprinted by chevron type folds, partly developing a new spaced crenulation cleavage (regional S3), which clearly predates the brittle slickenfibres occurring in the HU. Fault-slip analysis on such faults indicates NE-SW directed compression, which is 90° to what would usually be expected in the western Alps, where the main structures are typically related to regional SE-NW directed compression. However, the MB lies in the southwestward continuation of the Rhône-Simplon fault system, whose dextral movements clearly extend around both sides of the MB in both the Chamonix and Ferret valleys. The MB lies in the position of a restraining bend relative to these movements and the observed change in compression direction could be explained as due to this restraining bend geometry.

The strike of the MB turns from a roughly N-S orientation NE of Courmayeur to an ENE-WSW orientation further SW. It is noticeable that features such as the MC and the MBbt occur exactly at this corner point of the massif, which also happens to be the area where the topography of the MB reaches its maximum height. We postulate that this is an area stress concentration, induced by the geometry and position of the basement massif relative to the continuation of the Rhône-Simplon fault system, which would produce the observed thrust and back-thrust pair in an overall dextral transpressive regime.

REFERENCES

- Ceriani, S., Fugenschuh, B., and Schmid, S. M., 2001, Multi-stage thrusting at the “Penninic Front” in the Western Alps between Mont Blanc and Pelvoux massifs: *International Journal of Earth Sciences*, v. 90, no. 3, p. 685-702.
- Rolland, Y., Corsini, M., Rossi, M., Cox, S. F., Pennacchioni, G., Mancktelow, N., and Boullier, A. M., 2007, Comment on “Alpine thermal and structural evolution of the highest external crystalline massif: The Mont Blanc” by P. H. Leloup, N. Arnaud, E. R. Sobel, and R. Lacassin: *Tectonics*, v. 26.

1.D.6

Multi-disciplinary study for the exploration of deep low enthalpy geothermal reservoirs, Neuchâtel, Switzerland

Mauri Guillaume¹, Negro Francois ¹, Abdelfettah Yassine¹, Vuataz Francois-David¹, Schill Eva¹.

¹ *Laboratory for Geothermics (CREGE), Centre for Hydrogeology and Geothermics (CHYN), University of Neuchâtel, Neuchâtel, Switzerland, guillaume.mauri@unine.ch*

The authorities of the canton of Neuchâtel, in the Western part of Switzerland, is willing to develop geothermal energy for district heating in the two main cities of the canton: Neuchâtel, located along the Lake of Neuchâtel, and La Chaux-de-Fonds situated in a high valley of the Jura Massif. The geology of both areas is linked to the Jura Range and present complex structures, where the landscape is composed of anticlines associated with overthrust faults, which are overcut by strike-slip fault and secondary faulting events. The rock formations go from the Trias, which forms the detachment layer, up to the Quaternary rock. Bedrocks are mainly composed of limestones and marls, which can reach a thickness of several hundreds meters. The three main deep aquifers investigated in this area, from the shallowest (≤ 400 m below surface) to deepest (< 2000 m), are the Malm, the Dogger and the Muschelkalk. The estimated temperatures, based on previous studies, should range between 20 to 65 °C, which are function of depth, elevation and groundwater velocity. The expected low temperature is mainly due to the presence of karstic systems, which drains the heat towards the low elevation of the basin.

The present study is based on gravimetry surveys, 3D geological models and 3D gravimetry models to best characterize the underground structures and to find areas where the rock properties would be favourable to geothermal exploitation. This means targets where permeability and porosity are high in the potential aquifers, allowing a significant flow at the future production wells.

The results indicate that gravity anomalies are associated with both shallow and deep geological structures in the two exploration sites and that high resolution of dense grid gravity measurements combined with realistic 3D models of the geological structures allow to characterize interesting features for deep geothermal exploration. Gravity corrections were carried out with a computing code using different DEM resolution ranging from a very high resolution (0.5 m pixel in the vicinity of each station) toward a lower resolution (25 m for the distal areas as far as 110 km away from each station). The bathymetry of the Lake of Neuchâtel (218 km²) has been used to correct gravity effects from the large volume of water along the Lake shore of Neuchâtel.

The combination of 3D geological models with a high resolution gravity survey allows to better constrain the geometry of the Triassic formation, just above the detachment layer, as well to quantify the karstic processes, which could affect the three deep aquifers.

1.D.7

Strong rupture and postseismic response of the 8 June 2008 Achaia-Elia earthquake in Western Peloponnese, Greece

Panos Psimoulis^{3,1} Lujia Feng^{4,2} Andrew Newman², Stathis Stiros¹, Fanis Moschas¹, Sotiris Lycourghiotis¹, Grant Farmer^{5,2}

¹*Geodesy Lab., Dept. of Civil Engineering, University of Patras, 26500, Patras, Greece*

²*School of Earth and Atmospheric Sciences, Georgia Institute of Technology, USA*

³*currently: Geodesy and Geodynamics Lab., Inst. of Geodesy and Photogrammetry, ETH Zurich, Schafmattstr. 34, HPV F51, 8093, Zurich (panos.psimoulis@geod.baug.ethz.ch)*

⁴*currently: Nanyang Technological University, Earth Observatory of Singapore, 50 Nanyang Avenue, Block N2-01a-015, 639798, Singapore*

⁵*currently: Massachusetts Institute of Technology, Earth and Planetary Sciences, 77 Massachusetts Ave., Cambridge, MA02139, USA*

On 8th June, 2008 a strong earthquake occurred in western Peloponnese, only 30km SSW of the major port city of Patras of moment magnitude $M_w=6.4$. Fortunately no large population exists near the source region and thus loss of life and property damage was minimal. However the strong shaking associated with the event did cause significant damage to mostly unreinforced structures near the source region. The earthquake exhibits an approximately 25km long NE-SW tren-

ding aftershock distribution that together with fault plane solutions, clearly indicates right-lateral strike slip on a near vertical dipping fault which is not associated with existing mapped faults (Ganas et al., 2009). Thus it is suspected that these events form a newly-developed transform accommodating part of the Aegean-Eurasian boundary.

To record possible post-seismic surface deformation, a local network of nine continuous GPS sites was rapidly deployed in 24 to 48 hours and maintained for approximately six weeks (Fig.1a). The sites included one base station at the University of Patras and eight stations near the early aftershock locations, which were distributed almost longitudinally and laterally to the main trend of the aftershocks. Sites were installed either on rooftops of visibly undamaged 1-2 story houses, or on exposed bedrock in open fields.

Six weeks of daily point-position solutions were determined using JPL-GIPSY (Fig.1b) and for the first three days 15s kinematic solutions relative to site UPAT were determined using the Track software included with GAMIT/GLOBK (Fig.1c). Even though numerous aftershocks of magnitude $M_L=2-4$ continued in this region during the recording period, no discernible early post-seismic deformation was identified across the network using either the daily or the rapid kinematic solutions (Fig.1b,c). Some shifts which are observed in the kinematic solutions, are mainly short-lived (less than 1 day), not correlated across stations and are likely not tectonic in origin.

Furthermore based on analyses of InSAR images (ascending scenes on 2007.12.16 and 2008.07.13), it was shown that little interference consistent with coseismic activity is identifiable, implying probable buried or even detached slip in the sub-surface (Feng et al., 2010).

Thus based on GPS data and InSAR images analyses it was not revealed any significant post-seismic slip or coseismic surface deformation, respectively,

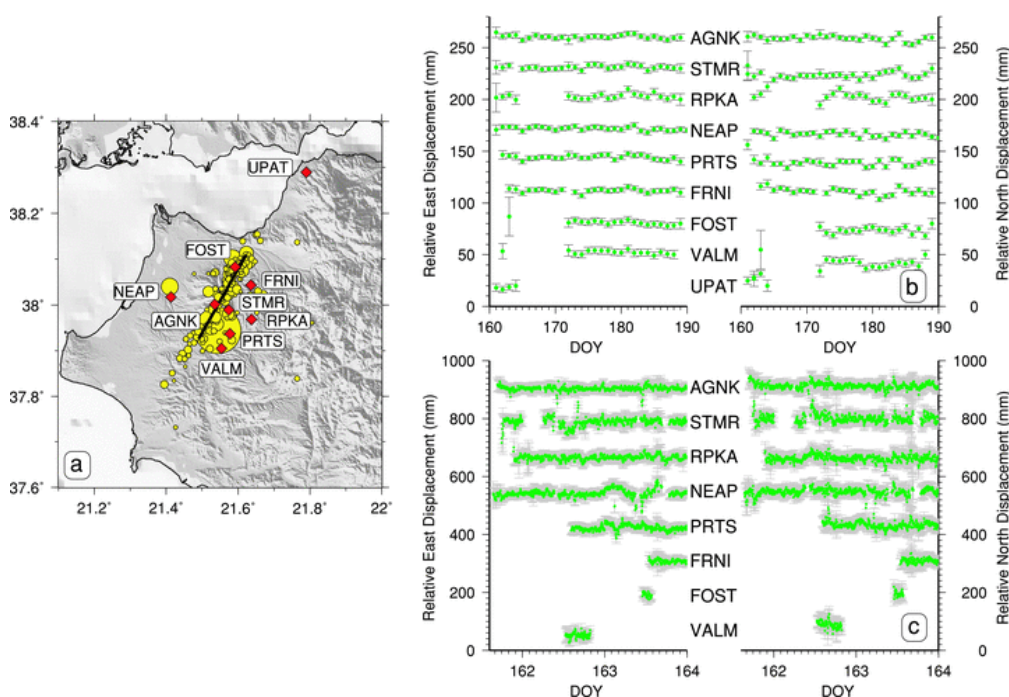


Figure 1. a) Location of the temporary network of nine continuous GPS sites (red diamonds). The solid line represents the approximate 25-km long projected fault trace estimated from main shock and 1-day of aftershocks (yellow circles). b) JPL-GIPSY daily solutions for post-seismic period. c) GAMIT-Track solutions for the first 3-day of recording. The data are 5-minute averaged 15-sec kinematic solutions relative to site UPAT.

which came in contrast with the highly energetic estimated rupture for an earthquake with hypocentre depth of ~25km. The suggestion is that the lack of surface deformation can be explained by a thick flysch layer, which covers the earthquake region, disassociates fault slip from the surface (Feng et al., 2010). Thus the geodetic evidence of the 2008 June 8, earthquake and numerous smaller strike-slip events reveal an immature NE-SW trending dextral transform fault zone in the western Peloponnese, making more clear the until then motion of the region (Hollenstein et al., 2008).

REFERENCES

- Feng, L., Newman, A.V., Grant, F.T., Psimoulis, P., Stiros, S.C., 2010: Energetic rupture, coseismic and post-seismic response of the Mw 6.4 Achaia-Elia Earthquake in northwestern Peloponnese, Greece: an indicator of an immature transform fault zone, *Geophys. J. Int.*, 183, 103-110
- Ganas, A., Serpelloni, E., Drakatos, G., Kolligri, M., Adamis, I., Tsimi, Ch., and Batsi, E., 2009: The Mw 6.4 Achaia-Elia (Western Greece) Earthquake of 8 June 2008: seismological, field, GPS observations and stress modeling, *J. Earthq. Eng.*, 13, 1101-1124
- Hollenstein, C., Muller, M.D., Geiger, A., Kahle, H.-G., 2008: Crustal motion and deformation in Greece from a decade of GPS measurements, 1993-2003, *Tectonophysics*, 449, 17-40

1.D.8

Fault-controlled formation of a primary turbiditic channel within the Gurnigel Flysch at the Voirons Massif (Haute-Savoie, France) during the Late Eocene.

Ragusa Jérémy¹, Ospina-Ostios Lina Maria¹ & Kindler Pascal¹

¹ Section of Earth and Environmental Sciences, University of Geneva, 13 rue de Maraîchers, CH-1205 Geneva
(Jeremy.Ragusa@unige.ch)

The Vachat Quarry outcrop is an exceptional exposure of the Vouan Conglomerates (Gurnigel Flysch) where primary turbiditic channel deposits were studied. The quality of the exposure has allowed the observation of a tectonically induced channel in the proximal part of a turbiditic system. The presence of a fault emphasizes the influence of tectonic activity in the geometry of this turbiditic system. Our results provide evidences of a tectonically generated canyon contrasting with the erosional model proposed by Frébourg (2006).

The studied section is located at about 20 km to the East of Geneva, on the western flank of the Mont Vouan (Voirons Massif). The outcrop called “The Vachat Quarry” is one of the most important and well-preserved millstone quarry of the area. About 100 m long and reaching a depth of 35 m in some places, this outcrop is crosscut by two vertical faults.

The Vouan Conglomerates consist of plurimetric beds of cobbly and pebbly sandstones with sparse conglomeratic layers. The matrix can be described as a feldspar-rich arkose (Ospina et al., submitted). Shaly intervals are extremely rare in this formation. This formation has been interpreted as the proximal part of a turbiditic system (Frébourg, 2006) of Late Eocene and Early Oligocene age (Ospina et al, submitted).

The outcrop exposes highly amalgamated beds composed of facies F1 to F2 (Mutti, 1992) (Fig. 1). At their base impressive load casts and bioturbation traces can be observed. Only one F3 layer was noticed. The latter is not laterally continuous and presents an erosional base. Along the section a massive and thick F5 facies bed was used as a “reference” level (Fig 1). Locally two really well-preserved F6 facies layers were observed.

The northern fault constitutes a major break. Beds from both fault blocks (1 & 2) cannot be correlated, implying a important offset. The “reference” bed is displaced by about 5 m by the southern fault, affecting fault blocks 2 & 3. This displacement has promoted the deposition of additional beds in fault block 2.

The good quality of the exposure allows to us to identify two primary turbiditic channels (facies F1 to F3) separated by transitional (channel to lobe) deposits (F5 facies). In the central part of the outcrop a decametric channel can be observed. The axial part of this channel shows erosional features (facies F3 and localized lens of pebbles). Transitional deposits are superimposed on the latter (facies F5, Mutti, 1992). The tectonic activity of the second fault has created a small hemigraben which controlled the formation of the channel. The depression generated was progressively filled by a second channel (F1 to F2 facies).

REFERENCES

- Frébourg, G. 2006: Les conglomérats du Vouan: un cañon turbiditique? MS Thesis, Univ. Geneva, 79 pp.
 Mutti, E. 1992: Turbidite sandstones. AGIP publisher, Parma, 275 pp.
 Ospina-Ostios, L. M., Ragusa, J., Wernli, R., & Kindler, P. (submitted to *Sedimentology*): New sedimentological and biostratigraphic data from the Voirons Flysch (Voirons massif, Gurnigel nappe, Haute-Savoie, France) : implications for Alpine geology.

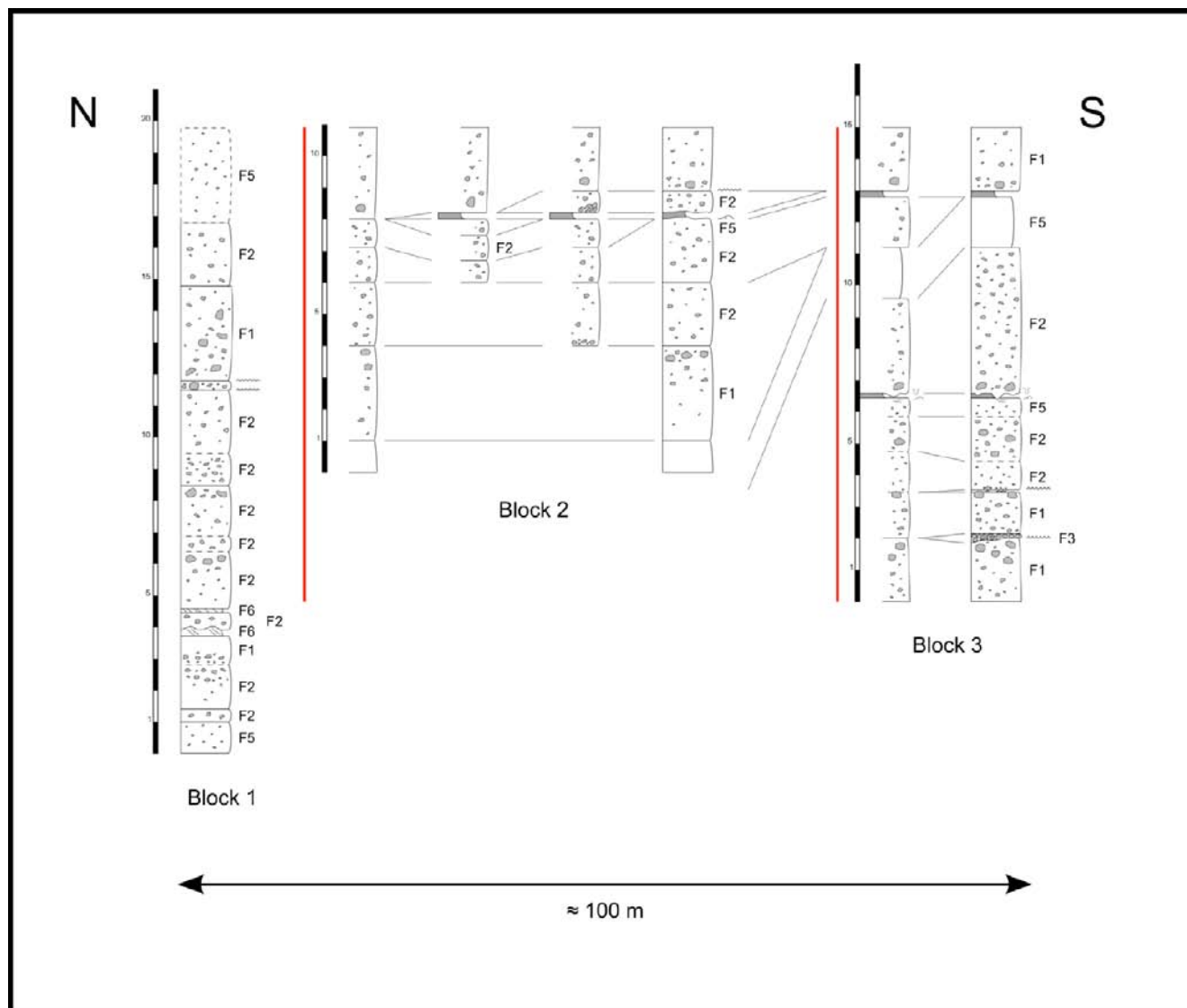


Figure 1: Lateral facies variations in Vachat Quarry section.

1.D.9

Large-scale geometry and structural evolution of the Bernhard nappe complex, Valais, Switzerland

Scheiber, Thomas¹, Pfiffner, O. Adrian¹, Schreurs, Guido¹

¹Institute of Geological Sciences, University of Bern, Switzerland
 thomas.scheiber@geo.unibe.ch

In order to understand the formation mechanisms of large-scale crystalline basement nappes within continental collision zones, the internal geometry and structural evolution of such basement nappes has to be assessed. The Bernhard nappe complex, exposed within the Penninic zone of western Switzerland, represents a major nappe complex which is ideal to study nappe-forming processes within continental collision zones. However, its large-scale geometry and structural evolution is still enigmatic. According to the classical model of Argand (1916), the Siviez-Mischabel nappe (which is the major and central part of the Bernhard nappe complex) represents a large-scale, isoclinal, basement-cored, recumbent and north-vergent fold, surrounded by Permo-Triassic sediments. In contrast, Markley et al. (1996) proposed that the Bernhard nappe complex consists mainly of thrust sheets which were placed on top of each other, without the development of large-scale isoclinal folds. In addition, Marthaler et al. (2008) proposed that the entire nappe complex is cross-cut by large subhorizontal post-nappe top-to-the-W shear zones, which might be kinematically linked with the Simplon-Rhone shear zone.

In this contribution we present three new N-S to NNW-SSE structural profiles across the central part of the Bernhard nappe complex between the Turtmann Valley and Val de Bagnes. We discuss the field evidence for the two models of Argand (1916) and Markley et al. (1996), and propose that the discrepancy between the models could be the result of the presence of a Permo-Carboniferous trough in the western part of the study area, which caused an overturned limb, and the absence of this trough in the eastern part of the study area, which exhibits mainly thrusting. We present a structural model for the investigated area, which includes (1) the preservation of a pre-alpine(?) fabric in parts of the crystalline basement, which is overprinted by (2) a south-dipping to subhorizontal top-to-the-N fabric associated with large-scale thrusts, which in turn is overprinted by (3) south-vergent folds with a N-dipping spaced cleavage associated with the large-scale Mischabel backfold. This basically two-phase alpine evolution with first a thrust-related, subhorizontal fabric overprinted by a second, backfolding-related fabric seems to be characteristic for the Middle Penninic basement nappes of the Alpine orogen (e.g. Suretta nappe, Scheiber et al., 2010).

REFERENCES

- Argand, E. 1916: Sur l'arc des Alpes occidentales. *Eclogae geologicae helveticae*, 14, 145-204.
 Markley, M., Teysier, Ch., Caby, R., 1999: Re-examining Argand's view of the Siviez-Mischabel nappe. *Journal of Structural Geology*, 21, 1119-1124.
 Marthaler, M., Sartori, M., Escher, A., Meisser, N., 2008: Feuille 1307 Vissoie. *Geologischer Atlas der Schweiz 1:25 000*, Notice explicative 122.
 Scheiber, T., Pfiffner, A., Schreurs, G., 2010: Strain accumulation during basal accretion: case study Suretta nappe (eastern Switzerland). *Swiss Geoscience Meeting*, Fribourg.

1.D.10

3D FEM modeling of fold nappe formation in the Western Swiss Alps

von Tschärner Marina & Schmalholz Stefan

Université de Lausanne, Institut de géologie et paléontologie, Quartier UNIL-Dorigny, Bâtiment Anthropole, CH-1015 Lausanne, (marina.vontschärner@unil.ch)

The fold axes of the Morcles fold nappe in western Switzerland plunges to the ENE whereas the fold axes in the more eastern Doldenhorn nappe plunges to the WSW. These opposite plunge directions characterize the Wildstrubel depression (Rawil depression). In the center of the Wildstrubel depression the ultrahelvetetic nappes lying above the Helvetic nappes are outcropping as isolated klippen (Ramsay, 1981, Fig. 1).

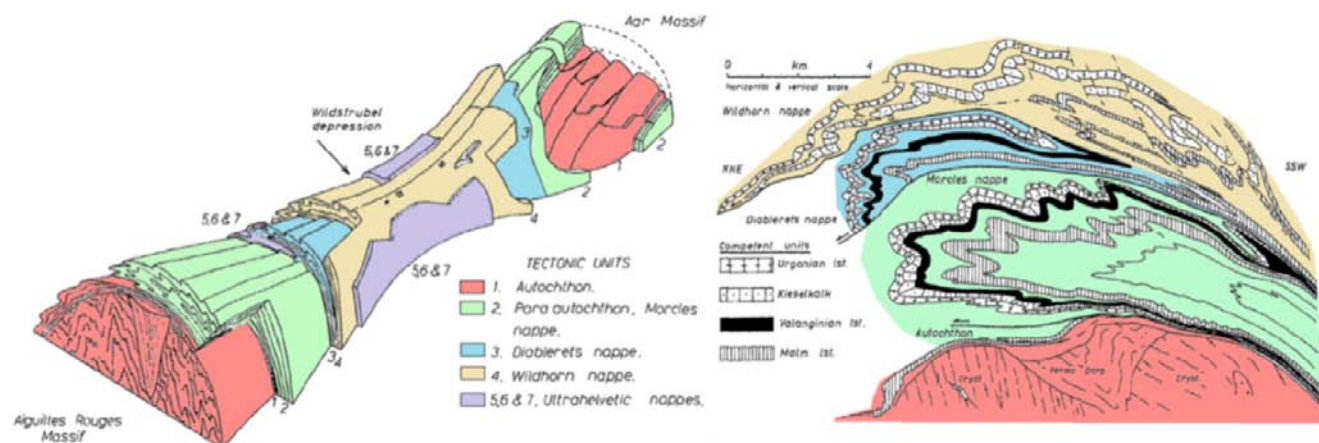


Figure 1: Left: 3D geometry model of the Helvetic nappes and the Wildstrubel depression. Right: 2D profile of the Morcles, Diablerets and Wildhorn nappe. (Ramsay, 1981)

The external basement in the western Swiss Alps exhibits significant ductile deformation. However, the higher units of the sedimentary cover often form more brittle thrust nappes where weak layers act as detachment horizons. An exception is the Morcles nappe which is the result of layer contraction and shearing (Ramsay, 1981). During the compression the massive limestones were more competent than the surrounding marls and shales, which led to the buckling characteristics of the Morcles nappe, especially in the north-dipping normal limb (Fig. 1).

There are no 3D numerical studies which investigate the dynamics of the formation of the large-scale 3D structure including the Morcles and Doldenhorn fold nappes and the related Wildstrubel depression. Such studies require a numerical algorithm that can accurately track material interfaces for large differences in material properties and for large deformations. We present a numerical algorithm based on the finite element method (FEM) which can simulate 3D fluid flow for a power-law viscous rheology. Our FEM code combines a numerical marker technique and a deformable Lagrangian mesh with re-meshing (Poliakov and Podladchikov, 1992) and is used to study the formation of 3D fold nappes similar to the ones in the Western Swiss Alps. The numerical method requires the interpolation of material properties to the integration points because the layer interface can lie within a finite element. To guarantee accuracy the number of integration points in the finite elements is increased considerably. The interpolation is only performed during several re-meshing steps when the deformed Lagrangian mesh is too distorted. During the re-meshing the global coordinates of the contour points specifying the interface between different materials remain unchanged and the new local coordinates of the contour points are interpolated from the element nodes of the new mesh (Fig. 2). Our new FEM code is tested for large strain density driven diapirism and single-layer folding of power-law viscous layers by comparing numerical results with analytical solutions. Also, the 3D results of the new code will be compared with 2D results of existing and tested 2D numerical codes for cylindrical folding.

In our first simulation with a simple set-up a recumbent fold with an overturned fold limb is modeled by compressing a strong layer against an even stronger block (Fig. 2). We will explain the applied numerical method and present preliminary results for the formation of the Morcles-Doldenhorn fold nappe system.

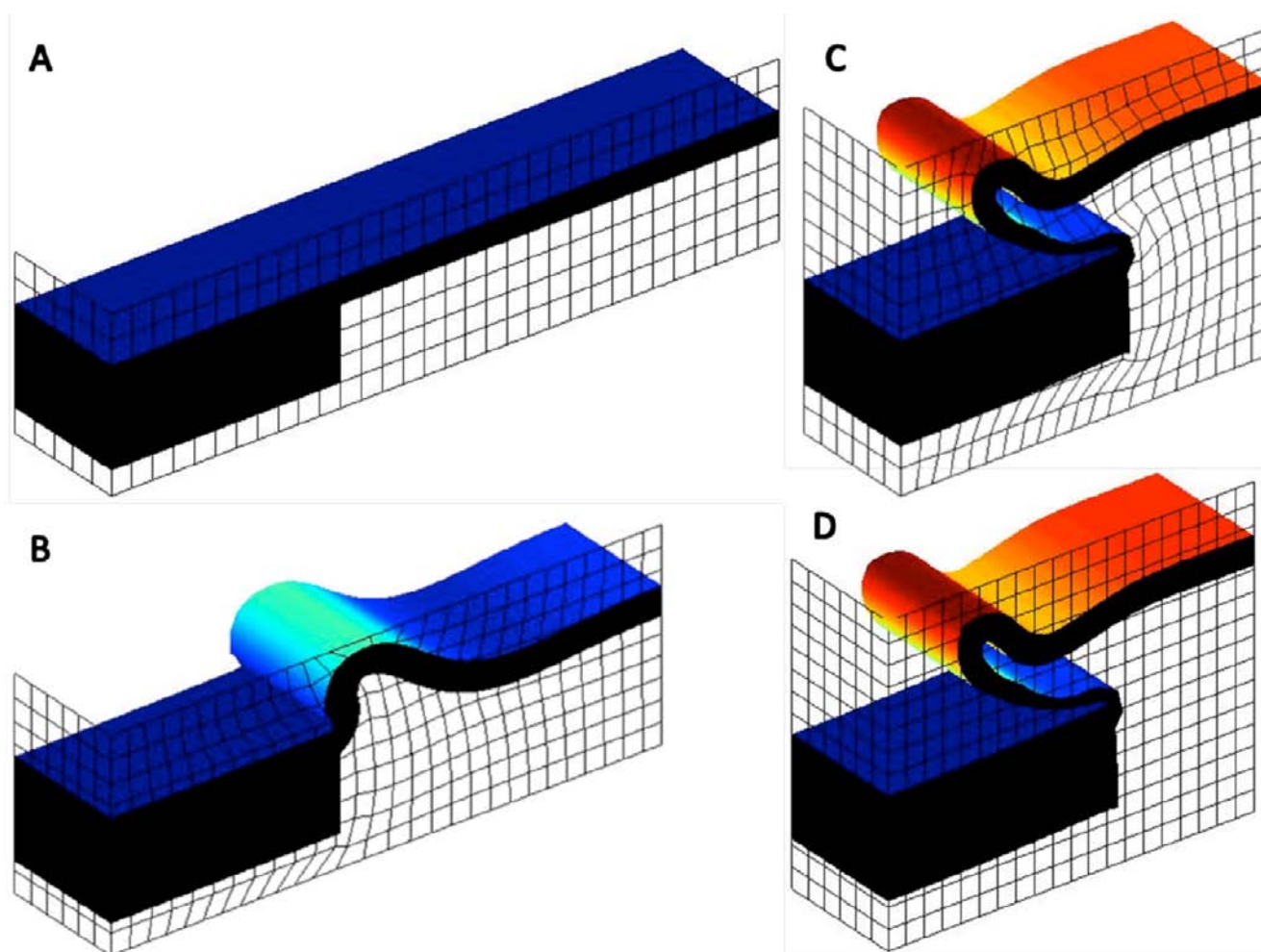


Figure 2: First results of a 3D simulation of a cylindrical single layer fold with overturned limb for a viscosity ratio of 50 between the layer and the matrix and 10000 between the rigid block and the matrix. A: Initial geometry. B: Geometry after 20% shortening. C: Geometry after 45% shortening before re-meshing. D: Geometry after 45% shortening after the re-meshing.

REFERENCE

- Poliakov, A. and Podladchikov, Y., 1992: Diapirism and topography. *Geophysical Journal International*, 109, 553-564
 Ramsay, J. G., 1981: *Tectonics of the Helvetic Nappes, Thrust and Nappe Tectonics*. The Geological Society of London, 293-309

1.E.1

Kinematics of Doruneh Fault in central Iran: two different behaviors since Eocene time

Bagheri Sasan¹, Madhani-Fard Razieh¹, Zahabi Foruzan¹ & Javadi-Zadeh Leila¹

¹Department of Geology, University of Sistan and Baluchestan, Zahedan, 98167-45785, Iran
Email: sasan_bagheri@yahoo.com

The Doruneh fault is one of the most striking transcurrent faults in Iran which an important part of convergence between Iran and surrounding plates has been accommodated along this fault since Cenozoic time. This northwardly curved fault with a 700 km length transects the Iranian crust wideness in a nearly N70 E direction (Fig. 1). The Doruneh fault has been known as the northwest border of the Central-East Iranian Micro-continent (CEIM) since the Paleogene time when the Neotethyan back-arc suture line was formed during the closure of the Sabzevar ocean.

Regarding the kinematics of the Doruneh fault, there are only a few data have been published without consensus about its movements and rate of displacement and convergence. What exists are the seismological data related to the neotectonic activities of its eastern part (Berberian, 1976). According to these evidences, the researchers consider a left-lateral displacement with different convergent rates related to its recent action. In this work we studied three and separate domains with proper outcrops along the fault: the Ashin, Pis-Kuh, and Zeber-Kuh complexes.

At the western termination of the Doruneh fault near Nain, the Ashin ophiolitic mélangé complex comprising the various units of the late Cretaceous Nain ophiolite accompanied by Eocene flysch and volcano-sedimentary deposits (Sharkovski et al., 1984) exposed as a crescent-shape structure in northern side of the Doruneh fault (This disrupted assemblage is unconformably overlain by Oligocene red detritus beds. The Ashin complex shows a restraining right-lateral strike-slip duplex structure seems to define the CEIM was largely displaced in respect to the Great Kavir Block.

Few ten of kilometers toward northeast, the second studied structure is the Pis-Kuh complex (Aistov et al., 1984) constructed exactly on the Doruneh fault near to the Jandaq town. Here, a thick pile of dominantly Eocene detrital beds is appeared in form of a positive flower structure including northeast-verging thrusts, Riedel and conjugate Riedel shears, and left-stepped en echelon folds overlies Oligo-Miocene folded beds and underlies the Pliocene unconformity surface. This structure seems to define a left-lateral displacement and northeast convergence during late Miocene time.

The Zeber-Kuh complex (Eftekhar-Nejad et al., 1977) southwest of Kashmar town as well as the same strike-slip duplexes in the south of Sabzevar basin, respectively at south and north side of the Doruneh fault emerges as an exotic duplex block. Half-folds with some northeast axial planes, asymmetrical stacked horses, and minor faults in the late Cretaceous-Paleogene volcano-sedimentary rocks around the Doruneh fault may give us some proofs related to the right-slip movement for the Doruneh fault.

The information come from mentioned areas direct us to propose the Doruneh fault has had two different behavior since Eocene time, if we imagine these complexes are all parts of blocks which affected by a single main fault. It seems the Doruneh fault has been governed by a transpressional stress field synchronous with the CEIM anticlockwise rotation and the Sabzevar ocean closing, so acted as a dextral strike-slip fault, while since Miocene time when it was pushed by the forces originated of the Iran-Arabia collision, it moved sinistrally.

REFERENCES:

- Aistov, L., Melanikov, B., Krivyakin, B., Morozov, L. and Kiristaev, V. (Eds.), 1984. Geology of the Khur Area (central Iran), Explanatory text of the Khur quadrangle map 1:250,000. Geological Survey of Iran, V/O "Technoexport" USSR Ministry of Geology, Reports, TE/No. 20, 1-132, Moscow.
- Berberian, M., 1976. Contribution to the Sestotectonic of Iran (part II), Geological Survey of Iran, Report No.39, 518 p
- Eftekhar-Nejad, J., Valeh, N., Ruttner, Nabavi, M. H., Hajian, J., Alavi, M., and Haghypour, A., 1977. Ferdows quadrangle map 1:250,000, Map no. J6, Geological Survey of Iran, Tehran
- Sharkovski, M., Susov, M. and Krivyakin, B. (Eds.), 1984. Geology of the Anarak area (central Iran). Explanatory text of the Anarak quadrangle map 1:250,000. Geological Survey of Iran, V/O "Technoexport" USSR Ministry of Geology, Reports, TE/No. 19, 1-143 Moscow.



Figure 1. The Doruneh fault satellite picture and location of studied complexes

1.E.2

New information on radionuclides concentration in phosphorites originating from Tunisia and Algeria

Jaloul Bejaoui^{1, 2}, Mohamed Samaali¹, Souad Baccouche¹, Nafaa Reguigui¹, Mohamed Fethi Ben Hamouda¹, Zohra Azzouz¹, Adel Trabelsi¹, Salah Bouhlef² and Boulamia Salim³

¹UR-MDTN, Centre National des Sciences et Technologies Nucléaires, Tunisie. ¹: Corresponding author: (bjaoui_geo@yahoo.fr)

² UR. de Minéralogie et Géochimie Appliquées, Département de Géologie, Faculté des Sciences de Tunis, Université de Tunis El Manar, 2092 Tunis, Tunisie

³Département de géologie et d'Aménagement, Faculté des sciences et sciences de la nature et de la vie, Université de Tébessa, Algérie.

Phosphorites were considered a source of radioactive materials, and the uranium behavior therein was discussed in several publications such as (Altschuler, 1980 and Volkov (1994). The principal constituent of phosphate rock (or phosphorite) is the mineral apatite. The typical phosphate (P_2O_5) concentration of the rock is about 15-40%, with clay, sand, carbonate and other impurities present in varying quantities.

In this study we investigate the radiological hazard of naturally occurring radioactive material in Tunisian and Algerian phosphorite deposits. Phosphorites samples were collected from the phosphorite mines (Fig.1). The Tunisian and Algerian phosphorites occur in the Late Paleocene and Lower Eocene (Ypresian-Lutetian) in age (Sassi, 1984 et Zaïer, 1999). Activity concentrations in all the samples were measured by alpha spectrometry and gamma spectrometry.

Alpha spectrometry analyses show that the specific activity values of ^{238}U , ^{234}U and ^{235}U in the samples of Tunisian phosphorite were 327 ± 7 (321–327), 326 ± 6 (325–331) and 14.50 ± 0.72 (13.90–15.57) Bq. kg⁻¹, respectively.

Specific activity measured by gamma spectrometry in the samples of the Tunisian and Algerian phosphorite show a small difference.

Specific activity levels of ^{40}K , ^{226}Ra , ^{232}Th , ^{235}U and ^{238}U in the phosphorite samples from Tunisia were respectively 71.10 ± 3.80 , 391.54 ± 9.39 , 60.38 ± 3.74 , 12.72 ± 0.54 and 527.42 ± 49.57 Bq.kg⁻¹ and Algeria were 15.72 ± 1.73 , 989.65 ± 12.52 , 12.08 ± 1.20 , 47.50 ± 1.52 and 1148.78 ± 7.30 Bq.kg⁻¹, respectively (Table1 and table2).

The measured value of specific activity of ^{232}Th and ^{40}K in the Tunisian phosphorite samples is relatively higher than that found in the samples of Algerian phosphorite. The measured activity of uranium (^{238}U) in the Tunisian phosphorite (527 ± 49) Bq.kg⁻¹ is lower than in Algerian phosphorite. The measured activity of ^{238}U in the Tunisian phosphorite samples was ($527-1315 \pm 65$) ^{238}U Bq.kg⁻¹ which is higher than its maximum background value of 110 Bq.kg⁻¹ in soils of the various countries of the world and similarities of a number of phosphorites mines in the world (M. Tufail et al., 2006 and ashraf et al., 2001). Different geological origins of phosphorites deposits are the main reason for the large spread in worldwide specific activities. Present study reveals that phosphorite deposits contain natural radioactivity higher than background level.

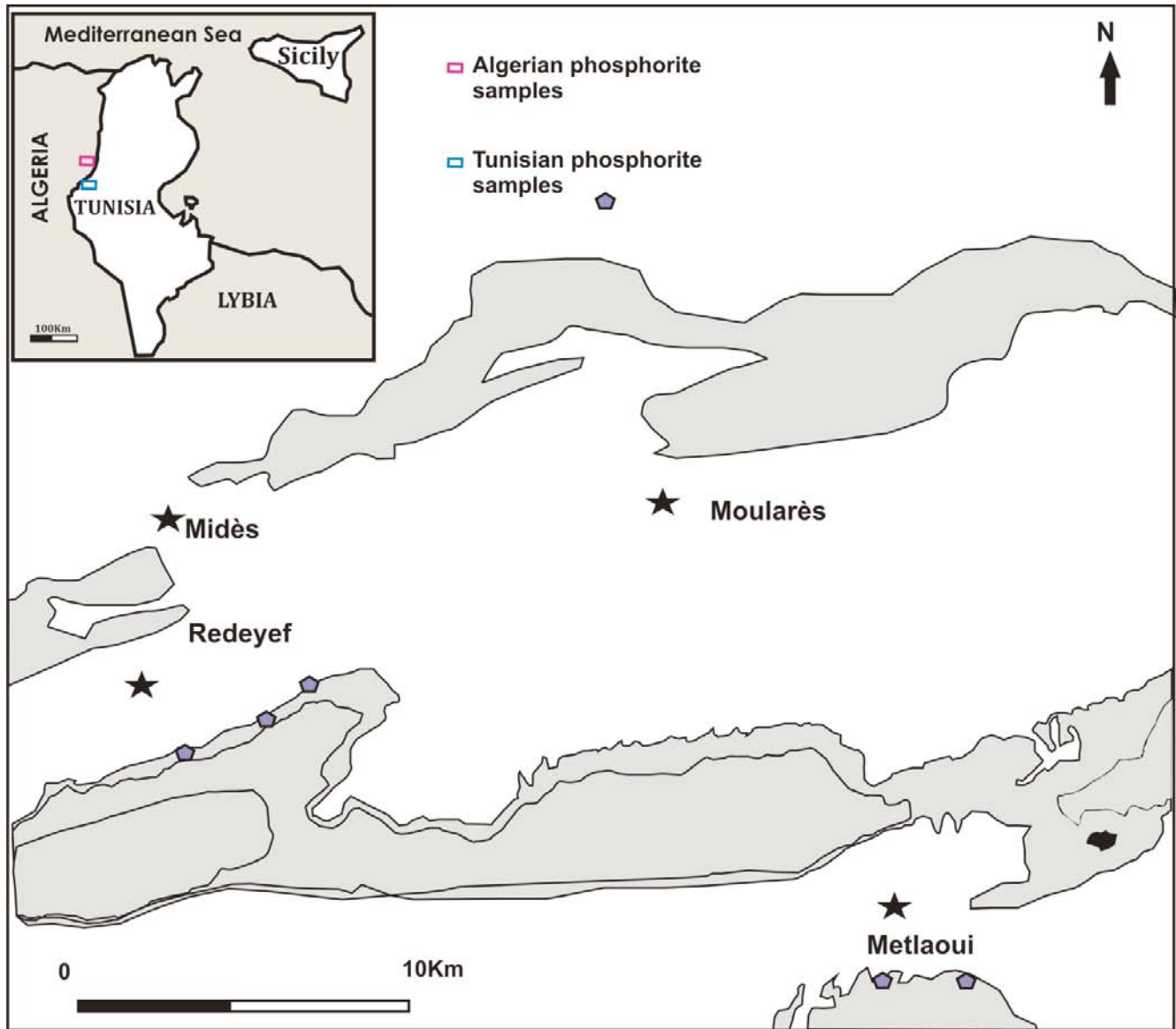


Figure 1. Location of phosphorite sampling sites in the area under study in Tunisia and Algeria.

Table 1 Specific Activity of ^{226}Ra series, ^{232}Th series and ^{40}K in Bq/kg dry weight in Tunisian and Algerian phosphorite samples.

Sample code and description	Sample	$^{226}\text{Ra} \pm E$	$^{232}\text{Th} \pm E$	$^{40}\text{K} \pm E$	^{226}Ra equiv
(Bq/Kg dry weight)					
<i>Phosphorite sample</i>					
Gamma spectrometry					
Tu1	ore rock	391,54±9,39	60,38±3,74	71,12±3,84	532,6158
Tu2	ore rock	283,37±8,31	58,17±3,25	68,09±2,91	418,9824
Tu3	ore rock	327,73±9,39	63,25±2,93	65,37±3,41	468,5124
Tu4	ore rock	384,08±7,85	72,63±2,61	73,10±2,78	544,2279
Tu5	ore rock	372,29±8,23	67,46±3,02	73,25±3,58	525,1603
Alg1	ore rock	989,65±12,52	12,08±1,20	15,728±1,73	1019,0349
Alg2	ore rock	1014,94±32,47	10,49±1,04	9,85±1,37	1037,5252
Alg3	ore rock	1109,16±28,34	11,15±2,04	13,71±1,26	1135,6612

Table 2. Specific Activity of uranium isotopes (^{238}U , ^{235}U and ^{234}U) in Bq/kg dry weight and uranium equivalent in ppm in phosphorite samples (1 ppm U=12.23 Bq ^{238}U /kg)

Sample code and description		$^{238}\text{U}\pm\text{E}$	$^{235}\text{U}\pm\text{E}$	$^{234}\text{U}\pm\text{E}$	Uranium equivalent (ppm)
Phosphorite sample		(Bq/Kg dry weight)			
Alpha spectrometry					
Tu1	ore rock	327.45±6.79	13.90±0.60	331.39±6.42	26.7913
Tu2	ore rock	327.21±6.82	15.57±0.65	326.61±6.35	26.7717
Tu3	ore rock	323.40±7.18	14.94±0.84	326.43±6.99	26.4600
Tu4	ore rock	321.81±7.61	14.94±0.83	326.43±6.99	26.3299
Tu5	ore rock	321.58±7.62	15.13±0.85	325.71±6.95	26.3110
Alg1	ore rock	889.40±7.18	32.94±0.84	627.43±6.99	72.7691
Alg2	ore rock	882.40±6.23	28.94±0.23	631.43±5.34	72.1504
Alg3	ore rock	879.40±5.17	37.18±0.15	627.43±4.28	50.3025
Gamma spectrometry					
Tu1	ore rock	527,42±49,57	12,72±0,54	nd	43,15
Tu2	ore rock	438,18±34,25	15,18±0,32	nd	35,8282
Tu3	ore rock	539,36±32,52	14,63±0,41	nd	44,1013
Tu4	ore rock	531,89±45,39	13,52±0,39	nd	43,4905
Tu5	ore rock	532,29±38,15	17,72±0,32	nd	43,5233
Alg1	ore rock	1148,70±87,30	47,50±1,52	nd	93,98
Alg2	ore rock	1315,28±94,17	44,96±1,21	nd	107,61
Alg3	ore rock	1248,15±91,23	48,96±1,05	nd	102.0564

REFERENCES

- Altschuler, Z.S. 1980: The Geochemistry of Trace Elements in Marine Phosphorites: Part 1. Characteristic Abundances and Enrichment, Marine Phosphorites (SEPM Spec. Publ.), no. 29, pp. 19-30.
- Beji Sassi, 1984: Pétrographie, Minéralogie et Géochimie des sédiments phosphatés de la bordure de l'île de Kasserine (Tunisia). In: Thèse 3ème cycle, Université d'Orléans, p. 230.
- M. Tufail, Nasim-Akhtar, M. Waqas 2006: Measurement of terrestrial radiation for assessment of gamma dose from cultivated and barren saline soils of Faisalabad in Pakistan, Radiat. Meas. (41) 443-451.
- Volkov, R.I. 1994: Geochemistry of Uranium in Vendian-Cambrian Phosphorites, Geokhimiya, no. 7, pp. 1042-1051.
- Zaïer A 1999: Evolution techno-sédimentaire du bassin phosphate du centre-Ouest de la Tunisie minéralogie, pétrographie, géochimie et genèse des phosphorites. Thèse Doct. Es-Sci. Univ. Tunis II.
- Ashraf E, R.H. Higgya and M. Pimpl 2001: Radiological impacts of natural radioactivity in Abu-Tartor phosphate deposits, Egypt. Journal of Environmental Radioactivity (55), 255-267.

1.E.3

Constraining collision events through arc magmatic record: The India / Arc / Asia collision

Bouilhol Pierre¹, Jagoutz Oliver¹, Hanchar John M.², Dudas Francis O.¹

¹Dept. of Earth, Atmospheric, and Planetary Sciences, Massachusetts Institute of Technology, 77 Massachusetts Ave, Cambridge, MA 02139 (pierreb@mit.edu)

² Dept. of Earth Sciences, Memorial University of Newfoundland, St John's, NF A1B 3X5, Canada

Three suture zones mark the Himalayan collision, and despite intensive research, the timing of the formation of these sutures is still debated. The Tsangpo suture separates India from Eurasia in central and eastern Himalaya with estimates ranging from 70 to 35 Ma. In the Western Himalaya, separated from the Eurasian plate (Karakoram) to the north by the Shyok suture, and from the Indian plate to the south by the Indus suture, lies the Kohistan-Ladakh Arc (KLA). This geological entity is recognized as a fully preserved oceanic arc, formed in the Tethys Ocean and now incorporated in the Himalayan collision system. The age collision estimate between the Arc and Eurasia ranges from Mid-Cretaceous to Oligocene, whereas the India / Arc collision is well constrained at ~50 Ma. The middle to upper crustal part of the KLA is made of plutonic rocks ranging from diorite to granites, together with volcano-sedimentary units. The crust-forming granitoids record a magmatic activity between >120 and 30 Ma, covering the range of estimated India / Arc and Arc / Eurasia collisions. Here, we present a detailed geochronological and isotopic study of the KLA granitoids in order to pinpoint the exact timing of the change in isotopic composition relating the colliding continent and to identify the possible sources accounting for those differences. This approach is based on the observation of modern Continent/Arc collision systems where the subduction of the leading edge of the colliding continent can be tracked in space and time by the composition of the magmatic products. We present U-Pb and Hf isotopic data on zircon coupled with Nd isotopic data on whole rocks from the KLA granitoids. In the southern part of the KLA, close to the Indus suture, a pronounced and abrupt shift in isotopic composition is observed from typical juvenile oceanic arc isotopic signature ($\epsilon\text{Nd}_{(t)} \approx +1$; $\epsilon\text{Hf}_{(t)} \approx +10$) during the Jurassic/Early Paleocene to more evolved but highly variable crustal-like composition in the Eocene/Oligocene ($-10 < \epsilon\text{Nd}_{(t)} < -4$; $-15 < \epsilon\text{Hf}_{(t)} < 0$). This change corresponds to the formation of the Indus suture. Inherited Paleozoic zircon crystals in the Eocene/Oligocene rocks indicate the participation of the Indian continental crust in their formation thus indicating that the Indian crust was underplated below the juvenile KLA therefore giving a minimum constraint on the India / KLA collision. In the North of the KLA, close to the Shyok suture, the change from juvenile arc signature to a more evolved crustal-like isotopic composition occurred 10 Ma later. Inherited zircon grain record identifies the Karakoram crust as being involved in the source of the young granitoids, thus constraining the final India-Arc / Karakoram collision in late Eocene. This collisional scenario can be transposed all along the Himalayan belt, defining the Shyok-Tsangpo suture zone as the locus of the final India / Eurasia collision.

1.E.4

Petit-spot-like volcano exposed in Costa Rica

Buchs David¹, Baumgartner Peter², Pilet Sébastien², Cosca Michael³, Flores Kennet⁴ & Bandini Alexandre⁵

¹IFM-GEOMAR, Kiel, Germany (dbuchs@ifm-geomar.de)

²Université de Lausanne, Switzerland

³US Geological Survey, Denver, USA

⁴University of Western Australia, Perth, Australia

⁵American Museum of Natural History, New York, USA

The study of intraplate ocean volcanoes is fundamental to better understand the dynamics of the Earth mantle and plate tectonics. An important question related to the origin of these volcanoes is the mode of production of basaltic melts at depth, which could be thermally-driven and related to the presence of deep mantle plumes, or tectonically-driven and related to fissure propagation in the lithosphere. Although access to intraplate ocean volcanoes is essential to determine their mode of formation, most of them develop entirely under submarine conditions and have remained unstudied. Accretionary complexes that expose fragments of ancient oceanic sequences can provide an alternate way of investigating intraplate ocean volcanism (Buchs et al., 2011).

Petit-spot volcanism recently found in the west Pacific is considered to represent a new type of tectonically-induced volca-

nism on Earth, which forms very small volcanic edifices in response to plate flexure near subduction zones (Hirano et al., 2006). Despite their significance to assess the extent to which tectonic processes can trigger intraplate ocean volcanism, few petit-spot volcanoes have been recognized to date and it remains unclear if they are common on the ocean floor. Documenting new occurrences of petit-spot volcanoes is therefore essential to improve our understanding of intraplate ocean volcanism. We report here on the first example of an accreted volcanic edifice similar to modern petit-spot volcanoes. The edifice is recognized based on a combination of field observations, geochemical analyses, radiometric dating and biochronologic data in the Santa Rosa Accretionary Complex (Baumgartner & Denyer, 2006) in northern Costa Rica.

The accreted volcano consists of tectonic stacks of volcano-sedimentary material that includes vesiculated pillow lavas, volcanic breccias and thick radiolarite beds intruded by igneous sills compositionally similar to the lavas. Major and trace element contents of the igneous rocks indicate an alkalic, moderately fractionated composition, and support very low degrees of partial melting in the garnet stability field. Three lines of evidence indicate that the studied volcano is volcanologically and compositionally analogous to modern petit-spot volcanoes: (1) tectonostratigraphic observations in the accretionary complex indicate that the accreted volcano was a once a small-sized edifice on the ocean floor; (2) the accreted volcano is composed of an unusual lithologic assemblage very similar to that of petit-spot volcanoes (Fig. 1); and (3) normalized trace element patterns of the basalts from the accreted volcano are very similar to those of petit-spot volcanoes in Japan, and distinct from those of typical OIB, MORB and off-axis seamounts. Step-heating ^{40}Ar - ^{39}Ar dating on co-magmatic amphiboles gave two ~ 175 Ma ages of formation for the accreted volcano. Tectonostratigraphic and biochronologic data (Bandini et al., 2011) clearly document a ~ 110 Ma age of accretion, and indicate that the volcano did not form close to a subduction zone or a mid-ocean ridge, and this constitutes an important difference with modern petit-spot volcanoes. Petrological modelling indicates that the accreted volcano may have been produced by low-degree partial melts from the low-velocity zone and metasomatic veins at the base of the lithosphere, without need for thermal anomalies in the mantle. Therefore, we propose that petit spot-like volcanoes such as that accreted in Costa Rica may represent a ubiquitous feature on the ocean floor, which reflects tectonically-induced leaking of melts pre-existing at the base of the lithosphere and can form far from mid-ocean ridges and subduction zones.

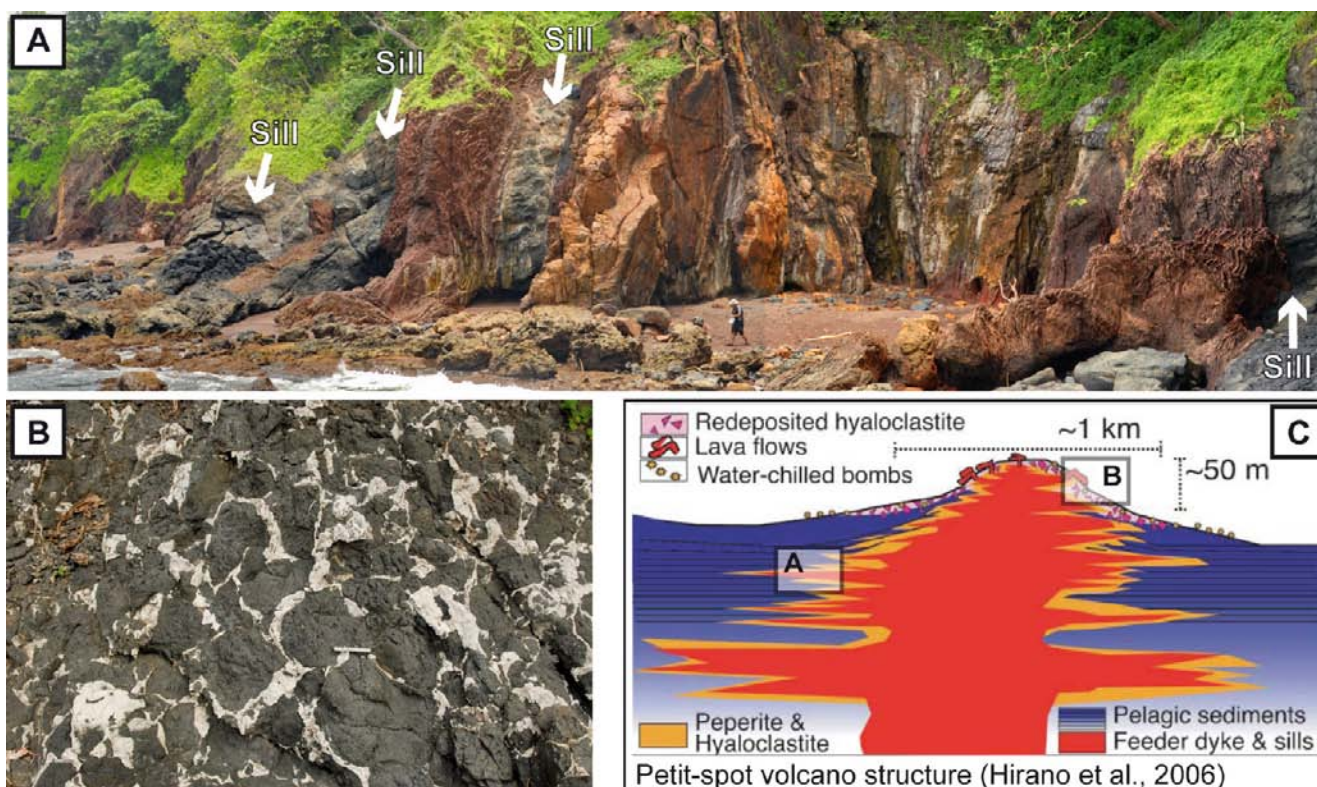


Figure 1. A-B) Selected lithologies of the petit-spot-like volcano accreted in Costa Rica. A) Sills and radiolarites forming the substrate of the volcano. B) Pillow breccia. C) Structure of petit-spot volcanoes in Japan (Hirano et al. 2006), with inferred positions of lithologies shown in (A) and (B).

REFERENCES

- Bandini, A.N., Baumgartner, P.O., Flores, K., Dumitrica, P. & Jackett, S.-J., 2011: Early Jurassic to early Late Cretaceous radiolarians from the Santa Rosa accretionary complex (northwestern Costa Rica). *Ofioliti* 36, 1-35.
- Baumgartner, P.O. & Denyer, P., 2006: Evidence for middle Cretaceous accretion at Santa Elena Peninsula (Santa Rosa Accretionary Complex), Costa Rica. *Geologica Acta* 4, 179-191.
- Buchs, D.M., Arculus, R.J., Baumgartner, P.O. & Ulianov, A., 2011: Oceanic intraplate volcanoes exposed: Example from seamounts accreted in Panama. *Geology* 39, 335-338.
- Hirano, N., Takahashi, E., Yamamoto, J., Abe, N., Ingle, S.P., Kaneoka, I., Hirata, T., Kimura, J.I., Ishii, T., Ogawa, Y., Machida, S. & Suyehiro, K., 2006: Volcanism in response to plate flexure. *Science* 313, 1426-1428.

1.E.5

Basin Dynamics in Taiwan

Eugster Patricia¹, Nagel Stefan¹, Castellort Sébastien¹, Kaus Boris J.P.²

¹Geologisches Institut, ETH Zürich, Sonneggstrasse 5, 8092 Zürich, (eugstepa@ethz.ch)

²Institut für Geophysik, ETH Zürich, Sonneggstrasse 5, 8092 Zürich

Taiwan has been created by collision of the Luzon Volcanic Arc with the Eurasian continental margin during late Miocene to early Pliocene. It is not a simple arc-continent collision. There are two opposite subductions involved. In the east the Philippine Sea plate is subducting below the Eurasian plate whereas in the south the Eurasian plate is plunging under the Philippine Sea plate. Due to the north-south orientation of the Luzon Arc and the northeast-southwest orientation of the Chinese continental margin the collision is assumed to propagate southwards. The velocity of the southward migration of the collision and therefore the orogen migration and the movement of the sedimentary basin was calculated by using geometrical constraints (84 km/Ma; Suppe (1981)) and tectono-sedimentary analyses (31 km/Ma; Simoes and Avouac (2006)) respectively. The foreland basin records the collision process and shows characteristic patterns of facies distribution, subsidence and deformation.

The aim of this study is to compare the subsidence of different scenarios of collision, plate loading and flexure with the known subsidence in the western foreland. By use of a Finite Differences model for elastic plates, different flexural scenarios were simulated. In order to achieve a best fit with the observed subsidence pattern in the foreland, a simple scenario with changeable flexural rigidity and tectonic scenarios that include the different continental and oceanic plates were chosen. In addition, the modern topography as well as the bathymetry were implemented as an additional load.

The observed facies distribution and the calculated subsidence show linear subsidence curves whereas the resulting subsidence curves of the numerical modelling are non-uniform subsidence curves. The depocenters do not correspond along the modern Taiwan mountain front. However, the exact shape of the different stages of evolution is still unclear. Concerning the FD modeling, the various flexural models show that an intra-plate stress of at least $1e9$ Pa is necessary for a significant influence on the deflection and therefore the forebulge evolution. In addition, the implemented bathymetry with topography as a load changes the pattern of the forebulge along the mountain belt and within the Taiwan Strait. More precise information about the tectonic behaviour of subduction zones on basin evolution would improve the model significantly (e. g. 3D models).

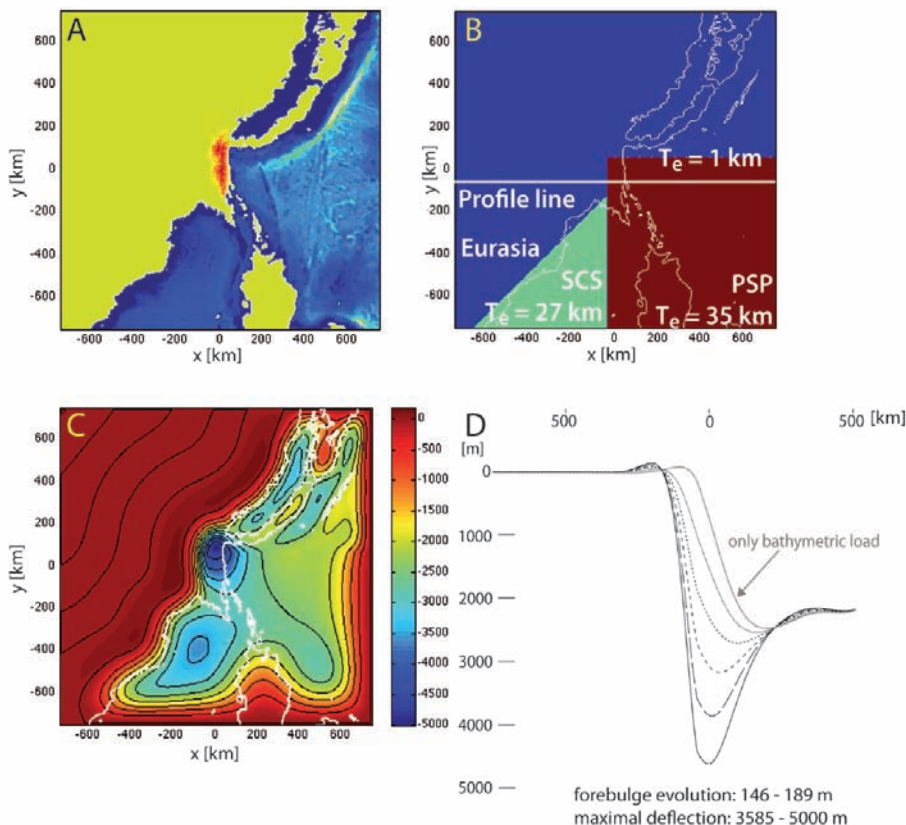


Figure 1. Simulation for experiments with an elastic thickness of 13 km. A: The load in the lithospheric plate: green no load, red the Taiwan orogeny, blue the Philippine Sea plate (water column); B: The tectonic situation including the Philippine Sea plate, the Eurasian plate and the South China sea plate. C: The resulting deflection of the lithosphere in meters. D: Evolution of the deflection with increasing load.

REFERENCES

- Simoes, M. and Avouac, J. P. 2006: Investigating the kinematics of mountain building in Taiwan from the spatiotemporal evolution of the foreland basin and western foothills. *Journal of Geophysical Research* 111.
- Suppe, J. 1981: *Mechanics of Mountain Building and Metamorphism in Taiwan*. Memoir of the Geological Society of China 4, 67 – 89.
- Van Wees, J. D. and Cloetingh, S. 1994: A Finite Difference Technique to Incorporate Spatial Variations in Rigidity and Planar Faults into 3D Models For Lithospheric Flexure. *Geophysical Journal International*, 117, 179 - 195.

1.E.6

Active crustal shortening in the Makran Accretionary Wedge (SE, Iran) revealed by deformed fluvial terraces

Haghipour Negar^{1,2}, Burg Jean-Pierre¹, Kober Florian¹, Zeilinger Gerold³, Ivy-Ochs Susan^{4,5}, Kubik Peter⁴, Faridi Mohammad²

¹Geological Institute, ETH Zurich, Sonneggstrasse 5, CH-8092 Zurich (negar.haghipour@erdw.ethz.ch)

²Geological Survey of Iran, Meraj Avenue, Azadi Square, P.O. Box 13185-1494, Tehran, Iran

³Institute für Geowissenschaften, Universität Potsdam, D-14476 Golm, Deutschland

⁴Laboratory of Ion Beam Physics, ETH Zürich, CH-8093 Zürich, Switzerland

⁵Department of Geography, University of Zürich, CH-8057 Zürich, Switzerland

We surveyed fluvial terraces over a wide area in order to decipher the Quaternary increment of crustal shortening, the rate of fold growth and the deformation pattern of the thin-skinned Makran Accretionary Wedge. We focused on three major fold systems associated with three crustal scale thrust faults where the rivers abandoned continuous terrace surfaces. Reconstructed terrace profiles revealed two regional dominant wavelengths, about 5 km in the northern part of the study area and about 15 km in the south.

The presence of two wavelengths suggests the existence of two décollement layers at two rooting depths. This result is consistent with published constructed cross sections in onshore Makran and subsurface data in offshore Makran. To estimate shortening rates, we used two methods:

- I. Conservation mass,
- II. Strain contour diagram.

Estimated crustal shortening rates based on conservation mass model are averaged over Pleistocene time to be 0.5 mm/a north of the Gativan Thrust and 0.9 mm/a toward the south, on the hanging wall of the Chahkhan Thrust. This change in shortening rate is consistent with thin-skinned tectonic regime where recent deformation is more active toward the front of the wedge.

The estimated long-term shortening rate across these fold systems accounts for ~20% of the total shortening rate (~6mm/a) and 2% of the total convergence rate (~19mm/a) recorded by kinematic GPS measurements between Arabia and Eurasia, across the Makran subduction zone. The strain contour diagram is derived by plotting two geometrical fold parameters: the thickness-to-wavelength (A/λ) and the amplitude-to-wavelength (H/λ) ratios.

Our data plotted in this diagram confirm that the strain accommodated by the studied folded terraces is <20% of total shortening on each individual fold structure and all data indicate together a very low viscosity contrast (< 10%) of the folded terraces with their shale-dominated basement. The shortening estimated with this method is in good agreement with estimates from the mass conservation model.

The geometry of deformed terraces combined with the strain contour diagram consistently indicates incipient fold growth and buckling as the dominant process responsible for recent folding. Despite active deformation and relatively high shortening rate across Makran, the geophysical record shows nearly absent seismic activity. We propose that strain accumulated in folds over intermediate décollement levels within a thick, incompletely lithified sedimentary cover explain the essentially aseismic recent tectonics in Makran.

1.E.7

Paleogeographical restoration and ramp tectonic evidence in Tunisian Tellian domain: Ain El Bey-Bou Awen area (northwestern Tunisia).

Kais Aridhi¹, Sabri Aridhi², Mohamed Abdoullah Ould Bagga³, Saâdi Abdeljaouad¹, Fouad Zargouni¹ & Eric Mercier⁴

¹ Faculty of Sciences of Tunis, Department of Geology, 2092 Tunis-El Manar-I-Tunisia-0021622533115.

² ETAP, entreprise tunisienne d'activité pétrolière, 54, avenue Med V-Tunis-Tunisia.

³ Faculty of Sciences of Gabès, Department of Geology, City Riadh Zrig-1030-Gabès-Tunisia-0021623587201.

⁴ Université de Nantes, Faculté des Sciences et Techniques UMR-6112 du CNRS-Planétologie et Géodynamique 2, rue de la Houssinière-BP 92208-44322 NANTES cedex 3-France.

Aridhikais@Gmail.com; mao_bagga@yahoo.com; Saadi_abdeljaouad@yahoo.fr; Fouadzargouni@yahoo.fr; Eric.Mercier@univ-nantes.fr.

Tunisian Alpine rang (fig.1-A), is a collision feature drawn after mi-lower Miocene compression between Kabyle block and Tethysian African margin (Cohen, 1989). Limited respectively, to Southern and Eastern by Saharan platform with sub-tabular structure and the Sahel hidden beneath recent formations (Castany, 1953; Zargouni, 1985; Frizon de Lamotte and al., 1995).

Internal part or Tellian area of Tunisian Alpine belt is a stacking gravitary thrust sheet in mi-Miocene, folded in upper Miocene and Quaternary (Rouvier, 1977). Numidian flysch or upper unit, overlap with tectonic contact underlying units or numidian underneath-units, which are from NW to SE: Adissa, Ain Draham, ED Diss and Kasseb units. On the other hand, regarding some authors (Ould Bagga and al., 2006; Aridhi and al., 2011), tectonic recovery between numidian underneath-units are not suitably significant to justify "thrust sheet" expression.

Studied area is localized in front of this internal zone which constitutes it's mainly external linkage. It corresponds to the SW tip imbrication zone of authors (Solignac, 1927 ; Castany, 1953 ; Kujawski, 1969 ; Rouvier, 1977), wholesale from Béja to Mateur and characterized by Paleocene and Eocene tectonic stacking, following their translation toward SE (Solignac, 1927). According Caire, 1973, this zone affected by large displacements, is qualified as "thrust sheet" continuity. Where, referring to Rouvier, 1977; it would be only affected by limited displacements, since did not leave its origin homeland. In the internal Alpine belt domain of Tunisia, NW "thrust sheet" area, tectonic inversion was drawn by thrusting system as flat and ramps.

These features produce imbricate tilted monocline the, how their tips are taken by local cylindrical anticlines over frontal ramp, orthogonal to displacement trend (Ould Bagga and al., 2006; Aridhi and al., 2011). Pronounced structures blocks, diversity of their geometry and their kinematic installation, are the mainly facts that qualified imbricate domain from Maghrebides belt. In this paper, will show that structures geometrical variability are related to both major effects, such as, position of this area in a more external alpine zone and tectonic Mesozoic heritage which its effect became as significant as horizontal constraint, at the front of this belt.

Fig.1

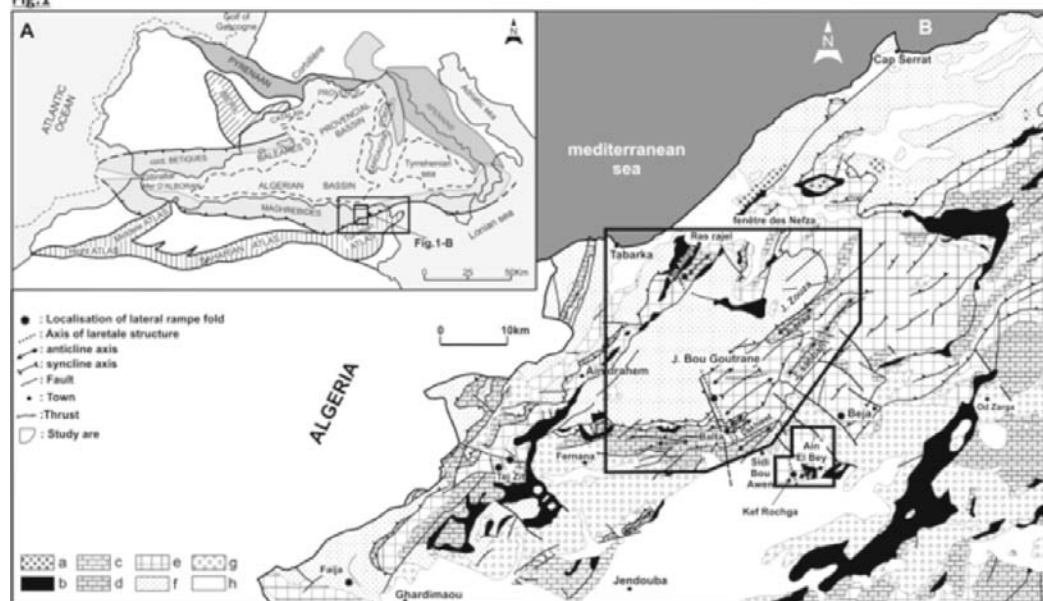


Fig.1: Geological map of northwestern Tunisia and location maps detail.

*A: The Maghrebides (DELGA Durand, 1980).

*B: Geological Map of northern Tunisia (Mining National Office, 1985, extracted and modified), and location of lateral folds.

a: Magmatic rocks; b:Triassic; c:Jurassic; d:Cretaceous; e:Palaeogene; f:Numidian (Oligo- Miocene flysch); g: Mio-Pliocene; h: Quaternary.

REFERENCE:

- Aridhi K., Ould Bagga M.A., Abdeljaouad S., Zargouni F. et Mercier E., 2011. Lateral Ramp-related Folding Evidences in the Tellian domain of Tunisia: Tectonic Implications (in press). *Comptes Rendus Géosciences*.
- Caire A., 1973. Les liaisons Alpines précoces entre Afrique du Nord et Sicile, et la place de la Tunisie dans l'arc Tyrrhénien. Livre jubilaire M. Solignac. *Ann. Min et Géol.*, Tunis, n° 26, pp. 87-110.
- Castany G., 1953. Le style tectonique de Hedhil et de la région de Béja (Tunisie septentrionale) ; ses rapports avec la « zone des flysch ». *C. R. Acad. Sci. Paris*, (7), t. 236, pp. 728-730.
- Cohen C.R., Schamel S., Boyd-Kaygi P., 1989. Neogen deformation in northern Tunisia: Origin of the eastern Atlas by microplate-continental margin collision. *Geological Society of America*, Part 1, Vol. 91, pp.225-237.
- Frizon De Lamotte D., Guezou J.C., Averbuch O. 1995. Distinguishing lateral folds in thrust-systems; examples from Corbières (SW France) and Betic Cordilleras (SE Spain). *Journal of Structural Geology*, Vol. 17, N°2, pp. 233-244.
- Kujawski H., 1969. Contribution à l'étude géologique de la région des Hedhil et du Béjaoua oriental. *Ann. Min. et Géol. Tunis*, N°24, 281p.
- Ould Bagga M.A., Abdeljaouad S., Mercier E., 2006. La « zone des nappes » de Tunisie : une marge méso-cénozoïques en blocs basculés modérément inversée (région de Tabarka/Jendouba; Tunisie nord-occidentale). *Bulletin de la Société Géologique de France*, Vol. 177, No. 3, pp. 145-154.
- Rouvier H., 1977. Géologie de l'extrême Nord Tunisien : tectonique et paléogéographie superposées à l'extrémité orientale de la chaîne maghrébine. Thèse Doc és Sciences, Univ. Paris VI, 898p.
- Solignac M., 1927. Etude géologique de la Tunisie septentrionale. *Dir. Gén. Trav. Pub.*, Tunis, Thèse Doct. Es-sciences. Lyon, 756p.
- Zargouni F., 1985. Tectonique de l'Atlas méridional de Tunisie. Evolution géométrique et cinématique des structures en zone de cisaillement. Thèse de doctorat ès Sci. Univ. de Strasbourg. *Rev. Des Sci. De la Terre*. Vol. 3, 304 p.

1.E.8

Link between topography and large-scale tectonics of Southern India: A preliminary study based on river profile analysis

Mandal Sanjay Kumar, Burg Jean-Pierre & Haghypour Negar

Structural Geology and Tectonics Group, Geological Institute, ETH, Zurich, CH-8092 Switzerland (sanjay.mandal@erdw.ethz.ch)

Spatial distribution and rates of active deformation provide important constraints on the geodynamics of deforming lithosphere. Yet, such data are often difficult to acquire in eroding landscapes where poor preservation of geomorphic or stratigraphic markers impedes strain reconstruction. Recent advances in the understanding of the relationship between bedrock channel profile and erosion rate have allowed applying them as an index of differential rock uplift rate in steady state landscapes. The current model suggests that the local rate of differential rock uplift should exert a primary control on the gradient of channel longitudinal profile form. In practice, discrimination of this effect from the influence of substrate heterogeneity, sediment flux, orographic precipitation, and transient changes in channel profile shape has proved difficult.

The west coast of Peninsular India is a high elevation passive margin that formed when India broke away from Madagascar around 88 Ma and then from the Seychelles-Mascarene platform at c.65 Ma. At the same time, the Réunion hotspot was reaching its peak activity. The approximately 1600 km long NNW-SSE trending mountain range of Western Ghats is characterized by a spectacular west facing 'great' escarpment and very youthful relief that suggest recent and ongoing uplift. Recent studies of exhumation and erosion rate suggest that the escarpment has been retreating eastward but the actual mechanism, timing and magnitude of retreat remain poorly understood. The rate and distribution of deformation along the Western Ghat and in the interior of Southern Indian Peninsula is needed to understand the evolution of high topography in intraplate settings. We investigated channels draining the western and eastern flank of Western Ghat between ~8°N and 21°6'N. We extracted and analyzed channel profiles from digital topographic data from the SRTM of 90m nominal resolution utilizing a group of built-in functions in ARC/INFO and a suite of MATLAB scripts developed by Snyder et al. (2000) and Kirby et al. (2003). In most cases, we observe smooth concave up profiles. Where channels exhibited distinct knickpoints separating reaches of varying gradient, we analyzed each reach independently. Our preliminary analysis of the longitudinal profile of bedrock channels reveals systematic differences in the channel steepness indices along the trends of Western Ghats. The well-defined Western Ghats escarpment is only partly associated with surface volcanics in the north, whereas the southern part is characterized by Precambrian basement. Therefore, the lithology has a limited influence on channel steepness. Our preliminary investigation shows that variation in channel steepness along the Western Ghats might instead result from differential rates of rock/surface uplift. Higher uplift rates are associated with the crest of the Western Ghats and they systematically increase towards south. This rate variation is also manifested by highest mountain elevation in the south.

REFERENCES

- Kirby, E., Whipple, K.X., Tang, W., Chen, Z., 2003. Distribution of active rock uplift along the eastern margin of the Tibetan Plateau: Inferences from bedrock channel longitudinal profiles. *Journal of Geophysical Research* 108 (B4), 2217 (10.1029/2001JB000861).
- Snyder, N., Whipple, K., Tucker, G., Merritts, D., 2000. Landscape response to tectonic forcing: Digital elevation model analysis of stream profiles in the Mendocino triple junction region, northern California. *Geological Society of America Bulletin* 112, 1250-1263.

1.E.9

Direct versus indirect thermochronology: What do we truly trace? An example from SE Peru and its implication for the geodynamic development of the Andes

Geoffrey M.H. Ruiz

IMG, Uni. Lausanne, CH-1015 Switzerland (geoffrey.ruiz@unil.ch)

To quantify long-term denudation rates, research groups commonly applied low-temperature thermochronometric methods to rock now exposed at the surface. This approach on bedrocks from the hinterland is sometimes limited since erosion has often removed the record of earlier stages of orogenic growth. To overcome this shortcoming, researchers have increasingly studied since 20 years orogenic sedimentary records combining detrital thermochronological analyses with sedimentary petrography but also modeled detrital age populations from true bedrock catchments.

We propose here to study the denudation history of a region located in the Eastern Cordillera of SE Peru. Our approach consists on analysing present-day erosional products along five different river catchments for the Apatite Fission-Track (AFT) thermochronometer. Up to four age populations were extracted from the analyses of 100 grains per sample. Age populations range between 80 and 0.5 Ma with a majority of age populations younger than 10 Ma. These AFT analyses from the 'true' present-day erosion product of the chain are compared with ones from an 'artificial' one we generated and this to investigate the recent evolution of the eastern Andes. The artificial detrital record was engendered by the combination of 197 individual grain ages we recently produced from a bedrock profile in the region. Interestingly, the 'artificial' sand express a clear homogeneous AFT signal with a single and pooled AFT age of 4.1 ± 0.1 Ma. This age is identical to the youngest age population (P1) we extracted from the 'true' sand within the same catchment (4.4 ± 0.4 Ma) and suggest that the 'true' dated grains of the P1 population were derived from, if not this one, a region with similar thermal record. Our results are of main importance because they indicate for the first time that a detrital age population, once statistically individualized and limitations of the method perfectly excluded, most likely reflects the erosion in a single part of a catchment. In the eastern Andes of Peru, the older age populations we extracted are probably derived from upper levels within the catchment that reflect by their presence, but not directly quantify, former denudation. Reversely, the youngest age populations for all present-day river sands are younger than 6.8 Ma. These data point towards lower levels of the eastern Andes that undergo rapid denudation and this since recent time because of the preservation of older thermal record.

The approach we developed is innovative and aims to reduce the amount of necessary analysis to constrain long-term denudation rates in different orogenic settings. It also hosts a methodological aspect by comparing results from direct (bedrock) and indirect (present-day river sands) thermochronological analyses within the same catchment.

1.E.10

Provenance studies in sands and sandstones from the Bay of Bengal, Myanmar

Tin Tin Naing¹, Winkler Wilfried¹, Mario Nold² & Albrecht von Quadt¹

¹ Department of Earth Sciences, ETH-Zentrum, Sonneggstrasse 5, 8092 Zurich, Switzerland (tintin.naing@erdw.ethz.ch, wilfried.winkler@erdw.ethz.ch, albrecht.vonquadt@erdw.ethz.ch)

² Dr. Mario Nold Think Tank, Project Managing & Consulting, World Trade Center, Leutschenbachstrasse 98, 8050 Zurich, Switzerland (marionold08@googlemail.com)

Since the discovery of the giant Shwe gas field offshore Myanmar, the Bay of Bengal has become the focus of one of the last unexplored deep water basins in the world. Due to the relative inaccessibility of the Arakan (Rakhine) area (Fig. 1) onshore and its offshore islands, we are faced with a lack of any modern integrated study, and hence of the understanding of the Total Petroleum System. One of the main problems is the origin of the sands, eg., do they all belong to the Bengal fan and are as such derived from the Himalayas, or can local fans be expected in addition, sourced from the onshore Rakhine area and possibly as far as from the Myanmar Central Basin (MCB).

The Rakhine hill ranges and the Rakhine coastal area (Indo-Burman Ranges, IBR, Fig. 1) are a result of the collision between the Indo-Australian plate and SE Asian plate. The IBR is a N-S oriented arc, which forms the tectonic barrier between the Assam shelf in the west and the MCB in the east. It represents an active accretionary wedge linked to the eastward subduction of the Bengal basin oceanic crust. The IBR comprises sedimentary, metasedimentary, intrusive and volcanic rocks forming the back-bone of an accretionary prism including slivers of dismembered ophiolite obducted over the east-dipping subduction zone.

The present research is aimed at tracing back the provenance of the Eocene to Miocene turbiditic sediments included into the accretionary wedge along the Bay of Bengal, western Myanmar (Fig. 1). The investigations will allow to understand the relationship between large scale tectonic processes during deposition of the sediments along the eastern margin of the Bengal fan.

Heavy mineral assemblages indicate the derivation of the clastic material from (1) granitoids, associated volcanics and/or recycled rock series (ultrastable zircon, tourmaline, rutile, ZTR-association), (2) medium-grade metamorphic rocks (garnet, epidote group, chloritoid), and (3) ophiolitic rocks (chromian spinell). This excludes the origin of the detritus from the Himalayan range and Bengal fan respectively, because these sediments are typically bearing high-grade metamorphic heavy mineral grains (Allen et al., 2008). In modal counts (e.g. Dickinson, 1985), the variably feldspar-bearing litharenites show a provenance from transitional to dissected arc sources and recycled orogenic terranes. Volcanic-hypabyssal lithoclasts strongly dominate over sedimentary and metamorphic lithic grains. These petrographic results clearly indicate the sources of the detrital material in the IBR and associated volcanic arcs.

Laser ablation ICP-MS detrital zircon U-Pb age results from 3 Eocene and 2 Oligocene sandstones show coherent patterns. The Late Cretaceous peaks ranging 95-85 Ma (\approx Cenomanian - Coniacian) dominate the age distributions. The Palaeogene is represented by peaks ranging from approx. 50-30 Ma (Eocene - Early Oligocene). The sources of these zircons are in majority the volcanic arcs within the IBR (Cretaceous) and Inner Volcanic Arc, MCB (Tertiary). Minor reworking of Early Mesozoic, Palaeozoic and pre-Cambrian zircons is observed. One particular sample of Eocene sandstone is characterized by a very broad Palaeozoic and pre-Cambrian zircon distribution pointing to a main provenance in the Shan Plateau.

REFERENCES

- R. Allen, Y. Najman, A. Carter, et al. 2008: Provenance of the Tertiary sedimentary rocks of the Indo-Burman Ranges, Burma (Myanmar): Burman arc or Himalayan-derived? *Journal of the Geological Society*, v. 165; p. 1045-1057.
- Bender, F. 1983: *Geology of Burma*. Gebr. Borntraeger: Berlin-Stuttgart, 293p.
- Dickinson, W.R. 1985: Interpreting provenance relations from detrital modes of sandstones, In: Zuffa, G.G., ed., *Provenance of arenites: NATO Advanced Study Institutes Series C; Mathematical and Physical Sciences* 148, 333-361.

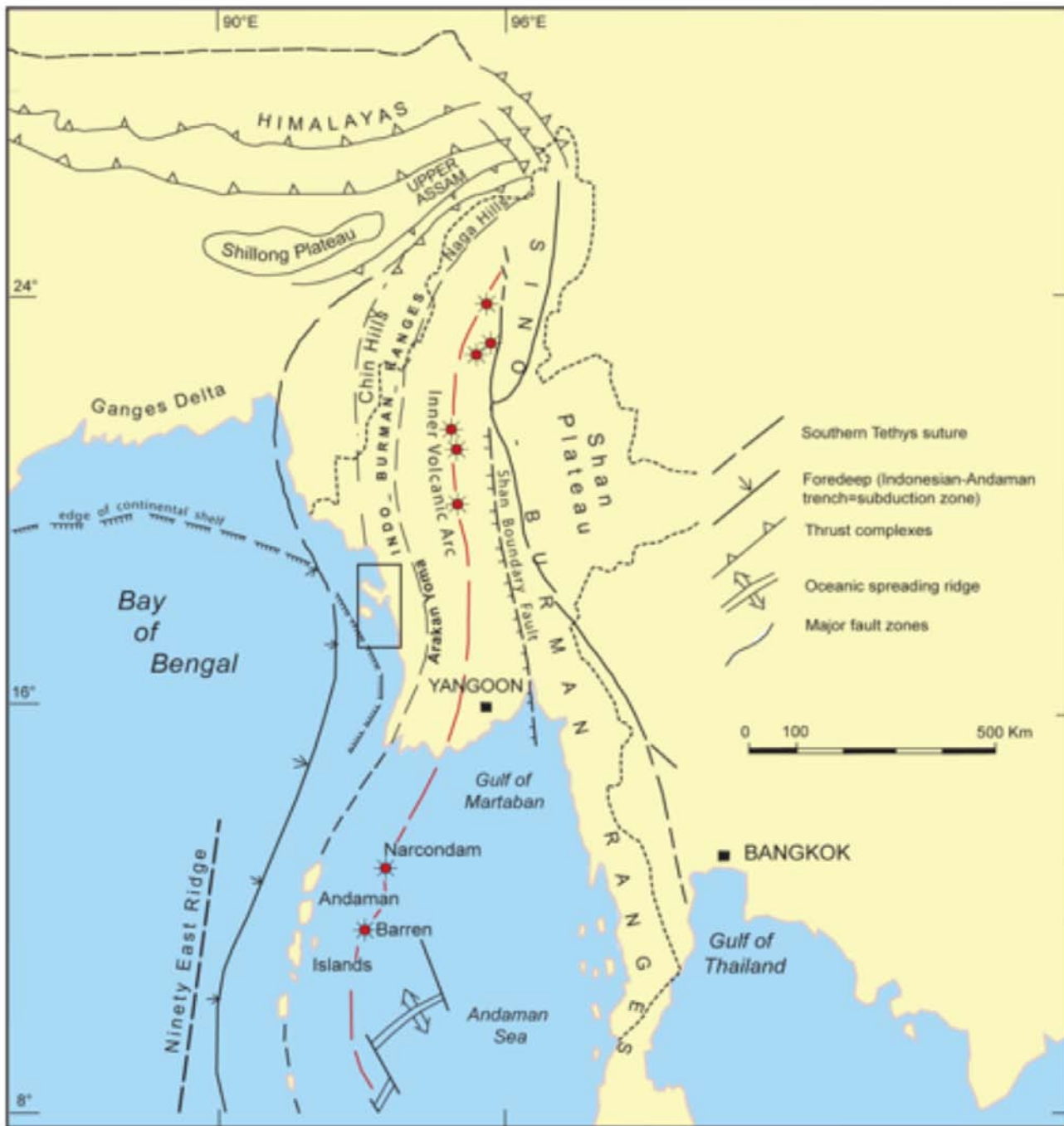


Figure 1: Schematic tectonic map of Myanmar (from Bender, 1983). The box indicates the working area in the Rakhine coastal area.

2. Mineralogy – Petrology – Geochemistry

Bernard Grobéty

Swiss Society of Mineralogy and Petrology (SSMP)

TALKS

- 2.1 *Ardia P., Withers A.C., Hirschmann M.M., Hervig R.L.:* C-O-H solubility under reduced conditions in a haplobasaltic liquid: implications for Mars degassing
- 2.2 *Baumgartner L.P., Floess D., Podladchikov Y., Foster C.T.:* Some consequences of mechanical and diffusional closure in garnets
- 2.3 *Bouvet de Maisonneuve C., Dungan M., Bachmann O., Burgisser A.:* Petrological insights into shifts in eruptive styles at Volcán Llaima (Chile)
- 2.4 *Buret Y., Kouzmanov, K.:* Polymetallic mineralization in the Laki mining district Southern Bulgaria: Paragenesis and fluid evolution
- 2.5 *Charilaou M., Löffler J.F., Gehring A.U.:* Probing solid-solution formation via magnetic freezing dynamics
- 2.6 *El Korh A., Schmidt S.Th., Vennemann T., Ulianov A.:* Evidence for trace element mobilisation in garnet-phengite eclogitic veins along a metabasite-micaschist contact during HP conditions: an example from the Ile de Groix, France
- 2.7 *Gasser, D., Bruand, E., Rubatto, D., Stuewe, K.:* The behaviour of monazite: a petrological, trace element and SHRIMP U-Pb study of greenschist facies phyllites to anatectic gneisses, Chugach Metamorphic Complex, Alaska
- 2.8 *Greber N., Hofmann B., Pettke T., Voegelin A., Villa I., Nägler T.:* Mo isotope composition of Mo-rich hydrothermal systems in the Aar Massif
- 2.9 *Hunziker D., Burg J.-P., Bouilhol P., Omrani J.:* Percolation and impregnation of a plagioclase-rich melt into the mantle-crust transition zone of the Makran ophiolites, SE Iran
- 2.10 *Marsala A., Wagner T., Wälle M., Heinrich C.:* Mass transfer processes and fluid composition of metamorphic quartz vein systems, Rhenish Massif (Germany)
- 2.11 *Martinek K., Wagner T., Wälle M., Heinrich Ch.:* Fluid chemistry and fluid-rock interaction of Alpine veins, Central Alps
- 2.12 *Mattsson H.B., Bosshard, S.A.:* Pyroclast textures in the explosive 2007-2008 eruption of Oldoinyo Lengai, Tanzania: Implications for magma ascent and fragmentation
- 2.13 *Mederer J., Moritz, R.:* The Kapan zone of the Somkheto-Karabakh island arc in the Lesser Caucasus: magmatism and ore deposits associated with Neotethys subduction
- 2.14 *Mewes K., Picard A., Rühlemann C., Kuhn T., Kasten S.:* Biogeochemical processes in sediments of the manganese nodule belt in the equatorial NE Pacific Ocean
- 2.15 *Miron G.D., Wagner T., Wälle M., Heinrich C.A.:* Fluid composition and mineral equilibria in low grade metamorphic rocks, Bündnerschiefer, Switzerland. Application of fluid inclusions and petrological modeling.
- 2.16 *Moritz R., Mederer J., Ovtcharova M., Selby D., Chiaradia M., Popkhadze N., Gugushvili V., Migineshvili R., Melkonyan R., Tayan R., Vardanyan A., Havokimyan S., Ramazanov V., Mansurov M.:* Major Cu, Au and Mo deposits of the Lesser Caucasus: Products of diverse geodynamic settings
- 2.17 *Mullis J., Tarantola A.:* PVTX evolution and reequilibration of prograde and retrograde fluid inclusions in diagenetic and metamorphic rocks, Central Alps, Switzerland.
- 2.18 *Seifert R., Malfait W.J., Petitgirard S., Sanchez-Valle C.:* Density of alkaline magmas at crustal and upper mantle conditions by X-ray absorption
- 2.19 *Wotzlaw J.F., Schaltegger, U., Frick D.A., Hüsing S.K., Bindeman, I.N., Hilgen, F.J., Günther D.:* Application of high-precision U-Pb geochronology to igneous petrology and stratigraphy: Potential and limitations

POSTERS:

- P 2.1 *Arlaux Y., Poté J., Thévenon F., Loizeau J.-L.*: Recent increase in Uranium Concentration in Lake Geneva Sediments: increased Inputs or enhanced chemical Precipitation?
- P 2.2 *Banerjee S., Robyr M.*: Monazite and Allantite's textural evolution from lower to higher grade pelites of Miyar Valley, NW India
- P 2.3 *Berghuijs J.F., Mattsson H.B.*: Explosion intensities and fragmentation modes of the Loolmurwak and Eledoi maar volcanoes, Lake Natron – Engaruka monogenetic field, northern Tanzania
- P 2.4 *Beridze T., Khutsishvili S., Popkhadze N., Moritz R., Gugushvili V.*: Stratigraphy and sedimentology of the Cretaceous host-rocks of the Madneuli gold-polymetallic deposit, Lesser Caucasus, southern Georgia, A new approach
- P 2.5 *Felix H., Mullis J.*: Evolution of composition, temperature and pressure of fluid inclusions through the NEAT Lötschberg base tunnel
- P 2.6 *Fulda D.*: Geology of Piz Duan: an oceanic sequence in the Avers schists, Grisons
- P 2.7 *Gauthiez L., Bussy F., Ulianov A., Gouffon Y., Sartori M.*: Ordovician mafic magmatism in the Métailler Formation of the Mont-Fort nappe (Middle Penninic domain, western Alps) – geodynamic implications
- P 2.8 *Hashemi Azizi S.H., Mirab Shabestari G.R., Khazaei A.R.*: Geochemistry of Paleocene-Eocene limestones from Chingdar syncline, west of Birjand, east of Iran
- P 2.9 *Hauser A., Müntener O.*: New age constraints on the opening of the Piemont-Ligurian Ocean (Tasna-Nauders area, CH-A)
- P 2.10 *Hovakimyan S.*: Origin and Paleotectonic Conditions of Formation of Ore-Containing Fractures of the Lichk-Aygedzor Ore Field of Southern Armenia, Lesser Caucasus
- P 2.11 *Hunziker D., Burg J.-P., Reusser E., Caddick M., Grolimund D.*: The influence of bulk and mineral ferric/ferrous ratios on thermobarometry of the Syros/Sifnos blueschists: Towards a new thermodynamic model for high pressure amphiboles
- P 2.12 *Kayani S.-A.*: X-ray diffraction and thermal analyses of a bangle shard from an Indus valley settlement
- P 2.13 *Klumb A., Franz L., Wetzel A. & de Capitani C.*: Petrographic and sedimentologic investigations of boulders of the river Wiese (southern Baden-Württemberg, FRG)
- P 2.14 *Martin L.H.J., Schmidt M.W., Hametner K., Mattsson H.B., Günther D.*: Element partitioning between immiscible carbonatite- and silicate melts from 1-3 GPa
- P 2.15 *McCarthy A., Müntener O.*: The Petrology and Geochemistry of the Civrari-Southern Lanzo Ophiolite, Piemonte, Western Italian Alps
- P 2.16 *Mert M., Mercan S., Gurler A.S., Sahin M.F., Aksoy N., Durmus K.*: Crime Scene Investigation And Forensic Mineralogy Applications At Gurpinar (Istanbul – Turkey) Murder
- P 2.17 *Monsef I., Rahgoshay M.*: Geochemistry and petrogenesis of the Dehsheikh Peridotitic Massif (South of Iran)
- P 2.18 *Monsef R., Emami M. H., Rashidnejad Omran N.*: Sr, Nd, and Pb isotopic constraints on the origin of the central Iran linear volcanic chains
- P 2.19 *Moulas E., Misra S., Burg J.-P., Kostopoulos D.*: Na-bearing garnets with oriented lamellar inclusions – are those majorite precursors? A case study from the Rhodope Massif (Greece)
- P 2.20 *Müller F., Mullis J.*: Investigations of fluid inclusions in quartz crystals in the dolomitic rocks of the Binn-Valley, Switzerland

- P 2.21 *Nievergelt, P.:* Stratigraphic successions in the Avers unit, southern Grisons, and comparison with the Tsaté nappe, W Alps
- P 2.22 *Ortelli M., Kouzmanov K., Wälle M.:* Minor and trace elements controlling the visible and near-infrared light transmittance of wolframite, pyrite and enargite
- P 2.23 *Popkhadze N., Beridze T., Moritz R., Gugushvili V., Khutsishvili S.:* Main volcano-sedimentary Lithofacies at the Cretaceous Madneuli copper-gold polymetallic deposit, Lesser Caucasus, Georgia
- P 2.24 *Serneels V., El Kateb A.:* Provenance of imported basaltic millstones in Switzerland during Roman times.
- P 2.25 *Siegel K., Wagner T., Trumbull R., von Quadt A., Jonsson E., Heinrich C. A.:* Isotope geochemistry of the Varuträsk pegmatite (northern Sweden)
- P 2.26 *Tayan R., Harutyunyan M., Hovakimyan S.:* Main Features of the Tectonic Pattern of the Zangezour Ore District of Southern Armenia, Lesser Caucasus
- P 2.27 *Tomé C.M., Tornos F., Seo J.H.:* Fluid inclusion evidence for magmatic-metamorphic fluid interaction in the copper-gold Sultana deposit at Huelva, Spain
- P 2.28 *Tornare E., Müntener O.:* Dunite formation in the Lanzo peridotites, Italy: a morphological, petrological and geochemical study.
- P 2.29 *Tumarkina E., Podladchikov Y., Connolly J.A.D.:* The coupling of deformation and reaction kinetics in the case of positive volume change reactions
- P 2.30 *Vardanyan A.:* Geological Setting of the Drmbon Copper-Gold Deposit, Nagorno Karabakh Republic, Lesser Caucasus
- P 2.31 *Zurfluh F., Hofmann B., Gnos E., Eggenberger U., Preusser F.:* When did the large meteorite shower Jiddat al Harasis 091 arrive on Earth?

2.1

C-O-H solubility under reduced conditions in a haplobasaltic liquid: implications for Mars degassing

Ardia Paola¹, Withers Anthony C.¹, Hirschmann Marc M.¹, Hervig Richard L.²

¹University of Minnesota, Dept. Earth Sciences, 108 Pillsburyhall, Minneapolis, MN, 55414, USA (paola.ardia@bluewin.ch)

** Arizona State University, School of Earth and Space Exploration, Tempe, AZ 85287, USA

Oxygen fugacity (fO_2) may have a critical influence on the solubility of volatiles in silicate liquids, which in turn influences fluxes of volatiles from planetary interiors to their atmospheres. Carbon dissolves in oxidized basic melts as carbonate but under reduced conditions is limited by precipitation as graphite or diamond. At conditions where melt is in equilibrium with Fe alloy, the carbonate solubility will not exceed few ppm (Hirschmann & Withers, 2009), limiting volcanogenic transport of C to the atmosphere. Therefore, dissolved C-H species may dominate C solubility and transport at low fO_2 (Mysen et al., 2009; Kadik et al., 2006, 2010)

In this study, we investigated the solubility of C-O-H fluid in a haplobasaltic melt ($Di_{40}An_{42}Ab_{18}$), adding C as $Si_5C_{12}H_{36} + H_2O$ to produce $SiO_2 + CH_4 + H_2$ and H_2O (Mysen et al., 2009). Experiments were performed using endloaded piston cylinder apparatus at pressure of 0.7, 1.5, 2.0 and 3.0 GPa, and at fix temperature of 1400°C. The fO_2 was buffered using a double Pt-capsule technique, where the external buffer (e.b.) fixed the fH_2 by transport across a H-permeable Pt barrier, and the internal buffer (i.b.) set the fO_2 of the silicate charge. In this study we used three buffer combinations: 1) e.b. with Fe-FeO- Fe_3C-H_2O , or Mo-MoO₂-Mo₂C-H₂O and i.b. powder graphite; 2) e.b. with Fe-FeO-H₂O and i.b. Si⁰, and 3) the more oxidized one using as e.b. Ni-NiO-H₂O and i.b. Si⁰.

After quench we checked the external capsule for water by piercing the Pt walls and afterward the capsule was opened using a Mo-wire along the capsule axis. At first we examined the capsules for the bufferphases and afterwards we examined resulting glasses, the bubbles and the solid phases by optical and SEM microscopy to establish equilibrium coexistence of the melt with a fluid phase and verified glass compositions with EMPA. Dissolved volatile species were identified by microRaman spectroscopy and OH and C concentrations were quantified by FTIR and SIMS, respectively.

Results show that C dissolves as methane together with OH, H₂O and H₂ in equilibrium with a volatile phase composed chiefly of CH₄ and H₂. At IW to IW-2 (buffer 1) the dissolved C increases linearly with pressure from 70 ppm at 0.7 GPa to 360 ppm at 3.0 GPa (Figure 1), and similar increase with pressure are found using the Fe-FeO-H₂O buffer (2; IW0 to -3). Hydrogen dissolved in the melt as OH, H₂O and H₂ speciation. Preliminary SIMS and FTIR results indicate large solubility of H₂ molecules in the quenched melt, showing a difference as a function of the hydrogen fugacity imposed by the different buffers, and the total water of the starting material. The results indicate that hydrogen dissolves almost equally as H₂ and total water (OH and H₂O).

Carbon dissolves as methane at reduced conditions, therefore methane is the dominant carbon species at low oxygen fugacity, which could be outgassed from reduced planetary mantles. Example of today and hystorical Mars atmosphere could be partially explained by large C emission into the atmosphere trough outgassing of CH₄ rich basalts.

REFERENCES

- Hirschmann, M.M., & Withers, A.C., 2008, Ventilation of CO₂ from a reduced mantle and consequences for the early Martian greenhouse. *Earth and Planetary Science Letters*, 270, 147–155.
- Kadik, A.A., Litvin, Y.A., Koltashev, V.V., Kryukova, E.B. & Plotnichenko, V.G., 2006, Solubility of hydrogen and carbon in reduced magmas of the early Earth's mantle. 1, 38–53.
- Kadik, A.A., Kurovskaya, N.A., Ignat'ev, Y.A., Kononkova, N.N., Koltashev, V.V. & Plotnichenko, V.G., 2010, Influence of oxygen fugacity on the solubility of carbon and hydrogen in FeO-Na₂O-SiO₂-Al₂O₃ melts in equilibrium with liquid iron at 1.5 GPa and 1400°C. *Geochemistry International*, 48, 953–960.
- Mysen, B.O., Fogel, M.L., Morrill, P.L. & Cody, G.D., 2009, Solution behavior of reduced COH volatiles in silicate melts at high pressure and temperature. *Geochimica et Cosmochimica Acta*, 73, 1696–1710.

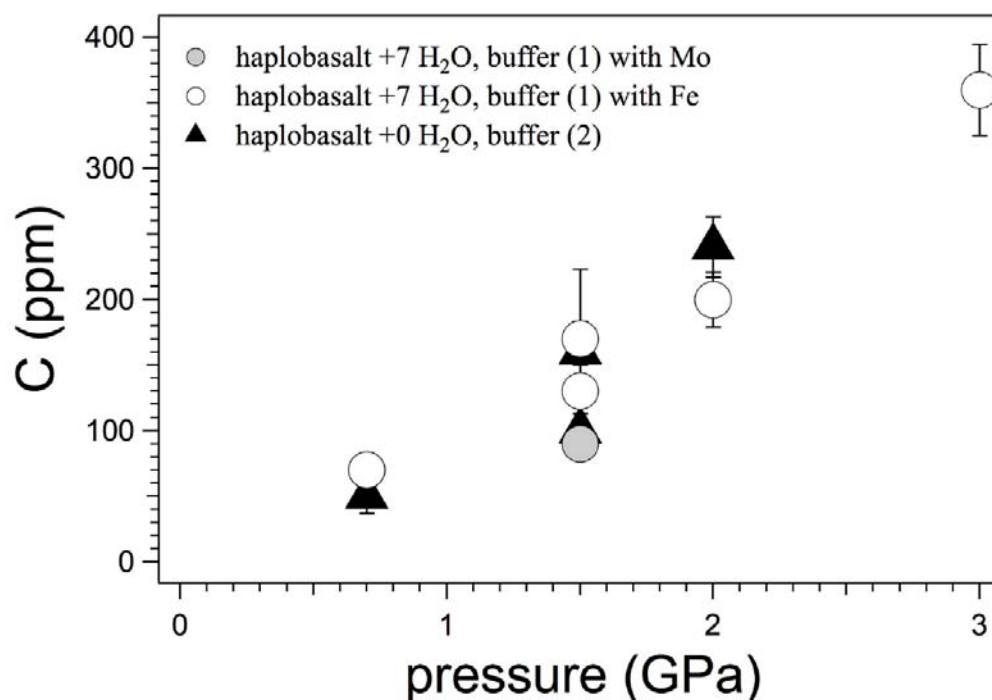


Figure 1. Carbon solubility in ppm with increasing pressure for the haplobasalt synthesised using the buffer (1), Fe-FeO-Fe₃C-H₂O (white circle), or Mo-MoO₂-Mo₂C-H₂O (grey circles) as external buffer and graphite internal buffer, and buffer (2) with Fe-FeO-H₂O as external buffer and Si⁰ as internal buffer (black triangles).

2.2

Some consequences of mechanical and diffusional closure in garnets

Baumgartner Lukas P.¹, Floess David¹, Podladchikov, Yuri² & Foster C. Thomas³

¹Institut de Minéralogie et Géochimie, Université de Lausanne, CH-1015 Lausanne (Lukas.baumgartner@unil.ch)

²Institut de Géophysique, Université de Lausanne, CH-1015 Lausanne (yuri.podladchikov@unil.ch)

³Department of Geosciences, University of Iowa, Iowa City, IA 52242 (tom-foster@uiowa.edu)

Partial molar volumes of components in solutions differ typically for several percent. As a consequence, diffusion of components will result in changes in volume. Such volume changes are easily accommodated in liquids, resulting in volume increase in one part of the diffusion zone, and volume decrease in the other. In crystals such volume changes result in stress. In the extreme case, in which a mineral behaves perfectly elastic (e.g. rigid), such volume changes result in large stresses. For example, assuming a garnet crystal to be accommodating a volume change accompanying diffusional mass transfer of 0.1 X (grossular) in a pyrope solid solution requires a local 15Kb pressure change to accommodate in an elastic fashion the induced volume change. Hence minute inclusions in garnets could report pressures, which are significantly higher (or lower) than the ambient pressure. Stress differences will of course be relaxed by the plastic behavior of minerals. If such Maxwell relaxation is faster than diffusion, the mineral will approach the diffusion behavior of a liquid. Hence the crucial question is if there is experimental or natural evidence for the rigid behavior of minerals?

Recently published experiments by Vielzeuf & Saul (2010) indicate that mechanical relaxation is slower than diffusion. In these experiments they used an overgrowth methodology to obtain coherent garnet crystal with a step discontinuity between seed and overgrowth. We calculated the molar volume for each part, seed and overgrowth, and found that the molar volume of the garnet remained constant for each zone in their experiments at 1150°C and 1200°C, at 1250°C, some mechanical relaxation seems to occur. This indicates that diffusion is faster than mechanical relaxation at lower temperatures. Hence mechanical closure of the system occurs at higher temperatures than diffusional closure, for these garnets. Following up in natural systems, we investigated the diffusion haloes surrounding coesite inclusions in garnets from Dora Maira. The observed Ca-depletion zones surrounding the inclusions can be interpreted to result from the pressure exerted from the inclusion onto the surrounding garnet. Here garnet volume did decrease due to pressure “pushing away” the

largest partial molar volume component, grossular. Hence, diffusion can be initiated by pressure gradients in minerals. The above observations are consistent with a Helmholtz approach for the chemical potential. We have also developed a simple model coupling mechanics with diffusion, to illustrate the difference of liquid-like diffusion and solid-like diffusion.

Finally, these observations lead us to speculate that micro-inclusions, such as diamonds, in garnets might indicate P conditions which were never experienced by the rock matrix as a whole. Similarly, using diffusion coefficients to analyze thermal cooling histories might result in erroneous time estimates, since pressure gradients – produced by diffusion or also prograde pressure during growth – will influence the diffusion behavior, if the concept of mechanical closure is neglected.

REFERENCES

Vielzeuf, D., & Saul A. 2011: Uphill diffusion, zero flux planes and transient chemical solitary waves in garnet, *Contributions to Mineralogy and Petrology*, 161, 683-702.

2.3

Petrological insights into shifts in eruptive styles at Volcán Llaima (Chile)

Bouvet de Maisonneuve Caroline¹, Dungan Michael¹, Bachmann Olivier², & Burgisser Alain³

¹Département de Minéralogie, University of Geneva, Rue des Maraichers 13, CH-1205 Genève (caroline.bouvet@unige.ch)

² Earth and Space Sciences, University of Washington, Seattle, WA 98195-1310, USA

³ ISTO, CNRS-University of Orleans, 45071 Orleans, France

Tephra and lava pairs from two summit eruptions (2008 and 1957 A.D.) and a flank fissure eruption (~1850 A.D.) are compared in terms of textures, phenocryst contents, and mineral zoning patterns in order to shed light on processes responsible for the shifts in eruption style during typical eruptive episodes at Volcán Llaima (Andean Southern Volcanic Zone, Chile). The mineralogy and whole-rock compositions of tephra and lavas are similar within eruptive episodes, suggesting a common magma reservoir for Strombolian paroxysms and lava effusion. The zoning profiles and textures of plagioclase record successive and discrete intrusions of volatile-rich mafic magma accompanied by mixing of these recharge magmas with the resident basaltic-andesitic crystal mushes that are commonly present at shallow levels in the Llaima system. The shallow magma reservoir of Volcán Llaima resembles that of Stromboli volcano (Italy) in that it contains a highly viscous crystal-rich magma, which is frequently refilled by low viscosity, nearly aphyric, and volatile-rich magma. Each recharge event destabilizes the plagioclase in equilibrium with the resident crystal mush and stabilizes relatively An-rich plagioclase, as is recorded by the numerous resorption zones. Lavas typically have ~15-20 vol% more phenocrysts than the tephra. Differences in plagioclase and olivine textures and zoning, combined with different phenocryst contents, indicate that a greater volume fraction of recharge magma is present in the explosively erupted magma than in the effusively erupted magma. We propose that Strombolian paroxysms at Volcán Llaima are triggered by interactions with large volume fractions of recharge magma, which decrease the bulk viscosity and increase the volatile contents of erupted magmas, favouring large expansion velocities required for the fragmentation of basaltic-andesite. Lava effusion ensues from reduced interactions with the recharge magma, after it has partially degassed and crystallized, thereby impeding rapid ascent. This process could be operating at other steady-state basaltic volcanoes, such as Stromboli or Villarica (Chile) volcanoes, wherein shallow reservoirs are periodically refilled by fresh, volatile-rich magmas.

2.4

Polymetallic mineralization in the Laki mining district Southern Bulgaria: Paragenesis and fluid evolution

Buret Yannick, Kouzmanov Kalin

Département de Minéralogie, Université de Genève, Rue des Maraîchers 13, CH-1205 Genève
(buret9@etu.unige.ch, kalin.kouzmanov@unige.ch)

The Laki mining district in southern Bulgaria is home to a number of Pb-Zn-Ag-(Cu) deposits. The district lies within the Central Rhodopian Dome (CRD), regarded as one of the most internal Alpine zones, related to the Aegean subduction system (Marchev et al., 2005). The CRD hosts several mining districts located in Madan, Laki, Ardino, Davidkovo and Enyovche, which have been dated as Oligocene (Kaiser et al., 2004). These districts show similar ore-body types of low- to intermediate-sulfidation mineralization, typically occurring in veins and metasomatic bodies. Four of the mining districts of the CRD are in close vicinity to the Middle Rhodopian detachment fault (Ivanov et al., 2000), which is cross-cut by rhyolite dykes and ore veins. The Laki district is made up of four linear ore-bearing NNE-trending faults, which also cross-cut sub-volcanic bodies associated with the Borovitsa caldera.

The focus of this study centres on the Djurkovo deposit, in the Laki district. Mineralization is concentrated in two main veins, named West 2 and the Eastern Apophysis, hosted in gneisses and marbles of the Asenitsa Unit (Ivanov et al., 2000). Both veins trend NNE-SSW, dip steeply towards the NW and reach a thickness of up to 2 meters. Average grades of West 2 are 3.76% Pb, 1.40% Zn, 0.29% Cu and 49 g/t Ag, while the Eastern Apophysis vein has grades of 5.29% Pb, 0.91% Zn, 0.46% Cu and 128 g/t Ag. Metasomatic bodies occur up to 140m from where veins cross-cut marble horizons. Ore grades from the metabodies vary from 2.9-3.6% Pb, 3.0-4.2% Zn, 0.2% Cu and 30 g/t Ag. All ore-bodies are cross-cut and displaced to various degrees by E-W normal faults, related to the late exhumation of the district. Detailed petrography and chemical analysis of ore and gangue minerals, is combined with fluid inclusion microthermometry, on samples collected from a vertical interval of 200m, in order to fully understand the P-T-X evolution of the ore-forming fluids.

The paragenetic sequence of the Djurkovo deposit can be simplified into three main stages for the veins: an early quartz-pyrite stage; a polymetallic stage; a late quartz carbonate stage, while the metasomatic bodies contain a prograde skarn stage caused by fluid-rock interaction. Chlorite occurs throughout all of these stages, as well as being one of the main alteration minerals of the host rocks, along with adularia, epidote and carbonate. This abundance and the tendency for chlorites to vary in composition due to variations in fluid conditions (temperature, chemistry, etc.) makes them useful indicators for the evolution of fluids at Djurkovo. Chlorite composition is represented by $(\text{Mg}, \text{Fe}^{2+}, \text{Fe}^{3+}, \text{Mn}, \text{Al})^{\text{VI}}_6 [(\text{Si}, \text{Al})^{\text{IV}}_4 \text{O}_{10}] (\text{OH})_8$, with cation substitution occurring in both octahedral and tetrahedral sites.

Careful petrography was carried out, followed by electron microprobe analysis of chlorites, from both veins and metasomatic bodies, to determine the compositional variation through time. Chemically the chlorites occur as tri-octahedral chamosites and clinochlores. Cation substitution observed occurs as $\text{Si}^{4+}\text{Mg}^{2+} \leftrightarrow \text{Al}^{\text{VI}}\text{Al}$; $\text{Fe}^{2+} \leftrightarrow \text{Mg}^{2+}$; $\text{Fe}^{2+} \leftrightarrow \text{Mn}^{2+}$; $\text{Fe}^{3+} \leftrightarrow \text{Al}^{\text{IV}}$; with anion substitution occurring in some areas as $\text{OH} \leftrightarrow \text{F}$.

Formation temperatures of the chlorites were calculated using the Cathelineau (1988) equation, based on the Al^{IV} content in the tetrahedral site, range from 390°C to 270°C in the veins and 390°C to 125°C within the metabodies. Variations in $\text{Fe}^{3+}/\text{Fe}^{2+}$ ratio appear to be inversely correlated to the temperature of formation. Elevated $\text{Fe}^{3+}/\text{Fe}^{2+}$ values may represent an increase in the oxidation state of the fluids through time, as well as a deficiency in aluminium required to balance the negative charge of the tetrahedral layer.

Electron microprobe analysis of sulfides has revealed that both galena and pyrite show varying compositions through time. The galena contains variable amounts of Bi and Ag. Observed substitutions within galena occur as $2\text{Pb} \rightleftharpoons \text{Bi}^{3+} + \text{Ag}^+$. Bonev (2007) observed that in the Madan district galena with elevated amounts of Bi are associated with high temperatures, while lower temperature galena does not show a presence of Bi. This study suggests that elevated values of (Bi+Ag) are present in the vein ore bodies for samples analyzed, while metabodies from the same locality exhibit up to 10 times lower (Bi+Ag). Maximum contents of Bi and Ag in the veins are 5 and 2.5 wt.% respectively. No significant difference is noted in the (Bi+Ag)/Pb between the two major veins. Metabodies show maximum values for Bi and Ag of 0.39 and 0.04 wt.% respectively. Minor quantities of Pb-Bi-Ag-Cu sulfosalt and aikinite, are present in some areas. Aikinites are present as a solid solution in the Bi_2S_3 - Cu_2S - Pb_2S_2 system and can be classified as hammarites.

X-ray mapping of pyrite grains indicate oscillatory zoning caused by As, and Co attributed to a minor amount of zonation. Arsenic rich zones are limited to the earlier generation of pyrite, while Co tends to form later.

Further work on fluid inclusions in both transparent and opaque minerals, including LA-ICP-MS trace element analysis provide insight to the fluid evolution in the Djurkovo deposit, with possible implications for the evolution of the Oligocene base metal deposits of the Rhodopian Dome.

REFERENCES

- Bonev, I. 2007: Crystal habit of Ag-, Sb-, and Bi-bearing galena from the Pb-Zn ore deposits in the Rhodope Mountains. *Geochemistry, Mineralogy and Petrology*, Sofia, 45, 1-18.
- Cathelineau, M. 1988: Cation site occupancy in chlorites and illites as a function of temperature. *Clay Minerals*, 23, 471-485.
- Ivanov Z., Dimov, D., Sarov, S. 2000: Structure of the Central Rhodopes. In: Ivanov, Z. (ed.) *Structure, Alpine evolution and mineralizations of the central Rhodopes area (south Bulgaria)*. ABCD-GEODE 2000 Workshop, Guide to Excursion B, 6-20.
- Kaiser-Rohrmeier, M., Handler, R., v.Quadt, A., Heinrich, C. 2004: Hydrothermal Pb-Zn ore formation in the Central Rhodopian Dome, south Bulgaria: Review and new time constraints from Ar-Ar geochronology. *SMPM*, 84, 37-58.
- Marchev, P., Kaiser-Rohrmeier, M., Heinrich, C., Ovtcharova M., von Quadt, A., Raicheva, R. 2005: Hydrothermal ore deposits related to post-orogenic extensional magmatism and core complex formation: The Rhodope Massif of Bulgaria and Greece. *Ore Geology Reviews*, 27, 53-89.

2.5

Probing solid-solution formation via magnetic freezing dynamics

Michalis Charilaou¹, Jörg F. Löffler², & Andreas U. Gehring¹

¹*Earth and Planetary Magnetism, Department of Earth Sciences, ETH Zurich, CH-8092 Zurich, Switzerland*

²*Laboratory of Metal Physics and Technology, Department of Materials, ETH Zurich, CH-8093 Zurich, Switzerland.*

The hemo-ilmenite solid solution $(x)\text{FeTiO}_3 - (1-x)\text{Fe}_2\text{O}_3$ is an important magnetism carrier in the Earth's crust. The system exhibits ferrimagnetism for compositions $0.5 < x < 0.95$ and antiferromagnetism for $0.0 < x < 0.5$, with an ordering temperature, that depends on the composition (Charilaou et al. 2011a). For compositions $0.6 < x < 0.95$, it exhibits a spin-glass-like freezing at low temperature ($T < 50$ K) due to Fe(II) – Fe(III) interaction-induced frustration (Charilaou et al. 2011b). The characteristics of the freezing can reveal the intrinsic mechanisms of magnetic interactions, which strongly depend on the crystalline homogeneity and cation order. Therefore, using well-defined synthetic hemo-ilmenites as comparison permits a deeper understanding of the physical properties of naturally formed solid solutions. In this report we compare data for synthetic and natural hemo-ilmenite solid solutions with composition 80% and 83% ilmenite, respectively. The comparison is based on quantitative analysis of the freezing dynamics using *ac* susceptibility (Charilaou et al. 2011c). From the experimental data we extract the effective relaxation times of the magnetic structure which reveal that naturally occurring solid solutions only exhibit short-range order, which clearly indicates the cooling rate effects on the formation of solid solutions.

REFERENCES

- Charilaou, M., Löffler, J. F., Gehring, A. U. 2011a: Fe–Ti–O exchange at high temperature and thermal hysteresis. *Geophys. J. Int.* 185, 647-652.
- Charilaou, M., Löffler, J. F., Gehring, A. U. 2011b: Slow dynamics and field-induced transitions in a mixed valence oxide solid solution. *Phys. Rev. B* 83, 224414, 1-7.
- Charilaou, M., Löffler, J. F., Gehring, A. U. 2011c: Freezing dynamics of spin-glass and superspin-glass in synthetic and natural mixed-spin oxide: a clustering scenario. *Phys. Chem. Miner.* (submitted).

2.6

Evidence for trace element mobilisation in garnet-phengite eclogitic veins along a metabasite-micaschist contact during HP conditions: an example from the Ile de Groix, France

El Korh Afifé¹, Schmidt Susanne Th.², Vennemann Torsten³, Ulianov Alexey³

¹ Institute of Geological Sciences, University of Bern, Baltzerstrasse 1+3, CH-3012 Bern, Switzerland (afife.elkorh@geo.unibe.ch)

² Department of Mineralogy, University of Geneva, Rue des Maraîchers 13, CH-1205 ³ Institute of Mineralogy and Geochemistry, University of Lausanne, Anthropole, CH-1015 Lausanne, Switzerland

A complex vein network in metabasites and micaschists on the Ile de Groix is thought to result from diverse fluid-rock interactions during both prograde and retrograde metamorphism (El Korh et al., 2011). Rare eclogitic HP–LT veins have a phe-grt-ep-rt-ilm-qtz-ab-pg-ap assemblage dominated by garnet and phengite. They are hosted in eclogite facies metabasites composed of grt-agr/jd-barr-gln-rt-ep-qtz-ab-chl-ilm-mt (peak conditions: ~ 2.0 GPa; 450–550°C) that are in contact with metapelites. Metasomatism of the host eclogite is evidenced by its high Na₂O content (6.0 wt%) and high proportion of Na-rich minerals (agr-jd and gln), and by its low MgO content (1.8 wt%).

Major and trace element compositions of minerals and the petrology support a multi-stage vein formation at HP conditions. During the first stage of vein formation, garnet cores, enriched in MREE and HREE, formed in equilibrium with LREE-, Th- and U-rich epidote I, and Ti- and Ta-rich rutile. During the second stage of vein formation, LILE-rich phengite and chloritoid have grown synchronously with garnet rims, HREE depleted compared to their cores, as well as with epidote II, with a flat REE pattern, and albite. Ilmenite formed after rutile and incorporated small amounts of Nb and Ta. Phengite is related to a strong LILE enrichment of the vein. Paragonite formed during the last stage of vein formation as a result of a reaction between albite and phengite. Paragonite consequently inherited a part of the LILE from phengite. A few inclusions of paragonite were detected in garnet rims, supporting paragonite growth during late garnet formation. The HREE-rich and LREE-depleted epidote III occurs in equilibrium with paragonite.

Eclogitic garnet-phengite veins hosted by eclogite facies metabasites along the contact metapelite-metabasalt, provide evidence of cumulate fluid flow. The strong HREE and HFSE enrichments in vein garnet and rutile, as well as the LREE enrichment in epidote, result from a mass transfer from the host metabasite involving an internally derived fluid during the first stage of vein formation. The fluid was able to mobilise the REE and HFSE on a small scale, but precipitation thereof within the vein minerals.

During the second stage of vein formation, the fluid responsible for the formation of phengite, chloritoid, ilmenite and garnet rims contained LILE and REE. Addition of an external fluid is necessary to explain the LILE enrichment. Phengite content, reaching 20–25% in the vein, is too high to originate from the host metabasites, which only contain 3–5% phengite. This fluid could originate from the neighbouring micaschists. The LILE composition of phengite is intermediate between the LILE compositions of phengite in metabasites and micaschists, suggesting an input of a pelite-derived fluid in addition to the internally derived fluid from the metabasic host rock. This fluid is able to transport LILE at least on a meter scale. Growth of paragonite and epidote III is related to re-equilibration during the last stage of vein formation.

The fluid d¹⁸O values of 10.8–12.1‰ (relative to VSMOW) calculated in equilibrium with garnet and phengite from the vein corresponds to an average between values estimated to be in equilibrium with massive metabasite hosts (8.9–9.6‰) and nearby micaschists (11.3–12.1‰). The fluid isotopic composition does not allow the internal and external fluid inputs to be quantified as the two sources (host metabasites and near-by metapelites) provide isotopic values that are relatively close (± 3‰).

Eclogitic garnet-phengite veins along metabasite-metapelite contacts provide evidence of local fluid migration, sourced in the surrounding rocks. Vein-forming fluids are responsible for significant mass transfer from source rocks to veins. The veins contain minerals with enrichments of HREE and HFSE, generally considered as immobile, but transported on a small scale from the host metabasites and host metapelites to the veins. HREE and HFSE mobility requires intense fluid-rock interactions, enhanced by fracturation along the foliation plane, and necessitates the destabilisation of the prograde HFSE- and HREE-rich minerals titanite and garnet of the vein-hosting rocks. The transport of HREE and HFSE is allowed through F and dissolved Na-Al-Si polymers in the fluid as complex formers (Haas et al., 2005; Antignano & Manning, 2008), as suggested by the presence of F-rich apatite and Na-rich minerals in the veins and their host rock (albite, paragonite, aegerine-jadeite).

REFERENCES

- Antignano, A. & Manning, C.E. 2008. Rutile solubility in H₂O, H₂O–SiO₂, and H₂O–NaAlSi₃O₈ fluids at 0.7–2.0 GPa and 700–1000 °C: Implications for mobility of nominally insoluble elements. *Chem. Geol.* 255, 283–293.
- El Korh, A., Schmidt, S.Th., Vennemann, T. & Ulianov, A. 2011. Trace element and O-isotope composition of polyphase metamorphic veins of the Ile de Groix (Armorican Massif, France): implication for fluid flow during HP subduction and exhumation processes. In Dobrzhinetskaya, L., Faryad, W., Wallis, S., Cuthbert, S. (Eds), "Ultrahigh Pressure Metamorphism: 25 years after discovery of coesite and diamond". Elsevier, Amsterdam, Netherlands, 243–291.
- Haas, J.R., Shock, E.L. & Sassani, D.C. 1995. Rare earth elements in hydrothermal systems: Estimates of standard partial molar thermodynamic properties of aqueous complexes of the rare earth elements at high pressures and temperatures. *Geochim. Cosmochim. Acta* 59, 4329–4350.

2.7

The behaviour of monazite: a petrological, trace element and SHRIMP U-Pb study of greenschist facies phyllites to anatectic gneisses, Chugach Metamorphic Complex, Alaska

Gasser, D^{1,2}, Bruand, E^{1,3}, Rubatto, D⁴, Stuewe, K¹

¹Department of Earth Sciences, University of Graz, Austria

²Department of Geological Sciences, University of Oslo, Norway (deta.gasser@geo.uio.no)

³ Earth and Environmental Sciences, University of Portsmouth, UK

⁴Research School of Earth Sciences, Australian National University, Australia

Monazite is a common accessory mineral in various metamorphic and magmatic rocks, and is widely used for U-Pb geochronology. However, linking monazite U-Pb ages with the *PT* evolution of the rock is not always straightforward. We would like to present the results of an investigation of the behaviour of monazite in a metasedimentary sequence ranging from greenschist facies phyllites into upper amphibolites facies anatectic gneisses. The sequence is exposed in the Eocene Chugach Metamorphic Complex of southern Alaska. We investigated the texture, chemical composition and U-Pb age of monazite in samples of differing bulk rock composition and metamorphic grade, with particular focus on the relationship between monazite and other REE-bearing minerals such as allanite and xenotime. In the greenschist facies phyllites, detrital and metamorphic allanite is present, whereas monazite is absent. In lower amphibolites facies schists, small, medium-Y monazite is wide-spread (Mnz1), indicating monazite growth at ~550°C and ≤3.4 kbar prior and/or simultaneous with growth of garnet and andalusite. In anatectic gneisses, new low-Y, high-Th monazite (Mnz2) crystallized from partial melts, and a third, high-Y, low-Th monazite generation (Mnz3) formed during initial cooling and garnet resorption. U-Pb SHRIMP dating of the second and third monazite generations revealed ages indistinguishable within error of the method and constrains these growth events to ~54-51 Ma. Monazite becomes unstable and is overgrown by allanite and/or allanite/epidote/apatite coronas within retrograde muscovite- and/or chlorite-bearing shear zones. This study documents polyphase, complex monazite growth and dissolution during a single-phase, relatively short-lived metamorphic event. The successive generations of monazite are related to metamorphic stages using microtextural observations combined with petrology, trace element geochemistry and geochronology.

2.8

Mo isotope composition of Mo-rich hydrothermal systems in the Aar Massif

Greber Nicolas D.^{1,2}, Hofmann Beda A.², Thomas Pettke¹, Voegelin Andrea R.¹, Villa Igor M.^{1,3}, Nägler Thomas F.¹

¹ Institut für Geologie, Universität Bern, Baltzerstrasse 3, CH-3012 Bern (greber@geo.unibe.ch)

² Naturhistorisches Museum der Burgergemeinde Bern, Bernastrasse 15, 3005 Bern.

³ Dipartimento di Scienze Geologiche e Geotecnologie, Università di Milano Bicocca, 20126 Milano, Italy.

The investigation of Mo isotopes has become increasingly popular in geosciences in the last decade. As molybdenite (MoS₂) is the only industrially valuable Mo mineral source, a number of studies have focused on its Mo isotope composition (IC). In this study, we analyzed the Mo IC from two MoS₂ mineralizations (Alpjahorn and Grimsel) and from a Mo-rich hydrothermal breccia (Grimsel) to broaden our knowledge about the Mo isotope behaviour in magmatic and hydrothermal systems. The two MoS₂ occurrences are related to late-magmatic processes in connection to residual hydrothermal fluids from the intrusion of the Central Aar granite, whereas the breccia has a Pliocene age and the Mo was transported via oxidized surface waters into the breccia system. In both cases, a reduction of Mo led to its precipitation.

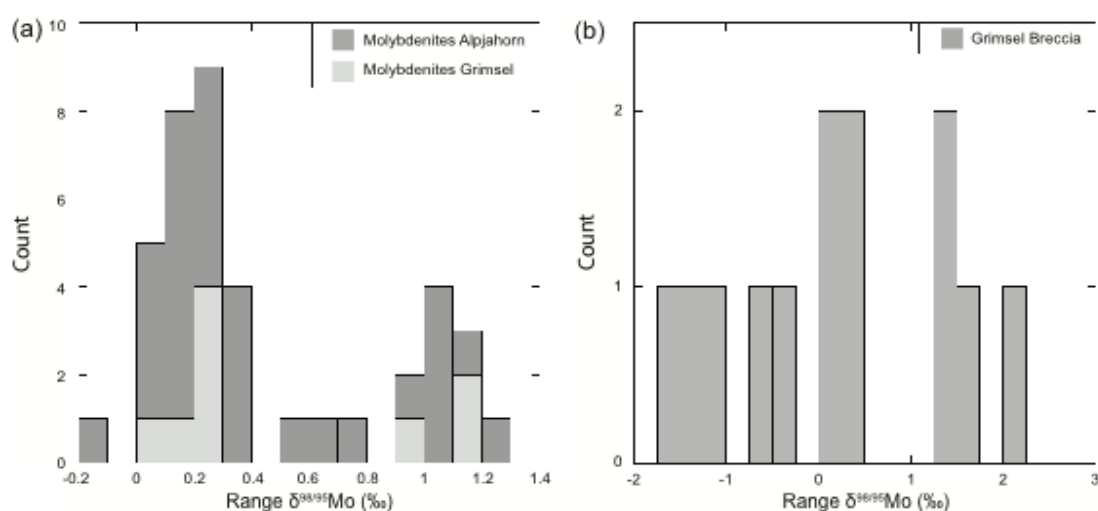


Figure 1. (a) Mo IC of MoS₂ from the Alpjahorn and the Grimsel Pass, showing two maxima. (b) Mo IC from the Mo-rich Grimsel breccia.

The breccia shows a wide and quite homogeneous Mo IC scatter of 3.0 ‰ (Figure 1). The $\delta^{98/95}\text{Mo}$ of the MoS₂ mineralizations varies over 1.35 ‰. Even in a single hand specimen it spans 0.45 ‰, indicating that fractionation processes during MoS₂ precipitation can vary on a cm scale. In contrast to the breccia, the MoS₂ of the Alpjahorn and the Grimsel Pass have an identical, bimodal Mo isotope pattern (Figure 1). This indicates that the same magmatic source and genetic evolution, in this case the intrusion of the central Aar granite, has formed both mineralizations. In addition, Rayleigh fractionation alone, as proposed in former studies, is unlikely to produce the observed bimodal Mo IC of molybdenites. Three explanations could account for this distinct Mo isotope signature of the MoS₂:

1. Alpine metamorphism might have caused additional Mo isotope fractionation. However, our petrographic observations do not hint at a redistribution of MoS₂.
2. If boiling of the hydrothermal fluid occurred, the transfer of dissolved Mo in a liquid hydrothermal phase and its uptake into a water vapour phase is also likely to produce Mo isotope fractionation. The precipitation of a first MoS₂ population from a vapour phase and of a subsequent one from a brine could account for the Mo IC pattern found in our samples.
3. The Central Aar granite has a Mo isotope value significantly lighter than that of most MoS₂ in the Aar Massif. The $\Delta^{98/95}\text{Mo}$ between granitic silicates and MoS₂ indicates that the former either preferentially incorporate light Mo isotopes during crystallization, or that hydrothermal fluids selectively precipitate heavy Mo isotopes. In either case, two discrete pulses of fluid exsolution from an increasingly fractionated magma could have produced the two isotopically different MoS₂ groups.

As reduction reactions are important considering Mo precipitation in both investigated systems (breccia and MoS₂), we suggest redox variations to be a main factor controlling the Mo IC in hydrothermal environments. To gain more information about the Mo fractionation processes in hydrothermal systems, the investigation of MoS₂ from the unmetamorph Questa porphyry deposit (USA) is in progress. Based on a detailed geochemical study, this deposit was formed by two different hydrothermal fluid exolutions and should therefore help to deny or strengthen at least the 3rd hypothesis explained above.

2.9

Percolation and impregnation of a plagioclase-rich melt into the mantle-crust transition zone of the Makran ophiolites, SE Iran

Hunziker Daniela¹, Burg Jean-Pierre¹, Bouilhol Pierre², Jafar Omrani³

¹Geological Institute, Structural Geology and Tectonics, ETH Zurich, Sonneggstrasse 5, NO E69, CH-8092 Zurich
(daniela.hunziker@erdw.ethz.ch)

²Department of Earth, Atmospheric and Planetary Science, Massachusetts Institute of Technology, 77 Massachusetts Avenue Cambridge, MA02139, USA

³Geological Survey of Iran, Meraj Avenue, Azadi Square, P.O.Box 13185-1494, Tehran, Iran

The Makran ophiolites are situated to the north of the accretionary wedge formed in the subduction zone between Arabia and Eurasia. The ophiolite sequence comprises harzburgite with rare lherzolites as the structurally lowest unit intruded by troctolite and gabbros that were covered by lavas and sediments after exhumation. Dunites occur next to extensive mafic intrusions and in the upper levels of the main outcrops as remnants of melt percolation. They mostly show cumulate textures and are only little serpentinized. Meter thick impregnation zones and bands of all sizes where plagioclase is interstitial make the often transitional contact to the troctolite difficult to locate. Only chemistry allows distinguishing olivine crystallized from the plagioclase-rich melt, identifying the rock as troctolite from olivine equilibrated after melt percolation in impregnated dunite. Plagioclase impregnation zones, troctolite and gabbro dykes intruding the re-equilibrated dunite mark the transition from depleted harzburgitic mantle to a lower oceanic crust consisting of cumulate dunites and various mafic intrusions.

HREE enrichment in all samples is attributed to melt percolation. Typically, dunites show an almost V-shape REE pattern, since they are the product of re-equilibration after the melt percolated; accordingly, they are enriched in HREE and demonstrate a steeper LREE trend. Dunite crystallized in melt channels yield a strongly positive Eu anomaly, which reflects plagioclase crystallization. Clinopyroxene in harzburgite is depleted in HREE and shows a flat trend in LREE, while clinopyroxenes of olivine-orthopyroxenite dykes and dunite are more enriched in HREE, suggesting stronger melt influence. Trace element features of plagioclase in impregnations and troctolites are identical.

The Makran ultramafic rocks represent a piece of oceanic lithosphere that has been percolated by plagioclase-rich melt at less than 1km depth, equivalent to the pressure at which plagioclase crystallizes before clinopyroxene at an estimated temperature of ~1000°C. The troctolite is being dated with Sm/Nd to get the age of intrusion. Other temporal constraints were obtained by SHRIMP and La-ICP-MS measurements of U-Pb isotopes in zircons of a trondhjemitic (~ 145 Ma) and a peraluminous granite dyke (~ 111 Ma). Granite dykes possibly intruded after obduction, since the youngest sediment covers are Barremian (125-130 Ma).

2.10

Mass transfer processes and fluid composition of metamorphic quartz vein systems, Rhenish Massif (Germany)

Marsala Achille¹, Wagner Thomas¹, Wälle Markus¹ & Heinrich Christoph¹

¹ Institute of Geochemistry and Petrology, ETH Zürich, Clausiusstrasse 25
CH-8092 Zürich (achille.marsala@erdw.ethz.ch)

Formation of metamorphic veins in fold-and-thrust belts is generally related to crustal fluid flow and fluid-rock interaction processes (Yardley, 1983; Oliver & Bons, 2001). Fluid inclusions in metamorphic veins record the chemical composition of metamorphic fluids and their evolution with time. This project investigates the fluid chemistry and mechanisms of mass transfer in metamorphic vein systems in the Rhenish Massif (Germany) by combination of field studies, fluid inclusion studies, isotope geochemistry and geochemical modeling. The project is part of the multidisciplinary research initiative FRACS (www.fracs.de) that aims at understanding the dynamics of vein formation processes at a fundamental level, and involves strongly linked collaboration between structural geologists, material scientists, hydrologists and geochemists. Based on field documentation and structural mapping, the relative time sequence of deformation and vein forming events in the central part of the Rhenish Massif has been established. Hosted by wall rocks of monotonous slates, two main generations of metamorphic quartz veins were identified. These are (1) en-echelon vein sets with tension gash shape located in faults and shear zones, related to progressive compressional deformation, and (2) extension veins related to the late-orogenic stage with tabular shape, abundant open vugs and fissures (containing euhedral quartz crystals) and pronounced laterally extensive alteration zones. They crosscut almost perpendicular the slate foliation (S1) that has NE-SW striking direction and subvertical dip. The second vein type is particularly important, because it likely channelized major amounts of comparatively hot fluids (Wagner et al., 2010).

Following petrographic investigation, the fluid inclusion study has concentrated on the extension veins, because they host abundant fluid inclusions with suitable sizes for fluid inclusion microanalysis using LA-ICPMS, and they show a complex multi-stage filling and growth history. The different stages are characterized by distinct textures, with the early stage comprising elongate-blocky quartz (Bons & Jessell, 1997), which gradually evolves to the late stage characterized by euhedral crystallization of quartz. Combining microthermometric and LA-ICPMS microanalysis of different fluid inclusion assemblages, we were able to produce one of the first datasets of the solute inventory in low-grade metamorphic fluids.

The salinity of the fluids is rather low, being in the range between 3 and 5 wt% NaCl in all the fluid inclusions analysed. With LA-ICPMS it was possible to analyse the concentration of several major and minor cations in each fluid inclusion. As expected, most of the alkali and alkali earth elements like Li, Na, K, Rb, Cs, Sr, Ba and B show consistent concentrations in all fluid inclusion assemblages measured. The concentrations of Ca, Mg, S, Mn, Zn, Sb are more variable among assemblages, likely reflecting their comparatively low concentrations and associated rather large analytical errors. From the data it is possible to calculate the K/Na ratio, which is an important first-order indicator for the status of fluid-rock equilibrium during vein formation. This is because for aqueous fluids that are in chemical equilibrium with quartzo-felspathic rocks, the K/Na ratio strongly decreases with increasing temperature (Yardley 2005; Dolejs & Wagner 2008). Our data give average K/Na ratios of 0.025 ± 0.013 indicating equilibration of the fluids at temperatures of around 250 ± 30 °C, in good agreement with other independent temperature estimates for the formation of the late-stage euhedral quartz crystals (Wagner et al. 2010).

REFERENCES

- Bons, P. D. & Jessell, M. W. 1997: Experimental simulation of the formation of fibrous veins by localised dissolution-precipitation creep, *Mineralogical Magazine*, 61 (1), 53-63.
- Dolejs, D. & Wagner, T. 2008: Thermodynamic modeling of non-ideal mineral-fluid equilibria in the system Si-Al-Fe-Mg-Ca-Na-K-H-O-Cl at elevated temperatures and pressures: Implications for hydrothermal mass transfer in granitic rocks, *Geochimica et Cosmochimica Acta*, 72 (2), 526-553.
- Oliver, N. H. S. & Bons, P. D. 2001: Mechanisms of fluid flow and fluid-rock interaction in fossil metamorphic hydrothermal systems inferred from vein-wallrock patterns, geometry and microstructure, *Geofluids*, 1 (2), 137-162.
- Wagner, T., Boyce, A. J. and Erzinger, J. 2010: Fluid-rock interaction during formation of metamorphic quartz veins: A REE and stable isotope study from the Rhenish Massif, Germany, *Am J Sci*, 310 (7), 645-682.
- Yardley, B. W. D. 1983: Quartz Veins and Devolatilization during Metamorphism, *Journal of the Geological Society*, 140 (Jul), 657-663.
- Yardley, B.W.D. 2005: Metal concentrations in crustal fluids and their relationship to ore formation. *Economic Geology* 100, 613-632.

2.11

Fluid chemistry and fluid-rock interaction of Alpine veins, Central Alps

Martinek Klara, Wagner Thomas, Wälle Markus, Heinrich Christoph

Institute of Geochemistry and Petrology, ETH Zurich, Clausiusstrasse 25, CH-8092 Zürich

The classical Alpine fissure veins are large cavities lined by occasionally giant quartz crystals and many other euhedral mineral assemblages. They occur in regionally metamorphosed terranes in the upper crust and record important information about the composition and evolution of metamorphic fluids (Mullis, 1996) and fluid sources and mass transfer during crustal fluid-rock interaction (Oliver & Bons 2001). Detailed fluid inclusion studies of Alpine veins along a Geotraverse in the Central Alps have established that the fluid composition shows a distinct evolution with increasing metamorphic grade, where consecutive zones are dominated by (1) heavier hydrocarbons, (2) CH₄, (3) H₂O-NaCl, and (4) H₂O-CO₂-NaCl (Mullis et al. 1994). This study addresses the chemical evolution of fluids in Alpine fissure veins in the Central Swiss Alps by integrating field work, fluid inclusion studies (microthermometry and LA-ICPMS microanalysis of individual fluid inclusions), and geochemical modeling.

The field locations were selected along a cross section through the Central Alps that covers different lithologies and metamorphic conditions. This includes vein systems in the Aar massif (Gauli glacier, Gerstenegg vein in the Grimsel power station), the Nufenen and Griess pass, the Bedretto valley, and the Maggia valley. Fluid inclusion studies have been completed for the two localities in the Aar massif, and it was possible to analyze a considerable number of elements with LA-ICPMS. These include Na, K, Rb, Cs, Li, Ca, Mg, Sr, Ba, Mn, B, As, Sb, S, Pb and Zn. The fluid inclusions from the Gauli and Gerstenegg vein systems are low-salinity aqueous two-phase. While the Gauli samples contain fluid inclusions with 4.5-5.0 wt% equivalent NaCl, those from the Gerstenegg have a considerably higher salinity of around 10 wt% eqv. NaCl.

This difference in salinity is correlated with consistently higher concentrations of those elements that are largely complexed by chlorine such as the alkali and earth alkaline metals, and divalent transition metals (Yardley 2005). Consequently, the fluid inclusions from the Gerstenegg yielded consistent data for Pb, Zn and Ag on the order of few ppm, whereas the concentrations of these metals were mostly below the detection limit in the Gauli samples. We will expand the fluid inclusion studies to Alpine fissure veins in the southern part of the cross section that record a higher metamorphic grade.

Of particular interest will be to compare the solute composition of aqueous-carbonic fluids with those of the more simple aqueous H₂O-NaCl type fluids. Comparing the measured fluid compositions with results from multicomponent-multiphase fluid-mineral equilibria modeling will then make it possible to evaluate the status of fluid-rock equilibrium along the metamorphic gradient.

REFERENCES

- Mullis, J., Dubessy, J., Poty, B., O'Neil, J. 1994: Fluid regimes during late stages of a continental collision: physical, chemical, and stable isotope measurements of fluid inclusions in fissure quartz from a geotraverse through the Central Alps, Switzerland. *Geochim. Cosmochim. Acta* 58, 2239-2267.
- Mullis, J. (1996) P-T-t path of quartz formation in extensional veins of the Central Alps. *Schweiz. Mineral. Petrogr. Mitt.*, 76, 159-164.
- Oliver, N.H.S., Bons, P.D. 2001: Mechanisms of fluid flow and fluid-rock interaction in fossil metamorphic hydrothermal systems inferred from vein-wallrock patterns, geometry and microstructure. *Geofluids* 1, 137-162.
- Yardley, B.W.D. 2005: Metal concentrations in crustal fluids and their relationship to ore formation. *Economic Geology* 100, 613-632.

2.12

Pyroclast textures in the explosive 2007-2008 eruption of Oldoinyo Lengai, Tanzania: Implications for magma ascent and fragmentation

Mattsson Hannes B.¹, Bosshard Sonja A.

¹*Institute of Geochemistry and Petrology, ETH Zurich, Clausiusstrasse 25, CH-8092 Zurich (hannes.mattsson@erdw.ethz.ch)*

After more than 25 years of effusive natrocarbonatitic activity the Oldoinyo Lengai (OL) volcano in northern Tanzania started erupting explosively in September 2007. The eruption continued for 8 months and was surprisingly vigorous (occasionally the plume reached up to 15 km in altitude). It has previously been proposed that thermal decomposition of older natrocarbonatites (and release of CO₂) inside the main crater of the volcano was responsible for the vigour associated with the explosive 1966-67 eruption.

From the recent eruption we sampled the initial ash-fall (3 days after the onset) in Al-canisters during a 24 hour period, which was later complemented by tephra samples collected from 140 profiles around the volcano during a field campaign in May 2011. Petrologically, bulk-rock analyses show a trend from being a mechanical mixture of natrocarbonatitic and nephelinitic material in the beginning of the eruption, to being dominated by nephelinitic composition at the end of the eruption.

SEM-studies of the first ash-deposits (i.e., September 7th) show a dominance of non-vesicular natrocarbonatitic droplets (containing nyerereite and gregoryite phenocrysts) mixed with a small amount of sub-spherical nephelinitic pyroclasts with low vesicularity (<25 vol.%). Deposits from the later phases of the eruption (as deduced from the tephra-stratigraphy) are dominated by well-sorted, near-spherical, lapilli. In these deposits, the natrocarbonatitic component is absent and individual tephra layers can be distinguished based on variations in grain-size. SEM studies of pyroclasts reveal that approximately 60% of the lapilli are cored by a crystal (predominantly nepheline, garnet, pyroxene, wollastonite) which is covered by a thin melt film. The nephelinitic melt film varies in vesicularity between 20 and 50 vol.% with a clear predominance of near-spherical vesicle shapes. An abundance of small particles and crystals are adhered/welded to the fluidal outer surface of the nephelinitic melt droplets. In addition to this, most of the studied deposits display an absence of particles produced by breaking/rupturing of vesicle walls.

Thus, the observed pyroclast textures in the OL-deposits strongly suggest that the nephelinitic magma was erupted in a similar fashion as an aerosol (i.e., melt droplets carried by a gas stream). Decomposition of carbonates which is required to generate such high gas-fluxes cannot occur inside the crater as this material is highly porous and only constitute the uppermost 80 m of the conduit (leaving little time for gas expansion to occur inside the conduit). Based on the observed pyroclast textures we find that the nephelinitic magma must have interacted with a deeper carbonatitic reservoir, in order to allow the CO₂ to expand during ascent (i.e., decompression). This interpretation is also supported by the petrological data.

2.13

The Kapan zone of the Somkheto-Karabakh island arc in the Lesser Caucasus: magmatism and ore deposits associated with Neotethys subduction

Mederer Johannes, Moritz Robert

Département de Minéralogie, Université de Genève, Rue des Maraîchers 13, CH-1205 Genève (johannes.mederer@unige.ch)

The present-day Lesser Caucasus forms part of the Tethyan belt, which is the result of complex processes of ocean openings, subductions, obductions and micro-plate accretions. Long lasting northwards subduction of the Neotethys (e.g. Khain & Koronousky 1997) below the Eurasian margin caused the evolution of the Jurassic-Cretaceous island arc of the Lesser Caucasus. It can be divided into the northwest-southeast striking Somkheto-Karabakh island arc, extending over 600 km from southern Georgia over northern Armenia into Nagorno Karabakh, and the subparallel Kapan zone further to the southwest which extends over 100 km from southeastern Armenia into northern Iran (Figure 1).

A pile of up to 7000 m of volcanic and volcanoclastic rocks characterizes the Jurassic-Cretaceous island arc of the Lesser Caucasus. In the Kapan zone, three magmatic complexes are distinguished from each other, which are by name the Middle Jurassic, Upper Jurassic-Lower Cretaceous and the Paleogene magmatic complexes (Achikgiozian et al. 1987). Intrusive rocks in the Kapan zone are rare but small bodies of gabbros and diorites occur. Most of the mineralization in the district is associated with the Middle Jurassic magmatic complex, minor uneconomic mineralization occurs in the unconformably overlying younger rocks. Other ore deposits along the Somkheto-Karabakh island arc such as the Drmbon deposit of Nagorno Karabakh or the Alaverdi deposits of northern Armenia are also related to similar volcanic and subvolcanic rocks of Middle Jurassic age.

Two different ore deposits are found in the Middle Jurassic volcanogenic complex of the Kapan mining district, distinct in mineral assemblage and host rock alteration: the Cu-Au-Ag-Zn±Pb Shahumyan deposit and the Cu±Au±Zn Centralni deposit are both located within a 4 km distance from each other. The currently operating Shahumyan deposit is hosted in subvolcanic quartz-dacite. Pyrite, chalcopyrite, sphalerite, fahlore and galena are the main ore minerals hosted in more than 100 east-west striking and steeply dipping extensional veins with phyllic alteration halos. Quartz and carbonates are the main gangue minerals. Gold and silver distribution in Shahumyan is controlled by different Au-Ag-tellurides. Northeast of the Shahumyan deposit, the abandoned Cu±Au±Zn Centralni deposit is divided into Centralni West and Centralni East. Centralni East and West are separated from each other by a major fault zone. Mineralization in Centralni West occurs in N100°±10° striking veins with variable 60°-80° dip to the south. Chalcopyrite and pyrite are the main sulfide minerals, together with minor amounts of fahlore and galena. Gangue minerals include quartz and carbonates. The ore-bearing volcanosedimentary sequence hosting the Centralni West mineralization is dark-green altered to chlorite, carbonate and epidote. Centralni East is characterized by stockwork-like mineralization within argillic altered andesite, with colusite, fahlore, chalcopyrite, minor luzonite and galena occurring as main ore minerals.

All magmatic rocks from the Middle Jurassic, Upper Jurassic-Lower Cretaceous and the Paleogene magmatic complex of the Kapan zone show subduction-related signature based on trace element geochemical data obtained by LA-ICP-MS analyses. However, igneous rocks of Middle Jurassic age can be distinguished from their overlying rocks by accentuated flat REE patterns and strong negative Nb- and Ta anomalies. A more depleted magma source and the pronounced participation of subduction-derived fluids during melt generation distinguish Middle Jurassic igneous rocks from the younger ones in the Kapan zone. In the subduction-related island arc of the Lesser Caucasus these processes might have been the key factors for the generation of fertile melts to which Middle Jurassic ore deposits are associated with.

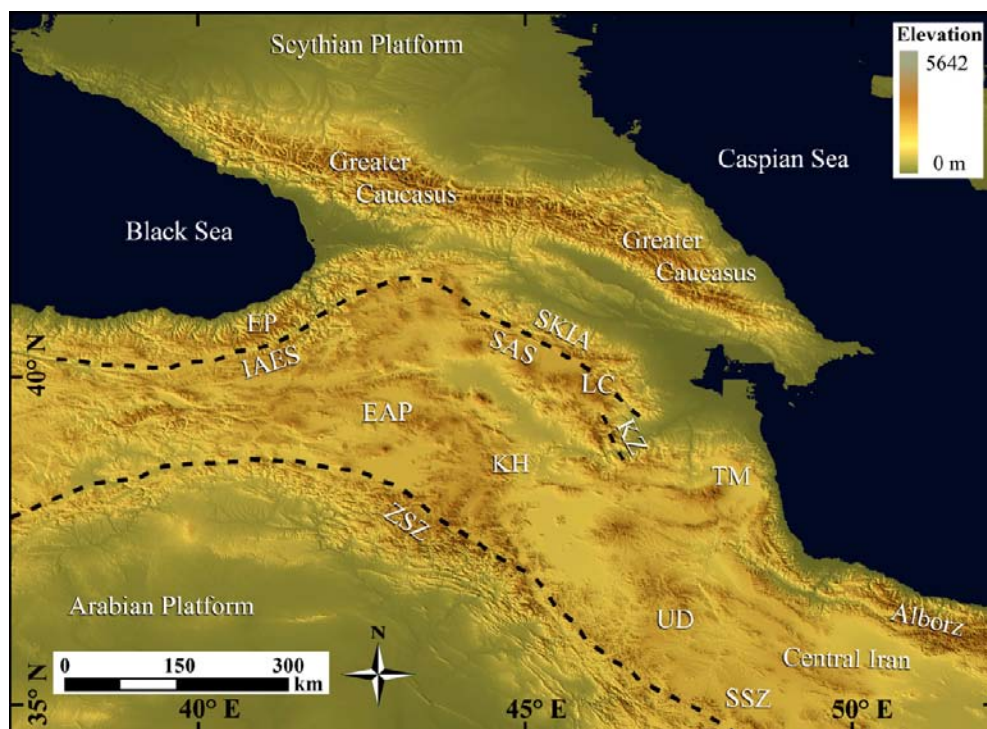


Figure 1. Digital elevation model of the Lesser Caucasus and adjacent regions. EAP-East Anatolian Platform; EP-Eastern Pontides; IAES-Izmir-Ankara-Erzincan suture; KH-Khoy ophiolitic complex; KZ-Kapan zone; LC-Lesser Caucasus; SAS-Sevan-Akera suture; SKIA-Somkheto Karabakh island arc; SSZ-Sanandaj-Sirjan zone; TM-Talesh mountains; UD-Urumieh Dokhtar magmatic arc; ZSZ-Zagros suture

REFERENCES

- Achikgiozian, S.O., Zohrabian, S.A., Karapetyan, A.I., Mirzoyan, H.G., Sargisyan, R.A. and Zaryan, R.N. 1987: The Kapan Mining district. Armenian Academy of Sciences SSR, 198 pp, (in Russian).
- Khain, V.E. & Koronousky, N.V., 1997. Caucasus. In: Moores, E.M. & Fairbridge, R.W. (Eds.), Encyclopedia of European and Asian Regional Geology. Chapman and Hall, London, pp. 127-136.

2.14

Biogeochemical processes in sediments of the manganese nodule belt in the equatorial NE Pacific Ocean

Mewes Konstantin¹, Picard Aude^{2,3}, Rühlemann Carsten⁴, Kuhn Thomas⁴ & Kasten Sabine¹

¹ Alfred Wegener Institute for Polar and Marine Research, Am Handelshafen 12, D-27570 Bremerhaven (konstantin.mewes@awi.de)

² Max Planck Institute for Marine Microbiology, Celsiusstrasse 1, D-28359 Bremen

³ MARUM - Center for Marine Environmental Sciences, Leobener Strasse, D-28359 Bremen

⁴ Federal Institute for Geosciences and Natural Resources, Stilleweg 2, D-30655 Hannover

During RV Sonne cruise SO-205 to the eastern part of the German manganese nodule exploration area, located in the Clarion-Clipperton Fracture Zone of the Pacific Ocean, we recovered sediments with a multiple corer and a box corer at 14 sites and with piston and gravity corers at 7 sites. These samples were geochemically analyzed to elucidate whether diagenetic processes contribute to manganese nodules growth.

High-resolution oxygen measurements revealed an oxygen penetration depth of 2-3m. This finding is in contrast to previous assumptions, which suggested oxic sediments over several tens of meters (Müller et al., 1988). Manganese nodule abundance was determined from the box core samples. The sediments recovered with a piston-/gravity corer at the same sites show neither dissolved Mn²⁺ in pore waters nor denitrification in sediments from sites with medium to high manganese nodule abundance. In contrary, sediments from nearby locations with no nodules or low manganese nodule abundance show an increase of pore water [Mn²⁺] with depth and denitrification. This result suggests that there is no diffusive flux of Mn²⁺ from underlying sediments to manganese nodules at the surface (no suboxic diagenesis). Furthermore we propose that these small scaled regional differences in the geochemical characteristics of sediments can be explained with variations in sedimentation rates and organic matter input, which in turn are probably controlled by differences in bottom water current strength due to lateral variations in seafloor roughness or the occurrence of seamounts (Turnewitsch et al., 2004).

REFERENCES

- Müller, P.J., Hartmann, M., Suess, E., 1988. The chemical environment of pelagic sediments. In: Halbach, P., Friedrich, G., von Stackelberg, U. (eds), *The manganese nodule belt of the Pacific Ocean. Geological environment, nodule formation, and mining aspects*. Enke Verlag, Stuttgart, pp.70-99.
- Turnewitsch, R., Reyss, J.-L., Chapman, D.C., Thomson, J., Lampitt, R.S. (2004). Evidence for a sedimentary fingerprint of an asymmetric flow field surrounding a short seamount. *Earth and Planetary Science Letters (Frontiers Article)* 222(3-4), 1023-1036.

2.15

Fluid composition and mineral equilibria in low grade metamorphic rocks, Bündnerschiefer, Switzerland. Application of fluid inclusions and petrological modeling.

George Dan Miron¹, Thomas Wagner¹, Markus Wälle¹, Christoph A. Heinrich¹

¹Institute for Geochemistry and Petrology, ETH Zurich, Clausiusstrasse 25, 8092 Zürich (dmiron@student.ethz.ch)

The composition of fluid inclusions hosted in quartz veins from low-grade metamorphic rocks of the Bündnerschiefer (north of Thusis and Schiers valley), Swiss Alps, was analyzed by combination of microthermometry and LA-ICPMS micro-analysis. Massive milky quartz and euhedral quartz crystals were sampled from two sets of veins, which are foliation parallel veins and open fissure veins that crosscut the main foliation. The host rocks are organic-rich metapelites, that additionally contain relatively high amounts of carbonate in the case of Schiers. Several metamorphic temperature indicators were used to determine the temperature and pressure during metamorphism of the host rocks: Kübler index for illite (Kübler & Jaboyedoff 2000), Raman spectroscopy on carbonaceous material (Beysac et al. 2002), mineral assemblages, chlorite geothermometry (Cathelineau 1988), and Na-Mg fluid solute geothermometry (Giggenbach 1988). All geothermometers point to equilibrium temperatures around 320 ± 20 °C for the Thusis rocks, placing them into the lower epizone (lower greenschist facies). The samples from Schiers show anchizone (subgreenschist facies) characteristics and have been metamorphosed at temperatures around 250 ± 20 °C. Most of the important rock forming elements have been successfully determined in individual inclusions. The fluid inclusions show very consistent element concentrations within petrographically defined fluid inclusion assemblages. They contain measurable concentrations of Na, K, Rb, Cs, Li, Ca, Mg, Mn, Sr, Ba, B, As, B, Zn, Pb, Cu and S. Typical elements concentrations are: Al (Thusis 30-40 ppm), Mg (Thusis 5-7 ppm, Schiers 3 ppm), Ca (Thusis 300-400 ppm, Schiers 200 ppm), Mn (both places 3-5 ppm), S (Thusis 300-350 ppm, Schiers 150 ppm), and Cu (Thusis 5-20 ppm) as well as the fluid inclusions have salinities of -2.3 ± 0.1 °C at Thusis and -1 ± 0.1 °C at Schiers. Homogenization temperatures are 122 to 140 °C at Thusis and 82 to 86 °C at Schiers. The total element concentrations are lower compared with bulk crush leach fluid composition data from similar metamorphic vein settings, and considerably lower than in mesothermal gold ore deposit fluids (Yardley et al. 1993; Yardley 2005). This likely reflects the lower bulk salinity of fluids in the Bündnerschiefer veins, which exerts a major control on those elements that are complexed by chloride (Yardley 2005). Combining fluid inclusion isocores with independent geothermometers results in pressure estimates between 2.8 and 3.8 kbars for Thusis, and around 3.4 kbars for Schiers. The geothermal gradient decreases from the southern location (27-22 °C/km: Thusis) to the northern location (19 °C/km: Schiers). The results of pseudosection modeling using Perplex (Connolly & Petrini 2002) show very close agreement between calculated and measured mineral assemblages and mineral modes, and further constrain the pressure-temperature conditions that were derived from conventional geothermobarometry. The fluid inclusion data, in conjunction with metamorphic indicators and petrological modeling suggest that fluid-rock equilibrium was reached during metamorphism. The comprehensive fluid composition dataset obtained in this study can be further used for fluid-rock equilibrium calculations and for improving mineral and fluid speciation thermodynamic models.

REFERENCES

- Beysac, O., Goffé, B., Chopin, C., & Rouzaud, J. N. 2002: Raman spectra of carbonaceous material in metasediments: a new geothermometer. *Journal of Metamorphic Geology*, 20(9), 859-871.
- Cathelineau, M. 1988: The chlorite and illite geothermometers. *Chemical Geology*, 70(1-2), 182-182.
- Connolly, J. A. D. & Petrini, K. 2002: An automated strategy for calculation of phase diagram sections and retrieval of rock properties as a function of physical conditions. *Journal of Metamorphic Petrology* 20(7), 697-708.
- Giggenbach, W. F. 1988: Geothermal solute equilibria. Derivation of Na-K-Mg-Ca geothermometers. *Geochimica et Cosmochimica Acta*, 52(12), 2749-2765.
- Kübler, B. & Jaboyedoff, M. 2000: Illite crystallinity. Concise review paper. *Comptes Rendus de l'Académie des Sciences - Series IIA - Earth and Planetary Science*, 331(2), 75-89.
- Yardley, B.W.D. 2005: Metal concentrations in crustal fluids and their relationship to ore formation. *Economic Geology* 100, 613-632.
- Yardley, B. W. D., Banks, D. A., Bottrell, S. H., & Diamond, L. W. 1993: Post-metamorphic gold-quartz veins from N.W. Italy: The composition and origin of the ore fluid. *Mineralogical Magazine* 57, 407-422.

2.16

Major Cu, Au and Mo deposits of the Lesser Caucasus: Products of diverse geodynamic settings

Moritz Robert¹, Mederer Johannes¹, Ovtcharova Maria¹, Selby Dave², Chiaradia Massimo¹, Popkhadze Nino³, Gugushvili Vladimer³, Migineshvili Ramaz³, Melkonyan Rafael⁴, Tayan Rodrig⁴, Vardanyan Arman⁴, Havokimyan Samvel⁴, Ramazanov Vagif⁵ & Mansurov Mamoy⁵

¹ *Section des Sciences de la Terre et de l'environnement, Université de Genève, Rue des Maraîchers 13, 1205 Genève (robert.moritz@unige.ch)*

² *Department of Earth Sciences, Durham University, United Kingdom*

³ *A.Janelidze Institute of Geology, M.Alexidze 1/9, 0171 Tbilisi, Georgia*

⁴ *Institute of Geological Sciences, National Academy of Sciences of The Republic of Armenia, Yerevan*

⁵ *Department of Mineral Resources, Baku State University, Baku, Azerbaijan*

The Lesser Caucasus sits astride on Georgia, Armenia and Azerbaijan, and is a favourable environment for investigating the formation of diverse ore deposits in successive geodynamic settings. It combines an evolution ranging from Jurassic-Cretaceous compressive tectono-magmatic events in subduction, Andean-style environments to Neogene, post-collisional, extensional tectono-magmatic events. The geodynamic evolution was accompanied by episodic ore formation in response to particular tectonic and/or magmatic events, which vary in style as a function of the different geodynamic settings. Recent studies in Anatolia, the Caucasus and Iran have improved our understanding about the Mesozoic to Tertiary geodynamic evolution of the Tethys orogenic belt. It formed during convergence and collision of the Eurasian, Arabian and African plates, in a complex setting including abundant microplates. Such contributions allow us to investigate the formation of ore deposits in a well-defined, regional geological framework. Ore deposit formation in the Lesser Caucasus occurred episodically. If one excludes basement rocks, four main metallogenic events can be distinguished: Middle-Late Jurassic, Late Jurassic-Early Cretaceous, Late Cretaceous, and Tertiary. Recent geochronological, litho-geochemical, and stable and radiogenic isotope data yield new constraints about the timing and genetic interpretations of various ore deposits during the geological evolution of the Lesser Caucasus.

The earliest metallogenic event consists of gold- and telluride-bearing, copper-rich pyrite veins and massive ore bodies hosted by Middle Jurassic volcanic and volcano-sedimentary rocks of the Somkheto-Karabakh island arc, with a mostly calc-alkaline composition. These deposits (Kapan, Alaverdi, Drmbon) remain the most enigmatic ones within the Lesser Caucasus, and it is debated whether they are volcanogenic massive sulphide (VMS) deposits, hydrothermal veins emplaced in a large volcanic edifice, or porphyry-style deposits. Middle to Upper Jurassic, and younger Cretaceous and Tertiary ages have been proposed. Sulphur isotopic compositions of barites mostly deviate from the ones of coeval Jurassic seawater, therefore questioning a typical VMS-only scenario.

The second metallogenic event consists of Cu-porphyry, skarns and epithermal gold deposits also located in the Jurassic-Cretaceous Somkheto-Karabakh magmatic arc, formed during subduction of the Neotethys below the Eurasian margin. They are mostly interpreted as Upper Jurassic to Lower Cretaceous in age, which is confirmed by a recent Re-Os molybdenite age of 145.85 ± 0.59 Ma and Rb-Sr isochrone ages of 156 ± 3 and 164 ± 6 Ma for the Toghout area, Armenia. Several porphyry copper deposits include zones of massive sulphide lenses, locally enargite, alterations consisting of silicification, sericite, kaolinite, and alunite, and gold-enrichments typical for deep porphyry to shallow epithermal transitional environments.

Upper Cretaceous volcano-sedimentary units, with abundant felsic volcanic and sub-volcanic rocks in an extensional setting including caldera formation, host polymetallic base and precious metal deposits, and mark the onset of arc rifting of the Somkheto-Karabakh belt and its Variscan basement, as documented at the Madneuli polymetallic deposit, Georgia and adjacent precious metal epithermal deposits. K-Ar and microfossil dating of the host rocks indicate, respectively, Coniacian - Middle Campanian and Middle - Upper Campanian ages. Detailed lithofacies studies document a mostly shallow marine depositional environment of the Madneuli host rocks. Litho-geochemistry of the magmatic rocks reveals a composition transitional between calc-alkaline and tholeiitic. The sulphur isotopic composition of ore sulphides and barite are consistent with magmatic and coeval Late Cretaceous seawater, respectively. Sr isotope data reveal a more radiogenic composition of the magmatic rocks at Madneuli ($^{87}\text{Sr}/^{86}\text{Sr} = 0.7046\text{-}0.7075$) in contrast with lower $^{87}\text{Sr}/^{86}\text{Sr}$ ratios (<0.7046) of the older Upper Jurassic - Lower Cretaceous magmatic rocks (see above) and the younger Tertiary magmatism (below). We conclude that these deposits are bimodal-felsic VMS-type deposits (Kuroko-Baimak) formed in a magmatic arc underlain by a continental basement, with transitional features to epithermal deposits, as recognised elsewhere in the Eastern Pontides.

The Tertiary evolution of the Lesser Caucasus is dominated by collisional and postcollisional tectonics and magmatism. The most important mineral district is the Tertiary Zangezur-Ordubad block (Meghri composite pluton) in the southern

Caucasus, close to the Iranian border, which consists of Eocene to Miocene calc-alkaline to alkaline mafic to felsic magmatic suites, and which hosts major Mo-Cu-porphyrries (including the world-class Kadjaran deposit) and subsidiary precious and base metal prospects. High-precision U-Pb zircon TIMS ages confirm the pulsating nature of magmatism revealed by previous Rb-Sr isochrone ages, with an early Eocene event (40-45 Ma) followed by events during the Oligocene (30-32 Ma) and the Miocene (20-23 Ma). On-going, high-precision Re-Os molybdenite dating from different Mo-Cu porphyry deposits indicate discrete ore forming events at 40-44 Ma (Agarak, Aygedzor, Dastakert deposits), 31 Ma (Kaler) and 27 Ma (Kadjaran), essentially overlapping with magmatic events. Studies are ongoing to understand the long duration of about 20 m.y. of repeated ore-forming processes in the postcollisional context of the Meghri pluton, as a result of slab break off and asthenospheric upwelling.

Postcollisional Tertiary magmatism is also at the origin of abundant, but poorly characterized epithermal gold deposits and prospects of the Lesser Caucasus, with uncertain Eocene to Miocene ages. Both low-sulphidation (e.g. Zod-Sotk, Miocene in age, mainly hosted by Jurassic ophiolites) and high-sulphidation deposits (e.g. Amulsar, best world gold discovery in 2006) are recognized.

2.17

PVTX evolution and reequilibration of prograde and retrograde fluid inclusions in diagenetic and metamorphic rocks, Central Alps, Switzerland.

Mullis Josef¹ & Tarantola Alexandre²

¹Mineralogisch-Petrographisches Institut, Bernoullistrasse 30, CH-4056 Basel, Switzerland (josef.mullis@unibas.ch)

²UMR G2R-7566, Faculté des Sciences - Université Henry Poincaré, BP239, F-54506 Vandoeuvre-lès-Nancy

Careful fabric, host mineral and fluid inclusion analyses of several hundred localities of the external parts of the Central Alps enable a critical discussion about their application to fluid evolution and fluid thermobarometry. Detailed investigations on fluid inclusions formed during prograde, PT-maximum and retrograde conditions in vein, Alpine fissure and slickenside systems from diagenetic to metamorphic terrains have been carried out.

Once trapped, fluid inclusions may re-equilibrate by changing their volume and content. This occurs by stretching, leakage and decrepitation of fluid inclusions when fluid pressure largely exceeds the confining pressure during further burial (e.g. McLimans 1987) and during heating (Mullis 1987; Tarantola et al. 2007). Fluid inclusions are reset by static or dynamic recrystallization of the host minerals (e.g. Wilkins and Barkas 1978). Furthermore, fluid inclusions are also modified under deviatoric stress and post entrapment ductile deformation (Tarantola & Diamond 2010). During retrograde evolution, stretching and decrepitation of high dense fluid inclusions might occur by isothermal pressure drop (Mullis 1987).

Our observations show that:

1. Fluids trapped at an early stage along the prograde path have mostly left the host mineral, due to fluid overpressure, decrepitation and recrystallization. Remaining fluid inclusions do not reflect composition and density of the fluid trapped during mineral growth.
2. Only very small fluid inclusions formed during prograde temperatures might be preserved and could reflect the prograde fluid composition, as recrystallization is not complete.
3. Hydrocarbon-saturated water-rich and water-saturated hydrocarbon-rich fluid inclusions formed at PT-maximum and during retrograde conditions are of reliable quality for geothermometry and geobarometry.
4. Fluid inclusions exposed to conditions of larger confining pressures than internal fluid inclusion pressure show tridimensional implosion features, and do not reflect the original trapping density.
5. Fluid inclusions exposed to post-entrapment ductile deformation by deviatoric stress form a bidimensional halo of neonate inclusions, revealing possible densities of the involved shearing event.
6. High dense fluid inclusions that were stretched or decrepitated by local and temporary pressure drop during retrograde conditions (due to seismic pumping or seismic valving) do not reflect the true composition and density of the original fluid.
7. High dense fluid inclusions that were stretched or decrepitated during "isothermal" uplift do not reflect composition and density of the original fluid.

REFERENCES

- McLimans, R.K. 1987: The application of fluid inclusions to migration of oil and diagenesis in petroleum reservoirs. *Applied Geochemistry* 2, 585-603.
- Mullis, J. 1987: Fluid inclusion studies during very low-grade metamorphism. In: *Low temperature metamorphism* (Ed. by Frey, M.). Blackie, Glasgow, pp.: 162-199.
- Tarantola, A. et al. 2007: Oxidation of methane at the CH₄/H₂O transition zone in the external part of the Central Alps, Switzerland: Evidence from stable isotope investigations. *Chemical Geology* 237, 329-357.
- Tarantola, A. & Diamond, L.W. (2011): Modification of fluid inclusions in quartz by deviatoric stress I: experimentally induced changes in inclusion shapes and microstructures. *Contributions to Mineralogy and Petrology* 160, 825-843.
- Wilkins, R.W.T & Barkas, J. P. (1978): Fluid inclusions, deformation and recrystallization in granite tectonites. *Contributions to Mineralogy and Petrology* 65, 293-299.

2.18

Density of alkaline magmas at crustal and upper mantle conditions by X-ray absorption

Rita Seifert¹, Wim J. Malfait¹, Sylvain Petitgirard² and Carmen Sanchez-Valle¹

¹ Institute for Geochemistry and Petrology, ETH Zurich, Zurich 8092, Switzerland

² European Synchrotron Radiation Facility, 38043 Grenoble, France

Silicate melts are essential components of igneous processes and are directly involved in differentiation processes and heat transfer within the Earth. Studies of the physical properties of magmas (e.g., density, viscosity, conductivity, etc) are however challenging and experimental data at geologically relevant pressure and temperature conditions remain scarce. For example, there is virtually no data on the density at high pressure of alkaline magmas (e.g., phonolites) typically found in continental rift zone settings.

We present *in situ* density measurements of alkaline magmas at crustal and upper mantle conditions using synchrotron X-ray absorption. Measurements were conducted on ID27 beamline at ESRF using a panoramic Paris-Edinburgh Press (PE Press). The starting material is a synthetic haplo-phonolite glass similar in composition to the Plateau flood phonolites from the Kenya rift [1]. The glass was synthesized at 1673 K and 2.0 GPa in a piston-cylinder apparatus at ETH Zurich and characterized using EPMA, FTIR and density measurements. The sample contains less than 200 ppm water and is free of CO₂. Single-crystal diamond cylinders ($\phi_{in} = 0.5$ mm, height = 1 mm) were used as sample containers and placed in an assembly formed by hBN spacers, a graphite heater and a boron epoxy gasket [2]. The density was determined as a function of pressure (1.0 to 3.1 GPa) and temperature (1630-1860 K) from the X-ray absorption contrast at 20 keV between the sample and the diamond capsule. The molten state of the sample during the data collection was confirmed by X-ray diffraction measurements. Pressure and temperature were determined simultaneously from the equation of state of hBN and platinum using the double isochor method [3]. The results are combined with available density data at room conditions to derive the first experimental equation of state (EOS) of phonolitic liquids at crustal and upper mantle conditions. We will compare our results with recent reports of the density of dry and hydrous rhyolite melts (Malfait et al., this meeting [4]) and discuss compositional effects on the density of melts and the implications for magmatic processes in the lower crust and magma chambers.

REFERENCES:

- [1] Hay D.E., Wendlandt R.F., 1995, *J. Geophys. Res.* 100, 401-410.
- [2] van Kan Parker M. et al., 2010, *High Pressure Research*, 30: 2, 332 – 341.
- [3] W.A. Chrichton, M. Mezouar, 2002, *High Temp.-High Press*, 34, 235.
- [4] Malfait W.J. et al., The density of dry and hydrous granitic magmas, AGU Fall Meeting 2011.

2.19

Application of high-precision U-Pb geochronology to igneous petrology and stratigraphy: Potential and limitations

Wotzlaw Jörn-Frederik¹, Schaltegger Urs¹, Frick Daniel A.², Hüsing Silja K.³, Bindeman Ilya N.⁴, Hilgen Frederik J.³ & Günther Detlef²

¹Section of Earth Sciences, University of Geneva, Geneva, Switzerland (Joern.Wotzlaw@unige.ch)

²Laboratory of Inorganic Chemistry, ETH Zurich, Zurich, Switzerland

³Department of Earth Sciences, Utrecht University, Utrecht, The Netherlands

⁴Department of Geological Sciences, University of Oregon, Eugene, USA

High-precision U-Pb geochronology of accessory minerals is an integral part of various Earth Science disciplines. Recent advances in U-Pb geochronology by isotope dilution – thermal ionization mass spectrometry (ID-TIMS) allow dating of high uranium accessory minerals (most commonly zircon) at permil precision and external reproducibility. Such high temporal resolution may result in complex zircon age populations, reflecting prolonged growth and magma residence, previously only resolvable by in-situ U-Th dating in Pleistocene magmatic systems. This allows to track the evolution of Cenozoic magmatic systems at unprecedented resolution and to add absolute time constraints to thermal and petrogenetic models (Crowley et al., 2007; Schaltegger et al., 2009). However, these complexities have also been considered to systematically bias zircon U-Pb derived eruption ages, to compromise chronostratigraphic applications of high-precision zircon U-Pb geochronology and to contribute to the systematic offset between the K-Ar and U-Pb systems (Simon et al., 2008; Renne et al., 2010). With this contribution, we aim to highlight [1] the potential of high-precision U-Pb geochronology in igneous petrology and [2] limitations for stratigraphic applications arising from pre-eruption residence time.

We obtained a large number of high-precision zircon U-Pb dates for some of the best-studied Cenozoic magmatic systems, i.e. the ~28 Ma Fish Canyon Tuff (Colorado, USA) and the ~56 Ma Skaergaard intrusive complex (East Greenland). In both cases, zircon U-Pb dates record 300,000 to 400,000 years of crystallization. Combined with zircon trace element and oxygen isotope geochemistry, respectively, high-precision zircon U-Pb dates provide snapshots of magma evolution. Chemical or isotopic differences within zircon populations as a function of age allow us to construct time-integrated petrogenetic models within the framework of independent petrologic constraints and thermal models.

In stratigraphic applications, where the desired age information is that of ash bed deposition, the pre-eruptive magmatic history recorded by zircons is a fundamental limiting factor. We present high-precision zircon U-Pb dates from ash beds intercalated with astronomically tuned Miocene sediments, aiming to quantify the effect of prolonged crystallization on zircon U-Pb derived ash bed deposition ages. All ash beds yield complex zircon age populations recording prolonged crystallization at the 10-100 ka scale. While the majority of zircons predate eruption, in most cases the youngest closed system zircons yield ²⁰⁶Pb/²³⁸U dates indistinguishable from the respective astronomical age and thus accurately date ash bed deposition. However, the conventional approach of averaging statistically equivalent zircon U-Pb dates to increase precision tends to overestimate the deposition age, if complexities are masked by uncertainties of individual analyses. We conclude that the precision of ash bed deposition ages is limited to the precision of individual single grain analyses.

REFERENCES

- Crowley, J.L., Schoene, B. & Bowring, S.A. 2007: U-Pb dating of zircon in the Bishop Tuff at the millennial scale. *Geology* 35, 1123-1126.
- Renne P.R., Mundil, R., Balco, G., Min, K. & Ludwig, K.R. 2010: Joint determination of 40K decay constant and ⁴⁰Ar*/⁴⁰K for the Fish Canyon sanidine standard, and improved accuracy for ⁴⁰Ar/³⁹Ar geochronology. *Geochim. Cosmochim. Acta* 74, 5349-5367.
- Schaltegger U., Brack, P., Ovtcharova, M., Peytcheva, I., Schoene, B., Stracke, A., Marocchi, M. & Bargossi, G.M. 2009: Zircon and titanite recording 1.5 million years of magma accretion, crystallization and initial cooling in a composite pluton. *Earth Planet. Sci. Lett.* 286, 208-218.
- Simon, J.I., Renne, P.R. & Mundil, R. 2008: Implications of pre-eruptive magmatic histories of zircons for U-Pb geochronology of silicic extrusions. *Earth Planet. Sci. Lett.* 266, 182-194.

P 2.1

Recent increase in Uranium Concentration in Lake Geneva Sediments: increased Inputs or enhanced chemical Precipitation?

Arlaux Yannick, Poté John, Thévenon Florian, & Loizeau Jean-Luc

Institut F.-A. Forel, Université de Genève, 10 route de Suisse, 1290 Versoix, Switzerland, Jean-Luc.Loizeau@unige.ch

Uranium concentration in Lake Geneva water is relatively high ($1.6 \mu\text{g U L}^{-1}$) compared to other freshwater bodies, due to a partly granitic, uranium-rich watershed. Moreover, intense works to collect and transport glacial melting waters to hydroelectric reservoir have enhanced the mobilization of U-enriched zones (Dominik et al. 1992). In order to reconstruct the uranium historical evolution in Lake Geneva, four sediment cores have been ^{137}Cs dated and analyzed using ICP-MS for their trace element composition. One core was recovered close to the Rhone River mouth (T52, 145 m depth; Fig. 1), whereas the other cores were collected in the deepest part of the lake (> 300 m depth, Fig. 1). The core close to the Rhone mouth didn't show any noticeable increase in U concentration during the last 50 years. On the other hand, the three sediment cores retrieved from the deep lake showed a clear increase in U concentration by a factor 2 to 3, with concentrations rising from 1 - 2 mg/kg to 4 - 5 mg/kg (Fig. 1). ^{137}Cs dating revealed that this increase occurred in the late 70's and was synchronous in the deep lake.

This period corresponded to the onset of two processes that could explain this variation: i) the increase in U inputs due to the large development of the water derivation in the watershed (tunnel under the Mont Blanc massif to Emosson dam), and ii) the eutrophication of the lake that induced increased flux of organic matter and hypoxia to anoxia in the deep lake, which can favor the precipitation of dissolved U. To decipher the origin of this U concentration increase, a mass balance model has been developed, to simulate the effect of the observed increased dissolved U inputs from the watershed. Results of the simulation showed that the additional dissolved load corresponded to an increase of about 2% of U in the lake water after 30 years, so that the observed enrichment in U might not be related to an increase in the source. Moreover, no U increase has been observed close to the Rhone river mouth which is the major tributary of the lake, then an increase of the particulate flux can be excluded. Therefore the other explanation pointed to an internal physicochemical origin for the enhanced U concentrations measured in Lake Geneva sediments. Eutrophication of the lake reached a maximum in the 70's, with extended periods of hypoxia in the deepest water layers. These conditions also occurred between 1986 and 1999, due to the absence of complete lake overturn. It is hypothesized that these hypoxic conditions favored the chemical precipitation and settling of dissolved form of uranium. Despite a marked increase in the U concentrations, the additional contribution to the sediments due to the eutrophication (200 kg/y) was minor compared to the dissolved U flux from the watershed (12500 kg/y).

REFERENCES

Dominik, J., Cuccodoro, S., Gourcy, L., & Santiago, S., 1992. Uranium enrichment in surface and groundwaters of the Alpine Rhône watershed. In Vernet, J.-P. (ed), Heavy metals in the Environment, Elsevier, Amsterdam, pp. 397-416.

P 2.2

Monazite and Allanite's textural evolution from lower to higher grade pelites of Miyar Valley, NW India

Banerjee Sriparna¹, Robyr Martin¹

¹*Institut für Geologie, Baltzerstrasse 1+3, CH-3012 Bern (1banerjee@geo.unibe.ch)*

The Himalayan metamorphic belt is a classic example of continent-continent collision (before 50-55 Ma), where ~1800-2500 km crustal shortening has occurred between the two plates of Indian and Eurasian. Number of thrust bounded slices has been developed within which the Higher Himalayan Crystalline (HHC), a 5-10 km thick sequence of amphibolite facies to migmatitic paragneiss preserves the metamorphic core of this orogen in Zaskar Himalayan terrain. The studied Miyar Valley section (Zaskar, NW India) consists of a single stratigraphic sequence of metapelites and -psammites which preserves a progressive increase in metamorphic conditions from the chlorite zone to the sillimanite zone and then in further migmatitic domain (Steck et al., 1999; Robyr et al., 2002; Robyr et al., 2006) (Fig. 1). The main aim of this work is to document any systematic variations in the chemistry and the texture of the identified accessory minerals and to estab-

lish the possible reaction path for the monazite formation. The extensive thin section study of this area reveals that the occurrence of the first metamorphic monazite coincides with the disappearance of allanite grains in metapelites. It should be emphasized that this transition in the stable LREE accessory phases occurs at the level of the staurolite-kyanite-in isograd, regardless whether the samples were collected in psammitic or pelitic layers. This observation strongly suggests that the LREE budget required for the monazite forming reaction is provided primarily by the breakdown of allanite. Textural observations indicate that the size and the complexity of the zoning pattern of the monazites significantly increase with the gradually increasing grade along the metamorphic field gradient. Below the sillimanite-in isograd, the size of the monazite grains generally does not exceed 50 μm , and the grains display no clear chemical zonation. Above the sillimanite-in isograd, the monazite grains preserve a complex zoning pattern, and the size of the grains is around 250-300 μm , where in further migmatite zone after muscovite out isograd, it may reach 400-500 μm having most complex zoning pattern. Allanite and monazite along with apatite also have been found as inclusions within garnet of the sillimanite zone rock, which strongly suggest that these allanites are from garnet zone captured within it. This textural arrangement is of major interest since it should permit the identification of an accurate P-T-t path for this specific garnet. The significance of this complex zoning and if there is any significant role of major silicates in formation of monazite are needed to assess further.

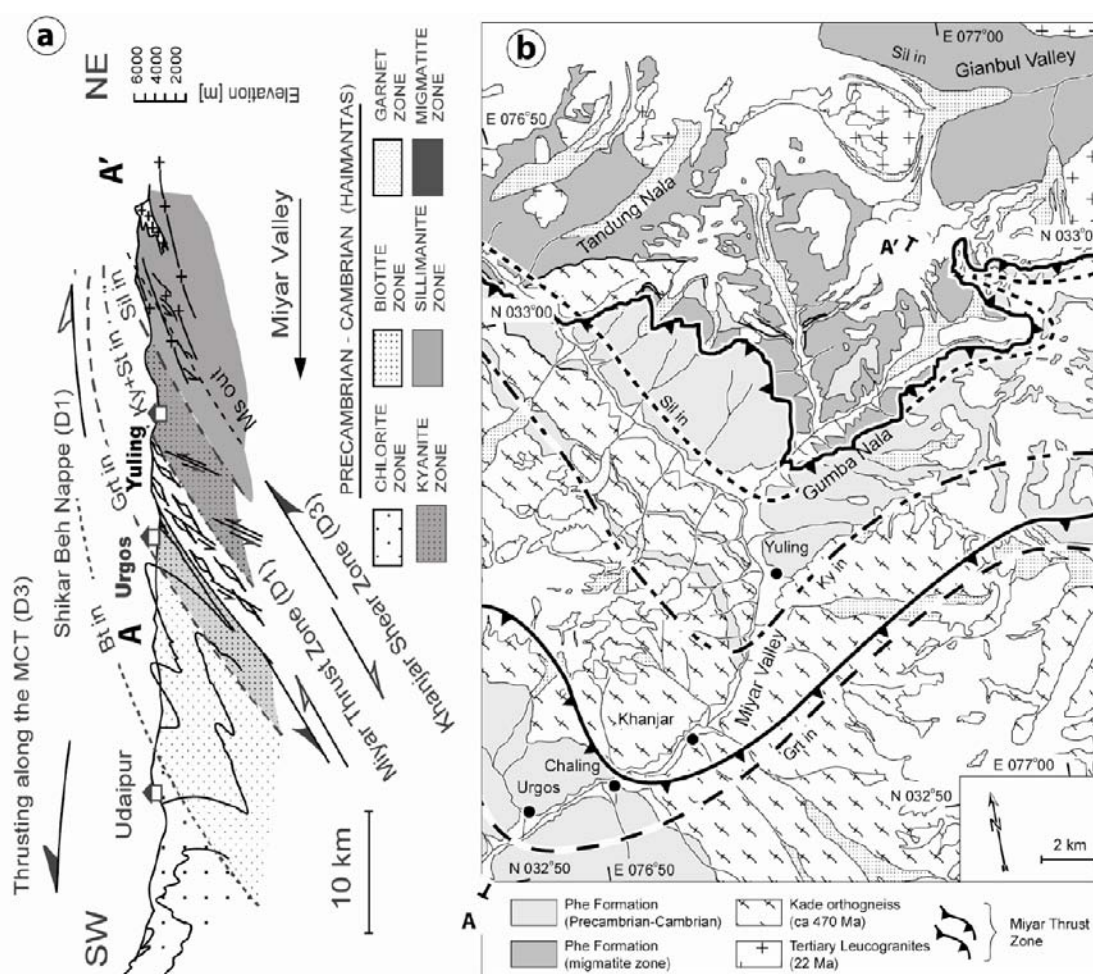


Fig. 1 : a) Cross-section along the Miyar Valley, b) Geological and metamorphic map of the Miyar Valley

REFERENCES

- Roby, M., Hacker, B.R., & Mattinson, J. 2006: Doming in compressional orogenic settings: New geochronological constraints from the NW Himalaya. *Tectonics*, v. 25, TC2007, doi:10.1029/2004TC001774
- Roby, M., Vannay, J.-L., Epard, J.-L., & Steck, A. 2002: Thrusting, extension and doming during the polyphase tectonometamorphic evolution of the High Himalayan Crystalline Sequence in NW India. *Journal of Asian Earth Sciences*, v. 21, p. 221-239.
- Steck, A., Epard, J.-L., & Roby, M. 1999: The NE-directed Shikar Beh Nappe - a major structure of the Higher Himalaya. *Eclogae Geologicae Helveticae*, v. 92, p. 239-250.

P 2.3

Explosion intensities and fragmentation modes of the Loolmurwak and Eledoi maar volcanoes, Lake Natron – Engaruka monogenetic field, northern Tanzania

Berghuijs Jaap F.¹, Mattsson Hannes B.¹

¹Institute of Geochemistry and Petrology, Swiss Federal Institute of Technology (ETH Zürich), Clausiusstrasse 25, 8092 Zurich, Switzerland

Two different theories currently exist on the explosion mechanism that is associated with diatreme volcanism. Some authors advocate a 'dry' eruption scenario in which gas exsolved from rising magma causes explosive activity, whereas others prefer a phreatomagmatic course of events in which diatreme formation is the result of interaction between magma and ground or surface water. However, only the later eruption mechanism is currently held viable for maar volcanoes, even though they are commonly, if not inevitably, associated with diatremes.

The Eledoi and Loolmurwak maars (Lake Natron - Engaruka monogenetic field, northern Tanzania) form two of the largest craters in an area of more more than 100 cones. Preliminary field evidence is in line with a recent study of Mattsson & Tripoli (2011) and suggests that craters in this area provide little evidence of wet deposition, such as accretionary lapilli and vesiculated tuffs. Rather, several observations point towards a dry mode of deposition, including a presumably wind-induced asymmetry of the crater rim (Eledoi) and the dominance of sub-spherical armoured lapilli, the core of which consists of olivine, pyroxene or amphibole phenocrysts (Loolmurwak, Fig. 1). Many of these lapilli show flattening parallel to the bedding plane, suggesting that they were molten droplets at the time of the eruption.

Magmas of both Loolmurwak and Eledoi are nephelinitic or olivine melilititic in composition. The abundance of phlogopite and amphibole megacrysts (up to 11 and 20 cm in diameter, respectively) indicates a high volatile content. Common in especially the Eledoi deposits is the occurrence of mantle xenoliths (predominantly dunites and wehrlites) that are frequently cut by several generations of metasomatic veins (containing amphibole, phlogopite, clinopyroxene and spinel). Mantle xenolith sizes suggest a minimum average magma ascent rate of 0.9 ms^{-1} for the Eledoi eruption.

The rapid ascent rate of the involved magmas from upper-mantle depths and the exsolution of abundant volatiles, together with pyroclast shapes and textures that indicate 'dry' magmatic fragmentation and deposition, indicate that the emplacement mechanism of the Eledoi and Loolmurwak maar craters is very similar to that typical for many kimberlites. Consequently, a more detailed study of pyroclast textures, mineralogy and chemistry of the Eledoi and Loolmurwak deposits can provide valuable new insights into maar emplacement processes.

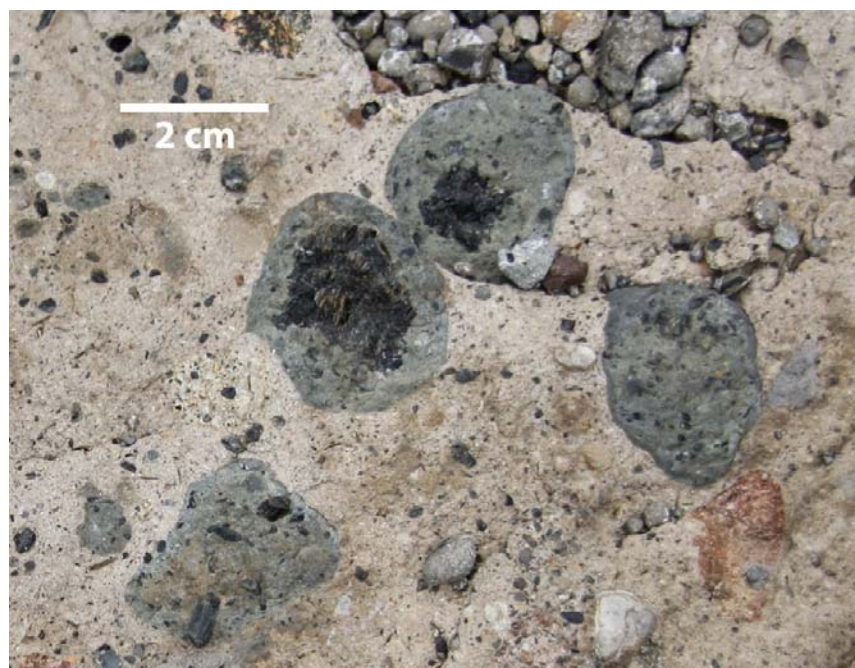


Figure 1. Subspherical armored lapilli within an ash matrix (Loolmurwak maar deposits). Lapilli cores predominantly consist of amphibole, pyroxene and olivine. Picture by J.F. Berghuijs.

REFERENCES

Mattsson, H.B., Tripoli, B.A., 2011: Depositional characteristics and volcanic landforms in the Lake Natron–Engaruka monogenetic field, northern Tanzania. *Journal of Volcanology and Geothermal Research*, 203(1-2), 23-34.

P 2.4

Stratigraphy and sedimentology of the Cretaceous host-rocks of the Madneuli gold-polymetallic deposit, Lesser Caucasus, southern Georgia: A new approach

Tamara Beridze¹, Sophio Khutsishvili¹, Nino Popkhadze¹, Robert Moritz², Vladimer Gugushvili¹

¹Alexandre Janelidze Institute of Geology of Ivane Javakishvili Tbilisi State University (tamara_beridze@yahoo.com)

² Université de Genève, Rue des Maraîchers 13, CH-1205 Genève

The Madneuli gold – copper – polymetallic deposit is located in the Bolnisi volcano tectonic depression between the Khrami and Loki pre-Alpine basement massifs. It is hosted by Cretaceous volcanic and volcano – sedimentary strata. In spite of intensive investigation and study of the deposit since its exploration in 1958, its origin is still debated. Recognition of sedimentary facies units within volcanic settings and especially those hosting ore bodies, based on process – oriented sedimentation has been neglected so far in our study area.

Our new sedimentological study of the Madneuli host rocks is focused on field and facies oriented analyses, and is based on the concept of flow transformations (gravity, body and surface types) that links the general volcanoclastic facies (single event) within a space – time framework from source to final deposition (proximal to distal, syn-, inter – or post eruptive, Fisher and Schminke, 1994). Based on this approach, we identified stratified tuff and lapilli tuff, subsidiary breccia – conglomerate and conglomerate – sandstone, slide – slump, accretionary lapilli-bearing tuff and tuffaceous units within the open pit and surrounding areas. Previous observations by Popkhadze et al. (2009) were confirmed and some were reinterpreted. The common transport mode operating within the area was deposition of volcanic and volcanoclastic – epiclastic material by debris, pyroclastic and ash flows, in some cases with flow transformation into density turbidity currents. Slide – slump units indicate downslope movement of sediments, either along the volcano flanks triggered by volcano – tectonic events or gravitational slumping within debris apron environments. Graded layers of accretionary lapilli and ash represent airfall pyroclastic deposits, interlayered with non-fall layers with current structures suggesting entering moving water. Bouma sequences developed in these layers are not related to transportation by turbidites (Lowe, 1988). Tuffites associated with slump units are interpreted as alteration of lapilli and fine ash – flow tuffs and might reveal a hemipelagic environment during deposition. Red – brown polymict volcanoclastic – epiclastic conglomerates and sandstones are products of channelized mass flow deposition.

In volcanic environments, volcanic eruptions control facies stratigraphy and geometry. Thus, stratification and correlation of the rocks units within the Madneuli ore field is complicated and is reflected in rapid lateral and vertical changes, with abundant structural – volcanic unconformities, poor fauna preservation, and lack of modern precise radiochronological data. The combined stratigraphic subdivision of the Cretaceous suites of the area is based on two different schemes used by Gambashidze et al. (1987) and Vashakidze et al. (1998). It also includes recent data based on a nanofossil study of the host rocks (Gavtadze et al., 2006) and existing K-Ar geochronological data. Our study clearly shows incompatibilities between the boundaries of the suites and in some cases their debatable ages. Modern stratigraphic studies are based on the fundamental understanding of global sedimentary and tectonic processes. That is why we suggest to define stratigraphic units on the basis of basin – wide relationships by paying great attention to the regional framework.

We conclude that detailed and complex stratigraphic – sedimentological study within the Madneuli ore field together with litho – and biostratigraphic, seismic, subsurface and basin mapping methods is essential in correct subdivision of the rock units.

REFERENCES

- Fisher R.V., Schminke H.U. (1994). Technical report from: Volcanoclastic sediment transport and deposition in K.Pye. Sediment transport and depositional processes. Blackwell Scientific Pub. p.351-388;
- Gambashidze R.A., Nadareishvili G.Sh. (1987). Structure and stages of development of the Upper Cretaceous volcanogenic – sedimentary formation of SE Georgia. In G.A. Tvalchrelidze (Ed) Volcanism and formation of useful minerals in mobile regions of the Earth «Metsniereba», Tbilisi.
- Gavtadze T., Migineishvili R., Khutsishvili S. (2006). New data on the age of enclosing rocks of the Madneuli copper – gold deposit. STII Journal Georgian Oil and gas. N7, p.33-37.
- Lowe Donald R. (1988). Suspended – load fallout rate as an independent variable in the analyses of current structures. Sedimentology, v.35, p.765-776;
- Popkhadze N., Beridze T., Moritz R., Gugushvili V., Khutsishvili S. (2009). Facies analyses of the Volcano – sedimentary host rocks of the Cretaceous Madneuli. VMS deposit, Bolnisi district, Georgia Bulletin of GNAS, vol.3, p.103-108;

P 2.5

Evolution of composition, temperature and pressure of fluid inclusions through the NEAT Lötschberg base tunnel

Felix Hélène¹ & Mullis Josef¹

¹Mineralogisch-Petrographisches Institut, Bernoullistrasse 30, CH-4056 Basel, Switzerland (felix.helene@unibas.ch)

The present research project is part of a multi-faceted research programme along the new alpine railway transverses NEAT. This project focuses on the investigation on fluid inclusions in the Lötschberg NEAT tunnels and boreholes.

Fluid inclusions are witnesses of the fluids from which the Alpine minerals precipitated in Alpine fissures several million years ago. Alpine fissures are generally small, closed ore opened hydrothermal systems that document the evolution of deformation, fluid composition, temperature and pressure during uplift and cooling (erosion) of the surrounding rocks.

The following aims are envisaged:

1. to understand the evolution of fluid composition, temperature and pressure during uplift and cooling along the Lötschberg transect;
2. to recognize the origin of the mineralizing fluids.

Microthermometric investigations on fluid inclusions in fissure quartz from boreholes, shafts and tunnels along the NEAT Lötschberg transect yield the following preliminary results:

1. Fluid composition evolves from higher hydrocarbon-bearing fluids (HHC-zone) close to Frutigen to methane-bearing fluids (methane-zone) at around 2 km South of Frutigen. Water-rich fluids with less than 2 mole % of CH₄ and CO₂ are characteristic for the sedimentary cover of the Northern Gastern Granit and all crystalline rocks of the Gastern and Aar massifs (water zone). The transition from the methane- to the water-zone occurs below the valley of Gasteretal. Up to 5 mole-percent of CO₂ within fluid inclusions are diagnostic for the Triassic metasedimentary cover of the Southwestern Aar massif.

2. Temperature and pressure develop from the HHC-zone at ≤150 °C and ~1.5 kbar to the HHC-methane transition at 200±5 °C and 2 kbar (Mullis 1979). The formation of methane is interpreted to be the maturation product of higher hydrocarbons, due to "burial" or "overthrusting". Methane break down occurs at 270 °C, due to redox-reactions between iron three bearing phyllosilicates and methane (Mullis et al. 1987; Tarantola et al. 2007). The dominance of aqueous saline fluids in the Gastern and Aar massifs is controlled by the lack of organic matter, dehydration reactions, as well as water-bearing metasediments situated probably below the massifs (Mullis et al. 1994). The increase of CO₂ in the Triassic metasedimentary cover is probably due to decarbonation reactions or oxidation of organic matter at temperatures and pressures of around 400 °C und 3.5 kbar.

REFERENCES

- Mullis, J. 1979: The system methane-water as a geologic thermometer and barometer from the external part of the Central Alps. *Bull. Minéralogy* 102, 526-536.
- Mullis, J. 1987: Fluid inclusion studies during very low-grade metamorphism. In: *Low temperature metamorphism* (Ed. by Frey, M.). Blackie, Glasgow, pp.: 162-199.
- Mullis et al. 1994: Fluid regimes during late stages of a continental collision: Physical, chemical, and stable isotope measurements of fluid inclusions in fissure quartz from a geotraverse through the Central Alps, Switzerland. *Geochimica Cosmochimica Acta* 58, 2239-2276.
- Tarantola, A. et al. 2007: Oxidation of methane at the CH₄/H₂O transition zone in the external part of the Central Alps, Switzerland: Evidence from stable isotope investigations. *Chemical Geology* 237, 329-357.

P 2.6

Geology of Piz Duan: an oceanic sequence in the Avers schists, Grisons

Fulda Donat

Schweizerische Geotechnische Kommission, Sonneggstrasse 5, CH-8092 Zürich (donat.fulda@erdw.ethz.ch)

A sediment-rich ophiolite unit can be mapped in the southern part of the Avers schists N of Val Bregaglia (southern Grisons). This so-called Duan-Cam unit (DCU) has a lenticular shape and is outlined by small lenses of serpentinite against the adjacent rock units. Its internal structure shows strong imbrication and folding, but the stratigraphic sequence is coherent and consists of three main rock types. The surrounding units (Avers schists above, Suretta nappe below) have a similar grade of deformation and metamorphism.

The main rock types comprise greenschists, banded quartz schists and calcite marbles. They represent the sequence of metamorphic basalt, radiolarite and limestone (pers. comm. P. Nievergelt). Both, the stratigraphy as well as preserved submarine volcanic structures (pillow lava) allow the DCU unit to be interpreted as a relic of an oceanic sequence in greenschist facies. This interpretation is confirmed by geochemical analysis which indicates a mid-ocean ridge basalt as protolith of the basic rocks. However, some of the metabasic rocks no longer show the original basaltic chemistry. These glaucophane-bearing metabasalts (prasinities, spilites) underwent strong oceanic hydrothermal alteration (Fe and Na-enrichment, Oberhänsli 1978).

The Duan-Cam unit is situated in the footwall of the Turba mylonite zone (TMZ) (Nievergelt et al., 1996), less than 1 km below this shear zone. The deformation of the Avers schists includes shearing to the SE and finally the development of the TMZ with top to the E movement. Five deformation phases (D1–D5) can be distinguished in the DCU, two of which (D2 and D3) are related to the TMZ. D1 and D2 are strong deformation events, which caused isoclinal folding, penetrative foliations and imbrication. The structures of D1, which were formed during mesoalpine nappe stacking (Schreurs, 1995),

have been largely overprinted by D2 structures. Phases D3 to D5 show increasingly weaker deformation from narrow folding to kinking. Apart from D3 all deformation phases within the DCU can be correlated with deformation events postulated by researchers for the surrounding units, e.g. in the Austroalpine-Pennine boundary (Liniger & Nievergelt, 1996), the Suretta and Tambo nappe (Huber, 1996), Schams nappes (Schreurs, 1995). In contrast, the prominent D3 phase, which shows open to narrow folding with developing axial plain foliation, seems to be a local structural phenomenon, which cannot be observed in the surrounding units. Whereas the prominent D2 overprint is a consequence of the main extensional episode of the TMZ, it is assumed that D3 was generated by a second, slightly weaker Turba extension event, which only affected the directly underlying DCU.

The most conspicuous formation of new minerals took place during early deformation of the DCU. Glaucophane was formed late post-D1 to syn-D2 and altered syn-D2 to barrosite under retrograde metamorphic conditions. Stability fields of glaucophane and barrosite (Ernst, 1979) indicate P-T conditions of 6.5 kbar and 400 °C for D2. Rutile occurs as inclusion in glaucophane and was therefore formed syn-D1. Similar to the Zermatt-Saas region in the Western Alps the occurrence of glaucophane and rutile could be a relic of a high-pressure metamorphic event (Dal Piaz & Ernst, 1979). Furthermore pseudomorphs after an unknown syn-D1 formed mineral can be observed. These facts indicate a metamorphic evolution that started earlier than reported so far in this area. However, because of the absence of additional high-pressure indicative minerals like e.g. lawsonite, unequivocal evidence for high pressure metamorphism in the DCU cannot yet be verified.

REFERENCES

- Ernst, W.G. (1979): Coexisting sodic and calcic amphiboles from high-pressure metamorphic belts and the stability of barrositic amphibole. *Mineralogical Magazine* 43, 269-278.
- Fulda, D. (2000): Geologisch-petrographische Untersuchungen am Piz Duan (Val Bregaglia, Graubünden). Unpubl. MSc thesis University of Zurich. 146 pages
- Huber, R.K., Marquer, D. (1996): Tertiary deformation and kinematics of the southern part of the Tambo and Suretta nappes (Val Bregaglia, Eastern Swiss Alps). *Schweiz. Mineral. Petrogr. Mitt.* 76, 383-398.
- Liniger, M. & Nievergelt, P. (1990): Stockwerk-Tektonik im südlichen Graubünden. *Schweiz. Mineral. Petrogr. Mitt.* 70, 95-101.
- Nievergelt, P., Liniger, M., Froitzheim, N. & Mählmann, F. (1996): Early to mid Tertiary crustal extension in the Central Alps: The Turba Mylonite Zone (Eastern Switzerland). *Tectonics* 15, 329-340.
- Oberhänsli, R. (1978): Chemische Untersuchungen an Glaukophan-führenden basischen Gesteinen aus den Bündnerschiefern Graubündens. *Schweiz. Mineral. Petrogr. Mitt.* 58, 139-156.
- Schreurs, G. (1995): Geometry and kinematics of the Schams nappes and adjacent tectonic units in the Penninic zone. *Beiträge zur Geologischen Karte der Schweiz* 167.

P 2.7

Ordovician mafic magmatism in the Métailler Formation of the Mont-Fort nappe (Middle Penninic domain, western Alps) – geodynamic implications

Gauthiez, Laure¹, Bussy François¹, Ulianov Alexey¹, Gouffon Yves², Sartori Mario³

¹Institut de Minéralogie et Géo chimie, Université de Lausanne, CH-1015 Lausanne (laure.gauthiez@gmail.com)

²Swisstopo, CH-3084 Wabern

³Université de Genève, Rue des Maraîchers 13, CH-1205 Genève

The Métailler Formation belongs to the basement of the Mont-Fort nappe, in the Middle Penninic domain of the western Alps. It consists of a heterogeneous volcanic detrital sequence dominated by mafic components including pillow-lavas and banded gabbros bodies. The age and significance of these lithologies have been debated since more than 50 years (e.g. Schaer, 1959; Chessex, 1995). These rocks have been strongly reworked by Alpine metamorphism and deformation in the greenschist facies. Metagabbro bodies are outcropping in the small Louvie valley, SE of Verbier (Wallis). They are composed of multiple coarse-grained bands (20cm to 5m thick) (Fig. 1a) of close but distinct chemical composition. Cm-long dark spots made of an actinolite ± chlorite ± epidote assemblage mimic former magmatic pyroxenes. These textural features as well as the shape and position of the gabbro bodies within the sedimentary host-rock suggest a sill-on-sill emplacement style in the volcanic-detrital sequence.

Magmas have a composition of continental tholeiites of E-MORB type, including differentiated facies as Ti-rich gabbros. Small volumes of albite-rich evolved liquids form discordant dikelets or segregates within the gabbros and contain zircons. The latter show unusual sponge-like textures (Fig. 1b) interpreted as the result of a metamorphic dissolution-recrystallization process triggered by Na-rich fluid circulation during Alpine metamorphism, in a similar way as described by Rubatto et al. (2008). LA-ICPMS U-Pb dating of preserved magmatic zircon cores yielded mean concordant ²⁰⁶Pb/²³⁸U ages of 456.7 ± 5 Ma and 462 ± 4/-7 Ma, respectively (Fig. 2).

Detrital zircons in the gneissic metasedimentary host rock display a large age range from Achaean rounded grains (3.5 Ga for the oldest) to Cambrian-Ordovician prismatic grains (550 to 475 Ma). As the youngest detrital zircon (456 ± 9 Ma) and the intruding gabbros have the same age within errors, deposition of the volcanic-detrital sequence occurred in a short time span. The mafic volcanic component in the sediments is also very close in composition to the gabbro intrusions and thus seems linked to the same magmatic event.

The Métailler Formation is interpreted as a sedimentary basin infill with a continental input documented by Achaean detrital zircons, located close to a mafic volcanic centre. The sedimentary context and the magma compositions are consistent with a back-arc environment. According to geodynamic reconstructions (e.g. Stampfli et al. 2011), the future Middle Penninic domain was part of the north-Gondwanan active margin at that time, which was progressively drifting off main Gondwana in response to the southward subduction of a northern oceanic domain. Thus the Ordovician Métailler Basin might document the early back-arc opening of north-Gondwana which ultimately gave birth to the eastern Rheic ocean.

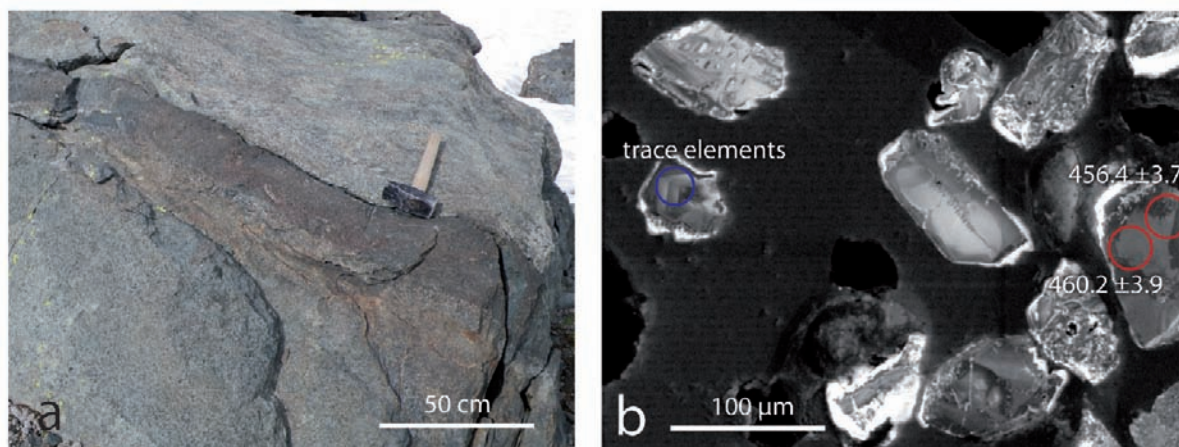


Figure 1. a) Banded gabbro body; b) Zircons of an albitic dikelet (epoxy mount, cathodoluminescence image, circles are LA-ICPMS (25µm) analysis spots.

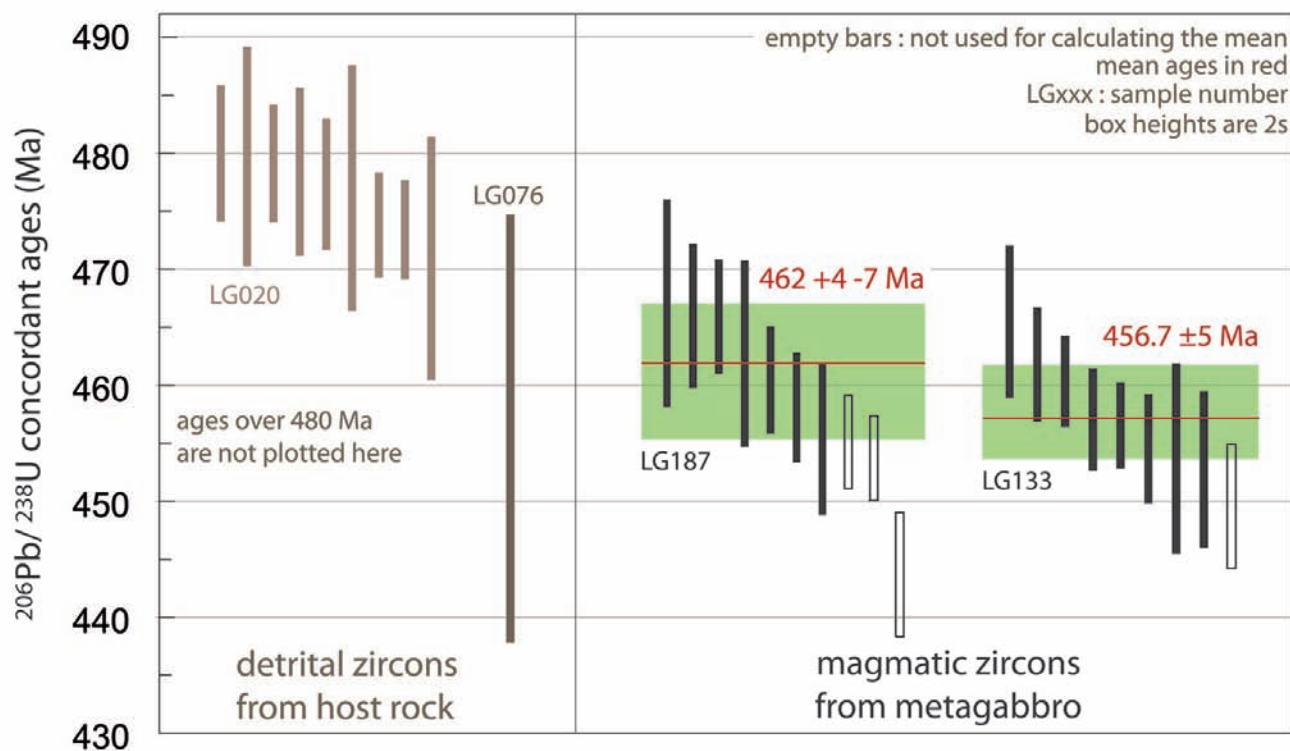


Figure 2. Summary of LA-ICPMS concordant $^{206}\text{Pb}/^{238}\text{U}$ zircon ages.

REFERENCES

- Chessex, R. 1995: Tectonomagmatic setting of the Mont Fort nappe basement, Penninic domain, Western alps, Switzerland. In: Proceedings of the international earth sciences colloquium on the Aegean region. - vol. 1, 19-35.
- Rubatto, D., Müntener, O., Barnhoorn, A., & Gregory, C. 2008: Dissolution-reprecipitation of zircon at low-temperature, high-pressure conditions (Lanzo Massif, Italy). - *American Mineralogist*. 93 (10), 1519-1529.
- Schaer, J.-P. 1959: Géologie de la partie septentrionale de l'éventail de Bagnes (entre le Val d'Hérémence et le Val de Bagnes, Valais, Suisse). - *Arch. Sci. (Genève)* 12/4, 473-620.
- Stampfli G.M., von Raumer, J. & Willhem, C. 2011: The distribution of Gondwana derived terranes in the early Paleozoic. Abstracts of the 11th Int. Symposium on the Ordovician System Alcalá de Henares (Madrid).

P 2.8

Geochemistry of Paleocene-Eocene limestones from Ching-dar syncline, west of Birjand, east of Iran

Hashemi Azizi S. Halimeh¹, Mirab Shabestari Gholamreza² & Khazaei Ahmadrza³

¹M.Sc. student, Department of Geology, University of Birjand/Iran (hashemi.azizi@gmail.com)

²Assistant Professor, Department of Geology, University of Birjand/Iran

³Assistant Professor, Department of Geology, University of Birjand/Iran

The Ching-dar syncline area is located in the east of Iran belt (after Alavi, 1991) (fig. 1). The studied sequence is about 500 m in thickness and consists of both skeletal and non-skeletal grains e.g. foraminifera, green algae, peloids, and intraclasts. They were deposited in a shallow marine carbonate ramp. The studied limestones were subjected to extensive diagenetic processes with varying intensities, the most important of which are cementation, compaction (mechanical and chemical), internal filling and stylolitization. Chemical analysis of the limestone samples revealed high calcium and low magnesium content.

Major and minor elements values were used to determine the original carbonate mineralogy of the Ching-dar limestones. Petrographic evidences and elemental analysis indicated that calcite was the original carbonate mineral in the Ching-dar limestones. The amounts of Mn and Sr/Na ratio in the studied samples, compared to the sub-polar cold-water Permian limestone, sub-tropical warm-water Ordovician aragonite (Rao, 1990, 1991), recent tropical shallow-marine aragonite (Milliman, 1974) and recent temperate bulk carbonate (Rao & Adabi, 1992; Rao & Jayawardane, 1994; Rao & Amini, 1995) indicate original carbonate mineralogy.

The elemental compositions of the Ching-dar carbonates also illustrate that they have been stabilized in a meteoric-phreatic diagenetic environment. Variations of Sr/Ca ratio versus Mn suggest that diagenetic alteration has occurred in an open system.

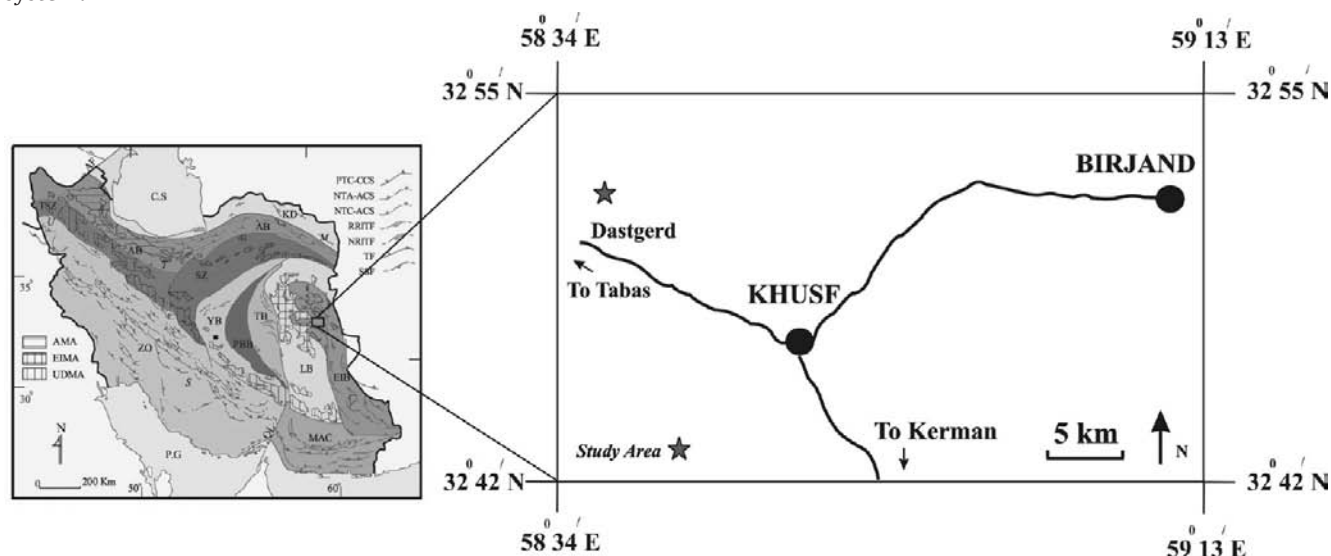


Fig 1. Left: Generalized tectonic map of Iran (after Alavi, 1991), EIB-east of Iran belt. Right: simplified location map of the studied area.

REFERENCES

- Alavi, M., 1991b: Tectonic map of the Middle East, 1:5000000, Geological Survey of Iran.
- Milliman, J.D., 1974: Marine carbonates, New York, Springer-Verlag, 375.
- Rao, C.P., 1990: Petrography, trace elements and oxygen and carbon isotopes of Gordon Group carbonate (Ordovician), Florentine Valley, Tasmania, Australia, *Sedimentary Geology*, 66, 83–97.
- Rao, C.P., 1991: Geochemical differences between subtropical (Ordovician), temperate (Recent and Pleistocene) and subpolar (Permian) carbonates, Tasmania, Australia, *Carbonates and Evaporites*, 6, 83–106.
- Rao, C.P., Adabi, M.H., 1992: Carbonate minerals, major and minor elements and oxygen and carbon isotopes and their variation with water depth in cool, temperate carbonates, western Tasmania, Australia, *Marine Geology*, 103, 249–272.
- Rao, C.P., Amini, Z.Z., 1995. Faunal relationship to grain-size, mineralogy and geochemistry in recent temperate shelf carbonates, western Tasmania, Australia. *Carbonates and Evaporites*, 10, 114–123.
- Rao, C.P., Jayawardane, M.P.J., 1994. Major minerals, elemental and isotopic composition in modern temperate shelf carbonates, eastern Tasmania, Australia: implications for the occurrence of extensive ancient non-tropical carbonates. *Palaeogeography, Palaeoclimatology, Palaeoecology*, 107, 49–63.

P 2.9

New age constraints on the opening of the Piemont-Ligurian Ocean (Tasna-Nauders area, CH-A)

Hauser Anne-Cécile¹, Müntener Othmar¹

¹*Institute of Mineralogy and Geochemistry, University of Lausanne, Anthropole, CH-1015 Lausanne (anne-cecile.hauser@unil.ch)*

The Engadine Window in Eastern Switzerland/Western Austria exposes the Lower-Middle Penninic Tasna nappe, which was recognized to preserve a pre-alpine Ocean-Continent-Transition (OCT) by Florineth (1994) and Florineth & Froitzheim (1994) in the Piz Minschun area. The present study confirms the observed OCT geometry in a more eastern part of the Tasna nappe at the border between Switzerland and Austria: Mapping of the area SW of Nauders reveals the contact between serpentinitized spinel-lherzolites and NE-ward out-wedging upper-continental crust which is sealed by a continuous layer of sediments. Compilation of geological maps of the South-Western part of the Window allows lateral connection of the newly mapped Nauders-OCT with the Tasna-OCT of Florineth (1994) around the border of the Window. The obtained overall geometry shows an approximately 8km long extensional allochthonous block comprising pre-, syn- and post rift sediments in normal position whose northern-, eastern- and southern border can be delimited. The lateral width of this block is undefined because it disappears beneath the Austroalpine nappes in the West.

Petrologic and geochemical investigations on serpentinites and (former-) garnet-pyroxenites confirm the subcontinental origin of the Tasna mantle and allow constraining its evolution. Pyroxenites formed at depths of at least 45km as indicated by the presence of garnet pyroxenites. Garnet subsequently almost completely decomposed to spl-opx-cpx symplectites by reaction with olivine in the spinel stability field at temperatures of initially ~830-950°C and shallower depth of 30-45km.

This corresponds to an uplift of the mantle rocks below a thinned continental crust and can possibly be linked with the late Carboniferous-Permian extension event. Almost complete decomposition of garnet associated with recrystallization and beginning equilibration of primary pyroxenes indicates relatively long residence at this sub-crustal depth during which the rocks cooled. The last event recorded in the mantle before exhumation is percolation of a K-rich Ca-poor alkaline liquid leading to formation of phlogopite and zircon in small, local veins. This event represents the rise of the first, unambiguous rift-related magmatic liquids in the area. Age determination on such a vein yields U-Pb ICP-MS crystallisation age of 167.3 ± 2.7 Ma for zircon and an Ar-Ar age of 167.55 ± 0.9 Ma and 167.9 ± 1.4 Ma for phlogopite, these ages are identical to the Ar-Ar phlogopite age of 170.5 ± 0.4 Ma and 169.1 ± 0.4 Ma obtained for the Tasna mantle (Manatschal et al. 2006).

These ages indicate Middle-Jurassic magmatism for low-degree mantle melts and are consistent with ages known for the South Penninic Piemont-Ligurian Ocean. They argue against a lower Cretaceous rifting of the NE part of the Valais domain and confirm the South Penninic origin of the Nauders-Tasna nappe already proposed by Manatschal et al. (2006).

REFERENCES

- Florineth, D. 1994: Neue Beobachtungen zur Ozeanbildung und zur alpinen Tektonik in der Tasna-Decke (Randbereich zwischen Nord- und Mittelpenninikum, Unterengadin). Unpublished Diplomathesis, ETH Zürich.
- Florineth, D. & Froitzheim, N. 1994: Transition from continental to oceanic basement in the Tasna nappe (Engadine window, Graubünden, Switzerland): evidence for Early Cretaceous opening of the Valais ocean. *Schweizerische Mineralogische u. Petrographische Mitteilungen*, 74, 437-448.
- Manatschal, G., Engström, A., Desmurs, L., Schaltegger, U., Cosca, M., Müntener, O. & Bernoulli. 2006: What is the tectono-metamorphic evolution of continental break-up: The example of the Tasna Ocean-Continent Transition. *Journal of Structural Geology* 28, 1849-1869.

P 2.10

Origin and Paleotectonic Conditions of Formation of Ore-Containing Fractures of the Lichk-Aygedzor Ore Field of Southern Armenia, Lesser Caucasus

Hovakimyan Samvel

Institute of Geological Sciences, National Academy of Sciences of The Republic of Armenia, Yerevan (samvel@geology.am)

The Lichk-Aygedzor ore field lies in the central part of the Megri composite pluton in Southern Armenia, between Kadjaran in the north and Agarak in the south. As opposed to the adjacent blocks, where large reserves of copper-molybdenum deposits are concentrated (Kadjaran, Agarak), the Lichk-Aygedzor block is distinguished by a spatial coincidence of deposits with average reserves of copper-molybdenum and gold-sulphide formations. They are: Terterasas, Tey, Lichkvaz gold-sulphide and Lichk, Aygedzor copper-molybdenic deposits.

The composite Meghri pluton consists of a broad spectrum of intrusive rocks of Upper Eocene-Lower Oligocene age, including olivine gabbro, monzonite, syenogranite, granodiorite, as well as porphyritic granite-granodiorite of Lower Miocene age (Melkonyan et al. 2008).

The controls of the ore deposits and prospects of the ore district are attributed by Hovakimyan & Tayan (2008) to circum-latitudinal and northeastern-oriented discontinuous fractures, particularly, the intersection with east-west-oriented fractures.

On the basis of our knowledge about the formation mechanism of fractures under shearing conditions (Sylvester 1988 and others), we made an effort to analyze the possible shifts of blocks during ore formation.

The investigated deposits were controlled by the above-mentioned circum-north-south-oriented fractures and the intersection with other fracture systems, particularly, circum-latitudinal and north-eastern extensions. The right-shearing displacements by the ore-controlling fractures analyzed on block-diagrams (Hovakimyan & Tayan 2008) contributed to open of northeastern-oriented fractures, containing copper-molybdenum and gold-sulphide mineralization. It is important to take into account the latter circumstance during projection of the numerous ore prospects and it can significantly contribute to the productivity of geological prospecting programs.

With the aim of reconstruction of the plan of deformation and spatial orientation of the axes of paleo-stresses (Gzovskiy 1975), during field work, we defined adjoint systems of spalling cracks, measured the orientation of lineations along fracture planes, which underwent shearing displacements. We also used the maximum data of circular crack diagrams.

For the axes of stresses, according to Gzovskiy (1975), we used the notation of axis of compression and extension- σ_3 and σ_1 , respectively. The intermediate axis being $-\sigma_2$, whereby $\sigma_3 \geq \sigma_2 \geq \sigma_1$.

Based on our results, the compressive forces were oriented along southwest and northeast directions and contributed to the spatial orientation of the axes of paleo-stresses and formation of tectonic fracturing of the Lichk-Aygedzor ore field. The axes of compression were oriented towards the horizon under average angles of 30-35°.

The dynamic conditions produced by stresses oriented northeast-southwest were favorable for the right shearing displacements by the plates of circum-meridional ore-controlling fractures with development (renewal) in the ore stage of north-eastern oriented ore-containing systems of cracks undergoing opening. Their orientation parallel to regional northeastern-southwestern compression and circum-horizontal location of axis of elongation, transverse to ore-containing fractures contributed to the conditions of extension.

The same direction of paleo-stresses together with the general orientation of axis of the north-south compression was obtained during recent regional investigations (Avagyan et al. 2005), and was related to the movement of secondary blocks during Arabian - Eurasian convergence.

REFERENCES

- Avagyan, A., Sosson, M., Philip, H., Karakhanian, A., Rolland, Y., Melkonyan, R., Rebai, S., Davtyan, V. 2005: Neogene to Quaternary stress field evolution in Lesser Caucasus and adjacent regions using fault kinematics analysis and volcanic cluster data. *Geodinamica Acta* 18/6. pp. 401-416.
- Gzovskiy, M.V. 1975: *Basis of Tectonic Physics*. M.: Science, 530p
- Hovakimyan, S.E. & Tayan, R.N. 2008. The Lichk-Aygedzor ore field ruptures and mineralization location conditions. *Izvestia of National Academy of Sciences of Armenia, Nauki o Zemle*, No 3, p.3-12.
- Melkonyan, R.L., Goukasyn, R.Kh., Tayan, R.N. & Harutyunyan, M.A. 2008: Geochronology of Monzonites of Meghri Plutonium (Armenia) –Results and Consequences. *Izvestia of National Academy of Sciences of Armenia, Nauki o Zemle*, volume LXI, No 2 p.3-9.
- Sylvester, A.G. 1988: Strike-slip faults. // *Geol. Soc. Amer. Bull.* vol.100, p.1666 – 1703.

P 2.11

The influence of bulk and mineral ferric/ferrous ratios on thermobarometry of the Syros/Sifnos blueschists: Towards a new thermodynamic model for high pressure amphiboles

Hunziker Daniela¹, Burg Jean-Pierre¹, Reusser Eric², Caddick Mark², Grolimund Daniel³

¹Geological Institute, Structural Geology and Tectonics, ETH Zurich, Sonneggstrasse 5, NO E69, CH-8092 Zurich (daniela.hunziker@erdw.ethz.ch)

²Institute for Mineralogy and Petrology, ETH Zurich, Clausiusstrasse 25, NW E85, CH-8092 Zurich

³Swiss Light Source, Paul Scherrer Institute, 5232 Villigen PSI, Switzerland

Blueschists are a key source of information regarding the thermo-mechanical evolution in subduction zones. They record temperature and pressure conditions of rock material transported down to great depths along the slab. The involved processes cannot be studied in situ so that investigations rely on recalculations and modeling based on thermodynamic properties of minerals. Current models based on charge balance may be inaccurate. In particular, elemental site occupations can vary dramatically in sodic amphiboles, which have a complex structure. Little is known on the ferric/ferrous iron ratio in glaucophane although it has been argued that changes in bulk or mineral values may have a drastic impact on the stability field of these minerals. To constrain our knowledge on subduction processes and the minerals defining the blueschist facies, we need to rely on realistic values. Otherwise, we might misestimate pressure and temperature conditions required to form such rocks.

Samples of varying pressure/temperature conditions and mineral parageneses have been selected in order to get a more general understanding on iron distribution under distinct conditions. Photometry is used to measure ferrous iron in both bulk and mineral compositions. For the mineral standards this values will be crosschecked with Moessbauer spectroscopy. Further measurements have been made with micro-XANES, which has the great advantage of in situ spot analyzes allowing to measure zoning in single crystals or contact zones within the original texture.

We present new data of bulk and mineral analyses of different types of blueschists focusing on samples from Syros and Sifnos (Cyclades, Greece). We chose these rocks because they contain garnet and white mica, which allow common thermobarometric estimations, thus some sort of calibration. Besides, the sodic amphiboles are fresh and chemically unzoned, which is crucial for using methods based on whole grain analyses. We found bulk and mineral ferric iron values higher than most charge balance recalculations yield. This result comforts the certainty that it is fundamental to incorporate measurements to ensure optimal results. The influence of measured ferric/ferrous iron contents on the thermobarometry of the Syros/Sifnos blueschists is discussed along with the potential for new constraints on amphiboles regarding recalculations of metamorphic conditions.

P 2.12

X-ray diffraction and thermal analyses of a bangle shard from an Indus valley settlement

Kayani Saheeb-Ahmed

National University of Sciences and Technology, Islamabad-44000, Pakistan (saheebk@ceme.nust.edu.pk)

In Pakistan, Harrappa is recognized as one of the most important and magnificent site of the Indus Valley Culture that flourished around 2600 BCE in this region. In order to determine the type of contents used in making bangles in Harrappa, a specimen shard was tested using the facilities available in Geoscience Advance Research Laboratories in Islamabad. The mineralogical make up of the clay used in the bangle shard was determined using XRD analysis while simultaneous TG/DT analyses were carried out to establish thermal properties and nature of phase changes that took place while the bangle was processed.

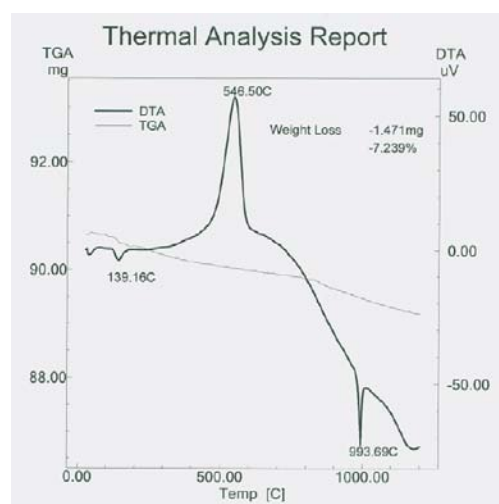


Figure 1. Results of simultaneous TG/DT analyses.

XRD analysis shows that the mineralogical make up of the clay used in the bangle shard includes montmorillonite ($(\text{Na,Ca})_{0.33}(\text{Al,Mg})_2(\text{Si}_4\text{O}_{10})(\text{OH})_2 \cdot n\text{H}_2\text{O}$), gypsum ($\text{CaSO}_4 \cdot 2\text{H}_2\text{O}$), and quartz (SiO_2). Results of thermal analysis have been included in Figure 1. The temperature was varied in steps of $20^\circ\text{C}/\text{min}$ from room temperature to 1200°C . For a sample mass of 20.32 mg, a loss of 1.471 mg or 7.239% was observed. There is a regular trend in mass loss over the entire heating range, which shows that the clay or clays used in the bangle shard are almost uniform in composition and properties. Mass loss in clays during thermogravimetric analysis can be divided into three stages: dehydration from room temperature to about 200°C , decomposition of hydroxyls from 400°C to 650°C , and decomposition of carbonates in the range 700 - 800°C (Drebushchak et al. 2005). The TGA curve for the specimen shows mass loss occurring in three distinct steps. The initial mass loss (0.15 mg) attributed to dehydration is very small, but it coincides with an endothermic peak at 139.16°C on DTA curve. (An endothermic effect attributed to presence of gypsum is also observed in the range 100 - 120°C (Moropoulou et al. 1995).) From this temperature onwards there is a gradual mass loss of 0.75 mg up till 850°C . Finally a mass loss of 0.5 mg is recorded from 850°C to 1200°C on the last portion of TGA curve. The mass loss around 400 - 650°C which coincides with a sharp exothermic peak at 546.5°C on DTA curve can be attributed to combustion of organic material in the tested specimen (Moropoulou et al. 1995). This organic material may have been added by ancient potters as a binder. (From XRD analysis, abundance of montmorillonite and the characteristic two endothermic peaks on DTA curve provide the evidence that the major constituent of the tested specimen is bentonite. The thermal analysis curves for the tested specimen can be compared with modern industrial bentonite (from India) and the trends are almost similar (Venkatathri 2006). A difference (in peaks and ranges) may exist due to addition of other components in the raw ceramic material of the bangle shard specimen.) Studies have shown that montmorillonite is destroyed when fired to a temperature of 860°C (Drebushchak et al. 2005). If montmorillonite has survived the firing stage during processing of the bangle, it appears that the temperature in the firing kiln was not in excess of 860°C .

Quartz has also been detected in XRD analysis. It is a non-plastic material where as bentonite is known to be very plastic and suited for complex shapes. Quartz may have been added in the raw ceramic material as a temper to allow water to evaporate smoothly (thus avoiding cracking) and also to improve handling and working of the raw clay. But unknown to ancient potters of Harrappa, this addition may have caused the bangles made out of this raw material to become less resistant to mechanical stresses while in use. An endothermic effect is observed from 600 - 950°C . There is a sharp endothermic peak at 993.69°C followed by an exothermic effect at about 1020°C . The endothermic effect especially around 800 - 950°C can be attributed to decomposition of any carbonates in the raw ceramic material used for making this particular bangle. No amount of calcite or dolomite has been identified in XRD analysis (given the limitation of the XRD apparatus not being able to detect minerals less than 10 wt% of the sample), the most usual carbonates in ancient ceramic materials (Moropoulou et al. 1995). The endothermic peak at 993.69°C can be interpreted as an indication of appearance of a crystalline phase (i.e. due to vitrification of quartz) in the sample (above 800°C), which might have undergone a solid-phase polymorphic transformation at this high temperature (Krapukaityte et al. 2008; Moropoulou et al. 1995).

REFERENCES

- Drebushchak, V.A., Mylnikova, L.N., Drebushchak, T.N., and Boldyrev, V.V. 2005: The investigation of ancient pottery: application of thermal analysis. *Journal of Thermal Analysis and Calorimetry* 82, 617-626.
- Moropoulou, A., Bakolas, A., and Bisbikou, K. 1995: Thermal analysis as a method of characterizing ancient ceramic technologies. *Thermochimica Acta* 269-270, 743-753.
- Venkatathri, N. 2006: Characterization and catalytic properties of a naturally occurring clay, bentonite. *Bulletin of the Catalysis Society of India* 5, 61-72.
- Krapukaityte, A., Tautkus, S., Kareiva, A., and Zalieckiene, E. 2008: Thermal analysis: a powerful tool for the characterization of pottery. *CHEMIJA* 19, 4-8.

P 2.13

Petrographic and sedimentologic investigations of boulders of the river Wiese (southern Baden-Württemberg, FRG)

Klumb Alexander¹, Franz Leander¹, Wetzel Andreas² & de Capitani Christian¹

¹Institute of Mineralogy and Petrography, Bernoullistrasse 30, Ch-4056 Basel (Alexander.Klumb@stud.unibas.ch)

²Institute of Geology and Palaeontology, Bernoullistrasse 32, Ch-4056 Basel

The river Wiese has its source in the southern Schwarzwald (south Germany) and carries a prominent amount of clastic material to the river Rhine. A petrographic and sedimentologic investigation aims to elucidate the changes in composition and maturity of boulders along the course of the Wiese river and its final supply to the Rhine river. At 5 sampling sites representative material was collected.

The first sampling station is located in the upper reach of the river Wiese, about 6 km downriver of its source at the Feldberg. High-grade metamorphic rocks (migmatitic gneisses) represent the largest proportion of the boulder population whereas fine to medium grained granites are subordinate. The gneisses, which crop out in the whole Feldberg area of the southern Schwarzwald, are mainly metapelitic types with prominent biotite, sillimanite, garnet, plagioclase, K-feldspar and quartz. The granites are mostly fine-grained and partly medium-grained. They are probably derived from smaller dykes and sills cutting through the metamorphic Variscan basement. The boulders from this site are moderately rounded.

The second sampling site is located north of the village Hausen, about 20 km downriver of the first site. It is situated at the boundary between the Schwarzwald and the Dinkelberg Block where Triassic sedimentary rocks crop out. Besides basement gneisses and porphyric granites, bioclastic limestones and sandstones form part of the boulder spectrum. Due to local erosion, the limestones form angular boulders, whereas the sandstones are well-rounded and relatively small while brought in by a tributary creek (Fig. 1). Intriguing is the occurrence of basaltic components probably delivered from the Badenweiler-Lenzkirch-Zone. The Wiese passes this Permo-Carboniferous structure a few kilometers upstream from this location. In addition, quartz porphyrites, conglomerates and subordinate quartzites are derived from this zone.

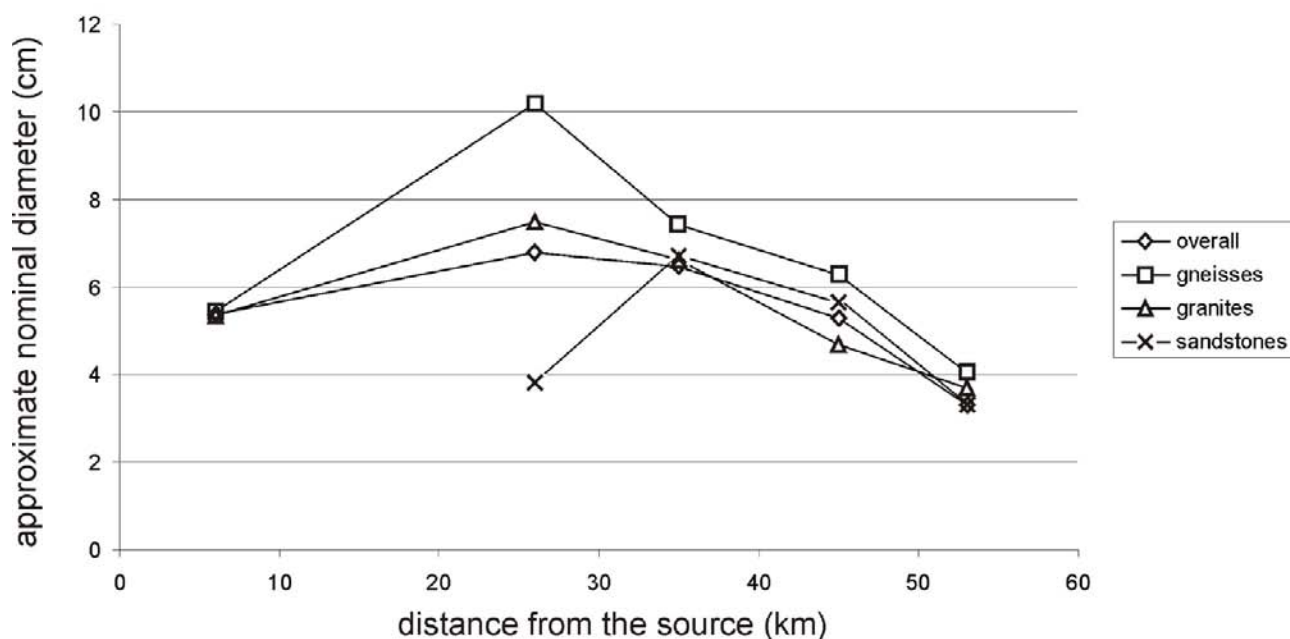


Figure 1: Diagram showing variation of approximate nominal diameter of boulders with distance

The third sampling site is located another 9 km downstream from Hausen at a retaining barrage near Maulburg. The boulders exhibit a wide variety in composition including basement gneisses, granites, porphyrites, basalts and Upper Permian sandstones. The amount of the latter is significantly enlarged as the Wiese actively erodes a cliff. Apart from the sandstones, the grain size of the boulders is decreasing (Fig. 1).

The fourth sampling location is at a retaining dam in Lörrach-Tumringen, which is another 10 km downstream from Maulburg. The lithology of boulders does not change but the proportion of Triassic rocks, in particular sandstone, markedly increases. Grain size decreases (Fig. 1) and roundness increases for all lithologies.

The last sampling station is an abandoned grave pit in Weil am Rhein, about 53 km downstream from the source of the Wiese river and close to the Rhine river. Here, a mixture of material derived from the Wiese catchment area, the Jura Mountains and the Alps occurs. For the first time, greenish granites showing a low-grade metamorphic overprint, are present. Furthermore, we observe fine grained amphibolites, radiolarites, flysch sandstones and quartzites from the Alps occur. The Jura Mountains delivered considerable amounts of greyish micritic limestones. Thus, the proportion of Wiese material is low. All the pebbles are fine-grained (Fig. 1) and quite well rounded.

A further quantification of textural and compositional data will be carried out.

REFERENCES

- Wimmenauer, W. 1985: Petrographie der magmatischen und metamorphen Gesteine, 382 pp.
 Sawatzki, G. 2000: Geologische Karte des Südschwarzwaldes 1:100000. Landesamt für Geologie, Rohstoffe und Bergbau Baden-Württemberg.
 Krumbein, W.C. & Sloss, L.L. 1963: Stratigraphy and sedimentation. Freeman, San Francisco, 660 pp.

P 2.14

Element partitioning between immiscible carbonatite- and silicate melts from 1-3 GPa

Lukas H.J.Martin¹, Max W. Schmidt¹, Kathrin Hametner², Hannes B. Mattsson¹ & Detlef Günther²

¹Institute for Geochemistry und Petrology, ETH Zürich, 8092 Zürich (lukas.martin@erdw.ethz.ch)

²Laboratory of Inorganic Chemistry, ETH Zürich, Wolfgang-Paulistr. 10, 8093 Zürich

The goal of this experimental study is to determine element partition coefficients (K_D^i) between conjugate and immiscible carbonatite and silicate melt pairs at pressures of 1-3 GPa in H₂O-free and H₂O-bearing systems. The determined K_D^i -values quantify the element partitioning between immiscible silicate-carbonatite melts and provide a tool to test for liquid immiscibility of natural melts from volcanoes erupting both silicate and carbonatite magmas.

Partition coefficients were determined for 3 water-free and 4 water-bearing systems with different silica contents between 1-3 GPa and 1150-1260°C. In the water-bearing experiments, the physical separation of the immiscible melts was sufficient to determine the partition coefficients. Major elements were analysed by electron probe microanalysis and trace elements by LA-ICP-MS for >40 elements. For the water-free systems, centrifugation at 700 g, at identical PT conditions as in the equilibrium experiments, was necessary to segregate the coexisting liquids in order to analyse them.

The partition coefficients of the dry systems are within a range of factor 4 for most elements. The alkali and alkali earth elements partition into the carbonatite melt as well as P and Mo, whereas the HFSE and most transition metals have a stronger affinity for the silicate melt. The LREE elements partition weakly into the carbonatite melt whereas the HREE prefer the silicate melt ($K_D^{La} / K_D^{Lu} = 1.6$ to 2.3).

For the water-bearing systems, the addition of water increased the width of the immiscibility gap, resulting in higher partition coefficients. The highest partition coefficients for Ca and the LREE (>30) were obtained in silica-rich water-bearing systems.

The alkali-rich compositions of carbonatite melts in our as well as previous studies indicate that primary carbonatites, which are immiscible with silicate melts, ought to be alkali-rich. As both, low degree of melting or fractionation of CO₂-rich melts (the two other mechanisms) also lead to alkali-enrichment in the carbonatites, we propose that pure calcite or dolomite carbonatites do not represent true liquid compositions. Nevertheless, we are not questioning the igneous characters of such calcio-carbonatites, but assume that these are primary cumulates or altered through weathering processes. It is likely that most carbonatites have lost at least part of their initial alkali-contents by leaching through magmatic- or meteoric fluids.

P 2.15

The Petrology and Geochemistry of the Civrari-Southern Lanzo Ophiolite, Piemonte, Western Italian Alps

McCarthy Anders¹, Müntener Othmar¹

¹*Institut de Minéralogie et Géochimie, University of Lausanne, Anthropole, CH-1015 Lausanne
(anders.mccarthy@unil.ch)*

Alpine-Apennine ophiolites have been found to represent subcontinental lithosphere emplaced at ocean-continent transition zones during lithospheric thinning and exhumation during the opening of the Alpine Tethys in Jurassic times [1,2]. Preserved mantle rocks have provided insight into mantle dynamics occurring at different depths, from melt-rock reaction and asthenospherization to melt intrusion. The presence of a small outcrop of peridotites within a sliver of slow-spreading oceanic crust, represented by the Civrari Ophiolite [3], has given us the ability to study peridotites and magmatism in a more oceanward environment. The Civrari peridotite consists of a small lense of both refractory and reactive lherzolites intruded by late stage low-pressure olivine-gabbros. The ultramafic massif in itself is strongly homogeneous and of refractory nature, with strongly contrasting compositions when compared to subcontinental mantle exhumed throughout the Alps. A detailed study suggests that the Civrari peridotite originated from a deeper part than the Lanzo peridotites, with preserved high temperatures (1200-1300°C) suggesting rapid exhumation to the ocean floor, without any prior accretion to the subcontinental lithosphere. These peridotites were formed through ~13% partial melting, beginning in the stability field of garnet, before reaching the spinel stability field. Localised percolation of small melt increments (very low melt/rock ratio) in the stability field of spinel caused some areas of the Civrari peridotite to become reactive lherzolites (dissolution of orthopyroxene, precipitation of ol + spl + cpx), before localised melt impregnation at shallower lithospheric levels dissolved clinopyroxene to form orthopyroxene + plagioclase. Preserved reacted clinopyroxene show trends of LREE, TiO₂ and Na₂O enrichment, with core to border zonations. Impregnation of lithospheric peridotites by orthopyroxene-saturated melts is consistent with migrating melts cooling and crystallizing during the exhumation of the peridotite. MORB-type aggregated magmas between the Civrari and Southern Lanzo domains intruded around 150 Ma as shown by plagioclase-clinopyroxene Nd mineral isochrons, and originated from a similar MORB-type depleted asthenospheric source. Increase in partial melting by the Civrari Ophiolite, coupled with the high temperatures recorded in peridotites, and the limited melt-interaction suggests that the Civrari ophiolite is found in a more oceanward environment than the Southern Lanzo peridotite, and might represent Jurassic-age oceanic crust.

REFERENCES

- [1] Müntener O. & Piccardo G.B., 2003, Melt Migration in ophiolitic peridotites: the message from the Alpine-Apennine peridotites and implications for embryonic ocean basins. *Ophiolites in Early history. Geol. Soc., London Spec. Publ.* 218, pp. 69-89.
- [2] Piccardo G.B., O. Müntener, A. Zanetti, T. Petke, 2004, *International Geology Review*, Vol. 46, pp. 1119-1159. Ophiolitic Peridotites of the Alpine-Apennine System: Mantle Processes and Geodynamic Relevance
- [3] Pognante U., Perotto A., Salino C., Toscani L. 1986, The Ophiolitic peridotites of the Western Alps. Record of the Evolution of a Small Ocean Type Basin in the Mesozoic Tethys. *Tschermak Mineralogische und Petrologische Mitteilungen*, vol 35, pp. 57-65.

P 2.16**CRIME SCENE INVESTIGATION AND FORENSIC MINERALOGY APPLICATIONS AT GURPINAR (ISTANBUL – TURKEY) MURDER*****GURPINAR (ISTANBUL – TURKEY) CİNAYETİNDE OLAY YERİ İNCELEMESİ VE ADLİ MİNERALOJİ UYGULAMALARI***

Murat MERT¹, Serkan MERCAN², A. Selçuk GÜRLER¹2, M.Feyzi ŞAHİN¹3, , Nurullah AKSOY², Kürşat DURMUŞ²

¹Council of Forensic Medicine, Istanbul – TURKEY, 1- Geology Engineer (PHD) muratmert@istanbul.edu.tr; 2,3 – Forensic Medical Doctor (MD) selcukgurler@gmail.com: feyzisahin@yahoo.com

² Istanbul Police Department , Crime Scene Investigation And Identification Unit
s.mrcn@hotmail.com; naksoy34@hotmail.com; kdurmus@hotmail.com

A reliable CSI is the most important step of Forensic Investigation to find out the crime and criminal. It is a fundamental legal principle to reach guilty from evidence and to judge the accused with the legally obtained evidence. In the recent years, using multidisciplinary studies are increased in Forensic Science by the development of science and technology. Compiling biological samples, finger prints researches, forensic materials is important to solve the crime, to ensure the justice and to relief.

The scope of this study is to highlight the using of forensic mineralogy and crime scene investigations in forensic science. For this purpose, the mineralogical findings were compared. The mineralogical findings were collected from crime scene and from a buried 50-55 aged male body found on the sea coast of Büyükçekmece Gürpınar. Also some of the findings were taken from the houses and cars of suspects who can be related to the crime.

ÖZET

Suç ve suçlunun ortaya çıkarılması için yapılan soruşturmanın en önemli ayağını iyi yapılacak bir olay yeri incelemesi oluşturmaktadır. Delilden sanığa ulaşmak ve sanığın yasal olarak elde edilecek delillere dayanılarak yargılanması temel bir hukuk prensibidir. Son yıllarda teknoloji ve bilimin gelişmesine bağlı olarak adli olayların çözümünde multi-disipliner çalışmaların kullanımı artmaktadır. Olay yerinde biyolojik örneklerin derlenmesi, parmak izi araştırmaları, adli mineralojik materyallerin toplanması vb. uygulamaların tümü olayın aydınlatılması, adaletin sağlıklı bir şekilde uygulanması ve mağduriyetlerin giderilmesi için önem arz etmektedir.

Bu çalışmada; adli mineralojinin adli bilimler alanında kullanımı ve olay yeri incelemesindeki öneminin anlatılması amacı ile Büyükçekmece Gürpınar sahilinde toprağa gömülü vaziyette bulunan 50 – 55 yaşlarındaki erkek cesedinde olay yeri ve otopsi sırasında toplanan mineralojik materyal ile ve olayla ilgisi olduğu düşünülen şüphelilerin ev, olayda kullanıldığı düşünülen arabalarının olay yeri ekiplerince yapılan incelemeleri sonucunda elde edilen bulguların karşılaştırılması anlatılmıştır.

P 2.17**Geochemistry and petrogenesis of the Dehsheikh Peridotitic Massif (South of Iran)**

Monsef Iman¹ & Rahgoshay Mohamad¹

¹ Shahid Beheshti University, Earth Sciences Faculty, Tehran, Iran (iman_monsef@yahoo.com)

Peridotitic tectonites from the Dehsheikh Massif record a spinel-peridotite facies condition, and indicated by deformation from tectonite to mylonitic fabrics in south of Iran. The ophiolitic peridotites are considered to represent by residual mantle that was tectonically formed by rifting and opening of the Jurassic Neo-Tethys embryonic ocean in fore-arc tectonic environment.

These peridotites include spinel-harzburgites and dunites, which display overall depleted geochemical signature.

Peridotites from the Dehshekh Massif are very refractory with low modal clino-pyroxenes, chrome-rich spinels with $Cr\# = 0.6 - 0.9$ and $Mg\# = 0.4 - 0.6$. Also, these samples show U-shaped rare earth element (REEs) profiles demonstrated that these peridotites have undergone extensive interaction with LREE-enriched subduction-derived fluids and depleted mantle residues.

Harzburgites and dunites are considerably characterized by more oxidized features, with calculated oxygen fugacities between FMQ +1 and FMQ +1.5, in comparison to other subduction zone related peridotites. Fractional melting modeling indicates that these peridotite samples are derived by 25-30 % melting of mantle in a supra-subduction zone environment.

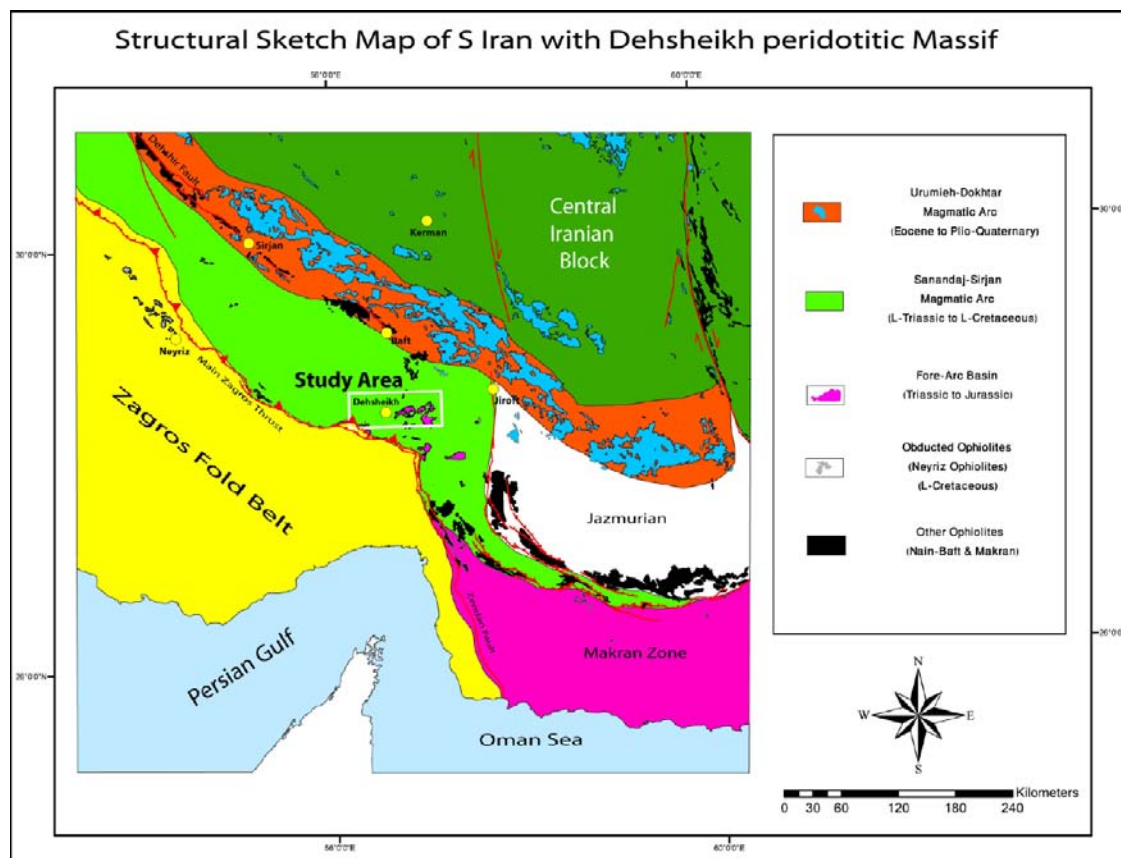


Figure 1. Simplified structural sketch map of Dehsheikh Peridotitic Massif in south of Iran. The location of study area with major structural zones consisting of Sanandaj-Sirjan Magmatic Arc, Central Iranian Block, Urumiyeh-Dokhtar Magmatic Arc, Makran Zone and Zagros Folded Belt are indicated.

REFERENCES

- Sachan, H.K., 2001. Supra-subduction origin of the Nidar ophiolitic sequence, Indus Suture zone, Ladakh, India: evidence from mineral chemistry of upper mantle rocks. *Ophiolite* 26, 23–32.
- Tamura, A., Arai, S., 2006. Harzburgite–dunite–orthopyroxenite suite as a record of supra-subduction zone setting for the Oman ophiolite mantle. *Journal of Asian Earth Sciences* 90, 43–56.
- Godard, M., Lagabrielle, Y., Alard, O., Harvey, J., 2008. Geochemistry of the highly depleted peridotites drilled at ODP sites 1272 and 1274 (Fifteen-Twenty Fracture Zone, Mid-Atlantic Ridge): implications for mantle dynamics beneath a slow spreading ridge. *Earth and Planetary Science Letters* 267, 410–425.

P 2.18

Sr, Nd, and Pb isotopic constraints on the origin of the central Iran linear volcanic chains

Monsef Reza¹, Emami Mohamad Hashem², Rashidnejad Omran Nematallah³

¹ Estahban Branch, Islamic Azad University, Estahban, Iran (r_monsef@iauestahban.ac.ir)

² Islamshahr Branch, Islamic Azad University, Tehran, Iran

³ Geology Department, Basic Science Faculty, Tarbiat Modares University, Tehran, Iran

The Miocene linear volcanic activity in the northwestern part of Iran is considered to be extensional basins after the Arabian – Eurasia collision. The samples are mainly andesitic basalt to andesite and were analyzed according to Nd-Sr-Pb isotopic compositions in order to understand the petrogenetic signature of volcanic rocks. The magmatism at these regions are calc-alkaline in affinity.

The analyzed samples are characterized by $^{87}\text{Sr}/^{86}\text{Sr}$ ratios (0.7056 to 0.7071), Epsilon Nd values (0 to -3.5) and $^{143}\text{Nd}/^{144}\text{Nd}$ (0.51246 to 0.51267) which indicate contribution of a mantle component in origin. The Pb isotope evidence is particularly high with $^{208}\text{Pb}/^{204}\text{Pb}$ ratios (38.731 to 39.097), $^{206}\text{Pb}/^{204}\text{Pb} = 18.770$ to 19.004 and $^{207}\text{Pb}/^{204}\text{Pb} = 15.645$ to 15.706.

This observation from the isotopic evidence for the volcanic chain implies that they probably originated from melting of enriched-mantle source, which ascribed to oceanic sediment played a major role in the origin of the volcanic rocks. The isotopic data suggest that the parent magma underwent fractional crystallization and were contaminated by crustal rocks similar to that of the lower crust.

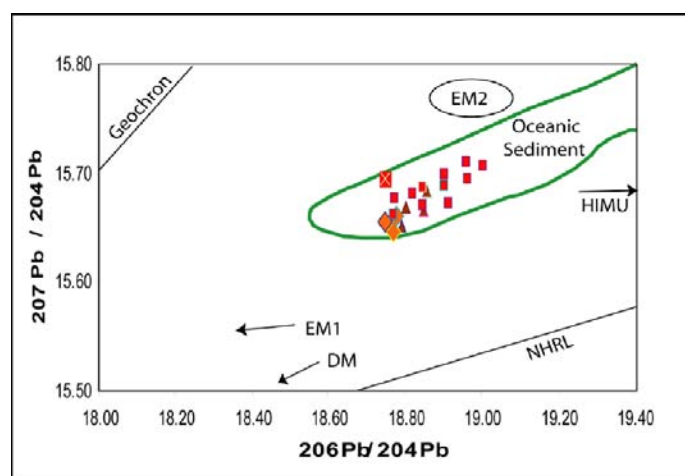
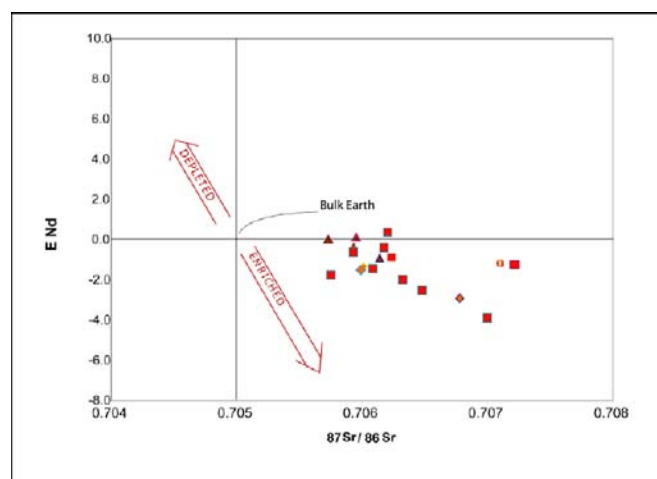


Figure 1. plot of Epsilon Nd versus $^{87}\text{Sr}/^{86}\text{Sr}$ ratios. Plot of $^{206}\text{Pb}/^{204}\text{Pb}$ versus $^{207}\text{Pb}/^{204}\text{Pb}$ ratios. NHRL (Hart, 1984).

REFERENCES

- Conticelli, S., Guranieri, L., Farinelli, A., Matti, M., Avanzinelli, R., Bianchini, G., Boavi, E., Tommasini, S., Tiepolo, M., Prelevic, D., Venturelli, G., 2009, Trace elements and Sr-Nd-Pb isotopes of K-rich, shoshonitic, and calc-alkaline magmatism of the western Mediterranean Region. Genesis of Ultra potassic to calc-alkaline magmatic associations in a Post-collisional geodynamic setting. *Lithos* 107, 68-92.
- Hart, S., Hauri, E.H., Oschmann, L.A., white head, J.A., 1992. Mantle plumes and entrainment. *Science* 256, 517-520.
- Shimoda, G., Fatsumi, Y., Nohda, S., Ishizaka, K., Jahn, B.M., 1998. Setouchi high-mg andesites revisited: Geochemical evidence for melting of subducting sediments. *Earth and planetary Science letters* 160, 479-492.

P 2.19

Na-bearing garnets with oriented lamellar inclusions – are those majorite precursors? A case study from the Rhodope Massif (Greece)

Moulas Evangelos¹, Misra Santanu¹, Burg Jean-Pierre¹ & Kostopoulos Dimitrios²

¹Department of Earth Sciences – ETH Zurich, Sonneggstrasse 5, CH-8092 Zurich (evangelos.moulas@erdw.ethz.ch)

²Department of Mineralogy and Petrology, National and Kapodistrian University of Athens, Panepistimioupoli Zographou, 15784 Athens

The Rhodope Massif in northern Greece – southern Bulgaria is an Alpine synmetamorphic nappe complex. The presence of microdiamonds as inclusions in metamorphic minerals of the intermediate thrust sheets is taken as evidence of ultra-high-pressure metamorphism (UHPM – $P > 2.5\text{GPa}$). One of the major UHP mineral indicators is garnet with lamellar inclusions of clinopyroxene, rutile ± apatite. Such lamellae are interpreted as the result of exsolving processes during decompression and cooling of majoritic garnet from UHP conditions.

We investigated an eclogite from the diamond-bearing tectonic unit in eastern Rhodope. The main mineral assemblage is grossular-almandine-rich garnet, omphacite, quartz, plagioclase, amphibole, clinozoisite, epidote and calcite; rutile, titanite, ilmenite and apatite are accessory phases. Omphacite and plagioclase form symplectites in the rock matrix. Garnets are zoned with respect to their manganese and sodium content whereas magnesium, calcium and iron are homogeneously distributed.

The chemical zoning in manganese is consistent with a fractional crystallization model and the sodium zoning follows the same trend. The mechanism responsible for the incorporation of sodium in garnet is the substitution $\text{MgAl}=\text{NaTi}$. Conventional thermometry using garnet-clinopyroxene pairs at the rim of the garnet yield temperatures of $650^\circ\text{C} (\pm 75^\circ\text{C})$.

All of the garnet grains exhibit lamellar inclusions of titanite, quartz and rutile which are oriented systematically within the crystal lattice of the garnet. Electron backscattered diffraction (EBSD) revealed that the lattice preferred orientation of these lamellar inclusions is not related to the lattice orientation of the host garnet. This crystalline relationship does not support an exsolution-type origin of the oriented lamellar inclusions, which would also require higher temperatures than that calculated.

P 2.20

Investigations of fluid inclusions in quartz crystals in the dolomitic rocks of the Binn-Valley, Switzerland

Müller Fabian¹, Mullis Joseph¹

¹Mineralogisch-Petrographisches Institut, University of Basel, Bernoullistrasse 30, CH-4056 Basel (fab.mueller@unibas.ch)

The aim of our investigations is a comparison of several sulfosalt bearing mineral localities in dolomitic rocks of the Binn-Valley (Wallis, CH), in terms of their mineralizing fluids. So it should be possible to improve the knowledge about the formation of the Lenggenbach deposit. The Lenggenbach quarry is one of the most famous mineral collecting sites in Switzerland. In the last decades, numerous investigations on geology, mineralogy and ore formation for this mineralization were done. The richness of sulfosalt minerals and the occurrence of Tl-sulfosalts is of specific scientific interest. The mineral deposit is located in Triassic meta-dolomites, underlayed by Jurassic schists (Bündnerschiefer). Over the dolomitic rocks different Pretriassic ortho- and paragneisses occur (Hügi 1988). Due to the tectonic settings the primary stratigraphic sequence of the rocks is reversed. Beside the Lenggenbach quarry, other sulfosalt bearing deposits are known, situated within dolomitic rocks. The most famous are Reckibach, Turtschi and Messerbach. Especially the localities Reckibach and Turtschi show considerable differences in their element dominances referred to the sulfosalt- and sulfide minerals. The outcrop Turtschi shows a Sb-Bi-dominance whereas Reckibach is clearly Ag-dominated. The Lenggenbach quarry in addition is characterized by the occurrence of Tl-sulfosalts and shows the largest mineral diversity of all outcrops (Graeser 1965). Quartz crystals from fissures and cavities are the host mineral of the investigated fluid inclusions. A differentiated inclusion petrography and microthermometric investigations are the basis of this work. It enables to evaluate the approximated composition and density of the mineralizing fluid. Daughter minerals, like halite, calcite and sphalerite were analyzed by Raman spectroscopy.

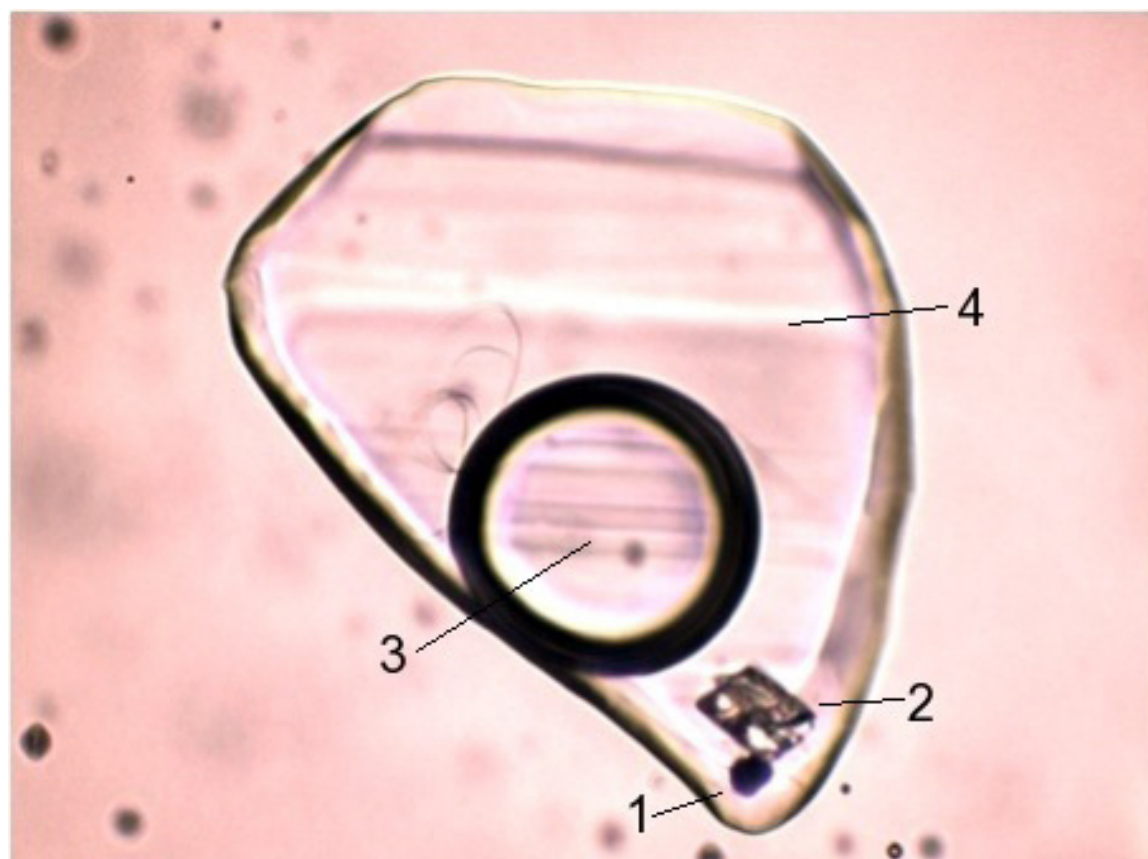


Figure 1. Fluid inclusion (180 μm) from the location Tschampigen Wyssi,
1: sphalerite, 2: calcite, 3: CO_2 (liq.), 4: aqueous solution

REFERENCES

- Graeser, S. 1992: Die Mineralfundstellen im Dolomit des Binntales, Schweiz. *Min. Petr. Mitt.*, Band 45, 601- 791
 Hügi, M. 1988: Die Quarze der Mineraliengrube Lenggenbach und ihre Einschlüsse, Lizentiatsarbeit (Uni Bern, Mineralogisch-Petrographisches Institut)

P 2.21

Stratigraphic successions in the Avers unit, southern Grisons, and comparison with the Tsaté unit, W Alps

Peter Nievergelt¹

¹Institute of Geochemistry and Petrology, ETH Zürich, Clausiusstrasse 25, CH-8092 Zürich (peter.nievergelt@erdw.ethz.ch)

The Avers schists are known as a complex of Mesozoic sediments with some ophiolitic rocks since the pioneering work of Rudolf Staub (1926). At that time serpentinites and basic rocks were attributed to lit-par-lit or sheet-like intrusions into basinal sediments in Cretaceous times. This mechanism fits at first sight with the map view, because ophiolitic rocks can be traced as narrow layers, including possible volcanoclastic deposits, over some distance. The abundance of ophiolites in the Avers unit increases towards the South. Staub also mapped in detail the overlying tectonic unit, the Platta ophiolites, that consist mainly of serpentinite, gabbro, pillow lava to greenschist and of associated sediments, namely thin layers of metaradiolarite (banded quartz schist) and bright marble.

The question remained whether the Avers ophiolites are sill-like intrusions or not. Field work in the southern part of the Avers unit (1977-1982) revealed wide spread occurrence of thin layers of metaradiolarite, sometimes with manganese mineralisation, and bright marble. Often associated with serpentinite lenses, the succession in the field is greenschist – metaradiolarite with Mn - bright marble – grey limestone/calcschist. This succession, reported here for the first time from the Avers unit, is similar to that from ophiolitic rocks in the Appennines, W Alps, the Platta nappe and to the stratigraphy in the Austroalpine Margna and Err nappes. Sediments associated with Avers greenschists are therefore correlated with the sequence also known as radiolarite (banded chert + Mn) - calpionella limestone - argille a palombini/Emmat-Fm (middle Jurassic - Early Cretaceous).

The distribution of ophiolitic rocks in the Avers schists is therefore mainly due to tectonic imbrication with other sedimentary series. The lower part of the Avers unit overlies Triassic quartzites and dolomite/calcite marbles of the Suretta nappe and consists mainly of carbonate sediments with some detrital layers. The breccias contain Triassic carbonates and indicate the break up of an adjacent platform. Sandstones and “silty green schists” made up of chlorite, some quartz and muscovite (and can be confused with basic greenschist in the field), partly represent material from the Roffna porphyry (basement of the Suretta nappe).

In the upper part of the Avers unit a stratigraphic succession can be mapped in areas with continuous outcrops. Age and stratigraphic younging is not verified, but comparison with the série grise and série rousse from the Tsaté nappe (Marthaler, 1984) suggest Early to Late Cretaceous and the following sequence of formations. (Instead of correct rock names in greenschist facies, e.g. calcschist, grey phyllite, Peters and Dietrich (2008), the terms for unmetamorphic rocks are used for description). The lower (?) series of alternating limestones and dark mudstones typically contain detrital layers of sandstones, siltstones, fine to medium grained (mm to cm) breccias with clasts from various dolomite and limestone source rocks (Triassic, Liassic....?). More visible in the field are 0.1 to 3 m thick layers of bright dolomite and dolomite-limestone breccias. The following dark “shaly” formation of black to grey siltstones and mudstones is 1-2 m thick. The overlying quartz-rich sandstone formation reaches 10 m. These mudstones and sandstones could represent rocks from the mid Cretaceous. The overlying formation can reach over 50 m and builds up Piz Piot. Alternating marly limestones and marls/mudstones without detrital layers are typical. This series is correlated with the série rousse of Marthaler (1984) and would then represent the Late Cretaceous. Towards the upper eastern tectonic boundary of the Avers unit another sandstone formation and a mappable “sandstone-rich tectonite formation” below the Turba mylonite zone can be distinguished.

Comparison of the Avers schists with rocks in the Tsaté nappe (Combin zone, below the Dent Blanche nappe in the Western Alps) revealed identical rock successions at very similar grade of deformation and metamorphism. Metaradiolarites, typically banded quartz schists with Mn mineralisations, are widespread and associated with many greenschists, from Val de Zinal, Val de Moiry, Val d’Arolla to Val de Bagnes S of lac de Mauvoisin. West and east of lac de Moiry the rocks are easily accessible along N-S trending crests. Thin metaradiolarite and marble layers (0.1 – 2 m) are generally still attached to greenschists, some are recognisable as former pillow lava. Packages of “argille a palombini”, dismembered from the original sequence, are prominent W of lac de Moiry, where also the série grise and rousse can be studied. Towards Pointe du Tsaté sandstones prevail in the upper part of the Tsaté unit. “Many rocks in the Avers unit” are therefore to be studied more easily in the lac de Moiry area.

The Avers and Tsaté units are very similar and are interpreted as accretionary wedges rich in sediments containing some oceanic rocks. They are known from many places in the Alpine chain. These units are distinguished from ophiolite-rich (sediment-poor) units such as the Platta nappe, Zermatt-Saas zone etc.

REFERENCES

- Staub, R. 1926: Geologische Karte des Avers (Piz Platta-Duan). Geol. Spezialkarte Nr. 97, 1:50'000. Schweiz. Geol. Kommission
- Peters, T. und Dietrich, V. 2008: Geologischer Atlas der Schweiz, 1:25'000, Nr. 124 Bivio, Bundesamt für Landestopografie swisstopo. Erläuterungen, 134 p.
- Marthaler, M. 1984: Géologie des unités penniques entre le val d'Anniviers et le val de Tourtemagne (Valais, Suisse). *Eclogae geol. Helv.*, 77/2, 395-448.

P 2.22

Minor and trace elements controlling the visible and near-infrared light transmittance of wolframite, pyrite and enargite

Ortelli Melissa¹, Kouzmanov Kalin¹, Wälle Markus²

¹ Earth and Environmental Sciences, University of Geneva, Rue des Maraîchers 13, CH-1205 Genève (melissa.ortelli@unige.ch, kalin.kouzmanov@unige.ch)

² Department of Earth Sciences, ETH Zurich, Clausiusstrasse 25, CH-8092 Zürich

In the ore deposit research, fluid inclusion studies can be conducted on ore minerals which are transparent to visible or near infrared radiations (Campbell and Robinson-Cook, 1987). The light transmittance of these semi-conducting minerals depends on the width of the band gap energy in their electronic configuration (Campbell 1984): if an incident light going through the mineral structure has an energy larger than its band gap energy, the light will be absorbed and the mineral will be opaque. Low-energy radiation (infra-red light, IR) is therefore used for transmitted light microscopy to observe internal features in minerals that are usually opaque to the visible light.

In this communication, we discuss the effect of minor and trace element content of wolframite, pyrite and enargite on the mineral transmittance to better assess the limits of visible and IR light ore microscopy.

Image analysis using the gray scale value (GSV) of visible and NIR transmitted-light photomicrographs allows having a rapid rough estimation of the mineral transmittance. Further analyses with FTIR micro-spectroscopy will quantify the IR transmittance of the following minerals as a function of the wavelength in the interval 1.0-3.0 mm.

The selected hübnerite crystals, Mn-rich wolframite from the Toromocho deposit in central Peru, are transparent to visible light and have growth zoning that has been investigated by electron microprobe (EMP) and LA-ICP-MS (Fig. 1). This growth banding is controlled by variable Fe, Mg and minor Zn content, which substitute for Mn in the wolframite structure. Therefore, a negative correlation between the GSV and Fe and Mg content has been observed (Fig. 1d) - an increase of Fe and Mg content from one to two orders of magnitude results in a decrease the GSV of up to 30% (Figs. 1b-c). Titanium (100's ppm level) positively correlates with the GSV.

IR microscopy of pyrite crystals associated with the studied wolframite revealed growth zoning, which has been investigated by EMP and is controlled by variable As and Co content, substituting for S and Fe respectively (Abraitis et al. 2004). Cobalt and arsenic content was often below LOD of the EMP, however in some of the dark growth bands (low GSV, ~ 20%) As concentration reaches 0.49 wt.%. Further LA-ICP-MS analyses will be processed to quantify the Co and As content variation in the pyrite.

IR microscopy revealed growth zoning in enargite from high-sulfidation epithermal veins (Kouzmanov et al. 2010), and has been investigated by EMP and LA-ICP-MS analyses. A clear negative correlation has been identified between the Fe and Sb concentrations and the GSV of the associated growth zones. High concentration of Fe and Sb, 160 and 10 000 ppm, respectively, are present in growth zones with 30% GSV, whereas lower concentration of Fe and Sb, 10 and 3000 ppm respectively, are present in growth zones with 80% GSV.

Image analysis of the GSV on transmitted visible and near IR light photomicrographs in combination with EMP and LA-ICP-MS allows first order estimation of the effect of minor and trace elements on the mineral transmittance, which is a crucial prerequisite for a successful fluid inclusion study. However, FTIR microspectroscopy measurements are required for quantitative analysis.

Acknowledgement

This study was supported by the Swiss National Science Foundation (grant 20021-127123).

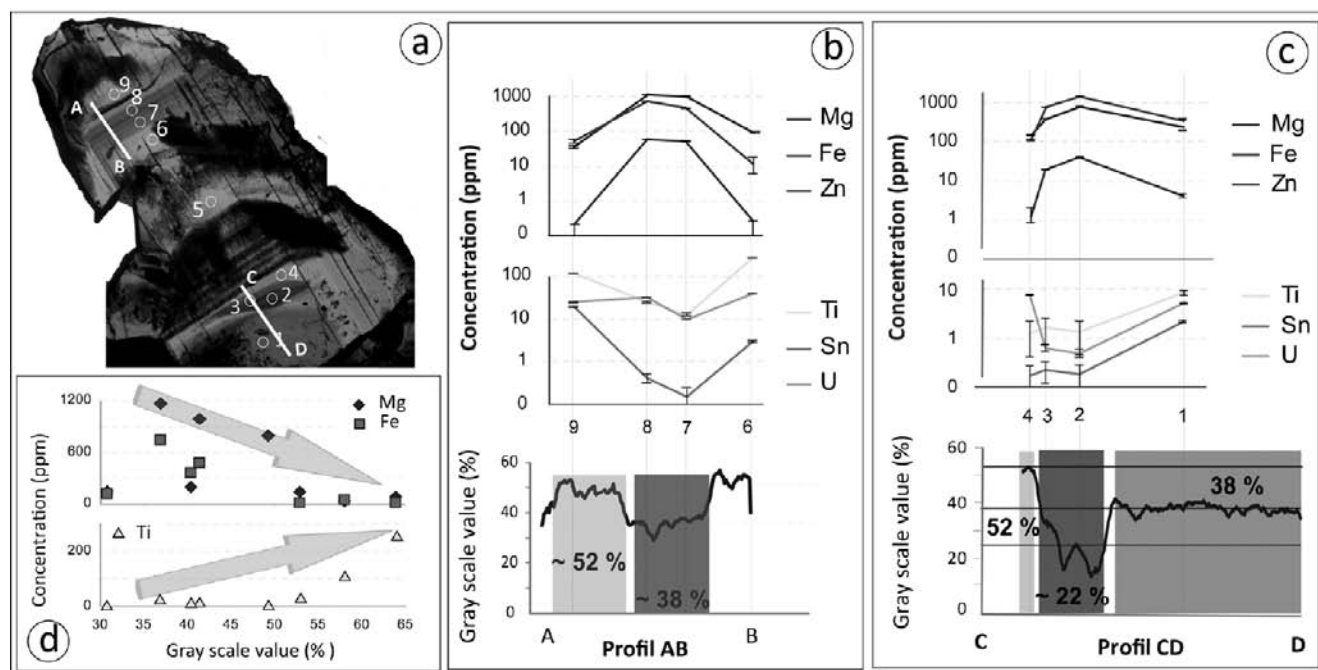


Figure 1. a) Transmitted-light photomicrograph of huebnerite with growth bands. Circles locate ablation pits from the LA-ICP-MS analyses and AB and CD lines correspond to profiles from 1b and 1c; b) Trace element content along profile AB and associated gray scale values; c) Trace element content along profile CD and associated gray scale values; d) Correlations between gray scale values of the huebnerite and trace element concentration.

REFERENCES

- Abratis, P.K., Patrick R.A.D., Vaughan D.J. 2004: Variations in the compositional, textural and electrical properties of natural pyrite: a review. *Int. J. Miner. Process.*, 74, 41-59.
- Campbell, A.R., Hackbarth, C.J., Plumlee, G.S. & Petersen U. 1984: Internal features of ore minerals seen with the infrared microscope. *Economic Geology*, 79, 1387-1392.
- Campbell, A.R. & Robinson-Cook, S. 1987: Infrared fluid inclusion microthermometry on coexisting wolframite and quartz: *Economic Geology*, 82, 1640-1645.
- Kouzmanov, K., Pettke, T., and Heinrich, C.A. 2010: Direct analysis of ore-precipitating fluids : combined IR microscopy and LA-ICP-MS study of fluid inclusions in opaque minerals. *Economic Geology*, 105, 351-373.

P 2.23

Main volcano-sedimentary Lithofacies at the Cretaceous Madneuli copper-gold polymetallic deposit, Lesser Caucasus, Georgia

Popkhadze Nino¹, Beridze Tamar¹, Moritz Robert², Gugushvili Vladimer¹ & Khutsishvili Sophio¹.

¹A.Janelidze Institute of Geology, M.Alexidze 1/9, 0171 Tbilisi, Georgia (nino_popkhadze@yahoo.com)

²Université de Genève, Rue des Maraîchers 13, CH-1205 Genève

The Cretaceous Madneuli barite-gold-copper-polymetallic mine is the major ore deposit of the Georgian Bolnisi mining district. The Bolnisi volcanic-tectonic depression is part of the Artvin-Bolnisi Unit, which is characterized by an arc association formed mainly during the Liassic-Campanian interval. It is located between the southeastern Black Sea-Adjara-Trialeti Unit to the north and the Bayburt – Karabakh Unit to the south. It represents the northern part of the southern Transcaucasus and the central part of the Eastern Pontides. The main ore bodies that were defined in the open pit include: (1) copper-pyrite, (2) barite polymetallic and (3) gold-bearing quartzites, from the base upward. Four structural-morphological ore body types are recognized at the Madneuli deposit: vein, disseminated, breccia and massive stratiform.

Subdivision and characteristics of the host rock units are based on detailed studies of each existing level of the open pit. The different units are characterized by variations in composition and texture. Eight lithofacies were singled out in our study for the first time in the Madneuli deposit. Further detailed studies are in progress. Descriptions and interpretations of the eight principal facies are summarized in Table 1.

The high proportion of volcanic glass, which is common in subaqueous lavas, the abundant pumiceous ash and lapilli, the absence of subaerial lithic clasts, a relatively good hydraulic sorting, and various forms of bioturbation, which are systematically associated with wavy parallel, graded tuffs and with accretionary lapilli tuffs are evidence for marine, mostly shallow marine conditions of the depositional setting of the Madneuli host rocks. Such a setting suggests that the Madneuli deposit was mostly formed under subaqueous conditions, as is common for volcanogenic massive sulfide deposits, and contradicts some previous investigations suggesting mostly subaerial conditions during some of the Madneuli host rock and ore deposit formation. This conclusion is supported by recently discovered radiolarian-bearing horizons within the open pit. The study of which is under progress.

Table 1 - Summary of the main volcano-sedimentary lithofacies of the Madneuli deposit

Lithofacies	Characteristics	Interpretation
Rhyolite pyroclastic lava-flow with flow foliation	Presence of shards of felsic rocks along flow foliations. Porphyry structure with plagioclase, feldspar and quartz phenocryst. Groundmass is perlitic, amygdales are filled with quartz. Locally strongly silicified.	Coherent facies of domes (cryptodomes) or volcanic sills.
Columnar-jointed ignimbrite	The shapes of columnar jointed ignimbrite are rectangular. Groundmass is typically perlitic, with a spherulitic texture of the volcanic glass, with oval shaped quartz crystals. High temperature devitrification of volcanic glass.	Depositional setting below a storm-wave environment.
Fine-grained accretionary lapilli tuffs and tuffs with bioturbation	Massive or normally graded. Recrystallized volcanic glass in the groundmass. Lapilli of various sizes, oval shapes, filled with quartz. Lapilli-rim type, with a core of coarse-grained ash, surrounded by a rim of finer grained ash.	Shallow water sedimentation; in part water settled volcanic ash.

Water-settled pyroclastic fall deposit	Inner flow stratification within a single layer shows fine-grained lamination, normal grading and lamination, thick units with clasts and reverse grading at the top and fine-grained pelitic in the upper part.	Resedimentation of shallow submarine pyroclastic flow; down-slope transport by high concentration turbidity currents.
Rhyodacitic intrusion	Massive. Evenly porphyritic groundmass micropoikilitic, rarely pumiceous.	Coherent facies of lavas or dome.
Non-stratified rhyolitic to dacitic breccias facies	Massive, poorly sorted, clast- to matrix-supported. The fragments of the rocks are slabby, irregular, blocky and oval shaped. Locally this unit is silicified and altered.	Autoclastic breccia from the margins of subaqueous lavas or cryptodomes.
Hyaloclastite	Carapace andesitic breccia flow. Hyaloclastite – with pillow like shapes and glass-like selvages. Groundmass with a perlitic structure. Fractures are defined by chlorite, and glass is replaced by quartz, feldspar, sericite and epidote.	Lobe hyaloclastite facies, reflects a continuous evolution of textures and structures that formed during extrusion in response to rapid chilling and quench fragmentation of lava by water or by wet hyaloclastite formed from previous lobes.

P 2.24

Provenance of imported basaltic millstones in Switzerland during Roman times.

Serneels V., El Kateb A.

In several areas of the Mediterranean, young vesicular lavas are cropping out. From the Bronze Age, the excellent abrasive properties of this type of rocks were noticed and they were used as millstone for grinding cereals. With the development of waterpowered mills during the Roman period, the high quality of this material makes it valuable enough to be traded at long distances.

In Switzerland, Roman watermills have been excavated in Avenches VD, the ancient town Aventicum capital for the Helvetii, and in Rodersdorf SO, a large farming villa. The millstones were made of light grey vesicular lavas.

We investigate 34 samples by mineralogical and petrological techniques (XRD, XRF, microscopy). We can characterize 7 different lithologies, each being typical for a single quarry. They are different from the wellknown sources in Italy (Eugean Hills, Vulcini, Somma-Vesuvius, Vulture, Etna, Sardinia), in Southern France (Agde) and Germany (Eifel). Geochemical affinities point to the recent volcanism of the French Massif Central but it is still impossible to point exactly specific localities. For several decades, the production of millstones during the Roman times in the Central Massif has been postulated, but no quarry remains are located. Our data provide a new insight on the complexity of the production and trade of this material.

P 2.25

Isotope geochemistry of the Varuträsk pegmatite (northern Sweden)

Karin Siegel¹, Thomas Wagner¹, Robert Trumbull², Albrecht von Quadt¹, Erik Jonsson³, Christoph Heinrich¹

¹*Institute of Geochemistry and Petrology, ETH Zurich, Clausiusstr. 25, CH-8092 Zurich (ksiegel@student.ethz.ch)*

²*Inorganic and Isotope Geochemistry, GFZ Potsdam, Telegrafenberg B125, D-14473 Potsdam*

³*Mineral Resources, Swedish Geological Survey, Box 670, SE-75128 Uppsala.*

The Varuträsk pegmatite, located in the Skellefte district in northern Sweden, is a classical representative of LCT-type (petalite subtype) rare element pegmatites (Cerny 1991; Cerny & Ercit 2005). Detailed geochemical and isotopic studies of this well-documented pegmatite body can help to address important questions in pegmatite petrogenesis, such as the processes controlling internal evolution and zoning, and the potential role of an aqueous fluid phase in the evolutionary history. The Varuträsk pegmatite shows a typical differentiation pattern, composed of well-developed border, wall, intermediate and core zones (Quensel 1952). Late stage assemblages are characterized by replacement features that might relate to interaction with a highly evolved melt or an aqueous fluid phase. Previous work (Matalin 2010) has focused on the major and trace element characteristics of key minerals (feldspars, micas, tourmaline, columbite-tantalite), constraining progressive magmatic fractionation trends in the primary pegmatite zones. Significant compositional changes observed in the late-stage mineral assemblages (e.g., reversals of magmatic fractionation trends, depletion in elements typically enriched in aqueous fluids) indicate that most likely an aqueous fluid exsolved after the development of primary pegmatite zonation.

The present study has been carried out to further constrain the role of an aqueous fluid phase, and additionally attempts to trace the source of the parental granitic magma. Stable isotope analysis (O, H, B) has been performed on quartz, mica and tourmaline of all principal mineral assemblages in the pegmatite. Radiogenic isotope (Rb/Sr and Sm/Nd) data have been obtained from two granite suites (Skellefte- and Revsund-type granites; Claesson & Lundquist 1995) that are likely source candidates, host rock amphibolites as well as pegmatitic apatites and feldspar minerals. The $\delta^{18}\text{O}$ values are in the range of 9.7 to 14.0 ‰, and the resulting equilibrium temperatures for quartz-mica pairs are 550°C for the wall zone and 450°C for the intermediate zones. Hydrogen isotope analysis of micas yielded δD values between -75.8 and -19.2 ‰. Both oxygen and hydrogen isotope data display an inward fractionation trend. Boron isotope data of tourmalines obtained using SIMS microanalysis are between -14.6 and -6.2 ‰. The $\delta^{11}\text{B}$ data of different tourmaline types conforming to the primary pegmatite zonation show a clear magmatic fractionation trend, whereas tourmalines related to late-stage assemblages show a reversed fractionation that is correlated with the trends shown by several major and minor elements in the tourmaline (Na, Fe, Mn, F). The radiogenic isotope data indicate an arc environment setting for the Revsund granitic suite, and a sedimentary (S-type granite) origin for the parental granite of the Varuträsk pegmatite which is most probably provided by the Skellefte type granites. This interpretation is supported by the elevated levels of phosphorus (London 2008) in the Varuträsk pegmatite, and the boron and oxygen isotope data that both point to an upper crustal S-type granitic origin.

REFERENCES

- Cerny, P. 1991: Rare-element Granitic Pegmatites. Part I: Anatomy and internal evolution of pegmatite deposits. *Geoscience Canada* 18, No. 2, 49-67.
- Cerny, P. & Ercit, T.S. 2005: The classification of granitic pegmatites revisited. *Can. Mineral.* 43, 2005-2026.
- Claesson, S. & Lundquist, T. 1995: Origins and ages of Proterozoic granitoids in the Bothnian basin, Central Sweden: isotopic and geochemical constraints. *Lithos* 36, 115-140.
- London, D. 2008: Pegmatites. *Mineral Assoc. Canada Spec. Publ.*, 10, 347 p.
- Matalin, G. 2010: Petrography and mineral chemistry of the Varuträsk pegmatite (Northern Sweden). Unpublished MSc thesis, ETH Zurich, 72 p.
- Quensel, P. 1952: The Paragenesis of the Varuträsk Pegmatite. *Geological Magazine* 89, 49-60.

P 2.26

Main Features of the Tectonic Pattern of the Zangezour Ore District of Southern Armenia, Lesser Caucasus

Tayan Rodrig, Harutyunyan Marianna, Hovakimyan Samvel

Institute of Geological Sciences, National Academy of Sciences of The Republic of Armenia, Yerevan (tayan@geology.am)

The Zangezour ore district is the southern segment of the Tsaghkounk-Zangezour structure metallogenic zone (Aslanyan 1958). It is located in the Lesser Caucasus of southern Armenian, generated during the collision of the southern margin of the Eurasian plate and the northern margin of the Arabian plate (Sosson et al. 2010).

The region is bounded by north-northwest oriented deep-seated tectonic zones: the Khustup-Giratakh fault in the east and the Ordubad-Salvard fault in the west. To the south, the folded and discontinuous structures are traced in the territory of Iran. The northern boundary with the Vayk synclinal block passes through the sub-latitudinal fractures of the upper parts of the Vorotan River.

The Khustup-Giratakh fault zone lies along the Shirak-Zangezour ophiolite zone. The Ordubad-Salvard fault zone, which delimits the blocks of Zangezour in the east and Nakhichevan in the west can be followed along the southern fragment of the Yerevan-Ordubad deep fracture zone (Aslanyan 1958). As the Zangezour block was uplifted, the Upper Eocene to Miocene sedimentation was concentrated in the Nakhichevan depression, to the west of the Ordubad-Salvard fault zone.

The Zangezour ore district is characterized by abundant Upper Eocene to Lower Miocene magmatism, which generated the composite Meghri-Ordubad pluton (covering an area of more than 1300 km², the largest pluton in Transcaucasia) and the Bargushat group of intrusions (Karamyan 1978; Melkonyan et al. 2008).

The large discontinuous intrablock faults, complicate the internal structure of the region, and consist of variably oriented extensive zones, among which the submeridional and sub-latitudinal ones are particularly remarkable (Tayan et al. 1976).

The central ore- and magma-controlling zone is located in the axial part of the Zangezour block, and is the product of a long and multi-stage evolution. It is manifested from the Lower Miocene by the formation of porphyritic granitoids prior to hydrothermal mineralization. This central zone is 10-12 km wide, which occupies a small area of the entire 60 km wide ore district.

The eastern border of the study zone in the southern part of the region is characterized by meridionally and submeridionally oriented fractures, which traced along the shores of the Meghri River and further to the north, and traced by dyke, rhyo-dacite, metasomatic rocks and the ore-bearing districts of Lernadzor, Pkhrou, Karmir-Kar, Tagamir, and Aygedzor (Eghnikasar district). The eastern Zangezour block was uplifted (Tayan et al. 1986), and resulted in the formation of the Meghri-Tey graben-synclinal structure within the limits of Central zone, the width of which is about 3,5-4 km. Its western limit is the Tashtoun fault. The formation of graben occurs essentially during the Mio-Pliocene accompanied by the deposition of terrigenous-fragmental lacustrine deposits of the Nor-Arevik Formation. It contains large fragments of ore-containing mid-Eocene volcano-sedimentary formations, which were derived from intrusions that are ore-containing in the Tey, and Terterasar gold-sulphide deposits. The formation of graben was favourable to preserve the economic copper-molybdenum and gold-sulphide deposits of the Meghri pluton from erosion.

In brief, three longitudinally oriented complex zones can be distinguished in the region, which were likely channel-ways for the circulation of hydrothermal solutions. They are the: 1. Giratakh; 2. Salvard-Ordubad and 3. Central- Zangezour zones.

The copper-molybdenum-porphyritic mineralization (Upper Eocene-Lower Miocene) conforming to the granite-granodiorite model (Melkonyan 1981), is the major one in the region. It was formed during complex geodynamic conditions and it consists of numerous ore prospects and deposits, among which the Kajaran deposit is the largest, with >2 milliards t. of ore.

REFERENCES

- Aslanyan A.T. 1958: Regional Geology of Armenia. Pub. "Haypetrat". Yerevan, p.430.
- Karamyan K.A. 1978: Geology, Geologic Structure and Conditions of Formation of Copper-Molybdenum Deposits of Zangezour Ore Region. Pub. Arm.SSR, Yerevan, p.180.
- Melkonyan R.L, Goukasyan R.H, Tayan R.N., Harutyunyan M.A. 2008: Geochronology of Monzonites of Meghry Plutonium (Armenia) –Results and Consequences. *Izvestia of National Academy of Sciences of Armenia, Nauki o Zemle*, volume LXI, No. 2 p.3-9.
- Sosson M. et al. 2010. Subductions, obduction and collision in the Lesser Caucasus (Armenia, Azerbaijan, Georgia), new insights. *Geological Society, London, Special Publications*, 340: p.329-352.
- Tayan R.N., Plotnikov E.P., Abduramanov R.U. 1976: Certain Peculiarities of Formation of Geologic Structure of Zangezour -Nakhichevan Region of Small Caucasus. *Izvestia of the Academy of Sciences of Arm.SSR, ser. Nauki o Zemle*, N 4, p.12-20.

P 2.27

Fluid inclusion evidence for magmatic-metamorphic fluid interaction in the copper-gold Sultana deposit at Huelva, Spain

M. Tomé Cristina¹, Tornos Fernando¹, Seo Jung Hun²

¹Geological Survey of Spain, IGME, Rios Rosas 23, Madrid (cris.martinez.tome@gmail.com)

²Institute of Geochemistry and Petrology, ETH Zurich, 8092 Zurich, Switzerland

The intrusion related copper-gold Sultana veinfield in Huelva (SW of Spain) formed 10 Ma after the Santa Olalla Plutonic Complex emplacement, during the Variscan orogeny which was dated at 341 Ma. The intrusion is hosted by volcanosedimentary rocks and black shales of Cambrian age that were affected by an intense aureole of contact metamorphism.

Combined techniques of scanning electron microscope cathodoluminescence imaging (SEM-CL), detailed fluid inclusion petrography, microthermometry, Raman analysis and laser ablation inductively-coupled plasma mass spectrometry (LA-ICPMS) in single inclusions are applied to reconstruct the physical and chemical evolution of the hydrothermal system in Sultana. The study suggests that a low saline (<4 to 15 wt % NaCl eq; avg of 5 wt % NaCl eq.), CO₂ bearing (up to 10.4 mole %) and intermediate density fluid with high ore-metal concentration (> 537 µg/g Cu, >539 µg/g S) is equivalent to an initial fluid pulse that was exsolved from an underlying carbonaceous melt. When this fluid rose reaching hydrostatic conditions, phase separation occurred by condensation of minor brine (~ 40 wt % NaCl eq.) and a low saline vapor phase (~ 2.4 wt % NaCl eq.) at ~ 350 °C and 100 - 300 bar, the latest carrying most of the copper, gold and sulfur (335 ± 123 µg/g Cu, 11.9 ± 8.7 µg/g Au and 1384 lld-µg/g S) into the system.

Coinciding with the dissolution of an early generation of quartz (Q1) during cooling and phase separation, sulfides were precipitated into open spaces together with the precipitation of a late generation of quartz (Q2) (Figure 1). In fact, Cu concentration drops from 700 µg/g to less than 0.1 µg/g in late fluid inclusions without proportional decrease in other elements. Gold was deposited in later stages in fractures within the chalcopyrite, probably due to the excess of sulfur in the vapor phase which could transport gold after the precipitation of Cu.

The Sultana orebody shares characteristics with intrusion-related Cu-Au deposits, with deeper parts of porphyry deposits and with mesothermal orogenic gold deposits, allowing the possible interaction of magmatic and metamorphic fluid components. With this study, we support that fluids originated from deep magmatic sources with some possible interaction of metamorphic fluids rather than mixing with external fluids at the depositional site of the mineralization.

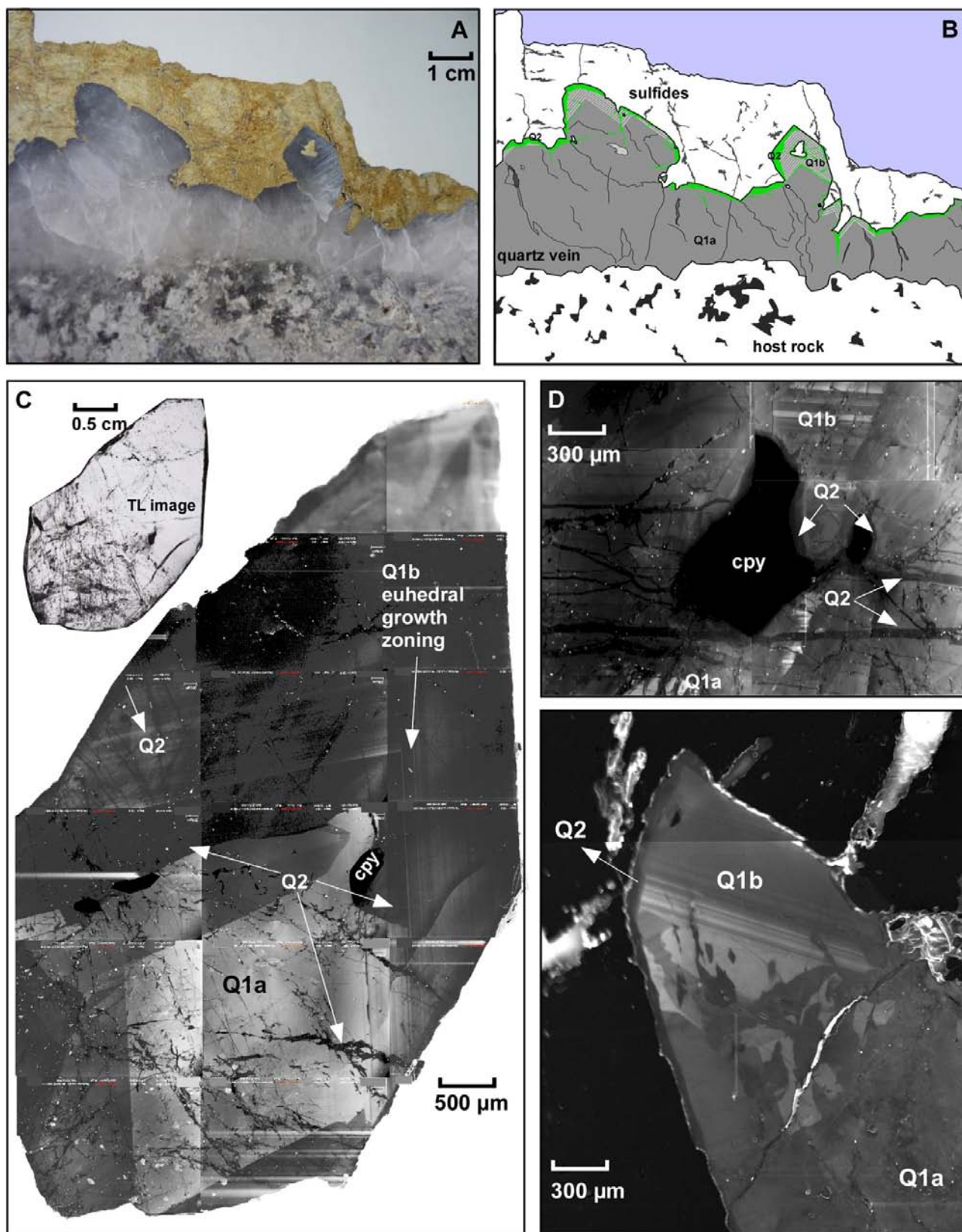


Figure 1. (A and B) Reconstruction of an area from the vein-sample CSU1 based on SEM-CL textures. Note that most of hydrothermal quartz vein infill is represented by the Q1 quartz generation, whereas Q2 forms a narrow rim of quartz around Q1 or fills fractures within Q1; (C) Photomosaic of a free standing quartz crystal (sample SUCH3) where the two quartz generations can be observed. This pattern can be observed in many samples where chalcopyrite and quartz formed in the center of the vein; (D) Detail of a small single grain of chalcopyrite that precipitated along a microfracture filled with quartz Q2 (sample CSU1A); (E) Thin rim of Q2 overgrowing euhedral Q1. The Q2 is always in direct contact with the main sulfide stage of chalcopyrite, bismutinite and gold-bearing minerals.

P 2.28

Dunite formation in the Lanzo peridotites, Italy: a morphological, petrological and geochemical study.

Tornare Evelyne¹, Müntener Othmar¹

¹*Institute of Mineralogy and Geochemistry, Anthropole, University of Lausanne, CH-1015 Lausanne, Switzerland*

The Lanzo ultramafic massif is located in the Western Alps, Northern Italy. This massif is formed by subcontinental mantle lithosphere peridotites and pyroxenites exhumed during Jurassic rifting related to the opening of the Piemont-Liguria ocean. During the early stages of exhumation this mantle portion underwent successive reactive and impregnating melt interaction phases. Intergranular porous melt percolation was first diffuse and then focused through high porous channels, which resulted in dunites bodies (Müntener and Piccardo, 2003). Dunites are clue for a better understanding of melt migration processes and evolution of mid-ocean ridge magmas and may develop during an advanced stage during the transition from a magma-poor margin to an (ultra)-slow spreading ridge. Here we present results from a morphological and geochemical study on olivine, spinel and clinopyroxene from Lanzo dunites.

Two distinct morphological and mineralogical types of dunite channels have been recognized. The first type is characterized by isolated straight and clinopyroxene-bearing dunite channels, with various and irregular size but especially as decametre-scale bodies. The second type is characterized by anastomosing networks of thin, braided clinopyroxene-free dunite channels. Olivine compositions are identical in both types in terms of Mg# (89.9 – 92.5) and trace element contents, while spinel compositions vary between the two types (TiO₂: 730 – 3230 ppm and even higher for the second type, Cr#: 29.3 – 44.2).

In clinopyroxene-bearing dunites, two clinopyroxene shapes have been identified: cumulate granular grains and typical interstitial grains. Granular grains are chemically homogeneous over the entire grain, while interstitial grains show incompatible trace element enrichment, including Na and Ti, and especially in Zr and Hf and a clear Zr/Hf ratio increase from core to rim of the grains. In addition, phlogopite and Ti-amphibole inclusions in dunite spinel surrounding small gabbroic dikes are enriched in incompatible elements, with positive Zr, Hf anomalies. Clinopyroxene chemistry and modal amounts may be related to conditions and time of the melt migration and allow us to establish a relative chronology of the dunite channel activity. Chondrite-normalized REE abundances of liquids in equilibrium with clinopyroxene have been calculated. The melt composition remains N-MORB type during the entire intergranular porous flow migration episode until the compaction event. At this point the melt composition seems to change and REE pattern of melt in equilibrium with interstitial clinopyroxene show a LREE enriched composition similar to E-MORB with a Zr and Hf positive anomaly.

The morphological and geochemical features can be related to two distinct crystallization regimes. The homogeneous granular grains crystallized in equilibrium from the cooling migrating melt; while the interstitial grains are the result of crystallization of interstitial trapped melt, probably induced by compaction and porosity decrease of the peridotites, during the final stages of melt migration. These last increments of melts probably represent refractory initial compositions that fractionate in the mantle forming metasomatic assemblages.

REFERENCES

- Müntener, O., Piccardo, G.B. (2003): Melt migration in ophiolitic peridotites: the message from Alpine Apennine peridotites and implications for embryonic ocean basins. In: Dilek, Y., Robinson, P.T. (eds.) *Ophiolites in Earth history*, vol 218, Geological Society of London Special Publications, pp 69-89

P 2.29

The coupling of deformation and reaction kinetics in the case of positive volume change reactions

Tumarkina Elizaveta¹, Podladchikov Yuri² & Connolly James A.D.¹

¹*Structural Geology and Tectonics group, Geological Institute, ETH, Sonneggstrasse 5, Zurich 8092, Switzerland (elizaveta.tumarkina@erdw.ethz.ch)*

²*Institute of Geophysics, UNIL, Quartier UNIL, Bâtiment Amphipôle, Lausanne 1015, Switzerland*

Common petrologic grids derived either by experimental or theoretical investigations do not consider the role of deformation during metamorphism. Moreover, rheological studies rarely take in the account mineral reactions in the system. In natural rocks, however, deformation and reaction are coupled. The majority of reactions in nature involve volume change. In some reactions volume change reaches almost 20% as for the transformation from jadeite to albite + quartz. Volume change causes reaction-induced stress. A number of studies have shown evidences for the existence of high transformation stresses in the materials as a consequence of the phase changes processes. The transformation-induced stresses initially produce elastic strain. Afterwards, if the reaction volume change is large enough than either plastic or viscous deformation occur.

In our previous studies we performed experiments on partial melting of quartz-muscovite system that has 3 % of positive volume change. It has been showed that deformation enhances reaction kinetics and during shear deformation melting rate is 1.7 times faster than at hydrostatic conditions. To explain this fact we considered few different hypotheses as shear heating, strain energy, surface energy, local pressure drops and effective viscosity. Our results suggest that the reduction in effective viscosity induced by macroscopic shear can have a profound effect on reactions that have a non-zero isobaric volume change. In contrast, all other explanations of increased melting as shear heating, strain and surface energies and local pressure drops effects are eliminated by our first order considerations. To verify the significance of effective viscosity effect we performed a model of the spherical liquid inclusion growth within an inert solid matrix. In this model thermodynamics of melting reaction and mechanical response of solid phase are coupled.

In this study we also propose a general version of the model of deformation and volume positive reaction coupling, expanding its relevance to many problems that exist in the current studies. For example, occurrence of highly deformed minerals in the contact with undeformed ones (Lenze et al. 2005) or kinetics of rim growth between quartz and olivine depending of geometrical relationships (Schmid et al. 2009).

REFERENCES

- Lenze A., Stockhert B. & Wirth R. 2009: Grain scale deformation in ultra-high-pressure metamorphic rocks - an indicator of rapid phase transformation. *Earth and Planetary Science Letters*, 229, 217– 230.
- Schmid D.W., Abart R., Podladchikov Y.Y. & Milke R. 2009: Matrix rheology effects on reaction rim growth II: coupled diffusion and creep model. *Journal of metamorphic Geology*, 27, 83–91.

P 2. 30

Geological Setting of the Drmbon Copper-Gold Deposit, Nagorno Karabakh Republic, Lesser Caucasus

Vardanyan Arman

Institute of Geological Sciences, National Academy of Sciences of The Republic of Armenia, Yerevan (arman_vrd@yahoo.com)

The Drmbon copper-gold deposit is located in the Mekhmana ore district (Nagorno Karabakh), which is the part of the Jurassic-Cretaceous Pont-Somkheti-Karabakh-Elburs island arc system of the Lesser Caucasus. The deposit was discovered in 1933. Recent mining of deposit, with mainly underground working, enabled us to clarify several important facts about the geological setting of the Drmbon deposit.

The Drmbon orefield occurs in a caldera setting of 4km in diameter. The lower volcanogenic suite of the Drmbon volcanic sequence consists of Lower Bajocian basaltic andesites, andesites and Upper Bajocian andesites, dacites and tuffs. The upper volcanogenic suite is composed of Bathonian basaltic andesites, andesites and their tuffs and volcano-sedimentary rocks. In addition, there are also Upper Jurassic volcanic agglomerates (basaltic andesite – andesite) and volcano-sedimentary rocks. There are abundant outcrops of subvolcanic rocks and dikes of different composition ranging from basaltic andesite to rhyolite, as well as felsic extrusions. Some of the subvolcanic rocks and dikes are located in arcual structures. In the northeastern part of the caldera there is a large outcrop of an Upper Jurassic stratiform diorite body.

In the northeastern part of the caldera, the rock sequences preserved their periclinal bedding. By contrast, in the southwestern part of caldera, the primary periclinal bedding of the rock sequences was modified and were inclined to the center of the caldera during subsidence. As a result of these movements, a domelike structure was formed in the southwestern peripheral part of the caldera, which was favorable for ore formation. The Drmbon deposit is located at the intersection of the caldera boundary and a northwest-striking fault.

The major rocks units in the ore deposit area are lower volcanogenic sequence (Lower and Upper Bajocian lavas and tuffs), Upper Bathonian subvolcanic quartz dacites and Upper Jurassic (Oxfordian) agglomerates. The main host rocks of the deposit are Upper Bajocian andesites and dacites, which were mainly brecciated during caldera formation. The thickness of the Upper Bajocian rocks in the deposit is between 50 and 65m.

An important role during ore deposit formation was played by subvolcanic (sill form) quartz dacites and a shear zone at the contact between the quartz dacites and the underlying host rocks, which stopped the main part of the hydrothermal fluids. As a result of this, massive ore zones are now located below the quartz dacites along their contacts. Quartz dacites were injected between the lower and the upper volcanogenic suites, parallel to the subsidence of the volcanic edifice. As a result of irregular movements of viscous magma along interlayer areas, quartz dacites acquired an ataxitic, fluidal and breccia texture. The thickness of the quartz dacite sill in the deposit reaches 200m.

Quartz dacites in the deposit crosscut Bathonian volcanic rocks and are crosscut by dike-form and vent bodies of agglomerates. On the southeastern flank of the deposit, agglomerates occur as beds, which in fill out and smooth out the irregularities of the paleorelief. Clasts in agglomerates are generally rounded, locally nearly isometric in size from 3-4cm to 1-2m, the percentage of which varies between 40 and 70%. Agglomerates show no sorting of clasts. Clasts consist predominantly of andesites and basaltic andesites, and subsidiary compact, fresh dacites. Agglomerates also include large blocks (10-20m) of early Oxfordian limestone.

Dikes in the Drmbon deposit consist of two varieties: dacites and andesites, which are mostly located in arcual faults and have a 55-75° dip toward the center of the caldera. They crosscut all volcanogenic rocks in the deposit. All dikes in the deposit are altered, but they do not contain any mineralization. Numerous observations in the mines and also studies of thin sections, collected from the contact of the dikes with the ore bodies, show evidence that the dikes pre-date ore formation.

In the deposit, there are abundant bodies of explosive-injection breccias. These rocks post-date the dikes, but pre-date or are coeval with mineralization. In the mine, there are explosive-injection breccias with numerous rounded fragments of plagiogranite, outcrops of which remain unknown in the whole ore district. A fragment of plagiogranite was also found in agglomerates. This suggests that there is a plagiogranite intrusion at depth below the Drmbon deposit.

The Drmbon deposit consists three main lens-form ore bodies. Their thickness varies between 20m and 80m. As a rule, the upper boundaries of the ore layers are clearly exposed and are characterized by a shear zone, at the contact of subvolcanic quartz dacites with underlying ore-bearing rocks. The richest massive sulfide ore lenses (2-6m of thickness) are located immediately below the shear zone. The lower parts of the ore bodies pass gradually into a zone of disseminated sulfide mineralization and into quartz - carbonate – sericite altered host rocks with pyrite dissemination.

REFERENCES

- Vardanyan A. 2008: Geological composition and peculiarities of The Drmbon gold-copper sulphide deposit. *Nauki o Ziemle series journal of The Izvestia of the National Academy of Sciences of the Republic of Armenia*, 2008, vol. LXI, No 1, 3-13 (in Russian, with English abstract).
- Vardanyan A. & Zohrabyan S. 2007: About subvolcanic character of quartz dacites of the Drmbon deposit. *Nauki o Ziemle series journal of The Izvestia of the National Academy of Sciences of the Republic of Armenia*, 2007, vol. LX, No 3, 46-49 (in Russian, with English abstract).
- Vardanyan A. & Zohrabyan S. 2008: Explosive-injection breccia-conglomerates of the Drmbon gold-copper sulphide. *Nauki o Ziemle series journal of The Izvestia of the National Academy of Sciences of the Republic of Armenia*, 2008, vol. LXI, No 1, 14-20 (in Russian, with English abstract).

P 2.31

When did the large meteorite shower Jiddat al Harasis 091 arrive on Earth?

Zurfluh Florian¹, Hofmann Beda², Gnos Edwin³, Eggenberger Urs¹ & Preusser Frank⁴

¹Institut für Geologie, Baltzerstrasse 1+3, CH-3012 Bern (florian.zurfluh@geo.unibe.ch)

²Naturhistorisches Museum Bern, Bernastrasse 15, CH-3005 Bern

³Muséum d'Histoire naturelle, route de Malagnou 1, CP 6434, CH-1211 Genève

⁴Department of Physical Geography and Quaternary Geology, Stockholm University, 106 91 Stockholm, Sweden

Jiddat al Harasis (JaH) 091 is a large meteorite strewn field in the desert of Oman (Russel et al. 2004, Gnos et al. 2006). About 670 fragments (different find places of paired samples, some of them are further fragmented) with a total mass of ~4 metric tons were so far recognized to belong to the same fall event. They are distributed over an ellipse of 51.2 km by 7.2 km. Some of the largest fragments formed a breccia that is composed of meteoritic fragments, iron hydroxides, a weathering product of the meteorite, and soil particles.

Terrestrial ages, the residence time of meteorites on Earth, are usually determined using the decay of spallation-produced radioactive isotopes such as ²⁶Al, ³⁶Cl (for meteorites with long terrestrial residence times, Antarctica) or ¹⁴C (shorter time scale, hot deserts) (e.g. Jull 2006). A limiting factor of radiocarbon dating is the size of the preatmospheric meteoroid since the production of cosmogenic ¹⁴C is restricted due to shielding. Such ages can be corrected with ¹⁰Be.

Beside this standard method we tried to estimate the terrestrial age of JaH 091 with several other indirect approaches: A well-known feature of meteorites recovered from hot deserts is the continuous accumulation of Sr and Ba (e.g. Al-Kathiri et al. 2005). By measuring natural and cut surfaces with handheld X-ray fluorescence (HHXRF), the degree of contamination can be evaluated. Another parameter is the degree of alteration of the primary minerals observed in thin section using reflected light (Wlotzka 1993). And finally, the presence of water soluble salts is an indicator of terrestrial alteration.

Since the degree of contamination with salts is size dependent and influenced by local soil composition, this parameter is not useful to determine the terrestrial age. The Sr and Ba accumulation is also a result of local soil composition, but seems to be more robust, since soil composition in Oman is relatively homogeneous. The degree of oxidation as represented by the weathering degree correlates with terrestrial age but can be inhomogeneous in a sample and is usually lower in large samples.

The find site of the largest fragments of the JaH 091 strewn field offered us the possibility to test a new approach: Some large meteorite pieces were completely buried into the soil. We took two soil samples direct under a large meteorite fragment from the main impact site and dated its last exposure to the sunlight, which is believed to be close to the terrestrial age of the meteorite, by optical stimulated luminescence (OSL). First results show a good agreement between the radiocarbon (19.3 ± 1.3 ka) and the OSL (15.2 ± 1.4 and 18.6 ± 1.5 ka) ages. The mean weathering grade of JaH 091 is W3, which is also in the range of ¹⁴C terrestrial ages of 15 – 20 ka from meteorites found in Oman. In addition, the amount of Sr and Ba contamination on exposed surfaces (~160 ppm and ~90 ppm, respectively) also fits this age range.

In conclusion, we can say that the terrestrial age of JaH 091 is between 15 and 20 ka and that the stones of this shower have undergone several kinds of alteration and contamination.

REFERENCES

- Al-Kathiri, A., Hofmann B. A., Jull A. J. T., and Gnos E. 2005: Weathering of meteorites from Oman: Correlation of chemical/mineralogical weathering proxies with ¹⁴C terrestrial ages and the influence of soil chemistry, *Meteoritics & Planetary Science*, 40, 1215-1239.
- Gnos, E., Eggimann M. R., Al-Kathiri A. and Hofmann B. A. 2006: The JaH 091 strewn field, *Meteoritics & Planetary Science* 41 Suppl., A64
- Jull, A.J.T., 2006, Terrestrial ages of meteorites in *Meteorites and the Early Solar System II* (Eds. Lauretta, D.S. & McSween, H.Y.), University of Arizona Press, 889-905
- Russell S. S., Folco L., Grady M. M., Zolensky M. E., Jones R., Righther K., Zipfel J. and Grossmann J. N. 2004: The Meteoritical Bulletin, No. 88, 2004 July. *Meteoritics & Planetary Science* 39, A215-A272.
- Wlotzka F. 1993: A Weathering scale for the ordinary chondrites (abstract). *Meteoritics* 28, 460.

3. Low-Temperature Isotope Geochemistry

Andrea Voegelin, Elias Samankassou

TALKS:

- 3.1 *Giorgioni M., Weissert H., Bernasconi S., Hochuli P., Coccioni R., Keller C.*: Late Albian Carbon Isotope Stratigraphy and new Insights into mid-Cretaceous Paleoceanography
- 3.2 *Grauel, A. L., Schmid T. W., Hu B., Bergami C., Capotondi L., De Lange G. J., Zhou L., Bernasconi S. M.*: Calibration and application of the 'clumped-isotope' thermometer to foraminifera for high-resolution climate reconstructions of the last 500 years from the Mediterranean Sea
- 3.3 *Jiskra M., Wiederhold J.G., Bourdon B., Kretzschmar R.*: Solution speciation controls mercury isotope fractionation during sorption of Hg(II) to goethite
- 3.4 *Kocsis L., Gheerbrant E., Mouflih M., Cappetta H., Ulianov A., Amaghaz M.*: Geochemical composition of marine vertebrates from Sidi Chenanne (Ouled Abdoun Basin, Morocco)
- 3.5 *Millán M.I., Bernasconi S.M., López-Horgue M.A., Iriarte E., Weissert H.*: Clumped isotope analysis of Pozalagua hydrothermal dolomite system (N Spain)
- 3.6 *Nägler T.F., Neubert N., Böttcher M.E., Dellwig O., Schnetger B.*: Molybdenum scavenging from anoxic waters of the modern Black and Baltic Seas
- 3.7 *Pretet C., Nægler T.F., Villa I.M., Böttcher M.E., Samankassou E.*: Barium isotope fractionation in carbonates
- 3.8 *Schmassmann Silvia, Mattias Fricker, Detlef Günther, Dominik Fleitmann*: Forest use and damages recorded by trace elements and stable isotopes in recent speleothems from Milandre cave (JU)
- 3.9 *Voegelin, A. R., Nægler, T. F., Neubert, N., Heri, A. R., Pettke, T., Schlunegger, F., Steinmann, M., Pourret, O., Villa, I.M.*: Molybdenum isotopes in river water: sources, fractionation processes and their importance for Mo cycling in the marine environment
- 3.10 *Wiederhold J.G., Bourdon B., Kretzschmar R.*: Mass-dependent and mass-independent fractionation of stable mercury isotopes as tracer for anthropogenic pollution in the environment
- 3.11 *Wille M, Sutton J., DeLeon A., Ellwood M., Eggins S., Maher W.*: Silicon isotopic fractionation in marine sponges: A model for understanding silicon isotopic variations in sponges

POSTERS:

- P 3.1 *Keller C.E., Hochuli P.A., Weissert H., Bernasconi S.M., Giorgioni M., Garcia T.I.*: A volcanically induced climate warming and floral change preceded the onset of OAE1a (Early Cretaceous)
- P 3.2 *Keller C.E., Weissert H., Hochuli P.A., Bernasconi S.M., Giorgioni M., Garcia, T.I.*: In the Tethys Ocean black shales commonly formed prior to Oceanic Anoxic Event 1a (OAE1a, Early Aptian, ~120 Ma ago)
- P 3.3 *Smith, R.S., Wiederhold, J.G., Jew, A.D., Brown, G.E., Bourdon, B., Kretzschmar, R.*: Mercury Isotope Fractionation as Biogeochemical Tracer in Ore Waste

3.1

Late Albian Carbon Isotope Stratigraphy and new Insights into mid-Cretaceous Paleoceanography

Giorgioni Martino¹, Weissert Helmut¹, Bernasconi Stefano¹, Hochuli Peter^{2,1}, Coccioni Rodolfo³, Keller Christina¹

¹Department of Earth Sciences, Geological Institute, ETH Zurich, Sonneggstr. 5, 8092 Zürich, Switzerland (martino.giorgioni@erdw.ethz.ch)

²Palaeontological Institute, University of Zurich, Karl Schmid-Strasse 4, 8006 Zürich, Switzerland

³Dipartimento di Scienze dell'Uomo, della Vita e dell'Ambiente, Università di Urbino, Campus Scientifico località Crocicchia, 61209 Urbino, Italy

We present new $\delta^{13}\text{C}_{\text{carb}}$ and $\delta^{13}\text{C}_{\text{org}}$ data from the Late Albian succession of the Umbria-Marche Basin showing the evolution of the ocean-climate system under the mid-Cretaceous greenhouse conditions. We observe long eccentricity cycles recorded both in the $\delta^{13}\text{C}_{\text{carb}}$ and in the $\delta^{13}\text{C}_{\text{org}}$ records, suggesting that orbital forcing affected both oceans and terrestrial environments. These cycles occur together with very variegated facies, with cyclic, thin black shale layers, suggesting that the oceanic circulation was unstable, very sensitive to orbital forcing, and prone to anoxic episodes.

During the Late Albian we observe the occurrence of more homogeneous and carbonate-rich sedimentation, accompanied by a stabilization of the $\delta^{13}\text{C}_{\text{carb}}$ curve. This suggests a switch of the global oceanic system into a more stable circulation mode, with deeper thermocline and permanent deep-water ventilation. On the other hand this change does not occur in the $\delta^{13}\text{C}_{\text{org}}$ record dominated by terrestrial organic matter, showing that this event concerned the oceanic but not the terrestrial system.

In the lattermost Albian, after the onset of the more stable circulation mode, the ocean was pushed back again into the unstable mode for a relatively short time. This event occurred at global scale, it was accompanied by a slight increase in carbon burial and was considered one of the minor Cretaceous Oceanic Anoxic Events (OAE 1d).

We hypothesize that the transition into the stable circulation mode was an oceanographic response to the opening and deepening of gateways during the mid-Cretaceous. On the other hand the short-term switch back to the unstable mode was due to a period of prolonged, exceptionally strong orbital forcing and/or to changes in atmospheric CO_2 concentrations. Our results show that anoxic conditions during the mid-Cretaceous could occur in response to different forcings, favored by the peculiar paleoceanographic conditions.

3.2

Calibration and application of the 'clumped-isotope' thermometer to foraminifera for high-resolution climate reconstructions of the last 500 years from the Mediterranean Sea

Grauel Anna-Lena¹, Schmid Thomas W.¹, Hu Bin ^{1,2}, Bergami Caterina³, Capotondi Lucilla ³, De Lange Gert J.⁴, Zhou Liping² & Bernasconi Stefano M.¹

¹ Geological Institute, ETH Zurich, 8092 Zurich, Switzerland (anna.grauel@erdw.ethz.ch)

² Department of Geography, Peking University, 100871 Beijing, China

³ CNR - National Research Council of Italy, ISMAR - Institute of Marine Sciences in Bologna

⁴ Institute of Earth Science, Utrecht University, 3584 Utrecht, The Netherlands

Clumped-isotope thermometry allows determination of the precipitation temperature of calcite via measurements of the abundance of ¹³C-¹⁸O bonds in carbonate and at the same time an estimation of the $\delta^{18}\text{O}$ of seawater in which the organism lived.

At ETH Zurich we utilize a newly developed technique for clumped-isotope measurements of small samples (Schmid and Bernasconi, 2010), which allows for the first time to produce combined high-resolution $\delta^{18}\text{O}$ and clumped-isotope records from sediment cores. In this contribution we present a calibration study on 8 species of foraminifera with growth temperatures ranging from 0.6°C to 29°C.

Our results are in good agreement with the published calibrations of Ghosh et al. (2006) and Tripathi et al. (2010). The clumped-isotope temperatures of the surface-dwelling planktonic foraminifera are similar to the measured sea surface temperatures (SST's), while the benthonic and deep-dwelling planktonic species show a larger variation, suggesting that they may not always precipitate their shells in isotopic equilibrium with seawater.

We also show that our measuring technique on small samples of foraminifera can be used to obtain high-resolution $\delta^{18}\text{O}$ and $\delta^{13}\text{C}$ time series, and at the same time to reconstruct lower-resolution clumped-isotope temperature records.

We present our $\delta^{18}\text{O}$ and clumped-isotope measurements of *Globigerinoides ruber (white)* from a short sediment core covering the last 500 years, at 3.5 years resolution, from the Gulf of Taranto (Mediterranean Sea). As it records both, marine and riverine influences, we deem this region well suited for reconstructing Holocene climate variability, especially for evaluating the potential of anthropogenic influence on climate.

The obtained clumped-isotope temperatures are in good agreement with measured SST's with accuracy of $\pm 2^\circ\text{C}$ over the last 50 years. This demonstrates that our method can serve as a robust new tool for reconstructing changes in temperature and $\delta^{18}\text{O}$ of seawater, and hence salinity, on the same sample.

We observe that SST's do not change significantly over the last 500 years. However, changes in salinity in the order of 1-2 PSU are common, which suggests changes in circulation and freshwater runoff. Additional analyses of core top samples and water samples from the same area support our calibration of the clumped-isotope signatures of *G. ruber (white)*.

REFERENCES

- Ghosh, P., Adkins, J., Affek, H., Balta, B., Guo, W., Schauble, E., Schrag, D., Eiler, J. (2006). ¹³C-¹⁸O bonds in carbonate minerals: A new kind of paleothermometer. *Geochim. Cosmochim. Acta* 70, 1439-1456.
- Schmid, T.W., Bernasconi, S.M. (2010). An automated method for 'clumped-isotope' measurements on small carbonate samples. *Rapid Comm. Mass Spectrom.* 24, 1955-1963.
- Tripathi, A.K., Eagle, R.A., Thiagarajan, N., Gagnon, A.C., Bauch, H., Halloran, P.R., Eiler, J.M. (2010). ¹³C-¹⁸O isotope signatures and 'clumped-isotope' thermometry in foraminifera and coccoliths. *Geochim. Cosmochim. Acta* 74, 5697-5717.

3.3

Solution speciation controls mercury isotope fractionation during sorption of Hg(II) to goethite

Jiskra Martin^{1,2}, Wiederhold Jan G.^{1,2}, Bourdon Bernard^{1,3} Kretzschmar Ruben²

¹ETH Zurich, Institute of Geochemistry and Petrology, Isotope Geochemistry, Clausiusstrasse 25, CH-8092 Zürich (martin.jiskra@erdw.ethz.ch)

²ETH Zurich, Institute of Biogeochemistry and Pollutant Dynamics, Soil Chemistry, Universitätsstr. 16, CH-8092 Zürich

³Laboratoire de Géologie de Lyon, ENS Lyon, CNRS and UCBL, 46 Allée d'Italie, F-69364 Lyon, France

Mercury is a pollutant of global concern because of its potential to be transported over long distances through the atmosphere and to form highly toxic organometallic molecules (e.g., methyl-Hg) which biomagnify along the food chain. Soils are the most important terrestrial sinks for atmospherically deposited Hg. Iron(oxyhydr)oxides are common soil minerals and can play an important role in the immobilization of Hg, especially in mineral soils with low organic matter content. Environmental changes like acidification, salinization, or land use change can lead to a leaching of mineral-bound mercury. The analysis of stable Hg isotope ratios has developed rapidly in the past years and represents a promising tool for pollution source identification and tracing the biogeochemical behavior of mercury. We use stable Hg isotopes to investigate the biogeochemical Hg cycle in soils. However, to interpret natural Hg isotope ratios, a better understanding of the processes causing Hg isotope fractionation in soils is needed. Therefore, we investigated the sorption of Hg(II) to goethite (α-FeOOH), an important Fe(III)-oxyhydroxide mineral in most soils, and the corresponding isotope fractionation mechanisms.

We performed laboratory scale sorption experiments with dissolved Hg(II) (nitrate salt) and goethite under different pH conditions (buffered at pH 7 with 2.5 mM MOPS, or unbuffered at pH 3-6), different Cl⁻ concentrations (0 and 0.5 mM) and different SO₄²⁻ concentrations (0 and 1M). Equilibration experiments from 18h to 30d were performed. The dissolved Hg was separated from the goethite by centrifugation and filtration, and the sorbed fraction was measured after dissolving the goethite in 6M HCl. Concentrations of Hg were measured by CV-AFS and isotope ratios by CV-MC-ICPMS (Nu Plasma) yielding a standard reproducibility of ±0.09 ‰ (2SD for δ²⁰²Hg, 16 measurements over 12 months) using Tl mass bias correction and sample-standard bracketing.

The experimental data revealed systematic mass dependent fractionation (MDF) during the equilibration experiments (72 h) with an enrichment of light Hg isotopes at the goethite surface (δ²⁰²Hg_{diss} - δ²⁰²Hg_{sorb} = 0.4 ‰). Low pH and increased Cl⁻ concentration reduced the sorbed fraction of Hg(II), but did not affect the isotope fractionation factor compared with pH 7. The amendment of 1M SO₄²⁻, resulting in a change of the Hg sorption complex from bidentate to monodentate (Kim et al., 2004), did not show any effect on the Hg isotope fractionation. Different equilibration times (18h – 30 d) did also not affect the observed isotope effect. These results strongly suggest that the observed isotope effect during sorption of Hg(II) to goethite is controlled by an equilibrium isotope effect between solution species. Computational chemistry calculations of mass-dependent and nuclear volume fractionation factors between solution species (Wiederhold et al., 2010) support this hypothesis by predicting for the sorption active Hg-cations (e.g. HgOH⁺) an enrichment of the lighter isotopes in the order of the experimentally observed 0.4 ‰ for δ²⁰²Hg relative to the dominant neutral solution species (e.g. Hg(OH)₂).

In combination with the previous findings on Hg(II) sorption to thiol groups (Wiederhold et al., 2010), a model study for sorption to organic matter, our data suggest that light Hg isotopes are preferentially sequestered in soils and one could expect an enrichment of heavy Hg isotopes in the mobile fraction which is leached from soils into surrounding ecosystems.

REFERENCES

- Kim, C.S., Rytuba, J., Brown, G.E. 2004: EXAFS study of mercury(II) sorption to Fe- and Al-(hydr)oxides – II. Effects of chloride and sulfate. *Journal of Colloid and Interface Science*, 270, 9-20.
- Wiederhold, J.G., Cramer, C.J., Daniel, K., Infante, I., Bourdon, B., Kretzschmar, R. 2010: Equilibrium Mercury Isotope Fractionation between Dissolved Hg(II) Species and Thiol-Bound Hg. *Environ. Sci. Technol.* 44, 4149-4197.

3.4

Geochemical composition of marine vertebrates from Sidi Chenanne (Ouled Abdoun Basin, Morocco)

Kocsis László¹, Gheerbrant Emmanuel², Mouflih Mustapha³, Cappetta Henri⁴, Ulianov Alexey¹, Yans Johan⁵ & Amaghaz Mbarek⁶

¹ Institut de Minéralogie et Géochimie, Université de Lausanne, Switzerland (laszlo.kocsis@unil.ch)

² Muséum National d'Histoire Naturelle, Département Histoire de la Terre, Paris, France

³ Faculté des Sciences Ben M'Sik, Casablanca, Morocco

⁴ «Institut des Sciences de l'Evolution», Université de Montpellier II, France

⁵ Facultés Universitaires Notre-Dame de la Paix à Namur, Belgium

⁶ Groupe Office Chérifien des Phosphates, Centre Minier de Khouribga, Morocco

Phosphate rich sediments are mined in several regions in Morocco. The most actively mined area is the Ouled Abdoun Basin which one of the largest producing mines in the world. The phosphate series cover a time span of about 25 million years from the Maastrichtian to early Lutetian. These layers are very rich in vertebrate remains, which often form bonebeds. The far most frequent fossils are shark teeth and bony fish remains, but several other groups like crocodiles, turtles, mosasaurs are also quite common in certain beds. Some of the rare curiosities are the fossils of pterosaurs, «dinosaurs», birds and mammals. The fossil richness of these beds has drawn the attention of many scientists for years, and not only paleontologists but also geochemists (e.g. Grandjean et al. 1988; Lécuyer et al. 1993; McFadden et al. 2004). These later studies mainly focused on oxygen isotope and rare earth element (REE) compositions of the vertebrate fossils in order to assess paleo-environmental conditions (climate, oceanography, early diagenesis).

Here, a similar but a more detailed study, involving also carbon isotope composition of the remains, has been carried out in the Sidi Chennane area. The different phosphate layers were systematically sampled largely for shark teeth and coprolites, and prepared for the geochemical analyses. One of the main aims of our study is to test whether the fossils reflect or preserved any of the observed perturbations in the carbon cycle during and after the Paleocene-Eocene (P/E) boundary, namely the abrupt negative carbon isotope shifts at different hyperthermals (cf. Lourens et al. 2005).

Shark teeth enameloid yielded often positive $\delta^{13}\text{C}$ values possibly reflecting dissolved inorganic carbon (DIC) of seawater at the time, while the $\delta^{13}\text{C}$ values of coprolites, bones and dentin are very negative linking to burial conditions and reflecting the special environment of phosphate formation with the intensive recycling of organic matter. The variation is quite large along the series in these fossils, especially in some of the bonebeds that is maybe due to reworked specimens and also maybe enhanced oxidation of organic matter at these levels. Between the phosphate layer-I and -II, that are Ypresian and Danian-Thanetian in age, more negative values appear which might relate to the P/E boundary event.

Oxygen isotope composition of shark teeth show habitat related variations, while along the series a general decreasing trend is observed till the top of layer-I possibly linking to warmer conditions.

Rare earth elements in apatite fossils originate almost entirely from early diagenetic pore fluid and thus they can be used as a fingerprint of burial conditions and they often applied in taphonomical studies (Trueman & Tuross, 2002). In the Sidi Chennane fossils the REE distribution is quite alike for the whole series showing typical seawater pattern with negative Ce-anomaly and heavy REE enrichment. Ypresian and Maastrichtian fossils are separated on La/Sm vs. La/Yb plot, while the Paleocene ones overlap between them.

REFERENCES

- Grandjean, P., Cappetta, H. & Albarède, F. 1988: The REE and eNd of 40–70 Ma old fish debris from the West-African platform. *Geophys. Res. Lett.*, 15, 389–392.
- Lécuyer, C., Grandjean, P., O'Neil, J.R., Cappetta, H. & Martineau, F. 1993: Thermal excursions in the ocean at the Cretaceous–Tertiary boundary (northern Morocco): $\delta^{18}\text{O}$ record of phosphatic fish debris. *Palaeogeogr. Palaeoclimatol. Palaeoecol.*, 105, 235–243.
- Lourens, L.J., Sluijs, A., Kroon, D., Zachos, J.C., Thomas, E., Röhl, U., Bowles, J. & Raffi, I. 2005: Astronomical pacing of late Palaeocene to early Eocene global warming events. *Nature*, 435, 1083–1087.
- MacFadden, B.J., Labs-Hochstein, J., Quitmyer, I. & Jones, D.S. 2004: Incremental growth and diagenesis of skeletal parts of the lamnoid shark *Otodus obliquus* from the early Eocene (Ypresian) of Morocco. *Palaeogeogr. Palaeoclimatol. Palaeoecol.*, 206, 179–192.
- Trueman, C.N. & Tuross, N. 2002: Trace elements in recent and fossil bone apatite. In: Kohn, J.M., Rakovan, J., Hughes, J.M. (Eds.), *Review in Mineralogy and Geochemistry*, vol. 48, pp. 489–521.

3.5

Clumped isotope analysis of Pozalagua hydrothermal dolomite system (N Spain)

M.I. Millán¹, S. M. Bernasconi¹, M.A. López-Horgue², E. Iriarte³ & H. Weissert¹

¹ Dept. of Earth Science, ETH Zürich, Sonneggstrasse 5, 8092 Zürich, Switzerland
(isabel.millan@erdw.ethz.ch)

² Dept. of Stratigraphy and Palaeontology, University of the Basque Country, Sarriena s/n, 48940 Leioa, Spain

³ Consejo Superior de Investigaciones Científicas. C/Egipcíacques 15, 08001 Barcelona, Spain

Carbonate clumped isotope geochemistry is an innovative technique that allows to estimate the precipitation temperature of carbonate minerals. In addition, the determined clumped isotope temperatures in combination with the $\delta^{18}\text{O}$ values of carbonates permit us to calculate the $\delta^{18}\text{O}$ of the fluid in equilibrium with the carbonate mineral. We tested this new tool in well-exposed outcrops of the hydrothermal dolomite system of the Asón Valley (Basque-Cantabrian Basin, western Pyrenees) to better characterize its thermal and fluid history.

The methodology used in the Stable Isotope Laboratory at ETH Zurich follows that described in Schmid and Bernasconi (2010). We measure the clumped isotope composition in multiple carbonate generations that were previously studied by microscopy and by fluid inclusion geochemistry. We analysed hydrothermal dolomites (saddle and fine replacive dolomites), early and late calcites, and host limestones at different burial depths and distances from the main dolomite body. The different generations of carbonates show a large range of D_{47} ranging between 0.356 and 0.590‰ corresponding to temperatures between approximately 40 and 200°C, using the Guo et al. (2009) theoretical calibration.

Dolomites give temperatures ranging from 117 to 169°C and reconstructed $\delta^{18}\text{O}$ water values from -3.6‰ to 6.6‰, indicating that they are the product of different fluid sources (hypersaline brines, marine and mixture of meteoric and marine waters). Yellow calcite filling transpressional Alpine fractures shows the lowest temperature value (40°C) with quite negative $\delta^{18}\text{O}$ water value (-12.4‰) indicating a late shallow depth origin influenced by meteoric waters. These results are in agreement with macroscopic (outcrop) and microscopic (petrography) analysis of the dolomites (López-Horgue et al., 2010). Host rock samples give the highest temperatures ranging from 130 to 200°C. Presuming a loading of sediments before Alpine compression of 1900 m, the paleogeothermal gradient obtained is 68.4 – 105.3°C km⁻¹. This elevated paleogeothermal gradient is related to extreme crustal thinning during the Mesozoic rifting stage previously documented in the Basque Cantabrian Basin (e.g.: García-Mondéjar et al., 2005).

The temperature reconstructions combined with petrographic and oxygen isotopic analysis provide an ideal opportunity to trace thermal and fluid history of the hydrothermal system of the Valle Asón in extraordinary quantitative detail. This study shows the great potential of the clumped isotope method to improve our understanding of low temperature hydrothermal systems and to trace thermal histories of sedimentary basins.

REFERENCES

- García-Mondéjar, J., López-Horgue, M. A., Aranburu, A., & Fernández-Mendiola, P. A. 2005: Pulsating subsidence during a rift episode: stratigraphic and tectonic consequences (Aptian-Albian, northern Spain): *Terra Nova* 17 (6), 517-525.
- Guo, W. F., Mosenfelder, J. L., Goddard, W. A., & Eiler, J. M. 2009: Isotopic fractionations associated with phosphoric acid digestion of carbonate minerals: Insights from first-principles theoretical modeling and clumped isotope measurements: *Geochimica Et Cosmochimica Acta*, 73 (24), 7203-7225.
- López-Horgue, M. A., Iriarte, E., Schröder, S., Fernández-Mendiola, P. A., Caline, B., Corneyllie, H., Frémont, J., Sudrie, M., & Zerti, S. 2010: Structurally controlled hydrothermal dolomites in Albian carbonates of the Asón valley, Basque Cantabrian Basin, Northern Spain: *Marine and Petroleum Geology*, 27 (5), 1069-1092.
- Schmid, T. W., & Bernasconi, S. M. 2010: An automated method for 'clumped-isotope' measurements on small carbonate samples: *Rapid Communications in Mass Spectrometry*, 24 (14), 1955-1963.

3.6

Molybdenum scavenging from anoxic waters of the modern Black and Baltic Seas

Nägler Thomas F.¹, Neubert Nadja^{1,2}, Böttcher Michael E.³, Dellwig Olaf³, & Schnetger Bernhard⁴

¹Institut für Geologie, Baltzerstarsse 3, 3012 Bern (naegler@geo.unibe.ch)

²Institut für Mineralogie, 30167 Hannover, Germany

³Leibniz Institut für Ostseeforschung Warnemünde, 18119 Rostock, Germany

⁴Institut für Chemie und Biologie des Meeres, 26111 Oldenburg, Germany

The isotope signature of molybdenum (Mo) is a relatively new proxy for paleo-redox conditions of the oceanic system. Mo is a redox-sensitive trace metal which is present in seawater as molybdate oxyanion with a long residence time of about 800 ka, resulting in a homogeneous seawater Mo isotope composition (Siebert et al. 2003). However, Mo is efficiently removed in the presence of sulfide and thus often enriched in reducing sediments. We analyzed samples from the Black Sea, the largest permanently euxinic basin and the type-system for sediment formation under anoxic conditions. Euxinic conditions prevail below the chemocline, at ~120 m water depth. A complementary sample set was taken from the Baltic Sea, the largest brackish basin of the world. Here, in two anoxic basins, the Gotland Deep and the Landsort Deep, have been included in the study. Most of the time, the water bodies are well stratified with a permanent pycnocline between 60 and 80 m depth. Water column profiles as well as surface sediment samples, were recovered from different water depths.

Dissolved Mo in all water samples is enriched in the heavy isotope ($\delta^{98}\text{Mo}$ values up to +2.9‰; $\delta^{98}\text{Mo}$ = deviation of $^{98}\text{Mo}/^{95}\text{Mo}$ from standard) compared to published isotope data of sedimentary Mo from the same water depths (Neubert et al. 2008). Furthermore, $\delta^{98}\text{Mo}$ values of all water samples from the Black Sea and anoxic deeps of the Baltic Sea are heavier than open ocean water (mean ocean Mo (MOMo) = +2.3 ‰). Near total removal of Mo from the water column is reached at aquatic sulfide concentration of ~11 μM (Erickson & Helz 2000). In the Black Sea this corresponds to a water depth of about 400 m. The corresponding sediment samples carry the signature of the main Mo source, ocean water, as expected from the mass balance. However, shallower sediments deposited under lower aquatic sulfide concentrations show significant Mo isotope fractionation. The sulfidity in the two deeps of the Baltic Sea is comparable to the Black Sea above 400m depth, and, as expected, the surface sediments show a similar Mo isotope fractionation.

While the observations are consistent, open questions remain concerning the of scavenging process: First, the extent to which Mo scavenging occurs in pore waters or within the sulfidic water column is still a matter of debate. Second, it is unclear whether the process is bidirectional (equilibrium) or unidirectional. Finally, the relative importance of the different oxythiomolybdates is not sufficiently constrained. These questions are approached applying a model (Nägler et al., 2011) involving published ab initio calculations of Mo isotope fractionation (Tossell 2005) and thermodynamic thiomolybdate distributions parameters (Erickson & Helz 2000). The model results indicate that the observed isotope fractionation between sediments and the anoxic water column of the Black Sea can readily be explained as decreasing importance of mono-, di-, or tri- thiomolybdate scavenging with increasing $\text{H}_2\text{S}_{\text{aq}}$. The model results further imply that Mo isotopic composition of the waters is in equilibrium with that of the sediments. The apparent equilibrium fractionation factor depends on the relative abundances of the different thiomolybdates, and thus $\text{H}_2\text{S}_{\text{aq}}$ abundance. An extrapolation to a theoretical pure MoS_4^{2-} solution indicates a fractionation factor between MoS_4^{2-} and authigenic solid Mo of $0.5 \pm 0.3\%$. Results from the Baltic Sea are in principle agreement with the model predictions, but may be affected by occasional large scale inflow events which lead to temporary disequilibrium distribution of thiomolybdates, due to the slow reaction kinetics of the MoOS_3^{2-} to MoS_4^{2-} transition.

$\delta^{98}\text{Mo}$ values of the upper mostly oxic waters of both basins are higher, and the Mo concentrations lower, than predicted by mixing models based on salinity. The results can be explained by non-conservative behavior of Mo under suboxic to anoxic conditions on the continental shelves, which, in case of the Black Sea, represent about 25% of its surface area. The suboxic to anoxic bottom water conditions favor preferential scavenging of lighter isotopes, leaving behind a heavy Mo isotopic composition in solution. Further, upwelling of deep saline water with heavy Mo isotopic signature and low Mo concentration may contribute to the $\delta^{98}\text{Mo}$ values of the upper waters.

In conclusion: 1) Data from euxinic water columns indicate in situ fractionation of Mo isotopes. 2) $\delta^{98}\text{Mo}$ of sulfidic waters and sediments are consistent with: a) Mo scavenging from the water column b) thiomolybdates scavenging c) equilibrium Mo isotope fractionation. 3) The apparent fractionation factor depends on relative abundances of the thiomolybdates and thus H_2S . The $\delta^{98}\text{Mo}$ between MoS_4^{2-} and sedimentary Mo is 0.5% +/- 0.3% . 4) $\delta^{98}\text{Mo}$ values of the upper waters of both basins indicate non-conservative behavior. This is most probably due to suboxic to anoxic Mo scavenging on the shelves.

REFERENCES

- Erickson, B.E., & Helz, G.R., 2000: Molybdenum(VI) speciation in sulfidic waters: Stability and lability of thiomolybdates, *Geochim. Cosmochim. Acta* 64, 1149-1158.
- Nägler, Th.F, Neubert, N., Böttcher, M.E., Dellwig, O. & Schnetger, B. 2011: Molybdenum isotope fractionation in pelagic euxinia: Evidence from the modern Black and Baltic Seas, *Chem. Geol.*, doi: 10.1016/j.chemgeo.2011.07.001
- Neubert, N., Nægler, T.F. & Böttcher, M.E. 2008: Sulphidity controls Molybdenum Isotope Fractionation into Euxinic Sediments: Evidence from the Modern Black Sea. *Geology*, 36; 10; 775–778
- Siebert, C., Nægler, T. F., von Blanckenburg, F., & Kramers, J. D., 2003: Molybdenum isotope records as a potential new proxy for paleoceanography, *Earth Planet. Sci. Lett.* 211, 159-171.
- Tossell, J.A., 2005: Calculating the partitioning of the isotopes of Mo between oxidic and sulfidic species in aqueous solution. *Geochim. Cosmochim. Acta* 69, 2981-2993.

3.7

Barium isotope fractionation in carbonates

Chloé Pretet¹, Thomas F. Nægler², Igor M. Villa^{2,3}, Michael E. Böttcher⁴, Elias Samankassou¹

¹ Département de Géologie et Paléontologie, rue des Maraîchers 13, CH-1205 Genève, (chloe.pretet@unige.ch)

² Institut für Geologie, Baltzerstrasse 3, CH-3012 Bern

³ Università di Milano Bicocca, I-20126 Milano

⁴ Leibniz Institute for Baltic Sea Research, Seestr. 15, D-18119 Warnemünde, Germany

In this study, we present first results from a current research on barium isotope fractionation in marine carbonates. This isotopic system could allow a better understanding of the evolution of oceanic water masses. In particular the Ba isotopic signature in carbonates could be linked with paleo productivity, given that Ba reacts like a nutrient in the water column. Further, continental weathering and upwelling influence the oceanic cycle of Ba. A Ba(NO₃)₂ standard solution and standard natural limestone BSC-CRM 393, obtained from the Bureau of Analysed Samples, Ltd., Middlesborough, England, have been analyzed to set up and optimize analytical procedures for the determination of Ba isotopes in carbonates.

We developed a method to separate Ba and measure its isotopic composition with sufficient precision to discriminate the expected variations in natural environments. Samples were dissolved in acids of different molarity in order to determine the most efficient method. A ¹³⁰Ba/¹³⁵Ba double spike (von Allmen et al., 2010) was added to all samples. Chemical separation on cation columns only made use of PTFE vessels to avoid the contamination introduced by softeners in other plastic materials. Measurements were carried out on a Nu Instruments multicollector ICP-MS. Sample digestion with hot concentrated acid (6.4 M HCl; 12h on the hot plate), yield isotopic compositions consistent within ±0.11 ‰ (2 standard deviation, referring to the ¹³⁷Ba/¹³⁴Ba ratio), while the use of 2.5 M HCl causes a significant fractionation to lighter isotopic compositions. Similarly, Ba concentrations determined on hot concentrated acid attacks are in line with independent concentration determinations, while 2.5 M HCl attacks recovered only about 50% of the Ba. These indications point to incomplete dissolution in the 2.5 M HCl attack. Probably disseminated small barites are present in the carbonate standard, with a Ba isotopic composition different from that of a coexisting, more soluble Ba phase. The internal reproducibility of the standard solution is 0.1 ‰ 2SD (N=14).

The precision and reproducibility of our refined method encourages us to measure natural carbonates, such as a vertical transect along a fossil carbonate platform (to constrain the oceanic evolution with depth), or corals (to constrain the influence of water masses on skeletal Ba).

REFERENCES

- von Allmen, K., Böttcher, M., Samankassou, E., Nægler, F.T. 2010: Barium isotope fractionation in the global barium cycle: First evidence from barium minerals and precipitation experiments, *Chemical Geology*, 277, 70-77.

3.8

Forest use and damages recorded by trace elements and stable isotopes in recent speleothems from Milandre cave (JU)

Schmassmann Silvia ^{1,2}, Mattias Fricker ³, Detlef Günther ³, Dominik Fleitmann ²

¹ Swiss Institute of Speleology and Karst Research, P.O. Box 818, CH-2301 La Chaux-de-Fonds, Switzerland (silvia.schmassmann@isska.ch)

² Institute of Geological Sciences, University of Bern and Oeschger Centre for Climate Change Research, Baltzerstrasse 1+3, CH-3012 Bern

³ Department of Chemistry and Applied Bioscience, Laboratory of Inorganic Chemistry, ETH Zürich, Wolfgang-Pauli-Strasse 10, 8093 Zürich

To test the suitability of speleothems from Milandre Cave (Boncourt, JU) for paleoclimatic and paleoenvironmental research, we analysed oxygen and carbon isotopes and a large range of trace elements in stalagmite M4 covering the period between 1822-2006 AC (chronology based on laminae counting).

Although many trace elements are probably of anthropogenic origin, the patterns of many pollution related trace elements do not correspond to the evolution of the concentrations in recognized archives for industrial pollution (e.g. Pb, Cu, Zn; cf. Fig 1). However, the sulphur in M4 corresponds to the SO₂ emissions (FOS) when considering an offset of about 30 years related to retention of S in the soil zone. The S-isotopic signature confirms a change in S-origin. The overlying soil acts thus probably as a reservoir for airborne and bedrock-derived elements. Mobilization of anthropogenic (e.g. Pb, Cu) and geogenic (e.g. Al, Ti) trace elements as solutes, colloids or particles is controlled mainly by soil stability and high infiltration events.

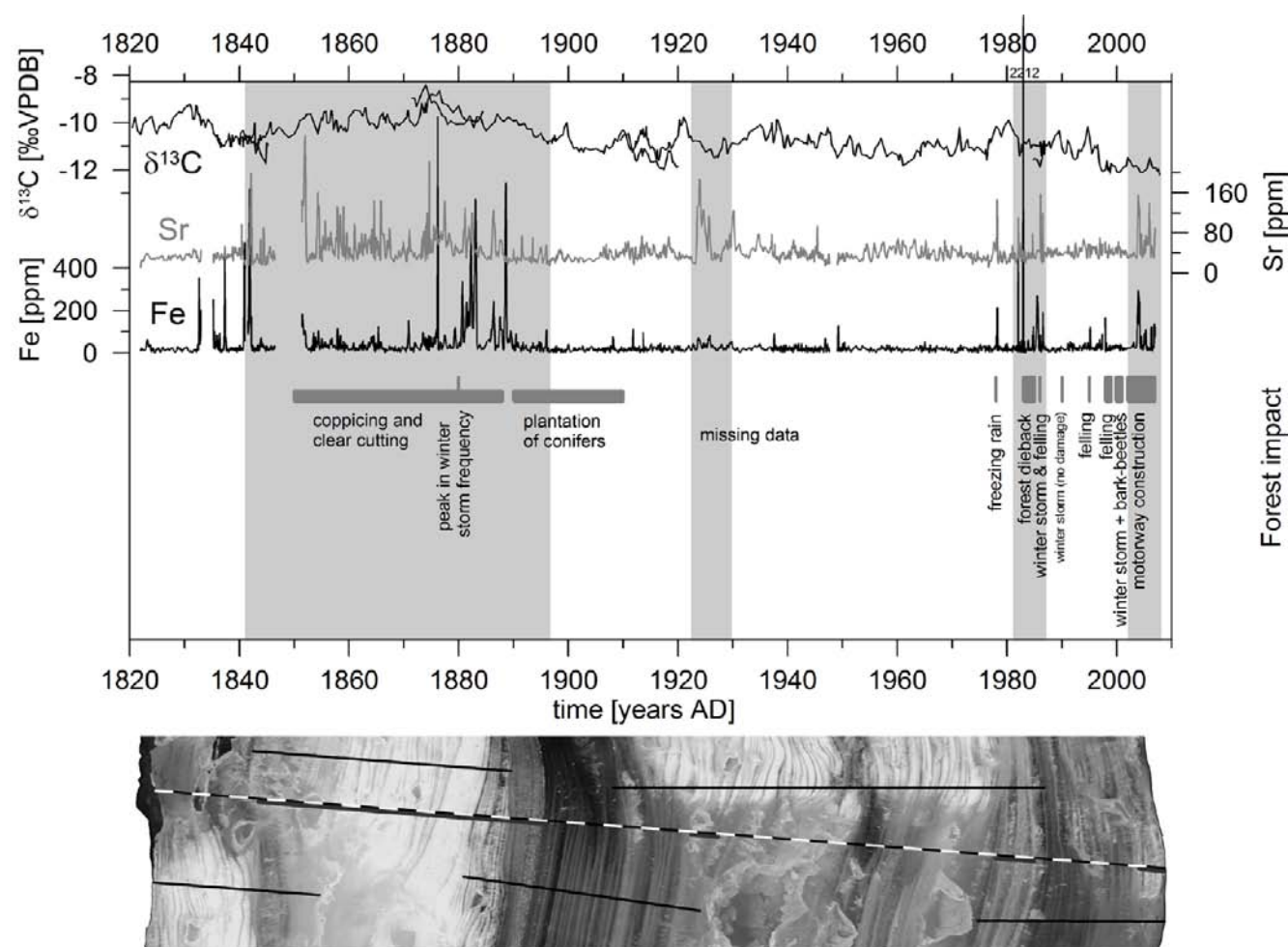


Figure 1. Comparison of Pb and S in stalagmite M4 from Milandre Cave with SO₂ emissions and an archive for anthropogenic Pb pollution (see legend for details). For Pb, no correlation is visible, S seems to record SO₂ air pollution with an offset of about 30 years.

Extreme events such as destructive storms (e.g. Lothar in 1999; winter storms in 1986), forest dieback due to air pollution (1980's), repeated coppicing and wood pasturing (19th century) are known to have affected the local forest and correspond well with the recorded high trace element concentrations in stalagmite M4 (Sr, Fe and many others ; Fig. 2). Stalagmite M4 is thus an appropriated archive for forest damages by extreme events and thus allows to extend the series of extreme events into the past. Some of them are confirmed by the reconstruction of forest damages (national level) by Usbeck et al. (2010).

The decrease in $\delta^{13}\text{C}$ in stalagmite M4 corresponds to a significant forest build-up and to increasing growing stock (i.e. forest density), confirming the importance of forest management practices and the soil for the M4 archive and the pertinence of $\delta^{13}\text{C}$ as a proxy for vegetation development in the Milandre Cave.

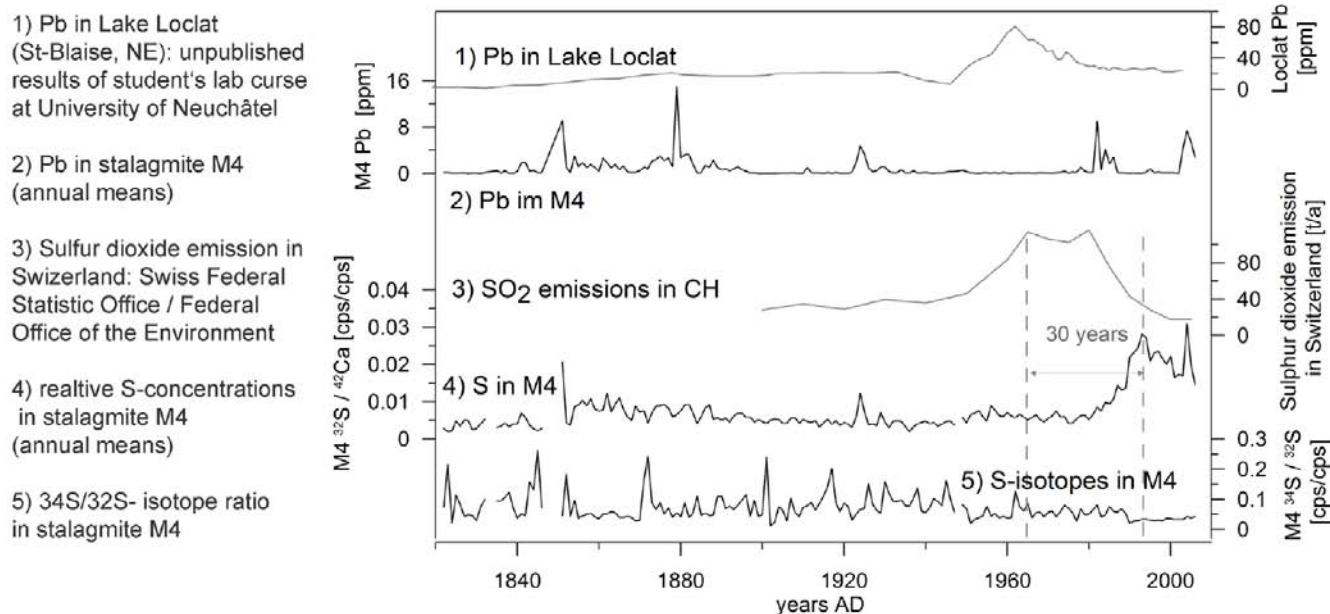


Figure 2:

$\delta^{13}\text{C}$, Sr and Fe concentrations in stalagmite M4 from Milandre Cave. Human and natural impact on the nearby forest (Augsburger & Monnin, 2009, personal communication). The sampling tracks for trace elements (1mm-scale bar) and stable isotopes (black lines) are indicated on a scan of M4.

REFERENCES

- Federal Office of Statistics (FOS) / Federal Office of the Environment (FOEN), www.bfs.admin.ch/bfs/portal/de/index/themen/02/06/indindicator.139201.1380.html
- Usbeck, T., Wohlgemuth, T., Dobbertin, M., Pfister C., Bürgi, A. & Rebetez, M. (2010). Increasing storm damage to forests in Switzerland from 1858 to 2007, *Agricultural and Forest Meteorology* 150, 47-55.

3.9

Molybdenum isotopes in river water: sources, fractionation processes and their importance for Mo cycling in the marine environment

Voegelin Andrea R.¹, Nägler Thomas F.¹, Neubert Nadja ², Heri Alexandra R.³, Pettke Thomas¹, Schlunegger Fritz¹, Steinmann Marc⁴, Pourret Olivier⁵ Villa Igor M.^{1,6}

¹Institut für Geologie, Universität Bern, CH-3012 Bern

²Institut für Mineralogie, Leibniz Universität Hannover, D-30167 Hannover

³Department of Earth Sciences, University of Hong Kong, Hong Kong, China

⁴UMR 6249 Chrono-Environnement, Université de Franche-Comté, F-25030 Besançon

⁵Institut Polytechnique LaSalle-Beauvais, Département de Géosciences, F-60026 Beauvais

⁶ Dipartimento di Scienze Geologiche e Geotecnologie, Università di Milano Bicocca, I-20126 Milano

The fluxes of most elements from continents to oceans are largely controlled by river transport. The marine isotope inventory is thus strongly dependent on fractionation processes during continental weathering and subsequent river transport to the ocean basins. In the case of the highly redox sensitive molybdenum (Mo), the continental contribution accounts for the predominant part of the marine Mo budget. Mo isotopes ($\delta^{98/95}\text{Mo}$) in marine sediments have been used to investigate the evolution of atmospheric O_2 and to quantify the extent of ocean anoxia in the geological record. Such models strongly rely on accurate assumptions regarding the riverine Mo isotope input signature. In the past, its isotopic composition has been assumed to be fairly stable, reflecting the $\delta^{98/95}\text{Mo}$ of igneous crustal rocks (-0.1 to +0.3‰). Recent studies by Archer & Vance (2008), Pearce et al. (2010), Neubert et al. (2011) and Voegelin et al., (submitted), however, have revealed not only a general preferential enrichment of river waters in the heavy Mo isotopes but also a large $\delta^{98/95}\text{Mo}$ variability (-0.13 to +2.3‰). This pronounced discrepancy between the assumed crustal background and the aquatic signature emphasizes the need for a better understanding of Mo behavior during weathering and transport.

We present a compilation of our recent findings on Mo sources and fractionation processes in the terrestrial weathering environment. We discuss data of samples collected in river catchments in Switzerland (Entlebuch and Aare) and France (Massif Central). Sampling was selected to monitor potential controlling factors, i.e. basement geology, fractionation during weathering, within river precipitation and soil retention of Mo. The sampling locations differ with respect to their bedrock lithologies: while the streams in the French Massif Central are underlain exclusively by igneous crustal rocks, the bedrock in the Entlebuch and Aare catchments comprise evaporites, marine sediments and molasses.

Generally, the Mo isotope data of water samples and their associated bedrocks have revealed that, independent of source rock type, the observed $\delta^{98/95}\text{Mo}$ variations of 0 to +1.9‰ are primarily controlled by bedrock lithology. In the case of the Swiss river systems, the heavy Mo isotopic compositions of the sedimentary rocks have shown to be reflected in the river water $\delta^{98/95}\text{Mo}$. Thereby two very prominent effects were identified to control the aquatic Mo signature: weathering of sedimentary (evaporitic) sulfates and oxidative weathering of sulfides. In the case of the French catchment, the heavy stream water $\delta^{98/95}\text{Mo}$ signatures do not reflect the bedrock composition. Given that the bulk rock $\delta^{98/95}\text{Mo}$ reflects a value typical for crustal magmatic rocks (ca. 0.1‰), Mo fractionation during incongruent rock dissolution can explain the observed isotopically heavy aquatic Mo signatures. The dominance of this process is supported by the excellent agreement of the stream water data with those of Mo released during experimental basalt leaching. Results of mass balance calculations, based on single grain and matrix laser ablation data, identify the rare, but in part highly Mo-enriched sulfide melt inclusions as the principal, isotopically heavy Mo source for the leach solutions and hence the stream waters. Incongruent crustal bedrock weathering may thus cause a preferential release of heavy Mo isotopes. This, however, is highly dependent on the primary bedrock mineralogy.

Despite being a potential pathway for the removal of light isotopes, soil retention of Mo or its adsorption to the particulate load do not play a dominant role in driving the river water Mo towards the heavy signatures observed in the catchments investigated here. Generally speaking, the isotopically heavy Mo of river waters is most likely the result of a complex interplay between various processes involved, and the mass balance between the competing factors likely controls the aquatic $\delta^{98/95}\text{Mo}$. The local system is thus highly dependent on rock mineralogy, degree of rock weathering and soil development, secondary mineral precipitation and adsorption. The finding that catchment geology exerts a primary control on the delivery of Mo to seawater indicates that the flux and isotope composition of molybdenum to seawater has likely varied in the geologic past. These variations are closely linked to e.g. the continents' configuration, the average age of the sediments exposed to erosion, weathering intensity and climate.

REFERENCES

- Archer, C. & Vance D., 2008: The isotopic signature of the global riverine molybdenum flux and anoxia in the ancient oceans. *Nature Geoscience* 1, 597–600.
- Neubert, N., Heri, A. R., Voegelin, A. R., Nägler, T. F., Schlunegger, F. & Villa, I. M. 2011: The molybdenum isotopic composition in river water: Constraints from small catchments, *Earth and Planetary Science Letters*, 304, 180-190.
- Pearce, C. R., Burton, K. W., Pogge von Strandmann, A. E., James, R. H. & Gislason, S. R. 2010: Molybdenum isotope behaviour accompanying weathering and riverine transport in a basaltic terrain, *Earth and Planetary Science Letters*, 295, 104-114.
- Voegelin, A. R., Nägler, T. F., Pettke, T., Neubert, N., Steinmann, M., Pourret, O. & Villa, I. M. submitted: The impact of igneous bedrock weathering on the Mo isotopic composition of stream waters: Natural samples and laboratory experiments.

3.10

Mass-dependent and mass-independent fractionation of stable mercury isotopes as tracer for anthropogenic pollution in the environment

Wiederhold Jan G.^{1,2}, Bourdon Bernard^{2,3}, Kretzschmar Ruben¹

¹ETH Zurich, Institute of Biogeochemistry and Pollutant Dynamics, Soil Chemistry, Universitätsstr. 16, CHN F23.2, CH-8092 Zurich (wiederhold@env.ethz.ch)

²ETH Zurich, Institute of Geochemistry and Petrology, Isotope Geochemistry, Clausiusstrasse 25, NW F82.2, CH-8092 Zurich

³Laboratoire de Géologie de Lyon, ENS Lyon, CNRS and UCBL, 46 Allée d'Italie, F-69364 Lyon, France

Mercury (Hg) is a toxic heavy metal that represents a serious hazard for human and ecosystem health at local and global scales. Anthropogenic activities (e.g., combustion, industry, mining) have increased global Hg cycling by about a factor of three compared with pre-industrial times. Although the biogeochemical cycling of mercury in the environment has been studied extensively over the last decades, many questions concerning sources, transformations, and the fate of Hg species in natural ecosystems still remain unclear.

The recent improvement of analytical methods, namely cold-vapor multicollector inductively-coupled plasma mass spectrometry (CV-MC-ICP-MS), has resulted in the detection of significant variations of Hg isotope ratios in natural samples caused by fractionation processes (Blum et al. 2011). Thus, stable Hg isotope signatures represent a promising new tool to trace Hg cycling in the environment by providing information on source materials and transformation processes which fractionate Hg isotope by various mechanisms.

The stable Hg isotope system is different compared to most other metal stable isotopes due to the occurrence of both mass-dependent (MDF) and mass-independent (MIF) fractionation which are affecting the even- and odd-mass Hg isotopes to a different extent (Figure 1). Thus, the Hg isotope signature of a natural sample contains multiple dimensions which can be exploited to track sources and transformation processes of Hg in nature.

Mass-independent fractionation of Hg isotopes was first reported for photochemical reactions (Bergquist & Blum 2007) which are also responsible for large MIF signatures in natural samples and probably caused by magnetic isotope effects during kinetic radical-pair reactions affecting only the odd-mass Hg isotopes which possess nuclear spin and a magnetic moment (Buchachenko 2009). In addition, smaller MIF effects of Hg isotopes can be caused by nuclear volume fractionation (Schauble 2007; Wiederhold et al. 2010) due to the non-linear increase of nuclear charge radii with isotopic mass.

Here, we present Hg isotope data from different anthropogenically polluted field systems (e.g., mining environments, sediments polluted by industrial sources) measured by CV-MC-ICP-MS to demonstrate the potential of Hg isotopes as environmental tracer and discuss ongoing laboratory studies to determine fractionation mechanisms and factors for individual Hg species transformations.

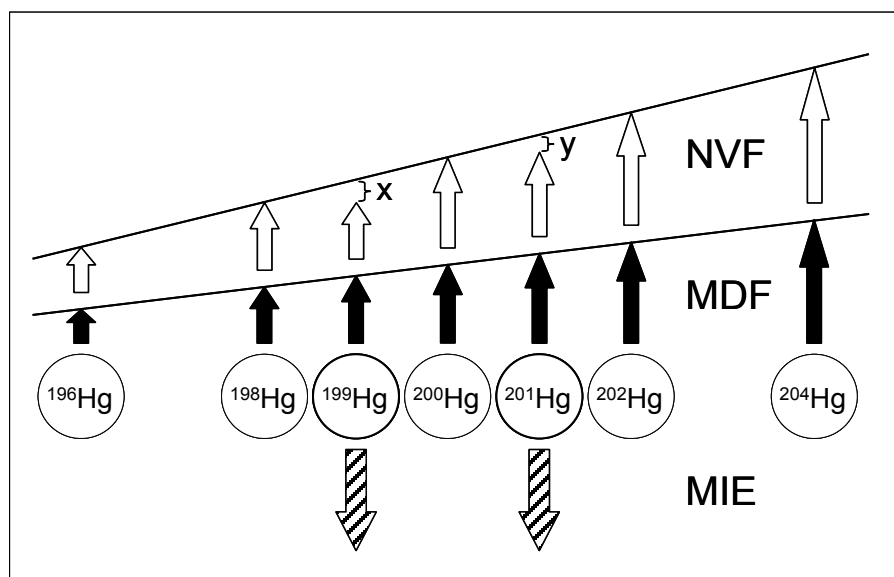


Figure 1. Schematic picture of stable Hg isotope fractionation by mass-dependent fractionation (MDF), nuclear volume fractionation (NVF), and magnetic isotope effect (MIE). Mass-independent fractionation (MIF) can be caused either by NVF (non-linear increase of nuclear charge radii with $x/y \sim 1.65$) or MIE (odd-mass isotopes with nuclear spin and magnetic moment are fractionated in kinetic radical-pair reactions relative to even-mass isotopes).

REFERENCES

- Bergquist, B.A. & Blum, J.D. 2007: Mass-dependent and -independent fractionation of Hg isotopes by photoreduction in aquatic systems. *Science* 318, 417-420.
- Blum, J.D. 2011: Application of stable mercury isotopes to biogeochemistry. In: *Handbook of environmental isotope geochemistry* (Ed. by Baskaran, M.), Springer, Chapter 12, 229-245.
- Buchachenko, A.L., 2009: Mercury isotope effects in the environmental chemistry and biochemistry of mercury-containing compounds. *Russian Chemical Reviews*, 78, 319-328.
- Schauble, E.A. 2007: Role of nuclear volume in driving equilibrium stable isotope fractionation of mercury, thallium, and other very heavy elements. *Geochimica et Cosmochimica Acta*, 71, 2170-2189.
- Wiederhold, J.G., Cramer, C.J., Daniel, K., Infante, I., Bourdon, B., Kretzschmar, R. 2010: Equilibrium mercury isotope fractionation between dissolved Hg(II) species and thiol-bound Hg. *Environmental Science and Technology*, 44, 4191-4197.

3.11

Silicon isotopic fractionation in marine sponges: A new paradigm and model for understanding silicon isotopic variations in sponges

Martin Wille¹, Jill Sutton², Andrea DeLeon³, Michael Ellwood³, Steve Eggins³ and William Maher⁴

¹ Department of Geosciences, University of Tübingen, Wilhelmstr. 56, 72074 Tübingen

² School of Earth Sciences, University of Victoria, Victoria, Canada

³ Research School of Earth Sciences, Building 47, Daley Road, Australian National University, ACT 0200, Australia

⁴ Ecochemistry Laboratory, Institute for Applied Ecology, Faculty of Applied Science, University of Canberra, Canberra, ACT 2601, Australia

The modern Southern Ocean plays a pivotal role in determine the air-sea balance of CO₂ and global biological production. However, there is debate regarding nutrient utilisation in Southern Ocean surface waters and how this transfers through to the deeper Southern Ocean, especially during the past. To fill this gap we have determined the silicon isotope composition of deep-sea sponges collected from near Antarctica, subantarctic waters (Tasmania Seamounts) and subtropical waters north of New Zealand with the aim of developing a new paleo-nutrient proxy. For deep-sea sponges, $\delta^{30}\text{Si}$ values widely between 0.87 ‰ and -3.40 ‰ (vs NBS). Depth profiles show that sponge $\delta^{30}\text{Si}$ compositions trend to lighter values with increasing depth. This is exemplified by sponges from the Tasmanian Seamounts which vary from 0.87 ‰ to -3.13 ‰ over a depth range from 100 to 1200 m. We find that silicon isotope fractionation ($\delta^{30}\text{Si}$ sponge - $\delta^{30}\text{Si}$ seawater) varies with seawater silicon concentration with more fractionated (lighter) isotope values being associated with specimens collected from water high in silicon. A mass-balance based model for silicon isotope fractionation is consistent with $\delta^{30}\text{Si}$ fractionation driven by changes in the difference between the silicon influx and efflux from the sponge. At higher seawater silicon concentrations efflux is correspondingly higher, and with $\delta^{30}\text{Si}$ having an apparent greater internal fractionation, this results in lighter $\delta^{30}\text{Si}$ spicule values. This model can also explain $\delta^{30}\text{Si}$ fractionation in diatoms and be used to reconstruct past seawater silicon concentrations from the $\delta^{30}\text{Si}$ signature of fossil sponges and diatoms.

P 3.1

A volcanically induced climate warming and floral change preceded the onset of OAE1a (Early Cretaceous)

Christina E. Keller¹, Peter A. Hochuli^{1,2}, Helmut Weissert¹, Stefano M. Bernasconi¹, Martino Giorgioni¹, Therese I. Garcia^{1,3}

¹Geological Institute, ETH Zurich, Sonneggstr. 5, CH-8092 Zürich
(Christina.Keller@erdw.ethz.ch)

²Palaeontological Institute, University of Zurich, Karl Schmid-Str. 4, CH-8006 Zürich

³Present address: Department of Geology, University of Toronto, Earth Sciences Center, 22 Russell Street, Toronto, Ontario, Canada M5S 3B1

The Aptian Oceanic Anoxic Event 1a (OAE1a) is preceded by a prominent negative C-isotope excursion (NCIE) attributed to major volcanism on the Ontong-Java plateau that is supposed to lead to a $p\text{CO}_2$ increase and a climate change. Lower Aptian sporomorph assemblages in two pelagic sections from the southern Tethys margin (N-Italy) were analysed in order to test if the postulated climate changes affected the terrestrial vegetation.

At the base of the NCIE the sporomorph assemblages comprise abundant bisaccate pollen reflecting a warm-temperate climate (Fig. 1). Several tens of kiloyears (ka) after the start of the NCIE decreasing bisaccate pollen and increasing *Classopollis* spp. and *Araucariacites* spp. suggest the beginning of a long-term temperature rise (Fig. 2). Palynomorphs indicate that maximum temperatures were reached several tens of ka after the end of the NCIE and the onset of OAE1a. The highest temperatures coincide with arid conditions, which could reflect a northward shift of the hot-arid Northern Gondwana floral province as a result of an increasing $p\text{CO}_2$. Over 200 ka after the onset of OAE1a reduced volcanic activity and/or increased black shale deposition allowed for a drawdown of most of the excess CO_2 and a southward shift of floral belts.

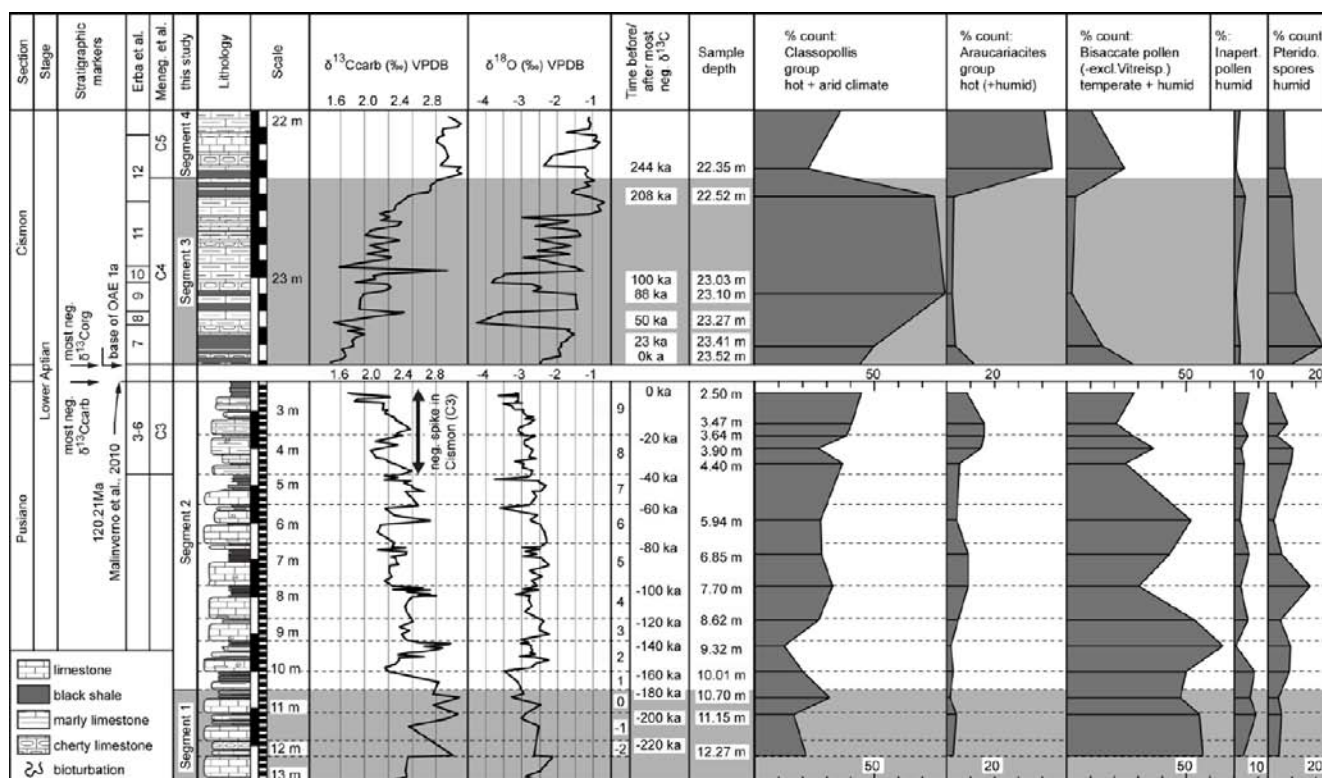


Figure 1 (Keller et al. 2011). Composite section of Pusiano and Cison showing the C_{carb} - and O-isotopes and the succession of sporomorph assemblages (%) through the negative C-isotope excursion (NCIE; Pusiano section, segment 2) and the onset of Oceanic Anoxic Event 1a (OAE1a; Cison section, segments 3–4, from Hochuli et al. 1999). Limestone-black shale couplets in Pusiano are considered to reflect orbital precession (~20 kiloyears (ka)). Timing for Pusiano: number of limestone-black shale couplets / time in estimated ka before the end of the NCIE. Timing for Cison: ka after onset of OAE1a (sedimentation rate from Malinverno et al., 2010). For further information see Keller et al. (2011).

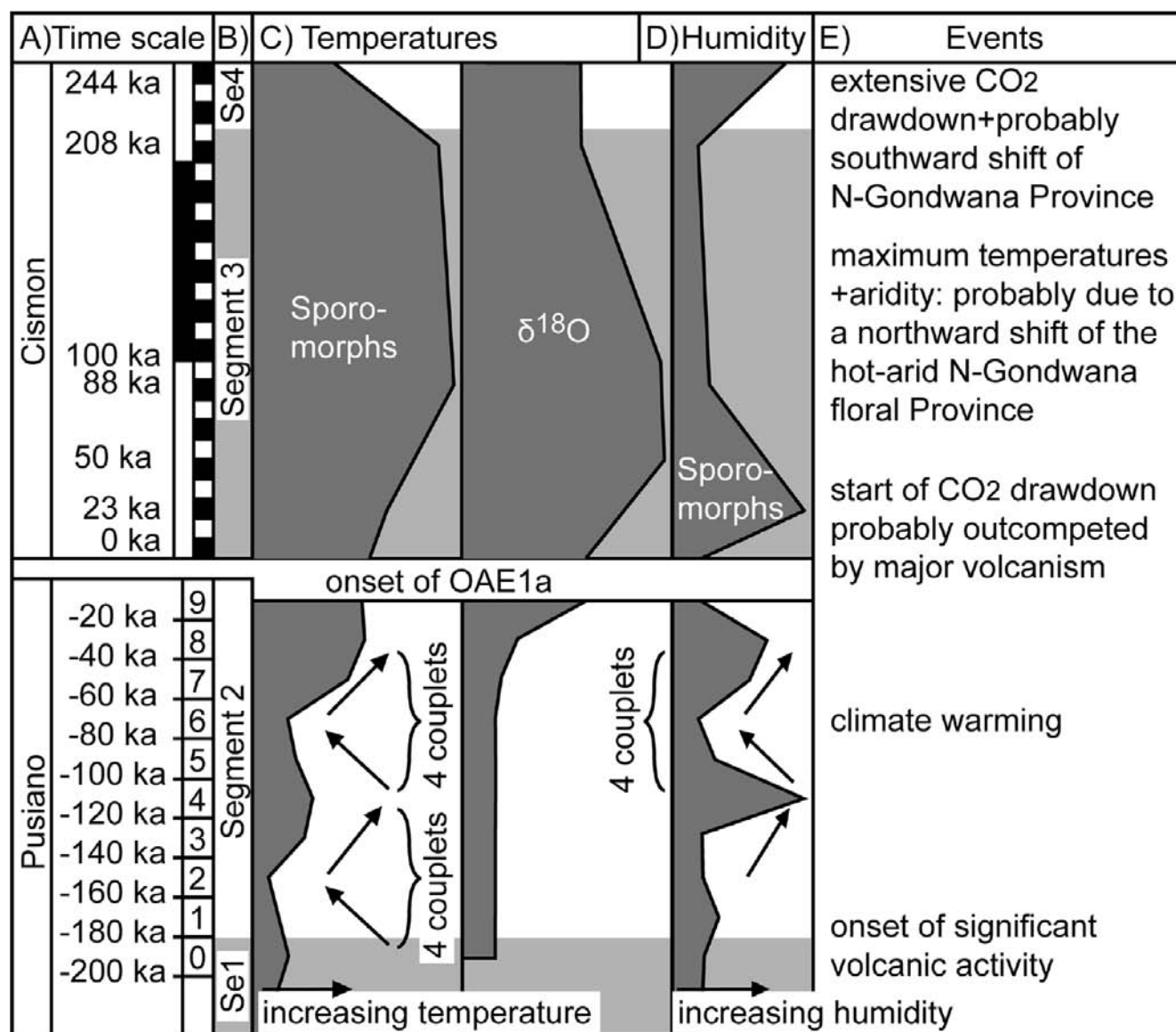


Figure 2 (Keller et al. 2011). Estimated evolution of temperature and humidity for the composite section of Pusiano and Cismon. A) Time scale. B) Segments (see Fig. 1). C) Relative temperature changes inferred from sporomorphs and $\delta^{18}\text{O}$. D) Relative humidity changes. E) Climate-related events. For further information see Keller et al. (2011).

REFERENCES

- Hochuli, P.A., Menegatti, A.P., Weissert, H., Riva, A., Erba, E. & Silva, I.P. 1999: Episodes of high productivity and cooling in the early Aptian Alpine Tethys. *Geology*, 27, 657–660.
- Keller, C.E., Hochuli, P.A., Weissert, H., Bernasconi, S.M., Giorgioni, M. & Garcia, T.I. 2011: A volcanically induced climate warming and floral change preceded the onset of OAE1a (Early Cretaceous). *Palaeogeography, Palaeoclimatology, Palaeoecology*, 305, 43–49, doi:10.1016/j.palaeo.2011.02.011.
- Malinverno, A., Erba, E. & Herbert, T.D. 2010: Orbital tuning as an inverse problem: Chronology of the early Aptian oceanic anoxic event 1a (Selli Level) in the Cismon APTICORE. *Paleoceanography*, 25, PA2203, doi:10.1029/2009PA001769.

P 3.2

In the Tethys Ocean black shales commonly formed prior to Oceanic Anoxic Event 1a (OAE1a, Early Aptian, ~120 Ma ago)

Christina E. Keller¹, Helmut Weissert¹, Peter A. Hochuli^{1,2}, Stefano M. Bernasconi¹, Martino Giorgioni¹, Therese I. Garcia^{1,3}

¹Geological Institute, ETH Zurich, Sonneggstr. 5, CH-8092 Zürich (Christina.Keller@erdw.ethz.ch)

²Palaeontological Institute, University of Zurich, Karl Schmid-Str. 4, CH-8006 Zürich

³Present address: Department of Geology, University of Toronto, Earth Sciences Center, 22 Russell Street, Toronto, Ontario, Canada M5S 3B1

The Early Aptian Oceanic Anoxic Event 1a (OAE1a) is attributed to increasing oxygen deficiency in the ocean waters as a result of climate changes triggered by major volcanic outgassing related to the formation of the Ontong Java plateau. However, onset of black shale deposition was not globally simultaneous and under specific palaeogeographic and palaeoceanographic conditions occurred already before OAE1a. In order to identify conditions favouring pre-OAE1a black shale formation, we compared four pelagic Tethyan sections (northern Italy and Switzerland), in which we analysed the evolution of CaCO₃/total organic carbon (TOC) content before and at the onset of OAE1a.

Throughout the studied stratigraphic interval, the sections record frequent precession controlled changes in carbonate content, which are reflected by limestone-marlstone alternations in the shallower sections and by limestone-black shale couplets in the deepest section, at the locality of Pusiano. Depth controlled suboxic to anoxic conditions in the water column are also suggested by the prominent OAE1a black shales, which occurred first in the deeper Pie del Dosso and Roter Sattel sections and only subsequently in the shallower Cismon section. However, contrary to expectations, the deepest Pusiano section exhibits – instead of an earliest onset of prominent OAE1a black shales – only a minor increase in TOC with a corresponding decrease in carbonate content.

This suggests that the orbitally driven climate changes most strongly influenced water stratification and hence are most prominently expressed in the deepest sections. Conversely, the volcanically induced long-term climate changes seemed to more strongly affect organic matter production, the extension of the oxygen minimum zone and hence had the strongest impact on sections at intermediate depth.

P 3.3

Mercury Isotope Fractionation as Biogeochemical Tracer in Ore Waste

Smith, Robin S.^{1,2}, Wiederhold, Jan G.^{1,2}, Jew, Adam D.³, Brown, Gordon E.³, Bourdon, Bernard^{2,4}, & Kretzschmar, Ruben¹

¹ ETH Zurich, Institute of Biogeochemistry and Pollutant Dynamics, Soil Chemistry, CHN F23.2, CH-8092 Zurich
(robin.smith@env.ethz.ch)

² ETH Zurich, Institute of Geochemistry and Petrology, Isotope Geochemistry, NW F82.2, CH-8092 Zurich

³ Department of Geological & Environmental Sciences, Stanford University, Stanford, CA, USA

⁴ Laboratoire de Géologie de Lyon, ENS Lyon, CNRS and UCBL, Lyon, France

High concentrations of mercury (Hg) can often be found in the environment around inactive Hg mines. During mine operation, rock containing the primary ore mineral HgS was crushed and heated in furnaces to temperatures of ~ 700 °C (calcination). Most of the resulting elemental Hg vapor was condensed and collected for various industrial uses. The remaining mine tailings (calcines) were then piled on site. This removal process was not complete and significant amounts of Hg remained in the calcines. Large pieces of calcine often exhibit a characteristic internal layering, with dark-grey cores, light-grey outer rims, and red outer surface layers. Previous studies have shown that Hg speciation in calcines is dominated by stable α -HgS & β -HgS, but consists of a small proportion of more soluble secondary Hg phases. The speciation of the Hg-bearing compounds in these wastes determines the solubility, volatility, and thus mobility of the Hg remaining in the calcines (Kim *et al.* 2004; Jew *et al.* 2011).

Various environmental processes fractionate the stable Hg isotopes via mass-dependent (MDF) and/or mass-independent fractionation (MIF); however, the controlling mechanisms are not fully understood. These fractionation signatures are a potentially useful “two-dimensional” tool to study the biogeochemical cycling of Hg and its transformations and fluxes from highly contaminated mining environments (Stetson *et al.* 2009). Here we report stable Hg isotope results for different layers in calcine cobbles collected from two sampling locations from the former New Idria Hg mine, San Benito County, CA, USA.

Differently colored layers in the calcines were carefully separated using a diamond saw or were chipped with chisels. The horizon pieces were then ground to a powder using a tungsten carbide rotary disk mill, followed by a total digestion in aqua regia. Mercury concentration analyses were conducted using cold vapor-AFS and isotopic analyses were performed on a Nu Plasma MC-ICP-MS with cold vapor introduction. Mass bias was corrected by a combination of standard-sample bracketing and Tl addition. Data for MDF are reported as $\delta^{202}\text{Hg}$ relative to the NIST-3133 standard. MDF is calculated by the following formula:

$$\delta^{202}\text{Hg} [\text{‰}] = 1000 \left(\left[\frac{(^{202}\text{Hg}/^{198}\text{Hg})_{\text{sample}}}{(^{202}\text{Hg}/^{198}\text{Hg})_{3133}} \right] - 1 \right)$$

Our analyses revealed significant concentration gradients across the different layers, with higher Hg concentrations in outer rims and lower concentrations in inner regions. Bulk calcine samples from one area sampled are isotopically heavier than ore and unroasted ore wastes, and significant MDF $\delta^{202}\text{Hg}$ gradients exist from isotopically heavy centers to lighter rims. Bulk samples from a second sampling site display smaller magnitude fractionation and the opposite MDF trend, with isotopically lighter centers and heavier rims. These findings suggest that incomplete roasting of ore rocks led to pronounced Hg isotope gradients which were presumably caused by kinetic effects during diffusive processes. The highly fractionated Hg isotope ratios of calcine materials, together with the higher solubility of secondary Hg phases which have formed during or after roasting, will have important implications for the isotope signature of Hg which is exported from the former mine into the surrounding ecosystems.

REFERENCES

- Jew, A.D., Kim, C.S., Rytuba, J.J., Gustin, M.S., Brown, G.E. 2011: New technique for quantification of elemental Hg in mine wastes and its implications for mercury evasion into the atmosphere. *Environmental Science and Technology*, 45, 412-417.
- Kim C.S., Rytuba, J.J., Brown, G.E. 2004: Geological and anthropogenic factors influencing mercury speciation in mine wastes: an EXAFS spectroscopy study. *Applied Geochemistry*, 19, 379-393.
- Stetson, S.J., Gray, J. E., Wanty, R.B., Macalady, D.L. 2009: Isotopic Variability of Mercury in Ore, Mine-Waste Calcine and Leachates of Mine-Waste Calcine from Areas Mined for Mercury. *Environmental Science and Technology* 43, 7331-7336.

4. Perspectives on batholith formation and evolution in 4D

Roel Verberne, Katharina Vogt and David Floess

Swiss National Science Foundation – ProDoc 4D Adamello
Swiss Society of Mineralogy and Petrology (SSMP)

TALKS:

- 4.1 *Blundy J., Annen C., Caricchi, L.:* Piecemeal Assembly of Shallow Crustal Magma Bodies
- 4.2 *Keller T., Kaus B.J.P.:* The importance of visco-elasto-plastic rheology in numerical modeling of two-phase flow
- 4.3 *Mantegazzi D., Sanchez-Valle C., Driesner T., Reusser E.:* The thermodynamic properties of saline-rich aqueous fluids at elevated P-T conditions from Brillouin spectroscopy measurements in a diamond anvil cell
- 4.4 *Melekhova E., Annen C., Blundy J.:* Andesite production in a deep crustal hot zone
- 4.5 *Menand T.:* Physical controls and depth of emplacement of sills and plutons
- 4.6 *Pattison D.R.M., de Capitani C. & Gaidies F.:* Petrologic consequences of variations in metamorphic reaction affinity
- 4.7 *Pistone M., Caricchi L., Ulmer P., Mancktelow N., Reusser E., Burlini L.:* Rheology of Volatile-rich Crystal Mush
- 4.8 *Pomella H., Klötzli U., Scholger R., Stipp M., Fügenschuh B.:* The tonalitic lamellae along the Giudicarie fault system: a multidisciplinary study
- 4.9 *Reverman R. L., Fellin M. G., Herman F., Willett S. D.:* Tectonic exhumation and relief development of the Alps: constraints from the Adamello Complex
- 4.10 *Schaltegger U., Broderick C., Wotzlaw J., Ovtcharova M., Schoene B.:* Timescales of pluton emplacement – insight from high-precision U-Pb dating
- 4.11 *Schubert M., Driesner T., Gerya T.,:* Injection of Mafic Magma as Trigger for Felsic Intrusion Processes
- 4.12 *Wagner T., Hennings S., Heinrich C., Ulmer P.:* Fluid evolution of the Monte Mattoni mafic complex, Adamello Batholith, northern Italy
- 4.13 *Weidendorfer D., Mattsson H.B., Ulmer P.:* Hybridization processes in a partially crystallized magma chamber (Austurhorn intrusion, SE Iceland): Multiple magma mixing scenarios
- 4.14 *Yoshinobu A.S.:* “Magma Emplacement Tectonics”: What can we learn from the oceans, ophiolites and arcs?

POSTERS:

- P 4.1 Broderick, C., Schaltegger, U., Frick, D., Günther, D., Brack, P.: A detailed reconstruction of emplacement and crystallization sequence in the Southern Adamello Batholith, N. Italy using the potential of accessory minerals
- P 4.2 Dymkova, D., Gerya, T., Podladchikov, Y.: 2D numerical modelling of fluid and melt percolation in the subduction zone
- P 4.3 Floess, D., Baumgartner, L., Brack, P.: Thermal evolution of the Western Adamello contact aureole
- P 4.4 Hürlimann, N., Müntener, O., Ulmer, P.: Trace-element partitioning in post-plutonic dike-suites S-Adamello (N-Italy)
- P 4.5 Leuthold, J., Blundy, J., Holness, M.: Trace elements geochemistry and experimental petrology as novel approaches to understand reactive flow through the Rum layered intrusion: preliminary results and perspectives
- P 4.6 Mettasch, S., Baumgartner, L.: Cordierite growth textures in the Permian sequence of the Adamello contact aureole, Italy
- P 4.7 Nandedkar, R., Ulmer, P., Müntener, O.: Liquid line of descent from olivine-tholeiite to granodiorite at 0.7 GPa
- P 4.8 Putlitz, B., Ramirez de Arellano, C., Ovtcharova, M., Müntener, O.: Textures and chemistry of zircons: implication on the interpretation of U-Pb zircon ages from observations of the Chaltén Plutonic Complex (Argentina)
- P 4.9 Skopelitis, A., Bindeman, I., Ulianov, A., Brack, P., Schaltegger, U.: Tracing episodic magma accretion by U-Pb dating and $^{18}\text{O}/^{16}\text{O}$ isotopes in zircon: the case of the Adamello batholith, Italy
- P 4.10 Stamper, C., Blundy, J., Melekhova, E., Arculus, R.: Experimental determination of the hydrous basalt liquidus: The Grenadan perspective
- P 4.11 Verberne, R., Ulmer, P., Müntener, O.: Field relations and consequences for emplacement of the Listino Ring Structure, Adamello Massif, N-Italy

4.1

Piecemeal Assembly of Shallow Crustal Magma Bodies

Blundy Jon¹, Annen Catherine¹, Caricchi, Luca¹

¹*School of Earth Sciences, University of Bristol, Wills Memorial Building, Bristol BS8 1RJ (jon.blundy@bris.ac.uk)*

The accumulation of large bodies of silicic magma in the shallow crust fuels volcanic eruptions, creates granite plutons and drives hydrothermal ore deposition. Granite batholiths testify to the very large volumes of magma that can accumulate, while caldera-forming eruptions prove that a significant portion of some silicic bodies contains eruptible magma at any one time. An enduring question in igneous geology is the timescales over which such shallow bodies accumulate. A variety of evidence has been mustered to argue for emplacement as large diapirs versus thin sills, for extreme longevity versus ephemerality, for large volumes of convecting eruptible magma versus small pockets of isolated melt. We will use evidence from a variety of plutonic and volcanic rocks to argue that the assembly of magma bodies is piecemeal, the presence of eruptible silicic melt is an ephemeral feature of such bodies, and that most bodies destined to form plutons rather than erupt.

The key evidence is as follows:

1. Trace element zoning in plagioclase phenocrysts in volcanic rocks is consistent with repeated interaction with magma of similar trace element chemistry, but slightly different temperature.
2. Textural variation in plutonic rocks tends to mask chemical variation suggesting that textural characteristics are imposed at a relatively late stage on melts whose chemistry is established at greater depth.
3. Diffusive timescales of phenocrysts tend to be quite short suggesting that individual pulses either grew shortly before eruption or spent only a fraction of their residence at high (eruption) temperatures.
4. Continuous influx of magma is required in order to sustain shallow magma bodies for substantially longer than is possible with a single large pulse.
5. Melt inclusions trapped at shallow level tend to show much greater diversity in major and trace elements than do the rocks in which they are found, consistent with additions of small volumes of melt to a larger reservoir with which they eventually become blended.
6. Melt inclusions often described curved liquid lines of descent in rocks whose chemical variations are typically linear, due to the prevalence of mixing processes.
7. Both plutonic and volcanic rocks show abundant textural evidence for the cannibalisation of ancestral magma, now preserved as xenocrysts, glomerocrysts and xenoliths.
8. Minerals and isotope systems with different closure temperatures often give quite discrepant timescales.
9. Most granite batholiths contain rocks with very similar bulk rock chemistry to coeval volcanics suggesting that the volumes of melt extracted from batholiths is modest to negligible, such that few batholiths are cumulates.
10. Magmatic fabrics in plutons show radial variations in intensity consistent with pulsed magma emplacement.
11. Few granite plutons appear to have the requisite volumes of complementary dense mafic cumulate rocks required to balance an overall basaltic composition.

In combination these observations can be reconciled with a model of magma differentiation that occurs on at least two discrete levels. In the deep crust differentiation of mantle-derived basaltic magmas generates a range of more evolved rock types on timescales of millions of years. The evolved melts ascend from the deep crustal hot zone (Annen et al, 2006), occasionally pausing en route to undergo further differentiation. Crystal cumulates in arc volcanics testify to such a process (e.g. Tollan et al, 2011). The volumes of ascending melt are small and ultimately accumulate in shallow reservoirs, characterised by repeated mixing of genetically-related magmas to construct large bodies. Textural development is primarily a consequence of these shallow-level processes, which include degassing, mixing and cannibalisation of ancestral plutonic rocks and their residues. Shallow bodies may grow to considerable size without ever containing appreciable volumes of low-crystallinity eruptible melt, or they may erupt frequently. The balance of magmatic addition versus volcanic losses likely reflects stress conditions in the overlying roof rocks, the rate of magma supply, and the non-linear relationship between temperature and melt fraction.

REFERENCES

- Annen, C., Blundy, J.D., Sparks, R.S.J., 2006. The genesis of intermediate and silicic magmas in deep crustal hot zones. *Journal of Petrology*, **47**, 505-539.
- Tollan, P.M.E, Bindeman, I., Blundy J.D., 2011. Cumulate xenoliths from St. Vincent, Lesser Antilles Island Arc: a window into upper crustal differentiation of mantle-derived basalts. *Contributions to Mineralogy and Petrology*, DOI 10.1007/s00410-011-0665-9

4.2

The importance of visco-elasto-plastic rheology in numerical modeling of two-phase flow

Keller Tobias¹, Kaus Boris J.P.²

¹*Institut für Geophysik, ETH Zürich, Sonneggstr. 5, CH-8092 Zürich (keller@erdw.ethz.ch)*

²*Institut für Geowissenschaften, Universität Mainz (DE)*

We investigate the behaviour of a two-phase system that involves production and percolation of partial melt through a visco-elasto-plastic continental lithosphere and crust under ongoing tectonic deformation. Using two-dimensional numerical simulations we examine the coupled magmatic and tectonic processes leading to intrusive rock formation.

The numerical modeling approach is based on the assumption that the melt fraction is equal to the porosity of the rock and that porosity changes reflects, apart from melting and crystallization, the compaction or dilation of the matrix framework due to visco-elasto-plastic processes. All modes of compaction are connected to the local effective pressure, which can be understood as the volumetric mean stress acting on the solid rock matrix.

The rheology of the solid phase largely determines the mode and efficiency of melt transport. Therefore it is of considerable importance to formulate a realistic visco-elasto-plastic rheology. In the case of two-phase flow modeling, we additionally formulate a volumetric viscosity to constitute compaction/ decompaction deformation along with a standard deviatoric rheology for shear deformation.

First results indicate that melt propagation is strongly related to the regional stress field, and that plastic failure zones (decompaction tubes, dikes and faults) form important conduits for the propagation of partial melt, especially through the more competent parts of lithosphere and crust. Where the partial melt reaches either mechanical barriers or neutral buoyancy with respect to the host rock, regions of magma accumulation may quickly evolve into magma chambers with melt content exceeding 50%. There, the melt may either reside until it crystallizes, or fractionate until the more evolved rest melt has obtained new buoyancy to force its way further through the crust.

A possible application of such models is to deepen the understanding of the processes involved in, and the geometry and field relations expected from, the emplacement of hydrated slab melts into the overriding continental plate in an ocean-continent subduction setting.

4.3

The thermodynamic properties of saline-rich aqueous fluids at elevated P-T conditions from Brillouin spectroscopy measurements in a diamond anvil cell

Mantegazzi Davide¹, Sanchez-Valle Carmen¹, Driesner Thomas¹ and Reusser Eric¹

¹*Institute of Geochemistry and Petrology, ETH Zürich, Clausiusstrasse 25, CH-8092 Zürich.*

1davide.mantegazzi@erdw.ethz.ch

Saline-rich aqueous fluids are of fundamental importance for a large number of geological processes. For instance, at convergent plate margins fluids are released from the hydrated phases present in the subducted oceanic crust through metamorphic devolatilization. These fluids are mainly H₂O- and CO₂ – rich, with different amounts of dissolved ions. As these fluids migrate to the overlying mantle wedge they act as metasomatic agent, modifying the mantle chemical composition. Moreover, the presence of fluid phases lowers the temperature of the mantle solidus, triggering the production of the magma at the origin of arc magmatism, resulting in the formation of batholiths at depth or volcanic arcs.

For a quantitative modeling of fluid-rock interactions at deep geological conditions the thermodynamic properties of the phases involved are a crucial prerequisite. While these data are available for most of the rock forming minerals, this is

not the case for aqueous fluids different than pure water. For instance, although the equation of state (EOS) for H₂O-NaCl solutions is valid up to 1000°C, the pressure range is limited to 0.5 GPa. There is therefore a lack of PVTx data of saline-rich aqueous fluids at high pressure conditions.

This work presents the PVTx properties of saline-rich aqueous fluids up to pressure and temperature conditions relevant for the lower Earth's crust and the upper Earth's mantle determined with Brillouin scattering measurements conducted in a diamond anvil cell (DAC).

Brillouin scattering spectroscopy is an accurate technique for measuring the velocity of acoustic waves propagating in a sample. The use of an externally heated membrane-type diamond anvil cell allows the performance of Brillouin measurements up to 500°C and 5 GPa. The densities of the saline-rich aqueous fluids analyzed in this work are inverted from the acoustic velocities measured, and successively fitted with an equation of state (EOS). This EOS is then used for deriving all other thermodynamic parameters, like for example, the coefficient of thermal expansion, the isobaric heat capacity, the isothermal compressibility, etc. Figure 1 shows the fit of the experimentally derived density data of H₂O-NaCl solutions with different concentrations performed with the EOS proposed in this work.

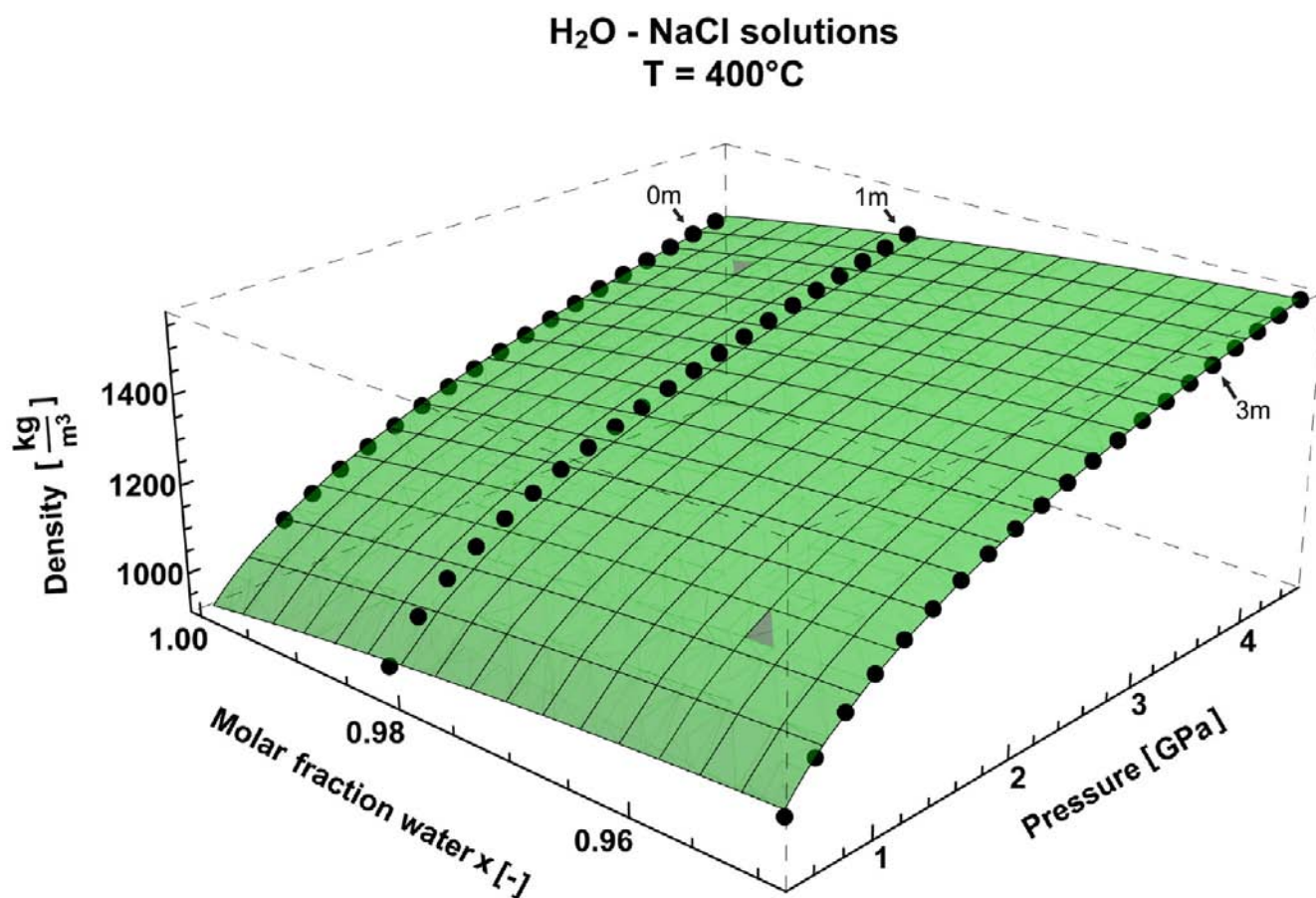


Figure 1. Density of H₂O-NaCl aqueous solutions at 400°C. The black points are density values calculated from Brillouin measurements in the DAC. The surface is a 3-dimensional fit of the data with the EOS proposed in this work.

REFERENCES

- Abramson, E., & Brown, M.J. 2004: Equation of state of water based on speeds of sound measured in the diamond-anvil cell. *Geochim. Cosmochim. Acta*, 68, 1827-1835.
- Driesner, T. 2007: The system H₂O-NaCl. Part II: Correlations for molar volume, enthalpy, and isobaric heat capacity from 0 to 1000 degrees C, 1 to 5000 bar, and 0 to 1 X-NaCl. *Geochim. Cosmochim. Acta*, 71, 4902-4919.
- Manning, C.E. 2004: The chemistry of subduction-zone fluids. *Earth and Planet. Sci. Lett.*, 223(1-2), 1-16.
- Schmidt M. W., & Poli S. 1998: Experimentally based water budgets for dehydrating slabs and consequences for arc magma generation. *Earth and Planet. Sci. Lett.*, 163(1-4), 361-379.
- Ulmer, P. 2001: Partial melting in the mantle wedge – the role of H₂O in the genesis of mantle-derived ‘arc-related’ magmas. *Phys. Earth Planet. Inter.*, 127(1-4), 215-232.

4.4

Andesite production in a deep crustal hot zone

Melekhova Elena¹, Annen Catherine, Blundy Jon

¹ Department of Earth Sciences, University of Bristol, Wills Memorial Building, Queen's Road, Bristol BS8 1RJ, UK (elena.melekhova@bristol.ac.uk)

Andesites represent the major proportion of eruptive product at the convergent margins and are considered a major component in the formation of continental crust. Several hypotheses of andesite petrogenesis have been developed, based on field observations and experimental studies, including, partial melting of peridotite under hydrous conditions (e.g. Wood & Turner, 2009), assimilation of plutonic roots of arcs by silicic magmas (Reubi & Blundy, 2008), and crystal fractionation of mantle-derived basalts (e.g. Muntener et al., 2001, Grove et al., 2003). However, all hypotheses have their weaknesses.

Andesitic magmas usually contain considerable volumes of crystals showing disequilibrium characteristic of magma mixing, assimilation, and fractional crystallization. Melt inclusions are considered as an essential source of information of magmagenesis, as they represent unequivocal liquid compositions. However, andesitic compositions in melt inclusions are very rare raising questions as to the mechanism by which andesites are produced (Reubi and Blundy, 2008). Here we present a plausible scenario for origins of pure andesitic melts (not magmas) in the deep crust based on a combination of high pressure phase equilibrium experiments and numerical simulations.

The compositional evolution of melts derived from the crystallisation of a primitive calc-alkaline basalt from St Vincent (Lesser Antilles) were investigated experimentally at 0.7, 1 and 1.3 GPa from liquidus to solidus temperatures with initial water contents of 2.3 and 4.5 wt%. The experiments show that the relationship between melt fraction (F) and temperature (T) is variously non-linear and varies with pressure (P) and H₂O content. The experimental T, P, F and melt compositions were used as input into numerical simulations of a deep crustal hot zone (Annen et al, 2006) where sills of basalts are periodically injected at the base of the crust. Basalt accretion rates of 2.5, 5, and 10 mm/yr were tested. The sills thermally equilibrate with the surrounding crust at temperatures that progressively increase with time. First melts to be generated are low temperature, low melt fraction and highly silicic. As the crust thermally matures the system produces higher melt fraction, lower in silica, melts.

Since a large proportion of crystals precipitates over a relatively small temperature interval, melt compositions become bimodal as the system matures when we have 2.3 wt% of initial water. The time needed for bimodalism to emerge at this water content varies between less than 0.5 to more than 8 millions years depending on the basalt emplacement rate. In a thermally mature deep crustal hot zone, 3 types of melts can coexist: a high melt fraction-low silica melt and a low melt fraction-high silica melt, both residual from basalt crystallisation and a crustal melt generated by partial melting of the preexisting crust. In marked contrast to the results at 2.3 wt% H₂O we do not see bimodalism developing if we have 4.5 wt% H₂O in the system and the sill emplacement takes place below 0.7 GPa. At such crustal pressures truly intermediate (andesitic) liquids emerge in a very short geological period, between 0.5 and 2 millions years (Figure 1), again depending on emplacement rate.

The numerical simulations are consistent with production of andesite liquids in deep crustal hot zones. The scarcity of andesitic melt inclusions could be that they are trapped at low pressures (< 0.5 GPa), following significant crystallisation and degassing.

Our preliminary results suggest that if there is more available water than 2.3 wt% in the parental liquid (melt) at low crustal conditions in the crustal hot zone truly andesitic liquids could be produced in considerable volume. Conversely, drier parental magmas tend to give rise to more bimodal melt compositions.

REFERENCES

- Reubi, O. & Blundy J. 2008: A dearth of intermediate melts at subduction zone volcanoes and the petrogenesis of arc andesites, *Nature*, 461, 1269-1274.
- Müntener, O., Kelemen, P.B. & Grove, T.L. 2001: The role of H₂O during crystallisation of primitive arc magmas under uppermost mantle conditions and genesis of igneous pyroxenites: and experimental study. *Contrib. Mineral. Petrol.*, 141, 643-658.
- Grove, T.L, and et al., 2003: Fractional crystallisation and mantle-melting controls on calc-alkaline differentiation trends. *Contrib. Mineral. Petrol.*, 145, 515-533.
- Annen, C., Blundy, J.D. & Sparks, R.S.J. 2006: The genesis of intermediate and silicic magmas in Deep Crustal Hot Zones. *J. of Petrol.*, 47, 505-539.

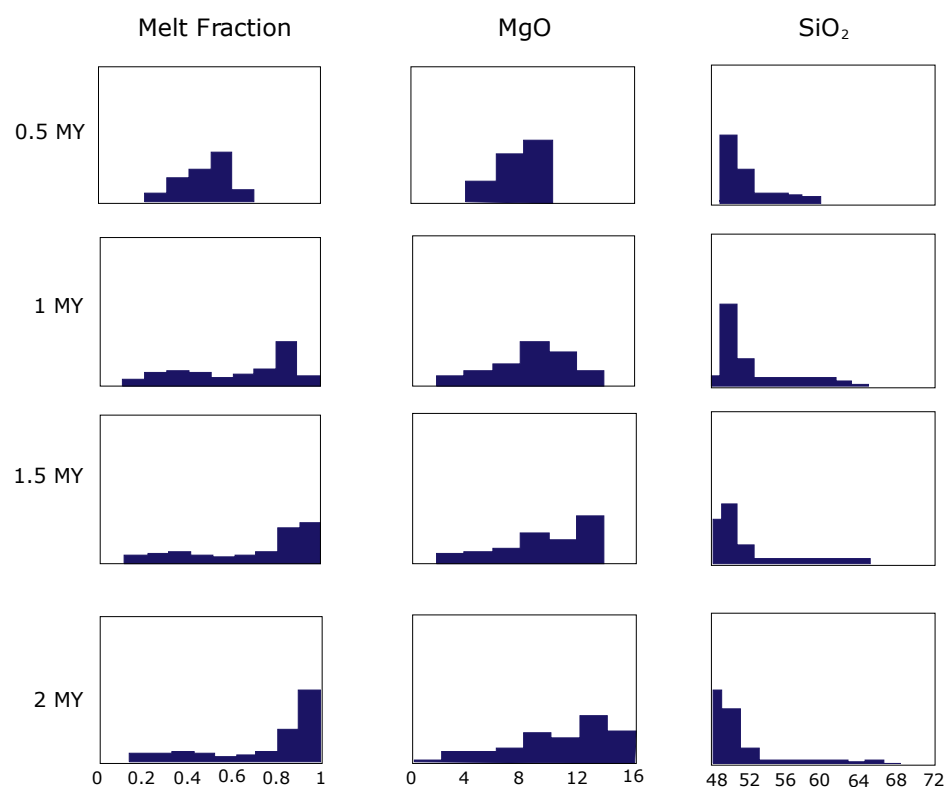


Figure 1. Simulation results at 1 GPa with 4.5 wt% of initial H₂O. Sill emplacement rate is 10 mm per year.

4.5

Physical controls and depth of emplacement of sills and plutons

Thierry Menand

Laboratoire Magmas et Volcans, Université Blaise Pascal, 5 rue Kessler, 63038 Clermont-Ferrand cedex (thierry.menand@univ-bpclermont.fr)

Emplacements styles and rates of magma bodies within the crust have fundamental implications for magma differentiation, country rock metamorphism and assimilation, as well as magma chamber formation. The formation and growth of magma bodies are now recognised as involving the amalgamation of successive, discrete pulses such as sills. Sills would thus represent the building blocks of larger plutons (*sensu lato*). Mechanical and thermal considerations on the incremental development of these plutons raise the issue of the crustal levels at which magma can stall and accumulate as sills. A critical analysis of the mechanisms that could a priori explain sill formation shows that principal physical controls include: rigidity contrast, where sills form at the interface between soft strata overlaid by comparatively stiffer strata; rheology anisotropy, where sills form within the weakest ductile zones; and rotation of deviatoric stress, where sills form when the minimum compressive stress becomes vertical. Comparatively, the concept of neutral buoyancy is unlikely to play a leading control in the emplacement of sills, although it could assist their formation. These different controls on sill formation, however, do not necessarily operate on the same length scale. The length scale associated with the presence of interfaces separating upper stiffer layers from lower softer ones determines the depth at which rigidity-controlled sills will form. On another hand, the emplacement depths for rheology-controlled sills is likely determined by the distribution of the weakest ductile zones. Whereas the emplacement depth of stress-controlled sills is determined by a balance between the horizontal maximum compressive stress, which favours sill formation, and the buoyancy of their feeder dykes, which drives magma vertically. Ultimately, the depth at which a sill forms depends on whether crustal anisotropy or stress rotation is the dominant control, i.e. which of these processes operates at the smallest length scale. Using dimensional analysis, it is shown that sill formation controlled by remote stress rotation would occur on length scales of hundreds of meters or greater. This therefore suggests that crustal heterogeneities and their associated anisotropy are likely to play a larger role than remote stress rotation in controlling sill emplacement, unless these heterogeneities are several hundred meters or more apart. This also reinforces the role of local stress barriers, owing to interactions between deviatoric stress and crustal heterogeneities, in the formation of sills.

4.6

Petrologic consequences of variations in metamorphic reaction affinity

Pattison David¹, de Capitani Christian² & Gaidies Fred^{1,3}

¹Department of Geoscience, University of Calgary, Calgary, Alberta, T2N 1N4, Canada (pattison@ucalgary.ca)

²Mineralogisch-Petrographisches Institut, Universität Basel, Bernoullistrasse 30, 4056 Basel, Switzerland

³Department of Earth Sciences, Carleton University, 1125 Colonel By Drive, Ottawa, ON, K1S 5B6, Canada

The extent to which kinetic barriers to nucleation and growth delay the onset of prograde metamorphic reaction, commonly known as overstepping, is related to the macroscopic driving force for reaction, termed reaction affinity. Reaction affinity is defined in the context of overstepping as the Gibbs free energy difference between the thermodynamically stable, but not-yet-crystallized, products and the metastable reactants. Mineral reactions which release large quantities of H₂O, such as chlorite-consuming reactions, have a higher entropy/volume change, and therefore a higher reaction affinity per unit of temperature/pressure overstep, than those which release little or no H₂O. The former are expected to be overstepped in T or P less than the latter. Different methods of calculating reaction affinity are discussed. Reaction affinity 'maps' are calculated that graphically portray variations in reaction affinity on equilibrium phase diagrams, allowing predictions to be made about expected degrees of overstepping. Petrologic consequences of variations in reaction affinity include: (1) metamorphic reaction intervals may be discrete rather than continuous, especially in broad multivariant domains across which reaction affinity builds slowly; (2) reaction intervals may not correspond in a simple way to reaction boundaries and domains in an equilibrium phase diagram, and may involve metastable reactions; (3) overstepping can lead to a 'cascade effect', in which several stable and metastable reactions involving the same reactant phases proceed simultaneously; (4) fluid generation, and possibly fluid presence in general, may be episodic rather than continuous, corresponding to discrete intervals of reaction; (5) overstepping related to slowly building reaction affinity in multivariant reaction intervals may account for the commonly abrupt development in the field of certain index mineral isograds; and (6) pressure-temperature estimation based on combined use of phase diagram sections and mineral modes/compositions on the one hand, and classical thermobarometry methods on the other, may not agree even if the same thermodynamic data are used. Natural examples of the above, both contact and regional, are provided. The success of the metamorphic facies principle suggests that these kinetic effects are second-order features that operate within a broadly equilibrium approach to metamorphism. However, it may be that the close approach to equilibrium occurs primarily at the boundaries between the metamorphic facies, corresponding to discrete intervals of high-entropy, dehydration reaction involving consumption of hydrous phases like chlorite (greenschist-amphibolite facies boundary) and mica (amphibolite-granulite facies boundary), and less so within the facies themselves. The results of this study suggest that it is important to consider the possibility of reactions removed from equilibrium when inferring the P-T-t evolution of metamorphic rocks.

4.7

Rheology of Volatile-rich Crystal Mush

Pistone M.¹, Caricchi L.², Ulmer P.¹, Mancktelow N.³, Reusser E.¹, Burlini L.¹

¹ Institute for Geochemistry and Petrology, Department of Earth Sciences, ETH, Zurich, Switzerland (mattia.pistone@erdw.ethz.ch)

² Department of Earth Sciences, University of Bristol, United Kingdom

³ Geological Institute, Department of Earth Sciences, ETH, Zurich, Switzerland

Large bodies of granite and their corresponding large eruptions have a dual nature: homogeneity at the large scale and spatial and temporal heterogeneity at the small scale (Burgisser and Bergantz, 2011). Such magma batholiths are commonly highly crystalline (> 50 vol%; crystal mush, Bachmann and Bergantz, 2008a) and possible modes of mobilization and emplacement have been intensively discussed in the last decades. Recently, it has been proposed that a stiff mushy batholith must be reheated to mobilize; this produces a reduction in crystallinity that leads to an increase of the magma buoyancy (Burgisser and Bergantz, 2011). Another way of batholith mobilization in the crust can be caused by addition of volatiles (mainly H₂O and CO₂) released by ascending hydrous mafic magmas coming from the mantle (Bachmann and Bergantz, 2008b). The enrichment in volatiles induces a drastic decrease of the bulk viscosity of the granitic body and, thus, in the rheological properties of the batholith. The rheology of such very crystal-rich highly viscous systems is still a matter of debate. To provide some additional experimental constraints relevant to this discussion, we deformed hydrous (2.52 wt% H₂O) haplogranitic magmas containing variable amounts of quartz crystals (from 55 to 65 vol%), and fixed

volume of gas-pressurized CO₂-bubbles (9-10 vol%), in simple shear using a HT-HP Paterson-type rock deformation apparatus. Strain rates ranging between $1 \cdot 10^{-5} \text{ s}^{-1}$ and $4 \cdot 10^{-3} \text{ s}^{-1}$ were applied at temperatures between 823 and 1023 K (subsolidus conditions) and constant confining pressure of 200 MPa (8 km depth). The results suggest that three-phase suspensions are characterized by strain rate-dependent rheology (non-Newtonian behavior). Two kinds of non-Newtonian behaviors were observed: shear thinning (decrease of viscosity with increasing strain rate) and shear thickening (increase of viscosity with increasing strain rate). The first effect dominantly occurs because of crystal size reduction and shear localization, enhanced by the presence of gas bubbles in the weak shear bands. However, when the solid crystal framework induces an internal flow blockage due to crystal interlock, the second effect becomes dominant. Comparing our results with previous ones for the rheology of crystal-bearing systems (Caricchi et al., 2007), the presence of limited amount of gas bubbles (12 vol% maximum) favors an evident decrease in viscosity; e.g., at about 70 vol% crystals a decrease of about 4 orders of magnitude in relative viscosity is caused by adding only 9 vol% bubbles. These experiments suggest that magma rheology is strongly controlled by the simultaneous presence of bubbles and crystals in the melt phase and their interactions during deformation. The localization in strain favors granite mobilization in the crust and the occurrence of large eruptions; in contrast, the crystal interlocking halts the batholith in the crust.

REFERENCES:

- Bachmann, O., Bergantz, G.W. (2008a). The magma reservoirs that feed supereruptions. *Elements* vol. 4 (no. 1), 17-21.
- Bachmann, O., Bergantz, G.W. (2008b). Rhyolites and their source mushes across tectonic settings. *Journal of Petrology* 49, 2277-2285.
- Burgisser, A., Bergantz, G.W. (2011). A rapid mechanism to remobilize and homogenize crystalline magma bodies. *Nature* 471, 212-215.
- Caricchi, L., Burlini, L., Ulmer, P., Gerya, T., Vassalli, M., Papale, P. (2007). Non-Newtonian rheology of crystal-bearing magmas and implications for magma ascent dynamics. *Earth and Planetary Science Letters* 264, 402-419.

4.8

The tonalitic lamellae along the Giudicarie fault system: a multidisciplinary study

Pomella Hannah¹, Klötzli Urs², Scholger Robert³, Stipp Michael⁴ & Fügenschuh Bernhard⁵

¹ *alpS GmbH, Grabenweg 68, A-6020 Innsbruck (Pomella@alps-gmbh.com)*

² *Department of Lithospheric Research, Althanstraße 14, A-1090 Vienna*

³ *Chair of Geophysics, University of Leoben, Peter-Tunner-Str. 25, A-8700 Leoben*

⁴ *Leibniz-Institute of Marine Sciences, IFM-GEOMAR, Wischhofstr. 1-3, D-24148 Kiel*

⁵ *Institute of Geology and Paleontology, Innrain 52, A- 6020 Innsbruck*

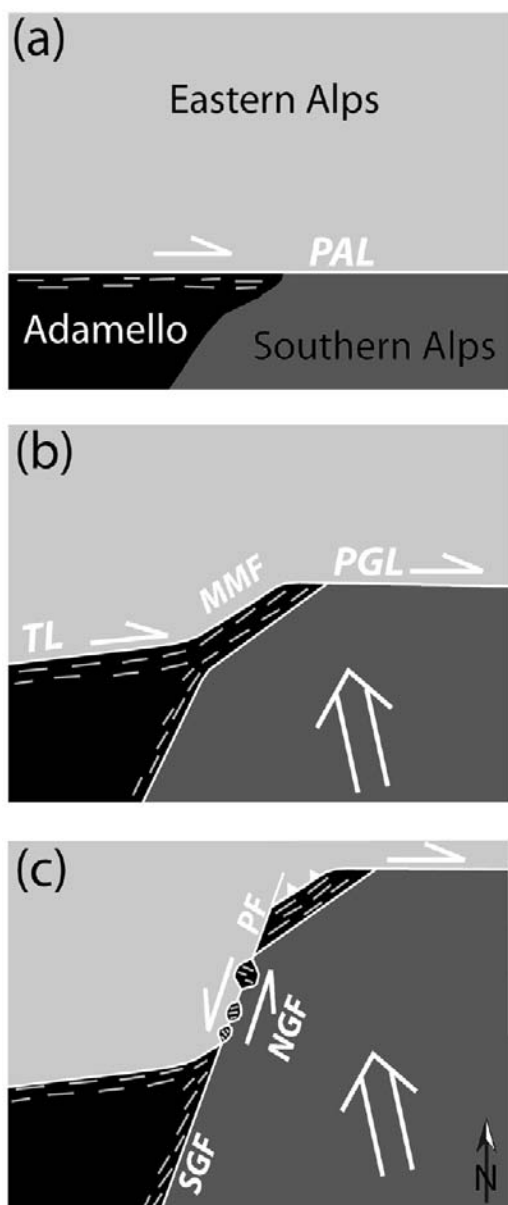
Numerous large and small magmatic bodies are exposed along the Periadriatic line (PAL) or close to it (e.g. Becke 1903; Rosenberg 2004). This study concentrates on small intrusions along two important faults of the Giudicarie fault system (GFS), the Northern Giudicarie (NGF) and the Meran-Mauls fault (MMF), summarised under the term tonalitic lamellae (Dal Piaz 1926).

Magnetic fabric analyses in combination with structural field data indicate dextral strike slip deformation along the NE-SW striking northern part of the GFS, the Meran-Mauls fault, overprinted by younger top-SE thrusting (Pomella et al. 2010). The regional stressfield was constantly oriented approximately NNW-SSE during Tertiary times. The distinctive change in deformation along the MMF from dextral strike slip to top-SE thrusting may be caused by a rotation or bending of the fault after the intrusion of the tonalites and the formation of their horizontal magnetic foliation.

U/Pb data on zircon (Pomella et al. 2010) show that some of the lamellae are of Oligocene (Rupelian), others of Late Eocene (Priabonian,) age. An amphibole-gabbro lens occurring on the Meran-Mauls fault provides a Middle Eocene (Bartonian) age. Among the major Periadriatic plutons, only the southern units of the Adamello batholith also intruded in the Eocene which suggests a strong correlation between the tonalitic lamellae and the Adamello batholith.

New zircon fission track data (Pomella 2010) show a corridor of young, Miocene zircon fission track ages from the tonalitic intrusions along the Northern Giudicarie fault. This corridor connects Early Miocene (17-23 Ma) Zircon fission track

ages of the NE-Adamello with the Miocene (23-9 Ma) zircon fission track ages of the Meran-Mauls basement and the Tauern window. To the SE the narrow corridor is bounded by Southalpine sediments characterized by only partially reset zircon fission track ages and towards NW by Oligocene zircon fission track cooling ages found in the Austroalpine units.



This multidisciplinary study provides evidence for a polyphase deformation along the Giudicarie fault system:

Oligocene (Fig. 1(a)): Intrusion of the northeastern units of the Adamello batholith adjacent to the straight, dextral strike-slip PAL. Late Oligocene / earliest Miocene (Fig. 1(b)): The NNW-ward movement of the Southalpine indenter leads to a bending of the fault, material from the northeastern part of the Adamello batholith is squeezed to the NE along the bent part of the fault. Early Miocene (Fig. 1(c)): The brittle Passeier fault, Northern and Southern Giudicarie fault dissect the bent part of the PAL. Along the northern part of the bend (MMF) a nearly continuous tonalitic body persists, whereas along the NGF only small boudinaged bodies rotated during brittle faulting are present

Figure 1. Schematic illustration of the emplacement of the tonalitic lamellae along the Giudicarie fault system (Pomella et al. 2010). PAL = Periodiadriatic line, MMF = Meran-Mauls fault, TL = Tonale line, PGL = Pustertal Gailtal line, NGF = Northern Giudicarie fault, SGF = Southern Giudicarie fault, PF = Passeier fault.

REFERENCES

- Becke, F. 1903: Exkursion durch das Westende der Hohen Tauern (Zillertal). Führer für Geologische Exkursionen in Österreich 9. Internationale Geologische Konferenz, 1-41
- Dal Piaz, G. 1926: Il confine alpino-dinarico dall'Adamello al massiccio di Monte Croce nell'Alto Adige. Atti dell'Accademia Scientifica Veneto-Trentino-Istria, 17, 3-7
- Pomella, H. 2010: The Cenozoic evolution of the Giudicarie fault system (Eastern/Southern Alps, northern Italy). A geochronological, structural and paleomagnetic study. PhD-thesis, Institute of Geology and Paleontology, University of Innsbruck
- Pomella, H., Klötzli, U., Scholger, R., Stipp, M., & Fügenschuh, B. 2010: The Giudicarie fault system in the light of new paleomagnetic and geochronological data from boudinaged Eo-/Oligocene tonalites. International Journal of Earth Sciences, DOI: 10.1007/s00531-010-0612-4
- Rosenberg, C.L. 2004: Shear zones and magma ascent: A model based on a review of the Tertiary magmatism in the Alps. Tectonics, 23, DOI:10.1029/2003TC001526

4.9

Tectonic exhumation and relief development of the Alps: constraints from the Adamello Complex

Reverman Rebecca L.¹, Fellin M. Giuditta¹, Herman Frederic¹ & Willett Sean D.¹

¹Eidgenössische Technische Hochschule Zürich, Switzerland (rebecca.reverman@erdw.ethz.ch)

The Adamello Complex is the largest of the Periadriatic intrusions, situated as a wedge between the Periadriatic Fault System (locally called the Tonale line), the South Giudicarie line and the Val Trompia thrust. A minimum of 5 kilometers of overburden has been removed since its emplacement in the late Eocene-early Oligocene and modern overall relief is over 2 km. Major rivers which dissect the complex flow into overdeepened valleys inferred to be areas of maximum incision from the Messinian Salinity Crisis (MSC). This makes it an ideal location to determine the role and magnitude of tectonic events (Giudicarie phase shortening in the late Miocene) and superimposed erosional events driven by climatic or other external environmental conditions (MSC and Neogene glaciation) as drivers of near surface exhumation.

Low-temperature thermochronometers, such as, apatite (U-Th-Sm)/He dating (AHe) and apatite fission-track dating (AFT), constrain near-surface (<5 km) exhumation rates that can be used to characterize climate or tectonic forcing. In this study we present AHe and AFT ages for samples collected in the three of the largest valleys of the Adamello Complex. The ages determined in this study span the Miocene and display a normal age-elevation relationship (AER), where age increases with elevation. All AFT ages along with high elevation AHe samples (3600-2700 m) record early to mid-Miocene ages, while samples located below 2300 m record nearly identical AHe ages, within error, of 6.5 ± 1 Ma. This pattern reveals the base of an exhumed AHe partial retention zone located at a modern elevation of ~2300m, which indicates 2-3 km of exhumation has occurred since ~8.5 Ma, and a minimum of 2 km of exhumation between 29 Ma and 8 Ma, as constrained by pluton emplacement age and depth. We use this data to calculate average exhumation rates and compare to those determined from AER and numerical modelling.

4.10

Timescales of pluton emplacement – insight from high-precision U-Pb dating

Schaltegger Urs¹, Broderick Cindy¹, Wotzlaw Jörn¹, Ovtcharova Maria¹, Schoene Blair^{1,2}

¹ Université de Genève, Sciences de la Terre et de l'environnement, 1205 Genève (urs.schaltegger@unige.ch)

² Princeton University, Department of Geosciences, Princeton NJ 08540, USA

Calibrating the timescales of magma generation, transport, and storage in the crust is important for building robust models for the thermal, rheological and geochemical evolution of the lithosphere. Models need to quantify volumes and rates of magma flux into the middle and upper crust, degrees of liquid-crystal separation, syn-intrusive deformation, degree of magma mixing and crustal assimilation and the fractionation paths of major and accessory minerals.

High-precision U-Pb geochronology has become an invaluable tool for calibrating the tempo of eruptive and intrusive igneous processes. The high closure temperature for Pb diffusion in zircon suggests that zircon U-Pb dates record the time of crystal growth in the magma. Age scatter of individual zircon grains suggest that large plutons are assembled over more than million year timescales by the amalgamation of small pulses of magma, thus downplaying the importance of large magma chambers in the generation of batholiths. As a result of increased age precision beyond the 0.1% level in U-Pb ID-TIMS geochronology of single- to sub-grain zircons, it is becoming increasingly common in plutonic rocks to find populations of zircons on the hand sample scale that record zircon growth over 10^4 - 10^6 years. Lead loss can be excluded as a source of scatter, since “chemical abrasion” techniques were used for the pre-treatment of analyzed zircons. Such data present difficulties because a zircon date does not necessarily represent the age of the intrusion of a magma or the eruption of a volcanic ash any more. On the other hand, the capability of such minerals to record crystal growth despite prolonged or subsequent exposure to magmatic temperatures can be used to our advantage because these minerals contain a geochemical record of the liquids from which they crystallized which can potentially provide information about the geochemical evolution of a magmatic system with time.

The example of the Adamello batholith shows that very different timescales are involved in its construction: 10-12 Ma for the intrusion of the whole Adamello batholith (Skopelitis et al. 2011), 1-2 Ma for the assembly of one pluton or unit (such as the Re di Castello unit; Schaltegger et al. 2009), 250-300 ka for the accretion of one intrusion series (such as the Val Fredda or the Lago di Vacca intrusion), 20-40 ka for the crystallization of a single magma batch (Broderick et al. 2011). Applying high-precision chemical abrasion – isotope dilution – thermal ionisation mass spectrometry techniques, using a double isotope EARTHTIME tracer solution for both Pb and U, lowest-blank chemical separation of Pb and U, and precise isotope ratio analysis on high-linearity secondary electron multiplier and high-precision ($10^{12}\Omega$) Faraday cups, we are able to achieve <0.1% uncertainty at 95% confidence level for individual analyses. For the Adamello batholith, we therefore can reconstruct crystallization processes at the $\pm 20'000$ - $30'000$ years level (see Fig. 1). With this unprecedented precision we are able to distinguish between *autocrystic zircon* (crystallized very late in the magmatic history in the lithology we see today), *antecrystic zircon* (crystallized earlier, in a magma but that broadly originated in the same magmatic system). Xenocrystic zircon is inherited from fully crystallized country rock.

By analyzing trace element ratios (e.g., Th/U, Gd/Yb, Eu/Eu*) and initial Hf isotopes of the same dated zircon volume (Schoene et al., 2010), we trace the geochemical evolution of the magmas during crystallization of zircon, involving assimilation, fractional crystallization, and magma mixing processes, which then can be resolved within high-precision time.

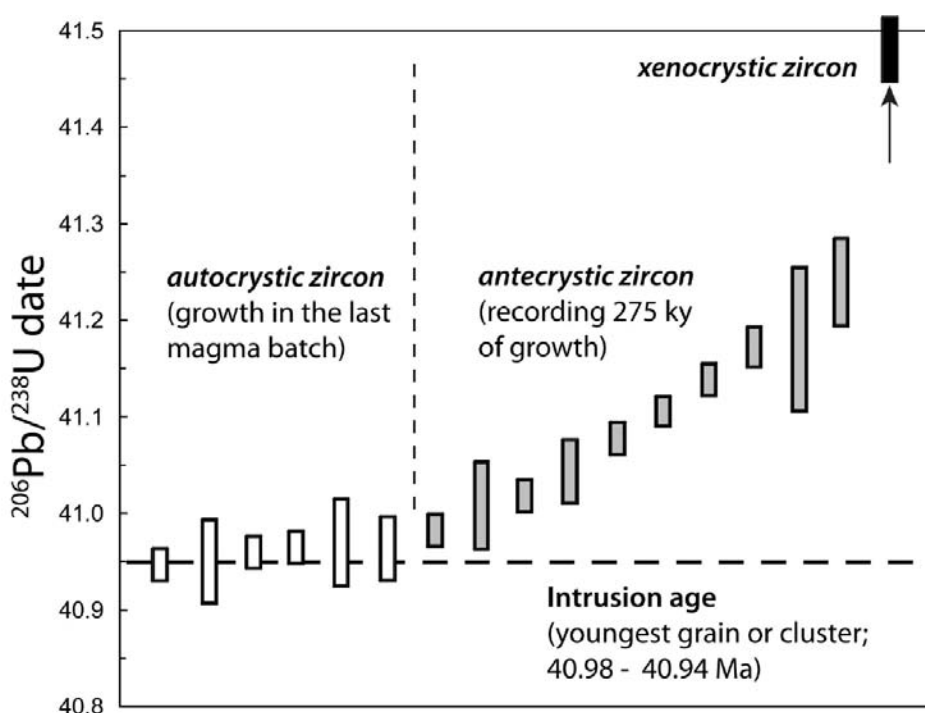


Figure 1: Example how to interpret plutonic zircon U-Pb ages

REFERENCES

- Broderick C.A., Schaltegger U., Frick D., Günther D., Brack P. (2011) Using the potential of accessory minerals: detailed reconstruction of emplacement and crystallization sequence in the Southern Adamello Batholith, N. Italy. AGU Fall Meeting, 5-9. 12. 2011, San Francisco.
- Schaltegger, U., Brack, P.B., Ovtcharova, M., Peytcheva, I., Schoene, B., Stracke, A., and Bargossi, G.M., 2009, Zircon U, Pb, Th, and Hf isotopes record up to 700 kyrs of magma fractionation and crystallization in a composite pluton (Adamello batholith, N Italy): Earth Planet. Sci. Lett., v. 286, p. 208-218.
- Schoene B., Schaltegger U., Latkoczy C. & Günther D. (2010) A new method integrating high-precision U-Pb geochronology with zircon trace element analysis (U-Pb TIMS-TEA). Geochim. Cosmochim. Acta 74, 7144-7159.
- Skopelitis A., Brack P., Ulianov A., Bindeman I., & Schaltegger U. (2011) Tracing episodic magma accretion by zircon $^{18}\text{O}/^{16}\text{O}$ isotopes and U-Pb dating in the Adamello batholith, Italy. Goldschmidt Conference, 14-19. 8. 2011, Prague.

4.11

Injection of Mafic Magma as Trigger for Felsic Intrusion Processes

Maike Schubert¹, Thomas Driesner¹, Taras Gerya², Peter Ulmer¹

¹Department of Earth Sciences, Institute of Geochemistry and Petrology, ETH Zurich, Switzerland

¹Department of Earth Sciences, Institute for Geophysics, ETH Zurich, Switzerland (maikeschubert@erdw.ethz.ch)

Plutons grow by melt transfer from a deep source to a higher emplacement level. However, the mechanisms leading to felsic magma transport through the crust is still a point of discussion (e.g. [1]). Geochronological data of exposed rocks in the Ivrea Zone, northern Italy, indicate a close spatially and temporally relation between intrusions of mantle derived mafic magma into the lower crust and crustal scale silicic volcanism [2].

Following up such observations on the correlation of mafic and felsic magma we used numerical modeling to identify potential physical mechanisms for the initiation of felsic magma ascent by injection of mafic material. The code I2ELVIS [3] has been used to study the emplacement of granitic intrusions into the upper crust in a self-consistent way including strong mechanical interaction between the ascending melt and the crustal rocks. It includes a visco-elasto-plastic rheology of the crustal rocks and it is possible to handle strong contrasts in the material properties between magma and crustal material. As initial setup we assume a region of high temperature in the lower crust where partially molten felsic magma is present and a mantle reservoir of mafic melt at a depth of 100km. This reservoir is connected to the bottom of the lower crust via a magmatic channel. We do not apply an initial stress field in the crust in order to get results independent from predefined stresses.

With our numerical experiments we show that the influx of mafic magma from a mantle source into a partially molten region in the lower crust is able to trigger the ascent of felsic material from the lower crust to a higher emplacement level. Furthermore, our study indicates which parameters determine timescale and final shape of upper crustal felsic intrusions and how they influence the development of the ascent and emplacement process.

REFERENCES

- [1] T. Menand, Physical controls and depth of emplacement of igneous bodies: A review, *Tectonophysics*, 500:11-19, November 2009.
- [2] J.E. Quick, S. Sinigoi, G. Peressini, G. Demarchi, J.L. Wooden, and A. Sbisà. Magmatic plumbing of a large permian caldera exposed to a depth of 25 km. *Geology*, 37(7):603-606, July 2009.
- [3] T.V. Gerya and D.A. Yuen. Characteristics-based marker-in-cell method with conservative finite differences schemes for modeling geological flows with strongly variable transport properties. *Physics of the Earth and Planetary Interiors*, 140(4):293-318, December 2003.

4.12

Fluid evolution of the Monte Mattoni mafic complex, Adamello Batholith, northern Italy

Wagner Thomas, Hennings Sibylle, Heinrich Christoph & Ulmer Peter

Institute for Geochemistry and Petrology, ETH Zurich (thomas.wagner@erdw.ethz.ch)

The fluid evolution of the Monte Mattoni mafic complex (John & Blundy 1993) in the southern Adamello batholith was reconstructed by combination of fluid inclusion studies (microthermometry and LA-ICPMS analysis of individual fluid inclusions) and fluid-mineral equilibria modeling. The Monte Mattoni complex consists of two main magmatic units, the Monte Mattoni and the Cadino gabbro, which both show textural evidence for fluid saturation. In the Mattoni gabbro, fluid saturation was likely reached due to rapid magma ascent and pressure decrease. The exsolved fluid phase is trapped in ocelli (miarolitic cavities of subcentimeter size) and segregated fluid pockets that formed from a more evolved, fluid-rich residual melt. In the Cadino gabbro, progressive crystallization and fractionation induced fluid saturation. Fluid inclusions are preserved in miarolitic cavities forming in the center of local pegmatitic pods. Five distinct fluid inclusion types (A to E) that are present as texturally and compositionally consistent assemblages (with clear relative chronology) were observed. The fluid evolution is characterized by several consistent features, most importantly changes in salinity, CO₂ concentration and the Ca/Na ratio. Fluid inclusion types A to C are aqueous-carbonic, and show a systematic decrease in salinity (from 7.8 to 5.5 wt%), coupled with a decrease in CO₂ concentration. The salinity in later aqueous fluid inclusion types D and E increases again (to 9.5 and 27.1 wt%), while the CO₂ concentration drops to very low values. The Ca/Na ratio in the aqueous fluids increases, and the late-stage type E fluids are concentrated calcic-sodic brines.

The initial decrease in salinity and CO₂ content is likely related to fluid-melt partitioning during successive stages of fluid exsolution (Cline & Bodnar 1991). Conversely, the substantial increase in salinity observed in late-stage aqueous fluids is the consequence of water-consuming fluid-rock reactions (formation of epidote and chlorite) at low fluid/rock ratios. This conclusion is strongly supported by fluid-mineral equilibria modeling in the system Si-Al-Fe-Mg-Ca-Na-K-C-H-O-Cl, using a Gibbs energy minimization approach that combines aqueous fluid speciation with nonideal mineral solid-solutions (Dolejs & Wagner 2008). The simulations predict the texturally observed mineral transformations and the chemical evolution of the fluids largely within their analytical uncertainties. The modeling does also predict the continuous decrease in CO₂ concentrations in the late-stage aqueous fluids resulting from calcite precipitation. From isochores constructed for the different fluid inclusion types an approximate pressure-temperature path has been derived. This path shows near isobaric cooling for the early aqueous-carbonic fluid inclusion types, followed by a substantial pressure decrease that resulted in entrapment of moderately saline aqueous inclusions. The late stage calcic brine inclusions were probably entrapped at temperatures as low as 250 °C. The concentrations of ore metals (Cu, Pb, Zn, W, and Mn) in the aqueous-carbonic fluid inclusions in the Monte Mattoni complex are rather low, both in comparison with mineralized intrusions and more differentiated barren plutons (Audetat et al. 2008). By contrast, the late-stage low-temperature calcic brines contain high concentrations of Pb and Zn which are comparable to base metal concentrations found in ore stage fluids of major sediment-hosted Pb-Zn deposits (Stoffell et al. 2008; Wilkinson et al. 2009).

REFERENCES

- Audetat, A., Pettke, T., Heinrich, C.A. & Bodnar, R.J. 2008: The composition of magmatic-hydrothermal fluids in barren versus mineralized intrusions. *Economic Geology* 103, 877-908.
- Cline, J. & Bodnar, R.J. 1991: Can economic porphyry copper mineralization be generated by a typical calc-alkaline melt? *Journal of Geophysical Research* 96, 8113-8126.
- Dolejs, D. & Wagner, T. 2008: Thermodynamic modeling of non-ideal mineral-fluid equilibria in the system Si-Al-Fe-Mg-Ca-Na-K-H-O-Cl at elevated temperatures and pressures: Implications for hydrothermal mass transfer in granitic rocks. *Geochimica et Cosmochimica Acta* 72, 526-553.
- John, B.E. & Blundy, J.D. 1993: Emplacement-related deformation of granitoid magmas, southern Adamello massif, Italy. *Geological Society of America Bulletin* 105, 1517-1541.
- Stoffell, B., Appold, M.S., Wilkinson, J.J., McClean, N.A. & Jeffries, T.E. 2008: Geochemistry and evolution of Mississippi Valley-Type mineralizing brines from the Tri-State and northern Arkansas districts determined by LA-ICP-MS microanalysis of fluid inclusions. *Economic Geology* 103, 1411-1435.
- Wilkinson, J.J., Stoffell, B., Wilkinson, C.C., Jeffries, T.E. & Appold, M.S. 2009: Anomalously metal-rich fluids form hydrothermal ore deposits. *Science* 323, 764-767.

4.13

Hybridization processes in a partially crystallized magma chamber (Austurhorn intrusion, SE Iceland): Multiple magma mixing scenarios

Daniel Weidendorfer¹, Hannes B. Mattsson, Peter Ulmer

Institute for Geochemistry and Petrology

Swiss Federal Institute of Technology (ETH Zurich), Clausiusstrasse 25, CH-8092 Zürich, Switzerland

¹(danielwe@student.ethz.ch)

The Tertiary Austurhorn intrusive complex in SE Iceland is believed to represent a large exhumed magma chamber with an extensive history of magma mixing and mingling. The basal part of the intrusion consists of granophyric host rocks which have been intensively intruded by different pulses of more mafic rocks. The association of granophyres, basic and hybrid rocks at Austurhorn are known as “net-veined complex” in the literature, but field relations suggests a much more complex history. Different mafic pillows can be distinguished in the field and morphologies range from near-ideal pillow shapes to fragmented pillows incorporated into intermediate rocks. Rapid quenching of some mafic pillows results in chilled margins, whereas others do not seem to follow the same thermal history. In pillows which lack a chilled rim plagioclase phenocrysts are randomly distributed and can be identified extending all the way to the outer rim compared to an absence of phenocrysts in outer parts of the quenched pillow margins. Complex cross-cutting correlations between different hybrid generations can be distinguished in numerous exposed outcrops. Trace element compositions of hybrid rocks suggest multiple replenishment events of mafic magma into a felsic host reservoir. Mixing proportions in different hybrid generations obtained from Rare Earth Element bulk partition coefficients show that in the beginning of magma mixing hybrid compositions are dominated by the felsic magma but with time hybrids get more mafic in composition as a result of an inversion of mixing endmember proportions. Plagioclase phenocrysts in hybrid rocks often display reverse and oscillatory zoning indicating replenishment events of mafic magmas. Distinct plagioclase zonation patterns represent the mixing history of a single hybrid generation and suggest in case of Austurhorn that magma mixing occurred between mafic, felsic and previously formed hybrid magmas. Near the contact of the intrusion the granophyric magma display brittle deformation indicated by the presence of sharp and blocky enclaves separated by mafic veins. The complexity of the mixing increases towards the center of the intrusion, where chaotic hybrid rocks dominate the lithology.

New magma input locally increases the host temperature and changes the rheology of both the felsic and basic magma. Repeated reheating episodes due to multiple magma injections decrease the viscosity of the granophyres and promote chemical diffusion. Compared to previous studies on the petrology of the Austurhorn intrusion our 65 bulk rock samples show linear trends suggesting mixing between the mafic and silicic end-members as well as mixing between different hybrid magmas. Textural observations in the field and bulk rock analysis suggest that hybrid rocks, in case of Austurhorn with andesitic composition, are formed by several mafic replenishment events into the basal part of an already partially crystallized felsic magma chamber.

4.14

Magma Emplacement Tectonics: What can we learn from the oceans, ophiolites and arcs?

Yoshinobu, Aaron Sei¹

¹Department of Geosciences, Texas Tech University, Lubbock, TX 79409, US (aaron.yoshinobu@ttu.edu)

Magma migration and emplacement remain the fundamental means by which large volumes of heat and mass are added to the lithosphere, ultimately resulting in crust formation. For example, the $\sim 170 \times 10^6$ km² Pacific Plate represents the quantum result of magma emplacement, solidification and crustal generation at the fast-spreading East Pacific Rise (EPR). Crustal accretion at the EPR occurs over a vertical region no more than ~ 6 km thick, perhaps as narrow as 50-500 m perpendicular to the strike of the ridge, and along 10's to 100's of km's of ridge strike length, indicating an extremely focused and efficient melt extraction and collection system. Island arcs and their plutonic underpinnings are considered the primary building block of continental lithosphere. The construction of large batholiths and the eruption of voluminous ignimbrite deposits point to the complex interaction of physical and chemical processes that lead to focused point sources for magma collection and/or eruption. Yet, there remains an incomplete understanding of the mechanisms of magma migration, emplacement, and solidification in the lithosphere. Are there similar operative processes in these diverse environments? If so, what insights may be gained by comparing these two systems?

From new data as well as an incomplete survey of the published literature a number of important paradigms in magma emplacement studies may be documented. These paradigms illuminate our understanding of "magma emplacement tectonics" in arc systems and oceanic spreading centers (OSC's) and provide a template for future studies.

- 1) Field, geophysical, textural, theoretical, and geochronological studies indicate that the construction of magma chambers may occur by the emplacement of successive batches of magma, the size of which vary by several orders of magnitude in *either* setting. Complexities arise when batches of different composition overlap in time and space.
- 2) The plutonic portions of these systems generally reflect an incomplete cumulate residue (gabbroic in OSC's vs. dioritic to mafic granodiorite in arcs) from which high-level, more evolved igneous rocks (or their eruptive equivalents) are derived.
- 3) Structural fabrics (hypersolidus foliations, lineations, folds, etc.) preserved within these systems form diachronously by i) strain associated with magma emplacement; ii) strain associated with regional deformation; and iii) a combination of the above. However, without an external kinematic reference frame (i.e., host rock configuration and structural orientation; regional displacement field orientation, etc.), these fabrics are difficult to interpret at best, and unintelligible, at worst.
- 4) Crystallographic, field, and geochemical data may be used to quantify near-solidus magma rheology. These studies point to the ability of magmas to undergo hypersolidus deformation at low melt fractions (e.g., < 10% melt in gabbroic systems), without preserving appreciable crystal-plastic deformation. Thus, the notion of a rheological transition (30-50% remaining melt), below which the magma behaves as a solid, must be called into question. Field and microstructural studies imply that low melt-fraction strain may be the norm in arc plutons. Such low-melt fraction (i.e., near-solidus) conditions may govern the formation of the final fabric patterns observed.
- 5) The thermal evolution of a given pluton may traverse the solidus multiple times due to cooling and reheating by subsequent intrusion of new batches of magma. Such "defrosting" may occur repeatedly and may be observed texturally in the form of resorbed crystals, truncated zoning profiles and new crystal growth.
- 6) "Traditional" magma emplacement mechanisms such as stoping, ductile flow (e.g., ballooning), roof uplift/floor down-drop (by rigid rotation/translation or by ductile flow) occur in both OSC's and arcs. However, field and mass-balance considerations indicate that the predominant displacement direction of the host material is downward in an integrated arc column, toward the region of magma generation by a combination of the above processes. In contrast, OSC's involve lateral material transfer parallel to transform faults; a transfer mechanism generally unaccounted for in arc systems. However, both roof uplift and floor down-drop have been documented in the plutonic portions of the Josephine and Oman ophiolites, indicating that vertical displacement also occurs.

Instead of focusing on various models for magma migration (e.g., dikes vs. diapirs), we suggest a method of defining the operative deformation mechanisms attending magma migration and emplacement. These include hypersolidus flow, dislocation creep, diffusion creep (both of which facilitate viscous flow), and elastic and inelastic failure (e.g., ductile fracturing, rigid body rotation/translation). The dominance of one mechanism over the other is primarily a function of the heat budget of the magma batch, host material temperature (viscosity), strain rate, and degree of melt overpressure. The observation that the plutonic sections of arcs, ophiolites, and in situ oceanic cores preserve evidence for multiple deformation mechanisms attending the emplacement of a *single magma batch* indicate that heat budget, strain rate, and degree of overpressure may vary in space and time during the emplacement of a single magma batch. The onus remains to establish testable predictions and thoughtful models that integrate the above paradigms to illuminate the nature of magma emplacement tectonics in these environs.

P 4.1

A detailed reconstruction of emplacement and crystallization sequence in the Southern Adamello Batholith, N. Italy using the potential of accessory minerals

Broderick Cindy¹, Schaltegger Urs¹, Frick Daniel², Günther Detlef² & Brack Peter³

¹ Department of Earth Sciences, Rue de Maraîchère 13, CH-1205 Genève (Cindy.Broderick@unige.ch)

² D-CHAB, Lab of Inorganic Chemistry, Hönggerberg HCI, CH- 8093 Zürich

³ Department of Earth Sciences, Sonneggstrasse 5, CH- 8092 Zürich

Recent advances in U-Pb zircon geochronology have revealed the complexities of pluton construction, by multiple injections on 10-100 ka to Ma timescales (Michel et al., 2008, Schaltegger et al., 2009). Using high precision U-Pb dating we are potentially able to describe the duration and evolution of magmatic systems, their crystallization and emplacement within the crust. The potential exists to better understand these processes by detailed study of accessory minerals. The trace element and isotopic characteristics of accessory minerals makes them important information carriers for tracking changes in a magma through time. High precision U-Pb dating, using CA-ID-TIMS and employing the ET2535 tracer solution for <0.1% precision and accuracy on ²⁰⁶Pb/²³⁸U zircon and titanite dates, and trace element analyses of zircon and titanite, combined with Hf isotope analysis of zircon are presented for the investigation of a complex magmatic system.

This study focuses on the Val Fredda Complex (VFC) in the southern tip of the 43 to 32 Ma Adamello batholith, N. Italy. The VFC displays complex relationships among mafic melts that were injected into solidifying felsic magmas. The mafic units crystallized potential antecrystic zircons over a duration of 100 ka, with the majority of zircons co-crystallizing with titanite. The TIMS-TEA method (Schoene et al., 2010) allows us to analyze trace elements on the same volume of zircon/titanite used for U-Pb dating. Mafic zircon and titanite trace elements (e.g., Eu/Eu* and Sr) suggest that these accessory minerals crystallized prior to plagioclase fractionation. Based on experiments (Ulmer et al., 1983) and the trace element data from this study, we suggest that the mafic zircons and titanites do not represent in situ crystallization and therefore are more likely antecrystic.

Data from the VFC felsic units show more complex zircon populations, including xenocrystic, antecrystic and autocrystic zircons. These felsic units have apparent autocrystic zircon growth over 100 to 200 ka, with zircons co-crystallizing with titanites during the final 20 to 50 ka. While zircon/chondrite normalized REE patterns do not vary with differentiation, titanite REE patterns reveal changes with differentiation, mostly within the LREEs and Eu/Eu*. Based on trace elements fractionation we suggest that felsic zircons and titanites crystallized in situ and represent autocrystic growth. The oldest autocrystic zircon may approximate the injection of the respective magma pulses into the host rock, whereas the youngest zircon and titanite indicate final crystallization at the solidus in a stagnant interstitial melt.

We acknowledge funding of FNS in the frame of ProDoc Adamello 4-D.

REFERENCES

- Michel, J., Baumgartner, L., Putlitz, B., Schaltegger, U., & Ovtcharova, M. 2008: Incremental growth of the Patagonian Torres del Paine laccolith over 90 k.y. *Geology* 36, 459-462.
- Schaltegger, U., Brack, P., Ovtcharova, M., Peytcheva, I., Schoene, B., Stracke, A., Marocchi, M., & Bargossi, G. M. 2009: Zircon and titanite recording 1.5 million years of magma accretion, crystallization and initial cooling in a composite pluton (southern Adamello batholith, northern Italy). *Earth and Planetary Science Letters* 286, 208-218.
- Schoene, B., Latkoczy, C., Schaltegger, U., & Günther, D. 2010: A new method integrating high-precision U-Pb geochronology with zircon trace element analysis (U-Pb TIMS-TEA). *Geochimica et Cosmochimica Acta* 74, 7144-7159.
- Ulmer, P., Callegari, E., & Sonderegger, U.C. 1983: Genesis of the mafic and ultramafic rocks and their genetical relations to the tonalitic-trondhjemitic granitoids of the of the southern part of the Adamello batholith, (northern Italy). *Mem. Soc. Geol. It.* 26, 171-222.

P 4.2

2D numerical modelling of fluid and melt percolation in the subduction zone

Dymkova Diana¹, Gerya Taras¹, Podladchikov Yury²

¹Institute of Geophysics, ETH Zurich, Sonneggstrasse 5, CH-8092 Zurich (diana.dymkova@erdw.ethz.ch)

²Institut de Geophysique, Quartier UNIL-Sorge, Batiment Amphipole, CH-1015n Lausanne

Subducting slab dehydration and resulting aqueous fluid percolation triggers partial melting in the mantle wedge and is accompanied with the further melt percolation through the porous space to the region above the slab. This problem is a complex coupled chemical, thermal and mechanical process responsible for the magmatic arcs formation and change of the mantle wedge properties.

We have created a two-dimensional model of a two-phase flow in a porous media solving a coupled Darcy-Stokes system of equations for two incompressible media for the case of visco-plastic rheology of solid matrix. Our system of equation is expanded for the high-porosity limits and stabilized it for the case of high porosity contrasts. Melting process is implemented according to the model of Katz (2003) where melting degree is a function of pressure, temperature, composition and water content. We use a finite-difference method with fully staggered grid in a combination with marker-in-cell technique for advection of fluid and solid phase.

We performed a comparison with a benchmark of a thermal convection in a porous media in a bottom-heated box to verify the interdependency of Rayleigh and Nusselt numbers with a theoretical one. We have demonstrated the stability and robustness of the algorithm in case of strongly non-linear visco-plastic rheology of solid including cases with localization of both deformation and porous flow along spontaneously forming shear bands.

We have checked our model for the forming of localized porous channels under a simple shear stress (channelling instability).

Current work includes implementation of non-linear viscous rheology and elaboration on the setup of self-initiating subduction. Later we plan to include solid elasticity and fluid/solid compressibility.

Also we have developed a full complexity system of equations for visco-elastic case and currently are working on numerical realisation of it to verify our simplifying assumptions for the general model.

Ultimate goal is to simulate in a realistic self-consistent manner fluid and melt generation and transport in subduction zones including fluid/melt focussing phenomena above slabs.

REFERENCES

Katz, R.F., M. Spiegelman, and C.H. Langmuir (2003), A new parameterization of hydrous mantle melting, *Geochem. Geophys. Geosyst.*, 4(9), 1073.

P 4.3

Thermal evolution of the Western Adamello contact aureole

Floess David¹, Baumgartner Lukas¹ & Brack Peter²

¹Earth Sciences – University of Lausanne (david.floess@unil.ch)

²Earth Sciences – ETH Zürich

The Western Adamello pluton (WAD, Northern Italy) intruded into the South Alpine basement and its permotriassic cover around 38 Ma ago. The thermal effects of the tonalitic intrusion on the host rock are (among other mineral reactions) a) partial melting of basement rocks and sediments up to 0.3 km from the contact due to breakdown of muscovite, b) garnet re-growth at 1.7 km from the contact and c) growth of andalusite at 2.4 km from the contact.

The occurrence of partially molten host rock requires temperatures >650 °C at 300 m from the contact and Grt/Bt thermometry of a sample at the same distance produced 637 ± 18 °C. Heat flow models can be used to describe the Temperature-time evolution in the contact aureole. For these, several parameters are crucial: A) initial host rock temperature, B) presence or absence of hydrothermal systems in the host rock, C) convection in the magma chamber, D) the emplacement style and E) the intrusion temperature. An initial attempt with a two-dimensional, thermal model (non-convecting) single batch intrusion with $T_{\text{int}} = 800$ °C and $T_{\text{host}} = 300$ °C yield temperatures at least 150 °C lower than those from the above petrologic evidence.

We varied, where appropriate, the above critical parameters to gain a better understanding of emplacement style by reproducing the observed temperatures in the contact aureole. A) The host rock temperature before intrusion is constrained to a maximum of 300°, since there was no post-Triassic resetting of Biotite Rb/Sr data outside the contact aureole (Pennacchioni et al. 2006) and Illite crystallinity from samples outside the contact aureole suggests, at most, anchizonal conditions (Riklin 1985). B) Significant convection in a large hydrothermal system in the host rock can be excluded in the inner aureole due to the low amount of partial melt observed in the proximity of the intrusion. C) Convection within the pluton is strongly depending on the intrusion geometry. The presence of a large batch of magma resulting in convection is often used to increase temperatures in the host rock. Bea (2010) showed that convection would only last in the order of a few thousand years for a single batch intrusion of a similar size to the WAD. The observed temperatures in the WAD contact aureole require the pluton to convect for at least 5 to 10x longer, unless intrusion temperatures are above 950°C.

Therefore, convection could contribute to higher contact metamorphic temperatures but cannot account for the entire temperature mismatch. D) Continuous or pulse-wise feeding of the magma chamber at the contact will significantly raise the temperatures in the contact aureole. The WAD (5 km) is mainly non-foliated, and non-layered with exception of a small marginal zone (500 m), showing a contact-parallel foliation and sub-vertical orientation of hornblendes. Structural elements in the host rock (foliation, boudinage, folding and microtextures) suggest a significant compressional component during the WAD emplacement.

Therefore, a scenario of a continuously growing pluton, fed over an extended period of time is favored. The emplacement has to be rapid enough to result in a large batch, allowing convection. More structural, petrographic and geochronologic data is needed to further constrain the emplacement style.

In any case, the intrusion temperature needs to be in excess of 800 °C to lead to the observed temperatures in the WAD contact aureole (E).

REFERENCES

- Bea F. 2010: Crystallization Dynamics of Granite Magma Chambers in the Absence of Regional Stress: Multiphysics Modeling with Natural Examples. *Journal of Petrology*, Vol. 51, Nr. 7, 1541-1569.
- Pennacchioni et al. 2006: Brittle–ductile–brittle deformation during cooling of tonalite (Adamello, Southern Italian Alps). *Tectonophysics* 427, Issues 1-4, 171-197.
- Riklin K. 1985: Contact metamorphism of the Permian red sandstones in the Adamello area. *Mem. Soc. Geol. Ital.* 26, 159-169.

P 4.4

Trace-element partitioning in post-plutonic dike-suites S-Adamello (N-Italy)

Hürlimann Niklaus¹, Müntener Othmar¹ & Ulmer Peter²

¹Institute of Mineralogy and Geochemistry, Anthropole, CH-1015 Lausanne (niklaus.hurlimann@unil.ch)

²Institute of Geochemistry and Petrology, Clausiusstrasse 25, CH-8092 Zürich

Mineral-melt trace-element partition coefficients are used to model the evolution of trace-element concentrations such as the rare earth elements (REE) in magmas through fractional crystallization. Recently, such mineral-melt coefficients were mainly determined by experiments. These partition-coefficients vary as a function of pressure, temperature and bulk composition. Here we present an approach to directly determine the partition coefficients from natural subvolcanic rocks where bulk composition for the primary magmas and pressure in the form of the emplacement level are confined. This is in the context of post-plutonic dike-suites from the S-Adamello, which is part of the batholith that emplaced during the late stage of the Alpine collision in N-Italy. Dike rocks generally closely approach liquid compositions, in particular mafic compositions, relative to plutonic rocks and thus are suitable to model the chemical evolution of magmas. The present case study explores the links of magma sources that formed the plutonic units and the later dikes.

A laser ablation study was carried out to determine the trace-element composition of the aphyric fine-grained matrix along the chilled margins representing the liquid, and the microphenocrysts such as pyroxene, hornblende and plagioclase to eventually calculate the partition coefficients between crystals and liquid. The aphyric matrix was analyzed by scanning with LA-ICP-MS. For performing the quantification of this analysis the whole rock composition was corrected for large crystals with their overall mineral chemistry and through detailed textural analysis to achieve a major-element composition for the aphyric-matrix. This in turn gives an internal standard for calculating liquid trace-element concentrations of the matrix scans with LA-ICP-MS.

Dike rocks display variation in cooling rates, which are very rapid at margins and decreases towards the center. Our calculations have to take into account the potential of increasing disequilibrium growth of the crystals towards the rapidly cooled dike margins due to kinetic effects (Mollo et al. 2011). Further the determined partition coefficients are assessed with the crystal structure lattice-strain model (Blundy & Wood 1994) for their consistency.

The range of different magma compositions of the Adamello dike-suites shows mingling or mixing of different magma sources for more evolved compositions through crystal textures. Different magma sources appear to have evolved along different liquid lines of descent. Differences in the crystallization sequence are revealed by mineral trace-element chemistry. Clinopyroxene in basalts has REE-patterns indicating co-crystallization with plagioclase through an Eu anomaly. Olivine occurs as pseudomorphs with spinel-inclusions in these basalts. Hornblende in basaltic andesite has generally lower concentrations in REE than hornblende in basalts. The slightly steeper light-REE patterns implies hornblende crystallizing after olivine rather than clinopyroxene. While in basalts olivine appears to have followed by clinopyroxene and plagioclase. These preliminary results imply that larger crystals from basaltic-andesites formed from a water-rich magma source in deep crustal reservoir. Such a water-rich magma source seems to have mixed with less differentiated drier basalts.

REFERENCES

- Mollo, S., Lanzafame, G., Masotta, M., Iezzi, G., Ferlito, C. & Scarlato P. 2011: Cooling history of a dike revealed by mineral chemistry: A case study from Mt. Etna volcano. *Chemical Geology*, in press.
- Blundy J. D. & Wood, B. J. 1994: Prediction of crystal-melt partition coefficients from elastic moduli. *Nature*, 372, 452-454.

P 4.5

Trace elements geochemistry and experimental petrology as novel approaches to understand reactive flow through the Rum layered intrusion: preliminary results and perspectives

Leuthold Julien¹, Blundy Jon¹, Holness Marian²

¹School of Earth Sciences, Wills Memorial Building, Bristol, United Kingdom (julien.leuthold@bristol.ac.uk)

²Department of Earth Sciences, Downing Street, Cambridge, United Kingdom

The well studied Rum Isle layered intrusion has built up by emplacement of a series of 16 macro-rhythmic units. Magma intruded 60.53 ± 0.08 Ma (Hamilton *et al.*, 1998), at a pressure < 0.5 kbar (Holness, 1999). Units are composed of feldspathic peridotite at the base, overlain by troctolite and gabbro. Layering is induced by fractional crystallization from picritic magma (Upton *et al.*, 2002; Holness *et al.*, 2007). Rum magma liquid line of descent is complicated by reactive melt percolation within crystal mushes, either originating from continuous cumulate pile compaction or from a newly injected reactive picritic magma (Figure 1). Field evidence is numerous: some troctolites, that display gabbroic enclaves, result from clinopyroxene primocryst dissolution from a gabbroic crystal mush, when intruded by subsequent clinopyroxene undersaturated peridotite dykes or protrusions. They are associated with a clinopyroxene-rich band in the overlying gabbroic mush. This horizon is wavy. In poikilitic gabbros, clinopyroxene occurs as cumulus grains, as interstitial crystals and as coronae around olivine cumulus grains. A distinct decrease in the Mg# and an increase in Ti content are observed between clinopyroxene primocrysts and oikocrysts (Holness *et al.*, 2007). Due to disequilibrium between crystals and invading magma, clinopyroxene is dissolved from the mush, leading progressively to saturation of the percolating magma (Holness *et al.*, 2007). After transport along grain boundaries, it is re-precipitated interstitially.

Rum is ideally suited to study interstitial melt migration through magmatic mushes. We are developing a novel approach to understand infiltration metasomatism, by coupling trace element geochemistry and experimental petrology. Appearance temperature for all mineral phases will be determined using (a) water-saturated, 200bar, f_{O_2} at QFM experiments on aphyric picrite in TZM pressure vessel, and (b) anhydrous, one-atmosphere, f_{O_2} at QFM in Gas-mixing furnaces, using a picritic starting material. Results will be used to define a relative timescale for infiltration processes, based on temperature. We will acquire high precision and space resolution microanalyses on natural samples and experiment run products, using FEG-probe, LA-ICP-MS and nanoSIMS. Equilibrium liquid composition with natural cumulus grains, thin rims and interstitial crystals will be determined, using calculated partition coefficients. The objectives of studying crystal zoning and mineral generations are to check if different infiltration episodes have occurred and to make precise timescale estimations using chemical diffusion through crystals. In a second stage, we will use a novel approach to study infiltration metasomatism process by producing synthetic mixes of crystals with reactive percolating melt.

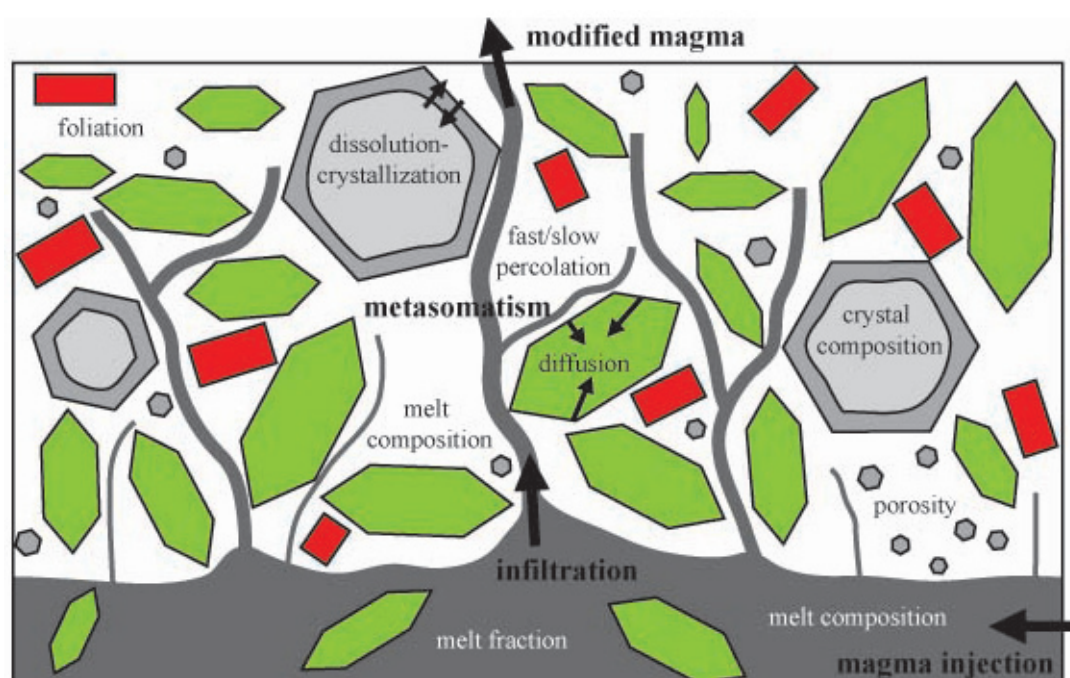


Figure 1. Schematic representation of reactive flow of residual interstitial melt through crystal mush.

REFERENCES

- Hamilton, M.A., Pearson, D.G., Thompson, R.N., Kelly, S.P. & Emeleus, C.H. 1998: Rapid eruption of Skye lavas inferred from precise U-Pb and Ar-Ar dating of the Rum and Cuillin plutonic complexes, *Nature* 394, 260-263.
- Holness, M.B. 1999: Contact metamorphism and anatexis of Torridonian arkose by minor intrusions of the Rum Igneous Complex, Inner Hebrides, Scotland; *Geol. Mag.* 136, 527-542.
- Holness, M.B., Hallworth, M.A., Woods, A. & Sides, R.E. 2007: Infiltration Metasomatism of Cumulates by Intrusive Magma Replenishment: the Wavy Horizon, Isle of Rum, Scotland, *J. Petrol.* 48(3), 563-587.
- Upton, B.G.J., Skovgaard, A.C., McClurg, J., Kirstein, L., Cheadle, M., Emeleus, C.H., Wadsworth W.J. & Fallick A.E. 2002: Picritic magmas and the Rum ultramafic complex, Scotland; *Geol. Mag.* 139, 437-452.

P 4.6

Cordierite growth textures in the Permian sequence of the Adamello contact aureole, Italy

Mettasch Sylvia¹ & Baumgartner Lukas¹

¹*Institute de Minéralogie et Géochimie, Batiment Anthropole, CH-1015 Lausanne (sylvia.mettasch@unil.ch)*

Metamorphic Permian rocks display different cordierite textures in the Adamello contact aureole in northern Italy. These rocks are pelitic sandstones of the Verrucano Lombardo unit and experienced low P/high T contact metamorphism due to the emplacement of the Adamello batholith, a Tertiary intrusion of mostly granodioritic to tonalitic composition (Callegari & Dal Piaz, 1973). The Adamello batholith is located between Lombardy and Trentino in the Southern Alps. The metamorphic overprint results in different metamorphic zones. With increasing grade these are (see also Ricklin, 1982): a) the biotite zone, which is characterized by the first appearance of small biotite and muscovite flakes growing around and into old detritic quartz, K-feldspars, deformed muscovites and biotites, or they form fine grained aggregates within the matrix; b) the cordierite zone, which is marked by the growth of cordierite around and within the biotite aggregates as well as the recrystallisation of K-feldspar in the matrix; c) the andalusite zone, which is characterized by the growth of andalusite at the margins of detritic quartz crystals and in many cases within the K-feldspar and muscovite rich zones between the cordierites; d) the sillimanite zone, with fibrolitic sillimanite occurring as aggregates, mostly replacing muscovite and biotite but rarely andalusite.

Cordierite growth textures show variable morphologies from egg-shaped, almost spherical porphyroblasts to irregular, dendrite- or tree-like patterns. Most of the cordierites were replaced by fine-grained pinnite increasing the contrast and therefore making the textures easily visible to the naked eye. Roundish, poikilitic cordierites vary from about 2 mm to 30 mm in size. Small crystals are typically spherical with well defined, straight margins, whereas larger crystals are more egg-shaped with rather lobate boundaries. Dendrite textures are up to 30 mm in size with more or less complex limbs. The overall shape of the dendrites is spherical and the geometry suggests a radial growth. They are either finely branched or thicker and less complex with thickened bifurcations. All different morphologies can occur with or without halos, which have variable sizes and shape. The halos are biotite-free, but contain otherwise the same mineralogy as the matrix (muscovite – K-feldspar – quartz – oxide – plagioclase). In most of the collected samples, the cordierites are randomly distributed throughout the rock but in some cases the textures are aligned within or even grow across the bedding. Thin section investigations suggest that the cordierite-producing reaction was muscovite + biotite + quartz = K-feldspar + cordierite + water.

Different morphologies were observed within a single outcrop, which experienced a unique temperature-time trajectory. Hence, the rate of temperature is not the major factor discriminating between the textures. We propose that differences mainly in whole rock chemistry and/or fluid composition were responsible for the generation of differences in textures.

REFERENCES

- Callegari, E. & Dal Piaz, G. 1973: Field relationships between the main igneous masses of the Adamello intrusive massif (Northern Italy), *Mem. Ist. Geol. Mineral. Univ. Padova*, 29, 39 p.
- Riklin, K. 1985, Contact metamorphism of the Permian “red sandstones” in the Adamello area, *Mem. Soc. Geol. It.*, 26, p. 159-169.

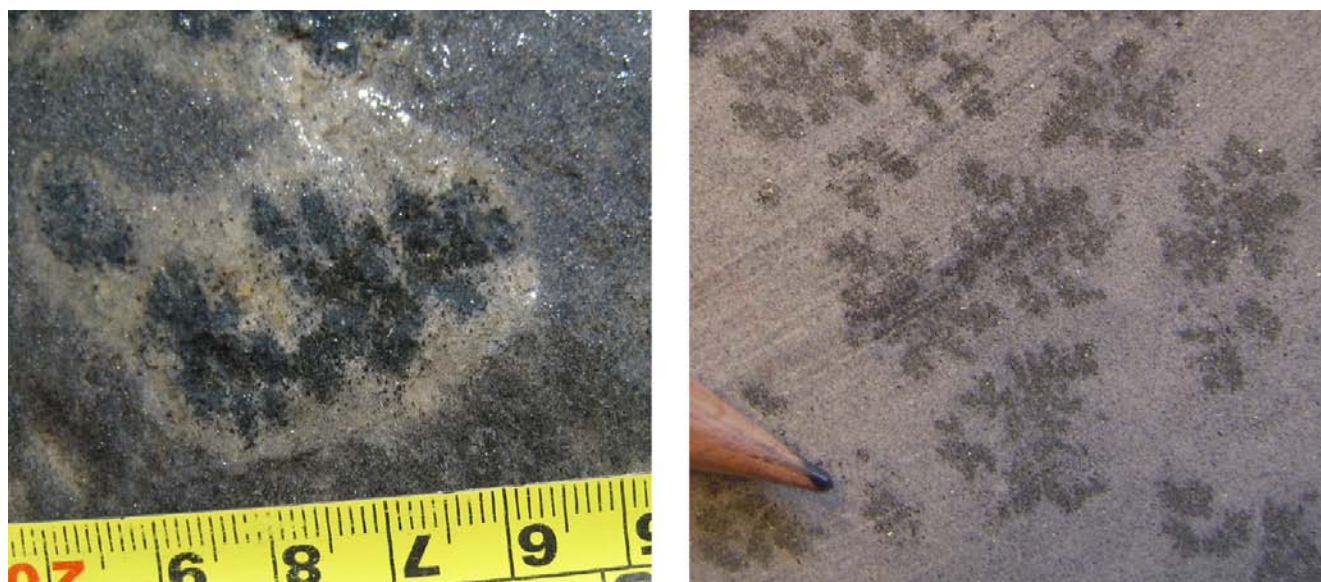


Figure 1 : Examples of dentritic cordierite growth with depletion halo (left) and without (right).

P 4.7

Liquid line of descent from olivine-tholeiite to granodiorite at 0.7 GPa

Nandedkar Rohit¹, Ulmer Peter¹, Müntener Othmar²

¹Institut für Geochemie und Petrologie, Clausiusstrasse 25, CH-8092 Zürich (rohit.nandedkar@erdw.ethz.ch)

²Institut de minéralogie et géochimie, Quartier UNIL-Dorigny Bâtiment Anthropole 4137, CH-1015 Lausanne

The isobaric fractional crystallization history of a cooling hydrous, primitive, calc-alkaline, basaltic magma at lower to intermediate crustal levels is investigated by this experimental study of the liquid line of descent. An end-loaded piston cylinder apparatus was used to perform these experiments at 0.7 GPa. The composition of an olivine-tholeiitic dike from the Adamello batholith (Northern Italy), was used to synthesize a synthetic equivalent containing 3 wt.% of water and 32 trace elements at 40 ppm level. Glass compositions, which represent the liquid composition in equilibrium with solid phases, were subsequently synthesized from oxides, hydroxides and silicates and used as new starting material for the following experiment conducted at 30°C lower temperature. Analyses were performed upon the recovered experimental charges using EPMA and LA-ICP-MS. Liquidus temperature of the synthetic equivalent of the natural olivine-tholeiitic dike has been found at 1165°C (±5°C). The experimentally obtained liquid line of descent follows a calc-alkaline fractionation trend as anticipated. The generated intermediate to granitic compositions closely resemble plutonic and volcanic rocks that compose arc-related igneous complexes (e.g. Adamello batholith, northern Italy). The following crystallization sequence has been determined: olivine (ol) => clinopyroxene (cpx) => plagioclase (plg), spinel (sp) => orthopyroxene (opx), amphibole (amph), magnetite (mag). The liquid line of descent evolves towards corundum-(Al₂O₃) normative (peraluminous) compositions at 780°C with a silica content of 68 wt.%. Comparing the study of Kägi (2000) on a similar initial starting material, it's noticeable that liquid compositions remained diopside-normative (metaluminous) down to 990°C at 1.0 GPa. Plagioclase fractionation, which occurred only at 0.7 GPa (this study), is not supposed to be responsible for this contrasting behavior. However, we state that a "branching" peritectic encompassing the amphibole stability field is causing the meta-versus peraluminous derivative liquids when respective phase equilibria are inspected: At 0.7 GPa, phase relations evolve from cpx+opx+plg+mag to amph+opx+plg+mag without cpx. In contrast, Kägi (2000) reported the coexistence of cpx+amph+mag at 1 GPa. This could be related to an inferred decrease of the amph stability field towards lower temperatures at 0.7 GPa or/ and a larger amount of opx compared to cpx crystallizing before amph at 1.0 GPa, driving the derivative liquids towards the other branch of the diverging peritectic point.

REFERENCES

Kägi, R., 2000. The Liquid Line of Descent of Hydrous, Primary, Calc-alkaline Magmas Under Elevated Pressure - An Experimental Approach. PhD-thesis, Diss ETH No. 13963, 163p., Zurich.

P 4.8

Textures and chemistry of zircons: implication on the interpretation of U-Pb zircon ages from observations of the Chaltén Plutonic Complex (Argentina)

Putlitz Benita¹, Ramírez de Arellano Cristobal¹, Ovtcharova Maria², Müntener Othmar¹

¹ *Institute of Mineralogy and Geochemistry, University of Lausanne, Anthropole, 1015 Lausanne (benita.putlitz@unil.ch)*

² *Département de Minéralogie, University of Geneva, Rue de Maraîchère 13, CH-1205 Genève*

The subject of this presentation is the high precision U-Pb dating of zircons from the Chaltén Plutonic Complex (CHPC) in Argentina. The CHPC is a mafic to granitic intrusive suite situated in a backarc position in Southern Patagonia. We could show that the precise absolute geochronology of this small plutonic complex has important consequences for the geodynamic interpretation, i.e. arc migration pattern in Patagonia (Ramirez et al. 2011). Here, we explore in more detail the textural and chemical characteristics of zircons from the different plutonic units of this composite intrusion to gain insights on the growth of zircons in magmas with variable degrees of differentiation. These features are of interest for the geological interpretation of zircon ages, especially since increasing precision of ages can be obtained (Schaltegger et al. 2009, Schoene et al. 2011).

The calc-alkaline gabbroic to granitic rocks of the CHPC were emplaced over a short time-span of 530 ky between 16.90 ± 0.05 Ma and 16.37 ± 0.02 Ma. The zircon ages are consistent with the relative geochronology inferred from field relations (8 plutonic units were distinguished). Where undulating ductile contacts are observed, the age difference between units cannot be resolved. In the case of brecciated contacts a minimum age difference of 80ky was obtained, which is at the limit of the obtained precision (± 40 ky). The petrographic textures of zircons in mafic rocks indicate crystallization in isolated pockets, i.e. interstitial. The application of the Ti-in-zircon thermometer yields consistently low temperatures ($\sim 760^\circ\text{C}$). This indicates that (most) of the zircons from these mafic samples might have crystallized near solidus temperatures, and consequently post-date the emplacement.

In contrast, the textures of zircons from diverse granitic rocks indicate a more protracted crystallization. The chemistry (LA-ICP-MS analysis) of zircons from granitic rocks displays systematic variations of U/Th and U/Ta ratios between core and rim. This pattern can be correlated with the variation of temperatures and $\text{Ce}^{\text{III}}/\text{Ce}^{\text{IV}}$ ratios. These observations suggest that several episodes of zircon crystallization at different temperatures exist in granitic melts. The calculated temperatures are 100°C to 200°C higher than the solidus, which would imply that many zircons crystallized prior to the emplacement (antecryst).

REFERENCES

- Ramírez de Arellano C, Putlitz B, Müntener O, Ovtcharova M & Chiaradia M (2011) Miocene Arc migration and subduction erosion in Patagonia – Evidences from the Fitz Roy Plutonic Complex. XVIII Geological Congress of Argentina, Neuquén, Argentina, 2011
- Schaltegger U., Brack P., Ovtcharova M., Peytcheva I., Schoene B., Stracke A. & Bargossi G. (2009) Zircon and titanite recording 1.5 million years of magma accretion, crystallization and initial cooling in a composite pluton (southern Adamello batholith, northern Italy) *Earth Planet. Sci. Lett.* 286, 108-218
- Schoene B, Latkoczy C, Schaltegger U & Günther D. (2010): A new method integrating high-precision U-Pb geochronology with zircon trace element analysis (U-Pb TIMS-TEA), *Geochim. Cosmochim. Acta*, 74, 7144-7159.

P 4.9

Tracing episodic magma accretion by U-Pb dating and $^{18}\text{O}/^{16}\text{O}$ isotopes in zircon: the case of the Adamello batholith, Italy

Skopelitis Alexandra¹, Bindeman Ilya², Ulianov Alexey³, Brack Peter⁴, Schaltegger Urs¹

¹ Département de Minéralogie, Rue de Maraichers 13, CH-1211 Genève 4 (Alexandra.Nowak@unige.ch)

² University of Oregon, OR 97403, USA

³ Institut de minéralogie et géochimie, Amphipôle, CH-1015 Lausanne

⁴ Inst. für Geochemie und Petrologie Clausiusstrasse 25, CH-8092 Zürich

Styles and timescales of batholith formation still remain a matter of debate. There is growing evidence that batholiths are not formed by a single ascent of magma but by accretion of multiple batches. In the latter case, are they derived from the same source or different ones, and do they suffer similar degrees of contamination?

In order to answer these questions, we study tonalites from the Adamello batholith (33–43 Ma) localized in the northern Italian Alps. Previous studies mainly based on cooling ages highlighted a younging of magmatic activity towards the north (Callegari & Brack 2002; Schaltegger et al., 2009; Del Moro et al., 1983) which is confirmed by our new U-Pb zircon LA-ICP-MS dating (Fig. 1). Isotopic compositions of both Sr and O indicated increased contribution from higher $\delta^{18}\text{O}$, more radiogenic supracrustal sources in the same direction (Cortecchi et al., 1979). We present new data from a $^{18}\text{O}/^{16}\text{O}$ isotope study on small quantities of freshest and refractory separates of quartz, amphibole, titanite and zircon, and best estimate $\delta^{18}\text{O}$ magma values (Bindeman 2008). The data confirm increasing crustal contamination towards the north indicated by elevated $\delta^{18}\text{O}$ values up to 7‰ in zircon. H isotope ratio is strongly negative (-97‰) for the amphibole in the most northerly sample suggesting an assimilation of hydrothermally-altered rocks or an assimilation of marine sediment. We will quantify the contamination by AFC modelling using geochemistry, whole rock and mineral isotopes. As a preliminary conclusion, the Adamello batholith was formed by different pulses over ca 10 m.y. coming from different in $\delta^{18}\text{O}$ magma reservoirs with contrasting oxygen isotope compositions, due to their different depth in a $^{18}\text{O}/^{16}\text{O}$ zoned crust.

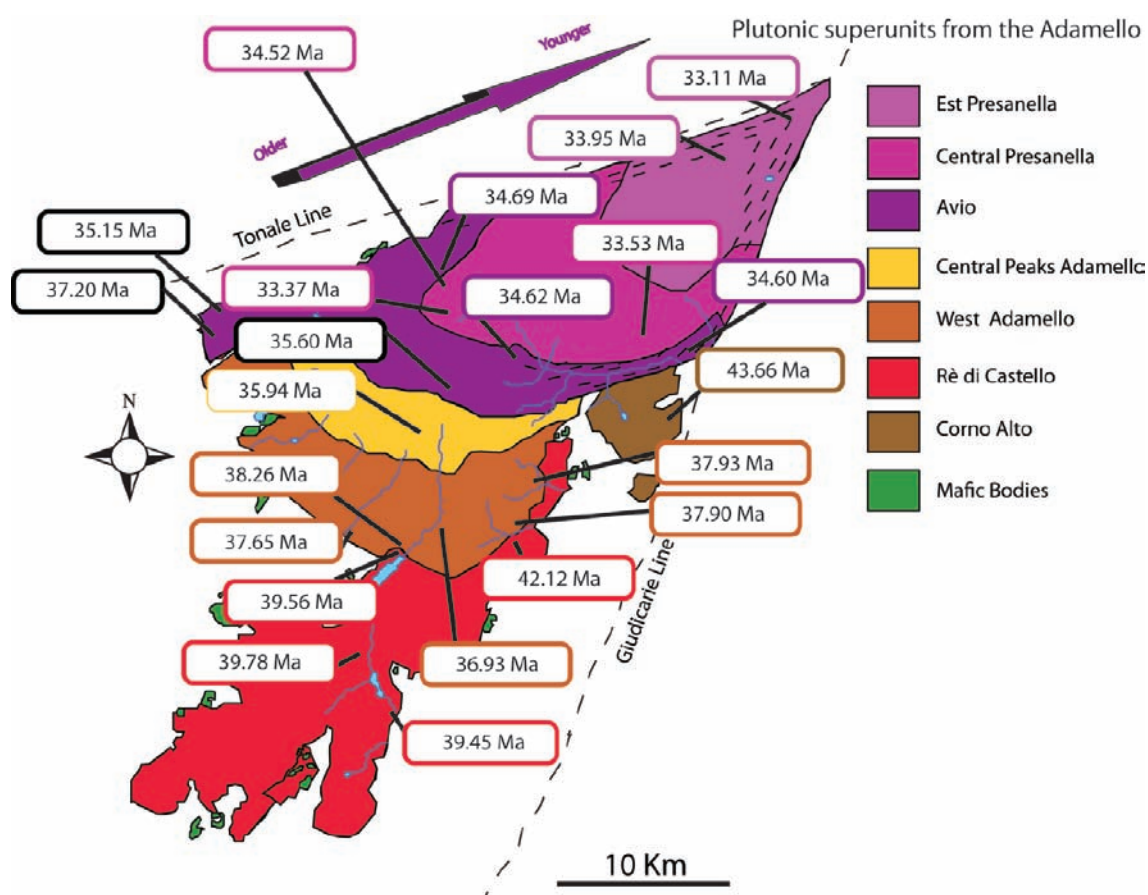


Figure 1. Simplified geological map of the Adamello batholith with the different superunits. New U-Pb ages analyzed by LA-ICP-MS on zircons.

REFERENCES

- Bindeman I. 2008 *Reviews in Mineralogy & Geochemistry*, 69, 445-478
- Callegari, E. & Brack, P. 2002 Geological map of Tertiary Adamello Batholith (Northern Italy) *Mem. Sci. Geol.* 54, 19-49
- Cortecci G., Del Moro, A., Leone, G. & Pardini, G.C. 1979 *Contributions to Mineralogy and Petrology*, 68, 421-427
- Del Moro, A., Pardini, G., Quercioli, C., Villa, I.M. & Callegari, E. 1983 *Mem. Soc. Geol. It.*, 26, 261-284
- Schaltegger, U., Brack, P., Ovtcharova, M., Peytcheva, I., Schoene, B., Stracke, A., Marocchi, M. & Bargossi, G.M. 2009 Zircon and titanite recording 1.5 million years of magma accretion, crystallization and initial cooling in a composite pluton (southern Adamello batholith, northern Italy) *Earth and Planetary Science Letters*, 286, 208-218

P 4.10

Experimental determination of the hydrous basalt liquidus: The Grenadan perspective

Stamper Charlotte¹, Blundy Jon¹, Melekhova Elena¹ & Arculus Richard²

¹*Department of Earth Sciences, University of Bristol, Wills Memorial Building, Queens Road, Bristol, BS8 1RJ, UK (c.stamper@bristol.ac.uk)*

²*Research School of Earth Sciences, Australian National University, Canberra 0200 Australia*

A series of experimental liquidus determinations have been carried out on a hydrous primitive basalt at a range of pressures pertaining to ≤ 60 km depth. The starting composition replicates the major element chemistry of a picrite from South East Mountain, Grenada, Lesser Antilles with 15.4 wt % MgO and whole rock Mg# = 73. The island of Grenada is known for erupting primary mantle melts and post-Miocene products of the arc volcanism yield evidence for magmatic water contents of ≤ 6.4 wt % H₂O (Bouvier et al. 2010).

The ultimate aim of this experimental series is to map out the topology of the hydrous basalt liquidus in P-T space. The position of the liquids relative to a mantle adiabat determines the amount of superheating experienced by magma as it ascends to lower pressures. This in turn has implications for the manner in which mantle-derived melts interact with the crust.

Equilibrium experiments have been conducted using both piston cylinder and TZM apparatus at pressures ≤ 1.7 GPa at an fO₂ corresponding to NNO. Both anhydrous and water-undersaturated conditions have been explored and the starting material is nominally carbon-free. All experiments have been conducted using the double capsule technique of Hall et al. (2004).

The 3.0 wt % H₂O liquidus is found to be parallel to the anhydrous liquidus and has a temperature gradient of $\sim 60^\circ\text{C}/\text{GPa}$, increasing from 1260°C at 1kbar to 1355°C at 1.7 GPa. At the lowest pressures the liquidus phase is Cr-rich spinel; at P > 6kbar the liquidus assemblage becomes olivine + spinel. Clinopyroxene-in occurs 50-100°C from the liquidus.

All experimental glasses have been analysed for CO₂ using SIMS. Significant carbon infiltration (< 1.2 wt %) has occurred in hydrous piston cylinder experiments but TZM run products remain relatively carbon-free (<500ppm), thus isolating graphite furnaces in the piston cylinder assembly as the source of the carbon. We discuss mechanisms for carbon diffusion and investigate techniques for limiting carbon contamination in piston cylinder experiments.

REFERENCES

- Bouvier A-S., Métrich N. & Deloule E. 2010: Light elements, volatiles, and stable isotopes in basaltic melt inclusions from Grenada, Lesser Antilles: Inferences for magma genesis. *Geochem. Geophys. Geosyst.*, 11, Q09004.
- Hall L.J., Brodie J., Wood B.J. & Carroll M.R. 2004: Iron and water losses from hydrous basalts contained in Au₈₀Pd₂₀ capsules at high pressure and temperature. *Min Mag* 68, 75–81.

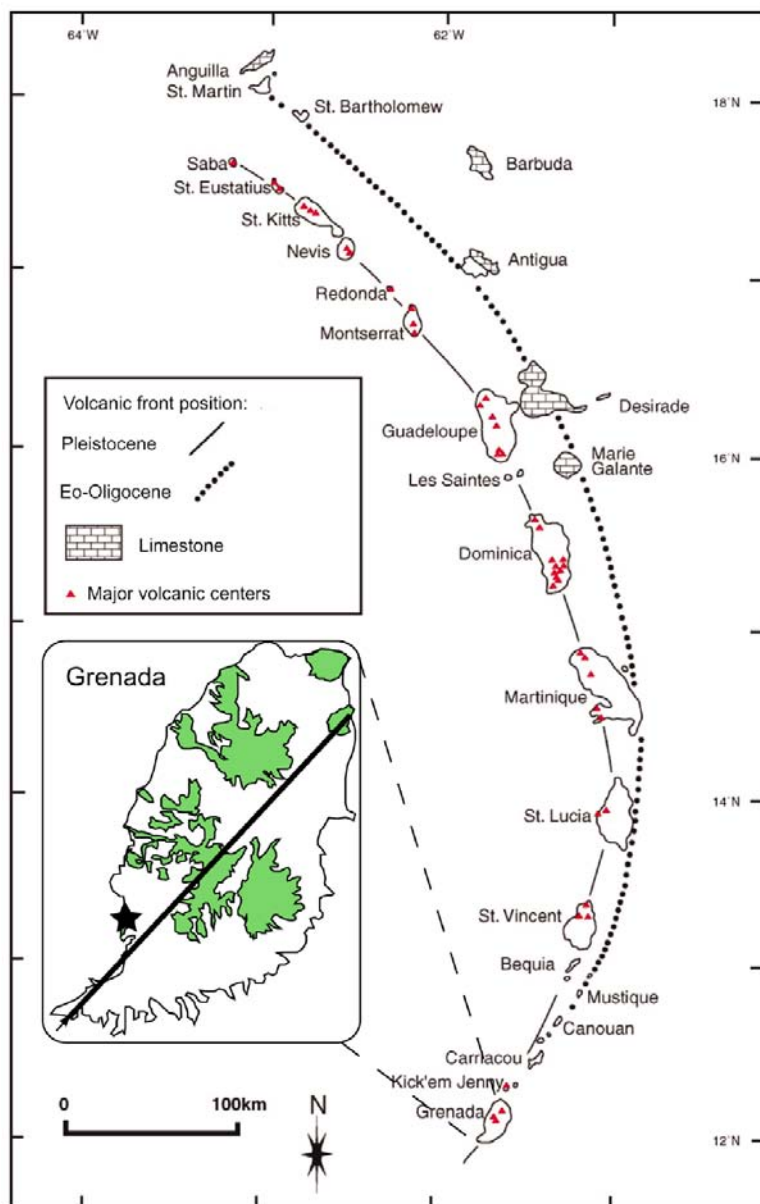


Figure 1. Position of Grenada within the island arc of the Lesser Antilles. Major volcanic centres on Grenada are shaded in green (Bouvier et al. 2010).

P 4.11

Field relations and consequences for emplacement of the Listino Ring Structure, Adamello Massif, N-Italy

Verberne Roel¹, Ulmer, Peter², Müntener, Othmar¹

¹*Institute of Mineralogy and Geochemistry, Bâtiment Anthropole, CH-1015 Lausanne (roel.verberne@unil.ch)*

²*Department of Earth Sciences, Clausiusstrasse 25, CH-8092 Zürich*

First described by Brack (1984, 1985), the Listino Ring Structure (LRS) in the tertiary Southern Adamello massif (Italy) consists of a 300-500 meter wide zone of well foliated, subvertical to steeply inwards dipping tonalite containing a large amount of elongated, mainly gabbroic, mafic enclaves, surrounding a core of fine-grained tonalite approximately 2.5 km in diameter. This zone itself is surrounded by fine- to medium-grained tonalites and is truncated by a granodiorite intrusion in the west. Deformation within the ring is mainly hyper-solidus (i.e. magmatic), although steeply dipping sub-solidus shears and joints are also present. The LRS is crosscut by several phases of syn- to post-plutonic dikes varying in composition from leucogranite to basalt. Recently, a more detailed study into the internal structure of the LRS, combining cross cutting and structural relations of the magmatic phases present has been made.

Cross cutting relationships found on the northeastern side of the LRS indicate the external tonalites (Monocola tonalite) are intruded by a gabbroic magma before they have completely crystallized. The resulting gabbroic enclaves can be up to several meters wide, have fine grained margins and form several 'enclave trains' parallel to the foliation in the tonalite. The tonalite within and immediately around these 'trains' contain coarse porphyritic plagioclase crystals and have diffuse margins with the Monocola tonalite. The tonalite in between the enclave trains is intruded by basalt dikes, which have been sheared into boudins. These are subsequently crosscut by diorite dikes, which form boudins in the tonalite between the enclave trains, but occur as enclaves within the enclave trains and can be found as nearly undeformed dikes outside of the LRS, giving insight into the localization of deformation around the LRS at the time of their intrusion. Two sets of tonalite dikes at right angles with each other crosscut all of these phases, still showing syn-magmatic deformation within the enclave trains of the LRS. These phases are crosscut by two-phase leucogranite dikes that appear to cut the LRS at right angles (radiating pattern) and may still record some syn-magmatic deformation. Plagioclase phyric granodiorite dikes that are closely associated with the LRS, but do not show any evidence for syn-magmatic deformation finally crosscut all of these.

As such, results from this study show an intricate relation between the relative timing, deformation and appearance in and outside of the LRS of magmatic phases present. At the conference, we will present geological models that may explain the development and evolution of the Listino Ring structure.

REFERENCES

- Brack, P. 1984: *Geologie der Intrusiva und Nebengesteine des Südwest-Adamello (Nord-Italien)*. PhD-thesis; Diss. ETH Nr. 7612, 253 p., Zürich.
- Brack, P. 1985: Multiple intrusions - examples from the Adamello Batholith (Italy) and their significance on the mechanism of intrusion. *Memorie della Società Geologica Italiana* 26, 145-157.

5. Geomorphology

I. Gärtner-Roer, M. Bollschweiler, R. Delaloye, C. Graf, N. Kuhn, S. Morard

Swiss Geomorphological Society

TALKS

- 5.1 Ambrosi C., Castelletti C., Soma L.: Quaternary Geologic Map of Osogna (Ticino), sheet 1293
- 5.2 Bennett, G.L., Molnar, P., Eisenbeiss, H., McArdell, B.W.: Probabilistic modeling and analysis of rock-slope failure in the Illgraben, Switzerland, 1963 – 2005
- 5.3 Caviezel C., Kuhn N.J.: Mass wasting in the Ursern valley (Switzerland): climate or land use change?
- 5.4 Champagnac J.-D., Molnar P., Sue C., Herman F.: Tectonics, Climate, and Mountain Topography
- 5.5 Meusbürger K., Steel A., Panagos P., Montanarella L., Alewell C.: Spatial and temporal variability of rainfall erosivity factor for Switzerland
- 5.6 Savi S., Schneuwly-Bollschweiler M., Stoffel M., and Schlunegger F.: Coupling – decoupling hillslope – channel system processes: a case study from dendrogeomorphology.
- 5.7 Stoffel, M., Trappmann, D., Schneuwly-Bollschweiler, M.: When science meets practice: Dendrogeomorphic documentation of rockfall trajectory frequencies, bounce heights and energies along a road in Valais
- 5.8 Trauerstein M., Norton K. P., Schlunegger F., Preusser F.: Climatic imprint on landscape morphology in the western escarpment of the Andes

POSTERS

- P 5.1 Barboux C., Delaloye R., Strozzi T., Christophe L., Raetzo H., Collet C.: InSAR Terrasar-X visibility assessment of moving landform monitoring in alpine periglacial environment: 30 case studies in the Valais Alps (CH)
- P 5.2 Bekaddour, T., Norton, K.P., Schlunegger, F.: Dip direction controls of bedrock on channel morphologies and denudation rates in the eastern Swiss Alps
- P 5.3 Büchi, M., Kober, F.: Landscape Evolution of the Hörnli-region: Landforms, Processes and Rates
- P 5.4 Dürst Stucki M., Schlunegger F., Christener F.: Deepening of inner gorges through subglacial meltwater - an example from the UNESCO Entlebuch area, Switzerland
- P 5.5 Juretzko G., Meusbürger K., Alewell C.: Suitability of Cesium-137 and USLE for soil erosion assessment in an Alpine valley (Val Piora, Switzerland)
- P 5.6 Khaksar K., Farboodi M.: Land Subsidence And Fissuring Due To Groundwater Withdrawal In The Neyshaboor Plain-Northeast Iran
- P 5.7 Kuhn N.J. : Teaching with Tolkien: environmental analysis of a fantasy world
- P 5.8 Moore J.R., Gischig V., Katterbach M., Loew S.: Crack air convection and resulting temperature disturbances at depth in an alpine rock slope
- P 5.9 Sorg, A., Rösch, A., Bolch, T., Shatravin, V.I., Solomina, O.N., Schneuwly-Bollschweiler, M., Stoffel, M.: Reconstruction of rock glacier activity in Northern and Inner Tien Shan based on tree rings and aerial photographs
- P 5.10 Tisato N., Sauro F., Bernasconi S.M., Bruijn R., De Waele J.: Hypogenic contribution to speleogenesis in a predominant epigenic karst system: a case study from the Venetian Alps, Italy

5.1

Quaternary Geologic Map of Osogna (Ticino), sheet 1293

Ambrosi Christian, Castelletti Claudio, Soma Linda

SUPSI, Institute of Earth Sciences, Campus Trevano, CH 6952 Canobbio (claudio.castelletti@supsi.ch)

In January 2011 the Swiss Federal Office of Topography (swisstopo) tasked SUPSI with the creation of quaternary deposits for Osogna (1293 – Osogna sheet), part of the project “Geocover”.

The study area is situated in Ticino, between Biasca on north and Bellinzona to south.

To recognize and identify the forms and deposits has been used different techniques:

- Analysis of a digital elevation model, 2 meters (DEM)
- Analysis of digital aerial photos
- Photo-interpretation

The map was made using two types of programs: ArcGIS 9.3 which had already been used successfully for the production of map of 1373 - Mendrisio, and a new program, ArcGDS.

ArcGDS is an extension of ArcGIS for viewing stereoscopic images and for capturing, editing and updating in stereoscopy (fig.1). This software allows a three-dimensional vision of the area by facilitating the recognition of the limits and forms of deposits and landslides especially in high altitude (above 2000 meters), where the DEM 2 meters is not available, thereby obtaining a detailed and comprehensive coverage of all the territory.

In the final phase of the project the verification of the results has been made directly with observations on the field.

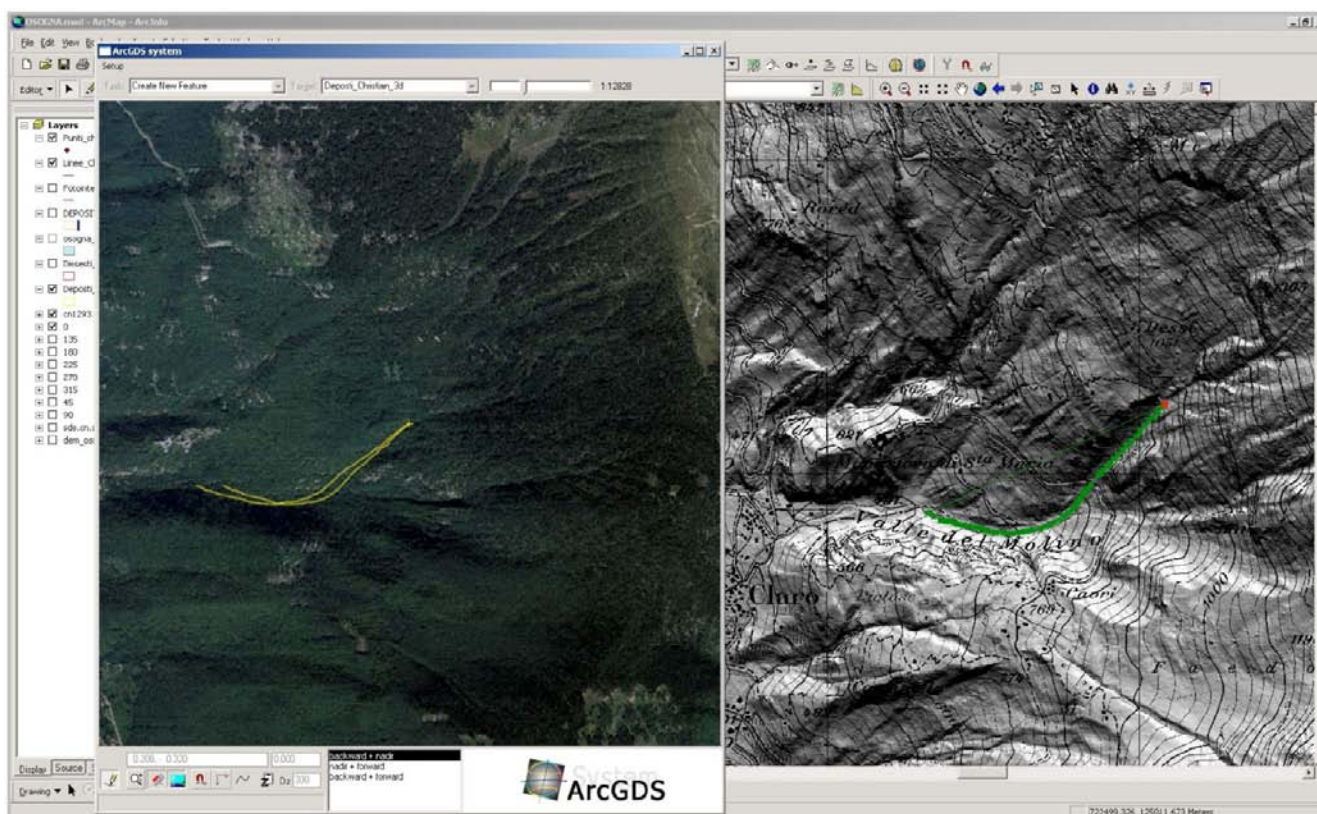


Figure 1: in the picture is visible the work page of ArcGDS (Geosoft), to the right the creation of a polygon in 3D, on the same time on the left its projection on a 2D DEM 2 meters (authorization of UMG, 08.01.08). Zone of Claro, 723770/124330

This method produces excellent and high quality results in a relatively short time, the resulting digitized maps are more homogeny and complete as the traditional. This method allows to recognize easier important structures, deposits and big landslides especially at high altitude.

5.2

Probabilistic modeling and analysis of rock-slope failure in the Illgraben, Switzerland, 1963 – 2005

Bennett, G.L.¹, Molnar, P.¹, Eisenbeiss, H.², McArdell, B.W.³

¹ Institute of Environmental Engineering, ETH Zurich, Wolfgang-Paulistrasse 15, CH-8093, Switzerland

² Institute of Geodesy and Photogrammetry, ETH Zurich, Wolfgang-Paulistrasse 15, CH-8093, Switzerland

³ Swiss Federal Research Institute WSL, Zürcherstrasse 111, CH-8903, Birmensdorf, Switzerland

Our understanding of slope failure is restricted by a lack of inventories of sufficient size and containing directly measured volumes. We used digital photogrammetry to produce a multi-temporal record of erosion of a rock-slope in the Illgraben catchment spanning 42 years. From this we extracted an inventory of ~2500 slope failures for 3 epochs of 6/7 years between 1986 and 2005 ranging over 6 orders of magnitude in volume. Through modeling the frequency-volume of these and analyzing relationships of volume-area, depth-area and depth-slope gradient we aimed to understand the characteristics of rock-slope failure at the head of this active alpine debris flow catchment.

The slope failures form a characteristic frequency-magnitude distribution with a roll-over at 50m³ and a power-law tail. We focused on modeling the exponent of this tail for the reason that it contains more than 90% of the total failure volume. We find that the accuracy of the exponent is compromised by fitting to the probability distribution and that it is advisable to estimate this using the complementary cumulative distribution function.

The low rock mass strength of the slope is indicated by the relatively small exponents in the frequency-volume and volume-area relationships as well as by the rapid rate of erosion. Our data suggest that the exceptionally rapid rate of erosion of ~350mm yr⁻¹ is achieved through two failure processes: (1) frequent small slumps and slides of restricted depth that occur across a range of slope gradients within the upper weathered layer of the slope; (2) rare larger and deeper fracture events that occur mainly on slopes greater than 45° along discontinuities within the slope.

Our study lends empirical support to the theoretical hypothesis that the characteristic probability distribution of landslides contains two separate processes: shallow slides in the top layer and deeper slides in the bottom layer.

5.3

Mass wasting in the Ursern valley (Switzerland): climate or land use change?

Chatrina Caviezel & Nikolaus J. Kuhn

Physical Geography, Environmental Sciences, University of Basel, Switzerland

Considerable changes in land use and management practices, as well as the increased frequency of extreme weather events in mountain regions, are considered to affect landscape susceptibility for mass wasting in the Alps. Analysing alp inspection reports, written each year by farmers commissioned to supervise pasture use and condition on the communal land in the Ursern Valley, Switzerland, a non-uniform distribution of mass wasting events between 1950 and 2000 was found. To investigate variations in mass wasting frequency, controlling parameters such as climate and grazing patterns and intensity were analysed using the regional archive. The results infer that land use changes and maintenance measures modified the effects of an increasing number of high magnitude rainfall events by changing landscape susceptibility to mass wasting and land degradation since 1950.

5.4

Tectonics, Climate, and Mountain Topography

Champagnac Jean-Daniel¹, Molnar Peter², Sue Christian³ & Herman Frédéric¹

¹Geological Institute / ESD, Swiss Federal Institute of Technology (ETHZ) Sonneggstrasse 5, CH-8092 Zürich, Switzerland. (jean-daniel.champagnac@erdw.ethz.ch)

²Department of Geological Sciences, Cooperative Institute for Research in Environmental Science (CIRES), Benson Earth Sciences Building, Campus Box 399, Room 462C, University of Colorado at Boulder, Boulder, Colorado 80309, USA.

³UMR 6249 Chrono-Environnement, Université de Franche-Comté, 16 route de Gray 25030 Besançon cedex, France

By regressing simple, independent variables that describe climate and tectonic processes against measures of topography and relief of 69 mountain ranges worldwide, we quantify the relative importance of these processes in shaping observed landscapes. Climate variables include latitude (as a surrogate for mean annual temperature and insolation, but most importantly for the likelihood of glaciation) and mean annual precipitation. To quantify tectonics we use shortening rates across each range. As a measure of topography, we use mean and maximum elevations and relief calculated over different length scales. We show that the combination of climate (negative correlation) and tectonics (positive correlation) explain substantial fractions (> 25%, but < 50%) of mean and maximum elevations of mountain ranges (Figure 1A and 1B), but that shortening rates account for smaller portions, <25%, of the variance in most measures of topography and relief (i.e. with low correlations and large scatter). Relief is insensitive to mean annual precipitation (Figure 1C and 1D), but does depend on latitude, especially for relief calculated over small (~1 km) length scales, which we infer to reflect the importance of glacial erosion (Figure 1C). Larger-scale (averaged over length scales of ~10 km) relief, however, correlates positively with tectonic shortening rate. Moreover, the ratio between small-scale and large-scale relief, as well as the relative relief (the relief normalized by the mean elevation of the region) varies most strongly with latitude (strong positive correlation) (Figure 1E and 1F). Therefore, the location of a mountain range on Earth and corresponding climatic conditions, not just tectonic forcing, appears to be a key factor in determining its shape and size. In any case, the combination of tectonics and climate, as quantified here, can account for approximately half of the variance in these measures of topography. The failure of present-day shortening rates to account for more than 25% of most measures of relief raises the question: Is active tectonics overrated in attempts to account for present-day relief and exhumation rates of high terrain?

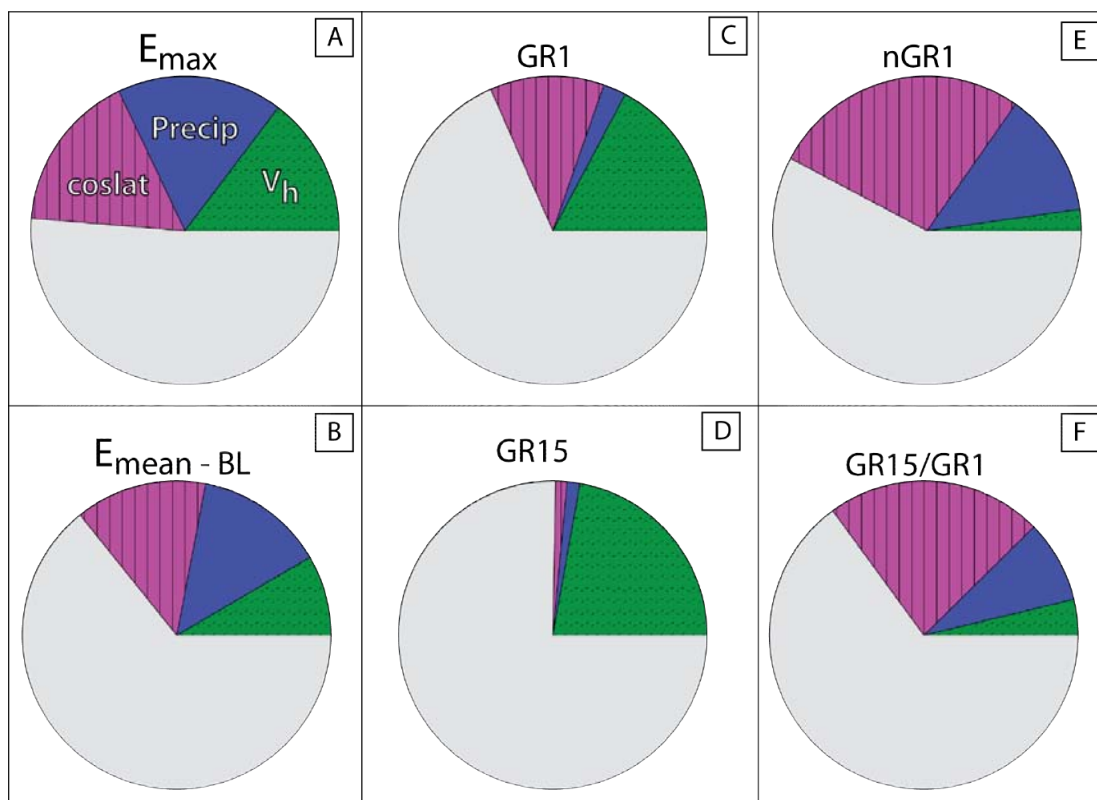


Figure 1: Pie charts of the relative contributions of each external variable – V_h (tectonic shortening rate), *precip* (mean annual precipitation), and *coslat* (cosine of the latitude)– to the observed variance of the topographic variables – E_{max} (maximum elevation of the topography average over a 10 km), $E_{mean-BL}$ (mean elevation of the range above the base level BL), $GR1$ and $GR15$ (mean geophysical relief over 1 and 15 km), $nGR1$ (relative relief, i.e. geophysical relief normalized by the mean elevation of each range), $GR15/GR1$ (Dimensionless ration between $GR15$ and $GR1$). The gray shading is the unexplained part of the variance that is due to unused variables and natural scatter.

5.5

Spatial and temporal variability of rainfall erosivity factor for Switzerland

Meusbürger K.¹, Steel A.², Panagos P.², Alewell C.¹, Montanarella L.²

¹ Institute for Environmental Geosciences, University of Basel, Bernoullistrasse 30, CH-4056 Basel, Switzerland,
Email: Katrin.Meusbuerger@unibas.ch, Tel.: +41-61-2673631, Fax: +41-61-2670479

² Joint Research Centre of the European Commission, Institute for Environment and Sustainability, E. Fermi 2749, IT-21027, Ispra (VA), Italy.

Rainfall erosivity, considering rainfall amount and intensity, is an important parameter for soil erosion risk assessment under future land use and climate change. Despite its importance, rainfall erosivity is usually implemented in models with a low spatial and temporal resolution. The purpose of this study is to assess the temporal- and spatial distribution of rainfall erosivity (R-factor) in Switzerland. Time series of 22 years for rainfall (10min resolution) and temperature (1h resolution) data were used to calculate rainfall erosivity as defined by Renard et al. (1997) for 71 automatic gauging stations distributed throughout Switzerland. Multiple regression was used to interpolate the erosivity values of single stations and to generate a map for Switzerland. Latitude, longitude, average annual precipitation, biogeographic units (Jura, Midland, etc.), aspect and elevation were used as covariates, of which average annual precipitation, elevation and the biogeographic unit (Western Central Alps) were significant predictors. The mean value of long-term rainfall erosivity is 1323 MJ mm ha⁻¹ h⁻¹ y⁻¹ with a range of lowest values of 124 MJ mm ha⁻¹ h⁻¹ y⁻¹ at an elevated station in Grisons to highest values of 5611 MJ mm ha⁻¹ h⁻¹ y⁻¹ in Ticino. All stations have highest erosivity values from July to August and lowest values in the winter month. Swiss-wide the months May to October show significantly increasing trends of erosivity (p<0.005). Only in February a significantly decreasing trend of rainfall erosivity is found (p<0.01). The increasing trends of erosivity in May, September and October when vegetation cover is susceptible are likely to enhance soil erosion risk for certain agricultural crops and alpine grasslands in Switzerland.

REFERENCE

Renard, K. G., Foster, G. R., and Weesies, G. A.: Predicting soil erosion by water; a guide to conservation planning with the revised universal soil loss equation (RUSLE), Agriculture Handbook No. 703, USDA-ARS, 404 pp., 1997.

5.6

Coupling – decoupling hillslope – channel system processes: a case study from dendrogeomorphology.

Savi Sara, Schneuwly-Bollschweiler Michelle, Stoffel Markus, and Schlunegger Fritz

Institute of Geological Sciences, Baltzerstrasse 1-3, CH-3012 Bern, (sara.savi@geo.unibe.ch)

We quantify the frequency distribution of debris flow events in the ca. 2.5 km²-large Schimbrig catchment that is located in the central Swiss Alps. We assess this distribution using patterns of tree-ring records that register growth perturbations caused by external forcing such as landsliding and debris flows. In particular, tree-ring analyses are used for the dating and understanding the modality of sediment transfer and for the assessment of connectivity between sediment sources and sinks.

The study catchment can be divided into two distinct tributaries: the eastern area, occupied by an active earth slide (Schimbrig landslide) that underwent high slip rates several centimetres to meters per day between September 1994 and May 1995, translating a total of 350,000 m³ of material; and the western segment, characterized by a deeply incised network of mixed debris flow and alluvial channels (50 m maximum incision) bordered by hillslopes that host shallow and deep-seated landslides less than 15,000 m² large. The entire catchment is mainly underlain by sandstone-mudstone alternations of the Eocene Subalpine Flysch that have been reworked by glaciers during the LGM. The unconsolidated sediments left by ice retreat are one of the main sediment sources causing instability in this region. The climate in the Schimbrig area is dominated by a very high precipitation rate.

Intense rainfall events may trigger landslides and debris flows from the steepest slopes of the channel network. Therefore we focused our study to this area of the catchment with the aim to understand the connectivity between hillslopes and channels using dendrogeomorphic techniques. We collected a total of 500 tree cores on the fan, along the main channel and in the catchment area. On the fan the analyzed trees allow the reconstruction of 16 debris-flow events occurred between AD 1857 and 2010. The most relevant event, affecting more than one-fourth of the trees on the entire fan, occurred in 1994-1995 and seems to be related to the highest activity of the Schimbrig landslide. Other important events, involving between 15 and 20% of the trees, occurred in 1997, 1967, 1964, 1957; 1951, 1881 and 1857-60. In the upper part of the catchment trees show a total of 52 events between AD 1905 and 2010 which were divided into different sectors depending on the trees' location. These events might represent several re-activation periods, as these areas are strongly affected by lateral landslides that showed different stages of movement. Particularly, periods with high activity are registered between the 1950s and 1960s, and at the end of the 1980s when growth disturbances have been registered in trees in all sectors. From the results describe above we can highlight some features of the Schimbrig catchment. The entire area is strongly affected by high instability that results in a large earth slide in the eastern tributary (Schimbrig landslide) and in a very instable channel network in the western area where several slides influence the stability of the channels' bordering slopes. The main processes affecting the upper part of the channel network seem to be related to slow slide or earth flows that continuously provide material into the channel bed so that the system might be classified as transport-limited. As the process is slow it cannot be related with single heavy rainstorm events but rather with long rainfall periods or snow melting that make infiltration and amount of soil water more important for sliding processes. From the analysis of the trees the decoupling between hillslope and channels processes becomes obvious with a mechanism of material supply from the hillslopes to the channels followed by some residence time of the sediment in the channel. Only with enough stream power (i.e. during heavy rainstorms) the river is capable to carry the material from the source areas to the depositional fan. Therefore, the timescale assessed by dendrogeomorphology allow establishment of a de-coupled system between hillslopes and channel network in the Schimbrig catchment.

5.7

When science meets practice: Dendrogeomorphic documentation of rockfall trajectory frequencies, bounce heights and energies along a road in Valais

M. Stoffel^{1,2}, D. Trappmann¹, M. Schneuwly-Bollschweiler^{1,2}

¹ *Laboratory of Dendrogeomorphology (dendrolab.ch), Institute of Geological Sciences, University of Berne, Baltzerstrasse 1+3, CH-3012 Berne, Switzerland*

² *Climatic Change and Climate Impacts, Institute for Environmental Sciences, University of Geneva, 7 Route de Drize, CH-1227 Carouge, Switzerland*

Rockfall is one of the most widespread geomorphic processes in mountainous regions, where its continuous occurrence regularly forms accumulations of rock fragments at the base of talus slopes. Sporadically, single rocks and boulders impinge on inhabited areas or transportation corridors, where they may destroy buildings or even cause fatalities. Nevertheless, data on past activity and on spatial patterns (spread and reach) of rockfalls is often sparse. The scarcity of inventory data is particularly a problem when hazards and/or risks need to be assessed or mitigation measures planned. The main road linking Stalden to Saas Fee (Valais, Swiss Alps) is particularly prone to rockfalls and cars have been affected several times in the recent past. For the purpose of rockfall net installations, their number, dimensioning (height, energy) and positioning within the slope, the Laboratory of Dendrogeomorphology was mandated by the cantonal authorities and local communities to study trajectory frequencies, bounce heights, energies and return periods of events on the slope and at the level of the main road. Work has been performed at three different segments of the road (Raaftearte, Falllowina, Huteggen–Bodenbrücke) with roughly 500 trees to document almost 2000 rockfalls of the past few decades. Results clearly show the added value of tree-ring reconstructions for the assessment of hazards and risks, as for instance at Raaftearte where we could document that almost one rock is passing the road per running meter and year. At Huteggen–Bodenbrücke, on the other hand, the frequency of rockfalls was smaller but the energies involved in frequent events trespassed several 1000 kJ which was much more than expected. As a consequence, we believe that these findings may help clearly authorities in prioritizing sectors and in dimensioning protective measures and lead to more realistic estimates of risks (and therefore much better cost–benefit estimates).

5.8

Climatic imprint on landscape morphology in the western escarpment of the Andes

Trauerstein Mareike¹, Norton Kevin P.², Schlunegger Fritz¹, Preusser Frank³

¹*Institute of Geological Sciences, University of Bern, Baltzerstrasse 1-3, CH-3012 Bern (trauerstein@geo.unibe.ch)*

²*School of Geography, Environment and Earth Sciences, PO Box 600, NZ-6140 Wellington*

³*Department of Physical Geography and Quaternary Geology, S-10691 Stockholm*

The western continental margin of northern South America is characterized by the active subduction of the Farallón-Nazca oceanic plate beneath the South American continental plate. Collision and arc magmatism started in the Early Jurassic followed by several phases of shortening and thrusting. The last phase (10-7 Ma) resulted in the formation of a steep ramp with a distinct escarpment edge (Victor et al. 2004, Farías et al. 2005). Upstream of this ramp on the Meseta/Altiplano (>3000 m a.s.l.), streams have remained graded to the Late Miocene base level broadly correlative with a series of Tertiary volcanic-volcaniclastic rocks that form a resistant cap rock lithology (Abbühl et al. 2011). Below the ramp, streams have incised more than 1000 m into Mesozoic plutonic and metasedimentary rocks along a series of steep, headward retreating knickzones that grade to the present-day base level defined by the Pacific Ocean (Schlunegger et al. 2006, Schildgen et al. 2007). The precipitation pattern is characterized by a strong negative north-south gradient, related to the positions of the Andean jet and the Intertropical Convergence Zone (Garreaud et al. 2003). Here, we present the results of a morphometric analysis of 36 watersheds, each separated in segments below and above the escarpment edge, in an effort to detect possible imprints of tectonics, lithology and climate on landscape metrics.

Our analysis shows no distinct relationships between rock type and landscape metrics, not only on the Meseta, but also within the incised zone. This suggests that lithology has little impact on the large-scale landscape form. Average local relief values, however, show a distinct correlation with precipitation rates, but only for the segments below the escarpment edge. Whereas previous work (e.g. from Rehak et al. 2010) found negative correlations between local relief and precipitation rates for landscapes where the drainage network is fully established, we find the opposite relationships for our study area, where the erosional response to the Late Miocene uplift pulse has not yet propagated through the entire drainage network. Additionally, the upstream distance of knickzone retreat correlates positively with the model discharge of the stream. Finally, also below the escarpment edge, we find negative relationships between the relative proportion of non-dissected palaeosurfaces and both mean annual precipitation rates and local relief, albeit with a poor correlation.

We conclude that in transient landscapes, local relief increases with increasing precipitation through a positive feedback response to fluvial incision, but that relief decays with increasing precipitation rates in landscapes where erosion has obliterated transient features related to an uplift pulse.

REFERENCES

- Abbühl, L.M., Norton, K.P., Jansen, J., Schlunegger, F., Aldahan, A. & Possnert, G. 2011: Erosion rates and mechanisms of knickzone retreat inferred from ¹⁰Be measured across strong climate gradients on the northern and central Andes Western Escarpment, *Earth Surf. Process. Landforms*, 36, 1464–1473.
- Farías, M., Charrier, F., Comte, D., Martinod, J., Hérail, G. 2005: Late Cenozoic deformation and uplift of the western flank of the Altiplano: evidence from the depositional, tectonic, and geomorphic evolution and shallow seismic activity (northern Chile at 19° 30'S), *Tectonics*, 24, TC4001.
- Garreaud, R., Vuille, M. & Clement, A.C. 2003: The climate of the Altiplano: observed current conditions and mechanisms of past changes, *Palaeogeography, Palaeoclimatology, Palaeoecology*, 194, 5–22.
- Rehak, K., Bookhagen, B., Strecker, M.R. & Echtler, H.P. 2010: The topographic imprint of a transient climate episode: the western Andean flank between 15.5° and 41.5°S, *Earth Surf. Process. Landforms*, 35, 1516–1534.
- Schildgen, T.F., Hodges, K.V., Whipple, K.X., Reiners, P.W. & Pringle, M.S. 2007: Uplift of the western margin of the Andean plateau revealed from canyon incision history, southern Peru, *Geology*, 35(6), 523–526.
- Schlunegger, F., Zeilinger, G., Kounov, A., Kober, F. & Hüsner, B. 2006: Scale of relief growth in the forearc of the Andes of Northern Chile (Arica latitude, 18°S), *Terra Nova*, 18(3), 217–223.
- Victor, P., Oncken, O. & Glodny, J. 2004: Uplift of the western Altiplano plateau: Evidence from the Precordillera between 20° and 21°S (northern Chile), *Tectonics*, 23, TC4004.

P 5.1

InSAR Terrasar-X visibility assessment of moving landform monitoring in alpine periglacial environment: 30 case studies in the Valais Alps (CH)

Barboux Chloé¹, Delaloye Reynald¹, Strozzi Tazio², Christophe Lambiel³, Raetzo Hugo⁴ & Collet Claude¹

¹ Department of Geosciences, Geography Unit, University of Fribourg, Ch. Du Musée 4, CH-1700 Fribourg, Switzerland (firstname.name@unifr.ch)

² Gamma Remote Sensing, Worbstr. 225, CH-3073 Gümligen, Switzerland, strozzi@gamma-rs.ch

³ Geography unit, Quartier UNIL-Dorigny, Bâtiment Anthropole 4056, CH-1015 Lausanne, Switzerland, christophe.lambiel@unil.ch

⁴ Federal Office for the Environment, CH-3003 Bern, Switzerland, hugo.raetzo@bafu.admin.ch

The topography of the Western Swiss Alps (Valais Alps) consists mainly of north-south oriented valleys and has proved to be an optimal situation for an application of the InSAR technique. However, inventories of active moving landforms (e.g. rock glaciers, landslides) located in mountain periglacial environment show that the objects of interest are sometimes located in areas polluted by irreversible geometric distortions in InSAR images and are moving more quickly than the maximal capabilities of InSAR technology (Delaloye et al. 2006, 2008, 2010).

The study aims to precisely determine the InSAR capability for monitoring the activity of alpine periglacial landforms based on test study sites located in Valais Alps. Geometrical distortions existing on invisible areas (shadows) and reverse imaged areas (layover) are already well explained in literature (Massonet & Feigl 1998) and the InSAR visibility is usually computed by a simple binary mask hiding them. In this study, the quality of observation of InSAR is evaluated taking into account the location and velocity of the landforms as well as the acquisition parameters of InSAR; here InSAR Terrasar-X (TSX) with high resolution X-band interferograms and 11 days time interval. Thus, under the hypothesis that the landform flow is directed toward the highest slope direction at 25m scale resolution, an index of visibility characterizing the velocity compression for each landform is computed. Then, the maximal observable deformation rate of each landform can be easily calculated. Comparisons and validations were performed by combining InSAR observations and differential GPS measurements on 30 active landforms.

According to this study, it is possible to monitor some very active rockglaciers ($1-2.5m.y^{-1}$) when geometrical distortions do not hide them with the shortest repeat pass of 11 days. Lower velocity rates could be well monitored using longer time lags. At higher rate velocities, decorrelation occurs in most of the cases and TSX appears to be unsuitable for a precise analysis of these kinds of surging landforms. Moreover, the high resolution of TSX looks suitable to monitor slope instabilities with narrow width (until 50 meters width). Thus, by combining it with field measurements needed in most of the cases to validate and confirm observations at local scale, TSX InSAR has a strong potential for moving landform survey of the alpine periglacial belt.

REFERENCES

- Delaloye R., Lambiel C., Lugon R., Raetzo H., Strozzi T. 2006: ERS InSAR for detecting slope movement in a periglacial mountain environment (western Valais Alps, Switzerland). High Mountain Remote Sensing and Cartography IX, Graz, 14-15 Sept. 2006
- Delaloye R., Strozzi T., Lambiel C., Perruchoud E., Raetzo H. 2008: Landslide-like development of rockglaciers detected with ERS1-2 SAR interferometry. Proceedings of FRINGE 2007 Workshop, Frascati, Italy, 26 – 30 November 2007 (ESA SP-649, February 2008)
- Delaloye R., Strozzi T., Lambiel C., Barboux C., Mari S., Stocker A., Techel F., Raetzo H. 2010 : The contribution of InSAR Data to the early detection of potentially hazardous active rock glaciers in mountain areas. Proceedings ESA Living Planet Symposium, Bergen, Norway, June28 – July2, 2010 (ESA SP-686, December 2010)
- Massonet D., Feigl K.L. 1998: Radar interferometry and its application to changes in the earth's surface. Reviews of Geophysics, 36, 4 / November 1998, pages 441–500

P 5.2

Dip direction controls of bedrock on channel morphologies and denudation rates in the eastern Swiss Alps

Bekaddour, T., Norton, K.P., Schlunegger, F.

Earth Surface Processes, Bern University, Baltzerstrasse, 1+3, CH-3012 Bern (toufik.bekaddour@geo.unibe.ch)

The bedding orientation of bedrock exerts a prime control on the nature and the rates of sediment transfer on mountainous landscapes. Here, we address one particular situation, in which the dip angle of the bedrock is subparallel to the topographic slope (termed dip-slope). Such an arrangement results in the potential for large-scale deep-seated landsliding with bedding or jointing acting as glide planes. Hillslopes with the opposite situation (non-dip slope) have no such preconditioning, and will denude through standard mechanisms. The Val Lumnezia, Eastern Swiss Alps (Graubünden) contains both dip-slope and non-dip slope valley flanks. The topographic slope of the western valley flank parallels Mesozoic metasediments (dip slope situation) whereas the Bündner schists on the opposite valley dip perpendicular to the topographic slope (non-dip slope situation). The dip slope case is transport limited, with deep-seated landslides of up to tens of km² large transferring material towards the trunk stream. The opposing, non-dip slope, valley side is dissected by <150 m deep, supply-limited, bedrock channels.

Quantifying these effects is however difficult as surface sediment transfer rates in the dip-slope case may not reflect the depth integrated sliding rate. Likewise, in non-dip slope catchments, failure events tend to be episodic. We approach this problem with multiple methods, complementing geodetic surveys with morphometric analysis and ¹⁰Be derived hillslope and channel denudation rates. In particular, we analyse the relationship between upstream size of drainage basins A and channel gradients S . In case where channels are graded and actively shaping the landscape, then channels gradients S are directly related to the size to the contributing area A following Flint's (1974) law:

$$S = k_s A^{-q} \quad (1)$$

where k_s and q denote the channels steepness and concavity, respectively. The type, magnitude, and relative contributions of hillslope and channel processes can result in deviations from this relationship, which are readily identified by changes in the concavity and steepness values. Accordingly, we calculated these parameters from tributary streams on dip slope and non-dip slope valley sides. Tributary channels on dip-slope valley side are characterized by low concavity values ranging from 0.1 to 0.2, and equally display low steepness indices of approximately 100 m^{0.9}. Streams on the non-dip slope valley side have substantially higher concavity values between 0.3 and 0.8 and higher steepness indices, reaching maximum values of ca. 200 m^{0.9}. Surface slip rates derived from geodetic data exceed 10 cm/yr on the dip-slope valley flank, but are below detection limits (~1 m horizontal shift) on non-dip slope hillsides (Schwab et al., 2009).

The high steepness and concavity values of streams on non-dip slope valley sides support the interpretation of rapid dissection of the channel network into landscape where low hillslope slip rates allow the channel network to stabilize and actively shape the landscape.

This is in contrast to the dip-slope valley side, where low steepness and concavity values suggest that the channel network is continually destabilized by rapid deep-seated landsliding. ¹⁰Be-derived denudation rates are expected to yield similar distinct relationships between landsliding, fluvial dissection and overall sediment yield.

REFERENCES:

- Flint, J. J. 1974. Stream gradient as a function of order, magnitude, and discharge. *Water Resour. Res.* 10:969– 973.
 Schwab, M., Schlunegger, F., Schneider, H., Stöckli, G., Rieke-Zapp, D., 2009. Contrasting sediment flux in Val Lumnezia (Graubünden, eastern Swiss Alps), and implications for landscape development. *Swiss J. Geosci.* 2: 211-222.

P 5.3

Landscape Evolution of the Hörnli-region: Landforms, Processes and Rates

Büchi Marius¹, Kober Florian¹

¹*Earth Surface Dynamics Group, ETH Zürich*

The Hörnli-region in NE Switzerland contrasts the surrounding lowlands by its high local relief and rugged landscape. This dichotomy can be mainly attributed to the nunatak position of the area during the Last Glacial Maximum, LGM.

30 catchments have been studied in this area combining field investigations, GIS-based landscape analysis of a high resolution DEM and catchment-wide denudation (CWD) rates based on terrestrial cosmogenic ¹⁰Be concentration in fluvial quartz sand. The investigated catchments are classified based on their morphometrics and processes as either glacially overprinted or fluvially, mass wasting dominated catchments. The former presence or absence of a glaciation in the catchments is identified to exert the principal control of the Holocene landscape evolution.

Transience is suggested for large parts of the formerly glaciated Thur river tributaries. Gorge-like incision reaches cut into the Quaternary deposits and the Tertiary bedrock and the distinct knickpoints are interpreted as the adjustment to a base level lowering of the Thur drainage system during the late-Glacial and Holocene. The landscape disequilibrium found in the Thur drainage system and the expected increased geomorphodynamics are, however, not reflected in the CWD rates with values in the order of 30 mm/ky. These values rank among the lowest rates measured in the Swiss Northern Alpine foreland. In fact, there is no significant difference in CWD rates between glacially overprinted catchments with and without incision reaches.

The Töss river drainage system was, to a large degree, not glaciated during the LGM. However, the establishment of a major glacier marginal melt water drainage channel with a strong melt water and debris discharge caused rapid bedrock incision during the late-Glacial. The base level in the melt water channel rose after its truncation from the glacier melt water supply. Today, the tributaries are partly still adjusting to the base level lowering initiated during the melt water phase. The TCN-derived CWD rates in the not formerly glaciated and fluvially, mass wasting dominated catchments are found to be in the order of 300 mm/ky. These values are in good agreement with comparable studies from the Swiss Northern Alpine foreland (e.g. Wittmann et al., 2007; Norton et al., 2008).

The comparison of catchment-wide and near-channel slope distributions was used to investigate hillslope-channel coupling. In catchments where slope distributions are mostly congruent when considering either the near-channel or the entire catchment a close hillslope-channel coupling was observed. These catchments were also found to be positively correlated with mean basin slope and drainage density. Where mixed surface processes (glacially overprinted surfaces, fluvially incised gorges) were observed the slope distributions are incongruent and indicate channels decoupled from hillslopes.

REFERENCES

- Norton, K. P., von Blanckenburg, F., Schlunegger, F., Schwab, M., Kubik, P. W. 2008: Cosmogenic nuclide-based investigation of spatial erosion and hillslope channel coupling in the transient foreland of the Swiss Alps. *Geomorphology*, 95, 3-4, 474-486.
- Wittmann, H., von Blanckenburg, F., Kruesmann, T., Norton, K. P., Kubik, P. W. 2007: Relation between rock uplift and denudation from cosmogenic nuclides in river sediment in the Central Alps of Switzerland. *Journal of Geophysical Research*, 112, F04010.

P 5.4

Deepening of inner gorges through subglacial meltwater - an example from the UNESCO Entlebuch area, Switzerland

Dürst Stucki M., Schlunegger F., Christener F.

Institute of Geological Sciences, University of Bern, Baltzersstrasse 1-3, CH-3012 Bern, (mirjam.duerst@geo.unibe.ch)

This paper explores the mechanisms by which inner gorges in the Alps were formed. It focuses on the ca. 1.5 km-long, 80 m-deep and a few hundreds of meters-wide *Lammschlucht* located at the northern foothills of the central Alps. We restored the glacial cover using lateral moraines and hanging talus cones that record the elevation of the ice surface at the deglaciation stage of the LGM. We use the restored ice thickness patterns to calculate the erosional potential of the subglacial meltwater. The applied model is based on the principle of energy conservation, and yields the pattern of downstream changes of the dynamic pressure, which is considered a measure for the erosional potential. The model results suggest a maximum of the dynamic pressure at the end of the inner gorge. We interpret, therefore, that the subglacial meltwater scoured the reach towards the end of the *Lammschlucht* due to the enhanced dynamic pressure, which was ultimately controlled by the ice overburden. Post glacial fluvial erosion then resulted in a readjustment through regressive shift of erosional front along the inner gorge farther upstream. The current location of this front lies almost in the middle of the *Lammschlucht* inner gorge where a step-pool channel changes into a straight plane bed channel flowing on a deeply scoured bedrock.

P 5.5

Suitability of Cesium-137 and USLE for soil erosion assessment in an Alpine valley (Val Piora, Switzerland)

Juretzko Gregor¹, Meusburger Katrin¹ & Alewell Christine¹

¹Institut für Umweltgeowissenschaften, University of Basel, Bernoullistrasse 30, CH-4056 Basel (Gregor.Juretzko@stud.unibas.ch)

Soil erosion constitutes an increasing global issue. Because of its special topographic situation, the Alps are a very complex and sensitive area and can be considered an early warning system for global climate change. However, the processes and recent trends of soil erosion are not well understood yet and tools and models for erosion assessment urgently need validation.

The aim of this study was to evaluate the suitability of the Cesium-137 (Cs-137) tracer technique and the Universal Soil Loss Equation (USLE) for soil erosion quantification in the Alpine Piora Valley. The valley (22.6 km²) is located in the Southern Alps and the elevation ranges from 1850 to 2773 m a.s.l.

Soil erosion rates can be determined with the Cs-137 tracer method by comparing Cs-137 inventories (kBq m⁻²) of investigated sites with those of reference sites not affected by erosion or sedimentation since the initial fallout of Cs-137. Sites with lower Cs-137 inventories as the reference inventory are defined as net erosion sites, whereby those with higher Cs-137 inventories are considered as net accumulation sites. Cs-137 inventories were measured at 10 evenly distributed transect sites (n = 60). The USLE estimates are based on measured physical soil properties and a digital elevation model (25 m grid). A prerequisite for the Cs-137 method is to establish the reference inventory. Several reference sites (n = 10) showed considerable Cs-137 variability. To evaluate this heterogeneity, additional 51 in situ measurements (in a regular grid with an edge length of 10 m) were implemented on a small plot (0.4 ha). Further, it could be shown that sites located in the western part of the valley had significantly higher Cs-137 inventories, which is assigned to higher precipitation rates and thus larger deposition of Cs-137 after the Chernobyl disaster. Complex patterns in snowfall, snow coverage and snow gliding in the days after the reactor accident might also have contributed to the heterogeneous deposition patterns. The USLE estimates were not related to the observed pattern of Cs-137 inventories. The potential and limitations of the two methods for Alpine areas and their relation to other soil erosion risk factors will be discussed in this contribution.

Small scale heterogeneity has been found, which is attributed to complex erosion dynamics and processes during Cs-137 deposition. Winter processes, particularly snow gliding, may be an important factor triggering erosion (Konz et al. 2009). Lowest Cs-137 inventories were observed at sites with considerable dwarf shrub coverage. Freezing and snow gliding processes are expected to interact with the dwarf shrubs, destabilising the slopes.

Most of the other factors like slope or soil organic carbon content were not correlated with Cs-137 inventories. Those factors could have been superimposed by other ones. Fractional vegetation cover is negatively correlated with Cs-137 inventories, assumed to be an indicator for accumulation processes.

Complex processes associated with alpine environments seem to constrain the applicability of the Cs-137 tracer method and the USLE.

REFERENCES

Konz, N., Schaub M., Prasuhn V., Baenninger D., & Alewell C. 2009: Cesium-137-based erosion-rate determination of a steep mountainous region. *Journal of Plant Nutrition and Soil Science* 172, 615–622.

P 5.6

LAND SUBSIDANCE AND FISSURING DUE TO GROUNDWATER WITHDRAWAL IN THE NEYSHABOOR PLAIN-NORTHEAST IRAN

Kaveh Khaksar¹, Manoocher Farboodi²

¹Department of Civil Engineering, Rudehen branch, Islamic Azad University, Rudehen City, Iran, E-mail: k.khaksar@riau.ac.ir,
²Department of Soil Science, Islamic Azad University, Mianeh branch, Mianeh City, Iran, E-mail: farboodi@miau.ac.ir

The Neyshaboor plain with 4100 km² is situated in the Khorasan province in the northeast of Iran, in the latitude 35° 40' and 39° 34' N and Longitude 58° 17' and 59° 20' E situation (Fig. 1).

The topography of the study area varies from plain to mountainous and includes old to young geological formations. The extrem altitude of Neyshaboor plain is 3200 meter and the mean altitude of plain is 1900 meter.

Studied area is located in Neyshaboor plain in north of Khorasan province, Northeast of Iran. The Neyshaboor plain is one of the most important plains of Khorasan province in agricultural products and crowded population. In recent years agricultural development along with the increasing population culminate in taking the groundwater resources and a lot of pressure on these resources. The subsidence in different parts of the plain due to decrease the level of the groundwater is observed. In this plain the soil has been subsided because of the withdrawal of the groundwater level, and there are also longitudinal fissures along the altitudes, the Neyshaboor catchment restrictor, due to enhance subsidence from the side-lines to the center of the plain.

According to the information which is obtained from 100 GPS installed devices, the rate of subsidence has been reported 5-15 cm per meter of the downfall of the groundwater level. After the groundwater withdrawal, soil has been compacted, reactivated of old faults and surface fissuring and has been considerable impact on human infrastructures. So in this and hard aquifer irrevocable climate condition we discern the flood and the steep of the plain has changed.

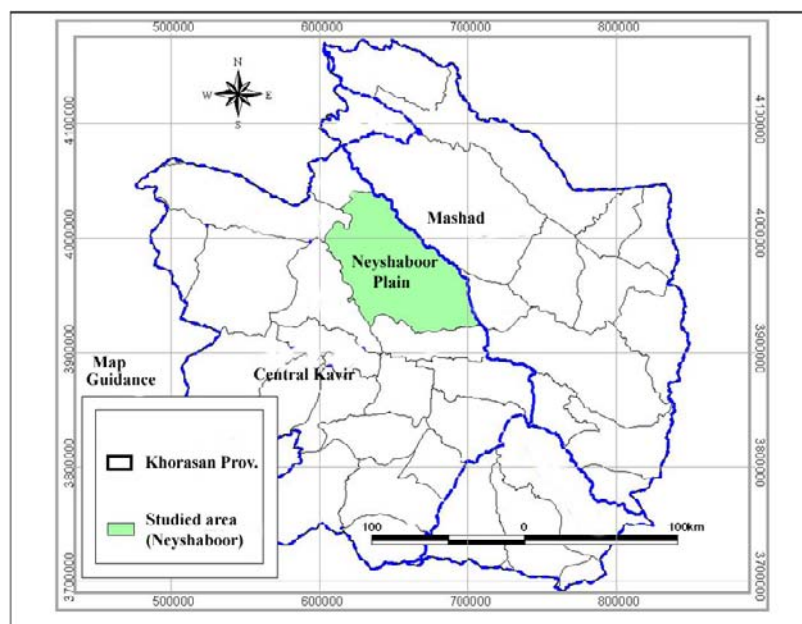


Figure. 1 Location of the study area.

Table 1. Statistics underground water resources during the year 2007 and 2010 (million cubic meters)

Total of annual Discharge	Total number of Water Sources	Fountain		Aqueduct		Well		Water resources
		Discharge	number	Discharge	number	Discharge	number	Year
791	2551	106/1	620	14/4	103	670/5	1828	2007
1175.4	4433	119/3	914	61/1	930	995	2589	2010

REFERENCE

- Belitz, K., Phillips, S.P., (1995). Alternatives to agricultural drains in California's San Joaquin Valley: Results of a regional-scale hydrogeologic approach, US Geological Survey Open-File Report 91-535, 71pp.
- Don, N. C., Hang, N. T. N., AraKi, H., Yamanishi, H., Koga, K. (2006). Groundwater resource and management for Paddy field irrigation and Associated environmental problems in an alluvial costal lowland plain, *Agricultural Water Management*, 84, 295-304.
- Hou, C. S., Hu, J. C., Shen, L. C., Wang, J. S., Chen, C. L., Lai, T. C. ,Huang, Yang, Y. R. ,Chen, R. F., Chen, Y. G., Angelier, J. (2005). Estimation of subsidence using GPS measurements and related hazard: the Pingtung Plain, southwestern Taiwan. *C. R. Geoscience* 337, 1184–1193
- Larson. K.J., Basagaoglu, H., Marino, M.A., (2001), Prediction of optimal safe ground water yield and land subsidence in the Los Banos–Kettleman City area, California, using a calibrated numerical simulation model, Vol. 242, pp. 79-102.
- Leake, S. A., 2004, URL: <http://geochange.er.usgs.gov/sw/changes/anthropogenic/subside>.

P 5.7

Teaching with Tolkien: environmental analysis of a fantasy world

Nikolaus J. Kuhn

University of Basel, Geography, Environmental Sciences, Basel, Switzerland (nikolaus.kuhn@unibas.ch)

In this study, the use of a fantasy world as a tool for teaching Geosciences especially in teacher training at the University of Basel is presented. J.R.R. Tolkien's *The Lord of the Rings* is one of the founding texts of fantasy literature and the centrepiece of a number of writings about the geography, history and mythology of „Middleearth“. The books have long become a cult phenomenon which has been transmitted to a new generation of followers by the massive success of the movie trilogy released between 2001 and 2003. The renewed interest in Tolkien's Middle-earth offers a unique opportunity to connect the Geosciences with literature studies and vice versa. Tolkien's Middle-earth is a distant and yet familiar enough world to allow for an analytical reflection of its geologic and ecologic coherence. The geographical analysis shows that the layout and description of Middle-earth roughly correlates with the paradigms of the Earth Systems Sciences. However, there are discrepancies between the spatial patterns of the various spheres which cannot be attributed just to artistic licence or ignorance, but point to significant issues connected with the moral and symbolic logic of Tolkien's work. For example, the absence of trees and woods in certain parts of "Middle-earth" where they would be expected in view of the description of climate throws into relief Tolkien's preservationist agenda. This setting, i.e. both the correlation between our world and Middle-earth, as well as the discrepancies, allow for a wide range of teaching activities. First and foremost, the geologic setting, both looking at Middle Earth as a self-contained world, but also a comparison of landmarks with their movie counterparts, offer pupils and students the opportunity to apply their knowledge of geosciences to a new world. For example, a typical question to be discussed is whether New Zealand volcanoes are of a similar type than those one would expect in Mordor. Further subjects for studies include methods, such as the reconstruction of environmental conditions from literature, but also GIS-based analysis of climate, vegetation, and land use. The lack of detailed information about the environment of Middle Earth offers students a new freedom to apply their knowledge and formulate a scientific hypothesis outside the pressure of delivering a correct answer. In our experience, this stimulates discussion and a vigorous exploration of the pupils' existing knowledge. Furthermore, a first case of breaking up the traditional barriers between humanities and natural sciences can be achieved by studying Middle-earth.

P 5.8

Crack air convection and resulting temperature disturbances at depth in an alpine rock slope

Moore Jeffrey¹, Gischig Valentin¹, Katterbach Maren¹, & Loew Simon¹

¹Department of Earth Sciences, ETH Zurich (jeffrey.moore@erdw.ethz.ch)

In this work, we analyze a unique set of temperature measurements from an alpine rock slope at ~2400 m a.s.l. in southern Switzerland. The monitored area encompasses part of an active slope instability above the village of Randa (VS) and is traversed by a network of open cracks, some which have been traced to >80 m depth. We first describe distributed temperature measurements and borehole profiles, highlighting deep steady temperatures and different transient effects. In a second step, we analyze the impact of air and water circulation in deep open fractures on the subsurface thermal field. On multiple visits to the study site in winter, we consistently noted the presence of warm air vents in the snowpack following the trace of deep tension cracks. Measurements showed that venting air changed temperature gradually from ~3 to 2 °C between December and May, which is similar to the rock temperature at around 50 m depth. Comparison with ambient air temperature suggests that winter conditions favor buoyancy-driven convective air flow in these fractures, which acts to cool the deep subsurface as rock gives up heat to incoming air. The impact of this process on the local thermal field is revealed by a disturbed temperature profile in one borehole and transient signals at depths well below the thermally active layer. Seasonal water infiltration during snowmelt appears to have little impact on the local temperature field.

P 5.9

Reconstruction of rock glacier activity in Northern and Inner Tien Shan based on tree rings and aerial photographs

A. Sorg^{1,2}, A. Rösch², T. Bolch³, V.I. Shatravin⁴, O.N. Solomina⁵, M. Schneuwly-Bollschweiler^{1,2}, M. Stoffel^{1,2}

¹ Climatic Change and Climate Impacts, Institute for Environmental Sciences, University of Geneva, 7 Route de Drize, CH-1227 Carouge, Switzerland

² Laboratory of Dendrogeomorphology (dendrolab.ch), Institute of Geological Sciences, University of Berne, Baltzerstrasse 1+3, CH-3012 Berne, Switzerland

³ Physical Geography Division, Department of Geography, University of Zurich, Winterthurerstr. 190, CH-8057 Zurich, Switzerland

⁴ Institute of Water Problems and Hydropower, National Academy of Sciences of the Kyrgyz Republic, Bishkek, Frunze str. 533, Kyrgyzstan

⁵ Department of Glaciology, Institute of Geography, Russian Academy of Sciences, Staromonetny 29, RU-119017 Moscow, Russia

Rock glaciers are a widespread geomorphic landform in continental Northern and Inner Tien Shan, where they expand from continuous permafrost regions above 3500 masl down to forested areas at 2700 masl. Rock glaciers generally respond to climate change with a larger time-lag than glaciers, which stresses their importance as fresh water resources in the future (e.g. for large cities like Almaty and Bishkek). Possibly a consequence of rising temperatures, Northern Tien Shan rock glaciers were found to have extraordinarily high downslope movements of >10 m yr⁻¹ (in the case of the Burkutty rock glacier). However, velocity rates vary strongly among the rock glaciers in this region and their complex behavior has not yet been fully understood. As long-term data from direct measurements is sparse, we analyzed tree rings and aerial photographs to reconstruct distinct periods of advance and to assess velocity rates for three rock glaciers in Northern and Inner Tien Shan. All juniper (*Juniperus sp.*) and Tien Shan spruce (*Picea shrenkiana*) trees growing in the immediate proximity to or even on the investigated rock glaciers were sampled. Responses such as the formation of reaction wood will be used as an indicator for periods of pronounced rock glacier advance. The results will then be complemented by velocity rates assessed from photogrammetric analysis of aerial photographs taken in the 1950s, 1960s, and 1980s as well as projected photographs taken in the early 2000s and 2011. The results will be checked for synchronous trends among the investigated rock glaciers and put into relation with historical climate data.

5.10

Hypogenic contribution to speleogenesis in a predominant epigenic karst system: a case study from the Venetian Alps, Italy

Nicola Tisato ^{*}, Francesco Sauro ², Stefano M. Bernasconi ^{*}, Rolf Bruijn ^{*} and Jo De Waele ²

¹ ETH Zurich, Geological Institute, Soneggstrasse 5, CH 8092 Zurich (nicola.tisato@erdw.ethz.ch)

² Istituto Italiano di Speleologia, Bologna University, Via Zamboni 67, I 40126 Bologna

Buso della Rana and Buso della Pisatela are two karstic caves located in the Venetian forealps (north-east Italy). They are part of the same karst system and are developed in the Castelgomberto calcarenitic marine sediment, which was deposited in a shallow Caribbean-type sea during the Eocene (Munier-Chalmas and De Lapparent, 1893). The Buso della Rana-Pisatela system developed mostly at the contact between the Castelgomberto calcarenite and underlying volcanic rocks. The system of caves is ~37 km long and has only three entrances, two of which are semi-artificial. The overlying karst plateau is not directly connected to the Buso della Rana-Pisatela system and, with the exception of one deep abyss, shows a rather scarcely developed karst. This is unexpected considering the presence of such a large and long cave at depth.

The genesis of the Buso della Rana-Pisatela system is considered to be epigenic (Allegranzi et al., 1960; Gleria and Zampieri, 1978). However, we present evidence that demonstrates how the genesis of this karstic system is strongly related to hypogenic mechanisms.

Gypsum ($\text{CaSO}_4 \cdot 2\text{H}_2\text{O}$) has locally been observed on the walls of the Buso della Pisatela cave. Energy dispersive X-ray spectroscopy (EDS), performed with a scanning electron microscope (SEM), reveals the presence of sulfur-bearing minerals within the host rock. Gypsum was formed by oxidation of these minerals as indicated by negative $\delta^{34}\text{S}$ values and Raman spectroscopy analyses. The oxidation of sulfide minerals forms a sulfuric-acid solution that dissolves the Castelgomberto calcarenite and, once it is oversaturated in calcium, precipitates as gypsum.

The lack of well-developed karst on top of the plateau and the analyses suggest that the formation mechanisms for the Buso della Rana-Pisatela system differ from classical epigenic speleogenesis. The “pyrite-effect” recognized in other caves is an example of hypo-speleogenetic process responsible for the dissolution of large portions of buried rocks in karst plateaus (e.g. Furman, 1993; Bottrell et al., 2001).

REFERENCES

- Allegranzi, A., Bartolomei, G., Broglio, A., Pasa, A., Rigobello, A., Ruffo, S., 1960: Il Buso della Rana (40 V-Vi). *Rassegna Speleologica Italiana* 12, 99-164.
- Bottrell, S.H., Crowley, S., Self, C., 2001: Invasion of a karst aquifer by hydrothermal fluids: evidence from stable isotopic compositions of cave mineralization. *Geofluids* 1, 103-121.
- Furman, F.C., 1993: Formation of East Tennessee, Knox MVT bodies by hypogenetic-interstratal-evaporite-TSR-sulfuric acid karstification. *Geology and Geochemistry of Mississippi Valley-Type Ore Deposits Proceedings Volume*, 133-148.
- Gleria, E., Zampieri, D., 1978: Contributo alla conoscenza del carsismo dell'altipiano Faedo-Casaron in relazione ai sistemi ipogei del rio Rana e del torrente Poscola. *Studi Trentini di Scienze Naturali* 55, 83-102.
- Munier-Chalmas, E., De Lapparent, J., 1893: Note sur la nomenclature des terrains sédimentaires. *Bulletin de la Société Géologique de France* III (21), 438-488.

6. Quaternary Research

Florian Kober, Susan Ivy-Ochs, Naki Akçar, Irka Hajdas

Swiss Society for Quaternary Sciences CH-Quat

TALKS

- 6.1 *Ariztegui D, Zvi Ben Avraham, Agnon A., Brauer A., Goldstein S., Haug G., Ito E., Stein M., Yasuda Y., Lazar M., Waldmann N. & the DSDDP Scientific Team: Filling gaps on the shrinking/swelling tale of the Dead Sea through continental drilling*
- 6.2 *Fleitmann D., Badertscher, S., Cheng, H., Edwards, R.L., Leuenberger, M., Zumbühl, A., Tüysüz, O.: Stalagmite evidence for a highly dynamic Pleistocene hydrological history of the Black Sea*
- 6.3 *Gierga M., Smittenberg R.H., Bernasconi S.M., Hajdas I. & Wacker L.: The chronology of Lake Soppensee (Switzerland) using a biomarker and a compound-specific isotope approach*
- 6.4 *Häuselmann A., Schmassmann S., Cheng H., Edwards L.R., Jeannin P.-Y., Häuselmann P., Fischer M., Fleitmann D.: Nature and Timing of Terminations I and II recorded in stalagmites from Switzerland*
- 6.5 *Heer A., Veit H., Bateman M.D., Adamiec G., Hajdas I., May J.H.: New findings concerning quartz properties important for luminescence dating of sediments in the Swiss NW Alpine foreland.*
- 6.6 *Hidalgo Staub R., Krüger Y., Marti D., Frenz M., Fleitmann D.: Fluid inclusions in stalagmites used as a quantitative thermometer in paleoclimate research*
- 6.7 *Kind J., Hirt A.M., Gehring A.U.: Evolution of the magnetic inventory in a lacustrine system since the late Pleistocene*
- 6.8 *Kwiecien O., Randlett M-E., Stockhecke M., Tomonaga Y., Unwin K. and the PALEOVAN scientific team: Paleoenvironmental changes in eastern Anatolia over the last 500 ka – first insights from the Swiss side of the ICDP Lake Van Drilling Project*
- 6.9 *Longchamp C., Derron M.-H., Jaboyedoff M.: Preliminary observations of small scale experiments for the characterization of large rock avalanches*
- 6.10 *Moernaut J., Van Daele M., Heirman K., Vandoorne W., Pino M., Urrutia R., De Batist M.: The recurrence pattern of megathrust earthquakes in South-Central Chile: semi-quantitative paleoseismology using lake sediments*
- 6.11 *Plotzki A., May J.-H., Preusser F., Roesti B., Veit, H.: Late Pleistocene to early Holocene fluvial dynamics in the southeastern Llanos de Moxos, Bolivian Amazon*
- 6.12 *Reber R., Akçar N., Zahno C., Lüthold A, Tikhomirov D., Ivy-Ochs S, Kubik P.W., Schlüchter C.: Exposure ages from erratic boulders on the northwestern flank of Rigi (Switzerland)*
- 6.13 *Scheidegger Y., Vogel N., Fleitmann D., Brennwald M.S., Figura S., Wieler R., Kipfer R.: Water concentrations in stalagmites as a potential new paleoclimate proxy – first results from two Holocene stalagmites from Socotra Island (Yemen)*
- 6.14 *Schweizer M., Darling K., Austin W.E.N.: Phylogeographic and morphological study of North East Atlantic benthic foraminifers*
- 6.15 *Tikhomirov D., Akçar N., Özkaymak Ç., Alfimov V., Ivy-Ochs S., Sözbilir H., Uzel B., Schlüchter C.: Reconstruction of seismic events using cosmogenic ³⁶Cl: An example from the western Anatolian Province of Turkey*

POSTERS

- P 6.1 *Brönnimann D., Ismail-Meyer K., Wild D., Ohnsorg P., Rentzel Ph.*: Oncoids, charales, and homogeneous silt: reconstruction of lake level and environment in the city of Zurich (Switzerland) between the Iron Age and Late Antiquity
- P 6.2 *Corella J. P., Anselmetti F. S., Loizeau, J.-L., Girardclos S.*: Sedimentology and geomorphology of the Rhone delta canyons (Lake Geneva, Switzerland-France)
- P 6.3 *Dietrich F., Golay A., Verrecchia E. P., Cailleau G.*: Calcium pools and sinks : the oxalate-carbonate pathway in tropical FERRALSOLS
- P 6.4 *Donadini F., Serneels V., Kapper L.*: Preliminary archeomagnetic results from Korsimoro, Burkina Faso
- P 6.5 *Hajdas I., Michczynski A.*: From Soppensee to Altai and New Zealand: Calendar times scales based on 14C chronologies and OxCal Models
- P 6.6 *Kapper K. L., Donadini F., Hirt A.*: Rock- and archeomagnetic study on central European artifacts for characterizing the geomagnetic field evolution during mid-Holocene
- P 6.7 *Khaksar K., Haghighi S.*: Correlation between Quaternary stratigraphy units in different Geological zones of Iran
- P 6.8 *Kocher M., Akçar N., Schlüchter C.*: Cosmogenic dating of unconsolidated sediments on Piz Starlex (at >3000m, Swiss-Italian border area)
- P 6.9 *Kremer K., Marillier F., Girardclos S.*: History of mass movements deposits in deep Lake Geneva during the last 3000 years
- P 6.10 *Leith K., Moore J.R., Sternai P., Ivy-Ochs S., Herman F., Loew S.*: A multidisciplinary approach to the reconstruction of a Lateglacial stadial in Canton Valais, Switzerland
- P 6.11 *Mohammadi A, Lak R, Burg J-P*: Sedimentology and sediment geochemistry of the Oman Gulf and Hormoz Strait coastal plain, SE Iran
- P 6.12 *Prizomwala S.P., Bhatt N., Castellort S., Hirt A.M., Winkler W.*: Mudflats of Gulf of Kachchh Coast: Archives of Sea Level Fluctuations and Palaeo-environmental Change since Mid Holocene
- P 6.13 *Reber R., Akçar N., Ivy-Ochs S, Kubik P.W., Schlüchter C.*: Maximal position and retreat phase of the Reuss-Piedmont Lobe during the LGM
- P 6.14 *Wiemann Ph.*: Understanding site manipulation and destruction in prehistoric lake-dwellings

6.1

Filling gaps on the shrinking/swelling tale of the Dead Sea through continental drilling

Ariztegui D¹, Zvi Ben Avraham^{2,3}, Agnon A.⁴, Brauer A.⁵, Goldstein S.⁶, Haug G.⁷, Ito E.⁸, Stein M.⁹, Yasuda Y.¹⁰, Lazar M.³, Waldmann N.³ and the DSDDP Scientific Team†

¹ Section of Earth and Environmental Sciences, University of Geneva, Rue des Maraichers 13, 1205 Geneva, Switzerland

² Department of Geophysics and Planetary Sciences, Tel Aviv University, POB 39040, 69978 Tel Aviv, Israel

³ Leon H. Charney School of Marine Sciences, University of Haifa, Mt. Carmel, 31905 Haifa, Israel

⁴ Institute of Earth Sciences, The Hebrew University, Givat Ram, 91904 Jerusalem, Israel

⁵ GeoForschungsZentrum (GFZ) Potsdam, Telegrafenberg, 14473 Potsdam, Germany

⁶ Lamont-Doherty Earth Observatory, Columbia University, POB 1000, Palisades, NY 10964, USA

⁷ Department of earth Sciences, Geological Institute, Swiss Federal Institute of Technology ETHZ, Sonneggstasse 5, 8092 Zürich, Switzerland

⁸ Department of Earth Sciences, University of Minnesota, 310 Pillsbury Drive SE, Minneapolis, MN 55455, USA

⁹ Geological Survey of Israel, 95501 Jerusalem, Israel

¹⁰ International Research Center of Japanese Studies, Kyoto University, 3-2 Oeyama-cho, Goryo Nishikyo-ku, 610-1192 Kyoto, Japan

Intensive investigations on outcrops and short core sediments in the Dead Sea Basin (DSB) have shown a Late Quaternary history containing a succession of expanding and shrinking lakes during glacial and interglacial intervals, respectively. Sedimentation on this basin located in the lowest continental exposed elevation on Earth has been continuously modulated by regional and global climate and rift tectonics. Hence, its sedimentary infill is comprehensively recording limnological, hydrological and seismic events. Moreover, the sections contain datable material such as primary aragonite that can be used to construct a chronology of the environmental history of lakes and their watershed and compare them to late Quaternary global climate archives. Yet, most of the studies carried out on the Dead Sea lakes during the past decades focused on the marginal terraces that are abandoned when the lake declines. Thus, we moved to drill within the framework of an ICDP (International Continental Scientific Drilling Program) two sets of nearly continuous sedimentary cores at water depth of ~300 m close to the deepest area of today's Dead Sea and at ~2.5m depth next the shore near Ein Gedi (Israel). These sedimentary cores fill in known (and estimated) gaps in the outcrop sediments and provide a nearly continuous and undisturbed record covering at least the past two glacial-interglacial cycles judging from changes in dominant lithology. The sedimentary record can be divided into two dominant lithologies: salt layers interbedded with laminated muds; and massive and laminated marl interbedded with thin salt layers. Silt and sand (and gravel) levels indicate intervals of extremely low lake level. The results of this study will provide crucial information to better understand the environmental conditions prevailing during human development and migration through the Dead Sea corridor.

† Complete list of DSDDP scientists @ www.icdp-online.org

6.2

Stalagmite evidence for a highly dynamic Pleistocene hydrological history of the Black Sea

Fleitmann Dominik¹, Badertscher Seraina¹, Cheng Hai², Edwards Lawrence R.², Leuenberger Markus³, Zumbühl Angela¹, Tüysüz Okan⁴

¹*Institute of Geological Sciences and Oeschger Centre for Climate Change Research, Baltzerstrasse 1+3, 3012 Bern, Switzerland (fleitmann@geo.unibe.ch)*

²*Department of Geology and Geophysics, University of Minnesota, Minneapolis, MN, USA*

³*Climate and Environmental Physics and Oeschger Centre for Climate Change Research, University of Bern, Bern, Switzerland*

⁴*Eurasia Institute of Earth Sciences, Istanbul Technical University, Istanbul, Turkey.*

The hydrological balance of the Black Sea is strongly governed by riverine input and exchange with the Mediterranean Sea through the shallow Bosphorus Strait (34 m below present sea level (mbsl)), both of which have distinctly different oxygen isotope signatures. Therefore, the oxygen isotope composition of Black Sea water is directly related to the presence of a Mediterranean connection and to climatically-driven hydrological changes in the vast watersheds of the Black Sea (2,410,840 km³) and the Caspian Sea (3,249,154 km³) further afield.

To date, very little is known about the Pleistocene hydrological history of the Black Sea because oxygen isotope records from its sediments only span the last 30 ka before present (BP). We present a stacked speleothem oxygen isotope record from Sofular Cave (Fleitmann et al., 2009; Badertscher et al., 2011) in Northern Turkey that tracks the isotopic signature of Black Sea surface water, allowing us to reconstruct the hydrological history of the Black Sea in unprecedented detail.

Our record, which extends discontinuously over the last 670,000 years, suggests that a connection between the Black and Mediterranean Seas persisted at least 12 times since 670 ka BP, more often than previously suggested. Each connection phase coincided with sea levels higher than the current Bosphorus sill depth, which was remarkably constant over the last 670 ka BP. Distinct minima in the Sofular oxygen isotope record indicate at least 7 intervals when isotopically depleted freshwater from the Caspian Sea overflowed into the Black Sea through the Manych-Kerch spillway. Our data provide the first detailed evidence for a highly dynamic hydrological history of the Black Sea.

REFERENCES

- Badertscher, S., Fleitmann, D., Cheng, H., Edwards, L., Göktürk, O.M., Zumbühl, A., Leuenberger, M. & Tüysüz, O. 2011. Pleistocene water intrusions from the Mediterranean and Caspian Seas into the Black Sea. *Nature Geoscience*, 4: 236-239.
- Fleitmann, D., Cheng, H., Badertscher, S., Göktürk, O.M., Mudelsee, M., Fankhauser, A., Pickering, R., Edwards, R.L., Matter, A., Kramers, J. & Tüysüz, O. 2009. Timing and climatic imprint of Dansgaard-Oeschger events in stalagmites from Northern Turkey, *Geophysical Research Letters*, doi: 10.1029/2009GL040050.

6.3

The chronology of Lake Soppensee (Switzerland) using a biomarker and a compound-specific isotope approach

Gierga Merle¹, Smittenberg Rienk H.^{1,3}, Bernasconi Stefano M.¹, Hajdas Irka² & Wacker Lukas²

¹Geological Institute, ETH Zürich, Sonneggstrasse 5, CH-8092 Zürich (merle.gierga@erdw.ethz.ch)

²Laboratory of Ion Beam Physics, ETH Zürich, Schafmattstrasse 20, CH-8093 Zürich

³Department of Geological Sciences, Stockholm University, SE-106 91 Stockholm

Chronologies of natural archives such as lake sediments are often based on radiocarbon ages of recognizable terrestrial macrofossils that are deposited soon after their biosynthesis. However, in many instances reliable dating is not possible due to a lack of macrofossils or other carbonaceous material that can be dated using radiocarbon (¹⁴C). Therefore dating of specific substances that contain a ¹⁴C signature of the time of sediment deposition can be a powerful tool to circumvent many chronological problems.

Here, we evaluate the potential of compound-specific radiocarbon analysis (CSRA) as a dating tool for lake sediments. We present the results of a biogeochemical study of the sedimentary record of the Swiss Lake Soppensee covering the last 14,000 years BP in combination with ¹⁴C ages given by certain organic compounds. The small, eutrophic, hard-water lake is situated on the central Swiss Plateau (596 m a.s.l.). This is a very well dated (Hajdas and Michczynski 2010) and studied (e.g. Lotter 2001, Fischer 1993) lake with undisturbed organic carbon-rich and partially laminated sediments. The master chronology of the record was established by the use of a varve chronology and ¹⁴C dating of terrestrial macrofossils (Hajdas and Michczynski 2010). It allows an evaluation of the potential of CSRA for dating approaches.

We show the radiocarbon ages of long-chain n-alkanes and fatty acids and of the total organic carbon (TOC) and compare them to the existing chronology. Additional information from biomarker profiles and compound-specific isotope analysis ($\delta^{13}\text{C}$) allows more insight into: a) The potential of using specific compounds for radiocarbon dating of the sediment core; b) The limnological and environmental history of the lake and of the soils in its watershed; c) Early diagenetic processes taking place in the lake environment.

In the sediment of lake Soppensee the main lipid signature derives from higher terrestrial plants. We isolated individual long-chain n-alkanes and fatty acids by the use of preparative gas and liquid chromatography for subsequent radiocarbon analysis. In the oldest parts of the record the age of these biomarker match well with the chronology, but with decreasing sediment age they show an increasing age difference. This phenomenon has already been described for other systems (Smittenberg et al., 2006) and gives a measure for residence time of these plant-derived compounds in soils before entering the lake.

REFERENCES

- Fischer, A. 1993: Isotopengeochemische Untersuchungen ($\delta^{18}\text{O}$ und $\delta^{13}\text{C}$) im Wasser und in den Sedimenten des Soppensees (Kt. Luzern, Schweiz), Diss. ETH Zürich No. 11924
- Hajdas, I. & Michczynski, A. 2010: Age-depth model of Lake Soppensee (Switzerland) based on high-resolution ¹⁴C chronology compared with varve chronology. *Radiocarbon*, 52, 1027-1040
- Lotter, A.F. 2001: The palaeolimnology of Soppensee (Central Switzerland), as evidenced by diatom, pollen, and fossil-pigment analyses. *J. Paleolimn.*, 25, 65-79.
- Smittenberg, R.H., Eglinton, T.I., Schouten, S. & Sinninghe Damsté, J.S.: Ongoing buildup of refractory organic carbon in Boreal soils during the Holocene. *Science*, 314, 1283-1286

6.4

Nature and Timing of Terminations I and II recorded in stalagmites from Switzerland

Häuselmann Anamaria¹, Schmassmann Silvia², Cheng Hai³, Edwards Lawrence R.³, Jeannin Pierre-Yves², Häuselmann Philipp², Fischer Martin⁴, Fleitmann Dominik¹

¹ Institute of Geological Sciences, University of Bern and Oeschger Centre for Climate Change Research, Baltzerstrasse 1+3, CH-3012 Bern (hauselmann@geo.unibe.ch)

² Swiss Institute of Speleology and Karst Research, P.O. Box 818, 2301 La Chaux-de-Fonds, Switzerland.

³ Department of Geology and Geophysics, University of Minnesota, Minneapolis, Minnesota 55455, USA

⁴ Postfach 13, CH-9050 Appenzell

One of the main objectives of a recently funded SINERGIA program called “STALCLIM- Multi-proxy climatic and environmental reconstructions from stalagmites from Switzerland, Turkey, Arabia and India” is to construct highly resolved and precisely dated paleoclimate records from stalagmites from caves in Switzerland by using a broad array of different analytical techniques. Since the beginning of “STALCLIM” in January 2011 we collected stalagmites from several caves (Figure 1). Based on preliminary results, two stalagmites from Milandre Cave (Jura Mountains; 400 m above sea level) and Cave R5/007 (Alpstein, Appenzell; 1890 m above sea level) cover the glacial-interglacial transitions corresponding to Termination I (Milandre Cave) and II (Cave R5/007) in close detail.

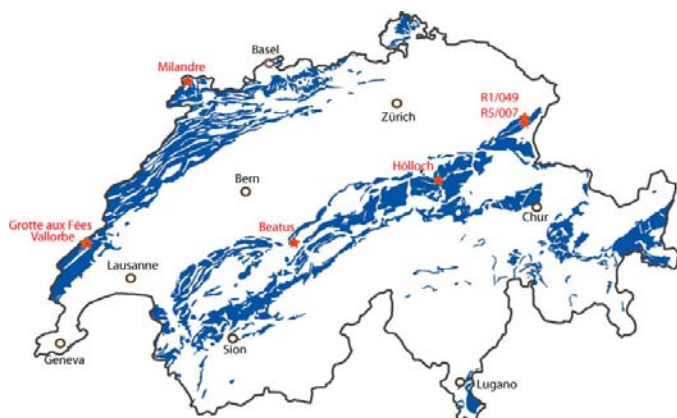


Figure 1. Map of Switzerland showing the location of studied caves (red stars) and spatial distribution of karst areas (blue shaded areas).

High resolution oxygen isotope profiles (Figure 2) indicate that Termination I and II are characterized by distinct positive shift of around 4.5 permil due to temperature dependent positive shifts in the oxygen isotopic composition of precipitation. While the timing and nature of Termination I is fairly well documented in numerous paleoclimate records from Switzerland, no detailed information exists for Termination II. The penultimate glacial termination is covered by stalagmite MF-3 from cave R5/007. Based on very precise Uranium-series ages with age uncertainties of only 500 to 900 years, we provide evidence for an early onset of the Eemian at around 133.000 ± 800 years before present. This timing is in good agreement with other absolutely-dated stalagmite records from Austria (Spötl et al., 2001) and Italy (Drysdale et al., 2009), providing additional support that glacial terminations are rather driven by changes in Earth's obliquity and not Northern Hemisphere summer insolation.

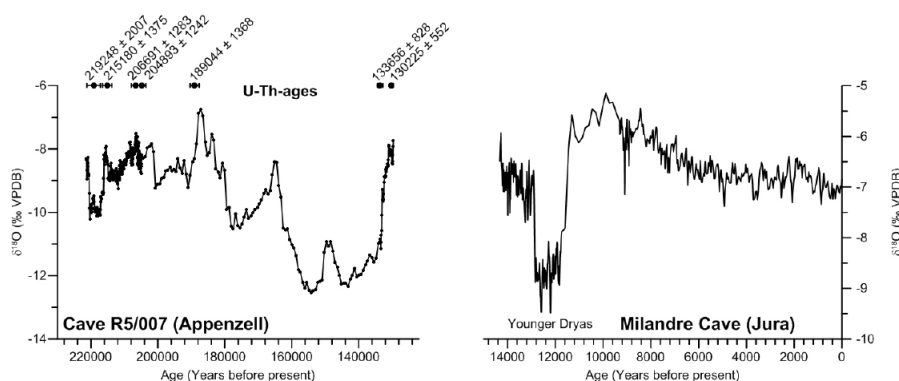


Figure 2. Oxygen isotope profiles of stalagmites from Milandre Cave and Cave R5/007 plotted versus age. Dots with error bars denote Uranium-series ages with age uncertainties.

REFERENCES

- Drysdale, R.N., Hellstrom, G.C., Zanchetta, G., Fallick, A. E., Sánchez Goñi, M. F., Couchoud, I., McDonald, J., Maas, R., Lohmann, R. & Isola, I. 2009: Evidence for Obliquity Forcing of Glacial Termination II. *Science* 323 (5947), 1527-1531
- Spötl, Ch., Mangini, A., Frenk, N., Eichstädter, R. Burns, S. 2002: Start of the last interglacial period at 135 ka: Evidence from high Alpine speleothem. *Geology* 30/9, 815-818

6.5

New findings concerning quartz properties important for luminescence dating of sediments in the Swiss NW Alpine foreland.

Heer Aleksandra¹, Veit Heinz¹, Bateman Mark D.², Adamiec Grzegorz³, Hajdas Irka⁴, May Jan-Hendrik ⁵

¹Geographisches Institut, Universität Bern, Hallerstrasse 12, 3012 Bern, Switzerland, (heer@giub.unibe.ch)

²Department of Geography, University of Sheffield, Sheffield S10 2TN, United Kingdom

³Institute of Physics, Silesian University of Technology, ul. Krzywoustego 4, 44-100 Gliwice, Poland

⁴IBP, SFTI (ETH Zürich), Schafmattstrasse 20, 8093 Zürich, Switzerland

⁵SEES, University of Wollongong, Wollongong, NSW 2522, Australia

Application of the Optically Stimulated Luminescence (OSL) and radiocarbon dating, with the aim of establishing the chronology of postglacial lake shore deposits from Grosses Moos (Swiss NW Alpine foreland), showed that the dimness of the sedimentary quartz and resultant poor counting statistics, required the use of large multi-grain aliquots for determining the equivalent doses. This is contrary to the common practice of using small aliquots or single grain luminescence measurements for sediments with complex depositional histories. L_x/T_x tests conducted at the single quartz grain (SG) level revealed that an extremely low proportion (0.5%) of bright grains were dominating the luminescence signal with the remainder being very dim and contributing little to the total signal. Thus large aliquots are equivalent to small aliquots of samples containing a larger proportion of bright grains.

The presence of lots of dim quartz also has implications for the statistical analysis applied to equivalent doses (D_e) replicates when trying to determine an age. Low overdispersion (OD) calculated for D_e replicates and a large number of SAR OSL measurements were required in order to also gain a representative number of bright grains and so reproducible results. The number of aliquots measured, but not their size was decisive for the resulting OD. The OD values obtained from the dose recovery experiments (formerly used as the arbitral σ_b when modelling age estimates) in fact reflected the OD of the photomultiplier tube (PMT) related to the average luminescence intensity (σ_{PMT}). Thus these OD values should not be further used for modelling purposes. For dim quartz data the additional OD (σ_b) value loses its physical importance of being an expression of microdosimetry, beta source inhomogeneity, crystallographic variability or complexity of environmental processes, because large standard errors obscure this information.

In the littoral sediments of Grosses Moos major D_e distributions dominated by a well bleached component with minor contributions from bioturbated and incompletely bleached sediment were anticipated. Because weighted models (e.g. Central Age Model: CAM, Minimum Age Model: MAM and Finite Mixture Model: FMM) favour D_e values resulting from sensitive grains, the final results are at least based on a small number of bright grains, thereby approaching results of modelling SG measurements. Model comparison showed that the FMM results surpass these of the MAM3 and CAM by yielding most consistent D_e values supported by radiocarbon dates.

6.6

Fluid inclusions in stalagmites used as a quantitative thermometer in paleoclimate research

Hidalgo Staub Rita^{1,3}, Krüger Yves^{1,3}, Marti Dominik¹, Frenz Martin¹ & Fleitmann Dominik^{2,3}

¹Institute of Applied Physics, University of Bern, Sidlerstrasse 5, CH-3012 Bern (hidalgo@iap.unibe.ch)

²Institute of Geological Sciences, University of Bern, Baltzerstrasse 1&3, CH-3012 Bern

³Oeschger Centre for Climate Studies, University of Berne, Zähringerstrasse 25, CH-3012 Bern

The fact that cave air temperatures reflect mean annual surface temperatures make speleothems potentially useful for determining absolute paleotemperatures. We have developed a new method to determine stalagmite formation temperatures from liquid-vapour homogenisation temperatures (T_h) of fluid inclusions in stalagmites (Figure 1). Fluid inclusions in stalagmites contain remnants of the drip water from which the calcite precipitated under atmospheric pressure. It is assumed that once they have formed, they do not undergo any changes in volume or composition. Therefore their T_h is expected to equal the stalagmite formation temperature i.e. the cave air temperature. Our approach is to determine the density of fluid inclusions by measuring the liquid-vapour homogenisation temperature after inducing vapour bubble nucleation in initially monophasic inclusions. This is achieved by ultra short laser pulses to overcome the metastable state of water (Krüger et al, 2007).

To test our paleothermometer T_h measurements were carried out using thick sections of an actively growing stalagmite from Milandre Cave (Swiss Jura). The observed homogenisation temperatures ($T_{h,obs}$) display a large variability with a maximum around the actual cave temperature of 9.5°C (Figure 2), because $T_{h,obs}$ values are influenced by various parameters. $T_{h,obs}$ values above 9.5°C result from density changes in the fluid inclusions induced during sample preparation. Therefore, these inclusions do not represent the original fluid density and are not considered for the determination of the stalagmite formation temperature (T_f). $T_{h,obs}$ values lower than 9.5°C can be explained by the effect of surface tension, which leads to a collapse of the vapour bubble below the nominal homogenisation temperature. In fluid inclusions formed at low temperatures this effect can amount to a temperature difference of several degrees. We have developed a theoretical model to calculate T_f based on $T_{h,obs}$ and the vapour bubble radius measured at different temperatures (Marti et al. in press). This results in a stalagmite formation temperature $T_f = 9.42^\circ\text{C}$ (median value), which is close to the present day cave temperature. The results show that our method allows us to determine paleotemperatures with an accuracy of $\pm 0.5^\circ\text{C}$.

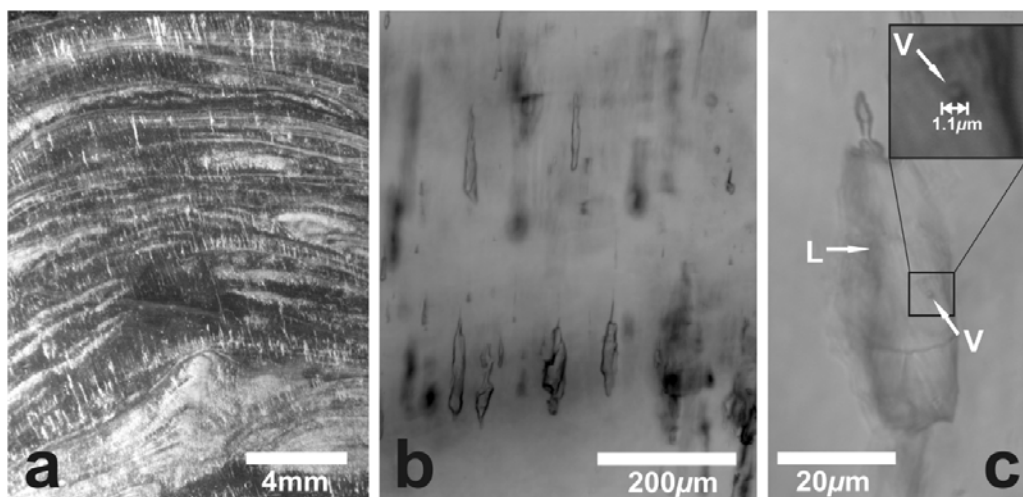


Fig. 1. a) Stalagmite section displaying numerous growth bands with fluid inclusions. b) Enlarged detail displaying typical monophasic fluid inclusions. c) Fluid inclusion after bubble nucleation with the vapour bubble (V) indicated.

REFERENCES

- Krüger, Y., Stoller, P., Ricka J. and Frenz M. 2007: Femtosecond lasers in fluid-inclusion analysis: overcoming metastable phase states. *Eur. J. Mineral.*, 19, 693–706.
- Krüger Y., Marti D., Hidalgo Staub R.; Fleitmann D., Frenz M. in press: Liquid-vapour homogenisation of fluid inclusions in stalagmites: Evaluation of a new thermometer for paleoclimate research. *Chemical Geology*.
- Marti D., Krüger Y., Fleitmann D., Ricka J., Frenz M. in press: The Effect of Surface Tension on liquid-vapour Homogenisation in low-temperature fluid inclusions. *Fluid Phase Equilibria*.

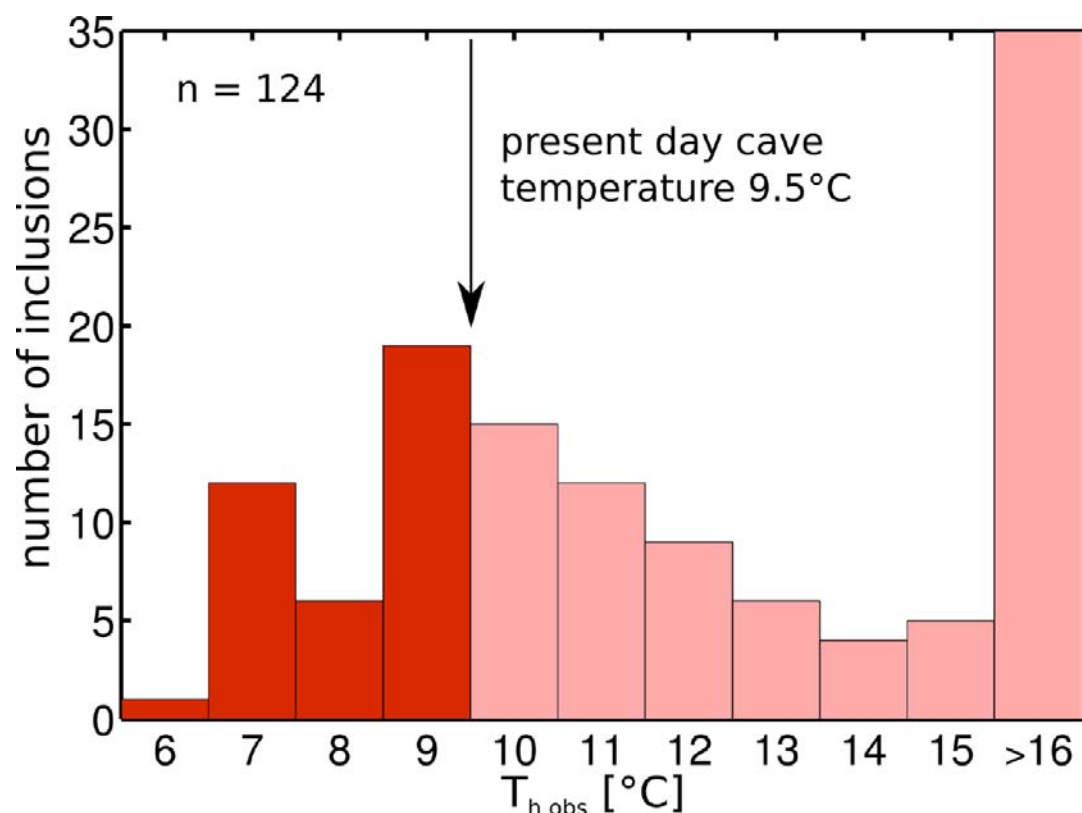


Fig. 2. Distribution of $T_{h\text{ obs}}$ values. Temperatures in light red (higher than the cave temperature) result from preparation induced density alterations. Temperatures in dark red are from fluid inclusions that have potentially preserved their density.

6.7

Evolution of the magnetic inventory in a lacustrine system since the late Pleistocene

Jessica Kind, Ann M. Hirt, Andreas U. Gehring

The magnetic inventory of a sedimentary record covering the last 18 kyr BP is taken to decipher the development of the Soppensee (Central Switzerland). A three-stage development of the lake is constraint from the analysis of the concentration, composition, grain size and configuration of magnetic iron oxides in the magnetic inventory. Stage 1 (18-14 kyr BP): The formation of the proto-lake is triggered by the retreat of the glacier and is characterized by detrital hematite which indicates prevailing oxic depositional conditions. Stage 2 (14-11 kyr BP): The setting of the lake is marked by a shift from an open to a close lake with low detrital input and reducing conditions denoted by the formation of magnetite and the precipitation of ferrous carbonates. This change is assigned to the Bølling/Allerød and the Younger Dryas period. Stage 3 (last 11 kyr): At the beginning of the Holocene a closed lake was established, documented by varves (approximately 11-6 kyr BP) with low magnetite content followed by considerable increase in magnetite production due to the bloom of magnetotactic bacteria (MTB) at approximately 6-2 kyr BP (Gehring et al., 2011, Kind et al. 2011). Intensified forest clearance to provide open areas for pastoral and arable farming at about 2.5 kyr BP affected the chemical conditions in the lakes unfavorable for MTB growth which in turn drop of the magnetite content in the magnetic inventory. With the continuing anthropogenic input the magnetite content in the magnetic inventory remains low and no clear environmental response to the magnetic record is evident. The detailed magnetic analysis of the Soppensee provides clear evidence that the magnetic inventory can be a puzzle piece in a big jigsaw puzzle to understand the paleolimnological development of lake systems.

REFERENCE:

- Gehring, A.U., Kind, J., Charilaou, M., Garca-Rubio, I., 2011. The detection of magnetotactic bacteria and magnetofossils by means of magnetic anisotropy. *Earth and Planetary Science Letters* 309, 113 – 117, doi:10.1016/j.epsl.2011.06.024.
- Kind, J., Gehring, A.U., Winklhofer, M., Hirt, A.M., 2011. Combined use of magnetometry and spectroscopy for identifying magnetofossils in sediments. *Geochem. Geophys. Geosyst.* 12, Q08008, 13 PP, doi:10.1029/2011GC003633.

6.8

Paleoenvironmental changes in eastern Anatolia over the last 500 ka – first insights from the Swiss side of the ICDP Lake Van Drilling Project.

Ola Kwiecien^{1,2}, Marie-Eve Randlett³, Mona Stockhecke², Yama Tomonaga², Katie Unwin² and the PALEOVAN scientific team

¹Swiss Federal Institute of Technology (ETH Zürich), CH-8092 Zürich (kwiecien@erdw.ethz.ch)

²Eawag, Swiss Federal Institute of Aquatic Science and Technology, CH-8600 Dübendorf

³Eawag, Swiss Federal Institute of Aquatic Science and Technology, CH-6047 Kastanienbaum

The PALEOVAN Project, aiming to reconstruct the climatic, tectonic and volcanic history of the eastern Mediterranean and the Near East is the first official Swiss contribution to the ICDP drilling enterprise. During the drilling campaign in summer 2010, our international team recovered a total of 800 m of sediment cores from two sites with multiple holes and reached the bedrock basement of Lake Van. This is a promise of a continuous and complete sedimentary succession covering the entire paleoenvironmental history of Lake Van and its surrounding region over the last ca. 500 ka. Here we present first results acquired within 5 research modules encompassing: (1) sedimentology and stratigraphy, (2) geochemical analyses of solid and fluid phase, (3) organic geochemistry and compound-specific radiocarbon dating, (4) ¹⁰Be as a tracer of solar and geomagnetic variability and erosion rate, and (5) noble-gas geochemistry in the pore water.

Lithological description and facies analysis establish the necessary correlative base for other modules. The 218m-long composite profile exhibits great variability and sharp lithological boundaries indicating rapid climate- and/or tectonic-driven changes in depositional conditions. Several annually laminated intervals enable paleo-reconstructions at seasonal resolution. Additionally, the TOC content, clearly showing glacial/interglacial variability, is a useful tool to construct a tuned age model. Pore water pH and elemental profiles (Mg, Ca, K, Na) reveal the geochemical evolution of Lake Van from a Ca-carbonate dominated freshwater basin to a Na-carbonate dominated saline water mass, while the isotopic composition of pore water ($\delta^{18}\text{O}$, dD) relates to the regional precipitation/evaporation balance. Lipid biomarker analysis suggests a significant amount of alkenones prospecting possibility of paleotemperature reconstruction. ¹⁰Be is used to test to what extent the solar variability and geomagnetic variability can be reconstructed from the production signal of cosmogenic radionuclides. In the first step the analysis focuses at a timeslice of 35-45ka BP (the Laschamp event), where the geomagnetic field was sufficiently reduced. Finally, noble-gas concentrations measured in the pore water allow (in particular He isotope concentration) for understanding of the fluid transport in the sediment column. Moreover the salinity calculated from the concentrations of heavier noble-gas species (i.e., Ar, Kr, Xe) seems to mimic the measured pore water salinity profile, suggesting that noble-gases in the sediments of Lake Van are promising proxies to reconstruct the past physical conditions of the overlying water body.

6.9

Preliminary observations of small scale experiments for the characterization of large rock avalanches

Longchamp Céline¹, Derron Marc-Henri¹, Jaboyedoff Michel¹

¹ Institute of Geomatics and Analysis of Risk, University of Lausanne, Quartier Sorge, CH-1015 Lausanne (celine.longchamp@unil.ch)

Rock avalanches are catastrophic events in which granular masses of rock debris flow at high speeds, commonly with unusual long runout. A great volume of material ($>10^6 \text{ m}^3$) is involved and the flowing mass can reach velocities up to ten meters per second. It can travel over long distances, in order of kilometers and easily cover an area over 0.1 km². These are extremely destructive and uncontrollable events. They present a particular scientific interest because the fundamental processes controlling the behavior of such masses are not well understood. In addition, they are often really costly in term of human lives and infrastructures. The laboratory experiments can play an important role in the understanding of the behavior of such extreme and destructive events.

Small scale experiments were performed on a slope with calibrated material in order to understand the behavior of a sliding mass. The installation is formed by a simple tilting plane where different substratum can be added as well as for the surface of deposition. A volume is released from a starting box, slides along the slope and stops on the horizontal surface. The mass is recorded during its motion by a high speed camera.

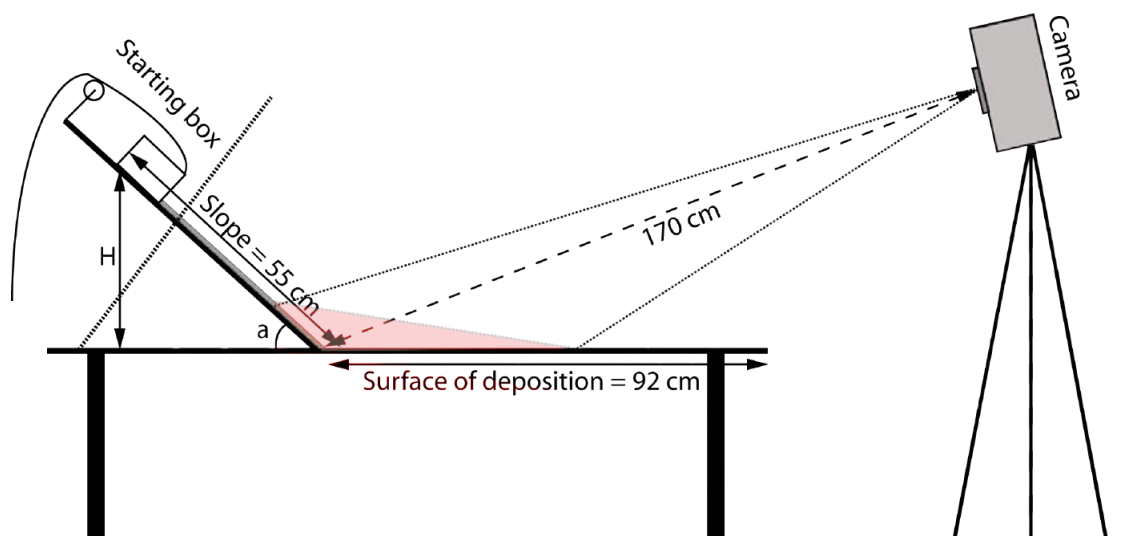


Figure 1. Scheme of the installation with H = height of fall and α = slope angle. The area filmed by the camera is represented in transparent.

We observe that some features and parameters are similar than these observed in some real cases. Deposits present features perpendicular and parallel to the flow direction similar to features identified in the Frank Slide deposit (Charrière, 2011). When a volume with different grainsize is used, the coarser grains tend to form the top of the deposit whereas the finer material forms the margins of the deposits. Different theories were proposed by several authors to explain this inverse grading of deposits (i.e. Middleton (1970), Bagnold (1954) or Takahashi (1980)). Cruden and Hungr (1986) observed this inverse grading in the Frank Slide deposit. An important parameter used to describe rock avalanche is the *Fahrböschung* or apparent coefficient of friction. This parameter, defined by Heim (1932), is the angle of a straight line that expresses the rate of frictional dissipation energy (Hsü, 1978). During our experiments, we observed *Fahrböschung* similar to past events such as: the Lecco rock avalanche, described by Scheidegger (1973), Airolo and Schächental events described by Hsü (1975).

The most important impacts of this study are a better understanding of the effects of grain size and spreading of rock avalanches, the relationship between grainsize and the substratum roughness. If the behaviour of those debris avalanches is better understood, the prediction and the risk assessment for such events will be better constrained.

REFERENCES

- Bagnold, R.A. 1954: Experiments on a gravity free dispersion of large solid spheres in Newtonian fluid under shear. *PRSL*, 225: 49-63.
- Charrière, M. 2011: Granulometrical, geological and morphological description of the Frank Slide deposit (Alberta, Canada). Master Thesis, University of Lausanne.
- Cruden, D.M. & Hungr, O. 1986: The debris of the Frank Slide and theories of rockSlide-avalanche mobility. *Canadian Journal of earth Sciences*, 23:425-432.
- Heim, A. 1932. *Der Bergsturz und Menschenleben*. Fretz und Wasmuth Verlag, Zürich, 218 p.
- Hsü, K.J. 1978: Albert Heim: observations on landslides and relevance to modern interpretations. B. Voight., Elsevier Science Publishers B.V., Amsterdam: 71-73.
- Hsü, K.J. 1975: Catastrophic debris streams (strurzstroms) generated by rockfall, *Geological Society of America Bulletin*, 86: 129-140.
- Middleton, G.V. 1970: Experimental studies related to the problems of flysch sedimentation. *Geological Association of Canada, Special Paper (7)*: 253-269.
- Scheidegger, A.E. 1973: On the prediction of the reach and velocity of catastrophic landslides. *Rock Mechanics and Rock Engineering*, 5 (4): 231-236.
- Takahashi, T. 1980: Debris flow on prismatic open channel. *ASCE Journal of the Hydraulic Division*, 106 : 381-396.

6.10

The recurrence pattern of megathrust earthquakes in South-Central Chile: semi-quantitative paleoseismology using lake sediments

Moernaut Jasper^{1,2}, Van Daele Maarten², Heirman Katrien², Vandoorne Willem², Pino, Mario³, Urrutia, Roberto⁴, De Batist, M.²

¹ Geologisches Institut, ETH-Zürich, Sonneggstrasse 5, CH-8092 Zürich (Jasper.Moernaut@erdw.ethz.ch)

² Renard Centre of Marine Geology, Ghent University, Krijgslaan 281 (S8), B-9000 Ghent, Belgium (Jasper.Moernaut@ugent.be).

³ Instituto de Geociencias, Universidad Austral de Chile, Valdivia, Chile.

⁴ EULA, Universidad de Concepcion, Concepcion, Chile

Megathrust earthquakes at the South-Central Chilean subduction zone (e.g. M_w 9.5 in 1960; M_w 8.8 in 2010) pose a major threat to society. A reliable seismic hazard assessment requires establishing if such mega-events occurred in the past, and determining their recurrence pattern. The Lake District (39-42°S) in South-Central Chile, located in the northern half of the 1960 rupture zone, contains several large glacigenic lakes, the sedimentary deposits in which are highly susceptible to earthquake-triggered slope instability.

To establish the recurrence interval of earthquakes during the Late Holocene, we mapped the spatial distribution of seismically-induced 'event' deposits and sedimentary structures in each lake using very-high resolution seismic data, and collected a series of short gravity cores and long piston cores. Multi-proxy sedimentary analyses (color, magnetic susceptibility, density, geochemistry, grain size), radiocarbon dating and varve-counting were used to identify 'event' deposits in each core and correlate paleoseismic horizons across basins. The sediment sequences investigated contain four main types of earthquake fingerprints: 1) multiple mass-wasting deposits and turbidites on a single stratigraphic level, which are relicts of basin-wide subaqueous slope failure; 2) homogenites indicative of lake seiches and tsunamis; 3) fluid-escape structures (e.g. sediment volcanoes), which reflect sudden liquefaction in buried mass-wasting deposits and subsequent vertical fluidization flow; 4) in-situ deformed units in nearly-flat layers, which reflect strong horizontal ground accelerations.

It appears that the distribution of (liquefiable) volcanic deposits and local sedimentation rates strongly controls the extent and timing of large subaqueous slope failures. However, comparison with historical earthquakes suggests that spatial extent and nature of turbidites can provide key quantitative information about local shaking intensity. For this, we estimated Intensity values using historical reports, instrumental data and empirically-derived attenuation formulae for the largest historical intra-plate and inter-plate ruptures in the region. Here, the well-documented 2010 megathrust event proved to be an ideal calibration point for our lacustrine paleoseismic method.

In three lake basins, we identified and correlated 12 paleoseismic 'events' during the last 3600 yrs with a sedimentary signature comparable to that of the giant 1960 earthquake. This paleoseismic reconstruction points out that strong 1960-like earthquake shaking occurred quasi-periodically with an average recurrence rate of 320 yrs along the northern part of the 1960 rupture zone. Sites characterized by a very-high earthquake recording capacity also recorded significantly smaller events and megathrust events at the adjacent subduction zone segment. New paleoseismic records (tsunami deposits, lake records) in the southern half of the 1960 zone are needed to constrain if the revealed events ruptured the entire 1960 zone, or whether partial ruptures might have taken place.

6.11

Late Pleistocene to early Holocene fluvial dynamics in the southeastern Llanos de Moxos, Bolivian Amazon

Plotzki Anna¹, May Jan-Hendrik², Preusser Frank³, Roesti Beda¹ & Veit Heinz¹

¹*Geographisches Institut, Universität Bern, Hallerstrasse 12, CH-3012 Bern (plotzki@giub.unibe.ch)*

²*School of Earth and Environmental Sciences, University of Wollongong, Northfields Avenue, 2522 Wollongong NSW, Australia*

³*Department of Physical Geography and Quaternary Geology, Stockholm University, 10961 Stockholm, Sweden*

The Llanos de Moxos, which are located in the lowlands of north eastern Bolivia (Beni), are one of the largest seasonally inundated savannahs in the world (150.000 km²). The region is characterized by a complex fluvial drainage pattern belonging to the Amazon system. Large-scale river migrations in the Beni basin have been reported for the Río Grande, Río Beni and Río Maniqui (ALLENBY 1988; DUMONT 1996; HANAGARTH & SARMIENTO 1990; HANAGARTH 1993; PLAFKER 1964). Nevertheless, no systematic analysis of the complex patchwork of palaeorivers has been attempted yet, and none of the river shifts can be placed into a temporal frame, complicating their interpretation with regard to their palaeoenvironmental significance and controlling mechanisms over late Quaternary timescales.

Here, we present first results from the southeastern Llanos de Moxos. The region is characterized by a dense pattern of different palaeoriver relicts and currently active rivers. Several large oxbows and numerous smaller palaeorivers have been identified on satellite imagery. A temporal succession of palaeorivers can be distinguished as younger (palaeo-) rivers are crossing older ones, and older fluvial features such as the large oxbows, appear less pronounced and have probably undergone some degradation. Given the clear difference in size, these large oxbows can not have been formed by the currently active fluvial regime.

Two infilled oxbows of these palaeochannel generations have been investigated in 2009 und 2010 and sediment cores have been taken. OSL dating and heavy mineral analysis has been conducted on the fluvial sands. The heavy mineral assemblage of the oxbow sands is similar to that of the today's Río Grande sands, giving clear evidence of the provenance of the fluvial traces. OSL dates indicate that the meanders were abandoned after 9.6 ka and 13.7 ka respectively. Three to four m of fine sediments, which have been deposited after meander cut-off, are overlaying the fluvial sands, and indicate limited but continued sediment supply. Soil formation in the infilled oxbows started between 8.2 and 4.8 cal ka BP, showing stable - non-sedimentary - conditions. This may be explained by i) intensified upstream avulsion dynamics during the mid-Holocene resulting in complete channel abandonment, and/or ii) a mid- to late Holocene reduction in flooding magnitudes and overall sedimentation rates. Both scenarios are indicative of significant changes in discharge and sediment supply of rivers with Andean headwaters, such as the Río Grande, which may be related to larger-scale environmental changes in South America.

In conclusion, our results represent the first available ages for late Pleistocene to mid-Holocene fluvial activity in the Llanos de Moxos. Thus, these data provide valuable information with regard to assessing timescales and styles of longer-term fluvial dynamics in southwestern Amazonia and interpreting their potential controls.

REFERENCES

- Allenby, R.J. 1988: Origin of rectangular and aligned lakes in the Beni Basin of Bolivia. *Tectonophysics* 145 (1-2), 1-20.
- Dumont, J.F. 1996: Neotectonics of the Subandes-Brazilian craton boundary using geomorphological data: the Marañon and Beni basins. *Tectonophysics* 259 (1-3), 137-151.
- Hanagarth, W. & Sarmiento, J. 1990: Reporte preliminar sobre la geocología de la sabana de Espíritu y sus alrededores (Llanos de Moxos, departamento del Beni, Bolivia). *Ecología en Bolivia* 16, 47-75.
- Hanagarth, W. 1993: Acerca de la geocología de las sabanas del Beni en el noreste de Bolivia. La Paz, Instituto de Ecología.
- Plafker, G. 1964: Oriented lakes and lineaments of northeastern Bolivia. *Geological Society of America Bulletin* 75, 503-522.

6.12

Exposure ages from erratic boulders on the northwestern flank of Rigi (Switzerland)

Regina Reber¹, Naki Akçar¹, Conradin Zahno², Aron Lüthold³, Dmitry Tikhomirov¹, Susan Ivy-Ochs⁴, Peter W. Kubik⁵, and Christian Schlüchter¹

¹Institut für Geologie, Universität Bern, Bern, Switzerland (regina.reber@geo.unibe.ch),

²Louis Ingenieurgeologie GmbH, Postfach 143, 6353 Weggis, Switzerland

³CSD Ingenieure AG, Postfach, 6460 Altdorf, Switzerland

⁴Labor für Ionenstrahlphysik (LIP), ETH Zürich, Zürich, Switzerland,

⁵Paul Scherrer Institut, c/o Institut für Teilchenphysik, ETH Hönggerberg, Zürich, Switzerland

As erratic boulders mark different stadial-positions of paleoglaciers, chronology of advance or retreat phases of paleoglaciers can be established with surface exposure dating with cosmogenic nuclides such as ¹⁰Be and ³⁶Cl. Nine erratic boulders on the Rigi of different lithologies (four Granitic, four Nagelfluh and one Carbonate) were exposure dated. Three of them are located on a lateral moraine of the Reuss-Piedmont Lobe. Exposure ages between ca. 19 ka to 24 ka reveal a moraine formation at around LGM (Last Glacial Maximum). The other six boulders are located on the northwestern flank of Rigi beyond this lateral moraine. Whether these are deposited by local or older glaciations was unknown. The exposure time of these boulders scatter between around 8 ka and 19 ka, among which five yielded younger exposure ages than LGM because of exhumation and human impact. Only one boulder may reveal local LGM glaciations of the Rigi, however more evidence is needed. Our results are synchronous with global LGM (21 ± 2 ka) (Mix et al. 2001) and in accordance with the existing exposure ages from the northern Alpine foreland.

REFERENCES

Mix, A.C., Bard, E., Schneider, R. (2001): Environmental processes of the ice age: land, oceans, glaciers (EPILOG). – *Quaternary Science Reviews* 20, 627–657

6.13

Water concentrations in stalagmites as a potential new paleoclimate proxy – first results from two Holocene stalagmites from Socotra Island (Yemen)

Scheidegger Yvonne^{1,2}, Vogel Nadia^{1,2}, Fleitmann Dominik³, Brennwald Matthias S.¹, Figura Simon¹, Wieler Rainer², Kipfer Rolf¹

¹Eawag, Swiss Federal Institute of Aquatic Science and Technology, Ueberland-strasse 133, CH-8600 Dübendorf, Switzerland (nadia.vogel@eawag.ch)

²ETH Zurich, Institute for Geochemistry and Petrology, Clausiusstrasse 25, CH-8092 Zurich, Switzerland

³Institute of Geological Sciences & Oeschger Center for Climate Research, University of Berne, Baltzerstrasse 1-3, CH-3012 Berne, Switzerland

Stalagmites represent excellent and increasingly studied paleoclimate archives as they not only preserve high resolution stable isotope records over long time scales but can also be dated with high precision (e.g., HENDERSON, 2006). As shown, e.g., by Kluge et al. (2008) and Scheidegger et al. (2010), the absolute temperature in which a stalagmite grew can be deduced from the amounts of atmospheric noble gases dissolved in fluid inclusion water entrapped by the growing stalagmite. As a “by-product” of these noble gas measurements, the water content of the samples (crushed calcite separates) is determined. We will argue below that this water content of stalagmite samples might be a valuable new paleoclimate proxy reflecting changes in drip water availability and thus precipitation outside the cave.

We have analyzed noble gases and water contents in 43 samples from two Holocene stalagmites from Socotra Island (Yemen). Stalagmite D1 (Dimarshim Cave; see Fleitmann et al. (2007) for absolute dating and the $\delta^{18}\text{O}_{\text{calcite}}$ record of D1) covers the last ~ 4.5 ka BP, while stalagmite P3 (Pit Cave) covers the time interval between ~ 10.4 and ~ 1.3 ka BP. We found that the water content of the samples traces shifts in the $\delta^{18}\text{O}_{\text{calcite}}$ records of the same stalagmites in a way that a progressively negative trend in the $\delta^{18}\text{O}_{\text{calcite}}$ record of stalagmite D1 coincides with a decrease of its water content, while a subtle positive trend of the $\delta^{18}\text{O}_{\text{calcite}}$ record of stalagmite P3 coincides with an increase of its water content (Fig. 1). Note that for the time being the age model for stalagmite P3 is anchored to two absolute age determinations only and consequently is rather uncertain.

Unlike many other speleothem's $\delta^{18}\text{O}_{\text{calcite}}$ records influenced by the Indian or Asian monsoon systems (see, e.g., Dong et al. (2010) for a recent compilation of own and published $\delta^{18}\text{O}_{\text{calcite}}$ records from these monsoon regions), stalagmites D1 and P3 show rather uniform or even slightly decreasing $\delta^{18}\text{O}_{\text{calcite}}$ records, which might imply that Socotra Island was less affected than the continental regions by the weakening of the summer monsoon precipitation caused by an orbitally induced decrease in northern hemisphere summer insolation (e.g., Dong et al., 2010; Fleitmann et al., 2007). Superimposed on this regional trend we find for P3 a positive $\delta^{18}\text{O}_{\text{calcite}}$ excursion which might hint to temporary dry conditions in Pit Cave causing evaporation effects, followed by the termination of growth of P3 at ~ 1.25 ka BP. Approximately coeval, D1 shows a major negative excursion with $\delta^{18}\text{O}_{\text{calcite}}$ values down to -5.3 ‰, which might be interpreted as reflecting a time with unusually intense precipitation. We therefore speculate that during this period the pathways for seepage water feeding stalagmite P3 were blocked, leading to its termination of growth. If the above interpretation is correct, increased precipitation and thus a higher drip rate correlates with lower water content (less water-filled inclusions due to undisturbed calcite growth) of the samples (D1), while a reduced drip rate would lead to the formation of more fluid inclusions and thus an increase of the water content of the stalagmite (P3). Based on these results we propose that the water content of stalagmite samples might be a valuable new paleoclimate proxy reflecting changes in drip water availability and thus might also hint to changes in the regional precipitation pattern. We anticipate to present at the conference an additional data set for stalagmite water content from a Swiss stalagmite ideally covering times of lower and higher drip water availability

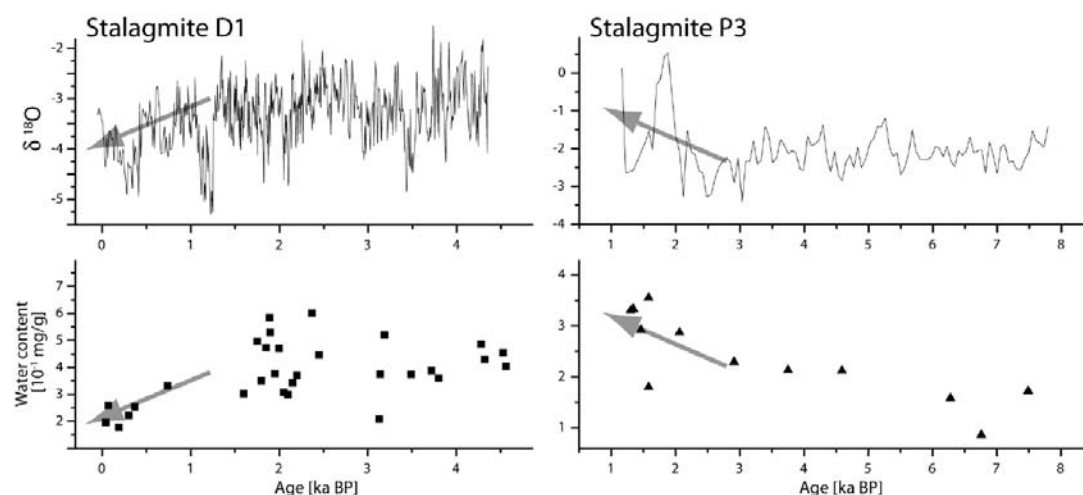


Figure 1: $\delta^{18}\text{O}_{\text{calcite}}$ records and water contents of stalagmites D1 and P3. Note that the water content released from the crushed samples is systematically lower than the total water content of the samples. Absolute dating and the $\delta^{18}\text{O}_{\text{calcite}}$ record of D1 were published by (FLEITMANN et al., 2007)

REFERENCES

- Dong J., Wang Y., Cheng H., Hardt B., Edwards R. L., Kong X., Wu J., Chen S., Liu D., Jiang X. & Zhao K. 2010: A high-resolution stalagmite record of the Holocene East Asian monsoon from Mt Shennongjia, central China. *The Holocene*, 20, 257-264.
- Fleitmann D., Burns S. J., Mangini A., Mudelsee M., Kramers J., Villa I., Neff U., Al-Subbary A. A., Buettner A., Hippler D. & Matter A. 2007: Holocene ITCZ and Indian monsoon dynamics recorded in stalagmites from Oman and Yemen (Socotra). *Quaternary Science Reviews*; 26, 170-188.
- Henderson G. M. 2006: Caving In to New Chronologies. *Science*, 313, 620-622.
- Kluge T., Marx T., Scholz D., Niggemann S., Mangini A. & Aeschbach-Hertig W. 2008: A new tool for paleoclimate reconstruction: Noble gas temperatures from fluid inclusions in speleothems. *Earth and Planetary Science Letters*; 269, 408-415.
- Scheidegger Y. M., Baur H., Brennwald M. S., Fleitmann D., Wieler R. & Kipfer R. 2010: Accurate analysis of noble gas concentrations in small water samples and its application to fluid inclusions in stalagmites. *Chemical Geology*, 272, 31-39.

6.14

Phylogeographic and morphological study of North East Atlantic benthic foraminifers

Schweizer Magali¹, Darling Kate¹ & Austin Bill²

¹*School of GeoSciences, University of Edinburgh, West Mains Road, UK-EH9 3JW Edinburgh (magali.schweizer@ed.ac.uk)*

²*School of Geography and Geosciences, University of St Andrews, Irvine Building, UK-KY16 9AL St Andrews*

The marine fossil record of benthic foraminifers is an important tool for quantitative faunal and geochemical reconstructions of past environments. Numerical data from assemblage counts can be used to infer bathymetry, ecosystem temperature/salinity conditions, productivity and deep water formation and shell calcitic signatures record the palaeo-environmental conditions of the benthos. The integrity of this approach is based upon the assumption that living communities are similar to their fossil counterparts. It is therefore vitally important to fully understand the relationship between present day environmental conditions and the living foraminiferal assemblages in conjunction with their shell geochemistry. All such numerical and geochemical proxies rely on strict recognition of taxonomic units, yet the morphological taxonomy of benthic foraminifera remains poorly constrained. This is partly due to the application of regional taxonomic systems by different workers, but a newly recognised problem has come to light. Recent genetic characterisation of major benthic foraminiferal groups indicates high levels of cryptic species diversity, compounding these taxonomic issues. Many individual morphospecies have been shown to represent several different genetic types with potentially distinct ecologies.

Here we present the first results of a study combining phylogeography and morphology of common neritic and bathyal benthic foraminifers from the North East Atlantic. The aims are to unify the taxonomy of benthic foraminifers from that region and to detect cryptic species.

6.15

Reconstruction of seismic events using cosmogenic ³⁶Cl: An example from the western Anatolian Province of Turkey

Tikhomirov Dmitry¹, Akçar Naki¹, Özkaymak Çağlar², Alfimov Vasily³, Ivy-Ochs Susan³, Sözbilir Hasan², Uzel Bora² & Schlüchter Christian¹

¹ *University of Bern, Institute of Geological Sciences, Baltzerstrasse 1+3, 3012 Bern, Switzerland (tikhomirov@geo.unibe.ch)*

² *Dokuz Eylül University, Engineering Geological Department, 35160 İzmir, Turkey*

³ *Institute of Particle Physics, ETH Hönggerberg, 8093 Zürich,*

Western Anatolia is one of the most seismically active and rapidly extending regions in the world. Therefore, it has been experiencing large earthquakes in the deaths of thousands of people and economic devastation for a long time. Seismological studies show that these destructive earthquakes occurred in relation to the western branches of the North Anatolian Fault System, which is located to the north of this extensional province.

In such tectonically active settings, long-term earthquake models are essential as for science as for society. Verification of these models with field observations requires records that contain well-dated earthquakes. However, such paleoseismic records are rare because landforms and sediments that record faulting are difficult to identify and easily buried or weathered; commonly the evidence of earlier earthquakes is obscured by later ones. Naturally exposed bedrock fault planes are the best evidence of paleoearthquakes and these can only be dated directly with cosmogenic nuclides.

In order to recover past seismic activity, we applied the new method of paleoearthquakes reconstruction to Mugirtepe scarp of the Manisa active fault system in western Anatolia. In this method, ³⁶Cl concentration curve along the foot wall surface of normal fault scarp is analysed to determine offsets caused by past earthquake events and their timing. We took 44 limestone samples in two slightly overlapping strips, which in total recovered 2.65 m of the fault scarp. First results from the Mugirtepe normal fault indicate at least two periods of high seismic activity around 8 ka and 14 ka, which resulted in sequences of earthquakes. Novelty of the method hampers to derive detailed results and provoke both methodological and computational improvements.

P 6.1

Oncoids, charales, and homogeneous silt: reconstruction of lake level and environment in the city of Zurich (Switzerland) between the Iron Age and Late Antiquity

Brönnimann David¹, Ismail-Meyer Kristin¹, Wild Dölf², Ohnsorg Petra² & Rentzel Philippe¹

¹Institute for Prehistory and Archaeological Science IPAS, University of Basel, Spalenring 145, CH-4055 Basel (david.broennimann@uni-bas.ch)

²Stadtarchäologie Stadt Zürich, Lindenhofstrasse 19, Amtshaus IV, CH-8021 Zürich

Several trenches and profiles around the Cathedral «Fraumünster» (Zurich, Switzerland) were documented and analysed in recent years. The sites are situated near the shore of Lake Zurich, on an ancient delta of the Sihl River which temporarily flowed through the area of study. Thus, the region around the «Fraumünster» has been influenced by both the Sihl and Lake Zurich. A characteristic stratigraphic sequence including a thin oncoid level, a layer with charales, and a thick deposit of homogenous silt was observed in most trenches. On the basis of micromorphology, granulometry, and chemical analysis the different sediments were attached to specific sedimentary milieu. In combination with radiocarbon data and archaeological features a reconstruction of the environment and water level of Lake Zurich can be postulated.

REFERENCES

- Hägele, D., Leinfelder, R., Grau, J., Burmeister, E.-G., & Struck, U. 2006: Oncoids from the River Alz (southern Germany): Tiny ecosystems in a phosphorus-limited environment. *Palaeogeography, Palaeoclimatology, Palaeoecology*, 237, 378-395.
- Magny, M. 2004: Holocene climate variability as reflected by mid-European lake-level fluctuations and its probable impact on prehistoric human settlements. *Quaternary International*, 113, 65-79.

P 6.2

Sedimentology and geomorphology of the Rhone delta canyons (Lake Geneva, Switzerland-France)

Corella Juan Pablo¹, Anselmetti Flavio S², Loizeau, Jean-Luc³ & Girardclos Stephanie¹

¹Institut des Sciences de l'Environnement (ISE) and Dept of Geology and Paleontology, University of Geneva, 1205 Genève

²Eawag (Swiss Federal Institute of Aquatic Science & Technology), 8600 Dübendorf

³Institut F.-A. Forel, University of Geneva, 1290 Versoix

The 'Elemo' scientific program (<http://www.elemo.ch>), coordinated at the Swiss Federal Institute of Technology in Lausanne (EPFL), aims to achieve a better understanding of subaquatic processes in Lake Geneva. The 'Elemo' workpackage 'The canyons of the Rhone delta' focuses on the geological and physical properties of the proximal Rhone delta area.

The Rhone delta is characterized by a complex underwater morphology with a slope deeply incised by canyons. The sediments of this delta system consist of channel and levee deposits punctuated by turbidite sequences and mass-movement deposits. A recent multibeam bathymetric survey of the sub-lacustrine Rhone delta (Fig. 1) greatly improved our knowledge of the underwater structures (Sastre et al., 2010) and raised new scientific questions and research goals in relation to the geomorphological and sedimentological processes in these environments.

From June to August 2011 two MIR submersibles have been exploring the submarine canyons of the Rhone delta, including *in-situ* observations of sediment structures, video-recording, and sediment sampling in the levees deposits and canyon beds and walls. These sedimentological and geomorphological data, complemented by regular core sampling from research vessels, will enable us: i) to understand the sedimentary processes and sedimentation rate affecting the channel/levee complex in proximal and distal areas of the active canyon (Fig. 1), ii) to compare the sedimentary sequences of active vs. old canyons; iii) to evaluate the lateral migration rate and the sedimentological processes and evolution of the old, non-active canyons and iv) to investigate the spatial distribution and triggering mechanisms of mass movements and turbiditic deposits in order to assess the contribution of delta failures to the meandering evolution of the deltaic complexes.

We thank the ELEMO Scientific Program for their financial support.

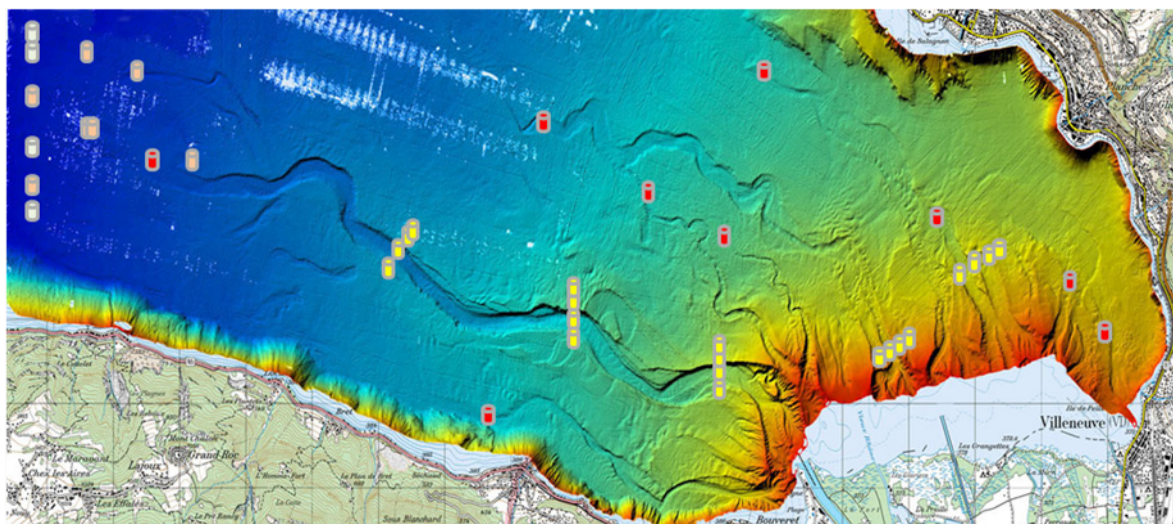


Figure 1. Rhone delta multibeam bathymetric map (Sastre et al., 2010) and location of the retrieved sediment cores

REFERENCE:

Sastre, V. et al., 2010. Morphology and recent history of the Rhone River Delta in Lake Geneva (Switzerland). *Swiss Journal of Geosciences*, 103: 33-42.

P 6.3

Calcium pools and sinks: the oxalate-carbonate pathway in tropical FERRALSOLS

Dietrich Fabienne¹, Golay Anne¹, Verrecchia Eric P.¹ & Cailleau Guillaume¹

¹ Laboratoire Biogéosciences, Institut de Géologie et Paléontologie, Bâtiment Anthropôle, Université de Lausanne, CH-1015 Lausanne (fabienne.dietrich@unil.ch)

In the African intertropical belt, recent research has identified an unexpected soil carbon sink related to the iroko tree (*Milicia excelsa*). Through photosynthesis, part of atmospheric CO₂ is transformed into oxalic acid, which accumulates in plant tissues as an insoluble calcium salt. Ca-oxalate crystals are released during tree decay, incorporated into the soil, and are then oxidised by soil oxalotrophic bacteria. This process, called the oxalate-carbonate pathway, increases the local pH and yields carbonate ions, which can precipitate as Ca-carbonate under certain conditions (Cailleau et al., 2011).

Calcium is present in both end-members of the oxalate-carbonate pathway (Ca-oxalate and Ca-carbonate). Consequently, calcium, as much as carbon, is a key element in the process. In acidic ferralsols, calcium pools are limited due to intense leaching, especially in these old studied soils (Leneuf, 1959). Moreover, in such environments, a carbon sequestration process is considered as a sink if calcium originates from a Ca-carbonate-free source (Elbersen et al, 2000). Therefore, the aim of this study was to quantify calcium pools and fluxes in a particular ecosystem in order to determine calcium behavior in the different ecosystem compartments.

The study site is located in the area of Bertoua (Cameroon), near a stump of a recently felled *M. excelsa*. Three soil profiles were sampled, one below the hollow trunk, one at 40cm from the tree, and a reference profile at 15m. All the identified calcium sources and outputs were collected (i.e. granitic bedrock, airborne particles,...). XRF and ICP-MS analyses were performed in order to quantify the total calcium content in samples. The calcium amounts present in the different soil compartments, i.e. exchangeable ions, carbonate substrates, and organic matter were quantified using a sequential extraction procedure and back titration.

The impact of an oxalogenic-oxalotrophic system on the local calcium cycle is discussed by comparing both *M. excelsa* and reference ecosystems (figure 1). The soil calcium content is 25 times higher near the tree than in the reference profile. Three main soil calcium compartments were identified: pedogenic calcium carbonate, soil available calcium, and calcium trapped in the organic matter.

Calcium is either sequestered, as CaCO_3 , or remains exchangeable, with 90% of it in the carbonate form below the hollow trunk. This figure tends to be inverted towards the reference profile, the other compartments becoming more important.

Finally, the 130kg of carbon sequestered as calcium carbonate into the soil during the tree's lifetime constitute a carbon sink as the input providing Ca is not related to calcium carbonate.

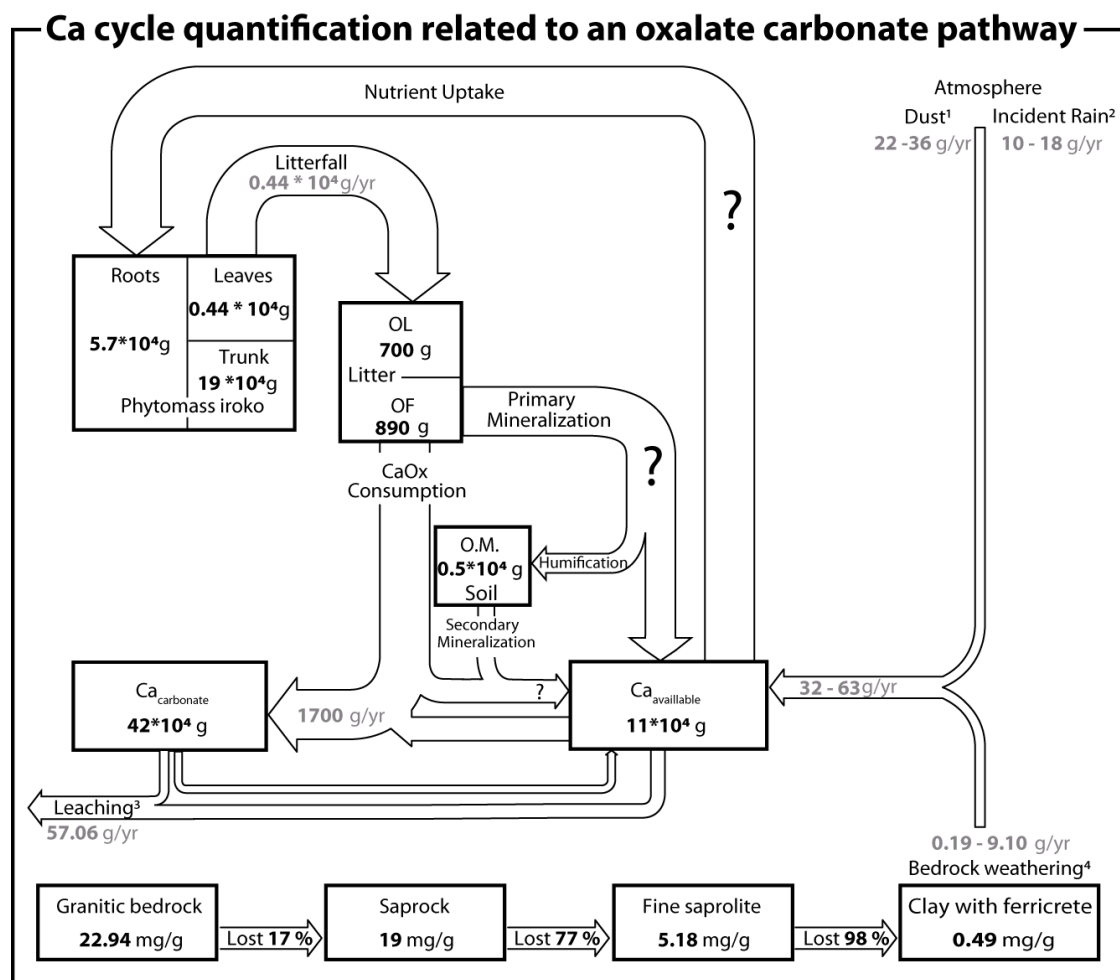


Figure 1. Ca cycle quantification related to an oxalate-carbonate pathway system (Bertoua, Cameroon). OL : recent litter, OF : fragmented litter, OM : organic matter, CaOx : calcium oxalate

1 Combined data from Stroorvogel et al (Biochemistry, 1997) and Dia et al (Chem. Geology, 2006)

2 Data from Braun et al (Geochem. Cosmochem. Acta, 2005) and Seyler et al (Hydrology of Warm Humid Regions, 1993)

3 Data from Bierman and Caffee (Am. Jour. Science, 2001) and Boeglin and Probst (Chem. Geology, 1998)

4 Data completed with the data of the University of Yaoundé

Acknowledgements: this research has been funded by the Fonds Matthey-Dupraz, The Swiss Academy of Sciences, and the FP7 EU "Co2SolStock" project (Agr. 226306).

REFERENCES

- Cailleau, G., Braissant, O. & Verrecchia, E.P. 2011: Turning sunlight into stone : the oxalate-carbonate pathway in a tropical tree ecosystem, Biogeoscience, 8, 1755-1767.
- Elbersen, GWW., Davie, G., Van Reeuwijk, LP. & Janssen RPT. (1999) : The carbon sink function of calcic horizons quantified by means of stable isotopes of strontium. In : 6th International Meeting on Soils with Mediterranean Type of Climate, Section II, Soil Chemistry, 150-107.
- Leneuf, N. 1959 : L'altération des granites calco-alcalins en Côte d'Ivoire forestière et les sols qui en sont dérivés. O.R.S.T.O.M, Paris, 210p.

P 6.4

Preliminary archeomagnetic results from Korsimoro, Burkina Faso.

Donadini Fabio¹, Serneels Vincent² & Kapper Lisa¹

¹Institut für Geophysik, ETH Zürich, Sonneggstrasse 5, CH-8092 Zürich (fabio.donadini@erdw.ethz.ch)

²Earth Sciences - Archaeometry Department Geosciences, University of Fribourg, Chemin du Musée 6, CH-1700 Fribourg

Reconstructions of the past geomagnetic field play an important role in understanding the evolution of the Earth's interior where it is generated. Prior the start of systematic measurements around 1600AD, geomagnetic field components can be indirectly measured from well baked archeological artifacts. Unfortunately archeomagnetic data from the equatorial regions and from the southern hemisphere are very scarce, yielding a global picture that is far from complete.

During the past three millenia the iron industry in West Africa flourished continuously, as witnessed by the large amount of kilns and slags found in that area. In January 2010 an excavation started at Korsimoro (Burkina Faso), aiming at studying the evolution of a complex metallurgical site in time.

In this occasion four kilns were sampled for archeomagnetic investigations. Four to eight samples were collected using the sun-compass technique, and were then cut in cubic specimens after consolidation in water-glass.

kiln 1 and 2 are rather small structures (about 30 cm in diameter) that were used to refine the smelted iron, whereas kiln 3 is a medium sized structure of about 80cm diameter, and finally kiln 4 was a large structure of 150cm diameter. It appears that kiln 4 is older than 1400 AD, because before that age rocks were smelted only once in large kilns. Kilns 1, 2, and 3 were instead used after 1400 AD, when the technique was improved. In these kilns the metal was first smelted in a medium sized oven, and then refined in a smaller one.

A viscous test measuring the changes in magnetization after three weeks storage in zero field shows that minimal changes (less than 6%) occur, indicating a very stable magnetic signal. This behavior is typical of well baked structures. High temperature susceptibility curves were measured to diagnose the various magnetic minerals based on their Curie temperature. In general the black part of the kilns, originated in reducing conditions, show a Curie temperature around 580°C indicating that magnetite is present. In contrast, samples showing a red color have Curie temperatures around 240°C and around 620°C, the latter most likely related to maghemite. A three-axial isothermal remanent magnetization experiment (Lowrie, 1990) was also carried out on selected specimens, and again proves the presence of magnetite and maghemite. Also hysteresis loops confirm the presence of two magnetic minerals when wasp-waisted loops are observed.

Alternating field demagnetization technique was applied to isolate the characteristic remanent component of the kilns. We selected directions that had a maximum angular deviation smaller than 1.5° and which consisted of at least 4 points. The first results yield a average declination of 9.7° and an inclination of 27.1° (number of specimens n = 10, confidence oval $\alpha_{95} = 4.7^\circ$, precision parameter k = 107) for kiln 1, 3.2° and 25.0° (n = 14, $\alpha_{95} = 3.8^\circ$, k = 112) for kiln 2, 11.5° and 23.2° (n = 25, $\alpha_{95} = 2.2^\circ$, k = 172) for kiln 3, and 15.9° and 9.2° (n = 35, $\alpha_{95} = 1.8^\circ$, k = 184) for kiln 4.

Preliminary intensity results from 26 specimens suggest that the field strength varied between 20 and 40 μT , and encompass the present field value at Korsimoro of 33 μT . Failure rate of this experiment was however high due to the fact that magnetomineralogical changes happened.

Radiocarbon ages are being determined and will serve to present the time variation of the field based on these four kilns. This work represents a preliminary step towards the construction of a reference curve of the geomagnetic field at Burkina Faso, and more sampling will be possible due to the abundance of sampling material at Korsimoro.

REFERENCES

Lowrie, W., 1990. Identification of ferromagnetic minerals in a rock by coercivity and unblocking temperature properties. *Geophysical Research Letters*, 2, 159-162.

P 6.5

From Soppensee to Altai and New Zealand: Calendar times scales based on ^{14}C chronologies and OxCal Models.

Hajdas Irka¹ and Michczynski Adam²

¹Laboratory for Ion Beam Physics, ETH Zürich, Schafmattstrasse 20, CH-8093 Zürich (hajdas@phys.ethz.ch)

²Silesian University of Technology, Institute of Physics, Radiocarbon Laboratory, GADAM Centre of Excellence, Bolesława Krzywoustego 2, 44-100 Gliwice, Poland

Radiocarbon chronologies are often applied in studies of past climate as well as archeology. Because of the nearly global nature of the ^{14}C , measurements of ^{14}C concentration and radiocarbon ages in various archives can be applied as a correlation and synchronization tool. However, correlation to other prominent climatic records such as ice cores or stalagmites can only be done using absolute time scales. Therefore, high-resolution calendar time scales of records dated by ^{14}C are needed. Using the Soppensee ^{14}C and Varve chronologies we have shown that such calendar chronology for events can be obtained when high-resolution ^{14}C chronology and Bayesian model available in OxCal4 (Ramsey 2009) are applied (Hajdas and Michczynski 2010).

As the next step of the study we apply this approach to other records. Moreover we will discuss application of other models that are available in OxCal4 (Ramsey 2009) and can be chosen dependent on the type of archive and the type of prior information (additional information about the ^{14}C chronology such as: sequence order, years in between samples, groups of ages).

REFERENCES

Ramsey, CB. 2009. Bayesian Analysis of Radiocarbon Dates. *Radiocarbon*, 51, 337-360.

Hajdas, I. & Michczynski, A. 2010: Age-depth model of Lake Soppensee (Switzerland) based on high-resolution ^{14}C chronology compared with varve chronology. *Radiocarbon*, 52, 1027-1040

P 6.6

Rock- and archeomagnetic study on central European artifacts for characterizing the geomagnetic field evolution during mid-Holocene

Kapper Kathrin Lisa¹, Donadini Fabio¹ & Hirt Ann¹

¹ Institute of Geophysics, Sonneggstrasse 5, CH-8092 Zurich (lisa.kapper@erdw.ethz.ch)

One of the major problems in deciphering geomagnetic field evolution prior to 1000 B.C. is the scarcity of archeomagnetic measurements. Nevertheless, recent studies have shown that a variety of burnt sediments from human activities are suitable for archeomagnetic investigations (e.g Carrancho et al. 2009). The Arconciel (ARC) shelter near Fribourg (CH), and the Riparo Gaban (RGB) shelter near Trento (IT) offered us the chance to collect a stratigraphic sequence (8000 to 7200 years BP, and 7000 to 6500 years BP) of burned sediments. In both cases these structures appear to be ancient hearths used for domestic purposes. Additionally, we received a collection of burned cherts and fragments of terracotta from Lugo, which is near Trento, and about 7000 years old. This particularly well burned materials should hold a magnetization stable enough to determine the ancient field strength.

We have performed several rock magnetic analyses to assess the suitability of various burnt, oriented sediments, and un-oriented cherts and fragments of terracotta. Both thermomagnetic curves and hysteresis loops indicate magnetite as the main carrier of magnetization. In some cases maghemite and hematite are also detected. In general, the thermomagnetic curves show that new magnetic phases are formed during heating to high temperatures. To quantify the viscous part of the magnetization we measured the change in natural remanent magnetization (NRM) of representative samples from each unit before and after storage for three weeks in a shielded environment. After three weeks the magnetization changes about 20 % maximum.

Anisotropy of magnetic susceptibility (AMS) was measured for RGB and ARC to assess the preferred alignment of the magnetic grains. The directions of the maximum (k_1) and intermediate (k_2) AMS are evenly distributed in the compaction plane, and the direction of the minimum AMS (k_3) is perpendicular to it. For samples from ARC the anisotropy ellipsoid is tilted by around 45° , and appears to agree with the tilt of these layers. The anisotropy degree $P = k_1/k_3$, does not exceed 6%, in general. For most of the specimens the anisotropy ellipsoid is oblate.

The characteristic remanent magnetization (ChRM) was isolated using alternating field (AF) demagnetization. In general, burned, reddish layers tend to yield directions that are more clustered compared to the intercalated ashy and organic layers. The characteristic direction has been defined for 17 of the sampled units from RGB, and 10 of the sampled units from ARC.

Analyses of the burned cherts and fragments of terracotta from Lugo show a single magnetic component carried by magnetite and low to moderate alteration with heating. This characteristic behavior suggests that the samples are suitable for paleointensity experiments. A set of 26 specimens was subjected to paleointensity determination, using the IZZI protocol (Tauxe and Staudigel 2004). Six specimens from Lugo yielded reliable paleointensity estimates. In contrast, all RGB and ARC samples from the burned sediments failed to yield a robust result. A comparison of our preliminary results is made with the recent CALS10K.1 global model (Constable et al. 2010), for which the mid-Holocene period mainly relies on lake sediment records (Figure 1). Our directional results show an easterly trend in declination from 6000 to 5500 B.C. and from 5000 B.C. to 4000 B.C., but a rapid shift to the west around 5500 to 5000 B.C. Inclinations appear to become progressively shallower during the entire time interval. Intensity results agree very well with the model value for that period.

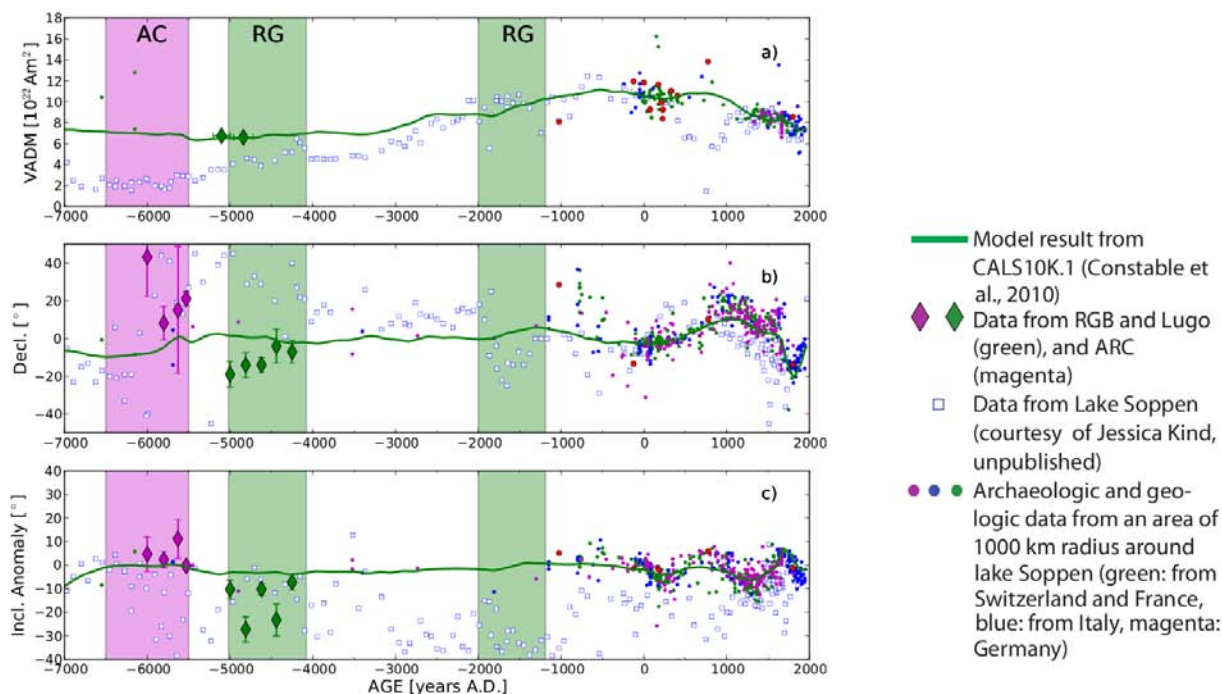


Figure 1. Preliminary results of RGB and ARC plotted together with measurements and model results. a) Virtual Axial Dipole Moment (VADM), b) declination, c) inclination anomaly, spanning a period from 7000 B.C. to 2000 A.D.

REFERENCES

- Carrancho, J. J., Villalan, D. E., Angelucci, M. J., Dekkers, J., Vallverdu, & J. M. Verges 2009: Rock-magnetic analyses as a tool to investigate archaeological fired sediments: a case study of Mirador cave (Sierra de Atapuerca, Spain). *Geophysical Journal International*, 179, 79–96. doi: 10.1111/j.1365-246X.2009.04276.x.
- Constable, C., Korte, M. C. & F. Donadini 2010: CALSK10k.1: A geomagnetic field model spanning 10~kyr. American Geophysical Union, Fall Meeting 2010, abstract #DI23B-1987.
- Tauxe, L. & H. Staudigel 2004: Strength of the geomagnetic field in the Cretaceous Normal Superchron: New data from submarine basaltic glass of the Troodos Ophiolite. *Geochemistry, Geophysics, Geosystems*, 5:Q02H06.

P 6.7

Correlation between Quaternary stratigraphy units in different Geological zones of Iran

Khaksar Kaveh¹, Haghghi Saeid²

¹Department of Civil Engineering, Rudehen branch, Islamic Azad University, Rudehen City, Iran, (k.khaksar@riau.ac.ir)

² Department of Soil Science, Rudehen branch, Islamic Azad University, Rudehen City, Iran.

In geology of Iran, generally, rocks and deposits related to post Pleistocene conglomeratic formations (Hezardarreh and Bakhtiari) have been attributed to Quaternary period, which have been covered older rocks as unconfirmed which alluvial – alluvial fan, eolian and desert – wilderness deposits have more portion among them. That is why there is this belief that after late Alpine tectonic event, Iranian plate has been emerged from water and it has formed its current morphology that one of its results is beginning of erosional cycles which have been imposed on Iran since that time to recent. Also, in some structural – sedimentary zones of Iran, such as Kopet Dagh mountains, mountains in east of Iran and even vast zones in Alborz and Central Iran, beginning of erosion phenomena is very older than Quaternary when Pyrenean event has more fundamental role in accomplishment of that. In addition to clastic accumulated strata in continental, lake and marine environments, magmatic activities in Quaternary period have created igneous rocks in this period. Regarded to factors just like sedimentary environment, origin, type of weathering processes and erosion, quaternary rocks of Iran can be as follow types. Unfortunately, our information's and data about Quaternary deposits of Iran are not sufficient because the principal geological study in Iran was begun to know more about minerals and hydrocarbourants materials. Therefore you may not find enough researches about the other geological periods. Another reason for lack of data of Quaternary may be the narrow thickness of these deposits. The scale of the most published geological maps in Iran is 1/250000 and 1/100000; therefore to separate horizons and narrow thickness of the sediments in these maps is difficult. A series of marine, heavily eroded mountain ranges surrounding Iran high interior basin. In sharp contrasts are the coastal regions outside the mountain rings. The Quaternary deposits comprising semiconsolidated to unconsolidated gravel, sand, silt and clay, occupy the greatest part of Iranian platform. These deposits have been used for example in construction aggregates for the residual, industrial and transportation segments of the population, ceramic clays, and laterites. Much of the groundwater essential to agriculture and human existence eminences from aquifers in quaternary sedimentary environments. The Quaternary deposits have been covered half past of Iranian territory and in order to important consist of alluvial, evaporate, eolian, beach sand, effusive activities, landslide-debris and glacial drift deposits. The late walachian minor events and pasadenian main pulsation vigorous were caused uplifting of mountains and subsidence of valleys. The Quaternary alluvial deposits have been composed of thick stratigraphic sediments, which formed by conglomerate, coarse gravels, boulders, pebbles, sand, silt and marls. Intervals of different stages have been distinct by changing in sedimentation. In the four distinguished areas of Iranian platform typically different, Quaternary deposits had similar characters, which indicated mentioned factors influence contemporaneous all part of Iran. In the central part of Iran, the Quaternary and recent Formations are mainly presented by extensive gravel sheets, deposited salt-water, brackish-water and fresh water lakes (Lake deposits, Lut and Kavir deposits, Recent salts), and by Aeolian sand, loess occurs in the western foothills of the Alborz and in the western spurs of the Kopet-Dagh. In the north part of Alborz mountains, Mazandran-Gorgan plain has been formed by marine deposits.

REFERENCES

- Haghghi, S. and Khaksar K. 2010 - The Quaternary sediments of Iran. Quaternary stratigraphy and paleontology of the southern Russia: connections between Europe, Africa and Asia, (2010 annual meeting INQUA-SEQS).
- Khaksar, K. 1998 - The Quaternary sediments of the Tehran region, 4th international Conference on the Geology of the Middle East, Beirut Lebanon.
- Khaksar, K. 2001 - Quaternary stratigraphy of Maharlu basin, Zagros mountains (South Iran), 4th International Symposium on Eastern Mediterranean Geology, Suleyman Demirel University, 21-25 May, 2001 Isparta, Turkey.
- Nabavi M.H. 1976. An introduction to geology of Iran. (in Persian), Geological Survey of Iran, Tehran.
- Stoklin J. 1977. Structural correlation of the Alpine ranges between Iran and central Asia. Mem. Hors-serie Soc. Geol. Fr., 8:333-353.

Chronostratigraphy		LITHOSTRATIGRAPHY				Tectono-stratigraphy
		Caspian Region	Piedmont areas			
QUATERNARY	Holocene	Recent Caspian deposits	Holocene alluvium	Holocene stage	Minab alluvium	Pasadenian main Pulsation Vigorous
	Upper Pleistocene	Baku Formation	Tehran alluvial F.	Young alluvial deposits	Sadich alluvium	
			Kahrizak Formation	Old alluvial deposits		
Lower Pleistocene	Apsheron Formation	Hezardareh Formation	Bakhtyari Conglomerate (Upper half)	Minab Conglomerate (Upper half)	Late Walachian minor events	

P 6.8

Cosmogenic dating of unconsolidated sediments on Piz Starlex (at >3000m, Swiss-Italian border area)

Mario Kocher¹, Naki Akçar¹ and Christian Schlüchter¹

¹Institut für Geologie, Universität Bern, Bern, Switzerland (m.kocher@students.unibe.ch)

In the Swiss Alps, few examples of unconsolidated, polymict, coarse sandy- gravelly deposits are known at high elevation. Their origin, age, and paleogeography are – with few exceptions – unknown. One of these sites is the top of Piz Starlex, a 3017m a.s.l. solitary mountain in the Swiss-Italian border area of the Val Mustair, SE-Switzerland. At the top of this exquisite mountain, crystalline-rich bouldery sandy gravel covers the almost flat mountaintop of approximately 8000m². Piz Starlex is composed of “eastern alpine dolomites” of the tectonic Scarl-Unit, which has been overthrust by the crystalline Ötztal complex. The aim of this study is to determine the origin, paleogeography and chronology of the Piz Starlex gravel. For that, first literature and rock collections were examined and then thin-sections of the crystalline components were analyzed. First results show that the unconsolidated crystalline components are from at least two major tectonic units: the Sesvanna-Scarl complex and the Ötztal complex. It is certain that the Piz Starlex gravel is not transported to its today’s high position (>3000m a.s.l.) by glacial processes, because the maximum vertical expansion of the Ice never exceeded 2700m a.s.l. in this area. It is, therefore, likely that the Piz Starlex gravels are a relict of an old (Paleogene to Neogene) river system in the Eastern Alps or/and has been tectonically uplifted over the past millions of years. To reconstruct the chronology of this deposit, crystalline components were sampled for cosmogenic nuclides analysis with ¹⁰Be and ²⁶Al.

P 6.9

History of mass movements deposits in deep Lake Geneva during the last 3000 years

Kremer Katrina¹, Marillier François² & Girardclos Stéphanie¹

¹ Institute of Environmental Sciences & Department of Geology and Palaeontology, University of Geneva, CH-1205 Geneva, Switzerland

² Institute of Geophysics, University of Lausanne, CH-1015 Lausanne, Switzerland

Lake sediments are excellent archives of past environmental changes, not only due to human activity and climate variations, but also to geological events such as earthquakes and slope collapses. Subaqueous mass movements recorded in lake sediments are often linked to historical earthquakes. However, numerous studies have shown that mass movements can also be triggered by aseismic processes such as delta and slope collapses due to sediment overloading, rockfalls, etc. Thus, the study of mass-movement deposits in lake sediments provides insights into past natural hazards at historic and prehistoric timescales.

In Lake Geneva, a previous seismic reflexion study showed that two large mass movements started on the lake slope off the city of Lausanne (Yrro 2010). In 2010, 100 km of high-resolution seismic reflection data (3.5 kHz Pinger source) were acquired on a dense grid to improve the imaging of the lake deep basin. The seismic data reveal six major mass movement units characterized by lense-shaped, transparent to chaotic seismic facies with irregular boundaries. These units alternate with sequences of parallel, continuous and high-amplitude reflections intercalated with transparent horizons. These sequences are interpreted as the “background” lake sediments composed of hemipelagic sediments interbedded with turbiditic deposits due to floods. The seismic facies interpretation is confirmed by correlation with lithological units of four 8 to 12 m-long sediment cores.

¹⁴C dating and the sediment core data reveal that the six major mass movements were deposited during the past 3000 years. These deposits vary in size, seismic and sedimentary facies revealing different deposition and trigger processes. The largest event deposit in this sequence is a 6 m-thick, thinning upwards bed with an erosive base that covers the entire deep basin with a minimum volume of 0.25 km³. This layer can be associated with the Tauredunum event of 563 AD that is historically known because of large human and material loss in the Rhone valley and in the old city of Geneva. Three older mass movement deposits are situated at the same sismo-stratigraphic level, meaning they were most probably deposited at the same time. As they originate from different locations and settings on the lake slope, they were most likely caused by an earthquake.

This project is funded by the Swiss National Fund nr. 200021-121666/1

REFERENCE

Yrro, B. J.-F. 2010: Etude sismique d'un glissement de terrain sous-lacustre au large de Lausanne. Master thesis, University of Lausanne, 123 pp.

P 6.10

A multidisciplinary approach to the reconstruction of a Lateglacial stadial in Canton Valais, Switzerland

Kerry Leith¹, Jeffrey R. Moore¹, Pietro Sternai¹, Susan Ivy-Ochs² Frédéric Herman¹, Simon Loew¹

¹ Geological Institute, ETH-Zürich, Sonneggstrasse 5, CH-8092 Zürich (kerry.leith@erdw.ethz.ch)

² Laboratory of Ion Beam Physics, ETH Zurich, CH-8093 Zürich

Remnant moraine deposits preserved on the walls of inner Alpine valleys provide valuable constraint on the timing and extent of Alpine glaciers during Lateglacial stadials. The Matter and Saas Valleys (Canton Valais, Switzerland) were major tributaries to the Rhone Glacier during the Last Glacial Maximum. They are oriented approximately north-south, and sub-parallel, approximately 10 km apart. The total catchment area of the Matter Valley is 450 km², while the Saas Valley has a catchment area of 250 km², valley floor elevations vary between 700 m and 2200 m. Detailed mapping of a prominent moraine sequence within the region has allowed us to delineate an extensive Lateglacial re-advance in each valley that coincides with a clear, and consistent change in the geomorphology of both. Moraine deposits interpreted to reflect the terminus of the principal valley glaciers are located at 1300 m elevation in the Matter Valley, and 1650 m in the Saas Valley, with lateral moraine deposits located between 300 m and 500 m above the present-day valley floor.

Although the geography of the two valleys is similar, the mapped extents reflect complicated dendritic glacier systems, and calculations of equilibrium line altitude, or correlation of the stadials are difficult. We use the numerical landscape evolution model ICE-CASCADE (Braun et al., 2008) to model glacial ice extents, and find a close correlation between modelled and mapped glaciers for a given equivalent ocean surface temperature. While the principal valley glaciers are particularly sensitive to this variation, it is likely that the mapped re-advance is contemporaneous. Cosmogenic ¹⁰Be exposure age dating is used to constrain the timing of moraine emplacement, and will allow us to both correlate this prominent stadial with Lateglacial advances recorded elsewhere in the Alps, and calibrate the ICE-CASCADE model for inferred climatic conditions during this stadial. Alongside results from our field mapping, we present a correlation of mapped extents with model results, as well as first results from ongoing surface exposure dating.

REFERENCES

J. Braun, D. Zwartz, and J. Tomkin. A new surface-processes model combining glacial and fluvial erosion. *Annals of Glaciology*, 28:282-290, 1998.

P 6.11

Sedimentology and sediment geochemistry of the Oman Gulf and Hormoz Strait coastal plain, SE Iran

Mohammadi Ali ¹, Lak Raziye², Burg Jean-Pierre¹

1- Geological Institute, ETH-Zurich, Switzerland

2- Research Institute for Earth Sciences, Iran

Due to low topography, strong wind systems and availability of fine and loose grains, coastal plains are important sources for aeolian sediments. The Makran coast of Iran and Pakistan with few dry playas produces 12 percent of dust storm of the world.

The main objective of this study is to find out the main controlling processes for sediment deposition and element distribution in the Makran coast.

The coastal plain of the Hormoz Strait and Oman Sea in southeastern Iran have huge watershed, dry climate and annual precipitation of less than 98mm. To study sedimentology and sediment geochemistry of the Oman Sea, 46 samples of surficial sediments were collected from Minab, near the Hormoz Strait, to the Guater Gulf near the Pakistan border.

Granulometry, calcimetry, elemental analysis (ICP), mineralogy and clay determination by XRD were carried out at the Geological Survey of Iran.

The analyses show that sediments are mostly very poorly to moderately sorted sandy mud, mud, muddy sand and sand. They statistically classify as coarse-skewed, fine-skewed, and near symmetrical with very leptokurtic to leptokurtic, platykurtic to very platykurtic and mesokurtic distributions.

Calcite, quartz and feldspar are the three dominant minerals in variable proportions. Halite is the fourth important constituent. Chlorite, illite, kaolinite and poligorskite are frequent clay minerals. Montmorillonite is found in the eastern part of the Oman coastal plain, from Chabahar to the Pakistan border. Conversely, poligorskite is found only in the coastal plain of the Hormoz Strait.

Cluster and factor analyses of elements reveal lead and cadmium of likely anthropogenic origin, yet at concentrations lower than authorized levels in sediments. Accordingly, they present no risk to the local population. Geochemical and mineralogical evidence shows that parts of sodium, calcium, strontium, barium, and phosphorus are chemically and biochemically produced in the region, as supported by their inverse relationship to the earth elements. Shell fragments and corals contribute Ca and Sr. Other elements (Al, Fe, Cr, Co, Zn, Zr, Mn, Ti, Mg, U, Th ...) have also a clastic origin, denoting erosion of ophiolite, mélange zones and turbidites of Makran. They entered the basin as clastic carbonates and aeolian sediments. Poligorskite, in particular, reached the Makran coast through the winds coming from the western part of the Persian Gulf.

This work shows that the clastic, chemical-biochemical and anthropogenic processes influence the elements distribution of Makran coastal sediments. The local rivers and winds are the important processes controlling present-day sedimentation there.

P 6.12

Mudflats of Gulf of Kachchh Coast: Archives of Sea Level Fluctuations and Palaeo-environmental Change since Mid Holocene

Prizomwala S.P.¹, Bhatt Nilesh¹, Castelltort S.², Hirt A.M.³ & Winkler W.²

¹Department of Geology, The M.S. University of Baroda, Vadodara, India (siddharth_prizomwala@yahoo.co.in)

²Geologisches Institut, ETH-Zentrum, Zürich CH-8092, Switzerland

³Institut für Geophysik, ETH-Hönggerberg, CH-8093 Zürich, Switzerland

Gulf of Kachchh, situated in western most part of India is a macrotidal regime with a tidal range of 4m at its mouth and 11m in intrinsic creeks (Ramaswamy *et al* 2007). It hosts sand and mud dominating coastal segments along its 450km long coastline. The mouth of gulf consists of sandy landforms like beaches, dunes, beach ridges etc. whereas, the inner gulf coastline is characterised by monotonous microenvironment as mudflats (Prizomwala *et al* 2010). The mineralogical and textural analyses of coastal sediments show that the sand fraction (>63 μ) is largely derived from the Kachchh mainland fluvial systems in the north and Saurashtra fluvial systems in the south. Whereas, the finer fraction (<63 μ) has dominantly been contributed by the River Indus. The presence of mica minerals (i.e. Muscovite and Biotite) has special significance in the region as they serve as a proxy for predominant River Indus load and is useful in understanding the offshore dynamics (Prizomwala *et al* 2011). We have studied the present day erosional engine and tried to document the sediment dispersal system along the Gulf of Kachchh coast (Fig 1).

A shallow sediment record (~2m) from the mudflats was recovered by trenching and shallow pipe coring. Seven major lithounits were identified on the basis of its sedimentological character and the entire sequence was then sub-sampled at 1cm interval for further studies. The lower most unit consists of loose unconsolidated coarse sand with clasts as larger as 3cm, which could be suggestive of either a beach microenvironment or a fluvial channel. It is overlain by a sandy silt unit with organic debris that marks a transition between underlying high energy regime to the above lying massive mud unit indicative of low energy regime. The massive mud unit is rich in foraminifera tests and is bluish green in colour. It is overlain by a trough cross bedded sandy unit, again suggestive of an increased energy condition (beach microenvironment). There is a conspicuous sand layer sandwiched between mud layers above it. The sharp contact of this sand layer, assorted texture and the abraded foraminifera tests point out towards their deposition on account of a high energy event

like tsunami. Further detailed studies pertaining to the mineralogical and textural character of this sequence is warranted as it could throw light on much sparsely documented sea level change and palaeo-environmental changes in the region. The generated multiproxy dataset on the present day active processes along the Gulf of Kachchh coastline would be immensely useful in studying temporal variations in the sediment sources.

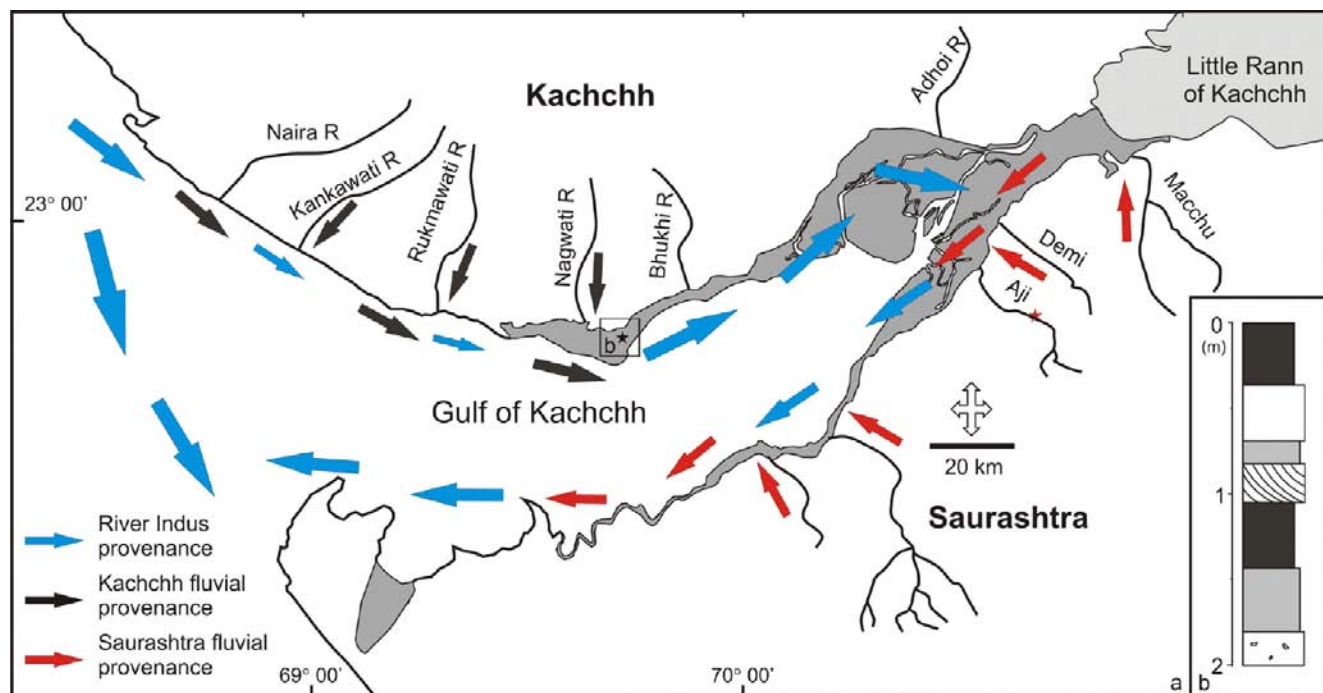


Figure 1. (a) Sediment dispersal system along the Gulf of Kachchh coast, (b) Litholog of shallow sediment sequence ~2m (black – laminated mud, gray – sandy mud and white - sand)

REFERENCES

- Prizomwala, S.P. Shukla, S.B., Bhatt Nilesh. 2010: Geomorphic assemblage of the Gulf of Kachchh coast, Western India: Implication in understanding the pathways of coastal sediments. *Zeitschrift fur Geomorphologie* 54 (1), 31-46.
- Prizomwala S.P., Shukla S.B. and Bhatt Nilesh. (in press 2011). Distribution of Indus born mica along Gulf of Kachchh coast: Implications in understanding offshore dynamics. *Journal of Geological Society of India*.
- Ramaswamy, V., Nagender, N.B., Vethamony, P., Illangovan, D., 2007. Source and dispersal of suspended sediment in macro-tidal Gulf of Kachchh. *Marine Pollution Bulletin* 54, 708-719.

P 6.13**Maximal position and retreat phase of the Reuss-Piedmont Lobe during the LGM**Regina Reber*, Naki Akçar*, Susan Ivy-Ochs², Peter W. Kubik³ and Christian Schlüchter*¹Institut für Geologie, Universität Bern, Bern, Switzerland (regina.reber@geo.unibe.ch)²Labor für Ionenstrahlphysik (LIP), ETH Zürich, Zürich, Switzerland ³Paul Scherrer Institut, c/o Institut für Teilchenphysik, ETH Höggerberg, Zürich, Switzerland

For understanding the timing of glacier retreat during Last Glacial Maximum (LGM) in the northern Alpine foreland Findlinge are sampled with regard to get surface exposure ages. With the exposure age of the Findling a minimum age for the presence of a paleoglacier at that locality can be determined. Three boulders in the lower Reuss-valley were exposure dated with cosmogenic ¹⁰Be. The study site is chronostratigraphically situated near to the terminal position of the LGM Reuss-Piedmont Lobe. ¹⁰Be exposure ages vary between 20 and 17 ka and are in good agreement with the field observations. The LGM advance is evidenced by the age of the “Kleiner Römerstein” (Reuss-22) and the “Grosser Römerstein” (Reuss-21). According the surface exposure ages of this boulders this advance was not later than around 20 ka ago. Moreover, a minimal age of a retreating stadial position is given by the exposure age of an erratic boulder located near by the “Erdmannlistein” (Reuss-20) at around 17 ka. The effect of human impact seems to be unlikely on these samples, thanks to careful choosing of sample position and general observations in field. These three boulders are comparable with boulders from the Rhone-Piedmont Lobe (Ivy-Ochs 2006) and are in good agreement with global LGM. Finally, more boulders need to be dated in order to verify the comparability of the data and to establish a clearer picture of the glaciation and deglaciation history in the northern Alpine foreland.

REFERENCES

Ivy-Ochs, S., Kerschner, H., Reuther, A., Maisch, M., Sailer, R., Schaefer, J., Kubik, P.W., Synal, H.-A., Schlüchter, C. (2006): The timing of glacier advances in the northern European Alps based on surface exposure dating with cosmogenic ¹⁰Be, ²⁶Al, ³⁶Cl, and ²¹Ne. In: Siame, L.L., Bourles, D.L., Brown, E.T. (Editors): In situ cosmogenic nuclides and their applications in earth sciences. – Geological Society of America Special Paper 415, 43–60.

P 6.14**Understanding site manipulation and destruction in prehistoric lake-dwellings**

Wiemann Philipp

Institute of Prehistory and Archaeological Science, University of Basel, Spalenring 145, CH-4055 Basel (philipp.wiemann@unibas.ch)

Lake-dwellings are well known for their remarkable preservation conditions. This applies to wooden artefacts, plant macro remains, and other organic materials. Contrastingly, features are often difficult to interpret, and cultural layers were affected by various syn- and post-sedimentary disturbances. In this study samples from Swiss Neolithic to Late Bronze Age lake-dwelling sites will be subjected to thin section analysis, in order to identify manipulating and destructive processes.

The poster gives first results from the study of the Neolithic lake-settlement of Zug-Riedmatt (Switzerland). This site has a remarkably thick (1.2 meters) highly organic stratigraphic sequence relating to the occupation(s) of the settlement, preserved by a covering of sediment several meters deep and below groundwater level. Identifiable within the organic sequence are several layers, homogenous in appearance across the site, which possibly indicate breaks in the occupation sequence. Geoarchaeological analysis suggests that these layers were deposited during low-energy inundations. This sediment type has not been identified in previous micromorphological lake-dwelling research, but a similar layer is possibly recognised at a recent lakeside excavation in Zurich.

Subsequently, such stratigraphic anomalies within the sites shall be linked to either cultural or natural phenomena. The aim of this study is to increase understanding of site formation and abandonment in lake-dwellings, in addition to assisting palaeoenvironmental reconstruction. Furthermore, it is hoped that micromorphology can be established as a site monitoring tool for the management of the lake-dwelling heritage in the future.

8. Hydrology and Sustainable Water Resources Management in View of Global Changes

Bruno Schädler, Michael Doering, Tobias Jonas, Petra Schmocker-Fackel

Swiss Hydrological Commission (CHy)

Swiss Society for Hydrology and Limnology (SGHL / SSSL)

Steering Committee NRP 61

TALKS:

- 8.1 *Bodmer P., Doering M., von Fumetti S., Robinson C.T., Nagel P.:* Respiration and microbial dynamics as indicators of floodplain heterogeneity: the alpine Urbach valley, Switzerland
- 8.2 *Brunner P., Irvine D., Hendricks Franssen H., Simmons Craig T.:* Implications of simplifying heterogeneous streambeds in models simulating surface water groundwater interactions
- 8.3 *Celio, M.:* Water management and allocation in semi-arid areas: lessons from Hyderabad water supply, India
- 8.4 *Finger D., Kauzlaric M., Jeannin P.-Y., Huss M., Wernli H.R., Schädler B., Rey E., Weber E., Hugentobler A. & Weingartner R.:* Identification Of Glacier Melt Routing Path Ways In A Karstic Environment: A Case Study Of The Glacier De La Plaine Morte
- 8.5 *Käser D., Brunner P., Renard P., Perrochet P., Schirmer M., Hunkeler D.:* How long can groundwater sustain stream flow during droughts? The influence of stream sinuosity on bank storage in alluvial plains
- 8.6 *Malard A., Vouillamoz J., Jeannin P.-Y., Eichenberger U., Weber E.:* Karst system characterization (KARSYS): a methodology for approaching the hydrogeology of karst systems in Switzerland (Swisskarst Project, NRP61)
- 8.7 *Moeck C., Brunner P., Schirmer M., Hunkeler D.:* Using high resolution lysimeter data to quantified current and future recharge rates and evaluating the uncertainty
- 8.8 *Mori N., Kanduc, T., Oz B., Brancelj A.:* Identifying ecological indicators for the alpine groundwaters in the context of future climate change: the interdisciplinary approach
- 8.9 *Rössler, O., Diekkrüger, B., Löffler, J.:* A Climate Change Impact Assessment Study on Mountain Soil Moisture with Emphasis on Epistemic Uncertainties
- 8.10 *Sideris I., Gabella M., Germann U.:* Real-time spatiotemporal combination of radar and raingauge measurements in Switzerland
- 8.11 *von Gunten D., Schaefli B.:* Modelling of Evaporation in high Alpine Catchments
- 8.12 *Zappa M., Fundel F., Jonas T., Jörg-Hess S.:* Quasi-operational estimation of water resources anomalies during the dry and wet spells of 2011

POSTERS:

- P 8.1 *Baillieux A., Moeck C., Hunkeler D.:* Effect of climatic forcing in nitrate concentration evolution of groundwater based on changing recharge rates
- P 8.2 *Diem S., Schirmer M.:* Impact of the uncertainty in river water levels on modeled groundwater residence times
- P 8.3 *Farinotti D., Usselman S., Huss M., Bauder A., Funk M.:* Hydrological changes in glacierized basins of the Swiss Alps: First attempt of a synthesis
- P 8.4 *Hänggi P., Bosshard Th., Angehrn S., Helland E., Job D., Rietmann D., Schädler B., Schneider R., Weingartner R.:* Einfluss der Klimaänderung auf die Stromproduktion der Wasserkraftwerke Löntsch und Prättigau
- P 8.5 *Oz B., Mori N., Brancelj A.:* Hydrogeological, physical and chemical differences influencing benthic macroinvertebrate communities in alpine springs of Slovenia
- P 8.6 *Vouillamoz J., Malard A., Weber E., Eichenberger U., Jeannin P.-Y.:* Swisskarst project (NRP61): Identification cards as tools for a sustainable management of karst systems.
- P 8.7 *Wirth S. B., Gilli A., Glur L., Anselmetti F. S., Magny M., Vannièrè B.:* Reconstructing the seasonality of Holocene flood events using varved lake sediments of Lake Ledro (S-Alps, Italy)

8.1

Respiration and microbial dynamics as indicators of floodplain heterogeneity: the alpine Urbach valley, Switzerland

Bodmer Pascal¹, Doering Michael², von Fumetti Stefanie¹, Robinson Christopher T.² & Nagel Peter¹

¹*Departement of Environmental Sciences, Section of Biogeography, University of Basel
St. Johans-Vorstadt 10, 4056 Basel, Switzerland (pascalbodmer@gmx.ch)*

²*EAWAG, Swiss Federal Institute of Aquatic Science and Technology, 8600 Dübendorf, Switzerland*

Natural floodplains can be considered as a heterogeneous mosaic of aquatic, semi-aquatic and terrestrial habitats, ranging from aquatic channels to terrestrial floodplain forests (Langhans et al. 2006). As such, they can serve as ideal model ecosystems to study the effects of environmental heterogeneity through different habitat properties on ecosystem processes (Tockner et al. 2010). The present study was conducted to improve the understanding of such linkages within floodplains. We investigated a 4-km long and up to 600-m wide alpine floodplain (800 m asl; Urbachtal (Büchi 1980), Innertkirchen, CH), which is characterized by a high hydrologic variability encompassing expansion and contraction as well as downwelling and upwelling dynamics. The focus of the study was two-fold: 1) Ecosystem respiration, an important process integrating the energy flow through biotic elements of aquatic and terrestrial ecosystems (Doering 2007), and 2) enzyme activities, which are responsible for the modification and remineralization of organic matter, thereby influencing its amount and composition (Sinsabaugh et al. 1991). We combined spatio-temporal assessment of habitat properties (temperature, organic matter content, grain size distribution and water content), aquatic (O₂ consumption in Plexiglas tubes) and terrestrial respiration measures (CO₂ production, IRGA) with microbial techniques (bacterial abundance by flow cytometry and enzyme bioassay) to (1) examine functional heterogeneity within the floodplain, (2) determine the main environmental drivers of respiration, and (3) find linkages between floodplain structure and function using respiration, bacterial abundance and enzyme activity data. Overall, we found high functional heterogeneity in measured habitat properties, respiration activities, bacterial abundance and enzyme activities. Lowest respiration and enzyme activities were generally measured in the harshest habitats including the river channel and exposed gravel, whereas activities were highest in more stable habitats such as alluvial forest and meadows. The main drivers of respiration were determined to be temperature and organic matter content. The results underline a tight and sensitive linkage between habitat heterogeneity and ecosystem functioning in this alpine floodplain which can serve as a framework to assess and monitor changes in floodplain ecosystems in terms of sustainable resource management or increasing environmental pressures such as from climate change or hydropower production.

REFERENCES

- Büchi, E. 1980: Geologie der autochthonen Sedimentbedeckung des Aar – Massivs im Urbachtal bei Innertkirchen. University of Bern.
- Doering, M. 2007: Environmental heterogeneity and respiration in a dynamic river corridor: Structural properties and functional performance. Diss. ETH no. 17046.
- Langhans, S.D., Tiegs, S.D., Uehlinger, U. & Tockner, K. 2006: Environmental heterogeneity controls organic-matter dynamics in river-floodplain ecosystems. *Pol. J. Ecol.* 54, 675-680.
- Sinsabaugh, R.L., Antibus, R.K. & Linkins, A.E. 1991: An enzymatic approach to the analysis of microbial activity during plant litter decomposition. *Agric. Ecosyst. Environ.* 34, 43-54.
- Tockner, K., Lorang, M.S. & Stanford, J.A. 2010: River flood plains are model ecosystems to test general hydrogeomorphic and ecological concepts. *River Res. Appl.* 26, 76-86.

8.2

Implications of simplifying heterogeneous streambeds in models simulating surface water groundwater interactions

Brunner Philip ^a, Irvine Dylan J.^{b,c}, Hendricks Franssen Harrie-Jan ^d, and Simmons Craig T. ^{b,c}

^a Centre de hydrogéologie et géothermie, Rue Emile-Argand 11, CH-2000 Neuchâtel (philip.brunner@unine.ch)

^b National Centre for Groundwater Research and Training, GPO Box 2100, Adelaide SA, 5001, Australia.

^c School of the Environment, Flinders University, GPO Box 2100, Adelaide SA, 5001, Australia.

^d Agrosphere, IBG-3, Forschungszentrum Jülich GmbH, Leo Brandtstrasse, 52425 Jülich, Germany.

A common approach in modeling surface water-groundwater interaction is to represent the streambed as a homogeneous geological structure with hydraulic properties obtained by means of model calibration. In reality, streambeds are among the most heterogeneous geological structures. Currently, no systematic analysis to quantify the implications of this modeling strategy exists. We aim to close this gap and estimate the errors associated with the simplification of the complexity of streambeds. The work builds on previous papers on the physics and the modeling of surface water groundwater interaction (Brunner et al 2009a, Brunner et al 2009b, Brunner et al 2010, Brunner et al 2011).

Using a fully coupled, physically based numerical model (HydroGeoSphere), synthetic observations of infiltration flux from a river to an aquifer were generated using heterogeneous streambeds. The streambeds themselves were constructed using geostatistical methods. These observations of infiltration flux were used to calibrate homogeneous substitute streambeds that reproduced the observation data. The calibrated models were subsequently used for predicting infiltration fluxes between the stream and the aquifer under different hydrological conditions.

An in-depth analysis of the errors revealed that two important factors determine the error in flux: In streambeds that allow for a simultaneous occurrence of both saturated and unsaturated flow the largest errors can be expected. Whether such unsaturated zones can occur in a stream-aquifer system is related to the spatial distribution of the hydraulic properties in the streambed. The second factor is related to the state of connection the observation was obtained from (e.g. connected, transitional or disconnected flow regime), and if the calibrated model is used to simulate a rising or a falling water table. Finally, we show that the maximum error in flux can often be easily estimated, even without a numerical model.

REFERENCES

- Brunner, P., P. G. Cook, and C. T. Simmons (2009a), Hydrogeologic controls on disconnection between surface water and groundwater, *Water Resour. Res.*, 45(1), W01422.
- Brunner, P., C. T. Simmons, and P. G. Cook (2009b), Spatial and temporal aspects of the transition from connection to disconnection between rivers, lakes and groundwater, *Journal of Hydrology*, 376(1-2), 159-169.
- Brunner, P., C. T. Simmons, P. G. Cook, and R. Therrien (2010), Modeling Surface Water-Groundwater Interaction with MODFLOW: Some Considerations, *Ground Water*, 48(2), 174-180.
- Brunner, P., P. G. Cook, and C. T. Simmons (2011), Disconnected Surface Water and Groundwater: From Theory to Practice, *Ground Water*, 49(4), 460-467.

8.3

Water management and allocation in semi-arid areas: lessons from Hyderabad water supply, India

Celio Mattia¹

¹ Embassy of Switzerland in India, Nyaya Marg, Chanakyapuri, 110 021 New Delhi (mattia.celio@eda.admin.ch)

Sustainable water management rests upon delicate fine tuning and orchestration of disparate fields of research and action, and is a process often frayed with latent or actual conflicts. A symbolic example is water allocation among water uses and users in water-scarce areas, that is, where water demand drifts critically close to what can be possibly supplied.

Drawing from research conducted on Hyderabad water supply (Celio et al., 2010), this contribution specifically explores the dynamics and implications of water allocation between the urban and the agricultural sectors. The city of Hyderabad, located in south peninsular India, has experienced a vibrant population growth over the last decades, and counts today a population of approximately 4 million. It is thus exemplar of the urban growth phenomenon observed in many other parts of the world, which poses tremendous challenges to municipal authorities and constantly redefines and strains rural-urban tradeoffs (on this particular aspect, see e.g. the seminal work by Swyngedouw, 2004)

From the city foundation in the late 1500s up to date, the response to Hyderabad growing water requirements fits within a generally observed pattern of urban water appropriation (see e.g. Molle & Berkoff, 2006): when local supply through withdrawals from shallow dugwells and artificially impounded water becomes insufficient to meet the growing demand, cities begin catching nearby sources and convey water via canals. Then, as demand growth outpaces supply, far located sources are tapped and/or water previously impounded and used for agricultural production is appropriated – water reallocation from agriculture to cities ensues.

The backdrop against which Hyderabad water supply has expanded and impinged upon water use in agriculture is a legal framework entirely handling over surface water (allocation) rights to the state government (Celio, 2010). While this supremacy of rights has eased the massive development of water resources during the so-called green revolution, it has actually had the opposite effect on Hyderabad. The historical reconstruction of the development of the city water supply clearly shows that the government representatives have been adverse to make any decisions regarding taking water from agriculture to meet Hyderabad needs, as such a move would have been politically risky as unpopular among farmers who make up the bulk of the electors. Thus, the increase of Hyderabad water supply was characterized by fears of negative impacts on agriculture, conflicts, party politics, and constant delays.

A research question triggered by the assumption that reallocation is harmful to farmers is: “to what extent agriculture, respectively farmers’ households, are *actually* affected by reallocations to Hyderabad”? While the mechanisms and actual development of water reallocation were studied by deciphering party politics, by retracing historical facts, and by reading through legal provisions and understanding how they translate in water rights, assessing actual impact requires a different approach and method.

First of all, a water balance was calculated for a water source shared by Hyderabad and an irrigation project (called “Nizamsagar”), so as to determine what variations in water supply to Nizamsagar could be specifically attributed to urban water supply. These variations were then translated into corresponding variations in agricultural output, notably using empirical data as crops water use, cropping patterns, and conjunctive use of groundwater in Nizamsagar command area. The study has yielded two main findings: firstly, that existing institutional arrangements – or rules – governing the daily sharing of water between Hyderabad and Nizamsagar have partially attenuated the potential negative impact on agriculture; secondly, that groundwater use in agriculture significantly compensates for the urban transfer.

The second component of the research question asked above still needs to be addressed: what does water transfer to Hyderabad entail for *farmers’ households*? Primary data collected through questionnaires interviews in Nizamsagar irrigation project show that water shortages, either brought about by withdrawals for urban supply or resulting from precipitations below average, tend to impact more heavily poor farmers located towards the tail end areas of the irrigation project. Besides being more exposed to drought as being situated the farthest from the water reservoir, these farmers are also unable to afford to pay for a borewell and thereby accessing groundwater, and only seldom rely on coping strategies as diversification of cropping patterns or shifting cropping calendars.

The plain simplicity of water pipelines easing their way through the landscape and supplying water to Hyderabad today tends to reassert engineering as being the challenge to overcome and the solution to water problems. The unfolding of Hyderabad water supply though, from its origins up to seemingly unrelated concerns as water provision to agriculture,

clearly demonstrates the multi-faceted complexity of water resources management and thereof the need to address the challenge through multidisciplinary research approach and action.

REFERENCES

- Celio, M., Scott, C. & Giordano M. 2010: Urban-agricultural water appropriation: the Hyderabad, India case. *Geographical Journal* 176(1), 39-57.
- Celio, M. 2010: More drops for Hyderabad city, less crops for farmers: water institutions and reallocation in Andhra Pradesh. In Cullet, P., Gowlland-Gualtieri, A. et al. (Eds.). *Water governance in motion – towards socially and environmentally sustainable water laws*. Cambridge University Press, New Delhi.
- Molle, F., Berkoff, J. 2006: *Cities versus agriculture: revisiting intersectoral water transfers, potential gains and conflicts*. International Water Management Institute, Colombo.
- Swyngedouw E. 2004: *Social power and the urbanization of water. Flows of power*. Oxford University Press, New York.

8.4

IDENTIFICATION OF GLACIER MELT ROUTING PATHWAYS IN A KARSTIC ENVIRONMENT: A CASE STUDY OF THE GLACIER DE LA PLAINE MORTE

Finger David ¹, Kauzlaric Martina ¹, Jeannin Pierre-Yves ², Huss Matthias ³, Wernli Hans Rudolf ¹, Schädler Bruno ¹, Rey Emmanuel ¹, Weber Eric ², Hugentobler Andreas ¹ and Weingartner Rolf ¹

¹*Institute of geography, University of Bern, Hallerstrasse 12, CH-3012 Bern (david.finger@unibe.ch)*

²*Swiss Institute of Speleology and karst-Research, P.O. Box 818, CH-2301 La Chaux-de-Fonds*

³*Department of Geosciences, University of Fribourg, Chemin du Musée 4, CH-1700 Fribourg*

Glaciers all over the world are expected to continue to retreat due to the global warming throughout the 21st century. Subsequently, future water management strategies will strongly be affected by changes in glacial melt runoff, as future water availability might become scarce once glacier area has declined below a certain threshold. Particular attention should be paid to glaciers sitting on top of the main water divide, thus providing melt water to two different mountain valleys. Predictions of such systems become even more complex, if the study site is located in a karstic environment, where significant parts of the melt water are drained through a karst system.

A typical study site of such a setting is the Glacier de la Plaine Morte, located at an elevation of 2,750 m asl, in the canton of Berne in Switzerland. The glacier covers about 9 km², and its thickness reaches up to 200 meters. The particular location of the glacier leads to meltwater runoff to the north, as well as to the south, providing both the canton of Berne and canton Valais with valuable glacial melt water. An accurate quantification of glacier melt water yields is very difficult, as a significant part of the runoff is routed through a karst system. Nevertheless, recent investigations reveal that a projection of future runoff into both valleys may be valuable for water management strategies, as climate change might mitigate vegetation, hydropower activities and subsequently the local economy.

In order to quantify the amount of runoff from Glacier de la Plaine Morte to the two regions, we performed an extensive tracer experiment, injecting three fluorescent dye tracers at three locations on the glacier and observing concentration of the tracer and discharge in major springs and rivers originating from the local karst system or directly from the glacier (Figure 1). On 22 August 2011 we injected 30kg Eosin at a north western location, 40kg Duasyn at a southern location and 12 kg Uranin at a south eastern location of the glacier. Dye tracers concentrations were monitored using automatic sampling devices, fluorimeters and active carbon filters. Altogether, we analyzed tracer concentration in over 1000 water samples at more than 20 locations north and south of the glacier.

Preliminary results indicate that during intense melt periods most of the glacier melt water is rapidly drained towards the north west of the glacier, alimending the River Simme in the Bernese Simmental (Figure 1). During the first two days of sampling we estimate that the entire amount of Eosin, about 50% of the Uranin and about 20% of the Duasyn was drained to the north east. While this result was expected for the Eosin tracer (injected in the north west), it is surprising that about half of the Uranin (injected in the south east of the glacier) traveled across the glacier to the north western surface runoff. These findings indicate that the rapid drainage system of the glacier follows primarily the thalweg at the bottom of the glacier. We expect to quantify the amount of melt water drained through the karst system by analyzing the remaining water samples. These results provide valuable insights into the structure of the Plaine Morte glacier as well as of the karst system. This is an essential contribution to the hydrological modeling activities within the MontanAqua project (NFP61).

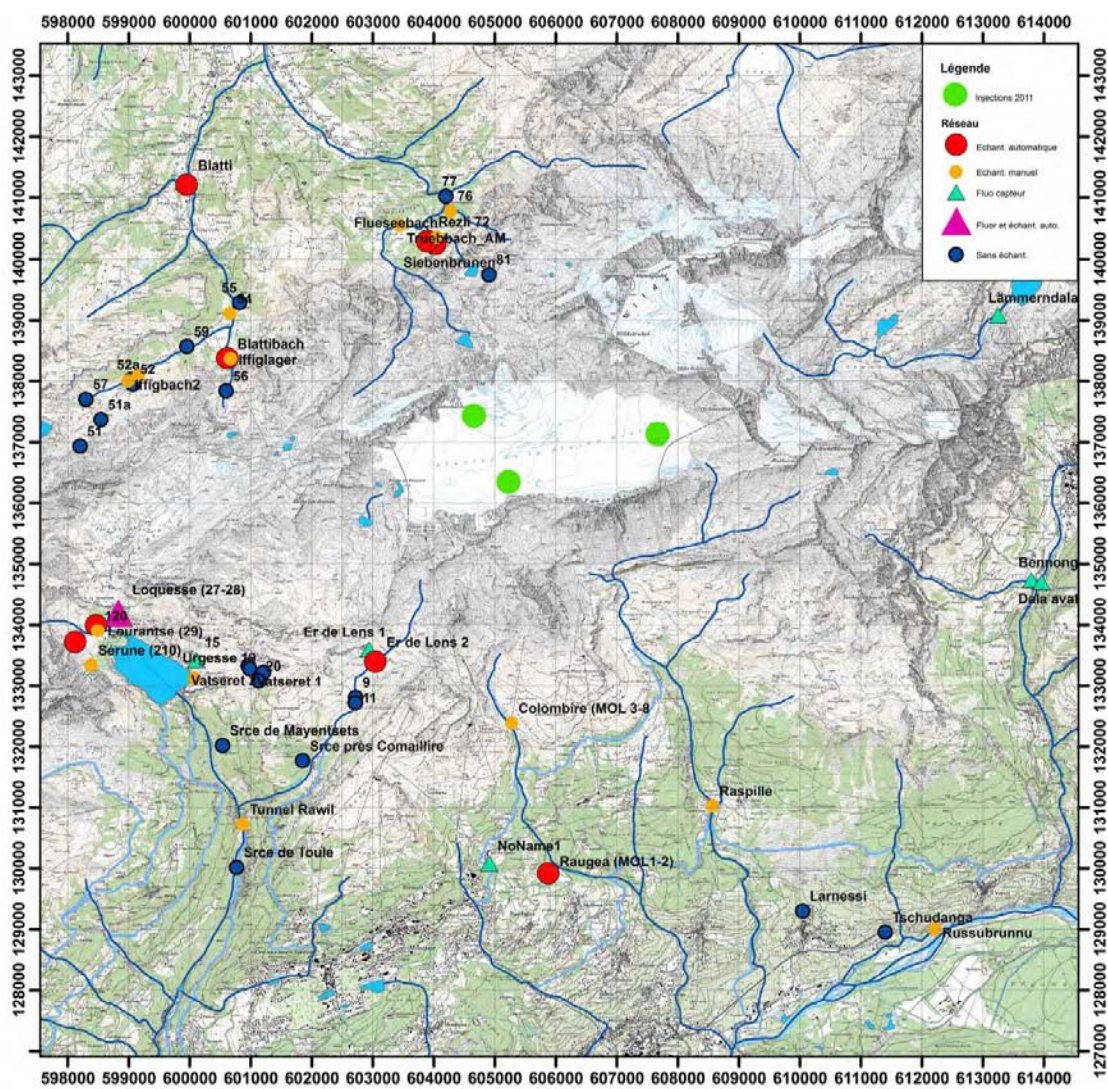


Figure 1: Glacier de la Plaine Morte and the two catchments: in the north the Bernese Simmental and in the south mountain stream in the Crans-Montana region. Symbols on the map locate sampling sites.

8.5

How long can groundwater sustain stream flow during droughts? The influence of stream sinuosity on bank storage in alluvial plains

Käser Daniel¹, Brunner Philip¹, Renard Philippe¹, Perrochet Pierre¹, Schirmer Mario^{1,2}, Hunkeler Daniel¹

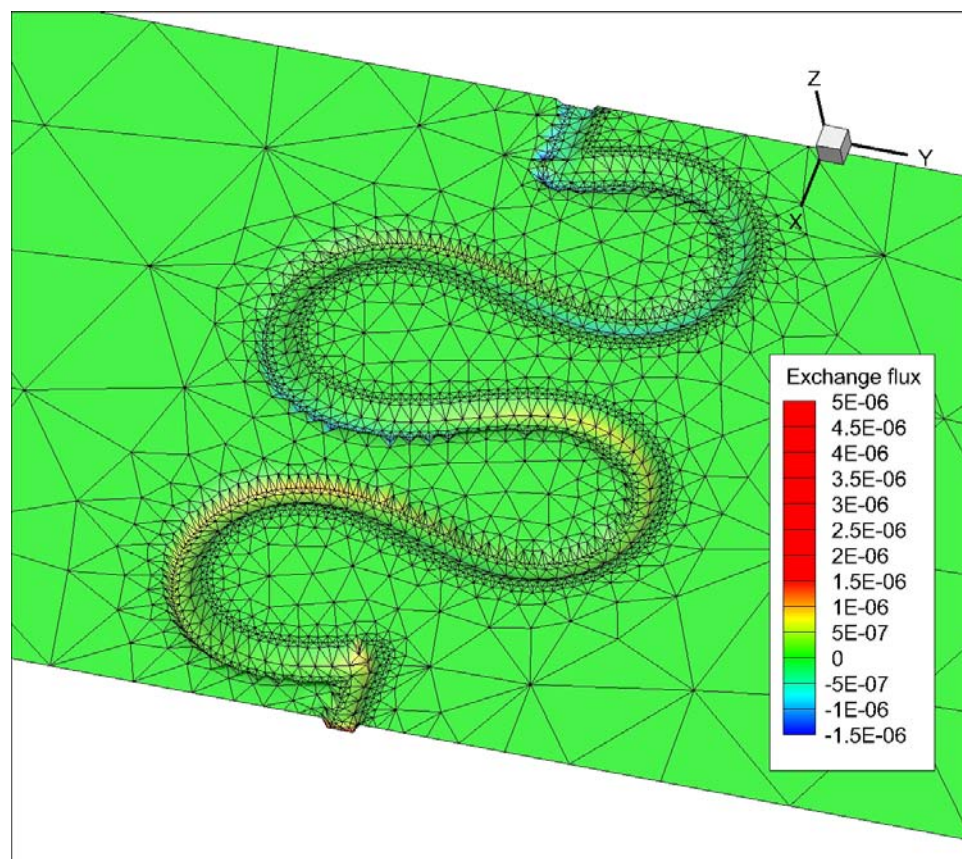
¹ Centre d'Hydrogéologie et de Géothermie de Neuchâtel, Rue Emile-Argand 11, CH-2000 Neuchâtel (daniel.kaeser@unine.ch)

² EAWAG, Überlandstrasse 133, CH- 8600 Dübendorf

In many regions, the role of groundwater during droughts is critical to sustain minimum stream flows. Among the processes that promote baseflow is the temporary storage of surface water in alluvial aquifers following high flow events. This study aims at understanding the potential significance of such bank storage in subalpine areas, where the narrow valleys imply a small surface area exposed to direct recharge by rain, but a large contact zone between groundwater and streams. This connectivity is partly controlled by the degree of meandering (or sinuosity) of the stream. Yet little is known about the influence of sinuosity on bank storage and its subsequent impact on the tail of stream recession curves. Understanding this geomorphologic control, which can be readily mapped, is likely to help improve low flow predictions.

To investigate the influence of bank storage on a stream hydrograph, we use a three-dimensional model that fully couples subsurface and surface flow (HydroGeoSphere). An idealised conceptualization of the hydrological system is used to evaluate the sensitivity of the hydrograph response to stream sinuosity.

The discussion covers an evaluation of the methodology and the quantitative relationship between sinuosity and bank storage. It addresses the following questions: how long, after peak flow, can bank storage maintain stream flow at least 5% above the steady-state flow? What are the surface and subsurface properties of an alluvial plain that can induce a significant change of a hydrograph recession curve? What is the effect of antecedent conditions, i.e., groundwater levels, on this modification? Is bank storage more sensitive to high flows of short duration (e.g. storms) or moderate flows of longer duration (e.g. snowmelt periods)? And how do these results pertain to the Swiss subalpine hydroscape?



Caption: Figure 1. Model output of a highly sinuous river and its floodplain representing the exchange flux between the stream and the aquifer. Zones of stream water infiltration are coloured in blue, and areas of groundwater discharge in red (ms^{-1}).

8.6

Karst system characterization (KARSYS): a methodology for approaching the hydrogeology of karst systems in Switzerland (Swisskarst Project, NRP61)

Malard Arnaud¹, Vouillamoz Jonathan¹, Jeannin Pierre-Yves¹, Weber Eric¹, Eichenberger Urs¹

¹Swiss Institute of speleology and karstology, Rue de la Serre 68, CP 818, CH-2300 La Chaux-de-Fonds

Karst hydrological systems are characterized by a highly heterogeneous structure including quick- and slow flow components (conduit network, phreatic and epikarstic storage). This induces an important hydrodynamic variability and complex flow dynamics. Furthermore, regional characteristics of karsts aquifers in Switzerland are poorly documented and a synthetic overview of karstic resource does not exist yet. This situation is not satisfactory and the management of karst water resources is far from being optimal. In the framework of the SWISSKARST Project, the Swiss Institute of Speleology and Karstology (SISKA) developed a methodology for approaching karst systems in their geometries and behaviours at the scale of Switzerland: This methodology has been called KARSYS for KARst SYStem Characterization. This approach combines several general characteristics of karst media with regional aspects leading to a pragmatic 3D conceptual model of a karst system. This model depicts systems boundaries, catchment areas, the aquifer basement, the location and extension of groundwater bodies and their boundaries in high water stage. Results of this approach are presented as Identification Cards for each main karst system, including hydrogeological karst maps (based on a new mapping methodology), 3D views, a basic data-base and a series of attachments (typically literature). Details on ID cards are presented in a separate paper (DEMARY *ET AL.* (2011)). Another part of the SWISSKARST project is dedicated to the development of a pragmatic hydrological modelling tool for the simulation of karst spring discharge from precipitation data. This part is presented in a separate paper (WEBER *ET AL.* (2011)). Application of this applied methodology cover a wide range of water uses and land uses as water supply, management (tunnel, dam,...), renewable energies (evaluation of power production potential or geothermic), natural hazards prediction,...

The present abstract focuses on the KARSYS part of the project. The first step of the KARSYS method consists in identifying all significant karst systems of a region by recognizing major springs through any kind of information such as the spring inventory of cantons, the existing literature, field campaigns or interviews of people knowing concerned region. Then, an iterative approach is applied, aiming at building a geological and hydrogeological conceptual model of karst systems. In this purpose, a 3D-geological model is assembled first, giving the framework for a hydrogeological model. This model describes the geometry of karst aquifer boundaries, of all major springs, and of karst groundwater bodies (assuming that the aquifer is saturated under the spring level). The respective catchment areas can be derived from this model. They usually considerably differ from topographic recharge areas, as they would be delineated in surface hydrology. This model also makes it possible to assess the main underground flowpaths. Data from tracing experiments can also be integrated into the model as a control. It appears frequently that application of KARSYS leads to identify water exchange between adjacent karst systems depending on the water table fluctuations. This methodology is therefore relevant to show the boundaries of systems and their interactions.

KARSYS was applied to the whole Vaud canton (2 822km²) in 2010 and is now extended to the Bern and Fribourg cantons demonstrating that the KARSYS method is applicable and provides much of meaningful information. Results can be viewed on the evolutionary SWISSKARST website: www.swisskarst.ch.

The KARSYS documentation approach of karst systems is an important step for a sustainable management of karst waters and it represents a necessary base for any further step including modelling of water quantity, regime, quality, or the assessment of global change on resources.

REFERENCES

- Demary, S., Vouillamoz, J., Eichenberger, U., Weber, E. & Jeannin, P. (2011): Identification Cards of karst systems as tools for a sustainable management of karst systems. , , .
- Weber, E., , Jordan, F., , Jeannin, P. Y., , Vouillamoz, J., , Eichenberger, U., , Malard, A. (2011): Swisskarst project (NRP61): Towards a pragmatic simulation of karst spring discharge with conceptual semi-distributed model. The Flims case study (Eastern Swiss Alps). , , .

8.7

Using high resolution lysimeter data to quantified current and future recharge rates and evaluating the uncertainty

Moeck Christian¹, Brunner Philip¹, Schirmer Mario², Hunkeler Daniel^{1,1}

¹ Centre de hydrogéologie et géothermie, Rue Emile-Argand 11, CH-2000 Neuchâtel (christian.moeck@unine.ch)

² Eawag, Überlandstrasse 133, CH- 8600 Dübendorf

Groundwater recharge is the key parameter for sustainable water resources management. However, quantifying its spatial and temporal distribution is difficult, because infiltration is affected by soil types and the presence of vegetation. Different soil types have a profound influence on how precipitation relates to groundwater recharge. The task is further complicated through climate change: The effect of climate change on groundwater recharge is still poorly understood.

Numerical models are an important tool in quantifying groundwater recharge. Typically, water flow and transport is simulated in 1-D models. Unfortunately, these models require a high number of parameters, which are difficult to measure. For example, water retention curves that describe the relation between saturation, matrix potential and hydraulic conductivity are required, yet their measurement in the laboratory is expensive and time-consuming. Pedotransfer functions are an alternative to direct measurements, but their reliability is highly questionable. Alternatively, the required parameters are calibrated to fit a set of available observations. However, in many cases only a few observations with low spatial and temporal resolution are available. Therefore, the unknown model parameters cannot be calibrated uniquely, resulting in large uncertainties associated with prediction.

In this project a large amount of high quality data through the lysimeter facility AGROSCOPE in Reckenholz is available to calibrate 1D soil column models. Data from 3 types of soils found in Switzerland are at our disposition. Data measured include deep drainage, evapotranspiration, as well as soil moisture and matrix potential at different depths. For the calibration of unknown parameters we use PEST, a model independent parameter estimation and uncertainty analysis program in combination with the numerical model HydroGeoSphere. Due to the quality and amount of observations, we expect to lower our uncertainty related to predictions significantly.

We use the calibrated models for the different soil types, in order to predict the effects of climate change on groundwater recharge for the main soil types in Switzerland. Additionally, we provide methodological insights into methods to quantify recharge. For instance, the relationship between temporal and spatial availability of observations and predictive uncertainty of the model will be investigated. These results will enable us to provide guidance on the required level of model complexity, amount and type of observation data required for future studies.

8.8

Identifying ecological indicators for the alpine groundwaters in the context of future climate change: the interdisciplinary approach

Mori Nataša^{1,2}, Kanduč Tjaša³, Oz Basak⁴, & Brancelj Anton¹

¹National Institute of Biology, Večna pot 111, SI-1000 Ljubljana (natasa.mori@nib.si)

²EAWAG, Überlandstrasse 133, CH-8600 Dübendorf

³Jozef Stefan Institute, Jamova 39, SI – 1000 Ljubljana

⁴University of Nova Gorica, Vipavska 13, SI-5000 Nova Gorica

Despite the fact that Alps are extremely rich with water, the increase in temperatures and redistribution of precipitations due to climate change together with the human overuse presents the serious threat for the water reserves. Within the EU project Alp-Water-Scarce (Water Management Strategies against Water Scarcity in the Alps, 2008-2011) several concurrent studies across Alpine countries have been carried out to characterize the hydrological systems and develop water management strategies against water scarcity. In the study from Slovenia an attempt was made to ecologically characterize and assess the vulnerability of the alpine aquifers combining hydrogeochemistry and faunistic surveys using springs as an ac-

cess points to the groundwater. Additionally, we tried to develop simple indicators for the rapid detection of significant decreases in groundwater levels.

Water from 12 springs located in the alpine region in Slovenia (Figure 1) was collected during high and low flows in 2009 and 2010 in order to carry out geochemical analyses (anions, cations, $\delta^{13}\text{C}_{\text{DIC}}$, $\delta^{13}\text{C}_{\text{POC}}$, $\delta^{18}\text{O}$, δD , tritium). Concurrently, discharge, temperature, oxygen and pH were measured, and invertebrates drifting from the aquifer and inhabiting springs were sampled.

The groundwaters studied represent waters strongly influenced by chemical weathering of Mesozoic limestone. The $\delta^{13}\text{C}$ of DIC ranged from -15.8‰ to -1.5‰ and indicated less and more vulnerable aquifers. Isotopic composition of oxygen ($\delta^{18}\text{O}_{\text{H}_2\text{O}}$), and tritium values range from -12.2 to -9.3‰ , and from 6.4 to 9.8 TU, indicate recharge from precipitation. The age of spring waters were estimated to be from 2.6 to 5.1 years. The invertebrates collected differed between the hydrogeological units identified by hydrological and geochemical measurements indicating to be a good predictor of aquifers hydrogeological characteristics. Moreover, the number of invertebrate species and their densities were significantly higher in 2009 than in 2010 which was a "dry" year by means of precipitation in comparison to 2010. It seems that lowering of groundwater water table stimulate more intense drifting of groundwater invertebrates. Hence, the monitoring of invertebrate drift from springs can be a useful tool to assess the level of stress in groundwater ecosystems due to decreasing water levels.

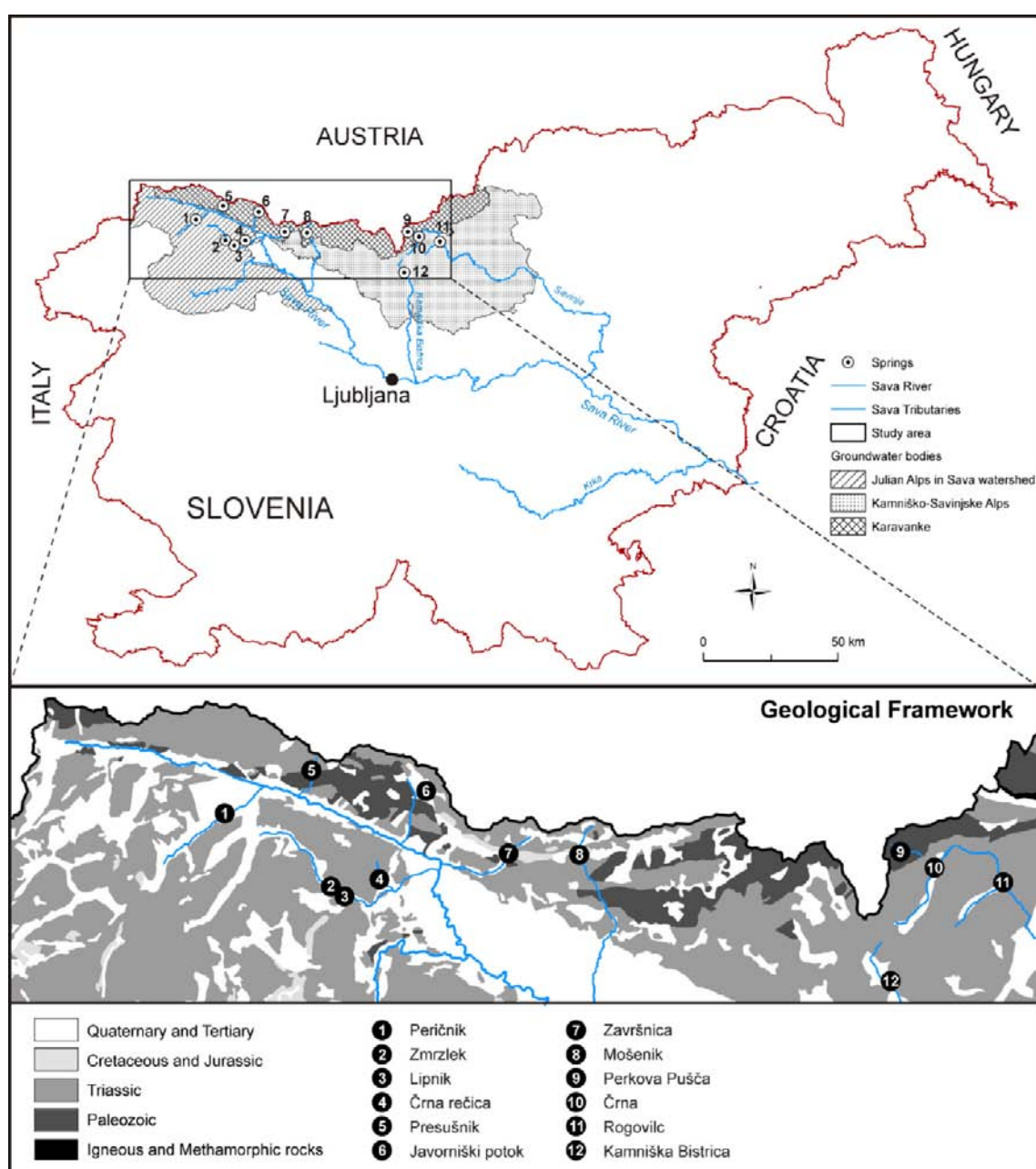


Figure 1. The map of the study area with geological settings and sampling locations.

8.9

A Climate Change Impact Assessment Study on Mountain Soil Moisture with Emphasis on Epistemic Uncertainties

Rössler Ole^{1,2}, Diekkrüger, Bernd², Löffler, Jörg²

¹Oeschger Centre for Climate Change Research, Institute of Geography, Uni Bern, Hallerstrasse 12, 3012 Bern

²Department of Geography, University of Bonn, Meckenheimer Allee 166, 53115 Bonn, Germany

Mountains are expected to respond sensitive to climate change. Thus, sound climate change impact assessment studies focusing on mountain areas are strongly needed to estimate changes and to develop adaptation strategies. Nowadays, climate change impact assessment studies (CCIAs) are a common approach and many publications on hydrological responses to climate change have been published. Nonetheless, CCIAs focusing on soil moisture are widely missing especially at the catchment scale; even more, as to our knowledge there are only two studies on mountain soil moisture at a coarse scale. The wide neglect of soil moisture in climate change impact assessment studies contrasts the key role of soil moisture in ecosystems. This clearly shows the strong demand for CCIAs on mountain soil moisture. In this study, a commonly used CCIAs approach was used, comprising (1) of a physically based model that was calibrated and validated under recent climate conditions, (2) that was driven by downscaled regional climate models (RCMs) for a reference and a future scenario climate conditions. A major challenge in CCIAs is the propagation of uncertainties that questions the model results. In this study a special focus is set on the structural uncertainties originating from the use of downscaling approaches and climate models. Therefore, an analytic framework was developed based on the both concepts of uncertainty propagation and the uncertainty cascade. The concept comprehensively summarizes all uncertainties occurring in climate change impact assessment studies and illustrates how the uncertainties propagate. We conducted the CCIAs in a mountain catchment (160 km²) in the Swiss Alps at a high spatial resolution (50m). At first, the frequently used, physically based, distributed hydrological model was successfully applied to the catchment for recent years (2001-2007) to provide a sound calibration and validation. The potentials and the limitations of WaSiM-ETH to simulate soil moisture dynamics and patterns were shown by comparing model results with extensive soil moisture measurements at an hourly time step. While WaSiM-ETH was able to reproduce discharge with a high accuracy ($R^2 = 0.95$, $ME = 0.8$, $IoA = 0.95$), the simulation of soil moisture for different altitudes and land use types is partly limited, since the model was unable to model the total variability of the soil moisture dynamic, but tended to mean values. An adjusted RMSE of 8.0 Vol-% that takes the intra-plot variability into account was calculated for soil moisture. A necessary prerequisite is the validation of the ability of the downscaled RCM data to drive the hydrological model in such that the hydrological processes are reproduced. A comparative study was conducted based on two common downscaling approaches (statistical downscaling (SD) and direct use (DU)) and two RCMs (CHRM, REMO). Uncertainties were found to be unsteadily distributed, both in terms of variables and time. The "one" model approach that shows least uncertainty for all kinds of hydrological variables like discharge, actual evapotranspiration, and soil moisture was not found. This finding adds considerable value to the scientific discussion, since most previous studies focus on one variable or one downscaling approach alone. In addition, we evaluated the spatial uncertainties of soil moisture and evapotranspiration. We showed that the choice of downscaling approaches is of circumstantial relevance for discharge and water balance, while for all spatial variables, we found SD approaches to perform better than DU approaches. Next, we simulated the impact of climate change on mountain soil moisture by applying three different downscaling approaches and two RCMs. In addition to the SD and DU-models, the very popular delta change approach (Δ) was applied that scales the climate observation by adding the climate signal. Therefore, uncertainty assessment for the Δ -approach was not necessary. The use of multiple downscaling techniques in an ensemble forecast is new for soil moisture impact studies. The study proved the partly superior role of downscaling approaches when focusing on the impact per se under future climate and thereby contrasting findings of recent publications. Moreover, it questions results from studies that are based on one downscaling approach alone. The study provided detailed data on climate change impact on the hydrology of the catchment that are completely in line with previous findings. The high spatio-temporal resolution of the study add value to previous mountain soil moisture studies of Jasper et al. (2004, 2006) by providing site specific data on soil moisture decrease and drought stress potential at the catchment scale. The consensus of six models driven by two threefold downscaled RCM reveals the forested areas below 1800 m a.s.l. to be most affected by climate change in 2070- 2100 (-10 vol-%). The variability of the results from the six ensembles were remarkably high, offering a bandwidth of possibilities from nearly unchanged soil moisture conditions to strong expansion of drought stress in the future. In addition we found uncertainties from the applied hydrological model and downscaling approaches in the magnitude of the predicted changes (+/- 10 vol-%). Therefore, the results have to be interpreted carefully. Probabilistic forecasting with several hundred model runs might confirm the found tendency of soil moisture decrease in future studies.

8.10

Real-time spatiotemporal combination of radar and raingauge measurements in Switzerland

Sideris Ioannis¹, Gabella Marco¹ & Germann Urs¹

¹MeteoSwiss, Stabile La Ferriera, Via Luini 12, CH-6600 Locarno (Ioannis.Sideris@meteoswiss.ch)

Merging raingauges and radar measurements to produce high quality rainfall fields has been a central problem in quantitative precipitation estimation. Although it has been attacked before (for instance see [1:10]) there is still demand for increased reliability, faster speed, and higher spatiotemporal resolution naturally motivating additional high-end improvements. Ideally one wants to produce reliable precipitation maps having the same spatial and temporal resolution as the corresponding radar cartesian composite. In the case of Switzerland this resolution is 1km² every 5 minutes. This presentation will describe techniques that indeed achieve such resolutions.

This work is part of project within MeteoSwiss which originated in 2009 and expected to be completed in 2012. Although real-time radar-derived precipitation maps have been existed in Switzerland for several years, the main goal of this project is the radar-raingauge adjustment of such maps. The context of this effort can be easily be recognized. Floods are not infrequent natural phenomena. In a real-life scenario it is critical for hydrological and meteorological models to be supplied as soon as possible with high quality, high spatiotemporal resolution precipitation maps.

Our algorithmic design has been constructed with such needs in mind. While most radar-raingauge schemes employ only spatial information, our technique does incorporate both spatial *and* temporal information. Time is introduced through co-krigged variables into a geostatistical scheme, leading to consistent improvements in the produced precipitation maps.

The involved complications in merging techniques are usually as complex as unavoidable: limited information by typically small numbers of real-time raingauges measurements, but also effects like topographic obstructions of the radar beam, common in the alpine regime, come easily to mind: efficient use of any correlated information such as temporal is of importance. Moreover, an operational-mode merging tool owes to be fully automatic ready to treat highly variable meteorological conditions without the need of any human intervention. This requires well-thought decisions in advance of the precipitation event. A continuous and focused effort has also been exercised by our team towards this direction. Our system has already been verified for extensive time-periods and a number of events and presents significant and consistent improvements over the existing maps.

REFERENCES.

- Koistinen, J., and T. Puhakka, An improved spatial gauge-radar adjustment technique, in Preprints of the 20th Conference on Radar Meteorology, Boston, MA, Amer. Meteor. Soc., 179-186, 1981.
- Krajewski, W.F., Cokriging Radar-Rainfall and Rain Gage Data, Journal of Geophysical research, 92, 9571, 1987.
- Creutin, J.D., Delrieu, G., and Lebel, T., Rain measurement by raingage-radar combination: a geostatistical approach, Journal of atmospheric and oceanic technology, 5, 102-114, 1987.
- Seo, D., Krajewski, W.F., Bowles, D.S., Stochastic interpolation of rainfall data from rain gages and radar using cokriging. 1. Design of experiments, Water Resources Research, 26, 469-477, 1990.
- Gabella M., Joss J., Perona G., Optimizing quantitative precipitation estimates using a non-coherent and a coherent radar operating on the same area, J. of Geophys. Research, 105, 2237-2245, 2000.
- Gabella, M., Notarpietro, R., Improving Operational Measurement of Precipitation Using Radar in Mountainous Terrain, IEEE Geoscience and Remote Sensing Letters, 1, 1545, 2004.
- Germann U, Galli G, Boscacci M, and M. Bolliger, Radar precipitation measurement in a mountainous region, Q. J. Roy. Meteor. Soc., 132, 1669–1692, 2006.
- Salek, M., Novak, P., Experience gained by five years of the utilization of the radar-based quantitative precipitation estimation at the Czech Hydrometeorological Institute, ERAD, 2008.
- Velasco-Forero, C.A., Sempere-Torres, D., Cassiraga, E.F., Gomez-Hernandez, J.J., A non-parametric automatic blending methodology to estimate rainfall fields from rain gauge and radar data, Advances in Water Resources, 32, 986-1002, 2009.
- Erdin, R., Master Thesis, ETH, Zurich, 2009.

8.11

Modelling of Evaporation in high Alpine Catchments

von Gunten Diane¹, Schaefli Bettina²

¹IACETH, Universitätsstrasse 16, 8000 Zürich and Laboratory of Ecohydrology (ECHO), School of Architecture, Civil and Environmental Engineering (ENAC), Ecole Polytechnique Fédérale de Lausanne (EPFL), Station 2, 1015 Lausanne (dvgunten@student.ethz.ch)

²Laboratory of Ecohydrology (ECHO), School of Architecture, Civil and Environmental Engineering (ENAC), Ecole Polytechnique Fédérale de Lausanne (EPFL), Station 2, 1015 Lausanne (bettina.schaefli@epfl.ch)

In Alpine catchments, evapotranspiration is a small part of the water balance (around 10% of precipitation, Lang, 1981). Accordingly, it is often neglected or very much simplified in glacio-hydrological models used to predict discharge. However, in the context of ongoing climate change, a better understanding of all water fluxes, including namely evaporation, seems essential to make reliable predictions of the future water balance. Indeed, global temperatures are expected to increase in the next century, and because evaporation is linked to temperature and radiation, it will probably increase in future. Furthermore, since glaciers are currently retreating, there is an increase in vegetated area and bare ground, which is likely to result in increasing evapotranspiration. In addition, total discharge of alpine catchments might decrease, which would increase evaporation importance. These changes might affect the water balance of Alpine catchment in a significant way and a more precise modelling of evaporation might become necessary.

In this context, the aim of this Master thesis research is to model evaporation in Alpine catchments and to estimate its real importance in a changing climate. Based on field measurements on Swiss glaciers, we first model ice evaporation and condensation from alpine glaciers and estimate its importance in future climates (Huss et al., 2008). We then use a classical Penman-Monteith approach to calculate potential evaporation from moraines, rocks and vegetation. These results are used in a hydrological simulation of the Rhone catchment (Switzerland) to estimate impacts of evaporation on discharge.

The main results of this study are that evaporation and condensation from glaciers are not likely to have an important impact on alpine discharge today or in the future. Indeed evaporation and condensation increase in a warmer climate but glacier area decreases. As a result, ice evaporation is higher but on a smaller area. Accordingly it has a similar impact on the total water balance in all climates.

However, impact of evaporation of the total catchment (rock, moraine and vegetation) could be more important than today in a warmer climate as shown in figure 1. The main reasons for this higher importance are discharge reduction, glacier retreat and reduced snow cover in our simulation. Potential evaporation is highly uncertain but has a low impact on the overall result. Transferability of these results to other models or other catchments is not known yet.

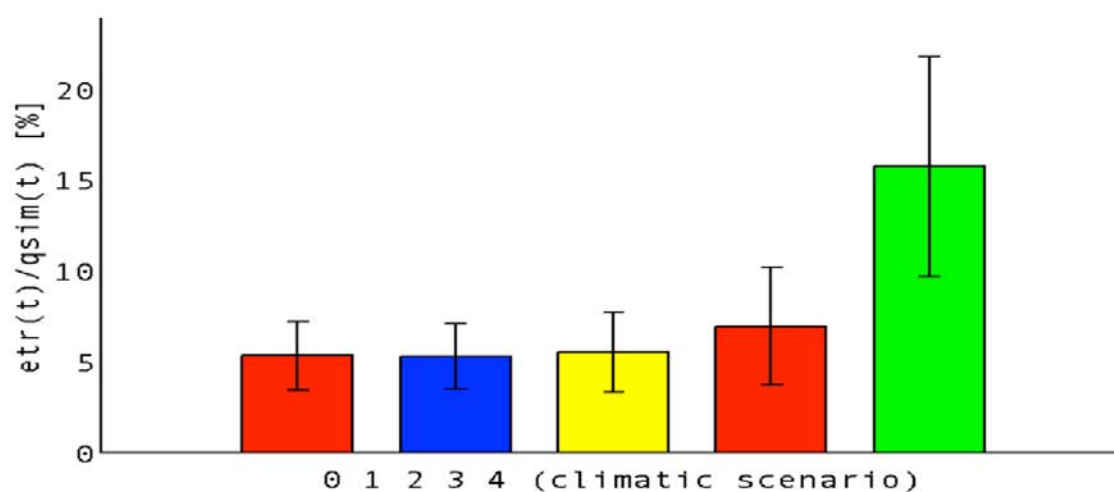


figure 1: evaporation divided by discharge in various climatic scenarios (0: actual climate, 1: wet climate, 2: median climate, 3: warm and dry, 4: small glacier - Huss et al., 2008)

REFERENCES

- Barnett T., J.Adam, and D. Lettenmaier, 2005: Potential impacts of a warming climate on water availability in snow-dominated regions. *Nature*, 438:303–309
- Lang H., 1981: Is evaporation an important component in high alpine hydrology? *Nordic Hydrology*, 12:217–224.
- Oelermans J. and E.J.Klok, 2002. Model study of the spatial distribution of the energy and mass balance of Morteratschgletscher, Switzerland. *Journal of Glaciology*, 48
- Schaepli B. and M. Huss, 2011: Integrating point glacier mass balance observations into hydrologic model identification. *Hydrology and Earth System Sciences*, 15:1227–1241
- Huss M., D. Farinotti, A.Bauder and M.Funk, 2008: Modelling runoff from highly glacierized alpine drainage basins in a changing climate. *Hydrological Processes*, 22:3888-3902

8.12

Quasi-operational estimation of water resources anomalies during the dry and wet spells of 2011

Massimiliano Zappa¹, Felix Fundel¹, Tobias Jonas² & Stefanie Jörg-Hess¹

¹ Swiss Federal Research Institute WSL, Zürcherstrasse 111, CH-8903 Birmensdorf, (massimiliano.zappa@wsl.ch)

¹ Swiss Federal Research Institute SLF/WSL, Flüelastrasse 11, CH-7260 Davos Dorf

During the last few years numerous research initiatives concerning climate impacts on water resources have been going on. Hydrological models have been applied to estimate current and future spatial and temporal availability of water resources in different areas of Switzerland and the European Alps.

In parallel large efforts have been allocated to the development and operational application of hydrological ensemble prediction systems, with focus on floods.

WSL has been active in all these fields and is now testing opportunities of combining the outcomes of climate impacts studies with operational forecasting. The goal is to establish a system for the early detection of anomalies in the temporal and spatial availability of water resources in Switzerland.

To this end the FOEN CCHydro Project water resources climatology for the control period 1980-2009 and probabilistic scenarios (10 members) for two 30-years periods in the future (2021-2050 and 2070-2099) have been created.

From the NRP61 project DROUGHT-CH tools are in preparation for the assimilation of snow water equivalent information for improving the prediction of water resources availability with lead times of up to 1 month. First simulation re-forecast experiments for the basins Thur and Alpine Rhine have been realized. In the presentation we will focus on the forecasts of the summer 2003 drought and the 1999 flood.

Finally, the experience obtained since 2007 with the operational implementation of the hydrological model PREVAH for probabilistic flood forecasts has been transferred to an early prototype focusing on the estimation of water resources anomalies.

A first demonstration period in April to June 2011 in the Thur river basin shows that in the first part of April a large deficit with respect to the 1980-2009 period on water availability was mostly caused a deficit in the snow resources. In the following weeks different situations occurred:

- At the begin of May a deficit of about -90 mm with respect to the median of the climatology (that means << 2.5% percentile with respect to the climatology) in the total water resources can be attributed to the deficit in snow (-20 mm), soil moisture (-50 mm) and “groundwater” (-20 mm) storages.
- At the begin of June a deficit of about -50 mm (~10% percentile) in the total water resources can be attributed to the deficit in snow (-10 mm), soil moisture (-35 mm) and “groundwater” (-15 mm) storages.

- At the begin of July the deficit is reduced to -10 mm (~45% percentile) .
- On July 18 a surplus of +30 mm (~75% percentile) is found after longer wet conditions. The surplus is owed to soil moisture (+17 mm) and “groundwater” (+7 mm) storages. Further surplus is split into the interception storage and the storage allocated by the model for generation of surface runoff and interflow.
- After further rainy days on August 8 a surplus of +40 mm is found (>97.5 percentile).

On August 21 2011 (Figure 1) the initial conditions indicate a small surplus of +7 mm in the total water resources in the Thur river basin, as compared to climatology. As compared to August 15, more than 40 mm surplus have been dissipated, mostly by evapotranspiration. Forecasts for the next 5 days indicate high probability of further reduction in the available resources. There is a 50% chance that on August 27 2011 the deficit will be of about -20 mm. Such deficit would result from a surplus of +5 mm in the “groundwater” storage and a deficit of -25 mm in the simulated soil moisture storage. However, the ensemble indicates, that there is also a small chance that five on August 27 the basin would have a surplus of +10 mm.

The presentation will end with some visions on possible further developments of this experimental system and its use for decision making for issues related to early detection of critical anomalies in the availability of water resources in Switzerland.

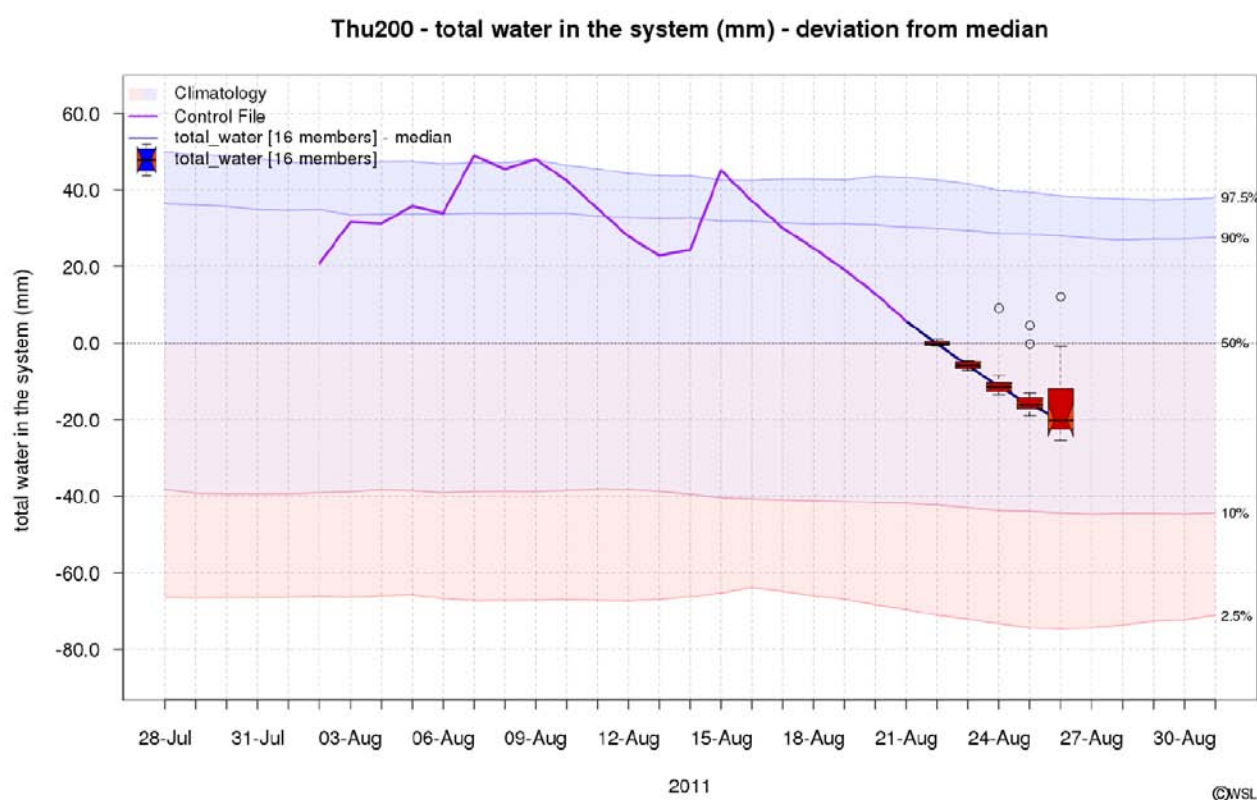


Figure 1. August 21 2011: Climatology (colour areas in the background) and current simulation (pink line and boxplots for COSMO-LEPS based numerical weather forecasts) of total water resources available in the Thur river basin. We plot the current deviation of the simulations from the climatology related to the period 1980-2009. Values above zero are sign of surplus, values below zero represent deficits. Research grants from: **CCHydro** (FOEN) and **Drought-CH** (NRP61).

P 8.1

Effect of climatic forcing on nitrate concentrations in groundwater based on changing recharge rates

Baillieux Antoine¹, Moeck Christian¹, Hunkeler Daniel¹

Centre d'Hydrogéologie et de Géothermie, Rue Emile-Argand 11, CH-2000 Neuchâtel (antoine.baillieux@unine.ch)

Climate changes can have an impact on the sustainability of groundwater resources not only in terms of groundwater quantity but also groundwater quality. For example after the dry period of 2003–2005 a significant increase of nitrate concentrations was observed at many public pumping wells of Switzerland (OFEV 2009).

In this study we present a simple approach to reproduce recent nitrate concentration trends and recharge rates and to estimate future trends under different climatic conditions. The aquifer of Wohlenschwil (canton of Aargau, Switzerland), where land use change are known since 1997, is taken as a case study site (Figure 1).

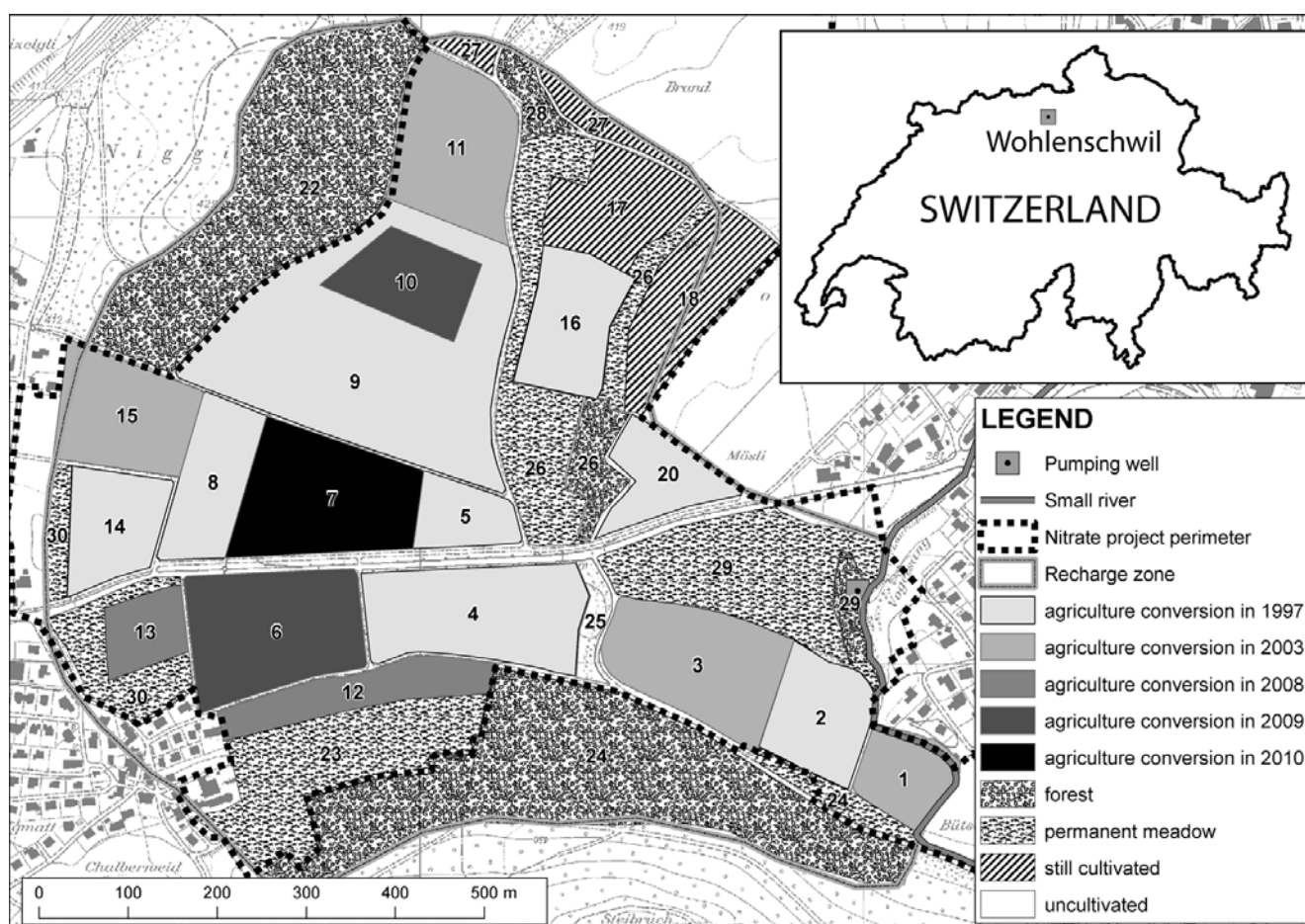


Fig. 1 Catchment area of the Wohlenschwil pumping well and land use changes

In a first step a numerical 1D soil column model estimates the recharge rates based on soil water content observations in different depth. Current recharge rates are compared with results from tracer tests in the unsaturated zone. Then groundwater recharge rates for future climate conditions are quantified using a delta change approach to estimate future temperature and precipitations trends.

In a second step a transfer function approach (Jury & Roth 1990) is applied to estimate the evolution of nitrate concentrations at the pumping well. For each subarea of the catchment with uniform land use (Figure 1), nitrate concentrations in recharge water were estimated based on culture-specific nitrate leaching rates and the estimated annual recharge rate. So far, the proposed approach does not take into account other changes in the nitrate leaching dynamics which could also be influenced by climate change (particularly modification of soil processes and crop productivity) (Stuart & al 2011).

Calculated nitrate concentrations for the period 1997-2010 agree well with the observed concentrations at the pumping well (Figure 2). With this approach it is possible to distinguish the change in nitrate concentration due to variations of recharge rates or due to land use changes. For instance in Wohlenschwil, about 5 mg/L of the nitrate concentration increase during the period 2005–2008 can be attributed to the decrease of recharge in the period 2003–2005 (Figure 2). The same approach can be used to evaluate the effect of climate change on future groundwater recharge rates and the evolution of the nitrate concentration.

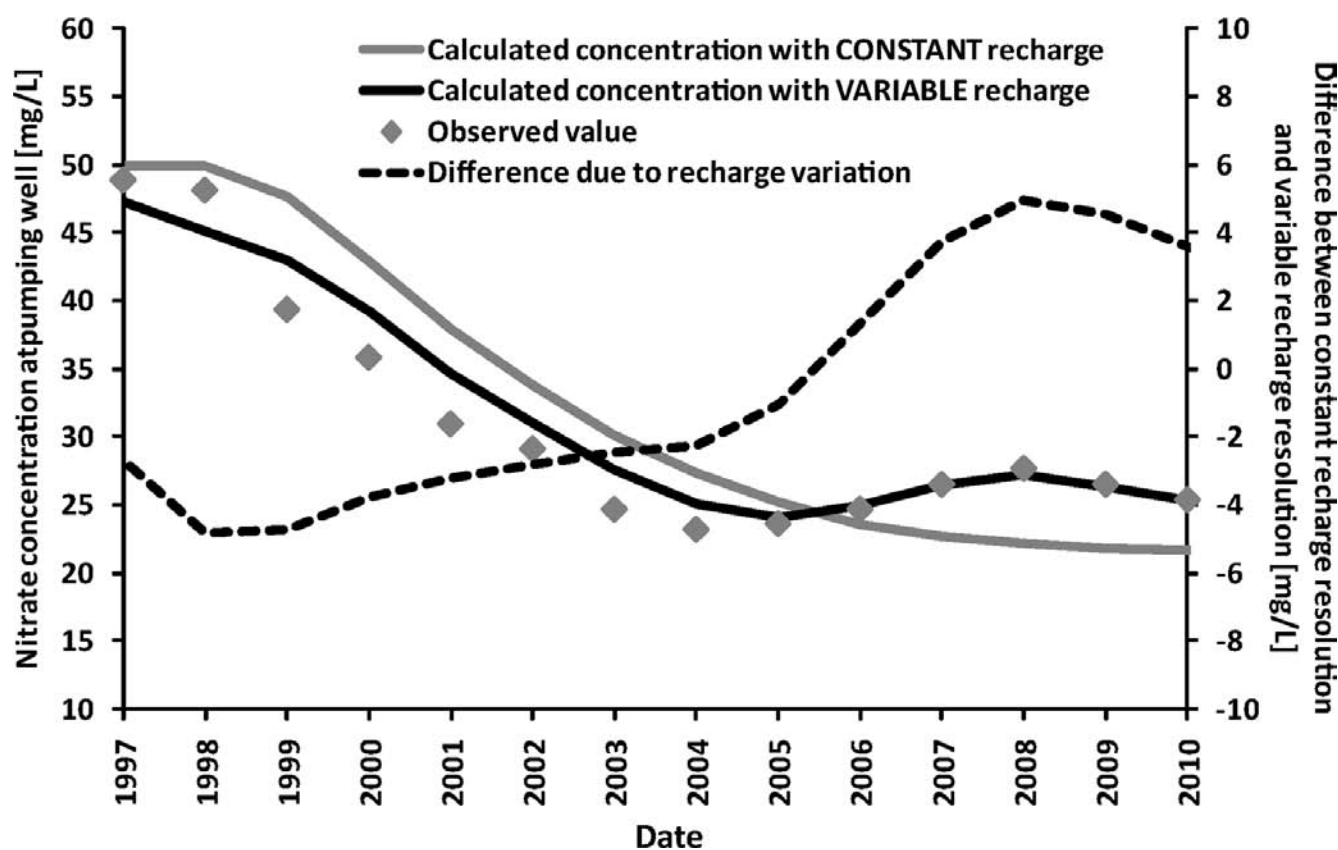


Fig. 2 Observed (grey triangles) and calculated (black line) evolution of the nitrate concentration at the pumping well of the Wohlenschwil aquifer considering annual variations of recharge rates for the period 1997 – 2010. A comparison with results computed with a constant mean annual recharge (grey line) reveals the effect of varying recharge rates on nitrate concentrations (dashed line).

REFERENCES

- Jury, W. A. & Roth, K. 1990: Transfer Function and Solute Movement through Soil: Theory and Applications. Birkhäuser Verlag, Basel, 228 p.
- OFEV 2009: Résultats de l'observatoire national des eaux souterraines (NAQUA) - Etat et évolution de 2004 à 2006. Etat de l'Environnement, Office Fédérale de l'Environnement, Berne, 144 p.
- Stuart, M. E., Goody, D. C., Bloomfield, J. P. & Williams, A. T. 2011: A review of the impact of climate change on future nitrate concentrations in groundwater of the UK. Science Of The Total Environment, 409(15), 2859–2873.

P 8.2

Impact of the uncertainty in river water levels on modeled groundwater residence times

Diem Samuel¹ & Schirmer Mario¹

¹Eawag, Swiss Federal Institute of Aquatic Science and Technology, Department of Water Resources & Drinking Water, Überlandstrasse 133, CH-8600 Dübendorf (samuel.diem@eawag.ch)

Riverbank filtration is a widely used method to produce drinking water. In Switzerland for instance, it accounts for 25% of the total drinking water supply. The residence time of the bank filtrate in the aquifer plays a key role in the purification process and therefore, modeling the travel times and groundwater flow paths in river-groundwater systems is important. The conceptual representation of the river boundary condition and the assigned river water levels are critical in this process. In past modeling studies, the assignment of river water levels has been accomplished using different methods, for instance by extracting data from a one or two dimensional hydraulic model (Derx et al. 2010; Doppler et al. 2007) or by interpolating measured water levels to the nodes in between measurement points (Lautz & Siegel 2006). These water level data are usually considered to be accurate and the calibrated model is used to extract quantitative information on parameters like residence time. However, there may be a considerable amount of uncertainty in the river water level information. Depending on the method used to derive water level data at specific points and depending on the interpolation approach to each boundary node, a different river water level distribution is likely to result due to the errors and assumptions within each method. This uncertainty would then impact the modeled groundwater flow paths, flow velocities and residence times.

To assess this possible impact we applied three different methods to define the river water levels at each river boundary node of a three dimensional groundwater flow model of a river – groundwater system, using the software FEFLOW (DHI-Wasy GmbH). The study site is located in northeastern Switzerland at the Thur River and has dimensions of 1x0.5 km. The corridor of the Thur River, flowing through the modeling domain, was restored in 2005 and currently has a width of 30-100 m. The first two methods used measured water level data to specify the river boundary condition, but incorporated two different interpolation approaches. The third method extracted river water level data from a two dimensional hydraulic model, which was established and calibrated several months before the data for the first two methods was collected. Each of the three methods was applied to the same steady-state modeling run of the calibrated groundwater flow model. Based on the groundwater flow field, the residence time from the river to several observation wells was calculated using particle backtracking.

The resulting residence times by applying method one and two differed by 15-20%. Compared to the residence times of method three however, the results of the first two methods differed by up to 70%, even if the model fit to groundwater level observations were equally accurate.

We found independent evidence that major flooding events in the period between the development of the different methods changed the riverbed morphology and subsequently the water levels for a given discharge condition. As a consequence, the variation in calculated river water levels may not be entirely due to the selected method.

REFERENCES

- Derx, J., Blaschke, A.P. & Blöschl, G., 2010: Three-dimensional flow patterns at the river-aquifer interface – a case study at the Danube. *Advances in Water Resources* 33(11), 1375-1387.
- Doppler, T., Franssen, H.J.H., Kaiser, H.P., Kuhlman, U. & Stauffer, F., 2007: Field evidence of a dynamic leakage coefficient for modelling river-aquifer interactions. *Journal of Hydrology* 347(1-2), 177-187.
- Lautz, L.K. & Siegel, D.I., 2006: Modeling surface and ground water mixing in the hyporheic zone using MODFLOW and MT3D. *Advances in Water Resources* 29(11), 1618-1633.

P 8.3

Hydrological changes in glacierized basins of the Swiss Alps: First attempt of a synthesis

Daniel Farinotti¹, Stephanie Usselmann¹, Matthias Huss², Andreas Bauder¹, Martin Funk¹

¹) Laboratory of Hydraulics, Hydrology and Glaciology (VAW), ETH Zurich, CH-8092 Zurich (farinotti@vaw.baug.ethz.ch)

²) Department of Geosciences, University of Fribourg, CH-1700 Fribourg

In Switzerland, water resources are often exploited for hydropower production, especially in the mountains. Assessing the impact of the current climate change on the hydrology of Alpine catchments is of both scientific and economic interest. Several stakeholders have invested considerable efforts in addressing this issue and have initiated several studies.

In this contribution we present the results of nine different case studies aiming at quantifying the impact of climate change on the hydrology of glacierized catchments and try to summarize the results in a quantitative but generalized way. The analyses are performed by using the glacio-hydrological model GERM (Huss et al., 2008, Farinotti et al., in press). A large data basis, including ice volume changes, direct mass balance and ice thickness measurements as well as recorded discharge time series, allowed to establish the link between climate and glacier change in the past. The model was then forced with climate scenarios provided by the Center of Climate System Modeling (C2SM) of the ETH Zurich and used to assess the expected future changes. Emphasis was put into quantifying the uncertainties deriving from the unknown climate evolution.

Although a strong glacier retreat is projected for all catchments, the results show a remarkably different evolution for runoff (Fig. 1): while several basins show the characteristic pattern expected for glacierized catchments, with a first phase of increasing runoff and a second one with decreasing annual discharge, the same pattern is not immediately recognizable for others. The reason can be found in the different glacierization, the different ice thickness distribution, and the different contribution of evapotranspiration to the water budget of the different catchments.

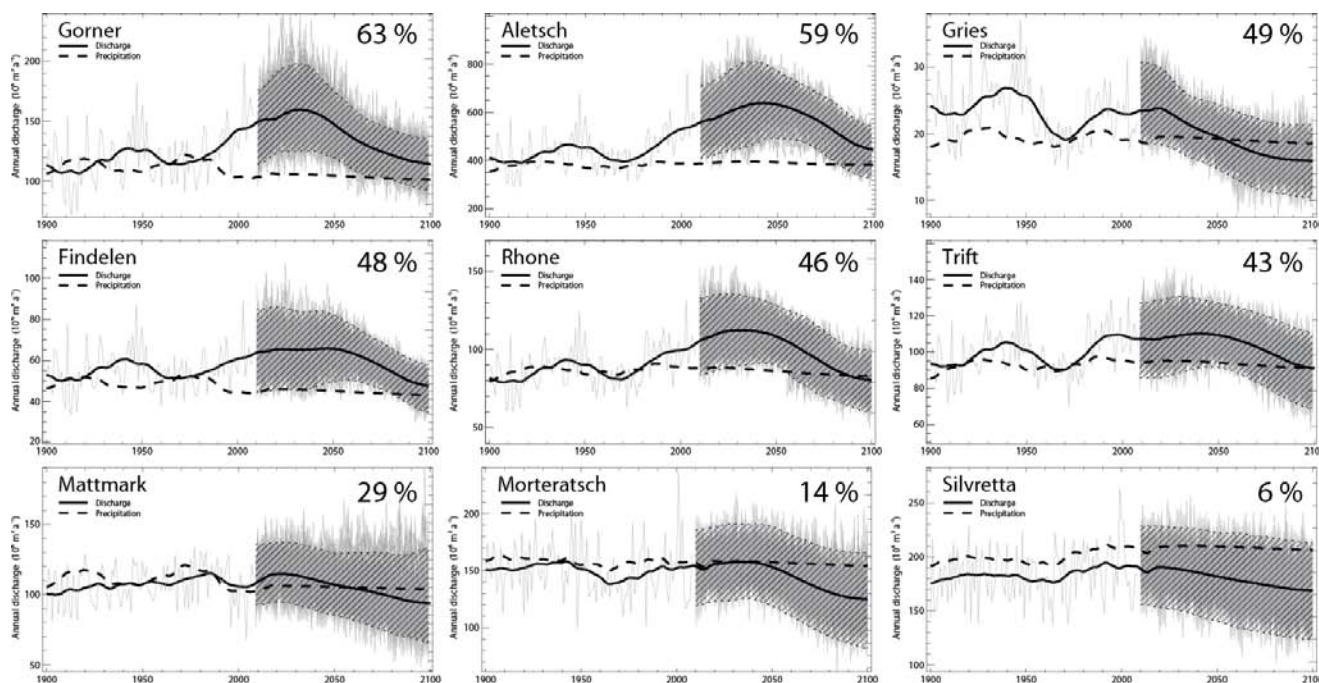


Figure 1. Evolution of annual discharge for the nine analyzed catchments. In the period 2010-2100 the model was forced with 100 different meteorological times series, reflecting the uncertainty in future climate evolution. Accordingly, 100 different time series for annual runoff are generated as well. The tick lines are 30-year running averages for runoff (solid) and precipitation (dashed), the hatched band is an empirical confidence band for runoff including 95% of all model realizations. Catchments are listed according to the present degree of glacierization (percentage shown on the upper right corner).

REFERENCES

- Farinotti, D., S. Usselmann, M. Huss, A. Bauder and M. Funk, in press. Runoff evolution in the Swiss Alps: Projections for selected high-alpine catchments based on ENSEMBLES scenarios. Accepted for publication in *Hydrological processes*. May 2011.
- Huss, M., D. Farinotti, A. Bauder and M. Funk, 2008. Modelling runoff from highly glacierized alpine catchment basins in a changing climate. *Hydrological Processes*, Vol. 22 (19), 3888-3902.

P 8.4**Einfluss der Klimaänderung auf die Stromproduktion der Wasserkraftwerke Löntsch und Prättigau**

Hänggi Pascal^{1,2}, Bosshard Thomas³, Angehrn Sonja⁴, Helland Eivind⁴, Donat Job⁵, Rietmann Daniel⁶, Schädler Bruno^{1,2}, Schneider Robert⁴ & Weingartner Rolf^{1,2}

¹Geographisches Institut der Universität Bern, Gruppe für Hydrologie, Hallerstrasse 12, CH-3012 Bern, (Pascal.haenggi@giub.unibe.ch)

²Oeschger-Zentrum für Klimaforschung, Universität Bern, CH-3012 Bern, Schweiz

³Institut für Atmosphäre und Klima, ETH Zürich, Universitätstrasse 16, CH-8092 Zürich

⁴Axpo AG, Handel und Vertrieb, Parkstrasse 23, CH-5401 Baden

⁵AF-Colenco AG, Wasserbau und Umwelt, Täferstrasse 26, CH-5405 Baden

⁶Axpo AG, Hydroenergie, Parkstrasse 23, CH-5401 Baden

An den Fallbeispielen des hydraulischen Speicherkraftwerkes Löntsch und der Wasserkraftwerksgruppe Prättigau wurde der Einfluss der Klimaänderung auf die Stromproduktion untersucht. Dabei wurden verschiedene Klimamodelle mit je einem hydrologischen und einem Betriebsmodell gekoppelt. Für die Berechnungen wurde die aktuelle Stromnachfrage unverändert belassen, sodass die Auswirkungen einer veränderten Zuflussmenge zu den Kraftwerken isoliert betrachtet werden konnten.

Beim Beispiel des Kraftwerkes Löntsch (Klöntalersee) gehen die Klimaprojektionen für die Periode 2021-2050 im Vergleich zur Referenzperiode 1998-2009 von einer Zunahme in den jährlichen Zuflüssen zum Wasserkraftwerk Löntsch aus (Median aller Klimaprojektionen: +2.2%; nicht signifikant). Das Zuflussregime verändert sich signifikant, mit höheren Werten im Winter und Herbst, und tieferen Werten während dem Sommer. Durch eine Anpassung des monatlichen Produktionsprofils kann eine Steigerung der Stromproduktion und des Umsatzes erreicht werden. Die Resultate liefern für hydrologisch ähnliche Gebiete mit gleichem Kraftwerkstyp Hinweise, wie ein sich änderndes Klima den Kraftwerksbetrieb beeinflussen könnte. Durch die Berücksichtigung von klimabedingten Veränderungen in der Stromnachfrage könnten weitere wichtige Hinweise erarbeitet werden.

Unter den gegebenen Klimaprojektionen für die Periode 2021-2050 wird beim Beispiel Prättigau im Vergleich zur Referenzperiode 1976-2004 eine Steigerung der Stromproduktion um 9.3% (Median aller verwendeten Projektionen) simuliert. Die Zunahme resultiert hauptsächlich aus einer Produktionssteigerung während dem Winter, im Sommer bleiben die Produktionsraten unverändert. Die Analyse der Dauerkurven zeigt, dass sich ein Ausbau der Hauptfassung in Klosters nicht lohnt, da die bestehende Fassungskapazität während des Sommers, wenn die grössten Abflussmengen auftreten, in Zukunft nur unwesentlich länger überschritten wird. Die Resultate liefern für hydrologisch ähnliche Gebiete mit gleichem Kraftwerkstyp Hinweise, wie ein sich änderndes Klima den Kraftwerksbetrieb beeinflussen könnte.

P 8.5

Hydrogeological, physical and chemical differences influencing benthic macroinvertebrate communities in alpine springs of Slovenia

Oz Basak ¹, Mori Nataša ² and Brancelj Anton ²

¹ University of Nova Gorica, Faculty of Environmental Sciences, Vipavska 13, 5000, Nova Gorica, Slovenia (basakozz@gmail.com)

² National Institute of Biology, Department of Freshwater and Terrestrial Ecosystems Research, Večna pot 111, 1000, Ljubljana, Slovenia

Springs are formed where the water table intersects with the land surface, or groundwater rises to the surface through rock faults, fractures or depressions as a result of geological structure. Springs are important ecotones within the interactions of groundwater, surface water and terrestrial ecosystems. In this paper, environmental variables were measured and benthic macroinvertebrate communities were studied in twelve springs from the alpine region of Slovenia. There are three different alpine components which indicate different hydrogeological characteristics such as limestone, dolomite and clastic rock, influencing physical and chemical characteristics of springs in Slovenia. Canonical Correlation Analysis (CCA), Shannon diversity index and similarity analysis classified different spring types and pointed out that invertebrate assemblages from Gastropoda, Amphipoda, Ephemeroptera, Plecoptera, Trichoptera and Chironomidae were different according to hydrogeological, physical and chemical characteristics of spring types.

P 8.6

Swisskarst project (NRP61): Identification cards as tools for a sustainable management of karst systems.

Vouillamoz Jonathan¹, Malard Arnould¹, Weber Eric¹, Eichenberger Urs¹, Jeannin Pierre-Yves¹

¹Swiss Institute of speleology and karstology, Rue de la Serre 68, CP 818, CH-2300 La Chaux-de-Fonds

SWISSKARST project aims at setting up a specific approach and a series of tools for improving the sustainable management of karst groundwater systems. The KARSYS methodology (Karst system characterization methodology) provides a framework for producing geologically and hydraulically meaningful conceptual models of karst systems (see Malard et al., this volume). The present paper focuses more on the way to present these results in a systematic and applicable way and introduces the idea of ID cards for karst systems.

Identification Cards intend synthesizing the main karst system characteristics. They have to be at once concise and enough complete. They must address questions from cantons, communities, water-supply associations or any further water-user of a karst area. For this reason, some aspects of the ID Cards are being adjusted to the respective demands and priorities of users. Furthermore, ID Cards consider the following potential user conflicts and interactions: drinking water supply, hydropower production, artificial snow, irrigation, geothermic, natural hazard management.

The ID Cards is formed of two parts. The first one consists in a documentation of the main systems characteristics. It documents the following 6 modules: (i) catchment area and recharge, (ii) karst morphology features, (iii) aquifer geology, (iv) groundwater bodies and underground flow paths, (v) related springs characteristics and (vi) resources uses. The second part graphically depicts those characteristics with an original hydrogeological interpreted map showing underground hydrological feature (height of the aquifer base, flow paths and groundwater bodies), surface hydrological behaviour (infiltration characteristics and multiple karst system appurtenances) and interaction between both surface and underground hydrology. ID Cards are placed on a free-access web-site (www.swisskarst.ch) together with 3D hydrogeological model (3Dpdf) to provide a homogenous documentation for further specific research.

REFERENCES

- GRETTILLAT, P.-A., 1992 : Carte Hydrogéologique de l'Ajoie (Canton du Jura, SUISSE). Eléments pour la gestion et la protection des eaux. 1/25 000
- KIRALY, L., 1973 : Notice et carte hydrogéologique du canton de Neuchâtel. Bulletin de la Société Neuchateloise de Sciences Naturelles, 96.
- MILANOVIC PT. 2004. Water Resources Engineering in Karst. CRC Presse (Ed.)
- STRUCKMEIER, W.-F., MARGAT, J., 1995 : Hydrogeological maps, a guide and a standard legend, International association of hydrogeologists, 17, 177p., Hannover.

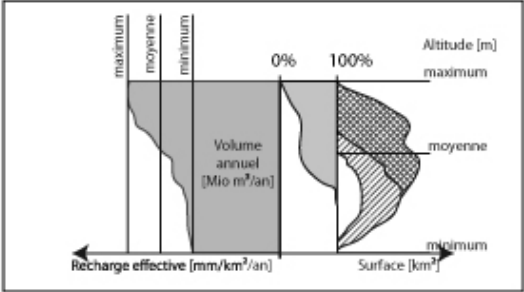
Présentation générale du bassin d'alimentation																																		
<p>Caractérisation du bassin d'alimentation - Recharge</p> <p>Nom du bassin d'alimentation <input type="text"/></p> <p>Surface [km²] Univoque Diffluent Localisation géographique (m)</p> <p>Karst découvert (KD) <input type="text"/> <input type="text"/> N <input type="text"/> N</p> <p>Karst sous couverture (KC) <input type="text"/> <input type="text"/> O <input type="text"/> E</p> <p>Non-karstique (NK) <input type="text"/> <input type="text"/> S <input type="text"/> S</p> 	<p>Indice de karstification - Transit dans la zone vadose</p> <p>Appréciation du développement des formes de surface</p> <p>Dolines <input type="checkbox"/> 1 = faible</p> <p>Lapiaz <input type="checkbox"/> 2 = moyen</p> <p>Vallée sèches <input type="checkbox"/> 3 = élevé</p> <p>Cavités explorées</p> <p>Nombre de cavités connues <input type="text"/></p> <p>Longueur des conduits explorés (m) <input type="text"/></p> <p>Nombre de pertes ponctuelles <input type="text"/></p> <p>Appréciation du développement du réseau karstique</p> <p><input type="checkbox"/> Peu développé <input type="checkbox"/> Moyennement développé <input type="checkbox"/> Très développé</p> <p>Autres / Remarques</p> <input type="text"/>																																	
Caractérisation hydrogéologique du système aquifère																																		
<p>Caractérisation géologique</p> <p>Toit</p> <p>Aquifère</p> <p>Formation <input type="text"/></p> <p>Lithologie <input type="text"/></p> <p>Epaisseur [m] <input type="text"/></p> <p>Mur</p> <p>Aquifère</p> <p>Formation <input type="text"/></p> <p>Lithologie <input type="text"/></p> <p>Epaisseur [m] <input type="text"/></p> <p>Aquifère</p> <p>Formation <input type="text"/></p> <p>Lithologie <input type="text"/></p> <p>Epaisseur [m] <input type="text"/></p> <p>Description de la formation aquifère</p> <input type="text"/>	<p>Caractérisation de la nappe</p> <p>Type hydrodynamique</p> <p><input type="checkbox"/> Nappe libre <input type="checkbox"/> Nappe captive <input type="checkbox"/> Mixte</p> <p>Extension de la nappe [km²]</p> <p>En basses-eaux <input type="text"/> En hautes-eaux <input type="text"/></p> <p>Volume de la nappe [km³]</p> <p>En basses-eaux <input type="text"/> En hautes-eaux <input type="text"/></p> <p>Chimisme des eaux de la nappe</p> <input type="text"/>  <p>Qualité des eaux : données disponibles</p> <p><input type="checkbox"/> Hydrogéochimie <input type="checkbox"/> Bactériologie</p> <p>Vulnérabilité:</p> <p><input type="checkbox"/> Zones de protection <input type="checkbox"/> Agriculture <input type="checkbox"/> Présence de sites pollués</p>																																	
<p>Comportement hydrodynamique de l'aquifère</p> <table border="1"> <thead> <tr> <th>Sources</th> <th>N°</th> <th>Perenne / Temporaire</th> <th>X</th> <th>Y</th> <th>Z</th> <th>Qmin</th> <th>Qmean</th> <th>Qmax</th> <th>T (°C)</th> <th>Cond (µS/cm)</th> </tr> </thead> <tbody> <tr> <td> </td> <td> </td> <td> </td> <td> </td> <td> </td> <td> </td> <td> </td> <td> </td> <td> </td> <td> </td> <td> </td> </tr> <tr> <td> </td> <td> </td> <td> </td> <td> </td> <td> </td> <td> </td> <td> </td> <td> </td> <td> </td> <td> </td> <td> </td> </tr> </tbody> </table>		Sources	N°	Perenne / Temporaire	X	Y	Z	Qmin	Qmean	Qmax	T (°C)	Cond (µS/cm)																						
Sources	N°	Perenne / Temporaire	X	Y	Z	Qmin	Qmean	Qmax	T (°C)	Cond (µS/cm)																								
<p>Utilisations actuelles ou potentielles</p> <p><input type="checkbox"/> Alimentation en eau potable <input type="checkbox"/> Irrigation <input type="checkbox"/> Géothermie <input type="checkbox"/> Production hydroélectrique</p> <p><input type="checkbox"/> Production neige artificielle <input type="checkbox"/> Protéger la ressource <input type="checkbox"/> Se protéger des risques karstiques</p>																																		

Figure 1 : Example of ID-Cards.

P 8.7

Reconstructing the seasonality of Holocene flood events using varved lake sediments of Lake Ledro (S-Alps, Italy)

Wirth Stefanie B.¹, Gilli Adrian¹, Glur Lukas², Anselmetti Flavio S.², Magny Michel³ & Vanni re Boris³

¹ Geological Institute, ETH Zurich, Sonneggstr. 5, CH-8092 Zurich (stefanie.wirth@erdw.ethz.ch)

² Eawag, Swiss Federal Institute of Aquatic Science and Technology, Department of Surface Waters,  berlandstr. 133, CH-8600 D bendorf

³ Laboratoire de Chrono-Environnement, UMR 6249 du CNRS, UFR des Sciences et Techniques, 16 route de Gray, 25030 Besan on, France

Floods as a result of extreme precipitation events represent a major natural hazard in the Alpine realm, causing enormous financial and social damage. Current climate models predict even an increase in heavy precipitation events in the future as a consequence of global warming (Frei et al. 2006). In particular, extreme summer events are expected to occur more frequently in the future. In order to assess this future flood hazard, knowledge about the natural variability and the climatic forcing factors of heavy precipitation events is required. Lacustrine sediments allow such a reconstruction of flood recurrence rates in the past, reaching beyond the time span covered by instrumental and historic data series. In special cases of annually laminated (i.e. varved) lake sediments, even the season in which the floods occurred can be determined.

Lake Ledro is one of the lakes investigated within the framework of the FloodAlp project aiming to reconstruct the Holocene flood history of the Central Alps. In total, 18 lakes are investigated but only few of them are annually laminated thus offering the possibility to resolve the seasonality of the events. Lake Ledro is located in the Trento Province in Northern Italy and has a surface area of 2.2 km² and a maximal water depth of 46 m. The lake is situated in a carbonate catchment built up by Mesozoic sediments, enabling the production of biogeochemical calcite varves. This annual lamination has been preserved for the past 9000 years and is intercalated by flood deposits of various thicknesses (sub-mm to 38 cm). Thus, based on the stratigraphic position of a flood layer within an annual varve cycle, the season, in which the flood occurred, can be determined.

To evaluate the potential of this approach, the past 500 varve-years have been analysed. As a result, a flood pattern dominated by summer and autumn events (78%) was discovered. The flood frequency during the same time period is strongly fluctuating, the highest flood frequencies occur around 1580 AD and between 1850 and 1950. Distinct lows in flood occurrence are observed around 1500 and 1700, corresponding to the Sp rer and Maunder sunspot minima. The observed seasonal distribution, as well as the frequency of the events, is in good agreement with the reconstruction of flood frequencies in the Northern Alps since 1500 by Schmocker-Fackel & Naef (2010). The seasonal record of Lake Ledro will be further expanded into the past, offering a unique high-resolution record for tracking the Holocene flood occurrence as well as related climatic forcing mechanisms.

REFERENCES

- Frei, C., Sch ll, R., Fukutome, S., Schmidli, J. & Vidale, P.L. 2006: Future change of precipitation extremes in Europe: Intercomparison of scenarios from regional climate models. *Journal of Geophysical Research*, 111: D06105, doi:10.1029/2005JD005965.
- Schmocker-Fackel, P. & Naef, F. 2010: Changes in flood frequencies in Switzerland since 1500. *Hydrological Earth System Science*, 14: 1581-1594.

9. Open Cryosphere Session

A. Bauder, M. Hoelzle, B. Krummenacher, C. Lambiel, M. Lüthi, J. Nötzli, J. Schweizer, M. Schwikowski

Swiss Snow, Ice and Permafrost Society

TALKS:

- 9.1 Dalban Canassy P., Funk M.: Study of the retreat of a lake-calving glacier terminus, Triftgletscher (Switzerland).
- 9.2 Faillettaz J., Funk M., Sornette D.: Prediction of alpine glacier sliding instabilities: a new hope
- 9.3 Gruber S.: Derivation and analysis of a high-resolution estimate of global permafrost zonation
- 9.4 Herren P-A., Eichler A., Eikenberg J., Machguth H., Papina T., Tobler L., Vogel E., Zapf A., Schwikowski M.: Ice core based climate reconstruction of the Mongolian Altai
- 9.5 Paul F., Frey H., Le Bris R., Linsbauer A., Haerberli, W.: Recent glacier changes in the Alps in response to atmospheric warming: Observations and consequences
- 9.6 Ryser C., Lüthi M., Funk M., Catania G., Hawley R., Neumann T.: Subglacial Controls of the Short Term Dynamics at the Margins of the Greenland Ice Sheet: Interaction between subglacial water pressure and ice deformation
- 9.7 Schmid M., Gubler S., Fiddes J., Keller M., Gruber S.: Using miniature temperature loggers for the analysis of snow cover distribution and melting
- 9.8 Walter, F., Husen, S., Clinton, J., Lüthi, M., Ryser, C., Funk, M.: Seismological Experiments on the Greenland Ice Sheet
- 9.9 Zapf A., Szidat S., Schwikowski, M.: Radiocarbon dating of glacier ice
- 9.10 Zwimpfer F., Mitterer C., Reiweger I., Schweizer J., Dual J.: Failure of wet snow

POSTERS

- P 9.1 *Alig C., Mitterer C., Schweizer J.*: On the reliability of indicator path avalanches for local avalanche forecasting
- P 9.2 *Bolch T., Chen F., Wei Y., Kang, S., Linsbauer, A.*: Past and future glacier changes in the western Nyainqentanglha Range on the Tibetan Plateau
- P 9.3 *Endrizzi S., Gruber S.*: Effects of subsurface lateral water flow on soil thaw
- P 9.4 *Gabbi J., Farinotti D., Bauder A., Maurer H.*: Ice volume distribution in the Mauvoisin region and implications on glacier fluctuations
- P 9.5 *Gärtner-Roer, I., Armstrong, R., Fetterer, F., Haeberli, W., Hoelzle, M., Käab, A., Kargel, J., Nussbaumer, S.U., Paul, F., Raup, B.H., Zemp, M.*: Integration of glacier databases within the Global Terrestrial Network for Glaciers (GTN-G)
- P 9.6 *Gärtner-Roer, I., Zemp, M., Koblet, T., Jansson, P., Thee, P., Haeberli, W., Holmlund, P.*: “Old-fashioned” photogrammetric analyses – still a key tool for the reassessment of long-term glacier changes: examples from Storglaciären, Sweden
- P 9.7 *Huss M., Farinotti D.*: Ice thickness distribution of 90'000 mountain glaciers around the globe using the GLIMS database and SRTM/ASTER DEMs
- P 9.8 *Köchle B., Schneebeli M.*: Numerical simulation of the Young's Modulus of snow
- P 9.9 *Machguth H., Salzmann N., Linsbauer A.*: The Swiss Alpine Glacier's Response to the “2 °C Air Temperature Target”
- P 9.10 *Monti F., Schweizer J.*: Stability information supplied by the snow cover model SNOWPACK
- P 9.11 *Morard S., Delaloye R.*: Thermal changes in ventilated overcooled talus slope: a mutli-methodological approach
- P 9.12 *Nuber A., Rabenstein L., Lehmann-Horn J. A.*: Surface Nuclear Magnetic Resonance Tomography on a First-Year Sea Ice Pressure Ridge
- P 9.13 *Rastner P., Bolch T., Paul, F.*: The first complete inventory of glaciers and ice caps for Eastern Greenland
- P 9.14 *Sanders, J. W., Cuffey, K. M., MacGregor, K. R.*: Short-term velocity variations of an alpine cirque glacier
- P 9.15 *Scherler M., Hauck C., Hoelzle M., Salzmann N.*: Projection of permafrost evolution under climate change scenarios and evaluation of sensitive influencing factors
- P 9.16 *Schmid L., Mitterer C., Schweizer J., Heilig A., Eisen O., Okorn R.*: Monitoring temporal changes within the snowpack utilizing upward-looking radar systems
- P 9.17 *Schneider S., Hauck C.*: Geophysical monitoring of three different permafrost forms within the Murtèl- Corvatsch Area, Upper Engadin
- P 9.18 *Wendl, I., Isaksson, E., Schwikowski, M.*: Study of a new Svalbard ice core
- P 9.19 *Wirz V., Beutel J., Buchli, B., Gruber S., Limpach P., Zhenzhong, S.*: Temporal characteristics of various cryosphere-related slope movements in high mountains: GPS measurements and analysis
- P 9.20 *Zemp, M., Haeberli, W., Huss, M., Joerg, P.C., Machguth, H., Morsdorf, F., Rastner, P., Schaepman, M.E.*: Glacier Laser-scanning Experiment Oberwallis: project overview and first results

9.1

Study of the retreat of a lake-calving glacier terminus, Triftgletscher (Switzerland).

Dalban Canassy Pierre¹, Funk Martin¹

¹Laboratory of Hydraulics, Hydrology and Glaciology (VAW), ETH Zurich, CH-8092 Zurich, Switzerland (dalban@vaw.baug.ethz.ch)

From 2000 to 2006, Triftgletscher (Bernese Alps, Switzerland) has retreated substantially and a proglacial lake containing 5.10^6 m³ water has progressively formed in the glacier forefield. One of the consequences of the tongue retreat is the destabilization of the steep part behind it, likely to result in the release of ice avalanches with several million m³ of ice plunging into the lake. Moreover, studies on the avalanches dynamics and lake hydraulics have shown that such avalanches could generate dangerous flood waves, thus posing a threat to the inhabitants of Gadmertal. In this context, the modelling of the terminus retreat appears relevant regarding the information it provides about how fast the lake forms and consequently about the steep part destabilization.

An important question regarding glaciers ending in lakes is to what extent the water contact influences their advances or retreat. Indeed, it is well known that iceberg calving can be a very efficient ablation mechanism. We propose to assess the role played by calving in the Triftgletscher tongue retreat using a simple mass balance model coupled with a calving model. The mass balance model is a temperature-index melt and accumulation model based on a linear relation between melt rate and positive air temperature. The calving criterion we use implies that as soon as the elevation of a surface point behind the calving front becomes equal to the flotation level, the portion between the point and the glacier terminus is removed.

Results show that the calving effect allows to explain 89% of the observed tongue retreat, whereas surface melting alone only accounts for 59 %. They also indicate that the total ice mass in the lake area would have disappeared two years later in the absence of calving. We point out some limitations of the modelling concerning its application at a yearly time scale. In this case, it appears that potential floating sustainments are likely to induce substantial delays in the calving at the front, affecting thus the model results relevance.

9.2

Prediction of alpine glacier sliding instabilities: a new hope

Faillietaz Jerome¹, Funk Martin¹ & Sornette Didier²

¹Laboratory of Hydraulics, Hydrology and Glaciology (VAW), ETH Zurich, CH-8092 Zurich, Switzerland (jerome.faillettaz@vaw.baug.ethz.ch)

² Department of Management, Technology and Economics, ETH Zurich, 8092 Zurich, Switzerland.

Mechanical and sliding instabilities are the two processes which may lead to breaking off events of large ice masses. Mechanical instabilities mainly affect unbalanced cold hanging glaciers (i.e. the snow accumulation is only partly compensated by break-off at the front). For the latter case a prediction of such an event could be achieved based on data of surface velocities and seismic activity (Faillietaz et al., 2011a). The case of sliding instability is more problematic. Sliding instabilities occur on temperate glacier tongues. Such instabilities are strongly affected by the subglacial hydrology: infiltrated melt water may cause (i) a lubrication of the bed and (ii) a decrease of the effective pressure at the glacier bed and consequently a decrease of basal friction. Available data from Allalingsletscher (Valais) indicate that the glacier tongue experienced an active phase during 2-3 weeks in summer or fall in most years with strongly enhanced surface velocities.

In order to scrutinize in more detail the processes governing the sliding instabilities, a numerical model developed to investigate gravitational instabilities in heterogeneous media (Faillietaz et al., 2010, Faillietaz et al. 2011b) was applied to Allalingsletscher. This model enables to account for various geometric configurations, interaction between sliding and tension cracking and water flow at the bedrock.

We could show that both a critical geometrical configuration of the glacier tongue and the existence of a distributed drainage network were the main causes of this catastrophic break-off. Moreover, this model casts a gleam of hope for a better understanding of the ultimate rupture of such glacier sliding instabilities.

REFERENCES

- Faillottaz, J., Sornette, D. & Funk, M. 2010: Gravity-driven instabilities: interplay between state-and-velocity dependent frictional sliding and stress corrosion damage cracking. *Journal of Geophysical Research*, 115, B03409, doi:10.1029/2009JB006512. arXiv/0904.0944.
- Faillottaz, J., Funk, M. & Sornette, D. 2011a: Icequakes coupled with surface displacements for predicting glacier break-off. *Journal of Glaciology*, 57, (203), 453-460.
- Faillottaz, J., Sornette, D. & Funk, M. 2011b: Numerical modelling of gravity driven instability of cold hanging glacier: reanalysis of the 1895 break-off of Aletschgletscher, Switzerland. *Journal of Glaciology*, 57 (205), 817-831.

9.3

Derivation and analysis of a high-resolution estimate of global permafrost zonation

Stephan Gruber

Glaciology, Geomorphodynamics & Geochronology, Department of Geography, University of Zurich, Switzerland
(stephan.gruber@geo.uzh.ch)

Permafrost underlies much of Earth's surface and interacts with climate, eco-systems and human systems. It is a complex phenomenon controlled by climate and (sub-) surface properties and reacts to change with variable delay. Heterogeneity and sparse data challenge the modeling of its spatial distribution. Currently, there is no data set to adequately inform global studies of permafrost. The available data set for the Northern hemisphere is frequently used for model evaluation, but its quality and consistency are difficult to assess.

A global model of permafrost extent and dataset of permafrost zonation are presented and discussed, extending earlier studies by including the Southern hemisphere, by consistent data and methods, and most importantly, by attention to uncertainty and scaling. Established relationships between air temperature and the occurrence of permafrost are reformulated into a model that is parametrized using published estimates. It is run with a high-resolution (< 1km) global elevation data and air temperatures based on the NCAR-NCEP reanalysis and CRU TS 2.0. The resulting data provides more spatial detail and a consistent extrapolation to remote regions, while aggregated values resemble previous studies. The estimated uncertainties affect regional patterns and aggregate number, but provide interesting insight.

The permafrost area, i.e. the actual surface area underlain by permafrost, north of 60°S is estimated to be 13–18 million km² or 9–14% of the exposed land surface. The global permafrost area including Antarctic and sub-sea permafrost is estimated to be 16–21 million km². The global permafrost region, i.e. the exposed land surface below which some permafrost can be expected, is estimated to be 22 ±3 million km². A large proportion of this exhibits considerable topography and spatially-discontinuous permafrost, underscoring the importance of attention to scaling issues and heterogeneity in large-area models.

REFERENCES

- Gruber, S. 2011: Derivation and analysis of a high-resolution estimate of global permafrost zonation, *The Cryosphere Discussions*, www.the-cryosphere-discuss.net/5/1547/

9.4

Ice core based climate reconstruction of the Mongolian Altai

Pierre-Alain Herren^{1,2}, Anja Eichler^{1,2}, Jost Eikenberg¹, Horst Machguth³, Tatyana Papina⁴, Leonhard Tobler^{1,2}, Edith Vogel², Alexander Zapf^{1,2} & Margit Schwikowski^{1,2}

¹Paul Scherrer Institut, CH-5232 Villigen (pierre-alain.herren@psi.ch)

²Oeschger Center University of Bern, Zähringerstrasse 25, CH-3012 Bern

³Glaciology and Geomorphodynamics University of Zurich Winterthurerstr. 190, CH-8057 Zurich

⁴Institute of Water and environmental problems, Molodyoznaya Street 1, RU-656038 Barnaul

In summer 2009 a 72 m ice core (56 m weq) reaching bedrock was drilled on Tsambagarav glacier in the Mongolian Altai (4140 m asl, 48°39.338'N, 90°50.826'E). The glacier temperatures ranging from -14.5 to -12.5°C indicate well-preserved paleoclimate records, suitable for climate reconstruction. Dating of the ice core was performed using four independent techniques, annual layer counting, identification of nuclear bomb as well as volcanic horizons, and nuclear dating with ²¹⁰Pb and ¹⁴C (Jenk et al. 2009). The upper 36 m weq contain the last two centuries with high resolution. The lower 20 m weq are characterised by a strong thinning of annual layers, with an age of 5500 years BP near bedrock suggested by the ¹⁴C method.

Analyzed species are stable isotopes ($\delta^{18}\text{O}$) and major ions by using standard analytical techniques such as mass spectrometry and liquid ion chromatography. The ion records allow reconstructing the air pollution of the Mongolian Altai, whereas $\delta^{18}\text{O}$ is assumed to be a temperature proxy. Former studies at Belukha glacier in the Siberian Altai showed a strong correlation between solar forcing and temperature in this region for the period 1250 to 1850 AD (Eichler et al. 2009). The Tsambagarav ice core will be used to investigate this findings and for a better understanding of the regional climate.

Occurrence of ice lenses in the upper part indicates melting in summer. This is confirmed by depletion of sulfate in the upper 10 m, due to relocation by percolating melt water. With increasing depth the occurrence of ice lenses declines, pointing to climatic changes during the last decades. The melt percent deduced from ice lenses is another potential temperature proxy (Henderson et al. 2006) and will be used combined with the $\delta^{18}\text{O}$ for regional temperature reconstruction.

REFERENCES

- Eichler, A. S. Olivier, K. Hendersen, A. Laube, J. Beer, T. Papina, H.W. Gäggeler, M. Schwikowski, Temperature response in the Altai region lags solar forcing, *Geophys. Res. Lett.* 36, L01808, doi:10.1029/2008GL035930 (2009).
- Henderson, K., Laube, A., Gäggeler, H., & Olivier, S. 2006: Temporal variations of accumulation and temperature during the past two centuries from Belukha ice core, Siberian Altai. *Journal of Geophysical Research*, 111, D03104. doi:10.1029/2005JD005819
- Jenk, T., Szidat, S., Bolius, D., Sigl, M., Gäggeler H.W., Wacker, L., Ruff, M., Barbante, C., Boutron, C., Schwikowski, M. 2009: A novel radiocarbon dating technique applied to an ice core from the Alps indicating late Pleistocene ages. *Journal of Geophysical Research*, 114, D14305, doi:10.1029/2009JD011860.

9.5

Recent glacier changes in the Alps in response to atmospheric warming: Observations and consequences

Paul Frank¹, Frey Holger¹, Le Bris Raymond¹, Linsbauer Andreas¹, Haeberli, Wilfried¹

¹ Department of Geography, University of Zurich, Winterthurerstr. 190, CH-8057 Zurich, (frank.paul@geo.uzh.ch)

The past two decades have seen massive loss of glacier volume in the Alps as a reaction to a sudden temperature increase of about 1 degree in the 1980s. Indirect signs of glacier downwasting (e.g. emerging rock outcrops, split of tributaries, disintegration) can be followed on satellite imagery over the entire Alps. Latest data from 2009 indicate a continuation of previous negative trends with strong changes now also observed for the larger glaciers. In particular the development of new lakes at the terminus is a widespread phenomenon that enhances ice melt. For an assumed further increase in temperature in the coming decades, glaciers will continue to shrink and lose mass at an accelerated rate due to positive feedbacks. For example, when the glacier surface comes to lower elevations due to the downwasting, glacier melt will further increase.

Modelling of glacier beds with a simplified approach revealed several interesting aspects for further glacier evolution. For example, the bed topography of the largest glaciers is less inclined than the surface, for some glaciers the slope is in some sections even close to zero. This implies that these glaciers cannot retreat to higher elevations to come in balance with a warmer climate and will completely lose their tongues. Furthermore, most glacier beds show several overdeepenings of partly considerable size that might transform to lakes in the future. Such lakes might compensate for the loss of glaciers from a touristic point of view, but they might also increase the hazard potential in some regions. For hydro-power companies the vanishing of glaciers and the appearance of new lakes has important consequences for their long-term planning.

9.6

Subglacial Controls of the Short Term Dynamics at the Margins of the Greenland Ice Sheet: Interaction between subglacial water pressure and ice deformation

Claudia Ryser¹, Martin Lüthi¹, Martin Funk¹, Ginny Catania², Robert Hawley³, Thomas Neumann⁴

¹ Versuchsanstalt für Wasserbau, Hydrologie und Glaziologie, Gloriastr. 37/39, CH-8092 Zürich

² University of Texas, Austin, TX

³ Dartmouth College, Hanover, NH

⁴ NASA Goddard Space Flight Center, Greenbelt, MD

With the aim of a better understanding of the processes responsible for peripheral thinning and seasonal flow velocity variations of the Greenland Ice Sheet (GrIS), we drilled 12 boreholes to bedrock during a field campaign this summer. The boreholes are located at two sites in the marginal area of the GrIS, downstream of SwissCamp.

In four boreholes, a newly devised borehole sensor systems, DIBOSS, was installed. DIBOSS is a digital borehole sensor system consisting of multi-sensor units (pressure sensor, inclinometer, magnetometer, thermistor), operated through a digital bus over a special extendable cable. It allows us to monitor subglacial water pressure, ice temperature, and shearing/stretching deformation of the ice body.

To get a comprehensive picture on the dynamics of the marginal areas also different surface measurements, e.g. surface velocity, complete the unique set of measurements.

We will present new data on the interaction between subglacial water pressure and ice deformation on the GrIS. We will also show data from pump tests which elucidate the development of the local subglacial hydrology.

9.7

Using miniature temperature loggers for the analysis of snow cover distribution and melting

Marc-Olivier Schmid¹, Stefanie Gubler¹, Joel Fiddes¹, Matthias Keller² & Stephan Gruber¹

¹ Department of Geography; University of Zürich, Switzerland (marc-olivier.schmid@geo.uzh.ch)

² Computer Engineering and Networks Laboratory, ETH Zurich, Switzerland

Mountain areas are characterised by an extreme lateral variability in elevation, exposure to solar radiation and ground material. This causes large differences in the seasonal snow cover distribution, snow melting and associated sub-surface phenomena such as ground temperatures and melt water infiltration. Because conventional techniques such as single point measurements of temperature or remote sensing are limited in the ability to reveal the spatio-temporal behavior at the snow-ground interface, this study investigates snow cover and snow melting based on spatial clusters of temperature measurements. Results are based on campaigns near Piz Corvatsch in the upper Engadin, Eastern Switzerland where ground surface temperatures (GST) were measured with miniature temperature loggers (iButtons) at 40 different locations, so called footprints. At each footprint up to 10 iButtons have been distributed randomly, measuring GST every 3 hours for 2 years. The footprints represent elevations of 2100 – 3300 m a.s.l.; aspects North, South, East, West and Slopes of 0 – 55°.

From a single temperature time series, two points in time are detected in a robust and precise way: The beginning of an isothermal snow pack, which also is the first time in the spring season when surface runoff is created, and the end of the snow cover. Furthermore (cf. Gubler et al. 2011), mean annual ground temperatures are calculated. For these three derived quantities, both the intra-footprint variability based on 10 measurements within 10 m x 10 m and the inter-footprint variability based on the comparison of values aggregated over footprints are analyzed and their patterns compared between measurement years.

Results provide important data for the validation of models and, especially though the analysis of considerable intra-footprint variability, point to the possible scaling conflict when comparing gridded models with single point measurements.

REFERENCES

Gubler, S., Fiddes, J., Gruber, S. & Keller, M. (2011): Measuring and analysis of scale dependent variability of ground surface temperatures in alpine terrain, *The Cryosphere*, 5, 431–443, doi:10.5194/tc-5-431-2011.

9.8

Seismological Experiments on the Greenland Ice Sheet

Fabian Walter^{1,2}, Stephan Husen², John Clinton², Martin Lüthi¹,
Claudia Ryser¹ & Martin Funk¹

¹Versuchsanstalt für Wasserbau, Hydrologie und Glaziologie, Gloriastr. 37/39, CH-8092 Zürich (walter@vaw.baug.ethz.ch)

²Schweizer Erdbebendienst, Sonneggstr. 5, CH-8092 Zürich

A critical gap in our current understanding of glaciers and ice sheets is how high sub-glacial water pressure controls the coupling of the glacier to its bed. Accordingly, some models predict that the Greenland Ice Sheet will lose ice in an accelerated manner through a feedback effect: High melt rates at the surface provide melt water which is routed through the sub-glacial drainage system and reduces basal friction, leading to high ice flow velocities and surface draw-down. This effect might induce a rapid decay of the ice sheet, and consequently contribute to global sea level rise.

In this context, the recent episodic increase of Greenland's ice discharge to the ocean (e. g. Rignot and Kanagaratnam, 2006) has received much attention and raised concerns about ice sheet stability in a warming climate. Although observations indicate that an increase in ocean temperatures triggered this event (e. g. Holland et al., 2008), correlation between ice discharge and surface melt has been observed in the past (Rignot et al., 2008). Furthermore, it is not clear how land-terminating portions of the ice respond to increased surface melt. The ice sheet's subglacial drainage system certainly plays an important role. Yet the question whether it will help enhance or diminish ice flow is currently subject to debate (e. g. Parizek and Alley, 2004; Sundal et al., 2011).

In order to better understand Greenland's subglacial drainage system and its role in ice flow, we conducted a series of seismological and glaciological experiments on the ice sheet in the summer 2011. In an international collaboration, over a dozen boreholes were drilled to the glacier bed at two sites and equipped with scientific instruments to measure englacial deformation, temperature, basal water pressure and glacier sliding rates. Another project component was the installation of an unprecedented high-density seismometer array around one of the drill sites. With an aperture of about 1.5 km, the array consisted of 17 seismometers, including three deep borehole seismometers (up to 400 m deep) and two broadband stations. The goal of this network is to detect englacial dislocation processes (icequakes) indicative of hydrofracturing and stick slip motion. In combination with the borehole geophysical measurements, the seismic monitoring will thus elucidate the effects of changes in the subglacial drainage system on glacier motion and ice fracturing.

We will describe the seismological experiment focusing on practical challenges of deploying seismometers in direct contact with glacier ice. We will also give a first impression of the icequake waveform variety, which we have recorded. As expected from previous studies of Alpine icequakes we recorded a large number of surface crevassing events. However, we also detected deeper fracture events, providing indications for englacial hydrofracturing. The high-quality waveform data allow for determination of important source parameters, such as hypocentral location, fracture volume, fault plane orientation and stress drop.

REFERENCES

- Holland, D. M., Thomas, R. H., de Young, B., Ribergaard, M. H., & Lyberth, B. (2008). Acceleration of Jakobshavn Isbræ triggered by warm subsurface ocean waters. *Nature Geoscience*, 1. doi:10.1038/ngeo316.
- Rignot, E. & Kanagaratnam, P. (2006). Changes in the Velocity Structure of the Greenland Ice Sheet. *Science*, 311(5763). doi:10.1126/science.1121381.
- Rignot, E., Box, J. E., Burgess, E., & Hanna, E. (2008). Mass balance of the Greenland ice sheet from 1958 to 2007. *Geophysical Research Letters*, 35(L20502). doi:10.1029/2008GL035417.
- Parizek, B. R. & Alley, R. B. (2004). Implications of increased Greenland surface melt under global-warming scenarios: ice-sheet simulations. *Quaternary Science Reviews*, 23(9-10), 1013–1027.
- Sundal, A. V., Shepherd, A., Nienow, P., Hanna, E., Palmer, S., & Huybrechts, P. (2011). Melt-induced speed-up of Greenland ice sheet offset by efficient subglacial drainage. *Nature*, 469, 521–524. 10.1038/nature09740.

9.9

Radiocarbon dating of glacier ice

Alexander Zapf^{1,2}, Sönke Szidat^{2,3}, Margit Schwikowski^{1,2}¹Paul Scherrer Institut, Villigen PSI, CH-5232 Villigen²Oeschger Centre for Climate Change Research, Zähringerstrasse 25, CH-3012 Bern³Departement für Chemie und Biochemie, Freiestrasse 3, CH-3012 Bern

In paleoclimatological investigations of ice cores from high-alpine glaciers dating is a non-trivial task mainly due to the complex impacts of glacier flow, accumulation, ablation etc. resulting in a strongly non-linear depth-age relationship. Particularly in the deepest parts of the ice core where thinning of the annual layers does not allow for conventional dating using annual-layer counting on seasonally varying parameters, other techniques are needed to establish precise age-depth models.

A novel radiocarbon method for dating ice cores has been developed by our group recently, utilizing carbonaceous particles contained in the ice. (Sigl *et al.*, 2009). Carbonaceous particles are extracted from the ice samples via filtration prior to a combustion step where the fractions of organic carbon (OC) and elemental carbon (EC) are separated (Szidat *et al.*, 2004). By means of the compact radiocarbon system MICADAS with a gas ion source (Ruff *et al.*, 2007) gaseous CO₂ samples from the combustion step are directly measured. This method proved to be applicable to high-alpine ice cores from the mid- and low-latitudes (e.g. Colle Gnifetti, 4450 m a.s.l., Swiss Alps; Nevado Illimani, 6300 m a.s.l., Bolivian Andes) resulting in ages covering a time-span from 1,000 to >10,000 years for both areas (Figure 1).

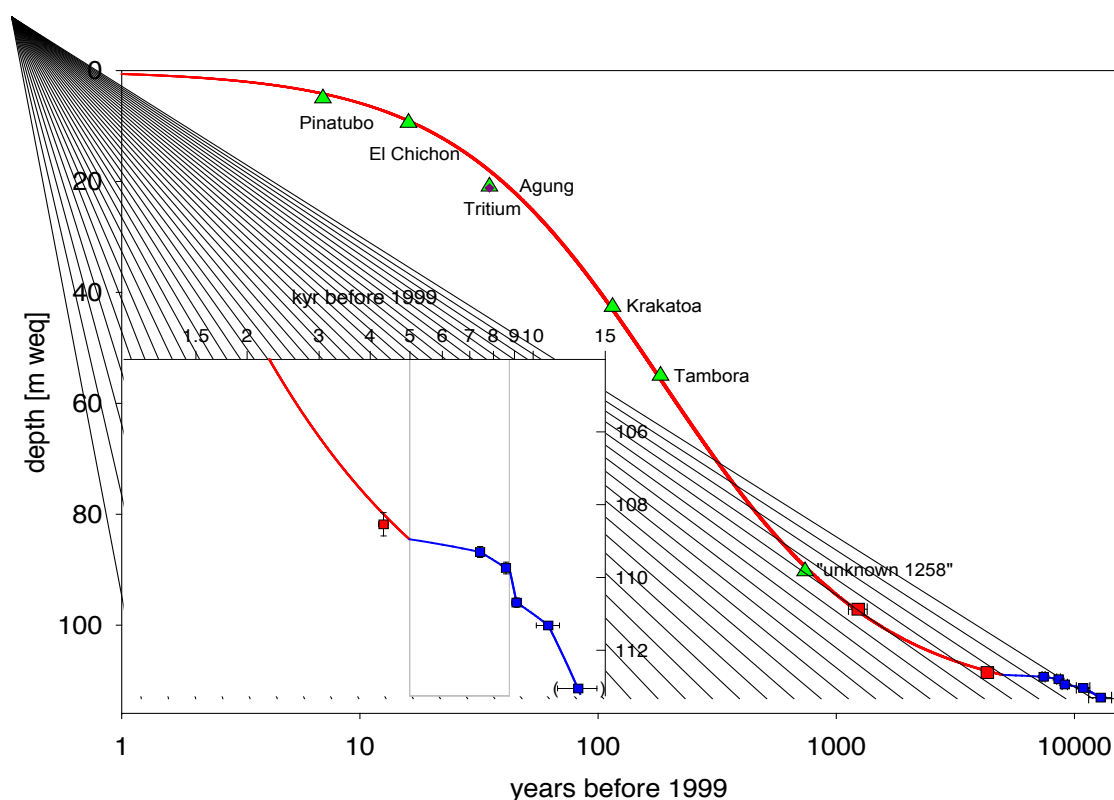


Figure 1. Age-depth relationship for the Illimani ice core applying different dating approaches: (i) Tritium peak (purple diamond). (ii) Volcanic eruption horizons (green triangles). (iii) Two-parameter model using volcanic horizons and two calibrated ¹⁴C ages (red line). (iv) Calibrated ¹⁴C ages (blue line/squares). Insert: Detail showing the calibrated radiocarbon ages with linear interpolation. Adopted from (Kellerhals *et al.*, 2010).

Applying this method to ice samples from various glaciated areas from the tropics to the poles yielded many interesting age estimations of these ice masses. Recently a ¹⁴C-based age-depth record was established for an ice core from the Mongolian Altai indicating a basal age of around 6000 years BP. Still, there are phenomena such as potential reservoir effects inherent in the carbonaceous aerosols which need to be better understood in terms of e.g. age offsets for the respec-

tive sites. Analyzing more samples together with previously well-dated reference samples will help us in the interpretation of the obtained results. Also thanks to recent improvements in small scale ^{14}C analysis of gaseous samples (sample size down to 3 $\mu\text{g C}$) we have a dating tool with great potential for ice core related paleoclimate studies to improve and extend new and existing chronologies.

Next projects will include ice sampling at the plateau glaciers of Kibo (Kilimanjaro massif, Tanzania) in order to provide an independent age estimate of these ice fields in the current discussion (Kaser *et al.*, 2010).

REFERENCES

- Kaser, G., Mölg, T., Cullen, N. J., Hardy, D. R. & Winkler, M. 2010: Is the decline of ice on Kilimanjaro unprecedented in the Holocene? The Holocene, doi: 10.1177/0959683610369498
- Kellerhals, T., Tobler, L., Brütsch, S., Sigl, M., Wacker, L., Gäggeler, H. W. & Schwikowski, M. 2010: Thallium as a tracer for preindustrial volcanic eruptions in an ice core record from Illimani, Bolivia, *Environ. Sci. Technol.*, 44, 888-893.
- Ruff, M., Wacker, L., Gäggeler, H. W., Suter, M., Synal, H. A. & Szidat, S. 2007: A gas ion source for radiocarbon measurements at 200 kV. *Radiocarbon*, 49, 307-314.
- Sigl, M., Jenk, T. M., Kellerhals, T., Szidat, S., Gäggeler, H. W., Wacker, L., Synal, H. A., Boutron C., Barbante, C., Gabrieli, J. & Schwikowski, M. 2009: Towards radiocarbon dating of ice cores. *J. Glaciol. Instrum. Meth.*, 55, 985-996.
- Szidat, S., Jenk, T. M., Gäggeler, H. W., Synal, H. A., Hajdas, I., Bonani, G. & Saurer M. 2004: THEODORE, a two-step heating system for the EC/OC determination of radiocarbon (C-14) in the environment. *Nucl. Instrum. Meth. Phys. Res. B*, 223-224, 829-836.

9.10

Failure of wet snow

Fabian Zwimpfer¹, Christoph Mitterer¹, Ingrid Reiweger¹, Jürg Schweizer¹, Jürg Dual²

¹ WSL Institute for Snow and Avalanche Research SLF, Flüelastrasse 11, 7260 Davos Dorf, Schweiz (mitterer@slf.ch).

² Center of Mechanics (Institute for mechanical Systems), Tannstrasse 3, 8092 Zürich, Schweiz

Liquid water changes the properties of snow in a highly non-linear manner and thus complicates the processes that lead to wet-snow avalanche formation. In previous studies, researchers investigated the influence of liquid water on the mechanical properties of snow in field studies (e.g. Brun and Rey, 1987; Bhutiyan, 1994). Since the reproducibility of field experiments is impaired by spatial and temporal variability of the snow, terrain, and weather conditions, systematic experiments under laboratory conditions are needed. The objectives of this study were to conduct first wet-snow experiments in a cold laboratory, test the experimental setup and gain primarily qualitative insights into the mechanical failure behavior of wet snow.

With a force-controlled loading apparatus (Reiweger *et al.*, 2010) natural, homogenous snow samples, i.e. without a prominent weak layer, were loaded to about ~75% of the dry-snow strength. In this way we achieved a critical state prior to the wetting. Using a tube network, water with 0°C was conducted to the top of the snow sample. The loading process was digitally recorded and the resulting stress at failure was compared to water content measurements. Two displacement sensors measured the horizontal and the vertical displacement of the upper sample holder and a displacement field for the whole snow sample was obtained by Particle Image Velocimetry (PIV). In addition, acoustic emissions were recorded as well and were supposed to act as a real-time monitoring system for crack formation processes in the material.

We carried out 24 experiments. A set of results for one experiment is shown in Figure 1. The loading apparatus was suitable for wet snow experiments, however, the tube network was not sophisticated enough to simulate natural precipitation or melting conditions. An average water content slightly larger than 6% by volume was measured at failure, the variance was substantial, though (Figure 1a). Results agree very well with previous findings. With 6% by volume water exists in continuous paths throughout the pore space and thus destroys bonds between the grains. Wet samples failed at an average critical stress $\sigma_{c,w} = 4.6 \text{ kNm}^{-2}$ which was about a factor of 2 lower than for the same dry sample. Again these

findings are in good agreement with those obtained by Bhutiyani (1994). The acoustic activity increased significantly during loading and a certain time before failure during water infiltration (Figure 1b) indicating that percolating water is very efficient in breaking bonds between snow crystals. PIV analysis showed that wet snow allowed much more deformation before failure and rather collapsed than fractured with a recognizable pattern compared to dry snow (Figure 1c).

The experimental setup is in general suitable; nevertheless the setup has to be optimized for recording water content and controlling the water influx.

Liquid water clearly influences the snow microstructure and alters the failure behavior. Water decreases the strength of the snow sample by a factor of 2 which leads to a pronounced collapse failure instead of a shear fracture (dry snow).

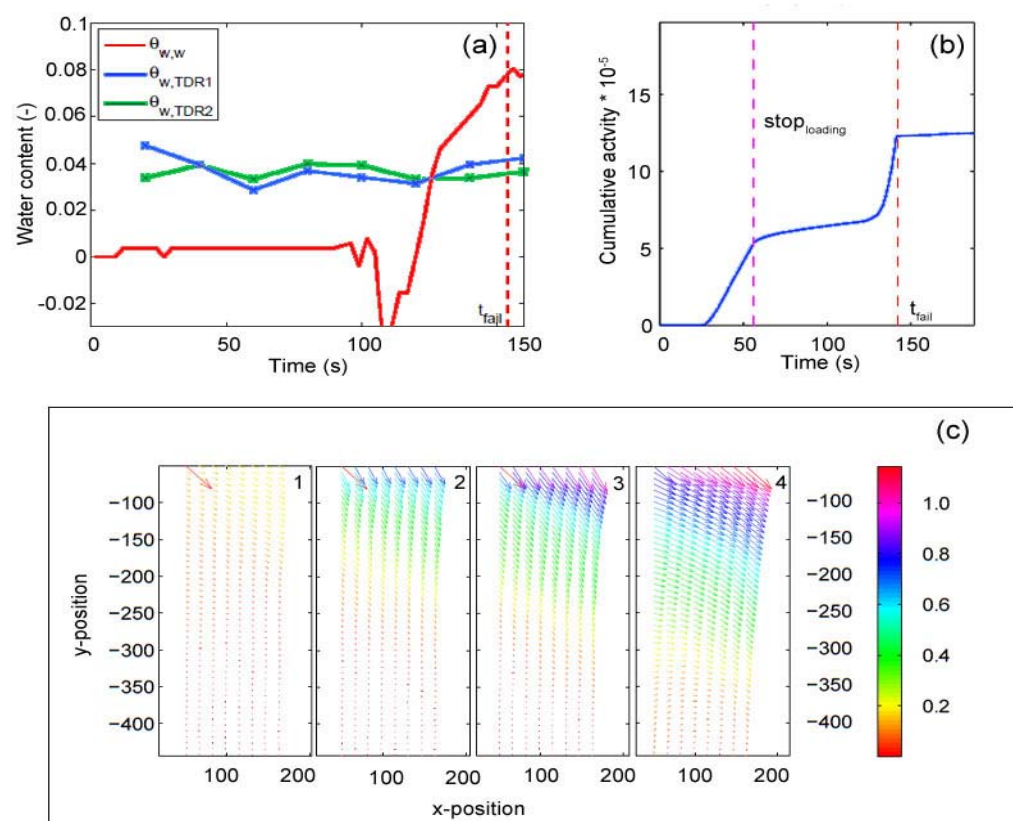


Figure 1: (a) Vol. liquid water content (θ_w) recorded with two TDR-probes ($\theta_{w,TDR1+2}$) and calculated using influx data ($\theta_{w,w}$) during experiment 19. Sample failure was at $t = 142$ seconds (red dashed line). (b) Acoustic emissions: typical example of cumulative count activity for experiment 19. Pink dashed line marks the end of loading and start of wetting, red dashed line marks failure of the sample. (c) Evolution of displacement field produced with PIV. 1 is showing the beginning of the experiment, 4 the last picture before failure of the wet sample. The red arrow is a reference arrow with constant length and direction; units are in pixel size (1 pixel ≈ 0.18 mm).

REFERENCES

- Bhutiyani, M.R., 1994. Field investigations on meltwater percolation and its effect on shear strength of wet snow. In: K.C. Agrawal (Editor), Proceedings Snow Symp - 94. Snow and Avalanche Study Establishment, Manali (H.P.), India, pp. 200-206.
- Brun, E. and Rey, L., 1987. Field study on snow mechanical properties with special regard to liquid water content. In: B. Salm and H. Gubler (Editors), Symposium at Davos 1986 - Avalanche Formation, Movement and Effects, IAHS Publ., 162. International Association of Hydrological Sciences, Wallingford, Oxfordshire, U.K., pp. 183-193.
- Reiweger, I., Schweizer, J., Ernst, R. and Dual, J., 2010. Load-controlled test apparatus for snow. Cold Regions and Technology, 62(2-3): 119-125.

P 9.1

On the reliability of indicator path avalanches for local avalanche forecasting

Claudia Alig, Christoph Mitterer, Jürg Schweizer

WSL Institute for Snow and Avalanche Research SLF, Flüelastrasse 11, 7260 Davos Dorf, Schweiz (mitterer@slf.ch).

Still today we cannot reliably predict the occurrence of snow avalanches at the local scale, e.g. for a section of a transportation corridor. As avalanches are clear signs of instability, they are often considered as the best predictor for further events. In fact, avalanches that release at the beginning of a period with high avalanche activity, are called indicator path avalanches by avalanche professionals as they indicate a high probability of further avalanche events in that specific area. In the present work, we will check whether such indicator path avalanches exist and whether they can be used to improve local avalanche forecasting.

Long-term avalanche occurrence data for three areas in Switzerland, namely the Urseren valley in canton Uri as well as for Davos and Zuoz in the Canton of Grisons are analysed. We focus on avalanche paths where avalanches frequently occur, which may have the potential to act as precursors. We define an avalanche path as indicator path, if the majority of all avalanches in the surrounding region release at the same day or on one of the consecutive three days. Releases on the days before would decrease the value of a typical indicator path avalanche. In the region of Davos, the Salezertobel avalanche with a return period of about one year was found to have a certain precursor function, but only if it is of a certain size (Figure 1). The return period of these large-sized avalanches is five years. In the Urseren valley which runs about west to east from Realp to Andermatt, two indicator path avalanches were found: the Böschenlauri on the northern slopes of the valley and the Lochthal-, Lauital- and Spitzegglaui avalanches on the southern slopes. These three avalanches can be grouped to one single precursor avalanche as they have similar aspect, incline and length. In the community of Zuoz, in the Upper Engadine valley, four adjoining avalanches were considered and analyzed as a single indicator path avalanche. All these four avalanches with precursory function are characterized by heavy precipitation before or during the event, in most cases in combination with strong wind.

Even if indicator path avalanches can predict other avalanches to follow, the quality of the forecast remains poor. Whereas there is a good chance that the release of an avalanche in an indicator path is followed by other avalanches, there are too many situations when some of these avalanches release but not the one in the indicator path. To sum up, based on our analysis, it seems not feasible to forecast other avalanches simply based on the avalanche occurrence in an indicator path.

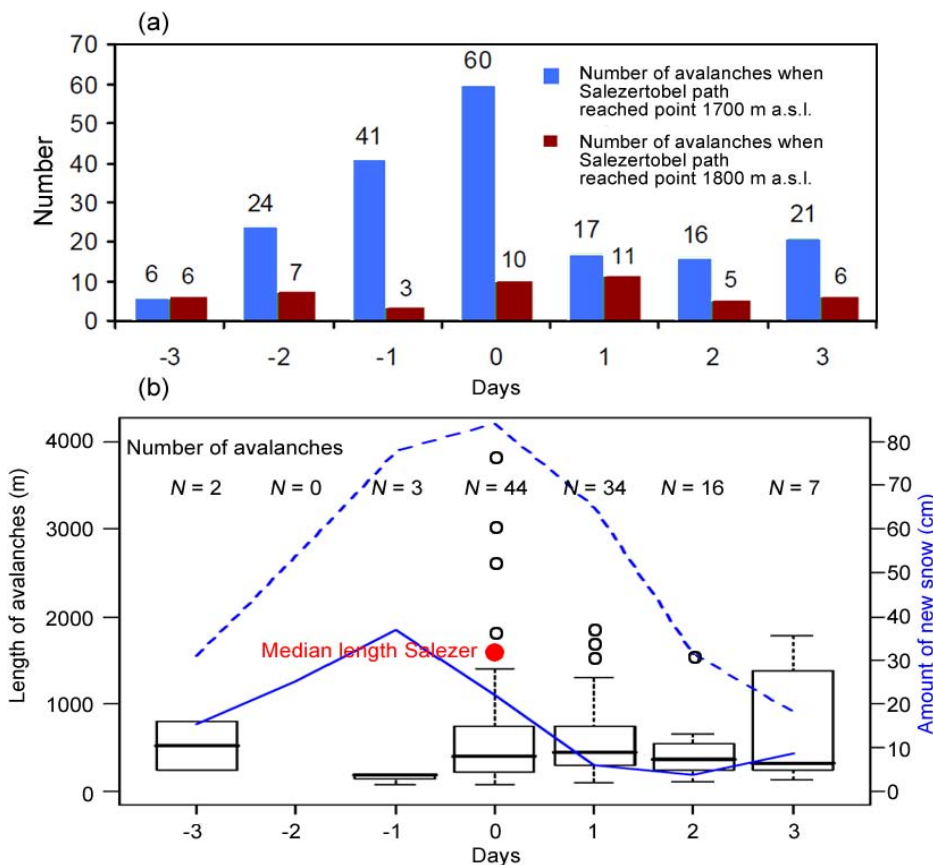


Figure 1. (a) Number of avalanches recorded in the surroundings of Davos on the 3 days before, on the day and during the 3 days after the Salezertobel avalanche run to an elevation of 1700 m a.s.l. (blue) and 1800 m a.s.l. (b) Length distribution of the avalanches recorded in the surroundings of Davos on the 3 days before, on the day and during the 3 days after the Salezertobel avalanche occurred. Boxes show interquartile range, black lines the median, whisker 1.5 times the interquartile range and open dots indicate extreme values. Red dot indicates median length of the Salezertobel avalanche. Blue solid line shows the new snow depth within 24 h, dashed blue line the 3-day sum of new snow.

P 9.2

Past and future glacier changes in the western Nyainqentanglha Range on the Tibetan Plateau

Bolch Tobias^{1,2}, Linsbauer Andreas¹, Chen Feng³, Wei Yang³, Kang Shichang³

¹Geographisches Institut, Universität Zürich, Zürich, Switzerland

²Institut für Kartographie, Technische Universität Dresden, Dresden, Germany

³Institut of Tibetan Plateau Research, Chinese Academy of Sciences, Beijing, China

Glaciers are characteristic elements on the Tibetan Plateau and are contributing to its water resources. The glaciers receded throughout the region during the last decades with few exceptions only. This shrinkage has not only caused an increase in runoff, but contributed also to the measured increase in lake levels which caused flooding of pastures. Knowledge about past and future glacier changes is therefore essential to understand the mechanisms and the importance of glacier runoff in the hydrological cycle.

We quantify these changes for the western Nyainqentanglha Range (Figure 1). The study region is located in the south-eastern centre of the Tibetan Plateau and is of special interest for glacio-climatological research: The region is influenced by both the continental climate of central Asia and the Indian Monsoon system and is situated in the transition zone between maritime and continental type glaciers.

The approach to determine past and model future changes requires multi-temporal satellite imagery, digital elevation models (DEMs) and representative time series of climate data. In a first step, a glacier inventory for the entire mountain range for the year ~2000 was generated using semi-automated remote sensing and GIS techniques based on Landsat ETM+ and SRTM3 DEM data. Furthermore, satellite data from Hexagon KH-9, Landsat MSS (year 1976), and Landsat TM/ETM+ (1991, 2001, 2005, 2009) were used to assess past changes through time.

The modelling of future glacier changes is based on two inputs: glacier elevation change in the past and a modelled glacier bed. A core element of the approach is the assumption that the thickness loss observed for the period 1970 – 2000 (by differencing the SRTM DEM from a DEM based on topographic maps) will continue in a similar way in the future. When future thickness change reaches the glacier bed, the respective part of the glacier area is removed in the model. Glacier thickness is estimated based on a mean basal shear stress for each glacier (derived from its elevation range) and local thickness values derived from an averaged surface slope angle (Linsbauer et al. 2009). Both information layers served as an input for a Geographic Information System (GIS) that is used to spatially extrapolate the local ice thickness values within the limits of the glacier. The results are calibrated and evaluated with direct thickness measurements and cumulative mass balance values. The latter are either derived from direct measurements or modelling on Zhadang Glacier, using climate data from surrounding stations and modelled climate data.

The entire western Nyainqentanglha Range contains about 960 glaciers covering an area of . The glacier area decreased by $6.0 \pm 3.0\%$ from 1976 to 2001, which is less than presented in previous studies based on topographic maps and Landsat data. However, the shrinkage rate increased in the period from 2001 to 2009 (Bolch et al. 2010). The ice thickness model gives a mean ice thickness of about 30 m in the year 2000 and the DEM comparison reveals an average thickness loss of 0.3 m/a with an increasing rate in recent years. At these rates the glacier will certainly survive the 21st century. The modelling of future glacier thickness is under way and results will be presented based on different climate change scenarios.

REFERENCES

- Bolch, T., Yao, T., Kang, S., Buchroithner, M. F., Scherer, D., Maussion, F., Huintjes, E. & Schneider, C. (2010). A glacier inventory for the western Nyainqentanglha Range and Nam Co Basin, Tibet, and glacier changes 1976–2009. *The Cryosphere*, 4.
- Linsbauer, A., Paul, F., Hoelzle, M., Frey, H. & Haeberli, W. (2009). The Swiss Alps Without Glaciers – A GIS-based Modelling Approach for Reconstruction of Glacier Beds, *Proceedings of Geomorphometry, Zurich, Switzerland*, 31.8 - 2.9. 2009, 243–247.

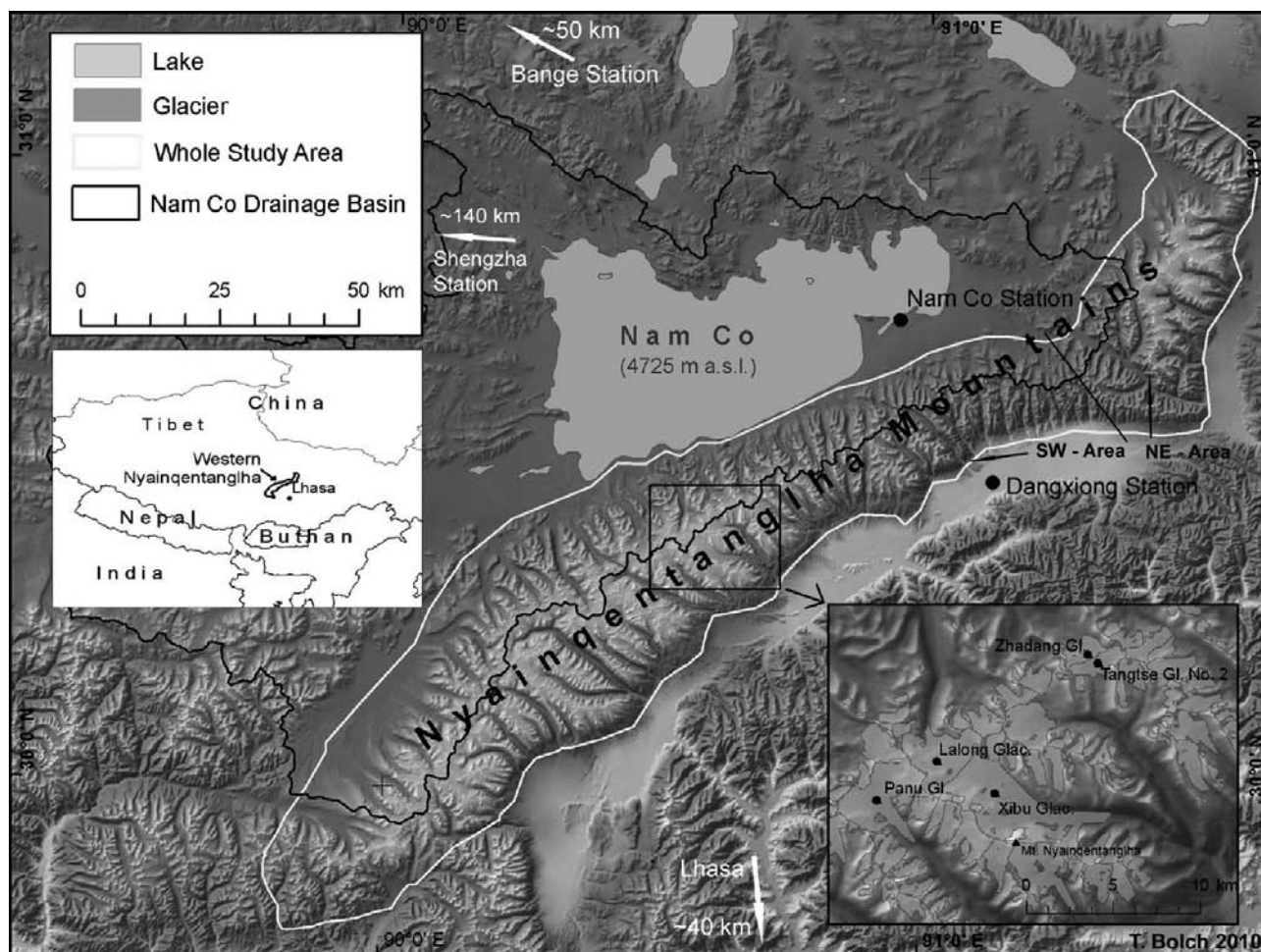


Figure 1. Overview of the study region, source: Bolch et al. (2010).

P 9.3

Effects of subsurface lateral water flow on soil thaw

Endrizzi S., Gruber S.

Glaciology, Geomorphodynamics & Geochronology, Department of Geography, University of Zurich, Switzerland

The effects of lateral water flow on the spatial distribution of depth of thaw in permafrost grounds have rarely been investigated with models. The GEOTop model, which solves the soil energy and water budgets in a coupled way and accounts phase change, has been here used to better understand how soil moisture spatial differences in the unfrozen upper part of the ground affect the thawing soil energy balance in an idealized hillslope topography. Results show that, in terrains with thermal conductivity highly variable with soil moisture, like organic soils, wetter areas absorb more efficiently heat from the atmosphere and, consequently, exhibit deeper thaw than drier areas. On the other hand, if thermal conductivity less markedly depends on soil moisture, as in mineral soils, the result is the opposite, since the effect of the higher thermal capacity resulting from higher soil moisture prevails.

P 9.4

Ice volume distribution in the Mauvoisin region and implications on glacier fluctuations

Gabbi Jeannette¹, Farinotti Daniel¹, Bauder Andreas¹ & Maurer Hansrudolf²

¹Versuchsanstalt für Wasserbau, Hydrologie und Glaziologie (VAW), ETH Zürich, Gloriastrasse 37/39, CH-8092 Zürich
(gabbij@vaw.baug.ethz.ch)

²Institut für Geophysik, ETH Zürich, Sonneggstrasse 5, CH-8092 Zürich

Profound knowledge of the ice volume distribution in a catchment is an important prerequisite for various glaciological applications. Different approaches, such as volume-area scaling relations, radio-echo soundings or borehole measurements, allow the determination of the ice volume with different levels of precision. In the Mauvoisin region, Valais Alps, five larger glacier (surface area between 5 and 18 km²) and several smaller glacier are found, which made up a total glacierized area of about 65 km². Extensive helicopter-borne ice radar measurements were carried out in this region in spring 2011. Almost 150 km of radar profiles were recorded. In order to obtain a continuous digital elevation model of the glacier bed topography, the information from the radar profiles has been integrated in the approach of Farinotti et al. (2009). First results indicate a total ice volume of about 4 km³ and a maximal ice-thickness of more than 250 m. We assessed the detailed changes in ice volume distribution and glacier geometry until the end of the 21st century by using the glacio-hydrological model GERM (Huss et al., 2008, Farinotti et al., in press) which is constrained by the most recent climate scenarios of C2SM (Bosshard et al., 2011). Extensive glacier retreat is projected independently of the scenario chosen. Smaller glaciers will disappear in the next decades. Only larger glaciers having substantial ice masses located at high elevations, will be partly left by 2100.

REFERENCES

- Bosshard T., Kotlarsky S., Ewen T. & Schär C. 2011: Spectral representation of the annual cycle in the climate change signal. *Hydrology and Earth System Sciences Discussion*, 8, 1161-1192.
- Farinotti, D., Huss M., Bauder A., Funk M. & Truffer M. 2009: A method to estimate the ice volume and ice-thickness distribution of alpine glaciers. *Journal of Glaciology*, 55(191), 422-430.
- Farinotti, D., Usselman S., Huss M. & Bauder A. & Funk M.: What will happen to runoff? Projections of runoff evolution for selected high-alpine catchments in the Swiss Alps. *Hydrological Processes*, (in press).
- Huss, M., Farinotti D., Bauder A. & Funk M. 2008: Modelling runoff from highly glacierized alpine drainage basins in a changing climate. *Hydrological Processes*, 22, 3888-3902.

P 9.5

Integration of glacier databases within the Global Terrestrial Network for Glaciers (GTN-G)

Gärtner-Roer, I.¹, Armstrong, R.², Fetterer, F.², Haeberli, W.¹, Hoelzle, M.³, Käab, A.⁴, Kargel, J.⁵, Nussbaumer, S.U.¹, Paul, F.¹, Raup, B.H.² and M. Zemp¹

¹ World Glacier Monitoring Service, University of Zurich, Zurich, Switzerland

² National Snow and Ice Data Center, University of Colorado, Boulder, U.S.A.

³ World Glacier Monitoring Service, University of Fribourg, Switzerland

⁴ Global Land Ice Measurements from Space, University of Oslo, Oslo, Norway

⁵ Global Land Ice Measurements from Space, University of Arizona, Tucson, U.S.A.

Changes in glaciers provide one of the clearest evidence of climate change and as such they constitute an Essential Climate Variable in the Global Climate/Terrestrial Observing System (GCOS, GTOS) in support of the United Nations Framework Convention on Climate Change (UNFCCC). As recommended by the International Council for Sciences (ICSU), free and unrestricted international sharing of high-quality, long-term and standardized data and information products is one of the basic requirements for advances in research as well as for political decisions.

The internationally coordinated collection and distribution of standardized information about glacier changes was initiated in 1894 and is today coordinated within the Global Terrestrial Network for Glaciers (GTN-G) under the auspices of FAO, ICSU, UNEP, UNESCO, and WMO. The GTN-G is jointly run by three operational bodies involved in glacier monitoring: the World Glacier Monitoring Service (WGMS, www.wgms.ch), the U.S. National Snow and Ice Data Center (NSIDC, www.nsidc.org), and the Global Land Ice Measurements from Space (GLIMS, www.glims.org) initiative.

With an online service (www.gtn-g.org), GTN-G provides fast access to regularly updated information on glacier distribution and changes. Currently, this includes glacier inventory data from about 100,000 glaciers mainly based on aerial photographs and maps, as well as digital outlines from about 100,000 glaciers mainly based on satellite images, length change series from 1,800 glaciers, mass balance series from 250 glaciers, geodetic thickness or volume changes from 430 glaciers, information on special events (e.g., hazards, surges, calving instabilities) from 130 glaciers, as well as 13,000 photographs from some 500 glaciers. In addition, for a number of 26 glaciers, fluctuation series (going back to the 16th century) are available as reconstructed from moraines, photographs, paintings and written documents. All of these datasets are freely available and have been used in numerous scientific publications as well as in the assessment reports of the Intergovernmental Panel on Climate Change (IPCC).

P 9.6

“Old-fashioned” photogrammetric analyses – still a key tool for the reassessment of long-term glacier changes: examples from Storglaciären, Sweden

I. Gärtner-Roer¹, M. Zemp¹, T. Koblet¹, P. Jansson², P. Thee³, W. Haeberli¹ and P. Holmlund²

¹ Department of Geography, University of Zurich, Switzerland

² Department of Physical Geography and Quaternary Geology, Stockholm University, Sweden

³ Swiss Federal Institute for Forest, Snow and Landscape Research, Birmensdorf, Switzerland

At Storglaciären, located in the Kebnekaise massif in northern Sweden, aerial photographs have been taken at decadal intervals since the beginning of the mass balance monitoring program, which was started in 1945/46. Early studies used the resulting vertical photographs to produce glaciological maps with which the in-situ observations could be verified. However, these maps as well as the derived volume changes are subject to errors which resulted in major differences between the derived volumetric and the glaciological mass balance. In this study, we reanalyzed dia-positives of the original aerial photographs of 1959, -69, -80, -90 and -99 based on consistent photogrammetric processing. From the resulting digital elevation models and orthophotos, changes in length, area, and volume of Storglaciären were computed between the survey years, including an assessment of related errors. Between 1959 and 1999, Storglaciären lost an ice volume of 19×10^6 m³, which corresponds to a cumulative ice thickness loss of 5.69m and a mean annual loss of 0.14 m. This ice loss resulted largely from a strong volume loss during the period 1959–80 and was partly compensated during the period 1980–99. As a consequence, the glacier shows a strong retreat in the 1960s, a slowing in the 1970s, and pseudo-stationary conditions in the 1980s and 1990s. In addition, we compared the calculated volumetric mass balances with the in-situ measured mass balances and were able to reassess the data series. The resulting data and findings promote the importance of aerial photographs in glacier research, especially for cross-checking in-situ measurements.

P 9.7

Ice thickness distribution of 90'000 mountain glaciers around the globe using the GLIMS database and SRTM/ASTER DEMs

Huss Matthias¹ and Daniel Farinotti²

¹Department of Geosciences, University of Fribourg, Chemin du Musée 4, CH-1700 Fribourg, Switzerland

²Laboratory of Hydraulics, Hydrology and Glaciology (VAW), ETH Zurich, Gloriastr. 37/39, CH-8092 Zurich, Switzerland

Mountain glaciers and small ice caps are expected to contribute significantly to eustatic sea level rise over the next decades. The ice volume of these more than 100'000 glaciers is normally estimated using volume-area scaling relationships (e.g. Bahr et al., 1997). Volume-area scaling does, however, not account for the characteristics of individual glaciers, and does not yield any information about the spatial distribution of the ice thickness which is required e.g. for the transient modelling of glacier ice flow dynamics. The GLIMS glacier database essentially provides 2D information about an important fraction of mountain glaciers and small ice caps on the earth. This study proposes and applies a method for adding the third dimension to glacier inventory data by inverting global digital elevation model (DEM) data to distributed ice thickness. This allows inferring additional glaciological variables that are vital for assessing the future retreat of glaciers around the globe and their contribution to sea level rise.

The method to estimate ice thickness distribution is based on glacier mass turn-over and the principles of ice flow mechanics. Using glacier elevation bands evaluated from a digital elevation model, volume balance flux is calculated and transformed into an initial guess of the local ice thickness using Glen's flow law (similar as in Farinotti et al., 2009). In an iterative procedure, the basal shear-stress distribution and the shape factor is determined along the glacier until convergence is reached. Finally, mean thickness in each elevation band is extrapolated transversal to the topographic gradient including local surface slope. Thus, for each glacier ice thickness on a regular grid can be calculated (Figure 1). The only input requirements are a glacier outline (given by the GLIMS glacier database) and a DEM.

DEMs between 60°N and 60°S are available from the Shuttle Radar Topographic Mission (SRTM) with a spatial resolution of about 90 m. North and South of 60° the Advanced Space-borne Thermal Emission and Reflection Radiometer (ASTER) DEM (30m resolution) is used.

Based on these readily available data sets, thickness distribution and ice volume of all mountain glaciers of the GLIMS data base is evaluated. Inferred thickness distribution is validated against in-situ measurements (radio-echo sounding) on about two dozens alpine glaciers, and against additional ice volume data indicating a good agreement with field data ($r^2=0.83$). The calculated ice volume of about 90'000 mountain glaciers evaluated using the presented method results in a total ice volume of 26'400 km³. Further research is required to better estimate the accuracy of the method for different mountain ranges and to overcome the many uncertainties arising from inhomogeneous elevation models or glacier inventory data.

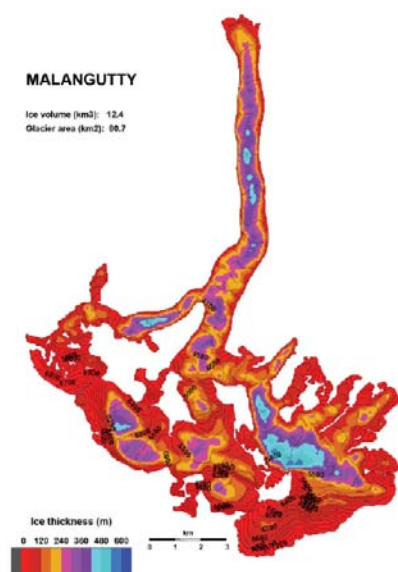


Figure 1. Calculated ice thickness distribution of Malangutty Glacier, Karakorum, 36°N 75°E.

REFERENCES

- Bahr, D. B., M. F. Meier and S. D. Peckham (1997). The physical basis of glacier volume-area scaling, *Journal of Geophysical Research*, 102(B9), 20355-20362.
- Farinotti, D., Huss, M., Bauder, A., Funk, M. and Truffer, M. (2009). A method for estimating the ice volume and ice thickness distribution of alpine glaciers, *Journal of Glaciology*, 55(191), 422-430.

P 9.8**Numerical simulation of the Young's Modulus of snow**

Köchle Berna¹, Schneebeli Martin¹

¹ WSL Institute for Snow and Avalanche Research SLF, Flüelastr.11, CH-7260 Davos
(koechle@slf.ch (B.Köchle), schneebeli@slf.ch (M.Schneebeli))

Snow is a porous, sintered material consisting of ice and air. As a highly metamorphic material its microstructure i.e the ice skeleton permanently restructures which leads to a great variability of snow types and thus to a great variability of mechanical properties. In literature the Young's modulus is empirically related to snow's density, neglecting microstructural information. With 3D images of the snow microstructure obtained by computer tomography we made voxel-based finite element calculations of the Young's modulus. For different snow types of the same density the Young's modulus can vary up to a factor of five, which can also be seen in our results. We also found that the size of the representative elementary volume (REV) for the Young modulus depends on the snow type and is, in general, much larger (up to a factor 3) than the REV for geometrical properties like density or specific surface area. Furthermore, we show that certain snow types exhibit a highly anisotropic elastic behaviour. Our results underline the importance of the microstructure of snow. At the current stage of our experiments, it remains to be seen if basic geometric descriptors of microstructure, as density (porosity) and specific surface area, are sufficient to correlate Young's Modulus uniquely.

P 9.9**The Swiss Alpine Glacier's Response to the "2 °C air temperature target"**

Machguth Horst^{1,2}, Salzmann Nadine^{2,3} & Linsbauer Andreas¹

¹ Department of Geography, University of Zurich, Winterthurerstrasse 190, CH-8057 Zurich (horst.machguth@geo.uzh.ch)

² Marine Geology and Glaciology, Geological Survey of Greenland and Denmark, Ø. Volgade 10, DK-1350 Copenhagen

³ Department of Geosciences, University of Fribourg, Chemin du Musée 4, CH-1700 Fribourg

Limiting global mean temperature increase to 2 °C ('2 °C target') is a major topic in the international climate debate. The effective impacts of a 2 °C temperature increase on regional scale systems like mountain glaciers, however, have yet received little attention.

Here, we combine homogenized long-term meteorological observations and Regional Climate Model (RCM) simulations to construct a plausible 2 °C warming scenario for the Swiss Alps. While the 2 °C target refers to a global average, a more pronounced climatic change in the Swiss Alps (Begert et al., 2005) has to be considered. Climate model output of the Alpine 2 °C scenario is then used as direct input for a glacier mass balance and glacier retreat model (Machguth et al., 2009; Huss et al., 2010). Distributed mass balance, glacier volume and area change is computed for the time span 1970 to 2150 and for 101 glaciers, representing about 50% of the glazierized area and 75% of the ice-volume in Switzerland.

The direct coupling of gridded climate scenario data to the distributed glacier mass balance model implies new challenges in model calibration. Furthermore, the experiment is challenging because both glacier retreat and subsequent adaptation of the glaciers to a new climate is modeled.

In our study, the Alpine 2 °C temperature target is reached at around 2045. From this point on no further warming occurs and glaciers adapt at various pace to the new climate: smaller glaciers reach a new equilibrium around 2080 to 2100 while the mass balance of the largest glaciers becomes zero only around 2140 to 2150. The different response times result in a characteristic curve of glacier volume and area loss: a phase of pronounced decrease ends around the year 2090 and is followed by reduced volume loss and eventually full stabilization. Relative to the year 2000 and after full adaptation in the year 2150, glacierized area and runoff are both reduced to about 45% while ice volume falls to about 25% (Figure 1).

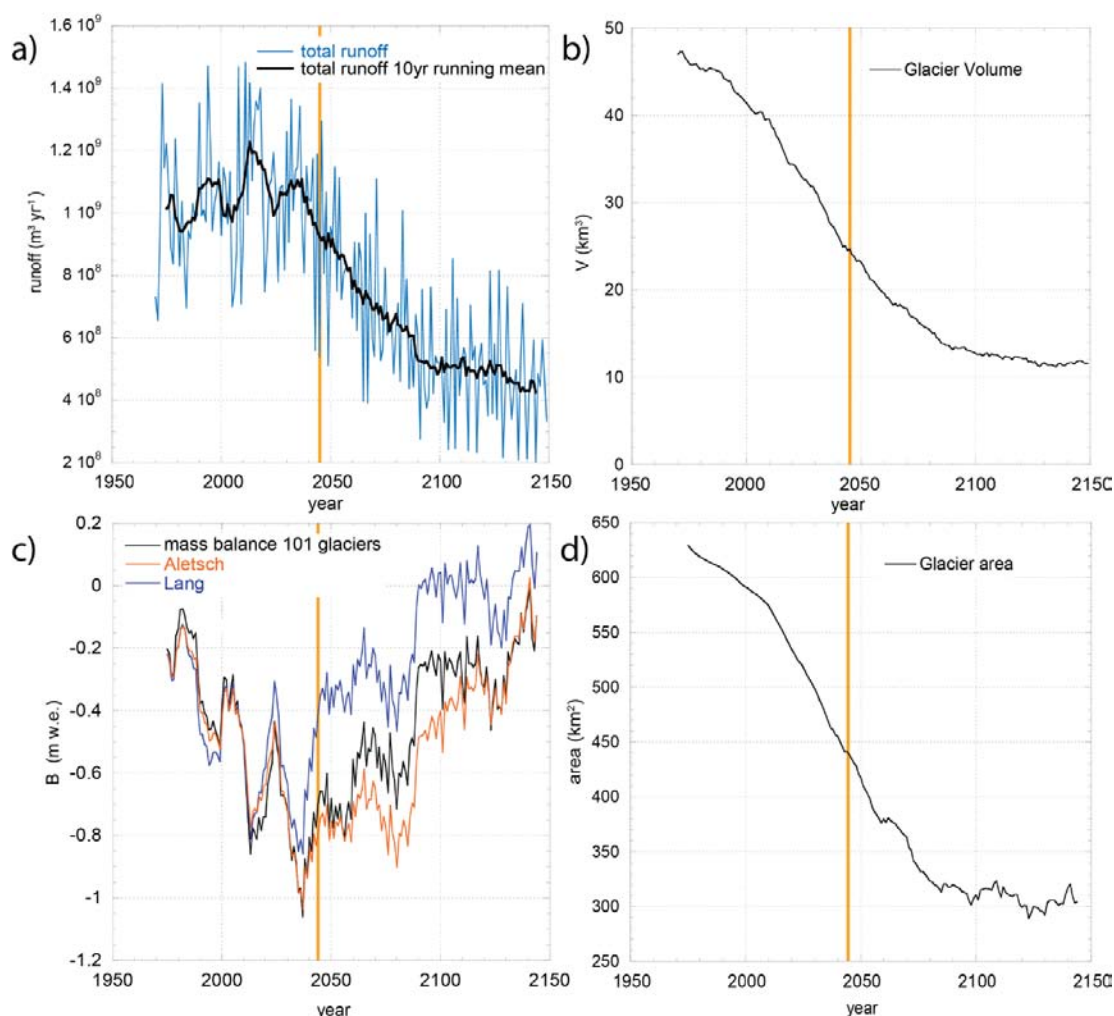


Figure 1. Model output for all 101 glaciers: (a) runoff; (b) volume, (c) mean mass balance and mass balance for Lang and Aletsch glacier (d) area.

The direct use of gridded RCM scenario is regarded as a step forward in the modeling of glacier change scenarios. Relevant feedback processes in glacier retreat like the mass balance-surface height feedback and the albedo feedback are considered. Modeled adaptation times of glaciers agree well with previously estimated response times for the Swiss Alps (Haeberli and Hoelzle, 1995). The model output provides for the first time a detailed assessment of expected changes in Alpine glaciation under a global 2 °C warming.

REFERENCES

- Begert, M., Schlegel, T. & Kirchhofer, W. (2005), Homogeneous temperature and precipitation series of Switzerland from 1864 to 2000, *International Journal of Climatology* 25(1), 65–80.
- Haeberli, W. & Hoelzle, M. (1995), Application of inventory data for estimating characteristics of and regional climate-change effects on mountain glaciers: a pilot study with the European Alps, *Annals of Glaciology* 21, 206–212.
- Huss, M., Juvet, G., Farinotti, D. & Bauder, A. (2010), Future high-mountain hydrology: a new parameterization of glacier retreat, *Hydrology and Earth System Science* 14, 815–829.
- Machguth, H.; Paul, F.; Kotlarski, S. & Hoelzle, M. (2009), 'Calculating distributed glacier mass balance for the Swiss Alps from RCM output: A methodical description and interpretation of the results', *Journal of Geophysical Research* 114, D19106.

P 9.10

Stability information supplied by the snow cover model SNOWPACK

Fabiano Monti, Jürg Schweizer

WSL Institute for Snow and Avalanche Research SLF, Flüelastrasse 11, 7260 Davos Dorf, Switzerland (monti@slf.ch).

The one-dimensional snow cover model SNOWPACK (Lehning et al., 1999) simulates snow stratigraphy using input data from automatic weather stations. The model provides information on the snow conditions reproducing most of the physical processes affecting the snow cover. For avalanche forecasting direct information on snow stability is most wanted. Lehning et al. (2004) introduced three stability indices, namely the natural stability index (S_N), the skier's stability index (S_{K38}) and the deformation index (S_d). They are mostly based on the shear strength of snow. Schweizer et al. (2006) modified the S_{K38} by introducing two parameters (difference in grain size and in hardness) which are related to snow stratigraphy (SSI). Further, they developed a classification, based on the SSI and S_{K38} that assigns a stability class (poor, fair, good) to simulated snow profiles (stability class index).

Schirmer et al. (2010) compared the characteristics of simulated and observed weak layers with observed stability conditions using the SSI to select the potentially most critical weak layer within a simulated snow profile. Based on their statistical analyses they concluded that SNOWPACK is useful to estimate snow stability. However, they noted that the relation of some weak layer properties to snow stability was counterintuitive and contrary to previous results derived from analysing manually observed profiles. Other analyses (e.g. Monti et al., 2009) did not find this discrepancy. The objective of the present work is therefore to solve the problem of these contradicting findings.

Picking the weak layer with the help of the SSI proved to be the most crucial step in estimating snow stability. We compared various versions of SNOWPACK and the corresponding implementation of SSI. In fact, with the presently implemented version, the SSI has in about 40% of the cases difficulties in finding the potentially most critical weak layer (Figure 1). Using the same data as Schirmer et al. (2010), but excluding all cases where we were sure that the weak layer was not detected correctly, we found that most weak layer parameters were either not related with stability, or the relation was not statistically significant. Integrating the simulated shear strength instead of the hand hardness index improved the discrimination power of the SSI. Based on our analyses, we suggest to recalibrate the SSI and/or to introduce a new method for assessing snow stability from simulated snow stratigraphy. The process of weak layer picking and the evaluation of its strength have to be separated. In any case, the new method must be robust against changes with in the modelling framework – otherwise repeated recalibration is needed.

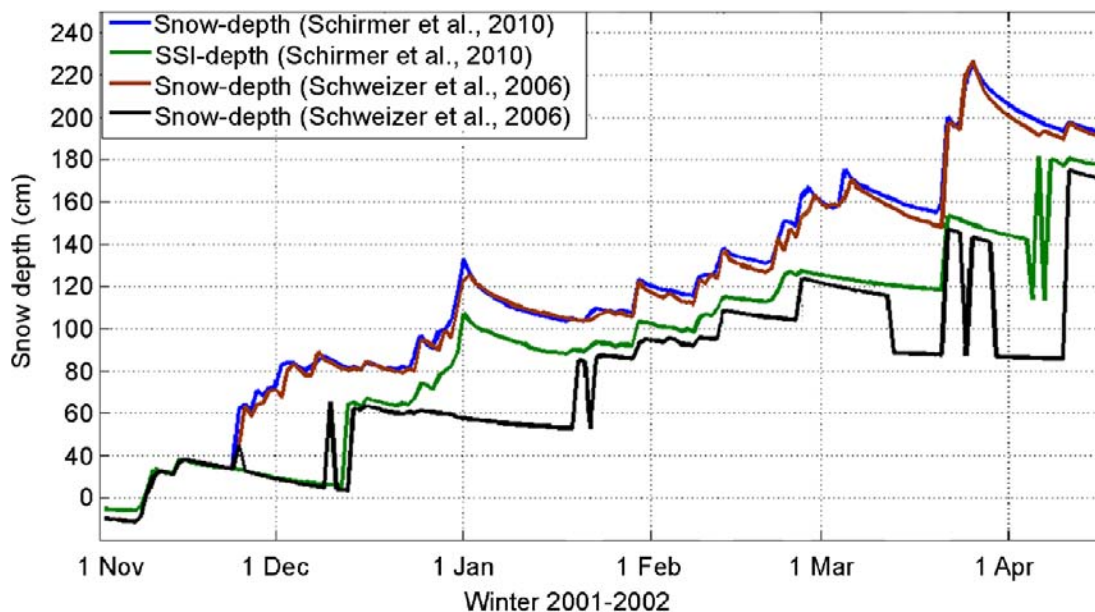


Figure 1: Comparison of the SNOWPACK simulations (winter 2001-2002) for the Weissfluhjoch study plot, used by Schweizer et al. (2006) and Schirmer et al. (2010). In the case of Schirmer et al. (2010), the SSI (green line) identifies the weak interface just below the depth of ski penetration from about the mid of December 2001 to the mid February 2002. Throughout this period, the depth indicated by the SSI is most probably not the depth of a truly critical weak layer. Therefore, these layer properties should not be used for the statistical analyses.

REFERENCES

- Lehning, M., Bartelt, P., Brown, R.L., Russi, T., Stöckli, U. and Zimmerli, M., 1999. Snowpack model calculations for avalanche warning based upon a new network of weather and snow stations. *Cold Reg. Sci. Technol.*, 30(1-3): 145-157.
- Lehning, M., Fierz, C., Brown, R.L. and Jamieson, J.B., 2004. Modeling instability for the snow cover model SNOWPACK. *Ann. Glaciol.*, 38: 331-338.
- Monti, F., Cagnati, A. and Valt, M., 2009. The 2008-2009 exceptional snowfalls in the Italian Alps: threshold sum approach and analysis of the SNOWPACK model stability indices, ISSW 2009. International Snow Science Workshop, Davos, Switzerland, pp. 318-322.
- Schirmer, M., Schweizer, J. and Lehning, M., 2010. Statistical evaluation of local to regional snowpack stability using simulated snow-cover data. *Cold Regions Science and Technology*, 64(2): 110-118.
- Schweizer, J., Bellaire, S., Fierz, C., Lehning, M. and Pielmeier, C., 2006. Evaluating and improving the stability predictions of the snow cover model SNOWPACK. *Cold Regions Science and Technology*, 46(1): 52-59.

P 9.11

Thermal changes in ventilated overcooled talus slope: a multi-methodological approach

Morard Sébastien¹, Delaloye Reynald¹

¹Geography Unit, Dept. Géoscience, University of Fribourg, Chemin du Musée 4, CH-1700 Fribourg (sebastien.morard@@unifr.ch)

Overcooled talus slopes are porous debris accumulations located in mid-latitude areas far below the regional mountain permafrost limit. These landforms are characterized by the occurrence of a negative thermal anomaly compared to the mean annual air temperature (MAAT) in the lower part of the slope, the preservation of ground ice during summertime and often by the existence of boreo-alpine species at elevation where MAAT is definitively positive. The main process leading to these cold environments is an internal and reversible mechanism of air circulation, the so-called “chimney effect” (Morard et al. 2010).

Since 2004, temperatures at the ground surface and in boreholes were recorded continuously in several sites in western Switzerland to better understand the ventilation process. In addition, the use of time-lapse electrical resistivity tomography (ERT) was used to document indirectly more precisely the 2D spatial pattern of temperature changes at depth (Hilbich et al. 2008).

The main results of this multi-methodological approach are:

- Despite differences in elevation, orientation, vegetation cover and material properties, the same seasonal thermal regime was observed in all the investigated sites. In the lower part of the talus slopes, a negative annual thermal anomaly reaching 3 to 7°C compared with MAAT is observed. This anomaly tends to increase at lower elevation. In contrast the upper part of the slope is characterized by a positive annual thermal anomaly.
- During wintertime, resistivity increases strongly (about 4 to 20 times) at the ground surface in the lower part of the talus slope, as at depth in the lower half of the debris accumulation. These modifications fit well with temperature records in borehole (figure 1). They illustrate both the deep penetration of freezing and the (re)filling of a cold reservoir inside the porous talus slope.
- The thermal conditions observed at the ground surface and in the shallow sub-surface in the blocky layer are mainly influenced by the intensity of winter cooling. The size of the cold reservoir is for instance more important during winters with cold atmospheric conditions. Winter air temperature is thus the main controlling factor for the evolution of the thermal regime of ventilated talus slope. However snowcover and summer temperatures play a less significant role.
- According to the observations of two boreholes in Dreveneuse d'en Bas (Valais Prealps, 1590m a.s.l., MAAT +4°C), a thin talus permafrost forms just a few meters below the surface in the lower part of the slope. This frozen ground extends to greater depth until the middle part of the slope, where it is found at 11.5m depth directly beneath the blocky material in finer sediments (till). This advective-induced permafrost is mainly temperate and its geometry and occurrence have suffered very rapid changes since November 2004: responding directly to contrasted interannual winter air temperature conditions, its growth has been reported between 2004 and 2006 and its thaw consecutive to the exceptional mild winter 2007. Only seasonal freezing was observed in 2008 and 2009. The little snowy but cold winter 2009-2010 led to the rebuilding of this particular extra-zonal permafrost.

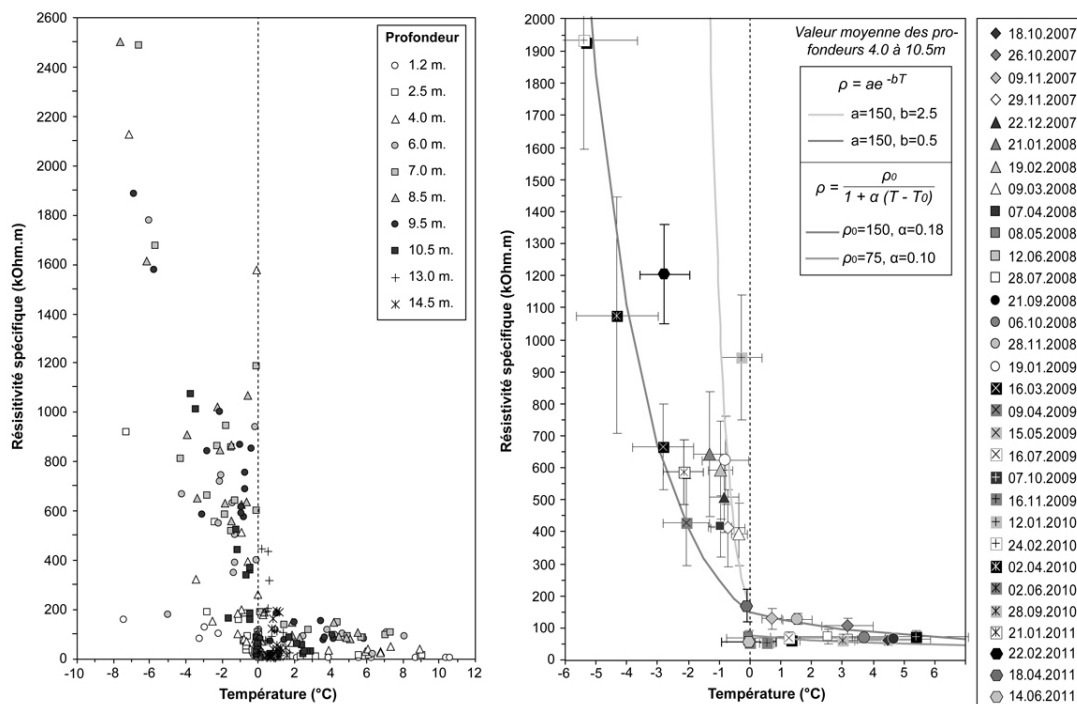


Figure 1. Resistivity – temperature relationships in the ventilated overcooled talus slope in Dreveneuse d'en Bas (Valais) (right: mean value).

REFERENCES

- Hilbich, C., Hauck, C., Delaloye, R., & Hoelzle, M. 2008: A geoelectric monitoring network and resistivity-temperature relationships of different mountain permafrost sites in the Swiss Alps, Proc. 9th Int. Conf. Permafrost, Fairbanks, 699-704.
- Morard, S., Delaloye, R., & Lambiel, J. 2010: Pluriannual thermal behavior of low elevation cold talus slopes (western Switzerland), *Geographica Helvetica*, Jg. 65, Heft 2, 124-134.

P 9.12

Surface Nuclear Magnetic Resonance Tomography on a First-Year Sea Ice Pressure Ridge

Nuber André¹, Rabenstein Lasse¹, Lehmann-Horn Jochen¹

¹Applied and Environmental Geophysics, ETH Zürich, Sonneggstrasse 5, CH-8092 Zürich (nubera@ethz.ch)

The porosity of the keel of a sea ice pressure ridge is one of the critical parameters in order to understand the evolution of the Arctic sea ice cover, since it accounts for its vulnerability against melting. Sea ice pressure ridges are built when drifting ice floes collide due to convergent forces, i.e. due to ocean currents or winds. Breaking ice blocks inclose water-filled cavities in the keel of the ridge. The determination of the keel porosity with drillings is inaccurate, because it only yields information about a few investigated points. Since the porosity within the keel equals its liquid water content, surface-NMR can be applied, a method which is directly sensitive to unbound hydrogen protons.

My master thesis (and therefore my presentation) describes the first application of surface-NMR on sea ice. A surface-NMR tomography using seven coincident soundings is performed on a first-year sea ice pressure ridge on the land fastened ice off Barrow, Alaska. The inversion yielded the water content of the shallow part of the ridge, $31 \pm 7\%$, and of deeper part, $49 \pm 7\%$ (see Figure 1).

The error range of 7% results from noise, but also from the uncertainty and the simplification of the ridge geometry, which was investigated with a synthetic modelling example. A further result of a preceding modelling study is the validation of the used numerical modelling algorithm for the calculation of the magnetic field induced by a transmitter loop at the surface.

The application of surface-NMR on sea ice is particular due to the high electric conductivity of the subsurface. The geometry of the ridge is known from drillings and yields, together with literature and the analysis of a drillcore, the conductivity distribution of the subsurface. The geometry and the conductivity distribution are successfully incorporated in the inversion of the surface-NMR data. Nevertheless, a misfit of around 30 nV (maximum amplitude around 200 nV) in the imaginary part of the sounding curves remains unexplained, giving rise to further research.

The presence of sea water on the one hand, and the absence of cultural noise due to the remoteness of the survey site on the other hand, yielded a very high signal-to-noise ratio. The good quality of the data allowed the demonstration of the effect of accounting for relaxation during the pulse (RDP). Neglecting RDP would lead to a severe underestimation of 8% water content within the deep keel. The incorporation of off-resonance effects in the forward modelling led to a reduction of 5.5 nV for the average misfit of the real part of the sounding curves.

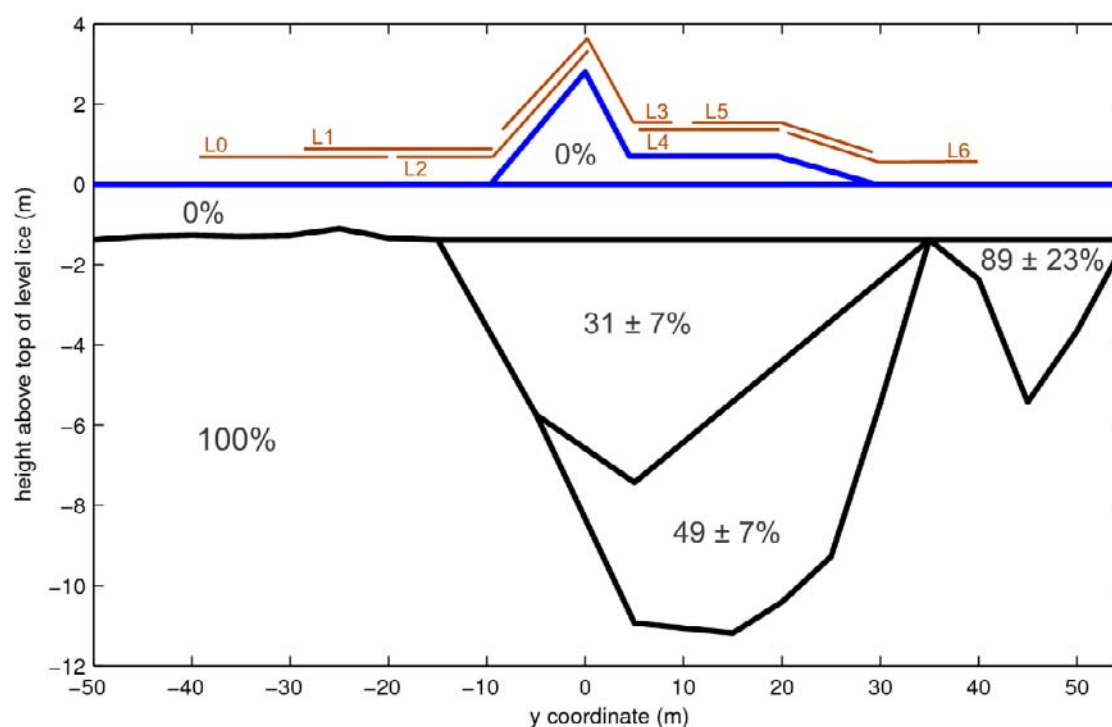


Figure 1. Profile throughout the investigated sea ice pressure ridge showing the water contents of the different blocks in %. The ridge geometry is obtained by drillings, the water contents are estimated from seven coincident surface NMR performed with the 20x20 m loops L0 to L6.

REFERENCES

- Haas, C. (2010). Dynamics versus Thermodynamics: The Sea Ice Thickness Distribution. In D. N. Thomas and G. S. Dieckmann (Eds.), *Sea Ice* (2nd ed.), Chapter 4, pp. 113–151. John Wiley and Sons.
- Hertrich, M. 2008: Imaging of groundwater with nuclear magnetic resonance. *Progress in Nuclear Magnetic Resonance Spectroscopy*, 53(4), 227-248.
- Lehmann-Horn, J. A. & Hertrich, M., Greenhalgh, S. A. & Green, A. G. (2010): 3-D Magnetic Field and NMR Sensitivity Computations Incorporating Conductivity Anomalies and Variable Surface Topography. *Earth X(X)*, 1–43.
- Walbrecker, J. O. & Greenhalgh, S. A. & Green, A. G. (2009). Accounting for relaxation processes during the pulse in surface NMR data. *Geophysics* 74(6), G27.
- Walbrecker, J. O. & Hertrich, M. & Green, A. G. (2011). Off-resonance effects in surface nuclear magnetic resonance. *Geophysics* 76(2), G1.

P 9.13

The first complete inventory of glaciers and ice caps for Eastern Greenland

Rastner, Philipp¹, Bolch, Tobias¹, Paul, Frank¹

¹*Geographisches Institut, Universität Zürich, Zürich, Switzerland*

Meltwater from glaciers and icecaps (GIC) provide a significant contribution to global sea-level rise, but estimates are uncertain due to the globally still incomplete information about glacier location and size, as well as large uncertainties in current Global Climate Models (GCMs). Recent studies that calculate global sea-level rise from GIC have developed simplified approaches using information from glacier inventories or gridded data sets and different GCMs. However, for several strongly glacierized regions very rough assumptions about the ice distribution have to be made and an urgent demand for a globally complete glacier inventory data is expressed.

The GIC on Greenland are one of these regions. Within the „EU-funded“ project ice2sea we map the Eastern part of Greenland using Landsat ETM imagery acquired around the year 2000 and the ASTER GDEM to derive topographic parameters and drainage divides. Up to now more than 5500 GIC with a total area of about 26.000 km² have been mapped between 62° and 80°N considering only glaciers with an area larger than 0.1 km² that have no direct connection to the ice sheet.

The largest valley glaciers are often debris covered, whereas smaller and mountain glaciers are often shaded due to the steep topography. Seasonal snow hiding the real glacier perimeter is a problem in some of the scenes that can only be solved by using scenes with better snow conditions. The artefacts in the GDEM are locally rather severe, but for the GIC considered for this inventory they were manageable. A comparison with the outline of the Greenland ice sheet as used in current models revealed that along the eastern coast a considerable amount of the local GIC is included in the extent of the ice sheet.

P 9.14**Short-term velocity variations of an alpine cirque glacier**Sanders Johnny¹, Cuffey Kurt² & MacGregor Kelly³¹*Geological Institute, ETH Zürich, Sonneggstrasse 5, CH-8092 Zürich (johnny.sanders@erdw.ethz.ch)*²*Department of Geography, UC Berkeley, Berkeley, CA 94020 USA*³*Geology Department, Macalester College, St. Paul, MN 55105 USA*

Since the pioneering work of Lewis and colleagues at several small glaciers in Norway (Lewis 1960), cirque glaciers have held the ignominious distinction of being simple. Given that Lewis' results predated modern glaciological theory, however, this reputation may be unwarranted. As part of a larger project designed to investigate the flow dynamics of West Washmawapta Glacier (Sanders et al. 2010), a small cirque glacier in the Canadian Rocky Mountains, we instrumented the ice surface with four GPS receivers mounted on metal conduit. Each receiver recorded its position once a day. We installed all four receivers in mid-May, when the glacier was still completely snow covered. When we returned to the glacier in early July, two of the antennas were still standing; the other two had tilted dramatically as a result of several meters of snowmelt. The average speeds of the four receivers over the course of the entire measurement period were between 6.2 and 8.0 m/yr. The highest average velocity occurred nearest the front margin of the glacier. The velocity record also shows three speedup events. We attribute the first and second speedup events to high water pressure at the glacier bed resulting from high melt rates. The third and final acceleration occurred immediately following one of the largest downpours of the summer season. The maximum speed reached at each receiver during this last speedup, which ranged from 18.1 to 20.1 m/yr, was the season high as well. We propose the development of an efficient subglacial stream network prohibited any further speedup events in the final month of the melt season, despite high temperatures and several rainstorms. Our results cast further doubt on the prevailing paradigm of cirque glacier behavior.

REFERENCES

Lewis, W. V. 1960: Norwegian Cirque Glaciers, R.G.S Research Series, 4, 104 p.

Sanders, J. W., Cuffey, K. M., MacGregor, K. R., Kavanaugh, J. L. & Dow, C. F. 2010: Dynamics of an alpine cirque glacier, *American Journal of Science* 310, 753 – 773.**P 9.15****Projection of permafrost evolution under climate change scenarios and evaluation of sensitive influencing factors**Scherler Martin¹, Hauck Christian¹, Hoelzle Martin¹ & Salzmann Nadine¹¹*Geographisches Institut, University of Fribourg, Chemin du Musée 4, CH-1700 Fribourg (martin.scherler@unifr.ch)*

Climate change as projected by contemporary global circulation and regional climate models will have a great impact on high latitude and high mountain permafrost. The impact of these changes for the time period of 1990 to 2100 has been evaluated for two characteristic high alpine permafrost sites using meteorological input of 6 different Regional Climate Models to drive a sophisticated one dimensional permafrost impact model. Statistical analysis of the modelled climate variables as well as the output of the impact model has been done to gain insight on the sensitivity of the active layer to changes in climate.

The projected snow cover at the two sites shows a general decrease in duration of about 50 to 80 days per year during the 21st century. Strong increases in active-layer thickness (ALT) of up to 100% can be seen at the sediment covered bedrock site Schilthorn followed by the formation of a talik around the year 2020 in most of the models. At the rock glacier site Murtèl the increase in ALT is less pronounced and the talik formation does not start until 2070. This thermal evolution is linked to an increase in unfrozen water content in the permafrost body at both sites.

Multiple linear regression analysis shows a strong dependence of ALT on ice content and summer soil surface temperatures and to a less significant degree on snow cover timing and duration. The ice content of the active layer in preceding years influences the ALT for about 3 to 7 years at both sites.

P 9.16

Monitoring temporal changes within the snowpack utilizing upward-looking radar systems

Lino Schmid¹, Christoph Mitterer¹, Jürg Schweizer¹, Achim Heilig^{2, 3, 4}, Olaf Eisen^{3, 4}, Robert Okorn⁵

¹ WSL Institute for Snow and Avalanche Research SLF, Flüelastrasse 11, Davos Dorf, Switzerland (schmidl@slf.ch).

² Department of Geosciences CGISS, Boise State University, Boise (ID), USA

³ Institute of Environmental Physics, University of Heidelberg, Heidelberg, Germany

⁴ Alfred Wegener Institute for Polar and Marine Research, Bremerhaven, Germany

⁵ Electronic & Technology Management (ETM) FH JOANNEUM, Kapfenberg, Austria

As the seasonal snow cover exists close to its melting point, the snow structure is constantly changing. Furthermore, the snowpack is spatially variable. Therefore, the evolution of snow stratigraphy can only be followed if using a non-destructive, continuously operating sensor system. Such systems should provide information on snow layering, snow settling, i.e. strain rates for specific layers after recent loading by precipitation, or the propagation of a wetting front.

For this study, two different upward-looking radar systems buried in the ground recorded continuous data of snow stratigraphy during the winter season 2010-2011. Under dry-snow conditions every three hours a measurement was performed; as soon as parts of the snowpack were wet, the sampling rate was changed to two measurements per hour. In addition to a previously installed and tested upward-looking impulse radar system (upGPR) a low-cost self-assembled frequency modulated continuous wave system (upFMCW) in a similar frequency range was buried in the ground. We compare the radar signals gathered with two different frequencies (600, 1600 MHz) with the upGPR to the signals recorded with the upFMCW in the frequency range of 1 - 2 GHz. Under dry-snow conditions, the radar offers the unique possibility to follow the evolution of internal snow layers, in particular to monitor settling rates of single layers. Under wet-snow conditions, the occurrence of strong multiple reflections as well as the daily increase in two-way travel time of reflection horizons allow one to determine the absolute amount of liquid water, the depth of a wetting front, the timing of the daily peak in volumetric liquid water content and its decreasing due to refreezing during the night.

9.17

Geophysical monitoring of three different permafrost forms within the Murtèl- Corvatsch Area, Upper Engadin

S. Schneider & C. Hauck

Alpine Cryosphere and Geomorphology (ACAG), Department of Geosciences, University of Fribourg, Switzerland

Permafrost in high mountain areas occurs in a great variation of surface and subsurface material and texture within short distances. Therefore, the thermal regime of the subsurface strongly depends on site-specific factors like the grain size, the pore volume and type of material beside climatic factors such as air temperature, incoming radiation and precipitation.

To fulfill a long-term aim, the analysis of the sensitivity of high mountain permafrost to climatic changes, an electrical resistivity tomography (ERT) as a regularly measured monitoring was installed. Performing geoelectrical measurements in permafrost regions implies that changes in the resistivity are due to different subsurface materials and to phase change processes of water/ice. A regularly monitoring of the subsurface allows to detect seasonal as well as annual changes of resistivity values and is therefore a useful method to analyse and predict the development of periglacial material. This poster presents two ERTM- data sets measured since 2009 for three different periglacial forms. It illustrates well the annual changes in the resistivity values and the different development of the active layer and the freezing front.

Two ERTM's were installed (one during summer 2009 and the other in 2010). Both are situated within the well investigated Murtèl-Corvatsch Area (Haeberli, W. et al 1988, Vonder Mühl et.al 2001), covering three different periglacial forms: bedrock, talus slope and rock glacier. To verify the ERTM- data, borehole temperature data (the ERTM- profiles are placed beneath two boreholes (Hanson, S. & Hoelzle, M., 2005)) was used and refraction seismic tomography (RST) was performed ones a year. For using the change of resistivity as an implication for changes in the water/ ice content, the resistivity for the frozen and unfrozen state of each investigated material was measured and verified by the borehole temperature data. To analyse seasonal changes in resistivity, ERTM-measurement were performed every 2 months and to estimate the annual changes in resistivity values, the summer ERT- data as well as the RST- data (measured in mid-august) of each year were compared.

Figure 1 presents an ERT from the Chastelets rock glacier, measured at the 09.08. 2010. Assuming that the frozen material at this site has a resistivity value of ≥ 12 kOhm, the active layer reaches until 3m depth and depth of the frozen layer is approximately 15m. The resistivity values at the other ERTM- profil which covers bedrock and talus slope, are much less probably due to the small ice content.

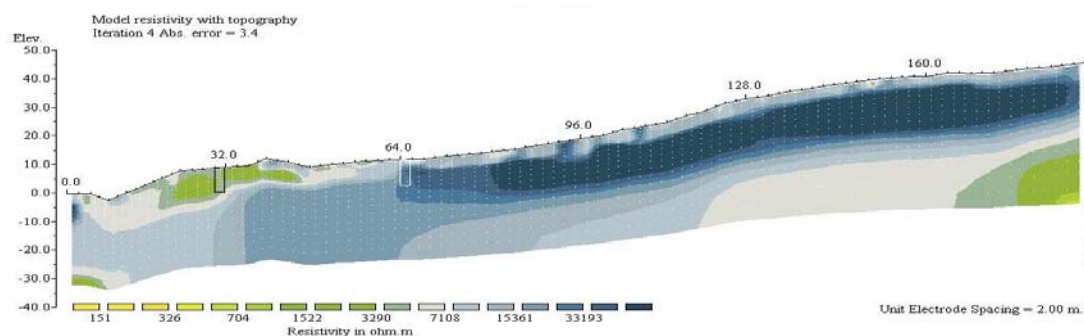


Figure1: ERT of the rock glacier "Chastelets" (09.08.2010). The places of the boreholes are marked by the rectangles.

The analysis of the ERTM and the RST data of the last three years show strong differences depending on the material. Especially the development of the freezing front of both sites varies. Regularly and longterm geophysical observation e.g. by ERTM is a useful method to understand and predict permafrost development and a first step to analyze the sensitivity of periglacial material to climatic changes.

REFERENCES

- Haeberli, W. and Huder, J. and Keusen, H.R. and Pika, J. and Rothlisberger, H., 1988. Core drilling through rock glacier-permafrost. In: *5th International Conference on Permafrost- Proceedings*. Tapir Publishers, Trondheim. p 937-942.
- Hanson, S. and Hoelzle, M., 2005. Installation of a shallow borehole network and monitoring of the ground thermal regime of a high alpine discontinuous permafrost environment. *Norsk Geografisk Tidsskrift- Norwegian Journal of Geography*. Oslo. 59: 84-93.
- Vonder Mühl, D. and Arenson, L. and Springman, S. 2001. Two new boreholes through the Murtèl-Corvatsch rock glacier, Upper Engadin, Switzerland. In: *1st European Permafrost Conference- Proceedings*. Rea, B., 26-28 March 2001, Rome., p. 48-49

9.18

Study of a new Svalbard ice core

Wendl Isabel^{1,2,3}, Isaksson Elisabeth⁴, Schwikowski Margit^{1,2,3}

¹Laboratory of Radiochemistry and Environmental Chemistry, Paul Scherrer Institut, CH-5232 Villigen PSI (isabel.wendl@psi.ch)

²University of Bern, Oeschger Centre for Climate Change Research, Zähringerstrasse 25, CH-3012 Bern

³University of Bern, Departement of Chemistry and Biochemistry, Freiestrasse 3, CH-3012 Bern

⁴Norwegian Polar Institute, Framsenteret, NO-9296 Tromsø

Svalbard is an archipelago north of Norway, surrounded by the Arctic Ocean. It ranges from 74 to 81°N and from 10 to 35°E and covers an area of 61022 km² of which 60% is glaciated.

Since the mid-1970's ice cores have been recovered from Svalbard, but very few have been studied in detail. The main issue occurring was dating due to melting processes. However, Lomonosovfonna, the highest ice field in Svalbard, was suggested to have a better preserved stratigraphy and thus be less influenced by melting than other sites on Svalbard (Pohjola et al. 2002; Moore et al. 2005).

In 1997, a 121 m long ice core was drilled at Lomonosovfonna by an expedition organized by the Norwegian Polar Institute (NPI). This core was studied in great detail, providing a historical record for the pollution and climate on Svalbard back to about 800 years (e.g. Divine et al. 2011). Furthermore, this study corroborated the assumption of less affection of the Lomonosovfonna by melting (Pohjola et al. 2002).

In the last years, the interest in black carbon (BC) has increased due to its potential impact on Arctic warming and the retreat of glaciers (Hegg et al. 2009). So far, no historical record for BC exists from Svalbard. In order to obtain this record a new 149 m long ice core was drilled at Lomonosovfonna (78°49'24.4"N, 17°25'59.2"E; 1202 m a.s.l.) in spring 2009.

This study deals with that new Lomonosovfonna ice core, focusing on the historical record of BC along with the analysis of the stable isotopes ($\delta^{18}\text{O}$, δD), ^3H and ^{210}Pb for dating purposes and other components related to climate variability and pollution such as Ca^{2+} , Na^+ , K^+ , Mg^{2+} , NH_4^+ , Cl^- , CH_3SO_3^- , NO_3^- , SO_4^{2-} .

The stable isotope record of the uppermost 2.6 m w.eq. (\approx four years) already indicated that the $\delta^{18}\text{O}$ record shows a distinctive seasonal cycle with higher values attributed to summer snow. However, the concentration records of the chemical species tend to peak in winter/ early spring in this uppermost core part which probably represents the Arctic haze phenomenon. The average ion concentrations were further found to compare well with long-term records from earlier ice core studies at Lomonosovfonna.

Moreover, the core is analyzed for BC with a single-particle soot photometer (SP2) to obtain a historical record that can then be compared to BC measurements from other Arctic sites such as Greenland, for example (McConnell et al. 2007).

Additionally, snow samples have been taken from several places around Longyearbyen and at Lomonosovfonna in March 2010. These samples have been analyzed for major ions as well as BC. In general, the concentrations of both major ions and BC are lower at Lomonosovfonna than at the other sampled sites. This can be explained by the greater distance to the potential sources, the sea or human activities, respectively, the latter being an important source for local BC pollution as already indicated by former studies.

REFERENCES

- Divine, D., Isaksson, E., Martma, T., Meijer, H.A.J., Moore, J., Pohjola, V., Van de Wal, R.S.W. & Godtliobsen, F. 2011: Thousand years of winter surface air temperature variations in Svalbard and northern Norway reconstructed from ice-core data. *Polar Research* 2011, 30, 7379.
- Hegg, D.A., Warren, S.G., Grenfell, T.C., Doherty, S.J., Larson, T.V. & Clarke, A.D. 2009: Source attribution of black carbon in Arctic snow. *Environmental Science & Technology* 43, 4016-4021.
- McConnell, J.R., Edwards, R., Kok, G.L., Flanner, M.G., Zender, C.S., Saltzman, E.S., Banta, J.R., Pasteris, D.R., Carter, M.M. & Kahl, J.D.W. 2007: 20th-century industrial black carbon emissions altered Arctic climate forcing. *Science* 317, 1381-1384.
- Moore, J.C., Grinsted, A., Kekonen, T. & Pohjola, V. 2005: Separation of melting and environmental signals in an ice core with seasonal melt. *Geophysical Research Letters* 32, L10501, 1-4.
- Pohjola, V.A., Moore, J. C., Isaksson, E., Jauhiainen, T., Van de Wal, R.S.W., Martma, T., Meijer, H.A.J. & Vaikmäe, R. 2002: Effect of periodic melting on geochemical and isotopic signals in an ice core from Lomonosovfonna, Svalbard. *Journal of Geophysical Research* 107, No.0, XX X1-X14.

P 9.19

Temporal characteristics of various cryosphere-related slope movements in high mountains: GPS measurements and analysis

Wirz, Vanessa¹, Beutel, Jan², Buchli, Bernhard² Limpach, Philippe³, Gruber Stephan¹ & Zhenzhong, Su³

¹ *Glaciology, Geomorphodynamics & Geochronology, Department of Geography, University of Zurich (vanessa.wirz@geo.uzh.ch)*

² *Computer Engineering and Networks Laboratory, ETH, Zurich*

³ *Institute of Geodesy and Photogrammetry, ETH, Zurich*

Permafrost slopes are sensitive to climate change and permafrost degradation can develop or accelerate slope instabilities. With predicted global climate change, it must be anticipated that instabilities of rock slopes and movement of ice-rich debris will increase (Haeberli and Burn, 2002). Knowledge of processes and factors affecting slope instability is essential for detecting and monitoring potentially hazardous slopes. The overall aim of this study is to detect and characterize differing slope movements in alpine periglacial environments, in order to better understand the broad range of phenomena and processes encountered. The main study site (Matter valley, Switzerland) includes exceptionally fast rock glaciers as well as various slopes where clear evidence for movement, e.g. open fractures, exist. However, the underlying mechanisms of these movements and the importance of subsurface ice for them are largely unclear.

This study is part of X-Sense, a joint research project between different research groups (geodesy, computer engineering, remote sensing and geography). Within X-Sense, new low-cost GPS devices suitable for high mountain environments have been developed (Beutel et al., 2011). Based on these measurements, high-accuracy daily differential GPS-positions and the corresponding velocities are calculated. The novelty of obtained data is that they have a high temporal resolution and can cover several years. This makes it possible to identify both velocity variations (a) within a short period (e.g. week or season) and (b) between different years. The exact timing of acceleration can help to detect influencing factors, such as snowmelt.

The low costs per GPS-device allow measuring at many locations. The high number of measurement points, located upon various slope movement types, will help to find common characteristics of cryosphere-related slope movements in high mountains. Since December 2010, 15 GPS stations on moving features have been installed.

First results from two GPS-stations, show strong short-term velocity fluctuations in spring. The velocity of a potentially destabilized rock-glacier tongue was slowly decreasing during winter. From the end of April, with increasing air-temperature and the disappearance of the snow cover, velocities increased up to nearly 2 cm/day in the middle of May, but again decreased to ~1.5 cm/day. These results demonstrate the importance of continuous (here daily) measurements over longer periods and their potential to enable the inference of factors and processes controlling slope movement.

The next analysis will include a more quantitative comparison of GPS data from the different locations and meteorological data, using descriptive statistical methods. To increase process understanding, we will apply statistical methods to combine measured data with physically-based computer simulations.

REFERENCES

- Beutel, J., Buchli, B. Ferrari, F. Keller, M. and Thiele, L. and Zimmerling, M. 2011: X-Sense: Sensing in Extreme Environments. Proceedings of Design, Automation and Test in Europe.
- Haeberli, W. and Burn, C. 2002: Natural hazards in forests: glacier and permafrost effects as related to climate change, in Environmental Change and Geomorphic Hazards in Forests. IUFRO Research Series, CABI Publishing, Wallingford/ New York (2002), edited by Sidle, R., 167–202.

P 9.20

Glacier Laser-scanning Experiment Oberwallis: project overview and first results

Michael Zemp¹, Wilfried Haeberli¹, Matthias Huss³, Philip C. Joerg¹, Horst Machguth¹, Felix Morsdorf², Philipp Rastner¹ & Michael E. Schaepman²

¹ *Glaciology, Geomorphodynamics and Geochronology Group, Dept. of Geography, University of Zurich, Winterthurerstr. 190, CH-8057 Zürich (michael.zemp@geo.uzh.ch)*

² *Remote Sensing Laboratories, Dept. of Geography, University of Zurich, Winterthurerstr. 190, CH-8057 Zürich*

³ *Department of Geosciences, University of Fribourg, Chemin du Musée 4, CH-1700 Fribourg*

Glacier mass balance is widely accepted as a key parameter in hydrological and climate change research. Traditionally, the mass balance of a glacier is measured in-situ, at an annual or seasonal basis, using ablation stakes and snow pits and compared with decadal volume changes derived from photogrammetric analysis of aerial photographs. A major drawback in glacier photogrammetry is the lack of contrast in shady and snow covered (accumulation) areas. Since the 1990s, pilot studies have repeatedly shown that airborne laser-scanning has the potential to overcome these problems and can provide accurate elevation changes at an even higher spatial resolution.

In this three-year project (2009-2012) we investigate the ability of airborne laser-scanning (ALS) for operational use in glacier monitoring at Findelengletscher in the Valaisan Alps, Switzerland. ALS flight campaigns were carried out by BSF Swissphoto in October 2005, October 2009, April and September 2010. The area of interest extends over 27 km² and is sampled with a mean point density of more than two laser echoes per square meter. In addition to the geometrical data, the laser-scanning systems used (Optech ALTM 3100 and Gemini) provided as well intensity data for every return which can be used for surface type classifications and albedo modeling. The flight campaigns were coordinated with direct glaciological mass balance measurements that have been carried out since 2004/05 and are today jointly run by the Universities of Fribourg and Zurich.

The main project goals are to (i) assess the accuracy of the ALS digital elevation products, (ii) compare the glaciological and the geodetic mass balances including a detailed uncertainty assessment, (iii) evaluate the further use of the ALS products for glaciological and hydrological applications, e.g. in combination with airborne radar surveys and airborne push-broom imaging spectrometer, and (iv) visualize the scientific findings for educational purposes and public outreach products.

This presentation provides an overview on the present state of the “Glacier Laser-scanning Experiment Oberwallis” and discusses first results of the project (see e.g. Figures 1 and 2).

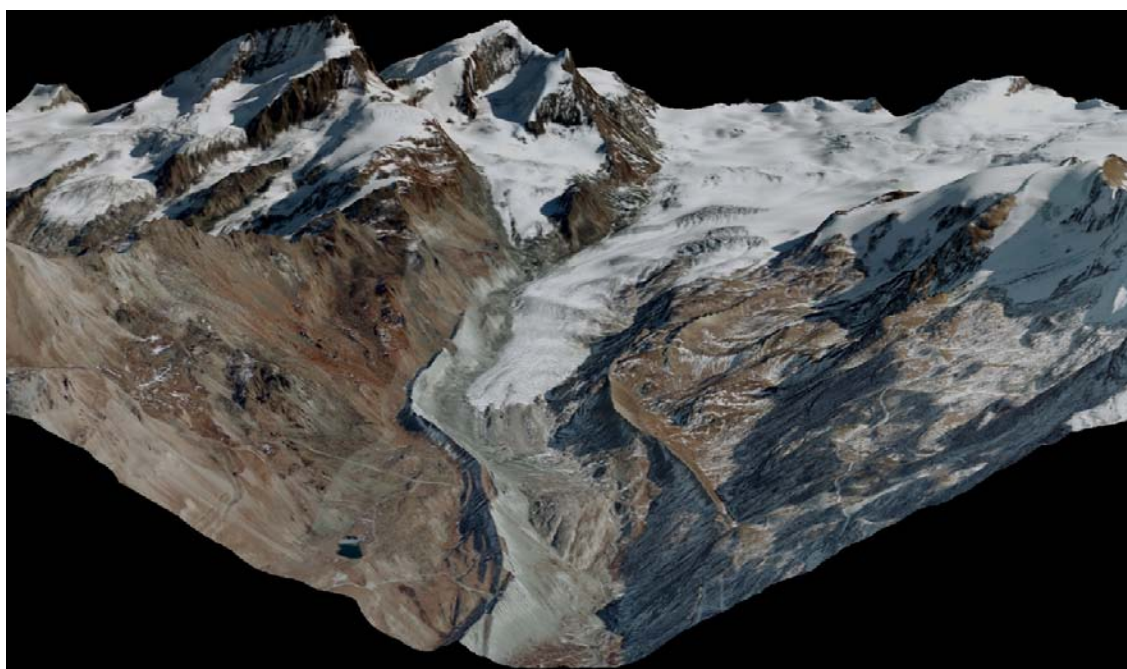


Figure 1. Virtual view of Findelengletscher, Valaisan Alps, Switzerland. The figure shows an overlay of the ALS elevation data from 2005 with an UltracamXP image mosaic from 2009.

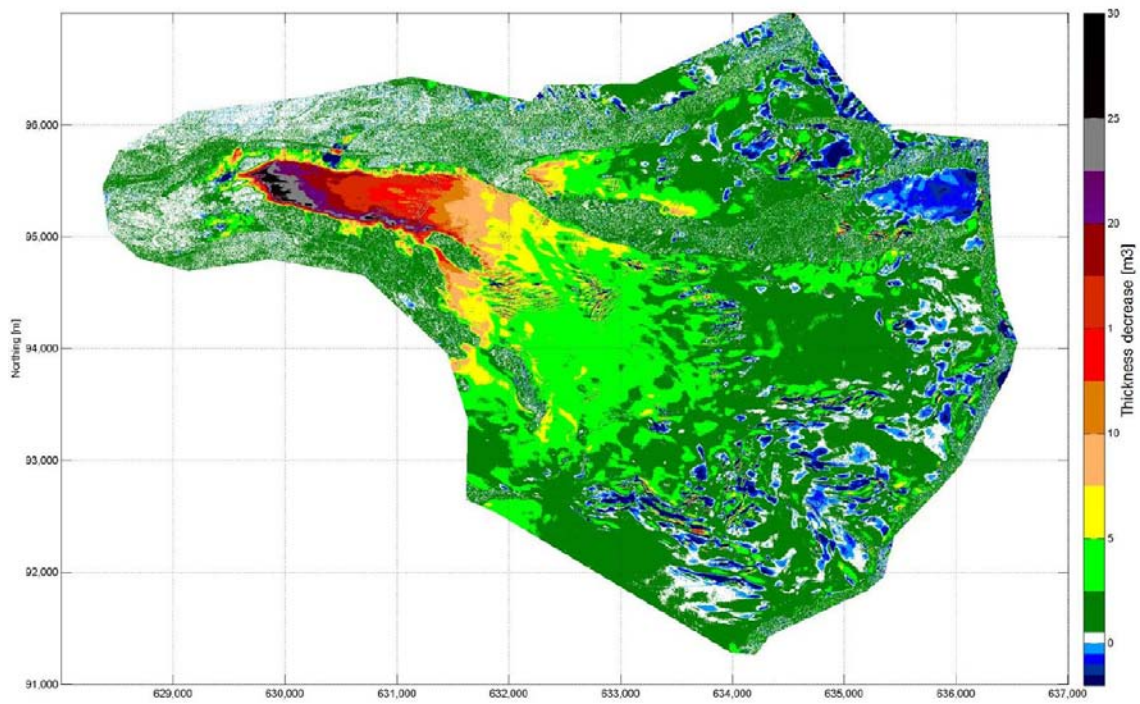


Figure 2. Elevation change as derived from differencing the digital elevation models produced by the two ALS surveys of October 2005 and October 2009.

10. Meteorology and Climatology + 11. Greenhouse Gases: Linkages between Biosphere and Climate

Rolf Philipona, Markus Furger, Werner Eugster, Christoph Ritz

*Swiss Meteorological Society,
Commission on Atmospheric Chemistry and Physics,
ProClim-,
Swiss Committee of IGBP*

TALKS:

- 10.1 Graf M., Sprenger M., Hofmann H., Seibt C., Lohmann U.: Numerical simulations of short-crested surface waves for a pre-Alpine lake using the SWAN wave model
- 10.2 Hiller R., Neiningen B., Brunner D., Künzle T., Buchmann N., Eugster W.: Regional scale methane emissions derived from concentration gradient measurements along the Reuss Valley, Switzerland
- 10.3 Kräuchi A., Philipona R., Romanens G., Levrat G.: New balloon sounding technic used to investigate the radiation error on radiosonde temperature measurements
- 10.4 Leutwyler D., Martius O., Folini D., Sprenger M., Wernli H.i: Heavy precipitation events in Europe and their connection to an upper-level stratospheric intrusion
- 10.5 Philipona R., Kräuchi a., Romanens G., Levrat G.: Radiation errors and uncertainty on radiosonde upper air temperature measurements
- 10.6 Schaller N., Cermak J., Knutti R., Wild M.: The response of the hydrological cycle to different forcing agents
- 10.7 Weibel B., Liniger M., Appenzeller C.: NCCR Climate related research at MeteoSwiss - The Swiss climate of today and tomorrow

POSTER:

- P 10.1 Lustenberger A., Knutti R., Fischer E.M.: A simple statistical model for estimating exceedance probabilities in a future climate

10.1

Numerical simulations of short-crested surface waves for a pre-Alpine lake using the SWAN wave model

Michael Graf¹, Michael Sprenger¹, Hilmar Hofmann², Christian Seibt², Ulrike Lohmann¹

¹ ETH Zurich, Institute for Atmospheric and Climate Science, Switzerland

² University of Konstanz, Limnological Institute, Germany

The spectral wave model SWAN (Simulation Waves Nearshore) was applied for Lake Zurich, a narrow pre-Alpine lake in Switzerland. It is able to simulate short-crested wind-generated surface waves. The model was forced by a dynamic wind field taken from the numerical weather prediction model COSMO-2. The winds are available in 1-h time steps. Model simulations were compared with measured wave data at one near-shore site during three different time periods dominated by: 1) low winds, 2) transient foehn winds, and 3) strong on-shore winds. The results suggest that the quality of the wave simulation highly depends on the accuracy of the input wind fields and varies strongly for different wind situations.

The influence of the temporal wind resolution is further studied with two sensitivity experiments. The first one considers a low-pass filtered wind field, based on a 2-h running mean of COSMO-2 output, and the second experiment uses a simple synthetic gust simulation, which is implemented into the SWAN model and takes into account short-term fluctuations of wind speed at 1 sec resolution. The wave field significantly differs for the 1-h and 2-h simulations, but is only negligibly affected by the gust simulation.

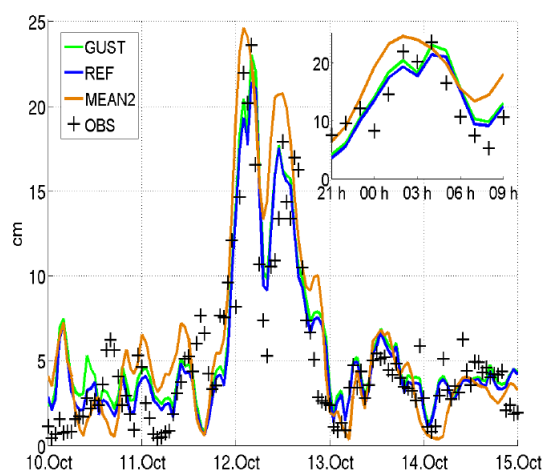


Figure 1: Time series of the significant wave height [cm] near Meilen. Grey crosses are in-situ measurements in Meilen. The solid lines are model outputs of the SWAN. The time resolution of the input winds for SWAN is given by one of the following three scenarios: (a) 1-hour resolution COSMO-2 data (REF); (b) 2-hour COSMO-2 running means (MEAN2); and (c) high-resolution (1 sec) synthetic wind speeds that take gustiness into account.

REFERENCES

- Cavaleri L. & Burgers G., 1992: Wind gustiness and wave growth. KNMI Tech. Memo., 62 pp.
 Holthuijsen L. H., 2007: Waves in Oceanic and Coastal Waters. Cambridge University Press, Cambridge, 387 pp.
 Janssen P., 2004: The interaction of Ocean Waves and Wind. Cambridge University Press, 300 pp.
 Jin K.-R. & Ji Z.-G., 2001: Calibration and verification of a spectral wind-wave model for Lake Okeechobee. J. Ocean. Eng., 28, 571-584.

10.2

Regional scale methane emissions derived from concentration gradient measurements along the Reuss Valley, Switzerland

Rebecca Hiller¹, Bruno Neininger², Dominik Brunner³, Thomas Künzle⁴, Nina Buchmann¹ & Werner Eugster¹

¹Institute of Agricultural Sciences, ETH Zurich, Universitätsstrasse 2, CH-8092 Zürich (hillerr@ethz.ch)

²Metair AG, Airfield Hausen a.A., CH-8915 Hausen a.A.

³Empa, Materials Science & Technology, Überlandstrasse 129, CH-8600 Dübendorf

⁴METEOTEST, Fabrikstrasse 14, CH-3012 Bern

Today's greenhouse gas inventories are typically based on bottom-up estimates, but comparisons to atmospheric measurements are scarce and can disagree by a factor of two or more (Nisbet & Weiss, 2010). Therefore, top-down assessments to verify the commonly used emission factors are needed. In Switzerland, 83% of the anthropogenic methane emissions are attributed to the agricultural sector (FOEN, 2010). To validate emission inventory estimates from this most relevant source in Switzerland, we performed aircraft measurements along part of the Reuss Valley, a pre-alpine valley dominated by agriculture.

Flight legs were mostly chosen to follow the terrain at constant heights of 50–400 m above ground surface. These transects showed distinct patterns in CH₄ concentrations depending on local changes in CH₄ source strength in combination with dynamic changes of atmospheric conditions. During periods with a steady valley wind system, a CH₄ concentration gradient was observed along the valley axis, with increasing concentrations along the direction of the prevailing wind. During these conditions it was possible to use a simple box model approach to calculate regional-scale fluxes. Additionally, fluxes were calculated with the help of the eddy covariance (EC) method. A spatially highly resolved CH₄ inventory allowed comparing aircraft-based regional scale flux estimates with fluxes based on default emission factors used for the Swiss national inventory report (FOEN, 2010).

In general, the regional scale fluxes derived by box and EC methods were comparable, but slightly higher than those suggested by the inventory. The scattering of fluxes based on the box model was larger than that based on the EC fluxes. However, biases are potentially present in both our estimates and the inventory. Aircraft measurements were only taken during the warm season at daytime, whereas the inventory represents mean annual flux estimates. A recent publication (Klevenhusen et al., 2010) further suggests 25% higher CH₄ emission factors for ruminants than used in the national inventory. This affects the most dominant CH₄ source in our study area. In addition, the inventory only accounts for the major anthropogenic CH₄ emissions (about 90%) and does not include natural fluxes, e.g. wetland emissions. Considering all the uncertainties, a good agreement between inventory and measurement based fluxes was found.

REFERENCES

- Nisbet, E. & Weiss, R. 2010: Top-Down Versus Bottom-Up. *Science* 328(5983), 1241-1243.
- FOEN 2010: Switzerland's Greenhouse Gas Inventory 1990–2008. National Inventory Report 2010 including reporting elements under the Kyoto Protocol. Submission of 15 April 2010 under the United Nations Framework Convention on Climate Change and under the Kyoto Protocol. <http://www.bafu.admin.ch/climatereporting/00545/10195/index.html?lang=en> (Accessed: May 27th 2011).
- Klevenhusen, F., Bernasconi, S., Kreuzer, M. & Soliva, C. 2010: Experimental validation of the Intergovernmental Panel on Climate Change default values for ruminant-derived methane and its carbon- isotope signature. *Anim. Prod. Sci.*, 50(3), 159-167.

10.3

New balloon sounding technic used to investigate the radiation error on radiosonde temperature measurements

Kräuchi Andreas¹, Philipona Rolf², Romanens Gonzague², Levrat Gilbert²

¹ETH-Zürich, IACETH, Universitätstrasse 16, CH-8092 Zürich (andik@rcm.ch) ²MeteoSchweiz, Chemin de l'Aerologie, CH-1530 Payerne (rolf.philipona@meteoswiss.ch)

Radiosondes are usually fixed with a single string of about 30 meters below a weather balloon. Analysis of video recordings and GPS data from several different flights showed that small gusts can lead to intense wobbling of the sonde. To get a smoother ascending, two balloons with a special triangle were attached to stabilize the whole radiosonde. This two balloon flight system allows releasing the carrier balloon with a controlling device inside the triangle once the sonde reached a given preset altitude. The second or parachute balloon is inflated such that the payload descends to the ground with the same speed as during ascent which leads to a much more predictable flight than before. With such a construction we were able to get rid of the wobbling which was a key element to our experiment were we need a stable platform for investigating the radiation error on radiosonde temperature measurements. The measurement of atmospheric temperature by radiosonde instruments is affected by heating from sources other than the air itself. Solar and infrared radiation, heat conduction to the temperature sensor from its attachment points, and infrared radiation emitted by the sensor are heat sources or sinks that make the temperature of the sensor different from that of the air in which it is embedded. Further we show experiments using special techniques that allow flying temperature sensors in shaded and unshaded conditions to investigate direct solar radiation effects on sensors. Results from first flights and the relation between measured radiative fluxes and the radiation effect on temperature sensors are presented.

10.4

Heavy precipitation events in Europe and their connection to an upper-level stratospheric intrusion

Leutwyler David¹, Martius Olivia², Folini Doris¹, Sprenger Michael¹ & Wernli Heini¹

¹Institute for Atmospheric and Climate Science, ETH Zurich, Universitätsstrasse 16, CH-8092 Zürich (davidle@ethz.ch)

²Oeschger Centre for Climate Change Research, University of Bern, Hallerstrasse 12, CH-3012 Bern

Floods and landslides caused by heavy precipitation (HP) events are an increasing threat to population and infrastructure. Massacand et al. (1998) and Schlemmer et al. (2010) show that along the Alpine south-side, HP events can be triggered by meridionally elongated and zonally narrow positive potential vorticity (PV) anomalies located at tropopause level over western Europe. These positive upper-level PV anomalies are filaments of stratospheric air intruding into the troposphere. In a climatological analysis, Martius et al. (2006) found that for HP events in the Alpine region upper-level PV anomalies “over western Europe occur in 73% of all HP days”. The question is whether or not this mechanism is also relevant for other areas in Europe.

Global climate models are widely used to estimate possible amplitudes, trends and impacts of future HP patterns, thus a correct representation of their link to the large-scale forcing is essential. Béguin (2009) assessed the capability of the global circulation model ECHAM5.5 to simulate upper-level PV anomalies for different model resolutions. For resolution T63 and T106 Béguin (2009) found good agreement between simulations and reanalysis data. However, regionally significant biases in the frequency of upper-level PV anomalies exist also in these high resolution simulations.

In this study we applied the methodology of Martius et al. (2006) to other areas in Europe using the ERA-40 reanalysis data set and data from the ECHAM5 global circulation model. A spatially confined, meridionally elongated frequency pattern of upper-level PV anomalies is observed on HP events in other European areas such as Eastern Europe (figure 1). The associated rain pattern is mostly limited to mountainous areas which suggests a close link between orographic lifting and the large-scale flow induced by the upper-level PV anomaly. ECHAM5 shows ambivalent performance in representing these upper-level PV anomalies. While the frequency pattern is well represented in areas with well resolved large scale mountain ranges (T63 and T106) it is mostly absent in areas with smaller orographic features.

The assessment reveals distinct large-scale flow situations leading to HP events in various regions in Europe. With the event based ECHAM5 verification we provide an approach to study the large-scale flow patterns associated with precipitation extremes in a future climate.

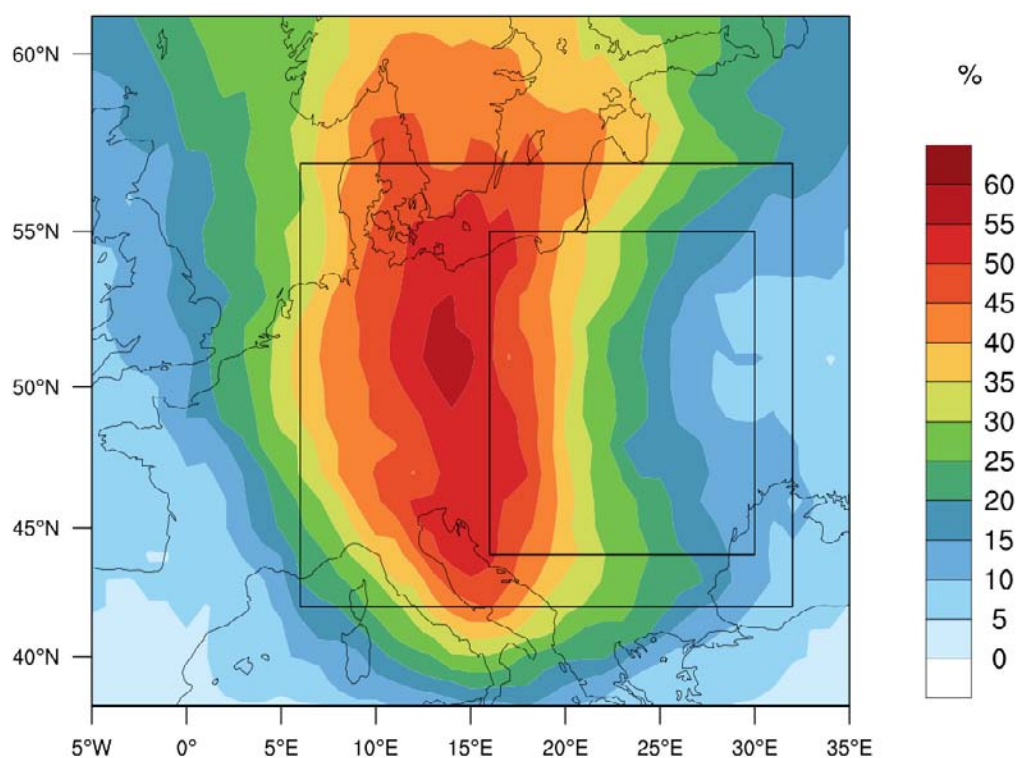


Figure 1. Frequency of upper-level PV anomalies touching the large box on days with a HP event over eastern Europe (small box).

REFERENCES

- Béguin, A. 2009. Rossby wave breaking in the global climate model echam5. Master's thesis. Institute for Atmospheric and Climate Science.
- Martius, O., Zenklusen E., Schwierz C., & Davies H.C. 2006. Episodes of Alpine Heavy Precipitation with an overlying elongated stratospheric intrusion: A climatology. *International Journal of Climatology*, 72, 172–186.
- Massacand, A., Wernli H., & Davies H C. 1998. Heavy precipitation on the Alpine southside: An upper level precursor. *Geophysical Research Letters*, 25, 1435–1438.
- Schlemmer, L., Martius O., Schwierz C., Twitchettand A., & Sprenger M. 2010. Disentangling the Forcing Mechanisms of a Heavy PRecipitation Event along the Alpine South Side Using Potential Vorticity Inversion. *Monthly Weather Review*, 138, 2336–2353.

10.5

Radiation errors and uncertainty on radiosonde upper air temperature measurements

Philipona Rolf¹, Kräuchi Andreas², Romanens Gonzague¹, Levrat Gilbert¹

¹MeteoSchweiz, Chemin de l'Aerologie, CH-1530 Payerne (rolf.philipona@meteoswiss.ch)

²ETH-Zürich, IACETH, Universitätstrasse 16, CH-8092 Zurich (andik@rcm.ch)

Atmospheric temperature profiles are long since important for meteorological purposes, but climate change issues now strongly enhanced interest in reference upper air observations. To improve radiosonde temperature measurements a new approach has been taken to determine the radiation errors on thermocouples. On the one hand shortwave solar and long-wave thermal radiation was accurately measured during radiosonde ascents. On the other hand air temperature was measured with several thermocouples on the same sonde under sun shaded and unshaded conditions, which allowed isolating heating effects of direct solar radiation. The experiments show that the very thin thermocouples (\emptyset 0.05 mm) used, experience solar radiation errors of only +0.1K at 1 km a.s.l. linearly increasing to +0.6K at 30 km. With thermal radiation being five to ten times lower than solar radiation, thermal radiative effects on thin thermocouples are negligible on day- and night measurements. Intercomparisons with other sondes however, revealed considerable larger day corrections on other sensor types. Our experiments suggest that remaining discrepancies on upper air temperature are most likely still due to large and ill corrected radiation errors.

10.6

The response of the hydrological cycle to different forcing agents

Schaller Nathalie¹, Cermak Jan¹, Knutti Reto¹ & Wild Martin¹

¹Institute for Atmospheric and Climate Science, Universitaetstrasse 16, CH-8092 Zürich (nathalie.schaller@env.ethz.ch)

This study investigates the response of the energy and water cycles to different forcing agents in global climate models. Human activities affect the climate system in several ways: greenhouse gases warm the oceans and the atmosphere by blocking outgoing longwave radiation, while aerosols have a predominantly cooling effect by scattering incoming shortwave radiation. Both forcings alter the energy budget of the Earth, which triggers responses through complex feedback mechanisms in order to reach a new equilibrium state. Among all these mechanisms, the ones modifying the processes leading to precipitation formation are of particular interest because human societies as well as ecosystems will likely have difficulties to adapt to changing precipitation patterns.

In order to better understand the sensitivity of the energy and hydrological cycles to different forcing agents, a set of idealised transient simulations with a fully coupled ocean has been performed with the NCAR CCSM3.5 climate model. First, the model is run with a transient increase of CO₂ from 355 ppm up to 710 ppm. Then the solar constant is transiently increased to reach a radiative forcing that corresponds to a doubling of CO₂ (i.e. 3.7 W/m²). In addition, simulations are also performed for CO₂ and solar forcings of doubled intensity along with a simulation combining both forcings. This allows for the investigation of the linear additivity in the response to forcings. Each simulation consists of 5 100-year runs intended to quantify the model internal variability. In a second step, ramp down simulations (CO₂ concentration is brought transiently back to 355 ppm) are run to assess if the system returns to its initial state or if it behaves non-linearly.

First results show that the temperature response to CO₂ and solar forcing of the same amplitude is significantly different, which indicates limitations in the definition of radiative forcing. The hydrological sensitivity is also found to be larger for solar forcing compared to CO₂ forcing in the global average in agreement with previous studies. Further, the response of most variables does not scale linearly with the forcing for several decades after stabilization. These results have important implications for the scaling of climate change patterns based on simple energy balance models.

REFERENCES

- Allen, M. R., & Ingram W. J. 2002: Constraints on future changes in climate and the hydrologic cycle. *Nature*, 419, 224-232.
- Held, I. M. & Soden B. J. 2006: Robust responses of the hydrological cycle to global warming. *Journal of Climate*, 19, 5686-5699.
- Wu, P. L., Wood R., Ridley J. & Lowe, J. 2010: Temporary acceleration of the hydrological cycle in response to a CO₂ rampdown. *Geophysical research Letters*, 37, L12705.

10.7

NCCR Climate related research at MeteoSwiss - The Swiss climate of today and tomorrow

Weibel Bettina, Liniger Mark, Appenzeller Christof

Federal Office of Meteorology and Climatology MeteoSwiss, Krähbühlstrasse 58, CH-8044 Zurich, Switzerland
(bettina.weibel@meteoswiss.ch)

Switzerland as an Alpine country is particularly sensitive to climate change. There is a demand and a social responsibility to present information about specific changes and possible adaptations. MeteoSwiss supports the public, research and decision makers in business and government by providing high quality climate information on the past, current and future climate conditions on different scales. This climate information and support with its interpretation and use is described as climate services (WMO, 2011).

MeteoSwiss is developing the scientific basis making high quality climate services possible bundling resources from different external fundings and a substantial internal contribution. MeteoSwiss is an active member of the C2SM (Center for Climate Systems Modeling) and participant of various research projects, in particular of the SNF NCCR Climate (Swiss National Center of Competence In Research – Climate), COST-Actions and projects funded by the European Union (FP7). MeteoSwiss coordinates the CH2011 Initiative, an update of climate scenarios for Switzerland within the framework of C2SM and NCCR Climate. The Swiss Climate Change Scenarios CH2011 will be published on September 28th.

The research project at MeteoSwiss runs from 2009 until 2012 and is divided into four subprojects: PreClim, Biotop, CombiPrecip and EURO4M. According to the key areas defined by the Stern Review (Stern et al., 2006), it is our goal to provide high resolution climate data (EURO4M, CombiPrecip) and to refine climate scenarios for user needs (Biotop, PreClim) in order to link the scientific community with real world applications.

PreClim provides climate scenarios for Switzerland for the current century based on regional climate models (Fischer et al., submitted; Weigel et al., 2010). Biotop links climate change scenario data to plant pest models, in order to investigate the potential threat of plant diseases under conditions of a changing climate. First results for codling moth (a key pest in apple plantations) for Northern Switzerland show a shift of important life phases towards earlier dates and a risk of an additional generation in the future (Hirschi et al., submitted). CombiPrecip combines information from the two classical rainfall measurements – radar and rain gauges – with statistical methods for climatological and near-real time applications such as hydrology (Erdin et al., submitted; Schiemann et al., 2010). EURO4M will provide a new high-resolution daily gridded Alpine wide precipitation data set over the last 40 years based on rain gauge observations.

REFERENCES

- Erdin, R., Frei, C. and Künsch, H.R. (submitted): Data transformation and uncertainty in geostatistical combination of radar and rain gauges. *Journal of Hydrometeorology*.
- Fischer, A.M., Weigel, A.P., Buser, C.M., Knutti, R., Künsch, H.R., Liniger, M.A., Schär, C. and Appenzeller, C. (submitted): Climate Change Projections for Switzerland based on a Bayesian multi-model approach. *International Journal of Climatology*.
- Hirschi, M., Stöckli, S., Dubrovsky, M., Spirig, C., Calanca, P., Rotach, M.W., Fischer, A.M., Duffy, B. and Samietz, J. (submitted): Downscaling climate change scenarios for apple pest and disease modeling in Switzerland. *Earth System Dynamics*.
- Schiemann, R., Erdin, R., Willi, M., Frei, C., Berenguer, M. and Sempere-Torres, D. (2010): Geostatistical radar rain-rain gauge combination with nonparametric correlograms: methodological considerations and application in Switzerland. *Hydrology and Earth System Science Discussion*, Vol. 7, 6925-6979.
- Stern et al. (2006): *Stern Review - The Economics of Climate Change*, HM Treasury, London.
- Weigel A.P., Knutti, R., Liniger, M.A. and Appenzeller, C. (2010): Risks of model weighting in multimodel climate projections. *Journal of Climate*, 23, 4175-4191.
- World Meteorological Organization. (2011): *Climate knowledge for action: A global framework for climate services – empowering the most vulnerable*. Report of the high-level taskforce for the global framework for climate services. WMO-No.1065, Geneva.

P 10.1

A simple statistical model for estimating exceedance probabilities in a future climate

Lustenberger Andreas¹, Knutti Reto², Fischer Erich³

¹Institute for Atmospheric and Climate Science, ETH Zurich, Universitätstrasse 16, CH-8092 Zurich (andreas.lustenberger@env.ethz.ch)

²Institute for Atmospheric and Climate Science, ETH Zurich, Universitätstrasse 16, CH-8092 Zurich (reto.knutti@env.ethz.ch)

³Institute for Atmospheric and Climate Science, ETH Zurich, Universitätstrasse 16, CH-8092 Zurich (erich.fischer@env.ethz.ch)

There is increasing confidence that certain types of climatic extremes will become more frequent and/or more intense under increased atmospheric greenhouse-gas concentrations. Not only the physical climate science community but also the climate impact community is interested in future trends of extreme events given their high potential impacts on infrastructure, society and ecosystems. Unfortunately, climate simulations are not available for all emission scenarios, time periods or spatial areas of interest. This raises the question whether reasonable estimations of expected changes for such cases are possible without simulating the missing information.

We here develop a simple statistical model for estimating changes in the exceedance probabilities for various percentile-related thresholds in a future climate given the expected change in the location and/or scale parameter. The applicability of this approach is investigated for a set of percentile-based temperature-related extreme indices. The underlying temperature distributions are the result of transient simulations for the SRES A1B scenario conducted by one-way nested regional climate models in the framework of the European ENSEMBLES project. First, the applicability of this simple model is evaluated for standardized temperature variables under the assumption of a constant scale parameter. In this context, the associated question is how reasonable this assumption is. Second, the complexity of this statistical model will be increased taking into account changes in the scale parameter because there is evidence that climate change affects not only the location parameter but also the variability. Finally, the skewness is taken into account using, for instance, skew-normal distributions since over parts of southern Europe the daily temperature distributions are often skewed.

12. Natural or man-made mineral dust and its influence on humans, environment and climate

Bernard Grobety, Reto Gieré, Barbara Kuhn, Nino Künzli, Urs Baltensperger

*Swiss Society of Mineralogy and Petrology (SSMP)
Commission on Atmospheric Chemistry and Physics (ACP)*

TALKS:

- 12.1 Kuhn B.K.: Dust analysis in human lungs
- 12.2 Maschowski Ch., Trouvé G., Gieré R.: Characterization of two different biomass pellets and their combustion products
- 12.3 Sodemann, H., Lai, M., Knippertz, P, Wernli, H., Stohl, A.: Validation of a Lagrangian dust transport model with data from the FENNEC/LADUNEX fieldcampaign
- 12.4 Sommer F., Gieré R., Dietze V.: Analysis of re-suspended ash from the Eyjafjallajökull
- 12.5 Stetzer O., Welti A., Lüönd F., Ladino L., Lohmann U.: The role of mineral dust particles and their surface properties for clouds
- 12.6 Wenzel M., Ebeling S., Merfort I., Dietze V., Gieré R.: Tire-wear particles and their effects on human A549 lung cells

POSTERS:

- P 12.1 Mariani I., Sigl M., Eichler A., Gabrieli J., Bolius D., Barbante C., Boutron C., Gäggeler H. W., Schwikowski M.: A 1000-year record of Sahara dust from an Alpine ice core
- P 12.2 Rahimzad Nasrin¹, Mohammadi Ali², Lak Raziye³: Sediments size characteristic of Sistan plain and Hamoon lakes as an important source of dust production in the world and adverse health effects of air pollution
- P 12.3 Spiegel J.K., Peter T., Mayol-Bracero O.L., Valle C.J., Zurcher F., Buchmann N., Eugster W.: Does long-range transported African Dust affect cloud droplet size distributions in a Tropical Montane Cloud Forest in Puerto Rico?

12.1

Dust analysis in human lungs

Kuhn Barbara K.¹

¹Zürcherische Arbeitsgemeinschaft zur Erforschung und Bekämpfung der Staublungen in der Schweiz, c/o Institut für Geochemie und Petrologie, Clausiusstr. 25, CH-8092 Zürich (barbara.kuhn@erdw.ethz.ch)

Every day, we inhale airborne dust from different sources. Natural dust sources are erosion, sandstorms, volcanic eruptions, sea spray or pollen. Forest and bush fires also contribute to the dust load as well as human activities like industry, traffic, construction and agriculture. Many people are exposed to high dust levels at their workplaces e.g. in mines, industry and construction.

Dust particles have various shapes, therefore the parameter used to describe and compare particles is the aerodynamical diameter. Particles with a diameter smaller than 8 µm are deposited in the lung. For fibrous material this means that fibers with a diameter smaller than 3 µm and as long as 100 µm can reach the alveoli. Clearance of particles/fibers mainly depends on the biopersistence of the material. So many materials get accumulated and cause health problems like silicosis (quartz), asbestosis, and hard metal (W, Ti, Ta, Nb, Mo) disease. Improvement of workplaces has led to reduced amount of inhaled dust. Silicosis has practically disappeared in Switzerland. Asbestos related diseases have a long latency period and are still diagnosed even so the use of asbestos has been banned in 1989 in Switzerland.

Workplace related dust induced lung diseases in Switzerland are insured by SUVA (Swiss Accident Insurance Fund). SUVA requires a work place investigation as well as a dust analysis on lung tissue for most insurance cases. The 'Staublungenlabor der SILAG' provides the analysis of dust separated from lung tissue or from bronchoalveolar lavage liquid (BAL).

At the 'Staublungenlabor der SILAG', the standard procedure comprises two different approaches to separate the dust from the lung tissue. One half of the sample is digested in sodium hypochlorite (Javelle) and the solution filtered on 1.2 µm Millipore filter. These filters are investigated by light microscopy to count the ferruginous bodies (see figure 1; Rüttner et al. 1991). The second half of the sample is dried and then ashed in an oxygen plasma at low temperatures. The remaining ash is dispersed in water and filtrated on 0.2 µm Nuclepore filter (Romer 1993). These filters are coated with carbon and placed on Cu-grids for TEM analysis. During TEM analysis fibers are counted, analysed by EDS, and if necessary identified by electron diffraction. The standard procedure allows the detection of fibers as short as 1 µm. Particle analysis consists of qualitative EDS spectra for approximately 100 particles.



Figure 1. Ferruginous body: asbestos fiber coated by ferro-protein, isolated from lung tissue. Photographed by B. K. Kuhn.

REFERENCES

- Romer, M. 1993: Präparation und mineralogische Analytik von Lungenstaub. Diss ETH Nr. 10129, pp.145.
 Rüttner, J.R., Romer, M., Spycher, M.A., Vogt, P. & Wälchli, P. 1991: Primäre Pleuratumoren. *Atemw.-Lungenkrkh.*, 17(6), 242-247.

12.2

Characterization of two different biomass pellets and their combustion products

Maschowski Christoph¹, Trouvé Gwénaëlle², Gieré Reto¹

¹ University of Freiburg, Institute of Geoscience Mineralogy - Geochemistry, Albertstr. 23b, D-79104 Freiburg (christoph.maschowski@neptun.uni-freiburg.de)

² Université de Haute-Alsace, Laboratoire de Gestion des Risques et Environnement, 3 bis, Rue de Alfred Werner – 68093 Mulhouse Cedex (gwenaëlle.trouve@uha.fr)

In this study, two different biomass pellets (DIN+ wood pellet and a new grass pellet “Miscanthus”) and their combustion products (bottom ash and fly ash) were investigated by Atomic Absorption Spectroscopy (AAS), Scanning Electron Microscopy (SEM) and Electron Microprobe Analysis (EMPA). Also, an attempt was made to characterize combustion derived particles by using SEM images and EDX spectra. Figure 1 shows a comparison of the particle types found for the two pellet types.

The fuels were combusted with a heating ramp (20°C to 820°C @ 20°C/min) using a glass tube reactor, and the particles were collected by an Electrical Low Pressure Impactor (ELPI) on twelve stages depending on their aerodynamic diameter. The results were compared with literature data. The main focus was put on the alkali, alkaline earth and silicon contents as these compounds lead to the formation of corrosive deposits in biomass power plants and hazardous primary and secondary particulate matter in the atmosphere.

The results reveal relatively higher potassium and calcium contents in the Miscanthus fuel and its combustion products (see figure 2 for bottom ash composition), whereas the silicon contents are almost the same for both fuel types. The unexpected high silicon and calcium content in the wood pellet is inferred to derive from contamination, probably from the pellet production process. Grains of calcite and quartz were observed in both pellet types by electron microscopy. In the grass pellet potassium and silicon were also found inside the cells (figure 3). In the bottom ash of the Miscanthus pellet, mineral phases from the melilite-group, quartz, calcite and sillimanite have been detected with X-ray diffraction. In the bottom ash of the DIN+ wood pellet, only quartz and calcite were detected.

In addition to the composition of the pellets and their combustion products, useful insights were gained on the suitability of sampling substrate materials for collecting the particles for further SEM analysis. Properties such as applicability with the ELPI, stability, purity and handling in the SEM and EMPA were taken in account while six different sampling substrate materials were used.

The main problem on the method of particle sampling and characterization for biomass combustion products was found to be the relatively large amount of organic condensates that appear to cover almost all of the ultra-fine particles on the sampling substrate and started to melt and evaporate during SEM measurements.

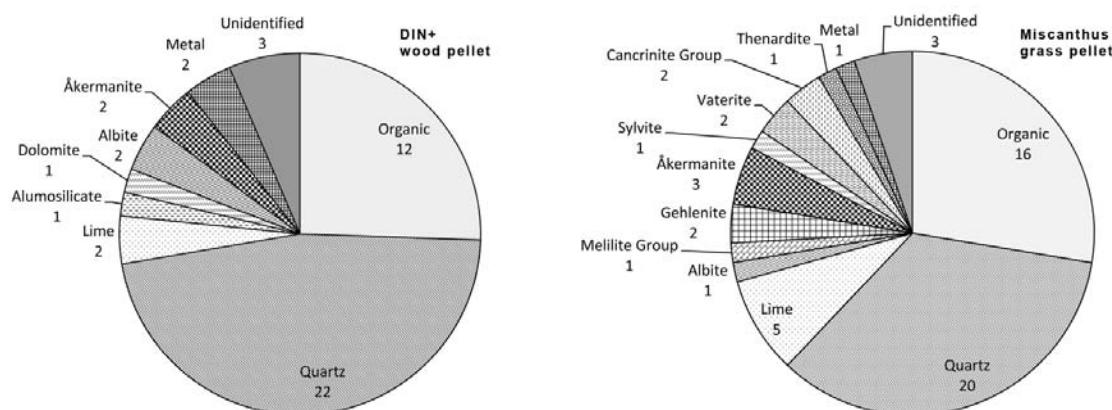


Figure 1: Distribution of particles formed during the combustion of the DIN+ wood pellet (left) and the Miscanthus grass pellet (right). Data obtained by Scanning Electron Microscopy (SEM) and EDX-Analysis.

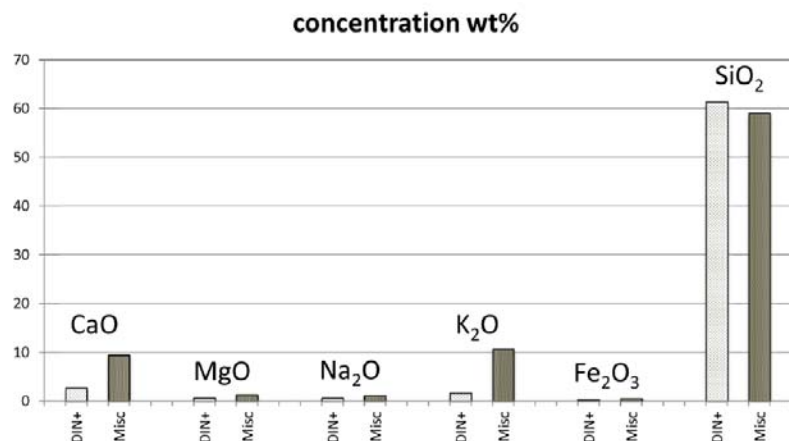


Figure 2: concentration of selected oxide components from the bottom ashes of the DIN+ wood pellet (light grey columns) and the Miscanthus grass pellet (dark grey columns) obtained by Atomic Absorption Spectroscopy (AAS).



Figure 3: Scanning electron image of a section through a Miscanthus grass pellet. The quartz grain is probably a contamination from the pellet production process or grass harvest. Spectra indicate 50 wt% silicon, 40 wt% potassium and 10 wt% calcium (roughly) inside the grass cells (probably biogenic).

12.3

Validation of a Lagrangian dust transport model with data from the FENNEC/LADUNEX field campaign

Sodemann, H.1, Lai, M.1, Knippertz, P.2, Wernli, H.1, Stohl, A.3

¹Institute for Atmospheric and Climate Science, ETH Zürich, Zürich, Switzerland

²SEE, University of Leeds, Leeds, UK

³NILU, Norway

Mineral dust aerosol is a key player in the Earth system. Strong winds over the world's major deserts mobilise and subsequently lift mineral dust high into the atmosphere. Due to the harshness and inaccessibility of desert regions, the exact processes of mobilisation and lifting, and layer formation are still unclear. One major unknown in the dust cycle is the dust source or emission strength. Despite better quantification being key for global models, the assessment of impacts on clouds, radiation and biogeochemical cycles, estimates in the literature from global and regional models span a wide range. Here, we validate the state-of-the-art Lagrangian particle dispersion model FLEXPART which has been made capable of simulating dust mobilisation and settling with airborne and ground-based mineral aerosol and turbulence measurements from the FENNEC/LADUNEX field campaign which was carried out over the western Sahara during June 2011. For selected case studies we compare in-situ data from the aircraft airborne and spaceborne LIDAR measurements and the FLEXPART model simulations. In combination, this will provide the data basis for the application of a dust inversion algorithm to provide a first step towards a new dust emission function from the inversion of airborne measurements of aerosol distribution and mass using the Lagrangian model.

12.4

Analysis of re-suspended ash from the Eyjafjallajökull

Frank Sommer¹, Reto Gieré¹ and Volker Dietze²

¹ Institut für Geowissenschaften Mineralogie - Geochemie, Albertstr. 23b, 79104 Freiburg (FrankSommer@t-online.de)

² Deutscher Wetterdienst, Research Centre Human Biometeorology, Air Quality Department, Stefan-Meier-Str. 4, D-79104, Freiburg

The 2010 eruption of the Eyjafjalla volcano had a great impact on international air traffic and illustrated the potential risks of active volcanism. It also showed the need for more investigations on the properties of airborne ash particles emitted by explosive vents. The explosive reaction between the magma and the ice from the glacier produced an extreme plume of ash up to 20 km in height in the atmosphere. The large particle fraction was deposited around the volcano and smaller sizes have been transported mainly southwards over Europe. The present study is focussed on particle re-suspension by wind conditions after the eruptions. It aims to examine the airborne particles and to develop automated analysis techniques.

Ambient air samples of airborne re-suspended ash were collected in winter 2010/11 with a passive sampler of the Sigma-2 type positioned 12 km south of the eruption zone. The first examination has been performed manually to ascertain the properties of the sample. Using an optical microscope under transmitted, polarized and cross-polarized light and an electron microprobe with BSE and EDX-analysis around 200 particles were characterized. Subsequently, the data were processed with an image analysis program. This procedure allowed for a categorization of the individual particles as glass, mineral, composite or agglutinated particles as well as to obtain chemical information about individual particles. To gain a statistically relevant overview about the composition of the sample and to minimize the analytic work, a larger area of the same sample, including the area studied manually, was examined using automatic single-particle SEM analysis (EDAX Genesis program), which resulted in characterisation of approximately 1600 particles. The results of both methods were compared against each other to evaluate the advantages and disadvantages of the different approaches and to develop the combined analytical approach further.

The examined particles range from 2.5 μm to 80 μm in size (equivalence diameters). The size distribution shows the typical character of ambient aerosol, i.e. increasing size with decreasing number of particles. The main fraction is contributed by particles larger than 10 μm . Only about 10 % (surface area) of the particles consist of glassy material; the main part is crystalline. With a surface-area fraction of 63 %, feldspar is the dominating mineral (plagioclase 43 %, K-feldspar 20 %), followed by pyroxene (18 %) and quartz (12 %). In minor quantities (1% or less) olivine, ilmenite and titanite can be found. The sample is also contaminated with salt of oceanic and/or volcanic origin.

To obtain optimal results a combination of automated and manual analysis is required. Only an automated method allows for an examination of a large number of particles, but the manual control is necessary to obtain more detailed information about the composition and the crystallinity of the particles.

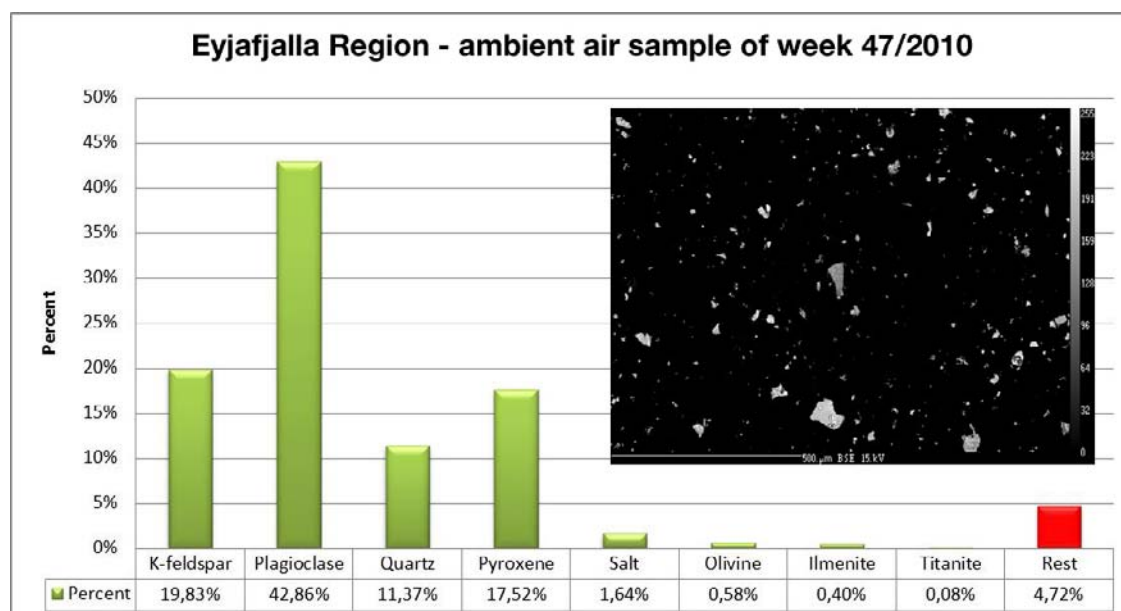


Figure 1. BSE image and the distribution of the surface area of the minerals in percent.

12.5

The role of mineral dust particles and their surface properties for clouds

Olaf Stetzer, André Welti, Felix Lüönd, Luis Ladino, Ulrike Lohmann

Institute for Atmospheric and Climate Science, ETH Zurich

Mineral dust particles are among the most abundant particle types in the atmosphere. They can serve as catalysts for chemical reactions in the atmosphere but also for phase transitions such as the formation of ice crystals in clouds. Once ice crystals start to form within a cloud it changes its radiative properties because they scatter light differently than cloud droplets. But ice crystals also often initiate precipitation and therefore reduce cloud lifetime. All these processes are important in the climate system and changes in the number of ice forming particles (ice nuclei) or their properties (temperatures at which they activate) can ultimately influence the global climate. But our knowledge of the underlying fundamental processes is still incomplete and especially the chemical and physical properties that govern the ice nucleation ability of a particle are still unknown. Classical Nucleation Theory may be applied for these processes and the important particle properties can be summarized here in the parameter called contact angle. It becomes even more complex when the variability of the particle surface is considered. It is a subject of current research how this variability can be parameterized with probability density functions of the contact angle.

Another degree of complexity results from the fact that different mechanism for ice nucleation in clouds exist. These are deposition nucleation, immersion freezing, condensation freezing, and contact freezing. Their relative importance is also a subject of current research. It is however unquestioned that the relative fraction of the different modes depends on the thermodynamic conditions within a cloud.

In our lab we investigate these different ice nucleation mechanisms with individual experiments for the different mechanisms using mineral dust aerosols (Ladino et al. 2011; Lüönd et al. 2010). In this paper, our recent results on the ice nucleation properties of mineral dust particles for immersion freezing, and contact freezing are presented and compared. The results demonstrate how different particle types differ in their ice nucleation ability as a function of temperature but also particle size. We also investigated the frozen fraction of droplets as a function of residence time. These measurements are compared with different model calculations, which are based on theoretical assumptions about the surface properties of the dust particles.

REFERENCES

- Ladino, L. A., O. Stetzer, F. Lüönd, A. Welti, and U. Lohmann. "Contact freezing experiments of kaolinite particles with cloud droplets." *Journal of Geophysical Research*. doi:10.1029/2011JD015727.
- Lüönd, F., O. Stetzer, A. Welti, and U. Lohmann. 2010. "Experimental study on the ice nucleation ability of size-selected kaolinite particles in the immersion mode." *Journal of Geophysical Research* 115: 14 PP. doi:201010.1029/2009JD012959.

12.6

Tire-wear particles and their effects on human A549 lung cells

Melanie Wenzel¹, Sandra Ebeling², Irmgard Merfort², Volker Dietze³, and Reto Gieré¹

¹ Institut für Geowissenschaften, Albert-Ludwigs-Universität, Albertstraße 23b, 79104 Freiburg, melanie.wenzel@venus.uni-freiburg.de

² Lehrstuhl für Pharmazeutische Biologie und Biotechnologie, Institut für Pharmazeutische Wissenschaften, Stefan-Meierstr. 19 (VF), 79104 Freiburg

³ Deutscher Wetterdienst, Research Center Human Biometeorology, Stefan-Meier-Str. 4, D-79104, Freiburg, Germany

In the recent time there has been a lot of discussion on the real properties of tire-wear particles, especially concerning their size and characteristic features but also with respect to their effects on health. In this study, three different tire-wear samples from the tire-test rig of the BAST in Bergisch-Gladbach (Germany) as well as one pure tire sample were analysed to specify parameters, such as, size distribution, chemical composition, particle structure, and optical behaviour. In a further step, the impact of tire-wear and tire particles on human lung cells, from the commonly used lung cell line A549, were investigated. An important goal was to develop standard treatment procedures, which lead to representative results and minimize the influence of preparation agents. The automated optical microscope analysis delivered information concerning the size and the grey value of the particles. In contrast to previous estimates, the pure tire sample contained both opaque and transparent particles. This result is not in agreement with the usual counting methods, for which so far only the opaque particles were regarded as tire material whereas the transparent particles were assumed to originate from the pavement only. Still, the transparent particles could result from pavement material, which stuck to the tires before they were shredded and ground for the experimental work. For the real tire-wear particles the size distributions were distinct for the different samples, but only one sample showed the often described bimodal size distribution with modes at approximately 7 µm and 20 µm. All samples contained particles smaller than 10 µm and opaque as well as transparent particles.

The experiments have shown that the lung cells, which were exposed for up to 8 h to the various samples at concentrations between 5 and 50 µg/cm², did not show any increase in NF-κB-DNA binding activity. An exception is one sample, for which an 8 h exposure to 50 µg/cm² sample material, led to a stronger increase in NF-κB-DNA binding activity measured by EMSA. Activation of the transcription factor NF-κB is closely linked to inflammatory processes.

Cytotoxicity tests revealed an increased cytotoxic potential for all the samples from the tire-test rig but not for the pure tire material. The extent of cytotoxicity, as measured by the MTT test, varies with concentration but is not always increasing with higher concentrations (Fig. 1). Whereas in most cases cytotoxicity is only slight, one sample induces cytotoxicity up to about 50%.

The preliminary results of this study indicate that there is a certain amount of particles smaller than 10 µm present, which is able to penetrate into the deeper part of the human lung and may cause health impacts.

The results from the cytotoxicity tests point to a negative impact on cells and health in general. However, additional tests are needed to corroborate the first conclusions. This study has so far also shown that there are significant differences between the samples from different tire types. Also the effects of pure material are distinct. This may either be due to structural differences or the cytotoxic effect resulting from the pavement material, which is present in small amounts and is abraded to a different extent by the different tire types. This question and the influence of size or chemical composition of the tire particles on the cells will be in the subject of further investigations.

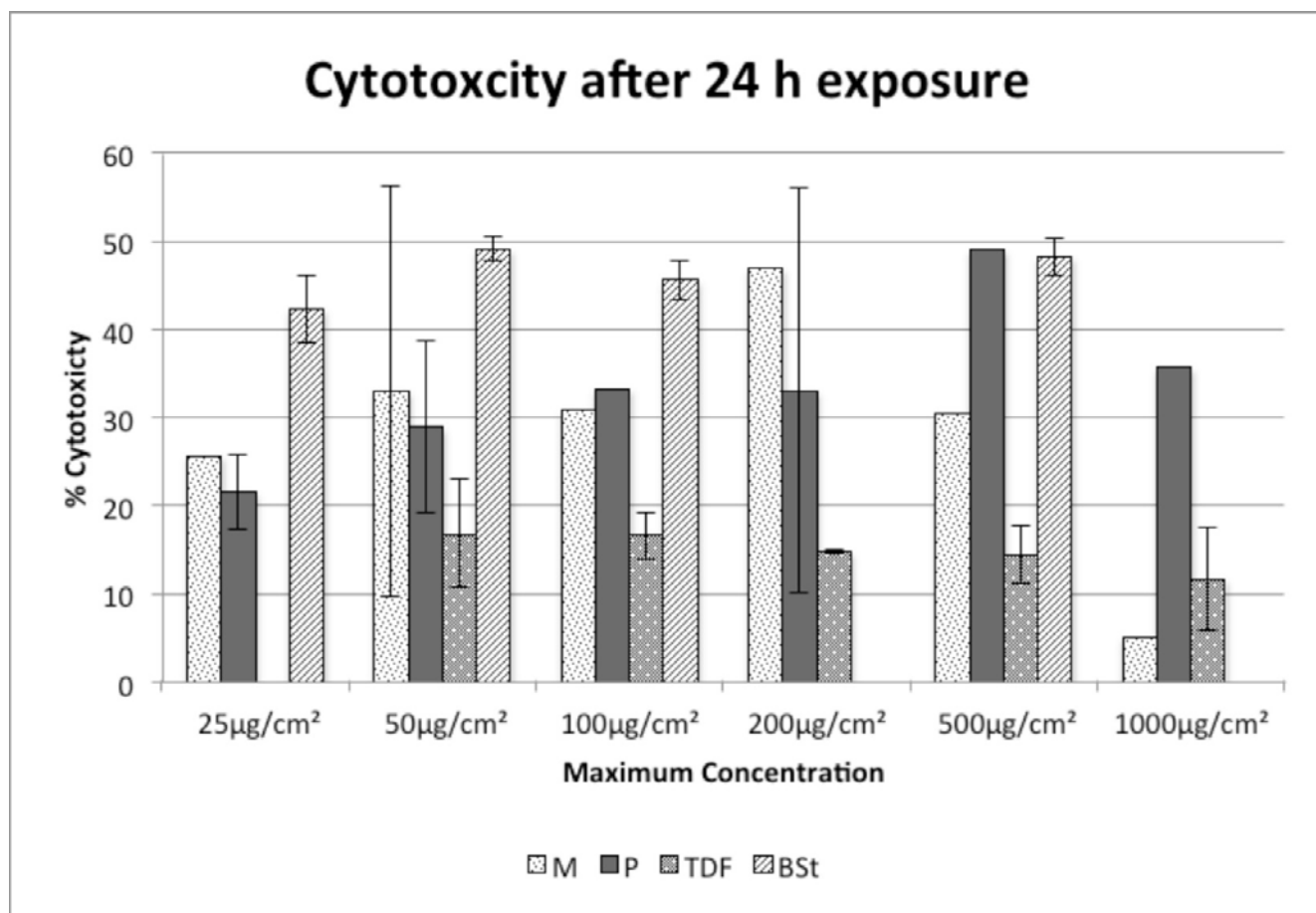


Figure 1. Comparison of the cytotoxic effect of different tire-wear particles measured by MTT test. TDF stands for tire-derived fuel and is the only analysed pure tire-particle sample. M, P and BSt are real tire-wear particles. The cytotoxicity was measured in A549 lung cells in six-well plates with 400 000 cells in each well. All the samples were measured in duplicate. Camptothecin and Actinomycin D were used as positive controls.

P 12.1

A 1000-year record of Sahara dust from an Alpine ice core

Mariani Isabella^{1,2}, Sigl Michael^{1,3}, Eichler Anja^{1,2}, Gabrieli Jacopo^{4,5}, Bolius David^{1,3}, Barbante Carlo^{4,5}, Boutron Claude⁶, Gäggeler Heinz Walter^{1,3} and Schwikowski Margit^{1,2,3}

¹ Paul Scherrer Institut, OFLB/102, CH-5232 Villigen PSI (isabella.mariani@psi.ch)

² Oeschger Centre for Climate Change Research, University of Bern, Zähringerstrasse 25, CH-3012 Bern

³ Department of Chemistry and Biochemistry, University of Bern, Freiestrasse 3, CH-3012 Bern

⁴ Department of Environmental Sciences, Informatics and Statistics, University of Venice, Calle Larga S.Marta 2137, I-30123 Venice

⁵ Institute for the Dynamics of Environmental Sciences - CNR, Calle Larga S.Marta 2137, I-30123 Venice

⁶ Laboratoire de Glaciologie et Géophysique de l'Environnement, University Joseph Fourier of Grenoble, 54, rue Molière, F-38402 Saint Martin d'Hères-Cedex

Saharan dust transport towards Central Europe is a common phenomenon, where mineral dust, mainly emitted from the Sahel and Saharan desert, is then transported northwards. Evidences of these events can be found in Alpine glaciers, where dust containing “red rain” or “yellow snow” is deposited.

The time duration of these phenomena, involving emission, transport and deposition, is of the order of magnitude of days. The atmospheric path can be quite variable, via direct or diverted transport (Sodemann et al. 2006). Most of the events generally occur in spring-summer (Collaud Coen et al. 2004).

Several studies show that at longer time scales dust emission at the source regions is controlled by the reduced rainfall in the previous years, leading to a slow adjustment of the vegetation (Engelstaedter & Tegen 2006).

We hypothesize that the interannual variability of Saharan dust deposition over the Alps depends on the drought conditions over Sahel and/or Sahara which seem to be related to the North Atlantic Oscillation.

For this purpose we investigate a highly resolved millennial record of mineral dust obtained from the Colle Gnifetti ice core, Swiss-Italian Alps.

Mean dust concentrations of the most recent 20 years are exceptional in the context of the last 1,000 years. This is consistent with direct and satellite-based observations of a widespread increase in dustiness and dust storm frequencies in Northern Africa over the last decades, also probably related to a human-induced desertification over Sahel (Moulin & Chiapello 2006).

REFERENCES

- Collaud Coen M., Weingartner E., Schaub D., Hueglin C., Corrigan C., Henning S., Schwikowski M. & Baltensperger U. 2004: Saharan dust events at the Jungfraujoch: detection by wavelength dependence of the single scattering albedo and first climatology analysis, *Atmospheric Chemistry and Physics* 4, 2465-2480.
- Engelstaedter S., Tegen I. & Washington R. 2006: North African dust emissions and transport, *Earth-Science Reviews*, 79, 73-100.
- Moulin C. & Chiapello I. 2006: Impact of human-induced desertification on the intensification of Sahel dust emission and export over the last decades, *Geophysical Research Letters*, 33, L18808.
- Sodemann H., Palmer A. S., Schwiertz C., Schwikowski M. & Wernli H. 2006: The transport history of two Saharan dust events archived in an Alpine ice core, *Atmospheric Chemistry and Physics* 6, 667-688.

P12.2

Sediments size characteristic of Sistan plain and Hamoon lakes as an important source of dust production in the world and adverse health effects of air pollution

Rahimzad Nasrin¹, Mohammadi Ali², Lak Raziye³

¹-Marine Geology Department, geological Survey of Iran

²- Geological Institute, ETH-Zurich, Switzerland

³- Research Institute for Earth Sciences, Iran

Since east of Iran have annual rainfall less than 100 mm, dust storms were occurred mainly from dried akes, wetlands and playas. Types of playa, area, location, morphological characteristics and the vegetation pattern, hydrology, climate and winds are important factors that control the dust storm. In this research 12 surface sediments collected from Sistan plain, Hamoon and Hirmand lakes. Each sample contains 64 subsamples belongs to 1600 m². Granulometry, mineralogy (XRD) and calcimetry analysis have been done in Geological survey of Iran. Frequency and cumulative curves for each sample were drawn. Results show that the types of sediments are sandy mud and mud. It's sorting sediments are bad to very bad. Grain size of sediments are between 4 micron to 2 mm. Kurtosis of sediments are leptokurtic to very platykurtic. Sediments are coarse skewed to strongly coarse skewed. A few gravel exist in the sediments. Carbonate minerals are 28 percents contain 25% calcite and 3% dolomite. Mineralogy of sediment contains Quartz, Calcite, Feldspar, Dolomite and Clay minerals respectively contain Chlorite, Montmorillonite, Illite and Kaolinite. Due to very strong wind system(120-days winds of Sistan and dray lake with low topography, soft and disconnected fine grain sediments this area is the most important source for producing dust in Iran and even South of Asia. Common health effects are respiratory tract, cardiovascular system, nervous system, cancer. Respiratory tract are cough, nose, throat and eye irritation, shortness of breath, exacerbation of allergic symptoms.

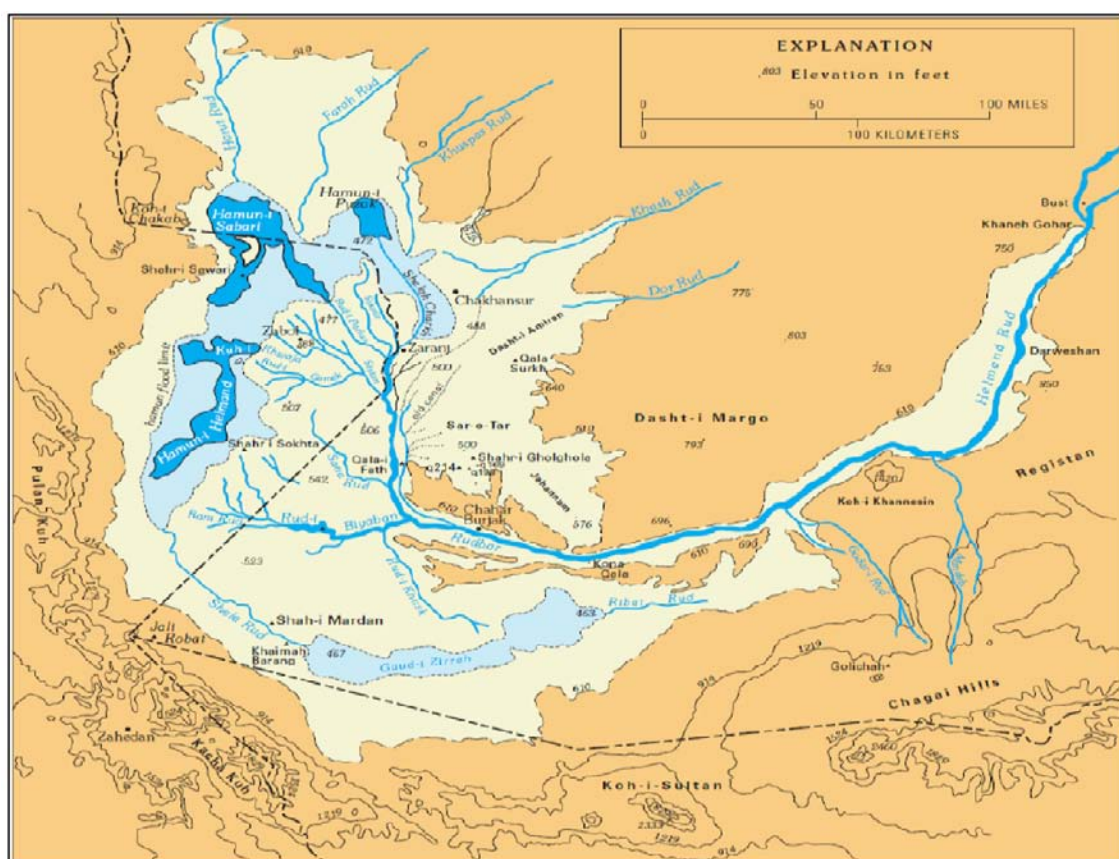


Figure 1: Geological map of Southern Helmand basin and along Helmand River and Puzak Saberi and Helmand Whitney, 2006)

REFERENCES:

Whitney, J.W., (2006). Geology, Water and Wind in the lower Helmand Basin, Southern Afghanistan. U.S. Geological Survey, scientific investigation report 2006-5182

P 12.3

Does long-range transported African Dust affect cloud droplet size distributions in a Tropical Montane Cloud Forest in Puerto Rico?

Johanna K. Spiegel¹, Thomas Peter², Olga L. Mayol-Bracero³, Carlos J. Valle³, Félix Zurcher³, Nina Buchmann¹ and Werner Eugster¹

¹*Institute for Agricultural Sciences, ETH Zurich, Zurich, Switzerland*

²*Institute for Atmospheric and Climate Science, ETH Zurich, Zurich, Switzerland*

³*Institute for Tropical Ecosystem Studies, University of Puerto Rico - Río Piedras, San Juan, Puerto Rico*

Long-range transport of dust on a global scale as well as the impact of dust on global climate has recently received special attention. Dust particles influence the Earth's radiative budget (a) directly by scattering and absorbing solar radiation, and (b) indirectly by affecting cloud formation and, consequently, cloud albedo. However, the underlying processes are poorly understood. We are particularly interested in how the dust hygroscopicity changes due to its aging during transport. In this study, we present preliminary results for droplet size spectra and derived variables such as liquid water content of clouds measured during an intensive sampling campaign of the "Puerto Rico African Dust And Clouds Study" (PRADACS), a project focusing on the impact of African Dust on clouds and precipitation in a tropical montane cloud forest. The cloud measurements were carried out in a tropical montane cloud forest on the Pico del Este at 1051 m amsl in July 2011. We used a forward scattering spectrometer probe (DMT Fog Monitor FM-100, Droplet Measurement Technologies, Boulder, CO, USA) which measures droplet size distributions in 40 size bins ranging from 2-50 μm . In a three days case study, we compared cloud data of three different days classified as (1) heavily dust-laden, (2) lightly dust-laden, and (3) dust-free, by using backward trajectories and aerosol data collected in the framework of PRADACS. We will discuss how long-range transported dust changes the cloud droplet size distributions. Preliminary results indicate that liquid water content, median volume diameter and effective diameter calculated for the measured size distributions are lowest for the heavily dust-laden day (1) and increase for the lightly dust-laden air mass (2). These parameters are highest for the dust-free day (3).

14. Traces of life on planet Earth: A tribute to the late Professor Lukas Hottinger

Lionel Cavin, Michael Hautmann

“Schweizerische Paläontologische Gesellschaft” (SPG/SPS)

“Kommission der Schweizerischen Paläontologischen Abhandlungen” (KSPA)

TALKS:

- 14.1 Geiger, M., Wilson, L. A. B., Costeur, L., Scheyer, T. M., Aguilera, O. A., Sánchez-Villagra, M. R.: Giant rodents from the northern Neotropics - taxonomic, phylogenetic and developmental aspects of their evolution within the caviomorph radiation
- 14.2 Hiard F., Mennecart B., Berger J.-P.: Palaeoenvironmental reconstruction of the Swiss Molasse Basin (Oligocene and Early Miocene) on the basis of postcranial remains of ruminants (Artiodactyla, Mammalia)
- 14.3 Hofmann R., Hautmann M., Bucher H.: Ecological structure and taxa distribution in near shore habitats of the Virgin Formation (south-western Utah): Implications for the Early Triassic recovery
- 14.4 Kolb, C.: Growth patterns deduced from bone histology of the dwarfed island deer *Candiacervus* from the Late Pleistocene of Crete
- 14.5 Mary Y., Knappertsbusch M.: Biogeographic morphological investigation of menardiform globorotalids in a time slice at 3.2 My (Mid-Pliocene)
- 14.6 Meister P.H.: Was the Triassic a plumeworld?
- 14.7 Mennecart B.: Was Europe an evolutionary DEAD END? Case of the Oligocene-Early Miocene ruminants.
- 14.8 Romano C., Brinkmann W., Goudemand N., Vennemann T., Ware D., Hermann E., Brühwiler T., Bucher H.: Recovery Patterns of Chondrichthyan and Osteichthyan Fishes after the end-Permian Mass Extinction
- 14.9 Scherler, L.: Paleobiogeographic and paleoecological considerations on European Anthracotheriidae (Cetartiodactyla, Mammalia)
- 14.10 Schneebeli-Hermann Elke, Hochuli Peter A., Kürschner Wolfram M., Bucher Hugo: Terrestrial ecosystems during and following the end-Permian mass extinction – or from spore spike to spore spike
- 14.11 Ware D., Bucher H., Goudemand N., Orchard M., Hermann E., Hochuli P.A., Brühwiler T., Krystyn L., Roohi G.: Nammal Nala (Salt Range, Pakistan), a potential GSSP candidate for the Induan/Olenekian Boundary (Early Triassic): detailed biostratigraphy and comparison with other GSSP candidates

POSTERS:

- P 14.1 *Costeur L., Domenici P., Ezquerra R., Rousseau M., Antognarelli F., Satta A., Simeone S., Pérez-Lorente F.*: A Cretaceous fish takes a fast start: insights from a recent analogue
- P 14.2 *Costeur L., Berthet D.*: A new skull of *Tapirulus* from the Late Eocene of France
- P 14.3 *Horath Th. D., Bachofen R., Neu Th.R., Strasser R. J.*: Endolithic microorganisms in Piora Dolomite
- P 14.4 *Knappertsbusch, M., Mary, Y.*: Mining morphological evolution in microfossils using volume density diagrams
- P 14.5 *Knappertsbusch, M., Mary, Y., Schorpp, R.*: AMOR does it for us
- P 14.6 *Och L., Shields-Zhou G.A.*: The Neoproterozoic Oxygenation Event: environmental perturbations and biogeochemical cycling
- P 14.7 *Pictet A.*: The *Exogyra aquila* Marls (Lower Aptian) on the Vivarais platform (Ardèche, France) : Sedimentology, stratigraphy, and biostratigraphy.
- P 14.8 *Thomas C., Vuillemin A., Pacton M., Waldmann N., Ariztegui D.*: Pushing life to the extreme: Investigating the subsurface biosphere in the Dead Sea Basin

14.1

Giant rodents from the northern Neotropics - taxonomic, phylogenetic and developmental aspects of their evolution within the caviomorph radiation

Geiger Madeleine¹, Wilson Laura¹, Costeur Loïc, Scheyer Torsten¹, Aguilera Orange³, Sánchez-Villagra Marcelo¹

¹ Paläontologisches Institut und Museum der Universität Zürich, Karl Schmid-Strasse 4, CH-8006 Zürich, Switzerland, (madeleine.geiger@uzh.ch, tscheyer@pim.uzh.ch, m.sanchez@pim.uzh.ch)

² Naturhistorisches Museum Basel, Konservator Geowissenschaften, Augustinergasse 2, CH-4001 Basel, Switzerland, (Loic.Costeur@bs.ch)

³ Museu Paraense Emílio Goeldi, Coordenação de Ciências da Terra e Ecologia, CCTE, Departamento de Geociências, Av. Perimetral, 1901, Terra Firme, CEP: 66077-830, Belém, PA, Brasil, (orangel.aguilera@gmail.com)

In the last decade, several fossils from giant caviomorph rodents from the Miocene of Venezuela were collected by teams from Zurich and Coro. These materials make possible the first examination of ontogenetic and taxonomic variation in these animals, in the context of the caviomorph evolutionary radiation. We examined continuous and discrete features in a sample of seven fossil specimens (cf. *Phoberomys*) and 149 recent ones representing 46 species. We investigated the order of maturation and fusion of the epiphyses of long bones (humeri and femora) and the pattern of evolution of nine discrete characters of the femur, the postcranial element most commonly preserved among the studied fossils. We found that the epiphyseal closure series of femora is conserved within the rodent clade. The ossification of the humeral epiphyses is similar in rodents and other mammalian clades (e.g. Carnivora, Eulipotyphla). The pattern of evolution of femoral features is largely homoplastic and there are no obvious correlations with ecology or phylogeny. Some but not all peculiarities of the fossils are most likely coupled with their gigantic size. The re-examination of a Miocene femur of giant rodent from Trinidad in the collections of the Naturhistorisches Museum in Basel lead to its identification as cf. *Phoberomys*, a taxon principally known from the Urumaco section in northwestern Venezuela. Current studies of its palaeohistology are revealing features on the growth pattern and functional architecture of the bone microstructure of these giants.

14.2

Palaeoenvironmental reconstruction of the Swiss Molasse Basin (Oligocene and Early Miocene) on the basis of postcranial remains of ruminants (Artiodactyla, Mammalia)

Hiard Florent¹, Mennecart Bastien¹, Berger Jean-Pierre¹

¹Department of Geosciences_Earth Sciences, Chemin du muse 6, 1700 Fribourg, Switzerland (florent_hiard@unifr.ch)

Some morphological features of the postcranial skeleton of ruminants are correlated to ecological features such as locomotion, body mass and habitat preferences. Here we propose to use these correlations to define terrestrial paleoenvironments of several Oligocene to Early Miocene Swiss Molasse Basin localities: La Beuchille (MP23), Grenchen 1 (MP24), Moutier-Gare (MP25), Mümliswil-Hardberg (MP26), Rickenbach (MP29), Küttigen (MP30), Engehalde (MN2), Wallenried (MN2), Tavannes (MN2), Benken and Wildensbuch (MN3/4).

Two different methods were used. The first is based on the morpho-functional study of Köhler (1993) and is applied on metapods and phalanges (53 specimens). The second one uses the morphology of astragalus to define habitat preferences of ruminants. It uses a PCA combined with a Support Vector Machine (SVM) calibrated with 209 astragalus of extant ruminants and is applied on 17 fossil specimens.

Between MP23 and MP26, the Swiss Molasse Basin presented essentially heavy forested environments. From MP29 to MP30, the environments seem to have been more open with wooded savannah or sparse forests (Mennecart et al. submitted). In MN2, the environments were more diversified with lightly wooded plains and more wooded environments (Becker et al. 2010). Finally, in MN4, the environments were more open with, however, some wooded area.

This succession of palaeoenvironments shows three different phases, which tend towards a general opening of the environments in the Swiss Molasse Basin. This evolution is consistent with the global evolution of environments in the Western part of Europe (Legendre 1989; Costeur 2005).

REFERENCES

- Becker, D., Antoine, P.-O., Engesser, B., Hiard, F., Hostettler, B., Menkveld-Gfeller, U., Mennecart, B., Scherler, L., & Berger, J.-P. (2011). Late Aquitanian mammals from Engehalde (Molasse Basin, Canton Bern, Switzerland). *Annales de Paléontologie*, DOI 10.1016/j.annpal.2011.03.001.
- Costeur, L. 2005: Les communautés de mammifères de l'Oligocène supérieur au Pliocène inférieur : Paléobiogéographie et paléobiodiversité des ongulés, paléoenvironnements et paléoécologie évolutive. PhD thesis, University Claude Bernard, Lyon, 124 pp.
- Köhler, M. 1993: Skeleton and Habitat of recent and fossil Ruminants, *Münchner Geowissenschaftliche Abhandlungen*, 25(A), 1-88.
- Legendre, S. 1989: Les communautés de mammifères du Paléogène (Eocène supérieur et Oligocène) d'Europe occidentale: structures, milieux et evolution, *Münchner Geowissenschaftliche Abhandlungen*, 16(A), 1-110.
- Mennecart, B., Scherler, L., Hiard, F., Becker, D., & Berger, J.-P. (submitted). Ungulates from Rickenbach (type-locality MP29, Late Oligocene, Switzerland): palaeoecologic and palaeoenvironmental implications. *Mémoire Suisse de Paléontologie*.

14.3

Ecological structure and taxa distribution in near shore habitats of the Virgin Formation (south-western Utah): Implications for the Early Triassic recovery

Hofmann Richard¹, Hautmann Michael¹ & Bucher Hugo¹

¹ Paläontologisches Institut und Museum, Universität Zürich, Karl Schmid Strasse 4, CH-8006 Zürich (richard.hofmann@pim.uzh.ch)

The recovery from the end-Permian biotic crisis is traditionally perceived to have been significantly delayed as a result of persistent deleterious environmental conditions and/or the extreme intensity of the extinction itself with an estimated species loss of 95% in the marine realm.

Previous studies on the Virgin Formation of the Western U.S. put forward the view that harsh environmental conditions still persisted during the Spathian, at least 2 ma after the main extinction. However, palaeoecological analyses on the basis of species-level abundance data have hitherto not been carried out. Thus, very little is known on the actual ecological structure of the Virgin palaeocommunities and their spatial distribution.

We present a quantitative palaeoecological data-set, which is analysed with respect to the identified sedimentary environments. This integrated approach helps to discriminate between possible effects of the end-Permian mass extinction event and local environmental factors on alpha-diversity and ecological structure of the Virgin Fauna. Shallow subtidal environments (see figure 1 for overview) yield the highest species richness and lowest dominance values as recorded in two benthic associations: the *Eumorphotis ericius*-association and the *Protogusarella smithi*-association, both of which contain 20 benthic species (bivalves, gastropods, brachiopods, echinoderms, and porifers). Tidal inlet deposits yield a low diverse fauna (*Piarorhynchella triassica*-association) with a very high dominance of filter feeders adapted to high energy conditions. Another comparably low diverse fauna is recorded by the *Bakevella exporrecta*-association, which occurs in deposits of the offshore transition zone encompassing unconsolidated, mostly silicilastic substrates with a low preservation potential for calcareous body fossils. A single sample containing five bivalve species (*Bakevella costata*-assemblage) is recorded from a marginal marine setting. The Virgin fauna yields a bulk diversity of 30 species (22 genera) of body fossils and 14 ichnogenera and, thus, represents the most diverse benthic fauna known so far from the Early Triassic.

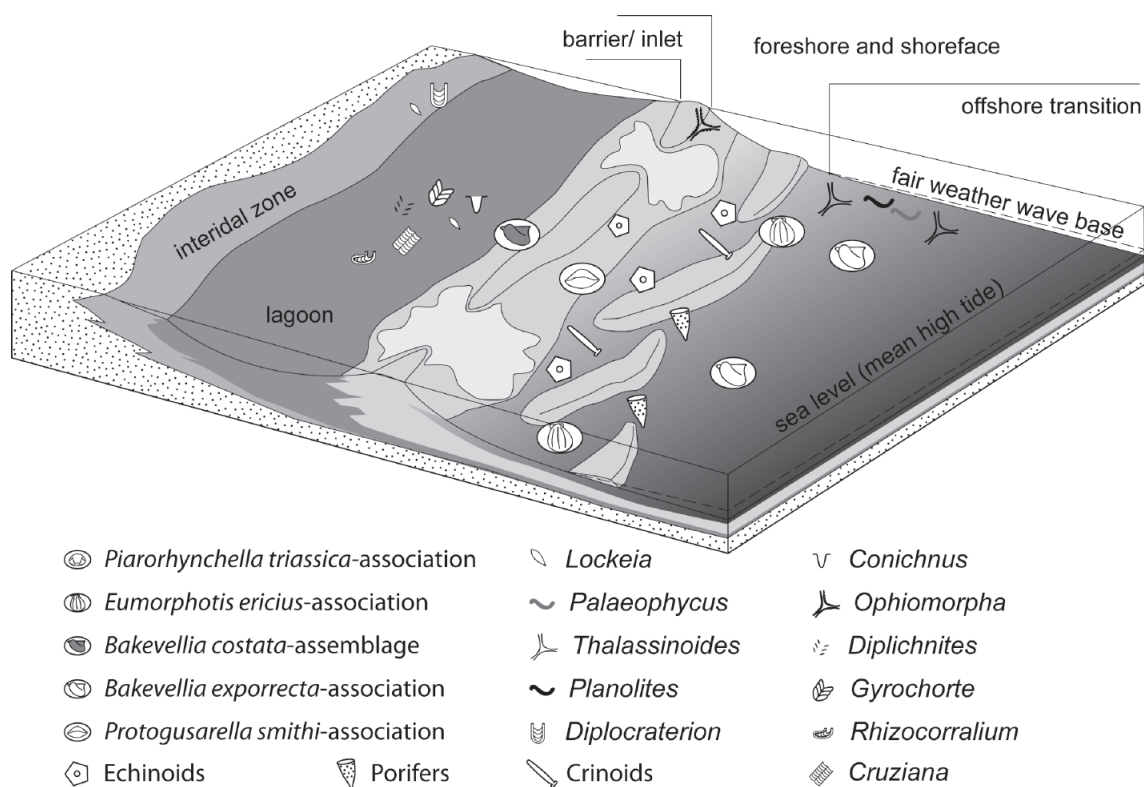


Figure 1. Sedimentological and palaeoecological model of the Virgin Formation as recorded in south-western Utah.

Our results suggest that oceanographic conditions during the Early Spathian enabled ecosystems to rediversify without major abiotic limitations. However, taxonomical differentiation between habitats was still low, indicating a time lag between increasing within-habitat diversity (alpha-diversity) and the onset of taxonomical differentiation between habitats (beta-diversity). We suggest that taxonomical habitat differentiation after mass extinction events starts only after competition within habitats exceeded a certain threshold, which was not yet reached in the Spathian of the investigated area. This interpretation is an alternative to previous suggestions that the prevalence of generalistic taxa in the aftermath of mass extinction events reflects ongoing environmental stress. The onset of increasing beta diversity is a potential criterion for distinguishing two major recovery phases: the first ending with habitat saturation and the second ending with completion of ecosystem differentiation.

14.4

Growth patterns deduced from bone histology of the dwarfed island deer *Candiacervus* from the Late Pleistocene of Crete

Christian Kolb¹

¹ Paläontologisches Institut und Museum der Universität Zürich, Karl Schmid-Strasse 4, CH-8006 Zürich (christian.kolb@pim.uzh.ch)

The Mediterranean island of Crete was connected to the mainland of Asia Minor since the Vallesian age of the Late Miocene, becoming later submerged. After re-emergence of the region at the end of the Pliocene, Crete gained its present shape and became colonized by overseas sweepstakes dispersal (van der Geer et al. 2010). Isolation and colonization led to natural experiments in geological time, as several lineages of mammals experienced rapid evolutionary increases or decreases in body size and life history. The Pleistocene endemic fauna of Crete included dwarfed forms of deer, hippopotamuses, proboscideans, and giant mice. In an analogous case, Köhler & Moyà-Solà (2009) investigated a dwarfed island bovid from the Late Pleistocene of Majorca, *Myotragus balearicus*, and based on palaeohistological studies found flexible synchronization of growth rates and metabolic needs within the bone tissue. This strategy is similar to that of ectothermic reptiles encountering resource limited environments. Whether this pattern is universal for extinct islands, mammals remain unexamined, and this study aims at testing this by deciphering growth and adaptive patterns of bone tissue types in the dwarfed Cretan deer *Candiacervus* as a case study.

The two smallest morphotypes of *Candiacervus* are represented by different ontogenetic stages in specimens from Liko and Gerani cave. Both morphotypes are characterized by a shortening of limb bones already present at birth (van der Geer et al. 2006) and a higher degree of bone fusions, typical evolutionary specializations of island ruminants (van der Geer et al. 2010).

Various long bones of newborn, juvenile, and adult specimens, housed in the Museum Naturalis Leiden, were sampled histologically. For the first time a bone histological examination of an ontogenetic series of *Candiacervus* is conducted.

Throughout limb bone development, ontogenetic changes of bone tissue patterns are observable including lines of arrested growth (LAGs). The number of LAGs indicates an age of about 2 years for juveniles and minimum 5 years for adults sampled.

Nevertheless, large parts of the growth record in the primary cortex were erased as a result of remodeling and resorption. Humeri and femora of newborn *Candiacervus* start with fibro-lamellar bone and show a plexiform arrangement of vascular canals. Layers of secondary deposited endosteal lamellar bone occur in the inner part of the cortex in juvenile and adult specimens as well as areas of Haversian bone or pockets of secondary osteons. Large areas of Haversian bone in adult specimens indicate strong bone remodeling during ontogeny. Metapodials of newborn specimens show woven-fibred bone. In the outer parts, woven-fibred bone is substituted by laminar or plexiform fibro-lamellar bone throughout ontogeny. Secondary deposition of lamellar bone is found in the anterior region of the inner cortex in juvenile and adult specimens as well.

The closely related continental deer *Megaloceros*, the giant Irish elk, shows a similar arrangement of bone tissue types in the metatarsals compared to *Candiacervus*. Both genera show a high amount of bone remodeling, i.e. the presence of Haversian bone is highest in the posterior cortical regions of the fused metatarsals.

Placing the fossil data into a larger phylogenetic context including also living species reveal common patterns of growth as well as life history changes in fossil forms which evolved in isolation or attained extreme sizes on the continent during Pleistocene times.

REFERENCES

- Köhler, M. & Moyà-Solà, S. 2009: Physiological and life history strategies of a fossil large mammal in a resource limited environment. *Proceedings of the National Academy of Sciences USA*, 106, 20354–20358.
- Van der Geer, A., Dermitzakis, M.D. & De Vos, J. 2006a: Relative growth of the metapodials of a juvenile island deer: *Candiacervus* (Mammalia, Cervidae) from the Pleistocene of Crete, *Hellenic Journal of Geosciences*, 41, 119-125.
- Van der Geer, A., Lyras, G., de Vos, J. & Dermitzakis M.D. 2010: *Evolution of Island Mammals: Adaptation and Extinction of Placental Mammals on Islands*, Oxford, Wiley-Blackwell, 496 p.

14.5

Biogeographic morphological investigations of menardiform globorotalids in a time slice at 3.2 (Mid-Pliocene)

Mary Yannick¹ & Knappertsbusch Michael¹

¹ Naturhistorisches Museum Basel, Augustinergasse 2, CH-4001 Basel (yannick.mary@unibas.ch).

Planktonic foraminifera are one of the most important tools for palaeoceanographic reconstructions and biostratigraphy. Recent outcomes of combined morphometrics and molecular studies have brought forward critical aspects of their classification: within traditionally defined morpho-species there exists genotypic variation that defines biogeographically and ecologically distinct cryptic species (Darling & Wade 2008). Morphological variability within these morphospecies is now considered as the result of genetic diversity, opening a wide field for biometrical investigations. Although fossil record of planktonic foraminifera contains several good candidates for studying morphological diversity, investigation of species-level composition remains difficult. The number of specimens to analyse is very high in order to reliably describe the differences cryptic forms and the morphological overlap of the cryptic forms is important.

The present work documents a new approach trying to tackle the above-mentioned problems. It combines size frequency analysis and morphological measurements with the use of a new automat, the robot AMOR, which orients and images microfossils under a binocular microscope (Knappertsbusch *et al.*, 2009). AMOR significantly increases the number of specimens to be analysed, while the construction of contoured frequency distributions allows to explore subgroups within morphologically convergent populations. Populations of up to 500 specimens are investigated in several locations. Size frequency distribution (SFD) is first calculated and described by superposition of several distinct Gaussian distributions.

Differences between SFDs are used in order to filter out specific frequency trends per locality. Morphological measurements including spiral height (δX), maximum diameter (δY), concavity (δS and δU), keel angles ($\Phi 1$ and $\Phi 2$), and profile view area (GA) employed as a proxy for shell volume, and therefore size estimator. These parameters are then used to characterise morphological variability within the previously defined subgroup.

As an experiment we studied the biogeographic variation of shell morphology of middle Pliocene Atlantic menardellids planktonic foraminifera. The Menadella group shows a high diversification during its timespan, as a consequence of the establishment of new ecological niches in the tropical Atlantic during the gradual closure of the ancient American Seaway (Chaisson, 2003). Two lineages which can be defined by their end members *Globorotalia (Menardella) multicamerata* and *Globorotalia (Menardella) pertenuis* evolved from the common ancestor *Globorotalia (Menardella) menardii*. These species strongly intergrade in a time-transgressive morphocline, a large proportion of the morphological overlap being caused by allometric growth of the shell (Cifelli & Scott 1986).

The combination of size frequency distributions with spiral height versus maximum diameter diagrams leads to the recognition of seven different *Menardellid* morphotypes in Mid-Pliocene tropical Atlantic populations: morphotype MA, MB, MC1, MC2, MC3, SH1 and SH2. Each morphotype covers a distinct range of size and is characterised by a distinct morphology, which suggests a distribution in different ecological niches (Al-Sabouni *et al.*, 2007).

Automatisation, morphological analysis and size frequency distribution solves the intergradation problems (without being too much time consuming), accounts for ontogenetic effects and opens prospects into population ecology in microfossils that are otherwise difficult to differentiate.

REFERENCES:

- Al-Sabouni, N., Kucera, M., Schmidt, D. N., 2007: Vertical niche separation control of diversity and size disparity in planktonic foraminifera. *Marine Micropaleontology* 63, 75-90
- Chaisson, W.P., 2003: Vicarious living: Pliocene menardellids between an isthmus and an ice sheet. *Geology* 31, 1085-1088.
- Cifelli, R., Scott, G., 1986: Stratigraphic record of the Neogene globorotaliid radiation (planktonic foraminifera). *Smithsonian contributions to Paleobiology*
- Darling, K., Wade, C., 2008. The genetic diversity of planktonic foraminifera and the global distribution of ribosomal RNA genotypes. *Marine Micropaleontology* 67, 216-238.
- Knappertsbusch, M.W., Binggeli, D., Herzig, A., Schmutz, L., Stapfer, L., Schneider, C., Eisenecker, J., Widmer, L., 2009. Amor - a new system for automated imaging of microfossils for morphometric analyses. *Palaeontologia Electronica* 12.

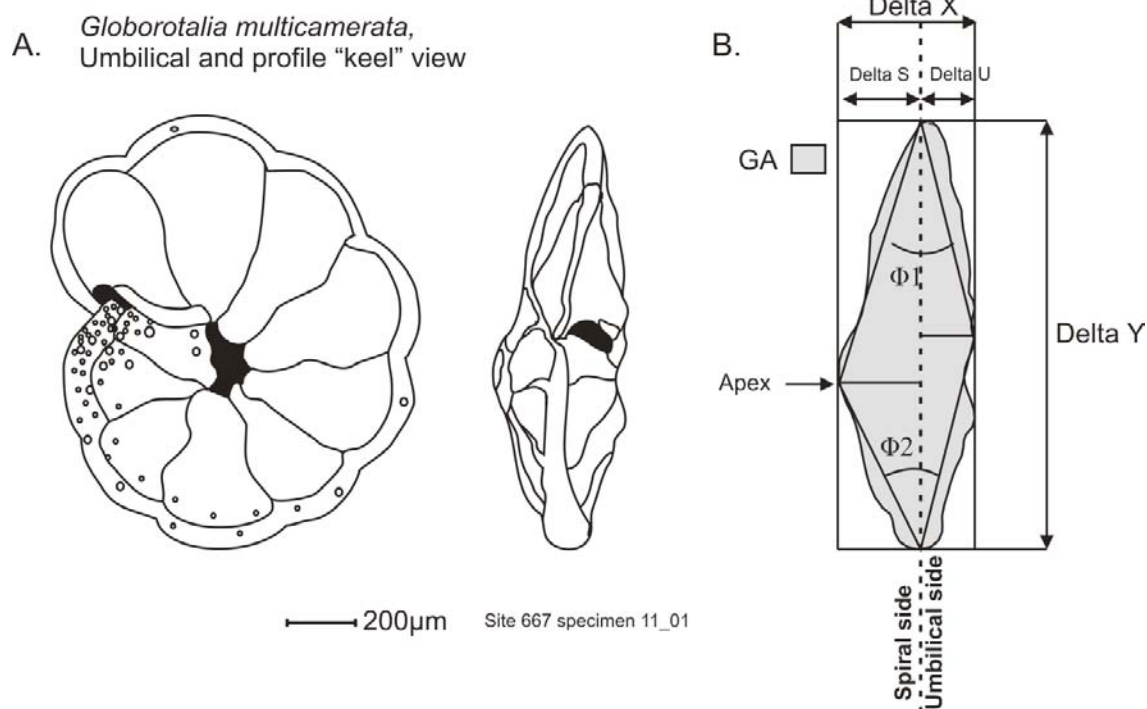


Figure 1: Morphological description of a globorotalid menardiform. A: detailed drawing of the test in umbilical and keel view. B: Outline of this specimen with associated measurements.

14.6

Was the Triassic a plumeworld?

Patrick H. Meister¹

¹ Max Planck Institute for Marine Microbiology, Celsiusstrasse 1, 28359 Bremen (pmeister@mpi-bremen.de)

The onset of pelagic biogenic carbonate production during the Cretaceous has strongly changed the mode of how carbonate is drawn down from ocean water. Before the “invention” of an elaborate mechanism of efficient carbonate precipitation by marine nannoplankton, this task was essentially carried out by benthic organisms and was mostly limited to the photic zone at ocean margins. Nevertheless, several intervals exist in the geological record that are rich in carbonates, and these carbonates often show a homogenous micritic texture draping considerable parts of the seafloor worldwide. According to the plumeworld hypothesis (Shields, 2005), such intervals may result from spontaneous precipitation of carbonate in the water column during times of high ocean water alkalinity. This mode of carbonate precipitation may explain abundant carbonates homogeneously draping the seafloor in the aftermaths of low latitude glaciations during the Neoproterozoic when atmospheric CO₂ levels were supposedly high compared to present levels.

Sedimentation style reminiscent of such cap carbonates is also abundant in the Triassic units of the Alps, even though these carbonates were mostly deposited in shallow seas surrounding the western end of the Palaeotethys embayment. Most of the Triassic carbonates show a predominantly micritic matrix, show features of soft sediment deformation and sometimes bioturbation indicating carbonate mud entirely unlithified at the time of deposition. The enormous quantity of micrite dwarfs the contribution of skeletal material and was unlikely produced by erosive mechanisms. At the same time, nannoplankton had not been produced in large amounts during the Triassic yet. Hence, spontaneous precipitation from the water column may provide an efficient mechanism to produce such carbonates.

Considerable amounts of the platform carbonates are dolomitic, and dolomitic units coincide with the most shallow water conditions as indicated by the sedimentary structures. The distribution of dolomite corresponds to particular conditions conducive to dolomite formation observed in a few modern environments, such as intertidal restricted lagoons or hypersaline sabkhas. Although most Triassic dolostones suffered considerable recrystallization during burial diagenesis, distribution of dolomites is often concordant with particular sedimentary units, and, in some cases, oxygen isotope signatures are preserved that indicate early precipitation at surface temperatures. Carbon isotope signatures of Triassic dolostones generally show marine values indicative of very early precipitation. If dolostones were formed in restricted environments, such values can also be the result of equilibration with atmospheric CO₂.

As a modern analogue we may consider Deep Springs Lake, an alkaline lake in eastern California. This lake also shows the formation of entirely unlithified clay-fraction dolomite ooze. A geochemical study (Meister et al., 2011) suggested dolomite in the water column because dolomite is not supersaturated in the porewater as a result of Ca limitation. Also, microbial sulphate reduction is insufficient to influence supersaturation by increasing the inorganic C pool and alkalinity. Even if the conditions in the lake are probably far more alkaline than in past seawater, the mode of precipitation in the lake may serve as a potential modern analogue for a plumeworld mode of carbonate formation in the past ocean.

The abundance of carbonate in the Alpine Triassic may be explained by high pCO₂ level, tropical and at times humid climate causing strong weathering of the continents and high alkalinity in the ocean. Additionally, uptake of bicarbonate by calcifying organisms was limited to sponges and microbialites in shallow environments while corals played a minor role during most of the Triassic. Hence the ocean was more supersaturated with respect to carbonate, most likely facilitating the spontaneous precipitation of carbonates under warm evaporative conditions. Based on these observations a plumeworld mode of carbonate precipitation may be locally suggested for the shallow platforms of the Triassic Palaeotethys. These platforms resemble ongoing carbonate precipitation in a few modern restricted environments but may have been the main pathway of carbonate formation during Proterozoic times. More research is necessary to understand the fundamental mechanisms of carbonate precipitation during the Triassic and earlier times in earth history.



Figure 1. Deep Springs Lake, California, showing ongoing authigenic formation of clay-fraction dolomite ooze. This mode of carbonate precipitation may have similarly occurred in Triassic marginal seas. (left: after rain; right dry season).

REFERENCES

- Meister, P., Reyes, C., Beaumont, W., Rincon, M., Collins, L., Berelson, W., Stott, L., Corsetti, F., and Nealson, K.H. (2011) Calcium- and magnesium-limited dolomite precipitation at Deep Springs Lake, California. *Sedimentology*, published online. DOI: [10.1111/j.1365-3091.2011.01240.x](https://doi.org/10.1111/j.1365-3091.2011.01240.x)
- Shields, G.A. (2005) Neoproterozoic cap carbonates: a critical appraisal of existing models and the plumeworld hypothesis. *Terra Nova* 17, 299-310.

14.7

Was Europe an evolutionary DEAD END? Case of the Oligocene-Early Miocene ruminants.

Bastien Mennecart

Department of Geosciences – Earth Sciences, ch. du Musée 6, Pérolles, CH-1700 Fribourg, Switzerland, bastien.mennecart@unifr.ch

Nowadays, the ruminants are the most diverse, ecologically dominant, group of the hoofed mammals. Including nearly 210 species, they occur in deserts to tropical forests, have a body weight from 3 kg to 2 tones, and cover feeding habits from selective browser to grazer (Mennecart et al. *subm.1*). The diversification of the current families in Europe seems to have occurred during the late Early to Middle Miocene with the Tragulidae (MN4), the sabertoothed Moschidae (MN5), the antlered Cervidae (MN3), and the horned Bovidae (MN4). The primitive Oligocene ruminants are mainly enigmatic and belong to extinct families or are uncertainly assigned to extant families (Mennecart et al. *subm.1*). Many authors suggest an early appearance of the ruminants in Europe during the Late Eocene. However, the latter are represented by isolated, poorly located, and lost specimens. Additionally, most of the time, the European Oligocene ruminant diversity is mainly related to a regional evolution with few migrations. Based on the review of specimens from 95 localities, this study aims to discuss a new insight into the diverse evolutionary pattern of European ruminants during the Oligocene and the Early Miocene.

The earliest undeniable European ruminants occurred only after the “Grande Coupure” event (MP20/21), at the same age of the Oi1 glaciation event (ca. 33.5 My; *Migr.1*, see Fig.), whereas the first true ruminants appeared earlier in the Middle Eocene in North America and Asia. Following this extinction/origination event, the earliest European families Lophiomerycidae and Gelocidae diversified rapidly and few later, at MP23, the new families Bachitheriidae and Tragulidae migrated from Asia (ca. 30.5 My). Swamps and forests dominated the European landscape, but at the beginning of MP24, a global change coinciding with the Oi2 glaciation event, occurred. In Switzerland, it was marked by the regression of the UMM and the Renish Sea, and drastic changes of the sedimentological context (Berger 2011), that generated a drier climate and a faunal renewal. Within the European ruminant community, we note the disappearance of the Gelocidae and the Tragulidae, and only the larger species of Bachitheriidae and Lophiomerycidae survived (*Ext.1*; Mennecart et al. *in press* and *subm.1*). At MP24/25 (ca. 29.2 My), the Bachitheriidae diversified and the nov. Family appeared in Europe (*Spec.1*). The European mammal evolution was relatively quiet and steady until MP27. In Switzerland, the environment was a wooded floodplain (Berger 2011).

Around MP28, large changes occurred in the faunal communities. First, a specific renewal resulted in more open habitat specialized ruminants (*Ext.2* and *Migr.2*). Then a rapid extinction occurred, during the emergence of new migrants, the Pecora (*Ext.3* and *Migr.3*; Mennecart et al. *subm.2*). In Switzerland, this short time interval coincided with sedimentological changes related to a drier environment (Berger 2011).

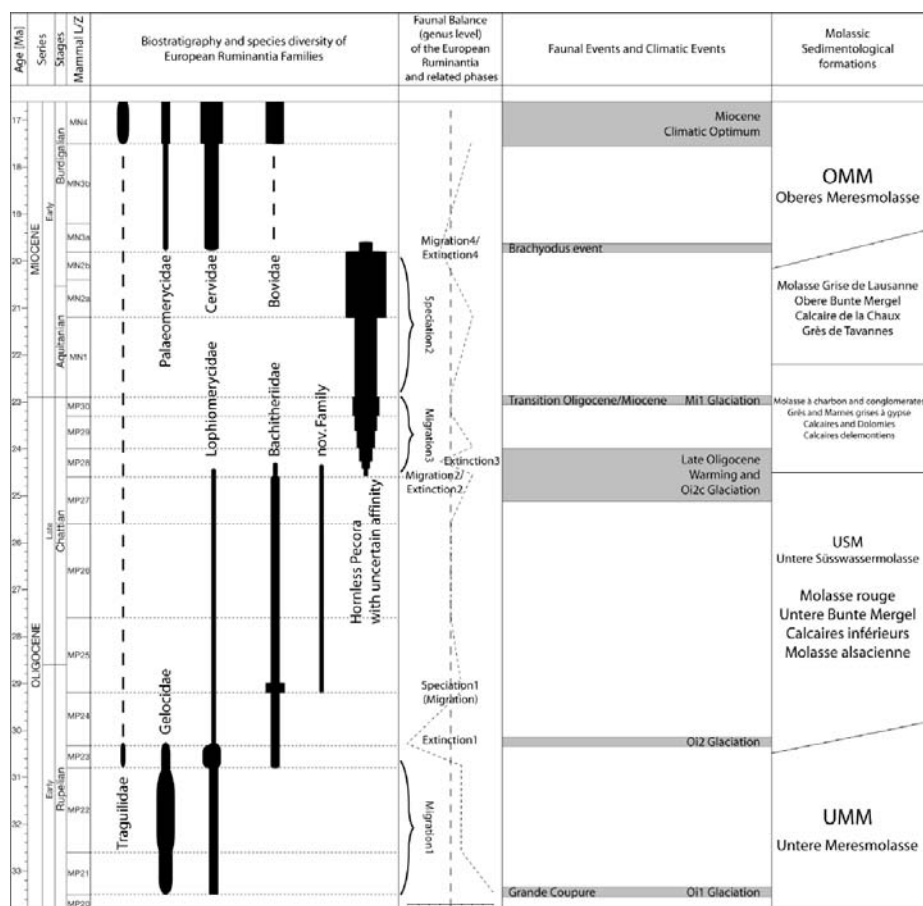
The Oligo-Miocene transition (ca. 22.9 My) was marked by the Mi1 glaciation event, which coincided with a general fragmentation of the environment. In spite of this, the ruminant community was not strongly affected. However, a general trend highlights size changes; the small species derived into smaller species and the medium size species into larger ones. At the end of MN2, a huge diversity of hornless sabertoothed ruminants belonging to uncertain families is recorded (*Spec.2*). The *Brachyodus* event, at the beginning of the Proboscidean datum (MN3a, ca. 19.8 My), coincided with the closing of the Tethys Ocean and, in Switzerland, to the transgression of the OMM. This major climate and faunal change led to the disappearance of old taxa and the emergence of the extant families (*Ext.4* and *Migr.4*).

As opposed to the regional evolution, proposed by older publications, which suggests few migrations, this study highlights an evolutionary pattern marked by several huge Asiatic migrations, strongly related with global and environmental changes and punctuated by some speciation phases. Europe should be considered more as a Dead End (Migration/Extinction) than an area with a normal evolutionary diversification (Speciation).

This project is supported by the FNS projects n°115995 and 126420 (supervised by Pr. Berger and Dr. Becker) and the paléojura project.

REFERENCES

- Berger, J.-P. (2011). *Géochronique*, 117, 47–49.
 Mennecart, B. et al. (*in press*). *Swiss J. of Geosciences*, Online.
 Mennecart, B. et al. (*subm.1*). in Mendes, R.E. (Ed), Nova Science Publishers.
 Mennecart, B. et al. (*subm.2*). *Swiss Journal of Palaeontology*.



14.8

Recovery Patterns of Chondrichthyan and Osteichthyan Fishes after the end-Permian Mass Extinction

Romano Carlo¹, Brinkmann Winand¹, Goudemand Nicolas¹, Vennemann Torsten², Ware David¹, Hermann Elke³, Brühwiler Thomas¹, Bucher Hugo¹

¹ Paleontological Institute and Museum, University of Zurich, Karl Schmid-Strasse 4, 8006 Zürich (carlo.romano@pim.uzh.ch)

² Institute of Mineralogy and Geochemistry, University of Lausanne, Anthropole, 1015 Lausanne

³ Institute of Earth Sciences, University of Utrecht, Budapestlaan 4, 3584 CD, Utrecht

The Permian-Triassic boundary (PTB) extinction event is the largest known crisis of the Phanerozoic, with more than 90% of marine species having been wiped out. The subsequent Early Triassic biotic recovery is traditionally considered delayed. However, although some groups apparently did not reach their pre-extinction diversity before Middle Triassic times (>6 million years after the PTB), others (e.g. ammonoids, conodonts, foraminifers, brachiopods) did recover in less than 1.4 million years after the PTB. Yet, soon after, near the Smithian-Spathian boundary, some clades like ammonoids and conodonts suffered an additional extinction.

Early Triassic recovery studies have mainly focused on marine invertebrates and, with the exception of the conodonts, only little is known about the timing and pattern of recovery of vertebrates. The relatively scarce fossil record and the often poor stratigraphic control of many vertebrate groups make it difficult to assess their diversity dynamics. Nonetheless, higher gnathostomian fishes (Osteichthyes and Chondrichthyes), which are the largest vertebrate group today, are relatively well-represented in the fossil record and, thus, useful for such studies.

Here we present an updated analysis of the diversity dynamics of Chondrichthyes (sharks and their relatives) and Osteichthyes (bony fishes) between the Lopingian (Late Permian) and Anisian (Middle Triassic). Our data reveal different trends in turnovers and generic richness of chondrichthyan and osteichthyan fishes across the PTB and during the Early Triassic. In general, the diversity of chondrichthyans seems to be more stable within the studied interval than that of the bony fishes. The results are discussed in the context of emerging evidence for profound environmental changes during the Early Triassic (e.g. ocean's chemistry, climate).

14.9

Paleobiogeographic and paleoecological considerations on European Anthracotheriidae (Cetartiodactyla, Mammalia)

Scherler Laureline¹

¹ OCC-SAP, PAL-A16, Hôtel des Halles, CP64, CH-2900 Porrentruy (laureline.scherler@net2000.ch)

This study 1) proposes a new vision on the paleobiogeographic repartition of European anthracotheres; 2) highlights surprising facts concerning their paleoecology and evolution; 3) brings new information for the understanding of the ecological dichotomy between the two modern species of hippopotamuses.

Anthracotheres lived almost worldwide from the Late Eocene to the Early Pliocene, migrating early from Southeast Asia towards North America, Europe, and Africa (e.g., Lihoreau & Ducrocq, 2007). The members of this family adapted to many different ecologies and colonized successfully various habitats throughout their evolutionary history.

The first anthracotheres arrived in Europe in the latest Eocene (FAD of *Elomeryx crispus* in MP18, Lutetian). A second migration wave in the “Grande Coupure” allowed an increase in diversity during the Oligocene, and at least five genera and eleven species coexisted until the latest Oligocene. One species survived shortly to this local extinction, until the earliest Miocene (LAD of *Elomeryx minor* in MN1, early Aquitanian). After the complete disappearance of anthracotheres on this continent, the bothriodontine *Brachyodus onoideus* temporarily occurred in Western Europe in the Burdigalian (MN3-4, late Early Miocene). This African genus, along with the proboscidean *Deinotherium*, migrated towards Eurasia when the continents reconnected. This marked the first dispersal episode linked to the Proboscidean Datum Event (e.g., van der Made, 1999).

During the Miocene, in Africa, an evolved subfamily of anthracotheres probably led to the modern hippopotamuses (e.g., Boisserie & Lihoreau, 2006). The latter are, today, only represented by two species, *Hippopotamus amphibius* and *Choeropsis liberiensis*, which display different adaptations to two very different ecological niches. The first one lives as a semi-aquatic mammal, whereas the dwarf hippo prefers forested habitats. The cranial morphology of this latter species is additionally not adapted to the amphibious mode.

The recent systematic review of European anthracotheres (Scherler, 2011) brought new data regarding their paleobiogeography and paleoecology. Firstly, the dispersal routes of this family highlight endemism during the Early Oligocene of Western Europe. Secondly, the description of the first complete skull of “*Anthracotherium*” pinpoints the fact that this very large representative was not amphibious, contrary to earlier thoughts expressed by many authors (e.g., Cuvier, 1822). Indeed, none of the sensitive organs (nasals, orbits, ears) are disposed in a periscopic position. Finally, the surprisingly high $\delta^{13}\text{C}$ values and the low standard deviation in $\delta^{18}\text{O}$ values measured for the tooth enamel of the small *Microbunodon* suggest either an amphibious mode of life, or a strong relation to an aquatic habitat (Scherler, in prep. a, b). Oligocene European anthracotheres may therefore be a key taxon to understand the ecological dichotomy between the two species of modern hippopotamuses.

All my gratitude goes to Prof. J.-P. Berger, Dr. D. Becker, Dr. F. Lihoreau, Dr. T. Tütken, B. Mennecart, C. Rambeau, University of Fribourg, SNF (126420), SAP-PAL A16 (Jura Canton), SPS, ESPP, MHNG (L. Cavin), MGL (R. Marchant), NMB (L. Costeur), NMBE (U. Menkfeld-Gfeller), NMO (P. Flückiger).

REFERENCES

- Cuvier, G. 1822: Recherches sur les ossements fossiles, où l'on rétablit les caractères de plusieurs animaux, dont les révolutions du globe ont détruit les espèces. Tome 5, Ed. d'Ocagne, Paris.
- Boisserie, J.-R. & Lihoreau, F. 2006: Emergence of Hippopotamidae: new scenarios. *Comptes Rendus Palevol*, 5, 749–756.
- Lihoreau, F. & Ducrocq, S. 2007: Family Anthracotheriidae. In: Prothero, D. R. & Foss, S. E. (Eds.): *The Evolution of Artiodactyls*. The John Hopkins University Press, Baltimore, 89–105.
- Scherler, L. 2011: Terrestrial paleoecosystems of large mammals (Tapiridae, Anthracotheriidae, Suoidea) from the Early Oligocene to the Early Miocene in the Swiss Molasse Basin: biostratigraphy, biogeochemistry, paleobiogeography, and paleoecology. Unpublished PhD Thesis, University of Fribourg, 225 pp.
- Scherler, L. in prep. a: Paleobiogeography of European Anthracotheriidae (Cetartiodactyla, Mammalia) highlights endemism in the Early Oligocene. To be submitted to PNAS.
- Scherler, L. in prep. b: Carbon and oxygen stable isotope compositions propose new interpretations for the paleoecology of European Anthracotheriidae (Cetartiodactyla, Mammalia). To be submitted to *Geochimica and Cosmochimica Acta*.
- Van der Made, J. 1999: Intercontinental relationship Europe-Africa and the Indian subcontinent. In: Roessner, G. & Heissig, K. (Eds.): *The Miocene land Mammals of Europe*, 457–472.

14.10

Terrestrial ecosystems during and following the end-Permian mass extinction – or from spore spike to spore spike

Schneebeili-Hermann Elke¹, Hochuli Peter A.², Kürschner Wolfram M.¹, & Bucher Hugo²

¹ *Palaeoecology, Institute of Environmental Biology, Faculty of Science, Utrecht University, Laboratory of Palaeobotany and Palynology, Budapestlaan 4, 3584 CD Utrecht, The Netherlands (ElkeSchneebeili@gmx.net)*

² *Paläontologisches Institut und Museum, Karl Schmid-Strasse 4, CH-8006 Zürich*

The impact of the end-Permian mass extinction on terrestrial ecosystems is still debated. It has been suggested that the destruction of forests left a low-diversity vegetation behind, which was dominated by pioneering plants unvaried for a time interval of 4-5 Ma (Looy et al., 1999).

Here we present an alternative view of the Early Triassic vegetation history based on the palynofloral records of the Permian-Triassic boundary succession in Norway, and the well-dated Upper Permian to Middle Triassic successions of Pakistan and South Tibet.

In Norway, the end-Permian floral succession is marked by a distinct spore spike, which is associated with the end-Permian mass extinction and coincides with the negative carbon isotope shift that has been reported from numerous other Permian-Triassic boundary sections. Its contemporaneous equivalent in Greenland has been interpreted as signal for terrestrial ecosystem destabilisation and the onset of a long recovery time dominated by pioneering lycopods (Looy et al., 1999; 2001). In contrast, the high resolution record from Norway shows that the end-Permian spore spike is immediately followed by the recovery of gymnosperms. Correlation with the Permian-Triassic stratotype section in Meishan (South China) suggests a recovery time of some 10 ka (Hochuli et al., 2010).

Preliminary results from a new Permian-Triassic boundary section in Pakistan (Amb, Salt Range) do not indicate an end-Permian spore spike so far, however, higher spore abundances close to the Permian-Triassic boundary have been observed from single occurrences at Narmia and Chitta-Landu (Surghar Range). The new results from Amb suggest a gradual floral change reflected in the increasing dominance of lycopod spores towards the Dienerian. In Pakistan palynofloras dominated by lycopod spores and low numbers of pteridosperm and conifer pollen prevail from the Dienerian until the early Smithian and are also known from the early Smithian of South Tibet. In Pakistan these assemblages are followed by a pronounced spore spike in the middle Smithian. Similar to the patterns of the end-Permian record, the middle Smithian spore spike coincides with a negative carbon isotope excursion and is followed by the late Smithian marine extinction event. The recurrent Early Triassic negative carbon isotope excursions have been interpreted to reflect volcanically induced CO₂ pulses (Payne and Kump, 2007), thus environmental perturbations in phases of volcanic degassing might be the common cause for both of these events.

In Pakistan and South Tibet palynofloras of early Spathian age (~2 Ma after the end-Permian extinction event) are characterised by increasing abundance of gymnosperm pollen (conifers and pteridosperms) associated with reduced numbers of lycopod spores indicating the onset of terrestrial ecosystems stabilisation.

The described palynofloral patterns are complex and closely related to the changes in the carbon isotope record, which suggests that the floral recovery dynamics were linked to the environmental conditions.

REFERENCES

- Hochuli, P. A., Hermann, E., Vigran, J.O., Bucher, H. & Weissert, H. 2010: Rapid demise and recovery of plant ecosystems across the end-Permian extinction event. *Global Planet. Change*, 74,144-155.
- Looy, C. V., Brugman, W. A., Dilcher, D. L. & Visscher, H. 1999: The delayed resurgence of equatorial forests after the Permian-Triassic ecologic crisis. *Proc. Natl. Acad. Sci. USA*, 96, 13857-13862.
- Looy, C. V., Twitchett, R. J., Dilcher, D. L., Van Konijnenburg-Van Cittert, J. A. H., Visscher, H. 2001: Life in the end-Permian dead zone. *Proc. Natl. Acad. Sci. USA*, 98, 7879-7883.
- Payne, J. L. & Kump, L. R. 2007: Evidence for recurrent Early Triassic massive volcanism from quantitative interpretation of carbon isotope fluctuations. *Earth Planet. Sci. Lett.*, 256, 264-277.

14.11

Nammal Nala (Salt Range, Pakistan), a potential GSSP candidate for the Induan/Olenekian Boundary (Early Triassic): detailed biostratigraphy and comparison with other GSSP candidates

David Ware*, Hugo Bucher*, Nicolas Goudemand*, Michael Orchard², Elke Hermann³, Peter A. Hochuli*, Thomas Brühwiler*, Leopold Krystyn⁴, Ghazala Roohi⁵

¹ Paläontologisches Institut und Museum, Universität Zürich, Karl Schmid-Strasse 4, CH-8006 Zürich, Switzerland

² Geological Survey of Canada, 625 Robson Street, Vancouver, BC, Canada V6B 5J3

³ Palaeoecology, Institute of Environmental Biology, Faculty of Science, Utrecht University, Laboratory of Palaeobotany and Palynology, Budapestlaan 4, 3584 CD Utrecht, The Netherlands

⁴ Department of Palaeontology – Geozentrum, Althanstrasse 14, A-1090 WIEN, Austria

⁵ Pakistan Museum of Natural History, Garden Avenue, Islamabad 44000, Pakistan

To improve our understanding of the biotic recovery in the aftermath of the Permian/Triassic mass extinction, a reliable high resolution biochronological frame of the Early Triassic period is crucial. This period is currently divided in two stages, the Induan and the Olenekian, but the boundary between the two is still not clearly defined and lacks a stratotype.

Here we present detailed biostratigraphical results based on new collections of ammonoids and conodonts from Nammal Nala (Salt Range, Pakistan), a classical locality for Early Triassic ammonoids, which had never been studied in detail. Our results show that this section provides by far the most complete profile for the definition of the Induan-Olenekian boundary (IOB). The GSSP's golden spike for the base of the Olenekian could be located at the first occurrence of Flemingitidae (a typical Smithian ammonoid family) and of the conodont genus *Novispathodus*. It also coincides with a positive shift of $\delta^{13}\text{C}_{\text{org}}$ of ca. 6‰, with a sequence boundary and with a palynofacies change (Hermann et al., 2011). In this expanded stratigraphical series the IOB falls within the Ceratite Marls without any significant facies change, an ideal configuration for the definition of a boundary.

The same sequence of faunal associations had previously been recognized in Mud (Spiti Valley, India; Brühwiler et al. 2010), another GSSP candidate for this boundary proposed by Krystyn et al. (2007a, b). Here, the faunal turnover occurs 1 m below the previously proposed IOB (in bed 10 instead of bed 13 of Krystyn et al. 2007a, b; Brühwiler et al. 2010), and is associated with a facies change (from dark shales with early diagenetic calcareous concretions to massive, bioturbated limestone beds) in a much more condensed section. Moreover, it has undergone strong diagenetic alteration, so no palynological record is available. Conodonts also allow detailed correlation with the section of Chaohu (SE China), another GSSP candidate for the IOB (Chinese Triassic Working Group 2007). The latter section is however condensed and lacks ammonoid and palynological record.

The use of multiple proxies to define the IOB allows its correlation with other sections throughout the world. However, pending similarly detailed analyses of other IOB localities (e. g. British Columbia, Arctic Canada, Siberia, Madagascar, etc.), detailed correlations with previous biostratigraphic schemes remain challenging.

REFERENCES

- Brühwiler, T., Ware, D., Bucher, H., Krystyn, L. And Goudemand, N. 2010. New Early Triassic ammonoid faunas from the Dienerian/Smithian boundary beds at the Induan/Olenekian GSSP candidate at Mud (Spiti, Northern India). *Journal of Asian Earth Sciences*, 39, 724-739.
- Chinese Triassic Working Group 2007. Final report of the GSSP candidate for the I/O boundary at West Pingdingshan Section in Chaohu, Southeastern China. *Albertiana*, 36, 10-21.
- Hermann, E., Hochuli, P. A., Méhay, S., Bucher, H., Brühwiler, T., Ware, D., Hautmann, M., Roohi, G., Ur-Rehman, K. And Yaseen, A. 2011. Organic matter and palaeoenvironmental signals during the Early Triassic biotic recovery: The Salt Range and Surghar Range records. *Sedimentary Geology* 234:19-41.
- Krystyn, L., Bhargava, O. N. And Richoz, S. 2007a. A candidate GSSP for the base of the Olenekian Stage: Mud at Pin Valley; district Lahul & Spiti, Himachal Pradesh (Western Himalaya), India. *Albertiana*, 35, 5-29.
- Krystyn, L., Richoz, S. And Bhargava, O. N. 2007b. The Induan-Olenekian Boundary (IOB) in Mud – an update of the candidate GSSP section M04. *Albertiana*, 36, 33-45.

P 14.1

A Cretaceous fish takes a fast start: insights from a recent analogue

Loïc Costeur¹, Paolo Domenici², Rubén Ezquerro³, Mathieu Rousseau⁴, Fabio Antognarelli², Andrea Satta², Simone Simeone² & Félix Pérez-Lorente⁵

¹ Naturhistorisches Museum Basel, Augustinergasse 2, CH-4001 Basel (loic.costeur@bs.ch)

² Istituto per l'Ambiente Marino Costiero, CNR, Località Sa Mardini, IT-09072 Torregrande-Oristano

³ Instituto de Estudios Riojanos, Portales 2, SP-26001 Logroño

⁴ CFTJF, Total S.A., F-64000 Pau

⁵ Universidad de La Rioja, C/Madre de Dios, 51, SP-26006 Logroño

We describe here a fish trail found in the Early Cretaceous sediments of the Oliván Group (late Aptian-Albian in age), La Rioja, Spain in the light of a modern analogue. We hypothesize that the trail was caused by a specific fish behaviour commonly observed in modern fish, i.e. a fast-start escape response, which was followed by a 2-meters long irregular swimming sequence. Fast-start behaviors are commonly used in predator-prey encounters either to attack or to escape (Domenici & Blake 1997). Such movements are achieved by most modern fish and are mediated by Mauthner cells in the hindbrain, albeit differences in swimming performance exist among species (Domenici & Blake 1997).

The finding occurred on a micaceous fine to medium sandstone slab taking place at the end of a fluvial channel infill. The whole sedimentary succession indicates continental deposits in fluvial environments (flood plains, channels and point bars). As far as we are aware the fish trail is one of the only traces of a specific behavior (other than routine swimming) ever recorded for fish. Indeed only abrupt turns (Martin & Pyenson, 2005) and a feeding trace (Martin et al., 2010) are known so far. Traces of specific behaviors are very informative since they unravel the range of possibilities allowed by body morphology. They also have an evolutionary significance since specific behaviors evolve in response to specific constraints.

As far as the trail maker is concerned, it should have been a fish with a rather strong anal and/or caudal fin and flexible enough to be able to produce a fast-start; such fishes can be found in the Teleostei or Amiiformes that occur in the Early Cretaceous of Spain although no fish remains is known from the Oliván group itself.

A modern-day species was used to back up the fast-start hypothesis. We built up an experiment using a grey mullet (*Liza aurata*) swimming in shallow water above a sandy sediment with a composition close to that of the fossil site. The fish, when threatened, responded with a fast start and produced a C-shaped trace on the sediment that grossly matches the fossil trail, albeit being not that strongly imprinted and slightly different in shape (Fig. 1). The environmental conditions and the fish species used (most probably not the same family than that of the fossil trail) may account for the differences. Nevertheless, the experiment allowed us to strengthen our hypothesis that the fossil trace refers to a specific swimming behaviour related to predator-prey interactions.

REFERENCES

- Domenici, P. & Blake, R.W. 1997: The kinematics and performance of fish fast-start swimming. *The Journal of Experimental Biology*, 200, 1165-1178.
- Martin, A.J. & Pyenson, N.D. 2005: Behavioral significance of vertebrate trace fossils from the Union Chapel site. In: Buta, R. J., Rindsberg, A. K. & Kopaska-Merkel, D. C., (eds.) *Pennsylvanian Footprints in the Black Warrior Basin of Alabama*. Alabama Paleontological Society Monograph, 1, pp. 59-73.
- Martin, A.J., Vazquez-Prokopec, G. & Page, M. 2010: First known feeding of the bottom-dwelling fish *Notogoneus osculus* and its paleontological significance. *PLoS ONE*, 5(5), e10420, doi:10.1371/journal.pone.0010420.

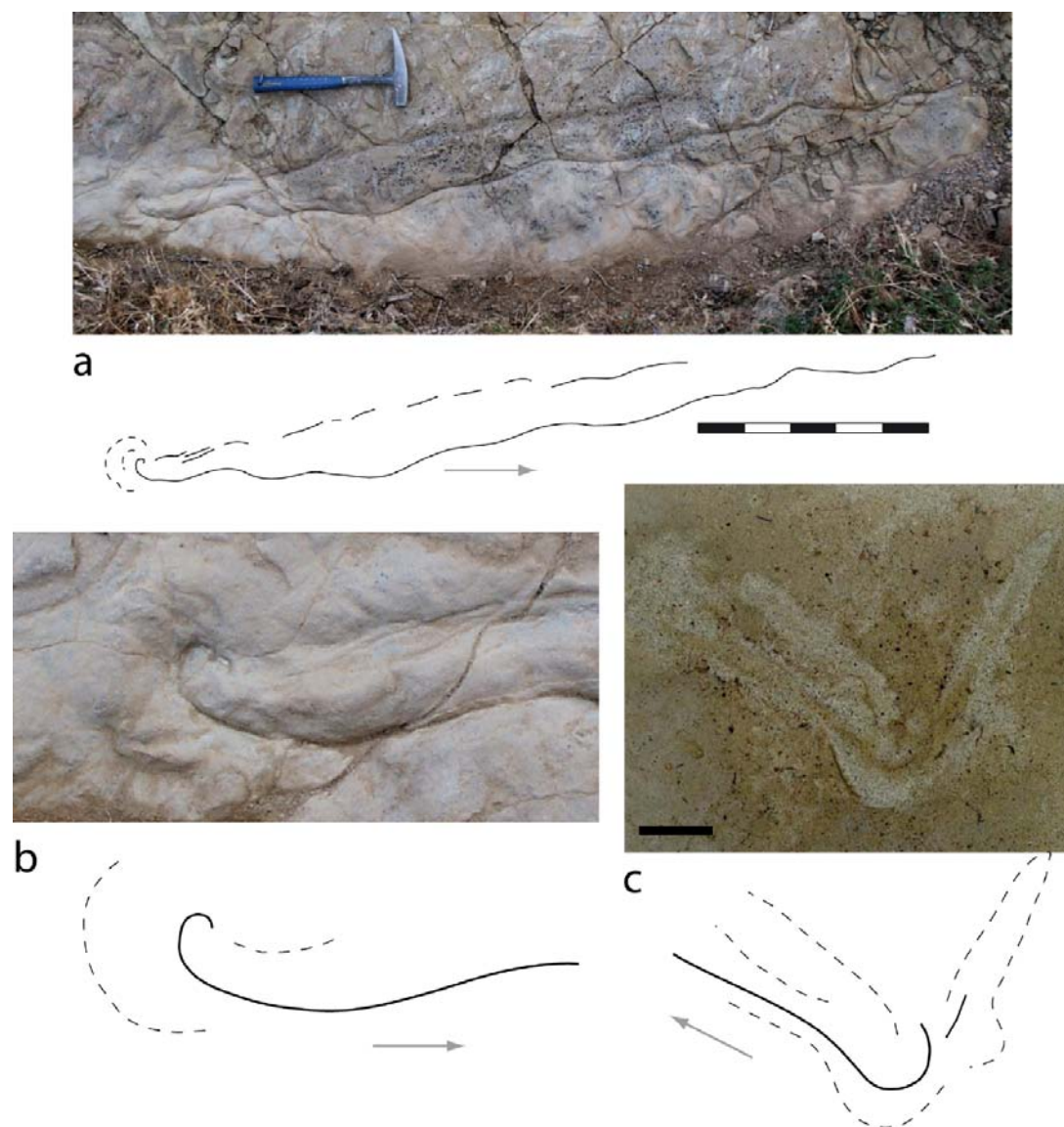


Figure 1. a, overall view of the Valtrujal fossil fish trail with explanatory drawing, scale bar: 50 cm; b, close-up of the C-shape starting point of the fossil trail with explanatory drawing; c, close-up of a fast-start C-shape trace left by a living grey mullet with explanatory drawing, scale bar: 5 cm. Dashed lines indicate mud rims or displaced sediment. Grey arrows indicate swimming direction.

P 14.2

A new skull of *Tapirus* from the Late Eocene of France

Loïc Costeur¹ & Didier Berthet²

¹ Naturhistorisches Museum Basel, Augustinergasse 2, CH-4001 Basel (loic.costeur@bs.ch)

² Centre de Conservation et d'Etude des Collections, 13 rue Bancel, F-69007 Lyon

Tapirus GÉRAIS, 1850 is an enigmatic small artiodactyl from the Late Eocene and Early Oligocene of Europe (Erfurt & Métais, 2007). The genus contains 5 species all characterised by a tapiroid bilophodont dentition which makes them quite different from the other European artiodactyls. The genus is endemic to Western Europe and is known from a relatively low amount of material (but with a rather good geographic distribution), albeit a very nice skull (Fig. 1) was recovered from the Quercy Phosphorites. It is one of the few genera to cross the Eocene-Oligocene famous “Grande Coupure”. The fossil we describe here is an almost complete skull with most of the dentition coming from a Late Eocene site in Central-Eastern France.

The site “Les Plantées” is situated in the vicinity of the city of Saint-Etienne not far from the shores of the Loire River. Geologically the sediments are fluvial in origin and the skull presented here was found in greenish coarse and not strongly consolidated sands. It's dated to MP18-20 (Huguency, 1997), thus Late Eocene. The site yielded few fossils and a preliminary faunal list was published in Huguency (1997).

The new skull is ascribed to *Tapirulus* cf. *hyracinus* STEHLIN, 1910. Preliminary comparisons to Eocene *Tapirulus* from the Middle to Late Eocene was carried out, and especially with skull NMB Q.B.185 (Fig. 1), one of the best preserved specimens from the Quercy Phosphorites and ascribed by Stehlin (1910) to *Tapirulus hyracinus*. Based on size alone, the four other species *T. majori*, STEHLIN, 1910, *T. depereti* STEHLIN, 1910, *T. schlosseri* STEHLIN, 1910, and *T. perrierensis* SUDRE, 1978 can be excluded as they are much smaller. Skull MHNL 20164554 is well preserved except in its basal part; the left tooththrow with I3-M3 together with the right tooththrow with P1-M3 are preserved; it is slightly smaller than that from Quercy, but overall proportions are similar. It is flat and has an elongated snout and thus a longer facial than posterior part. There seems to be two lacrimal orifices, or maybe a splitted orifice inside the orbit, while the skull from Quercy shows a clear situation of two separated orifices on its right virtually uncrushed orbit, one inside the orbit above a second one situated on the rim, both orifices being separated by a small projection of the lacrimal bone. A strong infraorbital foramen lies above the anterior part of the P3 just like on skull NMB Q.B.185. Teeth are worn so that few characteristics can be described in detail. However on molars, paraconules are absent and parastyles are rather strong; pre- and post-cinguli are strong especially on M3, much like on skull NMB Q.B.185 from the Quercy. The M1 and M3, although being larger than longer, do not reach the antero-posterior compression of the M2. P4 is triangular with strong labial styles and pre- and post-cinguli. Sudre (1978) mentions smaller sized *Tapirulus* (than *T. hyracinus*) from the Early Oligocene of Belgium and France and proposes to investigate this material in more details since he suggests that another Early Oligocene species might exist.

Comparisons to this material will be necessary to see if an intermediate sized species between the small *Tapirulus* and *T. hyracinus* did indeed exist. The locality “Les Plantées” is tentatively dated to MP18-20 (Huguency, 1997) and a Late Eocene age would fit well with *T. hyracinus* as this species is only known from the Late Eocene and Early Oligocene, the other species described so far being found in older localities.



Figure 1: Left, skull MHNL 20164554 and right, skull NMB Q.B.185 from the Quercy Phosphorites in dorsal, palatal and lateral view from top to bottom, respectively. Scale bar 10 mm

REFERENCES

- Erfurt, J. & Métais, G. 2007: Endemic European Paleogene artiodactyls - Cebochoeridae, Choeropotamidae, Mixtotheriidae, Cainotheriidae, Anoplotheriidae, Xiphodontidae, and Amphimerycidae. In: Prothero D.R. & Foss, S. (eds) *The Evolution of Artiodactyls*. The John Hopkins University Press, Baltimore, pp 59-84.
- Huguency, M. 1997: Biochronologie mammalienne dans le Paléogène et le Miocène inférieur du centre de la France : synthèse réactualisée. In: Aguilar, J.-P, Legendre S. & Michaux J. (eds) *Actes du Congrès BiochroM'97*. Mémoires et Travaux de l'E.P.H.E, Institut de Montpellier, 21, pp. 417-430.
- Stehlin, H.G. 1910: Die Säugetiere des Schweizerischen Eocaens. *Critischer Catalog der Materialien*. *Abhandlungen der schweizerischen paläontologischen Gesellschaft* 36, 855-1164.
- Sudre, J. 1978: Les artiodactyles de l'Eocène Moyen et Supérieur d'Europe occidentale (systématique et évolution). *Mémoires et Travaux de l'E.P.H.E, Institut de Montpellier*, 229 p.

P 14.3

Endolithic microorganisms in Piora Dolomite

Horath Thomas D.¹, Bachofen Reinhard¹, Neu Thomas R.², Strasser Reto J.³

¹Institute of Plant Biology, University of Zürich, Zollikerstr. 107, 8008 Zürich, Switzerland

²Department of River Ecology, UFZ Centre for Environmental Research, Leipzig-Halle, Brueckstrasse 3A, 39114 Magdeburg, Germany

³Laboratory of Bioenergetics, University of Geneva, Chemin des Embouchis 10, Jussy Lullier, 1254 Geneva, Switzerland

Endolithic microorganisms form a distinct band a few mm below the surface in dolomite rock in the Swiss Alps have been characterized using spectroscopical, optical and molecular methods. The light intensity in the band amounts for 1 to 5 % of the surface illumination. Reflection spectroscopy reveals pigments with *in vivo* absorption maxima around 715 nm, 680 nm, 625 nm and 500 nm, indicating the presence of eukaryotic algae, cyanobacteria and green phototrophic bacteria. Electron microscopy and confocal laser scanning microscopy display cyanobacteria of coccoid and filamentous morphotypes. Colonies of coccoid forms often are surrounded by pigmented sheaths and thick layers of exopolysaccharides protecting them against stress factors such as light, UV, or lack of water and nutrients. Cloning the small subunit ribosomal RNA gene resulted in 53 different clones, while the sequence of most of them was not present in data libraries. Besides *Bacteria* also *Crenarcheota*, eukaryotic *Amoebae* and a *Bryophytum* (moss) were found.

The fluorescence transients of chlorophyll a indicate that the photosynthetic activity of the cyanobacteria is strongly dependent on water availability.

We conclude that the small zone of endolithic microorganisms underneath the rock surface is a nearly closed micro-ecosystem harboring a broad variety of physiologically active species.



Figure 1. Opened dolomite rock from the Piora Valley with endolithic green phototrophs. The scale bar is in centimetres.

REFERENCES

- Strasser R, Srivastava A, Tsimilli-Michael M (2000) The fluorescence transient as a tool to characterize and screen photosynthetic samples. In: Yunus M, Pathre U, Mohanty P (eds.) Probing photosynthesis: Mechanisms, regulation and adaptation. Taylor & Francis, London, UK. Pp. 443-480.
- Neu TR, Woelfl S, Lawrence JR (2004) Three-dimensional differentiation of photo-autotrophic biofilm constituents by multi-channel laser scanning microscopy (single-photon and two-photon excitation). *J Microbiol Methods* 56:161-172
- Horath Th, Bachofen R (2009) Molecular Characterization of an Endolithic Microbial Community in Dolomite Rock in the Central Alps (Switzerland) *Microb Ecol* 58:290-306
- Horath Th D (2010) Endolithic Microbial Communities in Dolomite. Dissertation at the University of Zürich. <http://opac.nebis.ch/ediss/20111099.pdf>

P 14.4

Mining morphological evolution in microfossils using volume density diagrams

Michael W. Knappertsbusch¹ & Yannick Mary^{1,2}

¹Naturhistorisches Museum Basel, Augustinergasse 2, CH-4001 Basel (michael.knappertsbusch@unibas.ch)

²Geologisch-Paläontologisches Institut, Bernoullistrasse 32, CH-4056 Base

Morphometry is an important technique for the quantitative description of variations and differences between closely related extant and extinct species and their phylogenetic relationships. Morphotypes include a group of specimens, that most typically describe the morphological appearance in a fossil assemblage. They are characterized by a combination of meaningful, independent morphological characters. In the ideal case morphotypes are recognizable as well separated data clusters in a multivariate set of morphometric measurements. In reality however, there exists often overlap between such clusters and then statistical and/or graphical methods must be applied to best separate these clusters in a reliable way. Whether a morphotype also represents a biological species must further be clarified using independent evidence from biological, (paleo-) ecological, biogeographic, geochemical or molecular investigations. If the history of morphotype variation is studied in a sequence of successive samples in the geological record moments of evolutionary splitting and divergence may be uncovered, which eventually witness speciation of an ancestral species into a descendent one. Such analysis, however, requires a very large number of measurements through time, from several locations (Knappertsbusch 2011). Understandably, that these data are often difficult to analyse and interpret, even with the help of sophisticated statistical methods. Graphical analysis of the results is thus irreplaceable to reveal the morpho-phylogenetic relationships from one morphotype to another.

In the present contribution a graphical analysis and display software called Voxler from Golden Software is exploited, which allows to communicate complicate morphological evolutionary trends through geological time to researchers and to laymen. Two pre-existing and published data sets for the study of evolution in these organisms are used for the present exercise: The first example is taken from Knappertsbusch (2000), which describes the plexus of *Calcidiscus leptoporus* – *Calcidiscus macintyrei*, a group of Neogene marine calcareous planktonic algae including morphologically closely related extinct and extant morphotypes. These algae produce minute calcite platelets – coccoliths – that surround the cell and which after death accumulate to thick piles of calcareous deep sea oozes at the bottom of the oceans. The second example is taken from Knappertsbusch (2007), where *Globorotalia menardii* was studied, a representative of Neogene planktonic foraminifera, and which belongs to marine calcareous shell secreting planktonic protists. Also these shells - after settlement to the bottom of the ocean - are major contributors to worldwide deep-sea sediments.

In both cases, the original observations consisted of simple bivariate measurements of the hardparts along a number of deep-sea cores, i.e., coccolith size versus its number of sinusoidal ornamentations on the distal side for *C. leptoporus*, and the length versus width of shells in profile view in the case of *G. menardii*. The time-series of bivariate measurements were transformed into discrete time-series of bivariate frequency distributions, which themselves were interpolated to obtain continuous density diagrams of specimens throughout the bivariate morphospace and through geological time. These density variations could then be displayed in three dimensions and animated using Voxler.

The advantage of this graphical representation is, that morphotype evolution could be analyzed and visualized more comprehensively than with any of the previously applied methods (i.e., stacked series of scatter- or contoured frequency plots from one time-level to the next, or stacks of transversal sections of specimen frequencies parallel to the time axis, which were all quite difficult to present to the general audience). Using the animated density diagrams the authors are convinced, that they portray measured evolutionary patterns such as splitting and divergence more intuitively than without such tools.

The above abstract was submitted to Palaeontologia Electronica: Knappertsbusch, M. & Mary, Y.: in press. Mining morphological evolution in microfossils using volume density diagrams. Submitted to Palaeontologia Electronica.

Please follow also the links under "Research" from <http://pages.unibas.ch/museum/microfossils/index.html>

REFERENCES

- Knappertsbusch, M. 2011: Evolution im marinen Plankton. Mitteilungen der Naturforschenden Gesellschaften beider Basel, 13, 3-14.
- Knappertsbusch, M. 2007: Morphological variability of *Globorotalia menardii* (planktonic foraminifera) in two DSDP cores from the Caribbean Sea and the Eastern Equatorial Pacific. Carnets de Géologie / Notebooks on Geology, Brest, Article 2007/04 (CG2007_A04). URL: http://paleopolis.rediris.es/cg/CG2007_A04/index.html
- Knappertsbusch, M. 2000: Morphologic evolution of the coccolithophorid *Calcidiscus leptoporus* from the Early Miocene to Recent. Journal of Paleontology, 74, 712-730.

P 14.5

AMOR does it for us

Michael W. Knappertsbusch¹, Yannick Mary^{1,2} & Richard Schorpp^{3,1}

¹Naturhistorisches Museum Basel, Augustinerstrasse 2, CH-4001 Basel (michael.knappertsbusch@unibas.ch)

²Geologisch-Paläontologisches Institut, Bernoullistrasse 32, CH-4056 Basel

³Fachhochschule Nordwestschweiz, Institut für Automation, Steinackerstrasse 5, CH-5210 Windisch

AMOR (Automated Measurement system for shell mORphology) is a robot, which automatically positions, orientates and images isolate planktonic foraminifera, that are mounted in a standard micropaleontological slide under a binocular microscope (Knappertsbusch et al. 2009). It consists of a motorized four-axis tilting and gliding stage, that fits under a binocular and the latter being equipped with a digital video camera. The microscope is driven by a motorized zoom and has an autofocus. All components are controlled via custom developed software AMOR written in LabView 8.5 for a PC. The AMOR software was developed in several successive collaboration projects with students and engineers from the University of Applied Sciences of Northwestern Switzerland (FHNW). Since 2009 it was further improved to its present version 3.17. Using AutoIt v3 (a freeware automate and script language for windows tasks) individual functions from AMOR can be combined as needed and even allows for overnight-processing.

We use AMOR to collect images of shells of the planktonic foraminiferal group *Globorotalia menardii* in upside (keel) or spiral/umbilical view. AMOR first moves to the center of a field in the multicellular faunal slide, focuses, tilts the slide in x- and y direction until the specimen stands perfectly upright in keel position or is perfectly horizontal when spiral or umbilical position is selected. After re-calculation of the vertical position of the microscope and re-focussing and after image rotation for perfect “north-to-south” orientation of the shell on the computer monitor the optimum magnification for final imaging is sought. After auto-zooming and final refocussing a tiff image is saved to disc and the stage moves on to the next specimen repeating the cycle until the last field is completed. The magnification for every image is recorded for conversion of peripheral pixels to micrometers. A slide-calibration routine is implemented for usage of different types of faunal slides. Optionally, a character recognition can be activated in order to differentiate between the foraminiferal shell and white numerals, that are imprinted in the bottom of the slide. Next to operation in automated mode the user can choose a “single-specimen” mode to orientate and image individuals.

While AMOR orientates and collects digital images of isolated microfossils, additional software (MorphCol) developed by ourselves helps to automatically extract morphometric descriptors from the thousands of images, that we have collected so far. The following measurements are used to characterize shell variability: spiral height, axial length, keel angles, osculating circles of the keel region and surface area of the silhouette. For every specimen outline coordinates are extracted for fourier- and/or eigenshape analyses.

Our goal is to quantify inter- and intraspecific morphological shell variation in planktonic foraminifera like *Globorotalia menardii* and to better understand the biogeography of its morphological evolution and speciation (Knappertsbusch 2011). Menardiform globorotalids, our study objects, were selected because of their interesting radiation during the Pliocene. We use core materials from Holocene and ODP samples from a Late Pliocene (3.2 Ma) time-slice, and from from several DSDP and ODP cores considered to be interesting for testing speciation patterns through time. So far we have investigated cores from the Caribbean Sea (DSDP Site 502) and the Eastern Equatorial Pacific (503), and morphometric measurements from menardiform globorotalids are currently collected for the past 8 million years at ODP Site 925 (Ceara Rise).

Practical work with AMOR has proven its advantage for the routine collection of large data sets. However, as the system was especially developed for menardiform morphologies it is not always applicable to strongly different shell morphologies. Systematic shape changes, that other genera than flat globorotalids may have attained during their evolution may cause AMOR to fail for automatic positioning of shells (in such a case the operator has the possibility to escape to the “manual mode” of AMOR). For example, the umbilico-convex and asymmetric shells of *Globorotalia miocenica*, an extinct but related form within the *G. menardii* radiation, requires a slightly modified algorithm for auto-positioning than the bi-convex and almost symmetric shells of a typical *G. menardii*. Such difficulties were not inevitable during our studies and still need adaptation of the software, which is the next task in our effort to automate microfossil shell measurements.

REFERENCES

- Knappertsbusch, M., Binggeli, D., Herzig, A., Schmutz, L., Stapfer, S., Schneider, C., Eisenecker, J., & Widmer, L. 2009: AMOR - A new system for automated imaging of microfossils for morphometric analyses. *Palaeontologia Electronica*, Vol. 12, Issue 2; 2T: 20 p. URL: http://palaeo-electronica.org/2009_2/165/index.html
- Knappertsbusch, M. 2011: Evolution im marinen Plankton. *Mitteilungen der Naturforschenden Gesellschaften beider Basel*, 13, 3-14.

Knappertsbusch, M., 2004 – 2009: MorphCol - A collection of Fortran 77 programs for geometric morphometry. Technical Report. Naturhistorisches Museum Basel, Augustinergasse 2, 4001-Basel, Switzerland, 120 pages. URL: <http://pages.unibas.ch/museum/microfossils/Research/MORPHCOL/Start.html>

Please follow also the links under «Research» from <http://pages.unibas.ch/museum/microfossils/index.html>

P 14.6

The Neoproterozoic Oxygenation Event: environmental perturbations and biogeochemical cycling

Och Lawrence¹, Shields-Zhou Graham A.²

¹ Department of Earth Sciences, University College London, Gower Street, London WC1E 6BT, UK
Current address: Eawag, Seestrasse 79, CH-6047 Kastanienbaum

² Department of Earth Sciences, University College London, Gower Street, London WC1E 6BT, UK

The oxygen content of the Earth's surface environment is thought to have increased in two broad steps: the Great Oxygenation Event (GOE) around the Archean-Proterozoic boundary and the Neoproterozoic Oxygenation Event (NOE), during which oxygen possibly accumulated to the levels required to support animal life and ventilate the deep oceans. Although the concept of the GOE is widely accepted, the NOE is less well constrained and its timing and extent remains the subject of debate. We review available evidence for the NOE against the background of major climatic perturbations, tectonic upheaval related to the break-up of the supercontinent Rodinia and reassembly into Gondwana, and, most importantly, major biological innovations exemplified by the Ediacarian Biota and the Cambrian 'Explosion' (see Figure 1).

Geochemical lines of evidence for the NOE include perturbations to the biogeochemical cycling of carbon. Generally high $\delta^{13}\text{C}$ values are possibly indicative of increased organic carbon burial and the release of oxidative power to the Earth surface environment after c. 800 Ma. A demonstrably global and primary record of extremely negative $\delta^{13}\text{C}$ values after about 580 Ma strongly suggests the oxidation of a large dissolved organic carbon pool (DOC), the culmination of which around c. 550 Ma coincided with an abrupt diversification of Ediacaran macrobiota. Increasing $^{87}\text{Sr}/^{86}\text{Sr}$ ratios towards the Neoproterozoic - Cambrian transition indicate enhanced continental weathering which may have fuelled higher organic production and burial during the later Neoproterozoic.

Evidence for enhanced oxidative recycling is given by the increase in sulphur isotope fractionation between sulphide and sulphate, exceeding the range usually attained by sulphate reduction alone, reflecting an increasing importance of the oxidative part in the sulphur cycle. S/C ratios attained a maximum during the Precambrian – Cambrian transition, further indicating higher sulphate concentrations in the ocean and a transition from dominantly pyrite burial to sulphate burial after the Neoproterozoic. Strong evidence for the oxygenation of the deep marine environment has emerged through elemental approaches over the past few years which were able to show significant increases in redox-sensitive trace-metal (notably Mo) enrichment in marine sediments not only during the GOE but even more pronounced during the inferred NOE. In addition to past studies involving Mo enrichment, which has been extended and further substantiated in the current review, we present new compilations of V and U concentrations in black shales throughout Earth history that confirm such a rise and further support the NOE. With regard to ocean ventilation, we also review other sedimentary redox indicators, such as iron speciation, molybdenum isotopes and the more ambiguous REE patterns. Although the timing and extent of the NOE remains the subject of debate and speculation, we consider the record of redox-sensitive trace-metals and C and S contents in black shales to indicate delayed ocean ventilation later in the Cambrian on a global scale with regard to rising oxygen levels in the atmosphere which likely rose during the Late Neoproterozoic.

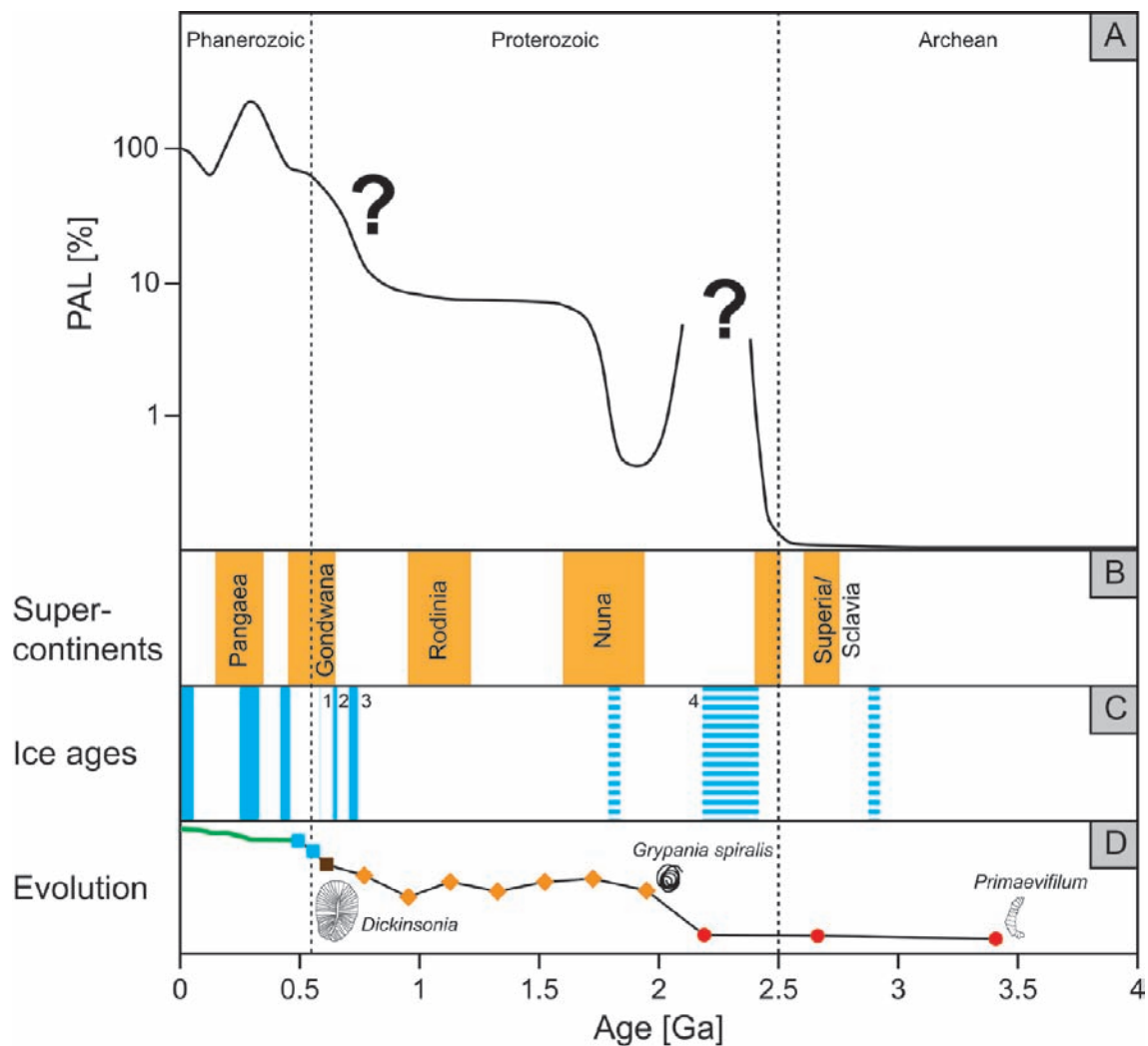


Figure 1: A) Proposed reconstruction of the atmospheric O_2 content through time expressed as the percentage of present atmospheric level of oxygen. B) Periods of supercontinent formation. C) Precambrian glaciations whereby the numbered blue bars are of presumably global extent: 1) Gaskiers glaciation, 2) Marinoan glaciation, 3) Sturtian glaciation, 4) Makganyene/Huronian glaciation. D) Biological innovations exemplified through increase of maximum size of organisms throughout Earth history. Red dots: prokaryotes, orange diamonds: protists, brown square: vendobiont (probable multicellular eukaryote, e.g. *Dickinsonia*), blue squares: animals, green line: vascular plants.

P 14.7

The *Exogyra aquila* Marls (Lower Aptian) on the Vivarais platform (Ardèche, France) : Sedimentology, stratigraphy, and biostratigraphy.

Pictet Antoine

Géology and Paléontology Institut, University of Lausanne, Anthropole – CH- 1015 Lausanne (sk8chmullen@hotmail.com)

The end of the Urganian carbonate platform is marked by the sudden disappearance of an entire oligotrophic ecosystem dominated by rudist, coral and stromatoporoids. On the Ardèche platform (SE France), this crisis is characterized by a regional discontinuity, polyphased, called DFU or DRBeS according to diverse authors. Petrographic and sedimentologic analyses carried out on this boundary and overlying “*Exogyra aquila* Marls” (Upper *Orbitolina* beds, Lower Aptian) have permitted to distinguish a karstified surface, whose cavities are commonly filled with continental sediments. Over this surface, is directly superimposed a deep-subtidal hardground, characterized by microbial mats (Stromatolites) that developed on internal platform, whose formation is probably linked to the Aptian transgression. Biostratigraphy by ammonites and orbitolinids allows to date this surface to the Forbesi Zone pro parte. This latter formed during a very short period, and indicates that brief eustatic variations of great amplitude must have occurred early in the Aptian, probably related to large-scaled climatic changes that significantly modified sediment and nutrient inputs.

The overlying “*Exogyra aquila* Marls” Formation, extremely well preserved on the Ardèche platform, can be structured into four members that constitute a shallowing-upwards sequence mainly comprised of hemipelagic, shaly limestones and echinoderm-rich limestones. During their deposition, an extensive tectonic activity took place, modifying the local depositional pattern and creating fluctuations within the shaly-calcareous sediments. Thanks to the abundance of ammonites, these sediments were easily dated from Forbesi and Deshayesi Zones.

The “Black Marls” Formation follows the *E. aquila* Marls, with a new transgression brutally interrupted by the highly erosive regional discontinuity DRBeT. The result of this erosion is a basal phosphatic breccia named Pélican Horizon, marking the base of this formation. The DRBeT discontinuity, as well as the “Horizon du Pélican”, were dated to be of the late Dufrenoyi subzone. This limit shows a significant erosion in the inner platform, along with large dissolved and recrystallized areas whose origin remains unclear.

REFERENCES

- Arnaud-Vanneau, A., Arnaud, H., & Masse, J.P. (1978): Les discontinuités sédimentaires du Barrémien supérieur et du Bédoulien sur le pourtour de la zone vocontienne. Livre jubilaire Jacques Flandrin – Docum. Lab. Géol. Fac. Sci. Lyon, 4, pp. 11-27.
- Elmi, S., Busnardo, R., Clavel, B., Camus, G., Kieffer, G., Berard, P., Michaely, B. (1996): Notice explicative de la feuille Aubenas à 1/50000. Editions du BRGM Service géologique national.
- Föllmi, K.B. & Gainon, F. (2008): Demise of the Tethysian Urganian carbonate platform and subsequent transition towards pelagic conditions: The sedimentary record of the Col de la Plaine Morte area, central Switzerland. *Sed. Geol.* 205, 142-159.
- Masse, J.P., Fenerci-Masse, M. (2011): Drowning discontinuities and stratigraphic correlation in platform carbonates. The late Barremian-early Aptian record of southeast France. *Cretaceous Research* (2011), doi:10.1016/j.cretres.2011.04.003.

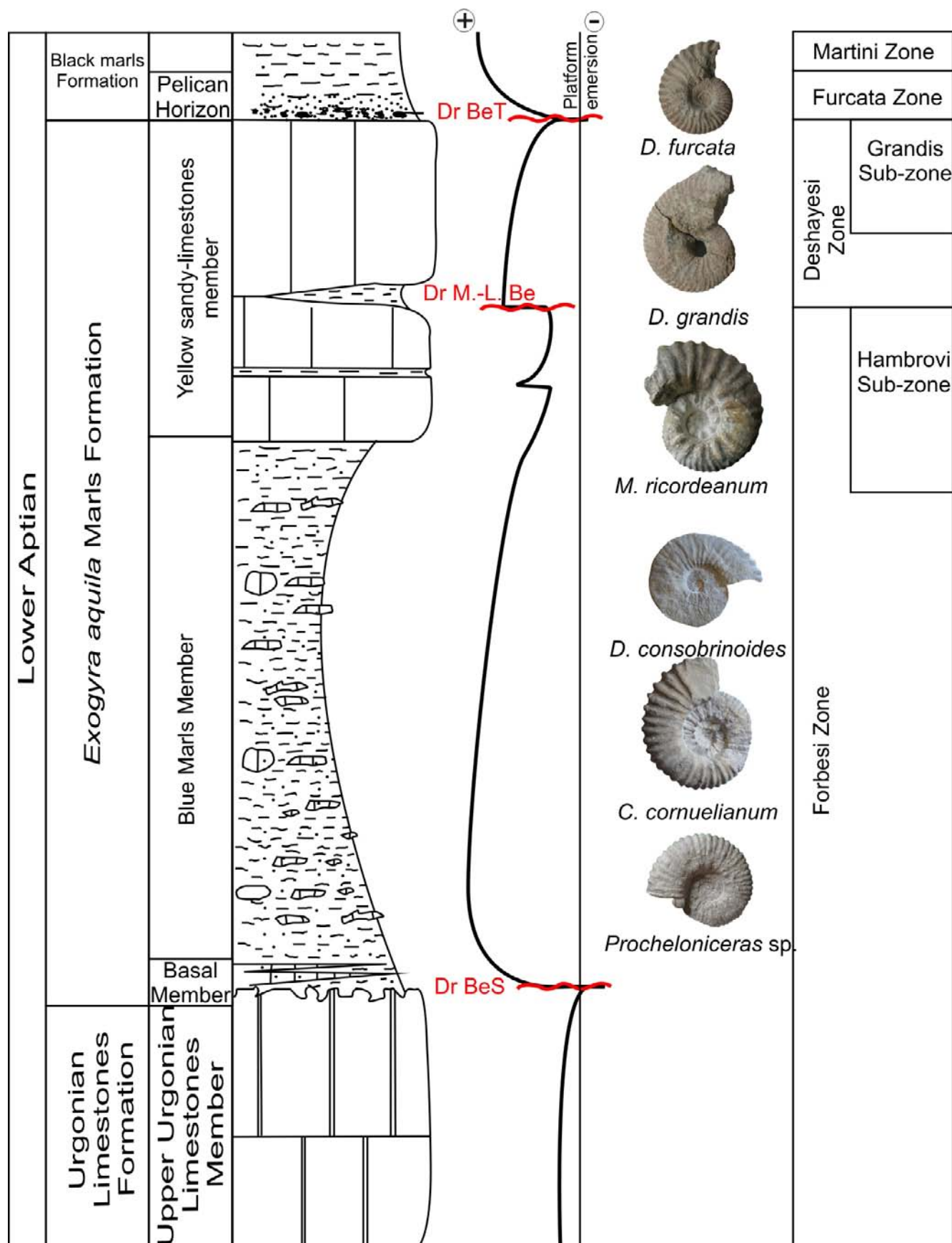


Figure 1. Simplified log of *Exogyra aquila* Marls on the Vivarais platform in regard with lithostratigraphy nomenclature, major discontinuities and eustatic curve, useful ammonites and corresponding biozonation.

P 14.8

Pushing life to the extreme: Investigating the subsurface biosphere in the Dead Sea Basin

Camille Thomas¹, Aurèle Vuillemin¹, Muriel Pacton², Nicolas Waldmann³, Daniel Ariztegui¹ and the DSDDP Scientific Team[°]

¹ University of Geneva, Department of Earth Sciences and Paleontology, CH-1205 Geneva, Switzerland (camille.thomas@unige.ch)

² ETH Zürich, Geologisches Institut, CH-8092 Zürich, Switzerland

³ University of Haifa, Department of Marine Geosciences, 31905 Mt. Carmel, Israel

[°] Complete list of DSDDP scientists at www.icdp-online.org

The Dead Sea Deep Drilling Project (DSDDP) is an internationally funded multidisciplinary initiative aiming to reconstruct the paleoenvironmental and paleoseismicity history of the Dead Sea Basin (DSB). Within this framework an ongoing geomicrobiological study in the recovered sediments aims to characterize the subsurface biosphere. The foci of this study are to identify the microbes surviving in this chemically peculiar environment and their participation in authigenic mineral precipitation.

A 450m long core consisting mainly of detrital mud, salt and primary aragonite has been recovered from the center of the present Dead Sea. DAPI-stained epifluorescence microscopy has allowed the observation and quantification of living bacteria in the uppermost 130m sediments. Several lithological intervals are dominated by needle and star-shaped aragonite interpreted as direct authigenic precipitation from the water column (Stein et al., 1997). SEM imaging and EDX spectroscopy have allowed the identification of precursors of Fe-S minerals within these intervals, pointing towards a microbially-related mineralization.

Similarly, in the superficial sediments of the core, where DAPI counting reaches a maximum, well preserved exopolysaccharide substances (EPS) are closely related to precursors of aragonite stars. We hypothesize that these EPS may act as a template for aragonite nucleation under the chemical conditions prevailing today. This is also supported by observations of dead microbial mats forming thin dark laminae interbedded with white laminae of aragonite in the modern western Dead Sea shore.

These observations have allowed the identification for a first time of a living subsurface biosphere in the Dead Sea sediments. Further investigations using a modern geomicrobiological approach will bring new light on the prevailing conditions behind its survival and its influence on the formation of the Dead Sea sediments throughout time.

REFERENCES

Stein, M., Starinsky, I. A., Katz, I. A., Goldstein, J. S. L., Machlus, M., & Schramm, A. 1997. Strontium isotopic, chemical, and sedimentological evidence for the evolution of Lake Lisan and the Dead Sea. *Geochimica et Cosmochimica Acta*, 61(18), 3975-3992.

15. Geoscience and Geoinformation - From data acquisition to modelling and visualisation

Nils Oesterling, Adrian Wiget, Massimiliano Cannata

*Swiss Geological Survey,
Swiss Geodetic Commission,
Swiss Geotechnical Commission,
Swiss Geophysical Commission,
Swiss Hydrogeological Society*

TALKS:

- 15.1 *Antonovic M., Cannata M.:* Managing authentication and permissions to OGC services with GeoShield: presenting the new GeoServer Resource Access Manager plug-in and the Sensor Observation Service protection
- 15.2 *Antonovic M., Cannata M., Molinari M.:* Protect-Me: web service for protection work catalogue
- 15.3 *Cannata M., Marzocchi R., Molinari M.:* GIS-based modeling for landslide-generated tsunami
- 15.4 *Dresmann H., Huggenberger P., Epting J., Wiesmeier S., Scheidler S.:* The geological 3D-model of the Basel region – new insights
- 15.5 *Friedel S.:* Earth modeling seen from a Multiphysics Perspective
- 15.6 *Kessler H., Mathers S., Wood B.:* Building the National Geological Model of Great Britain
- 15.7 *Khemiri Sami*, Kassebi Adnane*, Zargouni Fouad*:* Provision of 3D GIS (model GMS) for geospatial hydrogeologic modeling of Mio-Plio-Quaternary groundwater of Foussana (Central Tunisia)
- 15.8 *Michael C. S., Baumberger R., Oesterling N.:* Geological 3D modelling of Quaternary sequences using GSI3D – an example of the surroundings of Berne
- 15.9 *Molinari M., Cannata M., Ambrosi C., Begueria S.:* Numerical modelling for risk scenarios generation
- 15.10 *Novak D., Grimm D.E., Tokarczyk P.:* Modeling of the “Plan da Mattun” archeological site using a combination of different sensors
- 15.11 *Rogers S., Collet C., Lugon R.:* Determining archaeological potential in the Pennine Alps using GIS tools
- 15.12 *Sala P., Tisato N., Pfiffner O.A., Saenger E.H.:* Vp-Vs measurements of shallow formations in Chémery (FR): comparison between laboratory and field data and integration within a 3D geological model
- 15.13 *Strasky S., Oesterling N., Baland P., Michael C.S., Kühni A.:* The Swiss Geologic Data Model

15.1

Managing authentication and permissions to OGC services with GeoShield: presenting the new GeoServer Resource Access Manager plug-in and the Sensor Observation Service protection

Antonovic Milan¹, Cannata Massimiliano¹

¹ SUPSI Istituto Scienze della Terra, CP72 CH-6952 Canobbio (milan.antonovic@supsi.ch, massimiliano.cannata@supsi.ch)

Enterprises are increasingly feeling the need of more sophisticated data access control to OGC services. Nowadays there aren't many solution to manage data access control. Using actual techniques, administrators can mostly define read or write permission to specific services.

GeoShield meets this need by offering a centralized way to define security access-control to OGC services through a nice user friendly web interface. Basically it acts like a proxy, intercepting all the communications between clients and OGC compliant services (WMS, WFS, SOS). GeoShield is able to manage users and groups, it handles authentication and privileges settings among groups and registered services. It is capable to analyze requests applying the configured permission filters and/or manipulating the response accordingly.

This year GeoShield extends his capabilities introducing two major improvements: the Sensor Observation Services protection and the GeoServer Resource Access Manager plug-in.

The SOS protection introduces the definition of permissions for core and transactional profiles. Data managers can now set read permissions for each Observation Offering, and authorize writing permissions to transactional profile requests only to authorized users.

Thanks to the latest GeoServer release (2.1), GeoShield can be directly integrated with the new Resource Access Manager plug-in. This extension give some benefits in term of speed and reliability, GeoShield's proxy capabilities is bypassed, minimizing response time.

The presentation will introduce the attendees with GeoShield and the newly developed features throughout a practical demo.

REFERENCES

GeoShield project - <http://listgeo.ist.supsi.ch/site/projects/geoshield>

OGC Standards - <http://www.opengeospatial.org>

GeoServer – <http://www.geoserver.org>

15.2

Protect-Me: web service for protection work catalogue

Cannata Massimiliano¹, Milan Antonovic¹, Molinari Monia¹

¹ Institute of Earth Sciences – SUPSI, Campus Trevano, CH-6952 Canobbio (massimiliano.cannata@supsi.ch)

The executed study aims to realize a complete system for the catalogue, management and visualization of information related to the natural hazard protection works. Having a comprehensive understanding of where, how, when and in which status the executed mitigation works are is crucial for an effective natural hazard risk management.

The Institute of Earth sciences (IST) to fulfill the need expressed by the Swiss Confederation, at a national level, and by the Canton Ticino, at a local level, has design and realized a system (PMES, ProtectME Service) composed by: (i) a data model defined using XSD schema, (ii) a Web service, similar to those defined by the Open Geospatial Consortium (OGC) and (iii) a Web based user interface for the access to the developed service.

The system has been implemented by using the Python and JavaScript programming languages, throughout the usage of specific libraries, and taking advantages of the PostgreSQL database with the PostGIS spatial extension. This paper present the cognitive investigation on the state of the art in Ticino, the three components of the system and finally some conclusions and consideration.

Home | Admin | Login

Cerca per numero...

Ricerca progetto esistente: 1120.4

Progetti | Opere | Elementi

Costo totale: [Slider]

Utente: [Dropdown]

Data modifica: [Input]

Protegg-Me è un servizio Web per la catalogazione e diffusione d'informazioni sulle opere di protezione esistenti. Conoscere dove, come, quando ed in che stato le opere di protezione siano presenti sul territorio è, infatti, fondamentale per una corretta gestione del territorio in relazione ai pericoli naturali. Tali informazioni risultano di vitale importanza sia per i gestori delle opere (generalmente i consorzi, o i comuni) che, a livello più generale, alle amministrazioni (cantoni, regioni, province, nazioni): questi dati infatti consentono di pianificare come impiegare in maniera efficiente le risorse disponibili.

Titolo	category	Autore	Data
I2	element	Paolino Paperino	Oggi 11:04 am
io sono le note.. ma così non servono a niente..			
1120.4	work	Paolino Paperino	Oggi 10:29 am
è			
1120.5.3	element	Paolino Paperino	Oggi 9:07 am
None			
1120.5.2	work	Paolino Paperino	Oggi 9:00 am
È			
PPPPPP	element	Paolino Paperino	30-05-2011 17:49:10
quarto da sinistra prima fila			
qwertzu-001.01	element	Paolino Paperino	30-05-2011 17:21:30
None			
qwertzu-001	work	Paolino Paperino	30-05-2011 17:20:19

© Istituto Scienze della Terra - SUPSI

Figure 1. Home page of the developed Protect-Me application web interface.

15.3

GIS-based modeling for landslide-generated tsunamis

Cannata Massimiliano¹, Marzocchi Roberto¹, Molinari Monia¹

¹ Institute of Earth Sciences – SUPSI, Campus Trevano, CH-6952 Canobbio (massimiliano.cannata@supsi.ch)

The recent tragic events occurred in Japan have shown once again the high vulnerability of communities towards the risk of tsunamis and the need for continuous improvements both in terms of alarm systems and adoption of appropriate protection measures. From this point of view, numerical modelling is a very important resource because it allows to create flood maps which can provide useful information about the areas most likely at hazard and the probable intensity of an event.

At the Swiss Geoscience Meeting 2008 a procedure for the risk assessment of earthquake-induced tsunamis was presented; here the authors intend to present a model for the simulation of tsunami generated by subaerial landslides in lakes and artificial basins. The model, based on the equations proposed by Heller et al. (2009), has been spatially implemented within the GIS GRASS and allows to simulate the wave generation due to the landslide impact, its propagation toward the basin, the generation of run-up wave and the consequent inundation along the coast. A specific module named *r.impact.tsunami* has been specifically implemented.

Moreover the authors have compared the propagation and run up estimated using the empirical equations of Heller et al. (2009) with that obtained using an approach based on non linear shallow water equations (Cannata & Marzocchi, 2011). The case study, located on Como lake (Italy) concerns the falling of a rock column of 50'000 m³ into the lake and the successive generation of a tsunami wave.

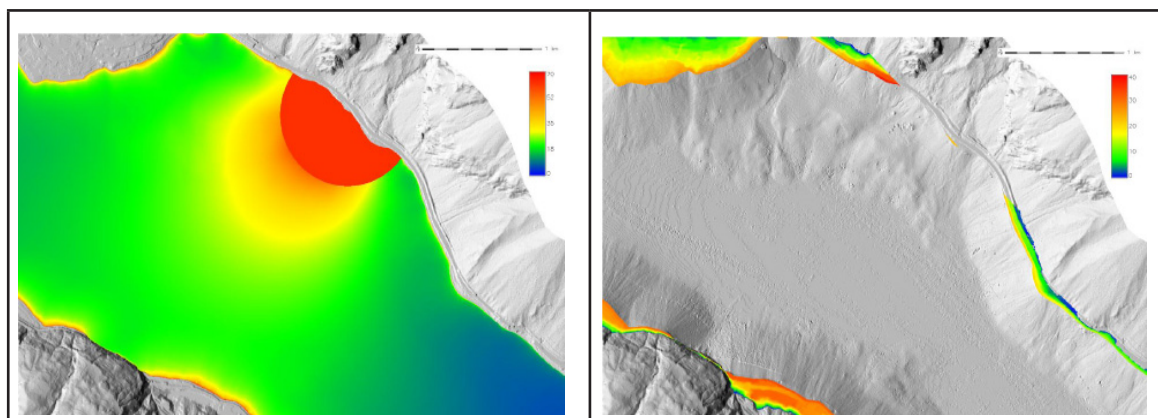


Figure 1. Wave height propagation and inundation maps estimated by the *r.impact.tsunami* model.

REFERENCES

- Cannata, M. & Marzocchi, R. 2011: Two-dimensional dam break flooding simulation: a GIS embedded approach, Natural Hazards, accepted for publication.
- Heller, V., Hager, W.H. & Minor, H-E. 1984: Landslide generated impulse wave in reservoirs: Basics and computation, in Boes, R. (Ed.), VAW Mitteilung 211, ETH Zurich, Zurich.

15.4

The geological 3D-model of the Basel region – new insights

Dresmann Horst¹, Huggenberger Peter¹, Epting Jannis¹, Wiesmeier Stefan¹ & Scheidler Stefan¹

¹ Applied and Environmental Geology, Department of Environmental Sciences, University of Basel, Bernoullistrasse 32, CH-4056 Basel, (Horst.Dresmann@unibas.ch)

In the last years, the use of subsurface geothermal resources (e.g. deep and shallow thermal energy) strongly increased. In addition, the research for the storage of nuclear waste and sequestration of carbon dioxide is intensified. As open space in urban areas is limited and infrastructure grows into the depth, and comparable to the space at the surface, the space in the subsurface is limited, too. Existing installations, e.g. for groundwater use, react very sensitive to changes of the subsurface environment. Therefore, use conflicts with new installations will be inevitably. Rules and management strategies for the subsurface use are needed to find solutions in potential or already existent conflicts.

Aware of these problems, in 2008 the geological surveys of France (BRGM), Baden-Württemberg (RPF-LGRB), Rheinland-Pfalz (LGB) and the Applied and Environmental Geology Group of the University of Basel initiated the EU project “GeORG” (www.geopotenziale.org) with the idea to establish a tool for 3D planning of the subsurface across political boundaries along the tri-national Upper Rhine Valley. The essential element of the project is the development of a geological 3D model between Basel (CH) and Mannheim (D), which can be used as a flexible tool for the evaluation of the possibilities and risks of the deeper underground. The main focus is the use of deep geothermal energy and issues as earthquake hazards and the sequestration of carbon dioxide.

In this context, the geological 3D-model of the Basel region (Fig. 1) was established as the Swiss contribution to the “GeORG”-project. Although, the development of the model is still in progress, it was already used to answer questions for urgent issues in the Basel region like risk evaluation in the context of deep geothermal energy, development of rules for the use of shallow geothermal energy, use of groundwater resources and construction of highway tunnels.

The example of the 3D model from the Basel area demonstrates the large potential of subsurface 3D models. It allows to set constraints and boundary conditions in different use conflicts and gives a rationale base for a sustainable management of the subsurface for the future.

The geological 3D-model of the Basel region comprises 600 km² and reaches to depth of about 6 km. 15 reflection seismic lines, geological maps and about 9000 boreholes represent the most important data for the geometric modelling process. The model comprises 20 different geological horizons between the Quaternary unconsolidated rocks and the Palaeozoic crystalline basement. About 150 faults are still integrated. Their distribution in space is strongly related to the basic data sets. Especially, the eastern part of the model, representing the Tabular Jura, shows a very distinct fault pattern in different scales.

The data density decreases with growing depth. In the canton of Basel-Stadt, there are about 3600 boreholes available, but only 14 reach depths of 250 m and more. Such heterogeneity in data distribution is influencing the quality of the different model areas. To communicate the geographical distribution of the model quality, it was tried to quantify and to visualize the resulting model uncertainties.

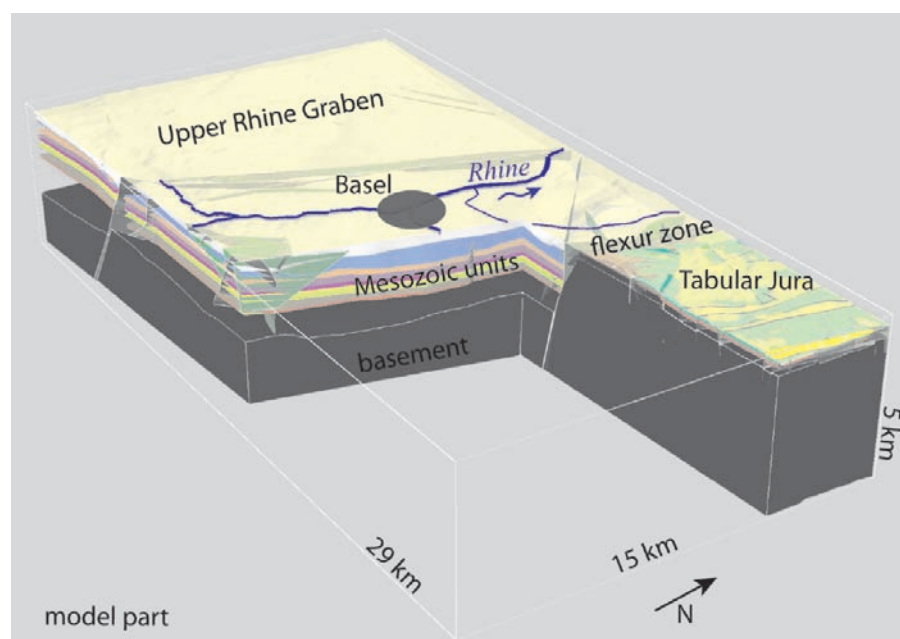


Figure 1. Part of the geological 3D-model of the Basel region (not all horizons shown)

15.5

Earth Modeling Seen from a Multiphysics Perspective

Friedel, S.

¹ COMSOL Multiphysics GmbH, Technoparkstrasse 1, CH-8005 Zürich (sven.friedel@comsol.com)

From the perspective of mathematical physics planet Earth can be seen as a huge spatial domain in which a multitude of physical, chemical and biological processes evolve in time, e.g. mechanical deformations, fluid flows, chemical reactions, electromagnetic fields, heat transfer but also the spread of diseases or even the evolution of organisms. Today, the perception of various Earth Science disciplines (geology, geophysics, geomechanics, geochemistry, hydrology, and related disciplines such as environmental, reservoir and civil engineering) moves towards a holistic view. We become aware of the various couplings of the above processes. Some of the most exciting science topics and most vital problems of the Earth are related to highly coupled, non-linear interactions of fields. This perception is reflected also in the need to model Earth's complexity in a more sophisticated way. Recent advances of computing hardware pave the way for the feasibility of such models not only on clusters but desktop computers. In our talk we focus on our project to provide the Earth Science community with a software tool, capable of modeling nearly arbitrary processes in the Earth on arbitrary scales of time and length. We report some of the latest achievements of users and invite further contributions to this platform.

Fundamentals and Key Requirements

Most processes on the Earth can be generally described in terms of transport of mass, momentum, charge, and energy but also general entities such biological species. Based on fundamental conservation laws and empirical material relations they can be described by systems of partial differential equations (PDEs). On a mathematical level, a vast class of problems can be described by the following general form PDE:

$$e \frac{\partial^2 u}{\partial t^2} + d \frac{\partial u}{\partial t} + \nabla \cdot \Gamma = f$$

where 'u' is a vector of unknown field variables, Γ is a generalized flux vector depending on spatial and time derivatives of 'u' and 'f' is a generalized source. Coupling and nonlinearities can arise from both material properties and loads depending on arbitrary field variables. By numerical discretization, such systems can be transformed into large sparse matrix systems. For an efficient and unified modeling tool in Earth Sciences we have identified the following key requirements regarding discretization, problem definition, solvers and interfaces:

- Geometry handling from digital elevation models to submicroscopic pores as well as built in 2D and 3D drawing
- Large repository of predefined equations and abstraction levels inviting multi-scale modeling
- Ability for user-defined equations and model interfaces
- Parallelized numerical algorithms (meshers and solvers) able to run on multiple OS and platforms from stand-alone PCs to clusters,
- Parameterization of material properties, loads and geometries
- Sensitivity analysis, optimization and parameter estimation
- Powerful Visualization without the need of external tools
- Interfaces to programming languages (C, Fortran, Matlab, Java)
- Interfaces to databases (e.g. geochemistry)
- Sustainable organization of the code: GUI, help system, support, community platform

Recent Applications

Recent contributions from Swiss geoscientists include applications from electromagnetic hydrogeophysics: (Maurer, Friedel & Jäggi, 2009, Bauer-Gottwein et al, 2010), geothermal modeling in permafrost areas, (Noetzli, Gruber & Friedel, 2007). Other applications include geomechanical stress analyses with Cam-Clay material model, mineral dissolution and crystal growth in anhydritic claystones, diffusion studies for nuclear waste deposits, and radar investigation of tunnel integrity. The openness of the code to couplings to other simulators is illustrated by Wissmeier and Barry (2010) who present a simulation tool for variably saturated flow with comprehensive geochemical reactions coupling COMSOL to PHREEQC.

The unified simulation platform COMSOL Multiphysics inspires to model real world processes with complex couplings between physical, chemical and even biological quantities. A large amount of predefined equations keeps the focus of the user on the model's experiment and theory rather than on numerical details. Openness to user-defined equations as well as couplings to other simulators invites further contributions to this novel multi-disciplinary approach to Earth modeling.

REFERENCES

- Bauer-Gottwein, P., Gondwe B. N., Christiansen, L., Herckenrath, D., Kgotlhang L. & Zimmermann, S. 2010: Hydrogeophysical exploration of three-dimensional salinity anomalies with the time-domain electromagnetic method (TDEM) *Journal of Hydrology*, 380 (3-4), 318-329.
- COMSOL AB, 2011: COMSOL Multiphysics Simulation Software, www.comsol.com
- Maurer, H., Friedel, S. and Jaeggi, D., 2009: Characterization of a coastal aquifer using seismic and geoelectric borehole methods, *Near Surface Geophysics*, 7(5-6), 353-366.
- Noetzli, J., Gruber, S. & Friedel, S. 2007: Modeling transient permafrost temperatures below steep alpine topography, *Proceedings of the 2007 COMSOL Conference, Grenoble, France, 23-24 October*
- Wissmeier, L. & Barry D.A. 2011: Simulation tool for variably saturated flow with comprehensive geochemical reactions in two- and three-dimensional domains *Environmental Modelling & Software*, 26(2), 210-218.

15.6

Building the national geological model of Great Britain

Holger Kessler, Steve Mathers, Benjamin Wood

British Geological Survey, Kingsley Dunham Centre, Keyworth, Nottingham, UK

There is a growing realisation in the environmental and social sciences that to address the grand challenges that face the world a whole system approach is required. These challenges including climate change, natural resource and energy security and environment vulnerability raise multi- and inter-disciplinary issues that require integrated understanding and analysis.

Many scientific disciplines have been modelling during the past 5 to 10 years in order to best understand and analyse the processes and conditions within their areas of interest. This has led to a multitude of discipline specific models, modelling system software and workflows with greater or lesser success depending upon the quantity and sources of data and complexity within the scientific discipline concerned. The challenge is to better link these models and enable users at all levels to make decisions based upon fully integrated environmental models. The fundamental role of a Geological Survey Organisation to support integrated environmental modelling is to develop a single, dynamically constructed multi-scaled 3D geological model of the UK and figure 1 shows progress being made towards this goal at the British Geological Survey (BGS). The difference to the core product of the past, the 2D map is that the model will be constructed at varying scales and will be maintained dynamically as geological understanding changes or new data becomes available.

The image below shows the initial fence diagram which was constructed using the GSI3D methodology and on which this geological model will be based (see figure 2). GSI3D (Geological Surveying and Investigation in 3 dimensions) is a methodology and associated software tool for 3D geologic modelling developed initially by INSIGHT GmbH and now by the BGS in conjunction with the GSI3D Research Consortium (www.gsi3d.org.uk). GSI3D utilizes a digital elevation model, surface geological linework and downhole borehole data to enable the geologist to construct cross sections by correlating boreholes and the outcrops to produce a geological fence diagram and corresponding coverage maps of geological units (outcrop plus subcrop). Scientists draw their sections based on facts such as borehole logs correlated by intuition - the shape 'looks right' to a geologist. This 'looks right' element pulls on the geologists' wealth of understanding of earth processes, examination of exposures and theoretical knowledge gathered over a career in geology

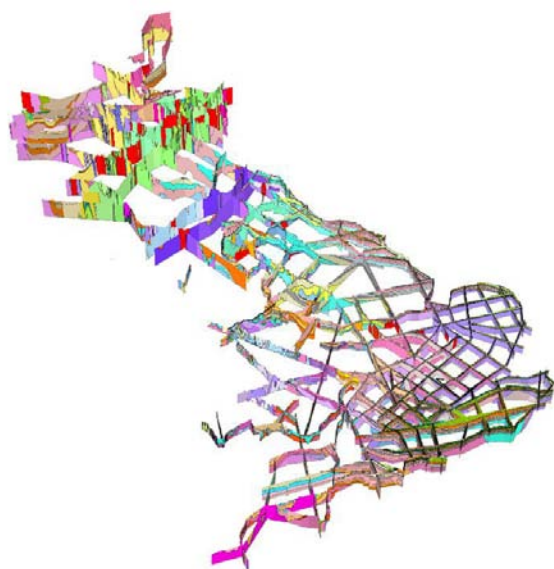


Figure 1 Current progress on developing the cross sections required to create a GSI3D framework model of onshore Britain. Note the scale differences and depths included, between Scotland and England and Wales

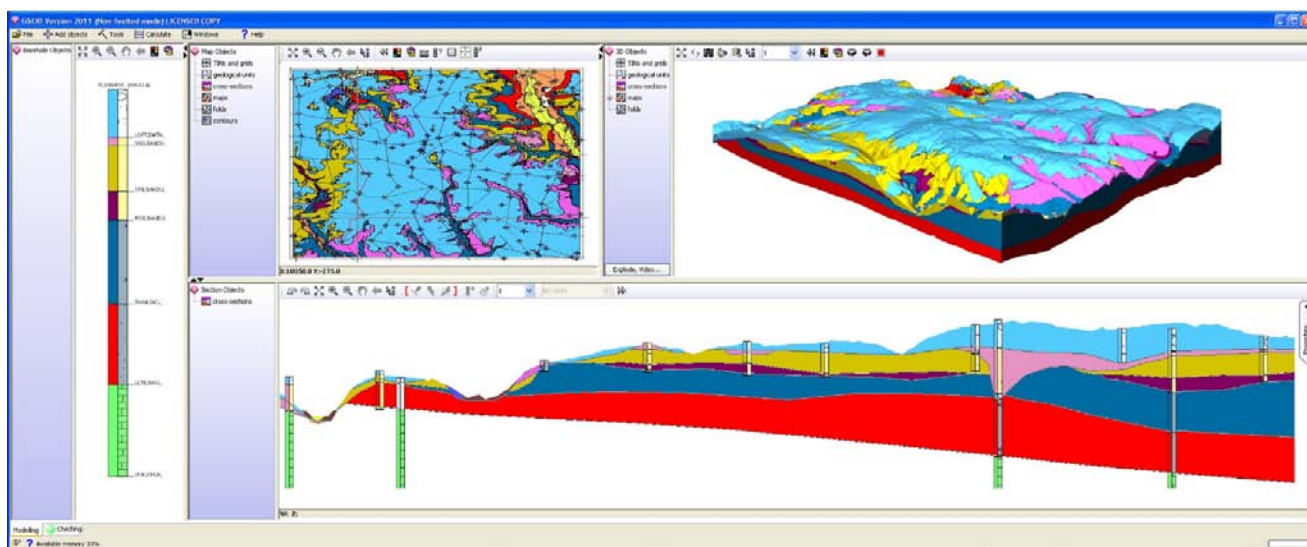


Figure 2 The GSI3D software interface

15.7

Provision of 3D GIS (model GMS) for geospatial hydrogeologic modeling of Mio-Plio-Quaternary groundwater of Foussana (Central Tunisia)

Khemiri sami¹, Kassebi Adnane¹, Zargouni Fouad¹

¹ *Department of Geology - Structural Geology Laboratory and applied, Faculty of Science of Tunis, 2092 University Campus - Tunis El Manar.*

Water is essential for all forms of life and crucial for human development. Water systems, including surface waters and aquifers, provide a vast majority of human need including drinking water, irrigation and industry. However, water resources are unequally distributed in space and time and therefore requiring an appropriate management especially in countries under arid and semi arid climate such as Tunisia where, an unlimited increasing of exploitation of the non-renewable water resources has been noted in the recent years. In this regard, irrigated agriculture, industry and energy supply consume the great part.

The aquifer of Foussana in central Tunisia constitutes an example showing signs of such over exploitation. The intensive exploitation of groundwater representing the mainstay of the Foussana area is becoming more pronounced and critical in the recent years resulting in over exploitation which requires a rigorous control of the management of groundwater resources. For tackling this problem and to properly ensure the management of groundwater resources, a good knowledge of both the quality and quantity of water is essential which requires a deep understanding of the evolution of the reservoir geometry and the characteristics of permeable formations.

In the present work we have used a new technique of interpretation and interpolations called "3D GIS". It allow a good management of the drilling data and help in the establishment of 3D schemes of the hydrostratigraphy and the aquifers with a simulated three-dimensional geometric which is very close to its actual condition.

Also, the understanding of the aquifer and its geometry was apprehended for the study of lithostratigraphic columns of wells and piezometers supported by GIS through the 3D model "Ground Modeling System" or "GMS". GMS is a geodata-base design for representing datasets in ArcGIS groundwater under the module "ArcHydro Groundwater" or AHGW. The data model allows storing, view and analyzing multidimensional data of groundwater, and includes several components to represent different types of datasets including representations of the aquifers, wells, boreholes, 3D hydrogeological models, timing information, and data from simulation models.

This model can explicitly represent the geological features highlighted in the interpretation of data in the form of hydrogeological horizons, so the form of solid or mesh Voxel.

The specific objectives of the intervention, corresponding to the expected results of the modeling can be formulated as follows:

- Assessment of regional patterns of flows in the area
- Identification of hydro reservoirs and their geometry;
- Evaluation of flow directions within the reservoirs identified, and quantification of groundwater flow in these tanks;
- Estimation of the regional distribution of hydrogeological parameters;
- Predictions of the effects of changes in groundwater recharge and the piezometric groundwater flow;
- Tool for decision support for the implementation of measures for monitoring and for the management and exploitation of groundwater;

The results of this intervention offers interesting perspectives for further developments in modeling of groundwater, both for the geometry contribution to the assessment of the renewable resource, and evaluation of its potential for exploitation; for the groundwater flow

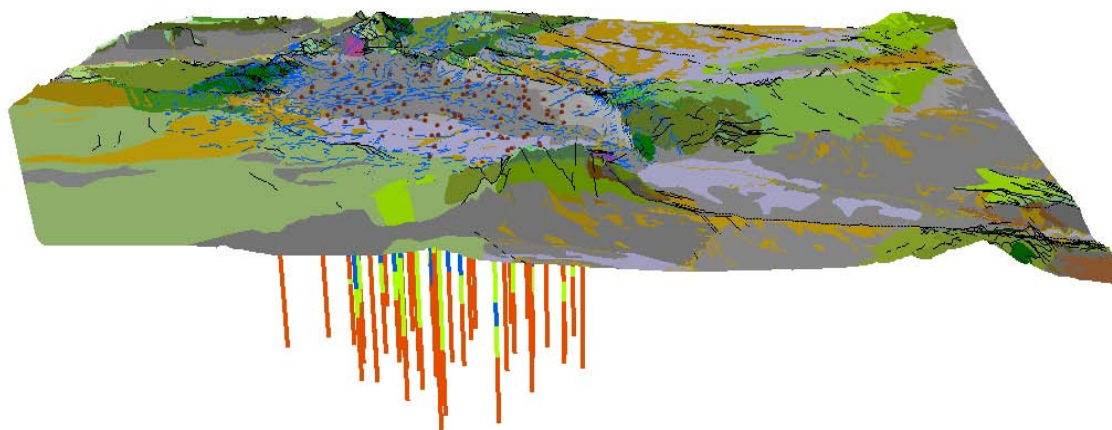


Fig.1: Numerical Model of the basin associated with the drilling of Foussana available

REFERENCES

- EL Morjane, Z. 2003. Design of a system of geographically referenced information for environmental management, application to the selection of potential storage sites for domestic and industrial wastes in semi-arid region (Souss, Morocco). Th Doct.Univ. Geneva, Forel Institute, 99.
- Kovar, K., & Nachnebel, H.P. 1993. Application of Geographic Information Systems in Hydrology and Water Resources Management. IAHS Publication No. 211, 693.
- Choi, Y.S. & Park, H.D. 2005. Development of an Intelligent Borehole Information System (IBIS) based on a Knowledge Approach. GIS Planet 2005 Proceeding CD, Estoril, Portugal, May 30-June 2.
- Johston, K., Ver Hoff, J.M., Krivoruchko, K., Lucas, N. 2003. Using ArcGIS Geostatistical Analyst. ESRI Press: Redlands, California.
- Zouari, H. 1984 Structural study of the Jebel Chaambi (central Tunisia). Relationship between the mineralization and structure, 3rd cycle thesis, University of Franche-Comté, Besançon, 335.
- Lee, H.J., Park, S.W., Yoo, S.D. & Kim, H.T. 2004. An Estimation of Long-Term Settlements in the Large Reclamation Site and Determination of Additional Sampling Positions using Geostatistics and GIS. Journal of the KGS, 20, 131-141 .

15.8

Geological 3D modelling of Quaternary sequences using GSI3D – an example of the surroundings of Berne

Michael C. Salomè, Baumberger Roland, Oesterling Nils

swisstopo, Swiss Geological Survey, CH-3084 Wabern, Switzerland

Contact: cristina.michael@swisstopo.ch

Federal Office of Topography swisstopo, Swiss Geological Survey, Seftigenstrasse 264, CH-3084 Wabern

swisstopo / Swiss Geological Survey (SGS) wants to build up geological 3D models at different scales and resolutions. These models visualise the structure of the earth's crust. Such information is important for many topics such as 3D urban planning, resource management etc. and can be easily understood by professional geologists as well as laymen.

A geological 3D model can comprise bedrock as well as superficial Quaternary formations. For modelling bedrock formations the SGS uses the Move software suite (Midland Valley Exploration) which provides various tools for model verification such as cross section balancing, kinematic forward and reverse modelling etc. In order to model the Quaternary sequences, the SGS applies in addition to Move the software GSI3D (Geological Surveying and Investigation in three dimensions) developed by the British Geological Survey (BGS). In GSI3D, especially the capability of vertical exaggeration while modelling is useful to build up Quaternary 3D models, because the shape of stratigraphic sequences can be visualised.

The following data has been used to build up the geological 3D model of Quaternary sequences of the surroundings of Berne:

- geological surface map of the Geological Atlas of Switzerland 1:25'000 (GA25) and its lithostratigraphic units
- Digital Elevation Model (DEM) of the earth surface
- borehole data (with two quality standards)
- cross sections
- DEM of the bedrock surface

All data has been combined within GSI3D and the 3D model has been constructed according to the following method:

- Construction of a geological fence diagram, based on the geological surface map (GA25)
- Refinement by adding further cross sections based on the data in GSI3D (correlation of boreholes, map and cross sectional data)
- Construction of geological unit maps with their area-wide extensions (subcrops) at the same time
- Construction of helper sections for specific areas, as proposed by Mathers et al. (2011)
- Topology check while digitising sections and geological units (snapping to intersections, outcrops and subcrops)

Combining the input data, the geological units are created in GSI3D in their lithostratigraphic order. Output is a 3D block model of the Quaternary units; they could also be displayed in an exploded layer view. For a general geological 3D model, this Quaternary block model is imported into Move and therein combined with a bedrock model.

Because the construction of a geological 3D model is always linked with a good deal of interpretation, the accuracy of such a model varies as a function of the distance to the trusted data, its quality and distribution. For a good quality control of a geological 3D model, it is useful to have a quality map of the trusted data, where the two-dimensional reliability of the model is represented. As the available borehole data in the surroundings of Berne, used in the introduced Quaternary 3D model, has a heterogeneous distribution and two different quality standards, the SGS created as a first approach a quality map with the inverse distance weighting (IDW) interpolation method. However for a final quality assessment further investigations are required.

REFERENCES

Mathers, S J, Wood, B & Kessler, H. 2011: GSI3D 2011 software manual and methodology, British Geological Survey Internal Report, OR/11/020, 152pp (<http://www.gsi3d.org.uk>)

15.9

Numerical modelling for risk scenarios generation

Molinari Monia¹, Cannata Massimiliano¹, Ambrosi Christian¹, Beguería Santiago²

¹Institute of Earth Sciences – SUPSI, Campus Trevano, CH-6952 Canobbio (monia.molinari@supsi.ch)

²Aula Dei Experimental Station - CSIC, Zaragoza, Spain

MIARIA (Adaptive Hydrogeological Monitoring supporting the Area Integrated Risk Plan) INTERREG project foresees, among other activities, the numerical modelling of instability phenomena.

The Swiss case study is located in Val Canaria (Tessin): a region particularly susceptible to landslides. In particular, the modelled landslide is of complex type. Its failure could generate an accumulation that may block the main river flow causing a temporary dam. Successive dam break would likely produce a flooding that could damage the buildings and the transport infrastructures of North-South axis of San Gottardo.

In 2009, an important event involving 350'000 m³ occurred: fortunately, even though the risk scenario presented above took place, the damages were limited because the flood didn't reach the critical infrastructures.

The availability of terrestrial laser-scanning data just before and after the event allows to generate detailed digital terrain models which are invaluable information in models set-up. In this study the authors applied MassMov2D (Begueria et al., 2009): a dynamic model that describes terrain movements by combining mass and momentum balance equations with rheological formulas able to characterize the material involved.

A three dimensional description of a phenomenon both in terms of run-out area and deposit heights can be obtained. This work illustrates (i) the phases of sensitivity analysis and calibration of the model on the 2009 event and, based on the parameters obtained from the calibration, (ii) the generation of a new hypothetical hazard scenario. Moreover, the implementation of the model within a GIS environment (GRASS) will be presented.

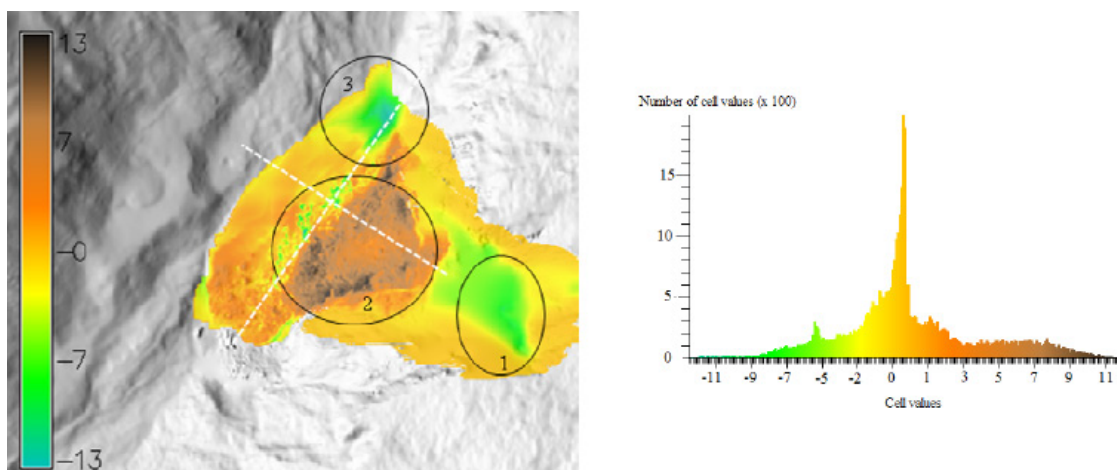


Figure 1. Difference map between observed and modelled deposit and histogram of the cell values

REFERENCES

Begueria, S., Van Asch, Th.W.J., Malet, J.P. & Gröndhal, S. 2009: A GIS-based numerical model for simulating the kinematics of mud and debris flows over complex terrain, *Natural Hazards and Earth System Sciences*, Vol. 9, Number 6, 1897-1909.

15.10

Modeling of the “Plan da Mattun” archeological site using a combination of different sensors

Novak David¹, Grimm David Eugen¹& Tokarczyk Piotr¹

¹ Institut für Geodäsie und Photogrammetrie, Wolfgang-Pauli-Strasse 15, CH-8093 Zürich
(david.grimm, piotr.tokarczyk, david.novak@geod.baug.ethz.ch)

Deep in the Tasna valley, finds dating back to the time of Ötzi, where discovered by archaeologists of University Zürich. The finds derive from early alpine dwellers, taking shelter below the overhanging boulders at Plan da Mattun, while they were hunting or before they crossed the mountain pass at the end of the valley. For expanded investigations of this archeological site, digital models of the terrain and of certain boulders were of larger interest. Additionally the digital models will be used for documentation and visualizations.



Figure 1 the archeological site “Plan da Mattun”

The goal was to obtain a digital terrain model of the rock stream located at the end of the valley, as well as detailed models of four larger boulders. The larger boulders are up to 15 meters high and the smaller rocks still average to about 2 meters in height and in diameter. The roughness of terrain (see Figure 1) makes it difficult to access certain areas and requires using multiple measuring techniques in order to cover all the objects of interest. That is why the digital terrain model was acquired using a combination of laser scanning (Leica Scanstation C10) and unmanned aerial vehicle (UAV) photogrammetry. The larger boulders were reconstructed with a Zoller&Fröhlich Imager 5006 laser scanner, terrestrial and UAV photogrammetry.

Georeferencing of the measured data

To georeference the obtained scans and images, a geodetic reference system had to be set up within the Swiss coordinate system LV95. Because of the lack of mobile phone reception at the end of the valley, the Swipos service could not be used. Therefore three reference points were measured by static GNSS and corrected with a virtual reference station (VRS) in advance. One of these was used to set up a local GNSS reference. Hence it was possible to measure the ground control points for the photogrammetry in real time. Accordingly to the GNSS accuracy, the control points had a horizontal accuracy of 2 cm and 5 cm in height. To georeference the scans done by the Scanstation, the scanner position was measured by GPS, force centered on the same tripod. The Scanstation C10 allows to directly setting the orientation by measuring a known sphere target. In contrast the scans done by the Zoller&Fröhlich Scanner, were georeferenced by using several sphere targets whose coordinates were measured before. For terrestrial photogrammetry, reflective targets were placed on the boulders and referenced with tacheometry.

Data processing

The scans from the Scanstation were edited in Cyclone and afterwards exported into Geomagic to edit the dataset. The UAV images were first processed with Photomodeler Scanner to obtain approximate camera positions and orientations. These orientations were then imported into Leica Photogrammetry Suite (LPS) and used to automatically measure tie points. The ground control points were measured manually. The digital terrain model was generated automatically and edited in Geomagic. Afterwards, the final orthophoto has been generated automatically using the mosaic tool from LPS. For the Z&F scanner the same processing chain as in the C10 case was performed. The terrestrial images as well as the UAV images were oriented and georeferenced in Photomodeler Scanner. The same software has been used in order to generate a dense point cloud. All the datasets used in this project were edited in Geomagic.

Results

The resulting dataset includes a coarse digital terrain model with a resolution of 10 cm and a relative accuracy of 2 cm in flat terrain. The larger boulders feature a resolution of 10 mm and a relative accuracy of 5 mm.

The datasets will be used for visualization purposes by the archaeologists and for analyzing purposes of the rock stream by geologists.



Figure 2. Orthophoto mosaic draped over DTM.

15.11

Determining archaeological potential in the Pennine Alps using GIS tools

Rogers Stephanie¹, Collet Claude¹ & Lugon Ralph¹

¹University of Fribourg, Chemin du Musée 4, CH-1700 Fribourg (stephanie.rogers@unifr.ch)

The accelerated melting of glaciers in the Alps is freeing up many archaeological relics which demonstrate the use of high altitude passes since prehistoric times. Until recently, scholars have neglected the study of these high altitude passes due to the fact that these areas were seen as marginal and uninhabitable by humans. There is an urgency to collect and conserve these archaeological findings as most objects consist of perishable material and, once exposed to the environment, they rapidly degrade and decompose. The disappearance of this prehistoric and/or historic material is an inestimable loss which would impede the understanding of how people have used these glaciated high altitude passages throughout history.

This project, which is funded by the Swiss National Science Foundation (SNSF) with the support of the Musée d'Histoire du Valais and the Service des Bâtiments, Monuments et Archéologie in Sion, proposes to develop methods using GIS tools to localize sites with the highest potential of artefact discovery in high altitude passes and trails in the Pennine Alps. This study area is one of the most glaciated territories of the whole Alpine arc and is located between the Canton of Valais (Switzerland) and the Italian border. We will use a multidisciplinary approach to develop a predictive model based on geographic, historic and cultural inputs. Some geographic inputs include: a 25 m digital elevation model (DEM), historic glacier delineations (since 1850), aerial photographs, trails and topographic maps. An archival text analysis is being conducted along with a critical analysis of historic publications to obtain more information about ancient trails and passes through these mountains. Archaeological find location information has been provided by the archaeological department in the Canton of Valais.

The theory behind our model is based on the model used by Dixon *et al.* (2005) for determining archaeological potential in glaciers and ice patches in Alaska's Wrangell-St. Elias National Park and Preserve. We will create potential 'influence' and 'restriction' layers, assign weights to each layer based on its importance for archaeological potential, and multiply 'influences' by 'restrictions' to create a model for archaeological potential.

REFERENCES

Dixon, J., Manley, W., & Lee, C. 2005: The Emerging Archaeology of Glaciers and Ice Patches: Examples from Alaska's Wrangell-St. Elias National Park and Preserve, *American Antiquity*, 70, 129-143.

15.12

Vp-Vs measurements of shallow formations in Chémery (FR): comparison between laboratory and field data and integration within a 3D geological model

Paola Sala¹, Nicola Tisato², Adrian Pfiffner¹, Erik H. Saenger³

¹Institut für Geologie, Baltzerstrasse 1, CH-3012 Bern (sala@geo.unibe.ch)

²ETH Zurich, Geologisches Institut, Sonneggstrasse 5, CH-8092 Zurich

³ETH Zurich; Spectraseis Denver, 1899 Wynkoop Street, Suite 350 Denver CO 80202 United States

Object of this study is an underground gas storage facility located in the south-western border of the Paris Basin. The geology of the site is well known and it is characterized by an anticlinal structure affected by a dense fault network (Fleury, 1997). This structural trap is exploited since late '70s as an artificial gas reservoir at a depth of 1200 m. The reservoir is located in Triassic strata of fluvial sandstones (Hamon and Merzeraud, 2001).

A passive seismic acquisition campaign was held in the area to record low frequency seismic waves above the reservoir (Artman et al 2011). The technique allows to define the areal extension of the gas cushion, detecting anomalies in the microtremor wavefield presumably caused by hydrocarbon (Saenger et al., 2009). Passive seismic can additionally be used to understand the influence of the near surface on the major wavefield. Therefore, a good knowledge of the velocity distribution within shallow formations is essential to understand possible anomalies in the seismic record.

Velocities of the shallow formations can be found in a public dataset which collects up-hole seismic data (BRGM online catalog: infoterre.brgm.fr/viewer). However, the velocity model can be better defined integrating laboratory measurements. We collected 24 hand specimen from which we drilled out core plugs. The sampled lithologies are 6 different sedimentary rocks, mostly calcarenites. The core plugs are 25 mm diameter and the length ranges from 23 to 50 mm. The measurements were conducted employing the pulse transmission method for compression (V_p) and shear (V_s) waves in dry and ~fully water saturated conditions. The samples were weighted, and the volume was measured accurately in order to obtain the density value in both saturation conditions. The porosity was measured with two different methods: (1) with a helium pycnometer, and (2) measuring the variation of weight for dry and fully saturated conditions. Porosity ranges between 45% and 0%.

The results obtained for dry samples are:

- Cretacic calcarenites exhibit V_p ranging between 1400 and 4700 m/s and V_s ranging 800 - 2800 m/s. Turonian Tuffeau Blanche and Tuffeau Jaune have average V_p ~2025 m/s and V_s ~1300 m/s, while the Senonian Craie Blanche à Silex has average V_p ~3600 m/s and V_s ~2000 m/s. Such differences were also observed by Hanot & Renoux (1991).
- Low cemented sample from the Palaeocene-Eocene Formation Détritique Continentale has V_p of ~1600 m/s and V_s of ~1050 m/s, while a sample from the same formation which is strongly cemented and silicified shows V_p of ~5600 m/s and V_s of ~3000 m/s.
- The Miocenic Calcaire de Beauce and the Falunian marine sands show V_p around 4500 m/s and V_s of ~2450 m/s.

In fully saturated conditions, V_p values increase on average by 10% while the V_s values decrease on average by 15%. Similar trends have been observed in the literature (Cadoret et al., 1992). Alteration of outcrop samples can affect the elastic modules of the materials significantly and has to be taken into account.

The velocities measured in the laboratory were then compared with the uphole velocity logs and the data were used to build a 3D model of elastic properties for the lithological units in the study area. This last task was performed employing the modeling software Petrel.

REFERENCES

- Artman B., Duclos M., Birkelo, B., Huguet, F., Dutzer, J.F. & Habiger, R., 2011- Low Frequency Seismic Survey at a Gas Storage Reservoir. 73rd EAGE Conference & Exhibition incorporating SPE EUROPEC 2011 Vienna, Austria, 23-26 May 2011.
- Cadoret, T., Marion, D., Zinszner, B., 1992 - Sonic wave velocities in partially saturated limestones: Evidence of microscopic fluid distribution effect on acoustic properties. Third European Core Analysis Symposium, Paris.
- Fleury, R., 1997 - Carte géol. France (1/50 000), feuille Romorantin (460). Orléans : BRGM. Notice explicative par R. Fleury, avec la collaboration de F. Charnet, J. Coppel, S. Debrand-Passard, Y. Gros, P. Maget (1997), 94 p.
- Hamon, Y., Merzeraud, G. (2001) - Sédimentologie, géométrie et signification géodynamique des dépôts réservoirs silico-clastiques du Trias de Chémery (Sologne, SW du Bassin de Paris). PhD Thesis. Université Montpellier 2.
- Hanot, F., and Renoux P., 1991 - Petrophysical variation in the Senonian chalk of the Paris Basin and their influence on static corrections. *First Break*, v. 9, n° 11, 1991, p. 515-526.
- Saenger, E.H., Schmalholz, S., Metzger, S., Habiger, R., Müller, T., Rentsch, S., 2009, A passive seismic survey over a gas field: Analysis of low-frequency anomalies. *Geophysics*, 74, 029-040.

15.13

The Swiss Geologic Data Model

Strasky Stefan, Oesterling Nils, Baland Pauline, Michael Cristina Salomè & Kühni Andreas

¹Federal Office of Topography swisstopo, Swiss Geological Survey, Seftigenstrasse 264, CH-3084 Wabern (stefan.strasky@swisstopo.ch)

Behind each geologic map is a concept that is visualised in its map legend. When converting a printed map into a Geographic Information System (GIS) dataset, the map legend is used to further extend this initial concept to meet the requirements of digital datasets. Although the concept for digital geologic datasets (database, structure and semantics) is often ignored by geologists, it turns out to be very important when putting data from different authors / sources together.

To facilitate the handling of different geologic datasets in a GIS-environment, the Swiss Geological Survey has established a data model (Strasky et al. 2011), which describes the structure of the geologic data and defines the specific objects and its attributes. A working group consisting of eleven members from various institutions of the Swiss Geological Community has contributed significantly to achieve a final draft version, which was then submitted to an external review board. Feedbacks from 22 external reviewers from federal and cantonal institutions (including the Swiss Geological Commission SGK, the Swiss Geotechnical Commission SGTk and the Swiss Association of Geologists CHGEOL) as well as private companies were included in the current version of the geologic data model. Today the model consists of 49 classes which organise the different geologic object types. The classes are further grouped into eight major topics. The documentation gives a detailed description of the content of the data model in French and German as well as UML-diagrams and the corresponding INTERLIS 2.3 code. Furthermore a standardised vocabulary for rock types, tectonic units and the geological time scale is provided. The data model is applicable for two-dimensional geologic data at any scale. The first official version of the Swiss geologic data model will be available by the end of 2011.

With the Swiss geologic data model we supply the basis for well-structured, homogenous geologic GIS data and we provide the standard for a future seamless, semantically harmonised, nationwide digital geologic map of Switzerland.

REFERENCES

Strasky, S., Baland, P. & Oesterling, N. 2011: Datenmodell Geologie / Modèle de données géologiques – Version 1.4, Swiss Geological Survey, swisstopo, 117 pp.

16. Earth System Science related Earth Observation

Michael E. Schaepman, Brigitte Buchmann, Manos Baltasvias

*Swiss Commission for Remote Sensing,
Swiss Geodetic Commission*

TALKS:

- 16.1 *Damm A., Kneubuehler M., Schaepman M.E.:* Investigating variations of gross primary productivity (GPP) over several ecotypes in Switzerland using the APEX chlorophyll fluorescence product
- 16.2 *Fontana F., Seiz G., Foppa N., Lugrin D.:* Satellite-based climate products for alpine studies within GCOS Switzerland
- 16.3 *Hüsler F., Wunderle S., Jonas T., Neuhaus C.:* Retrieval of the ECV „snow spatial extent“ from 25 years of AVHRR data over the European Alps for climate research
- 16.4 *Laurent V., Verhoef W., Clevers J., Schaepman M.:* Estimation of forest variables from multiangular radiance data using a coupled canopy-atmosphere model
- 16.5 *Papasaïka H., Baltasvias E., Schindler K.:* Fusion of Digital Elevation Models Using Sparse Representations
- 16.6 *Pasquali P., Riccardi P., Cantone A., Defilippi M., Holecz F.:* Methods and sensors for monitoring land subsidence phenomena based on satellite SAR interferometric stacking
- 16.7 *Popp C., Brunner D., Damm A., Buchmann B.:* High spatial resolution mapping of NO₂ from APEX imaging spectrometer data

POSTERS:

- P 16.1 *Fatehi P., Damm A., Kneubuehler M., Schaepman M.:* Ecosystem parameter mapping of Alpine regions using continuous fields derived from imaging spectrometer data
- P 16.2 *Galvez P., Ampuero J.-P., Dalguer T., Nissen-Meyer T.:* Modeling the complexity of the dynamic rupture process of the 2011 Mw 9 Tohoku earthquake.
- P 16.3 *Hocke, K., Kämpfer, N., Wacker, S., Gröbner, J., Vuilleumier, L.:* Consistent Trends in Water Vapour, Downwelling Radiation, and Temperature
- P 16.4 *Homolova L., Malenovsky Z., Schaepman M., Clevers J.:* Estimation of plant functional biochemical traits of subalpine and alpine grasslands from airborne images of high spatial and spectral resolution
- P 16.5 *Small D., Schubert A., Zuberbühler L., Meier E.:* Time series of radar backscatter: Moving towards simultaneous high temporal & spatial resolution observations of Alpine snow melting
- P 16.6 *Tuia, D., Verrelst, J., Alonso-Chordà, L., Camps-Valls, G.:* Acquiring the relevant samples for chlorophyll estimation with hyperspectral data

16.1

Investigating variations of gross primary productivity (GPP) over several ecotypes in Switzerland using the APEX chlorophyll fluorescence product

Damm Alexander¹, Kneubuehler Mathias¹ & Schaepman Michael, E.¹

¹Remote Sensing Laboratories, University of Zurich, Winterthurerstrasse 190, CH-8057 Zurich (alexander.damm@geo.uzh.ch)

Approximately 60 Gt of carbon are annually absorbed through plant photosynthesis. Slight alterations within terrestrial ecosystems may have significant changes on atmospheric carbon concentrations. Reliable monitoring systems are required to increase the knowledge on spatio-temporal dynamics of plant photosynthesis and related carbon fixation rates. Direct measurements of CO₂ uptake by plant canopies are well established using ground operated gas analyzer (eddy flux tower) (Baldocchi et al. 2001). Such systems are, however, limited as observations are only representative for local footprints of the underlying ecosystem. Remote sensing (RS) offers a unique possibility to spatially investigate carbon uptake by plant photosynthesis, which is commonly referred to as terrestrial gross primary production (GPP).

Remote sensing approaches used to quantify GPP are based on the light use efficiency (LUE) concept from Monteith (Monteith 1972, 1977), which relates GPP to the Absorbed Photosynthetic Active Radiation (APAR) and the efficiency of plants to utilize the absorbed radiation for photosynthesis, the LUE. There is evidence that APAR can be reliably derived from optical measurements. The estimation of the highly variable LUE, however, is challenging. A first generation of RS-GPP approaches relate optical vegetation indices to APAR and assume LUE either as constant or as a function of actual meteorological conditions. Research has currently focused on estimating both APAR and LUE directly from RS data because these approaches are expected to provide more realistic GPP estimates. In this context, the emitted chlorophyll fluorescence (Fs) provides a new powerful tool for assessing actual plant LUE and, consequently, for mapping GPP. FS is emitted by the core of the photosynthetic machinery and can be considered as direct indicator for the functional status of plant photosynthesis. Several studies proved the capability of this remote sensing parameter to predict GPP at leaf and canopy level (Damm et al. 2010; Meroni et al. 2008; Rascher et al. 2009).

The proposed contribution provides one of the first spatial explicit investigations of GPP at local/regional scale. Data of the new imaging spectrometer APEX (Airborne Prism EXperiment) were used to derive all relevant parameters needed to estimate GPP. Differences in spatial distribution of GPP are investigated for different ecosystems in Switzerland including an agricultural test site, a semi-natural grassland site, a mixed forest, and an alpine pine forest.

Results of this contribution are considered as important information, e.g. for the development of ESA's (European Space Agency) FLEX (FLUorescence Explorer), for the improvement of knowledge on ecosystem responses to environmental properties, or for evaluating common ecosystem monitoring approaches (eddy flux tower).

REFERENCES

- Baldocchi, D., Falge, E., Gu, L.H., Olson, R., Hollinger, D., Running, S., Anthoni, P., Bernhofer, C., Davis, K., Evans, R., Fuentes, J., Goldstein, A., Katul, G., Law, B., Lee, X.H., Malhi, Y., Meyers, T., Munger, W., Oechel, W., U, K.T.P., Pilegaard, K., Schmid, H.P., Valentini, R., Verma, S., Vesala, T., Wilson, K., & Wofsy, S. (2001). FLUXNET: A new tool to study the temporal and spatial variability of ecosystem-scale carbon dioxide, water vapor, and energy flux densities. *Bulletin of the American Meteorological Society*, 82, 2415-2434
- Damm, A., Erler, A., Gioli, B., Hamdi, K., Hutjes, R., Kosvancova, M., Meroni, M., Miglietta, F., Moersch, A., Moreno, J., Schickling, A., Sonnenschein, R., Udelhoven, T., Van der Linden, S., Hostert, P., & Rascher, U. (2010). Remote sensing of sun induced fluorescence yield to improve modelling of diurnal courses of Gross Primary Production (GPP). *Global Change Biology*, 16, 171-186
- Meroni, M., Picchi, V., Rossini, M., Cogliati, S., Panigada, C., Nali, C., Lorenzini, G., & Colombo, R. (2008). Leaf level early assessment of ozone injuries by passive fluorescence and photochemical reflectance index. *International Journal of Remote Sensing*, 29, 5409-5422
- Monteith, J.L. (1972). Solar-radiation and productivity in tropical ecosystems. *Journal of Applied Ecology*, 9, 747-766
- Monteith, J.L. (1977). Climate and efficiency of crop production in Britain. *Philosophical Transactions of the Royal Society of London Series B-Biological Sciences*, 281, 277-294
- Rascher, U., Agati, G., Alonso, L., Cecci, G., Champagne, S., Colombo, R., Damm, A., Daumard, F., De Miguel, E., Fernandez, G., Franch, B., Franke, J., Gerbig, C., Gioli, B., Gomez, J.A., Goulas, Y., Guanter, L., Gutierrez-De-La-Camara, O., Hamdi, K., Hostert, P., Jimenez, M., Kosvancova, M., Lognoli, D., Meroni, M., Miglietta, F., Moersch, A., Moreno, J., Moya, I., Neininger, B., Okujeni, A., Ounis, A., Palombi, L., Raimondi, V., Schickling, A., Sobrino, J.A., Stellmes, M., Toci, G., Toscano, P., Udelhoven, T., Van der Linden, S., & Zaldei, A. (2009). CEFLES2: The remote sensing component to quantify photosynthetic efficiency from the leaf to the region by measuring sun-induced fluorescence in the oxygen absorption bands. *Biogeosciences*, 6, 1181-1198

16.2

Satellite-based climate products for alpine studies within GCOS Switzerland

Fontana Fabio¹, Seiz Gabriela¹, Foppa Nando¹ & Lugrin David¹

¹ *Federal Office of Meteorology and Climatology MeteoSwiss, Swiss GCOS Office (fabio.fontana@meteoswiss.ch)*

The Global Climate Observing System (GCOS) was established in 1992 to ensure that the observations necessary to address climate-related issues are defined, obtained and made available to all potential users. Primarily, the GCOS observations should assist Parties in meeting their responsibilities under the UN Framework Convention on Climate Change (UNFCCC), as well as provide the systematic observations needed by the World Climate Research Programme (WCRP) and the Intergovernmental Panel on Climate Change (IPCC).

The Swiss GCOS Office at the Federal Office of Meteorology and Climatology MeteoSwiss has the task of coordinating all climate relevant measurements in Switzerland. These include measurements in both the atmospheric and terrestrial domains made by a variety of measurement systems, including satellite-based sensors. Latter have become increasingly important in recent years due to significant advances in space technology, and “a detailed global climate record for the future critically depends upon an observing system involving a major satellite component”, as stated in the satellite supplement to the GCOS Implementation Plan.

An important task of the Swiss GCOS Office is to foster the use of satellite-based data for alpine studies in Switzerland, to complement the long-term in situ observations. We will present an overview of the activities of the Swiss GCOS Office. In particular, the results of climatological studies of atmospheric and terrestrial Essential Climate Variables (ECVs) will be presented as a contribution to the National Climate Observing System (GCOS Switzerland).

REFERENCES

- Seiz, G. & Foppa, N. 2011. National Climate Observing System of Switzerland (GCOS Switzerland). *Advances in Science Research*, 6, 95-102, doi:10.5194/qsr-6-95-2011.
- Seiz, G., Foppa, N., Meier, M. & Paul, F. 2011. The Role of Satellite Data within GCOS Switzerland, *Remote Sensing*, 3, 767-780, doi:10.3390/rs3040767.

16.3

Retrieval of the ECV „snow spatial extent“ from 25 years of AVHRR data over the European Alps for climate research

Fabia Hüsler¹, Stefan Wunderle¹, Tobias Jonas² & Christoph Neuhaus¹

¹ Remote Sensing Research Group, University of Bern, Hallerstrasse 12, CH-3007 Bern (fabia.huesler@giub.unibe.ch)

² WSL Institute for Snow and Avalanche Research SLF, Flüelastrasse 11, CH-7260 Davos Dorf

Satellite time series can provide spatially and temporally consistent measurements of the Earth surface processes. In recent years, an increasing need for full resolution, multi-temporal satellite data sets has been identified to serve the purpose of climate change monitoring. Solely AVHRR offers the opportunity to analyze more than 25 years of medium resolution satellite imagery on a daily basis. Thereby it holds a great potential to detect, map and quantify long-term environmental changes, as this is the first satellite record approaching the length of statistical significance.

The University of Bern receives and archives daily full resolution (1.1 km) AVHRR data over Europe since 1984. This unique data set is used to generate a number of geophysical data records such as snow spatial extent, which has been declared an ECV. However, to compile a homogeneous data set for the use in climate studies, some inaccuracies, especially in the beginning stages of remote sensing techniques, have to be adequately corrected for. Therefore, a careful validation of the data is of major importance. In this study, we present an extended accuracy assessment of a modified snow cover retrieval from historical 1-km AVHRR data using a stable snow detection algorithm, which allows consistent snow sampling across the different AVHRR sensor generations. The spatial and seasonal validation includes a comparison to the quality assessed MOD10A1 snow cover product and a new approach of ground-truth validation using webcam imagery. The accuracy of the binary snow mask is found to be close to 90% (when compared to ground measurements) and correlations with MODIS snow masks exceed 0.9. In regard to time series compilation, assimilated station data were particularly valuable as a temporally stable reference to ensure sensor-to-sensor consistency. We will discuss snow product validation and present first time series results but also address the remaining challenges of a 25 year snow cover time series from space.

Given the importance of mountain regions for climate change assessment, the final objective is to provide a consistent database of snow extent that comes along with distinct accuracy parameters. This bears the potential to serve as a reference for climate models as well as supplement information for the assessment of trends over the last 25 years.

16.4

Estimation of forest variables from multiangular radiance data using a coupled canopy-atmosphere model

Laurent Valérie¹, Verhoef Wout², Clevers Jan¹ & Schaepman Michael³

¹Centre for Geo-Information, Wageningen University, P.O. Box 47 - 6700 AA Wageningen, the Netherlands (valerie.laurent@wur.nl)

²Faculty of Geo-Information Science and Earth Observation (ITC), University of Twente, P.O. Box 217, 7500 AE Enschede, the Netherlands

³Remote Sensing Laboratories, University of Zurich, Winterthurerstr. 190, CH-8057 Zurich, Switzerland

Many land targets have directional reflectance properties, including vegetation, and forests in particular. Since the launch of satellite platforms with angular sampling capabilities, the higher potential of multi-angular data for estimating vegetation structural and biochemical variables has been recognized. Many studies successfully estimated forest variables from atmospherically corrected multiangular data, but the use of physically based radiative transfer (RT) models is still limited. Because the atmosphere also has directional properties, it is important to understand the directional behaviour of the coupled canopy-atmosphere system in order to understand the multiangular radiance signal measured by the sensor at the top of the atmosphere (TOA). Coupling canopy and atmosphere RT models allows linking the vegetation and atmosphere variables directly to the TOA radiance. Such a coupled model is therefore a very interesting tool for estimating the forest variables directly from the multi-angular TOA radiance.

This case study investigated the potential of multi-angular radiance data as measured by CHRIS/PROBA for estimating structural and biochemical variables of three Norway spruce stands located at the Bily Kriz experimental site in Czech Republic. The soil-leaf-canopy RT model SLC and the atmospheric model MODTRAN4 were coupled using a method allowing to make full use of the four canopy angular reflectance components provided by SLC (Laurent et al. 2011a).

The coupled model provided good simulations of the measured spectral and angular signatures. The dimensionality of the data was investigated by performing singular value decompositions of the Jacobian matrices. The analysis showed that the dimensionality increased from 3 to 6 when increasing the number of angles from 1 to 4 (Table 1). Two cases were investigated for the estimation of the forest variables: 4 and 7 variables. The estimation was conducted by inverting the coupled model using look-up tables (LUT). The most influential variables were chosen for building the LUTs: vertical crown cover (Cv), fraction of bark material (fB), needle chlorophyll content (needleCab), needle dry matter content (needleCdm) for the 4-variable case, and additionally, tree shape factor (Zeta), dissociation factor (D), and needle brown pigments content (needleCs) in the 7-variable case. All angular combinations were tested, and the best estimates were obtained with combinations using two or three angles, depending on the number of variables and on the stand used. Overall, this case study showed that, although making use of its full potential is still a challenge, TOA multi-angular radiance data do have a higher potential for variable estimation than mono-angular data (Laurent et al. 2011b).

Table 1. Dimensionality based on the singular value decomposition for all possible angular combinations.

⊙	YOUNG	OLD1	OLD2
{m36}	3	3	3
{nadir}	3	3	3
{p36}	3	3	3
{p55}	4	4	4
{nadir, m36}	4	4	4
{nadir, p36}	4	5	5
{nadir, p55}	5	5	5
{m36, p36}	4	4	4
{m36, p55}	4	5	5
{p36, p55}	5	5	5
{nadir, m36, p36}	5	5	5
{nadir, m36, p55}	5	6	6
{nadir, p36, p55}	5	6	6
{m36, p36, p55}	5	6	6
{nadir, m36, p36, p55}	5	6	6

REFERENCES

- Laurent, V.C.E., Verhoef, W., Clevers, J.G.P.W., & Schaepman, M.E. (2011a). Estimating forest variables from top-of-atmosphere radiance satellite measurements using coupled radiative transfer models. *Remote Sensing of Environment*, 115 (4), 1043-1052.
- Laurent, V.C.E., Verhoef, W., Clevers, J.G.P.W., & Schaepman, M.E. (2011b). Estimating forest variables from multi-directional top-of-atmosphere radiance satellite measurements using coupled radiative transfer models. *Remote Sensing of Environment*, 115(10), 2603-2612.

16.5

Fusion of Digital Elevation Models Using Sparse Representations

Papasaika Haris¹, Baltsavias Emmanuel¹, Schindler Konrad¹

¹Institute of Geodesy and Photogrammetry, ETH Zurich, Wolfgang-Paulistrasse 15, 8093 Zurich, Switzerland, {haris.papasaika|manos.baltsavias|schindler}@geod.baug.ethz.ch

Digital Elevations Models (DEMs) are one of the most important types of geodata. They are needed in a large number of applications, ranging from virtual globes and visualization to engineering and environmental planning. DEMs of larger areas are usually generated either by photogrammetric processing of aerial and satellite images, SAR (Synthetic Aperture Radar) interferometry, or laser scanning (mainly from airborne platforms). Each sensing technology has its own strengths and weaknesses, and even within one technology the variations in DEM quality are large. DEMs are available at different scales from tailor-made local models to national and even global coverage. We are primarily interested in large-scale national and global products, whose resolution, accuracy, error characteristics, and homogeneity vary a lot. In most cases, the DEM producers provide users with information only on production technology, date of acquisition, and resolution, but only with coarse accuracy measures that fail to capture the local variations in data quality – sometimes only a single global number.

In an ideal world, one would of course obtain the raw measurements and sensor models from all sensors, and merge them by fitting a single DEM to the entire set of heterogeneous observations, along the way computing quality measures for every single height value. Unfortunately, this is usually not feasible in practice. Thus, one resorts to the next best solution, namely to fuse DEMs from different providers into a higher-quality product, and estimate its quality in the process from the available redundancy.

DEM fusion – and its necessary prerequisite, fine-grained quality characterization of the inputs – has several benefits: improved accuracy, homogeneity and completeness, as well as fine-grained quality information for the final product. We deal only with 2-D surfaces in regular grid format, which constitute the vast majority of large-scale DEMs (although our framework could in principle be extended to TINs).

In this work we make two contributions: we develop a computationally efficient and flexible mathematical method for robust fusion of 2-D surface models. The formulation is generic and can be applied with any two input DEMs, independent of the sensor technology and processing with which they were created, making it useful for practical applications; it takes into account both prior information about plausible terrain shapes (in the form of a dictionary), and the local accuracy of the inputs, controlled by interpretable weights; and it poses the complete fusion as a clean, convex mathematical optimisation problem that can be solved to global optimality, and in which the influence of the input DEMs is controlled by an interpretable set of local fusion weights.

We propose a data-driven method, which allows one to derive local measures of DEM quality (and thus also fusion weights) for each point or segment of a DEM, if no such information is available. To this end we use as input geomorphological characteristics of the terrain (slope, aspect, roughness) which are derived directly from the DEMs, as well as optionally semantic information such as land-cover maps. Using existing high-quality ground-truth DEMs as reference, we learn regression functions relating the available geomorphological characteristics to the DEM quality, which then allow one to estimate the local quality of a new DEM.

The proposed method is evaluated in detail with three different satellite datasets, and shows a significant improvement in DEM quality, consistently over all combinations of inputs.

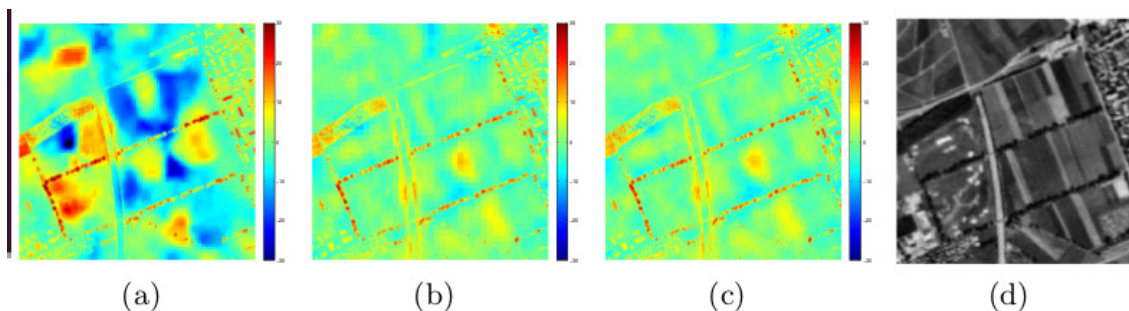


Figure 1. ALOS-SPOT fusion example. (a) Residuals between the L and A DEM, (b) Residuals between the L and S DEM, (c) Residuals between the L and F1 DEM. (d) SPOT orthoimage. The colored Z residuals are mapped in the interval $[-30,30]$. The bar unit is meters.

REFERENCES

- Papasaika, H., Kokiopoulou, E., Baltasvias, E., Schindler, K., & Kressner, D. 2011: Fusion of Digital Elevation Models Using Sparse Representations, In Proc. Photogrammetric Image Analysis, Munich, Germany, 5 - 7 October.
- Schindler, K., Papasaika, H., Schütz, S., & Baltasvias, E., & 2011: Improving Wide-Area DEMs Through Data Fusion - Chances and Limits, In Proc. Photogrammetric Week, 2011.

16.6

Methods and sensors for monitoring land subsidence phenomena based on satellite SAR interferometric stacking

Pasquali Paolo¹, Riccardi Paolo¹, Cantone Alessio¹, Defilippi Marco¹ & Holecz Francesco¹

¹sarmap SA, Cascine di Barico, CH-6989 Purasca (paolo.pasquali@sarmap.ch)

Interferometric stacking techniques emerged in the last decade as methods to obtain very precise measurements of terrain displacements, and in particular subsidence phenomena. In particular, the so-called Persistent Scatterers (Ferretti et al. 2001) and Small BASeline (Berardino et al. 2002) methods can be considered as the two most representative stacking approaches.

In both cases, the exploitation of 20 or more satellite Synthetic Aperture Radar (SAR) acquisitions obtained from the same satellite sensor with similar geometries on the interest area allows to measure displacements with an accuracy in the order of few mm / year, and to derive the full location history of “good” pixels with an accuracy of 1cm or better for every available date. A main difference between the two approaches is the type of objects and land cover that are favoured in the analysis: the PS technique focuses on so-called Point Targets, i.e. objects possibly of small size and with a very well characterized geometry like corner reflectors (e.g. buildings, rocks) and with a high temporal stability of the backscattered signal; the SBAS technique vice-versa is concentrating the analysis on so-called distributed targets, like open fields and not very geometrically characterized objects. The PS approach is then not making any assumption on spatial correlation of the displacement to be measured, but more on its linearity; the SBAS approach vice-versa is more robust in case of spatially correlated displacements, and allows in this case to monitor larger displacement rates.

This paper is performing an extensive analysis and comparison of the results that have been obtained with the two approaches in a same geographical area in Japan, characterized by subsidence due to water and natural gas extraction. The analysis is based on data acquired from the ALOS PALSAR (L-band), ENVISAT ASAR (C-band) and COSMO-Skymed (X-band) satellite instruments, and the validation of the results is based on GPS and leveling measurement.

The analysis allows to draw conclusions on the best approach and sensor to be selected for deriving the displacement measures for monitoring subsidence phenomena; the feasibility of exploiting the same approach in different geographical areas like Switzerland is also discussed.

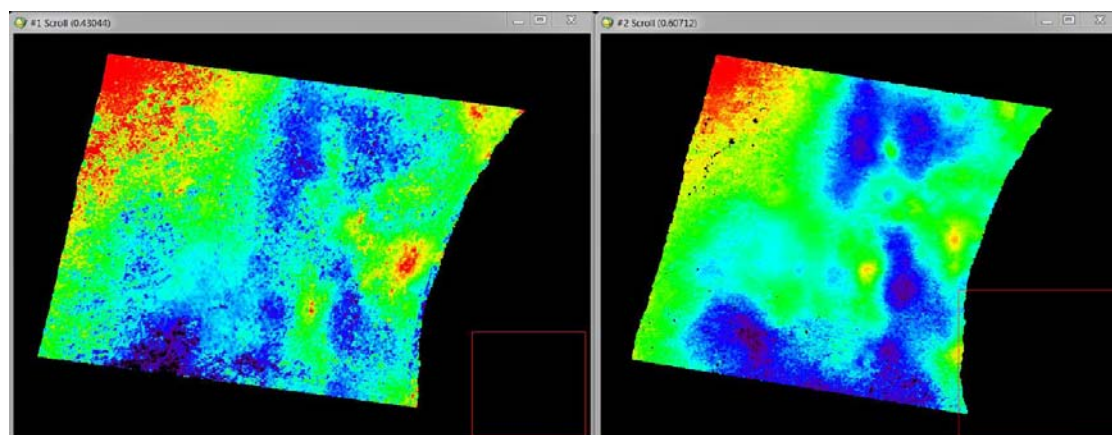


Figure 1. Comparison of average displacement rates (color scale between -25 mm/year in blue and +25mm/year in red) as derived from ALOS PALSAR (on the left) and ENVISAT ASAR (on the right) data.

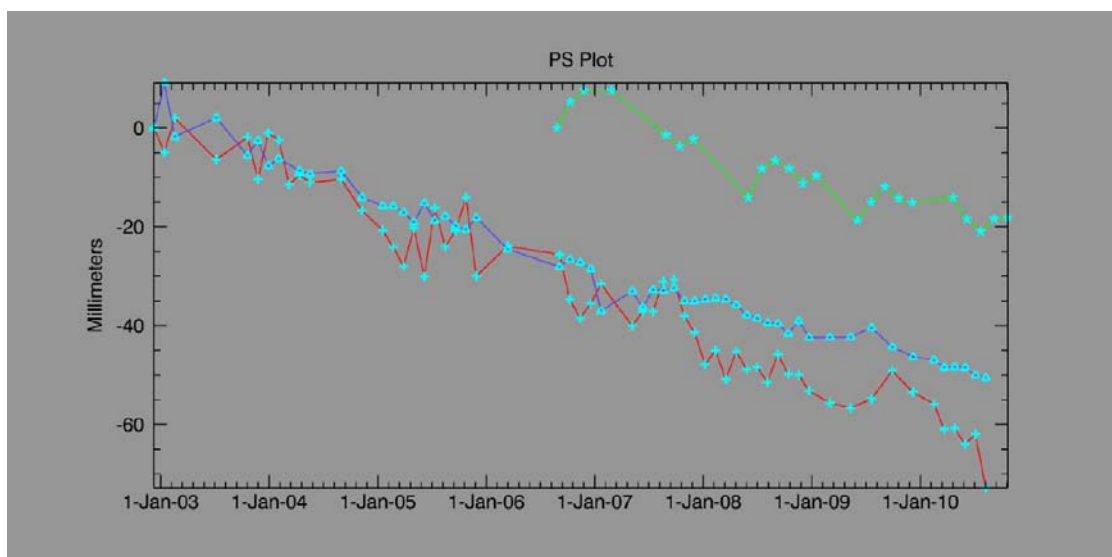


Figure 2. Comparison of displacement time series as derived from ALOS PALSAR + SBAS (star), ENVISAT ASAR + SBAS (triangle) and ENVISAT ASAR PS (plus).

REFERENCES

- Ferretti, A., Prati, C., & Rocca, F. 2001: Permanent scatterers in SAR interferometry, *IEEE Transactions on Geoscience and Remote Sensing*, 39, 8-20.
- Berardino, P., Fornaro, G., Lanari, R., & Sansosti, E. 2002: A new algorithm for surface deformation monitoring based on small baseline differential SAR interferograms, *IEEE Transactions on Geoscience and Remote Sensing*, 40, 2375- 2383.

16.7

High spatial resolution mapping of NO₂ from APEX imaging spectrometer data

Popp Christoph¹, Brunner Dominik¹, Damm Alexander² & Buchmann Brigitte¹

¹*Empa – Swiss Federal Laboratories for Materials Science and Technology, Überlandstr. 129, CH-8600 Dübendorf (christoph.popp@empa.ch)*

²*Remote Sensing Laboratories, University of Zurich, Winterthurerstr. 190, CH-8057 Zürich*

The investigation of small scale nitrogen dioxide (NO₂) distribution and concentration is of particular interest for local and regional air pollution assessment, for the identification and quantification of emission sources, or to assess the impact of small-scale variability on the comparison between coarse resolution satellite observations (e.g. from SCIAMACHY, OMI, GOME) and in-situ (point) observations. In this contribution, we present a methodological framework for NO₂ retrieval and first results using data of the Airborne Prism EXperiment (APEX) imaging spectrometer. APEX is a dispersive pushbroom imaging spectrometer for environmental monitoring covering the wavelength region between 380 nm and 2500 nm with a sampling interval between 0.4 nm and 10 nm. The radiometric and spectral performance of APEX allows mapping air pollution gradients and even individual strong NO₂ sources at an unprecedented resolution of about 50 m. Data used in this study were acquired during test flights on a Saturday in June 2010 over Zurich, Switzerland. NO₂ columns over Zurich were derived following a well-established two-step approach. First, the differential optical absorption spectroscopy (DOAS) technique is applied to raw APEX spectra in order to retrieve differential slant column densities (dSCD) using spectra obtained over pollution-free scenes as reference. Second, dSCD are converted to differential vertical column densities (dVCD) by computing air mass factors with a radiative transfer code. First results reveal very plausible spatial distributions of NO₂ over the greater Zurich area, e.g. peak concentrations in a shopping area as well as high concentrations along the major traffic pathways. APEX NO₂ maps are also evaluated by comparison with ground-based air quality measurements from the NABEL (National Air Pollution Network) and the inter-cantonal network Ostluft. Finally, we identify critical aspects for NO₂ retrieval from airborne imaging spectrometry data including sensor calibration. Further we outline requirements necessary to identify not only strong pollution sources but also to distinguish between background and moderately polluted regions.

P 16.1

Ecosystem parameter mapping of Alpine regions using continuous fields derived from imaging spectrometer data

Parviz Fatehi¹, Alexander Damm¹, Mathias Kneubuhler¹, Michael E. Schaepman¹

Remote Sensing Laboratories, Department of Geography, University of Zurich, WinterthurerStr. 190, CH-8507 Zurich, Switzerland.

Understanding and quantifying ecological processes and their spatio-temporal dynamics are crucial for monitoring and modeling ecosystems. Over the past two decades, remotely sensed data from imaging spectrometers have been used to accurately derive biogeochemical and biophysical ecosystem properties related to key ecological processes. The approach of Multiple Combined Continuous Fields (MCCF) is a promising alternative in representing the spatial and temporal distribution of ecosystem properties and offer advantages compared to traditional discrete classification approaches. In this contribution, the concept of continuous fields and a dedicated methodological framework for deriving continuous fields of ecosystem properties of Alpine regions is presented. The method includes abundance mapping of predominant land surface types and related quantitative maps of ecosystem parameters derived with empirical models from APEX (Airborne Prism Experiment) imaging spectrometer data.

P 16.2

Modeling the complexity of the dynamic rupture process of the 2011 Mw 9 Tohoku earthquake.

P. Galvez(1) , J.-P. Ampuero(3), L. Dalguer (1) and T. Nissen-Meyer(2).

1. Swiss Seismological Service (ETH-Zurich), 2. Institute of Geophysics (ETH-Zurich) 3. Seismological Laboratory, California Institute of Technology.

On March 11th 2011, a violent Mw=9 earthquake stroke Japan causing 28000 victims, including casualties and missing. This earthquake triggered a devastating tsunami causing severe damage in cities and nuclear facilities along the Japanese coast. The amount of data recorded from this earthquake is exceptional, with thousands of broadband, strong motion and continuous GPS sensors located all over Japan. This provides a great opportunity for seismologist and engineers to deeply investigate the rupture process in order to better understand the physics of this type of earthquakes and their associated effects like tsunamis.

Kinematic source inversion of strong ground motion, teleseismic, geodetic and tsunami data and source imaging by back-projection of body waves recorded by teleseismic arrays (e.g. Simons et al, Science 2011, Meng et al, GRL 2011) suggest that the earthquake featured a diversity of rupture styles, comprising distinct stages of fast and slow rupture intermingled with high-frequency radiation. Those results also revealed a clear spatial complementarity between the regions of low and high frequency radiation: the regions of large slip had long rise time dominating the low frequency radiation and the strongest high frequencies is originated along the bottom rim of the main slip areas, near the deep limit of interplate seismicity. A plausible interpretation of this high/low frequency complementarity, consistent with the presence of repeating earthquakes in the area, is that high frequency radiation arises from failure of brittle asperities embedded in the frictionally stable fault regions at the bottom of the seismogenic zone.

Here we investigate the proposed mechanism of this key feature of the rupture process of this event by means of dynamic rupture simulations. We employ the 3D spectral element code SPECFEM3D-SESAME, in which we recently implemented the capability of solving for dynamic fault rupture. Through the usage of an unstructured mesh, our model incorporates the non-planar geometry of the megathrust interface. We assume that the fault rupture is governed by slip weakening friction. Our first set of simulations is aimed at testing if the diversity of rupture phenomena during this earthquake can be overall reproduced by assuming the most basic friction law, linear slip-weakening friction, but prescribing a spatially heterogeneous distribution of the critical slip weakening distance D_c and initial fault stresses. Our initial model is composed of overlapping patches of a range of sizes which D_c correlates with the patch size. By trial-and-error we determine a range of asperity properties that are compatible with the main features of the Tohoku earthquake. In particular, we distribute a collection of small patches near the deeper transition zone of the fault, to account for the strong high frequency radiation in that region.

P 16.3

Consistent Trends in Water Vapour, Downwelling Radiation, and Temperature

Hocke, K., Kämpfer, N., Wacker, S., Gröbner, J., Vuilleumier, L.

Institute of Applied Physics, University of Bern, Sidlerstr. 5, 3012 Bern (klemens.hocke@iap.unibe.ch)

The motivation of the presentation is the challenging question: „Do we observe the rising greenhouse effect in time series of water vapour, downwelling long-wave radiation, and temperature measured by a Swiss ground station network?“

Observation data of the time interval 1994 to 2007 comes from pyrgeometers and thermometers at Davos, Payerne, Jungfrauoch, and Locarno-Monti (Alpine Surface Radiation Budget Network ASRB) and from the ground-based microwave radiometer TROWARA at Bern.

We performed a Mann-Kendall trend analysis and found consistent trends in integrated water vapour, downwelling long-wave radiation, and surface air temperature. Generally the seasonal trends were positive during summer with exception of August where all parameters showed a dip in the trend. Negative trends were present during winter in all parameters. These results are in a qualitative agreement with the consideration that the rising temperature due to man-made CO₂ emissions causes higher evaporation rates of water vapour. In turn, higher concentrations of tropospheric CO₂ and H₂O lead to an increase of downwelling long-wave radiation which was measured by means of the Alpine Surface Radiation Budget Network. This observation result is not trivial since it requires long-term stability of all measurement instruments.

REFERENCE

Wacker, J. Gröbner, K. Hocke, N. Kämpfer, L. Vuilleumier: Trend analysis of surface cloud-free downwelling long-wave radiation from four Swiss sites, *J. Geophys. Res.*, D10, D10104, 2011

P 16.4

Estimation of plant functional biochemical traits of subalpine and alpine grasslands from airborne images of high spatial and spectral resolution

Homolová Lucie^{1,2}, Malenovský Zbyněk¹, Schaepman Michael¹ & Clevers Jan²

¹ *Remote Sensing Laboratories, Department of Geography, University of Zurich, Winterthurerstrasse 190, CH-8057 Zurich (lucie.homolova@wur.nl)*

² *Laboratory of Geo-Information Science and Remote Sensing, Wageningen University, Droevendaalsesteeg 3, 6708 PB Wageningen, NL*

Plant functional traits (PFT) are any measureable feature that determines plants' responses to environmental factors and their effects on ecosystem processes. PFT are increasingly used to classify plants with similar function in an ecosystem, to quantify functional diversity of communities, or to parameterize e.g. dynamic global vegetation models. Even though field measurement protocols of many PFT are well established, they are time consuming and limited to discrete sampling points usually at local scale. Spatially continuous and non-destructive mapping of plant functional traits at larger areas using remote sensing methods is of interest to the plant ecology community.

Our research objective is to retrieve leaf biochemical traits, namely total chlorophylls (C_{ab}), water (C_w) content, and specific leaf area (SLA) of subalpine and alpine grasslands from high spatial and spectral resolution airborne imaging spectroscopy data. Further we are interested in interpretation of the spatial gradients of functional traits and their use for mapping of plant functional groups within the study area.

The airborne images, acquired with AISA Dual system (Specim, Ltd., Finland) during the vegetation season 2008 over sub-alpine and alpine grasslands in French Alps, were the main input into the physically based retrieval of functional traits.

The retrievals were based on look-up table inversion of integrated soil-leaf-canopy (SLC) radiative transfer model (Verhoef & Bach 2007). The model input parameters were adjusted to the local case study using field measurements to specify ranges and distributions of the model inputs. The ill-posed nature of the look-up table inversion, i.e. situations when different combinations of model inputs yield the same simulated top-of-canopy reflectance, was alleviated by retrieving individual traits from specific parts of the electromagnetic spectra.

Statistical analysis of field-measured leaf trait data revealed that trait variability is strongly driven by species (40-75%) and less by environmental gradients such as altitude (only less than 5% of the overall traits' variability could be explained by the altitude). Principal component analysis identified a triplet of leaf traits (Cab, Cw, and SLA) having high potential to distinguish functionally different plant groups, which is expected to be spatially revealed also at the canopy level from airborne spectral images.

REFERENCES

Verhoef, W. & Bach, H. 2007: Coupled soil-leaf-canopy and atmosphere radiative transfer modelling to simulate hyperspectral multi-angular surface reflectance and TOA radiance. *Remote Sensing of Environment*, 109, 166-182.

P 16.5

Time series of radar backscatter: Moving towards simultaneous high temporal & spatial resolution observations of Alpine snow melting

Small David¹, Schubert Adrian¹, Zuberbühler Lukas¹ & Meier Erich¹

¹Remote Sensing Laboratories, University of Zurich, CH-8057 Zurich (david.small@geo.uzh.ch)

Although snow provides a familiar strong signature at optical wavelengths, monitoring its presence and melting state is severely impaired by cloud cover and long wintry nights (and daytime shallow illumination) that often render meaningful observations by visible or infra-red sensors impossible. Radar sensors provide their own illumination source, penetrating through clouds to deliver backscatter observations day or night in all kinds of weather. Wet snow is characterised by very weak response to radars, observed as dark areas in the resulting imagery (Nagler & Rott, 2000).

Synthetic Aperture Radar (SAR) imagery is subject to both *geometric* and *radiometric* distortions caused by variations in the topography within an image. Corrections for the geometric properties of the images (topography and atmosphere) are being utilised to an increasing extent as SAR sensor positional accuracies also improve (Schubert et al., 2010).

High *geometric* accuracy is a pre-requisite for a well-defined local *radiometric* calibration throughout radar imagery. Correcting for the radiometric distortions induced by terrain has improved with a new technique recently developed within our group and demonstrated using data from ENVISAT ASAR, ALOS PALSAR, Radarsat-2, and TerraSAR-X. It is applicable to radar backscatter data available from any of over 10 satellites observing the Earth at a variety of microwave wavelengths (Small, 2011). A sample image acquired with the Canadian Radarsat-2 satellite in 2010 is shown in Figure 1. Open water and wet snow appears dark, fields dark grey, and forests intermediate grey. Cities and dry snow (above the freezing level) appear bright.

The technique is first demonstrated on a single image product, and then applied to a time-series of hundreds of radar images covering Switzerland. Improvements to multi-track inter-comparisons are shown. Wet snow observations in the springtime melting period are highlighted.

Given the upcoming European Sentinel-1 satellites due for launch in 2013, the potential of the technique to offer near daily high-resolution observations of wet snow throughout Switzerland and the Alpine chain is discussed.

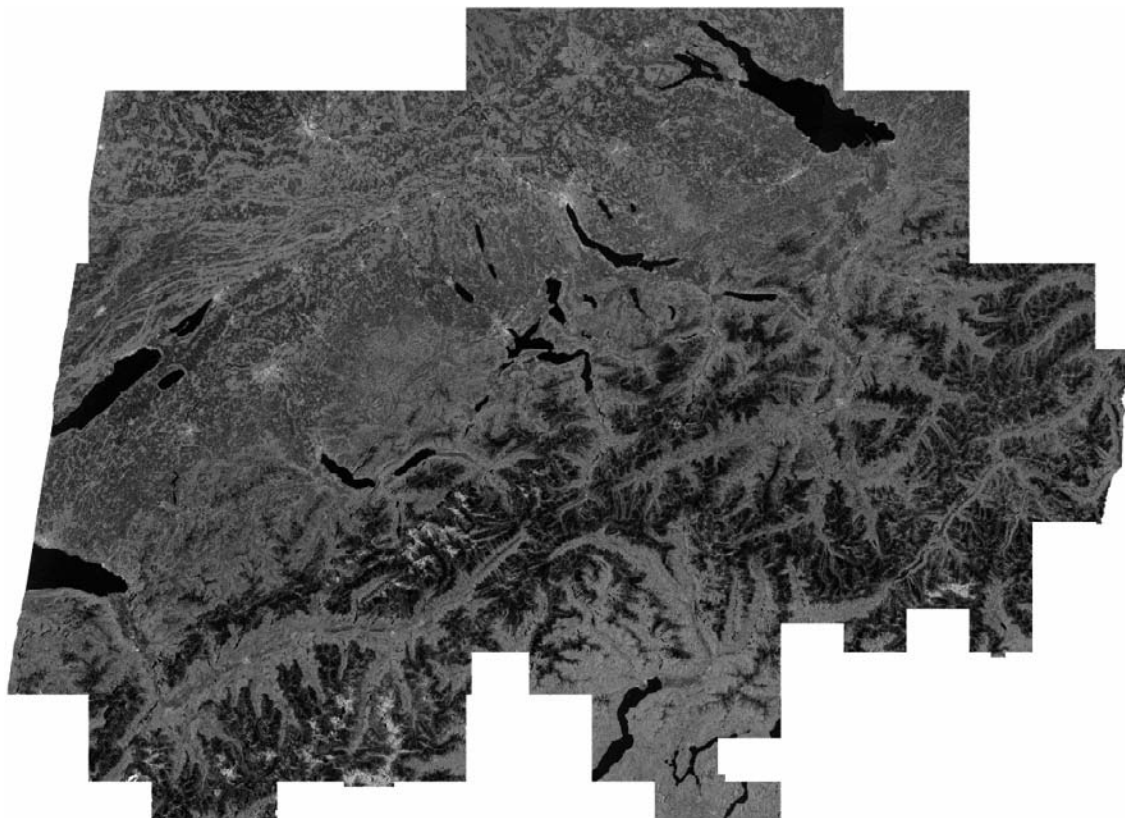


Figure 1. Melting snow observed in terrain-flattened gamma nought backscatter – Radarsat-2 ScanSAR 50m resolution VH polarisation, 27.04.2010, black= -26dB, white= -1dB – Radarsat-2 Data © Canadian Space Agency 2010, courtesy SOAR project #1985.

REFERENCES

- Nagler T. & Rott H. 2000: Retrieval of Wet Snow by Means of Multitemporal SAR Data, *IEEE Transactions on Geoscience and Remote Sensing*, 38(2), 754-765.
- Schubert, A., Jehle M., Small D. & E. Meier. 2010: Influence of Atmospheric Path Delay on the Absolute Geolocation Accuracy of TerraSAR-X High-Resolution Products. *IEEE Transactions on Geoscience and Remote Sensing*, 48(2), 751–758.
- Small D. 2011: Flattening Gamma: Radiometric Terrain Correction for SAR Imagery, *IEEE Transactions on Geoscience and Remote Sensing*, 49(8), 3081–3093.

P 16.6

Acquiring the relevant samples for chlorophyll estimation with hyperspectral data

Tuia Devis¹, Verrelst Jochem², Alonso-Chordà Luis² and Camps-Valls Gustavo²

¹Laboratoire des Systèmes d'Information Géographiques, Ecole Polytechnique Fédérale de Lausanne, Station 18, CH-1015 Lausanne (devis.tuia@epfl.ch)

²Image Processing laboratory (IPL), Universitat de Valencia, Spain

This contribution considers the problems of terrestrial campaign planning for the estimation of Chlorophyll using hyperspectral data. The advent of this new technology, as well as the forthcoming missions aiming at measuring fluorescence from satellite observations (FLEX among others) have created a strong research pole aiming at linking the biophysical parameters with remote sensing spectra (Verrelst *et al.* 2008, Stagakis *et al.* 2010, Tuia *et al.* 2011).

At present, many approaches rely on the definition of statistical models of prediction of the biophysical parameter and have proven their reliability and generalization capabilities. However, such models also depend on an appropriate training set, in particularly when dealing with situations where only few samples can be acquired at once.

There is thus the need for methods aiming at planning efficiently the next measurement campaigns, where the samples are acquired where the model needs them mostly. In this optic, the framework of *active learning* (Cohn *et al.* 1994) proposes a series of criteria for selecting new training samples (new measurements) so that the uncertainty of the model predictions is efficiently reduced. In this work, we present a strategy based on committees of prediction models (similarly to the strategy for classification proposed in Tuia *et al.* 2009), where the interest of acquiring a new sample is directly related to the variance in the predictions made by the committee for each potential new measurement site.

We focus on the estimation of Chlorophyll concentration using hyperspectral spectra acquired by the spaceborne sensor CHRIS-Proba. Field data were acquired during the ESA SPARC-2003 and SPARC-2004 campaigns in Barrax, Spain. The large variety of crop types and phenological stages represented by the data provide a very complete sample of possible Chlorophyll concentrations.

An ensemble of 135 samples is available for the analysis: 20 are used for training the initial models, and 3 additional samples are selected form a set of 88 potential sites and included iteratively to the training set, either randomly or using an active learning strategy. The remaining 27 samples are used to validate the generalization capabilities of the model in the prediction task.

Figure 1 illustrates the learning rates for an active acquisition versus a random selection of the sampling sites: the plots show that planning terrestrial campaigns using active learning leads to models requiring less samples for an efficient prediction. Figure 2 shows the prediction maps after 15 sample acquisitions for the random (left) and active (middle) strategy, while the right panel shows the uncertainty function leading the selection of new samples. The uncertainty criterion forces the new samples to be located in the central area of the image, whose predictions are considered more uncertain. As an effect, the predictions in that area are strongly improved (see the central panel of Fig. 2).

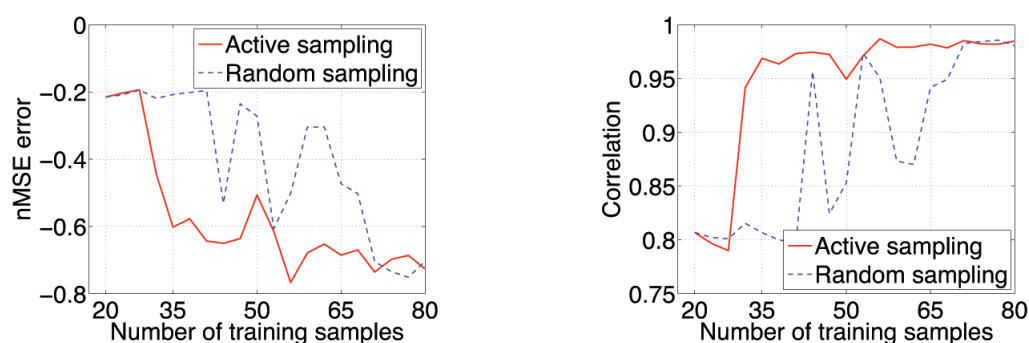


Figure 1. Comparison of random and active learning training points definition. (Left) normalized mean squared error

$$nMSE = \log_{10} \left(\sqrt{\frac{1}{N_S^2} \sum_i (y_i - \hat{y}_i)^2} \right)$$

as a function of the size of the training set; (right) Pearson correlation coefficient between predicted and real chlorophyll concentrations.

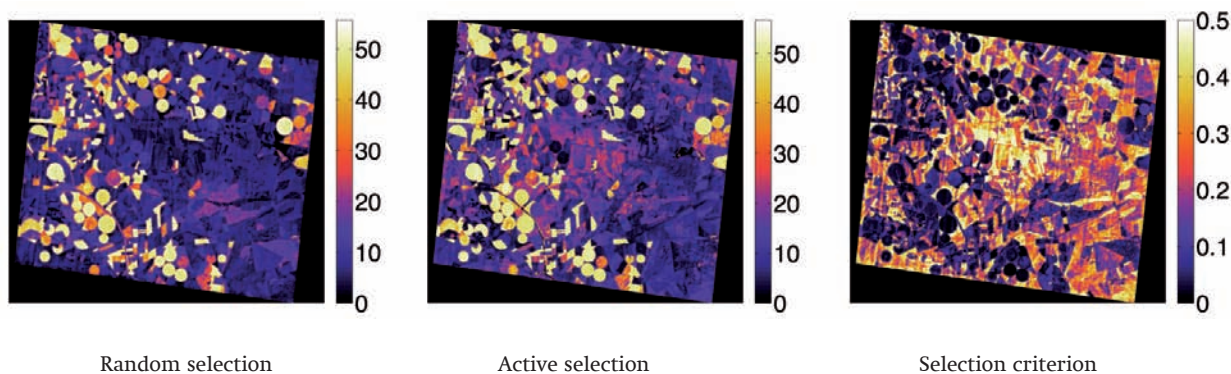


Figure 2. (Left) Chl prediction map when using random sampling (20 initial + 15 randomly selected); (middle) Chl prediction map when using active learning (20 initial + 15 actively selected); (right) Standard deviation of the prediction of the prediction models, used as a sample selection criterion.

Active learning seems a very promising way to minimize the number of training samples necessary to predict biophysical parameters using hyperspectral imagery. More results will be shown at the time of the conference.

REFERENCES

- Cohn, D., Atlas, L. & Ladner, R. 1994: Improving generalization with active learning, *Machine Learning*.15, 201-221.
- Stagakis, S., Markos, N., Sykioti, O. & Kyparissis, A. 2010: Monitoring canopy biophysical and biochemical parameters in ecosystem scale using satellite hyperspectral imagery: An application on a *phlomis fruticosa* mediterranean ecosystem using multiangular CHRIS/Proba observations. *Remote Sensing of Environment*.114(5) 977–994.
- Verrelst, J., Schaepman, M. E., Koetz, B. & Kneubühler, M. 2008: Angular sensitivity analysis of vegetation indices derived from CHRIS/Proba data. *Remote Sensing of Environment*. 112 (5), 2341–2353.
- Tuia, D., Ratle, F., Pacifici, F., Kanevski, M. & Emery, W. J. 2009: Active learning methods for remote sensing image classification. *IEEE Transactions on Geoscience and Remote Sensing*. 47 (7), 2218-2232.
- Tuia, D., Verrelst, J., Alonso, L., Pérez-Cruz, F. & Camps-Valls, G. 2011: Multi-output support vector regression for remote sensing biophysical parameter estimation, *IEEE Geoscience and Remote Sensing Letters*. 8 (4), 804-808.

17. Synergies between Advancements in Geodesy and other Geosciences

Markus Rothacher, Urs Marti, Pierre Yves Gilliéron, Rolf Dach

Swiss Geodetic Commission

TALKS:

- 17.1 Brockmann E., Schlatter A.: Station velocities in Switzerland derived from 20 years of geodetic satellite navigation observations
- 17.2 Buchli B., Sutton F., Beutel J.: GPS-equipped wireless sensor network for geodetic positioning applications
- 17.3 Dach R., Jäggi A., Schmid R., Lutz S., Steigenberger P., Beutler G.: Impact of troposphere modelling on GNSS satellite antenna PCV estimation
- 17.4 Hurter F., Geiger A., Perler D.: Geodetic water vapor monitoring campaign in Zermatt, summer 2010
- 17.5 Jäggi A., Meyer U., Prange L., Bock H., Dach R., Beutler G.: Gravity Field Determination at AIUB: From CHAMP and GRACE to GOCE
- 17.6 Salvini D., Studer M., Müller H., Spillmann T., Schnellmann M., Brockmann E.: Ein Permanentes Gns-Netz Zur Aufzeichnung Tektonischer Bewegungen In Der Nordschweiz
- 17.7 Wang K., Rothacher M.: Positioning improvements with stochastic clock modelling

POSTERS:

- P 17.1 Limpach P., Geiger A., Beutel J., Buchli B., Wirz V., Gruber S.: Permanent monitoring of rock glaciers with low-cost GPS
- P 17.2 Neyer F., Delaloye R.: Displacement detection on rock glaciers using webcam images: A case study in the Mattertal
- P 17.3 Su Zhenzhong, Limpach Philippe, Rothacher Markus, Geiger Alain: Improving sub-daily solutions of single-frequency GPS using antenna PCV
- P 17.4 Villiger A., Geiger A., Marti U., Brockmann E.: SWISS 4D: Estimation of the tectonic deformation field of Switzerland based on GPS measurements
- P 17.5 Zhang Y., Song S., Dalguer L., Clinton J., Haberling S.: Investigating the reliability of kinematic source inversion with dynamic rupture models and high rate GNSS data

17.1

Station velocities in Switzerland derived from 20 years of geodetic satellite navigation observations

Brockmann Elmar, Schlatter Andreas¹

¹Swiss Federal Office of Topography swisstopo, Geodesy Division, Seftigenstrasse 264, 3084 Wabern (elmar.brockmann@swisstopo.ch)

Between 1988 and 1995, the Federal Office of Topography (swisstopo) installed the Swiss Reference Network LV95 (Landesvermessung 95) as the national first network which is completely based on satellite observations to the global positioning system GPS. Together with the operation of the 30 permanent GPS stations of the automatic GNSS network Switzerland (AGNES) starting 1998, the LV95 stations represent the backbone of the geodetic reference frame and the national geodata infrastructure, the Swiss Terrestrial Reference Frame (CHTRF).

As a quality check and for studying the stability of the reference frame, swisstopo re-observed the whole network three times: 1998, 2004 and 2010. The comparison of the horizontal coordinates proved the stability of the reference frame on the cm level.

Furthermore, the detection of possible tectonic movements in the order of below 1 mm/year is achievable with the data set. Horizontal velocity vectors derived from the adjustment of the campaign data can also be compared with results of velocities derived from the permanent AGNES network. Reliable vertical velocities can be estimated only for the permanent stations and from the kinematic adjustment of all national leveling data since 1903. The analysis of the horizontal and vertical velocities is a further step towards the determination of a kinematic model for the recent crustal deformations in Switzerland.

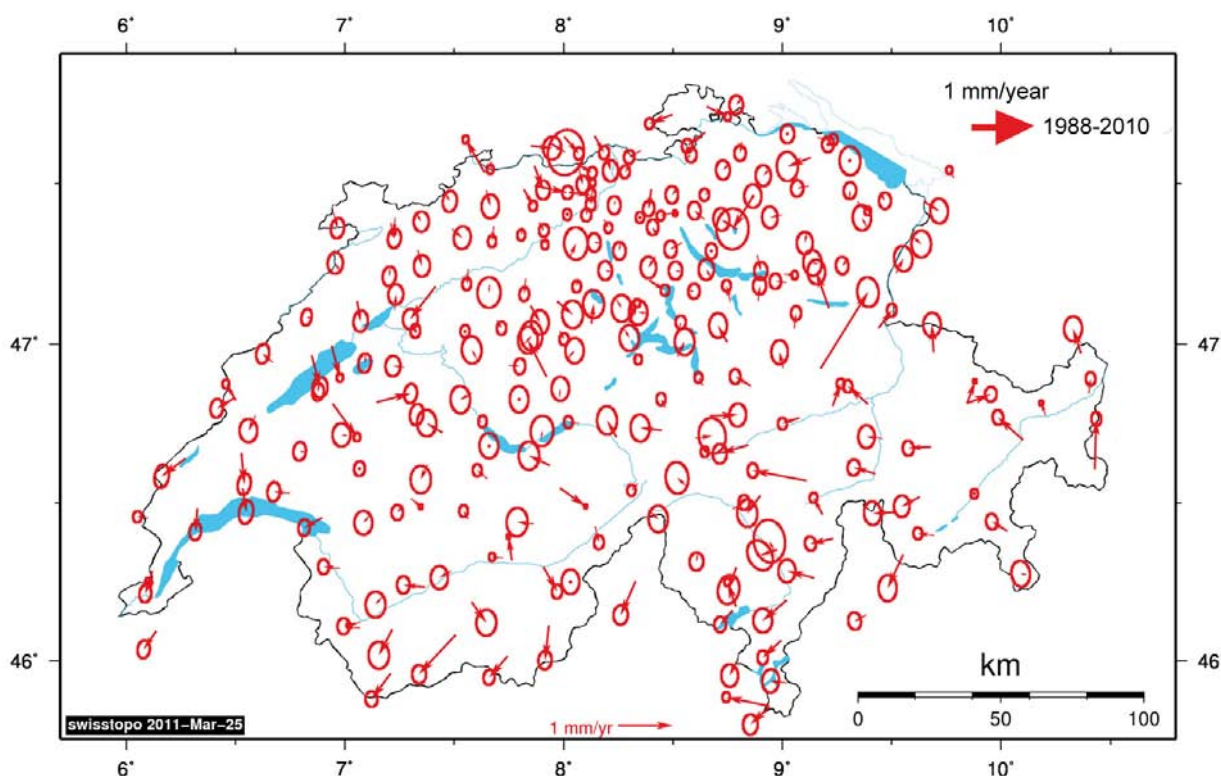


Figure 1. Horizontal velocities derived from GPS campaigns covering an time span of more than 20 years.

REFERENCES

Brockmann E., A. Schlatter (2011): 20 years of maintaining the Swiss Terrestrial Reference Frame CHTRF. In: Ihde, J. and H. Hornik (Eds): Subcommission for the European Reference Frame (EUREF), Chisinau, 2011 (in prep.)

17.2

GPS-equipped wireless sensor network for geodetic positioning applications

Bernhard Buchli, Felix Sutton, Jan Beutel

Computer Engineering and Networks Laboratory, ETH Zurich, 8092 Zurich, Switzerland
 {bbuchli, fsutton, janbeutel}@ethz.ch

We present the prototype architecture of a novel, power optimized and cost effective Wireless Sensor Network (WSN) node that allows the acquisition of L1 GPS data for highly accurate determination of position and motion based on differential processing of GPS signals [1]. With respect to the differential GPS processing involved it is mainly of importance that the required GPS data (RAW format) is synchronously captures at both a non-moving positions and positions in motion in order to be able to solve for position and velocity at great accuracy. The accuracy of the solutions resolved by this method [1] depends on the amount of GPS data captured, typically on the order of multiple hours for sub-cm accuracy. A configurable measurement schedule, power optimized operation and robustness against harsh environmental conditions makes it well suited for geodetic applications in remote areas, e.g. in high-alpine research. Compared to other approaches [5,6] we exploit low-power operation and real-time data access to allow longer lifetime and the application in natural hazard warning scenarios where data latency is critical [7].

The WSN node presented integrates seamlessly with the PermaSense WSN architecture [2]. In this architecture a multihop network of ultra-low power wireless sensor nodes is used to gather environmental monitoring data, i.e. crack dilatation or temperatures. The system is designed for delivering a continuously high data yield over long observation periods (multi-year) tolerating outages of system components at the node, base station, server and communication link level. Novel and challenging from the perspective of GPS sensors are the considerably higher amounts of sensor data generated and higher power requirements due to the long active time required for the GPS sensor.

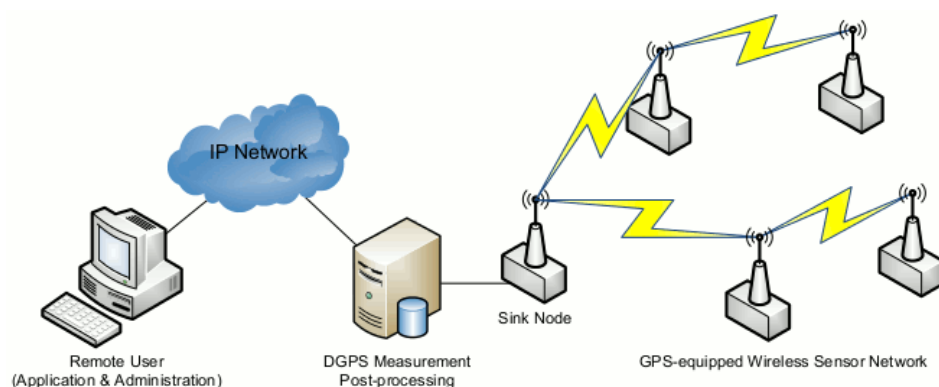


Figure 1. PermaSense GPS-equipped wireless sensor network.

The wireless sensor nodes are based on a commercial low power sensor module (TinyNode 184) coupled with a low-cost off-the-shelf single frequency GPS receiver (u-blox LEA 6T). Each node captures the range and timing information of all visible satellites, and communicates this data to the sink node for application-specific post processing on a backend server [3]. When not acquiring data, the GPS receiver is turned off for power savings. Network-wide synchronized GPS measurements are necessary for dGPS processing. This is achieved by periodically querying the timing information from the GPS unit to synchronize the schedule on the sensor node. The prototype system has been implemented and validated in a testbed setting [4]. A deployment for an outdoor application to monitor rock glacier creep is currently pending.

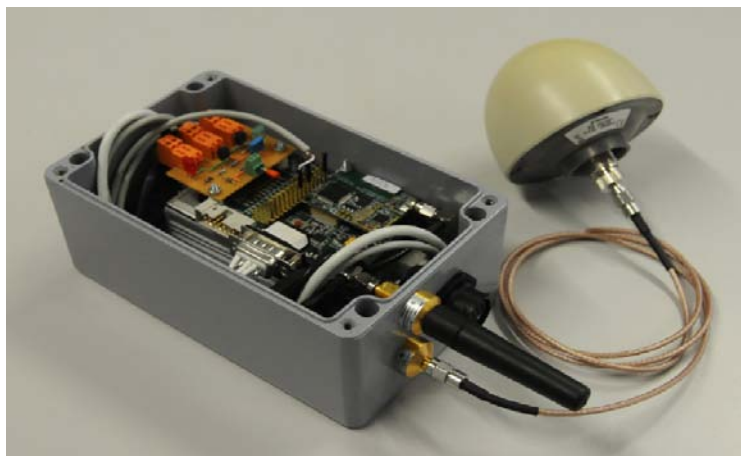


Figure 2. System prototype housed in a water-proof enclosure with EMP-protected antenna connectors for harsh environmental conditions.

REFERENCES

- [1] P. Limpach and D. Grimm, "Rock glacier monitoring with low-cost GPS receivers." in 7th Swiss Geoscience Meeting, August 2009.
- [2] J. Beutel, S. Gruber, A. Hasler, R. Lim, A. Meier, C. Plessl, I. Talzi, L. Thiele, C. Tschudin, M. Woehrle and M. Yuecel: PermaDAQ: A Scientific Instrument for Precision Sensing and Data Recovery under Extreme Conditions. Proc. 8th ACM/IEEE Int'l Conf. on Information Processing in Sensor Networks (IPSN/SPOTS '09), pages 265-276, April 2009.
- [3] N. Burri et al. Dozer: Ultra-low power data gathering in sensor networks. In ACM IPSN, 2007.
- [4] F. Sutton, GPS-equipped Wireless Sensor Node for PermaSense. Semester Thesis, ETH Zurich, 2010.
- [5] M. den Ouden et al. Stand-alone single-frequency GPS ice velocity observations on Nordenskiöldbreen, Svalbard. In *The Cryosphere*, Volume 4, Issue 4, pages 593-604, 2010.
- [6] L. Garin. Wireless sensor network-based distributed GNSS receiver architecture for infrastructure monitoring. In PhD Thesis, 2010.
- [7] Jan Beutel, Bernhard Buchli, Federico Ferrari, Matthias Keller, Lothar Thiele, Marco Zimmerling: X-Sense: Sensing in Extreme Environments. Proceedings of Design, Automation and Test in Europe, 2011 (DATE 2011), Grenoble, France, March, 2011.

17.3

Impact of troposphere modelling on GNSS satellite antenna PCV estimation

R. Dach¹, A. Jäggi¹, R. Schmid², S. Lutz¹, P. Steigenberger² & G. Beutler¹

¹*Astronomisches Institut, Universität Bern, Sidlerstrasse 5, CH-3012 Bern (rolf.dach@aiub.unibe.ch)*

²*Institut für Astronomische und Physikalische Geodäsie, Technische Universität München, Arcisstraße 21, DE-80333 München*

The antenna phase center variations (PCV) of GNSS-satellites (GNSS: Global Navigation Satellite system) are traditionally estimated from the data of a terrestrial tracking network (e.g., from the International GNSS Service, IGS). These measurements are affected (among others) by tropospheric delay considered in the data processing procedure by models (e.g., GPT/GMF or ECMWF/VMF1).

In particular Systematic deficiencies of the mapping function could map into the PCV estimates. We will assess this phenomenon by comparing the resulting GNSS satellite antenna PCV corrections when using different troposphere models for processing the data from the ground network.

On the other hand, GPS-data collected by low Earth Orbiters (LEOs) are not affected by the troposphere. When using these measurements for computing GNSS satellite antenna PCV corrections other problems arise, e.g., the number of different antenna models is very limited, the data are affected by multipath from the LEO environment, and only GPS-satellites can be calibrated in this way so far. Nevertheless, the results from such an analysis seems also be useful to evaluate the impact of troposphere models on the GNSS satellite PCV corrections derived from a terrestrial network of tracking stations.

17.4

Geodetic water vapor monitoring campaign in Zermatt, summer 2010

Hurter Fabian¹, Geiger Alain¹, Perler Donat¹

¹*Institut f. Geodäsie u. Photogrammetrie, Schafmattstr. 34, 8093 Zürich (fabian.hurter@geod.baug.ethz.ch)*

Extreme rain events as the one that occurred in the Valais in October 2000, often cause large fatalities and economic losses. This motivates our research to understand and predict the location, time and intensity of heavy precipitation in a river's catchment area. In the classical approach, radar images are used to predict rain several hours ahead (radar nowcasting). Since high humidity in the atmosphere is a precursor of heavy rain, additional knowledge of the tropospheric water vapor distribution might support radar nowcasting. Processed data of a Global Navigation Satellite System (GNSS) receiver delivers information on integrated tropospheric water vapor. A receiver network then allows 3D retrieval of atmospheric water vapor from the integrated values. This so-called water vapor tomography has been a research focus of the Geodesy and Geodynamics Lab, ETH Zurich, for several years. Our recent activities include software development, longterm validation and a GNSS campaign.

The Zermatt area in the Mattertal was chosen as study area to investigate water vapor and its relation to rainfall in an alpine catchment area. As the mountainous topography has a strong influence on both, rainfall and associated water vapor distribution with structures at kilometer-scale, a dense measurement network was required. In the campaign setup, 33 geodetic GNSS receivers with an average inter-station distance of 2 kilometers and 4 additional low-cost receivers were deployed during one month in summer 2010. For validation of the water vapor retrieval by GNSS, 25 radiosondes were launched. The network was supplemented by a rain gauge transect (hydrology group of Prof. Burlando, ETH Zurich).

Data collection and processing issues of the campaign data are discussed and first results are presented. These include integrated water vapor path delays from the GNSS processing and their validation using radiosonde measurements and numerical weather model data. Also preliminary tomographic reconstructions will be shown and it will be shortly outlined, how the GNSS information can be used to better understand the devolution of rain events in an alpine region.

17.5

Gravity Field Determination at AIUB: From CHAMP and GRACE to GOCE

A. Jäggi¹, U. Meyer¹, L. Prange¹, H. Bock¹, R. Dach¹ & G. Beutler¹

¹*Astronomisches Institut, Universität Bern, Sidlerstrasse 5, CH-3012 Bern (adrian.jaeggi@aiub.unibe.ch)*

Gravity field recovery at the Astronomical Institute of the University of Bern (AIUB) is rigorously treated as an extended orbit determination problem, which avoids the introduction of any a priori gravity field information from the CHAMP-, GRACE-, or GOCE-era. The so-called Celestial Mechanics Approach is applied to GPS high-low satellite-to-satellite tracking (hl-SST) data of low Earth orbiters (LEOs), via the use of previously established kinematic LEO positions, to K-band low-low satellite-to-satellite tracking (ll-SST) data of the GRACE mission, and to gradiometer data of the GOCE mission.

We use CHAMP and GOCE hl-SST data to fully exploit the long wavelength part of the Earth's gravity field. We validate the derived gravity field models by performing LAGEOS orbit determination using Satellite Laser Ranging (SLR) measurements and demonstrate that GPS hl-SST gives access to high-quality estimates of the lowest degree coefficients. We also assess the contribution of GPS hl-SST to the recovery of time variable gravity signals and show that large-scale variations may be captured.

We present the latest release AIUB-GRACE03S based on 6 years of K-band ll-SST and GPS hl-SST data, consisting of a static gravity field resolved up to degree 160 and a series of monthly gravity field models resolved up to degree 60. We compare the AIUB-GRACE03S release with results from other research groups and assess the quality of the monthly solutions.

As opposed to the commonly applied filtering techniques for GOCE gravity field recovery based on gradiometer data, empirical parameters are set up in addition to the gravity field coefficients to absorb the non-physical part of the gradiometer measurements. We study the impact of different empirical parametrizations on the GOCE gradiometer solutions and compare them with solutions relying on empirically derived covariance information.

17.6

Ein permanentes GNSS-Netz zur Aufzeichnung tektonischer Bewegungen in der Nordschweiz

Salvini Dante¹, Studer Mario¹, Müller Herwig², Spillmann Thomas², Schnellmann Michael² & Brockmann Elmar³

¹BSF Swissphoto AG, Dorfstrasse 53, CH-8105 Regensdorf (dante.salvini@bsf-swissphoto.com)

²Nationale Genossenschaft für die Lagerung radioaktiver Abfälle NAGRA, Hardstrasse 73, CH-5430 Wettingen

³Bundesamt für Landestopografie swisstopo, Seftigenstrasse 264, CH-3084 Wabern

Das bisher bekannte Muster der grossräumigen neotektonischen Bewegungen und Verschiebungsraten in der Schweiz basiert auf Präzisionsnivellements (Schlatter 2007), GNSS Kampagnenmessungen (Schlatter & Brockmann 2010) sowie Daten des GNSS Permanentnetzes AGNES (Brockmann et al. 2006). Die niedrigen Deformationsraten stellen diese Messungen allerdings vor einige technische Herausforderungen. Die Nationale Genossenschaft für die Lagerung radioaktiver Abfälle (NAGRA) initiierte deshalb das Projekt NaGNet, um die bestehenden tektonischen Modelle mittels Langzeitbeobachtungen permanenter GNSS-Stationen zu verfeinern.

Das entworfene Messnetz weist einen Stationsabstand von ca. 12 – 32 km auf (Abb. 1). Die Stationen wurden auf den wichtigsten tektonischen Blöcken abseits von bekannten regionalen Störungszonen platziert. Daneben wurde eine möglichst regelmässige gleichmässige Netzgeometrie angestrebt.

Weitere Faktoren bei der Standortwahl waren eine bestmögliche Anbindung an das anstehende Festgestein bzw. die Stabilität (Rutschanfälligkeit) und Setzungsempfindlichkeit des oberflächennahen Untergrundes (u.a. im Bereich der Stationsfundamentierung), der freie Horizont und die Qualität der empfangbaren GNSS-Signale (z. B. Signal-Rauschverhältnis, Multipath).

Potentielle Standortbereiche wurden zuerst mit topographischen und geologischen Karten voreingegrenzt und anschliessend begangenen; geeignete Standorte wurden entsprechend eines detaillierten Kriterienkatalogs bewertet und ausgewählt. Die Tauglichkeit der Standorte bezüglich des Empfangs von GNSS-Signalen wurde mit einer Testmessung von mindestens 72 Stunden Dauer geprüft. Nach dem Einholen des Einverständnisses der betroffenen Eigentümer und der Erteilung der Bewilligungen durch die zuständigen Behörden, konnten die Stationen gebaut werden.

Die mit dem Bau und Betrieb der Stationen betraute BSF Swissphoto AG hat mittlerweile neun der elf geplanten Stationen realisiert (Abb. 1) und in Betrieb genommen (die ersten Stationen im Oktober 2010).

Für die tektonische Interpretation der gewonnenen Messdaten ist die Qualität der Gründung von entscheidender Bedeutung. Eine direkte Gründung auf Festgestein kann lokale Einflüsse z. B. durch gravitative Bewegungen verhindern. Wo eine direkte Fundierung auf anstehendem Fels nicht möglich war, wurde das Fundament mit drei bis zu 15 m tiefen Injektionsbohrpfählen im Anstehenden verankert. Zusätzlich wird zur Erfassung etwaiger lokaler Bewegungsphänomene halbjährlich eine vermessungstechnische Kontrollmessung von Lage und Höhe der Stationen bezüglich Rückversicherungspunkten durchgeführt.

Auf dem Fundament wurde ein 2.5 m hoher Eisengittermast aufgeschraubt, der die GNSS-Antenne trägt (Abb 2). Das GNSS-Equipment an jedem Standort umfasst eine Choke-Ring GNSS-Antenne vom Typ Leica AR25 und einen GNSS-Empfänger von Typ Leica GRX-1200+. Neben dem Empfänger wurden die verschiedenen Komponenten zur Stromversorgung und für die Datenübermittlung in einer thermisch isolierten Kabine untergebracht. Bis zu einer mittleren Leitungslänge von 400 m wurden Kabel zur Strom- und Datenübertragung installiert. Wo dies nicht möglich war, liefert eine Photovoltaikanlage den Strom und die Daten werden über das GSM-Netz übertragen.

Die GNSS-Positionsdaten werden mit 0.1 s und 30 s Messintervall aufgezeichnet und in zwei Pufferspeicher geschrieben. Die hochauflösenden 0.1 s Daten werden nur lokal zwischengespeichert und können bei Bedarf (z.B. Analyse von co-seismischen Bewegungen) abgerufen werden. Die Übertragung der 30 s Daten erfolgt automatisch jede Stunde auf einen zentralen Rechner, wo die Daten auf Vollständigkeit und Qualität überprüft werden. Die aktuellen Resultate dieser automatischen Auswertung können auf einem web-basierten Kundenportal abgerufen werden. Sie dienen auch der Netzüberwachung und informieren bei Datenausfall oder ausserordentlichen Verschiebungsraten das zuständige technische Personal mit Email und SMS.

Die qualitätsgeprüften Rohdaten fliessen zum Rechenzentrum PNAC von swisstopo, wo sie zusammen mit den GNSS-Daten der AGNES-Stationen ausgewertet werden. Die präzisen Modelle, welche der Bernese-Software zu Grunde liegen, erlauben die Berechnung von hochgenauen Standortkoordinaten als Stunden-, Tages- oder Wochenlösungen. Die Wiederholbarkeit der bisher für die NaGNet-Stationen berechneten Wochenlösungen ist im Allgemeinen besser als 1 mm in der Lage und 2-3 mm in der Höhe. Diese Resultate werden in einigen Jahren zur Verfeinerung der bestehenden Modellvorstellung der neotektonischen Bewegungen in der Nordostschweiz beitragen.

REFERENZENZEN

- Brockmann, E., Grünig, S., Ineichen, D. & Schaer, S. (2006): Monitoring the Automated GPS Network of Switzerland AGNES. In: Torres, J.A. & Hornik, H. (Eds.): Rep. on the Symp. of the IAG Sub-commission for Europe (EUREF) in Riga, 14-17 Juni 2006, EUREF Publication No 16, pp. 176-83.
- Schlatter, A. & Brockmann, E. (2010): Dritte Wiederholungsmessung im GNSS-Landesnetz LV95, Messkampagne und erste Resultate. Swisstopo Kolloquium 1. April 2011. <http://www.swisstopo.admin.ch/internet/swisstopo/de/home/docu/Kolloquien/110401.parsys.14332.downloadList.31708.DownloadFile.tmp/chtrf2010teil2200.pdf>.
- Schlatter, A. (2007): Neotektonische Untersuchungen in der Nordschweiz und Süddeutschland. Kinematische Ausgleichung der Landesnivellementlinien CH/D. Nagra Arb. Ber. NAB 07-13.

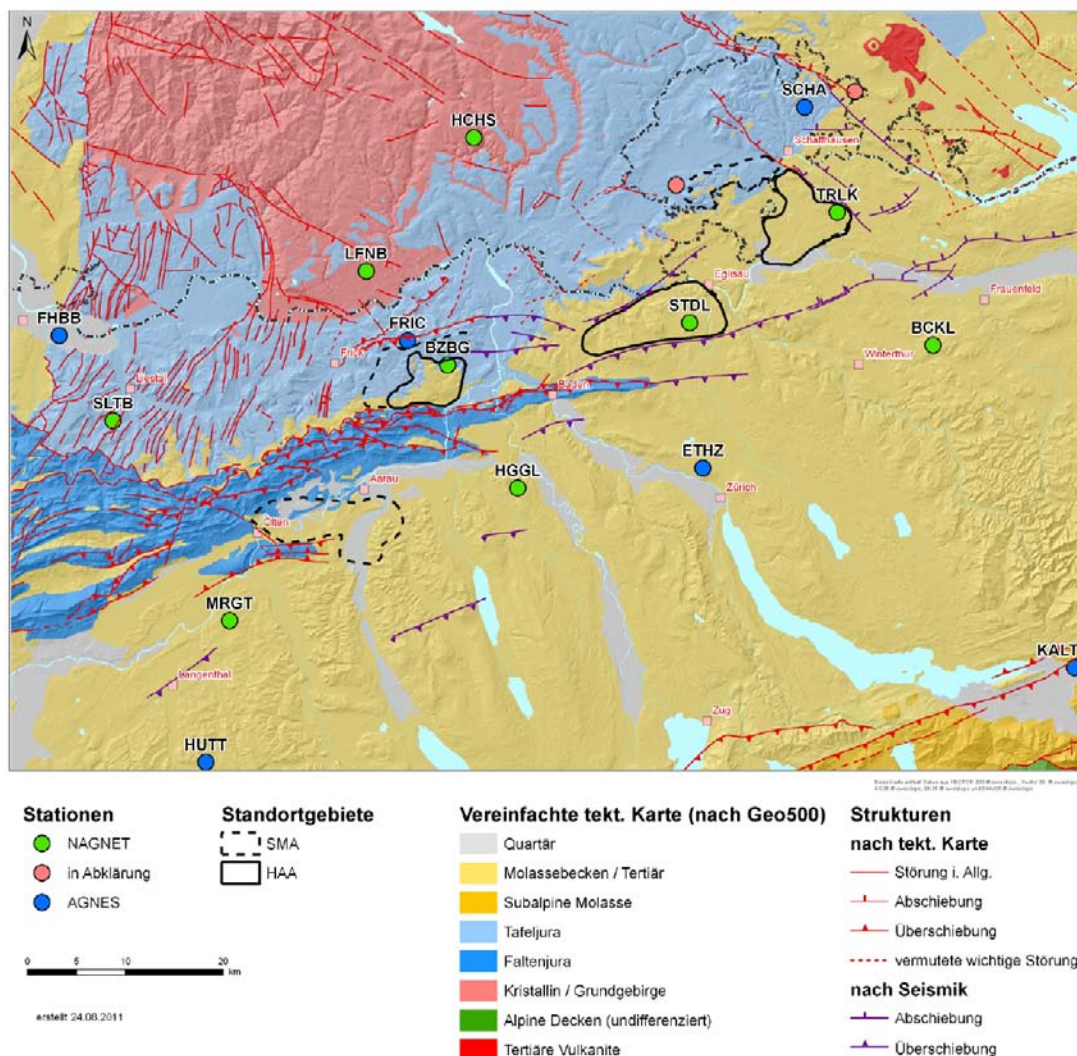


Abb. 1. Vereinfachte tektonische Karte und Verteilung der NaGNet- (grün) und AGNES-Stationen (blau) im Projektgebiet. Rot: NaGNet Standorte in Abklärung. Zur Orientierung sind die in der Nordostschweiz liegenden Standortgebiete für geologische Tiefenlager für schwach- und mittelaktive (SMA) sowie hochaktive (HAA) Abfälle eingezeichnet.



Abb 2. Eine fertig gestellte NaGNet-Station.

17.7

Positioning improvements with stochastic clock modelling

Wang Kan¹, Rothacher Markus¹Institute for Geodesy and Photogrammetry, ETH Zürich, Schafmattstr. 34, 8093 Zürich (wangk@ethz.ch)

The synchronization of the receiver clock with the satellite clocks is always an integral task of GNSS positioning. In current GNSS applications, all receiver clocks are typically determined for every measurement epoch to reach a high positioning precision. The fact that the clocks, especially very good clocks, do not jump by arbitrary values from one epoch to the next is hardly used at present. Making optimal use of the quality of the receiver clocks should, therefore, stabilize the solutions significantly and improve the positioning results.

Experiments with kinematic solutions for static stations equipped with H-Maser clocks have confirmed this. To access the achievable improvement, the least square adjustment algorithmus have been modified to allow for constraints between clock values of subsequent epochs. The weight of the relative constraint and the receiver clock quality are the essential factors for an improvement in the kinematic solutions. We will present first results of the investigation with different relative constraints on very good clocks showing that appropriate constraints improve the precision of the estimated kinematic coordinates, especially in the less accurate vertical direction, bis up to a factor of two. The improved performance of kinematic solutions is evaluated in detail and the benefit for the real-time monitoring of crustal deformation and earthquakes will be discussed.

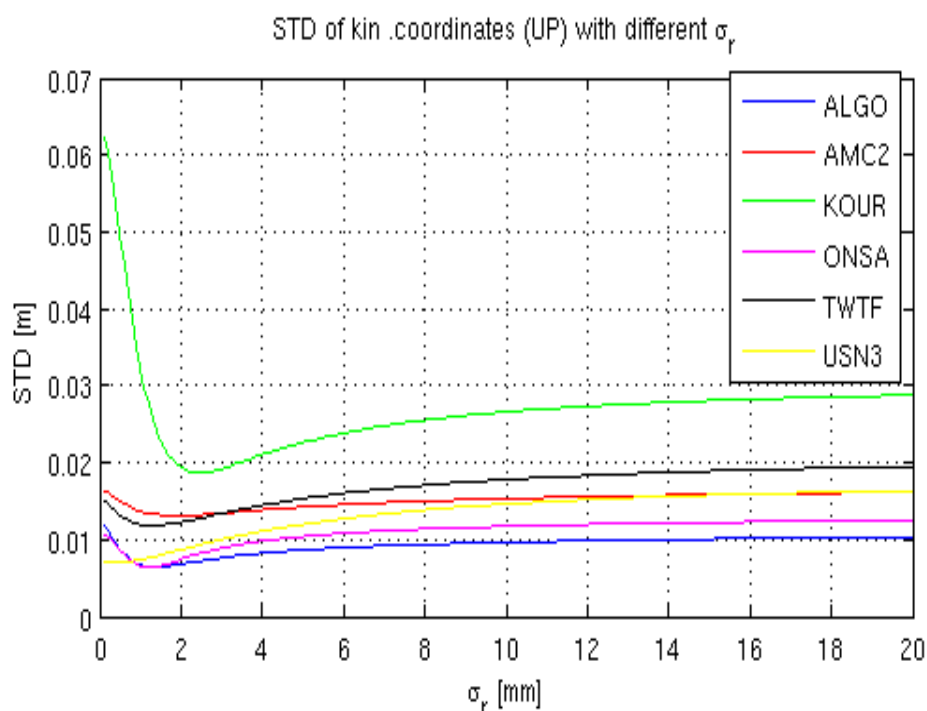


Figure 1. Repeatability of kinematic coordinates (height) using relative constraints $\sigma_r \sigma_r$ between subsequent epochs for clock parameters for some H-Maser clocks. X-axis represents the relative constraint $\sigma_r \sigma_r$ applied. As the constraint get smaller i.e. stronger the precision of the kinematic coordinates improves significantly per 5 minutes until an optimum is reached at about $\sigma_r \approx 1 \text{ mm}$.

REFERENCES

Dach, R. & Hugentobler, U. & Fridez, P. & Meindl, M. 2007: Bernese GPS Software Version 5.0. Astronomical Institute, University of Bern.

P 17.1

Permanent monitoring of rock glaciers with low-cost GPS

Limpach Philippe¹, Geiger Alain¹, Beutel Jan², Buchli Bernhard², Wirz Vanessa³, Gruber Stephan³

¹*Institute of Geodesy and Photogrammetry, ETH Zurich, CH-8093 Zurich (limpach@geod.baug.ethz.ch)*

²*Computer Engineering and Networks Laboratory, ETH Zurich, CH-8092 Zurich*

³*Department of Geography, University of Zurich, CH-8057 Zurich*

Since winter 2010/2011, a network of permanent GPS stations is being set up in the Matter Valley in the framework of the X-Sense project, currently totaling 20 stations. X-Sense is an interdisciplinary project for monitoring alpine mass movements at multiple scales, funded by the Swiss federal program Nano-Tera. The X-Sense stations consists of low-cost GPS receivers coupled with inclinometers. Some prototype stations allow for on-line data transmission.

The geodetic potential of low-cost GPS receivers for the precise monitoring of slope instabilities in mountain areas was previously investigated in a feasibility study. Based on a small GPS test network operated on Dirru rock glacier, Matter Valley, since June 2009, it was shown that low-cost GPS units are able to provide reliable and continuous time series of surface displacements at cm-level accuracy, using adequate differential processing techniques.

Enhanced algorithms were developed to derive accurate time series of surface velocities based on the GPS displacements. It was shown that the low-cost GPS receivers allow to reliably observe surface velocities even below 1 cm/day, as well as to detect small and short-term velocity changes. In addition, the time series of more than 2 years obtained from the test network reveals the capability to detect seasonal velocity variations, as well as inter-annual variations of the velocity pattern. By providing continuous observations of surface motion, the GPS-based permanent monitoring contributes to the understanding of processes linked to permafrost-related slope instabilities.

P 17.2

Displacement detection on rock glaciers using webcam images: A case study in the Mattertal

Fabian Neyer¹, Reynald Delaloye²

¹*Institute für Geodäsie und Photogrammetrie, ETH Zürich, Schafmattstrasse 34, CH-8093 Zürich (fabian.neyer@geod.baug.ethz.ch)*

²*Departement of Geosciences - Geography, University of Fribourg, Chemin du Musée 4, CH-1700 Fribourg*

Several fast moving rock glaciers in the Mattertal Valley, Switzerland, are exposed to intensive studies due to their possible harmful impact on human infrastructures. Historical but also very recent events show the high activity of the relatively fast moving rock masses. In order to understand possible correlations between environmental changes and the rock glacier behavior, displacement mapping is a good method to analyze these interactions. Over the last two years, several webcam observation platforms were installed by the University of Fribourg which deliver images of several rock glacier tongues on a relatively high sampling rate.

This work presents first results of motion detection based on webcam images taken over several months. Because of the coarse surface structures of the rock glaciers and hence the good small scale gradients in the images, feature tracking is the preferred method for the optical flow estimation. By applying a subpixel accuracy detection algorithm, highly accurate velocity fields can be extracted.

Due to an accuracy estimate of the displacement detections, a robust algorithm for outlier identification can be applied to clean the data. Having a clean dataset allows to compute displacement trajectories as well as strain and stress components of individual areas of the rock glacier.

By analyzing image sequences, the behavior of temporal and spatial variations of the rock glacier surface displacements can be studied. This is a fundamental data basis which might result in new insights of the complex behavior and interaction between a rock glacier and its environment.

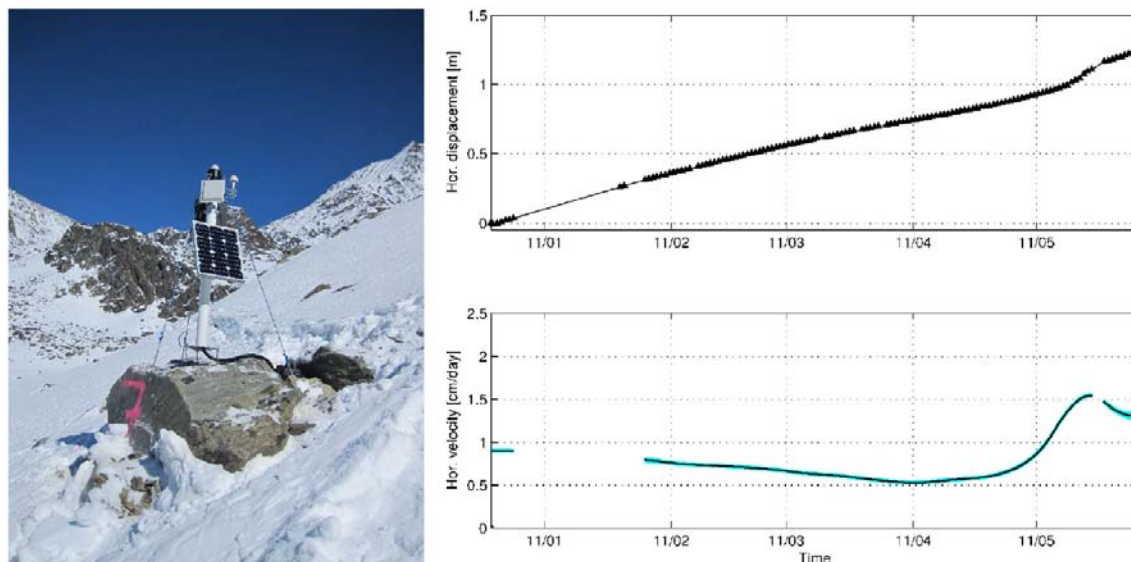


Figure 1. Example of an X-Sense GPS station at Dirru rock glacier, Matter Valley, with horizontal displacement and velocity as a function of time (year/month), from December 2010 to June 2011.

P 17.3

Improving sub-daily solutions of single-frequency GPS using antenna PCV

Su Zhenzhong, Limpach Philippe, Rothacher Markus, Geiger Alain

Institute of Geodesy and Photogrammetry, HPV G51, Schafmattstr. 34, CH-8093 Zurich (zhenzhong.su@geod.baug.ethz.ch)

Nowadays, GPS positioning is widely used as an efficient tool for mass movement monitoring. Geodetic-grade GPS equipment can easily achieve centimetre positioning accuracy in real-time and sub-centimetre accuracy in post-processing mode. However, deploying geodetic-grade equipment in hostile areas, like landslide or rock-glacier areas, is too expensive because of the high risk of damaging instruments due to rock fall, landslides, etc..

Meanwhile the investigation and research on low-cost, single-frequency GPS technology shows the possibility to provide an economical solution with a positioning accuracy comparable to geodetic-grade products. Therefore in the project X-Sense, low-cost, single-frequency GPS antennas and receivers are used and densely mounted in hostile areas.

The main factors that degrade the accuracy of low-cost, single-frequency GPS equipment are ionospheric delay, multipath, antenna PCV (phase center variations) and others. Investigations of each individual factor shall be carried out and algorithms for solving the problems shall be developed for short baseline processing, in order to achieve a high accuracy with a near real-time, single-frequency GPS positioning technique.

The influence of PCV is prominent especially for sub-daily coordinate resolution because of the satellite constellation change. In the first phase of the study, the PCV of the low-cost, single-frequency antennas are modelled and applied to test runs (using a 24-hour set of data with a 30-second time interval and baseline lengths around 15 meters) for computing 2-hour solutions. The result is shown in Figure 1. By applying antenna PCV, the RMS is improved by 57.68% in north, 28.95% in east and 49.30% in up direction (see Table 1).

Axis	RMS (Solution without PCV)	RMS (Solution with PCV)	Improvement
N [mm]	1.8	0.78	57.68%
E [mm]	1.6	1.1	28.95%
U [mm]	5.5	2.8	49.30%

Table 1. RMS of the estimated coordinates in north, east and up direction for both solutions with and without the applying of antenna PCV.

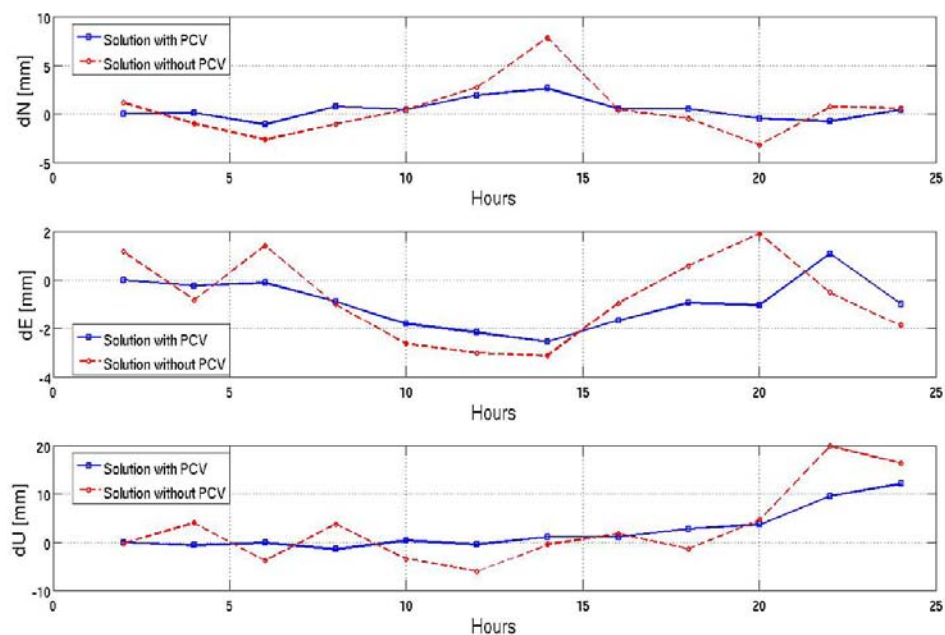


Figure 1. Time series of 2-hour solution (north, east and up) with and without applying antenna PCV

REFERENCES

- Geiger, A., 1988: Modeling of Phase Center Variation on its Influence on GPS Positioning, International GPS-Workshop, Darmstadt, FRG, April, 11-13, 1988
- Rothacher, M., Schaer, S., Mervart, L., & Beutler, G. 1995: Determination of Antenna Phase Center Variations Using GPS Data, Proceedings of the IGS Workshop "Special Topics and New Directions", Potsdam, May, 15-18, 1995, Gendt, G. / Dick, G., pp. 205-220, GeoForschungsZentrum Potsdam, Potsdam.
- Schwieger, V., 2009: Accurate High-Sensitivity GPS for Short Baselines, FIG Working Week 2009, Eilat, Israel, May, 3-8, 2009

P 17.4

SWISS 4D: Estimation of the tectonic deformation field of Switzerland based on GPS measurements

Villiger Arturo¹, Geiger Alain¹, Marti Urs² & Brockmann Elmar²

¹ Institute for geodesy and photogrammetry, ETH Zurich, Schafmattstrasse 34, CH-8093 Zurich (villiger@geod.baug.ethz.ch)

² Federal Office of Topography swisstopo, Seftigenstrasse 264, CH-3084 Bern

In 2010 the federal office of topography, swisstopo, carried out a GNSS measurement campaign for the CHTRF 2010. The measurements cover whole Switzerland and lead to an updated set of velocity data on more than 230 points. This dense network allows to search for tectonic deformations even though the magnitudes of deformation are very small. Velocities relative to station Zimmerwald are mostly below 1 millimeter per year. The small velocities increase the importance of separate the deformation into local and regional effects as both are of similar magnitude. The latter are assumed to represent the ongoing tectonic processes whereas local effects might be caused by landslides or monument instabilities.

To obtain a continuous velocity field representing the tectonic deformations from the noisy velocity data an adaptive least square collocation is used. It allows to extract a statistically significant velocity field separating tectonic and local deformation parts. This is achieved assuming tectonics is correlated over wider area whereas local effects are only correlated within a smaller area. Apart from the separation between the two effects the tectonic model is estimated introducing adjustments to the trend metric. Therefore, areas with high strain rates are decorrelated in an iterative process. This processing allows to extract information about the deformation field identifying regions with higher strain rates than surrounding areas.

P 17 5

Investigating the reliability of kinematic source inversion with dynamic rupture models and high rate GNSS data

Youbing Zhang¹, Seok Goo Song¹, Luis Angel Dalguer¹, John Clinton¹ and Simon Häberling²

* Institute of Geophysics, ETH Zurich

² Institute of Geodesy and Photogrammetry, ETH Zurich

An essential element of understanding the earthquake source processes is obtaining a reliable source model via geophysical data inversion. However, the epistemic uncertainties in the kinematic source inversion produce a variety of source models estimate for any given event. Thus, as done in the Source Inversion Validation (SIV) project, it is important to validate our inversion methods with synthetic data by testing forward Green's function calculation and comparing various inversion methods. Spontaneous dynamic rupture modeling, that incorporates conservation laws of continuum mechanics and constitutive behavior of rocks under frictional sliding, is capable of producing physically self-consistent kinematic description of the fault and its associated seismic wave propagation resulting in ground motions on the surface. Here we develop accurate dynamic rupture simulation of a vertical strike slip fault. Our source model is composed by well-defined asperities (patches of large stress drop) and we assume that fault rupture is governed by the linear slip weakening friction model. The resulting near-source ground motion dominated by low frequency (up to 1Hz) is used for testing our inversion method. We performed various inversion tests and compared estimated solutions with true solutions obtained by the forward dynamic rupture modeling. Our preliminary results show that estimated model spaces could be significantly perturbed, depending on data and modeling schemes used in the inversion, not only in terms of spatial distribution of model parameters, but also in terms of their auto- and cross-correlation structure. The Bayesian approach in source inversion becomes more and more popular because of the recent common availability of high performance computing capabilities. We adopted the Bayesian approach in our source inversion test, so that we can more effectively analyze the uncertainty of estimated models and also implement physically guided regularization in the prior. In addition, the recent emergence of high-rate Global Navigation Satellite Systems (GNSS) data can considerably improve the observation capabilities for dynamic surface movements (sampling up to 100 Hz) during large earthquakes. GNSS receivers are used to accurately measure both dynamic and static ground displacements without saturation or sensitivity to tilt and with a sampling interval below 1 second and sub-centimeter accuracy across the frequency spectrum. We expect that we can resolve an issue of relative weighting we often face in multiple data inversion, i.e., joint inversion of both geodetic and seismic data, by inverting ground displacement data recorded by the GNSS receivers.

18. Advances in GIScience and Remote Sensing

Michael Schaepman, Robert Weibel, Ross Purves, Markus Rothacher, Konrad Schindler

*Swiss Commission for Remote Sensing,
Interuniversitäre Partnerschaft für Erdbeobachtung und Geoinformatik (IPEG)*

TALKS:

- 18.1 *Breschan J., Heinimann H. R., Niederhuber M.:* Automatic identification of forest treatment units using LiDAR-data
- 18.2 *Demir N., Baltsavias E.:* Automated modelling of 3D building roofs using LIDAR and image data
- 18.3 *Derungs C., Purves R.:* Identifying and disambiguating toponyms
- 18.4 *Henke D., Meier E.:* Initial results of a low-frequency 3D-SAR approach for mapping glacier volumes
- 18.5 *Leinß S., Hajnsek I.:* Sensitivity of X-band SAR interferometry on the snow pack characterisation
- 18.6 *Waser, L.T., Ginzler, C, and Kuechler, M.:* Large-Area Tree Species Classification – Potential And Limits Of Airborne Digital Sensor (Ads40/80) Data For The Swiss Nfi

POSTERS:

- P 18.1 *D’Odorico P., Hueni A., Jehle M., Schaepman M.:* Recent efforts on APEX Calibration and Validation
- P 18.2 *de Jong R., Verbesselt J., Schaepman M.E., de Bruin S.:* Short-term variability within long-term trends in global vegetation activity
- P 18.3 *Saurer O., Baatz G., Köser K., Pollefeys M.:* Visual Localization Recognition and Photo-to-Terrain-Alignment in Mountainous Areas
- P 18.4 *Schubert A., Small D., Jehle M., Meier E.:* Long-term geolocation accuracy of TerraSAR-X high-resolution spotlight products
- P 18.5 *Torabzadeh H., Morsdorf F., Schaepman M.:* Data fusion methods of LiDAR and spectroscopy data for the derivation of forest biochemical and biophysical variables – a review
- P 18.6 *Weyermann J., Damm A., Kneubühler M., Schaepman M.:* Ross-Li BRDF correction of airborne imaging spectroscopy data for improved continuous field map generation in the Swiss National Park
- P 18.7 *Yáñez-Rausell L., Malenovsky Z., Schaepman M.:* Influence of gap fraction on coniferous needle optical properties measurements
- P 18.8 *V.L. Mulder, S. de Bruin, M.E. Schaepman:* Towards spectroscopic modelling of composite mineralogy

18.1

Automatic identification of forest treatment units using LiDAR-data

Breschan Jochen¹, Heinemann Hans Rudolf¹ & Niederhuber Monika¹

¹Institut für Terrestrische Ökosysteme ITES, ETH Zürich, CHN K73.1, CH-8092 Zürich (jochen.breschan@env.ethz.ch)

The management of forests requires the delineation of treatment units. Forest stands traditionally serve as treatment units. They are characterized by their stage-of-development (SoD). The SoD is classified into the six categories that represent ranges of the median diameter-at-breast-height (DBH) of the tallest trees within a forest stand (Schütz 2003). In the past, this delineation process was carried out by hand, i.e., using stand information gained from terrestrial inventories. However, the application of such an approach has become too expensive in the recent decades.

Here, we present an automated method of stand delineation that uses a spatially explicit forest inventory computed from high resolution LiDAR (Light Detecting And Ranging) surface- and terrain data. It is captured as a flow chart in Figure 1, that is structured into a forest inventory- and a stand delineation module.

The forest inventory module starts with the extraction of single trees on a Canopy Height Model (CHM, cell size 0.5 m) that was previously computed from the digital surface- and terrain model (DSM, DTM). Tree extraction algorithms have been widely studied in the recent decade (e.g., Kaartinen (2008) gives an overview on the performance of nine extraction methods). Here, we employ an algorithm inspired by Hyypäe (2001) that locates single trees at the local maxima of a filtered CHM. The biometric key figures, tree height and tree diameter, are then estimated based on the CHM.

The stand delineation module generalizes the forest inventory information, aiming to identify homogenous forest stands (i.e., aggregation of adjacent trees having a similar DBH). A fuzzy inference system first assigns the SoD to each tree based on its biometric key figures. This includes a DBH estimation as a function of tree height and crown diameter, using transfer functions (Ye 1995). The stand delineation is then processed based on the resulting "SoD-per-tree" raster by using a filter-method. It identifies the SoD with respect to the tallest trees (according their SoD-category) within the filter window for each cell on the grid raster.

This model has been implemented in Matlab, and was carried out on a coniferous forest in the Canton of Grisons. First results indicate that the method plausibly classifies the single trees according to the SoD. Stand delineation using the filter method retrieves plausible forest stands for filter windows $\geq 800\text{m}^2$. However, the perimeters of the single stands are zig-zag shaped and require more generalization to serve as operational treatment units. We are currently working on a clustering-approach that may overcome the shortcoming of the filter-method.

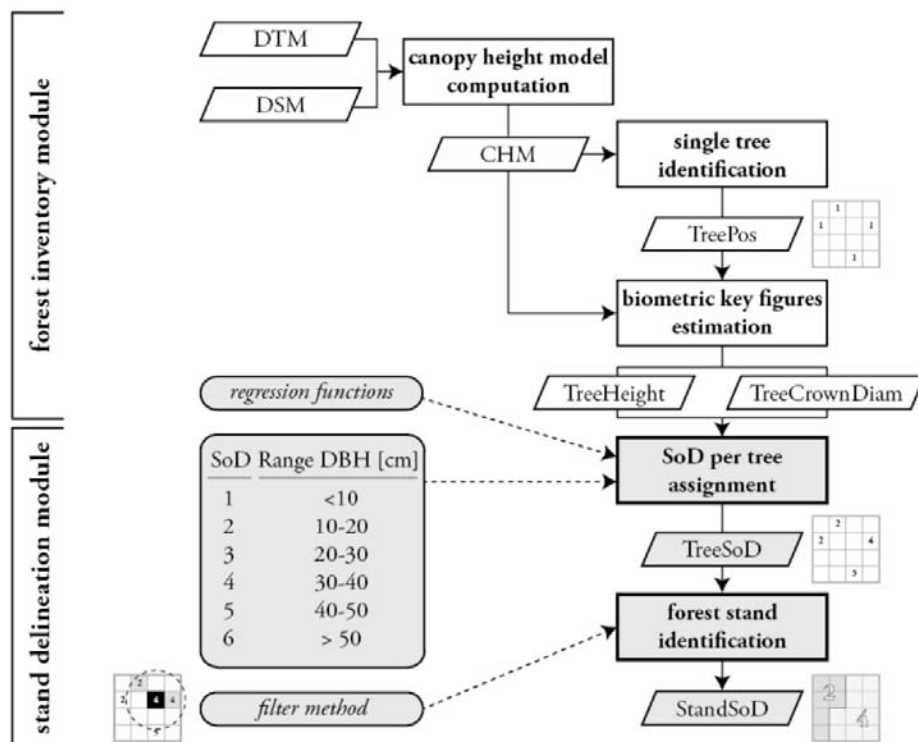


Figure 1. Model conceptualization of the automatic stand delineation method, consisting of a forest inventory- and a stand delineation module. The former module extracts single trees on a CHM raster grid and assigns biometric key figures. The latter module classifies each tree into its corresponding stage-of-development (SoD), and then aggregates the single trees into forest stands using a filter-method.

REFERENCES

- Hyypäe, J., et al. 2001. A segmentation-based method to retrieve stem volume estimates from 3-d tree height models produced by laser scanners, *IEEE Transactions on Geoscience and Remote Sensing*, 39, 969– 975.
- Kaartinen, H., et al. 2008: Accuracy of automatic tree extraction using airborne laser scanner data, *Proceedings of SilviLaser 2008: 8th international conference on LiDAR applications in forest assessment and inventory*, 467-476.
- Morsdorf, F., et al. 2004: LIDAR-based geometric reconstruction of boreal type forest stands at single tree level for forest and wildland fire management, *Remote Sensing of Environment*, 92, 353-362.
- Schütz, J.-P. 2003 : *Waldbau I – Die Prinzipien der Waldnutzung und der Waldbehandlung*, <http://www.wm.ethz.ch/docs/document/fm1>.
- Ye, R. 1995: *Waldsimulation auf der Basis automatischer Luftbildmessung und unter Kontrolle von GIS*, *Mitteilungen der Abteilung für Forstliche Biometrie* 95-1, Freiburg i. Brsg.

18.2

Automated modelling of 3D building roofs using LIDAR and image data

Demir Nusret¹, Baltsavias Emmanuel¹

¹ *Institute of Geodesy and Photogrammetry, ETH Zurich, 8093, Switzerland (demir,manos@geod.baug.ethz.ch)*

In this work, an automated approach has been developed for 3D roof modeling. The method consists of two main parts; the first one is the detection and the second is modeling of the roofs. A raw LIDAR point cloud with 5pts/1sqm resolution and DMC digital camera images with 8 cm GSD have been used for testing the developed methods.

For the detection of buildings, four different approaches are used and combined for achieving the best detection result. In the first approach, a slope-based morphological filter is used to detect all off-terrain objects (which include buildings, trees and other objects) using a DSM from image matching. After that, the trees are eliminated by unsupervised classification of the NDVI image. The second approach is based on a multispectral classification refined with height information from LIDAR data. In the third approach, above-terrain objects are detected from LIDAR data and the vegetation is eliminated using NDVI classification. The last approach is based on the detection and elimination of the trees using the vertical density of the raw LIDAR data. The results from the four alternative approaches are combined with Boolean operations in accordance with their advantages. The correctness of the detection has been calculated as 90% with 17% omission error. The detected regions are enlarged a bit to include, if possible, all points which belong to the roofs.

For the modeling part, the process chain starts with detection of planar features using the RANSAC approach using the LIDAR data in the previously detected building regions. Since the plane detection is a parameter sensitive approach, the detected planes are refined according to the neighborhood of the LIDAR points. During the refinement process, the distance of every point has been calculated to the assigned plane of the neighboring point. If the distance is in a certain threshold, (in our case it has been set as 0.2 m, the accuracy of LIDAR points), the plane assignment of the point has been changed to the plane of the neighboring point if its size is bigger than the actual plane size. After this refinement process, region growing is applied to split the over-segmented planes. In the next step, the planes are classified as wall, terrain and roof planes based on their slope and their relative height from the terrain surface. Existing neighboring tree points are eliminated by vertical density analysis. After that, only the roof points are used for the modeling approach. The alpha shape algorithm is used in the reconstruction of the roof outlines.

3D line segments from edge matching of stereo images are used to increase the positional accuracy and to eliminate the irregularity of the outlines. To generate 3D line segments, 2D line segments are extracted and matched across multiple images (Ok et. al. 2009). Additionally, the intersection edges are extracted from the intersection of the roof surfaces. 3D lines are assigned to the plane surfaces whenever they fit them within a certain distance threshold. Then the neighboring LIDAR points to 3D lines are eliminated and the alpha shape algorithm is applied again to generate the roof outlines. Since the 3D lines can not be fully extracted for all buildings, the final regularization of the roof polygons are needed.

For this regularization, the RANSAC approach is used to fit the roof outlines to the straight lines and all fitted lines are intersected between each other. The intersection points which are closest to the first generated roof outlines are selected as roof corner points. The consecutive points are converted to the line features, if their turning angle is not an acute angle. Then, LIDAR points which are neighbors to the generated line features are deleted and the line features are added into the set of LIDAR points. The alpha shape algorithm is applied again and final 3D roof models are generated.

3D reference data is measured manually using DMC images. It is used for assessing the accuracy of the generated roof models. A set of criteria are considered for the comparison of the models. The first criterion is defined as the area of intersection of the models in union of the models. The second criterion is called as correctness, and is obtained by finding the intersection area of the models in the modeled roof model. The third one is called completeness. It is the area of the intersection of the models in the reference roof model. The fourth criterion is the average absolute distance, and the last one is the shifts in x,y,z between the models. The pairs for the comparison between the generated roof models and the reference models are defined according to the maximum value of the first criterion.

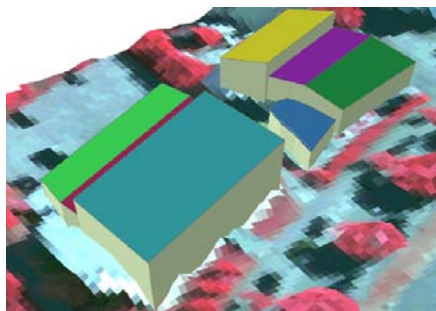


Figure 1. Some examples from the generated roof models

REFERENCES

- Demir, N., & Baltsavias., E., 2010. Use of image and laser scanning data for building detection., in APRS, Vol. 38, Part 4., Orlando, USA, 7 pp., on CD.
- Ok, A.O., & Wegner, J.D., & Heipke, C., & Rottensteiner, F., & Soergel, U., & Toprak, V.:2010. A new straight line reconstruction methodology from multi-spectral stereo aerial images, in IAPRS vol. 38, part 3A, Paris, pp. 25-30

18.3

Identifying and disambiguating toponyms

Curdin Derungs and Ross Purves

Department of Geography, University of Zurich, Winterthurerstrasse 190, CH-8057

Toponyms are place names or named spatial entities. We are all familiar with them through their use on topographic maps and in everyday language. A statement such as: “Ich bin beim Dynamo am baden” is a typical example of the use of toponyms. They are the most natural way that people explicitly refer to locations in space, and allow us to deal well with ambiguity and uncertainty. They are not only found in speech, but also in written text and thus recognition of toponyms in documents is a key way of linking written language to explicit coordinates through the use of lists of toponyms and their associated geographic coordinates.

A number of disciplines, including Natural Language Processing and Geographic Retrieval are concerned with the question of correctly identifying toponyms in text. For instance, in the example given above we must distinguish between a *Dynamo* used to power our bike lights and *Dynamo*, the restaurant on the Limmat. In this example the things that we explicitly know about ‘Dynamo’, together with the context of the sentence, help us find an adequate answer. Another hint for could be a vague understanding of where, geographically speaking, ‘Ich’ is assumed to be and that the place ‘Dynamo’ is likely to be visited by this person to go swimming. In a nutshell: to solve this problem in an everyday sense we use both the text and contextual knowledge we have about the place and the activity being described.

To date, most methods addressing identification of toponyms have used relatively simple methods, such as population or position in administrative hierarchies to distinguish between different instances of the same toponym (so called geo-geo ambiguity – are we referring to London, England or London, Canada) and other contextual information to distinguish between geo-non geo ambiguity (am I in the bath or going to the city of Bath near Bristol)?

Spatial granularity (does the toponym describe a rock in the Engadine or a city) has received limited attention. However, if we wish to correctly resolve toponyms, it is clear that we must consider whether a document describes the history of the last bear to be shot in Val Mingèr or a journey from Basel to Luzern. Val Mingèr and the surrounding alps, forest and mountains are unknown to most people, even in a small country like Switzerland. We do not know a lot about all these places and little explicit knowledge can be found in accessible data sources about candidate toponyms. By contrast, for a journey between Basel and Zürich we have much more knowledge about not only these cities, but what is found on the journey and this information can be used when deciding if Zürich or Basel are toponyms and if so which locations they are likely to refer to.

Within our work we try to address the issue of missing toponym knowledge by using other, mostly geographic, sources. The basic assumption is that toponyms that co-occur in a document have something in common. The more closely they co-occur the greater the similarity. Previous work has shown that geographic proximity (Euclidean distance) is one such measurement. Alternatively, we might search for a toponym using a search engine and use the number of responses as a basic measure of common a toponym is. This already is a very helpful piece of information as we can assume that the toponyms used in a document follow some predictable patterns, rather than being random (e.g. one fixed level of famousness, like Zürich, Basel, Bern or a constant zoom from famous to unknown toponyms, e.g. Dynamo in Zürich). One example of a more geographic and novel type of context that we can add to toponyms takes the form of geomorphometric scope. Here we explore the geomorphometry of candidate toponyms, again with the expectation that similar toponyms might be found in similar settings (e.g. the cities of Zürich and Basel in predominately flat areas, and locations around Val Mingèr in steeper, more rough terrain). In our talk we will illustrate how the combination of such knowledge can be used in the resolution of toponyms, and help to disambiguate between toponyms particularly for fine-grained cases where other knowledge such as population or web prominence is not available.

18.4

Initial results of a low-frequency 3D-SAR approach for mapping glacier volumes

Daniel Henke, Meier Erich

Remote Sensing Laboratories (RSL), University of Zurich, Winterthurer Strasse 190, CH-8057 Zurich, Email: daniel.henke@geo.uzh.ch

In the context of natural hazard prevention and water management, climate change and sea level predictions (Solomon, 2007), the retention of water in glaciers is a key factor. In traditional approaches, the ice thickness of glaciers is either roughly approximated by extrapolating field measurements (drilling or Ground Penetrating Radar) or by a set of empirical or physically based relationships as e.g. mass conservation and principles of ice flow dynamics (Farinotti, 2009). In recent years, remote sensing in general and SAR specifically (Prats, 2007) contributes to precise large-scale measurements of glacier parameters. However, these methods are all restricted to the top layer of the glacier and information about its volume can only be derived indirectly from methods described above. In this paper, we present preliminary results of a 3D-SAR processing approach using low-frequency radar waves capable of penetrating the glacier ice up to a certain depth. 3D-SAR in other applications has been shown to provide accurate height estimates using techniques ranging from interferometry and cross correlation in circular tracks (Oriot, 2008) to tomographic processing of dual-pol data (Frey, 2008). However, the data for this study come from a campaign with a low-frequency SAR system (i.e. CARABAS sensor operating at center frequency of ~50 MHz) in 2003 over the Aletsch Glacier area, Switzerland, and were originally not acquired for 3D applications. Based on only these few, arbitrary flight tracks a method to calculate the height of the maximal backscattering response in the glacier ice and to approximate its volume was developed demonstrating the potential of SAR for mapping glacier volumes.

To generate a 3D estimate of the glacier bed, first a 3D reconstruction grid matrix is initialized with the Digital Elevation Model (DEM) values at the top layer in z-direction. Then for each flight track a 3D time-domain back-projection algorithm calculates for each voxel an intensity value as a standard 2D back-projection algorithm (Frey, 2008) does it for each pixel. We introduce an additional processing step to account for the refractivity of the glacier ice. Consequently, at each radar pulse of the flight track the points of entry at the glacier surface have to be determined. We make use of the spatial and temporal interrelationship between adjusted pixels to achieve computational efficiency. The absolute values of the result-

ing 3D-matrices for each flight track are multiplied to incoherently merge the single track results to one voxel image. For the common and generally more precise coherent adding the number of tracks and the orientation of the flight pattern are not appropriate. The maximal value in each z-column of the final, merged matrix corresponds to the maximum backscattering response of the radar signal and thus indicates the height of a potential glacier bed. Finally, we apply a low-pass filter to suppress noise effects and get a smooth, more realistic estimate of the surface.

This method was applied to a 5x5 km² test site over the Konkordiaplatz with a horizontal resolution of 5m and a vertical resolution of 15m. Results are illustrated in Fig. 1. While for the snow and ice free surface (e.g. mountain tops) the highest backscattering response can be found in the top layers, in the glacier ice the low-frequency radar waves penetrate into the ice. It still has to be investigated whether the backscattering maxima is indeed caused by the bedrock or by other factors like a significant amount of moraine material, an unfavorable combination of crevasses, processing artifacts or poor signal-to-noise ratio.

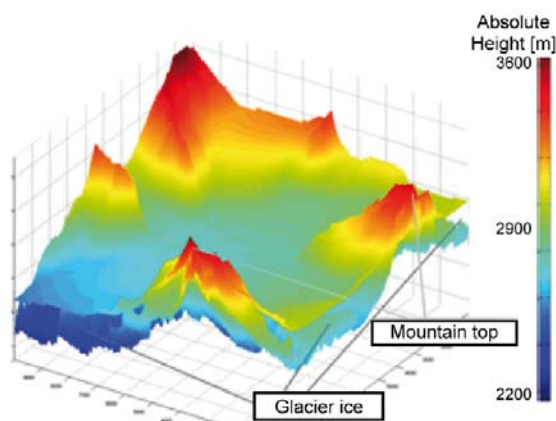


Fig. 1: DEM and 3D-SAR surface maps.

The results demonstrate the capability of low-frequency SAR sensors to potentially map glacier volumes in a large scale. Further campaigns with a flight track pattern optimized for the problem of 3D glacier mapping, and more research including ground truth validation, has to be done to verify the results. These ground truth validations are especially relevant to the question of how accurate the estimated height of the maximal backscattering is and how it is influenced by simplified physical assumptions and estimated processing parameters.

REFERENCES

- Farinotti D., M. Huss, A. Bauder, and M. Funk (2009), "An estimate of the glacier ice volume in the Swiss Alps," *Global and Planetary Change*, vol. 68, pp. 225-231.
- Frey O. and E. Meier (2008), "Tomographic Focusing by Combining Time-Domain Back-Projection and Multi-Looking Based Focusing Techniques," *European Conference on Synthetic Aperture Radar*, Friedrichshafen, Germany, vol. 2, pp. 73-75.
- Oriot H. and H. Cantalloube (2008), "Circular SAR imagery for urban remote sensing," *European Conference on Synthetic Aperture Radar*, Friedrichshafen, Germany, vol. 2, pp. 205-208.
- Prats, P., C. Andres, R. Scheiber, K. Macedo, J. Fischer and A. Reigber (2007), "Glacier Displacement Field Estimation Using Airborne SAR Interferometry," *IEEE Geoscience and Remote Sensing Symposium*, Barcelona, Spain, pp.2098-2101.
- Solomon, S., D. Qin, M. Manning, Z. Chen, M. Marquis, K.B. Averyt, M. Tignor and H.L. Miller (eds.) (2007), *Contribution of Working Group I to the Fourth Assessment Report of the Intergovernmental Panel on Climate Change, 2007*, Cambridge University Press, Cambridge, United Kingdom and New York.

18.5

Sensitivity of X-band SAR interferometry on the snow pack characterisation

Leinß Silvan¹, Hajnsek Irena^{1,2}

¹ Institute of Environmental Engineering, ETH Zürich, Switzerland

² Microwaves and Radar Institute, German Aerospace Center (DLR), Germany

The knowledge of the amount of snow cover and its structure is an important parameter for freshwater reservoirs, flood prediction, hydroelectric power plants as well as weather, climate, and avalanche models [Barnett, 2005]. Still, the precise knowledge of snow properties relies on local and work-intensive ground measurements which are of limited value due to the high spatial variability of the snow cover. Investigating the optical regime provide high spatial resolution but depends on clear weather conditions and provides only snow surface information while passive microwave systems suffering from the very low spatial resolution (km-scale).

Within the last few years the development in SAR technologies allows image resolution on the meter-scale from space while the microwave frequencies penetrate the snow cover. The obtained data are able to provide parameters for snow pack characterisation. Among a series of important snow parameter are the snow volume, snow water equivalent (SWE) and structural properties. The satellite mission TerraSAR-X equipped with a synthetic aperture radar (SAR) system operating at the X-band frequency of 9,65 GHz provides dual polarimetric radar scenes with a resolution of 3.5 m, which allow multi-pass interferometric acquisitions with a time resolution of 11 days [Werninghaus, 2010]. Exploiting the complex phase of high resolution interferograms of different polarisations gives access to snow cover related parameters [Deep, 2011].

Volume scattering in the snow layer causes decorrelation of the complex coherence of two consecutive images. A simple two layer volume model is adapted that relates the complex interferometric coherence of the volume scattering directly to physical parameters as volume height, volume media extinction, underlying topography and the ground-to-volume ratio. A first analysis of snow property extraction by using time series data of interferometric TerraSAR-X data available over three different snow test sites is performed.

REFERENCES

- Barnett, T. et al. D. 2005: Potential impacts of a warming climate on water availability in snow-dominated regions. *Nature* 438, 303-309.
- Werninghaus, R & Buckreuss, S. 2010: The TerraSAR-X Mission and System Design. *IEEE Transactions on Geoscience and Remote Sensing* 48 (2), 606-614.
- Deeb, E. et al. D. 2011: Monitoring snowpack evolution using interferometric synthetic aperture radar on the North Slope of Alaska. *International Journal of Remote Sensing* 32 (14), 3985-4003.

18.6

Large-area tree species classification – potential and limits of airborne digital sensor (ADS40/80) data for the Swiss NFI

Waser Lars¹, Ginzler Christian¹ & Kuechler Meinrad²

¹ WSL, Landscape Dynamics, Swiss Federal Research Institute WSL, 8903 Birmensdorf, Switzerland – phone: +4144 7392292; email: waser(ginzler, kuechler)@wsl.ch

² WSL, Biodiversity and Conservation Biology

Temporally frequent, cost-efficient and precise forest information requirements for NFIs, monitoring or protection tasks have grown over time and will continue to do so in the future. In Switzerland, the airborne digital sensors ADS40/ADS80 offers new opportunities as they can provide entire image strips with high geometric, radiometric and temporal resolution and cover the entire country every three years. This study presents an approach to semi-automated tree species classification on regional / state level for different types of forests using multispectral ADS40/ADS80 data to support some tasks of the Swiss National Forest Inventory (NFI).

Until now, most (semi)-automated species classification methods have been developed for small study areas of a few hectares with few field plots and for relatively homogeneous forests with only a few tree species. In the present study a robust model has been developed for an area located in the East of Switzerland with an extend of approx. 2500 km². The dominating deciduous tree species are *Fagus sylvatica* and *Fraxinus excelsior* and less frequently *Acer sp.*, *Alnus sp.*, and *Betula sp.* The main coniferous trees are *Abies alba*, *Larix deciduas*, *Picea abie*, and *Pinus sylvestris*.

Ground surveys were carried out in summer 2009 and 2010, focusing on the most frequent tree species (at least 5% coverage in Switzerland). ADS80-SH82 and ADS40-SH52 RGB and CIR images with a spatial resolution of 0.25-0.5 m were used. Additionally, canopy height models (CHMs) were generated automatically from the images and from additional LiDAR terrain data with a spatial resolution of 0.5m. Prior to the object-oriented tree species classification, homogenous image segments of individual tree crowns and tree groups were obtained using a multi-resolution segmentation procedure.

In a second step, several variables (geometric and spectral signatures) were derived from the remote sensing data using standard digital image processing methods (including colour transformation, principal components analysis, arithmetic combinations). To obtain good predictions, a small set of powerful variables has to be selected using a stepwise variable selection (AIC, both-directions). The final input variables used in this study consist of original image bands, IHS and their PCAs. As the response variable has more than two possible states, multinomial regression models had to be applied.

To determine the predictive power of the models, a 10-fold cross-validation was applied. The overall accuracies vary between 0.65 and 0.85, and Cohen's kappa values between 0.55 and 0.75. Lower accuracies (kappa < 0.5) were obtained for small samples of species such as non-dominant (mostly deciduous) tree species with similar spectral properties. Currently, NFI sample plots are being implemented for validation.

Further development is needed with the harmonization of the several image strips recording trees with a different phenological status. For this, radiometric correction between images stripes will be taken into account.

For the Swiss NFI, the tree species composition of larger areas, preferably on the national scale is required, the findings of this preliminary study provide a first important contribution. Furthermore, the continuity of this approach will be guaranteed since the required input data (field samples, images) is being provided every three years by other national campaigns or monitoring programs.

REFERENCES

- Waser, L.T., Küchler, M., Ecker, K., Schwarz, M., Ivits, E., Stofer, S., & Scheidegger, C. (2007). Prediction of Lichen Diversity in an Unesco Biosphere Reserve - Correlation of high Resolution Remote Sensing Data with Field Samples. *Environmental Modeling & Assessment*, 12(4), 315-328.
- Waser, L.T., Baltsavias, E., Ecker, K., Eisenbeiss, H., Ginzler, C., Küchler, M., Thee, P., & Zhang, L. (2008). High-resolution digital surface models (DSM) for modeling fractional shrub/tree cover in a mire environment. *International Journal of Remote Sensing*, 29(5), 1261 – 1276.
- Waser, L.T., Baltsavias, E., Ecker, K., Eisenbeiss, H., Feldmeyer-Christe, E., Ginzler, C., Küchler, M., Thee, P. and Zhang, L. (2008). Assessing changes of forest area and shrub encroachment in a mire ecosystem using digital surface models and CIR-aerial images. *Remote Sensing of Environment* 112(5): 1956-1968.
- Waser, L.T., Klonus, S., Ehlers, M., Küchler, M., and Jung, A., 2010. Potential of Digital Sensors for Land Cover and Tree Species Classifications - A Case Study in the Framework of the DGPF-Project. *Photogrammetrie, Fernerkundung und Geo-information*, Vol. 10 (2), pp. 132- 141.
- Waser, L.T., Ginzler, C.; Kuechler, M.; Baltsavias, E.; Hurni, L., 2011. Semi-automatic classification of tree species in different forest ecosystems by spectral and geometric variables derived from Airborne Digital Sensor (ADS40) and RC30 data. *Remote Sensing of Environment* 115: 76-85.

P 18.1

Recent efforts on APEX Calibration and Validation

Petra D'Odorico, Andreas Hueni, Michael Jehle, Michael Schaepman

Remote Sensing Laboratories, Dept. of Geography, University of Zurich, Winterthurerstrasse 190, 8057 Zurich

The generation of high-accuracy Earth System Science products based on remote sensing system relies on accurate system and data calibration, which ties data to international, physical standards.

The imaging spectrometer APEX (Airborne Prism Experiment) operates in the visible and near infrared region of the electromagnetic spectrum and has been designed to acquire Earth System related measurements.

In order to achieve the required accuracy, a detailed characterisation and calibration of the instrument is carried out on a regular basis on the Calibration Home Base (CHB) at DLR Oberpfaffenhofen.

The provision of calibrated data requires a stable and quality controlled data pool storing the vast amount of CHB data upon which calibration routines can be applied in a transparent, operational and repeatable manner.

The APEX Calibration Information System (APEX CAL IS) has been developed for the above reasons. It provides the means for monitoring the stability of the instrument over time. Comparison over time allows continuous quality checks during calibration at the CHB, reducing the risk of acquiring data with wrong or suboptimal CHB or instrument settings.

APEX takes calibration one step further by including in-flight monitoring of instrument performances. Differences between the laboratory and the airborne environment, in terms of environmental conditions and operational interfaces, can thus be taken into account during calibration. The instrument features onboard characterization equipment, such as an internal light source and spectral filters, known as the In-Flight Characterization (IFC) facility. Onboard characterization measurements are regularly acquired at closed shutter before and after every target, as well as on-ground. Performance correction coefficients can be derived from these measurements and applied to the imaging data acquired in flight. The APEX all-round calibration concept allows delivering physically meaningful data to the users and provides a data pool for calibration, simulation and validation of other optical airborne and spaceborne instruments.

P 18.2

Short-term variability within long-term trends in global vegetation activity

Rogier de Jong^{1,2}, Jan Verbesselt¹, Michael E. Schaepman³, Sytze de Bruin¹

¹ *Laboratory of Geo-Information Science and Remote Sensing, Wageningen University, The Netherlands*

² *ISRIC – World Soil Information, Wageningen, The Netherlands*

³ *Remote Sensing Laboratories, University of Zurich, Switzerland*

Continuous global time series of vegetation indices (VIs), which are available since early 1980s, are of great value to detect changes in vegetation activity at large spatial scales. Station-based phenological observations (e.g. Menzel et al., 2006) and these VI time series (e.g. Zhou et al., 2001) have shown evidence for greening and browning trends during the past decades in several regions in the world. These trends in vegetation activity may, over time, consist of an alternating sequence of greening and/or browning periods (e.g. Angert et al., 2005). Most change detection methods, however, assume a fixed change trajectory – defined by the start and end of the time series – and a linear or monotonic trend. We applied a change detection method, which detects abrupt changes within the time series in a data-driven manner, i.e. without prior knowledge on location or timing. This Breaks For Additive Season and Trend (BFAST) approach showed that large parts of the world were subjected to trend changes since the start of the satellite record in 1981. Many of these changes were found around large-scale natural influences like the Mt Pinatubo eruption in 1991 and the strong 1997/98 El Niño event, especially in grassland and shrubs. Shifts from greening to browning (or vice versa) occurred in 15% of the global land surface, which demonstrates the importance of accounting for trend breaks when analyzing long-term NDVI time series.

REFERENCES:

- Angert, A., Biraud, S., Bonfils, C., et al. (2005). DOI: 10.1073/pnas.0501647102
 Menzel, A., Sparks, T.H., Estrella, N., et al. (2006). DOI: 10.1111/j.1365-2486.2006.01193.x
 Zhou, L., Tucker, C.J., Kaufmann, R.K., et al. (2001). DOI: 10.1029/2000JD000115

P 18.3**Visual Localization Recognition and Photo-to-Terrain-Alignment in Mountainous Areas**

Olivier Saurer and Georges Baatz and Kevin Köser and Marc Pollefeys

Computer Vision and Geometry Group, ETH Zürich, CH-8092 Zürich

In this work we address the problem of registering terrestrial images to a digital elevation model, by estimating the six degree of freedom (rotation and translation) of the camera pose. What makes this problem lot harder than registration in urban environments is the different appearance of the mountains due to time of day and time of year. Relief-like structures and cracks cause very different image patterns depending on the illumination (shadows) and the appearance of the mountains varies a lot according to the amount of snow, the snow line, glaciers borders and vegetation which vary within and between seasons.

More stable features seem to be the contours and also other lines on the mountains. Although a large fraction of the line segments will not reappear under different conditions (time of day, shadows, time of year, different perspective), initial experiments show promising results. In particular, the skyline is virtually invariant (ignoring snow piles in winters and small changes by trees on the ridges) and often very discriminative even within 1000km².

To extract skylines of the model, we extract panoramic images from a 30km x 30km area with a 100m grid resolution, see figure[1]. The panoramas are represented as cubemaps, from which the contours can efficiently be extracted and represented on the unit sphere. In a similar way contours are extracted from a terrestrial image. The registration is achieved by comparing the contour lines of the panoramic and the terrestrial image.



Figure 1: Elevation model of 30km x 30km area size, textured with orthographic aerial images (left). The model resolution is 2 m² per grid point. Close-up view (middle). Right, cubemap representation of a 360 degree view. Top and bottom face of the cube (dark and light blue squares) represent the sky and the ground respectively.

We evaluate the algorithm by exhaustively searching for the best matching image on a 30 km x 30 km grid, sampled at a distance of 100m. The error term evaluated for each image pair, is visualized in figure [2] left. Figure [2] right, shows the best matching skyline overlaid onto the terrestrial image. For the first set of test images this method shows an optimum near the true position (light green), meaning that the registration could be solved reasonably well. In the future we plan to replace the computationally costly exhaustive search by efficient indexing methods known from web/test search.

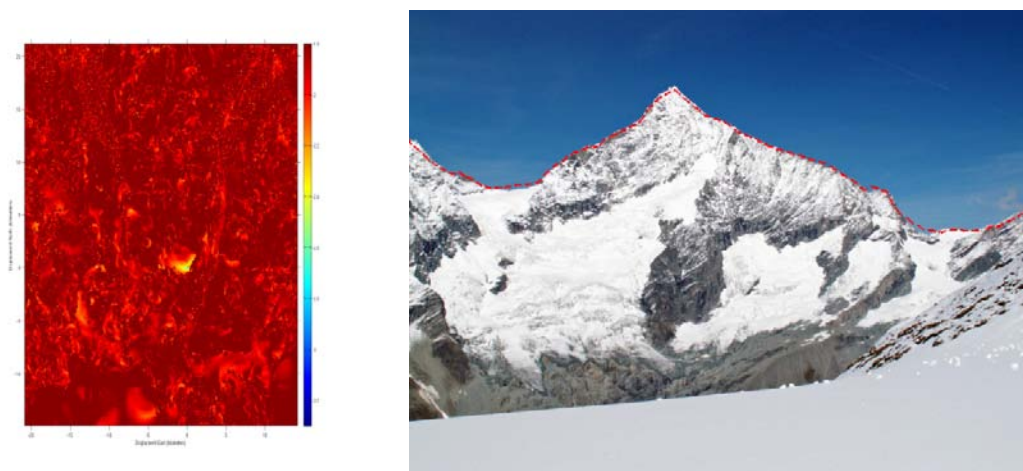


Figure 2: Left, evaluation of the error term over a grid size of 30km x 30km sampled at a distance of 100m. The optimal position (light green) is close to the true position. Right, overlay of the best matching synthetic skyline with the terrestrial image.

BIBLIOGRAPHY

1. *Vision-Based Localization*. Thompson, William B., et al. s.l. : ARPA, Morgan Kaufmann, 1993.
2. *Position Estimation from Outdoor Visual Landmarks for Teleoperation of Lunar Rovers*. Cozman, Fabio and Krotkov, Eric. s.l. : Proc. Third IEEE Workshop on Applications of Computer Vision, 96. pp. 156--161.
3. *Estimating Camera Position and Orientation from Geographical Map and Mountain Image*. Jr, Prospero C. Naval, et al. [ed.] Society of Instrument and Control Engineers 38th Research Meeting of the Pattern Sensing Group. 1997. pp. 9--16.
4. *Groups of Adjacent Contour Segments for Object Detection*. Ferrari, V., et al. s.l. : IEEE Computer Society, 2008. Vol. IEEE Transactions on Pattern Analysis and Machine Intelligence, pp. 36-51.
5. *Alignment by Maximization of Mutual Information*. Viola, Paul, Wells, III and M., William. s.l. : Kluwer Academic Publishers, 1997. pp. 137--154.
6. *Automatic Photo-to-Terrain Alignment for the Annotation of Mountain Pictures*. Baboud, Lionel, et al. Colorado Springs, USA : IEEE, 2011.
7. *VirtualPlanetBuilder*. s.l. : openscenegraph.org.
8. *Object Recognition from Local Scale-Invariant Features*. Lowe, D.G. [ed.] ICCV99. 1999.

P 18.4

Long-term geolocation accuracy of TerraSAR-X high-resolution spotlight products

Schubert Adrian¹, Small David¹, Jehle Michael¹ & Meier Erich¹

¹Remote Sensing Laboratories, University of Zurich, CH-8057 Zurich (adrian.schubert@geo.uzh.ch)

A SAR sensor with high geolocation accuracy greatly simplifies the task of combining multiple data takes with one another, not only simplifying their inter-comparison, but also dramatically speeding up applications such as near-real-time disaster mapping. Accurate geolocation also permits multiple image products to be quickly combined or layered with other data sources such as digital elevation models, cadastral maps, vegetation maps, forest maps, etc.

The extremely high orbital and product geolocation accuracy of TerraSAR-X (TSX) has been established in past validation studies conducted by various research groups (Eineder et al. 2011, Schubert et al. 2010, 2011). In particular the stripmap and high-resolution spotlight (HS) products, with their sample intervals ranging from 0.5 m to 2 m, offer one of the highest geometric resolutions currently available to the scientific community. However, achieving the highest-possible accuracy

cy from these products requires correcting for at least two perturbing factors: (a) atmospheric path delay due to refraction, and (b) solid Earth tides (SETs). In this study, ground measurements were surveyed using differential GPS (DGPS). Because of differences between the local and global geodetic reference frames caused by continental plate tectonics, a plate-drift model was also incorporated into our location estimates.

A time series of images spanning 16 months was obtained over a fixed test site in the west of Switzerland (*Torny-le-Grand*), making it possible to validate both an atmospheric refraction and a SET model, while at the same time establishing the instrument's long-term stability. These related goals were achieved by placing trihedral corner reflectors (CRs, two shown in Figure 1) at the test site, and estimating their phase centers with centimeter-level accuracy using DGPS. Oriented in pairs towards a given satellite track, the CRs could be seen as extremely bright points in the images, providing a geometric reference set.

SAR images from the TSX HS mode were obtained in alternating ascending and descending orbit configurations. The highest-resolution products were selected to enable determination of their positions at the best possible precision. Based on the delivered product annotations, the CR image positions were predicted, and these predictions were compared to the actual measured image positions both before and after compensation for atmospheric refraction and systematic solid-Earth deviations.

The study was able to demonstrate that when the delivered product timing annotations are corrected for path delay and SETs using simple models, the TerraSAR-X products deliver unprecedented geolocation accuracy. Furthermore, this accuracy was maintained for the duration of the 16-month test period.



Figure 1. Trihedral corner reflectors in *Torny-le-Grand* facing TerraSAR-X's descending orbit.

REFERENCES

- Eineder, M., Minet C., Steigenberger P., Cong X. & Fritz T. 2011: Imaging Geodesy – Toward centimeter-level ranging accuracy with TerraSAR-X, *IEEE Transactions on Geoscience and Remote Sensing*, 49(2), 661–671.
- Schubert, A., Jehle, M., Small, D. & Meier, E. 2010: Influence of Atmospheric Path Delay on the Absolute Geolocation Accuracy of TerraSAR-X High-Resolution Products. *IEEE Transactions on Geoscience and Remote Sensing*, 48(2), 751–758.
- Schubert, A., Jehle, M., Small, D. & Meier, E. 2011: Mitigation of atmospheric perturbations and solid-Earth movements in a TerraSAR-X time-series. *Journal of Geodesy* (cond. accepted).

P 18.5

Data fusion methods of LiDAR and spectroscopy data for the derivation of forest biochemical and biophysical variables – a review

Hossein Torabzadeh, Felix Morsdorf, Michael E. Schaepman

*Remote Sensing Laboratories, Department of Geography, University of Zurich, Winterthurerstr. 190, CH-8507 Zurich, Switzerland
(hossein.torabzadeh@geo.uzh.ch)*

Nowadays, multi-source data fusion is an important method to improve our understanding of forest functioning. Due to the available diversity of data sources in remote sensing, fusion methods play a critical role in estimating forest parameters. LiDAR (Light Detection and Ranging) systems and imaging spectrometers in particular have capabilities, which should ultimately provide reliable information on the state of forest ecosystem. LiDAR data can provide structural forest parameters such as tree height and fractional cover, while other parameters (e.g. true LAI or fAPAR) can only be determined accurately using complementing data sources. Imaging spectrometer data are used to assess biochemical variables of vegetation canopies, but their retrieval quality is strongly dependent on the structural heterogeneity of a forest. Like in any other data fusion method, choosing the appropriate method is a critical issue allowing the full exploitation of their complementarities. We review and analyze fusion approaches for these two acquisition methods. Structurally, we divide approaches into levels (fusion at data or product level) and methods (physically vs. empirical methods), and discuss these approaches in detail.

P 18.6

Ross-Li BRDF correction of airborne imaging spectroscopy data for improved continuous field map generation in the Swiss National Park

Weyermann Joerg¹, Damm Alexander¹, Kneubühler Mathias¹ & Schaepman Michael¹

*¹Remote Sensing Laboratories, Geographisches Institut, Universität Zürich, Winterthurerstr. 190, 8057 Zürich
(joerg.weyermann@geo.uzh.ch)*

Uncertainty in quantitative Imaging Spectroscopy (IS) data analysis can be introduced by a number of factors, e.g. sensor calibration, data pre-processing and atmospheric correction, anisotropy of the atmosphere or ground reflectance anisotropy issued by view angle changes over the across-track field of view (FOV). While much effort is put into sensor calibration and atmospheric correction, and anisotropy of the atmosphere plays a role only at very large off-nadir view angles and turbid atmosphere, ground reflectance anisotropy was found to cause significant uncertainties both on the hemispherical-directional reflectance factor (HDRF) data and on product level. While difficult especially for airborne IS data where no information on the angular reflectance behavior of a surface can be derived from the data, the normalization of HDRF anisotropy effects is absolutely critical for the reliability of a data products derived from the data. Advanced products like continuous field maps of surface parameters of interest (e.g. columnar surface water content) can only be generated with sufficient accuracy when the HDRF data were previously corrected for these effects. For operational correction, empirical or semi-empirical models can be used, which rely on a meaningful aggregation of data in order to estimate the surface BRDF shape over the FOV to generate a correction function. The semi-empirical Ross-Li model is well known and can also be used for airborne data (Weyermann et al. 2011). The model assumes that changes in the HDRF over the FOV are caused by ground HDRF anisotropy exclusively, which is only given when different factors causing illumination differences can be excluded. Solar angle changes can be disregarded in most cases, since no significant impact occurs during the acquisition of a single flight line. Topography, however, causes a spatial pattern that biases the estimation of ground HDRF and possibly overrides or fully hides the effect of the target anisotropy. The Ross-Li model can be applied also in case of mountainous terrain, but information on a pixels individual configuration regarding illumination and observation geometry must be taken into account.

This contribution reports on current achievements in BRDF correction in a 2010 APEX dataset acquired over the Swiss National Park (SNP). For Ross-Li parameterization, slope and aspect information is derived from a 25m digital elevation model (Swisstopo DHM25) in order to account for the topography- dependent relative illumination and observation geometry.

Results are evaluated with continuous field maps of various surface parameters and biochemical products calculated by inversion of the PROSPECT/SAIL radiative transfer model.

REFERENCES

Weyermann, J., Damm, A., Kneubühler, M. & Schaepman, M. 2011: Assessing the effect of BRDF on Imaging Spectroscopy data and products using the Ross- Li correction method. – in preparation.

P 18.7

Influence of gap fraction on coniferous needle optical properties measurements

Yáñez-Rausell Lucía^{1,2}, Malenovský Zbynek², Schaepman Michael²

¹Centre for Geo-Information, Wageningen University, Droevendaalsesteeg 3/PO Box 47, 6700 AA Wageningen, The Netherlands (lucia.yanezrausell@geo.uzh.ch)

²RSL, Department of Geography, Univ. of Zurich, Winterthurerstrasse 190, CH-8057 Zurich, Switzerland

Optical properties (OPs) of non-flat narrow leaves, i.e. coniferous needles, are extensively used by the remote sensing community, e.g. for calibration and validation of radiative transfer models at both leaf and canopy levels. Measurement of such small elements is, however, a technical challenge with a very little knowledge about related errors. Consequently two situations appear among the users of OPs: 1) the lack of such measurements forces them to make assumptions with a potentially negative impact on the interpretation of remote sensing data of coniferous forests (e.g. in radiative transfer modelling, needle transmittance is often assumed to be zero, or needle reflectance and transmittance are assumed to be equal); or 2) the used available datasets are of unknown reliability. This demonstrates a need for a robust, efficient and systematic measuring technique of narrow-leaf OPs.

Compared to the broad leaves, measurement of reflectance (R) and transmittance (T) of narrow leaves require adapting the conventional techniques (i.e. coupling a spectroradiometer to an integrating sphere) to a sample size smaller than the area illuminated by the incident light beam. Reduction of the illuminated area to the dimensions of one narrow leaf would result in a very low signal-to-noise performance. An alternative solution is to measure the signal from several needles simultaneously mounted next to each other in a carrier, and to correct such measurement for the portion of photons passing through the air gaps (gap fraction of the illuminated area – GF). The objective of this paper is to estimate an error budget of this technique by analysing errors originating from: 1) use of the carrier, 2) gap fraction estimation via digital image processing, and 3) multiple scattering caused by the non-flat nature of the needle leaves. To achieve this we measured OPs from an optically stable silicon material, which was cut in 1 mm thick strips to simulate needle shaped leaves. We build on the results presented by Mesarch et al. (1999) in which this technique was applied only on flat film paper, and we investigated the influence of the non-flat objects (needle leaves) on accuracy of the measurements. Computed R and T for different tested settings (i.e. carrier combinations, image processing settings, and distances between measured needles) were analysed to point out the best configurations and to estimate errors introduced by this technique.

REFERENCES

Mesarch, M.A., Walter-Shea, E.A., Asner, G.P., Middleton, E.M. & Chan, S.S. 1999: A revised measurement methodology for conifer needles spectral optical properties: evaluating the influence of gaps between elements. *Remote Sensing of Environment*, 68, 177–192.

P 20.8

Towards spectroscopic modelling of composite mineralogy

V.L. Mulder^{a,*}, S. de Bruin^a, M.E. Schaepman^{a,b}

^a *Laboratory of Geo-Information Science and Remote sensing, Wageningen University, Droevendaalsesteeg 3, P.O. Box 47, 6700 AA Wageningen, The Netherlands*

^b *Remote Sensing Laboratories, University of Zürich, Winterthurerstrasse 190, 8057 Zürich, Switzerland*

* *Titia.mulder@wur.nl*

Soil mineralogy is an important indicator for soil fertility, soil formation and suitability. However, the determination of mineralogy by powder diffraction is costly and labour-intensive. Therefore, soil scientist do have need for an efficient method to determine the mineral composition of the soil. VNIR spectroscopy has proven to be an efficient method for the determination of various soil properties. Currently, single soil minerals can be determined with absorption feature analysis or spectral unmixing. For the prediction of multiple minerals the determination becomes more complex since the minerals, but also vegetation components, do have similar absorption features which complicates unmixing. With unconstrained spectral mixture analysis based on a single model, the composite soil mineralogy cannot be determined. The use of multiple models does improve the unmixing but the dominant minerals with spectral similarity are in most cases not discriminated. Also, quantification of the different minerals present in the composite is not feasible. However, the unmixing does provide information on the type of minerals present in the sample. The results were successfully related to lithological indices derived from thermal infrared ASTER satellite data. The results demonstrate that the mineral composition is difficult to relate to the spectral data using a simple forward model approach. Therefore, we suggest to develop a linear spectral trend model which is capable of predicting the main composite mineralogy based on VNIR spectroscopy.

20. Deep Geothermal Energy

Keith Evans, Nicolas Deichmann, Christoph Heinrich

*Swiss Geological Society,
Swiss Geophysical Commission,
Swiss Geotechnical Commission,
Swiss Society of Mineralogy and Petrology*

TALKS:

- 20.1 Rybach L.: *Introduction: Status and prospects of deep geothermal energy, globally and in Switzerland*
- 20.2 Siddiqi G.: *Bringing Switzerland's geothermal resources to market – technological, economic and institutional challenges*
- 20.3 Schill E., Fisch, H., Uhde, J.: *Deep geothermal systems – advantages and limitations of using natural permeability*
- 20.4 Evans, K.F.: *Enhanced/Engineered Geothermal Systems (EGS) – experience to date and lessons learned*
- 20.5 Jung, R.: *Enhanced Geothermal Systems (EGS) - the way forward*
- 20.6 Deichmann N., Wiemer S.: *EGS and induced seismicity -- the good and the bad*
- 20.7 Driesner T., Jenny P.: *Process simulation: understanding and judging geothermal reservoir processes*
- 20.8 Gerber L., Maréchal F.: *Efficient conversion of geothermal resources for multiple energy uses*
- 20.9 Meier P., Burri P.: *Key success factors for Enhanced Geothermal Systems*

POSTERS:

- P 20.1 Evans, K.F., Zappone, A., Kraft, T., Deichmann, N., Moia, F.: *A survey of the induced seismic responses to fluid injection in geothermal and CO₂ reservoirs in Europe*
- P 20.2 Goertz-Allmann B. P., Bachmann C., Wiemer S.: *What can induced earthquake source properties tell us about reservoir geomechanics?*
- P 20.3 Kraft T., Husen S., Wiemer S.: *GEOBEST - A contribution to the long term development of deep geothermal energy in Switzerland*
- P 20.4 Schoenball M., Baujard C., Kohl T., Dorbath L.: *Changes of Coulomb Failure Stress due to dislocations during stimulation of well GPK2 in Soultz-sous-Forêts*
- P 20.5 Sikaneta S.G., Evans K.F.: *Natural fractures and stress heterogeneity in the host granite of the Basel Deep Heat Mining project*
- P 20.6 Zerlauth M., Ortner H., Pomella H., Schulz M., Fügenschuh B.: *Geothermal energy potential of Vorarlberg (Austria)*

20.1

Prospects of Deep Geothermal Energy in Switzerland

Ladislaus Rybach^{1,2}

¹Geowatt AG Zürich, Dohlenweg 28, CH-8050 Zürich (rybach@geowatt.ch)

²Institut für Geophysik ETHZ, Sonneggstrasse 5, CH-8092 Zürich (rybach@ig.erdw.ethz.ch)

Deep geothermal energy resources and utilization come in two main categories: hydrothermal and petrothermal. While the first is restricted to specific subsurface conditions and does not exist everywhere, the second is ubiquitous (in principle). The utilization is mainly for direct uses like district heating, for power generation or for both (“co-generation”). The –rather arbitrary– delimitation between shallow and deep is at 400 m depth.

Hydrothermal

The goal here is to find and develop ample thermal water in deep aquifers for space heating and/or co-generation. The problem of finding is that so far no method exists to determine the water content and/or the permeability of the subsurface from surface measurements. Only production tests in deep wells can prove the suitability of a given location. This constitutes a substantial finding risk. To mitigate this a system of risk coverage for deep geothermal drillings in Switzerland was applied in the years 1988–1998 for 13 wells 655–2690 m deep, with rather limited success: 5 successes, 1 partial success, 7 failures. Expenditure was 8.7 million CHF for risk coverage and 3.6 million CHF for development support (details in Rybach 2005). Currently a Federal risk guarantee fund (150 million CHF) has been established for geothermal power generation facilities. Hydrothermal targets are deep aquifers like karstified and/or fractured limestone formations (e.g. Malm or Oberer Muschelkalk). Whereas real, regionally extended deep aquifers exist elsewhere (Paris basin: Dogger limestones, Hungarian lowlands: Pannon sandstones, which can be tapped by drilling without much exploration) the Swiss deep aquifers are rarely regionally productive: the practically dry geothermal wells Thoney/GE, Reinach/BL, Triemli/ZH or Yverdon/VD testify this. Deep water-bearing fracture zones could be more frequent but their exploration (preferably with 3D seismics) is costly. Besides, such structures are often steeply dipping (i.e. with little area-wide coverage) and of limited extent only.

Petrothermal

Due to the above-mentioned facts a widespread development of deep hydrothermal resources is hardly possible in Switzerland. Significant utilization can arguably be envisaged only with petrothermal systems (in particular: EGS). However, many questions still remain. Nowadays there is general agreement about the requirements for a technically feasible and economically viable EGS heat exchanger at depth: fluid production rate 50-100 kg/s, fluid temperature at wellhead 150-200 °C, total effective heat exchange surface area $>2 \times 10^6$ m², total rock volume $>2 \times 10^8$ m³, flow impedance <0.1 MPa/(kg/s), water loss $<10\%$. Although the minimum requirements for an operable EGS reservoir are herewith set, their realization in a custom-made manner to comply with differing site conditions is not yet demonstrated. Local subsurface conditions (rock temperature, lithologies, stress field properties, kind and degree of natural fracturing) can be highly variable. The key issue is to have a technology for producing electricity and/or heat from a basically ubiquitous resource, in a manner independent of local subsurface conditions, i.e. to create EGS downhole heat exchangers, wherever wanted, with the properties quantified above. In addition it will be decisive to see whether and how the EGS power plant size could be upscaled, at least to several tens of MWe. A decisive parameter in this context is the recovery factor (the fraction “extractable heat/heat in place”). The recovery factor can change with time: permeability enhancement (e.g. new fractures generated by cooling cracks or dissolution of mineral species) could increase the recovery factor, while permeability reduction (e.g. due to mineral deposition) or short-circuiting could reduce heat production. Without having field-scale experience with long-term EGS production the economic estimates about production and maintenance costs remain unsubstantiated. It is obvious from all this that EGS is presently still at the “proof of concept” stage. More details about global EGS status and problems are given in Rybach (2010).

Legal and coordination needs

Contrary to other countries it is impossible in Switzerland to obtain a concession for exploration and development of deep geothermal resources. A general planning regulation of deep subsurface usage is also lacking. A federal working group has been set up to look into this; hopefully a suitable legislation will be soon formulated (and approved by Parliament) that facilitates the development of deep geothermal resources in Switzerland.

Another need is increasingly evident: enhanced coordination. Even in small Switzerland various geothermal groups are active, with often widely diverging interests. It is evident that the manifold problems can only be solved by a concerted and concentrated acting-together of the key players (Wyss & Rybach 2010), which underscores the need for coordination. Federal and Cantonal governments, City service companies like the ones of Zurich and St.Gallen, utilities and companies like Axpo AG or Geo-Energie Suisse AG as well as other actors should join forces. The various endeavours should be merged into a generalized concept and harmonized course of action (like the one described in FEGES 2007 (Mégel et al. 2007), in order to advance the development of deep geothermal resources in Switzerland.

REFERENCES

- Mégel, T., Wilhelm, J. & Wyss, R. 2007: Forschungs- und Entwicklungs-programm zur geothermischen Stromerzeugung in der Schweiz (FEGES) - Strategiepapier der Dachorganisation GEOTHERMIE.CH, 23 p.
- Rybach, L. 2005: Die Schweizer Risikodeckung für Geothermiebohrungen 1987-1997 – Ausgestaltung und Erfahrungen im Rückblick. In: Tagungsband, GtV Jahrestagung 2005, S. 18-23, ISBN 3-932570-53-7
- Rybach, L. 2010: The “Future of Geothermal Energy” and its challenge. In: Proceedings World Geothermal Congress 2010, Bali, Indonesia, 25-30 April 2010. Available at: www.geothermal-energy.org/pdf/IGAstandard/WGC/2010/3109.pdf
- Wyss, R. & Rybach, L. 2010: Developing deep geothermal resources in Switzerland. In: Proceedings World Geothermal Congress 2010, Bali, Indonesia, 25-30 April 2010. Available at: www.geothermal-energy.org/pdf/IGAstandard/WGC/2010/3169.pdf

20.2

Bringing Switzerland’s geothermal resources to market – technological, economic and institutional challenges

Siddiqi Gunter¹

¹Swiss Federal Office of Energy, CH-3003 Bern (gunter.siddiqi@bfe.admin.ch)

Switzerland’s energy sources have each their own large potential and highly variable paths to deliver what the Swiss population wants in terms of power, heat/cold and transport fuels. The Fukushima nuclear accident, consumer choices and technological progress fuel vigorous debates. Politically the Federal Council - in the framework of the Energy Strategy 2050 – has projected a scenario where power from nuclear sources is no more required. Many new energy sources need to come into play – in particular for power. Geothermal energy owing to its exceptional characteristics can and should play a significant role. Initially hydrothermal resources will feature strongly, where high temperature, geothermal brine from formations or geological structures with high productivity. But as experience grows, Engineered Geothermal Systems EGS are expected to come to the fore – substantially reducing, if not eliminating, costly exploration risk.

Bringing geothermal reserves to market in a commercially viable manner requires the lowering technological, economic and institutional barriers while reducing the risks related to geothermal development to a level as low as reasonably practicable. With technological progress and experience, unit technical cost of geothermal power can be substantially reduced from today’s Rp. 40-50 per kWh for geothermal resources. Hydrothermal resource development and operation are generally managed to low risk exposure and do not face insurmountable hurdles. Considering the response of the population of the Basel region, EGS induced seismicity - while very much a desired feature that testifies to reservoir development – is a major hurdle. But 5 years on, we are beginning to develop a more thorough understanding on how to reliably and predictably minimize the likelihood of causing an earthquake that harms people and the environment remains a major research topic.

Switzerland’s federal administration aims to support research and development, piloting and demonstration and project development through a number of programs, for example by sponsoring various research efforts into thermal spallation drilling, a technically challenging yet highly promising method to substantially reduce unit technical well cost.

20.3

Deep geothermal systems – advantages and limitations of using natural permeability

Eva Schill¹, Hansruedi Fisch² & Jörg Uhde²

¹ University of Neuchâtel, Emile-Argand 11, CH-2000 Neuchâtel, Switzerland (eva.schill@unine.ch)

² Axpo AG Neue Energien, Flughafenstrasse 54, CH-8152 Glattbrugg, Switzerland

The concept of hydrothermal systems in the sense of non-volcanic resources is based on the conceptual model of deep regional aquifers. In contrast, an Enhanced Geothermal System (EGS) is defined by improvement of the natural resource (ENGINE, 2009) usually either by hydraulic or chemical stimulation. In Switzerland, major regional aquifers have been distinguished in the Molasse basin in earlier studies: the Upper Malm, the Upper Muschelkalk and the upper crystalline basement. The Upper Marine Molasse and the Dogger are considered regional aquifers in northern and western Switzerland, respectively (e.g. Müller et al., 2001, Pasquier et al., 1999), but are usually too shallow for significant power production. One of the most productive examples world-wide for heat and electric power is the Upper Malm aquifer in the German Molasse basin. The permeable reef facies in the area of Munich, however, reveals also variable productivity depending on its degree of fracturation. The productivity can be naturally enhanced, when exploiting fracture zones within the aquifer, as most recently targeted in the Taufkirchen project, and it can be limited in undeformed areas or re-filled fractures. Thus, an expected hydrothermal project can turn into an EGS project such as the case of Mauerstetten. Analyzing recent hydrothermal projects and older wells in Switzerland, we come to the conclusion that the degree of fracturation is crucial for both hydrothermal and EGS projects and that our concept of regional aquifers lacks of confirmation by productive wells.

One of the few geothermal projects with long-term experience in central Europe is the heat exploitation of Riehen (BS). The geothermal system in Riehen is in operation since 1994 and produces 65 °C thermal water from the Upper Muschelkalk at a depth of 1547 m with a production rate of 18 l s⁻¹. It is used to feed the district heating system of Riehen (Switzerland) and Stetten (Germany) and supplies 26'000 MWh_{th} per year to 202 consumers. With the project "Riehen Plus" it is planned to increase the production rate to 23 l s⁻¹. Riehen is located at the Eastern boundary of the Upper Rhine valley with SSW-NNE-striking boundary faults. The development of the Upper Rhine graben in the Oligocene caused the formation of many small tectonic units. It is assumed that the sediments of the geothermally relevant Upper Muschelkalk in this area are highly fractured. Geochemical investigation proposes that a significant contribution of geothermal fluid is coming from the Permo-Carboniferous sediments which are related to deep trough structures in the crystalline basement. This indicates that the thermal anomaly observed at 1.5 km depth is caused by a regional circulation system along deep faults.

Current hydrothermal projects in Switzerland are planned along major fault zones. Examples are the projects of GP la Côte and St. Gallen in western and NE Switzerland, respectively. In both cases known existing fault zones have been further investigated by 2D or 3D seismic. Seismic investigations reveal the outline of fault zones in the sedimentary pile and the top basement. In general, the depth of the fault in the basement is difficult to access with any geophysical method. Tests of exploration methods at the Soultz site (Geiermann and Schill, 2010; Schill et al, 2010) have shown that gravity in combination with 3D geology or seismic investigation have potential to trace deep seated structures of anomalous porosity such as the Soultz reservoir area (Baillieux et al., this volume). Recently, the CHYN has applied similar methods in the deep target zone of St. Gallen, where on the basis of a 3D seismic survey we are able to distinguish different structural elements in the gravity data, which are relevant for the determination of the drilling path. First and preliminary estimates of porosity in the target fault zone have been made. This method is again applied for the EGS prospection of the deep underground of parts of Switzerland.

REFERENCES

- Baillieux, P., Schill, E., Dezayes, C., this volume. 3D structural regional model of the EGS site Soultz (Northern Upper Rhine graben, France): insights and perspectives
- ENGINE, 2009. Best Practice Handbook for the Development of Unconventional Geothermal Resources with a Focus on Enhanced Geothermal System. ENGINE Coordination Action (ENhanced Geothermal Innovative Network for Europe), www.engine.brgm.fr.
- Geiermann J., Schill E., 2010. 2-D Magnetotellurics at the geothermal site at Soultz-sous-Forêts: Resistivity distribution to about 3000m depth. C. R. Geosciences, 342: 587-599.
- Müller, W.H., Naef, H., Graf, H.R., 2001. Geologische Entwicklung der Nordschweiz, Neotektonik und Langzeitszenarien Züricher Weinland. Nagra Technischer Bericht, NTB 99-08, Wettingen.
- Pasquier, F., Bouzelboudjen, M., Zwahlen, F., 1999. Carte Hydrogéologique de la Suisse, Sarine, feuille 6. Commission Géotechnique Suisse et Service Hydrologique et Géologique National.
- Schill E., Geiermann J., Kümmeritz J., 2010. 2-D Magnetotellurics and gravity at the geothermal site at Soultz-sous-Forêts. World Geothermal Congress 2010, Bali, Indonesia, 25-29 April 2010.

20.4

Enhanced Geothermal Systems (EGS) – experience to date and lessons learned

Evans Keith F.

Engineering Geology, ETH Zürich, Sonneggstrasse 5, 8092 Zürich, Switzerland. (keith.evans@erdw.ethz.ch)

The first Enhanced or Engineered Geothermal System (EGS - previously known as Hot Dry Rock) to be constructed was at Fenton Hill, near Los Alamos, New Mexico in 1972. There, two 2-well systems at depths of 2.8 km and 4.2 km and temperatures up to 320°C were created in gneissic rocks. Extended circulation tests were performed to evaluate reservoir performance. Since then, a further three large-scale multi-well systems have been built and tested. These include: a 3-well system in granite at Rosemanowes in Cornwall, UK (depth 2.2 km and temperature 85°C); a four-well, multi-level system in granodiorite at Hijiori, Japan (depths 1.8 km and 2.2 km and temperatures of 250 and 270°C respectively); and a 2-well and 3-well system at 3.5 km and 5 km with temperatures of 160°C and 200°C respectively in granite at Soultz-sous-Forêts in France. All reservoirs were subject to extensive circulation testing. A long-held requirement of commercial reservoirs is that the circulation impedance (the pressure difference between wells required to produce unit production flow rate) should be less than 0.1 MPa/l/s. Whilst this is not the only requirement, it is particularly important because it largely dictates the maximum flow rate that can be produced from the reservoir. This is because there are limits to the maximum operational pressure difference that can be applied between the wells that are placed by geomechanical constraints (e.g. the injection pressure cannot exceed the minimum principal stress). Of the reservoirs built and tested to date, only the Soultz 3.5 km system has met the target for impedance. For the other reservoirs, the impedance could not be reduced to the level required to yield commercial production flow rates at sustainable pressures. Lower impedance can be promoted by placing the injection and production wells closer together, but this shortens the operation lifetime of the system set by the thermal breakthrough time (i.e. the time when the cooling front from the injection well reaches the production well). So there tends to be a trade-off between impedance and thermal breakthrough time. In this presentation I will show how close we have come to meeting the circulation performance target at the four large tests sites and indicate the principal factors that limited system performance at each site.

20.5

Enhanced Geothermal Systems (EGS) – the way forward

Jung Reinhard¹

¹JUNG-GEOTHERM, Gottfried-Buhr-Weg 19, D-30916 Isernhagen (jung.geotherm@googlemail.com)

The heat content of the crystalline basement is in almost every country and so in Switzerland by far the biggest energy resource of the earth crust. First attempts of the Los Alamos National Laboratory in New Mexico to access this resource date back to the early 1970´th and more than a dozen research projects have been performed since than in various countries. But still the technique, known as HDR (Hot-Dry-Rock) or EGS (Enhanced Geothermal Systems) is not mature and the thermal power achieved so far from HDR- or EGS-Systems does not meet economical standards. In addition further development of this technique is now hindered by the risk of induced seismicity.

The main reason for both problems is the present exploitation concept being applied in all major projects since the early 1980´th. Until that time the crystalline basement had been regarded as an almost un-fractured rock mass and the leading concept was to connect two inclined boreholes by a number of parallel vertical fractures created one after the other by hydraulic fracturing in short insulated borehole sections. After realizing that the crystalline basement already contains open natural fractures even at great depth it was assumed that it is not necessary or even impossible to create artificial fractures by fluid injection since the formation of artificial fractures will always be preceded by shearing of the natural discontinuities. Accordingly the term hydraulic fracturing was replaced by “hydraulic stimulation” and the corresponding mechanism interpreted as a pressure diffusion process in an existing fracture network accompanied by shearing and widening of favorably oriented fractures. As a result the overall permeability of a large rock volume is irreversibly enhanced. Size, shape, and orientation of the stimulated rock volume are determined by the spatial distribution of seismic events induced during the stimulation process. The remaining task to complete the circulation system is simply to drill a second or third borehole through this seismically defined volume.

The rapid adoption of this concept in the HDR-community was to a big part due to its technical simplicity. The original concept requires deviated boreholes and packers or other devices for insulating the borehole sections selected for the hydraulic fracturing tests and the pioneering HDR-project at Los Alamos was facing insurmountable technical problems with these devices at temperatures above 200 °C. The new concept in turn can be applied in vertical boreholes and is working without borehole packers since it is desirable to stimulate very long borehole sections containing a large number of natural fractures at once. The change in the leading concept had severe consequences:

- Much larger quantities of water were required for single tests.
- The development of high temperature directional drilling techniques and packers was no longer important.
- Heat exchanging area as a measure for the service life of a HDR-system was replaced by accessible rock volume.
- Fracture mechanics was no longer relevant.

By following this easy path HDR-research has maneuvered itself into a dead end street. It is evident today that industrial EGS-Systems after the present concept will need much higher flow rates and fluid volumes as being applied so far, e.g. in the European Soultz-project or in the Basel-project. This however increases the seismic risk and it is unlikely that this risk will be accepted by the public in densely populated and industrialized countries like Switzerland.

A more promising way is to go back to the original multi-fracture concept. Directional drilling and packer technology improved significantly during the last three decades and multi-fracture concepts are applied with great success in unconventional gas reservoirs. In the shale gas projects these multi-fracture-systems are approaching the dimensions of future industrial HDR-Systems. There are differences of course: The mass flow rate of HDR-systems, their depth and temperature will generally be higher, the rock type is different and in contrary to the shale gas application the fracture systems have to be intersected by a second or even a third borehole. But considering the experiences from both applications it seems almost certain that industrial HDR-Systems can be realized in this way in the near future.

20.6

EGS and induced seismicity – the good and the bad

Deichmann Nicholas¹ & Wiemer Stefan¹

¹Schweizerischer Erdbebendienst, ETH Zürich, Sonneggstrasse 5, CH-8092 Zürich (deichmann@sed.ethz.ch)

In contrast to hydrothermal systems, which attempt to exploit hot aquifers often found in pre-existing fault zones in sedimentary formations, Enhanced Geothermal Systems (EGS) rely on the possibility to create an artificial heat exchanger in the naturally more or less impermeable rock volume of the crystalline basement. In order to increase the permeability sufficiently to allow water to circulate between two or more production boreholes, large quantities of water are injected at high pressure through a first stimulation well into the potential heat reservoir. This procedure is invariably accompanied by high levels of microseismic activity and has, in a few cases, produced ground shaking strong enough to cause public concern or even some property damage.

Fluid-induced earthquakes are a common phenomenon and in many instances society has learned to live with the associated risk. They are known to occur not only in the context of the exploitation of deep geothermal energy but also as a consequence of reservoir impoundment, fluid-waste disposal in the deep underground, hydrocarbon exploitation and underground gas storage. In all cases, increased fluid pressure counteracts the normal stress on a given fault, thus decreasing its strength. In the common situation of a tectonically pre-stressed environment with numerous pre-existing faults at all scales, this can enable the differential stress acting on a fault to cause sudden slip, thereby producing an earthquake. Even massive rainfalls are known to have triggered earthquake swarms, and fluids probably play a significant role in most other naturally occurring earthquakes as well. Due to the inherent roughness of faults, earthquake related slip generally results in an increase in permeability along the fault. It is exactly this feature that is exploited for the stimulation of a deep heat reservoir. In addition, detailed monitoring of this microseismic activity and the precise location of the corresponding hypocenters delivers the decisive input for assessing the degree of permeability increase, that is being achieved by the stimulation, and thus for designing the final EGS. In other words, induced microseismicity is not only an inevitable but also a necessary attribute of EGS development.

The big challenge is to prevent this «good» microseismicity to reach magnitudes of those «bad» earthquakes that constitute a risk to society. Although the basic principles are well understood, it is still very difficult, particularly in the forefront of a proposed project, to quantify the relative role of each of the parameters that influence the probability of unwanted earthquakes, e.g. ambient tectonic stress, rock strength, density and orientation of pre-existing faults, injection pressure, rate at which fluid is injected and total volume of injected fluids. Case studies of the few projects already underway, laboratory experiments, numerical modeling and the development of statistical tools are being pursued in an attempt to quantify and minimize the seismic risk associated with EGS projects. However, just as with every other method of energy production, it is unlikely that it will ever be possible to reduce this risk to zero. Thus, for deep geothermal energy to offer a substantial contribution to the total energy mix of our society, the equally large challenge will be to actively engage the public in a dialogue about what risks it is willing to accept in view of the possible benefits of an abundant and environmentally friendly energy source.

20.7

Process simulation: understanding and judging geothermal reservoir processes

Driesner Thomas¹, Jenny Patrick²

¹Institute of Geochemistry and Petrology, ETH Zurich, Clausiusstrasse 25, CH-8092 Zürich (thomas.driesner@erdw.ethz.ch)

²Institute of Fluid Dynamics, ETH Zurich, Sonneggstrasse 3, CH-8092 Zürich (jenny@ifd.mavt.ethz.ch)

Permeability creation during stimulation, heat extraction, scaling in installations, early cold water breakthrough during production, and other reservoir processes are crucial for the economic viability of enhanced geothermal systems. Yet, the systematics of their behavior are still rather poorly understood, mainly because only few test sites have so far been operated and knowledge of the actual geological structure of the respective reservoirs is limited.

Numerical simulation is an attractive test bed to obtain fundamental insights into how geological parameters affect these physical and chemical processes. Depending on the problem, meaningful simulations reach from simple generic evaluations to studying coupled processes operating on complex geometries.

The latter can be addressed with a new generation of simulation tools that allow increasing realism in the model representation of geological structures, the accuracy with which the governing equations can be solved, and the size of models that can be handled within reasonable computing time. These developments center on simulating the mechanical behavior of complex fracture networks, the long-term permeability changes and scaling due to fluid-rock interaction, and the efficiency of heat extraction from reservoirs with heterogeneously distributed fracture permeability.

Such simulators allow building a knowledge base on optimal reservoir characteristics that may become a valuable tool for geothermal exploration models. Simulating “what if” scenarios may ultimately aid in decision making during reservoir engineering and operation.

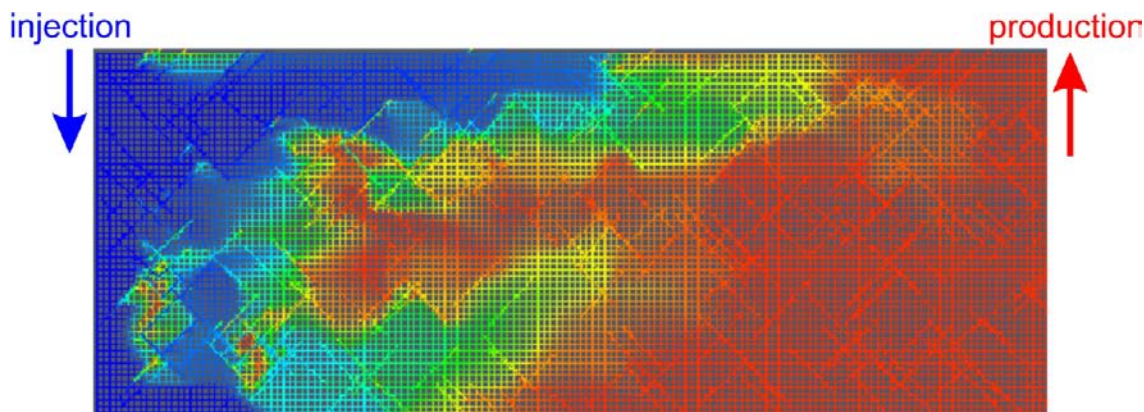


Fig. 1: Non-uniform progression of cold water front (blue) from injection well (left) towards production well (right) in a highly schematic geothermal reservoir model with heterogenous matrix and fracture permeability. Simulation by D. Karvounis, Institute of Fluid Dynamics, ETH Zurich.

20.8

Efficient conversion of geothermal resources for multiple energy uses

Gerber Léda¹ & Maréchal François¹

¹Industrial Energy Systems Laboratory, Ecole Polytechnique Fédéral de Lausanne, LENI-IGM-STI, Station 9, CH-1015 Lausanne (leda.gerber@epfl.ch)

Everything is not about obtaining hot water from the ground: it has as well to be decided how to realize the best use of the available resources, and which ones of them have to be targeted in priority. Important objectives that have to be accounted for in the design of the conversion system are the maximization of its economical profitability and of its efficiency.

High temperature geothermal energy from Enhanced Geothermal Systems (EGS) can be used for the polygeneration of multiple energy services: electricity, district heating and domestic hot water. Several conversion technologies can be used for this, such as flash systems and binary cycles.

In order to choose the best conversion technology and its operating conditions, the temperature levels of the geothermal resource and of the demand in district heating have both to be accounted for. Another important parameter is the seasonal variation of the demand in energy services.

By combining models of the different technologies with models of geothermal resources and of the seasonal demand in district heating, the overall conversion system can be simulated and designed. With a simulation of all the potential combinations of technologies and resources at different depths, it is possible to identify the technological orientations that have to be favored in the future development of cogeneration from EGS.

Results for a given case study, displayed at Figure 1, show that even at low electricity and district heating prices, cogeneration of electricity and district heating from EGS is profitable. The optimal depth of the exploited resource as well as the conversion technology to be used varies depending on these prices. Except at high electricity prices, where double-flash with an EGS at a depth of 8000m is the best combination, the optimal technology is an organic Rankine cycle with an EGS at 7000m.

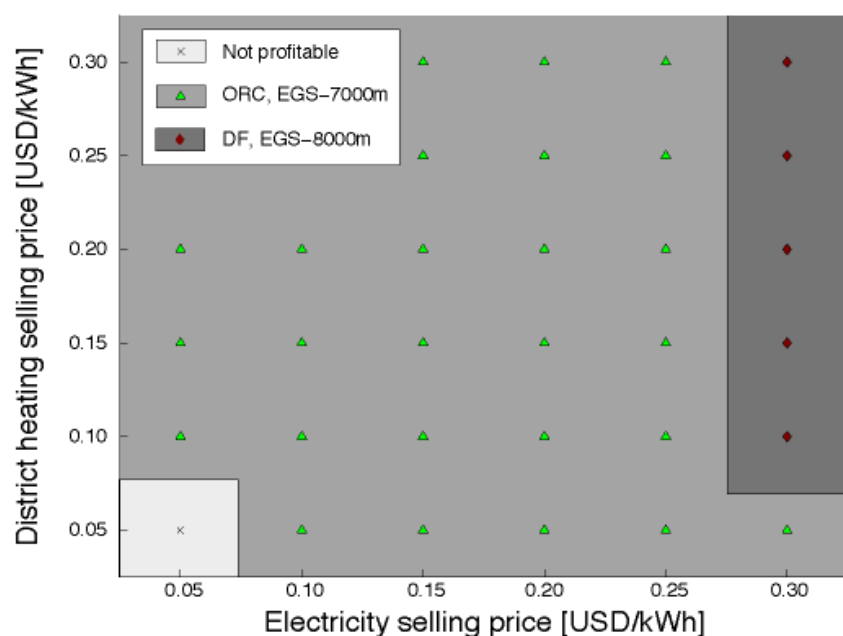


Figure 1. Best technology and depth of EGS in function of electricity and district heating selling prices

REFERENCES

- Hoban, M., Gerber, L. & Maréchal F. 2010: Integrated Thermo-economic Modeling of Geothermal Resources for Optimal Exploitation Scheme Identification, Proceedings of the 23rd International Conference on Efficiency, Cost, Optimization, Simulation and Environmental Impact of Energy Systems, 14-17 June 2010, Lausanne, pp. 2239-2246
- Gerber, L. & Maréchal F. 2011: Defining optimal configurations of geothermal systems using process design and process integration techniques, Chemical Engineering Transactions, 25, pp. 881-886

20.9

Key success factors for Enhanced Geothermal Systems

Meier Peter & Burri Peter

Geo-Energie Suisse AG, Steinentorberg 26, CH-4051 Basel (p.meier@geo-energie.ch)

Geo-Energie Suisse AG is the Centre of Competence for the development of deep geothermal energy created by seven Swiss utility companies. These shareholders want to join their forces and share the risks associated with the development of deep geothermal power generation in Switzerland. Most of them have already been partners of the Deep Heat Mining Project Basel. Therefore one of the most important assets of the newly founded company are the experience and the data from the project in Basel, which has been suspended in 2006 as a consequence of significant induced seismicity.

For Geo-Energie Suisse AG the focus lies on the development of Enhanced Geothermal Systems (EGS), since, given the geological setting of Switzerland, only EGS can lead to an important production of electrical power from geothermal energy (Rybach, 2011). The overall objective of the company lies a) in developing the EGS-concepts and technology further and b) in proving their technical feasibility by executing several pilot projects within the next three to five years.

The key success factors include reservoir creation, risk mitigation and predictability of induced seismicity, drilling technology especially in crystalline rocks, repeatability and long term economic feasibility and public acceptance.

Many international researchers are working since 2006 with the data from the project in Basel. Their work has resulted in a much better understanding of the processes involved with the creation of a large geothermal reservoir in crystalline rock in Switzerland and the risk of induced seismicity. A first task of Geo-Energie Suisse was therefore to compile the results from research and to identify the remaining open questions from a practical point of view. In cooperation with many specialists from industry and research the knowledge gaps are being filled by applying established techniques and tools from other geothermal research projects and also from nuclear waste disposal programs in crystalline rock.

The main objective is to identify and work on the key success factors for a new improved EGS-concept in comparison to the concept of the Basel project. Demonstrating considerable improvement since Basel-1 in understanding the mechanisms of creating artificial reservoirs and in predicting the impact of the methods, is essential to get the support of investors for a new project and gain the acceptance of authorities, politics and the population.

We will discuss the main conceptual ideas for the creation of an economically viable and safe EGS-System and show preliminary results for a horizontal multfrac-system, for which induced seismicity will be reduced and heat exchange area increased with respect to earlier used EGS-concepts. We will also discuss the main challenges for the further development and address some priority requirements in the interaction with government, politics, public opinion and universities.

REFERENCES

Rybach, L. 2011: Prospects of deep geothermal energy in Switzerland, 9th Swiss Geoscience Meeting, Zürich 2011

P 20.1

A survey of the induced seismic responses to fluid injection in geothermal and CO₂ reservoirs in Europe

Keith F. Evans¹ Alba Zappone², Toni Kraft², Nicolas Deichmann², Fabio Moia³

¹ *Engineering Geology, Swiss Federal Institute of Technology (ETH), Sonneggstrasse 5, 8092 Zürich, Switzerland.*

² *Swiss Seismological Service, Sonneggstrasse 5, 8092 Zürich, Switzerland.*

³ *RSE-Ricerca Sistema Energetico S.p.A., Milan, Italy.*

We document 41 European case histories that describe the seismogenic response of crystalline and sedimentary rocks to fluid injection. The work is part of an on-going study to identify factors that have a bearing on the seismic hazard associated with fluid injection. The data generally support the view that injection in sedimentary rocks tends to be less seismogenic than in crystalline rocks, although the presence of faults near the wells that allow pressures to penetrate significant distances vertically and laterally can be expected to increase the risk of producing felt events. All cases of injection into crystalline rocks produce seismic events, albeit usually of non-damaging magnitudes, and all crystalline rock masses were found to be critically stressed, regardless of the strength of their seismogenic responses to injection. Thus, these data suggest that criticality of stress, whilst a necessary condition for producing earthquakes that would disturb (or be felt by) the local population, is not a sufficient condition. The present data are not fully consistent with the concept that injection in to deeper crystalline formations tends to produce larger magnitude events. Injection at sites with low natural seismicity, defined by the expectation that the local peak ground acceleration has less than a 10% chance of exceeding 0.07g in 50 years, has not produced felt events. Although the database is limited, this suggests that low natural seismicity, corresponding to hazard levels at or below 0.07g, may be a useful indicator of a low propensity for fluid injection to produce felt or damaging events. However, higher values do not necessarily imply a high propensity.

P 20.2

What can induced earthquake source properties tell us about reservoir geomechanics?

Goertz-Allmann Bettina¹, Corinne Bachmann¹, and Stefan Wiemer¹

* ETH Zurich, Institute of Geophysics / Schweizerischer Erdbebendienst,
Sonneggstrasse 5, CH-8092 Zurich (bettina.allmann@sed.ethz.ch)

Hydraulic fracturing is an increasingly utilized technology to enhance the extraction of hot water or gas from a subsurface reservoir. Fluids are pressed into the reservoir formation from a treatment well at high pressures to open fractures and hence increase the permeability of the reservoir. Monitoring the seismic emission associated with the fluid injection allows to estimate the stimulated reservoir volume, and hence the effectiveness of the treatment. However, oftentimes little is known about the mechanical properties of the reservoir rocks, making it difficult to predict the response of the medium to the fluid injection. On the one hand, one would like to ensure that the fluid injection operation alters the medium sufficiently to make the reservoir economic, and on the other hand it needs to be insured that the magnitude of induced seismic events does not exceed values where shaking can affect surface infrastructure. A proper estimation of the in-situ mechanical properties of the reservoir is therefore necessary for an assessment of both the economics of reservoir treatment as well as the associated seismic hazard at the surface.

In this presentation, we show that the analysis of source properties of induced seismicity allows an estimation of the in-situ stress regime, and thus of the mechanical properties of the reservoir. For this purpose, we analyse seismicity induced by fluid injection in the Basel geothermal project in 2006. More than 10,500 events were induced since the beginning of stimulation, most of them during the actual 6-day stimulation period. The induced seismic activity culminated in several larger magnitude (up to $M_L=3.4$) earthquakes shortly after well shut-in, which were felt at the surface. The Basel case is an example for the potential seismic risk associated with hydraulic fracturing. The events were recorded by a six station seismic array installed in five monitoring boreholes within 5 km of the injection at depths between 317 m and 2740 m.

We estimate stress drops of the induced events from the best-fitting corner frequency of the P-wave source spectra. We also analyse spatial variations in the frequency-magnitude distribution of the seismicity. We observe significantly lower stress drops and higher b-values near the injection point. Stress drop increases by about a factor of five with radial distance from 10 m to 300 m. Comparison with forward-modeled pore pressure perturbation using a linear diffusion model reveals a correlation of both source properties with the pore pressure distribution in the reservoir. Stress drop is inversely proportional to the forward-calculated pore pressure perturbation within about 300 m of the injection point.

We can describe the observations by forward-modeling the pressure-induced stress changes and seismicity triggering based on Coulomb friction. We assume a stochastic heterogeneous stress distribution in the medium based on literature values of the minimum and maximum horizontal stresses, and the coefficient of friction. In an injection experiment, the stress field is mainly modified by the injection pressure. Increasing the pore pressure in the medium causes a reduction of the normal stress to an effective stress. If the stress is near the critical state (Mohr circle close to the Coulomb envelope) the reduction of the normal stress may cause the shear stress to exceed the Coulomb failure envelope and hence trigger an event. We model the spatio-temporal evolution of the effective stress based on a linear diffusion model and the actual wellhead pressure, and record an event once the Mohr circle has crossed the failure envelope. Stress drop and b-values are linked to differential stress in the modeling. The result is a forward-modeled seismicity cloud with origin time, stress drop, and magnitude assigned to each event location in the medium.

Our model is able to explain in principle the observation of reduced stress drop and increased b-values near the injection point where pore pressure perturbations are highest. The higher the pore pressure perturbation, the less critical stress states still trigger an event, and hence the lower the differential stress is before triggering an event. Less critical stress states (lower differential stresses) result in lower stress drops and higher b-values, if both are linked to differential stress.

We are therefore able to establish a link between the seismological observables and the geomechanical properties of the source region and thus a reservoir. Understanding the geomechanical properties is essential for estimating the probability of exceeding a certain magnitude value in the induced seismicity and hence the associated seismic hazard of the operation.

P 20.3

GEOBEST - A contribution to the long term development of deep geothermal energy in Switzerland

Toni Kraft¹, Stephan Husen¹ and Stefan Wiemer¹

¹Swiss Seismological Service @ ETH-Zurich, Sonneggstrasse 5, 8092 Zurich, Switzerland, (kraft@sed.ethz.ch)

Summary

The Swiss Seismological Service (SED) is implementing the GeoBest project on behalf of the Swiss Federal Office for Energy (SFOE) to provide cantonal and federal authorities with guidelines on how to handle seismic hazard in the framework of the environmental risk assessment. Within GEOBEST, selected pilot projects in Switzerland will be supported in the necessary seismic monitoring of natural and induced seismicity. GeoBest supports the pilot project in the first two years, that are most critical with respect to the financial risk, by providing seismological instrumentation from the GeoBest instrument pool and partial financial support for the installation and operation of the seismic monitoring network. In return the pilot projects grant SED access to project data needed for seismic hazard assessment and the development of best practice guidelines.

Background

With the global challenge to satisfy an increasing demand for energy while at the same time stabilizing or reducing carbon dioxide (CO₂) concentrations in the atmosphere, deep geothermal resources are being increasingly recognized by society as an attractive alternative energy source. Deep hydrothermal resources, such as aquifers at depths larger than 2km with sufficiently high productivity, have been successfully exploited for many years, but their distribution and potential for supplying electricity is limited. However, artificially created Enhanced or Engineered Geothermal Systems (EGSs) do not suffer this restriction.

In general, deep geothermal resources are exploited by circulating fluids through a geothermal reservoir using a number of deep injection and production wells, thereby extracting heat from the permeable or fractured rock mass. This operation

invariably alters the stress and pore pressure in the subsurface. The changes tend to be most pronounced during the EGS reservoir creation (i.e. stimulation) phase, but they also occur in the operational phase of EGS and deep hydrothermal systems (Giardini, 2009).

It has been realized over the last 20 years, that the Earth's crust generally supports high shear stress levels and is often close to failure. Thus, even small changes of the stress and pore pressure in the subsurface due to Earth engineering endeavors or even anomalously heavy rainfall can be sufficient to induce seismicity in natural systems (e.g., Hainzl et al. 2006, Husen et al. 2007). Historically, the most damaging events, are associated with the impoundment of reservoirs (Gupta, 1992). However, earthquakes of sufficient size to cause damage to localities have also been associated with mining activity (Gibowicz, 1990), long-term fluid withdrawal wells (Segall, 1989), and long-term fluid injection wells (Nicholson and Wesson, 1990; Evans et al. 2011).

Even though, massive stimulation injections have routinely been performed at EGS sites since the early 70s, the issue of the seismic hazard associated with these operations has only recently come to the fore. This is because the pioneering EGS developments at Fenton Hill (USA), Rosemanowes (UK), Hijiori (JP) and Soultz (F, 3.5 km reservoir) did not produce events large enough to disturb the local population. Recent attempts to develop EGS at 4.5-5.0 km at Soultz (F), Cooper Basin (AUS) and Basel (CH), and deep (~3km) hydrothermal systems in Landau (D) and Unterhaching (D) produced events approaching or exceeding magnitude $M_L=3$. A recent review of induced seismicity associated with deep fluid injections in Europe, including recapitulatory case histories, is given by Evans et al. (2011).

The processes and conditions underpinning induced seismicity associated with deep geothermal operations are still not sufficiently well understood to make useful predictions as to the likely seismic response to reservoir development and exploitation. The empirical data include only a handful of well-monitored EGS experiments; models are consequently poorly constrained. Unfortunately, datasets of well-monitored deep hydrothermal experiments are missing and empirical constraints of induced seismicity models for these cases do not exist. Given that the majority of the projects underway or planned in Europe are of the hydrothermal type, there is hope that this deficit can be remedied in the near future through a close cooperation of geothermal industry, science and public authorities.

This is where the GeoBest project comes to play. By supporting selected pilot project for a limited time, SED facilitates the dialog with geothermal industry. Besides of the unique opportunity to collect high quality seismic data and being able to access relevant project data, gaining first hand practical experience in this field is of paramount importance for the development of significant best practice guidelines.

Project Description

A detailed description of the goals of the GeoBest projects can be found in the document (www.seismo.ethz.ch -> Groups -> Special Seismic Networks -> GEOBEST).

REFERENCES:

- Evans, K.F., A. Zappone, T. Kraft, N. Deichmann and F. Moia (2011). A Survey of induced seismic response to fluid injection in geothermal and CO₂ reservoirs in Europe, accepted for publication in *Geothermics*.
- Giardini, D. (2009), Geothermal quake risks must be faced, *Nature*, 461, pp. 848-849.
- Gibowicz, S.J. (1990). Seismicity induced by mining. *Advances in Geophysics*, 32, pp. 1-74.
- Gupta, H.K. (1992). Reservoir-induced Earthquakes. Elsevier, Amsterdam, 364 pp.
- Hainzl, S., T. Kraft, J. Wassermann, and H. Igel (2006). Evidence for rain-triggered earthquake activity, *Geophys. Res. Lett.*, 33, L19303, <http://dx.doi.org/10.1029/2006GL027642>.
- Husen, S., C. Bachmann, and D. Giardini (2007). Locally triggered seismicity in the central Swiss Alps following the large rainfall event of August 2005. *Geophys. J. Int.*, 171, pp.1126-1134.
- Kraft, T., K.F. Evans, D. Giardini, N. Deichmann, and S. Wiemer (2010). Induced seismicity associated with the exploitation of deep geothermal resources, *European Geologist*, 29, pp.19-20.
- Nicholson, C. and R.L. Wesson, 1990. Earthquake hazard associated with deep well injection. *US Geological Survey Bulletin* 1951, 74 pp.
- Segall, P. (1989). Earthquakes triggered by fluid extraction. *Geology*, 17/10. pp. 942-946.

P 20.4

Changes of Coulomb Failure Stress due to dislocations during stimulation of well GPK2 in Soultz-sous-Forêts

Schoenball Martin^{1,2}, Baujard Clément¹, Kohl Thomas^{1,2} & Dorbath Louis³

¹GEOWATT AG, Dohlenweg 28, CH-8050 Zürich (schoenball@geowatt.ch)

²Karlsruher Institut für Technologie, Institut für Angewandte Geowissenschaften, Kaiserstr. 12, D-76131 Karlsruhe

³EOST, University Louis Pasteur, 5, rue René Descartes, F-67084 Strasbourg

The European deep geothermal research project at Soultz-sous-Forêts (Alsace, France) has been developed since 1987. The geothermal reservoir is situated in a horst structure within the granite basement of the Upper Rhine Graben. During the project for developing an Enhanced Geothermal System (EGS) several well stimulations have been conducted and induced several tens of thousands of microseismic events. During the stimulation of well GPK2 the maximum event recorded during stimulation reached magnitude 2.5.

In the field of seismology of tectonic earthquakes, aftershock sequences produced by a large magnitude main shock have been successfully described by changes of Coulomb failure stress due to the dislocation (in the following denoted as Δ CFS) by the main shock (e.g. King et al. 1994 and Toda et al. 2003).

We present 3D computations of Δ CFS by different geometries of the fault plane to find a computationally efficient way to approximate circular sources taking into account an appropriate slip distribution. We then compute transient Δ CFS in the Soultz reservoir during the stimulation of GPK2. For this analysis we use an extensive database of over 700 derived focal mechanisms (Dorbath et al. 2009). This allows us to conclude that the stress perturbation of all microseismic events during stimulation cannot be depicted by one single fault. Furthermore analysis of this dataset allows us to estimate the influence of Δ CFS by dislocation over the total change of Coulomb failure stress by other processes like the increase of pore fluid pressure, thermal stresses, hydraulic response of the reservoir and coupling of these.

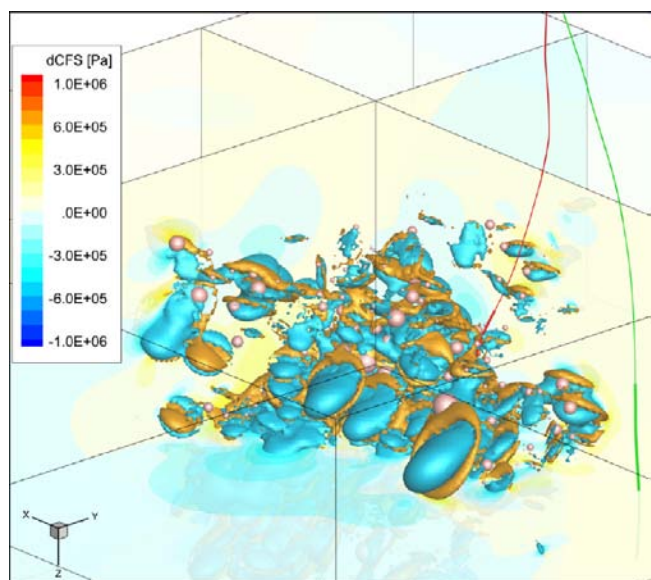


Figure 1. 3D views of Δ CFS in the Soultz reservoir with isosurfaces at ± 0.5 MPa. The wells GPK2 (red), and GPK3 (green) are displayed with bold open hole section. The microseismic events used for the computation are represented by sphere symbols that scale with the event magnitude.

REFERENCES

- Dorbath, L., Cuenot, N., Genter, A. & Frogneux, M. 2009: Seismic response of the fractured and faulted granite of Soultz-sous-Forêts (France) to 5 km deep massive water injections. *Geophysical Journal International*, 177(2), 653–75.
- King, G. C. P., Stein, R. S. & Lin, J. 1994: Static stress changes and the triggering of earthquakes. *Bulletin of the Seismological Society of America*, 84(3), 935–953.
- Toda, S. & Stein, R. 2003: Toggling of seismicity by the 1997 Kagoshima earthquake couplet: A demonstration of time-dependent stress transfer. *J. Geophys. Res.*, 108(B12), 2567.

P 20.5

Natural fractures and stress heterogeneity in the host granite of the Basel Deep Heat Mining project

Sikaneta Sakalima & Evans Keith

Engineering Geology, ETH Zürich, Sonneggstrasse 5, CH-8092 Zürich (sakalima.sikaneta@erdw.ethz.ch) (keith.evans@erdw.ethz.ch)

To understand of the processes underpinning permeability enhancement and attendant seismicity in the hydraulic stimulation of Enhanced/Engineered Geothermal Systems (EGSs) requires a geological model of the reservoir that includes discontinuity families and also knowledge of the state of stress. The ultrasonic borehole image (UBI) log provides high-resolution information on both these reservoir characteristics. A UBI log was acquired in the 2.6 km granite section of the Basel BS-1 well prior to the stimulation. We present evidence from borehole breakouts and drilling induced fractures visible on the UBI log that the stress profile within the BS1 well has a significant level of complexity. The stress orientation and stress magnitude fluctuate over the metre to hundreds of metre scales, with fluctuations demonstrably correlated to the occurrence of natural fractures visible on the UBI log. The complexity of the stress field in BS1 contrasts with the commonly held assumption that the state of stress in the subsurface has a constant orientation and magnitudes that vary in a simple, linear manner with respect to depth. The findings of this study emphasise the importance of including stress heterogeneity in geomechanical models of the reservoir seismic and hydraulic response to fluid injection. hence the associated seismic hazard of the operation.

P 20.6

Geothermal energy potential of Vorarlberg (Austria)

Zerlauth Michael¹, Ortner Hugo², Pomella Hannah¹, Schulz Marcel¹, Fügenschuh Bernhard²

¹*alps GmbH, Grabenweg 68, A-6020 Innsbruck (zerlauth@alps-gmbh.com)*

²*Institute of Geology and Palaeontology, Innrain 52, A-6020 Innsbruck*

Several tectonic units in Vorarlberg are potential targets for geothermal exploration, regarding the geological requirements for a hydrothermal system – a water bearing layer with an adequate permeability in an appropriate depth. From the top to the base of the Alpine nappe pile the Mesozoic cover (Bavarian Lechtal nappe) of the Silvretta nappe (Upper Austroalpine basement nappe), the Helvetic nappes as well as autochthonous units of the Northern Alpine foreland are comprised. Out of these units only the last two are probably present in a promising depth of more than 2500 m. The number of suitable locations for a deep hydrothermal system is additionally reduced by the required proximity to industrial customers. According to these limitations the focus in this study is on the Northern Alpine foreland and the Helvetic nappes in the area of the Rhine valley.

The most promising structure is a normal fault system offsetting the autochthonous sedimentary cover of the down-going European plate. This set of south to south-southeast dipping faults, located below Bregenz, was recognised by numerous seismic campaigns during the last 40 years, carried out in the course of the oil and gas exploration in the Molasse basin. Interestingly the currently realized St. Gallen deep geothermal project deals with a quite similar tectonic and stratigraphic setting and is therefore of substantial interest for our Vorarlberg study.

Concerning the southerly located site of interest in the Helvetic nappe stack, the situation is much more complex. Available seismic data reveal the lower and upper boundary of the whole Helvetic nappe stack without internal resolution and the reflectors are mostly afflicted with some uncertainties. Additionally to the seismic data, several deep drillings (V-Au 1, Maderhalm 1, Kierwang 1, Hindelang 1) have been carried out in the years 1961 to 1986. Based on the drill logs, seismic sections, and surface data, various cross sections have been constructed. Thereupon a model for the tectonic evolution of the Helvetic unit was created, in accordance with the situation in Eastern Switzerland and Lichtenstein and partly based on findings of previous authors (e.g. Wyssling 1985 & 1986, Zacher 1973). The facies development of the Helvetic shelf was reconstructed based on literature data and implemented in the model. Special attention was drawn to the Jurassic Quinten-Fm. and the Cretaceous Schrätenkalk-Fm. Both are prominent shelf limestones with a high hydrothermal potential, especially when fractured due to folding or faulting.

Based on all the so far available constraints, two blocks of some square kilometres around Bregenz and Feldkirch were defined for the construction of a 3D model, using the software package Move. These two 3D blocks will provide the basis for further planning of a 3D seismic campaign.

REFERENCES

- Wyssling, G. 1985: Palinspastische Abwicklung der helvetischen Decken von Vorarlberg und Allgäu. *Jb. Geol. B.-A.*, 127, Heft 4, 701-706.
- Wyssling, G. 1986: Der frühkretazische helvetische Schelf in Vorarlberg und im Allgäu - Stratigraphie, Sedimentologie und Paläogeographie. *Jb. Geol. B.-A.*, 129, Heft 1, 161-265.
- Zacher, W., 1973: Das Helvetikum zwischen Rhein und Iller (Allgäu - Vorarlberg). Tektonische, paläogeographische und sedimentologische Untersuchungen. *Geotekt. Forsch.*, 44,I-II, 1-74.

21. Geophysics and Rockphysics

Marcel Frehner

Swiss Geophysical Commission

TALKS:

- 21.1 *Gabriel A.-A., Ampuero J.-P., Dalguer L. A., Mai P. M.*: Macroscopic Source Properties from Dynamic Rupture Simulations in Plastic Media
- 21.2 *Girard L., Gruber S., Weber S., Amitrano D.*: Rock damage inferred from acoustic emissions in a partly frozen high-alpine rock-wall
- 21.3 *Kuteynikova M., Quintal B., Tisato N.*: Numerical modelling and laboratory measurements of seismic attenuation
- 21.4 *Madonna C., Almqvist B. S.G., Saenger E. H.*: Digital rock physics: numerical prediction of pressure-dependent ultrasonic velocities using micro-CT imaging
- 21.5 *Quintal B., Steeb H., Frehner M., Schmalholz S.M.*: S-wave attenuation due to wave-induced fluid flow in heterogeneous, partially saturated porous media
- 21.6 *Riahi N., Birkelo B., Saenger E. H.*: A statistical approach to ambient wave field analysis
- 21.7 *Saenger E.H., Enzmann F., Keehm Y., Steeb H.*: Digital rock physics: Effect of fluid viscosity on effective elastic properties
- 21.8 *van Dinther Y., Gerya T.V., Corbi F., Funicello F., Mai P.M., Dalguer L.A.*: The long-term seismic cycle at subduction thrusts: benchmarking geodynamic numerical simulations and analogue mode

POSTERS:

- P 21.1 *Abdelfettah Yassine, Schill Eva*: Accurate gravity data correction and 3D gravity forward modeling
- P 21.2 *Almqvist B.S.G, Aschwanden L., Diamond L., Ramseyer K., Zappone A.*: Characterization of the Upper Muschelkalk aquifer in northeast Switzerland using laboratory physical properties and imaging techniques
- P 21.3 *Baumann C.F.D., Dalguer L.A.*: Toward source characterization of local supershear ruptures in dip-slip faults
- P 21.4 *Benson, P., Heap, M., Lavallée, Y., Flaws, A., Hess, K., Cordonnier, B. and Misra, S.*: Laboratory simulations of tensile (hydro) fracture: current work and new directions
- P 21.5 *Frehner M., Quintal B.*: Physical mechanisms for low-frequency seismic wave attenuation in fractured media
- P 21.6 *Kaveh Khaksar, Marahem Rahmati*: Rock classification based on physico-mechanical analysis -case study: Poshtkuh basin, Alborze region-Iran
- P 21.7 *Madonna C., Tisato N., Saenger E. H.*: Low frequency measurements of seismic wave attenuation
- P 21.8 *Schoenball, M., Baujard, C, Köhl, T., Dorbath, L.*: Changes of Coulomb Failure Stress due to Dislocations during Stimulation of GPK2 at Soultz-sous-Forêts
- P 21.9 *Tisato N., Madonna C., Saenger E.H.*: Measurements and mechanisms of seismic wave attenuation in partially saturated rocks
- P 21.10 *Zappone A., Bruijn R., Tripoli B., Biedermann A.R., Burg J-P., Kissling E.*: The Swiss Atlas of Physical Properties of Rocks (SAPHYR): Progress and developments
- P 21.11 *Zappone A., Diamond L., Almqvist B., Evans K., Deichmann N., Werner M., Mazzotti M.*: Carma – Carbon Management in Power Generation: Geological CO₂ storage in Switzerland

21.1

Macroscopic Source Properties from Dynamic Rupture Simulations in Plastic Media

Gabriel Alice-Agnes¹, Ampuero Jean-Paul², Dalguer Luis Angel¹, Mai Paul Martin³

¹Swiss Seismological Service, ETH Zurich, Sonneggstr. 5, CH-8032 Zurich, Switzerland (alice@sed.ethz.ch)

²Seismological Laboratory, California Institute of Technology, 1200 E. California Blvd., MC 252-21, Pasadena, CA 91125, USA

³Division of Physical Sciences & Engineering, King Abdullah University of Science and Technology, Thuwal 23955-6900, Kingdom of Saudi Arabia

High stress concentrations at earthquake rupture fronts may generate an inelastic off-fault response at the rupture tip, leading to increased energy absorption in the damage zone. Furthermore, the induced asymmetric plastic strain field in in-plane rupture modes may produce bimaterial interfaces that can increase radiation efficiency and reduce frictional dissipation. Off-fault inelasticity thus plays an important role for realistic predictions of near-fault ground motion.

Guided by our previous studies in the 2D elastic case, we perform rupture dynamics simulations including rate-and-state friction and off-fault plasticity to investigate the effects on the rupture properties. We quantitatively analyze macroscopic source properties for different rupture styles, ranging from cracks to pulses and subshear to supershear ruptures, and their transitional mechanisms. The energy dissipation due to off-fault inelasticity modifies the conditions to obtain each rupture style and alters macroscopic source properties. We examine apparent fracture energy, rupture and healing front speed, peak slip and peak slip velocity, dynamic stress drop and size of the process and plastic zones, slip and plastic seismic moment, and their connection to ground motion. This presentation focuses on the effects of rupture style and off-fault plasticity on the resulting ground motion patterns, especially on characteristic slip velocity function signatures and resulting seismic moments.

We aim at developing scaling rules for equivalent elastic models, as function of background stress and frictional parameters, that may lead to improved “pseudo-dynamic” source parameterizations for ground-motion calculation. Moreover, our simulations might provide quantitative relations between off-fault energy dissipation and macroscopic source properties.

21.2

Rock damage inferred from acoustic emissions in a partly frozen high-alpine rock-wall

Girard Lucas¹, Gruber Stephan¹, Weber Samuel¹ & Amitrano David²

¹ 3G, Dep. of Geography, University of Zurich, Winterthurerstr. 190, CH-8057 Zurich, Switzerland. (girard@geo.uzh.ch)

² ISTerre, CNRS - Université Joseph Fourier, Grenoble, BP 53, 38041 Grenoble Cedex 9, France.

The formation of ice within rock is an important driver of rock damage near the surface and up to several meters depth. In steep terrain, this process may be crucial for the slow preconditioning of rock fall from warming permafrost areas. This presentation reports results from a pilot study where acoustic emission monitoring was used to investigate rock damage in a high-alpine rock-wall induced by natural thermal cycling and freezing/thawing.

Laboratory experiments as well as theoretical studies have contributed to clarify the basic mechanisms through which ice formation can damage rock: (i) the difference in density between the liquid water and the ice crystal, which results in the initial build-up of an in-pore pressure at the onset of crystallization and (ii) the cryo-suction process, which drives liquid water towards already frozen pores as the temperature further decreases. However, the transfer of corresponding theoretical insight and laboratory evidence to natural conditions characterized by strong spatial and temporal heterogeneity is nontrivial. The pilot experiment that we present here is intended to prepare the corresponding characterization of rock damage in natural conditions. The measurements were performed on a rock-wall located close to Jungfrauoch (Berner Oberland) at 3500m a.s.l. during 4 days in April 2010.

The results demonstrate the feasibility of such a technique: (i) the statistical properties of the acoustic emission events are shown to obey robust power-law distributions in the time and energy domains, expressing that rock damage and micro-fracturing are induced by stresses arising from thermal variations and associated freezing/thawing of rock; (ii) liquid water availability and rock temperature affect the acoustic emission activity, indicating the importance of freezing-induced stresses. These results suggest that the framework of further modeling studies (theoretical and numerical) should include damage, elastic interactions and poro-mechanics in order to describe freezing-related stresses.

21.3

Numerical modeling and laboratory measurements of seismic attenuation

Maria Kuteynikova¹, Beatriz Quintal¹, and Nicola Tisato¹

¹The Rock Physics Network at ETH Zurich (ROCKETH), Sonneggstrasse 5, CH-8092 Zurich, Switzerland
(maria.kuteynikova@erdw.ethz.ch)

Estimating pore fluid properties of saturated porous rocks from seismic data is very important in exploration geophysics for finding hydrocarbon reservoirs and in reservoir geophysics for monitoring and optimizing production. Theoretical studies show that pore fluid properties have a major effect on attenuation and velocity dispersion of seismic waves. This effect opens the potential of estimating fluid properties from seismic data. However, despite years of research on this subject, this link has not yet been exploited by the oil industry in exploration and production routines. For that to happen, the effect of fluid properties on seismic attenuation and velocity dispersion has to be quantified and better understood through laboratory and numerical investigations.

A major cause of attenuation and velocity dispersion in the frequency range of interest in seismic exploration (1-100 Hz) is wave-induced flow of pore fluid in the mesoscopic scale (e.g., Pride et al., 2004). The mesoscopic scale is much larger than the pore size (2-50 nm) and much smaller than the seismic wavelengths (hundreds of meters for seismic frequencies). In White's model (White, 1975) a partially saturated rock can be approximated by a medium with mesoscopic-scale heterogeneities fully saturated with one fluid and the background fully saturated with another fluid (so-called patchy saturation). The passing wave induces different fluid pressure in the regions saturated with fluids of different compressibilities.

Attenuation arises due to induced pressure gradients on the mesoscale, which causes fluid to flow and thus the loss of energy. White's model can be modeled using Biot's equations for wave propagation in poroelastic media with spatially varying petrophysical parameters. However, solving Biot's equations for wave propagation to calculate seismic attenuation due to wave-induced fluid flow is computationally inefficient because wave propagation and fluid flow occur on very different time scales. A method that is computationally efficient in calculating attenuation related to the fluid flow in the mesoscopic-scale is a quasi-static creep test (Masson and Pride, 2007). Furthermore, for calculating attenuation due to only wave-induced fluid flow at low seismic frequencies, inertial forces are negligible. Thus it is enough to solve a simpler mathematical problem, that is, Biot's equations of consolidation (Quintal et al., 2011).

In this work attenuation and velocity dispersion in porous saturated rocks due to wave-induced fluid flow are calculated by solving Biot's equations of consolidation with the software COMSOL. The finite element method is employed to simulate a creep test on a 2D numerical rock sample with mesoscopic-scale heterogeneities in fluid saturation. The resulting time-dependent stress-strain relations are transformed to the frequency domain with a fast Fourier transform and then used to calculate the undrained bulk and shear moduli. With these moduli, we determine the frequency-dependent P- and S-wave attenuation and velocity dispersion in the sample caused by the mechanism of wave-induced fluid flow.

Numerical modeling is useful to better understand the effect of rock-fluid properties on seismic waves. However, more than one physical mechanisms and complicated geometries and distributions of heterogeneities take place in real rocks. Thus, modeling needs a continuous comparison with laboratory data. Here we compare our numerical results to the data obtained using the Broad Band Attenuation Vessel (BBAV) (Tisato et al., 2011). The BBAV measures the phase angle between the force applied and the shortening of the sample, from which seismic wave attenuation at low frequencies (0.1-100 Hz) is calculated. The vessel can confine the sample, a cylinder of 0.25 m length and 0.038 m diameter, up to a pressure of 25 MPa to simulate subsurface in situ conditions. Attenuation ($1/Q$) measurements for two Berea sandstone samples with different permeability (about 300 and 800 mD), saturated with 90% water and 10% air, are shown in the figure below. The same physical parameters were input into the numerical model. Solid lines show the numerical results for different geometries and patch size, but the same saturation (90% water). As we see, different sizes of patches have an influence on the frequency-dependent attenuation. Further studies are needed in order to fit and understand the attenuation curves obtained in the laboratory.

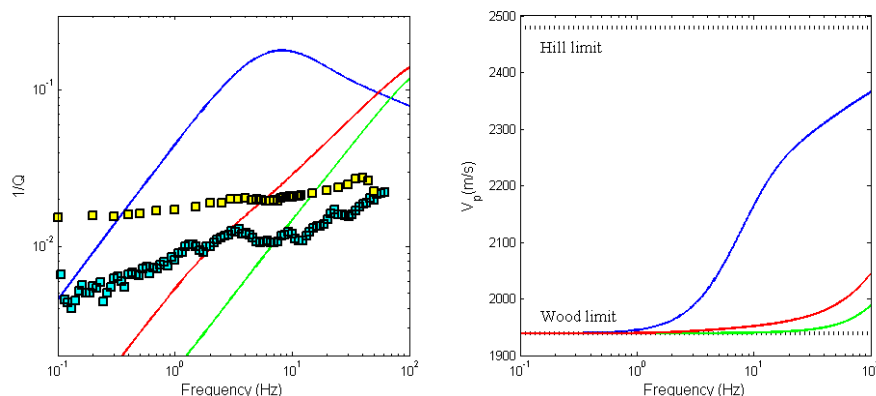


Figure 1. Numerical (solid lines) and laboratory (squares) results for attenuation ($1/Q$), and numerical results for the phase velocity (V_p), versus frequency. Phase velocities reach the Hills limit at higher frequencies.

REFERENCES

- Masson, Y.J., and Pride, S.R., 2007, Poroelastic finite-difference modeling of seismic attenuation and dispersion due to mesoscopic-scale heterogeneity: *Journal of Geophysical Research*, 112, B03204.
- Pride, S.R., Berryman, J.G., and Harris, J.M., 2004, Seismic attenuation due to wave-induced flow: *Journal of Geophysical Research*, 109, B01201.
- Quintal, B., Steeb, H., Frehner, and M., Schmalholz, S.M., 2011, Quasi-static finite element modeling of seismic attenuation and dispersion due to wave-induced fluid flow in poroelastic media: *Journal of Geophysical Research*, 116, B01201.
- Tisato, N., Madonna, C., Artman, B., and Saenger, E.H., 2011, Low frequency measurements of seismic wave attenuation in Berea sandstone: SEG International Exposition and 81st Annual Meeting.
- White, J.E., 1975, Computed seismic speeds and attenuation in rocks with partial gas saturation: *Geophysics*, 40, 2.

21.4

Digital rock physics: numerical prediction of pressure-dependent ultrasonic velocities using micro-CT imaging

Madonna Claudio¹, Almqvist Bjarne S. G.¹ and Saenger Erik H.¹

¹ *Geologisches Institut, Sonneggstrasse 5, CH-8092 Zürich (claudio.madonna@erdw.ethz.ch)*

Over the last decade, micro-tomography has rapidly evolved to become a common microscopy tool in the geosciences. Digital rock physics combines modern microscopic imaging with advanced numerical simulations for analysis of the physical properties of rocks, complementing laboratory investigations. X-ray micro-computed tomography (micro-CT) is among the emerging techniques used for digital rock physics. It allows analysis of a representative sample volume in a non-destructive way and enables the reconstruction of a realistic virtual 3D model of a porous material. Indeed, 3D micro-CT imaging and subsequent numerical determination of petrophysical properties have been applied in several studies, as well as the calculation of transport properties. Elastic-wave propagation modelling based on the microstructure images is used to estimate the effective elastic properties (Saenger et al. 2011).

As with every microscopic imaging technique, there is a trade-off between the maximum resolution and the investigated volume. Because a representative volume of a porous rock is imaged using the micro-CT technique, the smallest pores, micro-cracks, and grain-to-grain contacts remain unresolved. Such micro-structures may significantly influence the mechanical properties of a rock. For example, the elastic properties of granular material strongly depend on the grain-to-grain contacts which micro-CT imaging may not resolve.

The goal of this paper is to describe and understand how laboratory measurements of ultrasonic P-wave velocities compare with digital rock physics results based on the geometric microstructural details present in segmented micro-CT images. Using grain boundary reconstruction algorithms, we present a method for calibrating the numerically overestimated effective elastic properties based on experimental data obtained from a sample of Berea sandstone. We also suggest a strategy to predict pressure-dependent velocity using micro-CT images. A workflow is delineated that enables the identification of grain-to-grain contacts in the micro-CT images and, based on the laboratory calibration, the assignment of weaker micromechanical properties to the grain contacts for the subsequent numerical modeling.

REFERENCES

Saenger E.H., Enzmann F., Keehm Y. and Steeb H., 2011: Digital rock physics: Effect of fluid viscosity on effective elastic properties, *Journal of Applied Geophysics* 74, 236–241.

21.5

S-wave attenuation due to wave-induced fluid flow in heterogeneous, partially saturated porous media

Beatriz Quintal¹, Holger Steeb², Marcel Frehner¹, and Stefan M. Schmalholz³

¹*The Rock Physics Network at ETH Zurich (ROCKETH), Sonneggstrasse 5, 8092, Zurich, Switzerland (beatriz.quintal@erdw.ethz.ch; marcel.frehner@erdw.ethz.ch)*

²*Ruhr-University Bochum, Bochum, Germany (holger.steeb@rub.de)*

³*University of Lausanne, Lausanne, Switzerland (stefan.schmalholz@unil.ch)*

We study seismic S-wave attenuation caused by wave-induced fluid flow at the mesoscopic scale (Pride et al., 2004). Simple-shear relaxation experiments are performed by solving Biot's (1941) equations for consolidation of 2D poroelastic media with finite-element modelling (Quintal et al., 2011). The experiments yield time-dependent stress-strain relations used to calculate the undrained shear modulus, from which S-wave attenuation is determined. Our model consists of periodically distributed (simple-cubic packing) circular heterogeneities with much lower porosity and permeability than the conti-

nuous background medium. The continuous background is fully saturated with oil and the low porosity regions are saturated with water. The background contains 80% of the total pore space of the medium. The total saturation in the medium is then 80% oil, 20% water. Snapshots of the relaxation experiment are shown in Figure 1.

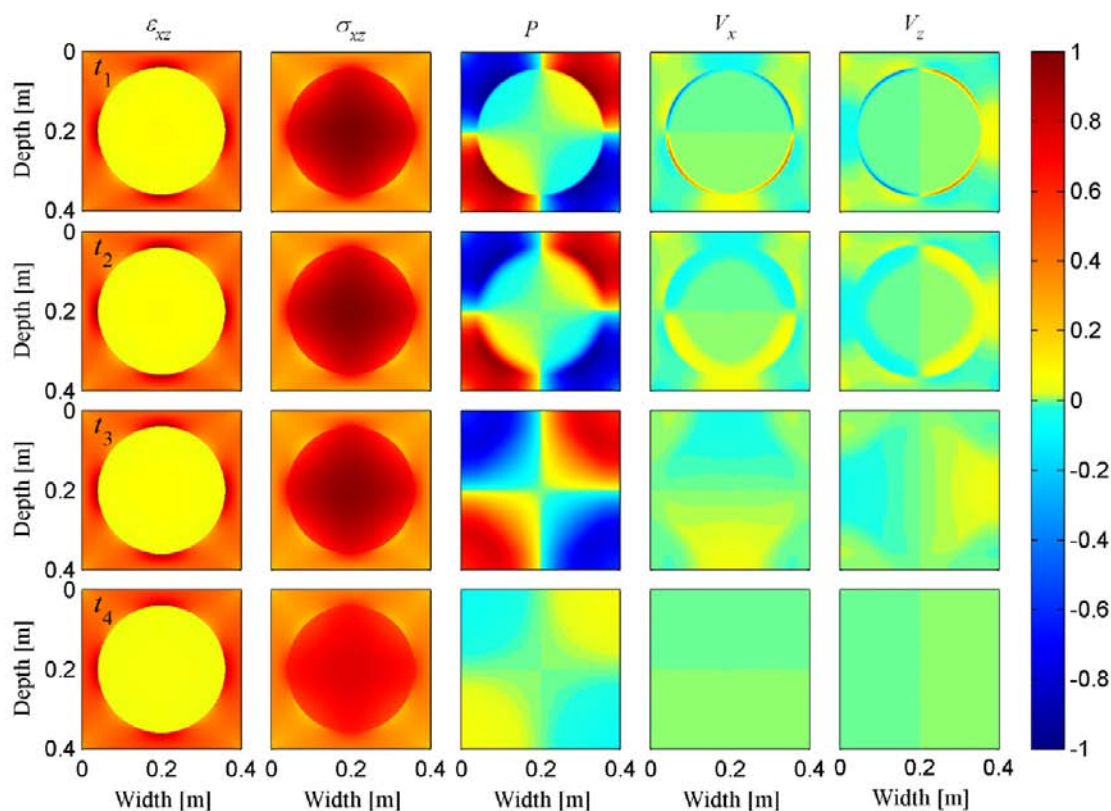


Figure 1. Snapshots at times $t_1 = 8.66 \times 10^{-6}$ s, $t_2 = 1.15 \times 10^{-4}$ s, $t_3 = 2.8 \times 10^{-3}$ s, and $t_4 = 0.1$ s, of the simple-shear relaxation experiment on the representative elementary volume with a circular heterogeneity saturated with oil. The fields ε_{xz} (shear strain), σ_{xz} (shear stress), P (pore fluid pressure), V_x and V_z (fluid velocity in the x- and z-directions) are normalized by their maximum values. The results are shown in Figure 2 (case A, oil-saturated heterogeneity).

For comparison, we also perform experiments for the background saturated with gas or water, instead of oil. The results are shown in Figure 2, where cases A to D differ in the values of the dry bulk and shear moduli (K and μ , respectively) in the background and in the heterogeneities. In case A, K and μ are, respectively, 36 and 32 GPa in the heterogeneity, and 4 and 2 GPa in the background. In case B, 36 and 32 GPa in the heterogeneity, 14 and 12 GPa in the background. In case C, 12 and 8 GPa in the heterogeneity, 4 and 2 GPa in the background. Case D is the opposite of case A, where K and μ are 4 and 2 GPa in the heterogeneity, and 36 and 32 GPa in the background.

The S-wave attenuation in this study is caused by flow of the pore fluid between the heterogeneity and the background caused by fluid pressure differences (see snapshots for P , V_x and V_z in Figure 1). A consistent tendency is observed in the relative behavior of the S-wave attenuation among the different saturation cases (Figure 2). First, in the gas-saturated media the S-wave attenuation is very low and much lower than in the oil-saturated or in the fully water-saturated media. Second, at low frequencies, the S-wave attenuation is significantly higher in the oil-saturated media than in the fully water-saturated media. Based on these tendencies, we suggest that S-wave attenuation could be used in seismic interpretation as an indicator and discriminator of fluid content in a reservoir, in addition to P-wave attenuation.

REFERENCES

- Biot, M. A., 1941: General theory of three-dimensional consolidation: *Journal of Applied Physics* 12, 155-164.
- Pride, S. R., J. G. Berryman, and J. M. Harris, 2004: Seismic attenuation due to wave-induced flow: *Journal of Geophysical Research* 109, B01201.
- Quintal, B., H. Steeb, M. Frehner, and S. M. Schmalholz, 2011: Quasi-static finite element modeling of seismic attenuation and dispersion due to wave-induced fluid flow in poroelastic media: *Journal of Geophysical Research – Solid Earth* 116, B01201.

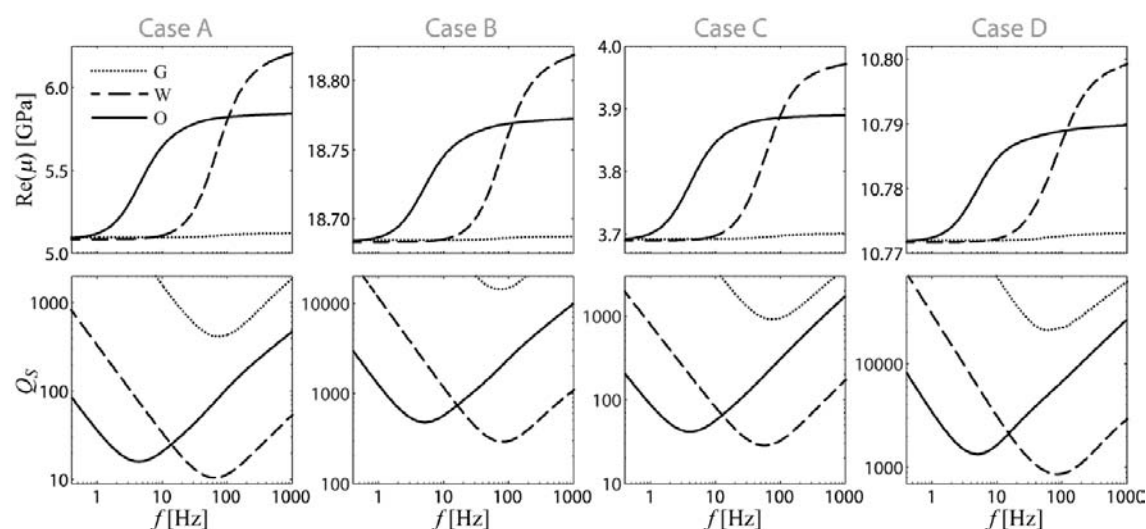


Figure 2. Numerical results for the real part of the undrained shear modulus, μ , and the S-wave quality factor, Q_s . The inverse of Q_s is a measure of S-wave attenuation. The legend terms refer to the fluid in the background: gas (G); water (W); or oil (O).

21.6

A statistical approach to ambient wave field analysis

Riahi Nima¹, Bradley Birkelo², Saenger Erik H.^{1,2}

¹ Earth Science Department ETH, Soneggstrasse 5, 8092 Zürich (nima.riahi@erdw.ethz.ch)

² Spectraseis, 1899 Wynkoop Street, Denver CO 80202, United States

The ubiquitous ambient seismic wave field at the surface can be used to estimate earthquake site response, monitor oceanic weather, and image the Earth's crust. It is also hypothesized to interact with hydrocarbon reservoirs at >800 m depth and exhibit seismic power variations, in particular on the vertical component (Saenger et al., 2009). Attempts to empirically validate this hypothesis require observed correlations between passive seismic power attributes and a reservoir but also a careful investigation of potential confounders such as shallow geologic structure, water table, seismic surface noise sources, and the overburden (Hanssen & Bussat, 2008; Ali et al., 2010).

To test the hypothesis a measurement campaign was conducted at Europe's second largest underground gas storage (UGS) facility in Chémery, France. In two surveys in April and November 2011 about 120 three-component, broadband particle velocity sensors were deployed over several days above and around the UGS. The reservoir is expected to exhibit the largest saturation and pressure changes between these two time snapshots. In the planned time-lapse analysis the constant overburden cannot act as a confounder. However, seasonal variations of the water table and surface noise sources (farming, ocean storms, local weather) must be considered.

We present a three-stage statistical approach that aids in identifying frequency ranges where neither single surface sources dominate nor changes in the near-surface are evident. These tests constitute minimal requirements to pass before analyzing potential correlations to reservoir structures. First, transient and/or high-power noise sources such as traffic and earthquakes are removed by selecting only the 10% of time periods with lowest seismic power (Riahi et al., 2011). Second, the distribution of the azimuth of the dominant polarization of these time periods is tested for isotropy to exclude the possibility that a small number of surface sources was dominating the recording. Lastly, H/V-ratio spectra (Bonney-Claudet, 2006) between the two time snapshots are compared to test if the shallow subsurface was constant, thereby reducing the likelihood of near-surface effects.

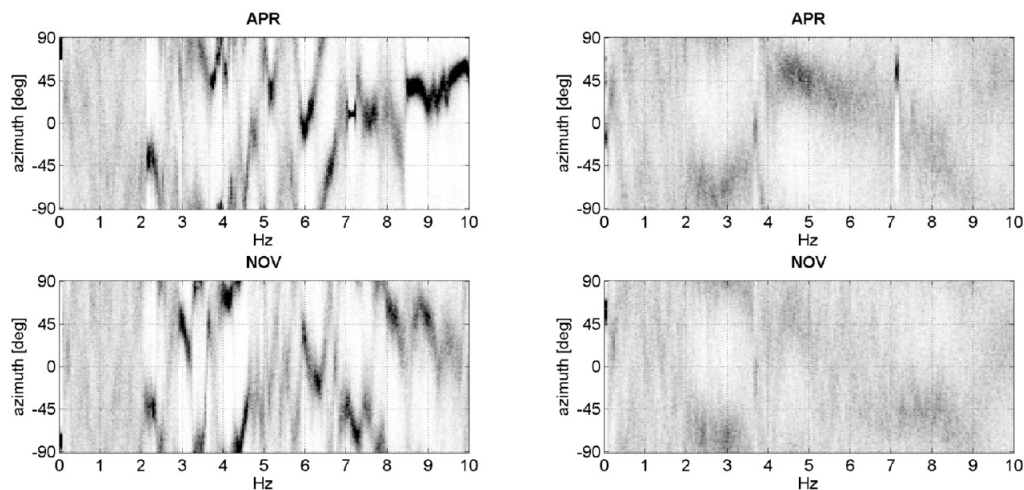


Figure 1 The distribution of polarization azimuth for a receiver near the surface-projected crest of the UGS (left hand side) and away from the UGS (right hand side). The top and bottom panels compare the situation between April and November. All panels reveal an isotropic particle motion below 2 Hz.

The method is illustrated on two sites selected from a larger set of measured locations. The example sites were situated away from the surface-projected crest of the UGS but above the gas storage and above a geologically similar, but gas-free aquifer. For these two particular sites the ambient wave field was found to be laterally isotropic below 2 Hz (Figure 1). Near-surface changes are unlikely to have affected that low-frequency band, as evidenced by stable H/V-spectra (Figure 2). The suggested tests can be applied to all measurements that are considered for a differential analysis to the reservoir.

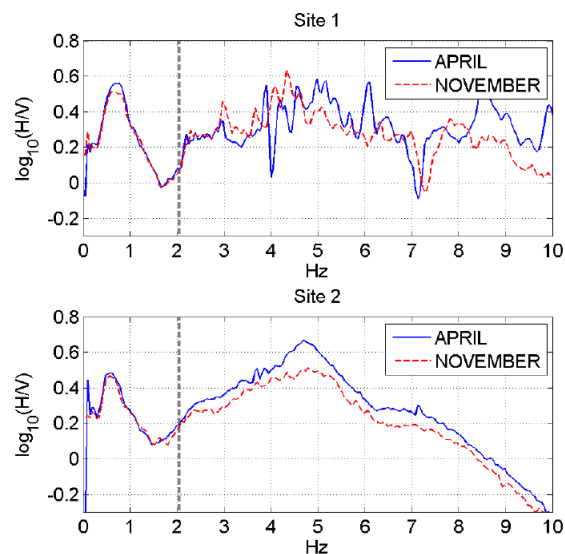


Figure 2 Comparison of H/V spectra observed in April and November for the location above the gas storage (top) and the aquifer (bottom). Below 2 Hz the spectral ratio is constant between the snapshots.

REFERENCES

- Ali, M. Y., Berteussen K. A., Small J., and Barkat B. 2010: Low-frequency passive seismic experiments in Abu Dhabi, United Arab Emirates: implications for hydrocarbon detection, *Geophys Prospect*, 58(5), 875-899.
- Bonnefoy-Claudet, S., Cotton F., and Bard P.-Y. 2006: The nature of noise wavefield and its applications for site effects studies: A literature review, *Earth Science Reviews*, 79, 205-227.
- Hanssen, P., and Bussat S. 2008: Pitfalls in the analysis of low-frequency passive seismic data, *First Break*, 26, 111-119.
- Riahi, N., Birkelo B., and Saenger E. H. 2011: Analyzing passive seismic attributes: a statistical strategy, paper presented at SEG Technical Program Expanded Abstracts, San Antonio.
- Saenger, E. H., Schmalholz S. M., Lambert M. A., Nguyen T. T., Torres A., Metzger S., Habiger R. M., Muller T., Rentsch S., and Mendez-Hernandez E. 2009: A passive seismic survey over a gas field: Analysis of low-frequency anomalies, *Geophysics*, 74(2), O29-O40.

21.7

Digital rock physics: Effect of fluid viscosity on effective elastic properties

Erik H. Saenger¹, Frieder Enzmann², Youngseuk Keehm³, Holger Steeb⁴

¹ETH Zurich and Spectraseis, Switzerland (erik.saenger@erdw.ethz.ch)

²Gutenberg-Universität Mainz, Germany

³Kongju National University, South Korea

⁴Ruhr-Universität Bochum, Germany

This paper is concerned with the effect of pore fluid viscosity on effective elastic properties using digitized rocks. We determine a significant velocity dispersion in wave propagation simulations by the variation of the pore fluid viscosity (Figure 1). Several attenuation regimes are considered which may contribute to this observation. Starting point is a virtual rock physics approach. Numerical simulations of effective transport and effective mechanical properties are applied to statistically representative rock samples. The rock microstructure is imaged by 3D X-ray tomography. Permeability values were estimated through Lattice-Boltzmann flow simulations. The dry rock moduli and the tortuosity are derived by dynamic wave propagation simulations (Figure 2). We apply a displacement-stress rotated staggered finite-difference grid technique to solve the elastodynamic wave equation. An accurate approximation of a Newtonian fluid is implemented in this technique by using a generalized Maxwell body. We give a practical description of how to use this approach and discuss the application limits. Additionally, we show the simulated signature of a theoretically predicted slow S-wave.

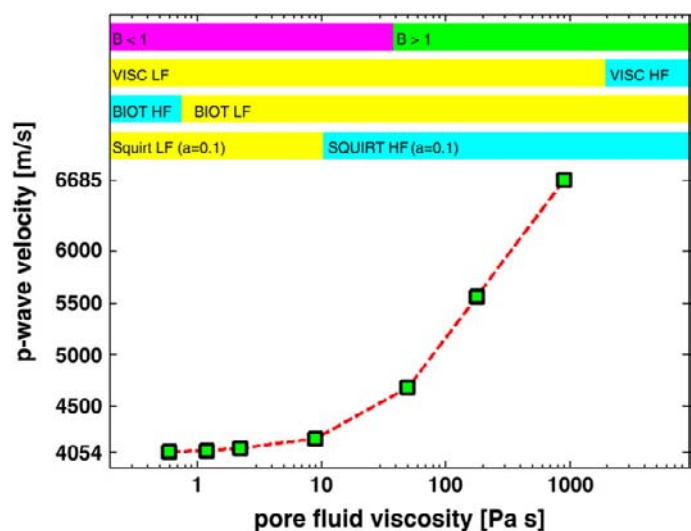


Figure 1. Numerically measured velocity vs. viscosity of the saturating fluid. Details of the corresponding simulations can be found in Saenger et al. (2011)

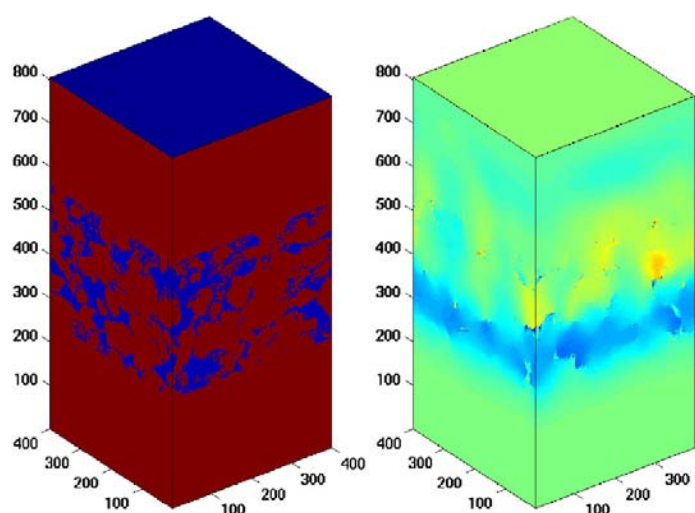


Figure 2. Left hand side: A digital rock with a homogeneous embedding. Red color and blue color indicate grain material and pores, respectively. The used units are grid points (1 [gp]=2.275 μ m). Right hand side: The 3D vertical displacement field of a plane P-wave generated at the top of the model after several timesteps.

REFERENCES

Saenger E.H., Enzmann F., Keehm Y. and Steeb H., 2011: Digital rock physics: Effect of fluid viscosity on effective elastic properties, *Journal of Applied Geophysics* 74, 236–241.

21.8

The long-term seismic cycle at subduction thrusts: benchmarking geodynamic numerical simulations and analogue models

Ylona van Dinther¹, Taras Gerya¹, Fabio Corbi², Francesca Funiciello², P. Martin Mai³, and Luis Dalguer¹

¹ Institute of Geophysics, ETH Zurich, Sonneggstrasse 5, CH-8092 Zurich

² Department of Geology, Università degli Studi 'Roma Tre', Roma, Italy

³ Division of Physical Sciences & Engineering, KAUST, Thuwal, Saudi Arabia

The physics governing the long-term seismic cycle in subduction zones remains elusive, largely due to its spatial inaccessibility, complex tectonic and geometric setting, and the short observational time span. To improve our understanding of the physics governing this seismic cycle, we benchmark a geodynamic numerical approach with a novel laboratory model. In this work we quantify and compare periodicity and source parameters of slip events (earth-quakes and gel-quakes) as a function of fault rheology (i.e. frictional properties).

Our fluid-dynamic numerical method involves a plane-strain finite-difference scheme with marker-in-cell technique to solve the conservation of momentum, mass, and energy for a visco-elasto-plastic rheology. The simulated gelatin laboratory setup constitutes a triangular, visco-elastic crustal wedge on top of a straight subducting slab that includes a velocity-weakening seismogenic zone.

Numerical and analogue results show a regular and roughly comparable periodicity of short, rapid wedge velocity reversals. Ruptures nucleating mainly around the bottom of the seismogenic zone, and propagating upward, cause a distinct and rapid drop in stress within the wedge. To mimic the short duration, high speed and regularity of the analogue results, the numerical method requires a form of steady-state velocity-weakening friction for acceleration, and healing. The necessity of including a variable state component into the numerical simulations is subject of ongoing work. Finally, we extend this analysis by observing the role of different friction laws in large-scale, geometrically more realistic models.

P 21.1

Accurate gravity data correction and 3D gravity forward modeling

Abdelfettah Yassine¹ & Schill Eva

¹ University of Neuchâtel, Emile-Argand 11, 2000 Neuchâtel, Switzerland (yassine.abdelfettah@unine.ch)

The correction of topographic effects on gravity data has been simplified in the past by introducing stepwise approximations to the far-field effect, for example, using the Hammer reticular method. This method computes the topography effect using the approximation of this on the gravity stations which came from the topography interpolation. This approximation causes the loss of the resolution especially at and near the gravity station.

In the present study, we propose a new and accurate gravity data correction approach. The area around the measurement point is subdivided into four zones with increasing radiuses: the inner zone, the near zone, the intermediate and the remote zones. Each zone has a specific weight following its distance to the observed gravity station. The accuracy of the calculation is increasing with decreasing distance. Our approach is based on the fact that any topography area can be described by Digital Elevation Model (DEM). Thus from any DEM, we can recover and construct the numerical topography which can be handled by a PC computer in a reasonable calculation time. From the DEM, we construct discrete prisms for which their gravity contribution to the measurement station is calculated. This calculation is carried out for all prisms until total gravity effect of the topography on the gravity station is assessed.

In order to increase accuracy of the topography effect on the gravity station and at the same time reduce computing time, two DEMs with different resolutions are used. The high resolution DEM is used in the inner zone. Sensitivity analyses have revealed the following recommendations to obtain optimum accuracy:

1. It is recommended to take the cell size resolution of the DEM < 5 m and to extend the inner zone up to 150 m from the gravity stations. The gravity effect is computed using the exact formula for a known prism. This prism has a parallelepiped rectangle form.
2. A DEM of lower resolution can be used for the three outer zones. It is first used in the near zone where the prism effect is computed again with the exact formula. Acceptable results are obtained with fixing the 2nd radius at 8 km, but to improve the accuracy, it is recommended to fix it at a distance more or equal to 20 km especially if there are not computing time constraint.
3. The 3rd sub-area is the intermediate zone which is delimited by the near zone and the 3rd radius. Here the DEM of lower resolution is used to assess the gravity effect of each prism by the theoretical basic formula where the gravity effect is concentrated in the center of the prism. This zone can be extended from 8 to 50 km.
4. The last subarea is the remote zone. It is delimited by the intermediate zone and the 4th radius. The DEM of lower resolution is used to generate a new DEM with cell size about 1 x 1 km. The altitude of these blocs is the average of all prisms located in the 1 x 1 km area. The gravity effect is assessed by the same approach as in the intermediate zone. This area can be extended from 40 to 167 km.

Specific considerations are taken an account between the intersection of these four zones especially between the inner and the near zones where the cell size resolution is not equal.

The following parameters can be chosen for the topographic correction: The radius which delimits the four zones, the densities will be use in the topography correction, if one or two DEM will be use, the format of these DEMs (xyz or ISRI), the input files, ...

Forward modeling of the gravity effect in particular for complex 3D geology is based on the same principal described above. Here the current input files are 3D geological models from 3D Geomodeller and Gocad. A selection of output forms, the different layers and their densities for a geological model can be chosen.

The code was tested and validated successfully on the real data for both gravity data correction and forward modeling. An example for the complete Bouguer anomaly obtained by the purposes is showed in Figure 1.

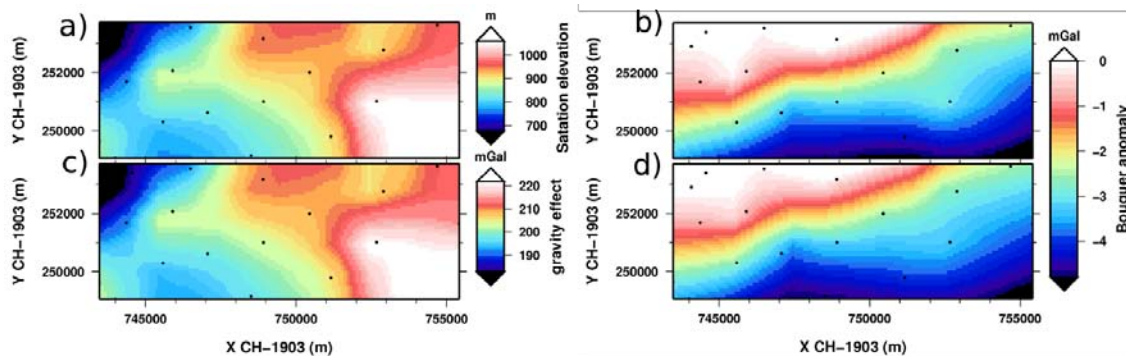


Figure 1: The results of the gravity data processing with a) the gravity station elevations denoted by the black points, b) Bouguer anomaly map computed by the SwissTopo using Hammer reticular method to achieve the topography data correction, c) terrain and the topography effects obtained assuming homogeneous density of 2.67 g/cm^3 . The gravity stations are located at the real elevation on the topography surface as showed in a). The gravity effect of the area is well recovered and as we can identify it is the Free Air anomaly for the homogeneous model. d) Bouguer anomaly obtained by our method. These results were obtained using 2 DEMs. The 1st used in the inner zone has cell size resolution of 2 m and the 2nd of 25 m. The inner zone is limited by 150 m radius and the near zone is limited by 50 km from the stations. The intermediate zone is bordered by the 3rd radius fixed at 70 km and the remote zone is bordered by 170 km radius.

P 21.2

Characterization of the Upper Muschelkalk aquifer in northeast Switzerland using laboratory physical properties and imaging techniques

Almqvist Bjarne S.G.¹, Aschwanden Lukas², Diamond Larryn², Ramseyer Karl², Zappone Alba³

¹ETH Zurich, Institute of Geological Sciences, Sonneggstrasse 5, CH-8092 Zurich (bjarne.almqvist@erdw.ethz.ch)

²University of Bern, Institute of Geological Sciences, Baltzerstrasse 1+3, CH-3012 Bern

³ETH Zurich, Institute of Geophysics, Sonneggstrasse 5, CH-8092 Zurich

Deeply buried levels of the Triassic Trigodonus Dolomite Formation of the Upper Muschelkalk aquifer (Swiss Molasse Basin) show potential for geothermal energy exploitation and for geological storage of gas – whether permanent storage of waste CO_2 (Chevalier et al., 2010) or seasonal storage of imported methane. All of these potential applications rely on high porosities and high permeabilities. Although some borehole intersections of the Formation look encouraging, very little is known about the regional distribution and magnitudes of porosity and permeability within the aquifer. In this context we are undertaking a quantitative and qualitative characterization of the porosity and permeability of the Trigodonus Dolomite using a variety of analytical techniques, including SEM imaging, He-pycnometry, mercury porosity, thin-section petrography, x-ray computer tomography (CT), as well as ultrasonic velocity and permeability measurements. These laboratory analyses will be integrated with field scale geophysical observations and laboratory geochemical and isotopic investigations.

The porosity of the Trigodonus Dolomite is mainly controlled by prevalent secondary dissolution of cm-scale anhydrite nodules and macrofossils as well as microporosity related to the dolomitization process. SEM imaging shows that large dissolution pores are often connected by inter-grain microporosity (Figure 1a). Additional macropore connectivity is provided by cm to dm long subvertical cracks, as is indicated by coarse resolution CT imaging and visual inspection of the drill core (Figure 1b). The timing of the dissolution of anhydrite nodules and formation of macroporosity is not well known and ongoing isotopic and fluid inclusion studies are aimed at pinpointing the dissolution event within the known temperature–burial depth history of the Formation.

The laboratory porosity measurements, on 2.54 cm diameter and ~3.5 cm length cores from the Benken drill core (Nagra, 2001), range from 8 to 25%. Ultrasonic P wave velocities, measured at ambient temperature and pressure conditions, vary from 3100 to 5800 m/s. The S wave velocities of the corresponding cores are between 1800 and 3500 m/s. In general there

is an inverse relationship between velocity and porosity, although a few samples do not follow this trend. Ongoing permeability measurements will help shed light on the micropore connectivity and hence on the injectivity of gas into storage space. However, the total permeability of the aquifer is likely determined by the subvertical sets of fractures, which are usually missed by drillcore-scale sampling. So far, the laboratory results show a good correlation with borehole geophysical data. This opens the way to calibrate the geophysical signals in order to derive a regionally extensive estimate of porosity and permeability.

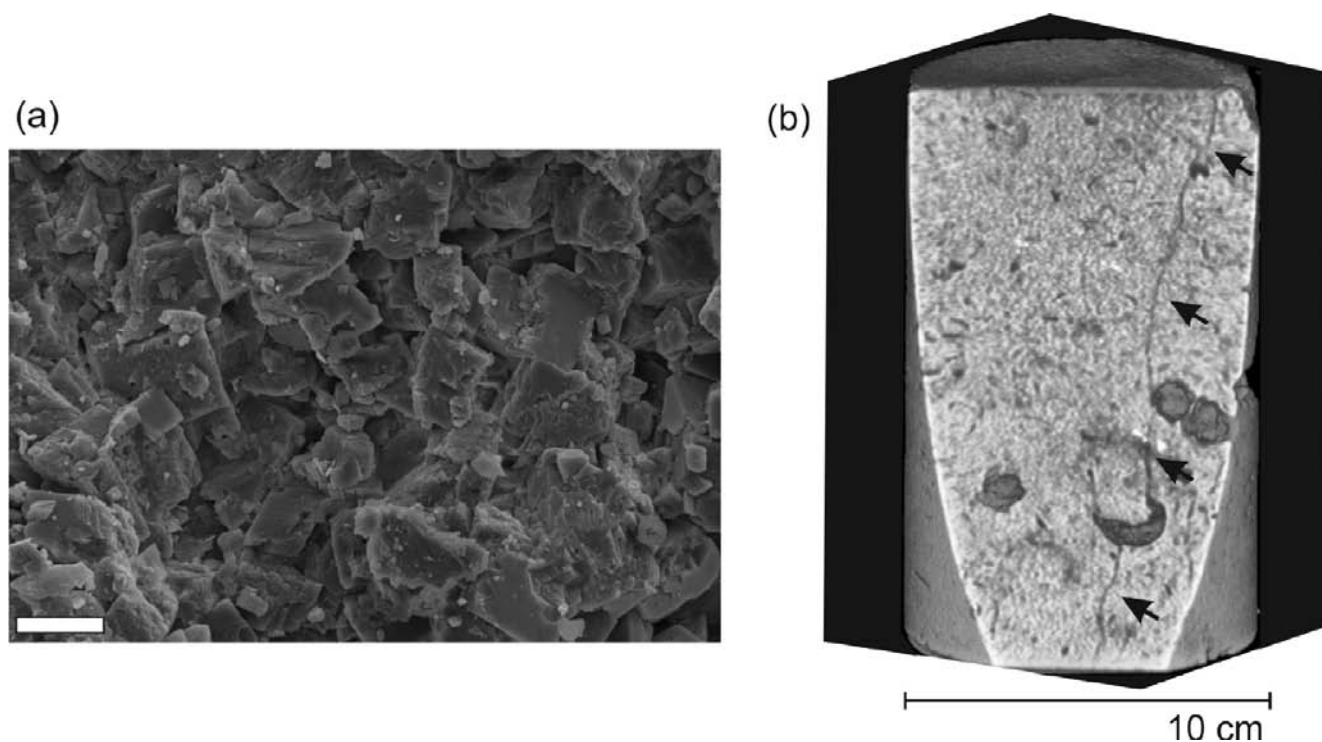


Figure 1. Different imaging techniques used to characterize the Trigodonus Dolomite (Benken, Nagra). (a) SEM image (secondary electron mode) illustrating the dolomite matrix grains and inter-grain porosity, at 825 m below surface (mbs); the scale bar is 20 μm (lower left). (b) A reconstructed CT-image from a core-segment at 827 mbs. A crack longer than 10 cm, with subvertical orientation, is outlined by the arrows. The x-ray tomography was performed at the Universitatspital in Zurich. Processing of the raw data and plotting was done using ImageJ, with the volume viewer 1.31 plugin.

REFERENCES

- Chevalier, G., Diamond, L. W. & Leu, W., 2010: Potential for deep geological sequestration of CO₂ in Switzerland: a first appraisal. *Swiss Journal of Geosciences* 103 (3), 427-455.
- Nagra, 2001: Sondierbohrung Benken - Untersuchungsbericht. Technischer Bericht 00-01 (288 pp). Wetztingen - Nagra.

P 21.3

Toward source characterization of local supershear ruptures in dip-slip faults

Cyrill Baumann¹, Luis Angel Dalguer¹

The speed at which a rupture propagates is an important factor that contributes to determine the character of the ground motion. Rupture speeds are bounded at the upper end by the maximum speed at which stresses are transmitted through the rock. Most earthquake ruptures propagate with velocities slower than the S-wave speed, while studies of some earthquake data, lab and theoretical physical models reveal the occurrence of rupture velocities exceeding the S-wave speed, i.e. supershear. Most of the attention of those studies has been given to large strike slip fault, because earthquakes in long faults predominantly ruptures in mode II, in which super-shear rupture speed is most likely to occur (see for instance Dalguer et al in this session)

Little attention has been given to evaluate the possibility and importance of the occurrence of supershear speed in dip-slip faults. Though rupture along the length of dipping faults predominantly rupture in mode III, there is also a portion of the rupture that propagate along the dip (mode II direction) in which supershear rupture speed may take place. Here we evaluate this possibility and quantitatively characterize the areas of supershear rupture speed in dip-slip faults. For such as purpose we develop suite of earthquake source physics-based dynamic rupture models. Stress distribution prior to earthquakes was assumed to be stochastic with heterogeneous stress consistent, in a statistical sense, with past earthquakes. We performed series of numerical simulations in 45° dipping normal faults with fault area between 30x20 Km, and 200x28 Km. The resulting earthquakes cover a range magnitude $M_w = 5.29-7.89$.

Our dynamic rupture simulations reveal that in rupture propagating along heterogeneities stress fields, the stress waves ahead of the rupture front encounter patches of pre-stress close to the yielding criteria. If these waves have sufficient amplitude, they can trigger short-lived periods of secondary rupture that can trigger localized supershear propagation. In the current simulations, this localized area is limited to areas along the width of the fault at the hypocenter zone, and increases with the earthquake size. For magnitude in the range $6.3 \leq M_w \leq 7.5$ this area increase respectively from 1% to 10% of the total rupture area.

Our final goal is to identify signatures of this localized supershear rupture speed on seismograms to assess the level and variability of ground motion in a certain areas for seismic hazard and risk mitigation.

P 21.4

Laboratory simulations of tensile (hydro) fracture: current work and new directions

Benson, Philip¹, Heap, Michael², Lavallée, Yan³, Flaws, Asher³, Hess, Kai³, Cordonnier, Benoit¹ and Misra, Santanu¹

¹ Geological Institute, Swiss Federal Institute of Technology, Zurich, Switzerland (philip.benson@erdw.ethz.ch)

² École et Observatoire des Sciences de la Terre, Strasbourg, France

³ Geo- und Umweltwissenschaften, LMU, Munich, Germany

During magma ascent, cracking and faulting of the host rock provide conduits for the movement of magmatic fluids. The spatial and temporal formation of such conduits, driven largely by pressurized magmas in the form of dykes, is of key importance in the volcano-tectonic system. In particular, it is known that both a fracture mechanical (brittle) mechanism (due to the propagating dyke tip) as well as a petrological mechanism (due to the elevated pressure-temperature environment), play roles in dyke propagation. As the use of elevated temperatures in the laboratory is technically challenging, early work has tended to concentrate either on analogue setups using gelatine and other materials that are fractured by injection of coloured water (Menand and Tait, 2001; Acocella et al., 2001; Walter and Troll, 2003), or – for simulation of representative pressures – a simplified setup at modest (room) temperatures. In this latter case, a relatively simple (room temperature) cylindrical setup is feasible using water as a pressurising fluid and with an axial conduit lined with a rubber membrane to isolate the fluid from the rock matrix (e.g. Vinciguerra et al., 2004).

Here, we overcome these difficulties by simulating magma intrusion in the laboratory through an experimental protocol that compresses a 'conduit' of magma encapsulated inside a hollow shell. A well-controlled stress is then imposed onto the conduit which has the effect of transmitting this force onto the inner wall of the surrounding shell. Although we present our work with a view to investigating fluid driven tensile fracture applicable to high temperature processes, this general protocol may be used to analyse a wide range of processes whereby direct fluid pressure is used to fracture a host medium. Common examples include hydrofracture in engineering geology applications (gas shale) as well as in engineered geothermal systems for the creation of injection and production water/steam wells. To analyse the system, we use a suite of well-known fracture mechanics methods allied to independently measured rheological parameters for the conduit to develop a model to explain (a) the stress relaxations, and (b) the peak stress measured at failure, as well as the observed interactions between the ductile inner conduit and brittle outer shell, interpreted as analogous to dykes driving through a volcanic edifice.

We conclude that (a), the coupling of stress, strain and seismic data through time can be used to infer the stability of volcanic conduits and/or the state of the magma during periods of unrest by calculating the viscoelastic relaxation parameters and hence the modulus or viscosity of the melt, (b), dyke propagation is initiated when the tensile strength of the country rock is overcome, between 7-11 MPa, in the case of basalt from Etna Volcano, and that the initial tensile failure is energetic enough to melt, and to produce shock waves in it, (c), that the fracture of silicate melt is strain rate dependent (Dingwell and Webb, 1989) and (d), that the material fracture parameters are largely temperature independent. Future plans in the rock deformation laboratory at ETH Zurich (Fig. 2) aim to extend this approach to elevated temperatures and confining pressures in order to simulate processes at depth.

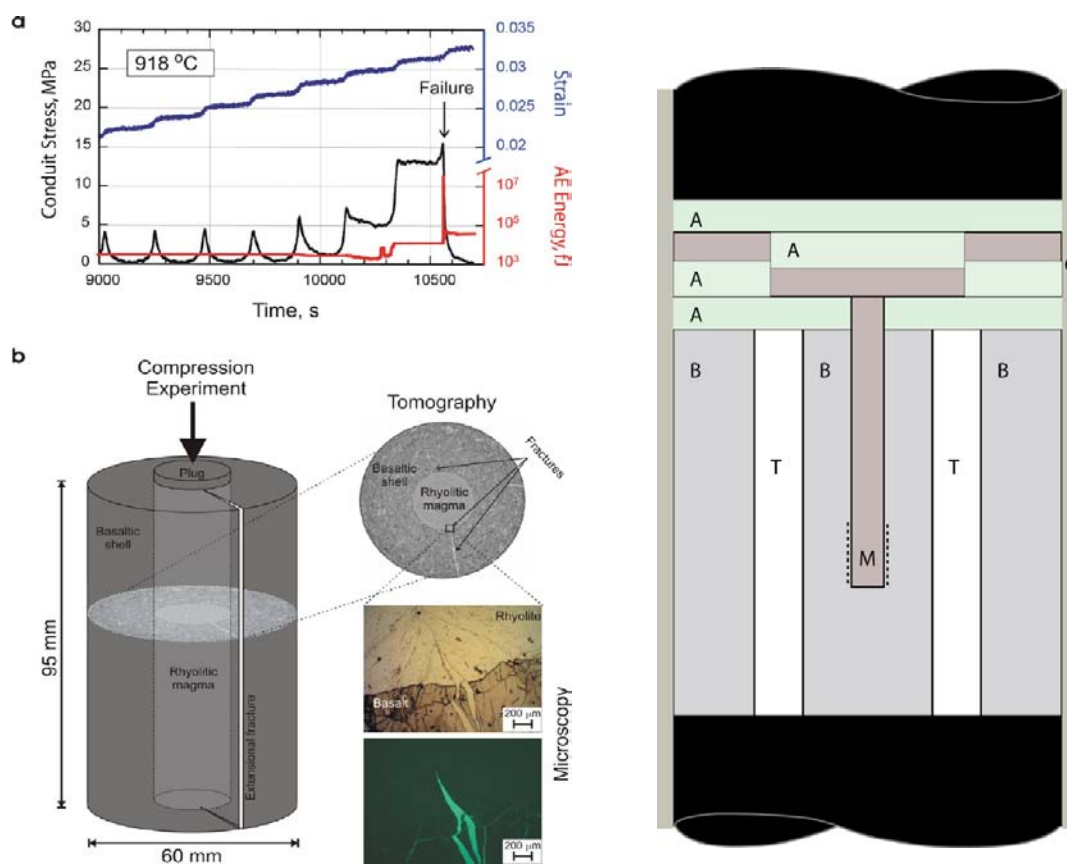


Fig. 1 (left). Magma/conduit interaction experiments. The application of pressure onto a solid basaltic plug compressed a rhyolitic magma (light grey) against the solid inner shell of basalt (dark grey). Fig. 2 (right): Concept of future experiments to add a confining pressure to the system via a Paterson type gas medium apparatus [A: Alumina spacers/piston; B: basalt; M: Melt, for internal pressurisation; T: Welded Tuff; C: Copper jacket].

REFERENCES

- Acocella, V., F. Cifelli, R. Funicello (2001), The control of overburden thickness on resurgent domes: insights from analogue models, *J. Volcanol. Geotherm. Res.*, 111, 137-153.
- Dingwell, D.B., Webb, S.L. (1989), Structural relaxation in silicate melts and non-Newtonian melt rheology in geologic processes. *Phys. Chem. Miner.*, 16 (5), 508-516.
- Menand, T., and S. R. Tait, (2001), A phenomenological model for precursor volcanic eruptions. *Nature*, 411, 678-680.
- Vinciguerra, S., P. G. Meredith, and J. Hazzard (2004), Experimental and modelling study of fluid pressure-driven fractures in Darley Dale sandstone, *Geophys. Res. Lett.*, 31, L09609, doi:10.1029/2004GL019638.

P 21.5

Physical mechanisms for low-frequency seismic wave attenuation in fractured media

Marcel Frehner¹ & Beatriz Quintal¹

¹The Rock Physics Network at ETH Zurich (ROCKETH), Sonneggstrasse 5, CH-8092 Zurich
(marcel.frehner@erdw.ethz.ch, beatriz.quintal@erdw.ethz.ch)

Attenuation and dispersion of seismic waves is an important parameter for analyzing seismic data, because it can provide additional information compared to analysis based only on velocity and density. Understanding the mechanisms causing attenuation is a challenging rock physics task. We present two physical mechanisms that can cause attenuation and dispersion of seismic waves.

1. Wave-induced fluid flow
2. Krauklis wave initiation

Both mechanisms are studied numerically using the finite-element method.

1. Wave-induced fluid flow

We performed numerical simulations of a quasi-static experiment to calculate attenuation ($1/Q$) caused by wave-induced fluid flow in a heterogeneous poro-elastic medium (with patchy saturation and double porosity). The methodology is described in Quintal et al. (2011) and COMSOL Multiphysics was used for these simulations. The finite element method using an unstructured mesh (Figure 1) was applied. The model consists of gas-saturated kerogen-rich shale with open fractures, which are saturated with water (injected during the fracturing). The fractures, also shown in Figure 1, are 4, 3, and 5 mm thick, respectively, from left to right. The medium is considered to be a repetition of the Representative Elementary Volume (REV) shown in Figure 1.

The results of the simulation are shown in Figure 2. The minimum value of Q is 10.2 at 1.6 Hz. H is the P-wave modulus, such that $V_p = \sqrt{H/\rho}$. From the simulation with closed calcite fractures, $Q = \text{infinite}$ (and constant), and $\text{Re}(H) = 2.5$ GPa (constant).

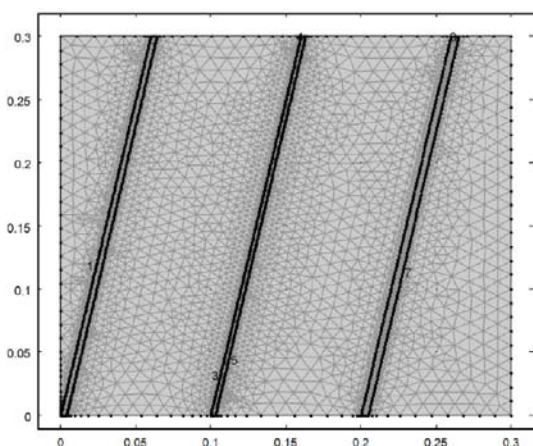


Figure 1: Model (0.3 x 0.3 m) and the unstructured triangular finite-element mesh of the fractured medium.

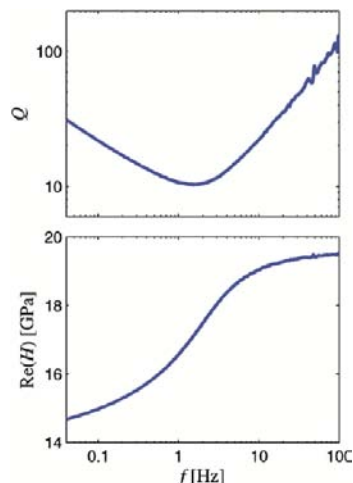


Figure 2: Results for the quality factor (Q) and the real part of the P-wave modulus (H).

2. Krauklis wave initiation

The Krauklis wave is a special wave mode that is bound to and propagates along fluid-filled fractures and can also influence seismic body waves. Krauklis waves can propagate back and forth along a fracture and emit a periodic signal (Frehner and Schmalholz, 2010). Seismic data can contain this characteristic frequency and eventually reveal fracture-related petrophysical parameters of the reservoir. Krauklis waves are well described mathematically for some theoretical cases. However, one key question that is still unclear is how Krauklis waves are initiated by a body wave passing a fluid-filled crack. Figure 3 shows a finite-element study for the case of a plane P-wave passing an elliptical water-filled crack with 45°

inclination. The P-wave is scattered and diffracted at the crack and two Krauklis waves are initiated, one at each crack tip (i.e., diffraction points). For more realistic crack geometries and/or intersecting cracks, more diffraction-points will lead to a higher probability to initiate Krauklis waves.

The initiation of Krauklis waves by a passing body wave represents an energy transfer from the body wave to the fracture, and therefore an attenuation mechanism for the body wave. By propagating back and forth the fracture, the Krauklis wave can emit a periodic body wave signal (Frehner and Schmalholz, 2010), which leads to a strong dispersion of the body wave. The efficiency of these processes remain to be studied in the future.

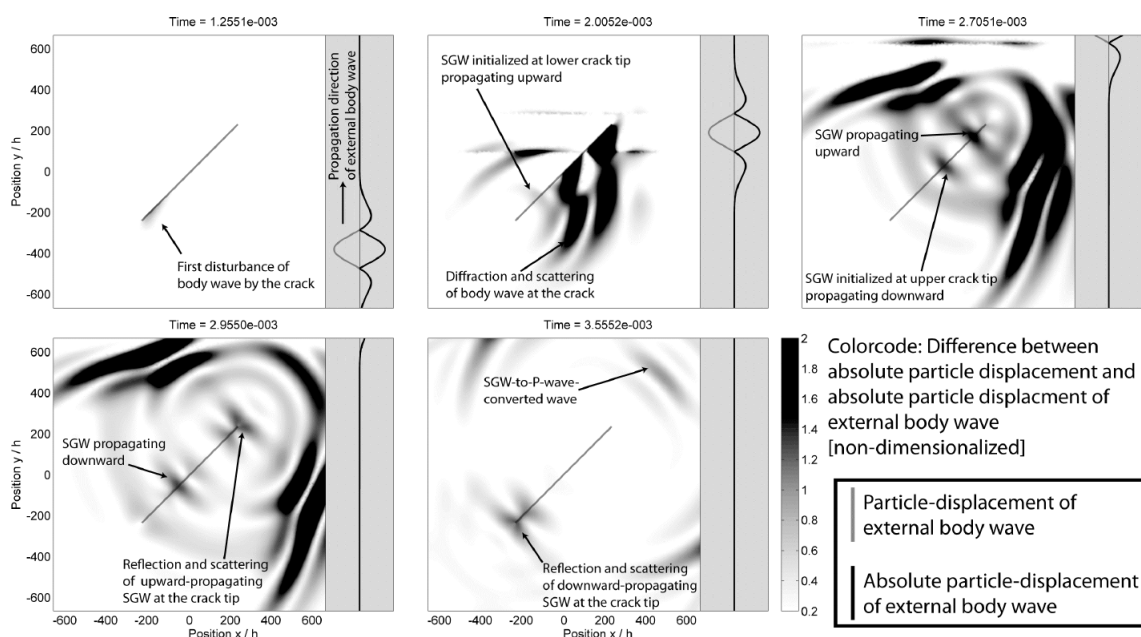


Figure 3: Snapshots of Krauklis waves being initiated by a passing plane P-wave. The single wavelet P-wave propagates from bottom to top and its profile is shown in the gray sidebars. The signal of the passing P-wave is subtracted from the total absolute particle displacement for better visibility.

REFERENCES

- Frehner, M. and Schmalholz, S.M., 2010: Finite-element simulations of Stoneley guided-wave reflection and scattering at the tips of fluid-filled fractures, *Geophysics* 75, T23–T36.
- Quintal, B., Steeb, H., Frehner, M. and Schmalholz, S.M., 2011: Quasi-static finite element modeling of seismic attenuation and dispersion due to wave-induced fluid flow in poroelastic media, *Journal of Geophysical Research – Solid Earth* 116, B01201.

P 21.6

Rock classification based on physico-mechanical analysis -case study: Poshtkuh basin, Alborze region-Iran

Kaveh Khaksar¹, Marahem Rahmati²

¹Institute of Scientific Applied Higher Education of Jihad-e-Agriculture, Dep. of Soil Science, Education and Extension Organization, Ministry of Agriculture, Iran. Email: kavehkhaksar@gmail.com

²Expert of Fishery Research Center, Tehran-Iran

This paper is derived from a research on rock classification using geological hammer, Schmitt hammer, fissure and joints, in the Maharlu basin in southwest of Iran.

The mechanical breaking and dissecting of rocks occurs in the regions, which the changes of temperature and humidity are considerable. The weathering of the geological formations depends on different factors, which have divided in two groups: 1) Superficial factors such as climatic conditions, topography, vegetation covering and human weathering system and 2) Bed rock and its physical and chemical characters.

Poshtkuh basin is located in Semnan province. The Middle Triassic and the Quaternary units are respectively the oldest and youngest rocks in the basin. Since the studied area is generally composed of sedimentary rocks and sediments like marl, shale, marly shale, conglomerate, sandstone and limestone rather have spread. The region is mainly composed of sedimentary deposits. The Poshtkuh basin lies in the North of Iran (Alborz range) and mainly calcareous rocks crop out in this area. It were carried out three physical and mechanical analyses to evaluate the sensitivity of rock units to weathering. The fissure and joints were measured, evaluation of mechanical properties and grade of weathering were also measured by using a Schmidt hammer and rock resistance was estimated by geological hammer. The acquired data from the various rock types constituting the basin were analyzed, and their sensitivity to weathering was determined. Finally, a map of erosion sensitivity was prepared for different geological units. In the base of the acquired results, the geological units of poshtkuh basin respect to erosion have been classified to:

Low: Member Jk^{l3}, Upper part of Lar Formation J₁², Tizkuh Formation k₁, Member k₁¹, Member k₁^{s.1}, Member k₂¹, Ziarat Formation (Pe₂), Member J₁¹

Low to medium: Elika Formation TRe3, Unit J_s^{1e}, unit k₂^{t.1}

Medium: Member J_s, Member k₂^v, Member k₁^{1m}, Fajan Formation (pg_f^c), Karaj Formation (E^k), Member J_s⁴

Medium to great: Member J_s³, Member E^{l.sh}

Great: Shemshak Formation TR3js, unit TR3JS1, unit J_s², Delichai Formation, unit (J_D), unit (E^{sh}), Quaternary deposits.

Finally the map of different geological unit resistivity to weathering of Poshtkuh basin has been assigned.

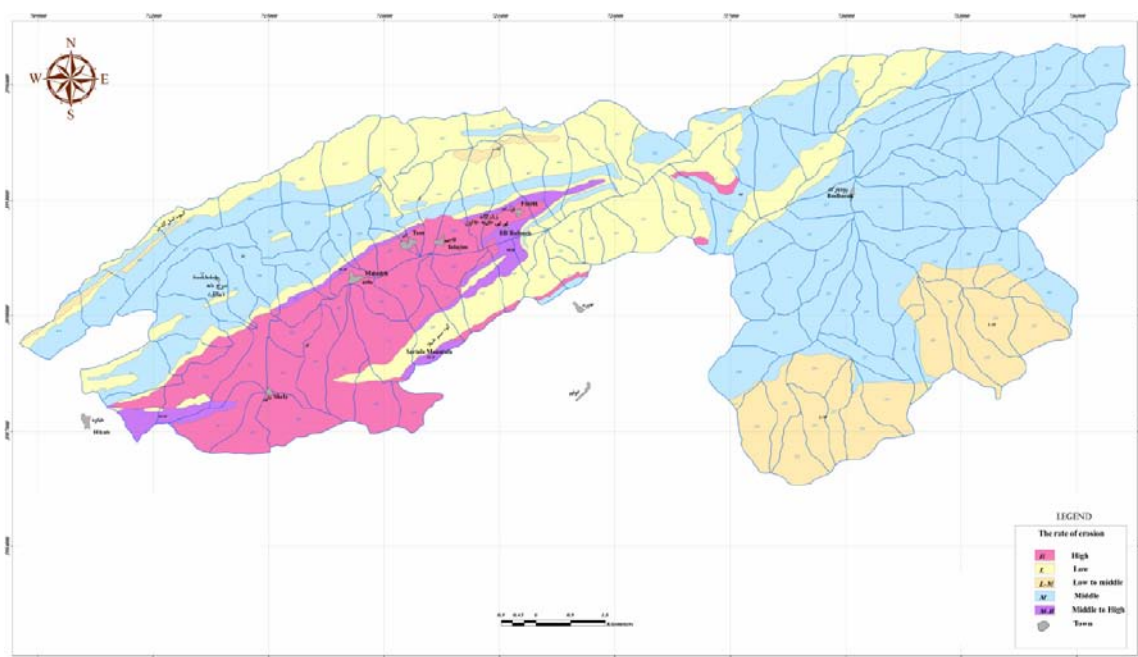


Figure. 1 Map of rock classification in the Poshtkuh Basin

REFERENCES

- Arzani, N. (2006) Primary versus diagenetic bedding in the limestone-marl/shale alternations of the eperic seas, an example from the lower Lias (Early Jurassic) of SW Britain, V. 21, N. 1, 94-109.
- Bieniawski, Z. T. (1989) Engineering rock mass classifications. Chichester, Wiley.
- Garnett, C. S. (2009) On a Local Alteration in Limestone Shales at Wensley, Derbyshire, Geological Magazine (1921), 58: 473-477.
- Gomez, F. P. (1995) Erosion E Inestabilidad en la Cuenca del Rio Patana (Alpujarra alta Almeriense), Instituto de Estudios Almerienses. Pp. 74.
- Hunt, R. E. (1984) Geotechnical Engineering Investigation Manual, Mc Graw Hill, 896 P.
- ISRM (1979) Suggested methods for determining in situ deformability of rock," ISRM Commission on Standardization of Laboratory and field Tests, Int. J. Rock Mech. Min. Sci. Geomech. Abstr., 16(3), 195-214.
- ISRM (1981a) Basic Geotechnical Description of rock masses, Int. J. Rock Mec. & Min. Sci.; Vol, 18, N 1. Pp. 85-110.
- Kent, P. E. (2009) The Limestone-Shale Rhythm in the British Lower Lias, Geological Magazine (1957), 94: 429-430.
- Khaksar & Roozkhsh (2007) Evaluation sensitivity classification of rock units and unconsolidated deposits to erosion, 6th International symposium on Mediterranean Geology, April 2-5, 2007, Amman-Jordan.
- Khaksar, Goodarzi, Rahmati, Gharibreza (2006) Sensitivity determination of geological formations, Maharlu basin, Quarterly of Geological Science, No: 62.

P 21.7

Low frequency measurements of seismic wave attenuation

Madonna Claudio ¹, Tisato Nicola ¹ and Saenger Erik H. ¹¹Geologisches Institut, Sonneggstrasse 5, CH-8092 Zürich (claudio.madonna@erdw.ethz.ch)

The study of wave attenuation in partially saturated porous rocks over a broad frequency range provides valuable information about reservoir fluid systems, which are inherently composed of multiple phase fluids. The main goal of our work is to experimentally measure the bulk attenuation on partially saturated rocks at frequencies between 0.01 and 100 Hz, using natural rock samples under in situ conditions. To fulfil this aim, we designed and set up a specific instrument: the Seismic Wave Attenuation Module (SWAM). We present its bench-top calibration, a series of data collected from different kind of rocks and the numerical simulations, which support the obtained results.

We employ the sub-resonance test. Assuming that the rock behaves as a linear time invariant (LTI) system, the attenuation factor Q^{-1} (Q is the quality factor) is equal to the tangent of the phase shift between the stress and the strain signal. This also corresponds to the ratio between the imaginary and the real part of the transfer function (Nowick and Berry; 1972, Jackson and Paterson, 1987). The phase lag (θ) is calculated by the difference obtained using the Fourier transform between phases of the stress and strain signals. Equation 10 of O'Connell and Budiansky (1978) shows the relation between attenuation Q^{-1} and the parameter gathered from the experiments can be expressed:

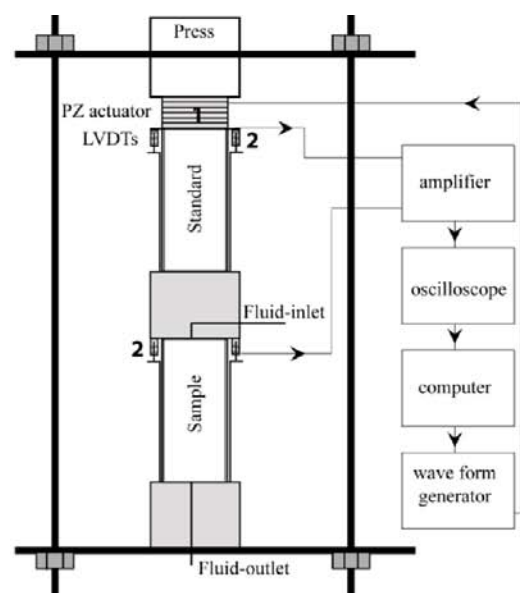
$$Q^{-1} = \frac{\Delta E}{2\rho E} = \tan|\varphi|$$

The phase lag, θ , can be seen as the ratio of the energy loss ΔE and total energy E introduced into the rock for each cycles.

Figure 1 is a sketch of the operating systems. To obtain precise and accurate measurements over a wide range of experimental conditions the SWAM apparatus measures, in an automated way, the bulk attenuation of non-homogeneous and partially saturated samples. Each sample is 60 mm long and 25.4 mm in diameter.

Our system makes a bulk attenuation measure across the whole sample length in contrast to the measurements using strain gauges. This is accomplished by measuring the strain across the whole sample with micro-linear variable differential transformers (micro-LVDT). This technique allows acquiring many values from all kinds of rocks: from consolidated granular materials up to highly dense and compact rocks. The magnitude of finite strain is in the order of 10^{-6} .

The device is comprised of two main elements: (1) A piezo-electric stack actuator (PZ) generates dynamic displacement. A sinusoidal axial compressive stress is applied by the relative vertical displacement of the PZ-actuator. The actual oscillating frequency ranges from 10^{-2} to 10^2 Hz with amplitudes from nanometers to micrometers. (2) Two displacement measurement modules consist of micro-LVDT's. These transformers measure the compression and extension strains of both the sample and a purely elastic standard with a nanometric resolution. The strain across the purely elastic standard is the reference signal to which we compare the strain across the sample for any phase lag induced by anelasticity.



Machine characteristics	
Name	S.W.A.M
Frequency range	0.01-100 Hz
Sample length	60-100 mm
Sample diameter	25.4 mm
Sensors	LVDT
Planned confining pressure	200 MPa

Figure 1. The stress is applied employing a piezo-electric actuator (1). Shortening of both the elastic element and the sample is measured through LVDTs (2).

REFERENCES

- Jackson, I., and M. S. Paterson, [1987] Shear modulus and internal friction of calcite rocks at seismic frequencies: pressure, frequency and grain-size dependence. *Phys. Earth Plan. Int.*, 45, 349-367.
- Nowick, A. S., and Berry, B. S. [1972], *Anelastic relaxation in crystalline solids*: Academic Press, New York.
- O'Connell and Budiansky [1978], Measures of dissipation in viscoelastic media, *Geophys. Res. Lett.*, 5(1), 5-8.

P 21.8 (see P 20.4)**Changes of Coulomb Failure Stress due to Dislocations during Stimulation of GPK2 at Soultz-sous-Forêts**

Schoenball, Martin^{1,2}, Baujard, Clément¹, Kohl, Thomas^{1,2} & Dorbath, Louis³

¹GEOWATT AG, Dohlenweg 28, CH-8050 Zürich (schoenball@geowatt.ch)

²Karlsruher Institut für Technologie, Institut für Angewandte Geowissenschaften, Kaiserstr. 12, D-76131 Karlsruhe

³EOST, University Louis Pasteur, 5, rue René Descartes, F-67084 Strasbourg

The European deep geothermal research project at Soultz-sous-Forêts (Alsace, France) has been developed since 1987. The geothermal reservoir is situated in a horst structure within the granite basement of the Upper Rhine Graben. During the project for developing an Enhanced Geothermal System (EGS) several well stimulations have been conducted and induced several tens of thousands of microseismic events. During the stimulation of well GPK2 the maximum event recorded during stimulation reached magnitude 2.5.

In the field of seismology of tectonic earthquakes, aftershock sequences produced by a large magnitude main shock have been successfully described by changes of Coulomb failure stress due to the dislocation (in the following denoted as ΔCFS) by the main shock (e.g. King et al. 1994 and Toda et al. 2003).

We present 3D computations of ΔCFS by different geometries of the fault plane to find a computationally efficient way to approximate circular sources taking into account an appropriate slip distribution. We then compute transient ΔCFS in the Soultz reservoir during the stimulation of GPK2. For this analysis we use an extensive database of over 700 derived focal mechanisms (Dorbath et al. 2009). This allows us to conclude that the stress perturbation of all microseismic events during stimulation cannot be depicted by one single fault. Furthermore analysis of this dataset allows us to estimate the influence of ΔCFS by dislocation over the total change of Coulomb failure stress by other processes like the increase of pore fluid pressure, thermal stresses, hydraulic response of the reservoir and coupling of these.

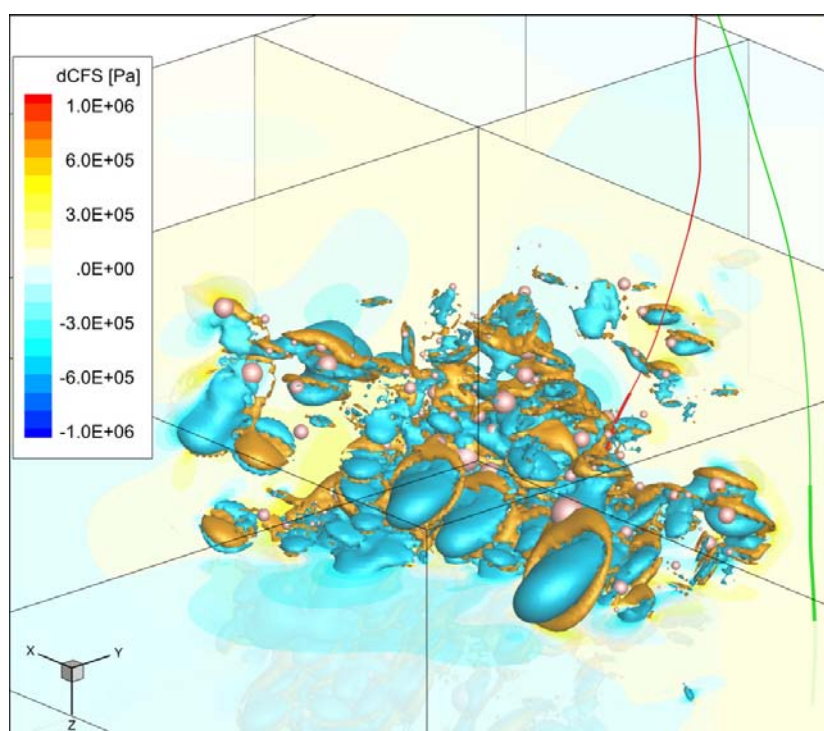


Figure 1. 3D views of ΔCFS in the Soultz reservoir with isosurfaces at ± 0.5 MPa. The wells GPK2 (red), and GPK3 (green) are displayed with bold open hole section. The microseismic events used for the computation are represented by sphere symbols that scale with the event magnitude.

REFERENCES

- Dorbath, L., Cuenot, N., Genter, A. & Frogneux, M. 2009: Seismic response of the fractured and faulted granite of Soultz-sous-Forets (France) to 5 km deep massive water injections. *Geophysical Journal International*, 177(2), 653–75.
- King, G. C. P., Stein, R. S. & Lin, J. 1994: Static stress changes and the triggering of earthquakes. *Bulletin of the Seismological Society of America*, 84(3), 935–953.
- Toda, S. & Stein, R. 2003: Toggling of seismicity by the 1997 Kagoshima earthquake couplet: A demonstration of time-dependent stress transfer. *J. Geophys. Res.*, 108(B12), 2567.

P 21.9

Measurements and mechanisms of seismic wave attenuation in partially saturated rocks

Nicola Tisato¹, Claudio Madonna¹ & Erik H. Saenger^{1,2}

¹ETH Zurich, Soneggstrasse, 5, CH 8092 Zurich (nicola.tisato@erdw.ethz.ch)

²Spectraseis, Giessereistrasse 5 CH 8005 Zurich

Seismic wave attenuation of low frequency seismic waves in the earth crust has been explained by partial saturation (Goloshubin, 2006) and permeability models (e.g. Pride et al., 2004). We present the latest results obtained with the Broad Band Attenuation Vessel (BBAV), which measures seismic wave attenuation in the range of 0.1 - 100 Hz under confining pressures up to 25 MPa. In addition, the apparatus can investigate fluid flow through the pore structure (White, 1975), which can explain the attenuation measurements. The description of the BBAV is also reported, B.B.A.V.

The calibration of the mono-frequency attenuation measurements was completed by testing aluminum and a PMMA (Plexiglas) sample. These two materials represent elastic and anelastic end-members, respectively. Calibrations match literature (Nowick and Berry, 1972; Lakes, 2009).

Two 76 mm diameter and 250 mm long Berea sandstone samples, with different permeability, were tested. The first sample (BS001) had 200-500 mD permeability, while the other sample (BS002) had 500-1000 mD permeability; both the specimens were 20% porosity. The stress conditions were: (1) $\sigma_1=3.5$ MPa, $\sigma_2=\sigma_3=0$ MPa (unconfined) and (2) $\sigma_1=18.5$ MPa, $\sigma_2=\sigma_3=15$ MPa (confined), where σ_1 was the vertical stress. For unconfined conditions, dry samples exhibit attenuation values of about 0.01; when they are 90% water saturated the same samples show attenuation values between 0.018 and 0.028 across the frequency range. For confined conditions, the samples exhibit always attenuation values around 0.01.

Five pore pressure sensors are inserted 38 mm deep in the specimen at different heights along the sample length. This allows continuous and local measurements of pore pressure changes generated by stress field changes. This additional capability of BBAV provides important information about the attenuation mechanisms during stress changes (Mavko et al., 2003). When the sample is 0% water saturated, there is no change in the pore pressure. This result is a benchmark that the measurements are not influenced by the deformation of the rock solid frame. When saturation is more than 60% pore pressure starts to be influenced by the stress field changes. Finally, when the rock is 90% water saturated, the increase of pressure is maximum for the two bottom sensors and around 8 mBar.

Attenuation measurements show that attenuation is frequency-dependent when the samples are unconfined. This observation can be explained by squirt flow (Mavko and Jizba, 1991). According to the characteristics of Berea sandstone, squirt flow should be active between 7 and 7000 Hz. On the contrary, the rock cracks could be closed when the samples are confined, impeding attenuation related to this mechanism. Additionally, pore pressure measurements indicate that stress induced fluid flow is active when the rock is more than 60% water saturated and unconfined.

REFERENCES

- Goloshubin, G., Van Schuyver, C., Korneev V., Silin, D., and Vingalov, V., 2006: Reservoir imaging using low frequencies of seismic reflections. *The Leading Edge*, 25, 527–531.
- Lakes, R., 2009: *Viscoelastic materials*, Cambridge University Press, Cambridge; New York.
- Mavko, G., Mukerji, T., and Dvorkin, J., 2003: *The rock physics handbook*. Cambridge University Press, Cambridge.
- Mavko, G., and D. Jizba, 1991: Estimating grain-scale fluid effects on velocity dispersion in rocks, *Geophysics*, 56(12), 1940, doi:10.1190/1.1443005
- McKavanagh, B., and Stacey, F. D., 1974: Mechanical hysteresis in rocks at low strain amplitudes and seismic frequencies. *Physics of the Earth and Planetary*, 8 (3), 246-250.
- Nowick, A. S., and Berry, B. S., 1972: *Anelastic relaxation in crystalline solids*. Academic Press, New York.
- Pride, S.R., Berryman, J.G., and Harris, J.M., 2004: Seismic attenuation due to wave-induced flow. *J. Geophys. Res.*, 109, B01201.
- White, J. E., 1975: Computed seismic speeds and attenuation in rocks with partial gas saturation. *Geophysics*, 40, 224-232.

P 21.10**The Swiss Atlas of Physical Properties of Rocks (SAPHYR): Progress and developments**

Zappone Alba ¹, Bruijn Rolf², Tripoli Barbara², Biedermann Andrea Regina³, Burg Jean-Pierre² & Kissling Eduard³

¹*Institute for Process Engineering, Sonneggstrasse 3, CH-8092 Zurich (alba.zappone@sed.ethz.ch)*

²*Geological institute ETH Zurich, Sonneggstrasse 5, CH-8092 Zurich*

³*Institute of Geophysics, ETH Zürich, Sonneggstrasse 5, CH-8092 Zurich*

Since 2006, a multi-year project supported by the Swiss Geophysical Commission (SGPK), aims to digitize all existing data on physical properties of rocks exposed in Switzerland and to place these data in a referenced geographical frame (GIS). The ultimate goal is to make these data accessible to an open public including industrial, engineering, land and resource planning companies as well as academic institutions.

The systematically measured physical properties are density and porosity, seismic, magnetic, thermal properties, permeability and electrical properties. For the time being, data from literature have been collected extensively for seismic and magnetic properties and only partially for the other physical properties.

In the past two years an effort has been placed on collecting samples and measuring the physical properties of the geologic formations that were poorly documented in the literature. The phase of laboratory measurements is still in progress. We present the updated outputs : a map of Switzerland with sample location, a density map, and maps with contoured and color-coded values of seismic V_p and V_s extrapolated to room conditions from the high pressure laboratory measurements (matrix or crack free properties). We expect to publish the first results of this Atlas of Switzerland by the end of 2011 ..

P 21.11

Carma – Carbon Management in Power Generation: Geological CO₂ storage in Switzerland

Zappone Alba^{1,4}, Diamond Larryn², Almqvist Bjarne³, Evans Keith³, Deichmann Nicolas⁴, Werner Mischa¹ & Mazzotti Marco¹

¹ Institute of Process Engineering, ETH Zurich, Sonneggstrasse 3, CH-8092 Zurich (alba.zappone@sed.ethz.ch)

² Institute of Geological Sciences, University of Bern, Baltzerstrasse 1+3, CH-3012 Bern

³ Geological Institute, ETH Zurich, Sonneggstrasse 5, CH-8092 Zurich

⁴ Swiss Seismological Survey, ETH Zurich, Sonneggstrasse 5, CH-8092 Zurich

The CARMA project aims to explore the potential for and the feasibility of the deployment of CCS in Switzerland within the framework of future energy scenarios. Moreover, we aim to exploit the available expertise to develop new CCS technologies and know-how, which might be applied in Switzerland and worldwide. As to the potential role of CCS, we intend to address and to evaluate the economical, environmental, societal, and institutional implications of CCS, as well as to assess the potential CO₂ geological storage capacity in Switzerland. As to the new technologies, we intend to build on the strengths, experience and available equipment of the research groups involved, focusing on the so-called pre-combustion capture, i.e. the production of hydrogen, its separation from CO₂ and its use in a gas turbine for power generation, and on mineral carbonation, as a means of fixing CO₂ in stable, mineral form. The CARMA consortium brings together the research groups at ETH Zurich, EPF Lausanne, FHNW, Paul Scherrer Institute and University of Bern. The project started in January 2009, with a total runtime of 4 years. This poster presentation shall report the achievements with respect to geological storage of CO₂ in Switzerland during the first half of the project.

An estimate of the theoretical storage potential in the subsurface of Switzerland was completed in August, 2010. The methodology followed an existing evaluation scheme developed in Canada, which is based on geological criteria only. Modifications were introduced to suit the geological setting and available data in Switzerland. The study relies on nine quantitative and semi-quantitative attributes derived from analysis of existing drillhole, geological, and geophysical data. The weighted combinations of these attributes have been ranked in order to visualize Switzerland's storage potential in the form of a contour map (resolution = a few km²). While the entire crystalline body of the Alps plus the southern part of Switzerland lack suitable geological formations for storage, the sedimentary rocks below vast parts of the Central Plateau, in contrast, show moderate to very good potential. The theoretical storage capacity of the suitable sandstone and limestone aquifers is approximately 2.6 Gtons of CO₂, i.e. 65 times Switzerland's current annual CO₂ emissions. Thorough geological investigations and one or multiple field tests would be imperative to prove its feasibility and safety.

Motivated by Switzerland's recent experience with injection-induced seismicity in Basel, the potential seismic hazard related to CCS operations is sought to be carefully assessed within CARMA. In particular, a catalogue of case histories has been compiled documenting the seismic response of the underground to fluid injection in Europe. The compilation includes Enhanced Geothermal Systems (EGS), hydrothermal plants (fault and aquifer utilization), and CCS projects. Data describing each case history includes the type of operation, the depth of the injection, the injection pressure, the net fluid volume injected, the duration and time distribution of the injection activity, the rock type, the tectonic regime and state of stress, and background seismicity of the injection area. Injection at sites with low natural seismicity, defined by the expectation that the local peak ground acceleration from natural earthquakes has less than a 10% chance of exceeding 0.08g in 50 years, has not produced felt events. Although the database is limited, this suggests that low natural seismicity, corresponding to hazard levels below 0.07g, may be a useful indicator of a low propensity for fluid injection to produce felt or damaging events.

An alternative approach to that offered by subsurface storage is ex-situ mineral carbonation in a controlled industrial setting. This involves the dissolution of CO₂ into an aqueous phase, leaching of magnesium/calcium from a natural mineral feedstock and the precipitation of Mg-/Ca-carbonates, thus fixing CO₂ in a stable, environmentally benign form. The reactions involved are exothermic overall, but their kinetics are slow under ambient conditions. This makes an energy intensive mechanical or thermal activation of the mineral feedstock inevitable. While this adds to costs, mineral carbonation offers the possibility of fixing CO₂ directly from an industrial off gas stream, thus obviating the costly capture step. Within the CARMA project, we are investigating an aqueous process, where a flue gas is bubbled through a stirred tank containing the mineral feedstock in suspension. Temperature is kept low to enhance gas solubility and the total pressure will be kept close to ambient to prevent co-pressurization of the non-CO₂ flue gas components. Carbonate precipitation takes place either in the same vessel, or from the filtered, Mg/Ca and CO₂ loaded solution in a second tank. We have built a set-up to perform mineralization experiments under a variety of temperature, pressure, gas composition and solution chemistry conditions, using several optical and physicochemical analytical techniques to monitor the different phases in-situ and online further downstream. Currently, the dissolution behavior of thermally activated serpentine is being studied. Hitherto, olivine was found to be the natural silicate feedstock exhibiting fastest dissolution kinetics. When directly compared to olivine, we found that activated serpentine dissolves 2 to 3 orders of magnitude faster under identical conditions.

22. Special symposium in honor of Daniel Bernoulli & Albert Matter

Karl Föllmi, Fritz Schlunegger, Helmut Weissert

Conférence universitaire de Suisse occidentale (CUSO)
International Union of Geological Sciences (IUGS)
Swiss National Science Foundation (SNSF)

TALKS:

- 22.1 *Allen P.A.*: Sediment budgets and fluvial drainage at mountain fronts, examples from the Pyrenees, Alps and Apennines
- 22.2 *Anselmetti F.*: From carbonate platforms to margin collapses: Comparing Alpine lake sediments with marine deposits
- 22.3 *Baumgartner P. O.*: Mesozoic radiolarites from oceans to mountains: Facies, ages and palaeo-environments
- 22.4 *Bertotti G.*: The Southern Alps from the Generoso Basin to the Dolomites: a unique natural laboratory for tectonic and structural studies
- 22.5 *Eberli G.P.*: The long goodbye of carbonate cycles as reliable recorders of orbitally driven sea-level fluctuations
- 22.6 *Fleitmann D.*: Albert of Arabia - Climatic and environmental reconstructions on stalagmites and lacustrine sediments from the Arabian Peninsula
- 22.7 *Immenhauser A., Buhl D., Riechelmann S., Spötl C., Richter D.K.*: Magnesium Isotopes: Establishing a new proxy in Earth Sciences
- 22.8 *Jenkyns H.C.*: Tectonics versus palaeoceanography in the evolution of the Alpine-mediterranean Tethys
- 22.9 *Manatschal G., Masini E., Mohn G.*: Stratigraphic and tectonic architecture of the Alpine Tethys margins
- 22.10 *Strasser M., Anselmetti F.S., Gorin G., Monecke K., Mosar J., Schnellmann M.*: Sedimentary archives of Northern Alpine and Molasse Basin neotectonics
- 22.11 *Winkler W., Beltrán A., von Quadt A.*: Tracing Alpine sediment sources through laser-ablation U/Pb dating and Hf-isotopes of detrital zircons - an appraisal

POSTERS:

- P 22.1 *Adatte T., Keller G., Khozyem Saleh H., Spangenberg J.*: The Cretaceous-Tertiary transition in the Alps, new insights from Gams, Austria:
- P 22.2 *Bonvallet L., Godet A., Spangenberg J. E., Föllmi K. B.*: The Urgonian Formation in the Helvetic Alps (late Barremian to early Aptian): new evidences from the Interlaken area.
- P 22.3 *Kindler P., Ospina-Ostios L-M., Ragusa J., Wernli R.*: The Voiron flysch (Voiron massif, Gurnigel nappe, Haute Savoie, France): a stack of km-sized flysch slices of Ultrahelvetic and north-Penninic origin
- P 22.4 *Morard A., Burkhalter R., Möri A., Strasky S.*: Lithostratigraphic harmonisation – a corner stone for a digital geological map with nationwide coverage
- P 22.5 *Stockar R., Baumgartner P.O., Kocsis L., Ulianov A., Dumitrica P., Condon D.*: The Meride Limestone (Monte San Giorgio, Ticino, Switzerland): a Ladinian archive of paleoenvironmental changes

22.1

Sediment budgets and fluvial drainage at mountain fronts; examples from the Pyrenees, Alps and Apennines

Philip A Allen

Department of Earth Science & Engineering, Imperial College, South Kensington Campus, London SW7 2AZ, UK

The treatment of the transfer of mass at the Earth's surface, from source to sink, as a bulk diffusive process over geological time scales permits the reconstruction of ancient sediment discharges from mountainous source areas and promotes an understanding of the tectonic and climatic driving mechanisms for long-term landscape dynamics. One of the important aspects of landscape dynamics is the nature of the drainage paths of alluvial rivers and specifically whether they flow longitudinally along the strike of the mountain belt, or transversely across the strike. The routing of sediment towards foreland basin systems and the preservation of stratigraphy in wedge-top and foredeep depocentres, depends on the balance between the sediment supply, which can be modeled as a number of point sources, and the spatial and temporal variations in tectonic uplift and subsidence controlling accommodation.

Frontal zones of mountain belts may consist of an array of regularly spaced anticlines separating narrow wedge-top basins, typically with low sediment discharges and low surface mean slopes, such as the northern Apennines. Early longitudinal sediment routing (Oligo-Miocene) has been replaced by transverse drainage, as seen for example in the Marche region. Other mountain belts are typified by a very narrow depositional wedge-top, with steep average surface slopes, high sediment discharges and a well-developed foredeep, such as the Alps of Switzerland. The mountain front zone is characterized by regularly spaced transverse fan systems such as the Napf and Hörnli. The southern Pyrenees show a diachronous east-to-west transition from longitudinal systems flowing along fault-controlled wedge-top troughs to late-stage transverse sediment routing systems that buried tectonic structures. These various possibilities are shown to reflect the balance between sediment discharge and tectonically generated accommodation.

A generic model is presented that shows how the slope-related sediment discharge from mountain catchments is estimated using a bulk diffusivity based on the length of fluvial concentrative flow. The sediment supply is delivered to depositional basins with spatial distributions of tectonically generated accommodation, which allows solutions of a 2-dimensional volumetric sediment budget for combinations of sediment discharge, depositional length and accommodation. A spin-off benefit is that we are able to make predictions of the regional trend in grain size, or alternatively, to invert tectonic variables from an observed grain size trend (Duller *et al.* 2010) The diffusion model is therefore dominated by parameters that can be constrained by geological datasets derived from sedimentary isopachs, thermochronology, and position of grain-size fronts in the depositional basin, as well as being informed by a range of provenance tools employed to make confident connections between source and sink. When applied to geological examples in the Pobla Basin of the south-central unit of the southern Pyrenees (deposited 42-27 millions of years ago) (Beamud *et al.* ; Whittaker *et al.* 2011), we recognize different types of sediment routing system ranging from small, middle Eocene fans with clasts derived primarily from local carbonate rock sources, filling small, tectonically active wedge-top basins, to an extensive, coalescing, gravel 'drape' of Oligocene age with clasts derived from catchments eroding back to the main drainage divide, built by transverse flow across the entire wedge-top zone. These different sediment routing systems in the Pobla Basin exhibit variations in their sediment budget over time that can be linked to the changing tectonic and topographic history through the mid Eocene to Oligocene interval.

REFERENCES

- Beamud, E., Garcés, M., Cabrera, L., Muñoz, J.A. & Almar, Y. 2003: A new middle to late Eocene continental chronostratigraphy from NE Spain. *Earth & Planetary Science Letters*, **216**, 501-514.
- Duller, R.A., Whittaker, A.C., Fedele, J.J., Springett, J., Smithells, R. & Allen, P.A. 2010: From grain size to tectonics *Journal of Geophysical Research – Earth Surface*, **115**, F03022, doi:10.1029/2009JF001495.
- Mellere, D. 1993: Thrust-generated, back-fill stacking of alluvial fan sequences, south-central Pyrenees, Spain (La Pobla de Segur Conglomerates). In: Tectonic controls and signatures in sedimentary successions (ed. by L.E. Frostick and R.J. Steel), *Special Publication International Association Sedimentologists*, **20**, 259-276.
- Whittaker, A.C., Duller, R.A., Springett, J., Smithells, R., Whitchurch, A.L. & Allen, P.A. 2011: Decoding downstream trends in stratigraphic grain-size as a function of tectonic subsidence and sediment supply. *Bulletin Geological Society America*, **123**, 1363-1382, doi:10.1130/B30351.1.

22.2

From carbonate platforms to margin collapses: Comparing Alpine lake sediments with marine deposits

Flavio S. Anselmetti

Eawag (Swiss Federal Institute of Aquatic Science & Technology), Department of Surface Waters, Überlandstrasse 133, 8600 Dübendorf, Switzerland (flavio.anselmetti@eawag.ch)

Historically, the discipline ‘sedimentology’ was developed in the marine realm (‘marine geology’) with Swiss institutions playing a major role at the forefront of sedimentologic research. Lacustrine sedimentology (‘limnogeology’) is a much younger discipline. It was as well initiated with prominent Swiss participation in the 1970s and thereafter, reflecting to a certain degree the speciality of a landlocked country. The two communities recognized from the beginning the joint methods, concepts and basic principles that underlie the sedimentologic processes, but nevertheless, a partly different terminology was established. This occurred despite the fact, that lakes were recognized early on as ‘model oceans’ offering small-scale analogues to the larger marine systems.

The greater Alpine realm offers two kind of sedimentologic playgrounds: 1) outcropping strata of various ages provide superb views in sedimentary architecture, which are interpreted using the principle of actualism, and 2) modern lacustrine basins that provide real-time actual sedimentary systems. These lakes allow the study of ongoing processes that can be observed using geophysical and sedimentologic methods so that their immediate sedimentary response can be validated. This symposium contribution compares these two systems: Some analogues will be presented that document the use of either system to better understand the other. As an example, sequence stratigraphic concepts developed in marine carbonate platform systems can be applied towards coastal lacustrine depositional systems from carbonate-producing perialpine lakes. In a similar fashion, high-density underflows, first described in river delta areas, provide a detailed understanding of turbidite processes, which in turn help to better interpret the marine systems.

22.3

Mesozoic radiolarites from oceans to mountains: Facies, ages and palaeoenvironments

Baumgartner Peter O.¹

¹ *Institut de Géologie et Paléontologie, University of Lausanne. Anthropole, CH-1015 Lausanne, Switzerland. (Peter.Baumgartner@unil.ch)*

Radiolarites are deep water sediments mainly composed of, besides minor amounts of clay, biogenic silica chiefly from radiolarians, but also from sponge spicules near margins, and possibly some diatoms in the late Mesozoic. Radiolarites generally contain few or no carbonate. Radiolarites are the dominant pelagic sediment associated with oceanic basalts of various geodynamic settings (“ophiolites” s.l.) throughout the pre-Late Cretaceous Phanerozoic. The creation of Palaeozoic and Mesozoic radiolarian biochronologic scales during the past 30 years has allowed to unravel the complex history of the Circumpacific oceanic terranes as well as of ophiolitic suture zones of the Alpine-Himalayan mountain ranges. Palaeozoic and Mesozoic radiolarites occur also in Alpine-Himalayan stratigraphic sequences representing marginal basins resting on (often thinned) continental crust.

Based on the observations during the early phase of deep sea drilling in the modern oceans, the calcite compensation depth (CCD) was thought by most geologists to be the key concept to explain the distribution of Mesozoic radiolarites. Based on the Cretaceous-Tertiary distribution of carbonate in the oceans, the CCD-concept predicted that radiolarites had to be deposited at depths exceeding 4-5 km. Obviously, this prediction was difficult to reconcile with palaeobathymetries derived from many plate tectonic settings of radiolarite occurrences such as mid-ocean ridges, oceanic island arcs and, above all, marginal basins.

Biochronologically controlled transects across marginal basins and highs of the Mesozoic Tethys show that the radiolarites accumulated in the troughs cannot be regarded as dissolution residues, formed beneath a hypothetical CCD, of siliceous limestones accumulated on shallower margins and highs: Radiolarians are rare or absent from the condensed pelagic limestones and overall accumulation rates of basinal radiolarites exceed by an order of magnitude those of the limestones.

A modern sedimentation model for radiolarites must take into account several parameters that have fundamentally changed through the Phanerozoic and especially since the Late Cretaceous:

1. The scarcity of calcareous plankton throughout the Palaeozoic and the early Mesozoic must be the principal reason of the dominance of radiolarite sedimentation in open-ocean settings (radiolarites as “default” pelagic sediment). It must be noted that many Mesozoic open ocean radiolarites have very low accumulation rates and contain often important amounts of autigenic clays making them resemble oceanic red clays. The CCD-concept in such a situation has no predictive value for palaeodepth – the CCD could have coincided with the thermocline throughout pre- Late Mesozoic times.
Calcareous plankton becomes “rock-forming” in the “intra-Pangean” ocean basins (Protocaribbean, Central Atlantic and Western Tethys) with the rise of Nannoconids (Biancone and Cat Gap facies) in the Latest Jurassic. In Panthalassa, radiolarites become replaced progressively by pelagic limestones, due to the growing abundance of calcareous nannoplankton and planktonic Foraminifera since the mid-Cretaceous.
2. Variations in the supply of periplatform carbonate must have controlled the spatiotemporal distribution of cherty limestone vs. radiolarite/spiculite in Mesozoic marginal settings, both on oceanic and continental basement. Here again, the CCD-concept has no palaeobathymetric value, since with high periplatform input calcite compensation may not occur at any depth.
3. High accumulation rates of radiolarites both in intra-Pangean oceanic and marginal basins and along panthalassan margins must be controlled by meso- to eutrophic surface water conditions that simultaneously cause high productivity of siliceous plankton and benthos and the stalling of the carbonate factory. In addition, lateral transport of the very low density radiolarian tests tend to increase their accumulation rates in current-protected depressions, while topographic highs typically show radiolarian-bearing spiculites or no siliceous deposits at all.

Radiolarite occurrences in Tethyan basins have been explained by upwelling either in a peri-equatorial ocean basin or in monsoonal circulation system. However, more elaborate reconstructions of the middle Jurassic Tethys show a complicated system of poorly interconnected oceanic basins with deeply submerged margins separated by submerged shelves on micro-continents. To produce upwelling in these relatively narrow basins, especially the Alpine Tethys, seems very difficult. An equatorial current system cannot be made responsible either, because palaeolatitudes of the mid Jurassic Tethyan basins are, according to most palaeotectonic reconstructions, between 20° and 40° N. Another fact speaks clearly against an equatorial current system crossing ancient Pangea: The Jurassic Central Atlantic and the Protocaribbean are devoid of biosiliceous sediments. This must be interpreted as the consequence of Atlantic surface waters that are more oligotrophic than those of the adjacent Tethys and Panthalassa. The Jurassic Atlantic was a “mediterranean” ocean basin such as the Modern Red Sea. Important bottlenecks (Palaeo-Gibraltar, S-Florida-Bahamas) exist through the middle and late Jurassic and must have prevented a voluminous water exchange between the Atlantic and its neighbouring basins.

Both pelagic and shelf areas of the central western Tethys were beyond the reach of detrital input, but experienced increased nutrient levels throughout most of the Middle Jurassic. While the mid Jurassic global setting is right for meso- to eutrophic (low C_{carb}) sedimentation, we need a mechanism to continuously supply nutrients to the Western Tethys. In analogy with the Caribbean-Gulf of Mexico we can imagine that the Tethyan N-Equatorial Current struck the Arabian Platform, was deviated to the N and may have entered the Jurassic Eastern Mediterranean. On its way, it interacted with freshwater plumes of large rivers draining tropical N-Africa. While the suspended load sedimented in the deep Eastern Mediterranean, freshwater plumes rich in dissolved nutrients were carried into the entire S-Tethyan realm providing a constant nutrient input. This input allowed for high accumulation rates of biosiliceous sediments, caused deep water anoxia during peak intervals and microbial carbonates on platforms.

22.4

The Southern Alps from the Generoso Basin to the Dolomites: a unique natural laboratory for tectonic and structural studies

Bertotti Giovanni^{1,2}

¹ Department of Geotechnology, Delft University of Technology, Stevinweg 1, 2628CN, Delft, Netherlands (g.bertotti@tudelft.nl)

² Department of Earth Sciences, VU University Amsterdam, De Boelelaan 1085, 1081HV Amsterdam

Following the work of numerous geologists, among which Ticino-loving Swiss geoscientists played a fundamental role, the sedimentology and stratigraphy of the Generoso basin and surrounding domains were fairly well-known. At this stage Daniel Bernoulli thought it was time for a more tectonic oriented research. Time to provide a quantitative reconstruction of the extension kinematics of the Generoso basin. Key was the intuition that, because of the general southward dip of Liassic to Triassic sediments, the northern part of the Generoso basin was reminiscent of a tilted paleo-vertical section exposing the deep geometry of the basin and its master fault (Bally et al., 1981) (Fig. 1). It was the right approach: in collaboration with S. Schmid we constrained the geometry of the Generoso basin down to depths of 12-15km (Fig. 2) and estimated vertical and horizontal movements. Analysing the fault rocks associated with the entire Lugano-Val Grande normal fault and integrating petrographic and geochronologic techniques the thermal evolution of the area was determined. Expanding our analysis we quantified the stretching history of the entire Lombardian basin, the major structure which developed during the initial stages of Mesozoic continental rifting (Bertotti et al., 1993). Such estimates are still rare in the literature but they are key for quantitative models of rifting.

The Generoso basin work highlighted two general phenomena which are still very much topics of research.

- i) Continental rifting began and developed in a frame of generalized cooling, fast during the first 10-20Myr and decreasing afterwards. This phenomenon, not foreseen in classic McKenzie-type models, caused a larger-than-normal Middle-Late Triassic subsidence and a change in the deformation style of the faults rocks associated with the deep segment of the Lugano normal fault (Bertotti, 2001). The occurrence of a thermal anomaly prior to rifting has been confirmed by other studies but its origin is debated. It is also unclear if such a thermal anomaly is a mechanic necessity to activate continental rifting as suggested by some numerical models.
- ii) The slow rate of extension enhanced by the mentioned cooling led to the progressive strengthening of the lithosphere underlying the Lombardian basin and the consequent West-ward migration of the site of extension. This phenomenon has been further developed in various margins e.g. Manatschal and co-authors) and modelled (van Wijk and Cloetingh, 2002); the Southern Alps, still remain one of the few places where a quantitative comparison is possible.

The Southern Alps natural laboratory had more to offer. In the Dolomites, the weakly dolomitized Latemar platform, turns out to be an excellent analog to investigate the influence of large-scale heterogeneities on strain patterns. Atoll-like carbonate platforms are of great structural interest because of the lateral juxtaposition of first-order domains (interior, margin and slope) with very different sedimentary architecture resulting in different mechanical properties. Indeed, the distribution of fractures as well as their mode, orientation and spacing, height and length are significantly different in the three domains. This introduces the idea that fractures can be tracers of bulk mechanic properties of platform domains. Interestingly, the geometric characteristics of the two fracture sets present in the Latemar are significantly different even when observed in the same domain (Boro & Bertotti, submitted). The two fractures system track then mechanical changes experienced by the platform from one fracturing episode to the other. These modifications are essentially controlled by the diagenetic evolution of the platform during its subsidence to its maximum burial depth. Fractures become then tracers of these platform-scale processes highlighting the added value of integrating sedimentology and structural geology.

REFERENCES

- Bally, A.W. Bernoulli, D. Davis, G.A., & Montadert, L. 1981: Listric normal faults. *Oceanologica acta*, 26th Int. Geol. Congr. Paris, 87-101
- Bertotti, G., Picotti, V., Bernoulli, D. & Castellarin, B. 1993: From rifting to drifting: tectonic evolution of the South-Alpine upper crust from the Triassic to the Early Cretaceous. *Sedimentary Geology*, 86, 53-76.
- Bertotti, G. 2001. Subsidence, deformation, thermal and mechanic evolution of the Mesozoic South-Alpine rifted margin: An analog for Atlantic-type margins. *Geol. Soc. Sp. Publ.*, 187, 125-141.
- Boro, H. & Bertotti, G. submitted. Low-strain, distributed fracturing affecting the Latemar, atoll-like carbonate platform (Dolomites, North Italy).
- Wijk, J. van & Cloetingh, S., 2002. Basin migration due to slow lithospheric extension. *Earth Planet. Sc. Lett.*, 198, 275-288.

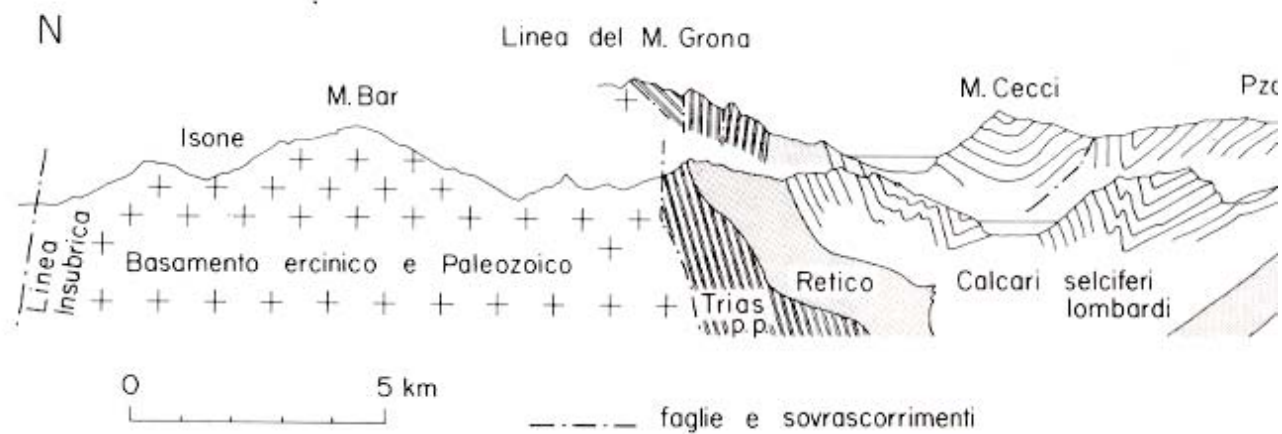


Fig. 1. Section across the N part of the Generoso Basin (Bernoulli 1995)

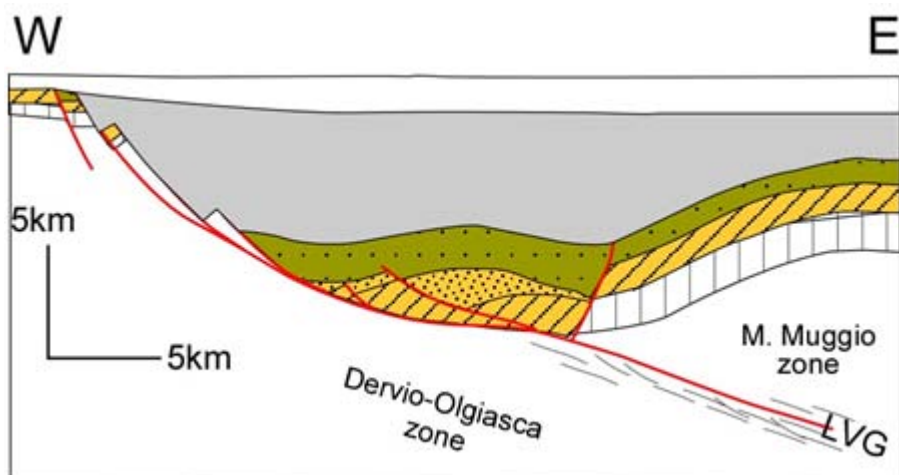


Fig. 2. The Generoso basin in Early Jurassic (Bertotti, 1991)

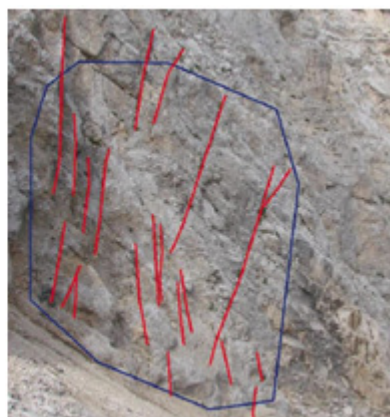


Fig. 3. Fractures in Latemar interior (3a) and slope (3b)

22.5

The long goodbye of carbonate cycles as reliable recorders of orbitally driven sea-level fluctuations

Gregor P. Eberli¹

¹*Comparative Sedimentology Laboratory, RSMAS-MGG, University of Miami, 4600 Rickenbacker Causeway, Miami, FL 33149, USA (geberli@rsmas.miami.edu)*

Shallow-water carbonates are deposited in pulses of relative sea-level change during which space is created to accommodate a new layer of sediment. There is, however, increasing evidence that these depositional cycles are unreliable recorders of both the frequency and the amplitude of orbitally driven sea-level fluctuations. Uncertainties in the assessment of the amplitude are caused by unfilled accommodation space and the inability to measure the amount of sea-level fall in these platform-top sediments. Uncertainties in the frequencies are caused by the variable amplitude of sea-level change, producing “missed beats” on the platform, and meter-scale oscillations of sea level within highstands that potentially produce cycles of very short durations.

Shallow-water carbonates often form spectacular vertically stacked, meter-scale depositional packages that are separated by exposure horizons or flooding surfaces. These smallest stratigraphic units, herein called carbonate cycles, vary in thickness and seem to be arranged in a hierarchical matter. Because the facies within carbonate cycles can be precisely tied to water depths, they are considered ideal for reconstructing past sea-level changes. Quantitative approaches include the computing cumulative cycle thickness variations through time (Fisher, 1964; Read and Goldhammer, 1988) and a variety of spectral analysis techniques for assessing their high-frequency cycling (e.g. Hinnow & Goldhammer, 1994). The underlying assumptions in these analyses are at odds with observations in the Holocene and Quaternary carbonate cycles that show a very sketchy record of both the amplitude and timing of known sea-level fluctuations during this time. A case can be made that the uncertainty in assessing both the amplitude of sea-level change from cycle thickness and the frequency from dating is too big to reconstruct a reliable record of past sea-level changes.

In regards to the amplitude of sea level the problem is twofold. First, the accommodation space is filled to different levels within the depositional environment. Most facies with the exception of shallow reefs, shoals and tidal flats are deposited within a certain water depth. This unfilled accommodation space is not recorded and, thus, the upper boundary of the mean sea level cannot be assessed precisely. Second, many carbonate cycles are capped by an exposure horizon that forms when sea level drops. The amount to which sea level drops below the exposed surface is, however, not recorded in the stacked shallow-water cycles. As a consequence, carbonate cycles record only a fraction of the amplitude of a sea-level cycle: a portion of the rise and nothing of the fall. Cores through the Pleistocene cycles on Great Bahama Bank illustrate this shortcoming. While the amplitudes of the last 9 sea level changes are each a hundred meters or more, the thickness of the cycles vary from a few meters to approximately 15 m. Although this lack of correlation between sea-level amplitude and cycle thickness might be extreme in the Neogene Ice House world, the uncertainty is not eliminated for cycles deposited during times of lower amplitudes because they also do not record the unfilled accommodation space and amount of sea-level fall.

In addition to the difficulty of accurate age model, the assessment of frequency has two main problems. The first is what is known as “missed beats”. A missed beat occurs when a sea-level rise is too small to produce new accommodation space in the shallow-water environment. This scenario is thought to occur preferentially during times of long-term sea-level fall. The benthic isotope record of the last 57 glacio-eustatic sea level changes documents that the amplitude variability is prevalent and seemingly random (Lisiecki & Raymo, 2005), resulting in many missed beats during the Plio-Pleistocene. The second problem is that new data document oscillations of the sea level during interglacials that occur in a sub-orbital timeframe. For example, Thompson and Goldstein (2005) proposed a sea-level drop of ~ 17 m within the last interglacial (MIS 5e). This sea level drop exposed the entire Great Bahama Bank and is recorded in exposure surfaces within marine deposits of MIS 5e. On Glovers Reef it produced stacked reefs separated by an exposure horizon. The combined effects of missed beats and oscillations within highstands are likely to produce cycles and hiatuses of variable durations that are most difficult to extract from the rock record.

In summary, carbonate cycles are produced by fluctuations of sea level but their incomplete record of both the amplitude and the frequency makes them an unreliable recorder of high-frequency sea-level changes.

REFERENCES

- Fischer, A.G., 1964: The Lofer cyclothems of the Alpine Triassic. *Kansas Geological Society Bulletin*. 169, 107-149.
 Hinnow, L.A. & Goldhammer, R.K., 1991: Spectral analysis of the Middle Triassic Latemar limestone. *Journal of*

Sedimentary Petrology. 61, 1173-1183.

Lisiecki, L.E. & Raymo, M.E. 2005: A Pliocene Pleistocene stack of 57 globally distributed benthic $\delta^{18}O$ records. *Paleoceanography*. 20, PA1003, doi:10.1029/2004PA001071.

Read, J. F. & Goldhammer, R. K. 1988: Use of Fischer plots to define third-order sea-level curves in Ordovician peritidal cyclic carbonates, Appalachians: *Geology*. 16, 895-899.

Thompson, W.G. & Goldstein, S.L. 2005: Open system coral ages reveal persistent suborbital sea-level cycles. *Science*. 308, 401-404.

22.6

Albert of Arabia - Climatic and environmental reconstructions on stalagmites and lacustrine sediments from the Arabian Peninsula

Fleitmann Dominik*

¹ *Institute of Geological Sciences and Oeschger Centre for Climate Change Research, Baltzerstrasse 1+3, 3012 Bern, Switzerland (fleitmann@geo.unibe.ch)*

In the late 1990's the Quaternary paleoclimatic history of the Arabian Peninsula was almost unknown. This was somewhat surprising considering that the climate on the Arabian Peninsula is strongly governed by the North Atlantic/Siberian pressure system and the African/Asian monsoon. Arabia is thus ideally situated to study how and to what extent both systems were dynamically linked in the past. Furthermore, Arabia is also a key area for the migration of *Homo sapiens* "out of Africa" at around 130 kyr before present, whereupon phases of human migration were most likely intimately linked to climate.



Figure 1. Albert Matter working on lacustrine sediments in the Nafud desert (picture taken by Dominik Fleitmann in 2010)

One of the main reasons for this distinct lack of knowledge of the paleoclimatic history of Arabia is the paucity of suitable paleoclimate archives. Fortunately, Albert Matter was one of the first scientists who realized that stalagmites, sand dunes and lake sediments can provide crucial information on paleoclimatic and –environmental changes on the Arabian Peninsula on time scales ranging from a few hundred to several hundred thousand years. Among several milestone achievements, Albert Matter's research on precisely-dated stalagmites from Oman and Yemen revealed that the occurrence of humid periods over the last 350 kyr before present was intimately tied to changes in the intensity of the Asian monsoon and latitudinal shifts of the Intertropical Convergence Zone and monsoonal rainfall belt respectively (e.g., Burns et al., 2001; Fleitmann et al., 2003a, 2007). Furthermore, it could be shown that decadal- to centennial-scale changes in monsoon intensity were caused by rather subtle changes in solar activity (Neff et al., 2001; Fleitmann et al., 2003b), triggering numerous new studies on the sun-climate relationship in the paleoclimate community. Albert Matter was also the first scientist who drilled into a mega dune to establish the timing of arid climatic phases in the Wahiba sands in Northern Oman (e.g., Preusser et al., 2002). His latest and ongoing research activities involved studies on lacustrine sediments in Saudi Arabia and stalagmites from Yemen to establish a link between human dispersal and climate (e.g., Fleitmann et al. 2011; Rosenberg et al., in press.).

The sentences by Benjamin Franklin “Energy and persistence conquer all things” and “To succeed, jump as quickly at opportunities as you do at conclusions” describe perfectly why Albert Matter’s paleoclimate research projects on the Arabian Peninsula were so successful. His profound knowledge of the Arabian language and way of life allowed him to create and foster a dense network of collaborators in Arabia. Therefore, it is absolutely justified to call him “Albert of Arabia”, in allusion to “Lawrence of Arabia” and his extraordinary variety of activities in Arabia.

REFERENCES

- Burns, S.J., Fleitmann, D., Matter, A., Neff, U. & Mangini, A. 2001. Speleothem evidence from Oman for continental pluvial events during interglacial periods. *Geology*, 29, 623-626.
- Fleitmann, D., Burns, S. J., Neff, U., Mangini, A. & Matter, A. 2003a. Changing moisture sources over the Last 330,000 Years in Northern Oman from fluid-inclusion evidence in speleothems. *Quaternary Research*, 60, 223-232.
- Fleitmann, D., Burns, S. J., Mudelsee, M., Neff, U., Kramers, J., Mangini, A. & Matter, A. 2003b. Holocene forcing of the Indian monsoon recorded in a stalagmite from Southern Oman. *Science*, 300, 1737-1739.
- Fleitmann, D., Burns, S. J., Mangini, A., Mudelsee, M., Kramers, J., Neff, U., Al-Subbary, A. A. & Matter, A. 2007. Holocene ITCZ and Indian monsoon dynamics recorded in stalagmites from Oman and Yemen (Socotra). *Quaternary Science Reviews*, 26, 170-188.
- Fleitmann, D., Burns, S.J., Pekala, M., Mangini, A., Al-Subbary, A.A., Al-Aowah, M., Kramers, J. & Matter A. 2011. Holocene and Pleistocene pluvial periods in Yemen, Southern Arabia. *Quaternary Science Reviews*, 30: 783-787; doi: 10.1026/j.quascirev.2011.01.004.
- Neff, U., Burns, S.J., Mangini, A., Mudelsee, M., Fleitmann & D., Matter, A. 2001. Evidence for solar forcing of the Indian Monsoon in a high-resolution speleothem record from Oman. *Nature*, 411, 290-293.
- Preusser, F., Radies, D. & Matter, A. 2002. A 160,000-year record of dune development and atmospheric circulation in southern Arabia. *Science* 296, 2018-2020.
- Rosenberg, T.M., Preusser, F., Fleitmann, D., Schwab, A., Penkman, K., Schmid, T.W., Al-Shanti, M.A., Kadi, K. & Matter, A. in press. Humid periods in southern Arabia: windows of opportunity for modern human dispersal. *Geology*.

22.7

Magnesium Isotopes: Establishing a new proxy in Earth Sciences

Adrian Immenhauser¹, Dieter Buhl¹, Sylvia Riechelmann², Christoph Spötl & Detlev K. Richter¹

¹ Ruhr-University Bochum, Institute for Geology, Mineralogy and Geophysics, Universitätsstraße 150, D-44801 Bochum, Germany (adrian.immenhauser@rub.de)

² Leopold-Franzens-University Innsbruck, Institute for Geology and Palaeontology, Innrain 52, A-6020 Innsbruck, Austria

The potential of magnesium isotope records is at present underexplored. This is mainly due to the analytical complexity related to this non-traditional isotope system and the limited knowledge regarding physico-chemical and biological disequilibrium fractionation processes in natural systems. Work under progress at Bochum involves $\delta^{26}\text{Mg}$ studies including marine biogenic (bivalve shells) and abiogenic (dolomite) carbonate archives as well as meteoric-vadose systems (speleothems). Here we present Mg isotope data from a monitored cave in Germany (Bunker Cave) and provides data on rain water ($\delta^{26}\text{Mg}$: $-0.70 \pm 0.14\text{‰}$), soil water ($\delta^{26}\text{Mg}$: $-0.51 \pm 0.10\text{‰}$) and drip waters ($\delta^{26}\text{Mg}$: $-1.65 \pm 0.08\text{‰}$) representing time series between November 2009 and May 2011. Field precipitation experiments, i.e., calcite precipitated on watch glasses ($\delta^{26}\text{Mg}$: $-3.56 \pm 0.26\text{‰}$; August 2006 to June 2010), were found to be of limited use. This is because of several experimental and sampling artefacts, probably combined with crystallographic problems related to the silica glass substratum and disequilibrium processes complicates this issue. Conversely, variations in soil- and drip water $\delta^{26}\text{Mg}$ over time are predominantly related to seasonal climate variations (mainly water availability and temperature changes) affecting the subtle weathering ratio between Mg-bearing clay minerals in the soil, here mainly chlorite and montmorillonite, and the low-Mg calcite hostrock. For fast drip sites, the direct correlation of $\delta^{26}\text{Mg}_{\text{soil water}}$ and $\delta^{26}\text{Mg}_{\text{drip water}}$ documents a relative short residence time of the fluid in the carbonate aquifer and thus limited isotope equilibration and mixing of different reservoirs. This result is encouraging and adds new evidence to the poorly understood hydro-geochemistry of carbonate aquifers. Slow (seepage flow) drip sites display an annual $\delta^{26}\text{Mg}_{\text{drip water}}$ pattern that is geochemically unrelated to that of the soil water. Bunker Cave $\delta^{26}\text{Mg}_{\text{drip water}}$ displays a significant dependency on the outside temperature, which influences CO_2 levels in the soil and hence rock-water interaction. Further research, including laboratory experiments, must focus on the complex fractionation between drip water and speleothem calcite Mg isotope record.

22.8

Tectonics versus palaeoceanography in the evolution of the Alpine-mediterranean Tethys

Jenkyns Hugh C.

¹*Department of Earth Sciences, University of Oxford, South Parks Road, Oxford OX1 3AN (hughj@earth.ox.ac.uk)*

One of the major events in the Jurassic evolution of the Alpine-mediterranean Tethys was the drowning of carbonate platforms. Shallow-water platforms installed on the continental margin subsided at different times and were mantled by pelagic sediment. The post-platform subsidence rates were variable, such that some areas rapidly became basinal, whereas others remained as topographic highs or seamounts. Although initially interpreted as a purely tectonic phenomenon, the coincidence in timing between drowning events and major disturbances of the global carbon cycle suggests that environmental change and water quality were contributory factors. Major drowning events took place around the Rhaetian–Hettangian (T/J) boundary, the Sinemurian–Pliensbachian boundary, and the Pliensbachian–Toarcian boundary. All of these intervals are associated with negative carbon-isotope excursions, recording the introduction of isotopically light carbon into the ocean–atmosphere system, probably associated with rises in global temperature and, at least in some cases, increased nutrient flux to the oceans and relatively elevated organic productivity. The most extreme case of this phenomenon was the early Toarcian Oceanic Anoxic Event (T-OAE). Where subsidence rates were relatively fast, inimical water quality favoured drowning; where subsidence rates and deepening were less extreme, a platform could re-establish itself when water quality improved. The Trento Platform/Plateau in the Southern Alps is an unusual case in that the T-OAE is registered in some areas by a change in facies to darker more clay-rich sediments, with ammonites, nannofossils and abundant spiculitic cherts, but local recovery to shallow-water carbonate-platform conditions (oolitic and crinoidal limestones) was achieved before ultimate drowning in the middle Jurassic. To understand the drowning of carbonate platforms, the interplay between local syn-sedimentary tectonics and global palaeoceanographic changes needs to be understood.

22.9

Stratigraphic and tectonic architecture of the Alpine Tethys margins

Gianreto Manatschal¹, Emmanuel Masini¹ and Geoffroy Mohn¹

IPGS - EOST, Université de Strasbourg – CNRS, 1, rue Blessig F-67084 Strasbourg Cedex, France

Research into the formation of passive rifted margins is incontestably undergoing a paradigm shift. The discovery of exhumed mantle and hyper-extended crust overlain by shallow marine sediments is proving fundamental in defining the controls and processes that thin continental lithosphere, lead to continental break-up and formation of oceanic domains. At present, little is known about the depositional environments, sedimentary facies, the kinematics and age of structures, or the subsidence and thermal history of syn-rift sediments of deep-water rifted margins. Moreover, the discovery of exhumed continental mantle and hyper-extended crust associated with large sag basins, hundreds of kilometres wide, has not yet been fully integrated in the understanding of collisional orogens. It is important to understand how these hyper-extended rift systems may control the structural and rheological evolution of Alpine type orogens.

In our presentation we present the key observations made along the Iberia-Newfoundland and Alpine Tethys rifted margins, review the paleogeographic evolution of this domain and discuss how the understanding of this domain may impact our thinking and understanding of the evolution of present-day rifted margins.

The study on the Iberia-Newfoundland rifted margins show that the transition from continental to oceanic crusts does not represent a sharp boundary, but is formed by an up to 160 km wide zone of exhumed sub-continental mantle. This observation questions the existence of a sharp and well-defined ocean-continent boundary at magma-poor rifted margins and the validity of the breakup unconformity and nature and significance of magnetic anomalies in ocean continent transitions.

Mapping of rift structures and depositional systems of the most distal parts of the ancient Alpine Tethys margins enabled to identify lithologies and structures similar to those drilled off Iberia. The most prominent structures observed in the Alps are a set of detachment faults. These structures can be traced from relatively little extended continental crust across the distal margin and ocean-continent transition towards embryonic oceanic crust. These faults are far more complex as proposed by the Wernicke model. Detachment faults interact with decollements in ductile layers and only when the crust is thinned to less than 10 km and is completely brittle, detachment faults can cut from the surface into mantle and exhume the latter at the seafloor. Fluids are intimately linked with this process, controlling rheological and thermal evolution.

The lesson from the Iberia-Newfoundland and Alpine Tethys rift systems might not be extrapolated directly to other margins, however, it may help to re-evaluate and rethink some of the concepts, the terminology and the processes that were (are) used to describe rifting and continental breakup along these less investigated rifted margins.

22.10

Sedimentary archives of Northern Alpine and Molasse Basin neotectonics

Strasser Michael¹, Anselmetti Flavio S.², Gorin George³, Monecke Katrin⁵, Mosar Jon⁶ Schnellmann Michael⁷

¹ Geological Institute, ETH Zurich, 8092 Zürich (strasser@erdw.ethz.ch)

² Eawag, Swiss Federal Institute of Aquatic Science & Technology, 8600 Dübendorf

³ Sciences de la Terre, Université de Genève 1205 Genève

⁵ Wellesley College, Department of Geosciences, Wellesley, MA, 02481, USA

⁶ Department of Geosciences, University of Fribourg, 1700 Fribourg

⁷ Nagra, Nationale Genossenschaft für die Lagerung radioaktiver Abfälle, 5430 Wetting

Switzerland lies tectonically in an intraplate area. Recurrence rates of strong earthquakes exceed the time span covered by historic chronicles. Consequently, they are not sufficient to document the full range of neotectonic processes. However, many lakes are present in the area that act as natural seismographs: their continuous, datable and high-resolution sediment succession allows to extend the earthquake catalogue from instrumental and historic periods to prehistoric times, all the way to the end of the last glaciation, when the modern lakes formed after glacier retreat.

Here we review and compile available data sets and results from more than 10 years of lacustrine paleoseismologic research in lakes of northern and Central Switzerland, and present an outlook of a new study starting in the Western Swiss Molasse Basin. The concept of using lacustrine mass-movement event stratigraphy to identify paleo-earthquakes is showcased by presenting data and results from Lake Zurich. The Late Glacial-to-Holocene mass-movement units in this lake document a complex history of varying tectonic and environmental impacts. Results include the documentation of 3 major (2200, 11 530, 13 840 cal yr. B.P. Strasser et al., 2006) and 3 minor (640, 3300 and 7270 cal yr. B.P), simultaneously-triggered basin-wide lateral slope failure events interpreted as the fingerprint of paleoseismic activity. In all lakes, historic calibrations were used to identify these “seismic fingerprints” in the sedimentary archives (Schnellmann et al., 2002, Monecke et al., 2004) a procedure which here is exemplarily discussed for the 1601 A.D. Unterwalden earthquake. These calibrations indicate that the macroseismic intensity threshold to trigger subaquatic slope failures is I=VII (Monecke et al., 2004). This quantitative calibration is reinforced by subaquatic slope stability assessment back-analyzing seismic ground shaking threshold conditions for landslide initiation in Lake Lucerne (Strasser et al., 2011).

We present a refined earthquake catalogue, which includes results from previous lake studies (Monecke et al., 2006). This compilation shows a non-uniform temporal distribution of earthquakes in northern and Central Switzerland. Higher frequency of earthquakes in the Late Glacial and Late Holocene period documents two different phases of neotectonic activity. They are interpreted to be related to isostatic post-glacial rebound and recent (re-) activation of seismogenic zones, respectively. Magnitudes and epicenter reconstructions for the largest identified earthquakes suggest that the latter may be related to ongoing alpine deformation and the release of accumulated NW-SE compressional stress related to an active basal thrust beneath the Aar massif (Strasser et al., 2006). However, even though these results reveal that also in Central Switzerland strong earthquakes with magnitudes (M) > 6.5-7 can occur, field-evidence for a neotectonically active fault zone capable of producing such large earthquakes remain absent.

In the Western Swiss Molasse Basin, in contrast, there is emerging evidence of neotectonic activity along the Fribourg Fault Zone (FFZ; Kastrup et al., 2007) and possibly also along the La Lance Fault Zone (LLFZ), which constitutes a conjugated fault system to the FFZ (Mosar et al., 2008). If not segmented, the total length of these fault zones may carry the potential of M 6+ earthquakes. Yet, this area so far lacks geological records of significant earthquakes. The obvious next step is to transfer the knowledge gained from studies in Central Switzerland and to apply the concept of “lakes as archive for quantitative paleoseismology and neotectonic reconstructions” in lakes of Western Switzerland (e.g. Lakes Neuchâtel, where airgun seismic data (Gorin et al., 2003) have shown that this lake also is prone for subaquatic landslides, the trigger mechanism(s) of which will be systematically investigated in a new project aiming at paleoseismologic and neotectonic reconstruction of this area).

REFERENCES

- Gorin, G., Morend, D., and Pugin, A., 2003, Bedrock, Quaternary sediments and recent fault activity in central Lake Neuchâtel, as derived from high-resolution reflection seismics: *Eclogae Geologicae Helvetiae*, v. 96, p. S3-S10.
- Kastrup, U., Deichmann, N., Fröhlich, A., and Giardini, D., 2007, Evidence for an active fault below the northwestern Alpine foreland of Switzerland: *Geophysical Journal International*, v. 169, no. 3, p. 1273-1288.
- Monecke, K., Anselmetti, F. S., Becker, A., Sturm, M., and Giardini, D., 2004, The record of historic earthquakes in lake sediments of Central Switzerland: *Tectonophysics*, v. 394, no. 1-2, p. 21-40.
- Monecke, K., Anselmetti, F., Becker, A., Schnellmann, M., Sturm, M., and Giardini, D., 2006, Earthquake-induced deformation structures in lake deposits: A Late Pleistocene to Holocene paleoseismic record for Central Switzerland:

Eclogae Geologicae Helveticae, v. 99, no. 3, p. 343-362.

Mosar, J., Ibele, T., and Matzenauer, E., 2008, Tectonics of the Molasse Basin of Western Switzerland: An Overview.

Schnellmann, M., Anselmetti Flavio, S., Giardini, D., McKenzie Judith, A., and Ward Steven, N., 2002, Prehistoric earthquake history revealed by lacustrine slump deposits: *Geology*, v. 30, no. 12, p. 1131-1134.

Strasser, M., Anselmetti, F.S., Fah, D., Giardini, D., and Schnellmann, M., 2006, Magnitudes and source areas of large prehistoric northern Alpine earthquakes revealed by slope failures in lakes: *Geology*, v. 34, no. 12, p. 1005-1008.

Strasser, M., Hilbe, M., and Anselmetti, F. S., 2011, Mapping basin-wide subaquatic slope failure susceptibility as a tool to assess regional seismic and tsunami hazards: *Marine Geophysical Researches*, p. in press.

22.11

Tracing Alpine sediment sources through laser-ablation U/Pb dating and Hf-isotopes of detrital zircons - an appraisal

Winkler Wilfried¹, Beltrán Alejandro¹, von Quadt Albrecht²

¹Geologisches Institut, ETH Zürich, Sonneggstrasse 5, CH-8092 Zürich, Switzerland (wilfried.winkler@erdw.ethz.ch)

²Institut für Geochemie und Petrologie, ETH Zürich, Clausiusstrasse 25, CH-8092 Zürich, Switzerland

In Alpine research provenance analysis on sandstones always played an important role. Conventional heavy mineral and sandstone modal framework grain analysis in the past have contributed to palaeogeographic reconstructions and geodynamic models. However, these methods appear to have reached their limits of evidence, because of the lack of geochronological precisions. Due to recent developments in in-situ laser ablation methods (e.g. Kosler et al. 2002; von Quadt et al., 2008) significant contributions from single detrital zircons can be gained (Figure 1).

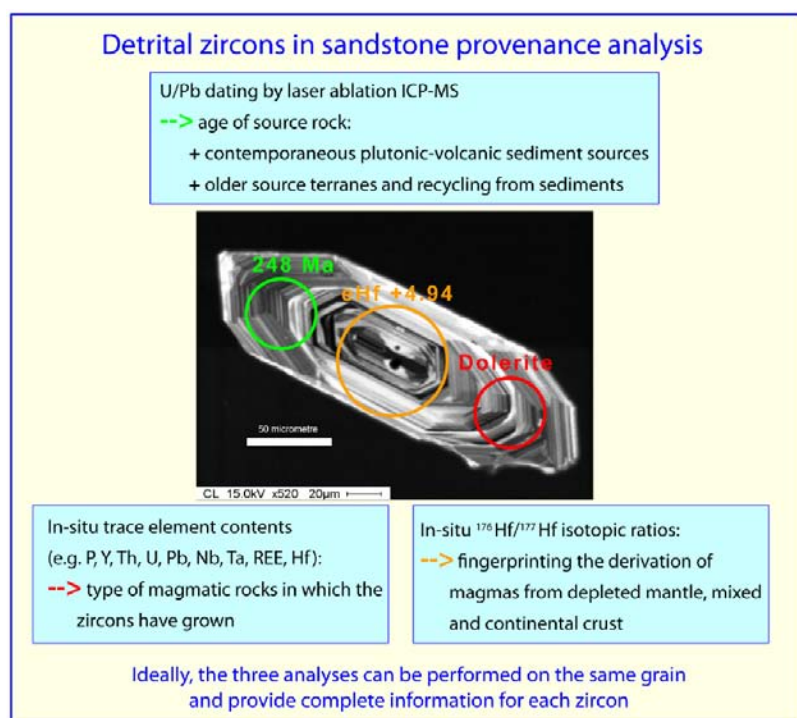


Figure 1: Provenance information on an Early Triassic detrital zircon from a Jurassic sandstone of the Mongol-Okhotsk Belt (Mongolia).

Triassic rifting-related sandstones in various/several Alpine palaeogeographic domains show variable zircon age compositions as major reworking of M. Cambrian - Devonian in the Helvetic Mels Fm (Scheidnössli, 09AB18, Fig. 2), the Lower Austroalpine Fuorn Fm (Punt de la Drossa Mb, 10AB14) depicts a dominating Permian population, and the Val Sabbia Fm in the Southern Alps (10AB08) an exclusive, contemporaneous Middle Triassic crustal magmatic source (Beltrán et al. 2011). Jurassic rifting-related series (Falknis Breccia 09AB28, Saluver Fm 10AB18, Inferno Series/Scopi Zone 09AB19) show

prominent/dominant Variscan - late Variscan peaks and intensive reworking of Early Palaeozoic and Proterozoic elements, in particular in the Gotthard Mesozoic para-autochthonous cover (09AB19). In the Prättigau Group (09AB23-27) the Ruchberg Fm is distinctive by a wide and old range of Early Jurassic - Proterozoic zircons revealing the activation of new sediment sources in comparison with older Bündnerschiefer formations. Except for the presence of rare Mesozoic zircons in the Niesen Flysch (09AB08), there is no significant distinction with the E. Jurassic sedimentary basement of the flysch (Leyderrey Conglomerate 09AB06) observed. Pre-alpine Flysches (Médianes 09AB01/02, Reidigen 09AB05, Mocausa/Rodomont 09AB03) show variable populations of Variscan and Pan-african detrital zircons with affinities with the Schlieren Flysch (Bütler et al. 2011). Bulk modal sandstone framework and heavy mineral analyses complete our data set.

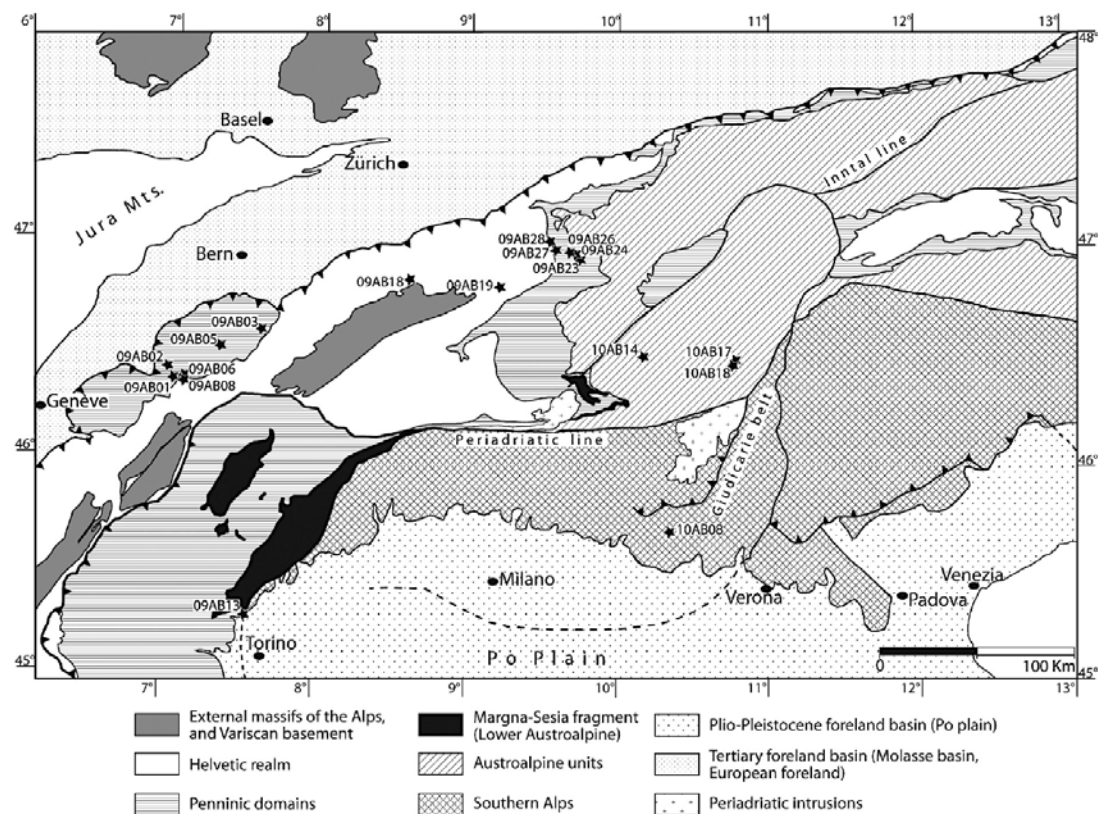


Figure 2: Palaeogeographic location of the discussed sandstone formations.

REFERENCES

- Beltrán, A., Winkler, W. & von Quadt, A. 2011: Triassic magmatism recorded by detrital zircons in South Alpine sedimentary units. Abstracts SGM 2011, Zurich (this volume).
- Bütler, A., Winkler, W. & Guillong, M. 2011: Laser ablation U/Pb age patterns of detrital zircons in the Schlieren Flysch (Central Switzerland): new evidence on the detrital sources. *Swiss J. Geosci.* doi 10.1007/s00015-011-0065-1.
- Košler, J., Fonneland, H., Sylvester, P., Tubrett, M. & Pedersen, R-B. 2002. U-Pb dating of detrital zircons for sediment provenance studies – a comparison of laser ablation ICPMS and SIMS techniques. *Chemical Geology*, 182, 605-618.
- von Quadt, A., Peytcheva, I., Reynolds, B. and Heinrich, C.A. (2008). In-situ Hf isotope and U-Th-Pb analyses within individual zircon growth zones. In: Winter Conference Plasma Spec. California, Jan. 2008, 310-311.

P 22.1

The Cretaceous-Tertiary transition in the Alps, new insights from Gams, Austria

Thierry Adatte¹, G. Keller², H. Khozyem Saleh¹, J. Spangenberg³

¹IGP, Lausanne University, 1015 Lausanne, Switzerland

²Dpt of geosciences, Princeton University, NJ 08544, USA

³IMG, Lausanne University, 1015 Lausanne, Switzerland

The Cretaceous-Tertiary (K-T) transition in eastern Austria (Gams, Styria) was analyzed in terms of lithology, mineralogy (bulk and clay minerals), stable isotopes, major and trace elements and biostratigraphy (planktic foraminifera). The Gamsbach section is part of the Nierental Formation and comprises a 6.4 m thick deep-water sequence composed of marlstones, marly limestones interbedded with sandy to silty turbidites, which become more frequent above the KTB. Age control is based on a high-resolution planktic foraminiferal biozonation of which permits evaluation of the continuity of the sedimentary record across the KTB transition based on the presence of relatively short interval zones and subzones. Presence of *P. hantkeninoides* in the 1.75 m below the KTB at Gamsbach indicates sediment deposition occurred in zone CF1, or during the last 150 ky of the Maastrichtian. Just below the KTB, an irregular wavy surface at the top of the marly limestone marks an unconformity, which is strongly bioturbated (Chondrites-type burrows) coincident with a 2.5 permil drop in $\delta^{13}\text{C}$ values and low calcite content (<2%). Most Maastrichtian species abruptly disappear at this level, except for survivor species that continue into the early Danian and a few reworked specimens. Above this surface, 0.2 to 0.4 cm of yellowish rusty clay marks the basal Danian overlain by 2–3 cm thick gray claystones both enriched in Ir, Co, Cr, Sc, Zn, Pb and Ni indicating an extraterrestrial source. Ten Danian species abruptly appear at that level, including *P. longiapertura* and *P. eugubina* the index species for zone P1a and abundant *Eoglobigerina edita*. The high species diversity and presence of *Parasubbotina pseudobulloides* 3 cm above marks subzone P1a(2). This indicates that zone P0 and subzone P1a(1) are mainly missing at this hiatus. Erosion of the top part of zone CF1 below the unconformity is also likely. Reworked Cretaceous species in Danian sediments are frequent in particular intervals and reflect downslope transport of eroded older sediments in upslope or shelf areas probably during times of intensified ocean circulation. Two hiatuses can be therefore identified in the Gamsbach section: 1) at the KTB where the basal Danian zone P0 and subzone P1a(1) are mainly missing above an undulating erosion surface of Upper Maastrichtian marly limestone, and 2) in the lower Danian where most of zone P1b is missing. Bulk and clay minerals indicate reduced detrital input in the Upper Maastrichtian becoming more significant during the lower Danian reflecting increased turbidite activity linked to growing Austro-Alpine tectonic subsidence and erosion. Weathering Index of Parker (WIP) that shows higher values in the Lower Danian confirms this change in detrital inputs.

P 22.2

The Urgonian Formation in the Helvetic Alps (late Barremian to early Aptian): new evidences from the Interlaken area.

Bonvallet Lucie ¹, Godet Alexis ¹, Spangenberg Jorge E. ² & Föllmi Karl B. ¹

¹Institut de Géologie et de paléontologie, University of Lausanne, Anthropole, CH-1015 Lausanne-Dorigny, Switzerland

(lucie.bonvallet@unil.ch)

²Institut de Mineralogie et de Geochemistrie, University of Lausanne, Anthropole, CH-1015 Lausanne-Dorigny, Switzerland

Urgonian platform carbonates are a common feature of subtropical and tropical shallow-water environments of late Early Cretaceous age. They include the remains of rudists, corals, chaetetids and stromatoporoids, which are interpreted as indicators of a predominantly photozoan, oligotrophic carbonate-producing ecosystem. The late Early Cretaceous is also marked by the occurrence of several oceanic anoxic episodes, such as the latest Hauterivian Faraoni and the early Aptian Selli Events, which are both interpreted as the consequence of generalized eutrophic conditions. These observations imply that the late Early Cretaceous underwent larger fluctuations in nutrient supply, which may have interfered with the evolution of the widespread Urgonian platforms.

Our goal is to study the interactions between paleoceanographic and paleoclimatic change, and Urgonian carbonate buildup in the northern, Helvetic Alps. This unit remains understudied relative to its counterparts in eastern and central France. We will examine a selection of stratigraphic sections along lateral and proximal-distal transects for their facies and microfacies, biostratigraphy, sedimentology, and geochemistry (stable isotopes, -phosphorus contents). We will also use high-resolution panoramas from a selection of mountain walls, in order to detect lateral changes in facies and geochemistry and establish a sequence-stratigraphic framework. We specifically intend to compare the Urgonian units of late Barremian age and early Aptian age, which are separated by the so-called "Lower Orbitolina Beds". The late Barremian was less affected by anoxia, whereas the early Aptian witnessed progressive change in paleoceanographic conditions, which led up to the Selli Event.

P 22.3

The Voirons flysch (Voirons massif, Gurnigel nappe, Haute Savoie, France): a stack of km-sized flysch slices of Ultrahelvetic and north-Penninic origin

Kindler Pascal¹, Ospina-Ostios Lina Maria¹, Ragusa Jérémy & Wernli Roland¹

¹ Section of Earth and Environmental Sciences, University of Geneva, 13 rue des Maraîchers, CH-1205 Geneva
(Pascal.Kindler@unige.ch)

New biostratigraphic, sedimentological and petrographic data and a thorough review of existing literature presented here modify existing knowledge on the age, the sedimentology, the petrography, the paleogeographic origin, and the structure of the Voirons flysch (Voirons massif, Gurnigel nappe, Haute Savoie, France).

The Voirons massif is situated in the Chablais Prealps, Haute-Savoie, France. It belongs to the Gurnigel nappe which is commonly thought to derive from an ultrabriançonnais or south-Penninic realm. The massif includes three stratigraphic units that have been dated so far with calcareous nannofossils and dinoflagellates (van Stuijvenberg & Jan du Chêne 1981): the Voirons Sandstones (Danian-Ypresian), the Vouan Conglomerates (Ypresian-Lutetian) and the Saxel Marls (Lutetian-Bartonian). These units have been interpreted as deep-water turbidites and characteristically contain igneous lithoclasts of south-alpine affinity. The Voirons massif is diversely described as one large, eastward-dipping tectonic slice (Lombard 1940), or as an imbricate structure including three slivers named, from bottom up, Branta, Saxel and Tête du Char, respectively (van Stuijvenberg 1980).

During the past 15 years, we have re-examined and re-sampled key outcrops in the Voirons massif to study benthic and planktonic foraminifer assemblages, as well as sandstone petrography and sedimentology. Our biostratigraphic results are the following: the Voirons Sandstones range from the Middle Eocene (planktonic foraminiferal zones P12 to P14) to the Late Eocene-Early Oligocene (P14 to P20); the Vouan Conglomerates span the Late Eocene and the Early Oligocene (P15 to P20); the Saxel Marls extend also from the Late Eocene to the Early Oligocene (P15 to P20). The nannofossil assemblages retrieved from the same samples systematically yielded older ages than those obtained from planktonic foraminiferal associations. Main fieldwork and sedimentological/petrographic results are the following: (1) some of the youngest exposures of the Voirons Sandstones occur near the base of the Gurnigel nappe and are overlain by older strata that are not overturned; (2) exposures of Voirons Sandstones of similar age were deposited in distinctive paleoenvironmental settings (e.g. differences in water depth and oxygenation); (3) the Saxel Marls (distal turbidites and/or basinal contourites) seem to be tectonically, and not stratigraphically, superimposed over the Vouan Conglomerates (proximal turbidites) and may further be affected by a recumbent fold; (4) preliminary petrographic investigation show that all exposures of the Voirons Sandstones do not contain the same heavy mineral assemblage; and (5) petrographic analysis of the Voirons Sandstones revealed the occurrence of rare, but unmistakable fragments of diabase, similar to those found in large quantity in north-Helvetic flyschs.

The occurrence of flysch exposures in reverse stratigraphic order combined with the lack of evidence of bed overturning, the variability of paleodepositional settings inferred from different flysch outcrops of similar age, diverse heavy mineral content, and the anomalous superimposition of distal turbidites and/or basinal contourites (Saxel Marls) over proximal turbidites (Vouan Conglomerates), all suggest that the Voirons massif comprises several stacked flysch units of various paleogeographic origin.

The young age of these km-sized flysch slices precludes a south-Penninic origin, but rather indicates an Ultrahelvetetic and/or Valais provenance for these units, confirming previous investigations in the NE part of the Gurnigel nappe (Trümpy 2006). In particular, the Vouan Conglomerates and the Saxel Marls could possibly represent the non-metamorphic equivalents of the Pierre Avoi Unit (Sion-Courmayeur Zone, internal Valais domain) that yielded an assemblage of planktonic foraminifers of late Middle Eocene to possibly Early Oligocene age (Bagnoud et al. 1998), similar to the assemblages found in the younger units of the Voiron flysch, and likewise contains schist and sandstone blocks derived from the Zone Houillière (Bagnoud et al. 1998).

Finally, the absence of nannofossil assemblages contemporaneous with the observed planktonic foraminifer associations suggests the former have been reworked, dissolved, or just simply diluted and not found by earlier researchers. This example from the Voiron massif shows that planktonic foraminifer associations are the most reliable biostratigraphic tool to obtain an accurate age from flysch successions.

REFERENCES

- Bagnoud, A., Wernli, R. & Sartori, M. 1998: Découverte de foraminifères planctoniques paléogènes dans la zone de Sion-Courmayeur à Sion (Valais, Suisse). *Eclogae Geologicae Helveticae*, 91, 421-429.
- Lombard, A. 1940: Géologie des Voiron. Mémoires de la Société helvétique de sciences naturelles, 74, 112 pp.
- Stuijvenberg, J. Van 1980: Stratigraphie et structure de la nappe du Gurnigel aux Voiron (Haute-Savoie). *Bulletin de la Société fribourgeoise de sciences naturelles*, 69, 80-96.
- Stuijvenberg, J. Van & Jan du Chêne, R. 1981: Nouvelles observations stratigraphiques dans le massif des Voiron. *Bulletin du BRGM*, 1, 3-9.
- Trümpy, R. 2006: Geologie der Iberger Klippen und ihrer Flysch-Unterlage. *Eclogae Geologicae Helveticae*, 99, 79-121.

P 22.4

Lithostratigraphic harmonisation – a corner stone for a digital geological map with nationwide coverage

Morard Alain¹, Burkhalter Reto^{1/2}, Möri Andreas¹ & Strasky Stefan¹

¹ Federal Office of Topography swisstopo, Swiss Geological Survey (SGS), Seftigenstrasse 264, CH-3084 Wabern (alain.morard@swisstopo.ch)

² President, Swiss Committee of Stratigraphy (SCS), c/o SGS

For more than 100 years, geologists have been striving to produce detailed geological maps in all parts of Switzerland, as a basis for process understanding, resource exploitation, and territorial management. The production of the *Geological Atlas of Switzerland 1:25'000 (GA25)* is still in progress. The published GA25 maps cover about 60% of the area of Switzerland. However, with the *GeoCover* project launched by swisstopo in 2009, the perspective of a nationwide coverage at an “adjusted” 1:25'000 scale is about to become a reality. Indeed, geological vector data sets for the entire surface of Switzerland will be available in 2012 as a result of the compilation and digitalisation of data from many different sources and variable quality (GA25, Geological Special Maps, unpublished original field records).

Although an immense step forward, this long awaited result will not reach its full scope till the individual mapped elements have been tied across the whole territory and uniformly attributed. As concerns rock bodies, the numerous lithostratigraphic units in usage have to be listed, clearly defined and correlated across the sheets of the Atlas. Their description according to the *Data Model Geology* (Strasky et al. 2011) and their consistent chronostratigraphic allocation are also necessary in order to run rapid and extensive queries in the GIS database. This is the basic aim of the HARMOS project (harmonisation of lithostratigraphic units), run by the Swiss Geological Survey (SGS), in close collaboration with the Swiss Committee of Stratigraphy (SCS; Burkhalter & Heckendorn 2009).

The nine workgroups of the SCS (Jura-East, Jura-West, Molasse, Helvetic, Prealps, Penninic-West, Penninic-East, East-/Southalpine, Quaternary), with coordination and support from the SGS, are in charge of this challenging task. Their work will be made available online through the Lithostratigraphic Lexicon of Switzerland (www.stratigraphie.ch), and serve as a harmonised geological map legend. Once achieved, this ambitious project will permit to revise and adapt the *GeoCover* dataset and serve as a basis for the completion of a seamless, nationwide vector data set of Switzerland at a scale of 1:25'000.

REFERENCES

- Burkhalter, R. & Heckendorn, W. (2009): Das Stratigraphische Komitee der Schweiz (SKS). – Swiss Bulletin for applied Geology 14/1+2, 159–162.
- Strasky, S., Baland, P., & Oesterling, N. (2011): Datenmodell Geologie / Modèle de données géologiques – Version 1.4. – Swiss Geological Survey, swisstopo, 117 pages.

P 22.5

The Meride Limestone (Monte San Giorgio, Ticino, Switzerland): a Ladinian archive of paleoenvironmental changes.

Stockar Rudolf^{1,2}, Baumgartner Peter O.¹, Kocsis László³, Ulianov Alexey³, Dumitrica Paulian⁵ & Condon Daniel⁶

¹Institut de Géologie et Paléontologie, Université de Lausanne, Anthropole, CH-1015 Lausanne (rudolf.stockar@unil.ch).

²Museo Cantonale di Storia Naturale, Viale Cattaneo 4, CH-6900 Lugano.

³Institut de Minéralogie et Géochimie, Université de Lausanne, Anthropole, CH-1015 Lausanne.

⁵Dennikofenweg 33, CH-3073 Gümligen

⁶NERC, Isotope Geoscience Laboratory, Keyworth, UK-NG12 5GG Nottingham.

New paleontological data, mainly based on palynomorphs and radiolarians (Figs 1a-b) in addition to daonellids and ammonoids, significantly improve the biostratigraphic resolution of the Ladinian sequence of the Monte San Giorgio (UNESCO WHL site, Southern Alps, Switzerland). Accordingly, the San Giorgio Dolomite and the Meride Limestone are now regarded as a 620 m thick sequence spanning from the *E. curionii* (early Fassanian) to the *P. archelaus* (Longobardian) ammonoid zones. The age of the world-famous fossil marine vertebrate faunas of the Meride Limestone has consequently been resolved to the substage and zone levels.

High-resolution single-zircon U–Pb dates have been obtained using ID-TIMS and CA (annealing/chemical abrasion) pre-treatment techniques on volcanic ash layers intercalated in the biostratigraphically constrained intervals of the Meride Limestone.

Our results suggest that the time interval bracketed by the vertebrate-bearing Middle Triassic section at Monte San Giorgio is around 4 Myr and thus significantly shorter than so far assumed. Accordingly, evolutionary rates inferable from the different faunal associations replacing each other throughout the section have to be reconsidered.

The San Giorgio Dolomite and the Meride Limestone prove to correlate with intervals of the Buchenstein Fm. and the Wengen Fm. in the reference section at Bagolino, where the Global boundary Stratotype Section and Point (GSSP) for the base of the Ladinian were defined. The new radio-isotopic ages are by 1.5–2 Myr older than those published for the bio-chronologically age-equivalent intervals at Bagolino but they are consistent with the recent re-dating of the underlying Besano Formation, also performed using the CA technique (Mundil et al. 2010). Moreover, the high-resolution U–Pb ages allow a correlation of the vertebrate faunas of the Lower Meride Limestone with the marine vertebrate record of the Upper Australpine (Prosanto Formation, Switzerland), so far precluded by the poor biostratigraphical control of the latter (Furrer et al. 2008).

The re-measurement of the whole section at the cm-scale and the new high-resolution geochronological constraints allow to assess sedimentation rates. At Monte San Giorgio sedimentation rates are higher by over one order of magnitude with respect to those assumed for the Buchenstein facies of the Southern Alps and its equivalents of the Western Tethys, which formed under sediment-starved, pelagic conditions. Such values mirror prevailing high subsidence and high supply of periplatform carbonate mud stirred up from the adjoining Salvatore/Esino shallow-water platform systems.

Palynofacies analysis has been carried out on the whole section and has been cross-correlated with a new continuous oxygen and carbon stable isotope record. The isotope record, as well as the ammonoid and radiolarian evidence, highlight a basin evolution that reflects open-marine but not deep-water connections for the lower part of the section. A major volcanoclastic event occurring in the *E. gredderi* Zone coincides with the shift to a more restricted sedimentation, recurrently influenced by storm events and increased continental input (Stockar 2010; Stockar & Kustatscher 2010). Finally, the late

evolution of the basin is characterized by a sedimentation typical for a proximal, near shore setting with a relative high supply of terrestrial organic matter (Fig. 1c).

Geochemical analyses performed on all the classic vertebrate-bearing Ladinian horizons have been supplemented with the study of new bone material from stratigraphic intervals so far never considered or even regarded as barren. Trace elements and isotope compositions of the vertebrate remains have been analyzed and used as paleoenvironmental proxies. REE concentrations are around 3 orders of magnitude higher than found in modern biogenic apatite. The stratigraphic changes in REE patterns after the mentioned volcanoclastic event provide an useful tool to reconstruct variations in early burial conditions.

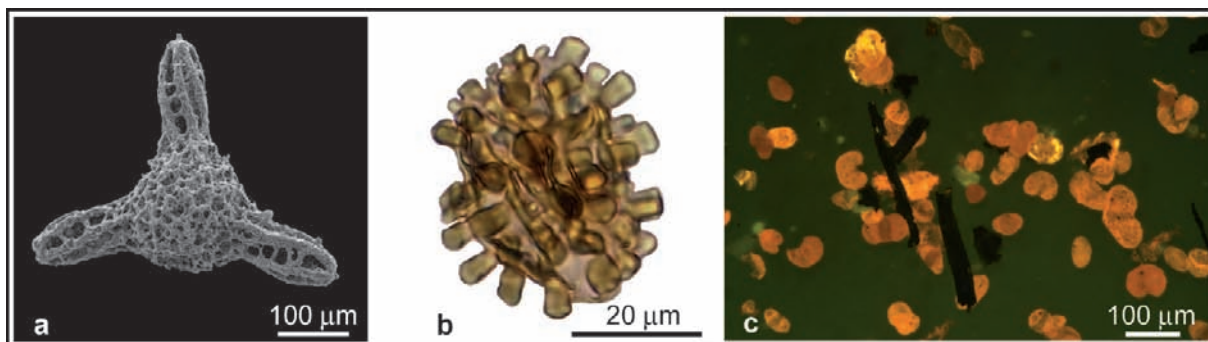


Fig. 1. (a) Radiolarian (*Eptingium manfredi*). (b) Sporomorph (*Echinitosporites iliacooides*). (c) Palynofacies (under blue light epifluorescence).

REFERENCES

- Furrer, H., Schaltegger, U., Ovtcharova, M. & Meister, P. 2008: U-Pb zircon age of volcanoclastic layers in Middle Triassic platform carbonates of the Austroalpine Silvretta nappe (Switzerland). *Swiss Journal of Geosciences* 101, 595–603.
- Mundil R., Pálffy J., Renne P. R., & Brack P. 2010: The Triassic timescale: new constraints and a review of geochronological data. In: *The Triassic Timescale* (Ed. by Lucas S. G.). Special Publications of the Geological Society of London, 334, 41–60.
- Stockar, R. 2010: Facies, depositional environment, and palaeoecology of the Middle Triassic Cassina Beds (Meride Limestone, Monte San Giorgio, Switzerland). *Swiss Journal of Geosciences* 103, 101–119.
- Stockar, R. & Kustatscher, E. 2010: The Ladinian flora from the Cassina beds (Meride Limestone, Monte San Giorgio, Switzerland): Preliminary results. *Rivista Italiana di Paleontologia e Stratigrafia* 116(2), 173–188.